Valence Bond Theory

David L. Cooper

editor

Valence Bond Theory

Valence Bond Theory

Edited by

David L. Cooper

Department of Chemistry
University of Liverpool
Liverpool L69 7ZD
UK

PREFACE

Over a decade ago, Elsevier published the much-cited volume "Valence-bond Theory and Chemical Structure" (Studies in Physical and Theoretical Chemistry, vol. 64) edited by Klein and Trinajstić. Since then, there have been very significant advances in methodology and many new researchers have entered the field. The last ten years have also seen a vast increase in the range of applications of methodology based on valence bond (VB) theory. As such, it seemed timely to publish a successor and complement to the earlier book.

The editor has attempted a selection of contributions by leading researchers from throughout the world. A wide range of work in the field is represented but, perhaps, with a greater emphasis on work in chemistry than in physics. The last two decades have certainly seen the re-emergence of *ab initio* valence bond theory as a serious tool for quantum chemical studies of molecular electronic structure and reactivity. Of course, one of the main attractions of VB approaches stems from the direct links between variational wavefunctions and more classical ideas of bonding. In physics there has been a vast change in attitude with extensive VB-based work following from the suggestion of P.W. Anderson in 1986 that a resonating valence bond (RVB) description was crucial in understanding high-temperature superconductivity. Various chapters in the present volume touch on such matters and provide a view of the extensive, predominantly semiempirical, research in this important area.

As is the nature of any such volume, a few people were unable to contribute and some important work will have been inadvertently overlooked. Nevertheless, the editor believes that a reasonable snapshot of the diverse field of VB theory is presented here. The general, historical development of VB theory is addressed in a few of the present chapters (such as those of Gallup and of Klein). Much more concerning this history may be found in the earlier Elsevier volume. Most of the present contributors were encouraged to focus particularly on work from the last decade, and to emphasize recent advances in methodology and recent applications. The editor is grateful to Doug Klein for advising on potential contributors and for his helpful comments on some of the manuscripts. It should certainly be clear from the exciting range of work described in this book that the future of VB theory looks very bright.

David L. Cooper

This Page Intentionally Left Blank

TABLE OF CONTENTS

This Page Intentionally Left Blank

1

Chapter 1

A short history of VB theory

G. A. Gallup

Department of Physics and Astronomy, University of Nebraska-Lincoln, Lincoln, Nebraska 68588-0111

1 INTRODUCTION

Shortly after quantum mechanics evolved Heitler and London[1] applied the then new ideas to the problem of molecule formation and chemical valence. Their treatment of the H_2 molecule was qualitatively very successful, and this led to numerous studies by various workers applying the same ideas to other substances. Many of these involved refinements of the original Heitler-London procedure, and within three or four years, a group of ideas and procedures had become reasonably well codified in what was called the valence bond (VB)* method for molecular structure.

A few calculations were carried out earlier, but by 1929 Dirac[2] wrote:

> The general theory of quantum mechanics is now almost complete, the imperfections that still remain being in connection with the exact fitting in of the theory with relativity ideas. These give rise to difficulties only when high-speed particles are involved, and are therefore of no importance in the consideration of atomic and molecular structure and ordinary chemical reactions . . . . The underlying physical laws necessary for the mathematical theory of a large part of physics and the whole of chemistry are thus completely known, and the difficulty is only that the exact application of these laws leads to equations much too complicated to be soluble . . . .

---

*A list of acronyms used in this chapter is in an appendix.

Since these words were written there has been no reason to feel that they are incorrect in any way. Perhaps the only difference between attitudes then and now are that, today, with visions of DNA chains dangling before our eyes, we are likely to have an even greater appreciation of the phrase "much too complicated to be soluble" than did early workers.

The early workers were severely hampered, of course, by the considerable difficulty of carrying out, for even small systems, the prescriptions of VB theory with sufficient accuracy to assess their merit. Except for H_2 and perhaps a few other molecules and ions, no really accurate VB calculations were possible, and, to make progress, most workers had to resort to many approximations. There thus arose a series of generalizations and conclusions that were based upon results of at least somewhat uncertain value. In their review of early results, Van Vleck and Sherman[3] comment upon this point to the effect that a physical or chemical result was not to be trusted unless it could be confirmed by several calculations using different sorts of approximations. It is perhaps only to be expected that such cross checking was rather infrequently undertaken.

In this chapter we have two goals. The first is to give a general picture of the sweep of history of VB theory. We restrict ourselves to *ab initio* versions of the theory or to versions that might be characterized as reasonable approximations to *ab initio* theory. Our second goal is to identify a few of the early ideas alluded to in the previous paragraph and see how they hold up when they are assessed with modern computational power. The list is perhaps idiosyncratic, but almost all deal with some sort of approximation, which generally will be seen to be poor.

2 History: PreWWII

In the next few sections we give an historical description of the activity and ideas that led to our current understanding of VB methods. As with so much other human activity, progress in the development of molecular theory was somewhat suspended by the second world war, and we use that catastrophe as a dividing point in our narrative.

Almost all of the ideas were laid down before WWII, but difficulties in carrying out calculations precluded firm conclusions in any but the simplest cases. The H_2 molecule does allow some fairly easy calculations, and, in the next section, we give a detailed description of the Heitler-London calculations on that molecule. This is followed by descriptions of early

work of a more qualitative nature.

2.1 Heitler-London Treatment

The original treatment of the H_2 molecule by Heitler and London[1] assumed a wave function of the form

$$\Psi = N[1s_a(1)1s_b(2) \pm 1s_b(1)1s_a(2)][\alpha(1)\beta(2) \mp \beta(1)\alpha(2)], \qquad (1)$$

where the upper signs are for the singlet state and the lower for the triplet, the "a" and "b" subscripts indicate $1s$ orbitals on either proton a or b, and α and β represent the $m_s = \pm 1/2$ spin states, respectively. When the function of Eq. (1) and the Hamiltonian are substituted into the variation theorem, one obtains the energy for singlet or triplet state of H_2 as

$$E^{(1,3)}(R) = 2E_H + \frac{J(R) \pm K(R)}{1 \pm T(R)}. \qquad (2)$$

Here E_H is the energy of a normal hydrogen atom, $J(R)$ was called the Coulomb integral, $K(R)$ was called the exchange integral, and $T(R)$ was called the overlap integral. The reader should perhaps be cautioned that the terms "Coulomb", "exchange", and "overlap" integrals have been used by many other workers in ways that differ from that initiated by Heitler and London. For the present article we adhere to their original definitions,

$$
\begin{align}
J(R) &= \langle 1s_a(1)1s_b(2)|V(1,2)|1s_a(1)1s_b(2)\rangle, & (3)\\
K(R) &= \langle 1s_a(1)1s_b(2)|V(1,2)|1s_b(1)1s_a(2)\rangle, & (4)\\
T(R) &= \langle 1s_a(1)1s_b(2)|1s_b(1)1s_a(2)\rangle, \\
&= \langle 1s_a(1)|1s_b(1)\rangle^2, \text{ and} \\
V(1,2) &= -1/r_{2a} - 1/r_{1b} + 1/r_{12} + 1/R_{ab}. & (5)
\end{align}
$$

These equations are obtained by assigning electron 1 to proton a and 2 to b, so that the kinetic energy terms and the Coulomb attraction terms $-1/r_{1a} - 1/r_{2b}$ give rise to the $2E_H$ term in Eq. (2). $V(1,2)$ in Eq. (5) is then that part of the Hamiltonian that goes to zero for the atoms at long distances. It is seen to consist of two attraction terms and two repulsion terms. As observed by Heitler and London, the bonding in the H_2 molecule arises from the way these terms balance in the J and K integrals. We show a graph of these integrals in Fig. (1). The energy of Eq. (2) can be improved in a number of ways, and we will discuss the way the Heitler-London theory predicts bonding after discussion of one of these improvements.
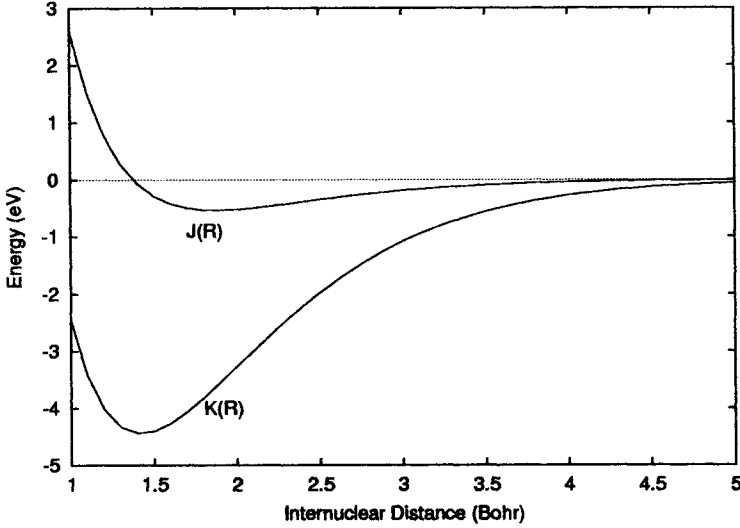
Figure 1: The relative sizes of the $J(R)$ and $K(R)$ integrals. The values are in eV.

The $1s$ orbitals in Eq. (1) represent the actual solution to the isolated H-atom. When we include an arbitrary scale factor in the exponent of the $1s$ orbital we symbolize it as

$$1s' = \sqrt{\alpha^3/\pi} \exp(-\alpha r). \qquad (6)$$

When the $1s'$ orbital is used in the place of the actual H-atom orbital, one has α as a variation parameter to adjust the wave function. The energy expression becomes

$$E^{1,3}(\alpha, R) = 2E_H + (\alpha - 1)^2 + \alpha \frac{J(\alpha R) \pm K(\alpha R)}{1 \pm T(\alpha R)}, \qquad (7)$$

which reduces to the energy expression of Eq. (2) when $\alpha = 1$. The changes brought by including the scale factor are only quantitative in nature and leave the qualitative conclusions unmodified.

It is important to understand why the $J(R)$ and $K(R)$ integrals have the sizes they do. We consider $J(R)$ first. As we have seen from Eq. (5), $V(1,2)$ is the sum of four different Coulombic terms from the Hamiltonian. If these are substituted into Eq. (3), we obtain

$$
\begin{aligned}
J(R) &= 2j_1(R) + j_2(R) + 1/R, \\
j_1(R) &= \langle 1s_a| - 1/r_b|1s_a \rangle = \langle 1s_b| - 1/r_a|1s_b \rangle, \\
j_2(R) &= \langle 1s_a(1)1s_b(2)|1/r_{12}|1s_a(1)1s_b(2) \rangle.
\end{aligned}
$$

The quantity $j_1(R)$ is seen to be the energy of Coulombic attraction between a point charge and a spherical charge distribution, $j_2(R)$ is the energy of Coulombic repulsion between two spherical charge distributions, and $1/R$ is the energy of repulsion between two point charges. $J(R)$ is thus the difference between two attractive and two repulsive terms that cancel to a considerable extent. The magnitude of the charges is one in every case. This is shown in Fig. (2), where we see that the resulting difference is only a few percent of the magnitudes of the individual terms.
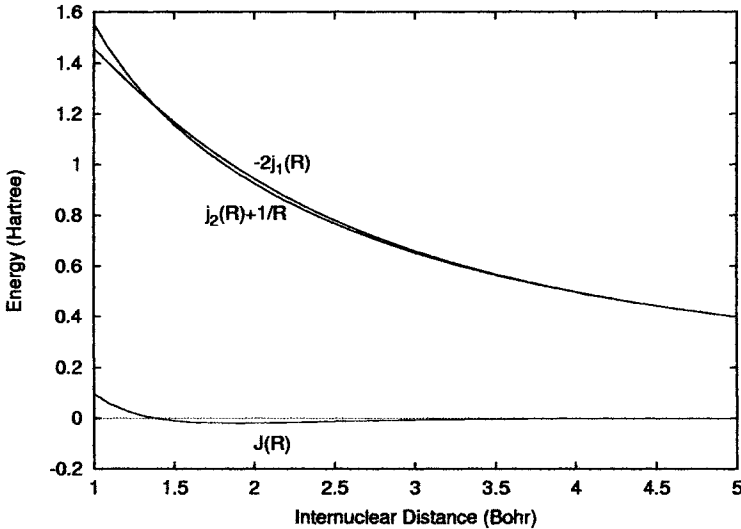
Figure 2: Comparison of the sizes of $j_2 + 1/R$ and $-2j_1$ that comprise the positive and negative terms in the Coulomb integral. Values are in Hartrees.

This is to be contrasted with the situation for the exchange integral. In this case we have

$$
\begin{aligned}
K(R) &= 2k_1(R)S(R) + k_2(R) + S(R)^2/R, \\
k_1(R) &= \langle 1s_a| - 1/r_b|1s_b\rangle = \langle 1s_a| - 1/r_a|1s_b\rangle, \\
k_2(R) &= \langle 1s_a(1)1s_b(2)|1/r_{12}|1s_a(2)1s_b(1)\rangle.
\end{aligned}
$$

The magnitude of the charge in the overlap distribution, $1s_a1s_b$, is $S(R)$, and here again, the overall result is the difference between the energies of attractive and repulsive terms involving the same sized charges of different shaped distributions. The values are shown in Fig. (3), where we see that
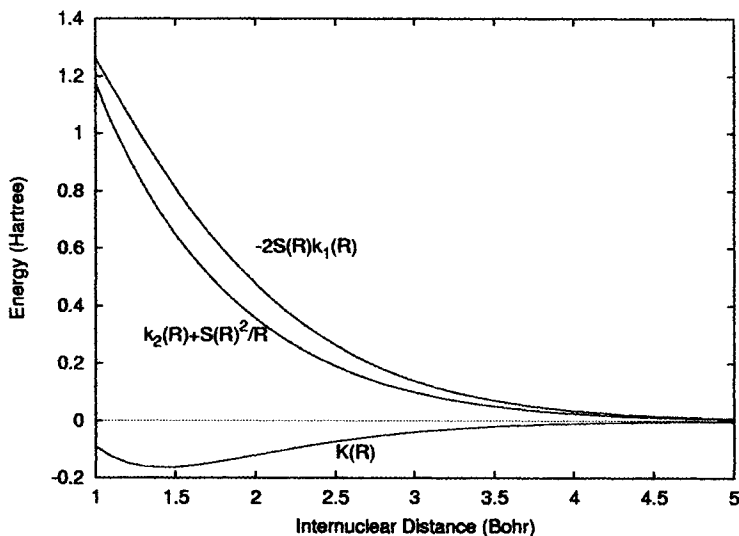
Figure 3: Comparison of the sizes of $k_2 + S^2/R$ and $-2k_1 S$ that comprise the positive and negative terms in the exchange integral. Values are in Hartrees.

now there is a considerably greater difference between the attractive and repulsive terms. This leads to a value about 20% of the magnitude of the individual terms.

These values for $J(R)$ and $K(R)$ may be rationalized in purely electrostatic terms involving charge distributions of various sizes and shapes.* From the point of view of electrostatics, $J(R)$ is the interaction of points and spherical charge distributions. The well-known effect, where the interaction of a point and spherical charge at a distance R is due only to the portion of the charge inside a sphere of radius R, leads to an exponential fall-off $J(R)$, as R increases.

The situation is not so simple with $K(R)$. The overlap charge distribution is shown in Fig. (4) and is far from spherical. The upshot of the differences is that the $k_2(R)$ integral is the *self-energy* of the overlap distribution and is more dependent upon its charge than upon its size. In addition, at any distance there is in $k_1(R)$ a portion of the distribution that surrounds the point charge, and, again, the distance dependence is decreased. The overall effect is thus that shown in Fig. (1).

---

*It should not be thought that the result $|J(R)| \ll |K(R)|$ is peculiar to the $1s$ orbital shape. It is fairly easy to show that a single spherical Gaussian orbital in the place of the $1s$ leads to a qualitatively similar result.
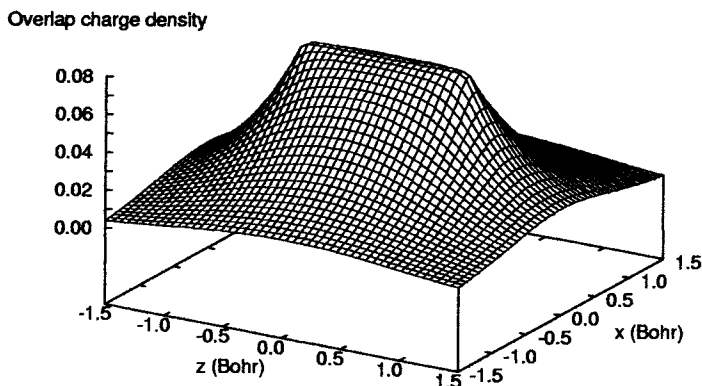
Figure 4: The overlap charge distribution when the H–H distance is near the molecular equilibrium value. We show an altitude plot of the value on the x-z plane.

We have not yet spoken of the effect of optimizing the scale factor in Eq. (7). Wang[4] showed, for the singlet state, that it varies from 1 at $R = \infty$ to about 1.17 at the equilibrium separation. Since both J and K have relatively small slopes near the equilibrium distance, the principal effect is to increase the potential energy portion of the energy by about 17%. The $(\alpha - 1)^2$ term increases by only 3%. Thus the qualitative picture of the bond is not changed by this refinement.

We have gone into some detail discussing the Heitler-London treatment of H_2, because of our conviction that it is important to understand the details of the various contributions to the energy. Our conclusion is that the bonding in H_2 is due primarily to the exchange effect caused by the combination of the Pauli exclusion principle and the required singlet state. Early texts (see *e.g.*, [5]) frequently emphasized the *resonance* between the direct and exchange terms, but this is ultimately due the principles in the last sentence. The peculiar shape of the overlap distribution leads to the major portion of the chemical bonding energy.*

---

*Those familiar with the language of the molecular orbital picture of bonding may be surprised that no parallel to the *delocalization energy* seems present in our description. That effect would occur in the VB treatment only if ionic terms are included. We thus conclude that delocalization is less important than the exchange attraction in bonding.

2.2 Extensions past the simple Heitler-London-Wang result

After the initial qualitative success of the simple VB calculation, further refinements that might be called multiconfigurational were investigated. These involve the introduction of *polarization*[6] and *ionic*[7] terms into the wave function. All of these refinements improve the quantitative agreement of the bond dissociation energy, D_e, with experiment, but any treatment so heavily dependent upon the H $1s$ and p_σ orbitals under-represents the electron correlation required to obtain better answers. At the time, such a treatment was carried out by James and Coolidge[8], but this was not really an extension of the Heitler-London-Wang calculation in any usefully physical sense.

2.3 Polyatomic molecules

The original Heitler-London calculation, being for two electrons, did not require any complicated spin and antisymmetrization considerations. It merely used the familiar rules that the spatial part of two-electron wave functions are symmetric in their coordinates for singlet states and anti-symmetric for triplet states. Within a short time, however, Slater[10] had invented his determinantal method, and two approaches arose to deal with the twin problems of antisymmetrization and spin state generation. When one is constructing trial wave functions for variational calculations the question arises as to which of the two requirements is to be applied first, antisymmetrization or spin eigenfunction.

1. Methods based upon Slater determinantal functions (SDF). When we take this approach, we are, in effect, applying the antisymmetrization requirement first. Only if the orbitals are all doubly occupied among the spin orbitals is the SDF automatically, at the outset, an eigenfunction of the total spin. In all other cases further manipulations are necessary to obtain an eigenfunction of the spin, and these are written as sums of SDFs.

2. Symmetric group methods. When using these we, in effect, first construct n-particle (spin only) eigenfunctions of the spin. From these we determine the functions of spatial orbitals that must be multiplied by the spin eigenfunctions in order for the overall function to be antisymmetric. It may be noted that this is precisely what is done in almost all treatments of two electron problems. Generating spatial functions

with the required properties leads to considerations of the theory of representations of the symmetric groups.

It is difficult to recreate today the attitudes that determined which of these approaches people chose. We can speculate that for small systems the basic simplicity of the SDF approach was appealing. The group theoretic approach seemed to some to be over-complicated. We quote from the Van Vleck and Sherman[3] review.

> . . . the technique of the permutation group is complicated, and more general than needed for practical purposes because the Pauli principle must be satisfied after the addition of spin. In the language of group theory, many "characters" for the orbital permutation group are not compatible with the Pauli principle. . . Thus the character theory is too general.

One must agree that the precise recipe implied by Van Vleck's and Sherman's language is daunting. The use of *characters* of the irreducible representations in dealing with spin state-antisymmetrization problems does not appear to lead to any very useful results. From today's perspective, however, it is known that some irreducible representation matrix elements (not just the characters) are fairly simple, and when applications are written for large computers, the systematization provided by the group methods is useful.

2.4 The Heitler-Rumer Method for polyatomic molecules

Heitler and Rumer[9] gave a generalization of the H_2 molecule results for polyatomic molecules. In these the quantities corresponding to the overlap in the normalization integral (the T in $(1 \pm T)^{-1}$) of Eq. (2) were set to zero, and permutations of higher order than binary were ignored in evaluating matrix elements. For the special case of a central atom, $\mathbf{C}$ of high multiplicity bonded to other atoms, $\mathbf{P}$, $\mathbf{Q}, \cdots$, they arrived at the total energy for the state of lowest multiplicity,

$$
E = E_{\mathbf{C}} + E_{\mathbf{P}} + E_{\mathbf{Q}} + \cdots + J_{\mathbf{CPQ}\cdots} + p_{\mathbf{P}} K_{\mathbf{CP}} + p_{\mathbf{Q}} K_{\mathbf{CQ}} + \cdots - p_{\mathbf{P}} p_{\mathbf{Q}} K_{\mathbf{PQ}} - \cdots ,
\tag{8}
$$

where $p_{\mathbf{P}}$ *etc.*, are the number of pairs of electrons in the $\mathbf{C}$–$\mathbf{P}$ bond *etc.*, $J_{\mathbf{CPQ}\cdots}$ is the simple sum of all of the Coulomb integrals and $K_{\mathbf{CP}}$ *etc.*, are the exchange integrals. In addition, this formula requires all of the

atoms be in S states. Eq. (8), although fairly impressive, has too many restrictions and approximations to be really satisfactory. In Section 4.1 we return to an examination of some of these approximations.

2.5 Slater's bond functions

Fairly soon after the Heitler-London calculation, Slater, using his determinantal functions, gave a generalization to the n-electron VB problem[10]. This was a popular approach and several studies followed exploiting it. It was soon called the method of *bond eigenfunctions*. A little later Rumer[11] showed how the use of these could be made more efficient by eliminating linear dependencies before matrix elements were calculated.

Slater's bond eigenfunctions constitute one choice (out of an infinite number) of a particular sort of basis function to use in the evaluation of the Hamiltonian and overlap matrix elements. They have come to be called the Heitler-London-Slater-Pauling (HLSP) functions. Physically, they treat each chemical bond as a singlet-coupled pair of electrons. This is the natural extension of the original Heitler-London approach. In addition to Slater, Pauling[12] and Eyring and Kimbal[13] have contributed to the method. Our following description does not follow exactly the discussions of the early workers, but the final results are the same.

Consider a singlet molecule with $2n$ electrons, where we wish to use a different atomic orbital (AO) for each electron. We can construct a singlet eigenfunction of the total spin as the product of n electron pair singlet functions

$$
\begin{aligned}
\Phi &= [\alpha(1)\beta(2) - \beta(1)\alpha(2)][\alpha(3)\beta(4) - \beta(3)\alpha(4)] \\
&\times \cdots \times [\alpha(2n-1)\beta(2n) - \beta(2n-1)\alpha(2n)],
\end{aligned}
\tag{9}
$$

where, clearly, $S_z\Phi = 0$. Consider the total *spin raising** operator,[14]

$$
S = S_x + iS_y = \sum_{k=0}^{2n} S_{xk} + iS_{yk} = \sum_{k=0}^{2n} S_k,
\tag{10}
$$

and we operate with it upon Φ. This results in zero, since for every pair function in Eq. (9) there is a corresponding pair of terms in S, and, *e.g.*,

$$
\begin{aligned}
(S_i + S_j)[\alpha(i)\beta(j) - \beta(i)\alpha(j)] &= [\alpha(i)\alpha(j) - \alpha(i)\alpha(j)] \\
&= 0.
\end{aligned}
$$

---

*The individual spin raising operator satisfies $S\alpha = 0$ and $S\beta = \alpha$

Now, the total spin operator may be written as $S^2 = S^\dagger S + S_z(S_z + 1)$, and, therefore, it is seen that $S^2 \Phi = 0$ and is a singlet spin function.

We now multiply Φ by a product of the orbitals, one for each particle, $u_1(1)u_2(2) \cdots u_{2n}(2n)$, where u_1, u_2, $\cdots u_{2n}$ is some particular ordering of the orbital set. When we apply the antisymmetrizer to the function of space and spin variables, the result can be written as the sum of 2^n SDFs. It is fairly easily seen that there are $(2n)!/(2^n n!)$ different $2n$-electron functions of this sort that can be constructed. Rumer's result, referred[11] to above, shows how to remove all of the linear dependences in this set and arrive at the minimally required number, $(2n)!/[n!(n+1)!]$, of bond functions to use in a quantum mechanical calculation.

2.5.1 *The perfect pairing function*

We have given a general discussion of the bond eigenfunction method and have pointed out that using all of the Rumer diagrams gives functions that completely span the subspace of the particular configuration addressed. Many of the early calculations used only one of the Rumer functions, and in this case the calculations were called perfect pairing results. Of course, each Rumer function represents perfect pairing between a particular set of orbitals, but the *perfect pairing* approximation always implied that the paired orbitals had a relation to the actual bonding of the molecule.

As an example, consider methane. If the carbon atom L-shell orbitals are arranged as tetrahedral hybrids, we can take the $t_a t_b t_c t_d$ configuration and combine this with an $s_a s_b s_c s_d$ configuration of the four hydrogen atoms. Table 1 shows some numbers of states associated with these orbitals. It is

Table 1: Numbers of states under various constraints for methane and four tetrahedral hybrids and four H-atom orbitals.

	Ionic	Number of States
All Singlet States	yes	1764
All States of $^1A_1$ Symmetry	yes	164
All States with $t^4 s^4$	no	86
All $^1A_1$ States with $t^4 s^4$	no	11
All States with $t_a t_b t_c t_d s_a s_b s_c s_d$	no	14
All $^1A_1$ States with $t_a t_b t_c t_d s_a s_b s_c s_d$	no	3
Perfect pairing State ($^1A_1$)	no	1

clear that using only the single perfect pairing function represents a consid-

erable constraint upon the wave function. Nevertheless, actual calculations show that it is the largest component of the full wave function, although not overwhelmingly so.

Pauling's criterion of maximum overlap led to the idea that the tetrahedral hybrids should be the most effective in the the perfect pairing wave function. People realized, however, that the effective state of the C atom in this wave function was not the ground state but a mixture of excited states determined by the detailed nature of the state. Van Vleck dubbed this the *valence state* of carbon, and one of the concerns of the early workers was the determination of the energy of this state and the corresponding influence this has upon the C–H bond energy in hydrocarbons. We examine these questions in more detail later in Sec. 4.4, but it must be emphasized that this whole question hinges upon the use of the perfect pairing wave function alone in determining energies.

2.6 Symmetric group theoretic approaches

The early workers, when treating two electron systems, usually made the observation that singlet states spin functions are antisymmetric while triplet spin functions are symmetric with respect to the interchange of particles, *i.e.,*

$$\sqrt{1/2}[\alpha(1)\beta(2) - \beta(1)\alpha(2)] \quad : \quad \text{singlet}$$

$$\begin{gathered} \alpha(1)\alpha(2) \\ \sqrt{1/2}[\alpha(1)\beta(2) + \beta(1)\alpha(2)] \quad : \quad \text{triplet} \\ \beta(1)\beta(2) \end{gathered}$$

Consequently, for the total wave function to be properly antisymmetric, the spatial function to be multiplied by the spin functions must be symmetric or antisymmetric for singlet or triplet states, respectively. Satisfying these requirements may be made more explicit in the following way.

The antisymmetrizer for two electrons may be written

$$\mathcal{A} = 1/2[I - (12)_r(12)_s], \tag{11}$$

where (12) stands for the binary interchange and the $_r$ subscript indicates this permutation is to be applied to spatial functions and the $_s$ subscript

indicates application to spin functions.* We thus factor the permutation into a space and a spin part. We may write idempotent symmetrizers or antisymmetrizers for either space or spin functions as

$$\mathcal{S}_i = \frac{1}{2}[I + (12)_i],$$
$$\mathcal{A}_i = \frac{1}{2}[I - (12)_i],$$

where $i = r$ or s. With this we obtain

$$\mathcal{A} = \mathcal{S}_r \mathcal{A}_s + \mathcal{A}_r \mathcal{S}_s, \tag{12}$$

as a "factored" form of $\mathcal{A}$. We work with Eq. (12) in the following way.

We can use one of the spin eigenfunctions above, symbolizing it by Θ_m^S, and multiply it by an arbitrary spatial function, Ξ, to obtain a function of both space and spin,

$$\Psi = \Xi \Theta_m^S, \tag{13}$$

which is, of course, not antisymmetric. Applying $\mathcal{A}$ to Ψ we obtain

$$\mathcal{A}\Psi = \mathcal{S}_r \Xi \mathcal{A}_s \Theta_m^S + \mathcal{A}_r \Xi \mathcal{S}_s \Theta_m^S. \tag{14}$$

If Θ_m^S is singlet, only the first term on the right of Eq. (14) survives, and the spatial part of the function, $\mathcal{S}_r \Xi$, is symmetric. For any one of the three triplet functions the other term on the right of Eq. (14) is the one that survives with the consequence that $\mathcal{A}_r \Xi$ is the required spatial function. These are the familiar results, of course.

We have given a short description of the two electron case. The important point is that there is a generalization of Eq. (12) to n electrons. It takes the general "factored" form

$$\mathcal{A}(1 \cdots n) = \sum_i (P_i^{op})_r (Q_i^{op})_s, \tag{15}$$

where P^{op} and Q^{op} are sums of permutations with coefficients that are determined by the irreducible representation matrices of the symmetric group, S_n. We write the general function to be used in our calculations as

$$\Psi = \Xi \Theta_M^S, \tag{16}$$

where Ξ is an n-electron spatial function and Θ_M^S is an eigenfunction of the total spin. The important result is that $(Q_i^{op})_s \Theta_M^S$ is zero for most of

---

*We write the antisymmetrizer as a properly idempotent operator for this discussion, contrary to the common practice that uses a $\sqrt{1/2}$ prefactor.

the terms,* and this is the source of the simplifications obtained by using symmetric group methods in atomic or molecular calculations. There is not room here to give further details of these methods, but we do discuss the nature of Θ_M^S.

The n-electron spin functions are sums of products of n α or β functions that satisfy

$$\begin{aligned} S^2\Theta_m^S &= \hbar^2 S(S+1)\Theta_m^S, \text{ and} \\ S_z\Theta_m^S &= \hbar m\Theta_m^S. \end{aligned}$$

Both the S^2 and S_z operators are symmetric sums of operators for each particle and, thus, both commute with every permutation of the n particle labels. Therefore, the eigenfunctions and eigenvalues of S^2 may be classified by the irreducible representations of the symmetric group. The important result is that there is a one-to-one relation between eigenvalues of S^2 and nonequivalent irreducible representations of the groups. We will not give the precise result here, there is a unique generalization of Eq. (12) for the n electron case. Therefore, applying the antisymmetrizer to an n-electron space-spin function of the form $\Xi\Theta_m^S$ results in a space function appropriate to the total spin quantum number S and satisfying the Pauli principle.

Serber[15] has contributed to the analysis of symmetric group methods as an aid in dealing with the twin problems of antisymmetrization and spin state. In addition, Van Vleck espoused the use of the Dirac vector model[16] to deal with permutations.[17] Unfortunately, this becomes more difficult rapidly if permutations past binary interchanges are incorporated into the theory. Somewhat later the Japanese school involving Yamanouchi[18] and Kotani et al.[19] also published analyses of this problem using symmetric group methods.

3   History: PostWWII and automatic computation

The period during and about ten years after WWII saw the beginnings of the development of automatic computing machinery. Although early workers made heroic efforts in many calculations, computers allowed calculations of molecular structure that were far too tedious to undertake by hand or to expect reliable results. The new computers thus allowed many of the quantitative procedures worked out earlier to be checked and accepted

---

*In the two electron case one term was zero and the other not.

or abandoned. Nevertheless, one of the principal developments in the late 1940s was a new way of arranging the orbitals in VB calculations. In this section we start with the Coulson-Fisher approach and follow with other proposals that grow naturally out of it. Much more recent developments in computers have also allowed multiconfigurational VB treatments of a size unimagined 45 years ago, and we also describe these in this section.

3.1   The Coulson and Fisher treatment of H_2

Coulson and Fisher[20] took a new step in molecular calculations with their treatment of H_2 in which the orbitals were non-orthogonal, but extended over both centers. They do not actually call their treatment a VB calculation, but their idea is an important step in the development of the ideas of others who do use the VB label in describing their treatments.

The essence of this method, when illustrated with H_2, is to write the two orbitals for the covalent Heitler-London function as

$$A(\vec{r}) = N(1s_a' + c1s_b'), \text{ and}$$
$$B(\vec{r}) = N(c1s_a' + 1s_b').$$

The constant c provides a parameter to vary during optimization. They, in effect, used molecular orbital (MO)s in the wave function, but this terminology is not usually used in the current context. The introduction of this sort of orbital provides the same effect as ionic terms in the more traditional treatment. The next two sections give modern extensions of this method.

3.1.1   *Goddard's generalized VB*

Goddard[21] made the earliest important generalization to the Coulson-Fisher method. Goddard's generalized VB (GGVB) wave function is written in terms of orbitals that are linear combinations of the AOs. Using the genealogical set of spin functions in turn and

$$\Psi = \mathcal{A}(1\cdots n)\Xi(1\cdots n)\Theta_{Mi}^{S}, \tag{17}$$

there are $i = 1, 2, \cdots, f$,

$$f = \frac{2S+1}{n+1} \binom{n+1}{n/2 - S} \tag{18}$$

different trial wave functions that can be constructed. Goddard designated these as the G1, G2,$\cdots$, Gf methods, the general one being Gi. For each of these functions the total energy may be optimized with respect to the coefficients in the orbitals. In general, the orbitals are grouped into two sets; orthogonality is enforced within the sets but not between them. Using the calculus or variations in the usual way, one arrives at a set of Fock-like operators that determine the optimum orbitals. The result is a set of f different energies, and one chooses the wave function for the lowest of these as the best GGVB answer. In actual practice only the G1 or Gf methods have been much used.

In simple cases the G1 is a HLSP function while the Gf wave function is a standard tableaux function, which we describe below in Sect. 3.3. For Gf wave functions one may show that the above orthogonality requirement is not a real constraint on the energy. On the other hand, no such invariance occurs with G1 or HLSP functions, so the orthogonality constraint has a real impact on the calculated energy in this case and with all other Gi wave functions.

Goddard and his coworkers applied the method to a number of chemical problems with an emphasis on orbital following results.

3.1.2 *The spin-coupled VB*

Somewhat later Pyper and Gerratt[22] proposed the spin coupled valence bond (SCVB) wave function. Further developments are reviewed by Gerratt, Cooper, and Raimondi[23] in an earlier volume of this series. These workers originally used genealogical spin functions, which produce the *genealogical representation* of the symmetric groups[24], but so long as the irreducible representation space is completely spanned, any representation will give the same energy and wave function. About the same time van Lenthe and Balint-Kurti[25] proposed using an equivalent wave function. The principal differences between these proposals deal with methods of optimization. We will continue to use the SCVB acronym for this method.

We have seen that with a system of n electrons in a spin state S there are, for n linearly independent orbitals, f (given by Eq. (18)) linearly independent spatial functions that can be constructed from these orbitals. In the present notation the SCVB wave function is written as the general

linear combination of these.

$$\Psi_{SCVB} = \sum_{i=1}^{f} C_i \phi_i(u_1, \cdots, u_n), \tag{19}$$

where the orbitals in ϕ_i are, in general, linear combinations of the whole AO basis.* The problem is to optimize the Rayleigh quotient for this wave function with respect to both the C_i and the linear coefficients in the orbitals. In contrast to the GGVB method the orbitals are subjected to no orthogonality constraints.

Using familiar methods of the calculus of variations, one can set the first variation of the energy with respect to the orbitals and linear coefficients to zero. This leads to a set of Fock-like operators, one for each orbital. Gerratt, *et al* use a second-order stabilized Newton-Raphson algorithm for the optimization. This gives a set of occupied and virtual orbitals from each Fock operator as well as optimum C_is.

The SCVB energy is, of course, just the result from this optimization. Should a more elaborate wave function be needed, the virtual orbitals are available for a more-or-less conventional, but non-orthogonal configuration interaction (CI) that may be used to improve the SCVB result. Thus improving the basic SCVB result here may involve a wave function with many terms.

SCVB wave functions for very simple systems appear similar to those of the GGVB method, but the orthogonality constraints in the latter have increasingly serious impacts on the results for larger systems.

3.1.3 *The BOVB method*

More recently Hiberty *et al.*[26] proposed the breathing orbital valence bond (BOVB) method, which can perhaps be described as a combination of the Coulson-Fisher method and techniques used in the early calculations of the Weinbaum.[7] The latter are characterized by using differently scaled orbitals in different VB structures. The BOVB does not use direct orbital scaling, of course, but forms linear combinations of AOs to attain the same end. Any desired combination of orbitals restricted to one center or allowed to cover more than one is provided for. These workers suggest that this gives a simple wave function with a simultaneous effective relative accuracy.

---

*The requirements of symmetry may modify this.

3.2 More recent developments in symmetric group methods

Earlier symmetric group procedures were usually based upon the irreducible representation matrices corresponding to the various schemes that had been developed for determining spin eigenfunction. After WWII the earlier work of Young on symmetric groups found application to the problems of implementing VB ideas. Matsen and coworkers[27] introduced what they termed a *spin-free* approach. Somewhat later the present author[30] introduced VB basis functions based upon Young's *standard tableaux* representation.

All methods produce one or another of the infinity of irreducible representations of the symmetric groups, and, if basis sets always completely span the representation, the quantum mechanical results are the same. One of the advantages of Young's procedure is the way it clearly shows the connections among the various ways that basis sets can be arranged.

The concept of the tableau is central to Young's theory, and we use only the portions of the theory necessary to discuss VB theory. For a particular set of n orbitals $u_1 \cdots u_n$ and n electrons, symbols for the orbitals may be arranged in a two-column table, in which the two columns are not necessarily the same length,

$$
\begin{bmatrix}
u_1 & u_{n-k+1} \\
\vdots & \vdots \\
\vdots & u_n \\
u_{n-k} &
\end{bmatrix}.
$$

The difference in the lengths of the columns is related to the spin; the total spin quantum number is $S = n/2 - k$. Clearly, $k \leq n/2$. In the tableau the orbitals are associated with particles labeled sequentially down the first and then down the second column. The subscripts on the orbitals label the functions, not the arguments.

Young defined two operators, the row symmetrizer $\mathcal{P}$ and the column antisymmetrizer $\mathcal{N}$, and we assume the these operate on (permute) the particle labels not the orbital labels. Each tableau designates a product of orbitals with a particular ordering

$$
\Xi = u_1(1)u_2(2)\cdots u_n(n). \tag{20}
$$

As the names suggest $\mathcal{P}$ is the product of k symmetrizing operators for the particles in the rows,

$$
\mathcal{P} = \frac{1}{2}[I + (1, n-k+1)] \cdots \frac{1}{2}[I + (k, n)], \tag{21}
$$

and $\mathcal{N}$ is the product of the two antisymmetrizers of the columns

$$\mathcal{N} = \mathcal{A}(1 \cdots n - k)\mathcal{A}(n - k + 1 \cdots n). \tag{22}$$

The (i, j) symbol in Eq. (21) stands for a binary interchange of the particles indicated. It will be observed that the particles operated upon in these operators are related closely to the way the particle labels occur in the tableau. As we have defined them, $\mathcal{P}$ and $\mathcal{N}$ are strictly idempotent.

Using the operators we have defined and the spatial function Ξ, new functions may be constructed, e.g., $\mathcal{P}\Xi$. It should be clear that this function now is insensitive to the positions of orbitals in the first k rows, i.e., one could interchange u_1 and u_{n-k+1}, for example, without changing $\mathcal{P}\Xi$. Similarly, any rearrangement (permutation) of the orbitals in a column will do no more that change the sign of $\mathcal{N}\Xi$. Permutations that change both the row and column position of orbitals will result in changing these projected functions.

Another central result of Young's work, when stated in our current language, is that $\mathcal{N}\mathcal{P}\Xi$ is equivalent to the perfect pairing function of Slater with the orbitals in the same rows paired.[27] At what might be called the other extreme, Heitler's and Rumer's early work assumed that diatomic molecules interacted with the atoms in their highest spin states consistent with the configuration, and these functions are equivalent to $\mathcal{P}\mathcal{N}\Xi$, where the orbitals in a column are associated with one of the atoms. A polyatomic analog of this situation exists. Thus, merely inverting the order in which the operators are applied, passes from one type of function to the other.

In discussions of the total spin[31] of multielectron systems the *spin branching diagram* is frequently used. Fig. (5) shows a version. The $\mathcal{N}\mathcal{P}$ operator corresponds to the branch in the diagram where the lowest line is always taken and the $\mathcal{P}\mathcal{N}$ operator to the branch where the highest possible branch is taken. The two Young operators thus correspond to the first and last rows of the genealogical irreducible representations of the symmetric groups, and, hence, to Goddard's G1 and Gf "methods", respectively. Therefore, Young's tableaux and the corresponding operators constitute a way of, at least partly, unifying the various techniques that have been devised for dealing with spin and antisymmetrization and VB calculations.

As a last point we note that the present author and his coworkers[36] devised an algorithm for the calculation of matrix elements of the overlap and Hamiltonian based upon the $\mathcal{P}\mathcal{N}$ operator that is n^5 in its worst case,
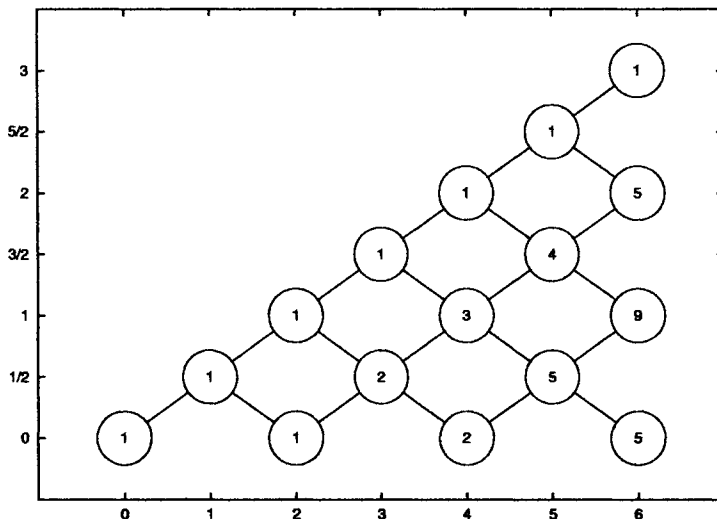
Figure 5: The spin branching diagram for 0 to 6 electrons (horizontal axis). The total spin quantum number is on the vertical axis. The numbers in the circles give the spin degeneracies.

where n is the number of electrons. There are reasons to believe that this is the best exponent that can be achieved. Transformation to the $\mathcal{NP}$ functions is possible when desired.

3.3 Multiconfiguration methods

The original Heitler-London treatment with its various extensions was a VB treatment that included several configurations, *e.g.*, the total wave function is a sum of terms with spatial functions made up of different subsets of the orbitals. This is the essence of *multiconfiguration* methods. The most direct extension of this sort of approach is, of course, the inclusion of larger numbers of configurations and the application to larger molecules. The computational power allowed calculations of this sort.

At the same time molecular orbital (MO) methods were seeing a rapid development, also because of increased computational ability. These, at least on the surface, appear to provide a simpler approach to molecular structure calculations. Nevertheless, Matsen and Browne[32] made a forceful case for the use of MCVB methods,* indicating the difficulties

---

*They called their suggested procedure an atomic orbital configuration interaction (AOCI) calculation.

that the enforced orthogonality in molecular orbital configuration inter-action (MOCI) calculations cause with processes that involve large scale relative motions of the nuclei.

3.3.1 *The multistructure procedure of Balint-Kurti and Karplus*

Balint-Kurti and Karplus[28] implemented an earlier suggestion of Moffit[29] for the evaluation of matrix elements of the Hamiltonian by transforming the AOs to an orthogonalized set. If carried out correctly, this involves no approximations. The method was applied to *ab initio* and empirically cor-rected calculations of LiF, F_2, and F_2^-. The transformation of the matrix elements to the orthogonalized form can be quite time consuming for large bases.

3.3.2 *The MCVB method*

The present author and his coworkers[36] devised the multiconfiguration valence bond (MCVB) procedure. These calculations involve a direct at-tack on the problem of evaluating matrix elements between n-electron func-tions of non-orthogonal orbitals. The algorithm depends upon the sym-metric group methods of Young and the $\mathcal{PN}$ operator. Although there is considerable flexibility allowed in the construction of basis sets, a treat-ment that uses a full or nearly full set of n-electron functions based upon a minimal AO set and "excitations" into n-electron functions containing orbitals designed to provide scaling has been a generally useful strategy. As was mentioned above, these wave functions are a generalization of the original Heitler-Rumer high spin atomic calculations. If the results are of interest a simple transformation to a wave function that is a sum of HLSP functions is possible. With today's computers calculations consisting of $> 10^5$ individual n-electron basis functions can be more or less routine.

4   Early ideas

In reviewing the history of VB methods there stand out a few ideas con-cerning approximations that might be made. The author has chosen four that allow simple computational tests in today's world, and these are dis-cussed in this section. There is little connection between them.

4.1 Overlap matrices and the neglect of some permutations

When the actual Heitler-London treatment of H_2 is generalized to n electrons, the matrix elements that arise involve permutations of higher order than binary. When calculations had to be done by hand, the complexities could mount rapidly. It was perhaps natural, if not strictly rigorous, for people to make the approximation of neglecting these higher order permutations. There was actually much debate about the validity of such an approximation, in general, in spite of its crudeness for H_2. Clearly in Eq. (2), if the binary permutation would be ignored completely, the same energy would be obtained for the singlet and triplet states. When it came to considering the denominator, however, it seemed to the early workers as if the $T(=S^2)$ might be a higher order effect, and suggestions were made that it might be safely ignored. Generalizing this led to the idea for n-electron systems that the above mentioned triple, quadruple, and higher permutations might be usefully ignored.

This question was not considered completely academic. In Heisenberg's[33] original theory of ferromagnetism the overlaps between the orbitals at the various sites were ignored. Inglis[34] criticized this, but suggested that including overlaps made the calculation meaningless since the correction due to them scales as n, the number of sites involved. Later, Van Vleck[35] showed that Inglis' objection ignored cancellations that mitigate the problem. We will not examine the ferromagnetism problem, but will undertake a less ambitious course and investigate the contribution of various orders of permutations to the value of the normalization constant for VB wave functions.

The $(1 \pm T)$ in Eq. (2) arises from the normalization of the wave function for H_2. In this section we will investigate the extent to which it might be permissible to ignore the permutations of some order and higher when normalizing a VB function for n electrons. We shall do this for a standard tableau function, where we have an expression for the wave function of any multiplicity.

Therefore, consider a standard tableaux function with orbitals $u_1, u_2,$ $\cdots, u_n$, where they need not all be different, of course,

$$\begin{bmatrix} u_1 & u_{n-k+1} \\ \vdots & \vdots \\ \vdots & u_n \\ u_{n-k} & \end{bmatrix}.$$

The orbitals are assumed real, normalized, but not necessarily orthogonal. The overlaps are symbolized by $S_{ij} = S_{ji} = \langle u_i | u_j \rangle$. It is shown elsewhere[36] that the normalization constant for such a standard tableaux function can be written as the integral of a functional determinant,

$$C^{-2} = (n - k + 1) \int_0^1 \begin{vmatrix} A & qB \\ qB^\dagger & C \end{vmatrix} (1 - t)^{n-k} dt, \qquad (23)$$

where $q = i\sqrt{t/(1-t)}$. It is observed that q is pure imaginary. The determinant is therefore that for a symmetric matrix, but not an Hermitian one. In Eq. (23) A is the $(n-k) \times (n-k)$ overlap matrix of the first-column orbitals, C, the corresponding $k \times k$ matrix for the second-column orbitals, and B the $(n-k) \times k$ matrix of the inter-column overlaps. A, C, and the overall matrix are symmetric. Eq. (23) is also written with all of the purely group theoretic factors implicit in the functions. This would make $C^{-2} = 1$ if the overlaps between all pairs of orbitals were zero, and, thus, we are considering only that part of the normalization constant that is affected by the overlaps. The overall matrix is diagonalizable by an orthogonal matrix, which is also a function of q, of course. We are actually not interested in the transformation matrix, but only the characteristic polynomial of the overall matrix. To proceed we prove a theorem.

Consider an $N \times N$ symmetric matrix S that has principal diagonal elements all equal to one.*

Theorem 1 *A simple transformation of the characteristic polynomial of such a matrix will present it in a form where the contribution from each order of permutation to the value of its determinant is displayed as an elementary symmetric function of the eigenvalues of $S - I$.*

Consider the determinant

$$|I + t(S - I)|,$$

which is a polynomial in t that may be written

$$|I + t(S - I)| = 1 + \sum_{l=2}^{N} s_l t^l. \qquad (24)$$

Clearly, the sum is just the determinant $|S|$ when $t = 1$, and a little reflection will convince one that s_l is the contribution from the l-order

---

*We write this with the symbol, S, since the overlap matrix is the sort we consider.

permuted indices. The term with $l = 1$ is zero, of course, since there can be no permutation of one object.

Let O be the orthogonal matrix that diagonalizes $(S - I)$. Then

$$(S - I) = O\text{diag}(d_1 d_2 \cdots d_N)O^\dagger, \tag{25}$$

and we rewrite the determinant of Eq. (24),

$$
\begin{aligned}
|I + t(S - I)| &= |I + tO\text{diag}(d_1 d_2 \cdots d_N)O^\dagger|, \\
&= \prod_{m=0}^{N} (1 + td_m), \\
&= \sum_{m=0}^{N} \sigma_m t^m, \tag{26}
\end{aligned}
$$

where σ_m is the mth-order elementary symmetric function[37] of the eigenvalues of $S - I$, each of which is one less than the corresponding eigenvalue of S. Equating coefficients of equal powers of t in our two expressions we have $s_l = \sigma_l$. The elementary symmetric functions are simple to determine recursively from the d_m.* Indeed, the algorithm is essentially that to determine binomial coefficients, as is evident from Eq. (26) if we were to set each $d_m = 1$. We note that σ_1 is the trace of $S - I$, which is zero, so that s_1 is also zero as it should be.

We consider the application of this theorem to the evaluation of the integral in Eq. (23) for an STO3G basis calculation of CH_4 and a π-only calculation of naphthalene. As indicated earlier, we do not attempt to address the ferromagnetism problem, but we can note that the overlaps in naphthalene much more resemble the magnetism system than do the overlaps in a small compact molecule like CH_4.

4.1.1 *Sums of permutations of the same order*

It is useful to examine the symmetric functions of Eq. (26) for the $n \times n$ matrix

$$
S = \begin{bmatrix}
1 & 1 & \cdots & 1 \\
1 & 1 & \cdots & 1 \\
\vdots & \vdots & \cdots & \vdots \\
1 & 1 & \cdots & 1
\end{bmatrix}, \tag{27}
$$

---

*For our work we really do not need to diagonalize $S - I$. A simpler procedure is to tridiagonalize it; the characteristic equation is available therefrom by an easy recursion.

which is, of course, invalid as a legitimate overlap matrix. It does, however, allow us to get some idea of the limits that the symmetric functions can attain when real overlap matrices are used.

The matrix of Eq. (27) minus the identity has for eigenvalues $n-1$ once and -1 $n-1$ times. Eq. (26) now gives us

$$\begin{aligned} |I + t(S - I)| &= (1-t)^{n-1}[1 + (n-1)t] \\ &= \sum_{k=0}^{n} (-1)^k (1-k) \binom{n}{k} t^k, \end{aligned}$$

where the standard symbol for the binomial coefficient has been used. The significance of this result should be clear. When we consider permutations that reorder k indices, the coefficient of t^k is the number of even permutations of that order minus the number of odd permutations of the same order. We note that the coefficient of t is zero, as it should be, and the coefficients of t^2 and t^3 are just minus the number of binary interchanges and plus the number of ternary permutations, respectively. All other terms involve differences between numbers of even and odd permutations. In the next two sections we consider the overlap matrices for realistic systems.

4.1.2 *Application to the π-system of naphthalene*

A ten electron system with each electron in a different orbital could have a multiplicity of 1, 3, 5, 7, 9, or 11. The singlet and possibly the triplet states are the only physically interesting cases, but we give all of them so that trends may be observed. The undecet case has some mathematical interest, since it just the determinant of the overlap matrix. Table 2 gives our results for the first three of the possible multiplicities and Table 3 gives the other three. The tables are arranged in columns showing the order of the permutation and the values and the accumulated sums for each order and the integral of Eq. (23). It should be clear that these orders represent the number of indices permuted at each stage. Except for orders 2 and 3, however, they involve permutations with different signatures. Order 4 can have, *e.g.*, the permutations (12)(34) and (1234). These both involve four indices, but the first is an even permutation and the second is odd. Of course, only the antisymmetrizer (undecet case) has ± 1 coefficients that exactly match the corresponding permutation's signature. The permutation operators giving other spin values are more complicated, and it would be difficult to give rules for the way the terms vary with order.

The $2p_z$ orbitals in naphthalene all have nearest neighbor distances that are quite close to one another, and the nearest neighbor overlaps do not vary much on either side of 0.32. With such a set of overlaps, the normalization constant does not vary greatly with spin state. Even with a

Table 2: Convergence of normalization constants for singlet, triplet, and quintet standard tableaux functions in the π-system of naphthalene.

Order	Singlet		Triplet		Quintet	
0	1.0000	1.0000	1.0000	1.0000	1.0000	1.0000
1	−0.0000	1.0000	0.0000	1.0000	−0.0000	1.0000
2	−0.7896	0.2104	−0.9204	0.0796	−0.9295	0.0705
3	0.0693	0.2796	0.1066	0.1862	0.1223	0.1927
4	0.2017	0.4814	0.2677	0.4539	0.2570	0.4497
5	−0.0320	0.4494	−0.0482	0.4057	−0.0481	0.4016
6	−0.0142	0.4351	−0.0262	0.3795	−0.0254	0.3762
7	0.0020	0.4371	0.0043	0.3837	0.0055	0.3817
8	0.0002	0.4373	0.0011	0.3849	0.0005	0.3823
9	−0.0000	0.4373	−0.0001	0.3848	−0.0002	0.3821
10	0.0000	0.4373	−0.0000	0.3848	0.0000	0.3821

Table 3: Convergence of normalization constants for heptet, nonet, and undecet standard tableaux functions in the π-system of naphthalene.

Order	Heptet		Nonet		Undecet	
0	1.0000	1.0000	1.0000	1.0000	1.0000	1.0000
1	−0.0000	1.0000	−0.0000	1.0000	0.0000	1.0000
2	−0.9346	0.0654	−0.9478	0.0522	−1.1902	−0.1902
3	0.1269	0.1923	0.1487	0.2009	0.2168	0.0267
4	0.2526	0.4448	0.2397	0.4407	0.4061	0.4327
5	−0.0422	0.4026	−0.0505	0.3901	−0.1051	0.3277
6	−0.0278	0.3748	−0.0173	0.3729	−0.0469	0.2808
7	0.0044	0.3792	0.0030	0.3759	0.0128	0.2936
8	0.0013	0.3805	0.0004	0.3763	0.0019	0.2955
9	−0.0001	0.3804	−0.0000	0.3763	−0.0004	0.2951
10	−0.0000	0.3804	0.0000	0.3763	−0.0000	0.2951

fairly small overlap such as we have here, the sums nevertheless require the inclusion of terms up to order 5 or 6 to reach a number close to their final values. As we see, the value of C^{-2} is smallest for the undecet case.

We note that the order 2 term for the highest multiplicity is the most negative. This must be the sum $-\sum S_{ij}^2$ in this case, and so it consists of all negative terms.

4.1.3 *Application to CH_4*

An STO3G basis applied to CH_4 at its equilibrium geometry yields 9 AOs, and, if the C $1s$ orbital is relegated to "core" [36] status, there are only eight orbitals and eight electrons to go into them. For illustration purposes we consider C^{-2} for the AO set $\{2s, 2p_x, 2p_y, 2p_z, 1s_a, 1s_b, 1s_c, 1s_d\}$. In Table 4 we show the values of each of the terms for different orders of permutations and also the accumulated sum, which gives information about the rate of convergence. Table 5 gives similar results for the heptet and nonet states.

Table 4: Convergence of normalization constants for singlet, triplet, and quintet standard tableaux functions in CH_4.

Order	Singlet		Triplet		Quintet	
0	1.0000	1.0000	1.0000	1.0000	1.0000	1.0000
1	−0.0000	1.0000	−0.0000	1.0000	−0.0000	1.0000
2	0.3824	1.3824	−0.1323	0.8677	−0.5916	0.4084
3	−0.0359	1.3465	−0.0798	0.7879	−0.1242	0.2842
4	0.2049	1.5514	−0.0101	0.7777	0.0590	0.3432
5	−0.0237	1.5277	−0.0113	0.7664	0.0383	0.3815
6	0.0916	1.6193	−0.0132	0.7532	0.0051	0.3866
7	−0.0065	1.6128	−0.0002	0.7530	0.0023	0.3889
8	0.0378	1.6506	−0.0038	0.7492	0.0025	0.3914

Among these values, only the singlet has any great physical interest, but we

Table 5: Convergence of normalization constants for heptet and nonet standard tableaux functions in CH_4.

Order	Heptet		Nonet	
0	1.0000	1.0000	1.0000	1.0000
1	−0.0000	1.0000	−0.0000	1.0000
2	−1.0190	−0.0190	−2.0434	−1.0434
3	−0.1690	−0.1880	0.2331	−0.8103
4	0.3249	0.1369	1.3421	0.5318
5	0.1228	0.2597	−0.1549	0.3770
6	−0.0166	0.2431	−0.3707	0.0063
7	−0.0227	0.2205	0.0261	0.0324
8	−0.0054	0.2151	0.0378	0.0702

again give all so that the trends can be seen. In general, as the multiplicity increases, the value of C^{-2} decreases. The overlaps within this basis are not all positive, so it is difficult to make specific predictions.

The overlaps in this molecule are rather larger than was the case with naphthalene. The largest is near 0.5. This results in a larger value for the singlet state and rather smaller value for the nonet state.

4.2 Orthogonalized AOs

In a fairly early discussion of solids Wannier[38] showed how linear combinations of the AOs could be made that rendered the functions orthogonal while retaining a relatively large concentration on one center. In more modern language we would now say that he used a *symmetric orthonormalization* of the AO basis. If we symbolize the overlap matrix for the AO basis by S, then any matrix N that satisfies

$$N^\dagger S N = I, \tag{28}$$

constitutes an orthonormalization of the basis. This requirement on N is insufficient to define it uniquely. Additional conditions could include:

1. Require N be upper triangular. This gives the traditional Schmidt orthonormalization.

2. Set $N = U\mathrm{diag}(s_1^{-1/2}, s_2^{-1/2}, \cdots, s_n^{-1/2})$ where U is the unitary matrix diagonalizing S and $s_1, s_2, \cdots, s_n$ are the eigenvalues. This gives the *canonical orthonormalization.*

3. Set $N = S^{-1/2}$. This gives the *symmetric orthonormalization,* so-called because this N is a symmetric matrix for real basis functions.

An important property of the symmetric orthonormalization is that it produces a new set of orbitals that are the closest possible to the original set in a least squares sense. Since evaluating matrix elements of the Hamiltonian is always much easier with orthonormal orbitals, this change had great attractions for early workers. Unfortunately, it has developed that this idea must be used with great care. The requirement of closeness in the least squares sense, although almost always well defined, does not guarantee that the resulting two orbital sets are close to one another in a physically useful sense.

We may demonstrate this difficulty by giving a result due to Slater.[39] Applying a symmetric orthonormalization to the basis normally used in the Heitler-London calculation we have a H1s function on each of two centers,

$1s_a$ and $1s_b$. The overlap matrix for this basis is

$$\bar{S} = \begin{bmatrix} 1 & S \\ S & 1 \end{bmatrix}, \tag{29}$$

and the inverse square root is

$$\bar{S}^{-1/2} = \begin{bmatrix} \frac{1}{2\sqrt{1+S}} + \frac{1}{2\sqrt{1-S}} & \frac{1}{2\sqrt{1+S}} - \frac{1}{2\sqrt{1-S}} \\ \frac{1}{2\sqrt{1+S}} - \frac{1}{2\sqrt{1-S}} & \frac{1}{2\sqrt{1+S}} + \frac{1}{2\sqrt{1-S}} \end{bmatrix}, \tag{30}$$

where $S = \langle 1s_a | 1s_b \rangle$, and the signs are appropriate for $S > 0$. This orthogonalization gives us two new functions

$$\begin{aligned} |A\rangle &= P|1s_a\rangle + Q|1s_b\rangle, \\ |B\rangle &= Q|1s_a\rangle + P|1s_b\rangle, \end{aligned}$$

where

$$\begin{aligned} P &= \frac{1}{2\sqrt{1+S}} + \frac{1}{2\sqrt{1-S}}, \\ Q &= \frac{1}{2\sqrt{1+S}} - \frac{1}{2\sqrt{1-S}}. \end{aligned}$$

We use these in a single Heitler-London covalent configuration, $A(1)B(2) + B(1)A(2)$, and calculate the energy. When $R \to \infty$ we obtain $E = -1$ au, just as we should. At $R = 0.741$ Å, however, where we have seen that the energy should be a minimum, we obtain $E = -0.6091$ au, much higher than the correct value of -1.1744 au. The result for this orthogonalized basis, which represents no binding and actual repulsion, could hardly be worse.

Slater says surprisingly little concerning this outcome, but, in light of present understanding, we may say that the symmetric orthonormalization gives very close to the poorest possible linear combination for determining the lowest energy. This results from the added kinetic energy of the orbitals produced by a node that is not needed. Alternatively, we may say that we have used *antibonding* rather than bonding orbitals in the calculation. We have here a good example of how unnatural orthogonality between orbitals on different centers can have serious consequences for obtaining good energies and wave functions.

We add another comment about this example and note that using symmetric orthonormalization on the simple two AO basis for the triplet state of H_2 gives the same answer as that obtained with unmodified orbitals.

Since the triplet state is represented by the antisymmetric combination of the orbitals, it is invariant to any nonsingular transformation of the two orbitals.

4.3 Relation of Hamiltonian matrix to overlap matrix

In work on the electronic structure of solids, Löwdin[40] pointed out that if the Hamiltonian matrix for a system were a polynomial function of the overlap matrix of the basis, H and S would have the same eigenvectors and the energy eigenvalues would be polynomial functions of the eigenvalues of S. A number of consequences of this sort of relationship are known, but so far as the author is aware, no tests of such an idea have ever been made with realistic H and S matrices. This may be accomplished by examining the commutator, since if

$$H = \sum_k a_k S^k, \tag{31}$$

H and S clearly commute, and this would be true even if the sum in Eq. (31) were a convergent infinite series, rather than a polynomial. Conversely, if the two matrices do not commute, no relation like Eq. (31) connects them.

Even if H and S are functionally independent, one still might argue that the commutator is likely to be small, and, thus, the idea could be a useful approximation. The difficulty here is with the subtleties of the concept of *smallness* in this context. We will not attempt to address this question quantitatively, but satisfy ourselves by examining the commutators of H and S for three systems. The first of these is a simple 2×2 system for which we may obtain an algebraic answer. The other two are matrices from real VB calculations of CH_4 and the π-system of naphthalene.

4.3.1 *A 2×2 system*

Let

$$H = \begin{bmatrix} A & B \\ B & C \end{bmatrix}, \tag{32}$$

and

$$S = \begin{bmatrix} 1 & s \\ s & 1 \end{bmatrix}. \tag{33}$$

The commutator of these two is

$$HS - SH = \begin{bmatrix} 0 & -(C - A)s \\ (C - A)s & 0 \end{bmatrix}, \tag{34}$$

and we see immediately that the commutator is zero if the two diagonal elements of H are the same.

We may write H as two terms, the first a part that is a polynomial function of S and the second a sort of remainder.

$$H = \begin{bmatrix} (A + C)/2 & B \\ B & (A + C)/2 \end{bmatrix} + \begin{bmatrix} (A - C)/2 & 0 \\ 0 & (C - A)/2 \end{bmatrix}. \tag{35}$$

Thus, we see in this simple case that the closeness of the approximation depends upon the size the second term in Eq. (35); whether it is really a small perturbation upon the system. With these matrices the approximation would be good only if the two diagonal elements of H are close in value. The 2×2 case is rather special, however, and we give further more complicated examples.

4.3.2 The π-system of naphthalene

For naphthalene we examine the H and S matrices based upon the both the HLSP functions and the standard tableaux functions for the system. In both cases we include the non-ionic structures, only. This will give a picture of how the situation compares for the two sorts of basis functions. In both cases, of course, the dimensions of the matrices are 42×42, the number of non-ionic Rumer diagrams for a naphthalene structure. Some statistics concerning the commutator are shown in Table 6. It is clear that,

Table 6: Statistics on commutator $HS - SH$ matrix elements for naphthalene. Lower triangle only. All are energies in Hartrees.

	HLSP	STF
Maximum element	6.8380×10^{-1}	3.5665×10^{-1}
Minimum element	-6.1237×10^{-1}	-1.4897×10^{-1}
Minimum absolute value	7.9021×10^{-9}	1.1904×10^{-4}
Average(Commutator)	1.5308×10^{-3}	1.0838×10^{-2}
RMS(Commutator)	2.0458×10^{-1}	5.7002×10^{-2}
Average($H_{ii} - H_{jj}$)	1.3997×10^{-1}	2.5172×10^{-1}
RMS($H_{ii} - H_{jj}$)	1.1386×10^{-1}	3.2597×10^{-1}

while there are quantitative differences between the two bases, qualitatively the results are similar. It should be emphasized that if the commutator $HS - SH$ were zero for one of the bases, it would also be for the other. The important point to be gleaned from Table 6 is that the root-mean-square (RMS) values of the commutator elements and the $H_{ii} - H_{jj}$ differences are all very similar. The conclusion is that the perturbation presented by the non-commuting part of H is not small in this case, and it would be a bad approximation to consider H to be a polynomial function of S.

4.3.3 The CH_4 molecule

When an STO3G AO basis full VB calculation of CH_4 is carried out, there are 1716 singlet standard tableaux functions all together. When these are combined into functions of symmetry $^1A_1$ the number of independent linear combinations is reduced to 164. Thus the symmetry factored H and S matrices are 164×164. We show the statistics for the $HS - SH$ matrix for standard tableaux functions in Table 7. The statistics for HLSP functions are not available in this case. It is immediately obvious that the numbers

Table 7: Statistics on commutator $HS - SH$ matrix elements for CH_4. Lower triangle only. All are energies in Hartrees.

	STF
Maximum element	$1.5946 \times 10^{+1}$
Minimum element	$-1.6021 \times 10^{+1}$
Minimum absolute value	1.3350×10^{-4}
Average(Commutator)	-2.0447×10^{-2}
RMS(Commutator)	4.0189
Average($H_{ii} - H_{jj}$)	-3.0335×10^{-1}
RMS($H_{ii} - H_{jj}$)	8.7425×10^{-1}

for CH_4 are considerably larger than they were in the case of naphthalene; the RMS value of the commutator elements is nearly 5 times the RMS value of $H_{ii} - H_{jj}$. When one considers this in comparison with the results for naphthalene, it is not too surprising, since the π system for that molecule involves AOs of only one kind, whereas with CH_4 there are AOs from both K and L shells of the carbon. In spite of the large deviations between diagonal elements of H, the RMS average of the commutator elements is still larger, as was emphasized above. The non-commuting part of H

is very large here and represents a large perturbation. Ignoring it would constitute a very crude approximation.

4.4 The perfect pairing wave function and the valence state of carbon

We have defined the "perfect pairing" wave function earlier, and in this section we will examine some of the effects using this function alone has on the energies. This will parallel some of the early treatments, but it is not simple to use the computer programs current today to give an exactly comparable calculation to those carried out in the early days of molecular theory. There are two significant differences. The first is that all early calculations on a molecule as large as methane were semiempirical, at least to some extent. The second is that they also neglected higher order permutations in the evaluation of matrix elements. These two approximations interact to some extent, of course, but, in any event, would be difficult to arrange in a modern program.

In Table 8 we give the results for several different wave functions and two different basis sets.

1. STO3G. This is the conventional representation of Slater type orbitals using three Gaussians apiece.[41]

2. EOP3G. This basis is the energy optimized three Gaussian basis set devised by Ditchfield et al.[42] This is very nearly the same as the (33/3) basis given by Huzinaga et al.[43]

In each of these there are four valence orbitals on carbon and one on each hydrogen for a total of eight.

Seven different results are given for each basis set, and in all of them the C $1s$ orbital is doubly occupied in a frozen core. They are coded as follows:

1. FV. The full valence MCVB. According to the Weyl dimension formula eight electrons and eight orbitals give 1716 basis functions, and these support 164 $^1A_1$ states. The energies for these wave functions at the geometry of the minimum are given as zero in Table 8. All other energies in each column are given relative to this one, which is the lowest in each case. The absolute energies are given in a footnote in

Table 8: Energies for various states and wave functions of CH_4.
These are valence only calculations with a C $1s$ frozen core.

Code[a]	STO3G		EOP3G	
	E_{Min}	$D_e{}^b$	E_{Min}	$D_e{}^b$
FV[c]	0.000 eV	19.491 eV	0.000 eV	17.307 eV
HFC	3.853	18.655	3.055	17.392
HPP	4.138	22.898	3.239	20.992
CFC	9.968	12.540	7.488	12.959
HSTF	10.912	11.596	8.525	11.922
CSTF	10.912	11.596	8.525	11.922
CPP[d]	23.895	5.405	19.575	6.795

[a]FV, full valence; HFC, hybrid full covalent; HPP, hybrid perfect pairing;
CFC, Cartesian full covalent; HSTF, hybrid stf; CSTF, Cartesian stf; CPP,
Cartesian perfect pairing. See the text for further details.
[b]The total four-bond dissociation energy for the corresponding wave function.
[c]The full valence total energies: STO3G, -39.80107 au; EOP3G, -39.97968 au
[d]Not an A_1 state. See text.

the table, and the absolute energy of any one of the states may be reconstructed if so desired. For this calculation we need not differentiate between tetrahedral hybrid and Cartesian p orbitals.

2. HFC. The carbon orbitals are formed into the standard tetrahedral hybrids, "pointing" at the H atoms. There are 14 covalent basis functions and the this row gives the relative energy for the 14 term wave function.

3. HPP. This is the single perfect pairing HLSP function with tetrahedral hybrids. At the geometry of the energy minimum this function is no more than 0.2–0.3 eV higher than the HFC wave function. This difference represents the deviation from perfect pairing that occurs with the covalent only functions. This row also has the largest dissociation energies, since the C atom is forced into the "valence state" of van Vleck at the dissociated geometry.

4. CFC. The standard Cartesian $2p_x$, $2p_y$, and $2p_z$ orbitals together with the unchanged $1s$ orbital are used in the 14 term covalent wave function. This change produces a considerably larger jump in the energy than those before.

5. HSTF. This is the single best standard tableaux function with the hybrid orbitals. It corresponds to the high-spin wave function of Heitler and Rumer and has C in its ^5S state exactly.

6. CSTF. These energies are the same as the previous set, since the C ^5S state is equally well described by the Cartesian or the hybrid orbitals.

7. CPP. The Cartesian perfect pairing wave function is by far the worst on the energy scale, but this arrangement of AOs is not really applicable to the present discussion. It is unclear, of course, even how to pair the orbitals in this case, and, although it is the energy of a singlet state, unlike all the others, a single function cannot have A_1 symmetry with this sort of wave function and, thus, does not approximate an energy eigenstate..

Voge[44] used the conventional techniques* of the time to determine the actual atomic carbon states in the "valence" state. Table 9 shows the populations of atomic states that Voge determined. Nevertheless, the

Table 9: Populations of carbon atom states in "valence state".

State		Population
s^2p^2	^3P	0.1406
	^1D	0.0466
sp^3	^5S	0.3125
	^3P	0.2820
	^1D	0.0313
p^4	^3P	0.1406
	^1D	0.0466

valence state concept, although well defined, seems artificial today, since it is not experimentally available and since full calculations are so easily accessible and give better results.

There is, however, interest in examining some energy differences from Table 8. We may estimate the energies of the valence and the ^5S states(above the calculated ground state), and these are are shown in Table 10. Thus, the HPP row shows the perfect pairing valence state to be around 7 eV above the ground state, similar to the value obtained by van Vleck. The row marked CSTF gives the estimated energy of the ^5S state, and it is

---

*I.e., neglecting higher order permutations in evaluating Hamiltonian matrix elements and even binary permutations in the overlaps.

Table 10: Energies of C atom states at asymptotic C + 4H distances.

	STO3G	EOP3G	Exp.
HPP	7.545	6.924	NA
CSTF	3.017	3.140	4.183

seen to be about 1 eV below the experimental value. This is expected since there should be more correlation energy in the ground state than in the ^5S state, and these bases are too restricted to give any good account of correlation.

Both the historical results and the modern indicate that, without a doubt, the excited valence configuration, sp^3, figures large in bonding in the CH_4 molecule. The hybridized orbitals give a better energy in the restricted calculations than do the Cartesian, but, of course, this difference goes away for the full calculations. These have no early counterpart, of course.

5 Acknowledgment

APPENDIX

A Acronyms

AO atomic orbital

AOCI atomic orbital configuration interaction

BOVB breathing orbital valence bond

CI configuration interaction

GGVB Goddard's generalized VB

HLSP Heitler-London-Slater-Pauling

MCVB multiconfiguration valence bond

MO molecular orbital

MOCI molecular orbital configuration interaction

RMS root-mean-square

SCVB spin coupled valence bond

SDF Slater determinantal functions

STF standard tableau function

VB valence bond

References

[1] W. Heitler and F. London,Z. Physik **44**, 619 (1927)

[2] P. A. M. Dirac, Proc. Roy. Soc. (London) **A123**, 714 (1929)

[3] J. H. Van Vleck and A. Sherman, Rev. Mod. Phys. **7**, 167 (1935)

[4] S. C. Wang, Phys. Rev. **31**, 579 (1928)

[5] L. Pauling and E. B. Wilson, "Introduction to quantum mechanics",(McGraw-Hill, New York 1935)

[6] N. Rosen, Phys. Rev. **38**, 2099 (1931)

[7] S. Weinbaum, J. Chem. Phys. **1**, 593 (1933)

[8] H. M. James and A. S. Coolidge, J. Chem. Phys. **1**, 825 (1933)

[9] W. Heitler and G. Rumer, Z. Physik **68**, 12 (1931)

[10] J. C. Slater, Phys. Rev. **38**, 1109 (1931)

[11] G. Rumer, Göttinger Nachr. **1932** 377

[12] L. Pauling, J. Chem. Phys. **1**, 280 (1933)

[13] H. Eyring and G. E. Kimbal, J. Chem. Phys. **1**, 239 (1933)

[14] A. Messiah, "Quantum mechanics", (North-Holland, Amsterdam, 1966), Chap. 8.

[15] R. Serber, Phys. Rev. **45**, 461 (1934); J. Chem. Phys. **2**, 697 (1934)

[16] P. A. M. Dirac, "The principles of quantum mechanics", Fourth Edition (Oxford, London 1958), Sec. 58.

[17] J. H. Van Vleck, Phys. Rev. **45**,405 (1934)

[18] T. Yamanouchi, Proc. Math.-Phys. Soc. Jpn. **19**, 436 (1937)

[19] M. Kotani, A. Amemiya, E. Ishiguro, and T. Kimura, "Tables of molecular integrals", (Maruzen, Tokyo, 1963)

[20] C. A. Coulson and I. Fisher, Phil. Mag. **40**, 386 (1949)

[21] W. A. Goddard, Phys. Rev. **157**, 81 (1967)

[22] N. C. Pyper and J. Gerratt, Proc. Roy. Soc. (London) **A355**, 407 (1977)

[23] J. Gerratt, D. L. Cooper, and M. Raimondi, in "Valence bond theory and chemical structure", Ed. by D. J. Klein and N. Trinajstić (Elsevier,Amsterdam, 1990) p. 287.

[24] D. E. Rutherford, "Substitutional Analysis"(Edinburgh University Press, reprinted by Hafner, New York,1968)

[25] J. H. Van Lenthe and G. G. Balint-Kurti, Chem. Phys. Lett. **76**, 138 (1980); J. Chem. Phys. **78**, 5699 (1983)

[26] P. C. Hiberty, S. Humbel, C. P. Byrman, and J. H. van Lenthe, J. Chem. Phys. **101**, 5969 (1994)

[27] F. A. Matsen, Ad. Quantum Chem. 1, 60 (1964); J. Phys. Chem. **68**, 3238 (1964); F. A. Matsen, A. A. Cantu, and R. D. Poshusta, j. Phys. Chem. **70**, 1558(1966)

[28] G. G. Balint-Kurti and M. Karplus, J. Chem. Phys. **50**, 478 (1969)

[29] W. Moffit, Proc. Roy. Soc. (London) **A218**, 486 (1953)

[30] G. A. Gallup, Intern. J. Quantum Chem. **6**, 899 (1972)

[31] See *e.g.*, R. Pauncz, "Spin eigenfunctions" (Plenum Press, New York, 1979)

[32] F. A. Matsen and J. C. Browne, J. Phys. Chem. **66**, 2332 (1962)

[33] W. Heisenberg, Zeits. f. Physik **49**, 619 (1928)

[34] D. R. Inglis, Phys. Rev. **46**, 135 (1934)

[35] J. H. Van Vleck, Phys. Rev. **49**, 232 (1936)

[36] G. A. Gallup, R. L. Vance, J. R. Collins, and J. M. Norbeck, Advances in Quantum Chem. **16**, 229 (1982)

[37] D. E. Littlewood, "The theory of group characters", (Oxford University Press, London, 1950), Second Ed., Section 6.2

[38] G. Wannier, Phys. Rev. **52**, 191 (1937)

[39] J. C. Slater, J. Chem. Phys. **19**, 220 (1951); see, also, J. C. Slater, "Quantum Theory of Molecules and Solids",(McGraw-Hill, New York, 1963)

[40] P.-O. Löwdin, J. Chem. Phys. **18**, 365 (1950)

[41] W. J. Hehre, R. F. Stewart, and J. A. Pople, J. Chem. Phys. **51**, 2657 (1969)

[42] R. Ditchfield, W. J. Hehre, and J. A. Pople, J. Chem. Phys. **52**, 5001 (1970)

[43] S. Huzinaga, "Gaussian Basis Sets for Molecular Calculations" (Elsevier Science Publishing Co.,New York, 1984)

[44] H. H. Voge, J. Chem. Phys. **4**, 581 (1936)

This Page Intentionally Left Blank

Chapter 2

Modern Valence Bond Description of Gas-Phase Pericyclic Reactions

David L. Cooper[a], Peter B. Karadakov[b] and Thorstein Thorsteinsson[a]

[a]Department of Chemistry, University of Liverpool,
Liverpool L69 7ZD, United Kingdom

[b]Department of Chemistry, University of York,
York YO10 5DD, United Kingdom

The combination of the spin-coupled formulation of modern valence bond theory with intrinsic reaction coordinate calculations provides easy-to-interpret models for the electronic rearrangements that occur along reaction pathways. We survey here the information revealed by such studies of the mechanisms of various gas-phase six-electron pericyclic reactions: the Diels-Alder reaction between butadiene and ethene, the electrocyclization of *cis*-1,3,5-hexatriene, the 1,3-dipolar cycloaddition between fulminic acid and ethyne, and the 1,3-dipolar cycloaddition of diazomethane. The fully-variational CASVB strategy proves particularly efficient for such studies.

1. INTRODUCTION

The elucidation of reaction mechanisms, and endeavours to predict the outcome of wide ranges of chemical reactions, lie at the very heart of chemistry. Electronic structure theory has made very significant progress in the quantitative description of one very important aspect, namely the changes in the geometry and energy of the reacting system on the way from reactants to products. The relevant potential surfaces can be studied using a wide range of correlated post-Hartree-Fock quantum-chemical approaches, the most advanced of which are already capable of providing essentially conclusive results for gas-phase processes involving relatively small molecules.

A second, equally important, aspect of the theoretical modelling of chemical reactions is related to the elucidation of the often radical changes in the electronic structure of a reacting system as it evolves from reactants, through one or more transition structures and/or reaction intermediates, to one or more sets of products. There is a well-recognized need to develop qualitative models based on *quantitative* wavefunctions but highlighting general features and tendencies in chemical structure and reactivity; this can be a very difficult task, especially if

one attempts to base such models on the multiconfigurational wavefunctions used in most post-Hartree-Fock approaches.

Most chemists still tend to think about the structure and reactivity of atomic and molecular species in qualitative terms that are related to electron pairs and to unpaired electrons. Concepts utilizing these terms such as, for example, the Lewis theory of valence, have had and still have a considerable impact on many areas of chemistry. They are particularly useful when it is necessary to highlight the qualitative similarities between the structure and reactivity of molecules containing identical functional groups, or within a homologous series. Many organic chemistry textbooks continue to use full and half-arrows to indicate the supposed movement of electron pairs or single electrons in the description of reaction mechanisms. Such concepts are closely related to classical valence-bond (VB) theory which, however, is unable to compete with advanced molecular orbital (MO) approaches in the accurate calculation of the quantitative features of the potential surface associated with a chemical reaction.

Modern valence bond theory, in its spin-coupled form, is an attractive approach for elucidating the changes in electronic structure that accompany the variations in energy and geometry of a reacting system on its way from reactants to products. Our recent work has indeed shown than the spin-coupled approach yields easy-to-interpret models for various organic reaction pathways, including the mechanisms of six-electron gas-phase pericyclic reactions. For such systems, the flexibility of the wavefunction allows it to describe, with equal ease, the various heterolytic and homolytic possibilities. In all cases, the spin-coupled wavefunction recovers a fairly consistent proportion (typically somewhat more than 90%) of the nondynamical correlation energy incorporated in the corresponding 'six electrons in six orbitals' CASSCF construction. In the present account, we survey the descriptions that emerge for the Diels-Alder reaction between butadiene and ethene [1], the electrocyclization of cis-1,3,5-hexatriene [2], the 1,3-dipolar cycloaddition between fulminic acid and ethyne [3], and the 1,3-dipolar cycloaddition of diazomethane to ethene [4].

2. SPIN-COUPLED APPROACH

As described in other Chapters in this book, the single-configuration spin-coupled wavefunction takes the form [5]

$$\Psi_{sc} = \mathcal{A}\left[\left(\prod_{i=1}^{n}\varphi_i\,\alpha\,\varphi_i\,\beta\right)\left(\prod_{\mu=1}^{N}\psi_\mu\right)\Theta_{SM}^{N}\right] \tag{1}$$

in which the active electrons are accommodated in N singly-occupied nonorthogonal spin-coupled orbitals ψ_μ, which are optimized as completely general linear combinations of atom-centred basis functions, without any overlap

or localization constraints. The corresponding total spin function, Θ_{SM}^N, which is labelled according to its eigenvalues of $\hat{S}^2$ and $\hat{S}_z$, is fully optimized in the full spin space. The orthonormal inactive orbitals φ_i may be optimized simultaneously with the spin-coupled orbitals and the total spin function, or they may be fixed to match those in appropriate preliminary calculations.

The closest MO-theory analogue of such a compact N-electron spin-coupled wavefunction is the corresponding many-configuration 'N electrons in N orbitals' CASSCF function. It is of course relatively straightforward nowadays also to construct fully-variational multiconfiguration VB wavefunctions for ground and excited states, should the need arise. However, high accuracy numerical results, as required for various applications, are normally achieved instead using nonorthogonal CI calculations involving excitations into fixed virtual orbitals. A common feature of such calculations is that the very compact spin-coupled descriptions dominate the final ground state wavefunction, so that we may claim that the essential physical picture remains essentially unchanged. As such, useful chemical insight may often be derived even from single-configuration spin-coupled wavefunctions, simply by examining the variations in the shapes of the spin-coupled orbitals and in the changes to the mode of spin coupling during the course of a chemical reaction. A convenient way to follow reactions is of course in terms of the minimum energy path or intrinsic reaction coordinate, IRC, which consists of the steepest-descent paths (in mass-weighted coordinates) leading from transition state(s) toward reactants or products.

A useful basic strategy for studying gas-phase organic reaction pathways could be to locate the transition states and several points along the minimum energy paths, to check that the 'N in N' CASSCF is qualitatively correct, and then to perform fully-variational spin-coupled calculations at each geometry. Efficient computational algorithms, often relying on group theory and/or on graphical indexing techniques, have led to tractable schemes for the direct optimization of spin-coupled wavefunctions [6,7], and these have been used in some of our work on organic reactions. An attractive alternative for carrying out fully-variational spin-coupled calculations is provided by codes which we have named CASVB [8]. Some key features of our CASVB strategy, which we have used in many of our studies of pericyclic reactions, are outlined in the next section.

3. OVERVIEW OF CASVB

As is well known, CASSCF wavefunctions are invariant to general (*i.e.* nonunitary) linear transformations of the active orbitals. As such, we may seek alternative, but equivalent, representations in which a small number of configurations are dominant. This is achieved in our case by means of efficient computational schemes for carrying out *exactly* the transformations of full-CI spaces induced by nonunitary transformations of orbital spaces [9].

In its simplest form, the CASVB approach may be used simply to generate representations of a CASSCF wavefunction Ψ_{CAS} in which a single- or multiconfiguration modern-VB component Ψ_{VB} is dominant. Writing

$$\Psi_{CAS} = S_{VB}\Psi_{VB} + (1-S_{VB}^2)^{1/2}\Psi_{VB}^{\perp} \tag{2}$$

in which $\Psi_{VB}^{\perp}$ denotes the orthogonal complement of Ψ_{VB}, such a task may be achieve by maximizing the overlap quantity S_{VB}, defined according to

$$S_{VB} = \frac{\langle\Psi_{CAS}|\Psi_{VB}\rangle}{\langle\Psi_{VB}|\Psi_{VB}\rangle^{1/2}} \tag{3}$$

This procedure is relatively inexpensive and, with suitable choices of the general form of Ψ_{VB}, it is fairly robust. An obvious alternative is to minimize the energy quantity E_{VB}, defined according to

$$E_{VB} = \frac{\langle\Psi_{VB}|\hat{H}|\Psi_{VB}\rangle}{\langle\Psi_{VB}|\Psi_{VB}\rangle} \tag{4}$$

By its very nature, minimization of E_{VB} is more expensive than the maximization of S_{VB}, because it requires the construction of quantities corresponding to applications of the hamiltonian operator, but this may be achieved by adapting the efficient procedures already available in various CASSCF codes. It turns out, however, that the two sets of orbital representations tend to be rather similar, and so maximization of S_{VB} tends to be preferred. In either case, the actual optimization uses reliable Newton-Raphson-like procedures that utilize first and second derivatives.

The CASVB strategy for the fully-variational optimization of modern VB wavefunctions relies on a linked two-step strategy, based on alternating steps, until convergence is reached. Active and inactive spaces are chosen, in the usual way, alongside an appropriate form for Ψ_{VB}. The 'nonorthogonal step' involves the minimization of E_{VB}, using the basic CASVB algorithms, whereas the 'orthogonal step' involves inactive-active, inactive-virtual and active-virtual orbital rotations using standard CASSCF procedures. Particularly when starting from a converged CASSCF wavefunction, convergence to the final VB wavefunction can involve a remarkably small number of iterations, such that, overall, the calculations tend to be somewhat cheaper than our traditional direct optimization of spin-coupled wavefunctions. The full CASVB module [8] is incorporated in the MOLPRO package [10], that has been used in most of our studies, and it has also recently been ported to the MOLCAS package [11].

4. PERICYCLIC REACTIONS

The choice of basis sets and the generation of geometries along the IRC are described in detail in our previous work [1–4,12], together with the corresponding energies. Instead, we concentrate here on the evolution of the electronic structure

revealed directly by the spin-coupled wavefunctions. For each of the gas-phase processes considered, six electrons were treated as active in the spin-coupled calculations, as in the usual organic chemistry descriptions of such systems.

4.1 Diels-Alder Reaction

Symmetry-unique spin-coupled orbitals for the Diels-Alder process are shown in Figure 1 for IRC values (in amu$^{\nu}$bohr) of 0.6 (towards reactants), zero (transition state, TS) and –0.6 (towards products) [1]. It is clear that each orbital remains associated with the same carbon atom throughout the reaction, with the main changes being in the degree of sp^x character and in the amount and direction of the deformations of the orbitals. Initially, the π bonds in butadiene are formed by the symmetry-related pairs (ψ_1,ψ_2) and (ψ_4,ψ_3), while (ψ_5,ψ_6) corresponds to the π bond in ethene (see right-hand column of Figure 1). Moving to the transition state (middle column of Figure 1), the distortion of ψ_2 towards ψ_3 (its symmetry-related counterpart) becomes much more noticeable, at the expense of reduced overlaps within the (ψ_1,ψ_2) and (ψ_4,ψ_3) pairs. At the same time, the overlap between ψ_5 and ψ_6 is reduced in favour of distortions towards the orbitals of the butadiene moiety. It is clear from the left-hand frame of Figure 2 that all of the key overlaps tend to much the same value in the vicinity of the transition state. Continuing towards reactants (left-hand column of Figure 1), orbitals ψ_6 and ψ_1 become much more sp^3-like, and correspond to one of the new σ bonds. Similarly, the pair (ψ_2,ψ_3) corresponds to the new π bond.

$IRC=-0.6$ TS $IRC=0.6$
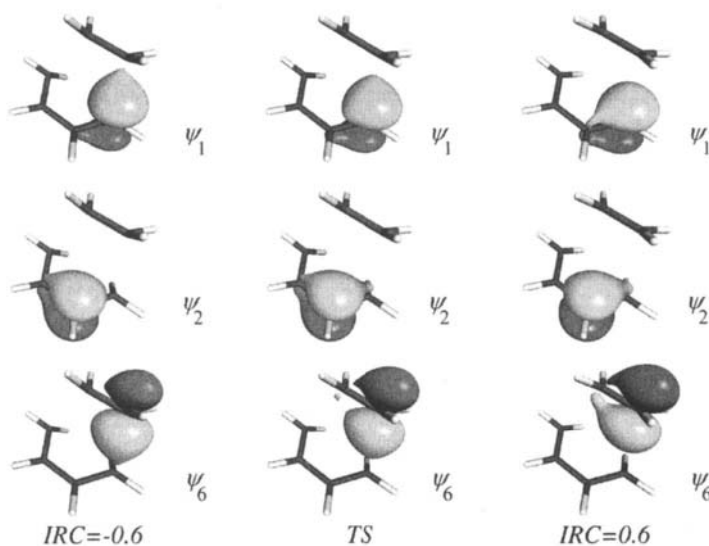
Figure 1. Symmetry-unique spin-coupled orbitals for the Diels-Alder reaction.
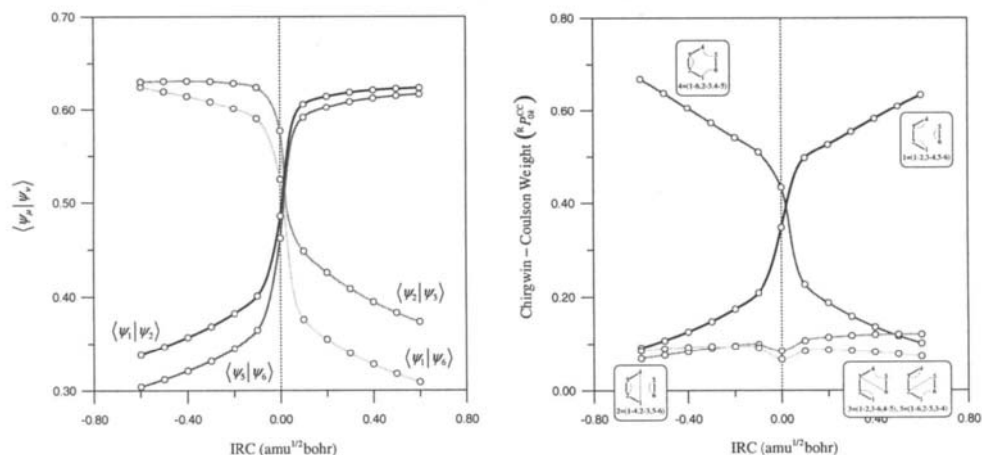
Figure 2. Overlap integrals (left) and spin-coupling weights (right) for the Diels-Alder reaction

These various changes to the shapes of the orbitals are accompanied by a recoupling of the electron spins. As shown in the right-hand frame of Figure 2, the total spin function Θ_{00}^6 is easily interpreted in the present case by means of the familiar Rumer basis. The two Kekulé-like functions (1–2,3–4,5–6) and (1–6,2–3,4–5) are dominant over the entire IRC segment considered, with one corresponding to reactants and the other to the products. They attain equal weight in the vicinity of the transition state. Indeed, the orbital overlaps, the mode of spin coupling, the estimated "resonance energy", and the location and nature of the first excited singlet state [1] are all strongly reminiscent of the spin-coupled description of benzene [13], and so it is tempting to argue in favour of an "aromatic" transition state.

Given that the orbitals remain associated with the same carbon atom throughout the reaction, but with a recoupling of the corresponding electron spins, it seems appropriate to label the changes as "homolytic", as might be represented by the following simplistic scheme:
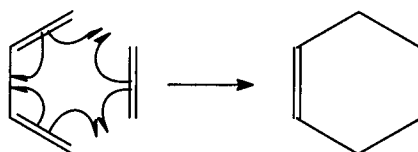
4.2 Disrotatory Electrocyclic Ring-Opening of Cyclohexadiene

The IRC was followed from the transition state, with twelve points in the direction of cyclohexadiene and a further twelve in the direction of *cis*-1,3,5-hexatriene, with steps of *ca.* 0.1 amu$^{1/2}$bohr [2]. Symmetry-unique spin-coupled

orbitals ψ_1–ψ_3 are shown in Figure 3 for IRC values (in amu$^{1/2}$bohr) of ≈ -1.2 (ring begins to open, left-hand column), zero (transition state, middle column) and $\approx +1.2$ (ring almost open, right-hand column). Reflection of ψ_1, ψ_2 and ψ_3 in the symmetry plane retained over this IRC interval results in ψ_6, ψ_5 and ψ_4, respectively.
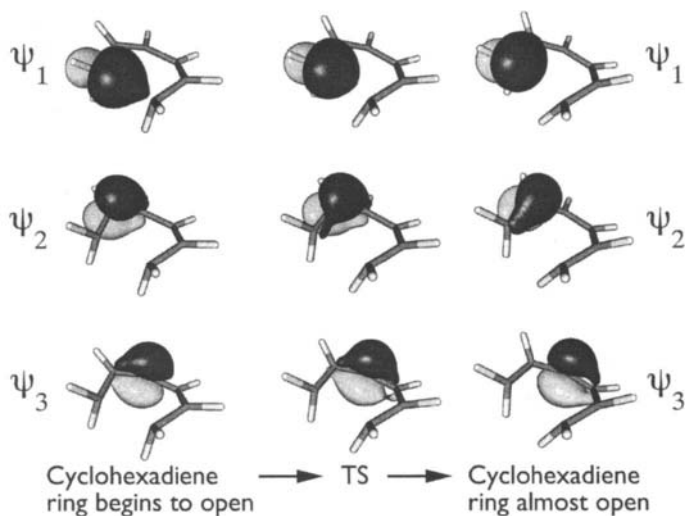
Figure 3. Symmetry-unique spin-coupled orbitals for the disrotatory electrocyclic ring-opening of cyclohexadiene.

At the start of the IRC interval, the length of the bond being broken is already 2.09 Å, but ψ_1 and ψ_6 still take the form of sp^x-like hybrids with significant s character. The pair (ψ_2,ψ_3) accounts for one of the π bonds in the cyclohexadiene ring. Orbitals ψ_2–ψ_5 at the transition state (middle column of Figure 3) are starting to attain much the same 'symmetrically-distorted' shape as orbital ψ_2 at the Diels-Alder transition state. The increased distance between the two terminal atoms (2.29 Å) is reflected in less distortion of ψ_1 and ψ_6 towards one another, and a reduced overlap. However, for this system, the most dramatic changes in the orbital overlaps and in the mode of spin coupling occur a little after the transition state (see Figure 4), when the carbon-carbon bond lengths in the chain become almost equal. The near-perfect 'resonance' of two Kekulé-type modes, as well as the near equalization of bond lengths and of orbital overlaps, suggests that this is another reaction that passes through an 'aromatic' structure.

At the end of the IRC interval, the distance between the terminal carbon atoms is 2.49 Å. Orbital ψ_1 is now essentially a π orbital. The three π bonds

correspond to the pairs (ψ_1,ψ_2), (ψ_3,ψ_4) and (ψ_5,ψ_6), and the corresponding perfect-pairing mode of spin coupling becomes the most important, as shown in Figure 4.
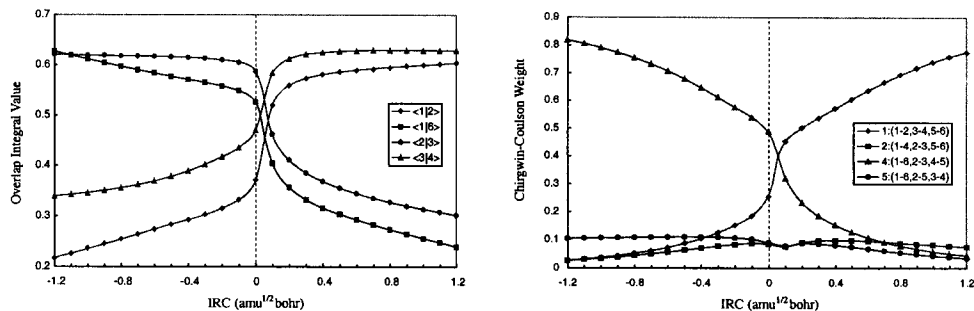
Figure 4. Overlap integrals (left) and spin-coupling weights (right) for the disrotatory electrocyclic ring-opening of cyclohexadiene.

The orbitals remain associated with the same carbon atom throughout the reaction, but with a recoupling of the corresponding electron spins. As in the case of the Diels-Alder reaction, it seems appropriate to label the changes as "homolytic", as might be represented using half-arrows as:
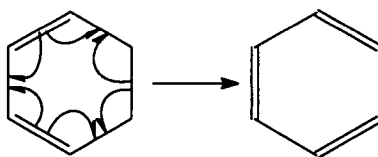
One difference from the Diels-Alder reaction [1], however, is that the aromatic structure in the present case occurs a little after the transition state [2].

4.3   1,3-Dipolar Cycloaddition of Fulminic Acid to Ethyne

Given the concerted, almost synchronous nature of this gas-phase reaction it might seem reasonable to suppose that the electronic mechanism would resemble those for the Diels-Alder and cyclohexadiene ring-opening reactions, described above. However, our spin-coupled calculations along the IRC reveal a somewhat different picture [3].

The right-hand column of Figure 5 corresponds to separated fulminic acid (HCNO) and ethyne moieties. Orbitals ψ_1, ψ_3, ψ_5 and ψ_6 are associated with the fulminic acid molecule and, taken together with the corresponding dominant mode of spin coupling, they suggest a 'hypervalent' central N atom, as described in previous work [14]. The remaining orbitals, ψ_2 and ψ_4, are associated with the 'in plane' ethyne π bond that is broken during the course of the reaction.

ψ_1 ψ_2 ψ_3 ψ_4 ψ_5 ψ_6

Isoxazole ← TS ← Fulminic acid and ethyne far apart
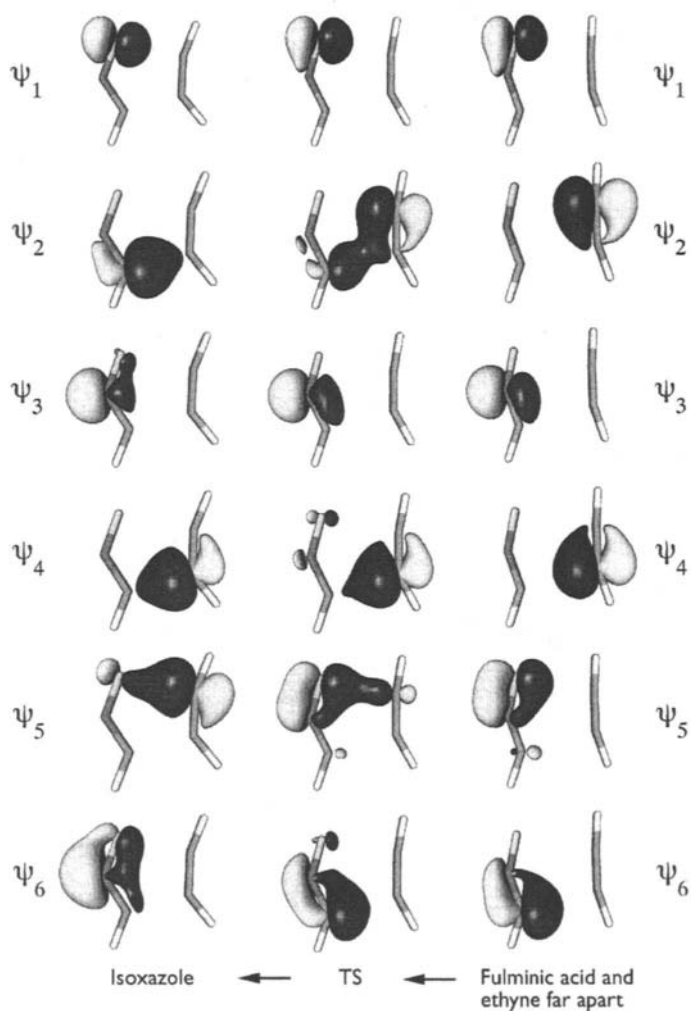
Figure 5. Symmetry-unique spin-coupled orbitals for the 1,3-dipolar cycloaddition of fulminic acid to ethyne.

For this system, we find that the spin-coupled orbitals do not remain associated with the same first-row atom throughout the reaction. Instead, orbital ψ_2 from the ethyne moiety becomes a linear combination of an sp^z-like hybrid from the ethyne and another such hybrid from the HCNO, as is shown for the transition state in the middle column of Figure 5. After the transition state, this orbital becomes almost entirely associated with the HCNO carbon atom.

Somewhat less dramatic changes are observed for orbital ψ_4, which undergoes rehybridization that is reminiscent of orbital ψ_6 in the Diels-Alder reaction. Ultimately, the (ψ_2, ψ_4) pair describes one of the two new bonds that close the isoxazole ring, as shown in the right-hand column of Figure 5.

Orbital ψ_5, originally from the highly polar 'in plane' N–O π bond, also 'moves' during the course of the reaction. At the transition state, it takes the form of the combination of two sp^z-like hybrids, one associated with its original location on oxygen and the other with the incoming carbon atom of ethyne. After the transition state, it becomes primarily associated with the ethyne carbon. Orbital ψ_1 changes relatively little during the course of the reaction. Ultimately, the pair (ψ_1, ψ_5) accounts for the other new bond that closes the isoxazole ring, as shown in the right-hand column of Figure 5. The remaining orbitals, ψ_3 and ψ_6, originally associated with the 'in plane' C–N π bond of HCNO, shift relatively little, so as to form a nonbonding pair on the isoxazole nitrogen atom (but with some polarization towards the oxygen atom).

Analysis of the total spin function reveals that the spins associated with the pairs (ψ_2, ψ_4), (ψ_3, ψ_6) and (ψ_1, ψ_5) remain essentially singlet coupled throughout the course of the reaction, with no evidence for any aromatic structure along the IRC. As such, the spin-coupled description corresponds to a mechanism that involves the simultaneous relocation of three orbital pairs, as might be represented by the following simplistic scheme:
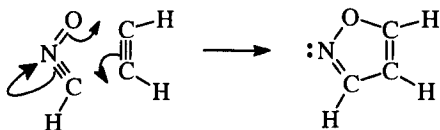
Using a somewhat different methodology, based on *orthogonal* localized molecular orbitals (LMOs), Nguyen *et al.* [15,16] conclude that the circulation of charge for this reaction is in the opposite direction to that described here. However, it is worth pointing out [17] that the weights of even the most important configurations within their CI-LMO-CAS wavefunctions tend to be fairly small. In the case of the 1,3-dipolar cycloaddition of fulminic acid to ethyne, the two configurations that are used to deduce the electronic reaction mechanism, never have weights that exceeding 0.28 and 0.16. As a rule, the spin-coupled wavefunction consistently accounts for more than 90% of the nondynamical correlation energy of a '6 in 6' CASSCF wavefunction using just *one* product of six singly-occupied active orbitals. The overlap between the spin-coupled and CASSCF wavefunctions is even higher (often more than 0.99). It is this proximity between the two wavefunctions that justifies the use here of changes to orbital shapes, orbital overlaps and/or the mode of spin coupling in order to describe the electronic mechanism of a chemical reaction. In a sense, we

are faced with choosing between a description that is backed by more than 90% of the CASSCF wavefunction, and another one which has behind itself a very much smaller proportion.

4.4 1,3-Dipolar Cycloaddition of Diazomethane to Ethene

In an analogous spin-coupled study [4] of the gas-phase concerted 1,3-dipolar cycloaddition of diazomethane (CH_2N_2) to ethene (C_2H_4), we found that the total spin function for the active electrons remains dominated by a single perfect-pairing mode (*i.e.* by singlet-coupled pairs) throughout the course of the reaction. Orbital pair shifts were observed, as in the previous example, indicating a heterolytic mechanism that does not pass through an aromatic structure. One minor difference arises from the fact that the N–O π bond in HCNO is much more polar than the corresponding N–N bond in CH_2N_2 [14,18]. The orbital pair responsible for this N–N bond is somewhat less mobile and shifts over to form one of the bonds closing the 1-pyrazoline ring well after the transition state, in contrast to the previous case, in which the corresponding orbital shifts were already well advanced at the transition state. Overall, the orbital changes in the present reaction may be summarized by the simplistic scheme
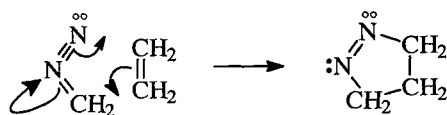
in which the hollow dots represent a nitrogen lone pair that was not treated as 'active' in the spin-coupled calculations, and the 'hypervalent' central N atom of the diazomethane molecule is represented as in our previous work [18].

5. CONCLUSIONS

For each of the gas-phase pericyclic reactions considered here, the spin-coupled approach produces a very clear picture of the electronic rearrangements that accompany the changes in geometry and energy along the IRC from reactants to products. In general, the changes in electronic structure in the vicinity of the transition state tend to be much more rapid than are the corresponding geometrical changes.

During the Diels-Alder reaction [1] and in the electrocyclization of *cis*-1,3,5-hexatriene [2], bonds break and form in a homolytic fashion, with orbitals remaining associated with the same centres throughout the reaction. For such systems, there is a major recoupling of the electron spins. This last takes place most rapidly at or near the transition state. The resonance pattern, taken together with other characteristics, is reminiscent of the spin-coupled description

of benzene. These gas-phase reactions appear to pass through an 'aromatic' structure.

An entirely different description emerges for the two 1,3-dipolar cycloaddition reactions that we have studied [3,4]. For such systems, the bond breaking and bond formation involves instead the shifts of well-identifiable orbital pairs, rather than any spin recouplings. Such heterolytic mechanisms, that do not pass through an aromatic structure, now seem to be a likely outcome of studies on other gas-phase concerted 1,3-dipolar cycloaddition reactions.

References

1. P.B. Karadakov, D.L. Cooper and J. Gerratt, *J. Am. Chem. Soc.* **120,** 3975 (1998).
2. P.B. Karadakov, D.L. Cooper, T. Thorsteinsson and J. Gerratt, in *Quantum Systems in Chemistry and Physics. Volume 1: Basic Problems and Models Systems*, ed. A. Hernández-Laguna, J. Maruani, R. McWeeny and S. Wilson (Kluwer, Dordrecht, 2000); p. 327.
3. P.B. Karadakov, D.L. Cooper and J. Gerratt, *Theor. Chem. Acc.* **100**, 222 (1998).
4. J.J. Blavins, P.B. Karadakov and D.L. Cooper, *J. Org. Chem.* **66**, 4285 (2001).
5. a) D.L. Cooper, J. Gerratt and M. Raimondi, *Chem. Revs* **91**, 929 (1991); b) J. Gerratt, D.L. Cooper, P.B. Karadakov and M. Raimondi, *Chem. Soc. Rev.* **26**, 87 (1997).
6. P.B. Karadakov, J. Gerratt, D.L. Cooper and M. Raimondi, *J. Chem. Phys.* **97**, 7637 (1992).
7. D.L. Cooper, J. Gerratt, M. Raimondi, M. Sironi and T. Thorsteinsson, *Theor. Chim. Acta* **85**, 261 (1993).
8. a) T. Thorsteinsson, D.L. Cooper, J. Gerratt, P.B. Karadakov and M. Raimondi, *Theor. Chim. Acta* **93**, 343 (1996); b) D.L. Cooper, T. Thorsteinsson and J. Gerratt, *Adv. Quant. Chem.* **32**, 51 (1998); c) T. Thorsteinsson and D.L. Cooper, in *Quantum Systems in Chemistry and Physics. Volume 1: Basic problems and models systems*, ed. A. Hernández-Laguna, J. Maruani, R. McWeeny and S. Wilson (Kluwer, Dordrecht, 2000); p. 303.
9. T. Thorsteinsson and D.L. Cooper, *Theor. Chim. Acta* **94**, 233 (1996).

10. MOLPRO is a package of *ab initio* programs written by H.-J. Werner and P.J. Knowles, with contributions from R.D. Amos, A. Berning, D.L. Cooper, M.J.O. Deegan, A.J. Dobbyn, F. Eckert, C. Hampel, G. Hetzer, T. Leininger, R. Lindh, A.W. Lloyd, W. Meyer, M.E. Mura, A. Nicklaß, P. Palmieri, K. Peterson, R. Pitzer, P. Pulay, G. Rauhut, M. Schütz, H. Stoll, A.J. Stone and T. Thorsteinsson.

11. MOLCAS Version 5.2: K. Andersson, M. Barysz, A. Bernhardsson, M.R.A. Blomberg, Y. Carissan, D.L. Cooper, M. Cossi, T. Fleig, M.P. Fülscher, L. Gagliardi, C. de Graaf, B.A. Hess, G. Karlström, R. Lindh, P.-Å. Malmqvist, P. Neogrády, J. Olsen, B.O. Roos, B. Schimmelpfennig, M. Schütz, L. Seijo, L. Serrano-Andrés, P.E.M. Siegbahn, J. Stålring, T. Thorsteinsson, V. Veryazov, M. Wierzbowska and P.-O. Widmark (Lund University, Sweden, 2001).

12. D.L. Cooper, N.L. Allan and P.B. Karadakov, in *The fundamentals of molecular similarity*, ed. R. Carbó-Dorca (Kluwer/Plenum, New York, 2001); p. 169.

13. a) D.L. Cooper, J. Gerratt and M. Raimondi, *Nature* **323**, 699 (1986); b) D.L. Cooper, S.C. Wright, J. Gerratt, P.A. Hyams and M. Raimondi, *J. Chem. Soc. Perkin Trans. 2*, 719 (1989); c) D.L. Cooper, J. Gerratt and M. Raimondi, in *Pauling's Legacy – Modern Modelling of the Chemical Bond*, ed. Z.B. Maksić and W.J. Orville-Thomas (Elsevier, 1999).

14. D.L. Cooper, J. Gerratt and M. Raimondi, *J. Chem. Soc. Perkin Trans. 2*, 1187 (1989).

15. M.T. Nguyen, A.K. Chandra, S. Sakai and K. Morokuma, *J. Org. Chem.* **64**, 65 (1999).

16. M.T. Nguyen, A.K. Chandra, T. Uchimaru and S. Sakai, *J. Phys. Chem. A* **105**, 10946 (2001).

17. P.B. Karadakov and D.L. Cooper, *J. Phys. Chem. A* **105**, 10946 (2001).

18. a) D.L. Cooper, J. Gerratt, M. Raimondi and S.C. Wright, *Chem. Phys. Lett.* **138**, 296 (1987); b) D.L. Cooper, J. Gerratt and M. Raimondi, in *Pauling's Legacy – Modern Modelling of the Chemical Bond*, ed. Z.B. Maksić and W.J. Orville-Thomas (Elsevier, 1999).

This Page Intentionally Left Blank

Chapter 3

Complete active space valence bond (CASVB) method and its application to chemical reactions

Haruyuki Nakano, Kazushi Sorakubo, Kenichi Nakayama, and Kimihiko Hirao

Department of Applied Chemistry, Graduate School of Engineering, University of Tokyo, 7-3-1 Hongo, Bunkyo-ku, Tokyo 113-8656, Japan

The complete active space valence bond (CASVB) method is an approach for interpreting complete active space self-consistent field (CASSCF) wave functions by means of valence bond resonance structures built on atom-like localized orbitals. The transformation from CASSCF to CASVB wave functions does not change the variational space, and thus it is done without loss of information on the total energy and wave function. In the present article, some applications of the CASVB method to chemical reactions are reviewed following a brief introduction to this method: unimolecular dissociation reaction of formaldehyde, $H_2CO \rightarrow H_2+CO$, and hydrogen exchange reactions, $H_2+X \rightarrow H+HX$ (X=F, Cl, Br, and I).

1. INTRODUCTION

The complete active space self-consistent field (CASSCF) method is one of the electronic structure theories that is employed most frequently in the study of chemical reactions. This method is feasible and gives potential energy surfaces of good quality, and hence it is also used as a starting point for higher-level multireference methods. In fact, the CASSCF method has many advantages: (1) it is well defined on the whole potential energy surface of a chemical reaction if an appropriate active space is chosen; (2) it is applicable to excited states as well as the ground state in a single framework, and (3) it provides size-consistent results, etc. However, it often generates too many configurations, and therefore there is a problem as to how we could extract a chemical description from the lengthy CASSCF wave functions.

The complete active space valence bond (CASVB) method [1,2] is a solution to this problem. Classical valence bond (VB) theory is very successful in providing a qualitative explanation for many aspects. Chemists are familiar with the localized molecular orbitals (LMO) and the classical VB resonance concepts.

If modern accurate wave functions such as CASSCF can be represented in terms of such well-known concepts, chemists' intuition and experiences will give a firm theoretical basis and the role of computational chemistry will undoubtedly expand.

The CASVB functions can be obtained by transforming the canonical CASSCF functions without loss of energy. First we transform the CASSCF delocalized MO to localized MO using the arbitrariness in the definition of the active orbitals. Then we perform the full configuration interaction (CI) calculation again in the active space. Here, we also use the arbitrariness in the definition of the expansion configuration functions. The configuration functions used are spin-paired functions based on the LMOs. This form of spin eigenfunctions plays a special role in the VB method. The CASVB wave functions can be readily interpreted in terms of the well-known classical VB resonance structures. The total CASVB wave function is identical to the canonical CASSCF wave function. In other words, the MO description and the VB description are equivalent, at least at the level of CASSCF. The CASVB method provides an alternative tool for describing the correlated wave functions.

With this method, we clarified the electronic structures of the ground and excited states of benzene, butadiene, methane, and hydrogen molecules [1,2]. We also applied the method to valence excited states of polyenes [3] and their cations [4]. In previous studies, we put our focus on the formalism of CASVB and its applicability to molecules in their equilibrium structures.

Even today, however, it is not a simple task to obtain chemical pictures at the transition state (TS) or along a reaction path. Discussion on the nature of TS is, for instance, often conducted using other features such as molecular structures and energy profiles rather than the wave functions themselves: if the bond length at TS is closer to that of the product than reactant, it is called a *late* TS, or if the reaction is highly exothermic, this reaction is assumed to proceed via an *early* TS. These discussions are qualitative and ambiguous. A more quantitative and clear-cut chemical description is necessary.

In this article, we present applications of CASVB to chemical reactions: the unimolecular dissociation reaction of formaldehyde, $H_2CO \rightarrow H_2+CO$ [5], and a series of hydrogen exchange reactions, $H_2+X \rightarrow H+HX$ (X=F, Cl, Br, and I). The method in this article is based on the occupation numbers of VB structures that are defined by the weights of the spin-paired functions in the CASVB functions, so that we could obtain a quantitative description of the nature of electronic structures and chemical bonds even during reactions.

In Sec. 2, we briefly survey the CASVB method. In Sec. 3, the CASVB method is applied to the unimolecular dissociation $H_2CO \rightarrow H_2+CO$ and the hydrogen exchange reactions $H_2+X \rightarrow H+HX$ (X=F, Cl, Br, and I), and the applicability to the reaction is discussed. Conclusions are given in Sec. 4.

2. OVERVIEW OF CASVB METHOD

We have proposed two types of CASVB method. The first one is a method where the valence bond structures are constructed from *orthogonal* localized molecular orbitals (LMOs) [1], and the second is one from *nonorthogonal* localized molecular orbitals [2].

The idea of CASVB is based on the fact that the densities of variational wave functions are invariant under the transformations which hold the variational space unchanged. In the CASSCF case, a complete active space (CAS) is invariant under the linear transformation of active orbitals and also that of configuration state functions (CSFs).

We may re-define the active orbitals utilizing the invariance of the active orbital space. In the CASVB with *nonorthogonal* LMOs, we employ Rueden-berg's procedure of projected localized MOs [6-8] and obtain quasi-atomic CASSCF MOs that have maximal overlaps with atomic orbitals (AOs) of the free atoms. Consider an AO, χ_A, centered on a nucleus A. Diagonalizing the matrix,

$$P_{ij} = \langle \psi_i | \chi_A \rangle \langle \chi_A | \psi_j \rangle \tag{1}$$

in the CASSCF MO basis, ψ_μ, and choosing the eigenvector with the largest eigenvalue gives the LMO, φ_A, which has the maximum overlap with χ_A. Similarly, we can define φ_B, φ_C, ... The LMOs, φ_μ, determined in this manner are nonorthogonal to each other. These atom-adapted LMOs are Ruedenberg orthogonalized, but we leave them as nonorthogonal. On the other hand, in the CASVB with *orthogonal* LMOs, we use LMOs produced by a Boys' localization procedure as $\{\varphi_i\}$ [9].

The full configuration space that is spanned by all possible configurations generated from these quasi-atomic CASSCF MOs is identical to that of full CI space that is constructed from the canonical CASSCF MOs. Thus, we use $\{\varphi_\mu\}$ as orbitals from which a CASVB wave function is constructed. To obtain the corresponding VB structures, we project a canonical CASSCF wave function onto a VB wave function. The projection does not modify the original wave function but simply re-expresses it in the VB language. Let Ψ^{CASSCF} be a CASSCF wave function,

$$\Psi^{CASSCF} = \sum_i C_i \Phi_i^{CSF}, \quad \Phi_i^{CSF} \equiv \Phi_i^{CSF}\left(\{\psi_i\}\right) \tag{2}$$

where Φ_i^{CSF} are the configuration state functions constructed by the orthogonal orbitals set $\{\psi_i\}$ and C_i are the known CAS-CI expansion coefficients. Simi-

larly define the CASVB function in terms of spin-paired functions as

$$\Psi^{CASVB} = \sum_i A_i \Phi_i^{VB}, \quad \Phi_i^{VB} \equiv \Phi_i^{VB}\left(\{\varphi_i\}\right) \tag{3}$$

where Φ_i^{VB} are spin-paired functions constructed by LMOs. The number of independent spin-paired functions is equal to the dimension of CAS, and the spaces spanned by $\{\Phi_i^{CSF}\}$ and $\{\Phi_i^{VB}\}$ are identical. Since Eqs. (2) and (3) are different expressions of the identical wave function, we may write

$$\sum_j A_j \Phi_j^{VB} = \sum_j C_j \Phi_j^{CSF}. \tag{4}$$

Left-multiplying Eqs. (2) and (3) by Φ_i^{CSF} and integrating the products, we get

$$\sum_j \Omega_{ij} A_j = C_i \quad \text{with} \quad \Omega_{ij} = \left\langle \Phi_i^{CSF} \middle| \Phi_j^{VB} \right\rangle, \tag{5}$$

whose dimension is equal to the dimension of CAS. Solving this linear equation, we obtain CASVB wave function Ψ^{CASVB}.

The occupation number (or weight) of a VB structure is calculated with

$$n_i = A_i^* \sum_j S_{ij} A_j, \tag{6}$$

where S_{ij} are overlaps between the structures i and j, defined by

$$S_{ij} = \left\langle \Phi_i^{VB} \middle| \Phi_j^{VB} \right\rangle, \tag{7}$$

and satisfies the normalization,

$$\sum_i n_i = 1. \tag{8}$$

Note that the occupation number n_i could be negative because of the nonorthogonality of resonance structures.

Fig. 1 is a schematic expression of coefficient A_i and occupation number n_i in a two dimensional case.

Thorsteinsson et al. also investigated the transformations of CASSCF functions to modern valence bond representations [10-12]. They examined trans-
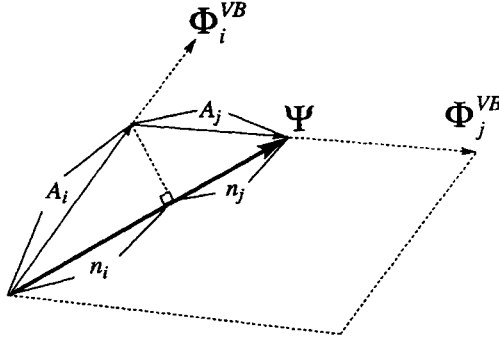
Fig. 1. Schematic expression of coefficient A_i and occupation number n_i in a two dimensional case: $\Psi = A_1 \Phi_1^{VB} + A_2 \Phi_2^{VB}$.

formations for which the total wave function is dominated by some VB structures (e.g. covalent structures) built from common products of nonorthogonal orbitals. This method was also named "CASVB method." Some recent works of their CASVB method can be seen in review articles [13-15] and references therein.

To obtain more insight into CASVB functions, let us consider the hydrogen molecule as an example [2]. Fig. 2 shows CASSCF, orthogonal localized, nonorthogonal localized, and generalized valence bond (GVB) molecular orbitals obtained for active space CAS(2,2) with correlation consistent valence double zeta (cc-pVDZ) basis set [16] at a bond distance of 0.7 Å. We observe that the orthogonal LMO is deformed significantly from the atomic $1s$ function and has a small tail on the other hydrogen atom due to the orthogonality constraint. The orthogonality requirement between LMOs forces small anti-bonding admixture from orbitals on neighboring atoms into each LMO. On the contrary, the nonorthogonal LMO looks very much like an atomic $1s$ function (the overlap is 0.9859) and the LMOs overlap strongly with each other (0.7775).

The CASSCF wave function for the hydrogen molecule is written as,

$$|CASSCF\rangle = 0.9948\sigma^2 - 0.1021\sigma^{*2}. \tag{9}$$

This wave function is transformed to CASVB function with orthogonal LMOs,

$$|CASVB_{OLMO}\rangle = 0.7799\mathscr{A}\left[\varphi_{H_A}\varphi_{H_B}(\alpha\beta - \beta\alpha)\right]\big/\sqrt{2}$$

$$+ 0.4426\left(\mathscr{A}\left[\varphi_{H_A}\varphi_{H_A}\alpha\beta\right] + \mathscr{A}\left[\varphi_{H_B}\varphi_{H_B}\alpha\beta\right]\right) \tag{10}$$

$$= 0.6082[H_A - H_B] + 0.3918\left\{\left[H_A^- \quad H_B^+\right] + \left[H_A^+ \quad H_B^-\right]\right\},$$

and with nonorthogonal LMOs,

CASSCF MOs

Orthogonal localized MOs

Nonorthogonal localized MOs

Generalized valence bond MOs
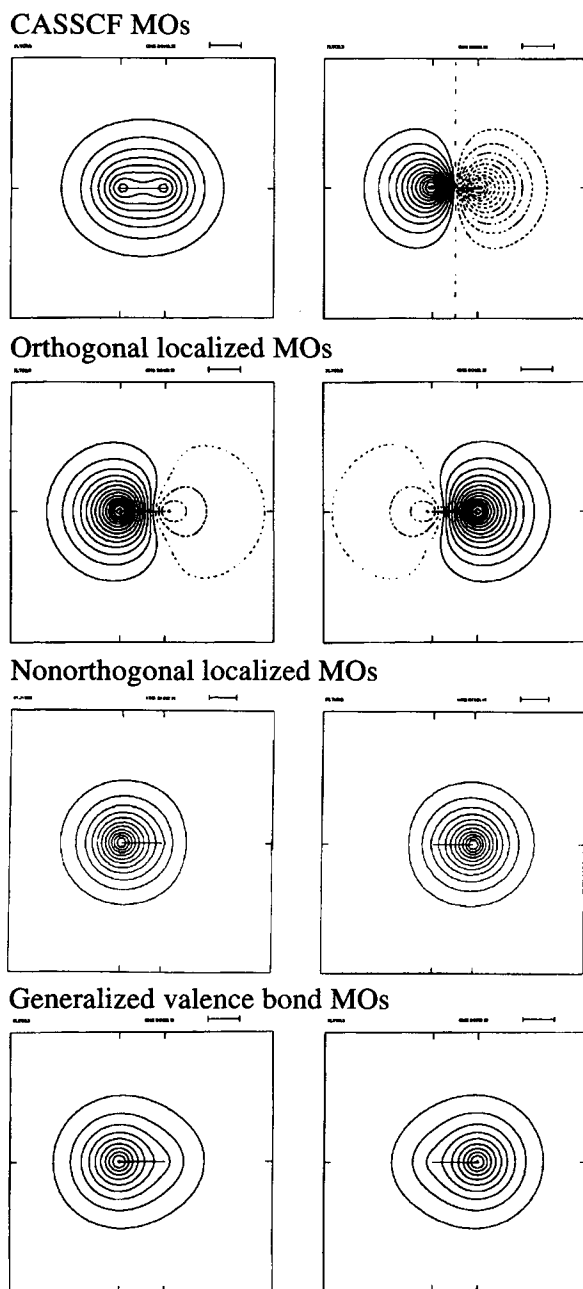
Fig. 2. CASSCF, orthogonal localized, non-orthogonal localized, and generalized valence bond molecular orbitals for the hydrogen molecule.

$$|\text{CASVB}_{\text{NLMO}}\rangle = 0.9124\mathscr{A}\left[\varphi_{\text{H}_\text{A}}\varphi_{\text{H}_\text{B}}(\alpha\beta - \beta\alpha)\right]/\sqrt{2}$$

$$+ 0.0503\left(\mathscr{A}\left[\varphi_{\text{H}_\text{A}}\varphi_{\text{H}_\text{A}}\alpha\beta\right] + \mathscr{A}\left[\varphi_{\text{H}_\text{B}}\varphi_{\text{H}_\text{B}}\alpha\beta\right]\right) \quad (11)$$

$$= 0.9122[\text{H}_\text{A} - \text{H}_\text{B}] + 0.0878\left\{\left[\text{H}_\text{A}^- \quad \text{H}_\text{B}^+\right] + \left[\text{H}_\text{A}^+ \quad \text{H}_\text{B}^-\right]\right\},$$

where the numbers before the VB structures are occupation numbers n_i (Eq. (6)) and $\mathscr{A}$ denotes the antisymmetrizer. Nonorthogonal LMOs change the
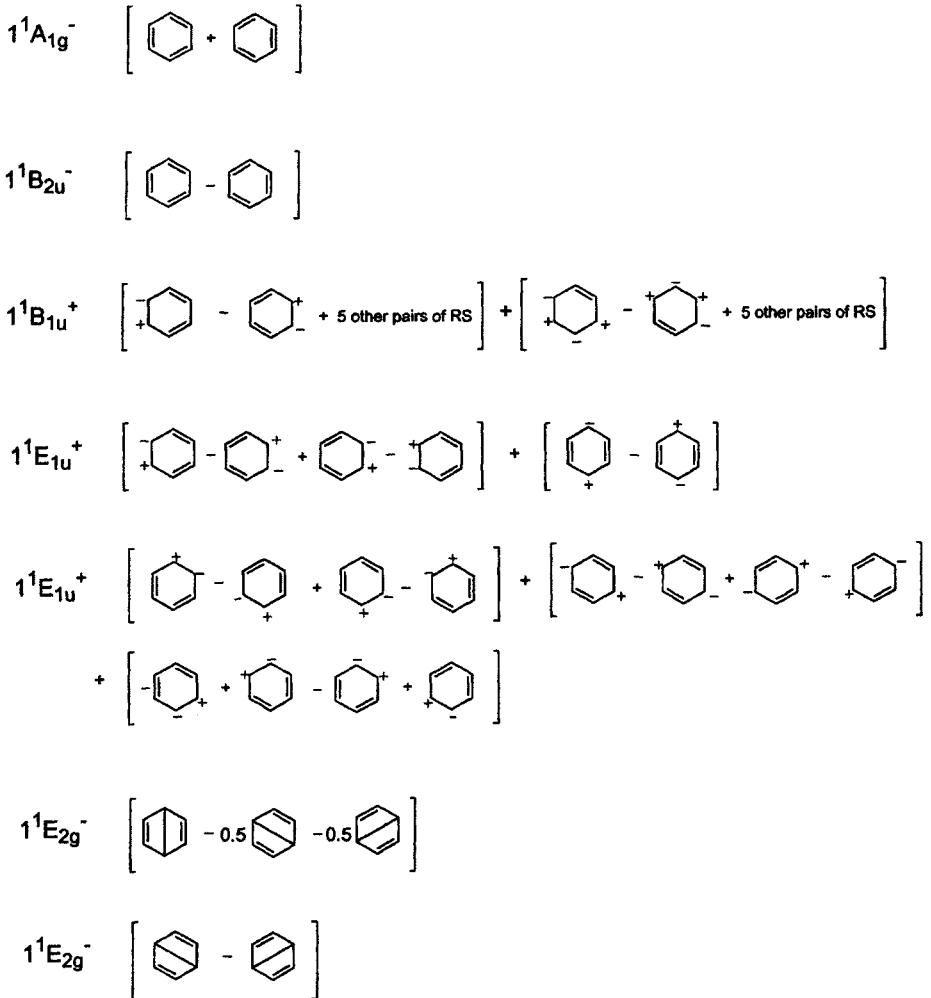
Fig. 3. CASVB description for the ground and $\pi \rightarrow \pi^*$ singlet excited states of benzene.

picture of ionic-covalent resonance dramatically from CASVB with the orthogonal LMOs. Orbital relaxation increases the covalent character of the HH bond and decreases the ionic character. Thus, the nonorthogonal description seems more reasonable conceptually.

The GVB function is also an equivalent expression to the CASSCF and CASVB functions in the CAS(2,2) case. In the GVB description, the wave function is written by the covalent structure only,

$$|\text{GVB}\rangle = \mathscr{A}\left[\varphi_{\text{H}_\text{A}}\varphi_{\text{H}_\text{B}}(\alpha\beta - \beta\alpha)\right]/\sqrt{2} = \left[\text{H}_\text{A} - \text{H}_\text{B}\right], \tag{12}$$

and no ionic structure contribution. The orbitals are distorted compared to the nonorthogonal LMOs due to this unphysical constraint.

For one more example, a CASVB description for benzene is given in Fig. 3. See Refs. 1 and 2 for the computational details. The CASVB affords a clear view of the wave functions for the various states. The excitation process is represented in VB theory in terms of the rearrangement of spin couplings and
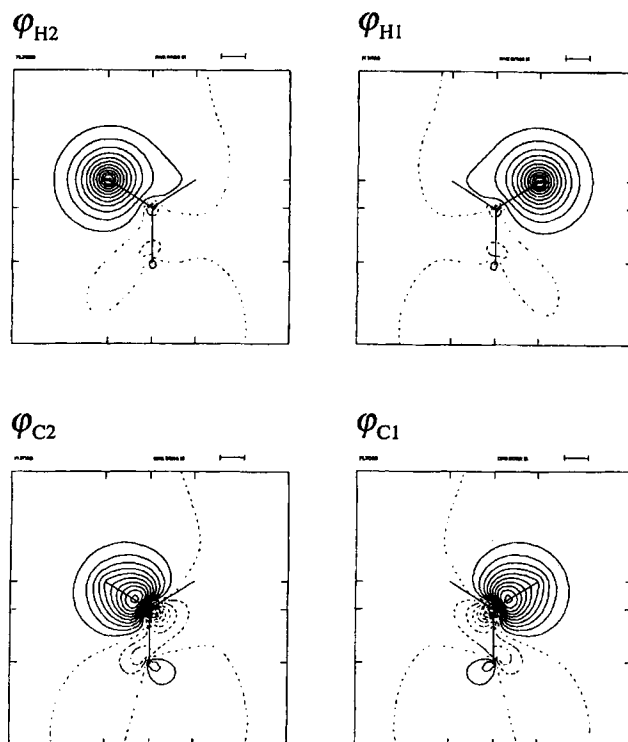
Fig. 4. The nonorthogonal LMOs at the equilibrium structure of H_2CO determined with Ruedenberg's projected localization procedure.

charge transfer. The former generates the covalent excited states and the latter gives rise to the ionic excited states, in which the covalent bond is broken and a new ionic bond is formed. Thus, the singly, doubly, ... , polar structures are generated from their respective *parent* ground state covalent (nonpolar), singly, ... , polar structures.

The ground state is represented by two covalent Kekulé structures as expected. The lowest excited $^1B_{2u}^-$ state is again described by a combination of the Kekulé structure. There are no significant contributions from the Dewar structures or the corresponding orthopolar structures. The linear combinations of the two equivalent Kekulé structures generate the plus and minus states. Their positive combination gives rise to the totally symmetric $^1A_{2g}^-$ ground state, while the negative combination yields the excited $^1B_{2u}^-$ state. The second and third $\pi \rightarrow \pi^*$ excited states are described by a number of ionic structures. There is no contribution from the covalent structures. The ionic character of these states can easily be found from a CASVB description. The highest valence excited states are the covalent $^1E_{2g}^-$ state. The state has a predominantly Dewar character with no contribution from the Kekulé structures. Thus, the Ke-

φ_{H2} φ_{H1}

φ_{C2} φ_{C1}
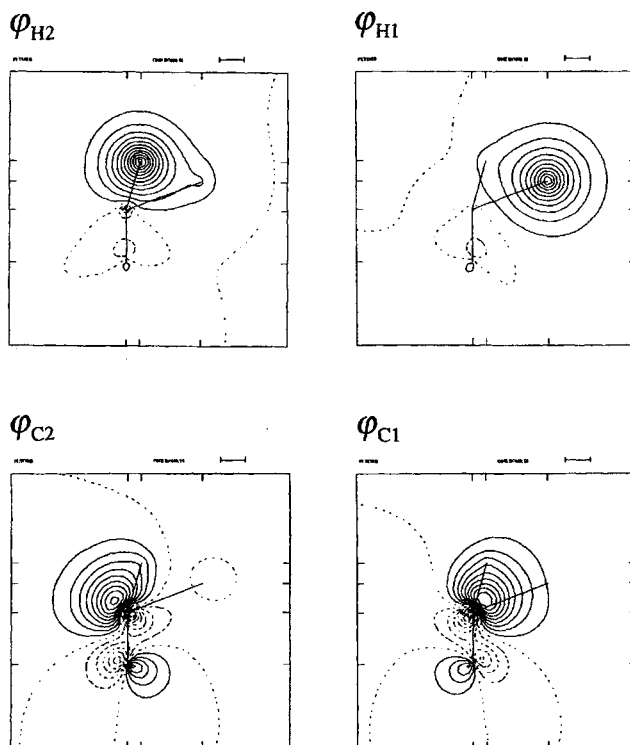
Fig. 5. The nonorthogonal LMOs at the TS structure of the $H_2CO \rightarrow H_2+CO$ reaction.

kulé structures dominate the ground state and the singly excited $1B_{2u}^-$ state while the Dewar structures dominate the doubly excited degenerate $^1E_{2g}^-$ states. The states described by Dewar structures are described by doubly, triply, ... excitations in an MO language.

In this article, we use only the CASVB description with nonorthogonal LMOs. Thus, it is hereafter referred simply as CASVB functions.

3. APPLICATION TO CHEMICAL REACTIONS

In this section, we examine how the electronic structures of molecules during chemical reactions are described by the CASVB method and how they are analyzed with the VB language. Two examples are shown: one is the unimolecular dissociation reaction of formaldehyde, $H_2CO \rightarrow H_2 + CO$ [5], and the other is the hydrogen exchange reactions, $H_2 + X \rightarrow H + HX$ (X=F, Cl, Br, and I).

Table 1
Spin-paired functions and VB structures of formaldehyde (Normalization and phase factors are omitted.)

Spin-paired function	VB structure	
$\varphi_{H2}\varphi_{C2}(\alpha\beta - \beta\alpha)\cdot\varphi_{C1}\varphi_{H1}(\alpha\beta - \beta\alpha)$	$H_2 \!-\! C \!-\! H_1$	(I)
$\varphi_{C2}\varphi_{C2}\alpha\beta\cdot\varphi_{C1}\varphi_{H1}(\alpha\beta - \beta\alpha)$ $\varphi_{C1}\varphi_{C1}\alpha\beta\cdot\varphi_{C2}\varphi_{H1}(\alpha\beta - \beta\alpha)$	$H_2^+ \ ^-C \!-\! H_1$	(II)
$\varphi_{H2}\varphi_{H2}\alpha\beta\cdot\varphi_{C1}\varphi_{H1}(\alpha\beta - \beta\alpha)$ $\varphi_{H2}\varphi_{H2}\alpha\beta\cdot\varphi_{C2}\varphi_{H1}(\alpha\beta - \beta\alpha)$	$H_2^- \ ^+C \!-\! H_1$	(III)
$\varphi_{H2}\varphi_{C2}(\alpha\beta - \beta\alpha)\cdot\varphi_{C1}\varphi_{C1}\alpha\beta$ $\varphi_{H2}\varphi_{C1}(\alpha\beta - \beta\alpha)\cdot\varphi_{C2}\varphi_{C2}\alpha\beta$	$H_2 \!-\! C^- \ ^+H_1$	(IV)
$\varphi_{H2}\varphi_{C2}(\alpha\beta - \beta\alpha)\cdot\varphi_{H1}\varphi_{H1}\alpha\beta$ $\varphi_{H2}\varphi_{C1}(\alpha\beta - \beta\alpha)\cdot\varphi_{H1}\varphi_{H1}\alpha\beta$	$H_2 \!-\! C^+ \ ^-H_1$	(V)
$\varphi_{C2}\varphi_{C2}\alpha\beta\cdot\varphi_{C1}\varphi_{C1}\alpha\beta$	$H_2^+ \ ^-C^- \ ^+H_1$	(VI)
$\varphi_{H2}\varphi_{H2}\alpha\beta\cdot\varphi_{H1}\varphi_{H1}\alpha\beta$	$H_2^- \ ^+C^+ \ ^-H_1$	(VII)
$\varphi_{H2}\varphi_{H1}(\alpha\beta - \beta\alpha)\cdot\varphi_{C2}\varphi_{C2}\alpha\beta$ $\varphi_{H2}\varphi_{H1}(\alpha\beta - \beta\alpha)\cdot\varphi_{C2}\varphi_{C1}(\alpha\beta - \beta\alpha)$ $\varphi_{H2}\varphi_{H1}(\alpha\beta - \beta\alpha)\cdot\varphi_{C1}\varphi_{C1}\alpha\beta$	$H_2 \ \ C \ \ H_1$	(VIII)
$\varphi_{H1}\varphi_{H1}\alpha\beta\cdot\varphi_{C2}\varphi_{C1}(\alpha\beta - \beta\alpha)$	$H_2^+ \ \ C \ \ ^-H_1$	(IX)
$\varphi_{H2}\varphi_{H2}\alpha\beta\cdot\varphi_{C2}\varphi_{C1}(\alpha\beta - \beta\alpha)$	$H_2^- \ \ C \ \ ^+H_1$	(X)
$\varphi_{H2}\varphi_{H2}\alpha\beta\cdot\varphi_{C2}\varphi_{C2}\alpha\beta$ $\varphi_{H2}\varphi_{H2}\alpha\beta\cdot\varphi_{C1}\varphi_{C1}\alpha\beta$ $\varphi_{C2}\varphi_{C2}\alpha\beta\cdot\varphi_{H1}\varphi_{H1}\alpha\beta$ $\varphi_{C1}\varphi_{C1}\alpha\beta\cdot\varphi_{H1}\varphi_{H1}\alpha\beta$	The other (doubly polarized) structures	(XI)

3.1. Unimolecular dissociation reaction of formaldehyde $H_2CO \rightarrow H_2 + CO$

This reaction is Woodward-Hoffmann forbidden and proceeds via a highly asymmetric TS structure. Diabatically H_2CO ($^1A_1$) dissociates to H_2 ($^1\Sigma_g^+$) + CO ($^1\Pi$), while H_2 ($^1\Sigma_g^+$) and CO ($^1\Sigma^+$) interact repulsively and correlate with an excited state of H_2CO. An avoided-crossing of these two diabatic potential energy surfaces gives rise to a barrier for dissociation on the adiabatic ground state potential energy surface.

A qualitatively correct description of the dissociation process requires at least four active electrons in the two CH bonds of H_2CO. During the dissociation process, two electrons, one from each CH bond, pair up to form the HH bond while the other two form a lone pair on C in CO.

The basis set used is Dunning's cc-pVDZ [16]. The CASSCF wave function was obtained with CAS(4,4). The geometries of the equilibrium and TS structures were determined with this basis set and active space. The orbitals were then localized in the active orbital space. The orbitals were transformed so as to have maximum overlap with two carbon sp^2 orbitals and hydrogen $1s$ orbitals. The sp^2 orbitals were used with the fixed hybridization ratio of $2s$ to $2p$ orbitals (1:2) and with a fixed angle of 120° relative to the CO axis

Equilibrium   Transition state

0.6748

+0.3506

−0.0657

+0.0057   −0.0186

−0.0111

−0.0036

+ ...

0.3891

+0.1973   +0.0442

+0.0907   −0.0179

+0.0036   −0.0159

+0.2232

+0.0544   +0.0041

+ ...
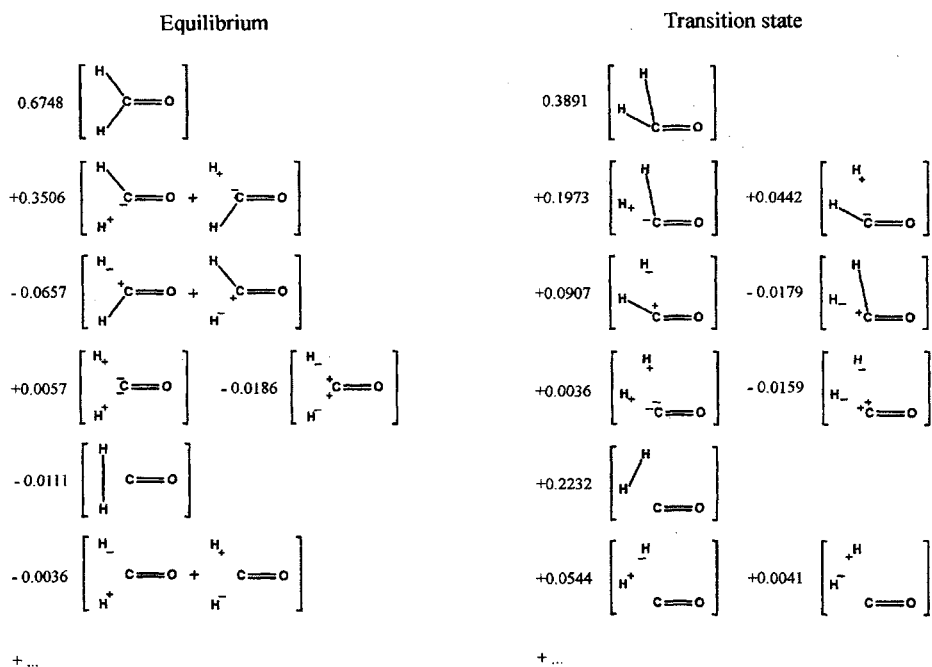
Fig. 6. The CASVB descriptions at the equilibrium and TS structures. The numerical values are occupation numbers.

throughout the reaction. The resulting orbitals are shown in Figs. 4 and 5. All the orbitals are well localized on the atomic centers, except LMOs on the carbon atom, which have a small contribution from the oxygen $2p$ orbital.

There are 20 linearly independent spin-paired functions corresponding to the dimension of CAS(4,4), which are listed in Table 1. Structures (I) to (VII) are classified as CH bond structures and the structures (VIII) to (X) as HH bond structures. Structure (XI) is classified as neither of the above, since these structures can be regarded both as structures polarized further from one of (II) to (V) and (IX) to (X).

The CASVB wave functions obtained for the equilibrium and TS structures are given in Fig. 6.

In the equilibrium structure, the main VB structure is the covalent CH bonds structure (I) as expected. The second most important are those where one of the CH bonds is connected with a covalent bond and the other with an ionic bond made by electron transfer from the hydrogen atom to the carbon atom, (II) and (IV). In contrast, the contribution from the structures that describe electron transfer from the carbon atom to a hydrogen atom is small and negative. The contribution from the HH bond structure (VIII) and ionic structures, (IX) and (X), is very small. The total occupation number of CH bonds is 0.9654, while that of HH bond is -0.0147. This indicates almost no bond formation between two hydrogen atoms in the equilibrium structure.

In the TS structure, the main structure is still the covalent structure (I), although the occupation number decreases. The structure (II), where the longer CH bond is covalent and the shorter CH bond is ionic, is also important, but
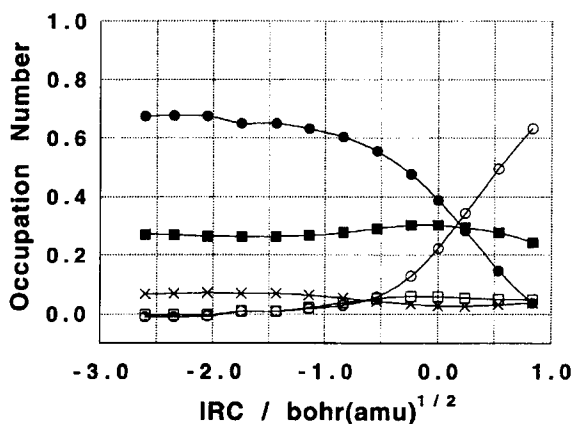
Fig. 7. Changes in the occupation numbers of the covalent CH bonds (●), ionic CH bonds (■), covalent HH bond (○), ionic HH bond (□), and the other (doubly ionic) (×) VB structures of H_2CO along IRC. The origin of the horizontal axis corresponds to the TS and the left end to the equilibrium structure of formaldehyde.

their occupation numbers also decrease. One the other hand, the structure (IV), where the shorter CH bond is covalent and the longer CH bond is ionic, is no longer important. The total occupation number of CH bonds structures is 0.6893, which shows a decrease from the value in the equilibrium structure 0.9654, but it is still large. The total occupation number of HH bond structures is 0.2817. Much of it comes from the covalent contribution (VIII), 0.2232. The contribution from the CH bonds overwhelms the contribution from the HH bond in the TS.

The occupation numbers of the covalent CH bonds, ionic CH bonds, covalent HH bond, ionic HH bond, and the other (doubly ionic) structures are defined by

$$n_{\text{Covalent CH}} = n_I, \qquad n_{\text{Ionic CH}} = \sum_{S=II}^{VII} n_S, \qquad (13)$$

$$n_{\text{Covalent HH}} = n_{VIII}, \qquad n_{\text{Ionic HH}} = n_{IX} + n_X, \qquad (14)$$

and

$$n_{\text{Doubly Pol.}} = n_{XI}. \qquad (15)$$

Using Eqs. (13) and (14), we may further define the total occupation numbers of the CH and HH bond structures,
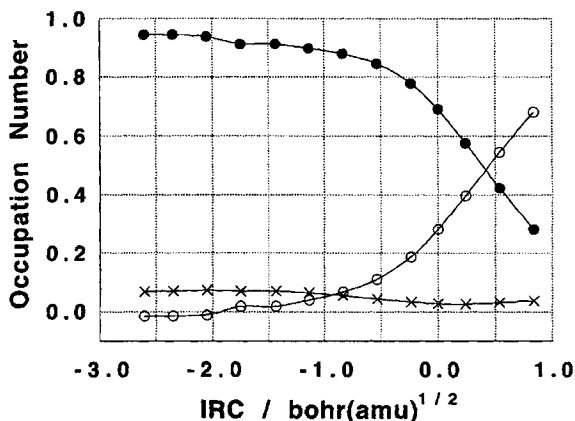
Fig. 8. Changes in the occupation numbers of the total CH bonds (●), total HH bond (○), and the other (doubly ionic) (×) VB structures of H_2CO along the IRC.
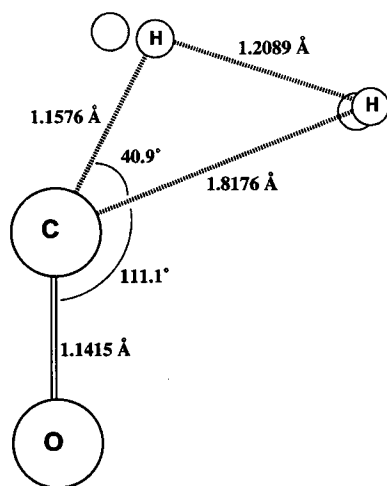
Fig. 9. The structure where the total occupation numbers of the CH bonds and HH bond valence bond structures are equal. The hydrogen atoms not bonded to the carbon atom represent the position at the TS.

$$n_{CH} = n_{Covalent\ CH} + n_{Ionic\ CH}, \qquad n_{HH} = n_{Covalent\ HH} + n_{Ionic\ HH}. \tag{16}$$

Fig. 7 shows the changes in the occupation numbers of the covalent CH bonds, ionic CH bonds, covalent HH bond, ionic HH bond, and the other (doubly ionic) structures along IRC. The origin of the horizontal axis corresponds to TS and the left end of each curve to the equilibrium structure. The occupation numbers of CH and HH covalent bond structures change rapidly near TS and the curves cross immediately after TS (0.1 bohr(amu)$^{1/2}$), while the occupation numbers of CH and HH ionic bond structures change slowly.

Fig. 8 shows the changes in the total occupation numbers of the CH and HH bond structures along the IRC. The crossing point is located after TS, 0.42 bohr(amu)$^{1/2}$. The structure at this point is given in Fig. 9. Compared to the TS, the longer and shorter CH bonds have stretched by 0.14 and 0.06 Å, respectively, and the HH bond has become shorter by 0.18 Å. These bond lengths are 1.03, 1.62, and 1.80 times longer than the corresponding equilibrium CH and HH bond distances. That point is the structure where the bonds switch; in other words, the point is the *transition state of chemical bond* between the CH bonds and HH bond.

The results here demonstrate the total occupation number defined in Eq. (16) is a useful concept for studying quantitative description of chemical bonds at TS and along reaction paths.

3.2. Hydrogen exchange reactions $H_2+X \rightarrow H+HX$ (X=F, Cl, Br, and I)

In the previous subsection, we applied the CASVB method to the unimolecular dissociation reaction $H_2CO \rightarrow H_2 + CO$, and examined how chemical bonds and electronic structures are described along the chemical reaction path. Our focus was on the chemical bond nature in the transition (TS) structure, that is, which bonds are dominant in TS, the dissociating CH bonds or the forming HH bond. The CASVB method shows that CH bonds are dominant in TS, based on the contribution of the VB structure of each bond. This kind of question is not easily answered using the CI picture with canonical molecular orbitals (MOs), and hence this is an example that demonstrates CASVB as a useful tool for analyzing electronic structures and chemical bond during chemical reactions. However, in this reaction the dissociating and forming bonds are both of covalent nature, that is, the bias of the charge is not so large, and thus the description is relatively easy compared to the reaction including ionic bonds.

In the this subsection, we examine a series of reactions including ionic bonds,

$$H_2 + F \quad \rightarrow H + HF, \tag{R1}$$
$$H_2 + Cl \rightarrow H + HCl, \tag{R2}$$
$$H_2 + Br \rightarrow H + HBr, \tag{R3}$$
$$H_2 + I \quad \rightarrow H + HI. \tag{R4}$$

The reaction for fluorine (R1) is highly exothermic, while the reactions for chlorine (R2), bromine (R3), and iodine (R4) are endothermic. The heats of these reactions are 30.8, -1.2, -16.7, and -32.7 kcal/mol for reactions (R1), (R2), (R3), and (R4), respectively. According to Hammond's postulate, reaction (R1) should have an early TS, and reactions (R2) and (R3) should have late TSs. On the other hand, the electronegativity (in Pauling's definition) for hydrogen, fluorine, chlorine, bromine, and iodine are 2.2, 4.0, 3.2, 3.0, and 2.7, respectively. This suggests that all the reactions (R1)-(R4) might have early TSs, since halogen atoms tend to receive an electron and form the bond with a hydrogen atom at early stage. What the electronic states are during these reactions, and how the CASVB method describes the electronic structure, are our interests in this subsection.

We first determined IRC for each reaction and then obtained the CASVB functions along IRC.

The basis sets used in the reactions including F and Cl are the augmented correlation consistent polarized valence double zeta (aug-cc-pVDZ) sets [16]. In the reactions including Br and I, the relativistic effective core potential (ECP) due to Stevens et al. [17,18] and their associated basis sets were used for Br and I, and the cc-pVDZ set for H. The basis sets of Br and I were augmented by adding a d polarization function with an exponent of 0.389 (Br) / 0.266 (I) and sp diffuse functions with an exponent 0.03574 (Br) / 0.03007 (I). The diffuse p polarization function of the aug-cc-pVDZ set of H was omitted for consis-

tency with the Br and I basis sets.

The active spaces were constructed by distributing three electrons in three orbitals consisting of $H_1(1s)$, $H_2(1s)$, and $X(2p\sigma)$, i.e. CAS(3,3). The dimension of the CAS is eight. According to this CAS, eight linearly independent VB structures,

$$\varphi_{H_A}\varphi_{H_B}(\alpha\beta - \beta\alpha)\cdot\varphi_X\alpha \qquad\qquad H_A - H_B \;\; \overset{\bullet}{X}, \qquad (I)$$

$$\varphi_{H_B}\varphi_{H_B}\alpha\beta\cdot\varphi_X\alpha \qquad\qquad H_A^+ \;\; {}^-H_B \;\; \overset{\bullet}{X}, \qquad (II)$$

$$\varphi_{H_A}\varphi_{H_A}\alpha\beta\cdot\varphi_X\alpha \qquad\qquad H_A^- \;\; {}^+H_B \;\; \overset{\bullet}{X}, \qquad (III)$$

$$\varphi_{H_A}\alpha\cdot\varphi_{H_B}\varphi_X(\alpha\beta - \beta\alpha) \qquad\qquad \overset{\bullet}{H_A} \;\; H_B - X, \qquad (IV)$$

$$\varphi_{H_A}\alpha\cdot\varphi_{H_B}\varphi_{H_B}\alpha\beta \qquad\qquad \overset{\bullet}{H_A} \;\; H_B^- \;\; {}^+X, \qquad (V)$$

$$\varphi_{H_A}\alpha\cdot\varphi_X\varphi_X\alpha\beta \qquad\qquad \overset{\bullet}{H_A} \;\; H_B^+ \;\; {}^-X, \qquad (VI)$$

$$\varphi_{H_B}\alpha\cdot\varphi_X\varphi_X\alpha\beta \qquad\qquad H_A^+ \;\; \overset{\bullet}{H_B} \;\; {}^-X, \qquad (VII)$$

and

$$\varphi_{H_A}\varphi_{H_A}\alpha\beta\cdot\varphi_{H_B}\alpha \qquad\qquad H_A^- \;\; \overset{\bullet}{H_B} \;\; {}^+X, \qquad (VIII)$$

were used to construct CASVB functions, where the normalization constants and antisymmetrizers are omitted.

The contributions of the covalent H_AH_B bond, ionic H_AH_B bond, covalent H_BX bond, ionic H_BX bond, and ionic H_AX bond are defined by

$$n_{\text{Covalent } H_AH_B} = n_I, \qquad\qquad n_{\text{Ionic } H_AH_B} = n_{II} + n_{III}, \qquad (17)$$

$$n_{\text{Covalent } H_BX} = n_{IV}, \qquad\qquad n_{\text{Ionic } H_BX} = n_V + n_{VI}, \qquad (18)$$

and

$$n_{\text{Ionic } H_AX} = n_{VII} + n_{VIII}. \qquad (19)$$

Furthermore, the contributions of the total H_AH_B and H_BX bond structures are defined by the sums of the covalent structure (I)/(IV) and ionic structures (II)/(V) and (III)/(VI),

$$n_{H_AH_B} = n_{\text{Covalent } H_AH_B} + n_{\text{Ionic } H_AH_B}, \qquad\qquad n_{H_BX} = n_{\text{Covalent } H_BX} + n_{\text{Ionic } H_BX}. \qquad (20)$$

Table 2
Occupation numbers of the VB structures in the products

			(H+) HF	(H+) HCl	(H+) HBr	(H+) HI
$\overset{\bullet}{\text{H}}$	H – X	(IV)	0.538	0.710	0.752	0.786
$\overset{\bullet}{\text{H}}$	H⁻ ⁺X	(V)	−0.018	0.041	0.064	0.101
$\overset{\bullet}{\text{H}}$	H⁺ ⁻X	(VI)	0.480	0.249	0.184	0.113

Let us first examine the electronic structure at the TS structure of the four reactions as well as those at the reactant and product structures.

The nonorthogonal LMOs were determined in the same manner as in the previous subsection. The atomic orbitals used for the determination are two $1s$ orbitals of the hydrogen atoms and $2p(\sigma)$ orbitals of the halogen atom. All the overlaps between the atomic orbital (AO) and the nonorthogonal LMO are greater than 0.9 (0.9004 at minimum). The molecular orbitals are therefore well localized.

The reactant in all the reactions is the system consisting of a hydrogen molecule and a halogen atom. Since the hydrogen molecule is expressed with VB structures as

$$\Psi_{\text{H}_2} = 0.889\left[\varphi_{\text{H}_A}\varphi_{\text{H}_B}(\alpha\beta - \beta\alpha)/\sqrt{2}\right] + 0.111\left[\varphi_{\text{H}_A}\varphi_{\text{H}_A}\alpha\beta + \varphi_{\text{H}_B}\varphi_{\text{H}_B}\alpha\beta\right], \quad (21)$$

Table 3
Occupation numbers of the VB structures at the TS

		H + H +F	H + H + Cl	H + H + Cl	H + H + Cl
H – H $\overset{\bullet}{\text{X}}$	(I)	0.485	0.328	0.217	0.172
H⁺ ⁻H $\overset{\bullet}{\text{X}}$	(II)	0.053	0.059	0.043	0.034
H⁻ ⁺H $\overset{\bullet}{\text{X}}$	(III)	0.017	−0.022	−0.023	−0.019
$\overset{\bullet}{\text{H}}$ H – X	(IV)	0.252	0.385	0.514	0.591
$\overset{\bullet}{\text{H}}$ H⁻ ⁺X	(V)	−0.005	0.018	0.042	0.073
$\overset{\bullet}{\text{H}}$ H⁺ ⁻X	(VI)	0.147	0.155	0.142	0.100
H⁻ $\overset{\bullet}{\text{H}}$ ⁺X	(VII)	0.006	0.013	0.011	0.010
H⁺ $\overset{\bullet}{\text{H}}$ ⁻X	(VIII)	0.045	0.064	0.053	0.039
HH bond		0.555	0.365	0.237	0.187
HX bond		0.394	0.558	0.698	0.764
Others		0.051	0.077	0.064	0.049

the reactant is written as

$$\Psi_{\text{Reactant}} = 0.889[(I)] + 0.111[(II) + (III)] \tag{22}$$

in all the reactions.

On the other hand, the products are the systems consisting of a hydrogen atom and a hydrogen halide. The VB structures are summarized in Table 2. As mentioned before, the electronegativities of all the halogen atoms are larger than that of the hydrogen atom. In particular, the difference between the electronegativity of F and H atoms, 4.0 and 2.2, respectively, is rather large. Hence, the bond nature of the HF molecule is thought to be ionic. However, the *covalent* nature is found to be dominant in all the hydrogen halide in the CASVB picture, even in the case of HF.

Table 3 shows the VB structure at the TSs of $H_2 + X \rightarrow H + HX$. Just as for the equilibrium structures, the covalent VB structures are dominant: the structures are well described by the superposition of the HH and HX covalent struc-
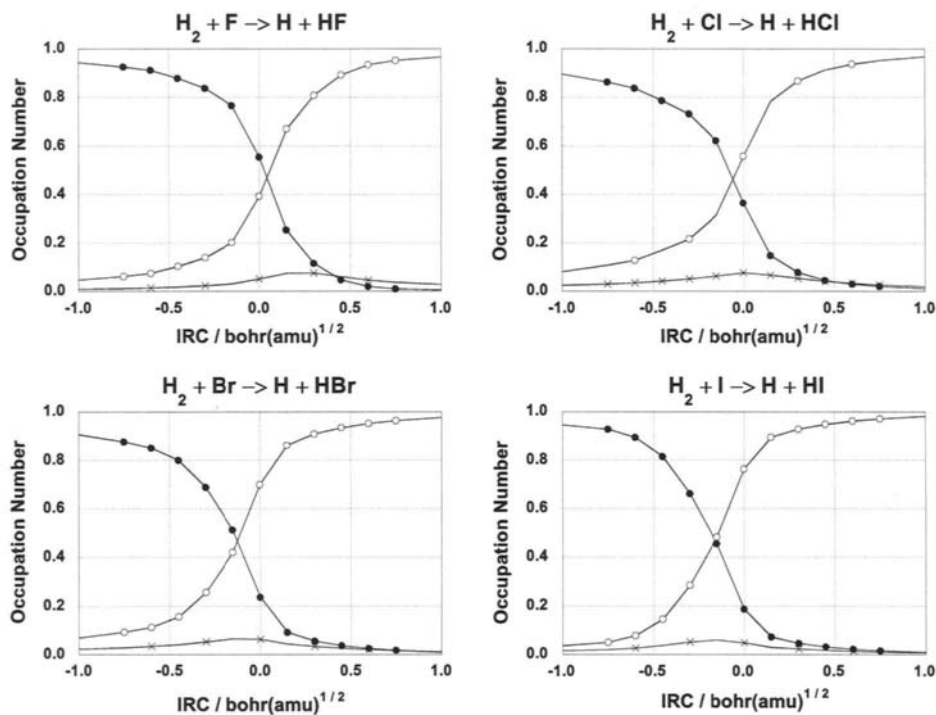
Fig. 10. Changes in the occupation numbers of the total HH bond (●), total HX bond (○), and the other (×) VB structures along IRC. The origin of the horizontal axis corresponds to the TS.

ture with small H$^+$H and H$^+$X$^-$ ionic contributions.

Using Eq. (20), these structures are further classified as the HH and HX bonds, as shown in Table 3. For X=F, the contribution of the HH bond (55.5%) is larger than that of the HX bond (39.4%). This relation is reversed for X=Cl, Br, and I. The contribution of the HH bond increases as the halogen atom becomes heavier (55.8 (Cl), 69.8 (Br), and 76.4% (I)). This means that *the TS of chemical bonds* (that is, the point where the occupation numbers of the two chemical bonds are equal) defined in the previous subsection is placed in the reactant side in the X=F case and in the product side for the case of X=Cl, and it shifts more to the product side as the halogen atom becomes heavier.

We now examine the bond nature during the reactions.

Fig. 10 shows the changes in the total occupation number of the HH and HX bond structures along the IRC. Similarly to the previous reaction, the occupation numbers of the HH and HX bond structures change rapidly and the curves cross near the TS. The crossing points are located at 0.07, −0.11, −0.25, and −0.33 bohr(amu)$^{1/2}$ for X=F, Cl, Br, and I, respectively, where a negative sign means the crossing point is located before the TS and a positive sign after the
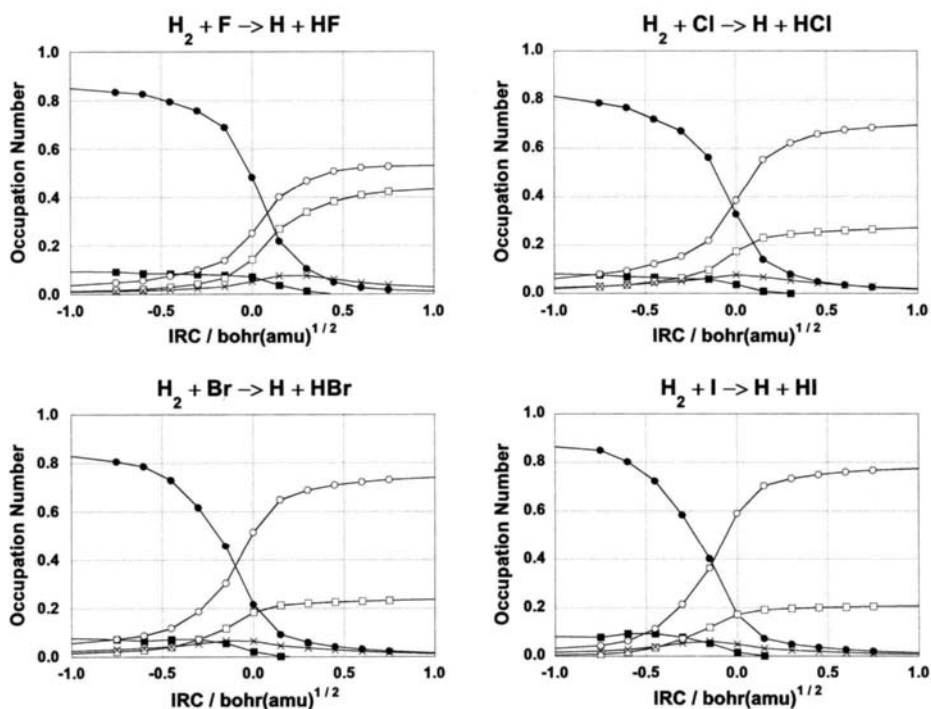
Fig. 11. Changes in the occupation numbers of the covalent HH bond (●), ionic HH bond (■), covalent HX bond (○), ionic HX bond (□), and the other (×) VB structures along the IRC.

TS. We can see the trend that the crossing point shifts from the reactant side to the product side as the halogen atom gets heavier. (We can also consider that the TS shifts from the product side to reactant side if we take the crossing point as the origin.)

The changes in the contents of the HH and HX bonds are plotted in Fig. 11. As expected in these reactions including ionic bonds, the contribution of ionic bond increases as that of the covalent bond increases. This feature contrasts with that in the dissociation reaction of H_2CO, where the ionic bonds do not change so much. However, the crossing point of HH and HX covalent bonds are still close to that of the HH and HX bonds in Fig. 10. Thus, also in these reactions, we can say that the covalent bonds are mainly responsible for determining the crossing points.

To analyze the crossing points, that is, *the TS structures of the HH and HX bonds*, we further examine the geometrical changes of the HH and HX bonds and the dipole moment of the systems.

Fig. 12 presents the difference of the HH and HX bond lengths from the equilibrium lengths along the IRC. It is rather difficult to determine the point
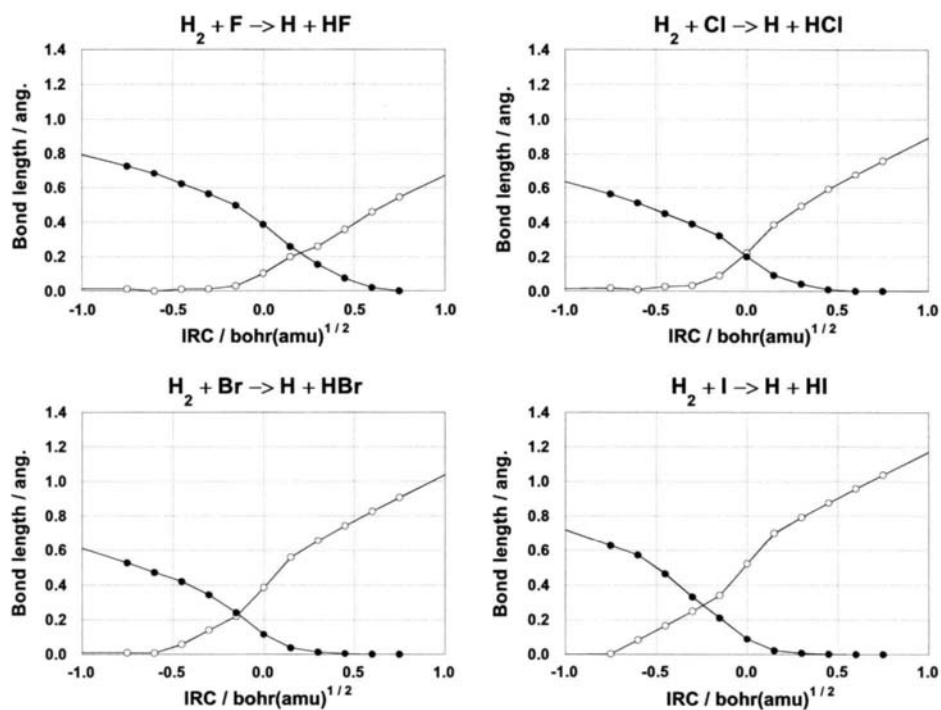
Fig. 12. Differences of the HH (o) and HX (•) bond lengths from the equilibrium lengths along the IRC.
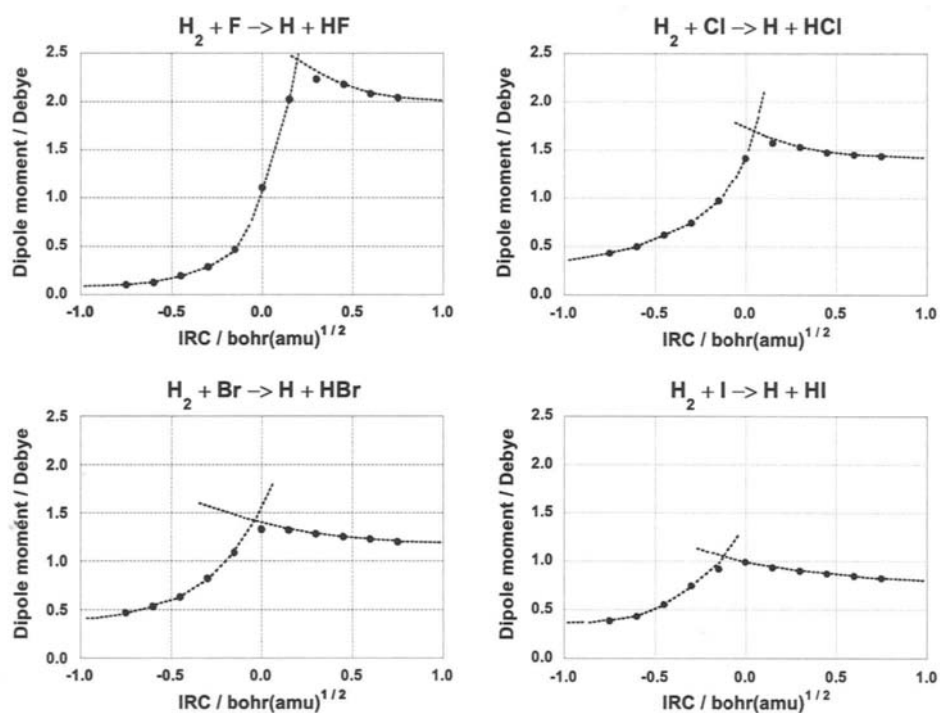
Fig. 13. Changes in dipole moment of the systems along the IRC.

that characterizes the TS. However, for qualitative discussion, the crossing points of the curves are enough to be the characterizing points: they are located at 0.20 (X=F), −0.02 (Cl), −0.14 (Br), and −0.25 bohr(amu)$^{1/2}$ (I). The trend in these positions is similar to the crossing points of the HH and HX bonds. The same can be seen in the changes in dipole moment of the systems plotted in Fig. 13. The curves are drawn so that either dipole moment value for HH+X or H+H$^{+\delta}$X$^{-\delta}$ could be smooth. The crossing points are considered the points where the charge transfer from H to X occurs (in other words, the points where the electronic structure changes drastically). The points are located at 0.19 (X=F), 0.04 (Cl), −0.04 (Br), and −0.13 bohr(amu)$^{1/2}$ (I).

We have now another TS, *the TS of the HH and HX bonds*, besides the real TS. What is the significance of this TS?

If we measure the crossing points in Figs. 12 and 13 from the crossing points of the HH and HX bonds, the values become 0.13 (F), 0.09 (Cl), 0.11 (Br), and 0.08 (I) for geometrical change, and 0.12 (F), 0.15 (Cl), 0.21 (Br), and 0.20 (I) for dipole moment. The ranges of the values are 0.05 for the former numbers and 0.09 for the latter numbers. These are rather small compared to those for the numbers measured from the real TS: 0.45 and 0.32. We may therefore say

that *the TS of chemical bonds* reflects the geometrical and electronic structure information more than the real TS. If we consider Hammond's postulate, probably we should not say that *the TS of chemical bonds* are shifted from the real TS, but instead say that the real TS is shifted from *the TS of chemical bonds* due to the systematic changes in heat of the reaction.

4. CONCLUDING REMARKS

In this article, we investigated the nature of bonds at TS and during the chemical reaction using the CASVB method with nonorthogonal LMOs. The nature of bond dissociation and formation can be viewed quantitatively by the use of the occupation number of the VB structure, which is defined by the weight of the spin-paired function of VB structure. The results in the previous section demonstrate that the occupation number is a useful concept for studying quantitative descriptions of chemical bonds at TS and along reaction paths. This analysis is applicable to reactions involving excited states as well as just the ground state. We believe that the CASVB occupation number analysis is a useful tool for understanding chemical reaction mechanisms.

ACKNOWLEDGMENT

REFERENCES

[1] K. Hirao, H. Nakano, K. Nakayama, and M. Dupuis, J. Chem. Phys. 105 (1996) 9227.

[2] K. Hirao, H. Nakano, and K. Nakayama, J. Chem. Phys. 107 (1997) 9966.

[3] K. Nakayama, H. Nakano, and K. Hirao, Int. J. Quantum Chem. 66 (1998) 157.

[4] Y. Kawashima, K. Nakayama, H. Nakano, and K. Hirao, Chem. Phys. Lett. 267 (1997) 82.

[5] H. Nakano, K. Nakayama, and K. Hirao, J. Mol. Struct. (Theochem) 461-462 (1999) 55.

[6] K. Ruedenberg, M.W. Schmidt, M.M. Gilbert, and S.T. Elbert, Chem. Phys. 71 (1982) 41.

[7] K. Ruedenberg, M.W. Schmidt, and M.M. Gilbert, Chem. Phys. 71 (1982) 51.

[8] K. Ruedenberg, M.W. Schmidt, M.M. Gilbert, and S.T. Elbert, Chem. Phys. 71 (1982) 65.

[9] J.M. Foster and S.F. Boys, Rev. Mod. Phys. 32 (1960) 300.

[10] T. Thorsteinsson, D.L. Cooper, J. Gerratt, P.B. Karadakov, and M. Raimondi, Theor. Chim. Acta 93 (1996) 343.

[11] T. Thorsteinsson and D.L. Cooper, Theor. Chim. Acta 94 (1996) 233.

[12] T. Thorsteinsson, D.L. Cooper, J. Gerratt, and M. Raimondi, Theor. Chim. Acta 95 (1997) 131.

[13] T. Thorsteinsson, D.L. Cooper, J. Gerratt, and M. Raimondi, in: R. McWeeny, J. Maruani, Y.G. Smeyers, and S. Wilson (Eds.), Quantum Systems in Chemistry and Physics: Trends in Methods and Applications, Kluwer, Dordrecht, 1997.

[14] D.L. Cooper, T. Thorsteinsson, and J. Gerratt, Adv. Quantum Chem. 32 (1998) 51.

[15] T. Thorsteinsson and D.L. Cooper, in: A. Herández-Laguna, J. Maruani, R. McWeeny, and S. Wilson (Eds.), Quantum Systems in Chemistry and Physics. Volume 1: Basic problems and models systems, Kluwer, Dordrecht, 2000.

[16] T.H. Dunning, Jr. J. Chem. Phys. 90 (1989) 1007.

[17] W.J. Stevens, H. Basch, and M. Krauss, J. Chem. Phys. 81 (1984) 6026.

[18] W.J. Stevens, M. Krauss, H. Basch, and P.G. Jasien, Can. J. Chem. 70 (1992) 612.

[19] M. Dupuis, S. Chin, and A. Marquez, in: G.L. Malli (Ed.), Relativistic and Electron Correlation Effects in Molecules and Clusters, NATO ASI Series, Plenum, New York, 1992.

[20] M.W. Schmidt, K.K. Baldridge, J.A. Boatz, S.T. Elbert, M.S. Gordon, J.H. Jensen, S. Koseki, N. Matsunaga, K.A. Nguyen, S. Su, T.L. Windus, M. Dupuis, and J.A. Montgomery, J. Comput. Chem. 14 (1993) 1347.

This Page Intentionally Left Blank

Chapter 4

TURTLE – A gradient VBSCF Program Theory and Studies of Aromaticity

Joop H. van Lenthe, Fokke Dijkstra, Remco W. A. Havenith

Theoretical Chemistry Group, Debye Institute, Utrecht University,
Padualaan 14, 3584 CH Utrecht, The Netherlands

The *Ab Initio* Valence Bond program TURTLE has been under development for about 12 years and is now becoming useful for the non-specialist computational chemist as is exemplified by its incorporation in the GAMESS-UK program. We describe here the principles of the matrix evaluation and orbital optimisation algorithms and the extensions required to use the Valence Bond wavefunctions in analytical (nuclear) gradient calculations. For the applications, the emphasis is on the selective use of restrictions on the orbitals in the Valence Bond wavefunctions, to investigate chemical concepts, in particular resonance in aromatic systems.

1. INTRODUCTION

Valence Bond theory has always struck a sympathetic chord in chemist's minds, because it can be linked so closely to the familiar Lewis structure. A bond is immediately translated in the wavefunction by two non-orthogonal orbitals on neighbouring atoms that are singlet coupled. An ionic structure may contain an atomic orbital, that is occupied twice, or alternatively two orbitals on the same atom. So it is simply possible to translate the assumed concept of the bonding in a molecule into a (small) set of structures. Alternatively, if the nature of the bonding is in question, the relative importance of the different structures may give insight. Vital for an unbiased wavefunction is the ability to optimise the wavefunction, both its orbitals and its structure coefficients. An efficient way to perform such an optimisation is implemented in the spin-coupled program and in its later incarnation the CASVB method [1,2]. These methods usually consider all spin-couplings and often a single set of singly occupied optimised orbitals.

In the development of the TURTLE program [3], we started by considering a multi-structure Valence Bond wavefunction and added the capability to optimise the orbitals. We tried to avoid putting restrictions on the way the wavefunction is built and to allow great flexibility in the choice of orbitals. For

instance if covalent and ionic structures are employed, the orbitals used in these structures may be identical, which just mimics the effect of orbital optimisations. Also all orbitals in an ionic structure, both doubly and singly occupied ones, may be chosen to be different from those in the covalent structure. This yields a very compact and accurate wavefunction (the Breathing Orbital Valence Bond method) [4,5] at the cost of a troublesome orbital optimisation, due to the near identity of the orbital spaces. The orbitals used may be fully optimised as in the spin-coupled approach, but they may also be restricted to a subspace of the full orbital space, e.g. just the one atom. This enhances the interpretability of the wavefunction considerably. Recently we added gradient capabilities to the program and integrated it into the GAMESS-UK [6] program.

We will describe the main features of our program and give examples of the use of the code for studying the aromaticity in various molecules.

2. WAVEFUNCTION OPTIMISATION

Our wavefunction is build as a linear combination of structures

$$\Psi = \sum_i C_i \Phi_i \tag{1}$$

Each structure is a spin-adapted linear combination of determinants. Both Rumer diagrams and Branching Diagrams may be chosen. If required, even individual determinants may be employed as building blocks. The coefficients in Eq. (1) are usually determined by solving the corresponding generalised eigenvalue problem

$$(\mathbf{H} - E\mathbf{S})\mathbf{C} = \mathbf{0} \tag{2}$$

Alternatively, they may be fixed from the outset. To the structures, weights can be attributed, which add up to one, using a formula given by Chirgwin and Coulson [7].

$$W_j = \sum_i c_i c_j S_{ij} \tag{3}$$

2.1 Orbital Optimisation
The orbital optimisation is based on the Generalised Brillouin Theorem [8] as extended to non-orthogonal wavefunctions [9,10]:

$$\left\langle \Psi_0 \left| H - E_0 \right| \Psi_{ij} \right\rangle = 0 \tag{4}$$

where Ψ_{ij} is the singly excited state, a Brillouin state, obtained by applying the unnormalised excitation operator $C_{i \to j}$ to the wavefunction:

$$\Psi_{ij} = C_{i \to j} \Psi_0 \tag{5}$$

The excitation operator does not have to adhere to the unitary condition, as is the case for orthogonal orbitals. Each Brillouin matrix element (Eq. (4)) represents the stationary condition for the mixing of orbitals ψ_i and ψ_j according to $\psi_i \to \psi_i + \partial \psi_j$. The wavefunction consisting of Ψ_0 and all singly excited states

$$\Psi = b_0 \Psi_0 + \sum_{i,j} b_{ij} \Psi_{ij} \tag{6}$$

is obtained by solving the corresponding generalised eigenvalue problem, the Brillouin state interaction problem. One can employ the coefficients b_{ij} to determine improved orbitals according to

$$\psi_i \to \psi_i + b_{ij} \psi_j \tag{7}$$

For orthogonal orbitals this procedure is often called the SuperCI method.

When the new orbitals are determined, the Valence Bond function is re-determined using Eq. (2), and the procedure is repeated until convergence is obtained, i.e. all b_{ij}'s in Eq. (6) are zero and the Generalised Brillouin theorem (Eq. (4)) is satisfied.

The usual convergence acceleration/stabilisation tools may be employed in this orbital optimisation. For instance, we have implemented level shifting and DIIS [11].

The SuperCI itself is usually quite stable, but involves solving a non-orthogonal CI of a considerable dimension, with each Brillouin state containing the same number of determinants as the Valence Bond wavefunction, which is rather time consuming. The SuperCI matrix can be approximated by its first row (the Brillouin theorem elements) and the diagonal at a considerable time saving. Then the Brillouin state coefficients b_{ij} are estimated following

$$b_{ij} = -\frac{\left\langle \Psi_0 \left| H - E_0 \right| \Psi_{ij} \right\rangle}{\left\langle \Psi_{ij} \left| H - E_0 \right| \Psi_{ij} \right\rangle} \tag{8}$$

which is the non-orthogonal equivalent of the first-order Raleigh-Schrödinger perturbation expression [12]. This approach produces, for not so complicated wavefunctions, acceptable convergence behaviour, especially when convergence aids like DIIS are invoked.

3. EXPRESSIONS FOR THE ENERGY AND ITS DERIVATIVES [13-15]

The wavefunction consists of a linear combination of structures, which themselves are spin-adapted linear combinations of determinants:

$$\Psi = \sum_p C_p \Delta_p \tag{9}$$

According to Löwdin [16] the interaction between two determinants Δ_p and Δ_q is:

$$\left\langle \Delta_p \left| \hat{H} \right| \Delta_q \right\rangle = \sum_{ik} h_{ik} \mathbf{S}^{(i,k)} + \sum_{i<j,k<l} \left\{ \langle ij|kl \rangle - \langle ij|lk \rangle \right\} \mathbf{S}^{(i,j,k,l)} \tag{10}$$

The overlap is obtained by expanding along an arbitrary column (k):

$$\left\langle \Delta_p \middle| \Delta_q \right\rangle = |\mathbf{S}| = \sum_i S_{ik} S^{(i,k)} \tag{11}$$

In these equations h_{ik} and S_{ik} are the one-electron matrix elements for orbital i and k $\langle \phi_i(1)|h(1)|\phi_k(1)\rangle$ and $\langle \phi_i(1)|\phi_k(1)\rangle$. The $<ij|kl>$ are the two-electron integrals $\langle \phi_i(1)\phi_j(2)|1/r_{12}|\phi_k(1)\phi_l(2)\rangle$. $\mathbf{S}_{ab}^{(i,k)}$ and $\mathbf{S}_{ab}^{(i,j,k,l)}$ are the first and second order cofactors of the overlap matrix, which are signed minors of it. The orbitals in Eqs. (10) and (11) are the orbitals occupied in the determinants Δ_p and Δ_q. So the indices i and j refer to the occupied orbitals in Δ_p, and the indices k and l to occupied orbitals in Δ_q. $\mathbf{S}$ is the overlap matrix between the occupied orbitals of Δ_p and Δ_q. More about cofactors and adjugates can be found in for example a book by Aitken [17]. The approach used to obtain the various cofactors will be discussed in the next paragraph.

Assuming a normalised wavefunction, we can now write the energy as

$$\cdot E = \left\langle \Psi \left| \hat{H} \right| \Psi \right\rangle = \sum_p \sum_q C_p C_q \left(\sum_{ik} h_{ik} \mathbf{S}_{pq}^{(i,k)} + \sum_{i<j,k<l} \left\{ \langle ij|kl \rangle - \langle ij|lk \rangle \right\} \mathbf{S}_{pq}^{(i,j,k,l)} \right) \tag{12}$$

By rearranging the summations and realising that $S_{pq}^{(i,k)}$ and $S_{pq}^{(i,j,k,l)}$ are sub-determinants of the determinant representing the overlap between Δ_p and Δ_q and that they are zero if the orbitals i,j and k,l do not appear in the respective determinants, we obtain

$$E = \left\langle \Psi \middle| \hat{H} \middle| \Psi \right\rangle$$
$$= \left(\sum_{ik} h_{ik} \sum_{p} \sum_{q} S_{pq}^{(i,k)} C_p C_q + \sum_{i<j,k<l} \left\{ \langle ij|kl \rangle - \langle ij|lk \rangle \right\} \sum_{p} \sum_{q} S_{pq}^{(i,j,k,l)} C_p C_q \right) \tag{13}$$

or

$$E = \left\langle \Psi|H|\Psi \right\rangle = \left(\sum_{ik} h_{ik} d_{ik} + \sum_{i<j,k<l} \left\{ \langle ij|kl \rangle - \langle ij|lk \rangle \right\} D_{ijkl} \right) \tag{14}$$

with the one and two electron reduced density matrices

$$d_{ik} = \sum_{p} \sum_{q} S_{pq}^{(i,k)} C_p C_q$$
$$D_{ijkl} = \sum_{p} \sum_{q} S_{pq}^{(i,j,k,l)} C_p C_q \tag{15}$$

This is of course the familiar expression from orthogonal MO theories. The complexity due to the non-orthogonality is now hidden in the cofactors in the reduced density matrices.

3.1 Hellmann-Feynman theorem

For exact wavefunctions, the Hellmann-Feynman [18,19] theorem states that the derivative of the energy with respect to a nuclear co-ordinate x equals the expectation value of the derivative of the Hamiltonian.

$$\frac{dE}{dx} = \left\langle \Psi \middle| \frac{\partial \hat{H}}{\partial x} \middle| \Psi \right\rangle \tag{16}$$

When the wavefunction is expanded, using expansion parameters c, this theorem still holds if $\partial E/\partial c = 0$, or when $\partial c/\partial x = 0$. The first is the case for completely optimised wavefunctions and the second for wavefunctions where some, or all, of the coefficients are frozen. This can be seen when we write the derivative of E with respect to x as a sum of two terms:

$$\frac{dE(x)}{dx} = \frac{\partial E(x;c)}{\partial x} + \frac{\partial E(x;c)}{\partial c}\frac{\partial c}{\partial x} \tag{17}$$

The first term contains the direct dependence on x, the second the dependence on x through c. When $\partial E/\partial c = 0$ (optimised), or $\partial c/\partial x = 0$ (frozen coefficients) the second part disappears:

$$\frac{dE(x)}{dx} = \frac{\partial E(x;c)}{\partial x} \tag{18}$$

Therefore, the dependence on the coefficients does not enter the gradient expression; not for fixed orbitals, which is the classical Valence Bond approach and not for optimised orbitals, irrespective of whether they are completely optimised or if they are restricted to extend only over the atomic orbitals of one atom. If the wavefunction used in the orbital optimisation differs, additional work is required. This would apply to a multi-reference singles and doubles VB (cf. [20,21]). Then we would require a yet unimplemented coupled-VBSCF procedure. Note that the option to fix the orbitals is not available in orthogonal (MO) methods, due to the orthonormality restriction.

3.2 Gradient expression

The only restriction for the gradient evaluation is that the wavefunction has to be normalised, i.e.

$$\langle \Psi | \Psi \rangle = 1 \quad or \quad [\langle \Psi | \Psi \rangle - 1 = 0] \tag{19}$$

To take this restriction into account, the Lagrange multiplier formalism is employed. We devise a Lagrangian by adding the restriction multiplied by a Lagrange multiplier λ.

$$L = E - \lambda[S - 1] = \langle \Psi | \hat{H} | \Psi \rangle - \lambda[\langle \Psi | \Psi \rangle - 1] \tag{20}$$

The Lagrange multiplier λ is determined by requiring that the derivatives of the Lagrangian with respect to all optimised variables like the structure coefficients C_k are zero:

$$\frac{\partial L}{\partial C_k} = \frac{\partial}{\partial C_k}\left\{\sum_{ij}C_iC_jH_{ij} - \lambda\left[\sum_{ij}C_iC_jS_{ij} - 1\right]\right\} = 2\sum_i C_i\{H_{ik} - \lambda S_{ik}\} = 0 \tag{21}$$

This is clearly equivalent to the secular equations

$$\sum_i C_i \{H_{ik} - ES_{ik}\} = 0 \tag{22}$$

Thus λ equals the energy E. Similarly one can derive the expression involving the orbital coefficients, which involves the generalised Brillouin theorem (Eq. (4)) which again yields $\lambda = E$.

The required energy derivative is

$$\frac{\partial E}{\partial x} = \frac{\partial L}{\partial x} = \frac{\partial}{\partial x} \langle \Psi | \hat{H} | \Psi \rangle - E \frac{\partial}{\partial x} \langle \Psi | \Psi \rangle \tag{23}$$

Another way to see that E is the required Lagrange multiplier is by taking the derivative of the energy expression for an unnormalised wavefunction:

$$\frac{\partial}{\partial x} \frac{\langle \Psi | \hat{H} | \Psi \rangle}{\langle \Psi | \Psi \rangle} = \frac{\langle \Psi | \Psi \rangle \frac{\partial}{\partial x} \langle \Psi | \hat{H} | \Psi \rangle - \langle \Psi | \hat{H} | \Psi \rangle \frac{\partial}{\partial x} \langle \Psi | \Psi \rangle}{\langle \Psi | \Psi \rangle^2} \tag{24}$$

Now add normalisation of Ψ so that $\langle \Psi | \Psi \rangle = 1$, and use:

$$E = \langle \Psi | \hat{H} | \Psi \rangle \tag{25}$$

and obtain:

$$\frac{\partial E}{\partial x} = \frac{\partial}{\partial x} \langle \Psi | \hat{H} | \Psi \rangle - E \frac{\partial}{\partial x} \langle \Psi | \Psi \rangle \tag{26}$$

Eq. (26) gives the final expression for the derivative of the energy. The derivatives of the energy (Eq. (14)) and the norm of the wavefunction have to be evaluated, using partial differentiation, since both one- and two-electron integrals and the density matrices (through the cofactors) may change with the geometry:

$$\frac{\partial \langle \Psi | H | \Psi \rangle}{\partial x} = \left(\sum_{ik} \frac{\partial h_{ik}}{\partial x} . d_{ik} + \sum_{i<j,k<l} \left\{ \frac{\partial \langle ij | kl \rangle}{\partial x} - \frac{\partial \langle ij | lk \rangle}{\partial x} \right\} D_{ijkl} \right)$$
$$+ \left(\sum_{ik} h_{ik} \frac{\partial d_{ik}}{\partial x} + \sum_{i<j,k<l} \left\{ \langle ij | kl \rangle - \langle ij | lk \rangle \right\} \frac{\partial}{\partial x} D_{ijkl} \right) \tag{27}$$

This equation has two parts. The first part contains derivatives of the one and two electron integrals. These are supplied by any standard gradient package and also appear in gradient expressions for orthogonal MO methods. The other part contains the derivatives of the density matrices, more specifically the derivatives of the first and second order cofactors. These are absent in the orthogonal methods by virtue of the fact that all cofactors are either 1 or 0. The orthonormality of the wavefunction is handled by the orthonormality restrictions, which in their turn give rise to Lagrange multipliers. We will gather all terms involving derivatives of the overlap in the derivatives expression into a matrix $\mathbf{L}$, which can take the place of the Lagrange multiplier matrix of MO based gradient packages.

3.3 Density matrices and Cofactors

As a cofactor is itself a determinant, we may just consider the determinant of an overlap matrix. A determinant can be expressed as a sum of products of its matrix elements. The derivative of a product of matrix elements is obtained by taking the derivative of one matrix element and multiplying this by the product of the other matrix elements. This has to be done for all the matrix elements in the product, and the results have to be added. Another way to look at a determinant is by expanding it in its first order cofactors (cf. Eq. (11)) :

$$|\mathbf{S}| = \sum_{i}^{N} s_{ik} S^{(i,k)} \tag{28}$$

Now the determinant is a linear combination of matrix elements of a row (or column) times the corresponding cofactors. The weight of a certain matrix element in the determinant is given by its first order cofactor. The derivative must be the sum of the derivatives of the matrix elements times their cofactors, like shown in the next equation:

$$\frac{d|\mathbf{S}|}{dx} = \sum_{rs} \frac{ds_{rs}}{dx} \mathbf{S}^{(r,s)} \tag{29}$$

Because cofactors are sub-determinants, one can immediately write down their derivatives. The first order cofactors of first order cofactors are second order cofactors, and first order cofactors of second order cofactors introduce third order cofactors.

$$\frac{d\mathbf{S}^{(i,k)}}{dx} = (sign)\sum_{rs}\frac{dS_{rs}}{dx}\mathbf{S}^{(i,r,k,s)}$$

$$\frac{d\mathbf{S}^{(i,j,k,l)}}{dx} = (sign)\sum_{rs}\frac{dS_{pq}}{dx}\mathbf{S}^{(i,j,r,k,l,s)}$$

(30)

In these equations there is also a sign involved, which depends on the relative positions of the original indices i,j,k and l with respect to r and s. The first indices refer to the original overlap matrix, while r and s should refer to the matrix where row i (and j) and column k (and l) have been removed. To keep the equations simple we will omit this sign in our equations[†].

Thus the derivatives of the density matrix elements are

$$\frac{\partial d_{ik}}{\partial x} = \sum_{rs}\frac{ds_{rs}}{dx}\sum_{p}\sum_{q}\mathbf{S}^{(i,r,k,s)}_{pq}C_pC_q = \sum_{rs}\frac{ds_{rs}}{dx}d_{irks}$$

$$\frac{\partial D_{ijkl}}{\partial x} = \sum_{rs}\frac{ds_{rs}}{dx}\sum_{p}\sum_{q}\mathbf{S}^{(i,j,r,k,l,s)}C_pC_q = \sum_{rs}\frac{ds_{rs}}{dx}d_{ijrkls}$$

(31)

Thus, we now need also a third order reduced density matrix, which involves the corresponding third order cofactors.

Eq. (28) can now be used to derive the expression for the derivative of the norm of the wavefunction, which is also required in Eq. (26).

$$\frac{\partial\langle\Psi|\Psi\rangle}{\partial x} = \sum_{p}\sum_{q}C_pC_q\frac{d|\mathbf{S}_{pq}|}{dx} = \sum_{rs}\frac{ds_{rs}}{dx}\sum_{p}\sum_{q}C_pC_q\mathbf{S}^{(r,s)}_{pq} = \sum_{rs}\frac{ds_{rs}}{dx}d_{rs}$$

(32)

Combining Eqs. (27), (31) and (32) the final expression for the derivative of the energy with respect to say a geometrical parameter is

$$\frac{\partial\langle\Psi|H|\Psi\rangle}{\partial x} = \left(\sum_{ik}\frac{\partial h_{ik}}{\partial x}.d_{ik} + \sum_{i<j,k<l}\left\{\frac{\partial\langle ij|kl\rangle}{\partial x} - \frac{\partial\langle ij|lk\rangle}{\partial x}\right\}D_{ijkl}\right) - \sum_{ik}\frac{\partial s_{ik}}{\partial x}.L_{ik}$$

(33)

[†] The sign depends on the relative position of the rows and the columns, which are removed. For instance, if $r<i$, the sign is unchanged when removing r, but if r lies beyond i the sign should reflect, that r actually should be moved 1 place back and therefore a -1 is produced cf. [22].

with

$$L_{ik} = E_0.d_{ik} - \sum_{rs} h_{rs} d_{risk} - \sum_{r<j,s<l} \{\langle rj|sl \rangle - \langle rj|ls \rangle\} D_{rjislk} \tag{34}$$

This expression is very similar to those in the normal orthogonal case. We may therefore use any general gradient package. Our VB program generates the density matrices and the matrix $\mathbf{L}$, which is used instead of the Lagrange multiplier matrix of for instance a MCSCF function.

3.4 Cofactors [23,24]

For the calculation of cofactors we use algorithms based on work by Löwdin [16], and Prosser and Hagstrom [25,26]. An overview of the theory of determinants, cofactors, adjugates and compound matrices can be found in a book by Aitken [17]. The symmetry and possible orthogonality in the orbital spaces give rise to a block-structure in the overlap matrices. This structure is exploited [22,27] to minimise the size of the matrices in the $\mathbf{L}$-$\mathbf{d}$-$\mathbf{R}$ decomposition, described below, an n^3 process for each matrix.

The calculation of the first order cofactors is simplified by performing an $\mathbf{L}$-$\mathbf{d}$-$\mathbf{R}$ decomposition of the overlap matrix. $\mathbf{L}$ and $\mathbf{R}$ are lower and upper diagonal matrices respectively. They have ones on the diagonal and therefore their determinant is one as well. $\mathbf{L}$ and $\mathbf{R}$ are chosen in such a way, that when $\mathbf{S}$ is pre-multiplied by $\mathbf{L}$ and post-multiplied by $\mathbf{R}$ the result is a diagonal matrix $\mathbf{d}$.

$$\mathbf{d} = \mathbf{L} \cdot \mathbf{S} \cdot \mathbf{R}$$

$$|\mathbf{L}| = |\mathbf{R}| = 1 \tag{35}$$

$$\mathbf{S} = \mathbf{L}^{-1} \cdot \mathbf{d} \cdot \mathbf{R}^{-1}$$

Because the determinants of $\mathbf{L}$ and $\mathbf{R}$ are one, the determinant of $\mathbf{S}$ equals the determinant of $\mathbf{d}$.

$$|\mathbf{S}| = |\mathbf{d}| = \prod_{i=1}^{N} d_{ii} \tag{36}$$

Now the adjugate matrix of $\mathbf{S}$, which contains the first order cofactors can be calculated using [17] and Eq. (38)

$$adj(\mathbf{S}) = adj(\mathbf{L}^{-1} \cdot \mathbf{d} \cdot \mathbf{R}^{-1}) = adj(\mathbf{R}^{-1}) \cdot adj(\mathbf{d}) \cdot adj(\mathbf{L}^{-1}) = \mathbf{R} \cdot adj(\mathbf{d}) \cdot \mathbf{L} \tag{37}$$

The nullity of the overlap-matrix $\mathbf{S}$, is its dimension minus its rank, so the nullity of $\mathbf{S}$ corresponds to the number of zero diagonal elements in $\mathbf{d}$. Nullity above 0, implies a singular $\mathbf{S}$-matrix. The algorithm depends on the nullity.

3.4.1 Nullity 0

Using the fact that the inverse of a diagonal matrix is a diagonal matrix with inverse elements, and that the adjugate of a matrix is directly related to its inverse

$$adj(d) = |d|.d^{-1} \tag{38}$$

the complete first order cofactor matrix can be calculated using Eq. (37) at a cost of $\sim n^3$ operations per overlap matrix, where n is the number of electrons. For the higher order cofactors we use the Jacobi ratio theorem to express higher order adjugates in terms of the compound matrices of the first order adjugate

$$adj^{(k)}(\mathbf{A}) = |\mathbf{A}|^{1-k}\left(adj(\mathbf{A})\right)^{(k)} \tag{39}$$

The kth order compound matrix $B^{(k)}$ is a matrix with the kth order minors (k^{th} order sub-determinants) as elements. So the kth order adjugate can be expressed in terms of the kth order compound matrix of the first order adjugate.

The 2nd order cofactors cost 2 multiplications each, at a total cost of $2.n^4$, no more than the cost of multiplying them by the two-electron integrals. Similarly, 3rd order cofactors take $6.n^6$ in total.

3.4.2 Nullity 1

Now the first order adjugate of the matrix $\mathbf{d}$ contains only 1 nonzero element, simplifying the application of Eq. (37). The Jacobi ratio theorem cannot be used straightaway for the higher order cofactors, when the overlap matrix is singular, since its determinant is zero. However, we can make use of the fact that determinants and thus cofactors, which are sub-determinants, are linear in their elements. If we change a matrix element of $\mathbf{S}$ as [13,28]

$$S'_{pq} = S_{pq} + t \tag{40}$$

then the determinant of $\mathbf{S}$ changes as:

$$|\mathbf{S}'(t)| = |\mathbf{S}| + t\mathbf{S}^{(p,q)} \tag{41}$$

The changes in the cofactors are similar.

$$\mathbf{S}'(t)^{(i,l)} = \mathbf{S}^{(i,l)} + (sign)t\mathbf{S}^{(i,p,l,q)}$$

$$\mathbf{S}'(t)^{(i,j,l,m)} = \mathbf{S}^{(i,j,l,m)} + (sign)t\mathbf{S}^{(i,j,p,l,m,q)}$$

$$\mathbf{S}'(t)^{(i,j,k,l,m,n)} = \mathbf{S}^{(i,j,k,l,m,n)} + (sign)t\mathbf{S}^{(i,j,k,p,l,m,n,q)} \qquad (42)$$

...

This procedure can be used to eliminate the singularities by changing the zero (diagonal) element of $\mathbf{d}$ after an $\mathbf{L\text{-}d\text{-}R}$ decomposition. The sign in these equations depends, like in the derivation of the derivatives of cofactors, on the ordering of p and q with respect to i,j,k,l,m and n. However, in a standard $\mathbf{L\text{-}d\text{-}R}$ decomposition the singularity is moved to the last position of $\mathbf{d}$ and the sign is just plus.

To obtain the nth order cofactors for a singular matrix, with nullity 1 we have to interpolate between two values of t, i.e. $t = +1$ and $t = -1$. The nth order cofactors of $\mathbf{S}'$ for $t=1$ and $t=-1$ are added to obtain the nth order cofactors of $\mathbf{S}$

$$adj^{(n)}(\mathbf{S}) = \frac{1}{2}\left(adj^{(n)}(\mathbf{S}'(1)) + adj^{(n)}(\mathbf{S}'(-1))\right) \qquad (43)$$

3.4.3 Nullity 2

When the nullity equals 2, all first order cofactors are eliminated. For the higher order adjugate matrices, two parameters have to be introduced and we need four points to interpolate and obtain

$$adj^{(n)}(\mathbf{S}) = \frac{1}{4}\left(\begin{array}{c} adj^{(n)}(\mathbf{S}''(1,1)) + adj^{(n)}(\mathbf{S}''(1,-1)) \\ +adj^{(n)}(\mathbf{S}''(-1,1)) + adj^{(n)}(\mathbf{S}''(-1,-1)) \end{array}\right) \qquad (44)$$

3.4.4 Nullity k

When the nullity is k there are also k parameters. The interpolated expression for the adjugate has now 2^k terms and we have to evaluate determinants of order n, where n is the order of the adjugates we require. When $n<k$ all cofactors are zero.

A special case is when k equals n, i.e. the nullity equals the order of the adjugates. Then one can extend an algorithm by Prosser and Hagstrom [25,26].

Writing $\mathbf{S}$ as $\mathbf{L}^{-1}\cdot\mathbf{d}\cdot\mathbf{R}^{-1}$ the adjugate of $\mathbf{S}$ is

$$adj^{(n)}(\mathbf{S}) = adj^{(n)}\left(\mathbf{L}^{-1}\cdot\mathbf{d}\cdot\mathbf{R}^{-1}\right)$$
$$= adj^{(n)}\left(\mathbf{R}^{-1}\right)\cdot adj^{(n)}(\mathbf{d})\cdot adj^{(n)}\left(\mathbf{L}^{-1}\right) \qquad (45)$$

The determinants of **L** and **R** are one, and we can introduce the nth order compound matrices of **R** and **L**.

$$adj^{(n)}\left(\mathbf{R}^{-1}\right) \cdot adj^{(n)}(\mathbf{d}) \cdot adj^{(n)}\left(\mathbf{L}^{-1}\right) = \mathbf{R}^{(n)} \cdot adj^{(n)}(\mathbf{d}) \cdot \mathbf{L}^{(n)} \tag{46}$$

The nullity equals n, and therefore the nth order adjugate of **d** has only one non-zero element. Now only one row of $\mathbf{R}^{(n)}$ and one column of $\mathbf{L}^{(n)}$ remain in the product, and the nth order adjugate of **S** reduces to the product of this row and column multiplied by the only element of the nth order adjugate of **d**.

4. PROGRAM

The formalisms derived above were implemented in the *Ab Initio* Valence Bond program TURTLE [3]. The logo for the program is shown in Fig. 1. This is the logo for the parallel version, as is obvious from the number of turtles depicted.

Currently the program has been parallellised using MPI[29,30], following the scheme in Fig. 2. This implies parallellising over 99% of the program, since contrary to MO programs, the matrix elements, both those needed when calculating the wavefunction and those required in the SuperCI, dominate completely. In the present implementation, a speedup of 54 is obtained when using 64 processors[31]. An implementation using Global Arrays[32-34] is in progress. In this implementation, the integral transformation and all calculations of density matrices are parallellised.

```
    t                    t     1
    t                    t     1
    tttt    u  u   rrrrr  tttt  1          eee
    t       u  u   r   r  t     1          eeeee
    t  t  u  u     r        t  t  1  1      e
    ttt     uu     r        ttt   111       eee


        ----            ----    )))))  --          ----   )))))
  --              ----        _ _ _  { o o }  ----    _ _ _   { o o }
          ----              _(_)_(_)_  ( ^ ) ---   _(_)_(_)_  ( ^ )
    ----                  _(_)_(_)_(_)_/ /        _(_)_(_)_(_)_/ /
  ----              ---- _(_)_(_)_(_)_(_)/      _(_)_(_)_(_)_(_)/
                          (_)_(_)_(_)_(_)_(_)    (_)_(_)_(_)_(_)_(_)
  ----      ----         //  //   //  //        //  //   //  //
```
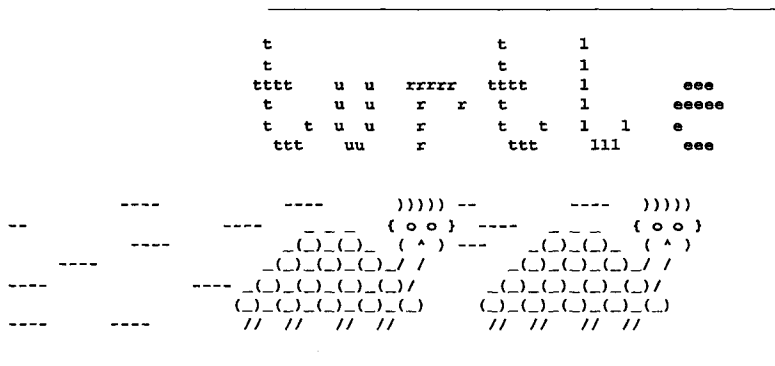
Fig. 1. TURTLE logo. The logo was originally developed by J. Verbeek.
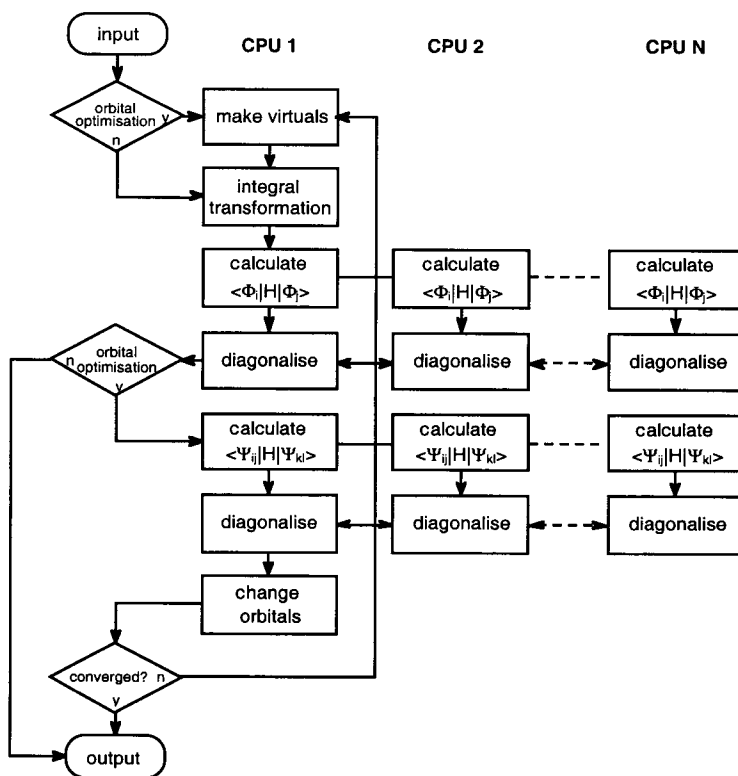
Fig. 2. The structure of the parallellised version of TURTLE.

5. APPLICATIONS

The concept of aromaticity has been intriguing chemists for years. An overview of the discussion about aromaticity and the various experimentally measurable effects can be found in textbooks as Garratt's [35], a paper by Von Schleyer and Jiao [36], and in a review by Wiberg [37].

There is still much dispute about what aromaticity really is. As a consequence of induced ring currents in aromatic π-systems [38,39] the magnetic properties of aromatic compounds differ with respect to those of non-conjugated alkenes. Hence, magnetic properties [36] (large anisotropy of the magnetic susceptibility [$\Delta\chi$], exalted magnetic susceptibility [Λ], deshielded ring protons and negative Nucleus Independent Chemical Shift (NICS) [40]) are also frequently used as aromaticity criteria. There are many other criteria, for instance based on geometric criteria [41-43]. The anomalous magnetic properties and bond equalisation all result from the cyclic electron delocalisation, with which aromaticity is associated.

The theoretical models start with Kekulé's [44] description of benzene, as having two structures. Later Hückel [45,46] discovered his [4n+2] and [4n] rules, and was able to account for the stability of benzene ([4n+2]) and the instability of cyclobutadiene and cyclo-octatetraene (both [4n]). The [4n+2] compounds were called aromatic after benzene, while the [4n] compounds were given the designation anti-aromatic.

A natural way to study aromaticity would be to make use of the concept of two structures, as introduced by Kekulé. The first to use this view were Pauling and Wheland [47]. They used an approximate form of the valence bond (VB) method developed by Heitler and London [48], for describing the aromaticity of benzene.

Classical VB calculations using fixed orbitals and containing all possible covalent and ionic structures for the π-system were done by Norbeck and Gallup [49] and by Tantardini *et al.* [50]. They both used σ-orbitals from an SCF calculation. The resonance energy used by them is the energy difference between benzene (described with all the structures) and 1,3,5-cyclohexatriene (described with a subset of structures) at a certain geometry. In these calculations, high resonance energies of -61.4 and -67.4 kcal/mol are obtained for benzene.

More recently, Mo and Wu [51] used this type of description for benzene and cyclobutadiene as well. They also optimised the geometries of these molecules and of the ones with localised bonds. In their calculation of resonance- and stabilisation energies, they took another set of structures for the description of the cyclohexatriene, which leads again to a different definition of the resonance energy.

The first calculations on benzene using optimised orbitals were done by Cooper *et al.* [52], using their spin-coupled VB method [20]. A review [53] has appeared with an overview of their work on aromatic and anti-aromatic compounds.

Resonating Generalised Valence Bond (GVB) calculations were performed on cyclobutadiene by Voter and Goddard [54]. They find a resonance energy of -22 kcal/mol for this molecule. According to them its geometry cannot easily be predicted, and is determined by the interaction between resonance and bond strain.

In the last 15 years new theories about aromaticity appeared. Since the discovery of the Hückel rules, aromaticity was considered as an effect of the interacting π-electrons. Shaik, Hiberty and co-workers [55-61] challenged that view, and stated that the π-system of benzene favours a distorted geometry with localised bonds, and that the σ-system forces the molecule to be symmetric. Glendening *et al.* [62] on the other hand conclude from their calculations on benzene with localised bonds that the interaction between the two Kekulé structures is necessary for the molecule to have a symmetric geometry.

In classical Valence Bond theory, a bond is simply defined as a singlet coupled orbital (electron) pair. Thus, a single bond is obtained using:

$$(Bond)_{12} = \left(\left|\phi_1\bar{\phi}_2\right| - \left|\bar{\phi}_1\phi_2\right|\right)\big/\sqrt{2} \equiv (12) \tag{47}$$

Then a total wavefunction is obtained by multiplying these units together and proper antisymmetrisation, thus

$$\Psi = (12)(34)(56)(78)\cdots \tag{48}$$

This resembles the GVB picture of chemical bonding as promoted by Goddard *et al.* [63]. However, in contrast to this, here we have no orthogonality imposed and the number of structures is, in principle, unlimited.

Ionic structures are most easily represented, as are lone pairs, by a doubly occupied orbital or, by two orbitals on one atom located in the same region [4], which is a more balanced picture. Finally, not all bonds have to be designated explicitly. Instead, one might define an orthogonal core, which contains these doubly occupied orbitals.

Thus, the simplest wavefunction describing say three bonds using the Valence Bond model in addition to an orthogonal core is given by

$$\Psi = \left|(core)(12)(34)(56)\right| \tag{49}$$

The wavefunction in Eq. (49) could be the wavefunction for a simple molecule, allowing for three bond dissociating, or it could be one of the structures of benzene. The wavefunction for benzene, containing two Kekulé structures for the π-system, is pictorially given in Fig. 3 and in formula by :

$$\Psi = c_1\left|(\sigma_{core})(12)(34)(56)\right| + c_2\left|(\sigma_{core})(23)(45)(61)\right| \tag{50}$$

The spin-space for the π-space of benzene is completed by adding the three Dewar structures shown in Fig. 4.

The wavefunction in Eq. (50) does describe the resonance between the two Kekulé structures through the interaction between the two structures.
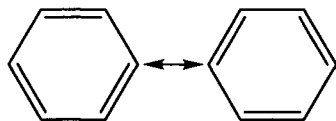
Fig. 3. The two Kekulé structures of benzene

Thus one can study the 'hypothetical' situation without resonance by just including one of the structures in the wavefunction, so as to assess the importance of resonance.

There is still freedom in the choice of "atomic" orbitals used in Eq. (50). For instance, one can use fixed atomic orbitals, which eliminates the (sometimes costly) orbital optimisation. One can also use fully optimised, potentially delocalised orbitals in the spin-coupled / Coulson-Fischer sense. Finally, one can use "real atomic" orbitals by limiting each orbital to its own atom. This often gives a clearer physical picture of chemical bonding. It generates for instance optimal hybrids [9,10].

Since a restriction is applied to the wavefunction, the energy goes up and the bond-strength is diminished. This is used in assessing the effects of the strengths of the bonds in cyclobutadiene. The orbitals may also be restricted to extend just over a part of the molecule [64], inhibiting delocalisation.

The applications we present are all related to the concepts of aromaticity, resonance and delocalisation.

5.1 The importance of resonance - benzene and cyclobutadiene[24,65-67]

Our VB program TURTLE [3] allows for both a more extensive and a more restrictive description of benzene and cyclobutadiene than was available in the previous studies. We included full orbital and full geometry optimisation. Two orbital models were used. The first has p-like (p_π) orbitals strictly localised on the carbon atoms. This corresponds to the classical Heitler-London model [48], but with optimal orbitals. The second uses delocalised fully optimised [68] p_π orbitals, which include tails to neighbouring atoms.

The main difference between them is that the delocalisation of the orbitals mimics the effects of ionic structures, giving stronger bonds in the molecule. This allows us to study the effect of the bond-strength in the π-system on the geometry. The local orbitals allow a description closer to the Pauling picture [47], since the orbitals lack freedom.

Since we can assign bonds at will, we may distinguish four molecules, some of which are not real in a chemical sense. First there is benzene which we described using just the two Kekulé structures (Fig. 3). The three Dewar structures (Fig. 4) were not taken into account.
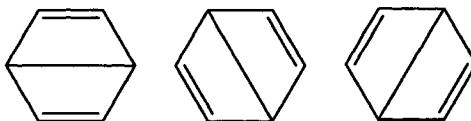
Fig. 4. The three Dewar Structures of benzene
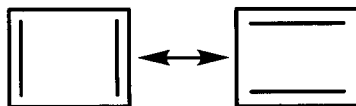
Fig. 5. The two resonance structures for cyclobutadiene

Earlier calculations [52,69] showed that they have a weight of about 6-7% each. Because these weights are relatively small, compared to the total weight of the Kekulé structures of about 80%, and since they obscure the view of the resonance, they were left out.

Next, we have cyclobutadiene, which is described using two structures as well (Fig. 5), though the two are not expected to have equal weight in the wavefunction.

Strictly adhering to the Pauling definition [47], the resonance energy (E_{res}) of an aromatic hydrocarbon is obtained as the difference between the total VB energy and the energy of the most stable structure ($E_{res}=E_{tot}-E_{lowest}$).

The energy difference between the two-structure calculation and a one-structure calculation at the same geometry with optimal orbitals but lacking resonance/π-electron delocalisation gives the vertical resonance energy (VRE) [70].

Finally, we can just use one structure, which for C_6H_6 gives the elusive cyclohexatriene (D_{3h} symmetry) (fig. 6). Of course, for cyclobutadiene, nothing out of the ordinary is observed and the normal 1,3-cyclobutadiene results. The difference in energy with the two-structure calculation gives the theoretical resonance energy (TRE) [51].

The energy of the hypothetical cyclohexatriene was previously estimated by Dewar *et al.* using experimental data by taking three times the C=C and C-C increment [71].

For all the compounds, orbitals and geometries were optimised using a 6-31G basis set [72].
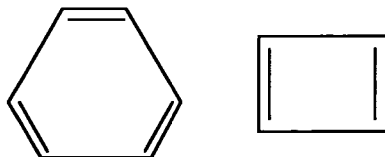
Fig. 6. 1,3,5-cyclohexatriene and 1,3-cyclobutadiene

5.1.1 Benzene and Cyclohexatriene

The benzene calculations using delocalised orbitals yielded a symmetric structure with a C-C bond length of 1.399 Å, in excellent, be it fortuitous, agreement with the experimental value (1.399Å [73]). In the calculations where orbitals were restricted to the atoms, the C-C bonds were weakened and correspondingly they lengthened to 1.426 Å. This elongation was also found when the local approximation was applied to the π-system of ethene [67]. The cyclohexatriene calculations (1 structure), resulted in a D_{3h} geometry, with C-C bond lengths of 1.433 and 1.369 Å, in reasonable agreement with linear 1,3,5–hexatriene (1.458 and 1.368 Å [74]). If the π-orbitals are restricted to the atoms the effect is only noticeable on the single bonds, which elongate to 1.509 Å, whereas the double bonds even contract very slightly to 1.368 Å.

This suggests, that in the delocalised calculation the formal single bonds still have some double bond character, as they have in 1,3,5-hexatriene. They lose this in the purely localised calculation. This throws some doubt on the clear interpretability of the delocalised calculation. However if a two-structure calculation is performed at the optimised geometry of cyclohexatriene, the weights according to Eq. (3) of the structures are quite similar in both models, viz. 0.74/0.26 for the delocalised calculations vs. 0.79/0.21 for the strictly localised ones.

In Table 1 we collect all resonance energies. The values for both the VRE and TRE are considerably lower than most previously reported values (range -5 to -95 kcal/mol [51,75-77]). We note that in previous calculations the 1,3,5-cyclohexatrienes (D_{6h} and D_{3h}) were accessed with non-optimised orbitals [76], or with pre-determined ethene π-orbitals [77]. Note the large difference between the Pauling resonance energy and the vertical resonance energy for the delocalised orbitals, whereas there is no difference for strictly localised orbitals. Obviously just for benzene, the extra freedom offered by the delocalisation is utilised to the full. If anything, the other resonance energies are remarkably similar, showing that the resonance persists even in cyclohexatriene. The two-structure calculation on cyclohexatriene does not represent a true minimum. It lies just 1.2 kcal/mol (delocalised orbitals) above benzene and will revert to that geometry if the geometry is relaxed.

Table 1

Resonance energies for benzene and cyclohexatriene

Molecule	Benzene		Cyclohexatriene	
model	delocalised	localised	delocalised	localised
Pauling Resonance Energy	-19.8	-25.4	-8.4	-7.7
Vertical Resonance Energy	-9.6	-25.1	-6.2	-7.7
Theoretical Resonance Energy	-7.4	-11.3		

The calculations show that the resonance energy is the driving force behind the symmetrisation of benzene (cf. [62]). Indeed benzene is easy to distort to e.g. a cyclohexatriene geometry [61]. This, however, should not be construed to be an indication of the unimportance of resonance but, on the contrary, to be taken as a sign of its persistence (cf. [69]).

Some of the previous calculations in the literature stressed the importance of ionic configurations. They are indeed needed for a proper description of the bonding when localised orbitals are used, as shown by the poor bond lengths obtained without. The calculations with ionic structures also give huge resonance energies, due to the large number of ionic structures used in the description of benzene. It is our feeling that the only reasonable definition for the resonance of benzene is the interaction between two Kekulé structures. Inclusion of the full set of ionic structures makes it difficult to obtain a balanced description of both cyclohexatriene and benzene. Different choices can be made for the description of cyclohexatriene as well (cf. [51] and [49]). The application of the spin coupled method[53], where the orbitals are optimised, gives essentially the same result (-20.0 kcal/mol) for the resonance energy as our calculations using delocalised orbitals. The only difference is that the Dewar structures of Fig. 4 were also present in the spin-coupled wavefunction.

5.1.2 Cyclobutadiene

A calculation using the delocalised orbital model yields a rectangular structure as expected [78], both with the two-structure and with the one-structure calculation. The bond lengths are 1.552 Å and 1.367 Å for the two-structure calculation and hardly different for the one-structure calculation. The resonance energy is quite small (-0.98 kcal/mol).

However when the π-bond strength is diminished, when using strictly localised orbitals, a molecule with equal C-C bondlengths (1.465 Å) is obtained. Now the resonance energy is quite large (Pauling E_{res}= -17.66 kcal/mol). So is the stabilisation energy of -7.85 kcal/mol with respect to the one-structure calculation, which obviously still yields a rectangular structure with bond lengths of 1.556 and 1.395 Å. The π-bonds are relatively weak in this system, due to the use of strictly localised orbitals. Thus, the square geometry can be explained by a preference of the σ-system for equal bond lengths.

In order to see if it is possible to neutralise this effect of the σ-system we performed a second calculation which used localised orbitals for the σ-system as well as for the π-system. In this calculation one perfect-pairing structure was used for the C-C bonds of the σ-system. All orbitals were localised on the C-H fragments. Doubly occupied orbitals were used for the C-H bonds, and strictly localised singly occupied orbitals for the C-C bonds. This calculation again yields a rectangular geometry with a much lower resonance energy. The bond

lengths are also longer than for calculations with only localised π-bonds, which shows that the bonds are indeed weaker.

We may conclude that the relative strengths of the σ- and the π-bonds determine the geometry of cyclobutadiene. For relatively weak π-bonds, the resonance, together with the σ-bonds, prevails to yield a square geometry. With stronger π-bonds or weaker σ-bonds the, expected, rectangular structure is produced.

5.1.3 Concluding remarks on the importance of resonance

Of the views expressed in the literature, we find two of them to be partly compatible with our findings. The model developed by Shaik, Hiberty and co-workers [55-61] states that the σ-system prefers equal bond lengths, while the π-system prefers alternating bond lengths. The resonance of the π-system is also a symmetrising influence.

The viewpoint expressed by Glendening *et al.* [62] is that the resonance between the structures is the key factor for delocalisation. We find this as well. When there is no resonance in cyclobutadiene (and benzene), the molecule becomes asymmetric. Just resonance is not enough, however. Both benzene and square cyclobutadiene have large resonance energies.

Finally, we have to disagree with Zilberg and Haas [79]. They state that the geometric distortion of cyclobutadiene is a fundamental property of [4n]-electron ring systems. We were able to generate a square symmetric system just by weakening the π-bonds. Voter and Goddard[54] correctly suggest that the geometry of cyclobutadiene is a result of a balance between bond strain and resonance.

We can therefore now conclude that there are three contributions that determine the geometry of benzene and cyclobutadiene. The first contribution is that of the σ-system which prefers equal bond lengths. The other two contributing factors are the π-bonds and the π-resonance. The π-bonds by themselves give rise to two states with a minimum at one of the geometries with alternating bond lengths. The resonance provides interaction between the two states and stabilises the symmetric structure.

5.2 Aromaticity of bent benzene rings [69]

An interesting question [80] is: "What happens when the benzene ring is bent from its planar structure?" Will it still be aromatic? The only experimental way to get insight into the possible behaviour of bent benzene molecules is by attaching bridges over the ring that put the ring under strain. Examples of such molecules are [n]meta- and [n]paracyclophane molecules, the number n denoting the length of the carbon chain that is attached to the benzene ring. The only way to study bent benzene molecules, without the disturbing influence of

the bridges, is to use theoretical methods, where the Born-Oppenheimer approximation [81] allows one to freeze the molecular geometry.

For the description of the bent benzene, the flat benzene ring was the starting point. For this system, there is a clear σ π separation. There is a clear distinction between the doubly occupied orbitals for the σ-core and the 6 non-orthogonal p-orbitals for the π-system.

The π-system is described by all five Rumer structures, which is the complete spin-space (i.e. Fig. 3 and Fig. 4). This allows a smooth transition from benzene, where the 2 Kekulé structures are most important, to the highly bent Dewar benzene, where only one of the Dewar structures (Fig 4) is important. All the orbitals, doubly occupied and singly occupied are fully optimised. For each bent structure, the orbitals from the preceding less bent structure were used as initial guess. This and the choice of wavefunction ensure that an aromatic "π-system" can be identified, even when no symmetry separation exists. All orbitals were completely optimised so we have a wavefunction of the spin-coupled type. This is the type of wavefunction used by Cooper *et al.* [52] in their study of benzene.

To obtain geometries, 10-orbital 10-electron complete active space self-consistent field (CASSCF) [82-84] calculations were performed with the GAMESS-UK program [6]. The occupied orbital order in an SCF for flat benzene is $\pi, 2\sigma, 2\pi$. In the bent molecule, there is no clear distinction between σ- and π-orbitals and we want to include all the π-orbitals in the CAS-space. Thus, 10 orbitals in the active space are required. Obviously, the 5 structure VB wavefunction would have been a preferable choice to use in the geometry optimisation. However, at that time, the VB gradients were not yet available. The energies of the VBSCF at the CASSCF geometries followed the CASSCF curve closely.

The geometry of the molecule at each point was optimised for a fixed bending angle ϕ (Fig. 7), while all the other geometrical parameters were free.
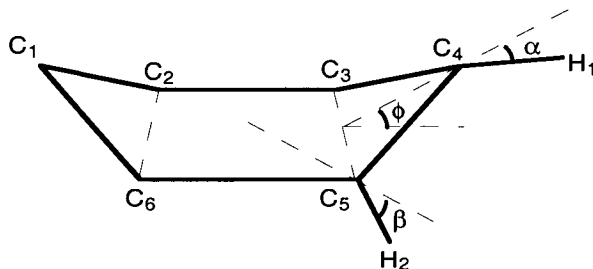
Fig. 7. Important geometrical parameters: ϕ is the angle between the plane of the displaced carbon atom 4 with carbon 3 and 5 and the plane of the 4 lower carbon atoms.

C_{2v} symmetry has been used throughout. Calculations were performed for ϕ from 0° to 90° with a step-size of 5°. All calculations were performed using the 6-31G basis set [72].

The carbon-carbon bond lengths remain very similar, with differences of less than 0.03 Å, up to a bending angle (ϕ) of 55°. The end-CH (α) bending increases up to 40° at ϕ=55°, thus maintaining the π-system as much as possible. Beyond ϕ=55°, the end-CH turns upwards (α=-1° at ϕ=60°), signalling the end of the aromatic ring. At that angle the equivalence between the C-C bonds is gone as well. There is a drastic change in the geometry between 55° and 60°, where the molecule attains the shape of Dewar benzene. The barrier in the potential energy curves is also here.

The clearest picture of the bonding is given by considering the weights of the Rumer structures (Eq. (3), Fig. 8). The weights for equivalent structures are added; So the weights of the two Kekulé structures are summed and the weights of two of the Dewar structures are summed. It is clear that at low angles the two Kekulé structures are the most important ones. They make up for more than 70 % of the wavefunction, up to 55°. Then one Dewar structure takes over completely and the molecule has become Dewar benzene.

The energies of the individual structures behave more smoothly. They are continuously rising (except for the bonding Dewar structure beyond 60°), though there is sudden change at 60° because of the change in geometry.

The resonance energy (Pauling definition [47]) is -20.30 kcal/mol for flat benzene and it decreases to -17.39 kcal/mol at 55°. Thus, we still have an aromatic molecule at 55°. After 55° one Dewar structure dominates the wavefunction and the resonance energy decreases to -0.10 kcal/mol; the aromaticity is gone.
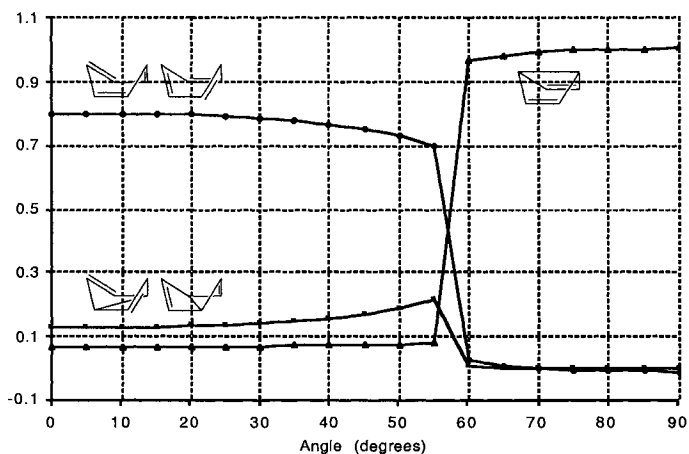
Fig. 8. Structure weights in bent benzene
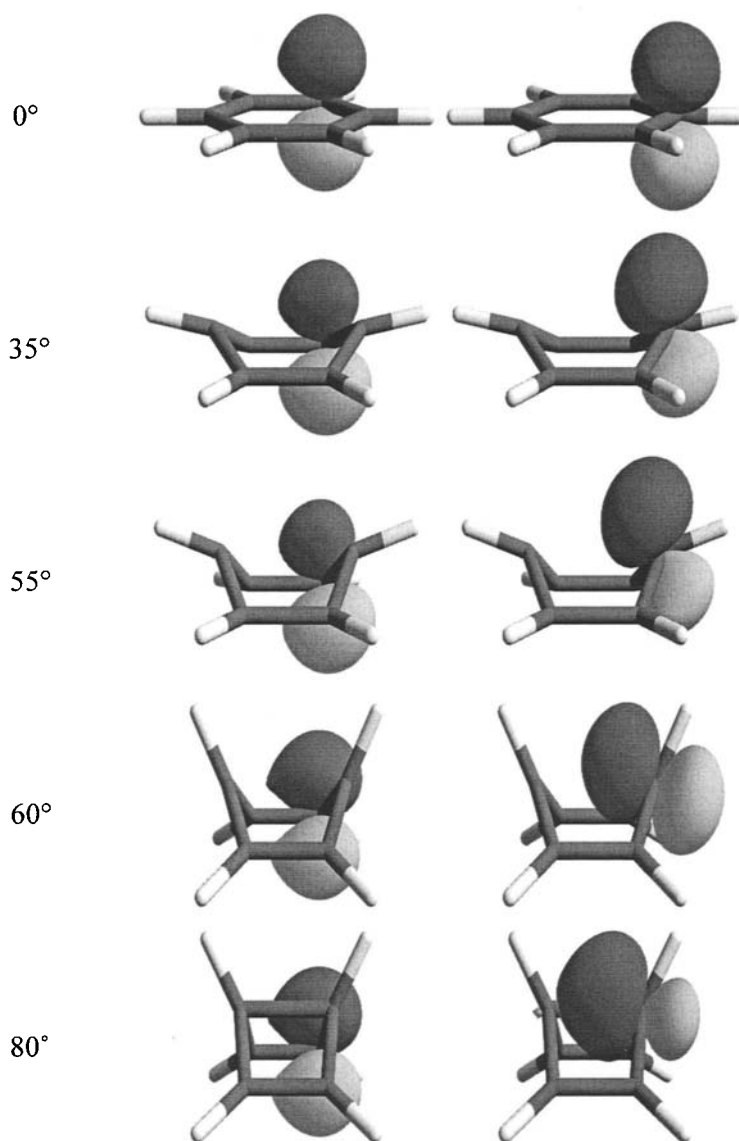
Fig. 9. π like orbitals on carbon atoms 3 and 4 for some important bending angles. The orbitals on the other atoms may be obtained by mirror-symmetry. The pictures were produced with the help of Molden [85]

Orbital pictures for the different bending angles are shown in Fig. 9. The pictures show iso-surfaces with an absolute value of 0.1. The different signs are shown by the dark and light grey-shades, and the orbitals extend to neighbouring atoms, reflecting the delocalised model employed. They show that the orbitals try to adapt to the form of the molecule and to maintain bonds for the Kekulé structures. At 60° the p-like orbitals on carbon atom 1 and 4 rotate to form a bond between those two atoms. So. first of all, the overlaps are maximised for the bonds in the Kekulé structures. Then the orbitals on the two carbon-atoms, which are bent out of plane (atom 1 and 4) rotate to form a bond in the Dewar structure with correspondingly much larger overlap.

The orbitals in bent benzene try to adapt to the bent ring as much as possible while still keeping large overlaps for the Kekulé structures. This also has to do with the geometry of the molecule, especially the hydrogen atoms attached to the carbon atoms 1 and 4. First, they are bent down making it possible for the p-orbitals on the carbons to stay perpendicular to the plane of the other 4 carbon atoms. In the Dewar form, they are bent up and the p-orbitals are again perpendicular to the plane of the hydrogen. So the geometry and the bonds adapt to each other.

If now the geometry would be forced to inhibit the aromatic system, as is the case in the experimental systems, where bridges are attached to bend the molecule, the aromaticity disappears at much lower angles. Test calculations [86], where the angle α is reversed to simulate this situation, indicate that then the aromaticity is only maintained up to 30°.

5.3 Aromaticity of Pyrene and its Cyclopentafused Congeners [65,87]

Polycyclic aromatic hydrocarbons (PAH's) with external cyclopentafused five-membered rings, such as the cyclopentafused pyrene derivatives (Fig. 10), belong to the class of non-alternant polycyclic aromatic hydrocarbons.

Several qualitative models, e.g. Platt's ring perimeter model [88], Clar's model [89] and Randić's conjugated circuits model [90-92] have either been or are frequently used for the rationalisation of their properties. All these qualitative models rationalise the properties of aromatic and anti-aromatic hydrocarbons in terms of the Hückel [4n+2] and [4n] rules. The extra stability of a PAH, due to π-electron delocalisation, can also be determined, computationally or experimentally, by either considering homodesmotic relationships [36] or by the reaction enthalpy of the reaction of the PAH towards suitable chosen reference compounds [93].

In a related study on the cyclopentafused pyrenes [94] in which regular *ab initio* methods were used (RHF/6-31G* and B3LYP/6-31G*), we found that the magnetic properties suggested that the aromatic character decreases upon cyclopentafusion. The aromatic stabilisation energies were unaffected, though.

These effects prompted us to study the effect of cyclopentafusion in the cyclopentafused pyrene series on the interaction between the different Kekulé resonance structures and thus on the resonance energy.

All geometries of **1-7** were optimised at the RHF/6-31G level. Structures **1-6** are really flat but **7** was found to be bowl-shaped [94]. In a treatment of the conjugated system in this geometry, the σ orbitals cannot easily be excluded, as the strict σ π separation is destroyed.

The deviation from the planar form of **7** is rather small. Since an aromatic structure is not easily destroyed by bending (cf. Section (5.2), [69]), the VB results obtained for the planar transition state are expected not to deviate much from those of bowl-shaped **7**. Of course, the calculation on planar **7** is computationally much cheaper.

The σ-core was taken from a preceding RHF/6-31G calculation. The π-system was described by strictly atomic non-orthogonal p-orbitals, which were optimised for benzene. Test calculations on cyclopenta[*cd*]pyrene (**2**) indicated that the structure energies and weights change only marginally upon optimisation of the p-orbitals.

For pyrene (**1**) 1430 covalent structures can be generated. Only six of those have all π-bonds along the σ-bonds. These six structures are the Kekulé resonance structures of pyrene. In the case of *tetra*cyclopenta[*cd,fg,jk,mn*]-pyrene (**7**), 208012 covalent structures can be generated. Only ten Kekulé resonance structures exist for this molecule. It is expected that only the Kekulé resonance structures are important in the description of these molecules and that the other structures can be ignored at a considerable saving in time and gain in interpretability.
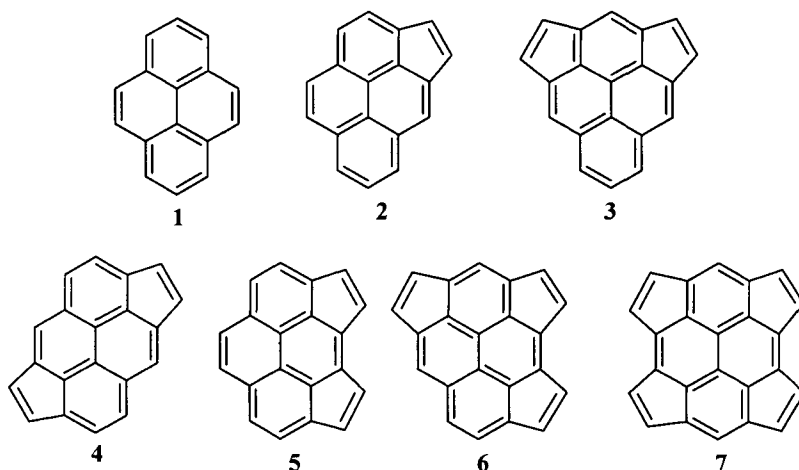
Fig. 10. The structures of **1-7**.

In the spirit of Pauling [95], only the Kekulé resonance structures were considered.

To identify the most important resonance interactions between Kekulé resonance structures and thus the most aromatic subsystems the total resonance energy had to be partitioned. Therefore the **H** matrix was transformed to an orthogonal basis using Löwdin-orthogonalisation [96], yielding $\mathbf{H}^{\perp}$. The total energy can then be partitioned in the weighted diagonal contributions of the structures and the weighted resonance contributions between them

$$E = \sum_{i}\sum_{j} c_i c_j H_{ij}^{\perp} = \sum_{i} c_i c_i H_{ii}^{\perp} + \sum_{i}\sum_{j>i} 2 c_i c_j H_{ij}^{\perp} = E_{diag}^{m} + E_{res}^{m} \qquad (51)$$

where c_i is the coefficient of structure i in the wavefunction.

The sum of the resonance contributions (E_{res}^{m}) is again another measure of the resonance energy, namely with respect to the weighted mean value of the energy of all structures. This mean resonance energy is thus more negative (stabilising) than the Pauling resonance energy (E_{res}). In Table 2 we give the total energies and resonance energies of the 7 compounds. The E_{res}^{m} values for **1–7** follow the same trend as the E_{res} values.

The contribution to E_{res}^{m} of a particular interaction between two structures is twice the weighted resonance contribution ($2 c_i c_j H_{ij}^{\perp}$). The differences between a pair of Kekulé resonance structures elucidate the conjugated circuit in which the π electrons are delocalised by resonance as shown in Fig. 11.

Table 2
Total energies of compounds **1-7** (a.u.) and resonance energies (kcal/mol).

Compound[a]	RHF	VB	E_{res} [b]	E_{res}^{m} [b]
1 (6)	-611.555550	-611.286631	-62.3	-100.9
2 (6)	-687.242053	-686.940798	-58.5	-101.1
3 (6)	-762.918242	-762.584880	-62.2	-101.8
4 (7)	-762.922606	-762.592661	-54.5	-101.5
5 (7)	-762.925727	-762.595225	-56.4	-101.8
6 (8)	-838.595341	-838.236025	-58.6	-102.7
7 (10)	-914.259921	-913.873884	-62.5	-104.2

[a]The number of Kekulé resonance structures is indicated between parentheses.

[b]For comparison the resonance energies of benzene, calculated with local p-orbitals (6-31G basis set) and two structures, are E_{res} = -25.4 kcal/mol (Table 1) and E_{res}^{m} = -44.2 kcal/mol.
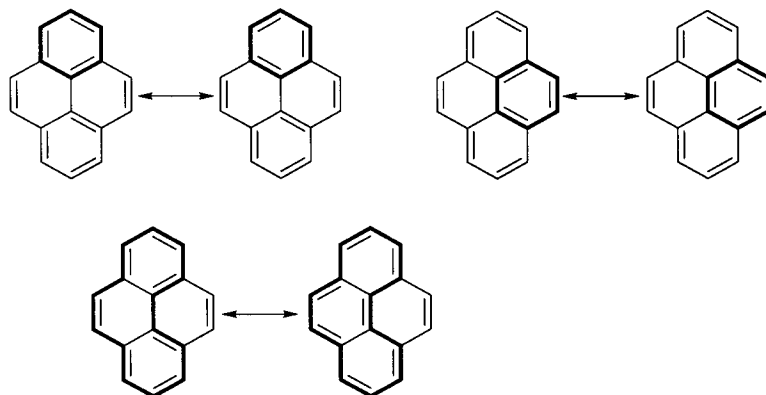
Fig. 11. Resonance between the structures leading to benzene-like resonance in the top six π electron, central six π electron and 14 π electron conjugated circuits, respectively.
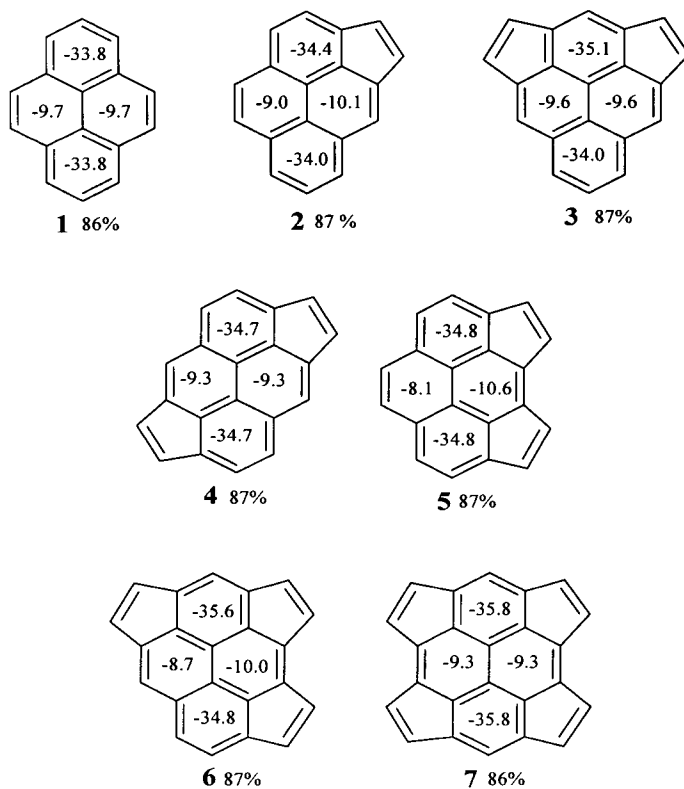
Fig. 12. Contributions of the individual rings to the resonance energy.

Using this method, the resonance energy was divided over the rings. The result is displayed in Fig. 12. The percentages below each structure give the amount of resonance energy accounted for by just the rings indicated. The remainder is resonance in 10/12/14/.. rings.

The partitioning of the resonance energy shows large contributions to the mean resonance energy (E_{res}^m) from the resonance interactions in the top and bottom six-membered rings. The right and left central six-membered rings contribute less than a third to the resonance energy.

In a previous study, it was shown that the aromatic stabilisation energies of the compounds **1-7** are all nearly equal [94] *i.e.* cyclopentafusion has no effect on the resonance energy. This conclusion is confirmed by the VB calculations. The resonance energy (both E_{res} and E_{res}^m) of the compounds **1-7** are all of the same magnitude (Fig. 12 and Table 2).

More generally, upon the addition of externally fused five-membered rings, the weights and energies of the pyrene sub-structures are only marginally affected. The contributions of the different conjugated circuits to E_{res}^m show for all compounds the same trends; the six π-electron (benzene-like) conjugated circuits in the top and bottom six-membered rings have the highest contribution to E_{res}^m, independently of cyclopentafusion. Hence, all compounds should be seen as substituted pyrene derivatives.
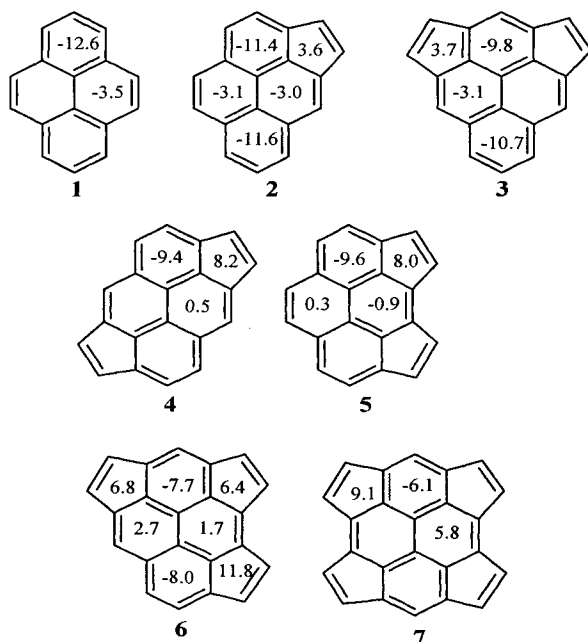
Fig.13. The NICS values of the individual rings.

Nucleus Independent Chemical Shift (NICS) values in the ring centres [40] were calculated using the Direct IGLO [39,97] program, at the RHF/6-31G geometry using the IGLO-III basis set. The chemical shift shielding tensor is given as a sum of the diamagnetic and paramagnetic part by the IGLO program.

The NICS values calculated at the ring centres for the compounds 1-7 are depicted in Fig.13. Large negative NICS values are found for the top and bottom six-membered rings. The NICS values for these rings are shifted 10 ppm upfield with respect to the NICS values of the central six-membered rings, which is in line with the resonance criterion, derived above.

Upon addition of externally fused five-membered rings, the NICS values at the ring centres suggest a reduction of the aromatic character in this series. The resonance criterion (both E_{res} and E_{res}^{m}), however, does not suggest that the aromatic character of 1-7 decreases.

This apparent discrepancy might be understood by realising that the diamagnetic contribution of the chemical shielding tensor perpendicular to the molecular framework ($NICS_{\perp}^{d}$) is indicative for the induced ring currents. Unfortunately, the paramagnetic contribution, which is zero in benzene due to symmetry, is included in the NICS values and the relation between dia- and paramagnetic contributions is gauge dependent. Thus, the NICS values can only be used for comparing the aromatic character of similar rings.

5.4 The enhanced acidity of carboxylic acids and enols relative to alcohols [98-100]

In this early application of the TURTLE program, the ability to restrict the wavefunction is used to ascertain the relative importance of π-electron delocalisation and induction to the enhanced acidity of carboxylic acids and enols compared to alcohols. These generic classes of molecules are represented by formic acid, vinyl alcohol and ethanol respectively.

The enhanced acidity of carboxylic acids and enols relative to alcohols has long been attributed to the stabilisation of the carboxylate and enolate anions by delocalisation of their π electrons (see 1 and 2 below). Alkoxide anions, as saturated systems, are not subject to resonance stabilisation.

The parent acids and alcohols, on the other hand, are not expected to display any significant mesomeric stabilisation, because this would involve the participation of some rather unreasonable Lewis structures with separated positive and negative charges. As a consequence, the π-delocalisation in 1 and 2 is a factor that lowers the deprotonation energy of carboxylic acids and enols, thus reinforcing their acidity, according to standard organic-chemistry textbooks.
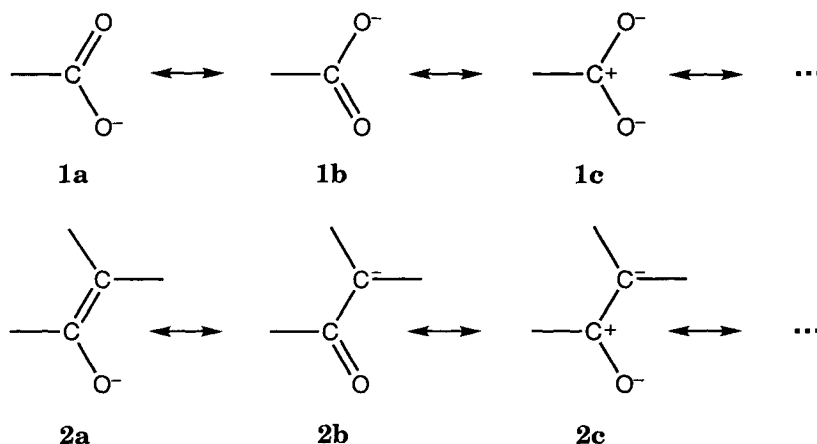
Fig. 14. Resonance structures for carboxylic acids and enols

Since the molecules are planar, there is a strict separation between the σ- and the π-system. In the calculations, the σ-system was handled with the usual delocalised orbitals. For the π-system two different models were defined.

In the localised VB the orbitals are only allowed to extend over part of the molecule. For instance, for an enolate anion, the basic wavefunction would have a doubly occupied π-orbital, localised only on the oxygen atom and a doubly occupied π-orbital extending over both carbon atoms. Thus, while describing structure 2a in Fig. 14, a single determinant is still employed. Since the orbitals are completely optimised, the σ-system can partly counteract the charge separation.

The delocalised model entails a normal Hartree-Fock calculation, allowing a complete delocalisation of both the σ- and π-systems, and thus describing the complete delocalisation of the π-system.

In both models inductive effects are included, so one can calculate the energetic effect of π-delocalisation in a direct way. The calculations were performed at three different levels of theory, with an increasing degree of electron correlation. For instance one might allow left-right correlation in the π-bond in the localised model and perform a corresponding CASSCF in the delocalised one. The results were found to be insensitive to the degree of electron correlation, so we present only the results of the simplest level here. It should be noted that in all cases inductive effects are fully operational, irrespective of the degree of localisation.

The calculations were performed with a standard 6-31G* basis set [101] augmented by diffuse p-functions [102]. The geometry optimisations of the delocalised states were carried out through a standard gradient technique with the GAUSSIAN92 program [103].

Table 3
Delocalisation energies of the deprotonated anions and their parent acids.

Anions	ΔE (kcal/mol)	Acids	ΔE (kcal/mol)
$HCOO^-$	40.2	HCOOH	17.5
CH_2CHO^-	34.9	CH_2CHOH	13.6
$CH_3CH_2O^-$	14.6	CH_3CH_2OH	6.6

Because no gradient routines were available at that time for the VB calculations, the geometries of the localised states were partly optimised by hand.

From a consideration of the optimised geometries, it could be concluded that both the acids and the deprotonated anions are subject to some π-electron delocalisation. In accord with chemical intuition, the effect of delocalisation is more important in the carboxylate and enolate anions than in the other species. However, the geometry changes that the acids undergo under deprotonation are only partly explained by π delocalisation.

The delocalisation energy (ΔE_{deloc}) of the parent acids and their anions is defined as the energy difference between the localised wavefunction, ϕ_{loc}, and the delocalised ground state, ϕ_{del} in their optimal geometry, i.e. the adiabatic delocalisation energy [104]

$$\Delta E_{deloc} = E_{\phi_{loc}} - E_{\phi_{deloc}} \qquad (52)$$

The energetic effects of π-delocalisation as calculated through Eq. (52) are summarised in Table 3.

The results show that the carboxylate and enolate anions have the largest delocalisation energies among the six species, in accordance with the principles of resonance theory. This is because none of these anions can possibly be described by a single Lewis structure. For example, the carboxylate anion, with its symmetrical geometry, requires besides structure **1a** at least the contribution of **1b**. This also applies to the enolate anion, but with an important difference: **1a** and **1b** are degenerate structures, a factor that is expected to maximise the resonance energy, while the structures **2a** and **2b** are not equivalent and have different energies. Accordingly, the delocalisation energy is expected to be smaller in the enolate anion than in the carboxylate anion, which is indeed found to be the case (see Table 3).

As expected, because the parent acids of these two anions can be reasonably well described by a single Lewis structure, they have much smaller delocalisation energies. In ethanol and its deprotonated anion, for which no resonance between low-lying Lewis structures may be expected, the delocalisation energy is relatively small.

As delocalisation reinforces acidity only if it stabilises the anion more than the parent acid, the contribution of delocalisation to the acidity is best defined as the difference of the two delocalisation energies: ($\Delta\Delta E = \Delta E$(anion) $- \Delta E$(acid)), Using this criterion, it appears that delocalisation contributes rather little (8 kcal/mol) to the acidity of ethanol, as expected from chemical intuition. In contrast, delocalisation contributes as much as 21–23 kcal/mol to the acidity of formic acid and of vinyl alcohol. Perhaps surprisingly, the $\Delta\Delta E$ values are the same for the two species, while one might have expected resonance effects to be more important in formic acid, for which the mesomeric description of its anion involves two equivalent structures. The explanation probably lies in the polar nature of the C-O bond, which results in a large contribution of structure **1c** to the anion. Since an ionic structure of the same type is also important in the undissociated acid, the nature of the π electronic system changes less than expected from acid to anion, so that the change in delocalisation energy remains relatively moderate. To push this reasoning to the limit: if the C-O bonds were entirely ionic, there would have been no resonance at all.

This does not mean that enols and carboxylic acids have comparable acidities, since inductive effects may also contribute to the acidities. In that respect, it is useful to compare the $\Delta\Delta E$ values obtained with the total acidity enhancements of formic acid and vinyl alcohol with respect to ethanol. The experimental gas-phase acidities of formic acid and ethanol are known to be 345 and 376 kcal/mol, respectively [105]. The acidity of vinyl alcohol has been accurately calculated by Streitwieser *et al.* [106], who predicted a value of 359.5 kcal/mol. So, the acidities of formic acid and vinyl alcohol are reinforced by 31 and 16.5 kcal/mol, respectively, relative to ethanol. The calculations indicate that delocalisation contributes 23, 21 and 8 kcal/mol, respectively, to the acidities of formic acid, vinyl alcohol and ethanol. Delocalisation therefore reinforces the acidities of the two former species by 15 and 13 kcal/mol, respectively, compared to ethanol. This is 48% and 78% of the total acidity enhancement, which is the major part of the acidity enhancement in vinyl alcohol. Delocalisation and inductive effects are found to be of equal importance to formic acid.

The calculations support the traditional view by showing that delocalisation is an important factor responsible for the enhanced acidity of carboxylic acids and enols relative to alcohols.

The same methodology was applied to the study of the role of conjugation in the stability and rotational barriers of formamide and thioformamide [100]. Here it was found that resonance accounts for roughly one-half of the rotational barrier of formamide and for two-thirds in the case of thioformamide.

6. CONCLUSIONS

We have given an account of some of the inner workings of the gradient VBSCF program TURTLE. The program is especially conceived to allow the optimisation of wavefunctions of arbitrary form. This feature is exploited in the study of resonance and delocalisation phenomena.

For instance it allows the complete optimisation, orbitals and geometry, of benzene (D_{6h} symmetry), which is described by two resonating structures and of the fictional molecule cyclohexatriene (D_{3h} symmetry), whose wave function consist of just one of the structures. A comparison of the results gives a better insight in the nature and the persistence of resonance.

ACKNOWLEDGEMENT

REFERENCES

[1]   D.L. Cooper, T. Thorsteinsson and J. Gerratt, Int. J. Quantum Chem. 65 (1997) 439.

[2]   T. Thorsteinsson and D.L. Cooper, Prog. Theor. Chem. Phys. 2 (2000) 303.

[3]   J. Verbeek, J.H. Langenberg, C.P. Byrman, F. Dijkstra and J.H. van Lenthe, TURTLE an Ab Initio VB/VBSCF program (1988-2000) .

[4]   P.C. Hiberty, S. Humbel, C.P. Byrman and J.H. van Lenthe, J. Chem. Phys. 101 (1994) 5969.

[5]   P.C. Hiberty, J. Mol. Struct. (Theochem) 398-399 (1997) 35.

[6]   M.F. Guest, J.H. van Lenthe, J. Kendrick, K. Schöffel, P. Sherwood and R.J. Harrison, GAMESS-UK, a package of *Ab Initio* programs (2001)
       With contributions from R.D. Amos, R.J. Buenker, M. Dupuis, N.C. Handy, I.H. Hillier, P.J. Knowles, V. Bonacic-Koutecky, W. von Niessen, V.R. Saunders and A.J. Stone.
       It is derived from the original GAMESS code due to M. Dupuis, D. Spangler and J. Wendolowski, *NRCC Software Catalog, Vol. 1*, Program No. QG01 (GAMESS) 1980.

[7]   B.H. Chirgwin and C.A. Coulson, Proc. Roy. Soc. (London) A 201 (1950) 196.

[8]   B. Levy and G. Berthier, Int. J. Quantum Chem. 2 (1968) 307.

[9]   J.H. van Lenthe and G.G. Balint-Kurti, Chem. Phys. Lett. 76 (1980) 138.

[10] J.H. van Lenthe and G.G. Balint-Kurti, J. Chem. Phys. 78 (1983) 5699 .

[11] J.H. van Lenthe, J. Verbeek and P. Pulay, Mol. Phys. 73 (1991) 1159.

[12] A. Banerjee and F. Grein, Int. J. Quantum Chem. 10 (1976) 123.

[13] J. Verbeek and J.H. van Lenthe, J. Mol. Struct. (Theochem) 229 (1991) 115.

[14] F. Dijkstra and J.H. van Lenthe, Chem. Phys. Lett. 310 (1999) 553.

[15] F. Dijkstra and J.H. van Lenthe, J. Chem. Phys. 113 (2000) 2100.

[16] P.O. Löwdin, Phys. Rev. 97 (1955) 1474.

[17] A.C. Aitken, Determinants and Matrices, (McGraw-Hill Book Company, New York, 1968).

[18] H. Hellmann, Einführung in der Quantenchemie, (Deuticke, Leipzig, 1937).

[19] R.P. Feynman, Phys. Rev. 56 (1939) 340.

[20] D.L. Cooper, J. Gerratt and M. Raimondi,Modern Valence Bond Theory, in: Ab Initio Methods in Quantum Chemistry, Vol. II, ed. K. P. Lawley (John Wiley & Sons Ltd., Chichester, New York, Brisbane Toronto, Singapore, 1987).

[21] M. Raimondi and D.L. Cooper, Topics in Current Chemistry 203 (1999) 106.

[22] F. Dijkstra and J.H. van Lenthe, Int. J. Quantum Chem. 67 (1998) 77.

[23] J. Verbeek, Nonorthogonal Orbitals in Ab Initio Many-Electron Wavefunctions, PhD Thesis, Utrecht University (1990).

[24] F. Dijkstra, Valence Bond theory, Implementation and use of analytical gradients, PhD Thesis, Utrecht (2000).

[25] F. Prosser and S. Hagstrom, Int. J. Quantum Chem. 2 (1968) 89.

[26] F. Prosser and S. Hagstrom, J. Chem. Phys. 48 (1968) 4807.

[27] J. Verbeek and J.H. van Lenthe, Int. J. Quantum Chem. 15 (1991) 201.

[28] W.I.I. van der Kallen and S.J. van Edixhoven, Private Communication (1987).

[29] W. Gropp, E. Lusk and A. Skjellum, Using MPI, (The MIT Press, Cambridge, Massachusetts, 1994).

[30] M. Snir, S. Otto, S. Huss-Lederman, D. Walker and J. Dongarra, MPI: The complete reference, (The MIT Press, Cambridge, Massachusetts, 1996).

[31] F. Dijkstra and J.H. van Lenthe, J. Comput. Chem. 22 (2001) 665.

[32] J. Nieplocha, R.J. Harrison and R.J. Littlefield, Global arrays: A portable "shared-memory" programming model for distributed memory computers, in: Supercomputing '94 (Washington D.C.,1994).

[33] J. Nieplocha, R.J. Harrison and R.J. Littlefield, SIAM News (1995) .

[34] J. Nieplocha, R.J. Harrison and R.J. Littlefield, Journal of Supercomputing 10 (1996) 169.

[35] P.J. Garratt, Aromaticity, (McGraw-Hill, London, New York, 1971).

[36] P.v.R. Schleyer and H. Jiao, Pure & Applied Chem. 68 (1996) 209.

[37] K. Wiberg,Aromaticity and its chemical manifestations, in: Pauling's legacy: Modern modelling of the chemical bond, Vol. 6, ed. Z. B. Maksic and W. J. Orville-Thomas (Elsevier, Amsterdam, 1999).

[38] L. Pauling, J. Chem. Phys. 4 (1936) 673.

[39] U. Fleischer, W. Kutzelnigg, P. Lazzeretti and V. Mühlenkamp, J. Am. Chem. Soc. 116 (1994) 5298.

[40] P.v.R. Schleyer, C. Maerker, A. Dransfeld, H. Jiao and N.J.R. van Eikema Hommes, J. Am. Chem. Soc. 118 (1996) 6317.

[41] C.W. Bird, Tetrahedron 41 (1985) 1409.

[42] C.W. Bird, Tetrahedron 42 (1986) 89.

[43] T.M. Krygowski, M.K. Cyrañski, Z. Czarnocki, G. Häfelinger and A.R. Katritzky, Tetrahedron 56 (2000) 1783.

[44] A. Kekulé, Liebigs Ann. 162 (1872) 77.

[45] E. Hückel, Zeitung zur Physik 70 (1931) 204.

[46] E. Hückel, Zeitung zur Physik 72 (1931) 310.

[47] L. Pauling and G.W. Wheland, J. Chem. Phys. 1 (1933) 362.

[48] W. Heitler and F. London, Z. Phys. 44 (1927) 455.

[49] J.M. Norbeck and G.A. Gallup, J. Am. Chem. Soc. 96 (1974) 3386.

[50] G.F. Tantardini, M. Raimondi and M. Simonetta, J. Am. Chem. Soc. 30 (1977) 2913.

[51] Y. Mo, W. Wu and Q. Zhang, J. Phys. Chem. 98 (1994) 10048.

[52] D.L. Cooper, J. Gerratt and M. Raimondi, Nature 323 (1986) 699.

[53] D.L. Cooper, J. Gerratt and M. Raimondi,The spin-coupled description of aromatic, antiaromatic and nonaromatic systems, in: Pauling's legacy: Modern modelling of the chemical bond, Vol. 6, ed. Z. B. Maksic and W. J. Orville-Thomas (Elsevier, Amsterdam, 1999).

[54] A.F. Voter and W.A. Goddard, III, J. Am. Chem. Soc. 108 (1986) 2830.

[55] S.S. Shaik and P.C. Hiberty, J. Am. Chem. Soc. 107 (1985) 3089.

[56] S.S. Shaik, P.C. Hiberty, J.M. Lefour and G. Ohanessian, J. Am. Chem. Soc. 109 (1987) 363.

[57] S.S. Shaik, P.C. Hiberty, G. Ohanessian and J.M. Lefour, J. Phys. Chem. 92 (1988) 5086.

[58] P.C. Hiberty, D. Danovich, A. Shurki and S.S. Shaik, J. Am. Chem. Soc. 117 (1994) 7760.

[59] S. Shaik, S. Zilberg and Y. Haas, Acc. Chem. Res. 29 (1996) 211.

[60] S. Shaik, A. Shurki, D. Danovich and P.C. Hiberty, J. Am. Chem. Soc. 118 (1996) 666.

[61] S. Shaik, A. Shurki, D. Danovich and P.C. Hiberty, J. Mol. Struct. (Theochem) 398-399 (1997) 155.

[62] E.D. Glendening, R. Faust, A. Streitwieser, K.P.C. Vollhardt and F. Weinhold, J. Am. Chem. Soc. 115 (1993) 10952.

[63] F.W. Bobrowicz and W.A. Goddard, III, Mod. Theor. Chem. 3 (1977) 79.

[64] J.H. van Lenthe and G.G. Balint-Kurti, VBSCF; The optimisation of non-orthogonal orbitals in a general (Valence Bond) wavefunction, in: 5th seminar on Computational Methods in Quantum Chemistry (Groningen,1981).

[65] R.W.A. Havenith, Ab Initio Organic Chemistry, A survey of ground- and excited states and aromaticity., PhD Thesis, Utrecht (2000).

[66] J.H. van Lenthe, R.W.A. Havenith, F. Dijkstra and L.W. Jenneskens, to be submitted for publication (2001) .

[67] F. Dijkstra, J.H. van Lenthe, R.W.A. Havenith and L.W. Jenneskens, Int. J. Quantum Chem. submitted (2001) .

[68] C.A. Coulson and I. Fischer, Phil. Mag. 40 (1949) 386.

[69] F. Dijkstra and J.H. van Lenthe, Int. J. Quantum Chem. 74 (1999) 213.

[70] R.S. Mulliken, J. Chem.Phys. 19 (1951) 1271.

[71] M.J.S. Dewar and C. de Llano, J. Am. Chem. Soc. 91 (1969) 789.

[72] W.J. Hehre, R. Ditchfield and J.A. Pople, J. Chem. Phys. 56 (1972) 2257.

[73] J.H. Callomon, E. Hirota, K. Kuchitsu, W.J. Lafferty, A.G. Maki, C.S. Pote, I. Buck and B. Starck,Structure data of free polyatomic molecules, in: Landolt-börnstein. Numerical data and functional relationships in science and technology, Vol. 7, ed. K.-H. Hellwege and A. M. Hellwege (Springer-Verlag, Berlin, 1976).

[74] J. Kao and N.L. Allinger, J. Am. Chem. Soc. 99 (1977) 975.

[75] R. Janoschek, J. Mol. Struct. (Theochem) 229 (1991) 197.

[76] F. Bernardi, P. Celani, M. Olivucci, M.A. Robb and G. Suzzi-Valli, J. Am. Chem. Soc. 117 (1995) 10531.

[77] H. Kollmar, J. Am. Chem. Soc. 101 (1979) 4832.

[78] B.R. Arnold and J. Michl,Spectroscopy of cyclobutadiene, in: Kinetics and spectroscopy of carbenes and biradicals, ed. M. S. Platz (Plenum Press, New York, 1990).

[79] S. Zilberg and Y. Haas, Int. J. Quantum Chem. 71 (1999) 133.

[80] D.J. Cram and J.M. Cram, Acc. Chem. Res. 4 (1971) 204.

[81] M. Born and R. Oppenheimer, Ann. Physik 84 (1927) 457.

[82] B. Jonsson, B.O. Roos, P.R. Taylor and P.E.M. Siegbahn, J. Chem. Phys. 74 (1981) 4566.

[83] B.O. Roos, P. Linse, P.E.M. Siegbahn and M.R.A. Blomberg, Chem. Phys. 66 (1982) 197.

[84] P.J. Knowles, G.J. Sexton and N.C. Handy, Chem. Phys. 72 (1982) 337.

[85] G. Schaftenaar, Molden (1998) .

[86] R.W.A. Havenith, Private Communication (2001).

[87] R.W.A. Havenith, J.H. van Lenthe, F. Dijkstra and L.W. Jenneskens, J. Phys. Chem. A 105 (2001) 3838.

[88] J.R. Platt, J. Chem. Phys. 22 (1954) 1448.

[89] E. Clar, Polycyclic Hydrocarbons, (Academic Press Inc., London, 1964).

[90] M. Randić, Chem. Phys. Lett. 38 (1976) 68.

[91] M. Randić, Tetrahedron 33 (1977) 1905.

[92] M. Randić, J. Am. Chem. Soc. 99 (1977) 444.

[93] Y. Mo, H. Jiao, Z. Lin and P. von R. Schleyer, Chem. Phys. Lett. 289 (1998) 383.

[94] R.W.A. Havenith, H. Jiao, L.W. Jenneskens, J.H. van Lenthe, M. Sarobe, P. von R. Schleyer, M. Kataoka, A. Necula and L.T. Scott, J. Am. Chem. Soc., accepted (2001) .

[95] L. Pauling, The Nature of the Chemical Bond and the Structure of Molecules and Crystals: An Introduction to Modern Structural Chemistry., (Cornell University Press, Ithaca, New York, 1960).

[96] P.O. Löwdin, Rev. Mod. Phys. 39 (1967) 259.

[97] U. Meier, C. van Wüllen and M. Schindler, J. Comput. Chem. 13 (1992) 551.

[98] P.C. Hiberty and C.P. Byrman, J. Am. Chem. Soc. 117 (1995) 9875.

[99] C.P. Byrman, Non-orthogonal Orbitals in Chemistry, PhD Thesis, Utrecht (1995).

[100] D. Lauvergnat and P.C. Hibery, J. Am. Chem. Soc. 119 (1997) 9478.

[101] P.C. Hariharan and J.A. Pople, Theor. Chim. Acta 28 (1973) 213.

[102] G.W. Spitznagel, T. Clark, J. Chandrasekhar and P.v.R. Schleyer, J. Comput. Chem. 3 (1982) 363.

[103] M.J. Frisch, G.W. Trucks, M. Head-Gordon, P.M.W. Gill, M.W. Wong, J.B. Foresman, B.G. Johnson, H.B. Schlegel, M.A. Robb, E.S. Replogle, R. Gomperts, J.L. Andres, K. Raghavachari, J.S. Binkley, C. Gonzalez, R.L. Martin, D.J. Fox, D.J. Defrees, J. Baker, J.J.P. Stewart and J.A. Pople, Gaussian 92, Revision C3 (1992) .

[104] S. Behrens, A.M. Köster and K. Jug, J. Org. Chem 59 (1994) 2546.

[105] J.E. Bartmess and R.T. McIver, Jr., Gas Phase Ion Chemistry, vol. 2 Academic Press: NY, 1979).

[106] M.R.F. Siggel, A. Streitwieser, Jr. and R.D. Thomas, J. Am. Chem. Soc. 110 (1988) 8022.

Chapter 5

Generalized Multistructural Method: Theoretical Foundations and Applications

A. G. H. Barbosa and M. A. C. Nascimento

Instituto de Química, Departamento de Físico-Química, Universidade Federal do Rio de Janeiro. 21949-900, Rio de Janeiro-RJ, Brasil

ABSTRACT

The Generalized Multistructural Wave Function (GMS) [1,2] is presented as a general variational many-electron method, which encompasses all the variational MO and VB based methods available in the literature. Its mathematical and physico-chemical foundations are settled. It is shown that the GMS wave function can help bringing physico-chemical significance to the classical valence-bond (VB) concept of resonance between chemical structures. The final wave functions are compact, easily interpretable, and numerically accurate.

1. THEORETICAL FOUNDATIONS

1.1. Introduction

Ab initio calculations of electronic wave functions are well established as useful and powerful theoretical tools to investigate physical and chemical processes at the molecular level. Many computational packages are available to perform such calculations, and a variety of mathematical methods exist to approximate the solutions of the electronic hamiltonian. Each method is based (or should be) on a well defined physical model, specified by a certain partition of the electronic hamiltonian, in such a way as to include a subset of all the interactions present in the exact one. It is expected that this subset contains the most important effects to describe consistently the situation of interest. The identification of which physical interactions to include is a major step in developing and applying quantum chemical theory to the study of real problems.

From the conceptual point of view, there are two general approaches to the molecular structure problem: the molecular orbital (MO) and the valence bond (VB) theories. Technical difficulties in the computational implementation of the VB approach have favoured the development and the popularization of MO theory in opposition to VB. In a recent review [3], some related issues are raised and clarified. However, there still persist some conceptual pitfalls and misinterpretations in specialized literature of MO and VB theories. In this paper, we attempt to contribute to a more profound understanding of the VB and MO methods and concepts. We briefly present the physico-chemical basis of MO and VB approaches and their intimate relationship. The VB concept of resonance is reformulated in a physically meaningful way and its point group symmetry foundations are laid. Finally it is shown that the Generalized Multistructural (GMS) wave function encompasses all variational wave functions, VB or MO based, in the same framework, providing an unified view for the theoretical quantum molecular structure problem. Throughout this paper, unless otherwise stated, we utilize the non-relativistic (spin independent) hamiltonian under the Born-Oppenheimer adiabatic approximation. We will see that even when some of these restrictions are removed, the GMS wave function is still applicable.

1.2. Molecular Orbital Theory

Proposed shortly after the VB theory, the MO theory became the most popular approach to molecular structure calculations, mainly because this theory is much more amenable than VB to computer implementation. As a consequence, there is a great number of results of MO calculations on many chemical systems. With the improvement of the numerical techniques and of auxiliary interpretative tools by many research groups, together with the wide availability of computer codes, MO theory was soon established as "the" computational (and for some also "the" conceptual) approach to the molecular structure problem. Due to its widespread use, MO theory is frequently pushed beyond its conceptual limits. In this section we will briefly outline some aspects of MO theory and highlight its physico-chemical interpretation.

Application of *ab initio* MO theory usually begins at the monoconfigurational level, with the Hartree-Fock-Roothaan or LCAO-SCF methodology [4,5]. In this scheme the wave function for a closed-shell molecule containing N electrons is approximated as an antisymmetrized product (determinant) of spin-orbitals $\{\varphi_i\}$:

$$\Psi(x_1, x_2, ..., x_N) = (N!)^{-1/2} \det | \varphi_1(x_1) \ \varphi_2(x_2) \ ... \ \varphi_N(x_N) |$$

The best spin orbitals will be the eigenfunctions of the one-electron Fock operator:

$F_i \varphi_i = \varepsilon_i \varphi_i$, where $F(i) = h(i) + g(i,j)$.

The Fock operator is divided into two general terms: h(i), called the core-hamiltonian, contains the one-electron terms (electron kinetic energy, electron nucleus attractions); g(i,j) contains the two-electron operator, composed of coulomb and exchange terms, which average the interactions among electrons. The spin-orbitals are almost always expanded in a basis of known functions (usually gaussians), and the expansion coefficients are variationally optimized to minimize the total electronic energy. At the end of the optimization process we have a set of orbital energies $\{\varepsilon_i\}$, and of spin-orbitals $\{\varphi_i\}$ associated with the electrons. Physically speaking, we have approximated the state of a *many-electron* system by an antisymmetrized product of N *one-electron* states, each one of them determined so as to respond to the average field generated by the other N - 1 electrons.

The Hartree-Fock wave function is only valid as an approximation to the many-electron state when it obeys the so-called SCF theorems [6], which govern the physical interpretation of the SCF solution functions. The Brillouin theorem states that singly excited determinants do not mix with converged ground state determinants in a configuration interaction expansion. The Delbruck theorem says that the spatial-spin symmetry of the SCF solutions must be the same of the exact many-electron wave function. In another words, the Hartree-Fock wave function must have a non-vanishing overlap with the exact many-electron wave function [7]. When either or both of these two restrictions are not met it is said that the Hartree-Fock solution presents instabilities [8], meaning that by removing the space-spin symmetry constraints one obtains a solution with lower energy. However, the physical meaning of the Hartree-Fock instabilities is a more complex subject, which will be addressed in a separate paper [9]. Unrestricted wave function based approaches [10] (UHF – unrestricted Hartree-Fock and GHF – general Hartree-Fock) will not be considered here. The corresponding wave functions are not eigenfunctions of the S^2 operator, and therefore do not obey Delbruck's theorem. This is a well known and documented problem of the UHF and GHF wave functions [4]. However, what is never mentioned is the fact that although the UHF wave function is antisymmetric in the α and/or β electrons, the full wave function is not antisymmetric and therefore it does not

obey the Pauli principle. For the moment we just anticipate that only closed shell many-electron systems can be approximated by a physically meaningful monoconfigurational wave function.

Chemically speaking there is little to say. Canonical Hartree-Fock molecular orbitals leave no place for classical chemical concepts such as bonds between atoms or groups, lone pairs, resonance hybrids, etc. However, chemists still utilize these concepts because they are extremely useful in correlating and understanding chemical facts. Even when one manages to localize the canonical molecular orbitals (which is not always straightforward) in regions such that they could be associated with lone pairs or individual chemical bonds, it is important to bear in mind that the orbitals represent *localized one-electron states*, and not a two-electron chemical bond between atoms or a lone pair of electrons, as will be discussed further.

From the physical point of view, we are representing a many-electron state by an antisymmetrized product of one-electron states. The density matrix formalism [4,11-13] allows one to analyse in the same footing calculations resulting from different levels of approximation. The density matrix is called reduced when is formed from a pure state:

$$\Gamma = |\psi\rangle\langle\psi|$$

If we form the reduced density matrix from the one-electron states obtained from a Hartree-Fock calculation, we will have the so-called Fock-Dirac reduced density matrix which is an approximation to the many-electron state. The analysis of this density matrix reveals the physical features of the many-electron state under the Hartree-Fock approximation. The first-order density matrix provides the natural 1-particle states (or natural states) of the system, that in some situations (especially in the presence of degeneracies or near-degeneracies) can differ considerably from the canonical Hartree-Fock orbitals. The pure many-electron state of a system, under a given approximation, is fully specified by the occupation numbers and natural orbitals of the reduced first-order density matrix (RDM1). In the Fock-Dirac DM, the occupation numbers are fixed, since we are dealing with a monoconfigurational wave function. The second-order reduced density matrix (RDM2) provides information on the interaction between the electrons in a given state. The total energy of a given state is determined by its first and second-order reduced density matrices. At the monoconfigurational level, one can see that there is no correlation between electrons of different spins. However, in the absence of any sort of correlation (dynamic or non-dynamic)

between electrons of different spins, it would be impossible to understand the formation and the breaking of a covalent bond as resulting from the pairing or unpairing of electrons of the atoms involved in the bond. Consequently, at the Hartree-Fock level we cannot speak of "chemical bonding" involving two electrons, but only of the binding energy of the whole system. However, electrons with the same spin factors are rigorously kept apart (Fermi hole) due to the antisymetrization imposed to the wave function.

Extensions of the monoconfigurational MO theory attempt to improve the description of the electronic correlation. In practice this means including in an explicit or implicit form other space-spin symmetry adapted orbital configurations (configuration state functions – CSF), and expanding the wave function in this extended basis. Under certain circumstances, this procedure allows one to obtain VB-type wave functions from MO calculations, that is, chemical bond descriptions. This is a manifestation of the Unitary Group invariance of the hamiltonian, meaning that if one performs an exact MO calculation ("full-CI" – superposition of all possible CSFs), the roots obtained ("many-particle" electronic states) are exactly the same ones that would have been obtained in an exact VB calculation [4]. It must be noted that the eigenfunctions are completely different in form, in spite of providing the same eigenvalues. In the next section we will briefly outline the VB theory, emphasizing the special form of the wave function and its physico-chemical interpretation.

1.3. Valence Bond Theory

VB theory is the quantum-mechanical translation of the classical ideas about chemical bond and chemical structure developed by Kekulé, Lewis, Pauling and others. From the most elementary levels, chemists are trained to regard molecules as a collection of atoms held together by individual chemical bonds. Specific properties of a molecule are assigned to atoms or groups of atoms present in its structure, and our chemical reasoning is based on these ideas. However, when one tries to ground these concepts into quantum mechanical language, many practical and some conceptual difficulties arise. This situation has led to an uneven development of the VB method in comparison to MO methods. In the last three decades, due to an increase of computational power and the development of new models, VB theory is slowly recovering its place as the conceptual basis for the quantum description of chemical phenomena [14,15]. In what follows we will sketch the main features of VB theory. An alternative view to the chemical structure

problem is presented by Bader [16] with his "Atoms in Molecules" theory. However his theory is subject to so many mathematical, physical and conceptual objections that it will not be considered here.

In its most general form, the *classical* VB wave function is the antisymmetric product of atomic centred singly occupied orbitals and their spin factors. Each spin coupling scheme defines a *"chemical structure"* by associating to each two singlet-paired electrons in two different orbitals a *"chemical bond"*. The spatial orbitals are not necessarily orthogonal, and their non-zero overlap is essential for the VB description of chemical bonding [4]. The linear superposition of all possible coupling schemes is the exact VB wave function for the molecule. The exact VB wave function (full-VB) has the same energy eigenvalues as the exact MO wave function. However, just as for its MO counterpart, it is computationally unpractical for all but the very small molecular systems. The use of only one kind of spin coupling, defines what is called the perfect pairing approximation. The Heitler-London wave function for the singlet H_2 molecule can be taken as example:

$$\Psi(x_1, x_2) = N \left[a(r_1)b(r_2) + b(r_1)a(r_2) \right] \times \left[\alpha(s_1)\beta(s_2) - \beta(s_1)\alpha(s_2) \right]$$

The first term in the product is associated with the spatial part and the second with the spin labels. The letters "a" and "b" stand for atomic orbitals centered in hydrogen atoms H_a and H_b respectively. To account for the indistinguishability of the electrons, spatial and spin factors appear in two products (configurations). Consequently, the VB approach is multideterminantal from the outset. This superposition of determinants causes the VB wave function, even in its most simple form, to maintain the indistinguishability of the electrons within the chemical bond. This effect is called "exclusion correlation", a non-dynamical correlation effect.

We can calculate the natural one-particle states from the density matrix generated by the VB wave function. However, for chemical interpretation purposes it is better to analyse the non-orthogonal singly-occupied orbitals since each one will correspond to an atomic localized electron overlapping (making a chemical bond) with another one. To illustrate the importance of a non-zero overlap among the spatial orbitals we can calculate the energy expression for this simple case:

$$E = \frac{Q + K}{1 + \Delta}$$

where

$$Q = \langle a|h|a \rangle + \langle b|h|b \rangle + \langle ab|g|ab \rangle$$

$$K = 2S_{ab} \langle a|h|b \rangle + \langle ab|g|ba \rangle$$

$$\Delta = \langle ab|ba \rangle = S_{ab}^2$$

The Q term contains the usual J (coulomb integral) plus the one electron diagonal terms among the electrons. The K term contains the Hartree-Fock exchange term plus an overlap dependent one-electron term. For singlet coupling this term is large and negative, contributing to the stabilization of the system. Thus, the chemist's view of the formation of the chemical bond through the overlap of atomic orbitals is preserved. In addition, since the VB wave function is built from individual atomic wave functions, it behaves correctly upon molecular dissociation, a feature not shared by MO monoconfigurational wave functions.

On the other hand, the non-orthogonality among atomic orbitals turns out to be a great problem in evaluating the matrix elements of the hamiltonian. While in the MO theory, developed with orthogonal orbitals, one can use the Condon-Slater rules to eliminate *a priori* many matrix elements from the calculation, in VB theory the number of these matrix elements increases enormously due to non-zero overlap. This fact, together with the problem of diagonalizing dense hamiltonian matrices, posed great difficulties to the computer implementation of the VB method. Another more serious problem, from a conceptual point of view, arises when one attempts to calculate classical VB wave functions. Most of the time, reasonable numerical accuracy can only be attained with the inclusion of highly unrealistic ionic structures. This is so, even for the simplest covalent system, the hydrogen molecule, causing VB theory to lose its most important characteristics: chemical interpretability and compactness of the wave functions. Coulson and Fischer [17] identified the origin of the problem and showed that the need for the ionic structures could be associated with the lack of orbital relaxation upon formation of the bond. However, the solution of this problem in feasible terms required new approaches to calculate VB wave functions that only began to appear almost 20 years later. In the meantime, unfortunately, VB theory fell into disuse, and the MO approach became the only practical model for molecular structure calculations.

In the late sixties, independent works of Goddard [18] and Gerratt [19], gave new impetus to VB theory. They explicitly considered the problem of orbital optimization, and generalized the definition of VB structure by considering a complete set of spin functions associated with a given orbital product. They named their models as GVB (generalized valence bond) and SCVB (spin coupled valence bond) respectively. These models optimize explicitly the form of the singly-occupied orbitals, (therefore, implicitly including the effect of ionic structures) yielding highly accurate monoconfigurational VB wave functions. Since the orbitals are non-orthogonal, the final wave functions incorporate a great deal of electronic correlation. Nowadays almost all VB related methods include orbital optimization to at least some extent.

Among the VB related methods existent in the literature, besides GVB and SCVB, it is worth mentioning the VB-SCF and the BOVB (breathing orbital valence bond) methods [3]. The VB-SCF method incorporates orbital optimization to the classical VB scheme. When one has more than one important perfect pairing scheme (or "resonance", but see the next Section) the BOVB method can be utilised. More recently McWeeny also presented his version of the classical VB method including orbital optimization and multistructural capabilities [20].

1.4. Resonance, Symmetry Breaking and Conical Intersections

One of the most characteristic concepts of VB theory is resonance. When just one perfect pairing scheme is unable to represent qualitatively the chemical structure of a given molecule, two or more perfect pairing schemes have equal or nearly equal importance for the representation of the molecule. The linear superposition of these "chemical structures" is called resonance in classical VB theory. Each chemical structure is called a resonance hybrid. Resonance is a concept to which chemists are deeply rooted [21]. In the classical VB literature it is stressed that the resonance hybrids have no individual physical significance, only their superposition. In quantum-mechanical terms, resonance is a coherent superposition of states. This superposition is sustained due to some sort of "mechanical stabilization" (energy lowering) originating in the coupled system. In applying the classical qualitative VB theory, chemists have made great (perhaps exaggerate) use of the concept of resonance. In spite of its great power in explaining and rationalizing many chemical facts, we have sometimes the unavoidable feeling when reading those classical works that the resonance concept brings

an artificial complexity to the description of some systems. In modern quantum chemistry literature, resonance is used in many contexts in very different forms. In what follows we will try to formulate the concept of resonance on more precise grounds and then analyse the arosed consequences.

Before getting into a deeper analysis of the concept of resonance, we must define precisely what we understand by *"chemical structure"*. One of the most basic concepts in molecular quantum mechanics is the one of potential energy surface (PES). It allows us to define a *"molecular structure"* as an arrangement of nuclear positions in space. The definition of "molecular structure" depends on the validity of the Born-Oppenheimer approximation for a given state. Actually, its validity is limited to selected portions of the entire Born-Oppenheimer PES. When a state is described by one PES, we call it an adiabatic state. It is clear that the concept of "chemical structure", depends on the existence of a previously defined "molecular structure". Only adiabatic states have a "molecular structure". From now on, we will always be dealing with adiabatic states.

Considering only the valence electrons, we define chemical structure as a configuration of singly occupied non-orthogonal atomic-localized spin-orbitals in a given molecular structure. We do not make restrictions on the topology of the spin pairing, that is, we can have two or more electrons involved in the same "bond". In fact, the reference to "spin" is somewhat misleading. There is no physical coupling between electron spins in a non-relativistic hamiltonian. Although the symmetry requirements imposed to the orbital part of an electronic wave function, as to conform to a given spin state, are very stringent, the final results can be analysed without specific reference to spin. In other words, provided that the orbital part possesses the correct permutational symmetry of a given spin state, they can be understood independently of spin. Thus, considering only the valence electrons, "chemical structure" can be redefined as a ***configuration of singly-occupied non-orthogonal atomic-localized orbitals***. These concepts are implicit in GVB and SCVB theories but we think that they are not thoroughly explored, since in the papers describing applications of VB theory, the authors are usually more interested in reproducing classical concepts than in exploring the new ones suggested by their own calculations. A good example is the SCVB calculation on the benzene molecule [22]. The classical Kekulé structures for benzene are the archetype of resonance hybrids. However, its SCVB wave function suggests that benzene is described by *one* configuration of equivalent singly occupied non-orthogonal atomic-localized orbitals, making a six-electron chemical bond, beautifully illustrating the "aromatic

effect". The Kotani spin functions used form an orthogonal set [23] defining unambiguously the total electronic wave function, allowing the spatial part to be considered independently of the spin part. In spite of that, the authors put more emphasis on the representation of this wave function in terms of the biased Rumer non-orthogonal spin basis to yield Kekulé and Dewar structures. These representations scramble the spin and spatial parts of the SCVB wave function, destroying the "chemical structure" originally defined, since the wave function is no longer monoconfigurational, the original spatial configuration topology being annihilated. Moreover, as we will show later in this paper, the spectroscopic ground state of benzene is not described by a superposition of Kekulé and/or Dewar structures.

Resonance is related to degeneracy or near-degeneracy effects. Degeneracy may arise in molecular quantum mechanics due to the existence of symmetry groups that commute with the molecular hamiltonian [24-26]. It is easily shown that the eigenfunctions of the exact hamiltonian must transform as irreducible representations of the commuting symmetry groups. When a given group has degenerate representations, some or all eigenstates of the hamiltonian of the system will reflect its degeneracy. A k-degenerate eigenvalue induces in the Hilbert space of functions, a k-dimensional subspace spanned by its eigenfunctions. Since they span the same subspace, the eigenfunctions can always be made orthogonal. This is the ordinary case of degenerate representations. However, under certain circumstances, another kind of degeneracy is possible. When the degenerate eigenvalues do not belong to the same subspace one says that there exists an "accidental degeneracy". In this case the tensorial Hilbert space is factored into irreducible non-overlapping subspaces, each one associated to an eigenvalue. The well known example of accidental degeneracy is the hydrogen atom. Its eigenfunctions should transform as irreducible representations (S, P, D, F, ...) of the SO(3) group. However the eigenfunctions associated with the same principal quantum number are degenerate: [1s], [2s,2p], [3s,3p,3d] ... In fact, the correct (non-relativistic) group of symmetry of the hydrogen atom is SO(4), which is the rotation group in four spatial dimensions. Accidental degeneracies signal that a given system has more symmetry than it appears to have. From the group theory point of view, it seems natural to relate degenerate resonance structures to point group degeneracy, or accidental degeneracies. This attribution is essential if one wants to relate "resonance" to identifiable physical effects, and to associate a "chemical structure" with the resonance hybrids. The structure of the resultant partitioned Hilbert space will

guide us in understanding the fundamental nature of the resonance phenomenon in each case.

A curious effect, prone to appear in near degeneracy situations, is the "artifactual" symmetry breaking of the electronic wave function [27]. This effect happens when the electronic wave function is unable to reflect the nuclear framework symmetry of the molecule. In principle, an approximate electronic wave function will "break" symmetry due to the lack of some kind of non-dynamical correlation. A typical example of this case is the allyl radical, which has C_{2v} point group symmetry. If one removes the spatial and spin constraints of its ROHF wave function, a lower energy symmetry broken (C_s) solution is obtained. However, if one performs a simple CASSCF or a SCVB [28] calculation in the valence "pi" space, the "symmetry breaking" disappears. On the other hand, from the classical VB point of view, the bonding of the allyl radical is represented as a superposition of two resonant structures.

However, as we will show below, a molecule possessing C_{2v} symmetry cannot possess two degenerate resonance hybrids. Thus, the allyl radical has a three electron "pi" bond, which cannot be described properly at the MO monoconfigurational level. This type of symmetry breaking is called "artifactual".

On the other hand there are other situations where the effects are difficult to identify precisely, and the wave function presents an intrinsic localization that breaks the symmetry. Typical examples are the core-hole states of homonuclear molecules. When one electron is removed from the core orbital of a molecule that has another equivalent core orbital, the symmetry broken ROHF wave function is usually 10eV more stable than the symmetry constrained one. In this case, we have two or more accidentally quasi-degenerate states, and their correct calculation demands a special wave function. The GMS wave function is perfectly suitable for these cases of "accidental degeneracy", since it can treat different states on the same footing. Apart from accidental degeneracies, there are the normal point group degeneracies, leading to Jahn-Teller nuclear framework distortions. In this case, the interaction between the degenerate states can also be treated, when they arise. Thus, there is a fundamental difference between artifactual and real "symmetry breaking". The first one is a calculation artefact and the other is a physical effect. More mathematical details on the symmetry character of wave

functions will be given in a forthcoming paper [9]. It should be clear that in the presence of either point group or "accidental" degeneracies, one configuration of singly occupied non-orthogonal atomic-localized orbitals is not enough to qualitatively describe the system. It is necessary to consider other configurations, leading naturally to the concept of resonance.

The study of nonadiabatic effects [29,30] in potential energy surfaces is one of the most active research areas of chemical dynamics. Conical intersections and intersection seams are found to be omnipresent in molecular potential energy surfaces. They seem to appear when different adiabatic states happen to have the same or nearly the same energy eigenvalues at the same region of nuclear configurations. That is precisely what happens when there is "resonance". In the presence of such degeneracies the Born-Oppenheimer approximation is no longer valid and different states interact directly giving rise to the so-called nonadiabatic effects, that include photochemical processes, charge transfer processes and spin forbidden reactions. The signature of a conical intersection is the so-called geometric phase effect; the sign of an adiabatic wave function is changed when transported along a closed loop, through a specific pseudorotation path around the conical intersection [31]. This pseudorotation connects the states at the vicinity of a conical intersection, and mediates their interaction. Since we are dealing with different adiabatic states, they will not cross each other, their adiabatic wave functions remaining intrinsically real by creating singularities in the hamiltonian. The pseudorotation that connects them is performed in the complex plane parametrized by an angle of mixing, allowing the total wave function to be single valued. *Thus, at a conical intersection, the total adiabatic wave function is described by the coupling of different states connected through a mixing angle. But this is the same idea behind the concept of resonance!* Thus, the resonance hybrids can be identified with adiabatic states which are related, through VB theory, to their individual chemical structures. With all these facts in mind it is easy to see that resonance *is* a nonadiabatic effect, derived from the superposition of many-electron states, which should always take place at conical intersection regions (except for diatomic molecules). At this point, the attentive reader may note that at a conical intersection, there is a breakdown in the Born-Oppenheimer approximation and it is not possible to define "molecular structure". Consequently it is also not possible to define "chemical structure" in the immediate vicinity of this point. However, around the conical intersection there are regions where the interaction between the adiabatic states is negligible, and the molecular and the "chemical structures" can be formally

defined from these nuclear configurations, as will be exemplified in the "applications" section.

In quantum chemistry literature resonance is sometimes considered to be equivalent to "delocalization". This happened mainly because of the "successful" MO monoconfigurational description of the "pi" system of benzene. However, the Hartree-Fock wave function for the benzene molecule (and for all aromatic molecules) is unstable [32], providing a *qualitatively* wrong description of its electronic structure. When dealing with pure states, delocalization reflects the failure of a given level of approximation to provide an *N*-representable wave function [9]. On the other hand, when there is resonance (in the precise sense defined above), we are dealing with mixed states, and the delocalization signals the intrinsic complex instability of degenerate or quasi-degenerate states.

1.5. Symmetry Conditions for Resonance Hybrids

It remains to state the symmetry conditions to be obeyed by resonance hybrids. For the total wave function to be able to split into different adiabatic states, it should be decomposable into independent parts. If the nuclear framework has some sort of spatial symmetry, it is easy to know the possible structures of the resonance hybrids. However, we must distinguish between two different situations: point group and accidental degeneracies [25,26].

When a given state belongs to a *k*-dimensional degenerate irreducible representation, the degenerate eigenfunctions belong to the same tensor subspace, and can always be made orthogonal. Point group degenerate states are always subject to Jahn-Teller distortions. The nuclear framework follows the symmetry descent coordinate until the complete removal of the degeneracy [33]. Consequently, it is not possible to have one PES minimum, or resonance, made by point group degenerate states. However, if these point group degenerate states are quasi-degenerate with a different state, the situation becomes much more complicated, and will not be considered in detail here. In these cases, resonance between these states may be possible, and the symmetries of the resonance hybrids will follow the symmetry descent path of the full point group of the system. An example of this situation recently described in the framework of MO theory is the NO_3 radical [34].

The real Hilbert space is always partitioned into a direct sum of subspaces, each representing a different energy eigenvalue of the spectrum of the hamiltonian operator:

$$\Lambda = \lambda_1 \oplus \lambda_2 \oplus \lambda_3 \ldots$$

When two or more eigenvalues happen to be equal, or nearly equal, we say that there is an "accidental degeneracy". Since the states belong to different subspaces, there is no symmetry descent path to follow. The direct product decomposition is the mathematical tool to analyse the symmetry of the allowed individual adiabatic states. It is related to the "ascent in symmetry" method [35] and justified by the Littlewood-Richardson rules for decomposition of tensor spaces in independent parts [36]. These rules define the only permissible decompositions of a tensor space (in our case, point group space), providing us with the possible symmetries of the resonance hybrids, which reproduce the total symmetry of the system. A simplified statement, suitable for our purposes, is that *"the direct product between the subsystem point group and the group that relates (maps) the subsystems should recover the full symmetry of the system"*. Notice that both the subsystems's point group and the group that maps the subsystems must be invariant subgroups of the full point group. In Table 1 all point groups are classified according to the possibility of being described by a direct product decomposition [37].

Table 1

Point groups decomposable in direct product forms	Point groups not decomposable in direct product forms
C_n, S_n ($n = 4k + 2$, $k=1, 2, \ldots$)	C_n, S_n ($n \neq 4k + 2$, $k=1, 2, \ldots$)
D_{nd} (n odd)	D_{nd} (n even)
C_{nh}, D_{nh}, T_h, O_h, I_h	C_i, C_s, C_{nv}, D_n, T, T_d, O, I

Table 2

Possible point group decompositions in direct products
$C_n = C_{n/2} \otimes C_2$ ($n = 4k + 2$, $k=1, 2, \ldots$)
$S_n = S_{n/2} \otimes C_i$ ($n = 4k + 2$, $k=1, 2, \ldots$)
$D_{nd} = D_n \otimes C_i$ (n odd)
$C_{nh} = C_n \otimes C_i$, $C_n \otimes C_s$ (n even); $C_n \otimes C_s$ (n odd)
$D_{nh} = D_n \otimes C_i$, $D_n \otimes C_s$, $C_{nv} \otimes C_s$ (n even); $D_n \otimes C_s$, $C_{nv} \otimes C_s$ (n odd)
$D_{\infty h} = C_{\infty v} \otimes C_i$, $C_{\infty v} \otimes C_s$
$T_h = T \otimes C_i$
$O_h = O \otimes C_i$
$I_h = I \otimes C_i$

Good examples are the core hole excited states of homonuclear molecules. When one electron is removed from a core orbital, the original $D_{\infty h}$ symmetry is lowered to $C_{\infty v}$. The $D_{\infty h}$ group can be decomposed into two $C_{\infty v}$ components related by a C_i or C_s operation, so it is fair to consider that the core-hole excited states are described by resonance between the two structures. The adiabatic subsystems have, by definition, zero overlap in the real space. Their interaction is defined only in complex space through the explicit overlap between the many-electron states.

An inspection on Table 2 shows that it is not possible to relate the benzene (D_{6h} symmetry) to Kekulé (D_{3h}) or Dewar (D_{2h}) structures. The ground state of benzene is not degenerate, and there is no theoretical or experimental evidence of a conical intersection with a degenerate state near the ground state geometry [38]. If there is no intersection of degenerate point group state, one cannot follow the symmetry descent path in this case. The only possibility would be that of an accidental degeneracy, but this is ruled out by the impossibility of direct product decomposition. Thus, as already stated before, the ground state of the benzene molecule is *not* described by a resonant mixture of Kekulé and/or Dewar structures.
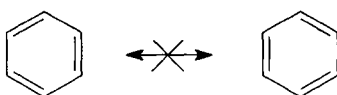
As the SCVB treatment had already shown [22], the "π" system of benzene is correctly described by a one configuration (one "chemical structure") of singly occupied atomic-localized non-orthogonal orbitals, making a *six-electron bond*, with no resonance.

Thus, the stabilization of the benzene molecule is due to the formation of the six-electron bond. From the MO point of view, the stability would be attributed to the "π" system delocalization. However, as previously mentioned, the Hartree-Fock wave function for benzene (and for all aromatic systems) is unstable [32], and the delocalization effect is exactly a manifestation of this instability [9]. Therefore, MO theory does not really explain the stability of these molecules.

At first sight it may appear that this model is difficult to reconcile with the traditional process of "molecular fragmentation" which is inherent to the classical VB description of the formation of a two-electron bond. However, Shaik and Hiberty presented in a series of papers a possible mechanism, through a nonadiabatic process, which can account for the formation of these multiply bonded systems retaining the classical concepts of molecular fragmentation [15,39,40]. The same reasoning equally applies to the allyl radical, whose "π" system is correctly described by one configuration representing a *three-electron bond* [28].

In summary, we have enlarged the concepts of chemical structure and resonance in such a way as to make then conform the more general theories of molecular quantum mechanics. Classical VB concepts have been extremely useful in rationalizing empirical facts but became inadequate in the light of the new theoretical developments. The new concepts presented here are consistent both with the mathematical models of quantum chemistry and with empirical chemical facts, and their formulation recognize the latest research advancements.

1.6. The Generalized Multistructural Wave Function (GMS)

The GMS wave function [1,2] combines the advantages of the MO and VB models, preserving the classical chemical structures, but dealing with self-consistently optimized orbitals. From a formal point of view, it is able to reproduce all VB or MO based variational electronic wave functions in its framework. Besides that, it can deal in a straightforward way with the non-adiabatic effects of degenerate or quasi-degenerate states, calculating their interaction and properties.

The GMS wave function can be defined as

$$\Psi_{GMS} = \sum_{I=1}^{N_{struct}} \sum_{i=1}^{N_{sef}} c_i^I \varphi_i^I,$$

where φ_i^I represents the ith spin eigenfunction (N_{sef}) of the Ith structure (N_{struc}) and the c_i^I its weight in the expansion. There are no restrictions whatsoever on the form of the wave function φ_i^I. Each of the φ_i^I can be individually optimized at the Hartree-Fock, or multiconfigurational (GVB, CASSCF) level, followed or not by configuration interaction (CI) treatment.

Each one of the φ_i^I is represented in a basis of orthogonal orbitals $\{\Phi_g^I\}$ optimized for the Ith structure. Although the orbitals of a given structure are taken to be orthogonal to each other,

$$\left\langle \Phi_\alpha^I \middle| \Phi_\beta^I \right\rangle = \delta_{\alpha,\beta}$$

no such restriction exists for the orbitals belonging to different structures I and II,

$$\left\langle \Phi_\alpha^I \middle| \Phi_\beta^{II} \right\rangle = S_{\alpha,\beta}^{I,II}$$

The coefficients c_i^I are obtained variationally by solving the equations,

$$\left\langle \delta\Psi_{GMS} \middle| H - E \middle| \Psi_{GMS} \right\rangle = 0$$
$$(H - SE)C = 0$$

where H and S are the interaction supermatrices containing the diagonal (same structure) and interstructural matrix elements. The matrix elements involving orbitals belonging to different structures are computed using a biorthogonalization procedure.

1.7. Equivalence between MO and VB based wave functions

The unitary group invariance of the hamiltonian assures that its exact eigenvalue spectrum is invariant to a unitary transformation of the basis. It means that a "full CI" calculation must provide the same eigenvalues (many-electron energy states) as a "full VB" calculation. However, at intermediate levels of approximation, this equivalence is not straightforward. In this section we will sketch out the main points of contact between MO and VB related wave functions.

The most simple and well known equivalence holds for the special case of two electrons in two orbitals, described by GVB(pp) and CASSCF(2,2) wave functions for covalent bonds [41]. When the bond has a mixed ionic-covalent character, the CASSCF(2,2) description is able to account approximately for this effect due to the presence of an extra ionic configuration. This problem is exactly replicated in a larger scale when

considering the equivalence between a CASSCF(N,N) and an unrestricted GVB(N) or SCVB(N), where N is the number of active electrons. The CASSCF natural orbitals can always be localized in approximately (sometimes exactly) atomic basis, providing as in VB theory, one configuration of non-orthogonal orbitals [42,43]. However, these orbitals are not necessarily singly-occupied, as they always are in single configuration VB theories. When they are singly occupied it is possible to extract VB wave functions from MO calculations. Being specific, the CASSCF(N,N) is qualitatively equivalent to a SCVB(N) or GVB(N) calculation when there is no net charge transfer between the N atomic-localized non-orthogonal orbitals, meaning that they are all strictly singly occupied [42].

In cases where this equivalence is not feasible, we are in the presence of degenerate or near-degenerate states of the many-electron system, and one configuration VB wave functions no longer represent the system correctly, since it is not possible to define real-valued reduced density matrices. In this situation we will have a mixing of many-electron states, and the non-orthogonal orbitals will not be strictly singly occupied, preventing the association of this density with a "chemical structure". In this case, multistructural or multistate theories are required. One should describe on the same footing the interaction among different many-electron states. In MO theory this can be accomplished approximately by MR-CI (multireference configuration interaction) on a basis of state-averaged CASSCF orbitals for the degenerate or near degenerate states [29]. Other MO based approaches are the B-CC (Brueckner orbitals coupled cluster) and QRHF-CC (quasi-restricted Hartree-Fock coupled cluster) [44], but since they are non-variational it is doubtful that they could treat excited states in an unbiased way. Moreover, in all MO based approaches, the idea of "chemical structure" is completely lost, avoiding a deeper understanding of the physico-chemical features of the coupled system. In VB theory one should consider a superposition of resonance structures. Each resonance structure should be associated with an adiabatic state, and with a "chemical structure", providing a clear picture of the physico-chemical features of the system. To meet simultaneously these requirements, it is necessary to consider explicitly the non-orthogonality effects between the structures. From a formal point of view, any multistructural VB method can deal with this situation, but in practice the existing methods generally are restricted to smaller domains, and the choice of which one to use will depend on the specific case [3].

Formally, all these wave functions, VB or MO based, can be reproduced at the GMS level. When using one structure, the GMS wave

function is equivalent to MO-CI, single or multireference, with complete flexibility as to the choice of configurations. It must be noted that any monoconfigurational VB (one "chemical structure") calculation can be reproduced exactly at the MO-CI level provided that the correct natural orbitals and CSFs are chosen. When using more than one structure, in the most general sense defined in this work, the resonance effects between adiabatic states (or "chemical structures") can be properly treated, since there are no orthogonality restrictions among different structures in the GMS methodology. Thus, the form of the GMS wave function allows a precise physico-chemical assessment to the unbiased defined concepts of chemical structure and resonance presented in this paper. It should be clear that the GMS method is formally suitable to treat all nonadiabatic processes that may occur in atoms or molecules, for bound and continuum states, as will be explored in forthcoming papers.

2. APPLICATIONS

In this section we will review briefly some of the recent applications of the GMS wave function. A previous review [45] covers most of the early applications of the GMS wave function. Our main goal is to illustrate some of the new ideas presented in the last section, using the most recent applications and some earlier but not unpublished material.

2.1. Core-hole excited states

The proper theoretical study of core-hole excited states has been one of the most challenging problems in molecular quantum mechanics. The difficulty stems from the fact that these states lie above the continuum part of the spectra, and their attainment as high-energy roots in an ordinary configuration interaction calculation is impossible [46]. However, core-hole excited states play an important role in the identification of chemical species by X-ray based spectroscopic techniques. Additionally, there are many interesting effects that are particular to this region of the spectra and their study are the object of active research [47].

When a given symmetric molecule contains indistinguishable nuclei, the associated core-hole spectra present extra complications. At the monoconfigurational level, symmetry broken localized ROHF solutions have

lower energy than the symmetry-constrained solution (about 10 eV in first row atoms). These localized states related to indistinguishable nuclei are "accidentally" degenerate and the correct approximation to their energies and properties should consider the superposition of the states in an unbiased way. The GMS wave function has been successfully applied to the accurate determination of transition energies, and optical and generalized oscillator strengths for core-hole states [48-52]. In this paper we will comment briefly on the latest applications of the GMS wave function to the study of core-hole states in molecules possessing identical nuclei.

The CO_2 molecule has two identical oxygen nuclei that can give rise to accidental degeneracy effects in its core-hole spectra. The total symmetry is $D_{\infty h}$, but the core-hole localized states have $C_{\infty v}$ symmetry. The superposition of these two symmetry broken degenerate solutions recovers properly the total symmetry of the molecule. The GMS wave function was used in conjunction with spectroscopic measurements to help the assignment of the electronic transitions of the inner-shell spectra of the CO_2 molecule [51]. Three structures were used in the calculations: two ROHF degenerate solutions with the hole localized in each one of the oxygen atoms, and one ROHF-CI delocalized structure. Transition energies and intensities were calculated, presenting excellent agreement with the experiments (Table 3).

Table 3
Transition energies for inner-shell excitation of the CO_2 molecule

Experimental (eV)	Calculated (GMS) (eV)	Assignment
535.4	535.5	$1\sigma_g \rightarrow 2\pi_u$
	535.7	$1\sigma_u \rightarrow 2\pi_u$
	535.7	$1\sigma_g \rightarrow 3s\sigma_g$
	536.9	$1\sigma_u \rightarrow 3s\sigma_g$
538.8	538.0	$1\sigma_g \rightarrow 3p\sigma_u$
	538.0	$1\sigma_u \rightarrow 3p\sigma_u$
538.8	539.3	$1\sigma_u \rightarrow 3p\pi_u$
	539.6	$1\sigma_g \rightarrow 3p\pi_u$
538.8	540.3	$1\sigma_g \rightarrow 4s\sigma_g$
	540.3	$1\sigma_u \rightarrow 4s\sigma_g$

It must be noted that the experiments did not resolve the bands of the quasi-degenerate states and the theoretical calculation is essential to get some understanding of the processes involved. The sum of the calculated optical

oscillator strengths for the $1\sigma_g \rightarrow 2\pi_u$ and $1\sigma_u \rightarrow 2\pi_u$ states (which are experimentally indistinguishable in an electron impact based experiment) agrees well with the measured one (calculated: 0.12; experimental: 0.11 to 0.13). The GMS wave function was able to reproduce not only the transition energies but also the optical oscillator strengths, which is a much more sensitive test for a wave function. For an extensive discussion on the profiles of the calculated and measured generalized oscillator strengths of the inner-shell spectra of the CO_2 molecule, the reader is referred to the original paper [51].

A similar theoretical study was undertaken for the core-hole states for the ethylene molecule [52]. There are two identical carbon atoms and the molecule has D_{2h} symmetry. The localized core-hole states have C_{2v} symmetry and the direct product $C_{2v} \otimes C_s$ recovers properly the full symmetry of the system. The results for transition energies and optical oscillator strengths agree well with those available in the literature.

2.2. Molecular Structure and Valence Spectroscopy

As an illustration of the new ideas presented in this review, we can consider the problem of determining a chemical structure of the ozone molecule (O_3). Traditionally, this molecule is regarded as a resonance hybrid between two zwiterionic structures. In the early seventies, the GVB(pp) method gave a very different picture, regarding the molecule as a singlet biradical, with a long "π" bond between the terminal oxygen atoms [53]. As already explained for the allyl radical, C_{2v} molecules cannot have degenerate resonance structures, since there is neither point group degenerate states nor accidentally degenerate states, because C_{2v} is not a direct product group.
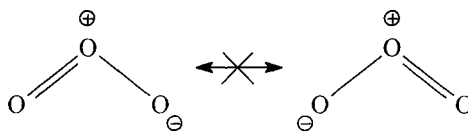
The GMS wave function for the ozone molecule supports the GVB(pp) picture for the ozone molecule in a straightforward way [54]. The two classical resonance structures were considered together with the biradical one in a three structure GMS-CI calculation. The ground state of the O_3 molecule

is solely described by the biradical structure, the contribution of the localized ones being completely negligible.
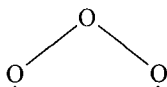
This is in perfect harmony with the theory presented in the first section. In fact, a simple qualitative application would allow an *a priori* deduction of the chemical structure of the O_3 molecule, since the biradical is the only non-degenerate symmetric structure possible.

The $(n \rightarrow \pi^*)^{1,3}$ excited states of the pyrazine molecule are a well-known case of wave function symmetry breaking [27,55]. An accidental degeneracy arises when one considers the valence electronic excitations within the equivalent nitrogen lone pairs. The pairs are in opposite and equivalent positions and, when there are two singly occupied orbitals in different symmetries, we will have a pair of accidentally degenerate states as shown below:
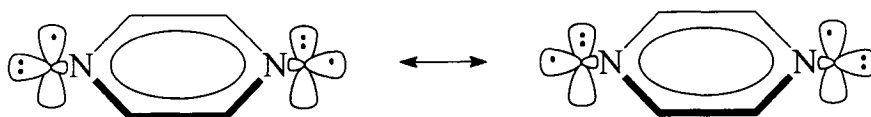
The total symmetry of the molecule is D_{2h}, so we cannot have point group degenerate states. The accidentally degenerate states represented above have C_{2v} symmetry. The direct product $C_{2v} \otimes C_s$ recovers properly the full symmetry of the system. Depending on the particular excitation and final spin state four states can be generated. In Table 4 we compare the results of Hartree-Fock (HF), configuration interaction with singles and doubles excitations (CI-SD) and the two structure GMS calculations, with the available experimental data.

Table 4
Transition energies (eV) for the $(n \to \pi^*)^{1,3}$ excited states of the pyrazine molecule

State	HF	CI-SD	GMS	Exp.
$^3B_{3u}$	4.52	3.51	3.27	3.33 [56,57]
$^1B_{3u}$	5.27	4.20	3.89	3.85 [56,58]
$^3B_{2g}$	6.23	5.21	4.77	4.59 [56]
$^1B_{2g}$	7.11	5.91	5.48	5.19 [56,59]

The results from the GMS calculation are always better than the HF and CI-SD ones, with the additional advantages of compactness of the wave function, and exact preservation of the full symmetry of the system.

3. FINAL REMARKS

In this chapter we presented the Generalized MultiStructural (GMS) method as the most general variational approach to calculate electronic wave functions. Emphasis was given to a proper understanding of the general conceptual features of the MO and VB methods and the relationship between them. Considering only valence electrons, we defined chemical structure as a configuration of singly occupied atomic-localized non-orthogonal orbitals, and stressed that it is valid only for an adiabatic state. The classical valence-bond concept of resonance was recast in a physically meaningful way, being exactly related to a nonadiabatic effect of point group or accidental degeneracy. In the case of accidental degeneracy, a set of point group based "selection rules" for the possible symmetries of resonant structures was discussed and applied to representative cases. It was shown that in these cases neither single configuration VB nor single state MO approaches could approximate the correct electronic wave function. Multistructural methodologies are then required, and the GMS method seems to be flexible and generally applicable. Finally, we briefly presented some applications of the GMS wave function.

At first sight, the concepts presented in this chapter may seem a little odd if compared to classical VB theory. However, in adopting these new concepts, we can bring physico-chemical significance to the resonance concept, establishing a common line of reasoning with MO theory. This is important because once one begins to increase the sophistication of the calculations, the numerical differences between MO and VB theories tend to

disappear. Secondly, VB theory has suffered for a long time the (unjustifiable) fame of not being physically motivated. Since the difference between chemistry and physics lies only in our heads, the ideas presented above put the two lines of thought in a single framework, while keeping the specific features of each one.

ACKNOWLEDGEMENTS

REFERENCES

[1] E. Hollauer and M. A. C. Nascimento, Chem. Phys. Lett. 184 (1991) 470
[2] E. Hollauer and M. A. C. Nascimento, J. Chem. Phys. 99 (1993) 1207
[3] P. C. Hiberty, J. Mol. Struc. (Theochem) 451 (1998) 237
[4] R. McWeeny, Methods of Molecular Quantum Mechanics, Academic Press, London, 1992
[5] A. Szabo and N. Ostlund, Modern Quantum Chemistry: Introduction to Advanced Electronic Structure Theory, McGraw-Hill, New York, 1989
[6] G. Berthier, Essay on the Theorems and Constraints if the SCF Theory, in Studies in Physical and Theoretical Chemistry 21 – Current Aspects of Quantum Chemistry 1981, R. Carbó ed., Elsevier, Amsterdam, 1982
[7] W. Kutzelnigg and V. H. Smith Jr., Int. J. Quantum Chem. 2 (1968) 531
[8] D. J. Thouless, The Quantum Mechanics of Many-Body Systems, Academic Press, New York, 1961
[9] A. G. H. Barbosa and M. A. C. Nascimento, to be published
[10] H. Fukutome, Int. J. Quantum. Chem. 20 (1981) 955
[11] R. McWeeny, Rev. Mod. Phys. 32 (1960) 335
[12] A. J. Coleman, Rev. Mod. Phys. 35 (1963) 668
[13] E. R. Davidson, Reduced Density Matrices in Quantum Chemistry, Academic Press, New York, 1976
[14] J. Gerratt, J. Mol. Struc. (Theochem) 229 (1990) 1
[15] S. S. Shaik and P. C. Hiberty, Adv. Quant. Chem. 26 (1995) 99
[16] R. F. W. Bader, Atoms in Molecules, Oxford, 1990
[17] C. A. Coulson and I. Fischer, Phil. Mag. 40 (1949) 386
[18] W. A. Goddard III, Phys. Rev. 157 (1967) 81; W. A. Goddard III, J. Chem. Phys. 48 (1968) 450
[19] J. Gerratt and W. N. Lipscomb, Proc. Nat. Acad. Sci. USA 59 (1968) 332; J. Gerratt, Adv. At. Mol. Phys. 7 (1971) 141
[20] R. McWeeny, Int. J. Quantum Chem. 74 (1999) 87
[21] G. W. Wheland, Resonance in Organic Chemistry, Wiley, New York, 1955

[22] D. L. Cooper, J. Gerratt and M. Raimondi, Nature 323 (1986) 699

[23] R. Pauncz, Spin Eigenfunctions: Construction and Use, Plenum Press, New York, 1979

[24] R. McWeeny, Symmetry, Pergamon Press, Oxford, 1963

[25] P.O. Lowdin, Rev. Mod. Phys. 39 (1967) 259

[26] C. D. H. Chisholm, Group Theoretical Techniques in Quantum Chemistry, Academic Press, London, 1976

[27] E. R. Davidson and W. T. Borden, J. Phys. Chem. 87 (1983) 4783

[28] J. M. Oliva, J.Gerratt, D. L. Cooper, P. B. Karadakov and M. Raimondi, J. Chem. Phys. 106 (1997) 3663

[29] D. R. Yarkony, Electronic Structure Aspects of Nonadiabatic Processes in Polyatomic Systems, in Modern Electronic Structure Theory; D. R. Yarkony Ed; World Scientific: Singapure, 1995

[30] D. R. Yarkony, Acc. Chem. Res. 31 (1998) 511

[31] A. J. C. Varandas and Z. R. Xu, Chem. Phys. 259 (2000) 173

[32] D. Dehareng and G. Dive, J. Comp. Chem 21 (2000) 483

[33] A. D. Liehr, J. Phys. Chem., 67 (1963) 389

[34] W. Eisfeld and K. Morokuma, J. Chem Phys. 113 (2000) 5587

[35] D. J. Klein, C. H. Carlisle and F. A. Matsen, Adv. Quantum Chem. 5 (1970) 219

[36] X. Li and J. Paldus, J. Math. Chem. 13 (1993) 273

[37] S. L. Altmann and P. Herzig, Point Group Theory Tables, Claredon Press, Oxford, 1994

[38] E. C. Silva, D. L. Cooper, J. Gerratt and M. Raimondi, J. Chem. Phys 101 (1994) 3866

[39] S. S. Shaik and P. C. Hiberty, J. Am. Chem. Soc. 107 (1985) 3089

[40] S. S. Shaik, P. C. Hiberty, G. Ohanessian and J. M. Lefour, J. Phys. Chem. 92 (1988) 5086

[41] F. W. Bobrowicz and W. A. Goddard III, Self-Consistent Field Equations for Open-Shell Hartree-Fock and Generalized Valence Bond Wave Functions, in Modern Theoretical Chemistry, vol. 3, H. F. Schaeffer III Ed., Plenum, New York, 1977

[42] J. J. W. McDouall and M. A. Robb, Chem. Phys. Lett 142 (1987) 131

[43] T. Thorsteinsson, D. L. Cooper, J. Gerrat and M. Raimondi, A New Approach to Valence Bond Calculations: CASVB, in Quantum Systems in Chemistry and Physics, R. McWeeny, J. Maruani, Y. G. Smeyers and S. Wilson Ed., Kluwer, Dordrecht, 1997

[44] J. F. Stanton, J. Gauss and R. J. Bartlett, J. Chem. Phys. 97 (1992) 5554

[45] M. A. C. Nascimento, Studies on Chemical Structure, Spectroscopy and Electron Scattering Using Generalized Multistructural Wavefunctions, in Quantum Systems in Chemistry and Physics, R. McWeeny, J. Maruani, Y. G. Smeyers and S. Wilson Ed., Kluwer, Dordrecht, 1997

[46] I. Shavitt, The Method of Configuration Interaction, in Modern Theoretical Chemistry, vol. 3, H. F. Schaeffer III Ed., Plenum, New York, 1977

[47] A. P. Hitchcock, Theory and Applications of Inner-Shell Spectroscopy, classnotes, unpublished, 1996

[48] C. E. Bielschowsky, M. A. C. Nascimento and E. Hollauer, Phys. Rev. A. 45 (1992) 7942

[49] M. P. Miranda and C. E. Bielschowsky, J. Mol. Struc. (THEOCHEM) 282 (1993) 71

[50] M. P. Miranda, C. E. Bielschowsky, H. M. B. Roberty and G. G. B. de Souza, Phys. Rev. A. 49 (1994) 2399

[51] I. G. Eustatiu, T. Tyliszczak, A. P. Hitchcock, C. C. Turci, A. B. Rocha and C. E. Bielschowsky, Phys. Rev. A. 61 (2000) 042505

[52] A. B. Rocha and C. E. Bielschowsky, J. Chem. Phys. 113 (2000) 7971

[53] W. A. Goddard III, T. H. Dunning, W. J. Hunt and P. J. Hay, Acc. Chem. Res. 6 (1973) 368

[54] W. B. Floriano, S. R. Blaszkowski and M. A. C. Nascimento, J. Mol. Struc. (THEOCHEM) 282 (1995) 51

[55] R. L. Martin, J. Chem. Phys. 74 (1981) 1852

[56] Y. Okuzawa, H Fujui, M. Ito, Chem. Phys. Lett. 171 (1990) 341

[57] G. Fischer, Chem. Phys. Lett. 79 (1981)

[58] K. K. Innes, J. B. Byrne and I. G. Ross, J. Mol. Spect. 22 (1967)

[59] A. Bolovinos, P. Tsekeris, J. Philis, E. Pantos and G. Andritsopoulos, J. Mol. Struc. 103 (1984) 240

Chapter 6

A spin–free approach for valence bond theory and its applications

Wei Wu, Yirong Mo, Zexing Cao, and Qianer Zhang

Department of Chemistry, The State Key Laboratory for Physical Chemistry of Solid Surfaces, and Institute of Physical Chemistry, Xiamen University, Xiamen, Fujian 361005, China

A spin-free approach for valence bond (VB) theory, based on symmetric group techniques, is introduced in this chapter. Bonded tableaux (BT) are adopted to represent VB structures, and a paired-permanent-determinant algorithm is developed to solve the so-called "$N!$" problem in the nonorthogonal VB method, followed by the introduction of our *ab initio* VB program, Xiamen-99. Furthermore, applications of *ab initio* VB method to the resonance effect, chemical reactions, and excited states are carried out by the Xiamen package.

1. INTRODUCTION

The striking difference between the molecular orbital (MO) theory and the valence bond (VB) theory[1] lies in the fact that all orbitals in the former are delocalized and orthogonal, while orbitals in the latter are localized and nonorthogonal. The nonorthogonality of orbitals leads to the notion that chemical bonds originate from the overlap of the bonding orbitals, which is the heart of the chemical theories. Thus, the MO and VB methods are complementary rather than exclusive. However, the notorious $N!$ problem due to the nonorthogonality of orbitals in the VB method hindered the development of *ab initio* VB approaches, although significant progress has been made by a few groups [2-7]. Particularly, Goddard's generalized VB (GVB) [4], which makes a compromise between the MO and VB methods by introducing the strong orthogonality approximation and thus notably reduces the computational costs, still enjoys great popularity. In the past decade a significant resurrection of interests in the *ab initio* VB methods [8-11] has been observed. This trend is partially promoted by the advancement of computation technology, however, the growing demand for *ab initio* VB methods to solve many tricky computational chemistry problems, for which MO methods

are unable to give definite answers, nevertheless is the driving force.

In the MO theory, the most reliable approach for the study of reaction pathways perhaps is CASSCF [12, 13], but multi-VBSCF is essentially at the same level with CASSCF [14]. Since a VB wave function can be expanded into the combination of numerous Slater determinants that are used to define configurations in the MO theory, the VB theory provides a very compact, accurate description for chemical reactions. While both MO and VB theories have their own advantages as well as disadvantages, in our opinions, there are some areas where the VB theory is particularly superior to the MO theory: 1) the refinement of molecular mechanics force field; 2) the development of empirical or semi-empirical VB approaches; 3) the impact of intermolecular charge transfer or intramolecular electron delocalization on the structure and properties; 4) the validation of classical chemical theories and concepts at the quantitative level; 5) the elucidation of chemical reactions and excited states intuitively.

As one of the most remarkable progresses in chemistry, molecular simulations of condensed states such as solution and biosystems are receiving more and more attentions [15]. Generally molecular simulations are based on molecular mechanics (MM) methods, where the force field is normally expressed as the summation of bonded and non-bonded terms [16]. Unfortunately, very few leads are available to guide the formulations and parameterization of these energy terms. For example, whether and how the polarization effect is important in the simulation of protein and DNA interactions is still an open question [17], although there is much interest to develop polarizable force fields [18]. Since in the VB theory, wave functions for diabatic states (or resonance structures), where each bonding electron pair is localized in the bonding region, can be easily constructed, it is possible to derive various energy terms such as polarization and charge transfer energy and compare their contributions to the complexation energy between monomers [19], and this type of information is indispensable for the validation and refinement of MM force fields [20]. Notably, the importance of electron transfer between protein and aqueous solution is especially difficult to evaluate. Most recently, Thompson and Hynes tried to estimate the charge transfer effect in simple hydrogen bonding systems at the MM-VB level [21].

Closely related to the above merit of VB methods, the unique definition of diabatic states also allows us to derive the energy profiles for diabatic states. Since for many reactions the whole process can be described with very few resonance structures, the comparison between the diabatic and adiabatic state energy profiles can yield insight into the nature governing the reactions [22-24]. In fact, even for complicated enzymatic reactions, simple VB ideas have shown unparalleled value [25, 26]. However, the further utilization of the VB ideas at the empirical and semi-empirical levels should be carefully verified by benchmark *ab initio* VB

computations.

While the concept of resonance has been broadly but qualitatively used in chemistry, the exploration of the nature of some chemical reactions and the understanding of structure-activity relationships call for the quantification of the resonance effect. For example, conventionally, it is believed that π electron delocalization is responsible for the greater acidity of carboxylic acids compared to aliphatic alcohols. However, this explanation was challenged by Siggel and Thomas [27], who attributed the difference in acidity to electrostatic interactions. The controversies went on due to the lack of absolute data to support either side [28], until *ab intio* VB calculations by Hiberty and Byrman [29] presented reliable data to show the importance of electron delocalization in carboxylic anions. Similarly, our studies on the delocalization in allyl cation, radical and anion also solved the arguments about the magnitude of the resonance stabilization in these systems and showed that in the cation and anion the resonance stabilization is comparable, which leads to the conclusion that the averaging of charges inside a system is the main driving force for electron delocalization at least in these allyl ions [30].

Although at the present *ab initio* VB methods are still limited to small systems, the impact of this development on the reformation of our chemical knowledge is significant and diverse. In brief summary, the small benchmark calculations can not only enhance the reliability and legitimization of simple VB models and monitor the development of semi-empirical VB approaches, but also provide the guidelines for the refinement of MM force fields, which have been widely applied to the simulation of biosystems. The VB project in Xiamen University started in 1986, when a spin-free form of VB method was independently derived [31]. The same form was also proposed by McWeeny [32]. In the earlier years we wrote a simple VB code and applied it to some simple systems [33, 34]. The systematic development of a complete and efficient VB code nevertheless started in 1992 [35], when an algorithm based on the left coset decomposition of the symmetric group was proposed and programmed [36]. While this approach has been further pursued by Li after his moving out of our group [37], later we developed a more efficient algorithm called the paired-permanent-determinant approach [38, 39], on which our present code, Xiamen-99, is based. A similar algorithm for $S = 0, \frac{1}{2}$ was also presented by Li and Pauncz [40].

The arrangement of this chapter will be as following. Firstly, we discuss the construction of the bonded tableau basis and its properties. Secondly, the paired-permanent-determinant method is derived, followed by the introduction of our Xiamen-99 *ab initio* VB program. Then we show the applications of the *ab initio* VB method to the resonance effect, chemical reactions, as well as to excited states. Finally, we give a brief summary and an outlook for our future work.

2. BONDED TABLEAU VALENCE BOND APPROACH

2.1 Bonded tableau basis

The most general many-electronic wavefunction in spin-free quantum chemistry, which should be a spin eigenfunction and share anti-symmetry of electron indices, is of the form,

$$\Psi_K = \hat{A}\Omega_0\Theta_K, \tag{1}$$

where $\hat{A}$ is an antisymmetrizer, Ω_0 is an orbital product

$$\Omega_0 = \phi_1(1)\phi_2(2)\cdots\phi_N(N) \tag{2}$$

and Θ_K is a spin function. For VB approaches, spin functions are Rumer bases

$$
\begin{aligned}
\Theta_K &= 2^{-1/2}[\alpha(i_1)\beta(j_1) - \beta(i_1)\alpha(j_1)] \times 2^{-1/2}[\alpha(i_2)\beta(j_2) - \beta(i_2)\alpha(j_2)]\cdots \\
&= \prod_{(ij)} 2^{-1/2}[\alpha(i)\beta(j) - \beta(i)\alpha(j)]\prod_k \alpha(k),
\end{aligned} \tag{3}
$$

where (ij) runs over all bonds and k over all unpaired electrons. Given an orbital product Ω_0, a complete set of VB functions is constructed by choosing the spin functions Θ_K. Using the antisymmetry property of electron indices in VB functions, one can rewrite the VB function, Eq. (1), as

$$\Psi_K = \hat{A}\Omega_K\Theta_0, \tag{4}$$

where

$$\Theta_0 = 2^{-1/2}[\alpha(1)\beta(2) - \beta(1)\alpha(2)] \times 2^{-1/2}[\alpha(3)\beta(4) - \beta(3)\alpha(4)]\cdots \tag{5}$$

and

$$\Omega_K = 2^{-1/2}[\phi_{i_1}(1)\phi_{j_1}(2) + \phi_{j_1}(1)\phi_{i_1}(2)] \times 2^{-1/2}[\phi_{i_2}(3)\phi_{j_2}(4) + \phi_{j_2}(3)\phi_{i_2}(4)]\cdots \tag{6}$$

Eq. (4) shows that a complete set of VB functions can also be given by fixing

a spin function and changing the orbital product Ω_K.

The antisymmetrizer can be decomposed into $e_{rs}^{[\lambda]}$ and $e_{\tilde{r}\tilde{s}}^{[\tilde{\lambda}]}$, the operators which operate on the orbital and spin spaces, respectively, as [41]

$$\hat{A} = \sum_r \Lambda_r^{[\lambda]} e_{rs}^{[\lambda]} e_{\tilde{r}\tilde{s}}^{[\tilde{\lambda}]}, \tag{7}$$

where $\Lambda_r^{[\lambda]} = (\pm 1)$ is a coupling coefficient, $[\tilde{\lambda}]$ is the conjugate representation of $[\lambda]$, and the projector is defined through the irreducible representation matrix elements, $D_{rs}^{[\lambda]}(P)$, as

$$e_{rs}^{[\lambda]} = \left(\frac{f_\lambda}{N!}\right)^{1/2} \sum_P D_{rs}^{[\lambda]}(P) P. \tag{8}$$

Thus, one can have

$$\Psi_K = N_K \sum_r \Lambda_r^{[\lambda]} e_{rs}^{[\lambda]} \Omega_K e_{\tilde{r}\tilde{s}}^{[\tilde{\lambda}]} \Theta_0, \tag{9}$$

where N_K is a normalization factor and $[\lambda] = [2^{N/2-S}, 1^{2S}]$. It can be easily proved that

$$e_{rs}^{[\lambda]} \Omega_K = \delta_{s1} e_{r1}^{[\lambda]} \Omega_K. \tag{10}$$

Using Eq. (10) and the properties of the first Young tableau [31], one can reduce Eq.(9) to

$$\Psi_K = N_K \sum_r \Lambda_r^{[\lambda]} e_{r1}^{[\lambda]} \Omega_K e_{\tilde{r}1}^{[\tilde{\lambda}]} \Theta_0, \tag{11}$$

where Ω_K is now simply an orbital product,

$$\Omega_K = \phi_{i_1}(1)\phi_{j_1}(2)\phi_{i_2}(3)\phi_{j_2}(4)\cdots. \tag{12}$$

In spin-free quantum chemistry, matrix elements of a spin-independent

148

Hamiltonian are determined only by the spin-free function

$$\Phi_K = N_K e_{r1}^{[\lambda]} \Omega_K, \tag{13}$$

which is called a bonded tableau (BT) state [31, 42], and where N_K is a new normalization factor. In Eq. (13) one omits r from Φ_K since the matrix elements are independent of r in the spin-free treatment. A BT basis can be denoted as

$$\begin{vmatrix} a & a' \\ b & b' \\ c & c' \\ \cdot & \cdot \\ \cdot & \\ \cdot & \end{vmatrix} = N_K e_{r1}^{[\lambda]} \phi_a(1)\phi_{a'}(2)\phi_b(3)\phi_{b'}(4)\cdots, \tag{14}$$

which clearly corresponds to a VB structure with bonds a-a', b-b', c-c', ...

It is proved that BTs have the following symmetry properties, which exactly echo the symmetries of VB structures:

$$\begin{vmatrix} a & b \\ \cdot & \cdot \\ \cdot & \cdot \\ \cdot & \\ \cdot & \end{vmatrix} = \begin{vmatrix} b & a \\ \cdot & \cdot \\ \cdot & \cdot \\ \cdot & \\ \cdot & \end{vmatrix}, \tag{15}$$

$$\begin{vmatrix} a & b \\ \cdot & \cdot \\ c & d \\ \cdot & \\ \cdot & \end{vmatrix} = \begin{vmatrix} c & d \\ \cdot & \cdot \\ a & b \\ \cdot & \\ \cdot & \end{vmatrix}, \tag{16}$$

$$\begin{vmatrix} \cdot & \cdot \\ \cdot & \cdot \\ \cdot & \cdot \\ a & \\ b & \end{vmatrix} = -\begin{vmatrix} \cdot & \cdot \\ \cdot & \cdot \\ \cdot & \cdot \\ b & \\ a & \end{vmatrix}, \tag{17}$$

$$\begin{vmatrix} a & b \\ c & \cdot \\ \cdot & \cdot \\ \cdot & \\ \cdot & \end{vmatrix} = -\begin{vmatrix} b & c \\ a & \cdot \\ \cdot & \cdot \\ \cdot & \\ \cdot & \end{vmatrix} - \begin{vmatrix} a & c \\ b & \cdot \\ \cdot & \cdot \\ \cdot & \\ \cdot & \end{vmatrix}, \tag{18}$$

$$\begin{vmatrix} a & b \\ b & \cdot \\ \cdot & \cdot \\ \cdot & \\ \cdot & \end{vmatrix} = -\begin{vmatrix} b & b \\ a & \cdot \\ \cdot & \cdot \\ \cdot & \\ \cdot & \end{vmatrix}. \tag{19}$$

For a given orbital configuration, various BTs can be constructed by taking different orbital pairing schemes. Like VB structures, all possible BTs form an overcomplete set and are not independent of each other. The construction of a complete BT set from an overcomplete one is not unique. For the VB approach, one can define the functions corresponding to canonical VB structures as the canonical BTs (CBTs). By this definition, all doubly occupied orbitals are placed in the upper part of the tableau. In the lower part, each two bonding orbitals occupy the same row, while the unpairing orbitals are inserted in the single-column part. Another simple way to construct CBTs is to follow the Weyl rules [31], which is more suitable for CI procedures in molecular orbital theory.

2.2 Matrix elements of the Hamiltonian and overlap

In the spin-free VB theory, the many-electron wavefunction for a system is expressed as a linear combination of spin-free VB functions

$$\Psi = \sum_K C_K \Phi_K. \tag{20}$$

Clearly Φ_K may be a BT, defined by Eq. (13). The Hamiltonian and overlap matrix elements are now written as

$$H_{KL} = \langle \Phi_K | H | \Phi_L \rangle = \sum_{P \in S_N} D_{11}^{[\lambda]}(P) \langle \Omega_K | HP | \Omega_L \rangle \tag{21}$$

and

$$M_{KL} = \langle \Phi_K | \Phi_L \rangle = \sum_{P \in S_N} D_{11}^{[\lambda]}(P) \langle \Omega_K | P | \Omega_L \rangle, \tag{22}$$

respectively. The coefficients C_K in Eq. (20) are easily determined by solving the usual secular equation $\mathbf{HC} = E\mathbf{MC}$. The orbital products Ω_K and Ω_L in Eqs. (21) and (22) are given according to their corresponding VB structures. For the sake of convenience, they are supposed to be

$$\Omega_K = U = u_1(1)u_2(2)\cdots u_N(N), \tag{23a}$$

$$\Omega_L = V = v_1(1)v_2(2)\cdots v_N(N), \tag{23b}$$

and follow the notations

$$s_{ij} = \langle u_i | v_j \rangle, \quad f_{ij} = \langle u_i | f | v_j \rangle, \quad g_{ij,kl} = \langle u_i u_j | g | v_k v_l \rangle. \tag{24}$$

It is evident that the matrix elements of the Hamiltonian and overlap are independent of the index r of BT in Eq. (13) and only the first diagonal element of the irreducible representation matrix, $D_{11}^{[\lambda]}(P)$, is required, which has been well discussed [31, 33, 42, 43], and is easily determined. It is worthwhile to emphasize that Eqs. (21) and (22) are the unique formulas of the matrix elements in the spin-free approach, even though one can take some other forms of VB functions. For example, it is possible to construct VB functions by Young operator [2], but the forms of the matrix elements are identical to Eqs. (21) and (22) [44].

Both of Eqs. (21) and (22) involves $N!$ terms due to $N!$ permutations of the symmetric group S_N, which is similar to a determinant expansion or a permanent, except for different coefficients. If one-electron functions are orthogonal, only a few terms are non-zero and make contributions to the matrix elements [42], and consequently the matrix elements are conveniently obtained. However, the use of

non-orthogonal orbitals is one of the most important characterstics of a VB approach, and thus all $N!$ terms make contributions to the matrix elements. There have been very efficient algorithms for the evaluation of a determinant, and it is not too difficult to evaluate a permanent. Unfortunately, there is still no efficient algorithm for the evaluation of Hamiltonian and overlap matrix elements. This is the well-known "$N!$" difficulty in valence bond theory. In the next section, we will define a new function, called paired-permanent-determinant (PPD) [39], to discuss how to calculate Hamiltonian matrix elements as efficiently as possible, which will enable one to implement a spin-free VB program.

3. PAIRED-PERMANENT-DETERMINANT ALGORITHM FOR NONORTHOGONAL VALENCE BOND METHOD

In this section, a new function, called paired-permanent-determinant (PPD), is introduced, which is an algebrant. An overlap matrix element in the spin-free VB method may be obtained by evaluating a corresponding PPD, while the Hamiltonian matrix element is expressed in terms of the products of electronic integrals and sub-PPDs.

3.1 Paired-permanent determinant (PPD) function

Given an $N \times N$ square matrix $A = \{a_{ij}, i, j = 1, 2, \cdots, N\}$, the PPD of A for the irreducible representation $[\lambda]$ is the number

$$\mathrm{ppd}(\lambda, A) = \sum_{P \in S_N} D_{11}^{[\lambda]}(P) a_{1p_1} a_{2p_2} \cdots a_{Np_N}, \qquad (25)$$

where

$$P = \begin{pmatrix} 1 & 2 & \cdots & N \\ p_1 & p_2 & \cdots & p_N \end{pmatrix} \qquad (26)$$

and the summation extends over all $N!$ permutations of S_N. In a similar fashion to a determinant, one can denote a PPD by

$$\mathrm{ppd}(\lambda, A) = \begin{Vmatrix} a_{11} & a_{12} & \cdots & a_{1,n} & a_{1,n+1} & \cdots & a_{1N} \\ a_{21} & a_{22} & \cdots & a_{2,n} & a_{2,n+1} & \cdots & a_{2N} \\ \vdots & \vdots & & \vdots & \vdots & & \vdots \\ a_{n,1} & a_{n,2} & \cdots & a_{n,n} & a_{n,n+1} & \cdots & a_{n,N} \\ a_{n+1,1} & a_{n+1,n+1} & \cdots & a_{n+1,n} & a_{n+1,n+1} & \cdots & a_{n+1,N} \\ \vdots & \vdots & & \vdots & \vdots & & \vdots \\ a_{N,1} & a_{N,2} & \cdots & a_{N,n} & a_{N,n+1} & \cdots & a_{N,N} \end{Vmatrix}, \tag{27}$$

where $n = N - 2S$. The right hand side of Eq. (27) may be divided into 4 zones. Two diagonal zones of $n{\times}n$ and $(N - n){\times}(N - n)$ are, respectively, the "paired zone" [39], which describes bonding electron pairs in the VB method, and the "unpaired" zone, which is for unpairing electrons. Two off-diagonal zones are for the interactions between paring and unparing electrons. For simplicity, one may also denote $\mathrm{ppd}(\lambda, A)$ as

$$\mathrm{ppd}(\lambda, A) = \left\| a_{(1,2,\ldots,i,\bar{i},\ldots,n;n+1,\ldots,N)}^{(1,2,\ldots,i,\bar{i},\ldots,n;n+1,\ldots,N)} \right\|, \tag{28}$$

where the superscript $(1, 2, \ldots, n; n + 1, \ldots, N)$ of a is the order of the row in array A, and the subscript $(1, 2, \ldots, n; n +1, \ldots, N)$ is the order of the column. In a similar fashion to a determinant or a permanent, the PPD is an algebrant that depends not only on the matrix A, but also on the irreducible representation $[\lambda]$. For $S = 0$, only the "paired" zone exists, which is also called paired-permanent [38], while for $[\lambda] = [1^N]$, only the "unpaired" zone exits, which is exactly a determinant.

According to the symmetry properties of $D_{11}^{[\lambda]}(P)$, one can divide row and column indices of a PPD into two sets: paired symmetry indices (PSI) $i, i \leq N - 2S$, and anti-symmetry indices (ASI) $i, i > N-2S$. Furthermore, $2k-1(2k)$ is refered to as the partner of $i = 2k (2k-1)$, denoted as $\bar{i}$, if i is a PSI. Evidently, PPDs shares symmetries similar to the BTs, as follows:

1. $\mathrm{ppd}(\lambda, A)$ is invariant under transposition, and one may write

$$\mathrm{ppd}(\lambda, A) = \mathrm{ppd}(\lambda, A^{\mathrm{T}}), \tag{29}$$

2. $\mathrm{ppd}(\lambda, A)$ is invariant under exchange between row (column) i and row (column) $\bar{i}$,

$$\left\| a_{(1,2,\ldots,i,\bar{i},\ldots,n;n+1,\ldots,N)}^{(1,2,\ldots,i,\bar{i},\ldots,n;n+1,\ldots,N)} \right\| = \left\| a_{(1,2,\ldots,i,\bar{i},\ldots,n;n+1,\ldots,N)}^{(1,2,\ldots,\bar{i},i,\ldots,n;n+1,\ldots,N)} \right\|, \tag{30}$$

3. $ppd(\lambda, A)$ is invariant under exchanges between row (column) i and row (column) j and between row (column) $\bar{i}$ and row (column) $\bar{j}$,

$$\left\| a_{(1,2,\ldots,i,\bar{i},\ldots,j,\bar{j},\ldots,n;n+1,\ldots,N)}^{(1,2,\ldots,i,\bar{i},\ldots,j,\bar{j},\ldots,n;n+1,\ldots,N)} \right\| = \left\| a_{(1,2,\ldots,i,\bar{i},\ldots,j,\bar{j},\ldots,n;n+1,\ldots,N)}^{(1,2,\ldots,j,\bar{j},\ldots,i,\bar{i},\ldots,n;n+1,\ldots,N)} \right\|, \tag{31}$$

4. $ppd(\lambda, A)$ changes its sign under exchange between row (column) i and row (column) j, if $i, j \in API$.

Various PPDs may be obtained by exchanging the row (column) indices for a given matrix A. The total number of the PPDs is

$$\frac{N!}{2^{N/2-S}(N/2-S)!(2S)!}, \tag{32}$$

due to the row (column) symmetries of the PPD. Like BTs, all PPDs obtained from a given A form an overcomplete set. One can refer to the independent PPDs as canonical PPDs. The definition of canonical PPD may be given by either the standard Young tableaux or the Rumer rule.

Eq. (25) may be rewritten as

$$ppd(\lambda, A) = \sum_{P \in S_N} D_{11}^{[\lambda]}(P) P \overline{\Omega_0}, \tag{33}$$

where

$$\Omega_0 = a_{11} a_{22} \cdots a_{N-1,N-1} \, a_{N,N}, \tag{34}$$

and permutation P operates on the second index of a_{ij}. Exchanging the columns of the matrix A, one can have various PPDs,

$$\Phi(g) \equiv \text{ppd}(\lambda, A_g) = \sum_{P \in S_N} D_{11}^{[\lambda]}(P) P g^{-1} \Omega_0, \tag{35}$$

where g is the permutation permuting the column indices of the matrix A to get the new matrix A_g. It is clear that the canonical PPDs may be defined as

$$\Phi_i \equiv \Phi(\sigma_{i1}) = \sum_{P \in S_N} D_{11}^{[\lambda]}(P) P \sigma_{1i} \Omega_0, \tag{36}$$

where σ_{i1} is the permutation permuting the index numbers of the first Young tableau to those of Young tableau i. It can be shown that a PPD associated with permutation g may be expressed as

$$\Phi(g) = \sum_{i,j} B_{ij}^{-1} D_{j1}^{[\lambda]}(g) \Phi_i, \tag{37}$$

where the matrix B is defined as

$$B_{ij} = D_{i1}^{[\lambda]}(\sigma_{j1}), \tag{38}$$

which is in upper triangular form [44]. Thus, $\Phi(g)$ may be expressed in terms of the linear combination of canonical PPDs,

$$\Phi(g) = \sum_i C_i(g) \Phi_i, \tag{39}$$

where

$$C_i(g) = \sum_j B_{ij}^{-1} D_{j1}^{[\lambda]}(g). \tag{40}$$

3.2 Evaluation of PPDs

It is clear from the above discussion that the difference between a PPD and its corresponding determinant solely lies in the coefficients of the permutation P. Unfortunately, this makes PPDs unable to share many of the nice properties of determinants. For instance, the basic multiplicative law valid for determinants

$$\det(AB) = \det(A)\det(B) \tag{41}$$

is flagrantly false for PPDs. Also, the addition of a multiple of one row (column) of A to another does not leave $ppd(\lambda, A)$ invariant. These facts greatly limit the exploration of computational techniques for $ppd(\lambda, A)$. Fortunately, the Laplace expansion for determinants has a simple counterpart for PPDs. A procedure for evaluating $ppd(\lambda, A)$, which is similar to the Laplace expansion method, has been presented. We now briefly describe the procedure and give an example.

It can be shown that a PPD of order N may be obtained by evaluating $N(N-1)/2$ PPDs of order $N-2$ as follows,

$$ppd(\lambda, A) = \sum_{k<l} d_{kl} A_{ii}^{kl} \, ppd(\lambda_1, A_{(ii)}^{(kl)}), \tag{42}$$

where $d_{kl} = 1$, if $k, l \in$ PSI, and $l = \bar{k}$; $d_{kl} = -1/2$, if $k \in$ PSI, but $l \neq \bar{k}$; $d_{kl} = 0$, if $k, l \in$ ASI, A_{ii}^{kl} is a PPD with order 2

$$\begin{Vmatrix} a_{ki} & a_{k\bar{i}} \\ a_{li} & a_{l\bar{i}} \end{Vmatrix} = a_{ki} a_{l\bar{i}} + a_{k\bar{i}} a_{li}, \tag{43}$$

and $ppd(\lambda_1, A_{(ii)}^{(kl)})$ is a sub-PPD of $[\lambda_1] = [2^{N/2-S-1}, 1^{2S}]$ obtained by removing rows k, l and column $i, \bar{i}$ of A, whose order is such that the column indices remain unchanged, and the row indices remain unchanged if $l = \bar{k}$, otherwise l is replaced by $\bar{k}$.

Example. A PPD with $N = 6$ and $S = 1$ is expanded as

$$\mathrm{ppd}([2^2,1^2],A) = m_{12}\Delta_{12} + m_{34}\Delta_{34} - \frac{1}{2}\sum_{i=1}^{2}\sum_{j=3}^{4} m_{ij}\Delta_{ij} - \frac{1}{2}\sum_{i=3}^{4}\sum_{j=5}^{6} m_{ij}\Delta_{ij} \ ,$$

where m_{ij} is a minor, defined as

$$m_{ij} = A_{12}^{ij} = \begin{Vmatrix} a_{i1} & a_{i2} \\ a_{j1} & a_{j2} \end{Vmatrix},$$

and Δ_{ij} is its corresponding complement $\mathrm{ppd}([2^1,1^2],A_{(12)}^{(ij)})$.

Furthermore, a complementary minor can be evaluated as follows:

$$\mathrm{ppd}([2^1,1^2],A_{(12)}^{(12)}) = \begin{Vmatrix} a_{33} & a_{34} \\ a_{43} & a_{44} \end{Vmatrix}\begin{Vmatrix} a_{55} & a_{56} \\ a_{65} & a_{66} \end{Vmatrix} - \frac{1}{2}\begin{Vmatrix} a_{33} & a_{34} \\ a_{53} & a_{54} \end{Vmatrix}\begin{Vmatrix} a_{45} & a_{46} \\ a_{65} & a_{66} \end{Vmatrix}$$

$$- \frac{1}{2}\begin{Vmatrix} a_{33} & a_{34} \\ a_{63} & a_{64} \end{Vmatrix}\begin{Vmatrix} a_{55} & a_{56} \\ a_{45} & a_{46} \end{Vmatrix} - \frac{1}{2}\begin{Vmatrix} a_{53} & a_{54} \\ a_{43} & a_{44} \end{Vmatrix}\begin{Vmatrix} a_{35} & a_{36} \\ a_{65} & a_{66} \end{Vmatrix} \qquad (44)$$

$$- \frac{1}{2}\begin{Vmatrix} a_{63} & a_{64} \\ a_{43} & a_{44} \end{Vmatrix}\begin{Vmatrix} a_{55} & a_{56} \\ a_{35} & a_{36} \end{Vmatrix}$$

With Eq. (42), one expands a PPD by choosing a PPD of order 2 as a minor, and the complementary minor is still a PPD. One can also take a minor from the ASI part.

It can be shown [39] that a PPD can also be expanded as follows:

$$\mathrm{ppd}(\lambda, A) = \sum_{k=1}^{N} a_{kl}\, \mathrm{cppd}(\lambda_2, A_{(l)}^{(k)}), \quad l \in \mathrm{ASI}, \qquad (45)$$

and

$$\text{cppd}(\lambda_2, A_l^k) = \begin{cases} -\dfrac{1}{2S+1}\sum_{q \in Q}(-1)^q\, \text{ppd}(\lambda_2, A_{q(l)}^{(k)}), & k \in \text{PSI} \\ -\text{ppd}(\lambda_2, A_{(l)}^{(k)}), & k \in \text{ASI, but } k \neq l \,, \\ \text{ppd}(\lambda_2, A_{(l)}^{(l)}), & k = l \end{cases} \tag{46}$$

where $\text{cppd}(\lambda_2, A_{(l)}^{(k)})$ may be considered as the complementary minor of a_{kl}, $[\lambda_2] = [2^{N-2S}, 1^{2S-1}]$, $A_{(l)}^{(k)}$ is an $(N-1) \times (N-1)$ array obtained by interchanging the kth and the lth rows of A and then removing the kth row and the Nth column, A_q is an $N \times N$ array obtained by operating q on the row indices of A, and the Q contains all transposition (kl), $l \in \text{ASI}$, which is to act on the row indices of $A_{(l)}^{(k)}$.

Clearly, Eq. (45) reduces to the formula for the Laplace expansion of a determinant, if $[\lambda] = [1^N]$.

Example. A PPD with $N = 6$ and $S = 1$ is also expanded as

$$\text{ppd}([2^2, 1^2], A) = -\frac{1}{3}\sum_{i=1}^{4} a_{i6}(\text{ppd}([2^2, 1^1], A_{(6)}^{(i)}) - \text{ppd}([2^2, 1^1], A_{(56)(6)}^{(i)}))$$
$$- a_{56}\,\text{ppd}([2^2, 1^1], A_{(6)}^{(5)}) + a_{66}\,\text{ppd}([2^2, 1^1], A_{(6)}^{(6)})$$

Generally, Eq. (45) is much more troublesome than Eq. (42) and it is not essential to the evaluation of a PPD. However, it is of great importance to the application in the VB approach. Using Eq. (45) successively, one can expand a PPD by taking a determinant with order 2 as a minor [39], which is also required in the VB approach.

The discussion so far is applicable to any given spin number S. It is clear that the expansion of a PPD, Eq. (42), will be greatly simplified if the spin number $S = 0$. In this case there are not ASI indices any more, and only two values, 1 or $-1/2$, are taken for d_{kl}. Furthermore, it is possible to choose a PPD with any even order m as a minor.

It can be shown that

$$\text{ppd}(\lambda, A) = \sum_{(m)} d_{(m)}\,\text{ppd}(\lambda_1, A_{(m)})\,\text{ppd}(\lambda_2, A_{(N-m)})\,, \tag{47}$$

where $[\lambda_1] = [2^{m/2}]$, $[\lambda_2] = [2^{(N-m)/2}]$, $A_{(m)}$ is an $m \times m$ array by taking m rows and m

columns $1, 2, \ldots, m$ from A, the summation runs over all possibilities of choosing m indices from N indices and all possibilities of the index arrangements of the m: indices that partner each other in A still remain in pairs, while indices that are unpaired in A should be paired with each other. $\text{ppd}(\lambda_2, A_{(N-m)})$ is the complementary minor of $\text{ppd}(\lambda_1, A_{(m)})$, whose index order is such that indices that partner each other in A still remain in pairs, indices should be paired if their partners are paired in $A_{(m)}$ but not in A. $d_{(m)}$ is given by

$$d_{(m)} = \frac{(-1)^{m'}}{(m'-1)!} \, , \tag{48}$$

where m' is the number of pairs whose indices are unpaired in A.

3.3 Formulas for Hamiltonian and overlap matrix elements in the PPD algorithm

It is evident from the definition of the PPD, Eq. (25), that the spin-free form of VB function, Eq. (13), is a PPD associated with matrix $V = \{v_j(i)\}$, i.e.,

$$\Phi_K = \left(\frac{f_\lambda}{N!}\right)^{1/2} \text{ppd}(\lambda, V) \, , \tag{49}$$

where the normalization factor N_K is neglected, and the overlap is also a PPD, given by

$$M_{KL} = \text{ppd}(\lambda, S) \, , \tag{50}$$

where S is the matrix of orbital overlap, $S = (s_{ij})$.

Clearly, the overlap matrix elements can be simply obtained by the procedure for evaluating a PPD discussed above.

The expression of the Hamiltonian matrix elements is a little complicated. For simplicity, only the case of $S = 0$ is discussed here. The treatment for systems with arbitrary spin number has been described elsewhere [39].

The Hamiltonian operator is

$$H = \sum_{i=1}^{N} f(i) + \sum_{i,j}^{N} g(i,j). \tag{51}$$

Using the definition of partner indices, Eq. (51) is rewritten as

$$H = \sum_{i=1}^{N} H(i) + \sum_{i,j}^{N} G(i,j), \tag{52}$$

where

$$H(i) = f(i) + f(\bar{i}) + g(i,\bar{i}), \tag{53}$$

$$G(i,j) = g(i,j) + g(i,\bar{j}) + g(\bar{i},j) + g(\bar{i},\bar{j}), \tag{54}$$

and the summation runs over $i,j = 1,3,\cdots,N-1$.

Using Eq. (42), the contribution from $H(i)$ to the Hamiltonian matrix element H_{KL} is

$$H_{KL}(i) = \sum_{k<l} d_{kl} H_{ii}^{kl} \, \text{ppd}(\lambda_1, S_{(i\bar{i})}^{(kl)}), \tag{55}$$

where

$$H_{ii}^{kl} = f_{ik} s_{\bar{i}l} + f_{il} s_{\bar{i}k} + f_{\bar{i}k} s_{il} + f_{\bar{i}l} s_{ik} + g_{i\bar{i},kl} + g_{i\bar{i},lk}, \tag{56}$$

and $S_{(i\bar{i})}^{(kl)}$ is an $(N\text{-}2)\times(N\text{-}2)$ array obtained by removing rows k and l and columns i and $\bar{i}$ of the overlap matrix S.

Using Eq. (42) successively, the contribution from $G(i,j)$ to H_{KL} is

$$G_{KL}(i,j) = \sum_{\substack{k<l,m<n \\ k<m,l\neq m,n}} d_{kl,mn} G_{iijj}^{klmn} \, \text{ppd}(\lambda_2, S_{iijj}^{klmn}). \tag{57}$$

In the above equation, $[\lambda_2] = [2^{N/2-2}]$, S_{iijj}^{klmn} is an $(N-4)\times(N-4)$ array obtained by removing rows $k,l,m,$ and n and columns $i,\bar{i},j,$ and $\bar{j}$, The value of $d_{kl,mn}$ is given as follows:

a. $d_{kl,mn} = 1$, if $l = \bar{k}, n = \overline{m}$; $\tag{58a}$

b. $d_{kl,mn} = -\dfrac{1}{2}$, if $l \neq \bar{k}, n = \overline{m}$, or $l = \bar{k}, n \neq \overline{m}$; $\tag{58b}$

c. $d_{kl,mn} = -\dfrac{1}{2}$, if $k = \overline{m}, l = \bar{n}$; $\tag{58c}$

d. $d_{kl,mn} = \dfrac{1}{4}$, if $l \neq \bar{k}, \bar{n}, m \neq \bar{n}$, $\tag{58d}$

and G_{klmn}^{iijj} involves 32 terms as follows:

$$G_{klmn}^{iijj} = \sum_{\substack{t=i,\bar{i},t'=j,\bar{j} \\ r=k,l,s=m,n}} (g_{tt',rs} s_{\bar{t}r'} s_{\bar{t}'s'} + g_{tt',sr} s_{\bar{t}s'} s_{\bar{t}'r'}). \tag{59}$$

With Eqs. (55) and (57), the Hamiltonian matrix elements are finally written in the form of PPDs as

$$H_{KL} = \sum_{k<l} d_{kl} \sum_i H_{ii}^{kl} \, \text{ppd}(\lambda_1, S_{ii}^{kl}) + \sum_{\substack{k<l,M<n \\ k,m,l\neq m,n}} d_{kl,mn} \sum_{i<j} G_{iijj}^{klmn} \, \text{ppd}(\lambda_2, S_{iijj}^{klmn}). \tag{60}$$

4. XIAMEN-99 – AN *AB INITIO* SPIN-FREE VALENCE BOND PROGRAM

Xiamen-99 is an *ab initio* spin-free valence bond package. It is based on the

paired-permanent-determinant algorithm. The Hamiltonian and overlap matrix elements are derived from the evaluation of PPDs. In this section, a description of the package is briefly given, including the algorithm and its capabilities.

4.1 The implementation of the evaluation of a PPD

As shown in the last section, Hamiltonian and overlap matrix elements are expressed in terms of PPDs. A practical VB package highly depends on an efficient routine for the evaluation of a PPD. Although a PPD may be expressed in terms of sub-PPDs of any given order and their complementary minors, in the present version of Xiamen-99, an algorithm of $2 \times (N\text{-}2)$ expansion is used. This is because the 1-e and 2-e electron integrals may be built as "effective" 2×2 PPDs.

A procedure for the evaluation involves two parts: one being the numerical operations of matrix elements, the other being the index operations of the sub-PPDs. It is obvious that the index operation is independent of the system that is being studied. To save CPU time in VB applications, all index operations are pre-computed and stored in the file that accompanies the source code of the package. In addition, all sub-PPDs that are required in the evaluation are computed first and are labeled. This will enable one to avoid repeated computations of sub-PPDs and minimize the computational effort in the calculation.

4.2 The evaluation of the energy and its gradient vector

From Eq. (50), an overlap matrix element is exactly a PPD and can easily be evaluated from the routine for PPDs, while Hamiltonian matrix elements may be obtained by a similar routine to that for PPDs, where 2×2 sub-PPDs are replaced with "effective" sub-PPDs of one-electron and two-electron integrals.

As mentioned in Section 1, in a traditional VB treatment, a VB wavefunction is expressed as the linear combination of 2^m Slater determinants, where m is the number of covalent bonds in the system. For some applications in which only a few bonds are involved in the reaction, it is too luxurious to adopt the PPD algorithm, as the number of Slater determinants is still not too large to deal with. It would be more efficient to use a traditional Slater determinant expansion algorithm than the PPD algorithm. Therefore, as a complement, a Slater determinant expansion algorithm is also implemented in the package.

It is well known that energy gradient vectors play an important role in orbital optimization procedure. Because analytical energy gradient vectors in nonorthogonal VB approach are much more complicated than those of canonical molecular orbital method, and it is difficult to evaluate exact energy gradient vectors, in Xiamen-99, an approximate energy gradient vector is derived by using the generalized Brillouin theorem [45]. It is shown from our applications that this

approximation works well and removes much computational effort.

4.3 Valence bond orbital optimization

The most important feature of modern VB theory is that orbitals are allowed to optimize flexibly. The use of overlap-enhanced orbitals (OEOs) provides the key to the construction of VB functions of considerable accuracy and compactness. The disadvantage of OEOs is that they obscure the classical interpretation of covalent and ionic structures. Hybrid atomic orbitals (HAO), which are purely localized, provide a clear understanding of the nature of chemical bonding and are widely applied to VB studies of chemical reactions. But the VB function with HAOs is usually not as compact as that of OEOs, unless the breathing orbital valence bond (BOVB) [46] approach is applied. Bond-distorted orbital (BDO) sets are a balance between OEO and HAOs, where only bonding orbitals are allowed to mix. A wavefunction for a covalent structure using BDOs covers 3 localized VB structures: one being covalent, and the other two being ionic. Therefore, it provides a very clear and compact VB wavefunction for diabatic curve in a valence bond state correlation diagram (VBSCD) [47]. In the Xiamen-99 package, VB orbitals may be defined and optimized flexibly. One can take OEOs, HAOs, or BDOs as VB orbitals, or any other forms for some special purposes in applications.

The orbital optimization method adopted in the package is based on the Davidon-Fletcher-Powell (DFP) family of variable metric methods [48]. In these methods, only the energy and its gradient vector are required, with information from successive line minimizations being accumulated and used to build up an approximate Hessian matrix. It is necessary but time consuming to perform the line minimization needed in most multidimensional optimization methods. A simple algorithm is implemented in the package, in which only one evaluation of energy and gradient vector is required in each iteration (except on rare occasions – which are tested for and corrected). In addition to the use of the generalized Brillouin theorem to build approximate gradient vectors, a routine using a numerical difference algorithm is also available in the package to evaluate gradient vectors. Furthermore, Powell's steepest descent algorithm is also implemented, but our experience shows that it is inferior to other options.

4.4 Capabilities of Xiamen-99

Xiamen-99 is a "pure" *ab initio* valence bond program. One can use the package to do any types of VB calculations with any forms of VB orbitals. This means that VBSCF, BOVB, and VBCI calculations may be carried out with the package, and it is also feasible to combine the valence bond method with some advanced molecular orbital methods, like VB-DFT [49].

Coefficients and weights of VB structures are given in the output file, and optimized orbitals and charge population analysis are also available from the output file.

5. APPLICATIONS

5.1 Resonance

5.1.1 Synopsis
Resonance was introduced when it was found that there are many molecules whose properties cannot be accounted for by means of a single electronic structure of the VB type, but rather by a combination of several structures [1]. Although there is an element of arbitrariness in the resonance theory, in the sense of choosing VB structures, Wheland [50] systemized the basic principles to select the important resonance structures as well as to estimate their relative contribution to the ground state of a molecule. In fact, the qualitative resonance theory enjoyed such a great success due to its convenience and usefulness that resonance has become one of the most fundamental concepts in chemical theory.

With the advent of the computer era, it is now possible to reexamine and rethink the resonance theory at the *ab initio* level. For example, throughout Pauling and Wheland's books, benzene is supposed to be a hybrid of two Kekulé structures, by noting that Dewar and other ionic structures make little contribution to the resonance in benzene. However, classical *ab initio* VB calculations with all possible 175 resonance structures by Norbeck et al. [51] and Tantardini et al. [3], where strictly atomic orbitals are used to construct VB functions, manifested that the five covalent Kekulé and Dewar structures make even less contribution to the ground state of benzene than the other 170 ionic structures. This prompts us to reconsider the mathematical formulations for resonance structures [52].

From the viewpoint of classical VB, a bond between two atomic orbitals χ_A and χ_A centered on atoms A and B, respectively, can be expressed as a combination of a covalent structure and two ionic structures

$$\Psi_{AB} = C_1\Phi(A:B) + C_2\Phi(A^+B^-) + C_3\Phi(A^-B^+),$$ (61)

where

$$\Phi(A:B) = N_1 e_{11}^{[2]}(\chi_A\chi_B),$$ (62)

$$\Phi(A^+B^-) = N_1 e_{11}^{[2]}(\chi_B\chi_B),$$ (63)

$$\Phi(A^-B^+) = N_1 e_{11}^{[2]}(\chi_A\chi_A).$$ (64)

In the case of A = B, it was previously presumed that the two ionic structures are unimportant, but *ab initio* calculations verified the necessity to include the two ionic structures to describe accurately the A-B bond dissociation energy profile.

Bearing in the mind that a real bond should be described by three classical VB structures, we return to the case of benzene. Across the whole history of resonance theory, Kekulé structure has been treated as the hypothetical 1,3,5-cyclohexatiene whose double bonds are comparable to ethylene. However, it is clear from the previous paragraph that the π bond in ethylene should be expressed as a sum of three classical VB structures. Furthemore, there are three π bonds in a Kekulé structure. Consequently, from the mathematical point of view, the wave function for a Kekulé structure should be expanded by 3^3=27 classical VB structures as follows:

(1) (6) (3) (6) (3) (2) (6)
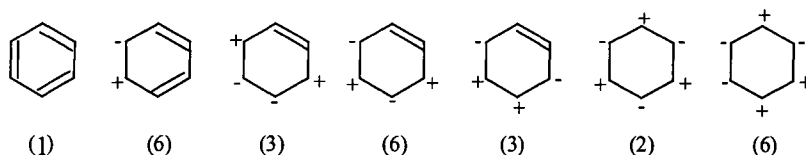
where the number in parentheses indicates the equivalent structures. In other words, there is no one-to-one correspondence between resonance structures and classical VB structures. This clarification is important since otherwise we can derive very different resonance energies with difference interpretations of the resonance theory.

The only notable difference between classical *ab initio* VB and modern *ab initio* VB lies in the one-electron orbitals. As we already mentioned, in the classical *ab initio* VB method, all one-electron orbitals are strictly atomic orbitals. In contrast, in modern *ab initio* VB methods, one-electron orbitals are not restricted to atomic orbitals anymore and are allowed to extend over the whole molecule in the form of OEOs

$$\chi'_\mu = \chi_\mu + \sum_{v\neq\mu}\lambda_{\mu v}\chi_v.$$ (65)

The significant advantage of this type of MO-like orbitals is that most of the correlation energy can be recovered with only a small number of VB structures. For example, for benzene, use of just the five covalent structures can recover 93%

of the correlation energy [53]. However, due to the delocalized nature of OEO's, they are not suitable for the construction of an individual resonance structure, e.g., when the resonance energies are to be evaluated. In that case, we proposed a type of localized orbitals called bond-distorted orbitals (BDOs) as[54]

$$\chi'_\mu = \chi_\mu + \lambda_{\mu\nu}\chi_\nu, \tag{66}$$

where $\lambda_{\mu\nu}=0$ if there is no bond between χ_μ and χ_ν. By adopting BDO's as one-electron orbitals, we are able to achieve almost the same energy as a VB-CI calculation with the 27 classical VB structure as shown above with only one VB structure.

5.1.2 Benzene vs. cyclobutadiene

Benzene and cyclobutadiene are the well-known examples for aromaticity and antiaromaticity, which have been the subject of extensive studies [55, 56]. While many criteria based on geometry, magnetism or energy have been proposed to discern the aromaticity/antiaromaticity, all of the energetic criteria are based on the design of model homodesmic and isodesmic reactions, where both the steric effect and the hyperconjugation effect are inevitably involved and cannot be distinctly screened from the reaction enthalpies. A more suitable refinement is to determine the aromaticity or antiaromaticity by the difference of the resonance energies, which are based on the Pauling-Wheland definition, between a cyclic conjugated compound and its corresponding linear polyene. Here we show the calculated results of resonance energies, which by definition are always positive, in benzene and cyclobutadiene.

In the framework of *ab initio* classical VB method, totally there are 175 and 20 VB structures for benzene and cyclobutadiene, respectively. On the other hand, for the hypothetically localized 1,3,5-cyclohexatriene and 1,3-cyclobutadiene, 27 and 9 classical VB structures are needed to run the VB-CI calculations. For all calculations, a STO-6G basis set is employed.

At first we define two types of resonance energies, namely vertical resonance energy (VRE) and theoretical resonance energy (TRE). The former is the energy difference between the optimal delocalized molecule such as benzene and the localized reference molecule such as 1,3,5-cyclohexatriene whose geometries are kept the same. The latter is the energy difference between the delocalized molecule and the optimal localized reference molecule, whose geometries are not kept the same. Fig.1 shows the relationship between VRE and TRE. The computed results are listed in Table 1.

Table 1

Optimized bond lengths and (R_{cc}) resonance energies (RE) in benzene and cyclobutadiene

	R_{CC} (Å)		Number of	RE
	Short	Long	VB structures	(kcal/mol)
Benzene	1.404	1.404	175	
Rigid 1,3,5-cyclohexatriene	1.404	1.404	27	-74.3
Stable 1,3,5-cyclohexatriene	1.343	1.521	27	-44.5
Cyclobutadiene	1.369	1.538	20	
Rigid 1,3-cyclobutadiene	1.369	1.538	9	-3.7
Stable 1,3-cyclobutadiene	1.355	1.555	9	-3.2
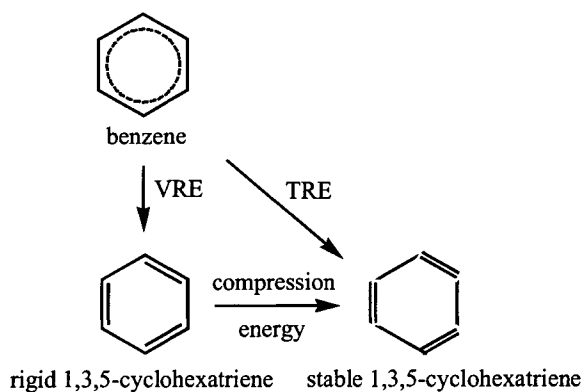
Fig. 1 Definitions of vertical resonance energy (VRE) and theoretical resonance energy (TRE)

The optimal bond lengths in the delocalized forms of benzene and cyclobutadiene are in good agreement with experimental or high-level computational data. However, the optimal bond lengths in the localized forms are nevertheless experimentally unavailable, and thus of particular interest. In 1,3,5-cyclohexatriene, the double bond length is 1.343 Å, almost identical to that of ethylene at the same full π-CI level. The single Csp^2-Csp^2 bond length, 1.521 Å, is somewhat shorter than the Csp^3-Csp^3 bond length in ethane [54]. Compared with 1,3,5-cyclohexatriene, both double and single bond lengths in 1,3-cyclobutadiene are longer, indicating the ring strain in the rectangular cyclobutadiene.

Experimentally, the estimation of resonance energy is based on the heat of hydrogenation or combustion, and the value for benzene is -36 kcal/mol, which is comparable to the TRE of -44.5 kcal/mol. The small discrepancy between the experimental resonance energy and TRE is due mainly to the hyperconjugation

effect in the reference system, cyclohexene [57].

5.1.3 Resonance effect in formamide

An understanding of the internal rotation about the amide bond is important because of its relevance to protein structure. Formamide is the simplest amide. The coplanarity and the remarkable rotational barrier about the C-N bond in formamide can be rationalized by resonance between the π electrons of the carbonyl group and the lone pair of the nitrogen atom [1, 50]. According to VB theory, the π electronic structure of formamide may be described by six resonance structures.
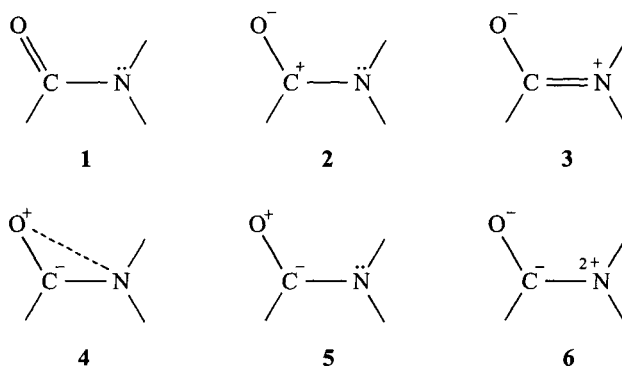
Contribution from resonance structure **3**, which contains a formal double bond between carbon and nitrogen, is considered to be primarily responsible for the coplanarity and the high rotational barrier about the amide bond [58]. The introduction of resonance structure **3** also implies that there is significant charge-delocalization from the nitrogen lone pair to the carbonyl oxygen.

However, the validity of the VB resonance model for formamide has been challenged on the basis of various population analyses. Wiberg et al. [59] found that the population on the carbonyl oxygen, which was calculated via integration of charge density difference maps, was essentially unchanged as a function of the torsional angle about the amide bond, and that the charge variation mainly occurs on the amide nitrogen and the carbonyl carbon. The oxygen is essentially a spectator during the rotation. It was further suggested that the VB resonance theory was not valid for formamide [60]. In contrast, Fogarasi and Szalay [61] analyzed geometric changes, charge shifts from Mulliken population analysis and NMR data as a function of rotation, and suggested that there is compelling evidence to support the simple amide resonance model, which was also confirmed

by the natural atomic orbital population analysis [62]. Lauvergnat and Hiberty [63] usefully probed the validity of the resonance model in formamide and thioformamide using the *ab initio* VB method, which allows one to turn on or off the electronic delocalization in these two molecules. The electronic delocalization energies are measured by comparing the fully delocalized (adiabatic) ground state and the localized, diabatic state, in which the nitrogen lone pair is constrained to remain strictly localized.
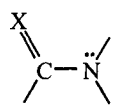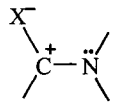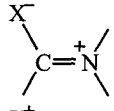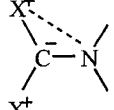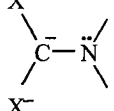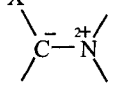
Here we revisit the VB resonance model in formamide by taking all six resonance structures into account. Such a study allows us to compare the individual contributions from resonance structures **1-6** to the resonance effect in formamide. For comparison, the isoelectronic systems vinylamine and formamidine are also investigated to gain insights into the trends of resonance stabilization. A 6-31G(d) basis set is employed in the calculations, and the orbitals in the VB functions are self-consistently determined for each resonance structure, but restricted to be atomic orbitals. The structural weights of the six resonance structures are listed in Table 2.

To derive the VRE's in these three conjugated systems, calculations with the three resonance structures **1**, **2** and **5** are also performed and the results are presented in Table 2.

It is clear that the covalent structure **1** makes the largest contribution to the ground state of the planar $HCXNH_2$ (X=O, CH_2 and NH) and its structural weight increases with the decreasing electronegativity of X or the polarization of the C=X bond. On the contrary, as the second most important resonance structure, the structural weight of **2** decreases in the order of X=O > NH > CH_2. The resonance structure **3**, which is essential to highlight the partial double bond between C and N, contributes only 13.1%, 9.8% and 7.0% to the ground states of formamide, formamidine and vinylamine, respectively. However, energetically the importance of the structure **3** cannot be overlooked. In fact, both resonance structures **3** and **4** are responsible for π electronic delocalization and the hindered rotational barrier in formamide. Our calculations are slightly different from the VB study on formamide by Felgg and Harcourt [64] using the minimal basis set, where the structural weights of **2** and **3** are underestimated (about 0.180 and 0.051, respectively) and the latter is even lower than that of structure **4** (0.074). However, the overall conclusions derived from the present VBSCF calculations are similar to those of Felgg and Harcourt, namely structures **1-4** should all be used to describe formamide. It is interesting to point out that numerous studies reported in the literature included only structures **1** and **3** to describe the resonance in formamide. Pauling[1] estimated that these two resonance structures contribute 60% and 40%, respectively, to the ground state of formamide, whereas Glendening et al. [62] found that the structural weights of **1** and **3** are 65.4% and

Table 2

Individual structural weights, total energies and VRE's from the VBSCF calculations with the 6-31G(d) basis set

Resonance structure		X=O		X=NH		X=CH$_2$	
		6VBSCF	3VBSCF	6VBSCF	3VBSCF	6VBSCF	3VBSCF
(structure)	1	0.4608	0.6007	0.5448	0.6775	0.6106	0.7250
(structure)	2	0.3180	0.3663	0.2463	0.2677	0.1902	0.1962
(structure)	3	0.1313		0.0976		0.0696	
(structure)	4	0.0649		0.0698		0.0689	
(structure)	5	0.0234	0.0330	0.0406	0.0548	0.0607	0.0788
(structure)	6	0.0016		0.0009		0.0000	

Total energy (a.u.)	-168.95863 -168.91937	-149.10165 -149.06855	-133.08376 -133.05673
VRE (kcal/mol)	-24.6	-20.8	-17.0

28.5%, respectively. The difference between the latter results and our present *ab initio* VB calculations is due to the definition of the one-electron orbitals used to construct the VB wave function. If the one-electron orbitals are not strictly atomic orbitals, the basis set polarization contribution can lead to the mixing of various classical VB structures. Thus, the "localized" structures of the forms **1** and **3** in *modern* VB can actually be expanded into the *classical* VB structures **1, 2, 5** and **3, 2, 6**, respectively.

Energetically, the resonance effect in the three systems decreases in the order of formamide > formamidine > vinylamine, which is consistent with the rule of atomic electronegativity. It is worthwhile to note that Wheland [50] estimated the resonance energy of formamide based on the heats of combustion and gave a

value of 22 kcal/mol, which is very close to our data. The significant resonance stabilization energy in formamide validates the applicability of the resonance model to formamide.

5.2 S_N2 reactions

The S_N2 reactions are good examples to highlight the different merits of VB and MO theories in quantum chemistry [65]. In the VB method, the atomic features are preserved and the focus is the two-electron-two-center bonds, and each molecule is formed with bonds (plus the lone and core pairs). Whereas one resonance structure is not enough to describe a molecule, multi-resonance structures are adopted. In fact, the resonance theory can also be applied to illustrate the reactions in an intuitive way. For example, for the chloride-exchange reaction

$$Cl^- + CH_3Cl \rightarrow ClCH_3 + Cl^-$$
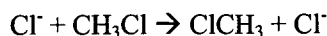
normally three resonance structures are used to describe the whole reaction potential energy profile,

$$\underset{a}{Cl^-\ CH_3\!-\!Cl} \qquad \underset{b}{Cl\!-\!CH_3\ Cl^-} \qquad \underset{c}{Cl^-\ CH_3{}^+\ Cl^-}$$
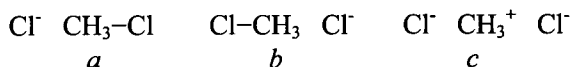
where a is the reactant structure and there is no chemical interaction between the left hand chloride anion and the carbon atom, and b is the product structure where no bond exists between the hand right chloride anion and the carbon atom. The last resonance structure c, whose energy is the highest in the gas phase, may play an important role in solutions due to its high ionicity. A useful qualitative description of the S_N2 reactions has been presented by Shaik and Pross using their empirical VB configuration-mixing model [66], which shows qualitatively how various substituents in different solvents may affect the reaction barrier [22]. Warshel and his coworkers [25] proposed an empirical VB (EVB) approach, which uses experimental information to evaluate the energies of the VB resonance structures and then calculate the environment-dependent stabilization of the ionic structures in the enzyme and in solutions.

Here we employed modern *ab initio* VB method to study several typical S_N2 reactions including chloride, fluoride and hydrid exchanges with the three resonance structures a, b and c, whose VB wave functions are expressed as

$$\Phi_a = N_a e_{11}^{[2^2]}(\chi_{Cl1}\chi_{Cl1}\chi_C\chi_{Cl2}), \tag{67}$$

$$\Phi_b = N_b e_{11}^{[2^2]}(\chi_{Cl1}\chi_C\chi'_C\chi_{Cl2}),\tag{68}$$

$$\Phi_c = N_c e_{11}^{[2^2]}(\chi_{Cl1}\chi_C\chi_{Cl2}\chi_{Cl2}),\tag{69}$$

where we omit the remaining electrons and orbitals which do not take part in the reaction explicitly. However, in our present code all orbitals are optimized simultaneously. The whole reaction path is explored along the reaction coordinate (x^R) that is the difference between the CX1 and CX2 bond lengths. To get the accurate adiabatic energy profile, we performed VBSCF with two resonance structures a and b with the breathing orbitals (BOs) (2BOVB in short). The reason not to include the resonance structure c is due to the delocalized nature of BOs, since BOs are expanded in the whole system. Consequently, the resonance structure c has already implicitly been taken into account. For a diabatic state, nevertheless, only 1VBSCF is performed and the orbitals are strictly localized. At each point, the geometry of the whole supermolecular system is optimized at the HF level. Then a BOVB calculation is performed to get the reaction energy profile, and 1VBSCF calculations are run to derive individual energy curves of Φ_a, Φ_b and Φ_c, respectively. In all calculations, the 6-31G(d) basis set is adopted.

Fig.2 shows the state correlation digrams for the three identity S_N2 reactions, and the major numerical results derived from Fig.2 are reported in Table 3. In both Fig.2 and Table 3, $\Delta E^{\neq}$ denotes the reaction barrier, B represents the coupling between two covalent resonance structures a and b, and T measures the magnitude of the participation of the ionic resonance structure c.

It is of interest to note that the chloride exchange reaction has the lowest coupling term B, although it has a similar reaction barrier from the stable ion complex to the transition state as the fluoride exchange reaction. While for both chloride and hydride reactions, their ionic structure c has a minimum energy at the transition state, the ionic structure for the fluoride exchange reaction has two minimum at $x^R = \pm 0.86$Å, due to the strong electrostatic interaction resulting from the small ionic radii of fluoride anion.

Table 3
VBSCF computation results for the $X^- + CH_3X \rightarrow XCH_3 + X^-$ reactions (kcal/mol)

X	$\Delta E^{\neq}$	B	T
Cl	17.8	21.0	29.6
F	19.3	33.2	45.7
H	52.6	33.2	72.5
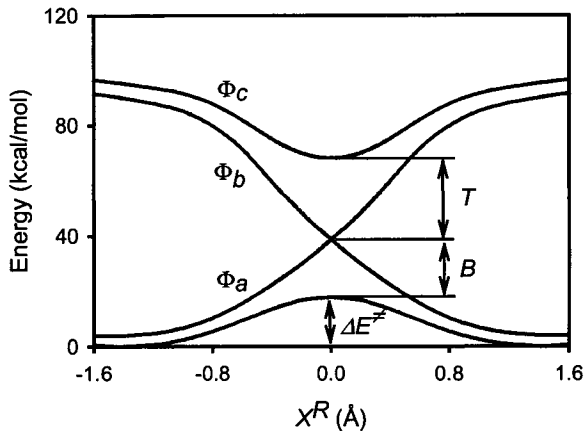
(1) Chloride exchange reaction
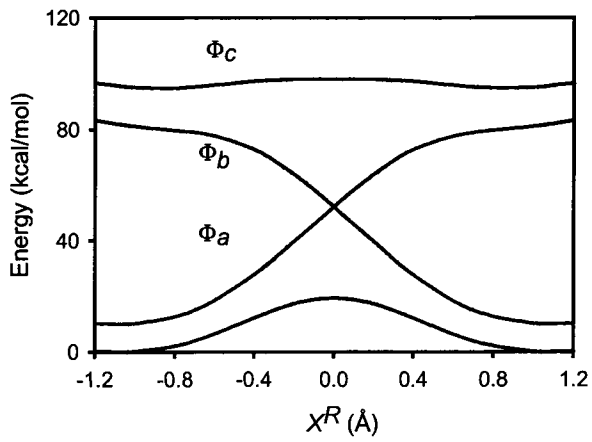
(2) Fluoride exchange reaction
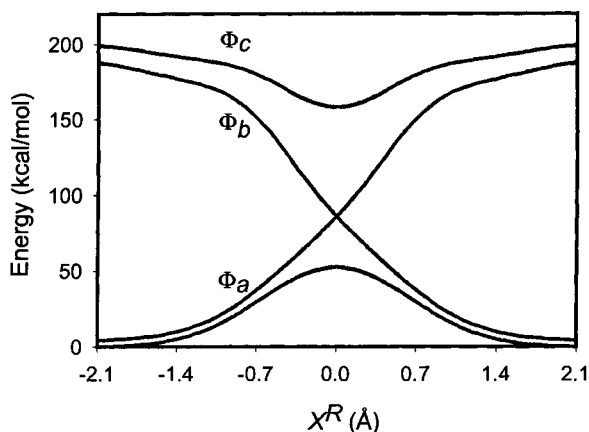
(3) Hydride exchange reaction

Fig. 2. State correlation diagrams for the $X^- + CH_3X \rightarrow XCH_3 + X^-$ S_N2 reactions based on *ab initio* VBSCF computations: (1) X = Cl; (2) X = F; (3) X = H

5.3 The visual VB rule for chemical reactions

A chemical reaction always involves bond-breaking/making processes or valence electron rearrangements, which can be characterized by the variation of VB structures. According to the resonance theory [1, 50], the evolution of a system in the elementary reaction process can be interpreted through the resonance among the correlated VB structures corresponding to reactant, product and some intermediate states. Because only symmetry-adapted VB structures can effectively resonate, all VB structures involved in the description of a reaction will thus retain the symmetry shared by both reactant and product states in the elementary process. Therefore, we postulate that the VB structures of the reactant and the product states for concerted reactions should preserve symmetry-adaptation, called the VB structure symmetry-adaptation (VBSSA) rule.

In fact, chemical reactions are generally very localized, and most parts of the reactants and products are therefore conserved. This feature lingers in VB structures, e.g., only partial VB structural segments are directly involved in the

reaction. The valence electrons forming these segments, as the electrons in the frontier orbitals of Fukui [67], would be the most important and essentially dominate the reaction pathway. As a consequence, the VB structure symmetry-adaptation analysis should be concentrated on these VB structural segments. Considering the possibility of energy partitioning and the geometrical conformation constraint, we can divide a resonance structure into certain sub-VB structures. For different sub-VB structures, the symmetry analysis of the VB structures can be independently carried out, i.e. interactions among different sub-VB structures could be ignored. For example, we could presume no resonance interaction between the σ electrons and π electrons in a C=C double bond in the fixed nucleus approximation, and these four bonding electrons can be divided into two sub-VB structures corresponding to one σ bond and one π bond, respectively.

5.3.1 Symmetrization of the VB wavefunction

In VB theory, all electrons are assigned to localized two-centered bonds, lone pairs and unpaired components. Each collective pattern of such components constitutes a VB structure. The corresponding VB structure function can be expressed as Φ_K, namely, a bonded tableau (BT) state as mentioned before. The wavefunction for the whole system is defined as the superposition of all possible VB structure functions

$$\Psi_{VB} = \sum_K C_K \Phi_K . \tag{70}$$

Usually, an individual VB structure assembled from the localized bonding components does not share the point group symmetry of the molecule anymore. However, the overall VB wavefunction, Ψ_{VB}, should retain the same symmetry properties as the MO wavefunction (in the sense of full CI, they are in fact identical). Therefore, Ψ_{VB} can be classified by an irreducible representation associated with a given point group. In order to sort $\{\Psi_{VB}\}$ by symmetry, a project operator can be introduced as follows:

$$P_i = \frac{n_i}{g} \sum_i \chi_i(R)R, \tag{71}$$

where R is the symmetry operation, $\chi_i(R)$ is the character of the point group, g is the order of the point group, n_i is the dimension of the irreducible representation

Γ_i. Combining the symmetry properties of the bonded tableau [68] and applying the projection operation P_i to a bonded tableau (or a VB basis function) corresponding to a VB structure, we can construct the symmetry-adapted BT function (SABTF) and the symmetrized VB-type wavefunction.

5.3.2 Application of the VBSSA rule

We now consider the isomerization of Dewar benzene into benzene:
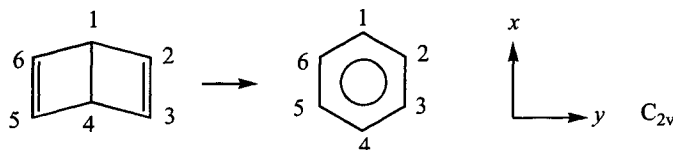
In the above reaction, the product benzene is of D_{6h} symmetry, but only C_{2v} symmetry elements are common for both Dewar benzene and benzene. We can perform therefore the symmetry analysis of the VB structures within the C_{2v} point group framework. There are 6 essential valence electrons involved in the reaction, numbered from 1 to 6. These six valence electrons form three localized bonds (two π bonds and one σ bonds) in Dewar benzene, and a Π_6^6 delocalized bond in benzene, which can be described by five independent BTs within the OEO formalism (see Eq.(65)). Their corresponding BTs are

Dewar benzene $|\,1\,4\,|$, $|\,2\,3\,|$, $|\,5\,6\,|$
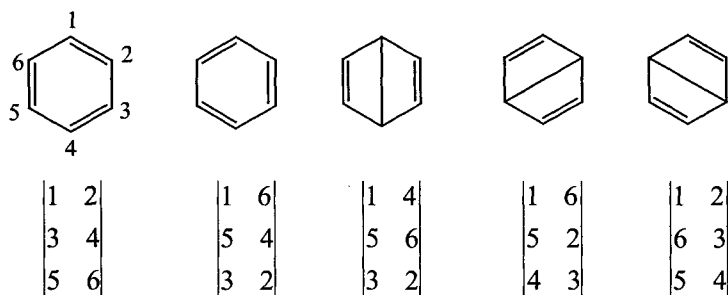
Benzene

Applying the projection operators associated with C_{2v} point group on these BTs results in Dewar benzene

A_1: $|1\,4|$, $|2\,3| + |5\,6|$ B_2: $|2\,3| - |5\,6|$

Benzene

$$A_1: \begin{vmatrix} 1 & 2 \\ 3 & 4 \\ 5 & 6 \end{vmatrix} + \begin{vmatrix} 1 & 6 \\ 5 & 4 \\ 3 & 2 \end{vmatrix}, \ \begin{vmatrix} 1 & 4 \\ 5 & 6 \\ 3 & 2 \end{vmatrix}, \ \begin{vmatrix} 1 & 6 \\ 5 & 2 \\ 4 & 3 \end{vmatrix} + \begin{vmatrix} 1 & 2 \\ 6 & 3 \\ 5 & 4 \end{vmatrix}$$

$$B_2: \begin{vmatrix} 1 & 2 \\ 3 & 4 \\ 5 & 6 \end{vmatrix} - \begin{vmatrix} 1 & 6 \\ 5 & 4 \\ 3 & 2 \end{vmatrix}$$

$$A_2: \begin{vmatrix} 1 & 6 \\ 5 & 2 \\ 4 & 3 \end{vmatrix} - \begin{vmatrix} 1 & 2 \\ 6 & 3 \\ 5 & 4 \end{vmatrix}$$

Obviously, the conversion from Dewar benzene to benzene is forbidden by the VBSSA rule because no A_2 symmetrized VB structure segment in the reactant Dewar benzene can match the A_2 symmetrized VB structure segment of benzene. More examples, including generally allowed and forbidden chemical process, can be found in our previous study[69].

The VBSSA rule can be used to select relevant VB structures and construct the semiquantitative and quantitative curve-crossing VB diagram. Combining the MO method and VB calculations, we investigated atom exchange reactions: H + HLi $\rightarrow$ H$_2$ + Li and H + LiH$\rightarrow$HLi + H, and discussed the effect of energy differences between the VB structures on the activation energy and properties of the transition state [70].

5.4 Excited states

In the MO formalism it is quite straightforward to deal with the excited states of a molecule. An adequate wavefunction of an excited state can be constructed according to the resultant configuration and its symmetry arising from electron promotion among MO series. Compared with numerous MO-based methods, VB approaches are far less employed to study excited states due to the difficulty in VB computations. Recently, by observing the correlation between MO theory and resonance theory, as well as the symmetry-adapted VB wavefunction described in the last section, we performed VB calculations on low-lying states of some molecules [71, 72].

5.4.1 VB-type wavefunctions of excited states

For simplicity, the σ-π separation is imposed in the VB calculations for the ground and excited states since low-lying excitations only involve the π electrons in selected species O_3^-, C_3^- and C_3H_5. After the σ-π separation, the symmetry of both the ground electronic state and the π excited states only depends on π valence electronic structures because a doubly occupied σ core within the MO formalism is always total symmetric, and does not affect the symmetry of electronic states. If the three p orbitals forming π bonds in O_3^- are numbered as
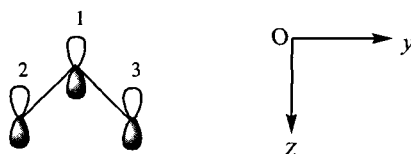
the three possible VB structures and corresponding BTs for O_3^- would be

$$\begin{vmatrix} 1 & 1 \\ 2 & 2 \\ 3 & \end{vmatrix} \phi_1 \qquad \begin{vmatrix} 1 & 1 \\ 3 & 3 \\ 2 & \end{vmatrix} \phi_2 \qquad \begin{vmatrix} 2 & 2 \\ 3 & 3 \\ 1 & \end{vmatrix} \phi_3$$
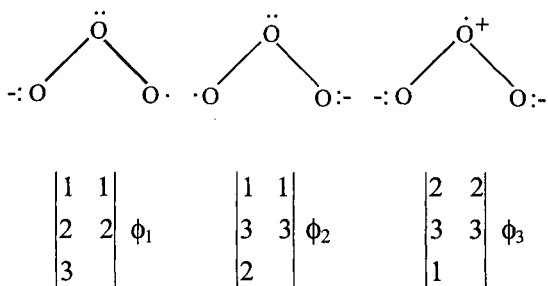
Applying projection operators P_{A_1}, P_{A_2}, P_{B_1} and P_{B_1} to the above BTs ϕ_1, ϕ_2 and ϕ_3, respectively, we obtain

$$P_{A_1} = \frac{1}{4}\sum_R \chi_{A_1}(R)R\phi_1 = \frac{1}{4}\left(1\begin{vmatrix} 1 & 1 \\ 2 & 2 \\ 3 & \end{vmatrix} + 1\begin{vmatrix} -1 & -1 \\ -3 & -3 \\ -2 & \end{vmatrix} + 1\begin{vmatrix} 1 & 1 \\ 3 & 3 \\ 2 & \end{vmatrix} + 1\begin{vmatrix} -1 & -1 \\ -2 & -2 \\ -3 & \end{vmatrix}\right)$$

$$= \frac{1}{4}\left(\begin{vmatrix} 1 & 1 \\ 2 & 2 \\ 3 & \end{vmatrix} - \begin{vmatrix} 1 & 1 \\ 3 & 3 \\ 2 & \end{vmatrix} + \begin{vmatrix} 1 & 1 \\ 3 & 3 \\ 2 & \end{vmatrix} - \begin{vmatrix} 1 & 1 \\ 2 & 2 \\ 3 & \end{vmatrix}\right) = 0$$

(72)

$$P_{A_1}\phi_2 = P_{A_1}\phi_3 = P_{A_2}\phi_3 = P_{B_2}\phi_1 = P_{B_2}\phi_2 = P_{B_2}\phi_3 = 0, \tag{73}$$

$$P_{B_1}\phi_1 = P_{B_1}\phi_2 = \frac{1}{2}(\phi_1 + \phi_2), \tag{74}$$

$$P_{A_2}\phi_1 = P_{A_2}\phi_2 = \frac{1}{2}(\phi_1 - \phi_2), \tag{75}$$

$$P_{B_1}\phi_3 = \phi_3. \tag{76}$$

Similarly, the SABTFs for O_3 and O_3^+ are

O_3

$$S = 0 \quad A_1 : \begin{vmatrix} 1 & 1 \\ 2 & 3 \end{vmatrix},\ \frac{1}{2}(\begin{vmatrix} 1 & 1 \\ 2 & 3 \end{vmatrix} + \begin{vmatrix} 1 & 3 \\ 2 & 2 \end{vmatrix});\quad B_2 : \frac{1}{2}(\begin{vmatrix} 1 & 1 \\ 2 & 3 \end{vmatrix} - \begin{vmatrix} 1 & 3 \\ 2 & 2 \end{vmatrix}). \tag{77}$$

$$S = 1 \quad A_1 : \frac{1}{2}(\begin{vmatrix} 2 & 2 \\ 1 & \\ 3 & \end{vmatrix} + \begin{vmatrix} 3 & 3 \\ 1 & \\ 2 & \end{vmatrix}),\quad B_2 : \frac{1}{2}(\begin{vmatrix} 2 & 2 \\ 1 & \\ 3 & \end{vmatrix} - \begin{vmatrix} 3 & 3 \\ 1 & \\ 2 & \end{vmatrix}),\ \begin{vmatrix} 1 & 1 \\ 2 & \\ 3 & \end{vmatrix}. \tag{78}$$

O_3^+

$$S = 1/2 \quad A_2 : \frac{1}{2}(\begin{vmatrix} 1 & 2 \\ 3 & \end{vmatrix} - \begin{vmatrix} 1 & 3 \\ 2 & \end{vmatrix})\quad B_1 : \frac{1}{2}(\begin{vmatrix} 1 & 2 \\ 3 & \end{vmatrix} + \begin{vmatrix} 1 & 3 \\ 2 & \end{vmatrix})\ \text{or}\ \begin{vmatrix} 2 & 3 \\ 1 & \end{vmatrix} \tag{79}$$

For the case of linear C_3^-, the symmetries of the ground and π excited states are determined by five π valence electrons in the six p orbitals numbered from 1 to 6 as
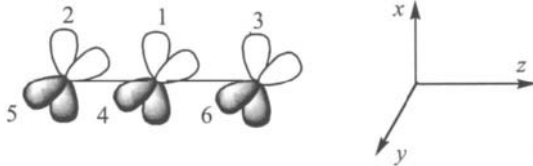
Here the p orbitals are OEOs, and they have the same symmetry as the localized one-center p orbitals. Thus, the chemical bond generated by p orbitals 1 and 2 can be described by one covalent structure $|12|$; the ionic structures $|11|$ and $|22|$ can be ignored. The five π valence electrons and six p orbitals can form 4 BTs as follows

$$
\begin{vmatrix} 1 & 2 \\ 4 & 6 \\ 3 & \end{vmatrix} \phi_1 \qquad
\begin{vmatrix} 1 & 2 \\ 4 & 6 \\ 5 & \end{vmatrix} \phi_2 \qquad
\begin{vmatrix} 1 & 3 \\ 4 & 5 \\ 2 & \end{vmatrix} \phi_3 \qquad
\begin{vmatrix} 1 & 3 \\ 4 & 5 \\ 6 & \end{vmatrix} \phi_4
$$

For the $D_{\infty h}$ point group, we can use the projection operators from the subgroup D_{4h}. Applying the project operators P_{E_g} and P_{E_u} to the above 4 primary BTs, we obtain

$$
P_{E_g}\phi_1 = \frac{2}{16}\sum_R \chi_{E_g}(R)R\phi_1 = \frac{1}{2}(\phi_1 - \phi_3) \tag{80}
$$

$$
P_{E_g}\phi_2 = \frac{1}{2}(\phi_2 - \phi_4), \quad P_{E_u}\phi_1 = \frac{1}{2}(\phi_1 + \phi_3), \quad P_{E_u}\phi_2 = \frac{1}{2}(\phi_2 + \phi_4). \tag{81}
$$

Other projection operators on the primary BTs from ϕ_1 to ϕ_4 result in a null outcome, suggesting that these BTs have no contribution to other irreducible representations in the subgroup D_{4h}. In fact, the SABTFs $\frac{1}{2}(\phi_1 - \phi_3)$ and $\frac{1}{2}(\phi_2 - \phi_4)$ are equivalent, so are $\frac{1}{2}(\phi_1 + \phi_3)$ and $\frac{1}{2}(\phi_2 + \phi_4)$, and they account for the states ^2E_g and ^2E_u, respectively, i.e. $^2\Pi_g$ and $^2\Pi_u$ corresponding to the $D_{\infty h}$ point group.

5.4.2 π–electron excitation energies

The excitation energies of the transitions $^2B_1 \rightarrow {}^2A_2$ for O_3^-, $^2A_2 \rightarrow {}^2B_1$ for C_3H_5 and $^2\Pi_g \rightarrow {}^2\Pi_u$ for C_3^- were calculated by different methods. A comparison of calculated results with available experimental data is presented in Table 4. In these calculations, optimized geometries of the ground and π electronically excited states are located by the restricted open-shell Hartree-Fock (ROHF) energy-gradient method in GAMESS [73]. In subsequent VB calculations only the π electrons are involved, and the σ electron contribution to the total energy was considered within the ROHF formalism.

Table 4

π electron excitation energies

species/method	transition	I_e (eV)	basis set
O_3^-	$X^2B_1 \rightarrow 1^2A_2$		
ROHF		2.71	6-311+G
VB(3, 2)[a]		2.71	6-311+G
VB(15,10)		2.15	6-311+G
CASSCF[b]		2.13	11s7p2d/7s4p2d
Expt.[c]		2.03	
C_3^-	$X^2\Pi_g \rightarrow 1^2\Pi_u$		
ROHF		5.16	6-31G
VB(2, 2)		3.69	6-31G
MCSCF[d]		4.18	6-31G
C_3H_5	$X^2A_2 \rightarrow 1^2B_1$		
ROHF		4.86	6-31G
VB(2, 2)		3.28	6-31G
CI[e]		3.13	DZ+P
Expt.[f]		3.07	

a Numbers in parentheses are the numbers of bonded tableaus used in the VB calculations for the ground and excited states, respectively.

b reference [75]

c reference [76]

d The MCSCF wavefunction is generated by the CISD method, and the active space is composed of 17 lower MOs in energy exclusive of three core orbitals.

e reference [77]

f reference [78]

For O_3^-, there are five π electrons in three p orbitals, and there is no typical 2-electron 2-center bond. Primary VB and ROHF calculations predict the same transition energy of 2.71 eV, which is larger than the experimental value of 2.03eV. When the VB wavefunction is expanded with additional bonded tableaus formed by the split valence orbitals along with the inclusion of single excitations of π electrons from 2p to diffuse p basis functions, a reasonable excitation energy of 2.15 eV is obtained. For C_3H_5, VB calculation gives a better excitation energy of 3.28 eV compared with 4.86 eV from ROHF calculations. VB calculations of π electrons in C_3^-ca n recover partial correlation energies, and obtain lower total energies, especially for the excited state $1^2\Pi_u$ in comparison with the ROHF calculation.

Alternatively, the correspondence between MO theory and resonance theory in the description of electronic structures can be used to construct VB wavefunctions for the low-lying states of diatomic molecules. Test calculations

on transition energies of excited states in B_2 [74] and in LiB [72] molecules have been performed, and comparisons of VB calculations with other post-SCF calculations and available experiments show that these approaches are promising for the VB study of excited states.

5.4.3 Bonding features of the ground and π excited states of S_3

S_3 is the simplest poly-sulfur cluster, whose valence electronic structure is similar to O_3 and SO_2, and four 3p valence electrons contribute to π bonding. The visual picture of bonding for S_3 can help us understand the chemistry of polysulfides. In order to ensure an unambiguous definition of a covalent or an ionic description of the bonding, the active orbitals forming π bonds are restricted to an expansion in a set of symmetry-adapted primitive functions from one atom. The σ-π separation was used to reduce computational cost, and six fully occupied 2p orbitals after the σ-π separation were frozen in the VB calculation. Possible singlet and triplet VB structures and corresponding BTs for S_3 in singlet and triplet states are as follows (with the same orbital numberings as for O_3^- shown before):

$$S = 0$$

$$S = 1$$
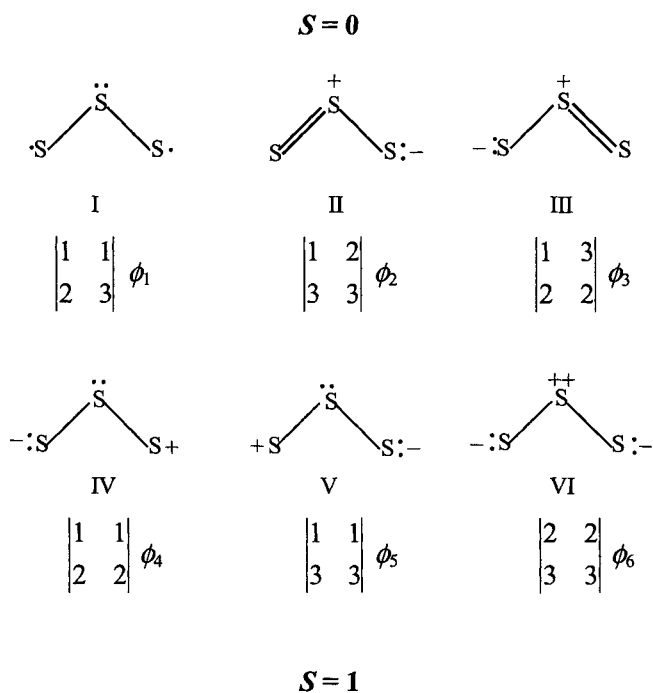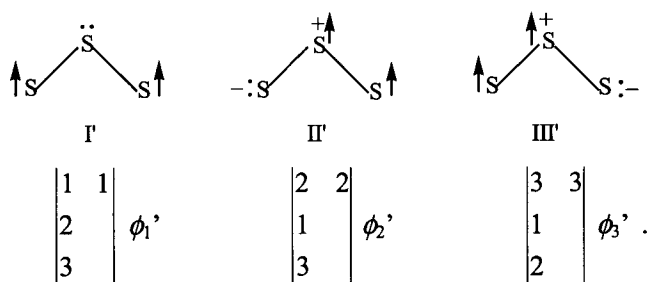
Table 5 lists the computed results for the ground and first π singlet and triplet excited states with the 6-31G basis set. The weights in Table 5 demonstrate the significant differences in chemical bonding amongst the ground and π excited states. E.g., in the ground state, the VB structure I (biradical in singlet) has a large weight of 54.30%, and the dipolar structures II and III have also a significant contribution of 41.16%. This bonding feature implies that S_3 in the ground state is active for radical, nucleophilic and electrophilic processes. The dipolar structures II and III are predominant for the excited state 1^1B_2. The structure I' (biradical in triplet) has a weight of 90%, and dominates the excited state 1^3B_2.

Table 5

Optimized geometries and bonding features of S_3

State	VB structure	coefficient	weight	geometry [a]
X $^1A_1$	ϕ_1	0.6673	0.5430	
	ϕ_2	-0.3724	0.2058	$r = 2.052$
	ϕ_3	-0.3724	0.2058	$\theta = 115.1$
	ϕ_4	-0.0526	0.0089	
	ϕ_5	-0.0528	0.0089	
	ϕ_6	-0.0865	0.0275	
1^1B_2	ϕ_2	0.6951	0.4874	
	ϕ_3	-0.6951	0.4874	$r = 2.267$
	ϕ_4	0.0647	0.0126	$\theta = 97.9$
	ϕ_5	-0.0647	0.0126	
1^3B_2	ϕ_1'	0.9240	0.9000	$r = 2.186$
	ϕ_2'	-0.1625	0.0500	$\theta = 106.0$
	ϕ_3'	0.1625	0.0500	

a Bond lengths in Ångstrom, angles in degree.

6. SUMMARY

With the persistent efforts for one and half decades, we have developed a state-of-the-art *ab initio* VB code, Xiamen-99, which is based on our proposed paired-permanent algorithm. This algorithm makes use of the symmetries in the spin-free VB wavefucntions in an attempt to ease the $N!$ problem which has hampered the development of *ab initio* methods for a long time. The applications of the *ab initio* VB method by our group and other groups have already generated numerous interesting and fruitful findings, and more studies by the means of *ab initio* VB calculations are highly expected. Computational results have demonstrated the different merits of the VB method and MO method, and confirm the necessity to pursue *ab initio* VB approaches, separately from MO-based approaches. While continuous efforts to expand the applicability of *ab initio* VB methods are guaranteed, we also anticipate the combination of the VB method with high level MO methods, in an attempt to derive accurate results with reasonable computational resources.

ACKNOWLEDGEMENTS

REFERENCES

[1] L. C. Pauling, The Nature of the Chemical Bond, Cornell University Press, Ithaca, NY, 1960.
[2] F. A. Matsen, Adv. Quantum Chem., 1 (1964) 59.
[3] G. F. Tantardini, M. Raimondi, and M. Simonetta, J. Am. Chem. Soc., 99 (1977) 2913.
[4] W. A. Goddard, Phys. Rev., 117 (1967) 73.
[5] J. Gerratt, At. Mol. Phys., 7 (1971) 141.
[6] C. R. Sarma and S. Rettrup, Theor. Chim. Acta., 46 (1977) 63.
[7] G. A. Gallup, R. L. Vance, J. R. Collins, and J. M. Norbeck, Adv. Quant. Chem., 16 (1982) 229.
[8] D. L. Cooper, J. Gerratt, and M. Raimondi, Chem. Rev., 91 (1991) 929.
[9] R. Mcweeny, Int. J. Quantum Chem., 74 (1999) 87.
[10] P. C. Hiberty, J. Mol. Struct. (THEOCHEM), 398-399 (1997) 35.
[11] F. Dijkstra and J. H. van Lenthe, J. Chem. Phys., 113 (2000) 2100.
[12] J. Cullen, J. Comput. Chem., 20 (1999) 999.
[13]S. Clifford, M. J. Bearpark, and M. A. Robb, Chem. Phys. Lett., 255 (1996) 320.

[14] M. Raimondi and D. L. Cooper, Top. Curr. Chem., 203 (1999) 105.

[15] M. P. Allen and D. J. Tildesley, Computer Simulation of Liquids, Clarendon Press, Oxford, 1987.

[16] U. Burkert and N. L. Allinger, Molecular Mechanics, American Chemical Society, Wanshington D.C., 1982.

[17] Y. Mo, M. Lin, W. Wu and Q. Zhang, to be published.

[18] J. Gao and X. Xia, Science, 258 (1992) 631.

[19] Y. Mo, J. Gao, and S. D. Peyerimhoff, J. Chem. Phys., 112 (2000) 5530.

[20] C. R. Landis, T. Cleveland, and T. K. Firman, J. Am. Chem. Soc., 120 (1998) 2641.

[21] W. H. Thompson and J. T. Hynes, J. Am. Chem. Soc., 122 (2000) 6278.

[22] S. S. Shaik, H. B. Schlegel, and S. Wolfe, Theoretical Aspects of Physical Organic Chemistry. The SN2 Mechanism, Wiley-Interscience, New York, 1992.

[23] S. Shaik and P. C. Hiberty, Adv. Quantum Chem., 26 (1995) 99.

[24] M. Cuma, U. W. Schmitt, and G. A. Voth, Chem. Phys., 258 (2000) 187.

[25] A. Warshel and R. M. Weiss, J. Am. Chem. Soc., 102 (1980) 6218.

[26] J. Villa, J. Bentzien, A. Gonzalez-Lafont, J. M. Lluch, J. Bertran, and A. Warshel, J. Comput. Chem., 21 (2000) 607.

[27] M. R. F. Siggel and T. D. Thomas, J. Am. Chem. Soc., 108 (1986) 4360.

[28] P. Burk and P. v. R. Schleyer, J. Mol. Struct. (THEOCHEM), 505 (2000) 161.

[29] P. C. Hiberty and C. P. Byrman, J. Am. Chem. Soc., 117 (1995) 9870.

[30] Y. Mo, Z. Lin, W. Wu, and Q. Zhang, J. Phys. Chem., 100 (1996) 6469.

[31] X. Li and Q. Zhang, Int. J. Quantum Chem., 36 (1989) 599.

[32] R. McWeeny, Int. J. Quantum Chem., 34 (1988) 25.

[33] W. Wu, A Study on Valence Bond Theory in Quantum Chemistry, Ph.D. Thesis, Xiamen University, Xiamen, 1990.

[34] Y. Mo, Valence Bond Method and Its Applications, Ph.D. Thesis, Xiamen University, Xiamen, 1992.

[35] J. Li, W. Wu, and Q. Zhang, Chinese Sci. Bull., 37 (1992) 2243.

[36] J. Li and W. Wu, Theor. Chim. Acta., 89 (1994) 105.

[37] J. Li, Theor. Chim. Acta 93 (1996) 35.

[38] W. Wu, A. Wu, Y. Mo, and Q. Zhang, Science in China (Chinese Ed.) B25 (1995) 1247; (English Ed.) B39 (1996) 456.

[39] W. Wu, A. Wu, Y. Mo, M. Lin, and Q. Zhang, Int. J. Quantum Chem., 67 (1998) 287.

[40] J. Li and R. Pauncz, Int. J. Quant. Chem., 62 (1997) 245.

[41] M. Hamermesh, Group Theory and Its Application to Physical Problems, Addison-Wesley, MA, 1962.

[42] Q. Zhang and X. Li, J. Mol. Struct., 189 (1989) 413.

[43] R. McWeeney, Methods of molecular quantum mechanics, Academic, London, 1989.

[44] W. Wu and Q. Zhang, J Phys., A 25 (1992) 3737.

[45] B. Levy and G. Berthier, Int. J. Quantum Chem., 2 (1968) 307.

[46] P. C. Hiberty, S. Humbel, C. P. Byrman and J. H. van Lenthe, I. Chem. Phys., 101 (1994) 5969.

[47] S. Shaik and A. Shurki, Angew. Chem. Int. Ed., 38 (1999) 586.

[48] R. Fletcher, Practical Methods of Optimization, Wiley, New York, 1987.

[49] W. Wu and S. Shaik, Phys. Chem. Lett., 301 (1999) 37.

[50] G. W. Wheland, Resonance in Organic Chemistry, Wiley: New York, 1955.

[51] J. M. Norbeck and G. A. Gallup, J. Am. Chem. Soc., 96 (1974) 3386.

[52] Y. Mo and S. D. Peyerimhoff, J. Chem. Phys., 109 (1998) 1687.

[53] D. L. Cooper, J. Gerratt, and M. Raimondi, Nature, 323 (1986) 699.

[54] Y. Mo, Z. Lin, W. Wu, and Q. Zhang, J. Phys. Chem., 100 (1996) 11569.

[55] V. I. Minkin, M. N. Glukhovtsev, and B. Y. Simkin, Aromaticity and Antiaromaticity: Electronic and Structural Aspects, Wiley, New York, 1994.

[56] P. v. R. Schleyer and H. Jiao, Pure and Appl. Chem., 36 (1996) 209.

[57] Y. Mo and Q. Zhang, J. Mol. Struct. (THEOCHEM), 357 (1995) 171.

[58] A. Streitwieser, C. H. Heathcock, and E. M. Kosower, Introduction to Organic Chemistry, Macmillan, New York, 1992.

[59] K. B. Wiberg and P. R. Rablen, J. Am. Chem. Soc., 117 (1995) 2201.

[60] K. E. Laidig and L. M. Cameron, J. Am. Chem. Soc., 118 (1996) 1737.

[61] G. Fogarasi and P. G. Szalay, J. Phys. Chem. A, 101 (1997) 1400.

[62] E. D. Glendening and J. A. Hrabal, J. Am. Chem. Soc., 119 (1997) 12940.

[63] D. Lauvergnat and P. C. Hiberty, J. Am. Chem. Soc., 119 (1997) 9478.

[64] R. H. Felgg and R. D. Harcourt, J. Mol. Struct. (THEOCHEM), 164 (1988) 67.

[65] Y. Mo and J. Gao, J. Comput. Chem., 21 (2000) 1458.

[66] A. Pross and S. Shaik, Acc. Chem. Res., 16 (1983) 363.

[67] K. Fukui, T. Yonezawa, and H. Shingu, 20 (1952) 722.

[68] W. Wu, Y. Mo, and Q. Zhang, J. Mol. Struct. (THEOCHEM), 283 (1993) 227.

[69] Z. Cao, H. Xian, W. Wu, and Q. Zhang, Theor. Chem. Acc., 101 (1999) 352.

[70] Z. Cao, W. Wu, and Q. Zhang, Science in China (English Ed.), B41 (1998) 660.

[71] Z. Cao, W. Wu, and Q. Zhang, Int. J. Quantum Chem., 66 (1998) 1.

[72] Z. Cao, W. Wu, and Q. Zhang, Int. J. Quantum Chem., 70 (1998) 283.

[73] M. W. Schmidt, K. K. Baldridge, J. A. Boatz, S. T. Elbert, M. S. Gordon, J. H. Hensen, S. Koseki, N. Matsunaga, K. A. Nguyen, S. J. Su, T. L. Windus, M. Dupuis, and J. A. Montgomery, J. Comput. Chem., 14 (1993) 1347.

[74] Z. Cao, W. Wu, and Q. Zhang, Science in China (English Ed.), B41 (1998) 660.

[75] K. A. Peterson, R. C. Mayrhofer, and R. C. Woods, J. Chem. Phys., 93 (1990) 5020.

[76] J. F. Hiller and M. L. Vestal, J. Chem. Phys., 74 (1981) 6096.

[77] T. K. Ha and H. Baumann, J. Chem. Phys., 85 (1986) 1438.

[78] C. L. Currie and D. A. Ramsay, J. Chem. Phys., 45 (1966) 488.

This Page Intentionally Left Blank

Chapter 7

BOVB - A valence bond method incorporating static and dynamic correlation effects

P.C. Hiberty[a] and S. Shaik[b]

[a]Laboratoire de Chimie Physique, CNRS UMR 8000, Groupe de Chimie Théorique, Bat. 490, Université de Paris-Sud, 91405 Orsay Cedex, France

[b]Department of Organic Chemistry and Lise Meitner-Minerva Center for Computational Chemistry, Hebrew University, 91904 Jerusalem, Israel

The BOVB method is aimed at combining the qualities of interpretability and compactness of valence bond wave functions with a quantitative accuracy of the energetics. The fundamental feature of the method is the freedom of the orbitals to be different for each VB structure during the optimization process. In this manner, the orbitals respond to the instantaneous field of the individual VB structure rather than to an average field of all the structures. As such, the BOVB method accounts for the differential dynamic correlation that is associated with elementary processes like bond forming/breaking, while leaving the wave function compact. The use of strictly localized orbitals ensures a maximum correspondence between the wave function and the concept of Lewis structure, and makes the method suitable for calculation of diabatic states.

1. INTRODUCTION

Despite the quantitative victory of molecular orbital (MO) theory, much of our qualitative understanding of electronic structure is still couched in terms of local bonds and lone pairs, that are key conceptual elements of the valence bond (VB) picture. VB theory is essentially the quantum chemical formulation of the Lewis concept of the chemical bond [1,2]. Thus, a chemical bond involves spin-pairing of electrons which occupy valence atomic orbitals or hybrids of adjacent atoms that are bonded in the Lewis structure. In this manner, each term of a VB wave function corresponds to a specific chemical structure, and the isomorphism of the theoretical elements with the chemical elements creates an intimate relationship between the abstract theory and the nature of the

chemical structure and its transformation. As such, VB theory and its simplest variant, resonance theory [3], have given rise to fundamental concepts such as hybridization, covalency, ionicity, hybrid nature of resonance structures, resonance stabilization, and so on. These concepts served chemists extremely well and enabled them to rationalize and predict reaction mechanisms or molecular properties by simply writing down VB structures on a back of an envelope.

Alongside this conceptual aspect, VB theory offers the quantitative facility that enables us to study a variety of problems and thereby extract unique chemical insight that is not available by standard *ab initio* MO based computations. Such a wide ranging use of VB theory is the generation of diabatic states, which represent electronic structures that must remain as invariant as possible throughout a reaction coordinate. The so generated diabatic states apply to numerous problems, such as : (i) Chemical dynamics, in cases where the Born-Oppenheimer approximation breaks down; (ii) chemical reactivity, with the Shaik-Pross diagrams, in which a reaction barrier originates in the avoided crossing of two diabatic state curves, one representing the bonding scheme of the reactants and the other that of the products [4]; (iii) photochemistry, with the harpooning and charge transfer mechanisms [5]; (iv) fundamental principles of organic chemistry, e.g. the role of electronic delocalization as a stabilizing factor [6,7,8,9]; (v) solvation, with theoretical models treating the solvation effects separately on covalent and ionic components of a bond [10]. For such applications, it is not only important to be able to interpret the wave function in terms of chemical structural formulas (Lewis structures), but also to be able to estimate the energy of each of these individual Lewis structures and their variations along a reaction coordinate prior to their interaction to form the adiabatic states. Clearly, the usefulness of a quantitative VB method derives from the combination of quantitative rigor and conceptual lucidity. These desirable qualities typify the breathing orbital VB (BOVB) method that has been proposed recently [11-13], and is being reviewed here.

2. ELECTRON CORRELATION IN VB THEORY

The term "electron correlation energy" is usually defined as the difference between the exact nonrelativistic energy and the energy provided by the simplest MO wave function, the mono-determinantal Hartree-Fock wave function. This latter model is based on the "independent particle" approximation, according to which each electron moves in an average potential provided by the other electrons [14]. Within this definition, it is customary to distinguish between non dynamical and dynamical electron correlation.

2.1 Non dynamical electron correlation

Non dynamical electron correlation is the part of the total correlation that is taken into account in a CASSCF calculation that correlates the valence electrons in valence orbitals. Physically, the non dynamical electron correlation is a Coulomb correlation that permits the electrons to avoid one another and reduce their mutual repulsion as much as possible with respect to a given zero order electronic structure defined by the Hartree-Fock wave function. In VB terms, the non dynamical correlation ensures a correct balance between the ionic and covalent components of the wave function for a given electronic system. The dynamical correlation is just what is still missing to get the exact nonrelativistic wave function.

The essential part of non dynamical correlation energy for polyatomic molecules is the " left-right electron correlation ", which is concerned with the ionic-covalent balance within a given two-electron bond. Let us therefore discuss this type of correlation.

2.1.1. Left-right electron correlation in the MO and VB theories

Historically, the first calculation of the electronic structure of a neutral molecule was carried out by Heitler and London [15], who treated H_2 using the valence bond (VB) method. In this early paper, the molecular wave function for H_2 was considered to be purely covalent, and constructed from the atomic orbitals (AO's) χ_a and χ_b of the separate atoms. Dropping the normalization constant hereafter, the wave function is given in equation 1.

$$\Psi_{HL} = \chi_a(1)\chi_b(2) - \chi_b(1)\chi_a(2) \tag{1}$$

This simple wave function, so called the Heitler-London (HL) wave function, was able to account for about 66% of the bonding energy of H_2, and performed a little better than the rival MO method that appeared almost at the same time.

In the MO framework, The Hartree-Fock wave function Ψ_{HF} takes the form of an antisymmetrized orbital product, which in the case of H_2 is the Slater determinant involving the spin-up and spin-down counterparts of the bonding orbital σ_g, as in eq 2:

$$\Psi_{HF} = |\sigma_g \bar{\sigma}_g|; \qquad \sigma_g = \chi_a + \chi_b \tag{2}$$

The physical constitution of the Hartree-Fock wave function appears most clearly by expanding the MO determinant of eq 2 as a linear combination of determinants constructed from pure AO's, eq 3:

$$| \sigma_g \, \overline{\sigma}_u | \; = \; | \chi_a \, \overline{\chi}_b | + | \chi_b \, \overline{\chi}_a | + | \chi_a \, \overline{\chi}_a | + | \chi_b \, \overline{\chi}_b | \tag{3}$$

Here the first two determinants are the determinantal form of the Heitler-London function (eq 1), and represent a purely covalent interaction between the atoms. The remaining determinants represent zwitterionic structures, H^-H^+ and H^+H^-, and contribute 50% to the wave function. The same constitution holds for any interatomic distance. This weight of the ionic structures is clearly too much at equilibrium distance, and becomes absurd at infinite separation where the ionic component is expected to drop to zero. Qualitatively, this can be corrected by including a second configuration where both electrons occupy the antibonding orbital, σ_u, i.e. the doubly excited configuration. The more elaborate wave function Ψ_{CI} is shown in eq. 4, where C_1 and C_2 are coefficients of the two MO configurations:

$$\Psi_{CI} = C_1 | \sigma_g \, \overline{\sigma}_g | + C_2 | \sigma_u \, \overline{\sigma}_u | \tag{4}$$
$$\sigma_g = \chi_a + \chi_b \; ; \; \sigma_u = \chi_a - \chi_b$$

This is the essence of the configuration interaction (CI) method. When both the coefficients of the configurations and their orbitals are optimized simultaneously in flexible basis sets, the method is called multi-configuration SCF (MCSCF). The doubly excited configuration in eq. 4 also involves too a 50:50 mixture of covalent and ionic components but with a negative sign between them. Consequently the combination of the two configurations deletes the excess ionic character of Ψ_{HF}, thereby leading to the wave function in eq 5. The corrected wave function displays a qualitatively correct behavior, with an optimal covalent/ionic ratio of typically 80:20 at equilibrium distance [16] all the way to 100:0 at infinite separation.

$$\Psi_{CI} = \lambda (| \chi_a \, \overline{\chi}_b | + | \chi_b \, \overline{\chi}_a |) + \mu (| \chi_a \, \overline{\chi}_a | + | \chi_b \, \overline{\chi}_b |) \tag{5}$$

The early VB point of view was based solely on the purely covalent HL wave function. In this wave function the electrons are never allowed to approach each other and therefore their electron repulsion is minimized and their Coulomb correlation is at maximum. Thus, while the Hartree-Fock model has no electron correlation, giving equal weight to covalent and ionic structures, the early VB models overestimated the correlation. The true situation is about half-way in-between. In the same way as the Hartree-Fock wave function is improved by CI, the purely covalent VB function can be improved by admixture of ionic structures as in eq 5, in which the coefficients λ and μ would be directly optimized in the VB framework. Both improved models thus lead to wave functions that are strictly equivalent and physically correct, even though their initial expressions appear entirely different. This

statement can be generalized: Since both *ab initio* VB and *ab initio* MO theories exploit a subspace of the same configuration space, the VB and MO wave functions of a given electronic structure are mutually interconvertible and become equivalent when both theories are driven to their higher level of refinement.

A severe inconvenience of describing each bond of a polyatomic molecule by one covalent and two ionic components is that the number of VB structures grows exponentially with the size of the molecule. Coulson and Fischer [17] proposed a very elegant way to incorporate left-right correlation into a single and formally covalent VB structure of the HL type. To this end they used deformed or rather slightly delocalized orbitals as exemplified in eq 6 for H_2.

$$\Psi_{CF} = |\varphi_l \, \overline{\varphi}_r| + |\varphi_r \, \overline{\varphi}_l| \tag{6}$$

$$\varphi_l = \chi_a + \varepsilon\chi_b, \quad \varphi_r = \chi_b + \varepsilon\chi_a$$

Here each orbital, φ_l or φ_r, is mainly localized on a single center but involves a small tail on the other center, so that the expansion of the Coulson-Fischer wave function Ψ_{CF} (eq 7) in AO determinants is in fact equivalent to Ψ_{CI} in eq 5, provided the coefficient ε is properly optimized.

$$\Psi_{CF} = (1+\varepsilon^2)(|\chi_a \, \overline{\chi}_b| + |\chi_b \, \overline{\chi}_a|) + 2\varepsilon(|\chi_a \, \overline{\chi}_a| + |\chi_b \, \overline{\chi}_b|) \tag{7}$$

The Coulson-Fischer proposal gave rise to the "separated electron pair theory" which was initiated by Hurley, Lennard-Jones and Pople [18]. Its further development by Goddard [19], resulted in the "Generalized Valence Bond" (GVB) method. In the latter method, each bond in a polyatomic molecule is considered as a pair of non-orthogonal and spin-coupled orbitals, as in the HL wave function. The different GVB pairs can in turn be constrained to be mutually orthogonal, without much loss in numerical accuracy. Much as the Coulson-Fischer orbitals, each GVB orbital is centered on one atom with delocalization tails on the neighboring atoms. The resulting GVB wave function that formally displays purely covalent bonds implicitly contains ionic structures, necessary for a reasonable description of the bonds. The most popular version of GVB theory is the so-called "perfect pairing" approximation, which considers a single spin-coupling scheme in which spin pairing is restricted to the electrons and orbitals of the bonded atoms in the Lewis structure. For example, in methane, the perfectly paired GVB wave function couples the electrons of each sp^3 hybrid of carbon to the hydrogen that faces it. In fact, for this case of 8 electrons in 8 orbitals there are 14 possible spin coupling schemes in all rigor. As such, the perfectly paired GVB approximation constitutes a tremendous simplification of the wave function, often with no serious loss of accuracy. The closely related method is the Spin-

Coupled (SC) theory of Gerratt, Raimondi and Cooper [20]. This method removes any orthogonality restrictions and consider all possible spin-coupling schemes between the singly occupied orbitals. Note that the shape of the orbitals (e.g. sp^3-like in the carbon atom of methane) and their degrees of delocalization are not *a priori* imposed, but naturally arise from the optimization of the orbitals for self-consistency. The lone pairs can be treated either as doubly occupied localized orbitals, or as pairs of strongly overlapping singly occupied orbitals.

2.1.2 Remaining part of non dynamical electron correlation

The GVB and SC methods take care of the left-right correlation for each bond of a polyatomic molecule. However, these methods do not include the totality of the "non-dynamical" correlation since the various local ionic situations are not interconnected with these methods. For example, the two ionic situations **1** and **2** below are expected to have different weights, **2** being more important than **1**,

but this feature is not taken into account in the wave functions of Coulson-Fisher type. To include all non dynamical electron correlation, one should abandon the Coulson-Fisher idea and go back to VB structures constructed with strictly atomic orbitals, without any delocalization tails, and generate all possible VB structures, allowing their coefficients and orbitals to be optimized simultaneously.

Technically, the simultaneous optimization of orbitals and coefficients for a multistructure VB wave function can be done with the VBSCF method due to Balint-Kurti and van Lenthe [21,22]. The VBSCF method has the same format as the classical VB method with an important difference. While the classical VB method uses orbitals that are optimized for the separate atoms, the VBSCF method uses a variational optimization of the atomic orbitals in the molecular wave function. In this manner the atomic orbitals adapt themselves to the molecular environment with a resulting significant improvement in the total energy and other computed properties.

2.2 Dynamical electron correlation

The importance of left-right correlation for the description of the bond is best appreciated in the case of the F_2 molecule. Here the experimental bonding energy is 38 kcal/mol, while the Hartree-Fock bond energy is *negative*, -36

kcal/mol [23], i.e., the energy of the molecule is found *higher* than that of the separated fluorine atoms. The situation improves considerably at the GVB or CASSCF levels (see Tables 1 and 2 below) which are nearly equivalent for this molecule. Despite the improvement, the calculated bonding energy is still disappointingly small, reaching only half of the full CI estimation with the same basis set. Thus, while GVB (and CASSCF) calculations take care of the Coulomb correlation, they do not treat the dynamic correlation which is accounted for in the extensive CI calculation. The qualitative defect of the GVB or CASSCF wave function of F_2 appears instantly once the wave function is expanded in terms of covalent and ionic VB structures with strictly localized AOs, in a manner similar to eq 7, and as pictorially represented in eq 8:

$$\Psi_{GVB} = \qquad\qquad \longleftrightarrow \qquad\qquad \longleftrightarrow \qquad\qquad \qquad (8)$$

$$F\bullet\!-\!\bullet F \qquad\qquad\qquad F^- \ F^+ \qquad\qquad\qquad F^+ \ F^-$$
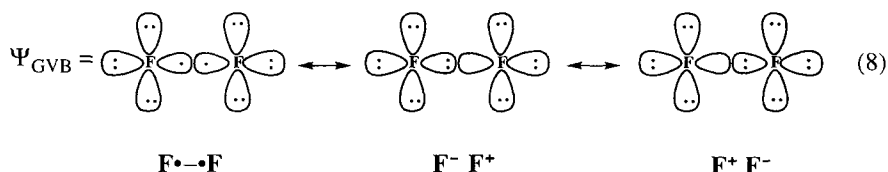
In the GVB wave function the orbitals and coefficients of the covalent and ionic structures are optimized. However, the atomic orbitals are nearly identical for the covalent and ionic structures, i.e. the orbitals are adapted to the mean-field of the three structures. In fact, all the orbitals are optimized for an average neutral situation, which is about correct for the covalent structure but disfavors the ionic ones. However, common sense suggests that the molecular energy would be further lowered if the AO's were allowed to assume different sizes and shapes, depending on whether they belong to the neutral atoms in the covalent structure or to the ionic atoms in the ionic structures. This is dictated not only by common sense but also from the wave-like property of the electron. Thus, as a wave the electron wave function should exhibit an instantaneous response to the local fields of the VB structures rather than to their mean-field. One can therefore anticipate that the mean-field constraint of GVB underestimates the weight of the ionic structures, leading to a poor description of the bond. Relaxing this constraint during the orbital optimization should allow each VB structure to have its own specific set of orbitals, different from one structure to the other, and would improve the description of the bond without increasing the number of VB structures. In such a wave function, the orbitals can be viewed as instantaneously following the charge fluctuation by rearranging in size and shape. Such orbitals were dubbed "breathing orbitals" and the method itself was named the "breathing-orbital valence bond" (BOVB) method. Our working hypothesis is that the qualitative improvement brought by this breathing-orbital effect closely corresponds to the contribution of dynamical correlation to the formation of the bond.

3. THE BREATHING ORBITAL VALENCE BOND METHOD

The idea of using different orbitals for different VB structures is not new, and has been successfully applied to molecules qualitatively represented as a pair of resonating degenerate Lewis structures, e.g., formyloxyl radical, carboxylate anions, etc. [24-26]. In this context, the non orthogonal CI of Jackels and Davidson for the formyloxyl radical [24], the RGVB method of Voter and Goddard [25], and the generalized multistructural wave function of Nascimento [26] should be mentioned. What we advocate here is just the systematic application of this principle to the description of the chemical bonds in reacting systems, with the aim of defining a VB method that possesses the following features: (i) Unambiguous interpretability of the wave function in terms of Lewis structures. (ii) Compactness of the wave function. (iii) Ability to calculate diabatic as well as adiabatic states. (iv) Reasonable accuracy (say a few kcal/mol) of the calculated energetics. (v) Consistency of the accuracy at all points of the calculated surfaces. The latter two points require that the method is able to describe the elementary events of a reaction, i.e. bond-breaking or bond-forming, in a faithful manner. Thus, a crucial test for the method will be its ability to reproduce dissociation curves, for two-electron as well as odd-electron bonds.

3.1 General principles

The general philosophy is that the representation of an electronic state in terms of Lewis structures is not just a model but rather an intimate picture of the true nature of the chemical interactions. The picture needs only a rigorous quantum mechanical formulation to become a quantitative computational method. The procedure that derives from this philosophy and underlies the BOVB method is straightforward. It consists of generating *all* the Lewis structures that are necessary to describe a reacting system in VB terms, and providing the corresponding VB structures with the best possible orbitals to minimize the energy of the final multi-structure state. This kind of "absolute" optimization of the orbitals is attained by getting rid of the above discussed mean-field constraint (e.g., of GVB, VBSCF, etc.), and allowing different orbitals for different VB structures. The method is thus grounded on the basic postulate that *if all relevant Lewis structures of an electronic state are generated and if these are described in a balanced way by a wave function, then this wave function should accurately reproduce the energetics of this electronic state throughout a reaction coordinate.*

The requirement that all Lewis structures be generated requires in turn that both covalent and ionic components of the chemical bonds have to be considered. As the number of VB structures grows exponentially with the number of electrons, it is already apparent that the BOVB method will not be

applied to large systems of electrons, but rather to that small part of a molecular system that effectively "takes part" in a reaction, so called the "active subsystem". The rest of the electrons are considered as spectators and treated at the MO level. These MO's do undergo however optimization during the BOVB procedure.

3.1.1. Choice of an active subsystem

Consider a typical S_N2 reaction as an example (eq 9). The reaction consists of the breaking of a C-F bond followed by the formation of a new C-Cl bond.

$$Cl^- + CH_3\text{-}F \rightarrow [Cl...CH_3...F]^- \rightarrow Cl\text{-}CH_3 + F^- \tag{9}$$
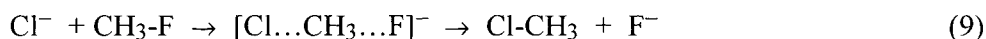
The four electrons and three orbitals involved in the C-F bond and in the attacking lone pair of Cl^- will constitute the heart of the reaction, and will form the "active" system. Three lone pairs of fluorine, three other lone pairs of chlorine and three C-H bonds of carbon will keep their status unchanged during the reaction and will form the "spectator" or "inactive" system. More generally, the active system will be composed of those orbitals and electrons that undergo bond-breaking or bond-forming in a reaction. While the inactive system will be treated at the simple MO level, i.e. the corresponding lone pairs or bonds will be described as localized doubly occupied MOs, the active system will on the contrary be subject to a detailed VB treatment involving the complete set of chemically relevant Lewis structures.

In the above example, this would mean consideration of the full set of the six VB structures (3-8) that one can possibly construct for a system of four electrons in three orbitals.

$$
\begin{array}{cccccc}
| & | & | & | & | & | \\
Cl^- \; C\bullet\text{-}\bullet F & Cl\bullet\text{-}\bullet C \; F^- & Cl^- \; C^+ \; F^- & Cl^- \; C^- \; F^+ & Cl^+ \; C^- \; F^- & Cl\bullet \; C^- \; F\bullet \\
/\backslash & /\backslash & /\backslash & /\backslash & /\backslash & /\backslash \\
\mathbf{3} & \mathbf{4} & \mathbf{5} & \mathbf{6} & \mathbf{7} & \mathbf{8}
\end{array}
$$
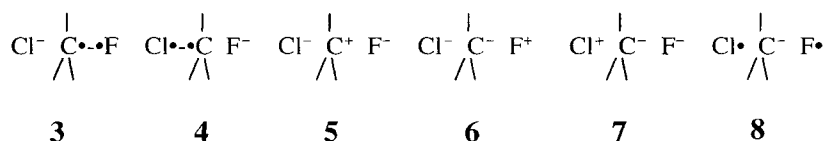
The active electrons are thus explicitly correlated, while the inactive electrons are not. One expects that the lack of correlation in the inactive subsystem will result in a constant error throughout the potential surface and therefore just uniformly shift the calculated energies relative to fully correlated surfaces. Note that in this model the inactive electrons are still affected by the progress of the reaction, since their orbitals rearrange and optimize at all points of the reaction coordinate. It is simply their mutual correlation that is considered as constant.

The above definitions of active/inactive subsystems is of course not restricted to the study of reactions but can be generalized to all static systems

whose qualitative description can be made in terms of resonating Lewis structures, like conjugated molecules, mixed valence compounds, etc.

3.1.2. VB formulation of the Lewis structures

After the choice of the relevant Lewis structures has been made, the following step involves their quantum mechanical formulation. Each Lewis structure corresponds to a set of atomic orbitals which are singly or doubly occupied, as illustrated in **9-11** for the F_2 molecule.

9   **10**   **11**
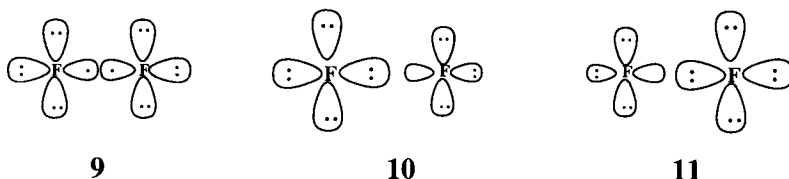
Each such Lewis structure is represented by a single VB spin-eigenfunction (Ψ_9-Ψ_{11}), hereafter called a "VB structure". These VB structures are linear combinations of Slater determinants involving the same occupied AOs as the corresponding Lewis structures, as in eqs 10-12.

$$\Psi_9 = \left|...\varphi_i...L_n\overline{R}_n\right| + \left|...\varphi_i...R_n\overline{L}_n\right| \tag{10}$$

$$\Psi_{10} = \left|...\varphi_i{'}...L_a\overline{L}_a\right| \tag{11}$$

$$\Psi_{11} = \left|...\varphi_i{'}...R_a\overline{R}_a\right| \tag{12}$$

Here φ, φ' and φ'' represent the set of inactive orbitals for each VB structure, L and R are the active orbitals of the left and right fragments, respectively, and the subscripts n and a stand for neutral and anionic fragments, respectively (recall that the cationic fragments have only inactive orbitals and no active ones). Note that the inactive orbitals φ_i, φ_i' and φ_i'' of Ψ_9-Ψ_{11} are all different from each other, as are the active orbitals L_n, L_a, or R_n, R_a. These differences are pictorially represented in **9-11** by drawing orbitals with different sizes depending on the identity of the species as neutral, cationic or anionic.

An important feature of the BOVB method is that the active orbitals are chosen to be strictly localized on a single atom or fragment, without any delocalization tails. If this were not the case, a so-called "covalent" structure, defined with more or less delocalized orbitals like, e.g., Coulson-Fischer orbitals, would implicitly contain some ionic contributions, which would make the interpretation of the wave function questionable [27]. The use of pure AOs is therefore a way to ensure an unambiguous correspondence between the concept of Lewis structural scheme and its mathematical formulation. Another reason for the choice of local orbitals is that the breathing orbital effect is

effective only when the charge fluctuation is truly reflected in the VB structures. This means that the ionic structures are really ionic and the covalent ones really covalent. When the orbitals are not local, a formally ionic structure is in fact contaminated by covalent ones and can at best reflect some damped charge fluctuation. Moreover, since one uses the full set of the VB structures, allowing the orbitals to delocalize would lead to artificial redundancy of the VB structures. It follows therefore that, the choice of purely localized active orbitals is in fact *not* a restriction on the orbital optimization, but rather a way to ensure a correct procedure.

On the other hand, there is no conceptual problem in letting the inactive orbitals be delocalized. For example, either the local p_x lone pairs of F_2 (in **9-11**) or their doubly occupied bonding and antibonding combinations represent two lone pairs facing each other. Thus, qualitatively both representations keep the same physical picture of this four-electron interaction. However, in flexible basis sets, the delocalized representation has more degrees of freedom over the localized one, since the building block AOs of the bonding and antibonding combinations can be different, thereby leading to a slightly better description of the four electron interactions. Therefore, the delocalization of inactive orbitals will be used as one of the possible options in the BOVB method.

3.1.3. BOVB levels

Several theoretical levels are conceivable within the BOVB framework. At first, the inactive orbitals may or may not be allowed to delocalize over the whole molecule *(vide supra)*. To distinguish the two options, a calculation with localized inactive orbitals will be labeled "L", as opposed to the label "D" that will characterize delocalized inactive orbitals. The usefulness and physical meaning of this option will be discussed below using particular cases.

Another optional improvement concerns the description of the ionic VB structures. At the simplest level, the active ionic orbital is just a unique doubly occupied orbital as in **10** or **11**. However this description can be improved by taking care of the radial correlation (also called "in-out" correlation) of the two active electrons, and this can be achieved most simply by splitting the active orbital into a pair of singly occupied orbitals accommodating a spin-pair, much as in GVB theory. This is pictorially represented in **12** and **13** which represent improved descriptions of **10** and **11**.
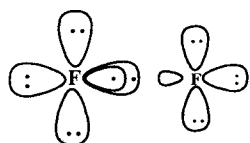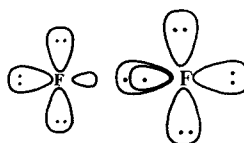
12   **13**

This improved level will be referred to as "S" (for "split") while the simpler level will carry no special label. Combining the two optional improvements, the BOVB calculations can be performed at the L, SL, D or SD levels.[†]

These levels are tested below on bond energies and/or dissociation curves of classical test cases, representative of two-electron and odd-electron bonds.

3.2. Dissociation of 2-e bonds

3.2.1. The difluorine molecule

The dissociation of difluorine is a demanding test case used traditionally to benchmark new computational methods. In this regard, the complete failure of the Hartree-Fock method to account for the F_2 bond has already been mentioned. Table 1 displays the calculated energies of F_2 at a fixed distance of 1.43 Å, relative to the separated atoms. Note that at infinite distance, the ionic structures disappear, so that one is left with a pair of singlet-coupled neutral atoms which just corresponds to the Hartree-Fock description of the separated atoms.

Since extensive basis sets are required to reproduce properties of this molecule, and we are using only 6-31G*, we cannot hope to reproduce the experimental bond energy. Therefore the best bonding energy is taken as the full CI value, in the region of 30 kcal/mol. The classical VB level, referred to in the Table as iteration 0, is a simple non-orthogonal CI between one covalent and two ionic structures, the orbitals being the pure atomic orbitals of fluorine as optimized in the free atoms. As can be seen, the bonding energy at this latter level is extremely poor (though better than Hartree-Fock) and does not even have the right sign. The GVB level, which nearly corresponds to the same VB calculations but with optimized orbitals (all VB structures sharing the same set of orbitals), is much better but still far from quantitative. However, as soon as the orbitals are allowed to adapt themselves to the individual VB structures (entries 1-5), the bonding energy increases and converges rapidly to a value close to the full CI estimation. Thus, the breathing orbital effect just corresponds to that part of the dynamical electron correlation that vanishes as the bond is broken. This provides a clear picture for the physical meaning of the dynamical correlation associated to the single bond, which is nothing but the wave-like quality of the electron manifested as the instantaneous adaptation of the orbitals to the charge fluctuation experienced by the two bonding electrons. Table 1 displays also the weights of the covalent and ionic structures, as calculated by means of the popular Chirgwin-Coulson formula,[‡]

[†] The L, SL and SD levels were referred to as levels I, II and III in ref. 12.

[‡] The weight W_n of a VB structure V_n is calculated as: $W_n = \sum_m C_n C_n S_{nm}$, where C_n and C_m are

Table 1

L-BOVB calculation on the F_2 molecule at a fixed interatomic distance of 1.43 Å. The 6-31G* basis set has been used. See Ref. 11 for more details.

Iteration	Energy (au)	D_e (kcal/mol)	Coefficients (Weights)	
			Covalent **9**	Ionic **10** or **11**
0	-198.71314	-4.6	0.840 (0.813)	0.194 (0.094)
1	-198.75952	24.6	0.772 (0.731)	0.249 (0.134)
2	-198.76494	27.9	0.754 (0.712)	0.258 (0.144)
3	-198.76572	28.4	0.751 (0.709)	0.260 (0.246)
4	-198.76600	28.5	0.752 (0.710)	0.259 (0.145)
5	-198.76608	28.6	0.750 (0.707)	0.261 (0.146)
Projected GVB[a]	-198.74554	15.7	(0.768)	(0.116)

[a] The VB weights are calculated after projecting the GVB wave function onto a basis of pure VB functions defined with strictly localized AOs.

thus emphasizing the imbalanced ionic/covalent ratio that characterizes low levels of calculation. The classical VB calculation, with its orbitals taken from the free atoms, severely disfavors the ionic structures with a weight that is much too small when compared with the best calculation, entry 5. The GVB wave function (projected on a basis of VB functions defined with pure atomic orbitals), with its orbitals optimized for the bonded molecule, is a little better, but it still suffers from the mean-field constraint. Now, when full freedom is given to the ionic structures to have their orbitals different from the covalent ones, the ionic weights gradually increase after each iteration. This clearly supports the above stated intuitive proposal that the lack of dynamical correlation, that characterizes the classical VB, GVB, SC or valence-CASSCF levels, results in an imbalance in the treatment of covalent vs ionic situations, and disfavors the latter structures.

The above best calculation [11] corresponds to the simplest level of the BOVB method, referred to as L-BOVB. All orbitals, active and inactive, are strictly local, and the ionic structures are of closed-shell type, as represented in **10** and **11**. However the theory can be further improved, and the corresponding levels are displayed in Table 2. It appears that the L-BOVB/6-31+G* level, yields a fair bonding energy, but an equilibrium distance that is rather too long compared to sophisticated estimations. This is the sign of an incomplete description of the bond. Indeed this simpler level does not fully account for the

---

the coefficients of V_n and V_m in the wave function and S_{nm} is their overlap.

Table 2
Dissociation energies and optimized equilibrium bond lengths for the F_2 molecule.

Method	R_{eq} (Å)	D_e (kcal/mol)	Ref.
6-31+G* Basis Set			
GVB	1.506	14.0	[12]
CASSCF	1.495	16.4	[12]
L-BOVB	1.485	27.9	[12]
SL-BOVB	1.473	31.4	[12]
SD-BOVB	1.449	33.9	[12]
Estimated full CI		< 33	[23]
Dunning-Huzinaga Basis Set [a]			
SD-BOVB	1.443	31.6	[12]
Estimated full CI	1.44 ± 0.005	28 - 31	[28,29]
Experimental	1.412	38.3	[30]

[a] A modified Dunning-Huzinaga basis set used by Laidig, Saxe and Bartlett [28]. The normal (4,1) p contraction is extended to (3,1,1) and a set of six d functions of exponent 1.58 is added.

correlation of the active electrons, which are located in doubly occupied orbitals in the closed-shell ionic structures **10** and **11**. Splitting the active orbitals of the ionic structures as in **12** and **13**, i.e., the SL-BOVB level, remedies the deficiency. The corresponding SL-BOVB level displays an increased bonding energy and a shortened bond length as compared to L-BOVB in Table 2.

The optimized equilibrium distance is still too large, however, and now the interactions between inactive electrons have to be considered. In the F_2 case, the inactive electrons involve the three lone pairs of each atom, facing each other. While their local AO or delocalized MO descriptions would be strictly equivalent in a minimal basis set, this is not the situation in more flexible basis sets. In a flexible basis set the delocalized MO description implicitly allows some charge transfers from one lone pair of an atom to some outer-valence orbitals of the other atom [31]. Most of this charge transfer corresponds to some back-donation in the ionic structures, i.e. the fragment F^- that has an electron excess in its sigma orbitals donates back some charge to the F^+ fragment through its π orbitals. Indeed, allowing the π lone pairs to delocalize (SD-BOVB entries in Table 2) results in a significantly shortened calculated bond length which is now in the expected range.

For the sake of comparison, Table 2 displays also some full CI estimations by Laidig, Saxe and Bartlett [28] (LSB), along with SD-BOVB calculations using the same basis set. The BOVB bonding distance appears perfectly correct, while the bonding energy seems slightly too large, but still within an acceptable error margin.

3.2.2. The hydrogen fluoride molecule

Hydrogen fluoride is another classical test case, representing a typical polar bond between two atoms of very different electronegativities. As such, the molecule is expected to possess one ionic structure, F^-H^+ (**14**) that is nearly as important as the covalent one (**15**). Thus, any deficiency in the description of ionic structures should result in significant error in the bonding energy and dissociation curve. Another distinctive feature of the F–H bond is its very high experimental bonding energy of 141 kcal/mol. With such strength of the bonding, one may wonder if the inactive electrons may still keep their identity, as assumed by the basic hypothesis of the BOVB method. For these two reasons, hydrogen fluorine is a challenging case, especially when the BOVB method can be assessed *vis à vis* benchmark full CI calculations that are available for the bond energy and the full dissociation curve.

As usual, the single bond is described by three VB structures, **14-16**.

| 14 | 15 | 16 |
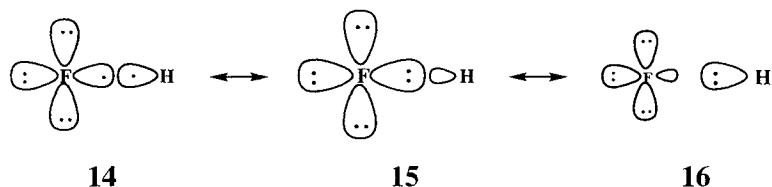
The F^+H^- (**16**) structure is expected to be very minor but is nevertheless added for completeness. Table 3 displays the optimal bond lengths and bonding energies calculated at various theoretical levels, in the 6-31+G** basis set and in an additional basis set comparable in quality to the one used by Bauschlicher and Taylor [32].

Dynamic electron correlation effects appear once again to be an important component of the bonding energy, since the GVB/6-31+G** calculation yields a value of only 113 kcal/mol, quite far from the experimental value. However the simple L-BOVB level also proves to be quite insufficient, with a bonding energy that is still much too small. This is expected (*vide supra*), owing to the importance of the F^-H^+ ionic structure **15** that is rather poorly described without splitting the doubly occupied orbitals. Splitting the active orbital of this structure, as in **17**, leads to a spectacular improvement of the bonding energy, by *ca* 12 kcal/mol, (SL-BOVB/6-31+G** entry in Table 3). As in the F_2 case, further improvement is gained by delocalizing the π inactive orbitals to reach

Table 3

Dissociation energies and optimized equilibrium bond lengths for the FH molecule

Method	R_{eq} (Å)	D_e (kcal/mol)	Ref.
6-31+G** Basis Set			
GVB(1/2)	0.920	113.4	[12]
L-BOVB	0.918	121.4	[12]
SL-BOVB	0.911	133.5	[12]
SD-BOVB	0.906	136.3	[12]
Extended SD-BOVB	0.916	137.4	[12]
BT Basis Set [a]			
SD-BOVB	0.906	136.5	[12]
Extended SD-BOVB	0.912	138.2	[12]
Full CI [b]	0.921	136.3	[32]
Experimental	0.917	141.1	[30]

[a] A double-zeta + polarization + diffuse basis set used by Bauschlicher and Taylor [32].
[b] The 2s orbitals are not included in the CI.
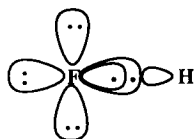
17

the SD level that yields a bonding energy of 136.3 kcal/mol, in very reasonable agreement with the experimental value.

Due to its polar nature, hydrogen fluoride is a stringent test for the key assumption that the correlation of the inactive electrons remains nearly constant throughout the dissociation process. Since the inactive electrons of F^- in the F^-H^+ structure feel a different electric field than those of the neutral F fragment at infinite separation, one might have expected the intra-pair correlation energy of the active electrons to vary with the interatomic distance, owing to the importance of the ionic structure at the equilibrium geometry. To probe whether the assumption breaks down, we pushed the BOVB calculation to a higher level. Here, *all* doubly occupied orbitals, in the two main VB structures, are splitt, leading to **18** and **19**.

This test calculation, referred to as "Extended SD-BOVB" in Table 3, results in an improvement of only 1.1 kcal/mol of the bonding energy relative to the standard SD level, thus confirming the assumption of near-constancy of the correlation within inactive electrons. It follows therefore that going beyond the SD-BOVB level is not necessary.

| 18 | 19 |
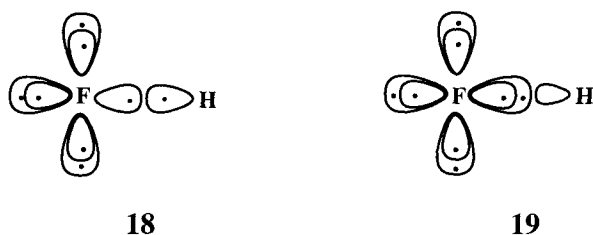
Table 3 displays also a comparison of a full CI calculation by Bauschlicher and Taylor [32] with the best BOVB levels using a common basis set. Once again the SD-BOVB level is entirely sufficient, while its extended version leads to a meager improvement. In any case, both levels are in excellent agreement with the full CI results.

By nature, the BOVB method describes properly the dissociation process. As a test case, the dissociation curve of the FH molecule was calculated at the highest BOVB level (extended SD-BOVB), and compared with a reference full CI dissociation curve calculated by Bauschlicher et al. [33] with the same basis set. The two curves, that were compared in Ref. 12, were found to be practically indistinguishable within an error margin of 0.8 kcal/mol, showing the ability of the BOVB method to describe the bonding interaction equally well at any interatomic distance from equilibrium all the way to infinite separation [12].

3.2.3. First row transition metals hydride cations

Bonds that involve transition metals are difficult to handle computationally, owing to two factors : (i) The reshuffle of electronic configurations that accompanies the dissociation, and (ii) the presence of a large number of inactive electrons that exert a great influence on the bonding electrons. In this context, previous theoretical studies of transition metal hydride cations (TMH^+) showed that accurate predictions of bond dissociation energies require extended wave functions, which account for both static and dynamic electron correlation effects [34,35]. Goddard et al. [34] showed that the GVB function by itself is unable to provide quantitative accuracy, but it predicts correct trends and elucidates the bonding patterns in first-row TMH^+. The factors which determine the bonding patterns [35] are the promotion energy of the metal cation from the $3d^{n+1}$ state to the bond-forming $4s^13d^n$ state, the loss of exchange in the $4s^13d^n$ state following bond-formation, and the ground state

symmetry determined by the electrostatic repulsion between the d electrons. It is apparent therefore that VB theory is capable of providing very useful insight into bonding because it involves a compact, easily interpretable wave function. Further insight can be gained by employing the BOVB method that uses explicit covalent and ionic structures and can provide bonding patterns in terms of covalency, covalent-ionic resonance energy and orbital relaxation of the 3d and $3s^23p^6$ shell electrons. Can the BOVB wave function, despite its extreme simplicity, still provide reasonable bonding energies in such difficult cases?

To answer this question, Galbraith et al. [36] used BOVB to study the bond energies of TMH$^+$ species (TM = Sc, Ti, V, Cr, Mn, Fe, Co, Ni, Cu and Zn). The basis set involved a relativistic effective core potential for the $1s^22s^22p^6$ core and a triple-ζ (8s,7p,6d//6s,5p,3d) basis for the 3s, 3p, 3d and 4s shells of the metal, augmented with an f-type polarization function. For hydrogen, the triple-ζ (5s//3s) basis of Dunning was augmented with a p-type polarization function. At the dissociation limit the BOVB wave function correlates with the restricted open-shell Hartree-Fock (ROHF) states of TM$^+$ and H. This level treats poorly the atomic states and especially the $3d^{n+1}$ state. To correct for this non-VB-related deficiency, Galbraith et al. [36] used the technique recommended by Goddard [34,35] and Bauschlicher [37], of shifting the energies of the TM$^+$ fragment using experimental data. Thus, the TMH$^+$ species are first dissociated into the atomic state most closely resembling their situation in the molecule (i.e. the $4s^13d^n$ state for TM$^+$), and whenever necessary, the experimental atomic state splitting is used to correct the energy of the TM$^+$ fragment to the corresponding atomic ground state.

The bond dissociation energies, calculated at the various computational levels, are displayed in Table 4 and compared with experimental values. The VBSCF results are seen to be slightly better than the GVB results. Both results qualitatively reproduce the characteristic zigzag pattern of the experimental trends across the first TM row. However these two sets of bond energies are systematically too weak, by 10-20 and sometimes by more than 30 kcal/mol, thus projecting the importance of dynamic correlation. Accordingly, a significant improvement is found upon moving from GVB or VBSCF to L-BOVB. The added flexibility of the BOVB method is seen to bring the predicted bond dissociation energies closer to the benchmark CCSD(T) values and to experimental results. Thus, while VBSCF (as well as GVB or SC methods) captures the essential non dynamic correlation effects due to the bonding event, the BOVB retains this qualitative picture, but adds the dynamic relaxation of all the electrons in response to bond pairing.

Still, the BOVB bonding energy for CuH$^+$ remains too small, by *ca* 10 kcal/mol, a rather unusually large error for this method. However, CuH$^+$ is a particularly difficult case as can be judged by the VBSCF and GVB values which are in error by 38 and 44 kcal/mol, respectively. Another source of

Table 4

Bond dissociation energies (kcal/mol) of TMH$^+$ species, at the GVB, VBSCF, L-BOVB and CCSD(T) levels. The M-H bond lengths are optimized at the VBSCF level.

	GVB	VBSCF	L-BOVB	CCSD(T)	experimental
ScH$^+$	47.4	46.4	57.5	55.2	57 ± 2
TiH$^+$	43.4	44.2	54.3	54.6	54 ± 3
VH$^+$	33.8	41.6	53.1	48.0	48 ± 2
CrH$^+$	8.9	9.5	26.1	37.3	32 ± 2
MnH$^+$	25.9	30.6	44.0	44.2	48 ± 3
FeH$^+$	31.2	36.0	53.9	51.9	50 ± 2
CoH$^+$	21.3	27.2	48.8	39.5	47 ± 2
NiH$^+$	9.7	16.1	40.3	39.3	40 ± 2
CuH$^+$	-22.2	-16.3	11.4	24.4	22 ± 3
ZnH$^+$	46.5	46.2	55.7	56.0	55 ± 3

inaccuracy comes from the use of VBSCF-optimized bond lengths, which were found generally too long by an average of 0.09 Å at this crude level [36]. Moreover, the BOVB calculation was limited to the simplest L-BOVB. It would be interesting to test the SD-BOVB level on these systems, with proper geometry optimization, to make a more critical evaluation of this unusual case.

3.2.4. General procedure for low-symmetry cases

Up to now we have dealt with molecules which makes the distinction between active and inactive orbitals an obvious task based on simple symmetry considerations. Such symmetry is not always present in the general case, and this poses a danger that there could be flipping between the sets of active and inactive orbitals during the BOVB orbital optimization,

The simplest level, L-BOVB, presents no particular practical problem. Fast convergence is generally obtained by using well adapted guess orbitals, that can be chosen as the Hartree-Fock orbitals of the isolated fragments with the appropriate electronic charge. Thus, the guess orbitals for the covalent structure are those of the isolated radicals, while the orbitals of the isolated anions and cations can be taken for the ionic structures.

Moving to the more accurate SL-BOVB level, merely requires checking that the orbital that is being split (in an ionic structure) is indeed an active orbital, and that the pair of singly occupied orbitals does not end up belonging to the inactive space after the optimization process. While this condition is generally met by choosing an appropriate guess function in high symmetry cases (F$_2$ or HF above), in the general case nothing guarantees *a priori* that this

exchange between the active and inactive spaces will not take place, leading for example to **20** instead of the correct structure **21** in the case of $H_2N\text{-}NH_2$.
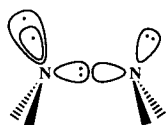
20	**21**

To circumvent this difficulty, a general procedure was developed. After the L-BOVB step, the orbitals are initially subject to localization[†] using any standard method, then the active orbital are split while the inactive ones are kept frozen during the optimization process.

Delocalization of the inactive orbitals (D-BOVB or SD-BOVB) is important for getting accurate energetics, especially in cases where the inactive orbitals are not lone pairs but are instead bonding orbitals (e.g. C-H bond in $H_3C\text{-}F$). This is because this degree of freedom allows for charge transfer to take place between inactive orbitals of the two fragments. The antibonding orbitals of a bond like C-H are better suited than high-lying outer-valence lone pair orbitals to accept an extra electron from the neighboring fragment e.g., F in $H_3C\text{-}F$. Once again, it is important to make sure that the orbitals that are delocalized are the inactive ones, while the active set remains purely localized which is the basic tenet of the method. Otherwise, any artefactual solution might be found. To avoid any spurious exchange between the active and inactive spaces during the orbital optimization process, it is possible to start from an L-BOVB or D-BOVB wave function, then allowing delocalization of the inactive orbitals while freezing, this time, the *active* orbitals during the subsequent optimization process that leads to the D-BOVB or SD-BOVB levels, respectively.

3.3. Dissociation of Odd-e Bonds

Alongside electron-pair bonds, odd-electron bonds play an important role in chemistry, and constitute therefore a compulsory test case for any computational method. Odd-electron bonds can be represented as two resonating Lewis structures that are mutually related by charge transfer, as shown in (13) for two-center, one-electron (2c,1e) bonds and in (14) and (15) for typical two-center, three-electron (2c,3e) bonds.

$$A\bullet\ B^+\ \leftrightarrow\ A^+\ \bullet B \tag{13}$$
$$A\bullet^+ :B\ \leftrightarrow\ A: \bullet B^+ \tag{14}$$
$$A\bullet\ :B^-\ \leftrightarrow\ A:^-\ \bullet B \tag{15}$$

[†] This requires prior orthogonalization of the orbitals within each fragment.

According to qualitative VB theory, such bonds owe their strength to the resonance energy associated with the mixing of the two limiting structures. A significant resonance energy requires degeneracy of the two resonating structures, or nearly so. As a result most of the observed odd-electron bonds are homonuclear (A=B).

In MO theory the stability of these bonds is readily understood by inspection of orbital interaction diagrams **22** and **23**, where σ and $\sigma*$ are bonding and antibonding combinations of active orbitals, respectively. Both

22   **23**
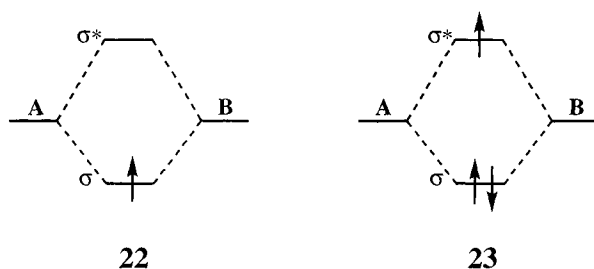
diagrams display one net bonding electron. These diagrams can be further considered to question the role of left-right electron correlation. In **22**, the active space reduces to a single electron, and this eliminates the need for electron correlation within this space. On the other hand, the active space of **23** involves three electrons; however, the only configuration one might have added to improve the simple Hartree-Fock wave function is the singly excited $\sigma^1\sigma*^2$ one, which by virtue of Brillouin's theorem does not mix with $\sigma^2\sigma*^1$. It follows that the concept of left-right correlation is meaningless in such systems, and that the description of both one-electron and three-electron bonds is already qualitatively correct at the Hartree-Fock level, contrary to two-electron bonds.

In view of the preceding analysis, the complete failure of Hartree-*Fock ab initio* calculations to reproduce three-electron bonding energies might seem to be a paradox. Clark [38] and Radom [39] carried out systematic calculations on series of cation radicals involving three-electron bonds between atoms of the second and third rows of the periodic table, and showed that the Hartree-Fock error is always large, sometimes of the same order of magnitude as the bonding energy itself. Thus, F_2^- that is experimentally bound by 30 kcal/mol is found to be unbound at the ROHF level [23]. The error is much smaller in the case of one-electron bonds [38], yet it may be as large as 13 kcal/mol in the $H_3C\bullet CH_3^+$ cation. Interestingly, the Hartree-Fock error is not constant, but gradually increases as the bonded atoms are taken from left to right or from bottom to top of the periodic table.

Focusing on the three-electron case, the puzzling Hartree-Fock deficiency can be analyzed by expanding the corresponding wave function into its VB constituents, as we did above in the two-electron case. Taking the F_2^- case as an example, the Hartree-Fock wave function Ψ_{HF} (3-e) reads:

$$\Psi_{HF}(3-e) = \left|...\varphi_i...\sigma_g \overline{\sigma}_g \sigma_u\right| \tag{18}$$

where φ_i represent the inactive orbitals, and the active orbitals σ_g and σ_u are defined already in eq 4 above. Expanding σ_g and σ_u leads to eq 19:

$$\Psi_{HF}(3-e) = \left|...\varphi_i...\chi_a \overline{\chi}_a \chi_b\right| + \left|...\varphi_i...\chi_a \overline{\chi}_b \chi_b\right| \tag{19}$$

Thus, the Hartree-Fock wave function is equivalent to a two-configuration VB wave function. The same VB structures, **24** and **25**, were in fact used in the original VB treatment of three-electron bonds by Pauling [40].

| **24** | **25** |
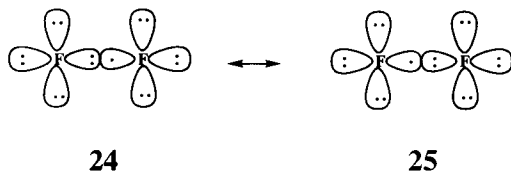
Even though it is physically correct, the ROHF wave function suffers from the same defect as the GVB wave function for two–electron bonds. Thus, the active AOs are common for the two structures and are not adapted to their instantaneous occupancies, while the inactive orbitals are not adapted to the instantaneous charge of the fragments. Once again, this defect can be removed by use of the BOVB wave function that allows for different orbitals for different structures, as in eq 20 :

$$\Psi_{BOVB}(3-e) = C_1\left|...\varphi_i...L_a \overline{L}_a R_r\right| + C_2\left|...\varphi_i...L_r \overline{R}_a R_a\right| \tag{20}$$

$$L_a \neq L_r; \quad R_r \neq R_a; \quad \varphi_i \neq \varphi_i'$$

Here the orbitals are defined in the same way as in eqs 10-12. Some representative test cases are discussed below.

3.3.1. The F_2^- radical anion

As is the case for its neutral homologue, the difluorine radical anion is a difficult test case for the calculation of its bonding energy. At the Hartree-Fock level, the bonding energy is about ± 4 kcal/mol, depending on whether the ROHF or UHF method is used. The experimental bond energy is 30 kcal/mol.

In contrast, the MP2 and MP4 methods of theory are successful, and this success emphasizes the dynamic nature of electron correlation for this molecule.

The computed equilibrium distance and bonding energy of F_2^- are displayed in Table 5. To appreciate better the sensitivity of active vs inactive orbitals to the breathing orbital effect, the latter has been introduced by steps: In the first step no breathing orbitals are used ($L_a = L_r$, $R_a = R_r$, $\varphi_i = \varphi_i'$): this VBSCF calculation is nearly equivalent to the ROHF level. In the second step, only active orbitals are included in the breathing set ($L_a \neq L_r$, $R_a \neq R_r$), while in the next step full breathing is permitted ($L_a \neq L_r$, $R_a \neq R_r$, $\varphi_i \neq \varphi_i'$). The latter wave function, at the L-BOVB level, can be represented as in **26**, **27** below.

26   **27**
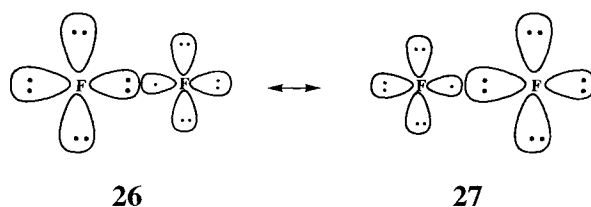
The breathing orbital effect, restricted to the active orbitals that are directly involved in the three-electron bond, already improves the bonding energy by some 17 kcal/mol relative to the ROHF value (Table 5). Extension of the

Table 5

Calculated equilibrium distances and dissociation energies for the F_2^- radical anion, (6-31+G* basis set). BOVB calculations are performed with all valence orbitals being included in the set of breathing orbitals (fully-breathing option) unless otherwise specified (entry 2).

Entry	Method	R_{eq} (Å)	D_e (kcal/mol)	Ref.
1	ROHF		-4	[23]
2	L-BOVB (active set only)	1.954	13.3	" "
3	L-BOVB	1.964	29.7	[13]
4	D-BOVB	1.954	30.1	" "
5	SD-BOVB	1.975	28.0	" "
6	SD-BOVB (4-structure)	1.976	28.0	" "
7	MP2	1.916	26.2	[13]
8	PMP2	1.935	29.5	" "
9	MP4	1.931	25.8	[41]
10	Experiment		30.2	[30]

breathing orbital effect to the inactive orbitals brings another 16 kcal/mol, yielding a final bonding energy of 29.7 kcal/mol, in excellent agreement with the experimental bonding energy of 30.2 kcal/mol [30].

The Hartree-Fock error is thus completely corrected by the breathing orbital effect. On a "per orbital" basis, each active AO contributes for 8.6 kcal/mol to the overall BO stabilization, while the inactive lone pairs have a lesser influence, about 2.8 kcal/mol each.

The calculation can be further improved by allowing the inactive π orbitals to delocalize over the molecule, at the D-BOVB level. As a result, the equilibrium bond length is shortened by 0.01 Å, and the bonding energy is increased by 0.4 kcal/mol relative to the L-BOVB level (Table 5). This rather meager return from increasing the level of theory indicates that the fully localized atomic orbitals are, right at the outset, well adapted to the description of the three-electron interaction, contrary to what is observed in two-electron bonds. This difference may be due in part to the long equilibrium distance that characterize three-electron bonds, which results in weak interatomic repulsions between inactive lone pairs. Another reason for the ineffectiveness of π delocalization is that neither of the VB structures **24** or **25** displays a polar σ bond that needs to be counter-polarized by π back-donation as in two-electron bonds.

Somewhat more significant is the effect of splitting the active orbitals, leading to structures **28** and **29** at the SD-BOVB level, where the local singlet

28   **29**
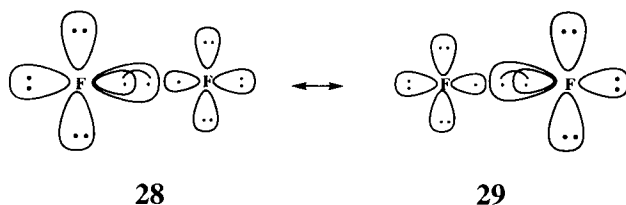
spin-couplings are indicated by curved lines. However this improvement does not lead to an increase, but rather to a small decrease (1.7 kcal/mol) of the bonding energy. This is because the effect of splitting the active orbitals stabilizes both the separated fragments and the bonded molecules, so that both stabilizations nearly compensate each other and may lead to a small correction of any sign in the bonding energy. In contrast, in the case of two-electron bonds, splitting the doubly occupied active orbitals always benefits the ionic structures that are present at equilibrium distance but which vanish at infinite separation, leading thereby to an increased bonding energy.

Up to now we have dealt with the two Lewis structures that a chemist might write down to describe the three-electron interaction. However, mathematically, there are two spin-coupling modes of three electrons in three orbitals both

leading to doublet spin eigenfunctions. Thus, the complexity of the SD-BOVB wave function could be further increased by adding structures **30** and **31**. These structures exhibit the same orbital occupancy as **28** and **29** but exhibit different spin couplings. The calculation using **30** and **31** is referred to as "SD-BOVB (4-structure)" in Table 5, and is seen to give a bond energy virtually the same as the standard SD-BOVB level. This result fully confirms the validity of Pauling's simple model based on chemical intuition.

30   **31**
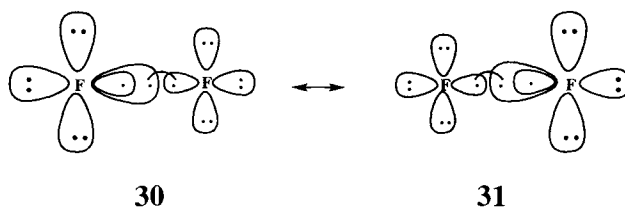
The performances of the various BOVB levels can be compared to those of Møller-Plesset (MP) perturbation theory, yet with some caution since the various MP orders do not converge well. This is due to a rather large spin contamination at the unrestricted MP2 level, which leads to a wave function with an $<S^2>$ value of 0.78. Keeping in mind that the breathing orbitals of F_2^- are not much polarized [13], the bonding energy is not expected to be very basis set dependent, so that the SD-BOVB value of 28.0 kcal/mol is entirely reasonable relative to the experimental value of 30.2 kcal/mol. The BOVB calculated equilibrium bond lengths are rather long relative to the values calculated at the various MP levels (no experimental value is available), and both sets of values display significant variations from one level to the other. This inaccuracy is however normal, owing to the extreme flatness of the potential surface near the energy minimum. Indeed, at the MP4 level the force constant is only 0.55 mdyn/Å, which means that stretching the bond by 0.02 Å away from equilibrium results in an energy rise of only 0.03 kcal/mol.

A final point is in order concerning the avoidance of symmetry-breaking artefacts by the BOVB method as opposed to others. Three-electron bonds, just like any electronic system that must be described by more than one Lewis structure, are subject to the symmetry-breaking artefact with most computational methods of MO type: Hartree-Fock, MP2 or MP4, and even CCSD and CCSD(T)) [42,43]. This symmetry breaking is observed beyond a critical interatomic distance which may actually happen to be shorter than the equilibrium bond length, and it is due to a competition, during orbital optimization, between the resonance effect and the breathing orbital effect (called " size effect " by other authors [44,45] in this case). Assuming for example that the orbital optimization is performed at the Hartree-Fock level, the wave function is subject to the so-called " symmetry dilemma ": that is, if

the symmetry of the wave function is broken, it converges to a solution like **26** alone, in which the orbitals are adapted to their occupancy but where the resonance is lost. On the other hand, if the symmetry is maintained, the wave function converges to a solution of the type **24↔25**; this benefits from the resonance energy, but the orbitals are optimized in a mean field, and are consequently poorly adapted to their instantaneous occupancy. In cases where the resonance is dominant, the wave function displays the correct symmetry. However, as soon as the resonance becomes too weak to overcome the breathing orbital effect, the wave function departs from the molecular symmetry and leads to unphysical geometries, frequencies and energetics. This problem, which is rather difficult to overcome with standard computational methods, vanishes at the BOVB level: as the wave function involves *both* the size effect and the resonance effect at any molecular geometry, the root cause for the symmetry breaking disappears. *The BOVB method is, by nature, entirely free from the symmetry breaking artefact.*

3.3.2. The Cl_2^- radical anion

The valence orbitals of Cl_2^- are spatially larger than those of F_2^-. Accordingly, the breathing orbital effect is expected to be less important in Cl_2^- than in F_2^-, since two electrons occupying the same orbital are now less confined than in the compact orbitals of F_2^-.

Table 6 displays some bonding energies for Cl_2^-, as calculated at the D-BOVB level and at other theoretical levels, including Hartree-Fock and Møller-Plesset perturbation theory. Unlike the F_2^- case, the Møller-Plesset series converges well around the values of 24-25 kcal/mol which can be taken as references for the bonding energy in this basis set.

The fully breathing D-BOVB result is once again in good agreement with the various Møller-Plesset values and with the POL-CI calculation of Wadt and Hay [46] in a similar basis set. The breathing orbital effect of the inactive orbitals, estimated by comparing the bonding energies in entries 1 and 2 in Table 6, only amounts to 7.1 kcal/mol, which is significantly smaller than the corresponding value of 16.4 kcal/mol in F_2^-. Moreover, the effect for the active orbitals alone (compare entries 2 and 3) brings only 4.5 kcal/mol of stabilization in Cl_2^- relative to the Hartree-Fock level, to be compared to the value 17.3 in F_2^-, thus fully supporting the qualitative expectations based on orbital size.

Basis set effects begin to be important in three-electron bonds involving atoms of the third-row, since polarization functions are important for reproducing atomic polarizabilities, which are important in atom-ion interactions. For this reason, the BOVB result that was calculated in the modest 6-31+G* basis set yields a bonding energy which is some 4-5 kcal/mol smaller than more accurate G2 [47] and CPF [48] calculations, using a close to

Table 6

Calculated dissociation energies for the Cl_2^- radical anion, in 6-31+G* basis set, with an MP2-optimized bond length of 2.653 Å, except otherwise specified.

Entry	Method	D_e (kcal/mol)	Ref.
	D-BOVB		
1	fully-breathing	22.6	[13]
2	active set only	15.5	[13]
3	ROHF	11.0	[13]
4	MP2	24.7	[13]
5	PMP2	25.5	[13]
6	MP4	24.4	[13]
7	POL-CI [a]	24.0	[46]
8	G2 [b]	27.5	[47]
9	CPF/6s5p4d3f2g [c]	27	[48]

[a] Optimized bond length of 2.69 Å. [b] Optimized within the G2 procedure.
[c] Optimized bond length of 2.59 Å.

complete basis set. It is clear that using a more sophisticated basis set for Cl_2^- would have brought the BOVB calculated bonding energy close to the accurate value. In support of this assertion, Archirel [49] has calculated the bonding energy of another three-electron-bonded molecule of the third-row, Ar_2^+, and got disappointing results with a simple double-zeta polarized basis set. Then, using a better basis set of 4s4p2d1f quality, he obtained a bonding energy of 30.2 kcal/mol at the D-BOVB level, in good agreement with the experimental value of 30.7 kcal/mol, or 32.0 kcal/mol after compensating for the estimated spin-orbit interaction [50].

3.3.3. The $(NH_3)_2^+$ radical cation

The atomic orbitals of nitrogen are larger than those of fluorine, with optimized exponents of 1.96 for NH_3 vs 2.40 for F^-, in a minimal basis set. Therefore, one can once again predict a smaller breathing orbital effect for both the active and inactive orbitals of $(H_3NNH_3)^+$, relative to F_2^-. However, the inactive orbitals in this case represent single N-H bonds as opposed to the lone pairs in the F_2^- case. It is clear that the inactive electrons are on average closer to the nuclei for lone pairs than for bonds, and are therefore more sensitive to the charge fluctuation of the active space. This effect, together with the orbital size effect, leads to the expectation that the breathing orbital effect should be definitely weaker in $(H_3NNH_3)^+$ compared with F_2^-, and probably even more

Table 7
Calculated dissociation energies for the $(H_3N\text{-}NH_3)^+$ radical cation in its D_{3h} conformation (6-31G* basis set). MP2-optimized geometries are used throughout.

Method	D_e (kcal/mol)	Ref.
D-BOVB		
fully-breathing	37.9	[13]
active set only	30.8	" "
ROHF	20.3	" "
MP2	40.0	" "
PMP2	41.4	" "
MP4	38.9	" "

so in the inactive orbital space.

The bonding energies of the $(H_3NNH_3)^+$ cation, calculated at the D-BOVB level and at various levels of MO theory, are reported in Table 7 and support the above qualitative deductions. The total breathing orbital effect amounts to 17.6 kcal/mol, that could be decomposed into 7.1 kcal/mol for the inactiveorbitals and 10.5 kcal/mol for the active ones, which is much less than in F_2^-. As in the preceding case, the BOVB-calculated bonding energy of $(H_3NNH_3)^+$ is in satisfying agreement with the results of the Møller-Plesset series which is rather well converged and probably reflects the basis set limit.

3.3.4. One-electron bonds

As shown by Clark [38] in a comprehensive computational study of $(H_nX\bullet XH_n)^+$ radical cations (X= Li to C, Na to Si), one-electron bonds are already rather well described by simple Hartree-Fock theory. This is because the active system contains a single electron, so that the breathing orbital effect is ineffective in the active subspace, where each orbital is either empty or singly occupied as illustrated in **32, 33** for the C•C bond.

32   **33**
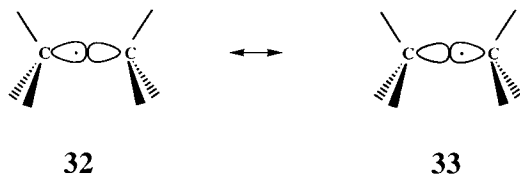
Therefore, the effect is restricted to the inactive space and, accordingly, the Hartree-Fock error is nearly proportional to the number of inactive orbitals. It

increases gradually in the series (X = Li to C), reaching 13 kcal/mol in $(H_3C \cdot CH_3)^+$, compared with the total bonding energy of 51.0 kcal/mol [51], calculated at the MP4/6-31G* level. In accord with the above qualitative analysis of the breathing orbital effect in terms of orbital size, compounds of the third row atoms (X = Na to Si) exhibit less correlation effects than analogs of the second row of the periodic table.

The $(H_3C \cdot CH_3)^+$ radical cation was selected, to test the ability of the BOVB method to describe one-electron bonds, since this bond exhibits the largest correlation effect in the series. The bonding energy, calculated at the D-BOVB level, amounts to 48.7 kcal/mol, in fair agreement with the MP4 value.

3.4. Summary of the Computational Tests

The BOVB method has not been subject to systematic tests of accuracy, except for the F_2, HF, F_2^-, Cl_2^- and $(NH_3)_2^+$ species. However, some bonding energies have been calculated here and there in studies dedicated to other aspects of bonding, e.g., charge-shift bonding in H_3M-Cl (M = C, Si, Ge, Sn, Pb) [52,53], the lone pair bond weakening effect [54], etc. These studies provide additional tests of the accuracy of the BOVB method. However it must be kept in mind that in these studies, the best accuracy was not the aim and hence was not sought. In particular, basis sets of modest size were used, so that the calculated dissociation energies should not be compared directly to experimental values.

Naturally then, the accuracy of the results, displayed in Table 8, follows the adequacy of the basis set that has been used. As a rule, basis sets involving high-ranking polarization functions are needed for third-row atoms and/or for atoms involving lone pairs. Accordingly, the calculated C-H bonding energy is quite close to the experimental value for CH_4, a molecule made of first and second-row atoms and devoid of lone pairs, for which the 6-31G** basis set is sufficient. For NH_2 and H_2O, which bear lone pairs, the lack of f-type polarization functions begins to down-grade the numerical accuracy, and the

Table 8

Some BOVB-calculated bonding energies in double-zeta polarized basis sets

	BOVB level	Basis set	D_e (theor.)	D_e (exp.)	Ref.
H_3C-H	SL	6-31G**	114.5	112.0	[54]
H_2N-H	SL	6-31G**	114.4	116.0	[54]
HO-H	SL	6-31G**	119.1	125.4	[54]
H_3C-Cl	SD	6-31G*	79.9	87.3	[52]
H_3Si-Cl	SD	6-31G*	101.7	110.7	[52]

basis set deficiency gets more severe in H_3C-Cl and H_3Si-Cl that involve lone pairs as well as third-row atoms. Nonetheless, the bonding energies remain very reasonable in all cases, as has been found above for transition metal hydrides [36].

This generally good performance demonstrates that the BOVB wave function, despite its very small size, captures the essence of the chemical bond, be it of the odd-electron or two-electron type, polar or non-polar. The complete neglect of Coulomb correlation within the inactive space has no significant consequences for the relative energies. This in turn means that the inactive electrons require dynamic correlation, associated with the fact that their orbitals undergo changes in size, polarization or hybridization. However these electrons have some nearly constant Coulomb correlation energy. In fact, just the bare minimum electron correlation is taken into account since the method becomes equivalent to a Hartree-Fock calculation of the separated fragments at the dissociation limit. Thus, the method only calculates the differential electron correlation, that involves the left-right electron correlation of the active electrons, and the dynamical correlation associated with the formation of the bonds. Since the latter term is nascent from the instantaneous adaptation of the orbitals to the charge fluctuation of the active electrons, dynamical correlation effects are particularly important in three-electron bonds, because in such systems the stabilizing interaction originates only in the charge fluctuation between the two VB structures.

While all levels provide nearly equally good bonding energies for the three-electron bonds, the same does not hold true for two-electron bonds which often require the best levels for an accurate description. Splitting the active orbitals in the ionic structures is important when the bond is polar. Moreover, the interatomic interactions between inactive orbitals are important in two-electron bonds, owing to their short equilibrium bond lengths. Such interactions are adequately taken into account by delocalizing the inactive orbitals.[†] This effect is particularly important when the bond is very polar as in H_3C-Cl and H_3Si-Cl. Thus polar bonds are better described at the SD-BOVB level while bonds that are mainly covalent in nature are less demanding.

Finally, a few remarks are in order concerning the non dynamic correlation of the inactive electrons. Normally, these electrons are left uncorrelated (except in the extended SD-BOVB calculation for H-F, above) in the molecule as well as in the dissociated fragments or in any conformation of a molecular system throughout a potential surface. However, since the inactive orbitals are somewhat different in the HL and ionic VB structures, it is impossible to avoid

---

[†] It has been checked by counterpoise calculations that the stabilization due to the delocalization of the inactive orbitals is much larger than the spurious basis set superposition effect [12,13].

the fact that such a difference in a multistructure wave function will bring in some correlation of the inactive electrons. This explains why, when medium basis set are sufficient or when the calculation is compared to estimated full CI (as for H_3C-H or F-F above), the SD-BOVB dissociation energy tends to be a few kcal/mol too high. This is a rather fortunate systematic error, since generally the basis set that is used is far from complete and the slight BOVB overbinding compensates for the basis set deficiency. However, some cases may be encountered in which this spurious correlation of the inactive electron *replaces* the breathing orbital effect of the active electrons, leading to nonsensical bond energies. This may happen, for example, if the active orbitals were allowed to delocalize freely as in the GVB method. The outcome might be that the active orbitals are all the same in the HL and ionic structures, being of Coulson-Fisher type, thus representing a triplicate active system of GVB type. On the other hand, the degree of freedom of the BOVB wave function would be used to make the inactive orbitals very different from each other in the three structures, so that the resulting wave function would display some correlated inactive electrons. This would bring an additional correlation effect that stabilizes only the molecule but not the fragments because, at the asymptotic geometry, the HL structure is the only VB configuration that remains. This stresses the importance of keeping the active orbitals as strictly localized on their respective atom or fragment. *A BOVB calculation would become meaningless if the active orbitals were freely allowed to delocalize.*

The energy collapse due to spurious correlation of inactive orbitals may be exceptionally encountered, even if the active orbitals are not delocalized, as has been observed for ZnH^+ above [36]. Such an artefact is however easy to detect, based on the fact that an inactive pair in an ionic structure occupies an orbital that is mostly virtual in the HL structure, e.g. an orbital displaying a node. The remedy consists of effectively giving the inactive electrons the level of correlation that they try to achieve. This can be done by going to the extended SD level as in FH above, however this rigorous solution makes the calculation rather cumbersome. A much easier corrective procedure is to double the major VB structure at any point of a potential surface all the way to the dissociated products, if any. In this way, the " excess " stabilization of the inactive orbitals carries over to the whole potential surface, which deletes any artefactual overbinding effect. This procedure has been used successfully in the ZnH^+ case.

3.5. Diabatic states

One of the most valuable features of theoretical methods based on classical VB structures is their ability to calculate the energy of a diabatic state. For practical uses, some diabatic bond energy curves of chemical interest can be, for example, the separate dissociation energy curves of the ionic and covalent components of a bond, or the energy curves of the effective VB structures of a

chemical reaction which are traced individually along a reaction coordinate. Such diabatic curves are plotted in the curve-crossing VB diagrams which are used to predict and interpret reaction barriers [4]. Diabatic states have also some applications related to the concepts of organic chemistry, like resonance energy.

3.5.1. Definition

While the definition of an adiabatic state is straightforward, as an eigenfunction of the Hamiltonian within the complete set of VB structures, the concept of diabatic state is less clear-cut and accepts different definitions. Strictly speaking, a basis of diabatic states (ϑ, ϑ'...) should be such that eq 21 is satisfied for any variation ∂Q of the geometrical coordinates.

$$< \vartheta \mid \partial/\partial Q \mid \vartheta'> = 0 \tag{21}$$

However this condition is impossible to fulfill in the general case with more than one geometrical degree of freedom, so that one has to search for a compromise in the form of a function whose physical meaning remains as constant as possible along a reaction coordinate. Clearly, a single VB structure, that keeps the same bonding scheme irrespective of the geometry of the system, is the choice definition for a general diabatic state. For example, if we consider the A-B molecule in the BOVB framework, the ground state (made of three VB structures) will be adiabatic, while the three VB structures, respectively A•——•B, A^+B^- and A^-B^+, will be the diabatic states. Note however that a diabatic state can possibly be made up of more than one formal VB structure. For instance, in the S_N2 reaction (eq. 9), one diabatic state could be the bonding scheme of the reactants, $Cl^- + H_3C\text{-}F$, while the other would represent the products, $Cl\text{-}CH_3 + F^-$. In this case, each diabatic state would be made of three VB structures, respectively **3**, **5**, **6** and **4**, **5**, **7**, corresponding to the covalent and two ionic components of the carbon-halogen bond. Such diabatic states constitute the crossing curves of the VB correlation diagrams of Shaik and Pross [4].

3.5.2. Practical calculation

Having defined a diabatic state as a unique VB structure, or more generally as a linear combination of *a subset* of the full VB structure set that describes the adiabatic state, in the next step one has to specify the orbitals needed to construct the VB structure(s) of this diabatic state. One first possibility is to keep for the diabatic state the same orbitals that optimize the adiabatic state. This has the advantage of simplicity. Practically, once the orbitals have been determined at the end of the BOVB orbital optimization process, the hamiltonian matrix is constructed in the space of the VB structures and the

adiabatic energies are calculated by diagonalization of the hamiltonian matrix while the energies of the diabatic states are just the respective diagonal matrix elements.

An inconvenience of this practical procedure is that it does not guarantee the best possible orbitals for the diabatic states. Indeed, the BOVB orbitals are optimized so as to minimize the energy of the multi-structure ground state and are therefore the best compromise between the need to lower the energies of the individual VB structures and to maximize the resonance energy between these VB structures. This latter requirement implies that the final orbitals are not the best possible orbitals to minimize each of the individual VB structures taken separately. It follows that the diabatic states calculated in this way are not the best possible diabatic states to represent the respective bonding schemes and, in practical calculations, they may appear surprisingly high in energy. For instance, the purely covalent H_3C—Cl bond appears to be repulsive, if calculated this way, which is unreasonable.

An alternative approach which we recommend consists of optimizing each diabatic state separately, in an independent calculation. As a result, the orbitals of the diabatic states come out different from those of the adiabatic states, and we now get for each diabatic state its best possible set of orbitals. The diabatic energies are obviously lower compared with those obtained by the previous method. Using again the H_3C-Cl bond as an example, the second procedure now yields an energy profile for the purely covalent structure, with a bonding energy of 34 kcal/mol, in agreement with common sense as opposed to the repulsive covalent interaction obtained in the first procedure. We therefore believe that the separate calculations of the diabatic states yields the best possible results in terms of chemical interpretation.

It might be argued that the diabatic states, calculated separately as we recommend, are subject to basis set dependency. It is true that, in the limit of an infinite basis set, there would be so many and so diverse polarization functions that the optimized orbitals could not be considered as localized, so that the diabatic state would converge to the ground state rather than to a specific VB structure. However, some tests have been done which show that, as long as standard basis sets are used, such basis set dependency remains marginal. As an example, adding a set of diffuse functions to the 6-311G* basis set was found in one of our applications to change the energy of the diabatic state by only 0.1-0.2 kcal/mol relative to the ground state [55].

3.5.3. Resonance energies

Many molecules are represented as a set of resonating structures. For example, the ground state of formamide is the optimized mixture of the VB structures **34** and **35**. The resonance energy, which is responsible for the

rotational barrier, is the energy difference between the major VB structure **34** and the ground state.

Thus, the resonance energy characterizes the insufficiency of structure **34** for accurately representing the ground state. It is clear therefore that this concept is best quantified by comparing the energy of the optimized ground state with that of the *best possible* wave function for **34**, and this is meaningful
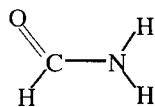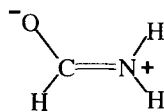
34   **35**

only if the orbitals of the diabatic state that represents structure **34** are optimized for this specific state alone, as recommended above. Accordingly, the method for calculating resonance energies in the BOVB framework consists of separate optimizations of the ground state and of the major VB structure (the one that has the largest weight in the wave function). The resonance energy is the difference between the variational energies of the full state and the reference VB structure. In this manner the resonance energy itself is variational.

4. SUMMARY AND CONCLUSION

It is striking that, while the great majority of quantitative calculations are done in the framework of MO theory, the language of chemists has remained faithful to the valence bond theory with its Lewis structures, hybrid orbitals, mesomeric stuctures and so on. In a way, one might say that MO theory has won the battle of computations while VB has won the battle of language and epistemology, so that the most commonly employed computational tool is not fully commensurate with the chemical concepts. This has occasionally created some confusion with respect to the great paradigms of chemistry. To take only a few examples, the role of electronic delocalization in aromaticity, the role of resonance in the rotational barriers of the peptide bonds in a protein or in the strength of carboxylic acids has long been debated, mainly because of the inadequacy of MO methods to settle these questions.

Clearly, there has been a need for a computational method that would speak the language of chemists while being reasonably quantitative as far as geometries, force constants and energetics in general are concerned. The BOVB method is an endeavour to fill this gap by bringing together the qualities of lucidity, compactness and reasonable accuracy. The requirements necessary to achieve the goal were as follows :

    (i)   As a first condition, it is necessary to ensure a maximum correspondence between the mathematical formulation and the

concept of Lewis structure displaying a specific bonding scheme. This requirement leads to the use of strictly localized orbitals, at least in the active space.

(ii)   A second condition was that the method should be capable of describing the elementary events that characterize a chemical process: the breaking and forming of chemical bonds, be they of the one-electron, two-electron or three-electron type. This is a requirement for a balanced description of an electronic system throughout a potential surface. To achieve this balance, it is essential to take care of the *differential* electron correlation types associated with the bonds that are created or broken along the reaction coordinate. A unique feature of the BOVB method is that it brings not only the non dynamic but also the dynamic part of this differential correlation, which can be very significant in some cases.

The leading principles of the method are straightforward. To calculate a given electronic state, all the Lewis structures that are relevant for the qualitative VB description of this state are generated, and the covalent forms are distinguished from the ionic ones. Each of these Lewis structures is represented by a single VB function which has its specific set of orbitals. The orbitals and the coefficients of the VB structures are optimized simultaneously, to minimize the energy of the final multi-structure state.

Practically, only a small part, called the active part, of a molecular system is treated in the VB framework, while the rest is treated at the ordinary MO level. The active part includes these orbitals and electrons that undergo effective changes throughout a potential surface, like bond-breaking or bond-forming. The inactive part undergoes orbital optimization to follow the changes of the active part, but its electrons are not explicitly correlated, in keeping with the assumption that the absolute error so introduced is quasi-constant throughout a potential surface. This ensures an extreme compactness of the wave function. As a typical example, the study of an S_N2 reaction would necessitate a BOVB wave function involving only six VB configurations, from the reactants to the products *via* the transition state.

The VB structures can be defined in different ways according to the desired level of accuracy, but all levels agree on the principle that the active orbitals should be strictly localized on their specific atom or fragment, and not allowed to delocalize in the course of the orbital optimization process. This latter condition is important for keeping the interpretability of the wave function in terms of Lewis structures, but also for a correlation-consistent description of the system throughout a potential surface.

The computational tests that have been performed in a variety of difficult cases show that the description is consistent and reasonably accurate, in view of

the compactness of the wave functions. Some applications of the BOVB method to effective chemical problems have already been made by various authors. Langenberg et al. [56] have used the BOVB method as a mean to solve the symmetry-breaking artefact in the potential energy surface of the glyoxal cation. This property of the method has also been exploited by Humbel et al. in the investigation of the $H_2O_2^-$ potential surface [57]. Basch et al. applied the method to study the SiH_3-F bond [58] and to calculate the covalent vs ionic dissociation curves of CH3-Y molecules (Y = F, OH, NH_2, CH_3, BH_2, CN, NO) [59]. Calculations of diabatic states were performed by Lauvergnat et al. to characterize the lone pair bond weakening effect in the H-NH_2, H-OH and H-F bonds [54]. The diabatic states were also used in the generation of VB curve crossing diagrams for hydrogen transfer reactions between X groups (X = H, CH_3, SiH_3, GeH_3, SnH_3, PbH_3) [60], and for identity radical exchange reactions of the type H + XH'$\rightarrow$ HX + H' and X + HX'$\rightarrow$ XH + X' (X = F, Cl, Br) [61]. The covalent vs ionic nature of homonuclear and heteronuclear π bonds was investigated [55], and a new type of bonding, in which the strength of the bond is primarily due to an exceptional energy of resonance between the covalent and ionic forms, has been discovered [55,61]. The reader is referred to the original papers.

The BOVB method does not of course aim to compete with the standard *ab initio* methods. BOVB has its specific domain. It serves as an interface between the quantitative rigor of today's capabilities and the traditional qualitative matrix of concepts of chemistry. As such, it has been mainly devised as a tool for computing diabatic states, with applications to chemical dynamics, chemical reactivity with the VB correlation diagrams, photochemistry, resonance concepts in organic chemistry, reaction mechanisms, and more generally all cases where a valence bond reading of the wave function or the properties of one particular VB structure are desirable in order to understand better the nature of an electronic state. The method has passed its first tests of credibility and is now facing a wide field of future applications.

REFERENCES

[1]   (a) L. Pauling, J. Amer. Chem. Soc. 53 (1931) 1367; (b) L. Pauling, J. Amer. Chem. Soc. 54 (1932) 998, 3570; (c) L. Pauling, The Nature of the Chemical Bond, 3rd edn. Cornell University Press, Ithaca, NY, 1960.

[2]   (a) J. C. Slater, Phys. Rev 35 (1930) 509; (b) J. C. Slater, Phys. Rev 38 (1931) 1109; (c) J. C. Slater, Phys. Rev 41 (1932) 255.

[3]   G. W. Wheland. Resonance in Organic Chemistry, John Wiley New York, 1955.

[4]   S. S. Shaik, J. Amer. Chem. Soc. 103 (1981) 3692; (b) A. Pross, S. S. Shaik. Acc. Chem. Res. 16 (1983) 363; (c) A. Pross, Adv. Phys. Org. Chem. 21 (1985) 99; (d) A. Pross, Acc. Chem. Res. 18 (1985) 212; (e) S. S. Shaik. in: J. Bertran, I. G. Csizmadia (Eds)

New Concepts for Understanding Organic Reactions, Kluwer, Dordrecht, 1989: NATO ASI Series Vol. C267; (f) S. S. Shaik, P. C. Hiberty, in: Z. B. Maksic (Ed) Theoretical Models of the Chemical Bonding, Part 4, Springer, Heidelberg, 1991, pp 269-322. (g) S. Shaik, A. Shurki, Angew. Chem. Int. Ed. 38 (1999) 586. (h) S. S. Shaik, Prog. Phys. Org. Chem. 15 (1985) 197. (i) S. Shaik, P.C. Hiberty, Adv. Quant. Chem. 26 (1995) 100.

[5]   (a) A. Sevin, P. C. Hiberty, J.-M. Lefour, J. Am. Chem. Soc. 109 (1987) 1845; (b) A. Sevin, P. Chaquin, L. Hamon, P. C. Hiberty, J. Am. Chem. Soc. 110 (1988) 5681; (c) A. Sevin, C. Giessner-Prettre, P.C. Hiberty, E. Noizet, J. Phys. Chem. 95 (1991) 8580.

[6]   (a) S.S. Shaik, P.C. Hiberty, J.M. Lefour, G. Ohanessian, J. Amer. Chem. Soc. 109 (1987) 363; (b) S.S. Shaik, P.C. Hiberty, G. Ohanessian, J.M. Lefour, J. Phys. Chem. 92 (1988) 5086; (c) S. Shaik, A. Shurki, D. Danovich, P.C. Hiberty, J. Amer. Chem. Soc. 118 (1996) 666; (d) S. Shaik, A. Shurki, D. Danovich, P.C. Hiberty, Chem. Rev. in press.

[7]   D. Lauvergnat, P.C. Hiberty, J. Amer. Chem. Soc. 119 (1997) 9478.

[8]   P.C. Hiberty, C. P. Byrman, J. Am. Chem. Soc. 117 (1995) 9875.

[9]   J.D. da Motta Neto, M.A.C. Nascimento, J. Phys. Chem. 100 (1996) 15105.

[10] (a) J.-K. Hwang, G. King, S. Creighton, A. Warshel, J. Am. Chem. Soc. 110 (1988) 5297. (b) S.S. Shaik, J. Am. Chem. Soc. 106 (1984) 1227.

[11] P.C. Hiberty, J.P. Flament, E. Noizet, Chem. Phys. Lett. 189 (1992) 259.

[12] P.C. Hiberty, S. Humbel, C.P. Byrman, J.H. van Lenthe, J. Chem. Phys. 101 (1994) 5969.

[13] P.C. Hiberty, S. Humbel, P. Archirel, J. Phys. Chem. 98 (1994) 11697.

[14] Hartree-Fock: (a) V. Fock, Z. Phys. 61 (1930) 126; (b) J.C. Slater, Phys. Rev. 35 (1930) 210.

[15] H. Heitler, F. London, Z. Phys. 44 (1927) 455.

[16] S.S. Shaik, P.C. Hiberty, J. Amer. Chem. Soc. 107 (1985) 3089.

[17] C.A. Coulson, I. Fischer, Phil. Mag. 40 (1949) 386.

[18] A.C. Hurley, J. Lennard-Jones, J.A. Pople, Proc. Roy. Soc. A220 (1953) 446.

[19] (a) W.J. Hunt, P. J. Hay, W.A. Goddard, J. Chem. Phys. 57 (1972) 738; (b) W.A. Goddard, L.B. Harding, Ann. Rev. Phys. Chem. 29 (1978) 363; (c) F. B. Bobrowicz, W.A. Goddard, in : Methods of Electronic Structure Theory, H.F. Schaefer (ed.), Plenum Press, New York, 1977, pp. 79-127; (d) A. F. Voter, W. A. Goddard, J. Chem. Phys. 75 (1981) 3638.

[20] D.L. Cooper, J. Gerratt, M. Raimondi, Adv. Chem. Phys. 69 (1987) 319; (b) D.L. Cooper, J. Gerratt, M. Raimondi, Int. Rev. Phys. Chem. 7 (1988) 59; (c) D.L. Cooper, J. Gerratt, M. Raimondi, in : Valence Bond Theory and Chemical Structure, D.J. Klein, N. Trinajstic (eds.), Elsevier, 1990, p. 287; (d) D. L. Cooper, J. Gerratt, M. Raimondi,Top. Current Chem. 153 (1990) 41. (e) P.B. Karadakov, J. Gerratt, D.L. Cooper, M. Raimondi, Chem. Rev. 91 (1991) 929.

[21] (a) J. Verbeek, Ph.D. Thesis, University of Utrecht, 1990; (b) J. Verbeek, J.H. van Lenthe, J. Mol. Struc. (Theochem) 229 (1991) 115; (c) J. Verbeek, J.H. van Lenthe, Int. J. Quant. Chem. 40 (1991) 201.

[22] J. Verbeek, J.H. Langenberg, C.P. Byrman, J.H. van Lenthe, TURTLE-An ab initioVB/VBSCF/VBCI program: Theoretical Chemistry Group, Debye Institute, University of Utrecht, 1993.

[23] M.B. Lepetit, J.P. Malrieu, J. Phys. Chem. 97 (1993) 94.

[24] C.F. Jackels, E.R. Davidson, J. Chem. Phys. 64 (1976) 2908.

[25] (a) A.F. Voter, W.A. Goddard III, Chem. Phys. 57 (1981) 253; (b) A.F. Voter, W.A. Goddard III, J. Chem. Phys. 75 (1981) 3638; (c) A.F. Voter, W.A. Goddard III, J. Amer. Chem. Soc. 108 (1986) 2830.

[26] (a) E. Hollauer, M.A.C. Nascimento, Chem. Phys. lett. 184 (1991) 470; (b) E. Hollauer, M.A.C. Nascimento, J. Chem. Phys. 99 (1993) 1207; (c) E. Hollauer, M.A.C. Nascimento, Chem. Phys. 177 (1993) 79; (d) C.E. Bielscowsky, M.A.C. Nascimento, E. Hollauer, Phys. Rev. A 43 (1992) 7942.

[27] G. Ohanessian, P.C. Hiberty, Chem. Phys. Lett. 137 (1987) 437.

[28] W.D. Laidig, P. Saxe, R.J. Bartlett, J. Chem. Phys. 86 (1987) 887.

[29] M. Merchan, J. P. Daudey, R. Gonzales-Luque, I. Nebot-Gil, Chem. Phys. 141 (1990) 285.

[30] K.P. Huber, G. Herzberg, in : Molecular Spectra and Molecular Structures. IV. Constants of Diatomic Molecules, van Nostrand Reinhold, New York, 1979.

[31] P.C. Hiberty, J.M. Lefour, J. Chim. Phys. 84 (1987) 607.

[32] C.W. Bauschlicher, P.R. Taylor, J. Chem. Phys. 86 (1987) 887.

[33] C.W. Bauschlicher, S.R. Langhoff, P.R. Taylor, N.C. Handy, P.J. Knowles, J. Chem. Phys. 85 (1986) 1469.

[34] J.B. Schilling, W.A. Goddard, J.L. Beauchamp, J. Phys. Chem., 91 (1987) 5616.

[35] G. Ohanessian, W.A. Goddard, Acc. Chem. Res. 23 (1990) 386.

[36] J.M. Galbraith, A. Shurki, S. Shaik, J. Phys. Chem. A 104 (2000) 1262.

[37] L.G.M. Petterson, C.W. Bauschlicher, S.R. Langhoff, H. Partridge, J. Chem. Phys. 87 (1987) 481.

[38] T. Clark, J. Amer. Chem. Soc. 110 (1988) 1672.

[30] P.M.W. Gill, L. Radom, J. Amer. Chem. Soc. 110 (1988) 4931.

[40] (a) L. Pauling, J. Amer. Chem. Soc. 53 (1931) 3225. (B) L. Pauling, J. Chem. Phys. 1 (1933) 56.

[41] Nguyen, M. T.; Ha, T.-K. J. Phys. Chem. 91 (1987) 1703.

[42] B. Braïda, P.C. Hiberty, J. Phys. Chem. A 104 (2000) 4618.

[43] B. Braïda, D. Lauvergnat, P.C. Hiberty, J. Phys. Chem. A, in press.

[44] A.D. McLean, B.H. Lengsfield III, J. Pacansky, Y. Ellinger, J. Chem. Phys. 83 (1985) 3567.

[45] Y. Xie, , W.D. Allen, Y. Yamaguchi, H.F. Schaefer III, J. Chem. Phys. 104 (1996) 7615.

[46] W.R. Wadt, P.J. Hay, J. Chem. Phys. 82 (1985) 284.

[47] L.A. Curtiss, K. Raghavachari, G.W. Trucks, J.A. Pople, J. Chem. Phys. 94 (1991) 7221.

[48] L. Eberson, R. Gonzalez-Luque, J. Lorentzon, M. Merchan, B.O. Roos, J. Amer. Chem. Soc. 115 (1993) 2898.

[49] P. Archirel, personal communication.

[50] F.X. Gadea, J. Savrda, I. Paidarova, Chem. Phys. Lett. 223 (1994) 369.

[51] P.C. Hiberty, S. Humbel, D. Danovich, S. Shaik, J. Amer. Chem. Soc. 117 (1995) 9003.

[52] D. Lauvergnat, P.C. Hiberty, D. Danovich, S. Shaik, J. Phys. Chem. 100 (1996) 5715.

[53] A. Shurki, P.C. Hiberty, S. Shaik, J. Am. Chem. Soc. 121 (1999) 822.

[54] D. Lauvergnat, P. Maître, P.C. Hiberty, F. Volatron, J. Phys. Chem. 100 (1996) 6463.

[55] J.M. Galbraith, E. Blank, S. Shaik, P.C. Hiberty, Chem. Eur. J. 6 (2000) 2425.

[56] J.H. Langenberg, P.J.A. Rutink, Theor. Chim. Acta 85 (1993) 285.

[57] S. Humbel, I. Demachy, P.C. Hiberty, Chem. Phys. Lett. 247 (1995) 126.

[58] H. Basch, J.L. Wolk, S. Hoz, J. Phys. Chem. A 101 (1997) 4996.

[59] H. Basch, P. Aped, S. Hoz, Mol. Phys. 89 (1996) 331.

[60] S. Shaik , W. Wu, K. Dong, L. Song, P.C. Hiberty, submitted.

[61] P.C. Hiberty, C. Megret, W. Wu, L. Song, S. Shaik, manuscript in preparation.

This Page Intentionally Left Blank

Chapter 8

The Biorthogonal Valence Bond Method

Joseph J.W. McDouall

Department of Chemistry, University of Manchester, Oxford Road,
Manchester M13 9PL, United Kingdom

The theoretical basis and certain computational aspects of the biorthogonal valence bond (BOVB) method are presented. A number of calculations on small molecules are used to illustrate the description of electronic structure and bonding that can be obtained from BOVB calculations. Calculations are reported that include up to 30 electrons in nonorthogonal orbitals outside a closed shell. It is suggested that calculations involving up to 60 electrons, accommodated in nonorthogonal singly-occupied orbitals, can be contemplated realistically. The combination of the BOVB method with layering techniques, in which a molecule is partitioned into different layers and each layer is treated at a different level of theory, provides a viable route to valence bond studies on large molecular systems. Recent calculations on the pseudohalide acid HCS_2N_3 and a large diphosphaallene radical anion are also reported.

1. INTRODUCTION

The biorthogonal valence bond method has its origins in the work of Moshinsky and Seligman on group theory and second quantization for nonorthogonal orbitals [1]. Essentially, by introducing a dual (biorthogonal) orbital space, they showed how the difficult problem of evaluating matrix elements of the electronic hamiltonian, between functions built from nonorthogonal orbitals, could be simplified. Moshinsky and Seligman applied their formalism to the potential energy surface of H_3 using a minimal basis of orbitals, with the resultant complete configuration basis expressed as Gelfand states. Following this seminal work, Cantu, Klein, Matsen and Seligman [2] discussed the use of this formalism in a valence bond context using a Rumer-Weyl basis [3, 4] of configuration state functions (CSF). However, these authors did not provide any examples of numerical calculations. The biorthogonal technique was investigated in the context of classical valence bond

wavefunctions, including varying numbers of covalent and ionic terms with fixed orbitals, for H_2, LiH and H_2O by Norbeck and McWeeny [5]. Payne [6] also provided a theoretical exposition on the biorthogonal method for general configuration interaction (CI) calculations in a nonorthogonal orbital basis. The biorthogonal approach was introduced in the context of modern valence bond calculations by McDouall [7]. Initial biorthogonal valence bond (BOVB) studies on HF, H_2O and F_2O_2 involved optimizing the nonorthogonal orbitals involved in bond formation for a single spin-coupling mode (perfect-pairing approximation) with all other electrons assigned to doubly-occupied molecular orbitals, which were simultaneously optimized. Following this work, optimization for more general wavefunctions was considered [8], with special emphasis on the requirements for accurate evaluation of the dynamic electron correlation energy in an extended biorthogonal CI. Malcolm and McDouall [9] implemented a BOVB method in which the configuration expansion in the nonorthogonal orbital space was complete. This yields energies identical to the corresponding N-electron/N-orbital orthogonal complete active space self-consistent field (CASSCF) wavefunctions, thus ensuring a variational bound. Application of this method to the electronic structure of some 1,3-dipoles [10] showed that the results obtained, in terms of nonorthogonal orbital shapes and overlaps, are essentially identical with those of spin-coupled valence bond studies [11, 12]. However, the realm of applicability of this approach is limited to the same size of problem as can be handled in CASSCF calculations ($\approx$ 12-14 electrons) since the configuration expansion increases very rapidly with N. Despite this limitation, a major advantage of this approach is that it is a simple matter to evaluate derivatives of the energy with respect to geometrical parameters, thus enabling geometry optimizations and reaction path searches to be carried out. Indeed the simplest way to do this is to use an efficient CASSCF procedure and then transform to the BOVB representation. A similar idea has been used more recently in the CASVB methodology [12]. Thorsteinsson and Cooper [13] have also discussed the implementation of the biorthogonal method using techniques similar to those used in their spin-coupled valence bond studies.

In the next section we review some of the theoretical and practical details of the BOVB method. In particular we consider means by which much larger calculations may be attempted. In section 3, we present some illustrative calculations to expose the properties of BOVB wavefunctions and familiarize the reader with the BOVB description of electronic structure. This is followed by a description of some recent calculations on the pseudohalide acid HCS_2N_3 and a large diphosphaallene radical anion. We conclude by summarizing the strengths and weaknesses of the BOVB method as a general quantum chemical tool and suggest areas for future development.

2. PRINCIPLES OF BIORTHOGONAL VALENCE BOND THEORY

2.1. Theory

In most modern valence bond calculations the wavefunction takes the form of a multiconfigurational expansion

$$\Psi = \sum_K C_K \psi_K \tag{1}$$

in which ψ_K is an antisymmetrized space-spin product. The set $\{\psi\}$ is usually constructed from an orbital set, $\{\phi\}$, which contains a number of doubly-occupied orbitals which accommodate the energetically low lying electrons. Above the doubly-occupied orbitals sit a group of orbitals which are allowed different occupancies and spin-couplings in different members of $\{\psi\}$. $\{\phi\}$ also contains a number of virtual orbitals which are not occupied in $\{\psi\}$. The doubly-occupied orbitals are chosen to be orthogonal amongst themselves and to all other orbitals. In contrast, the orbitals which are allowed variable occupancies and spin-couplings are allowed to be nonorthogonal amongst themselves, but are required to remain orthogonal to the doubly-occupied 'core'.

The main difficulty in performing calculations with an orbital set containing nonorthogonal orbitals is that of evaluating matrix elements over the hamiltonian. These matrix elements contain complicated products of orbital overlap integrals [14]. In the BOVB approach, the set $\{\psi\}$ is used in setting up the electronic Schrödinger equation

$$\hat{H}\big|\Psi\big\rangle = E\big|\Psi\big\rangle \tag{2}$$

but when integrating for the energy (taking scalar products from the left) a second set of functions $\{\tilde{\psi}\}$ is introduced to expand the wavefunction

$$\tilde{\Psi} = \sum_K \tilde{C}_K \tilde{\psi}_K \tag{3}$$

giving

$$E = \frac{\big\langle \tilde{\Psi}\big|H\big|\Psi\big\rangle}{\big\langle \tilde{\Psi}\big|\Psi\big\rangle} \tag{4}$$

The members of $\{\tilde{\psi}\}$ have a one-to-one correspondence with the members of $\{\psi\}$ with respect to orbital occupancy and spin-coupling, except that the orbitals used in their construction belong to a *dual* set defined by

$$\tilde{\Phi} = \Phi T = \Phi S^{-1} \tag{5}$$

where S is the orbital overlap matrix. The set $\{\tilde{\phi}\}$ can always be defined in this way provided the set $\{\phi\}$ is not linearly dependent. The two sets of orbitals $\{\phi\}$ and $\{\tilde{\phi}\}$ possess a biorthogonality property

$$\langle \tilde{\phi}_p | \phi_q \rangle = \delta_{pq} \tag{6}$$

Thus the reduction of the matrix element $\langle \psi_K | H | \psi_L \rangle$ in a nonorthogonal valence bond calculation, which contains complicated products of orbital overlap integrals, $\langle \phi_p | \phi_q \rangle$, is replaced by the corresponding element $\langle \tilde{\psi}_K | H | \psi_L \rangle$ which contains the biorthogonal overlaps in Eq. (6) and consequently may be evaluated as if the orbitals were orthonormal. The matrix elements, using conventional notation, may be written as

$$\langle \tilde{\psi}_K | H | \psi_L \rangle = \sum_{pq} \langle \tilde{\phi}_p | h | \phi_q \rangle \gamma_{pq}^{\tilde{K}L} + \sum_{pqrs} (\tilde{p}q | \tilde{r}s) \Gamma_{pqrs}^{\tilde{K}L} \tag{7}$$

The integrals over the one- and two-electron operators have the dual basis to the left of the operator and the primary basis to the right. The one- and two-electron vector coupling coefficients, $\gamma_{pq}^{\tilde{K}L}$ and $\Gamma_{pqrs}^{\tilde{K}L}$ respectively, may be evaluated as though over orthogonal orbitals but it must be remembered that the introduction of the dual basis reduces the symmetry properties of these to

$$\gamma_{qp}^{\tilde{L}K} = \gamma_{pq}^{\tilde{K}L} \qquad \text{and} \qquad \Gamma_{qpsr}^{\tilde{L}K} = \Gamma_{pqrs}^{\tilde{K}L} \tag{8}$$

These quantities may be evaluated by a variety of techniques [15-18]. In the dual basis the one-electron integrals have no exploitable symmetry and the two-electron integrals possess only a two-fold symmetry

$$\left(\tilde{\phi}_r \phi_s | \tilde{\phi}_p \phi_q \right) = \left(\tilde{\phi}_p \phi_q | \tilde{\phi}_r \phi_s \right) \tag{9}$$

A consequence of this is that $\langle \tilde{\psi}_K | H | \psi_L \rangle \neq \langle \tilde{\psi}_L | H | \psi_K \rangle$ and we must deal with an unsymmetric eigenvalue equation

$$\sum_L \langle \tilde{\psi}_K | H | \psi_L \rangle C_L = E \sum_L \langle \tilde{\psi}_K | \psi_L \rangle C_L \tag{10 a}$$

or in matrix notation

$$\tilde{\mathbf{H}}\mathbf{C} = \tilde{\mathbf{S}}\mathbf{C}\mathbf{E} \tag{10 b}$$

In general Eq. (10) is not equivalent to the secular equations obtained from the variation method, unless $\{\psi\}$ is complete. An analysis of the error in the energy obtained from Eq. (10) was given by Boys [19]. Error vectors may be defined for the left and right eigenvectors of Eq. (10) as

$$\tilde{\Delta} = \tilde{\mathbf{C}} - \tilde{\mathbf{C}}_\infty \tag{11}$$

$$\Delta = \mathbf{C} - \mathbf{C}_\infty \tag{12}$$

where $\tilde{\mathbf{C}}$, $\mathbf{C}$ are the left and right eigenvectors in a truncated expansion and $\tilde{\mathbf{C}}_\infty$, $\mathbf{C}_\infty$ are the corresponding eigenvectors of Eq. (10) in a complete basis, respectively. Boys showed that the error in the energy is proportional to ε, defined as

$$\varepsilon = \sqrt{\tilde{\Delta} \cdot \tilde{\Delta}} \sqrt{\Delta \cdot \Delta} \tag{13}$$

The significance of this is that the error contains the product of both error vectors. Hence, if $\{\psi\}$ is a good set for representing Ψ, then the norm of Δ will be small and an accurate energy should be obtained since it will not depend too heavily on the set $\{\tilde{\psi}\}$. However it is not possible to know how the error will decrease as the set $\{\psi\}$ is systematically extended.

2.2. BOVB wavefunctions

Given the preceding discussion of the error in the energy obtained from Eq. (10) it is clear that complete expansions, analogous to orthogonal CASSCF methods, provide a useful limiting case against which to explore the properties of more general BOVB wavefunctions. We have recently been interested in using highly truncated expansions which, if necessary, can be systematically improved to the limiting case. To this end it is useful to introduce a notation

$$\text{BOVB}(N,M+X) \tag{14}$$

which we use to clearly label different wavefunctions. In this notation, N is the number of electrons accommodated in N nonorthogonal orbitals. M is the number of spin-couplings of the N electrons included in the wavefunction and X is the level of orbital replacements (Single, Double, etc. excitations) generated from *each* of the M spin-couplings. All other electrons in the system

are deposited in doubly-occupied molecular orbitals. For example, consider a BOVB wavefunction for water describing the two O—H bonds in 4 nonorthogonal orbitals
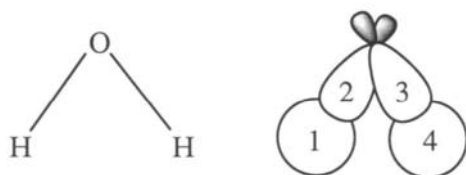
With the orbitals numbered as shown above, two linearly independent spin-couplings would be
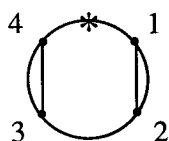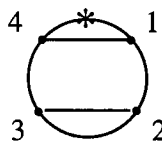
$$\psi_1 = A[\phi_1\phi_2(\alpha\beta-\beta\alpha)\ \phi_3\phi_4(\alpha\beta-\beta\alpha)] \qquad \psi_2 = A[\phi_1\phi_4(\alpha\beta-\beta\alpha)\ \phi_2\phi_3(\alpha\beta-\beta\alpha)]$$

and these would be denoted BOVB(4,2). If we were to include all single orbital replacements (necessary in our scheme for optimizing the nonorthogonal orbitals) the corresponding wavefunction would be denoted BOVB(4,2+S). If a complete expansion was to be used we would simply denote this as BOVB(4,V) indicating the variational limit (equivalent to a 4-electron/4-orbital CASSCF wavefunction). In general the total number of CSF of ionicity, i, which may be constructed from N electrons distributed in n orbitals with total spin, s, is [20]

$$D_{Nns} = \frac{(2s+1)n!}{i!(n+i-N)!\left(\frac{1}{2}N+s-i+1\right)!\left(\frac{1}{2}N-s-i\right)!} \qquad (15)$$

i, the ionicity gives the number of orbitals which are doubly occupied. In Eq. (15) the values of i are restricted to lie in the range

$$(N-n) \le i \le N/2 \qquad (16)$$

Another set of configurations which it is sometimes useful to add to each spin-coupling is based on the restricted CI (RCI) ideas of Goddard and coworkers (e.g. see [21]). We have found that on some problems the variational bound is

violated when the BOVB wavefunction is limited to a small number of spin-couplings and their single excitations. This sometimes happens when a BOVB orbital optimization is started from a particularly poor set of orbitals. In such cases spurious lower energy roots appear in the solutions to Eq. (10), making any type of orbital optimization a hazardous undertaking. Clearly, under these conditions, the eigenspectrum of Eq. (10) does not lie close to that of Eq. (2). We have found that a stabilization (elimination of spurious lower roots) can be achieved by increasing the number of functions included in the BOVB wavefunction, in accord with the expectations of Eq. (13). In particular, the RCI expansion allows up to *(N-2s)/2* simultaneous single excitations. While we have been unable to provide a rigorous proof of the efficacy of the RCI type expansion in BOVB calculations, we have not observed any problematic cases which have not been tamed by the use of a RCI expansion. The RCI expansion is generated by allowing *each* spin-coupled pair to have all possible occupations in the paired orbitals, i.e.

1) ϕ_1—|— ϕ_2—|—

2) ϕ_1—||— ϕ_2——

3) ϕ_1—— ϕ_2—||—

The total wavefunction is then obtained by taking the direct product of all such structures. This leads, for P pairs, to a total of 3^P spatial configurations

$$
\begin{pmatrix} \phi_1-|- & \phi_2-|- \\ \phi_1-||- & \phi_2-- \\ \phi_1-- & \phi_2-||- \end{pmatrix} \otimes \begin{pmatrix} \phi_3-|- & \phi_4-|- \\ \phi_3-||- & \phi_4-- \\ \phi_3-- & \phi_4-||- \end{pmatrix} \otimes \ldots\ldots
$$

The RCI expansion produces a relatively small number of additional terms and can be used for problematic cases to stabilize the energy obtained from Eq. (10). A wavefunction including these additional configurations for the example above would be denoted BOVB(*4,1+S+RCI*).

2.3. Orbital optimization

In the BOVB procedure the orbital space is partitioned into three subspaces: (1) a core of doubly-occupied orbitals which are orthogonal amongst themselves and also to all other orbitals, (2) an 'active' space of orbitals which are mutually nonorthogonal but are orthogonal to the core orbitals, and (3) a complementary virtual space which is orthogonal within itself and also to all other subspaces. With this partition of the orbital space, the optimization may be formulated in terms of a general rotation, $\mathbf{R}$, of the orbitals. $\mathbf{R}$ may be separated into the product of a transformation, $\mathbf{R_O}$, amongst orbitals which are required to remain orthogonal to each other and a general transformation, $\mathbf{R_N}$, amongst the nonorthogonal orbitals

$$\mathbf{R} = \mathbf{R_O}\,\mathbf{R_N} \tag{17}$$

$\mathbf{R_O}$ is usually expressed as an exponential transformation

$$\mathbf{R_O} = e^{\mathbf{X}} = \mathbf{I} + \mathbf{X} + \tfrac{1}{2}\mathbf{X}^2 + \dots \tag{18}$$

Where $\mathbf{X}$ is an antisymmetric matrix containing the independent (orthogonal) rotation parameters. Expanding the energy in $\mathbf{X}$ about the origin

$$E(\mathbf{X}) = E(0) + \mathbf{g}\mathbf{X} + \tfrac{1}{2}\mathbf{X}^+\mathbf{G}\mathbf{X} \tag{19}$$

allows $\mathbf{X}$ to be obtained from

$$\mathbf{X} = -\mathbf{G}^{-1}\mathbf{g} \tag{20}$$

where the components of $\mathbf{g}$, the gradient vector, are given by

$$\frac{dE}{dX_{pq}} = L_{pq} + \tilde{L}_{pq} - L_{qp} - \tilde{L}_{qp} \tag{21}$$

The matrices $\mathbf{L}$ and $\tilde{\mathbf{L}}$ are defined as

$$
\begin{aligned}
L_{pq} &= \sum_r \langle \tilde{\phi}_p | h | \phi_r \rangle \gamma_{qr} + 2\sum_{rst} (\tilde{p}r | \tilde{s}t)\Gamma_{qrst} \\
\tilde{L}_{pq} &= \sum_r \langle \tilde{\phi}_r | h | \phi_p \rangle \gamma_{rq} + 2\sum_{rst} (\tilde{r}p | \tilde{s}t)\Gamma_{rqst}
\end{aligned}
\tag{22}
$$

The one- and two-body density matrices are formed by contraction of the vector coupling coefficients with the left and right eigenvectors of Eq. (10) (assuming $\tilde{\mathbf{C}}\tilde{\mathbf{S}}\mathbf{C} = \mathbf{I}$)

$$\gamma_{pq} = \sum_{KL} \tilde{C}_K \gamma_{pq}^{\check{K}L} C_L$$

$$\Gamma_{pqrs} = \sum_{KL} \tilde{C}_K \Gamma_{pqrs}^{\check{K}L} C_L$$

(23)

Further details of the evaluation of $\mathbf{R_O}$, such as approximate expressions for the hessian matrix, $\mathbf{G}$, in Eq. (20), may be found in Ref. 10.

In our earlier work the transformation, $\mathbf{R_N}$, was evaluated using a super CI method [7-9]. Super CI includes single excitations from the reference wavefunction into the expansion space and uses the eigenvector from this extended CI calculation to rotate the orbitals [22]. The super CI strategy is not without problems in optimizing BOVB wavefunctions. When the expansion space is complete the energy is invariant to the nonorthogonal orbital rotations. If a truncated expansion is used, the energy is not variational and minimization is not necessarily the best way to proceed. However, the super CI formalism is particularly simple to implement and lends itself to large scale application. Consequently, we now develop a projection criterion for optimizing the nonorthogonal orbitals in a BOVB calculation which is motivated by the super CI method and reduces to super CI exactly in the limit of a single reference function. As we have mentioned previously, we wish to be able to extend the configuration expansion systematically to the complete limit. This means that it is most convenient to work with uncontracted configuration expansions. However, the super CI formalism (for more than a single reference function) is a contracted CI method in which single excitation operators are applied to the reference wavefunction rather than to individual configurations. Furthermore if we wish to expand the configuration space systematically, it is necessary to use some form of 'standard' expansion functions to avoid linear dependence. To illustrate this consider the application of an excitation operator (a product of creation and dual annihilation operators which transform as the generators of $GL(N)$, see Ref.s 1 and 7) to a Rumer CSF (all our calculations employ the Rumer basis), $\left| \psi_K \right\rangle$, where $N=6$ and $s=0$
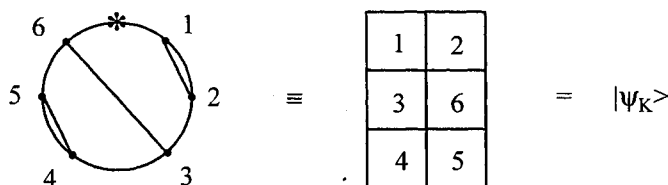
Now apply the excitation operator $\tilde{E}_{14}$

$$\tilde{E}_{14}\;\begin{array}{|c|c|}\hline 1 & 2 \\\hline 3 & 6 \\\hline 4 & 5 \\\hline\end{array}\;=\;\begin{array}{|c|c|}\hline 1 & 2 \\\hline 3 & 6 \\\hline 1 & 5 \\\hline\end{array}\;=\;-\frac{1}{2}\;\begin{array}{|c|c|}\hline 1 & 1 \\\hline 2 & 5 \\\hline 3 & 6 \\\hline\end{array}\;\equiv\;$$

This produces a non-standard Rumer function as shown by the representation on the right hand side. These non-standard functions, which correspond to a Rumer diagram in which the lines cross, are not used in calculations. A standard set of functions can be selected using the following procedure: the open shell orbitals are represented by a 1 if their number occurs in the left hand column of the Weyl tableau or a 2 if it appears in the right hand column. Hence for the example above

$$\begin{array}{lcccc}\text{Orbital Number:} & 2 & 3 & 5 & 6 \\\text{Term:} & 1 & 1 & 2 & 2 \end{array}$$

We now pair the left most "2" with the closest "1" to its left, i.e.

$$\begin{array}{lcccc}\text{Orbital Number:} & 2 & 3 & 5 & 6 \\\text{Term:} & 1 & 1 & 2 & 2 \end{array}$$

Thus we obtain the standard function

$$\begin{array}{|c|c|}\hline 1 & 1 \\\hline 2 & 6 \\\hline 3 & 5 \\\hline\end{array}\;\equiv\;$$

which is to be used in the calculation. Hence we can write

$$\tilde{E}_{14} \quad \begin{array}{|c|c|} \hline 1 & 2 \\ \hline 3 & 6 \\ \hline 4 & 5 \\ \hline \end{array} \quad = \quad \rho^K_{14} \quad \begin{array}{|c|c|} \hline 1 & 1 \\ \hline 2 & 6 \\ \hline 3 & 5 \\ \hline \end{array}$$

ρ^K_{14} indicates that this is the result of applying $\tilde{E}_{14}$ to $\left| \psi_K \right\rangle$. The best way to keep track of such transformations is to calculate the overlap between the raw Rumer function generated and the standard Rumer function to be used in the super CI calculation. This phase/overlap must be included in the transformation process. In general all doubly-occupied orbitals are written first, in ascending order, then paired orbitals are ordered, first within each row of the Weyl tableau and then by the left column into ascending order, and finally the high-spin orbitals are inserted in ascending order.

$\mathbf{R_N}$ is obtained from the eigenvector of this pseudo super CI calculation. If we are optimizing the orbitals for M reference functions, $\mathbf{R_N}$ is obtained as

$$\mathbf{R_N} = \mathbf{I} + \sum_K^M \mathbf{X}_K \tag{24}$$

where

$$\left(\mathbf{X}_K \right)_{pp} = 0$$
$$\left(\mathbf{X}_K \right)_{pq} = sign(C_K)\Delta^{-1}C_K C^K_{pq}\rho^K_{pq} \tag{25}$$
$$\Delta = \sum_K^M \left| C_K \right|$$

In Eq. (25) C_K is the right eigenvector component of reference function $\left| \psi_K \right\rangle$ and C^K_{pq} is the eigenvector component corresponding to the application of $\tilde{E}_{pq}$ to $\left| \psi_K \right\rangle$. With these definitions we can generate the rotation matrix, $\mathbf{R}$, and assume convergence when $\mathbf{R=I}$. In the case of a single reference function (M=1) Eq.s (24) and (25) reduce to the regular super CI procedure [23]. Other definitions of the projection for defining the nonorthogonal orbital transformation are possible. The transformation as defined in Eq.s (24) and (25) produces results which, in terms of orbital shapes and overlaps, are very similar to those obtained within the spin-coupled valence bond approach. Many examples illustrate that this process does converge, but we have found it

essential to include some form of convergence accelerator. In particular we have employed DIIS extrapolation [24] of the orbital coefficients using gradients of the orthogonal rotation parameters and the off-diagonal elements of $\mathbf{R_N}$ to define the error vector. We have also implemented the space efficient form of the BFGS hessian updating method of Fischer and Almlöf [25]. By default our procedures use DIIS extrapolation, but we have found that the quasi-Newton technique can force convergence when extrapolation fails. More elaborate optimization techniques are certainly possible but only at an increased computational cost.

2.4. Weights in BOVB wavefunctions

Given that we intend to employ a wide range of different expansions in our BOVB calculations it is important to know which types of configurations dominate the wavefunction and which simply serve to condition Eq. (10). The usual way to analyze a wavefunction is to calculate the weight of each configuration within the total wavefunction. The most widely used definition of weight is that of Chirgwin and Coulson [26]

$$W_K = \sum_L C_K S_{KL} C_L \tag{26}$$

in which S_{KL} is a configuration overlap and $\mathbf{C}$ is the eigenvector. $\mathbf{C}$ is usually normalized such that

$$\sum_{KL} C_K S_{KL} C_L = 1 \tag{27}$$

In the BOVB approach, we must deal with both left and right eigenvectors. Hence we use a symmetric form for the weights

$$\tilde{W}_K = \tfrac{1}{2}\left\{ \tilde{C}_K \tilde{S}_{KL} C_L + \tilde{C}_L \tilde{S}_{LK} C_K \right\} \tag{28}$$

which given the normalization of the left and right eigenvectors

$$\sum_{KL} \tilde{C}_K \tilde{S}_{KL} C_L = 1 \tag{29}$$

implies

$$\sum_K \tilde{W}_K = 1 \tag{30}$$

All weights reported in this chapter were evaluated using Eq. (28).

3. ILLUSTRATIVE CALCULATIONS

In this section we outline some simple calculations which illustrate the nature of the results we can expect from the BOVB method we have described. Our purpose here is not to report new applications, those will be given in the next section, but rather to illustrate the utility of what we have proposed and enable a comparison to be made with other valence bond schemes.

All of our computer programs have been interfaced with the GAUSSIAN 98 suite of programs [27]. All one- and two-electron integrals and integral derivatives over atomic basis functions are evaluated using standard procedures within GAUSSIAN 98. These are passed to our programs which have been coded as a link within the GAUSSIAN structure. All other standard *ab initio* and semiempirical calculations are performed with GAUSSIAN 98. Orbital surface plots presented in this chapter are produced with MOLDEN [28].

3.1. $C_{2n}H_{2n+2}$ Polyenes

Polyenes provide a good example to illustrate BOVB calculations based on a single covalent configuration (perfect-pairing approximation). It is possible to treat a very large number of electrons within this type of approximation. For a $BOVB(N, 1+S)$ calculation the single excitations necessary for orbital optimization add only $N(N-1)$ configurations to the super CI problem. This coupled with our use of essentially linear methods for the orbital optimization, which reduce the number of transformed two-electron integrals required to a minimum, prompts us to believe it is possible to treat perhaps up to $N=60$. In this work we report calculations for up to $N=30$ using our current code. For larger problems it will be necessary to write a very efficient direct biorthogonal two-electron integral transformation, since this process will now dominate the calculation. A revised strategy for this transformation is currently being developed. We also note that if we wish to include more than a single perfect-pairing configuration the extension of the super CI space goes roughly in steps of $N(N-1)$ per additional spin-coupling. So several spin-couplings can be treated without difficulty.

Since our purpose is to show the number of electrons/nonorthogonal orbitals that can be handled we have simply used a minimal STO-3G basis [29]. The polyene is set up with alternating double and single bonds. The double bond length is taken as 1.335 Å, the single bond length as 1.45 Å and the C—H bond as 1.089 Å, in all cases. The CCC and HCC angles are assumed to be 120°. We also report, for comparison, Hartree-Fock energies and CASSCF energies. The CASSCF calculations are limited to up to $N=12$. In these $C_{2n}H_{2n+2}$ systems there are $2n$ π-electrons and we include all of these in our calculations. The wavefunction used may be denoted $BOVB(2n, 1+S)$ in the notation of Eq. (14). As may be anticipated the outcome of the BOVB
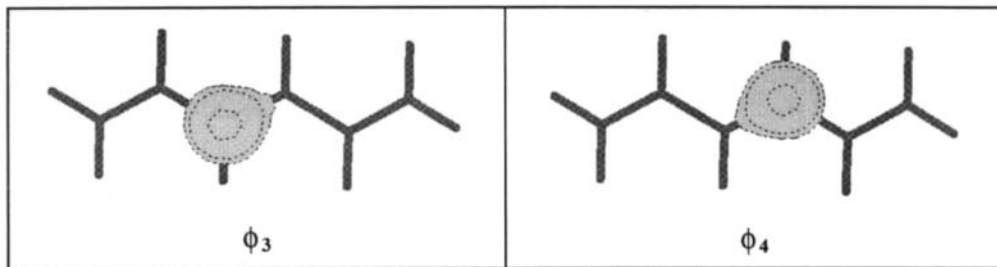
Fig. 1. The innermost paired orbitals in C_6H_8 obtained at the BOVB($6,1+S$)/STO-3G level. The molecule is oriented so that it lies in the plane of the paper.

orbital optimization is a set of $2n$ carbon-centred, highly localized $2p$-like nonorthogonal orbitals which are distorted towards their bonding partner. Fig. 1 displays the innermost paired orbitals in C_6H_8 viewed from above the molecular plane. The overlap integral between these orbitals is 0.601. For the outer pairs the overlap integral is reduced slightly to 0.597. This pattern persists through all of the polyenes we have studied ($N=2n$=2-30). The overlap integrals between adjacent spin-coupled pairs is 0.329 indicating that our perfect-pairing calculation does not impose any type of inter-pair orthogonality restriction.

It is interesting to look at the differences in energy between the Hartree-Fock, CASSCF N in N and BOVB($N,1+S$) calculations. The Hartree-Fock and CASSCF energies scale linearly with the number of electrons for these systems (size extensive). To be able to compare the BOVB and CASSCF energies, as a function of the number of electrons, these quantities are plotted in Fig. 2 as energies relative to the Hartree-Fock energy for each polyene. A straight line has been fitted to each set of data: in both cases, the correlation coefficient is 1.0000. This shows the stability of the BOVB results even for very large numbers of electrons. A further point to note is that accurate energies can be obtained even with this very restricted type of BOVB wavefunction. The highly localized form of the orbitals introduces a large amount of electron correlation, despite the fact that only a single spatial configuration and spin-coupling are included.

The energies reported are from the super CI calculation, as described in the previous section. The orbitals are transformed until the norm of the orbital gradient falls below 1×10^{-5}. In all cases, at convergence, the weight of the perfect-pairing configuration is 1 (see Eq. (28)). This illustrates that for a single configuration Eq. (25) is equivalent to the regular super CI method.
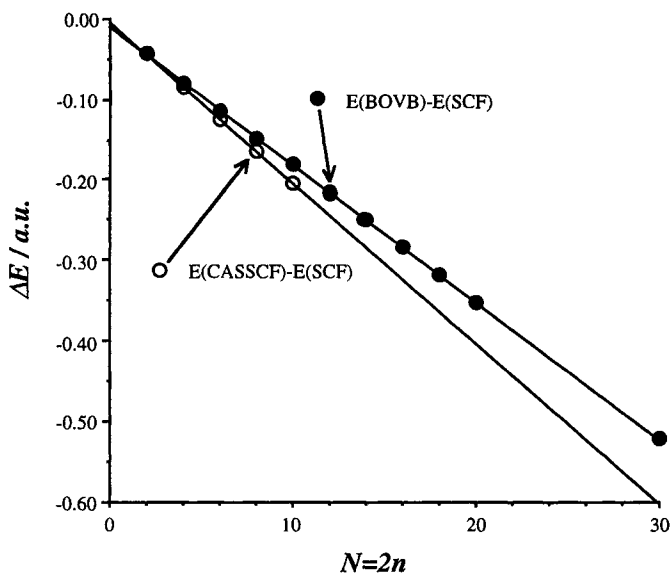
Fig. 2. Comparison of CASSCF N in N, BOVB($N,1+S$) and Hartree-Fock energies for polyenes $C_{2n}H_{2n+2}$ ($N=2n=$2-30).

3.2. Benzene

The classic spin-coupled valence bond description of benzene [30] is by now well known. The description comprises six equivalent, carbon-centred $2p$-like orbitals which are distorted equivalently towards neighbouring carbons. The BOVB description is qualitatively identical to that of the spin-coupled valence bond method. Using a cc-pVDZ basis [31] and allowing the six π orbitals and electrons to become nonorthogonal we have performed BOVB($6,V$), BOVB($6,5+S$) and BOVB($6,2+S$) calculations. Fig. 3 shows one of the six equivalent carbon-centred orbitals which are obtained. The molecule has been tilted out of the plane of the paper to show clearly the $2p$-like shape and the symmetric distortion towards both neighbouring carbon atoms. Table 1 shows the total energies, and orbital overlap integrals between adjacent and next nearest orbitals, obtained at different levels. Also given is a breakdown of the weights from each class of function included: covalent, singly ionic, doubly ionic etc. The covalent functions comprise the two equivalent Kekulé structures and the three equivalent Dewar structures:

Kekulé   Dewar
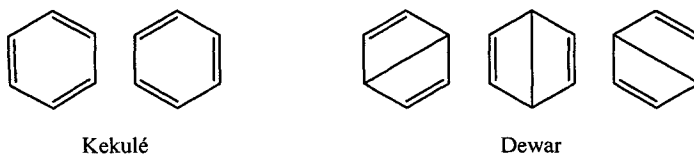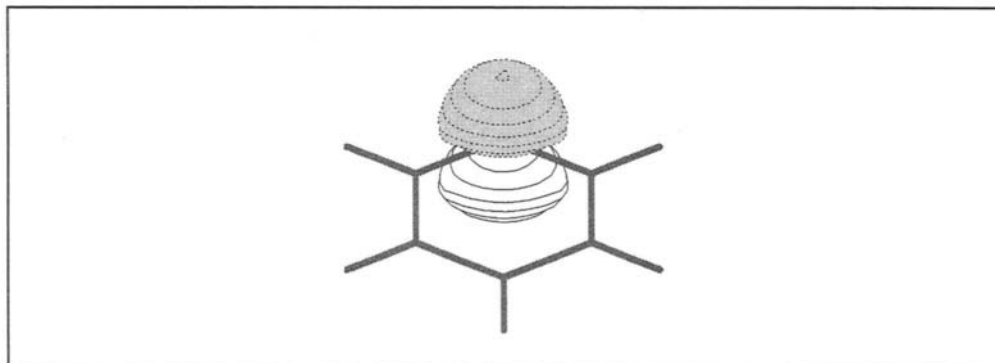
Fig. 3. One of the six equivalent carbon-centred benzene orbitals obtained from BOVB calculations.

The energy of the BOVB($6, V$) calculation is identical to an orthogonal CASSCF 6-electron/6-orbital calculation. Note that the contribution of the singly ionic terms is not zero but, when combined via Eq. (25), a zero orbital rotation is obtained. Qualitatively the picture emerging from all three BOVB calculations is the same. It is useful to compare the BOVB wavefunctions with those in Ref. 32. Spin-coupled valence bond calculations do not contain any ionic configurations and so give summed weights for the Kekule and Dewar structures of 0.812 and 0.188, respectively. CASVB calculations do include ionic configurations but their weights are effectively reduced to zero and so yield weights in the range of 0.819-0.627 for the Kekulé structures and 0.181-0.373 for the Dewar structures, depending on the type of optimization used.

Table 1

Total energies (a.u.), overlap integrals and configuration weights for benzene obtained with the cc-pVDZ basis with different wavefunctions. The geometry used is HF/cc-pVDZ

Wavefunction	Energy	Orbital overlap integrals	
		Adjacent	Next nearest
HF	−230.702913		
BOVB($6, V$)	−230.775933	0.526	0.112
BOVB($6,5+S$)	−230.771032	0.533	0.115
BOVB($6,2+S$)	−230.756827	0.527	0.102

	Sum of weights					
	Kekulé + Dewar = covalent			singly ionic	doubly ionic	remainder
BOVB($6, V$)	0.555	0.277	0.832	0.129	0.038	0.001
BOVB($6,5+S$)	0.573	0.254	0.827	0.173	—	—
BOVB($6,2+S$)	0.826	—	0.826	0.174	—	—

3.3. Dioxirane

The next example we consider is the three-membered ring dioxirane. Here we treat the electrons involved in the bonds of the ring. The geometry we use was obtained at the HF/cc-pVDZ level. We carried out BOVB($6,V$) and BOVB($6,1+S+RCI$) calculations. In contrast to π systems, we have observed that nonvariational BOVB calculations are quite difficult to converge for σ systems. Faced with this problem, as we have discussed above, we include as well as all single excitations from the reference covalent function also the RCI configurations. This usually stabilizes the optimization process. Table 2 shows the energies obtained at various levels and the weights of different functions in the total wavefunction. The wavefunction is dominated by a single spin-coupling with a weight of 0.954:
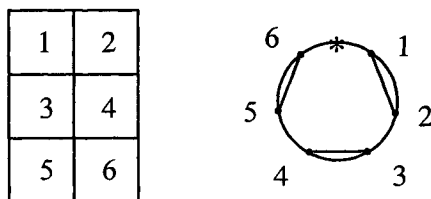
$$\psi = A[\phi_1\phi_2(\alpha\beta-\beta\alpha)\ \phi_3\phi_4(\alpha\beta-\beta\alpha)\ \phi_5\phi_6(\alpha\beta-\beta\alpha)]$$

Other spin-couplings have small but negative weights and so reduce the contribution of covalent functions in the BOVB($6,V$) wavefunction to 0.892. This is a consequence of the Chirgwin-Coulson definition of weights which can produce negative weights. Fig. 4 shows the BOVB symmetry unique orbitals. There are three equivalent orbitals on the opposite side of the mirror plane perpendicular to the plane of the ring. The numbers of these orbitals are indicated in parenthesis in Fig. 4. Table 3 shows the matrix of orbital overlap integrals. The powerful oxidizing reactivity of the dioxirane molecule is generally initiated by rupture of the O—O bond rather than the C—O bonds.

Table 2
Total energies (a.u.) and configuration weights for dioxirane obtained with the cc-pVDZ basis with different wavefunctions.

		Sum of weights			
		covalent	singly ionic	doubly ionic	remainder
Wavefunction	Energy				
HF	–230.702913				
BOVB($6,V$)	–230.775933	0.892	–0.007	0.079	0.036
BOVB($6,1+S+RCI$)	–230.756827	0.889	0.000	—	0.111
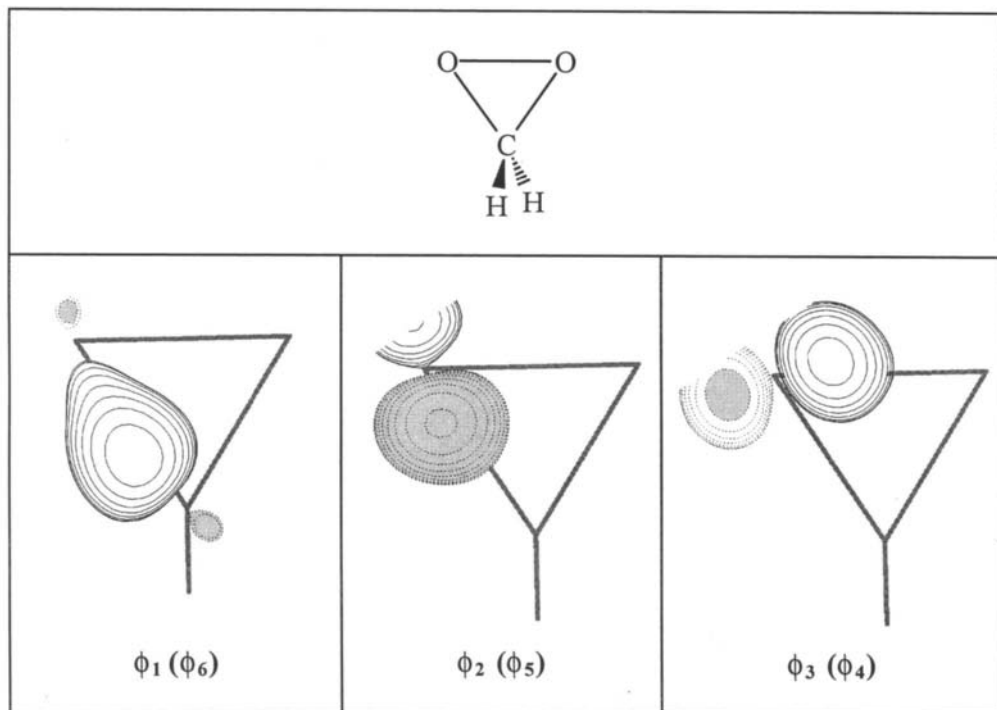
Fig. 4. Symmetry unique orbitals of dioxirane obtained with BOVB(6,1+S+RCI) wavefunction using a cc-pVDZ basis. Parts of the orbitals have been cut off by the bounding box used for plotting.

This preference is reflected in the overlap integral of 0.627 between the O—O orbitals, compared with an overlap of 0.800 for the C—O orbitals. The largest inter-pair overlap (0.128) is between the two symmetry equivalent carbon-centred orbitals (ϕ_1 and ϕ_6).

Table 3

Overlap integrals obtained from BOVB(6,1+S+RCI) wavefunction for dioxirane in a cc-pVDZ basis

	ϕ_1	ϕ_2	ϕ_3	ϕ_4	ϕ_5	ϕ_6
ϕ_1	1.000					
ϕ_2	0.800	1.000				
ϕ_3	0.021	−0.054	1.000			
ϕ_4	0.060	0.033	0.627	1.000		
ϕ_5	0.124	0.084	0.033	−0.054	1.000	
ϕ_6	0.128	0.124	−0.060	0.021	0.800	1.000

3.4. Methane

Historically there have been many valence bond descriptions of methane. Here we report a BOVB(*8,1+S+RCI*)/cc-pVDZ calculation at the HF/cc-pVDZ geometry. The BOVB description is dominated by a single spin-coupling with a weight of 0.766. This spin-coupling corresponds to four equivalent spin-coupled pairs, each of which consists of the two orbitals shown in Fig. 5. The overlap integral between the paired orbitals is 0.810, with all other overlap integrals being $< 1 \times 10^{-4}$. The singly-ionic terms do not contribute to the final wavefunction, but the additional RCI terms have a summed weight of 0.234. The RCI terms serve to condition the eigenproblem and produce a good estimate of the energy. The BOVB(*8,1+S+RCI*) energy lies approximately 0.005 a.u. above the BOVB(*8,V*) energy. This is remarakbly close given the compactness of the BOVB(*8,1+S+RCI*) expansion (129 CSF) compared with the BOVB(*8,V*) expansion (1764 CSF). The bonding picture that emerges is consistent with the classical hybrid description which may be found in most undergraduate textbooks. It must be stressed that while the individual orbitals do not transform as irreducible representations of the molecular point group, the total *N*-electron wavefunction does possess full T_d symmetry.
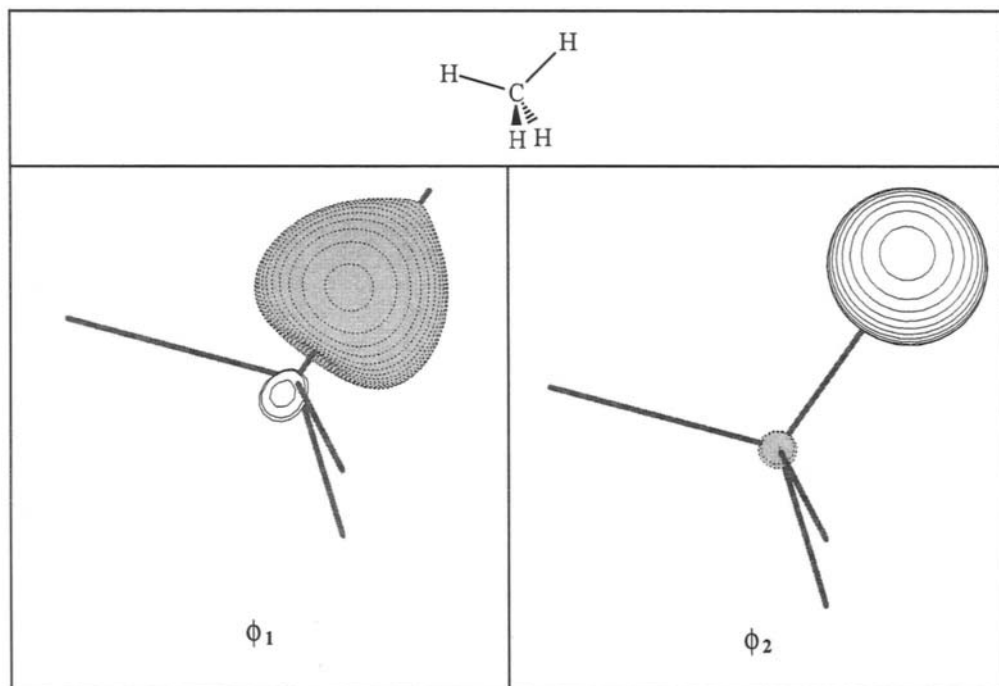
Fig. 5. Symmetry unique orbitals of methane obtained with BOVB(*8,1+S+RCI*) wavefunction using a cc-pVDZ basis.

3.5. Water

We have shown the BOVB description of π and σ bonds in the previous examples. We conclude this section with the BOVB description of the water molecule in which we allow both the bonding and lone-pair electrons to be described in nonorthogonal orbitals. This leads to an eight electron problem which we describe with a BOVB($8,1+S+RCI$)/cc-pVDZ wavefunction. Again the geometry is HF/cc-pVDZ. The BOVB($8,1+S+RCI$) energy lies approximately 0.008 au above the BOVB($8,V$) energy.
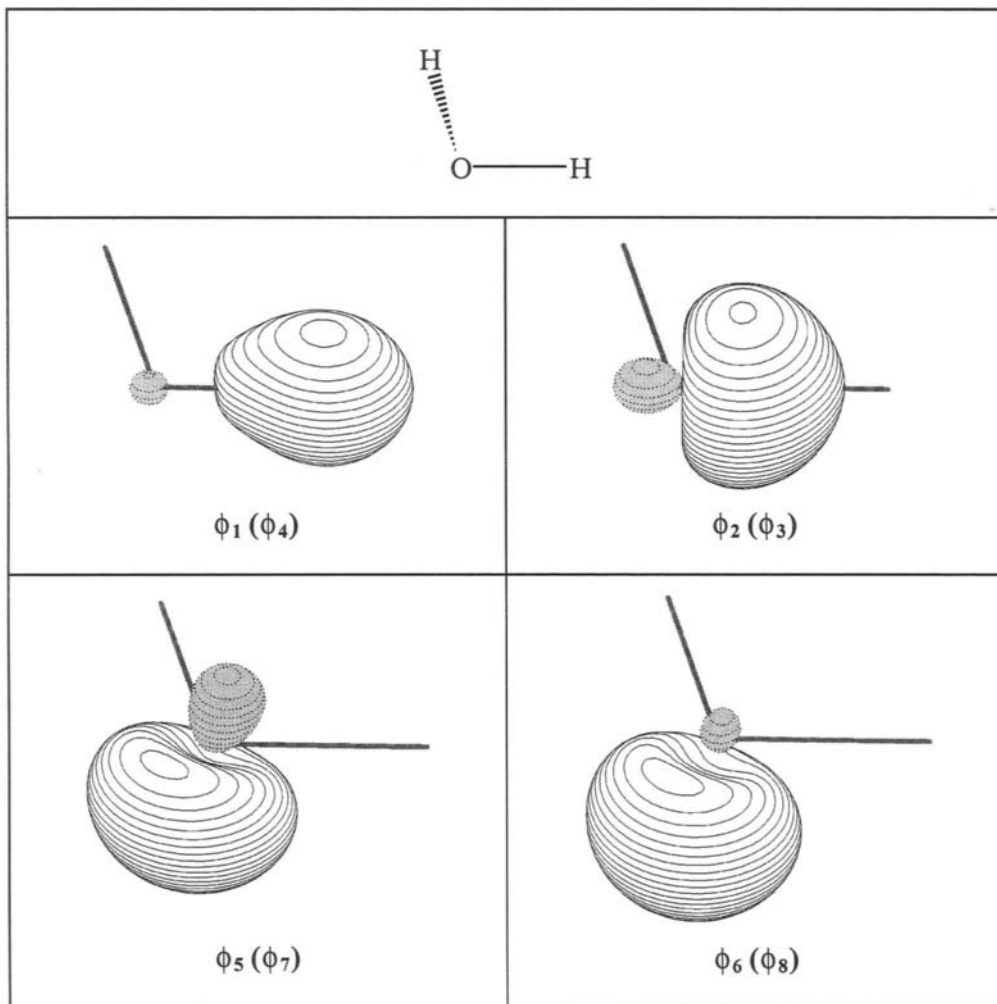
Fig. 6. Symmetry unique orbitals of water obtained with BOVB($8,1+S+RCI$) wavefunction using a cc-pVDZ basis.

It is well known that there are two viewpoints on the description of the lone-pairs in water. They differ in whether the lone-pairs are equivalent or not.

(a)   (b)
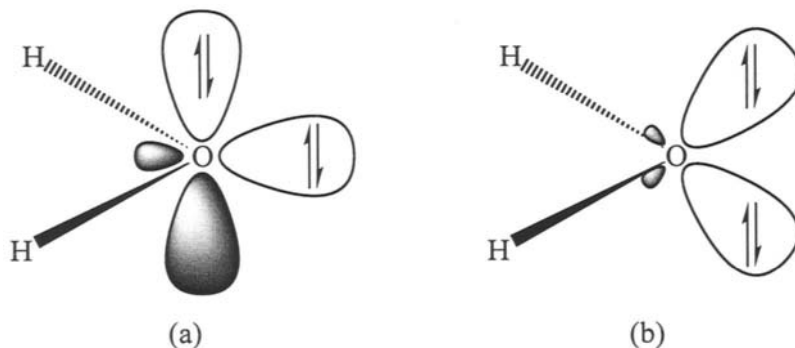
Both descriptions, depicted above, are equally valid and lead to a total N-electron wavefunction which possesses the full symmetry of the molecular point group. However, we note that we have found it impossible to converge our BOVB method to any solution mimicking (a) above. The description given in Fig. 6 is the only one we have been able to fully optimize. In this description we obtain two equivalent lone-pairs, one above and one below the molecular plane in radially split nonorthogonal orbitals. The matrix of overlap integrals is given in Table 4. The weight of the perfect-pairing configuration is only 0.571. The singly-ionic terms have zero weight but the RCI terms contribute 0.429 to the final wavefunction. Again, this large contribution from the RCI terms probably explains why the energy obtained is so close to that obtained with a complete expansion. Conversely, the energy obtained with just the perfect-pairing term can be expected to lie well above the variational limit.

Table 4
Overlap integrals obtained from BOVB($8,1+S+RCI$) wavefunction for water in a cc-pVDZ basis (see Fig. 6 for numbering)

	ϕ_1	ϕ_2	ϕ_3	ϕ_4	ϕ_5	ϕ_6	ϕ_7	ϕ_8
ϕ_1	1.000							
ϕ_2	0.773	1.000						
ϕ_3	0.191	0.353	1.000					
ϕ_4	0.089	0.191	0.773	1.000				
ϕ_5	0.106	0.226	0.226	0.106	1.000			
ϕ_6	0.026	0.139	0.139	0.026	0.817	1.000		
ϕ_7	0.106	0.226	0.226	0.106	0.054	0.015	1.000	
ϕ_8	0.026	0.139	0.139	0.026	0.015	−0.074	0.817	1.000

4. APPLICATIONS

4.1. The pseudohalide acid HCS_2N_3

The term pseudohalogen is used to refer to strongly bound, linear or planar univalent radicals which can form anions, hydracids, neutral dipseudohalogens and interpseudohalogens. Recently the $CS_2N_3\bullet$ radical has been shown to satisfy all these conditions and so is classed as a pseudohalogen [33]. It is the only cyclic pseudohalogen currently known.

Our investigation is concerned with the electronic structure of the hydracid, H—(CS_2N_3). Early semiempirical calculations [34] indicated two stable geometric forms,

| I | II |
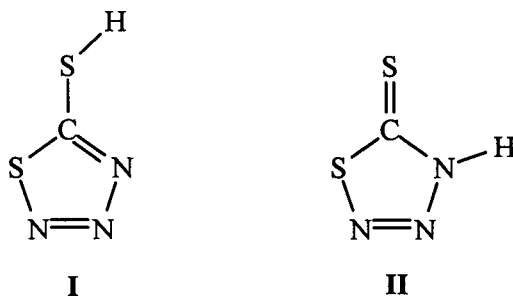
with the thiol form (**I**) being the more stable. However, recent experimental studies [33] have shown that the N—H form (**II**) is the one adopted in the X-ray structure. There has also been much reference [33-35] to the "aromatic" or "pseudoaromatic" character of the underlying $CS_2N_3^-$ ion. We have investigated this system with our BOVB method using the cc-pVDZ basis.

H—(CS_2N_3) contains eight valence π electrons. It should be borne in mind that the sulfur atom outside the ring also contributes two electrons to the π system. We have optimized the geometries of both forms of the acid using a BOVB($8, V$) wavefunction with no symmetry constraints. Both optimized structures are very slightly non-planar. Table 5 gives the total and relative energies of the two forms. We see accord with the experimental situation in that the N—H form (**II**) is predicted to be the most stable.

Table 5

Total energies (a.u.) and relative energies (kcal mol⁻¹) in parenthesis for the two forms of H—(CS_2N_3) obtained with the cc-pVDZ basis

Wavefunction	Form I	Form II
HF	–996.785519 (7.1)	–996.796858 (0.0)
BOVB($8, V$)	–996.864375 (4.8)	–996.872056 (0.0)
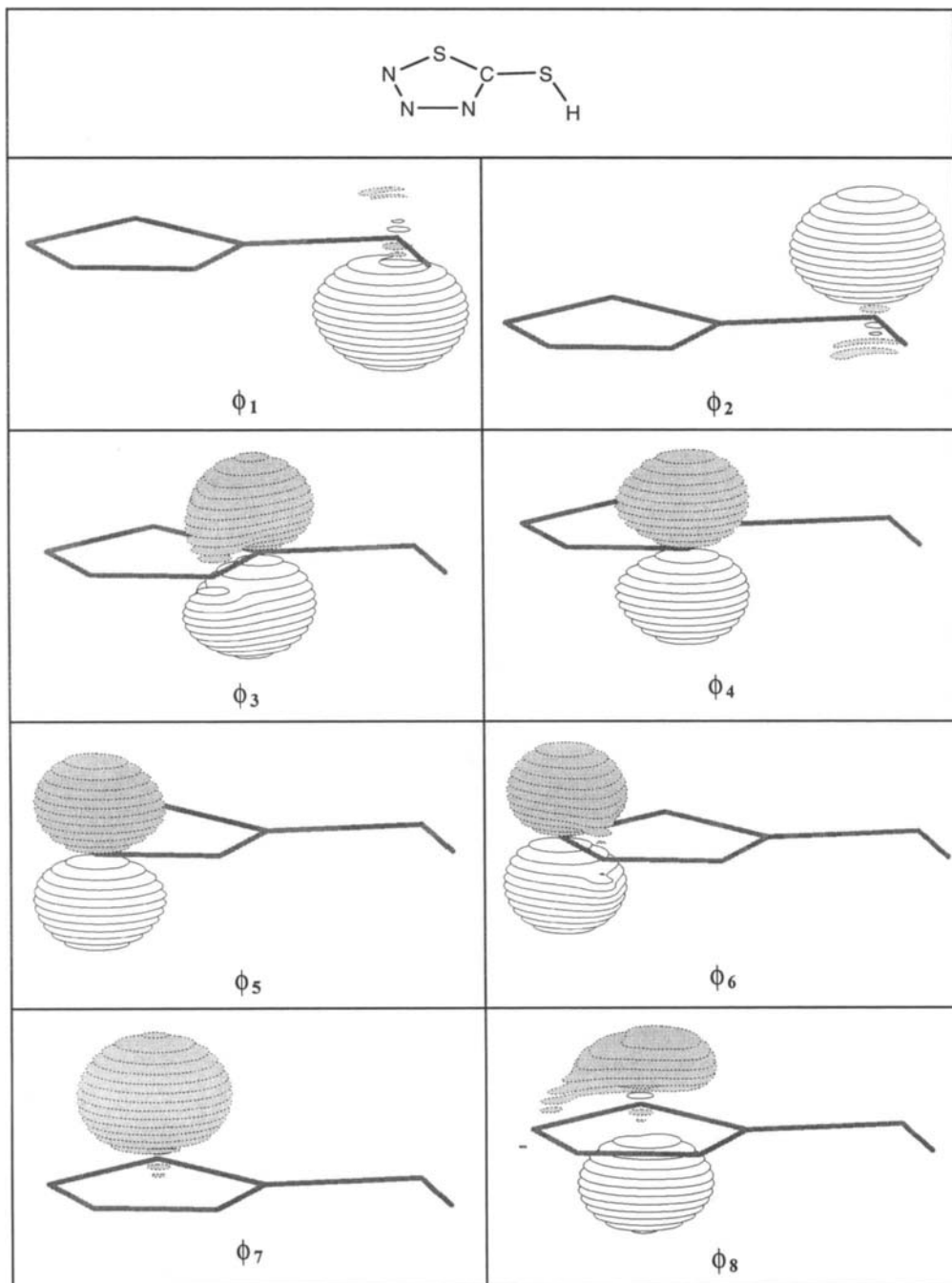
Fig. 7. BOVB($8, V$)/cc-pVDZ orbitals of form **I** of H—(CS_2N_3)

Table 6
Overlap integrals obtained from BOVB($8,V$) wavefunction for form **I** of H—(CS$_2$N$_3$) in a cc-pVDZ basis (see Fig. 7 for orbitals)

	ϕ_1	ϕ_2	ϕ_3	ϕ_4	ϕ_5	ϕ_6	ϕ_7	ϕ_8
ϕ_1	1.000							
ϕ_2	0.849	1.000						
ϕ_3	0.208	0.207	1.000					
ϕ_4	0.025	0.024	0.670	1.000				
ϕ_5	−0.041	−0.042	0.191	0.290	1.000			
ϕ_6	−0.018	−0.020	0.051	0.093	0.614	1.000		
ϕ_7	0.061	0.061	0.172	0.010	0.019	0.179	1.000	
ϕ_8	0.104	0.090	0.236	−0.006	0.003	0.234	0.853	1.000

In both structures the wavefunction is dominated by a single spin-coupling in which the orbitals are paired ϕ_1—ϕ_2 ϕ_3—ϕ_4 ϕ_5—ϕ_6 ϕ_7—ϕ_8. In the S—H form (**I**) this function has a weight of 0.899 in the final wavefunction. In the N—H form (**II**) the weight of this spin-coupling is 0.972. The BOVB($8,V$) orbitals for **I** are shown in Fig. 7 and those of **II** in Fig. 8. The corresponding overlap integrals are given in Tables 6 and 7. We find no indication of any 'aromaticity', since both structures are dominated by a single spin-coupling. From our results, the distribution of the π electrons in these systems is best denoted as
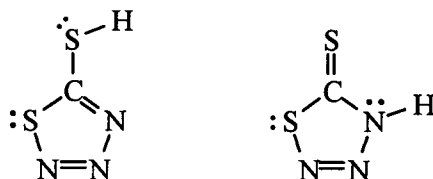
Table 7
Overlap integrals obtained from BOVB($8,V$) wavefunction for form **II** of H—(CS$_2$N$_3$) in a cc-pVDZ basis (see Fig. 8 for orbitals)

	ϕ_1	ϕ_2	ϕ_3	ϕ_4	ϕ_5	ϕ_6	ϕ_7	ϕ_8
ϕ_1	1.000							
ϕ_2	0.701	1.000						
ϕ_3	−0.010	0.112	1.000					
ϕ_4	−0.110	0.181	0.834	1.000				
ϕ_5	0.033	−0.042	0.183	0.293	1.000			
ϕ_6	0.032	−0.005	0.042	0.029	0.616	1.000		
ϕ_7	−0.021	0.119	0.038	0.079	0.036	0.173	1.000	
ϕ_8	−0.076	0.115	0.045	0.104	0.028	0.230	0.852	1.000
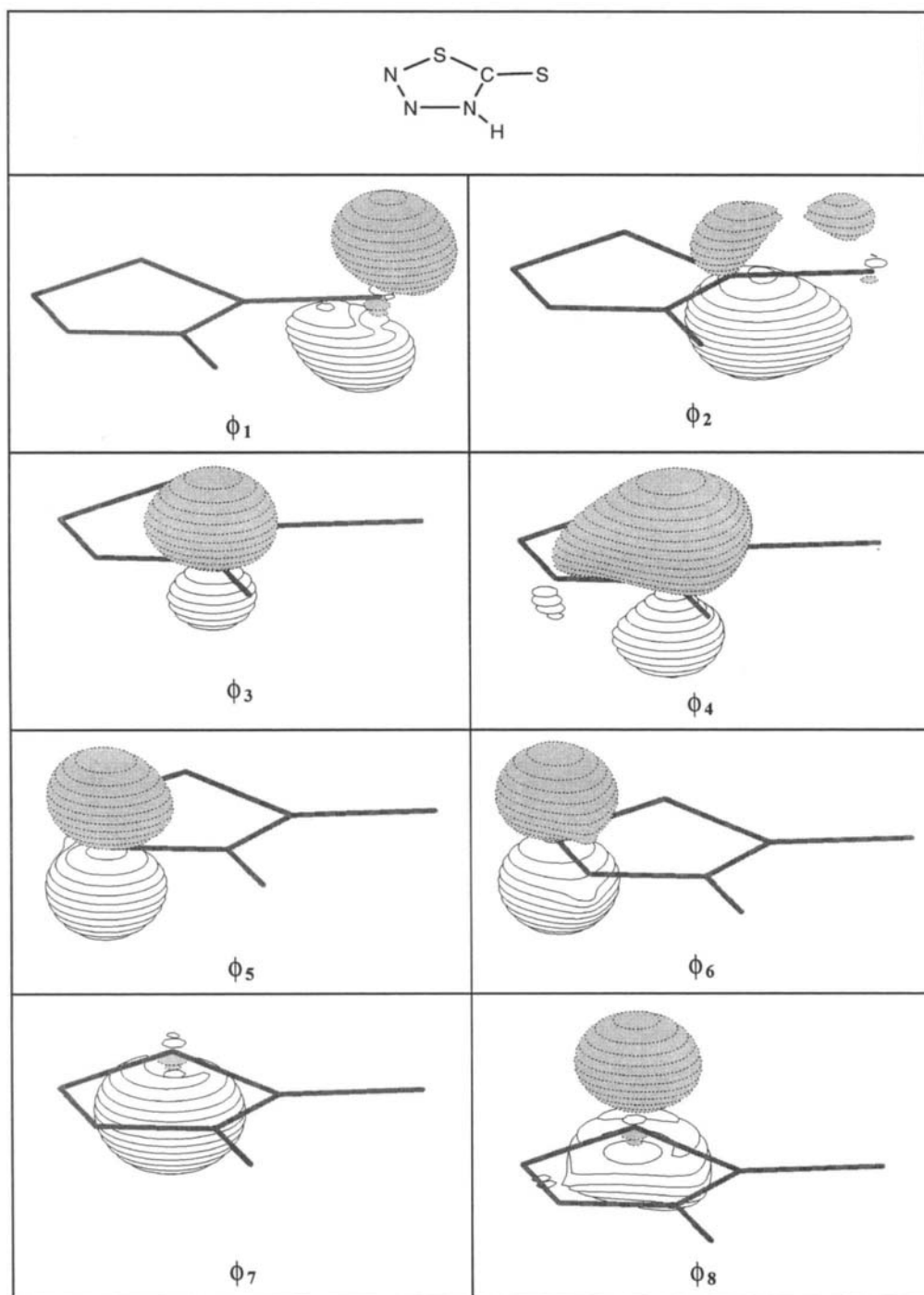
Fig. 8. BOVB($8, V$)/cc-pVDZ orbitals of form **II** of H—(CS$_2$N$_3$)

4.2. Diphosphaallene radical anion

The formation of anions provides an interesting challenge to electronic structure methods. Not only from the point of view of providing quantitatively accurate predictions, but also from the perspective of what happens to the electronic structure when an extra electron attaches. Recent studies on the diphosphaallene system
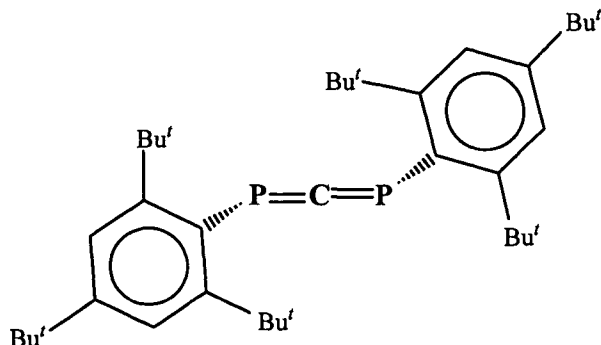
(which we shall denote Ar–P=C=P–Ar) and its radical ions [36, 37] have suggested that it is an electronically intriguing system. Essentially, when the anion is formed, by electrochemical reduction, two conformations are obtained. These two conformations have been referred to as "*cis*-like" and "*trans*-like" [37] and differ principally in the Ar–P...P–Ar dihedral angle.

cis-like   *trans*-like
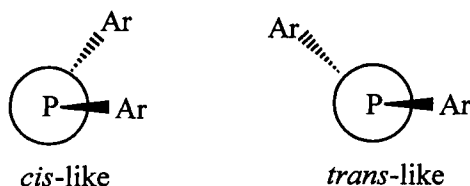
In the *cis* structure the dihedral angle is in the region of 45° while in the *trans* structure it is in the region of 135°. These structures lie very close to each other in energy. Semiempirical AM1 studies on the complete system suggest a preference for the *trans* conformation of 0.3 kcal mol^{-1}. Conversely, *ab initio* and density functional methods applied to the model H–P=C=P–H system predict the *cis* structure to be more stable by 0.3-1.5 kcal mol^{-1}, depending on the level of theory used [37]. It has been suggested that the calculated EPR couplings of the *trans* structure agree better with the results of EPR experiments. The *cis* structure possesses C_2 symmetry with both P atoms equivalent. The *trans* structure is of C_1 symmetry with the two P atoms slightly inequivalent. This inequivalence rises from the bending of the PCP

angle. It has been found that this angle has an essentially flat potential which gives the P–C–P linkage a fluxional nature, allowing it to invert easily. This, and the results of EPR experiments, have led to the suggestion that the radical anion [Ar–P=C=P–Ar]⁻ is best described by two equivalent allylic structures

$$\overset{\bullet}{\text{Ar–P}}\text{–}\overset{-}{\text{C}}\text{=P–Ar} \quad \leftrightarrow \quad \text{Ar–P=}\overset{-}{\text{C}}\text{–}\overset{\bullet}{\text{P}}\text{–Ar}$$
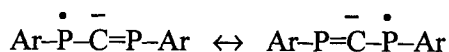
where the 'resonance' is brought about by the fluxional P–C–P linkage. These resonance forms are suggested by the molecular orbital viewpoint which involves the additional electron entering an antibonding allylic orbital and thus weakening/breaking the P=C bond.

Clearly, obtaining an *ab initio* description of a system as large as this with a reasonable basis set is an unrealistic undertaking. Thus we have chosen to use the layering method (IMOMO) of Morokuma and coworkers [38], in which the full system is divided into three sets with coordinates denoted by $\mathbf{R_1}$, $\mathbf{R_2}$ and $\mathbf{R_3}$, respectively.

Real system   Model system
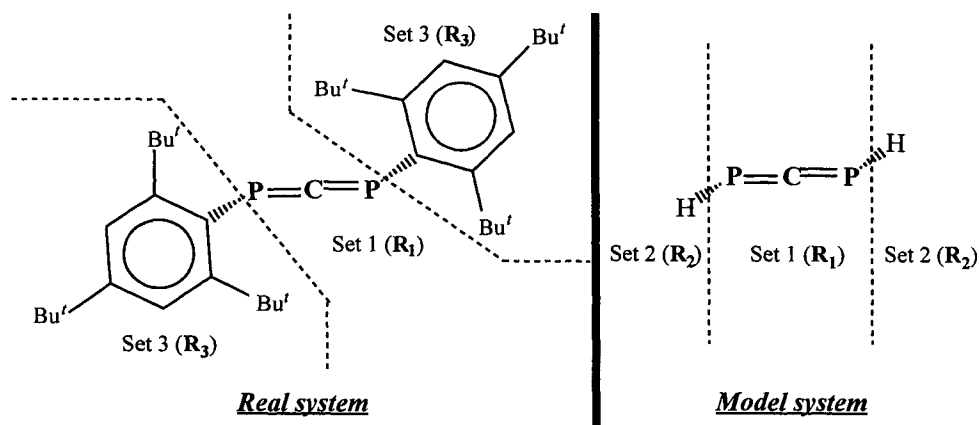
The model system we have treated with the BOVB method and the full system with the PM3 semiempirical method. The total energy is evaluated as

$$E\left(R_1, R_3\right) = E_{BOVB}\left(R_1, R_2\right) + E_{PM3}\left(R_1, R_3\right) - E_{PM3}\left(R_1, R_2\right) \tag{31}$$

The gradients of Eq. (31) with respect to geometrical parameters may be evaluated straightforwardly.

For the BOVB description of the neutral system we chose the four electrons of the allylic π system and used a 6-31++G(d,p) basis [39]. We carried out geometry optimizations at the BOVB(*4,V*)/6-31++G(d,p):PM3 level for the neutral and found very good agreement with the X-ray structure. For

the radical anion we included in the BOVB orbital space one additional allylic orbital from the starting set of spin-restricted open-shell Hartree-Fock orbitals. We located both *cis* and *trans* forms of the radical anion at the BOVB(*5,V*)/6-31++G(d,p):PM3 level. Our calculations agree with the findings of previous *ab initio* calculations, on the model HPCPH system, in that we find the *cis* structure is more stable than the *trans* structure by 2.0 kcal mol^{-1}.
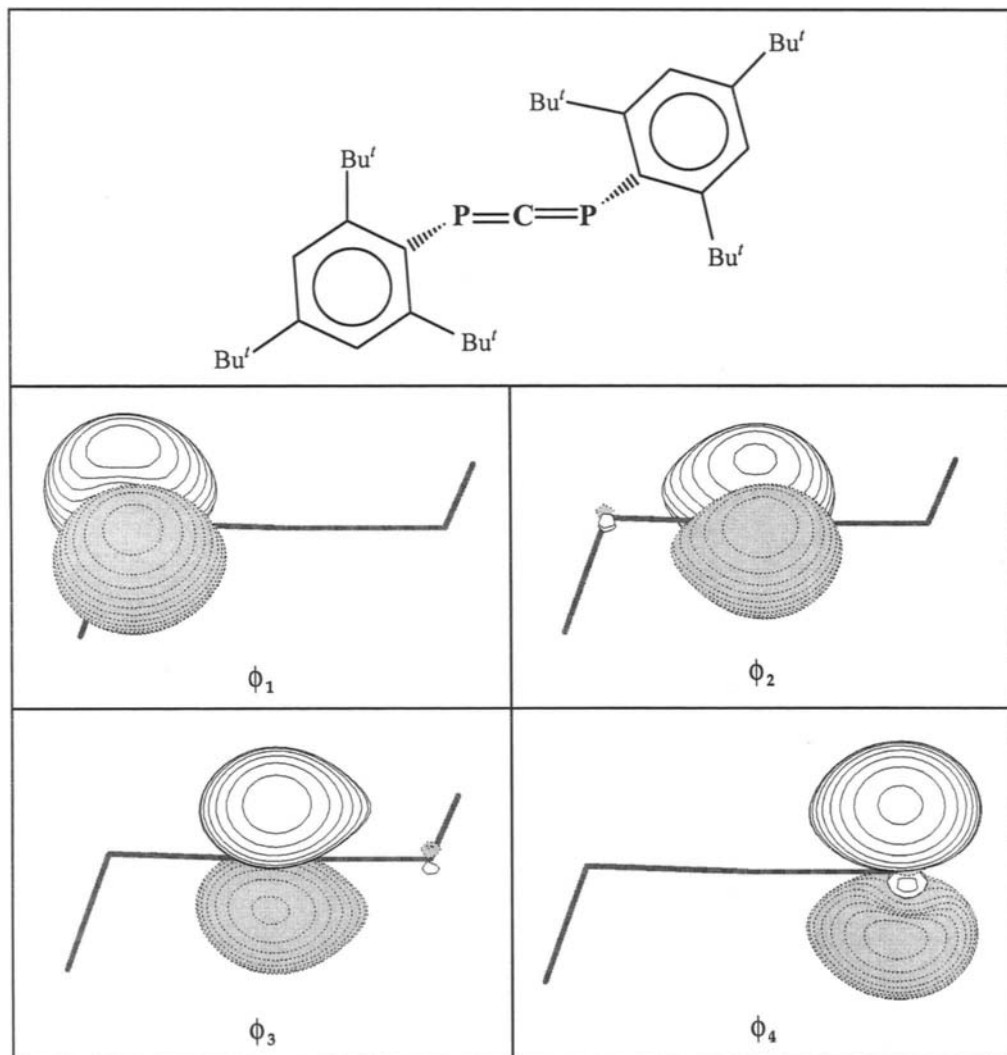
Fig. 9. BOVB(*4,V*)/6-31++G(d,p) orbitals of the —P=C=P— fragment of Ar–P=C=P–Ar (see text for description)

Our concern here is the nature of the radical anion. In Fig. 9 the BOVB(4, V) orbitals of the neutral are shown. The wavefunction is dominated by a single spin-coupling, ϕ_1—ϕ_2 ϕ_3—ϕ_4, with a weight of 0.981. The overlap integrals $\langle \phi_1 | \phi_2 \rangle = \langle \phi_3 | \phi_4 \rangle = 0.600$, with all other overlap integrals being two orders of magnitude smaller.

Fig. 10 shows the BOVB(5, V) orbitals of the *trans* radical anion. Two spin-couplings make a significant contribution: ϕ_2—ϕ_3 ϕ_4—ϕ_5 ϕ_1, with a weight of 0.727 and ϕ_1—ϕ_4 ϕ_2—ϕ_3 ϕ_5, with a weight of 0.129. The orbital overlap integrals are given in Table 8. Clearly the double bonds of the P–C–P linkage still appear intact. Although ϕ_4/ϕ_5 have been distorted by having the high-spin electron largely localized on the P atom on the left hand side. A small amount of high-spin character is also attributed to ϕ_5 by the second spin-coupling. From these results we suggest a better scheme for depicting the radical anion might be

$$
\overset{\overset{\textstyle -}{\textstyle \bullet}}{\text{Ar--P}}\text{=C=P--Ar} \quad \leftrightarrow \quad \text{Ar--P=C=}\overset{\overset{\textstyle -}{\textstyle \bullet}}{\text{P}}\text{--Ar}
$$
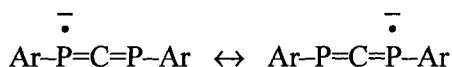
which emphasizes that the attachment of an electron does not automatically lead to the disruption of the P=C bond.

The use of the layering scheme combined with our BOVB methods provides one route to valence bond studies of large molecular systems. These types of studies merit much more investigation. The layering technique can of course be adapted to any form of energy calculation and hence any type of valence bond calculation. It opens up new horizons for *ab initio* valence bond methods, which have traditionally been used mostly for small molecule studies. Ironically (perhaps), the small molecule *ab initio* calculation gets to stay (which pleases the theoretician), but it takes on the appearance of 'reality' through the intermediation of Eq. (31). For systems very much larger than those studied here it is possible to add a further layer to Eq. (31), and introduce a yet lower level of theory (molecular mechanics) to produce a three-layer calculation.

Table 8

Overlap integrals obtained from BOVB(5, V)/6-311++G(d,p) wavefunction for [Ar--P=C=P--Ar]⁻ (see Fig. 10 for orbitals)

	ϕ_1	ϕ_2	ϕ_3	ϕ_4	ϕ_5
ϕ_1	1.000				
ϕ_2	−0.165	1.000			
ϕ_3	0.129	0.656	1.000		
ϕ_4	0.813	0.103	0.247	1.000	
ϕ_5	0.399	0.081	0.263	0.730	1.000
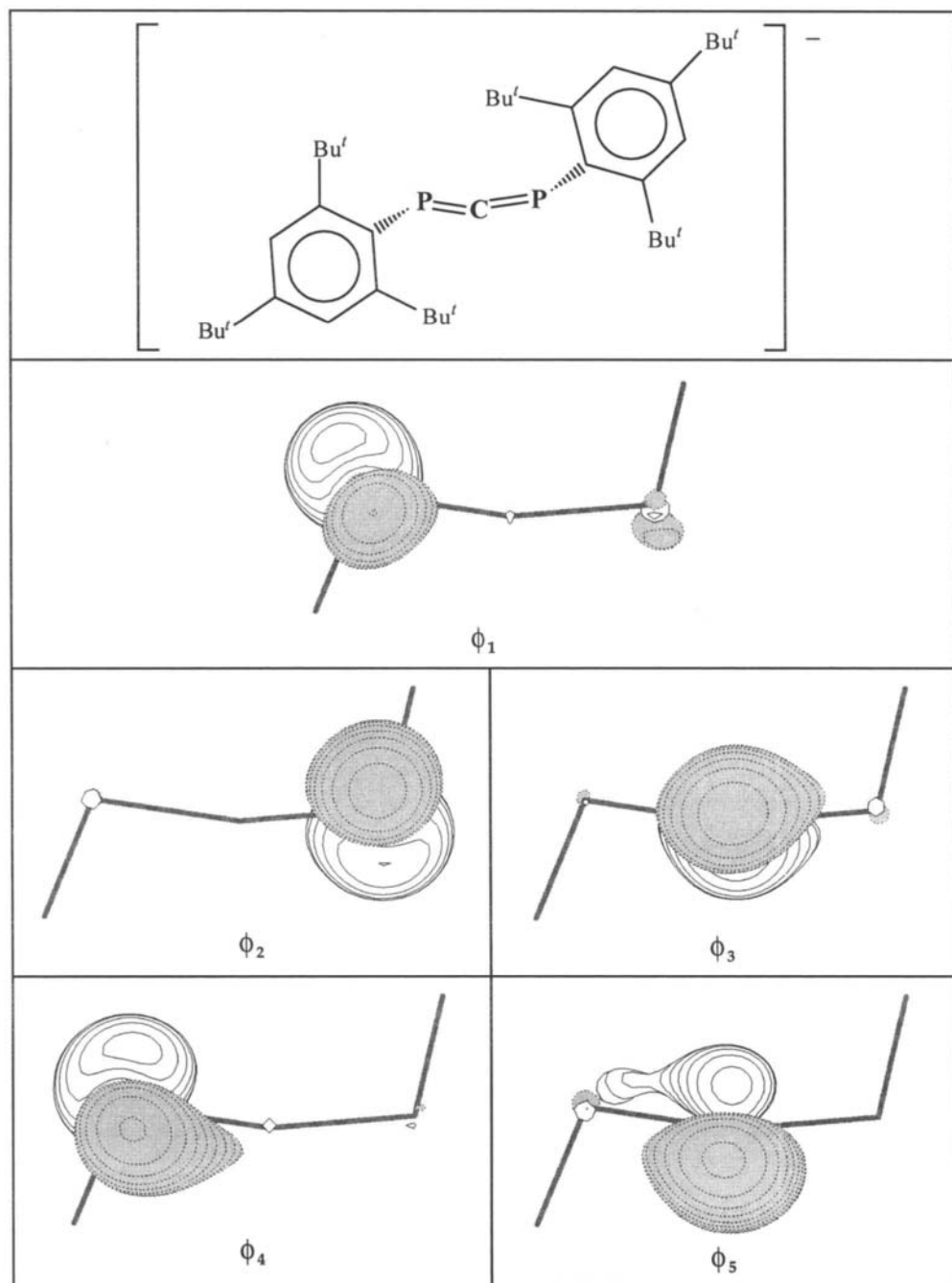
Fig. 10. BOVB($5, V$)/6-31++G(d,p) orbitals of the —P=C=P— fragment of [Ar–P=C=P–Ar]⁻
(see text for description)

5. CONCLUSIONS

It is appropriate to conclude by asking what the BOVB method has to offer valence bond theory in general and, perhaps more importantly, what it may offer the larger area of quantum chemistry as a whole.

The BOVB method does not lend itself for use as a 'black box' method. The same is true of any valence bond approach. The user must have some understanding of the underlying electronic structure of the system under study. Only then will they be able to make sane choices for the orbital partitioning and spin-coupling problems. This aspect may be viewed as a strength or a weakness, depending on one's point of view. However, it does mean that the 'preparative' stage of a calculation is very much more labour-intensive than a corresponding calculation using, for example, a Hartree-Fock based or density functional method. Computationally, like any multiconfigurational method, there are significant overheads in obtaining transformed molecular integrals and dealing with a sometimes large eigenvalue problem. To treat large molecular systems some form of layering and/or hybrid and/or semiempirical methodology must be employed. The wavefunctions obtained from BOVB calculations are not always as compact as those from spin-coupled valence bond studies, but they are sufficiently compact and accurate to be a useful extension of valence bond methods. There also remain essential developments in the BOVB method which are required, such as gradients for general BOVB wavefunctions and a compact treatment of the dynamic electron correlation problem.

At present, the BOVB method is able to treat large numbers of electrons in nonorthogonal orbitals, provided some restriction of the spin space is imposed. This combined with layering techniques for managing large numbers of atoms should provide a route into many areas of molecular research which have traditionally been 'too big' for all atom valence bond calculations. The developments of the last decade bear witness to the fact that as the number of valence bond studies on *real* problems increases, so the following for the valence bond approach grows. The future of valence bond methods appears bright.

REFERENCES

[1] M. Moshinsky and T.H. Seligman, Ann. Phys., 66 (1971) 311.
[2] A.A. Cantu, D.J. Klein, F.A. Matsen and T.H. Seligman, Theor. Chim. Acta, 38 (1975) 341.
[3] T.H. Seligman, J. Math. Phys., 13 (1972) 876.
[4] T.H. Seligman, Group Theoretical Methods in Physics, Nijmegen, Netherlands, 1973.
[5] J.M. Norbeck and R. McWeeny, Chem. Phys. Lett., 34 (1975) 206.
[6] P.W. Payne, J. Chem. Phys., 77 (1982) 5630.

258

[7] J.J.W. McDouall, Theor. Chim. Acta, 83 (1992) 339.

[8] J.J.W. McDouall, Theor. Chim. Acta, 85 (1993) 395.

[9] N.O.J. Malcolm and J.J.W. McDouall, J. Comput. Chem., 15 (1994) 1357.

[10] N.O.J. Malcolm and J.J.W. McDouall, J. Comput. Chem., 15 (1994) 1365.

[11] D.L. Cooper, J. Gerratt and M. Raimondi, J. Chem. Soc., Perkin Trans. 2, (1989) 1187.

[12] T. Thorsteinsson, D.L. Cooper, J. Gerratt, P.B. Karadakov and M. Raimondi Theor. Chim. Acta, 93 (1996) 343.

[13] T. Thorsteinsson and D.L. Cooper, Mol. Phys., 93 (1998) 663.

[14] R. McWeeny, Methods of Molecular Quantum Mechanics, 2nd Ed., Academic Press, London, 1989.

[15] J. Paldus, S. Rettrup and C.R. Sarma, J. Mol. Struct. (Theochem), 199 (1989) 85.

[16] I.L. Cooper and R. McWeeny, J. Chem. Phys., 45 (1966) 226.

[17] C.M. Reeves, Commun ACM, 9 (1966) 276.

[18] B.T. Sutcliffe, J. Chem. Phys., 45 (1966) 235.

[19] S.F. Boys, Proc. Roy. Soc. A, 309 (1969) 195.

[20] M. Raimondi, M. Simonetta and G.F. Tantardini, Comput. Phys. Reps., 2 (1985) 171.

[21] E.A. Goddard and W.A. Goddard III, J. Chem. Phys., 88 (1988) 3132.

[22] J.H. van Lenthe and G.G. Balint-Kurti, J. Chem. Phys., 78 (1983) 5699.

[23] F. Grein and T.C. Chang, Chem. Phys. Lett., 12 (1971) 44.

[24] P. Pulay, Chem. Phys. Lett., 73 (1980) 393.

[25] T.H. Fischer and J. Almlöf, J. Phys. Chem., 96 (1992) 9768.

[26] B.W. Chirgwin and C.A. Coulson, Proc. Roy. Soc. A, 201 (1950) 196.

[27] Gaussian 98, Revision A.7, M. J. Frisch, G. W. Trucks, H. B. Schlegel, G. E. Scuseria, M. A. Robb, J. R. Cheeseman, V. G. Zakrzewski, J. A. Montgomery, Jr., R. E. Stratmann, J. C. Burant, S. Dapprich, J. M. Millam, A. D. Daniels, K. N. Kudin, M. C. Strain, O. Farkas, J. Tomasi, V. Barone, M. Cossi, R. Cammi, B. Mennucci, C. Pomelli, C. Adamo, S. Clifford, J. Ochterski, G. A. Petersson, P. Y. Ayala, Q. Cui, K. Morokuma, D. K. Malick, A. D. Rabuck, K. Raghavachari, J. B. Foresman, J. Cioslowski, J. V. Ortiz, A. G. Baboul, B. B. Stefanov, G. Liu, A. Liashenko, P. Piskorz, I. Komaromi, R. Gomperts, R. L. Martin, D. J. Fox, T. Keith, M. A. Al-Laham, C. Y. Peng, A. Nanayakkara, C. Gonzalez, M. Challacombe, P. M. W. Gill, B. Johnson, W. Chen, M. W. Wong, J. L. Andres, C. Gonzalez, M. Head-Gordon, E. S. Replogle, and J. A. Pople, Gaussian, Inc., Pittsburgh PA, 1998.

[28] G.Schaftenaar and J.H. Noordik, Molden: a pre- and post-processing program for molecular and electronic structures, J. Comput.-Aided Mol. Design,14 (2000) 123.

[29] W.J. Hehre, R.F. Stewart and J.A. Pople, J. Chem. Phys., 51 (1969) 2657.

[30] D.L. Cooper, J. Gerratt and M. Raimondi, Nature, 323 (1986) 699.

[31] T.H. Dunning Jr., J. Chem. Phys., 90 (1989) 1007.

[32] T. Thorsteinsson, D.L. Cooper, J. Gerratt and M. Raimondi, Theor. Chim. Acta, 95 (1997) 131.

[33] M.-J. Crawford, T. M. Klapötke, P. Klüfers, P. Meyer and P.S. White, J. Am. Chem. Soc., 122 (2000) 9052.

[34] M. Conti, D.W. Franco and M. Trisic, Inorg. Chim. Acta, 113 (1986) 71.

[35] M.-J. Crawford and T. M. Klapötke, Phosphorus, Sulfur and Silicon, 155 (1999) 201.

[36] M. Chentit, H. Sidorenkova, A. Jouaiti, G. Terron, M. Geoffroy and Y. Ellinger, J. Chem. Soc., Perkin Trans. 2, (1997) 921.

[37] H. Sidorenkova, M. Chentit, A. Jouaiti, G. Terron, M. Geoffroy and Y. Ellinger, J. Chem. Soc., Perkin Trans. 2, (1998) 71.

[38] S. Humbel, S. Sieber and K. Morokuma, J. Chem. Phys., 105 (1996) 1959.

[39] W.J. Hehre, R. Ditchfield and J.A. Pople, J. Chem. Phys., 56 (1972) 724; P.C. Hariharan and J.A. Pople, Theor. Chim. Acta, 28 (1973) 213; T. Clark, J. Chandrasekhar, G.W. Spitznagel and P.v.R. Schleyer, J. Comput. Chem., 4 (1983) 294.

This Page Intentionally Left Blank

261

Chapter 9

Recent developments of the SCVB method

M. Sironi[a], M. Raimondi[a], R. Martinazzo[b], F.A. Gianturco[b] and D.L. Cooper[c]

[a]Dipartimento di Chimica Fisica ed Elettrochimica, CNR Centro CSRSRC, Università di Milano, Via Golgi 19, 20133 Milano, Italy

[b]Department of Chemistry, University of Rome, Città Universitaria, 00185 Rome, Italy

[c]Department of Chemistry, University of Liverpool, Liverpool L69 7ZD, United Kingdom

Ab initio modern valence bond theory, in its spin-coupled valence bond (SCVB) form, has proved very successful for accurate computations on ground and excited states of molecular systems. The compactness of the resulting wavefunctions allows direct and clear interpretation of correlated electronic structure. We concentrate in the present account on recent developments, typically involving the optimization of virtual orbitals via an approximate energy expression. These virtuals lead to higher accuracy for the final variational wavefunctions, but with even more compact functions. Particular attention is paid here to applications of the methodology to studies of intermolecular forces.

1. INTRODUCTION

Various methods are now available for computing highly accurate total energies and molecular properties for ground and excited states of small molecular systems. Unfortunately, the ever-increasing sophistication of such wavefunctions tends to make it more and more difficult to obtain direct insight into the physical and chemical details of the molecular electronic structure. As such, there is of course much interest in developing alternative strategies that can obtain useful accuracy with relatively compact wavefunctions, thereby allowing the development of appropriate models that provide reliable predictions for larger systems. Of course, as well as being compact, the descriptions need to be accurate if we are to trust the predictions of the derived models. At least in principle, valence bond theory has always offered direct and clear interpretation of the wavefunction, but intrinsic difficulties linked to the nonorthogonality of the orbitals, as well as to the apparent high contributions from ionic structures, have

meant that VB approaches have received relatively minor attention from the chemical community.

As evidenced by numerous contributions to this volume, recent years have seen a significant resurgence of interest in *ab initio* VB approaches, with a prominent role being played by algorithms for computing so-called 'modern VB' wavefunctions, such as in spin-coupled valence bond (SCVB) theory. In the present account, we summarize key features of the basic spin-coupled and SCVB approaches, before describing recent extensions that combine the required degrees of compactness and accuracy by utilizing optimized virtual orbitals. Particular attention will be devoted to the application of the methodology to studies of intermolecular forces, which pose additional problems.

2. SC APPROACH

The SC method describes an N-electron molecule through a set of N singly occupied SC orbitals $\{\phi_i\}$ which are completely free to overlap with one another. The coupling of the spins is described by a linear combination of the full space of f_S^N spin eigenfunctions $\{\Theta_{SM;k}^N\}$, where S,M are the usual spin quantum numbers, and

$$f_s^N = \frac{(2S+1)N!}{(\tfrac{1}{2}N+S+1)!(\tfrac{1}{2}N-S)!} \tag{1}$$

The most general single-configuration wavefunction that can be set up using the N SC orbitals may be written [1,2]:

$$\Psi_{SC} = \mathcal{A}\left(\phi_1\phi_2\dots\phi_N \sum_{k=1}^{f_S^N} c_{Sk}\Theta_{SM;k}^N\right) \tag{2}$$

in which $\mathcal{A}$ is the antisymmetrizer, needed to satisfy the Pauli principle, and the c_{Sk} are called spin-coupling coefficients.

The N SC orbitals are expanded in a proper basis set of m basis functions $\{\chi_p\}$:

$$\phi_i = \sum_{p=1}^{m} c_{ip}\chi_p \tag{3}$$

Hence the expectation value of the energy becomes a function of the $\{c_{ip}\}$ and $\{c_{Sk}\}$ coefficients:

$$E = \frac{\langle \Psi_{SC}|\hat{H}|\Psi_{SC}\rangle}{\langle \Psi_{SC}|\Psi_{SC}\rangle} = E(\{c_{ip}\},\{c_{Sk}\}) \tag{4}$$

in which $\hat{H}$ is the usual nonrelativistic clamped-nucleus hamiltonian. The various free parameters are evaluated on the basis of the variational principle, using a

robust minimization algorithm based on a stabilized Newton-Raphson procedure. This last requires the evaluation of first and second derivatives of the energy with respect to the variational coefficients, using density matrices up to third order (for the gradient) and up to fourth order (for the hessian).

It is straightforward also to include a 'core' of doubly-occupied orthonormal orbitals, which may either be taken unchanged from prior calculations or optimized, simultaneously with the $\{c_{ip}\}$ and $\{c_{Sk}\}$ coefficients, as linear combinations of the $\{\chi_p\}$. Multiconfiguration variants of the SC wavefunction may also be generated, if required, and calculations may be performed directly for excited states.

In general, SC wavefunctions are not invariant to linear transformations of the $\{\phi_i\}$, so that the converged solution is a unique outcome of the optimization procedure. There is slightly more flexibility in the numerical values of the spin-coupling coefficients, which depend on the particular choice of full basis used in the calculations, but it is routine to transform exactly between different spin bases. The shapes of the SC orbitals, and their variations with nuclear geometry, provide direct insight into the spatial arrangements of the electronic clouds, the hybridization of the atoms, and processes of bond making and bond breaking. The spin-coupling coefficients, and/or matrix elements of appropriate spin operators, furnish a quantitative description of the relative importance of the different modes of spin coupling. This gives the possibility, for example, of elucidating the role of different resonance structures to the overall wavefunction.

In this way we may obtain a compact single-configuration wavefunction of comparable accuracy to a many-configuration 'N electrons in N orbitals' CASSCF description. It must be stressed that no constraints are imposed on the SC orbitals, which are determined solely only on the basis of the variational principle, but a *typical* outcome is a set of functions mostly localized on individual atoms but distorted towards all neighbouring atoms, especially along the direction of bonds. As such, it is often straightforward to interpret SC wavefunctions in terms of traditional chemical concepts. An important consequence of these 'overlap enhancing' orbital distortions is a much reduced role for ionic configurations.

Basis set superposition error (BSSE) is a particular problem for supermolecule treatments of intermolecular forces. As two moieties with incomplete basis sets are brought together, there is an unavoidable improvement in the overall quality of the supermolecule basis set, and thus an artificial energy lowering. Various approximate corrections to BSSE are available, with the most widely used being those based on the counterpoise method (CP) proposed by Boys and Bernardi [3]. There are indications that potential energy surfaces corrected via the CP method may not describe correctly the anisotropy of the molecular interactions, and there have been some suggestions of a bias in the description of the electrostatic properties of the monomers (secondary basis set superposition errors).

Not surprisingly, there have been various attempts to develop methods for the *a priori* elimination of BSSE, including the development of appropriate effective hamiltonians. Of particular relevance to the present work is the idea of partitioning the supermolecule basis set between the various molecular fragments, of identifying the total number of electrons associated with each fragment, and then of developing each orbital using only the basis functions of the particular fragment. At the RHF level, this procedure has been termed self-consistent field for molecular interaction (SCF–MI) [4,5]. The SCF–MI method has been applied successfully to a variety of systems, ranging from the well known problem of the water dimer up to pairs of nucleic acids [5]. Much the same type of approach can be implemented almost immediately within the SC methodology.

Indicating with $\{\chi_p^A\}$ and $\{\chi_p^B\}$ the atomic basis functions centred on the moieties A (with N_A electrons) and B (with N_B electrons), respectively, the SC orbitals are expanded in the form:

$$\phi_i^A = \sum_{p=1}^{m_A} c_{ip}\chi_p^A \qquad \text{for} \quad i=1,2,...,N_A$$

$$\phi_i^B = \sum_{p=1}^{m_B} c_{ip}\chi_p^B \qquad \text{for} \quad i=1,2,...,N_B \tag{5}$$

Of course, the SC orbitals associated with a particular fragment are completely free to overlap with one another, *and* with all of the SC orbitals of the other fragment(s). In particular, the $\{\phi_i^A\}$ are free to extend spatially over the nuclei of the B molecule, using the tails of the atomic functions $\{\chi_p^A\}$, thereby taking into account also effects connected to charge transfer interactions. Various calculations have confirmed that such a SC wavefunction is able to describe in a compact way the ground state of a weakly-bound system, without biasing the results with BSSE.

3. SCVB

The converged SC orbitals satisfy orbital equations of the form [6]:

$$f^{(i)}\phi_i^{(j)} = \varepsilon_i^{(j)}\phi_i^{(j)} \qquad i=1,...,N \quad \text{and} \quad j=1,...,m \tag{6}$$

such that one of the solutions coincides with the SC orbital ϕ_i already determined by the variational procedure and the higher solutions are virtual orbitals. Due to the mathematical structure of the hermitian operators $\{f^{(i)}\}$, each orbital 'feels' a field generated by only the remaining $N-1$ electrons, so that low-lying virtuals provide rather good descriptions of actual excited states. Each of the $f^{(i)}$ generates its own 'stack' of m orthonormal functions, but orbitals in different stacks may overlap one another.

Starting from the ground-state SC configuration and/or from other appropriate reference configurations, additional configurations may be generated by replacing one or more occupied orbitals with virtual orbitals. 'Vertical' excitations are those within individual stacks. Configurations with doubly occupied orbitals, obtained by means of 'cross excitations', are termed ionic. Once all the desired structures have been generated, the best linear combinations of them are determined by constructing and resolving the corresponding secular problem using efficient VB strategies [7,8]. The various roots are called SCVB wavefunctions and correspond, of course, to different electronic states.

Calculations on quite a large variety of systems have shown that the SCVB approach can generate molecular properties and relative energies of an accuracy comparable to MO–CI methods, but using expansions built from orders of magnitude fewer configurations. In addition, it is very common to find that very few VB structures have an appreciable weight in any given excited state, thereby making it very straightforward to deduce a reliable and insightful qualitative interpretation of the electronic structure.

In recent years, the SCVB approach has proved particularly useful in studies of low-energy charge transfer collisions in astrophysical plasmas [9]. The usual strategy is to consider only vertical excitations into low-lying virtuals, plus associated ionic configurations, taking as reference functions the dominant structure for each state of interest. It is important to achieve good accuracy for several asymptotic energy separations, as these determine to a large extent the positions and the nature of (avoided) crossings. However, it is just as important to maintain this high accuracy for all geometries, and for many states of different spin and spatial symmetry. The compactness of the final SCVB wavefunctions proves particularly beneficial for the computation of the required radial (nonadiabatic) couplings. The ease of identifying the qualitative character of each state, over the entire range of nuclear geometries, is an important asset when transforming the adiabatic molecular data to the p-diabatic representation that it is used in the fully-quantal scattering calculations.

4. SCVB*

We are especially interested in calculating accurate intermolecular potentials to be used with classical and quantum dynamics programs. Particularly for systems with larger numbers of valence electrons, we need to be able to obtain very accurate SCVB wavefunction by means of even smaller numbers of structures. To accomplish this we have devised a new approach in order to generate one or more 'optimal' virtual orbitals for each occupied SC orbital [10]. We concentrate here on the case of a single properly optimized virtual orbital ϕ_i^+ for each SC occupied orbital ϕ_i.

The determination of these virtual orbitals $\{\phi_i^+\}$ is carried out by augmenting the converged SC wavefunction with all double vertical excitations into the unknown virtuals:

$$\Psi_D = c_0 \Psi_{SC} + \sum_{i>j}^{N} c_{ij} \Psi_{ij} \tag{7}$$

where

$$\Psi_{ij} = \mathcal{A} \left(\phi_1 \phi_2 \ldots \phi_i^+ \ldots \phi_j^+ \ldots \phi_N \sum_{k=1}^{f_S^N} c_{Sk}^{(ij)} \Theta_{SM;k}^N \right) \tag{8}$$

Our task is to find virtual orbitals $\{\phi_i^+\}$ that minimize the total energy of the wavefunction Ψ_D but, in order to reduce the overall computational effort, we now invoke the following approximations:

1) the spin coupling coefficients $c_{Sk}^{(ij)}$ appearing into the excited configurations are fixed to the values found for the SC reference configuration.
2) the virtual orbitals are optimized with respect to the energy of the overall wavefunctions by means of a second order perturbation approximation.

The use of this perturbation approximation to compute optimized virtual orbitals introduces a major saving. We need only compute diagonal and first row elements of the hamiltonian and overlap matrices, because the relevant energy expression takes the form:

$$E^{(2)} = H_{00} + \sum_{i>j}^{N} \frac{[H_{(0,ij)} - H_{00} S_{(0,ij)}]^2}{H_{00} S_{(ij,ij)} - H_{(ij,ij)}} \tag{9}$$

in which $H_{00} = \langle \Psi_{SC} | \hat{H} | \Psi_{SC} \rangle$, $S_{(0,ij)} = \langle \Psi_{SC} | \Psi_{ij} \rangle$, and so on. The hamiltonian and overlap matrices are computed using the usual Löwdin formula for the evaluation of matrix elements between Slater determinants built from non-orthogonal orbitals. Many of the efficient computational strategies adopted in the SC methodology [11] have been used in this new approach. However, the bra and ket orbitals are now different, with the resulting loss of symmetry in the density matrices elements leading to some additional computational overhead [10].

The most convenient procedure for attaining the minimum of the second order perturbation expression of the energy, so as to generate the optimized virtual orbitals, depends on the kind of problem being studied. In the case of intermolecular interactions, convergence is quite easy with just a gradient-based procedure. The minimization scheme can be recast in such a way that the coefficients of the improved virtual orbitals can be obtained, at each step, by a resolution of a linear system of $N_A + N_B$ equations. Specifically:

$$F^A C_i^A = -\varepsilon_i^A$$

$$F^B C_i^B = -\varepsilon_i^B \tag{10}$$

in which F^A (F^B) is a square matrix of order m_A (m_B), and C_i^A (C_i^B) is a column vector of dimension m_A (m_B) containing the new updated coefficients corresponding to the virtual orbital ϕ_i^+.

Ultimately, the SC occupied orbitals and the optimized virtuals are used to construct the final, variational SCVB* wavefunctions. These take the form:

$$\Psi_{SCVB*} = c_0\Psi_{SC} + \sum_i^N c_i\Psi_i + \sum_{i>j}^N c_{ij}\Psi_{ij} \tag{11}$$

and thus consist of:

a) The SC reference configuration Ψ_{SC}, i.e. f_s^N structures.

b) Singly-excited configurations Ψ_i, where the occupied SC orbital ϕ_i has been replaced by its own optimized virtual orbital ϕ_i^+, i.e. $N \times f_s^N$ structures. These are included to improve the description of molecular properties and to take account of orbital relaxation.

c) Doubly-excited configurations Ψ_{ij} in which pairs of occupied orbitals ϕ_i and ϕ_j have been replaced by their own optimized virtual orbitals ϕ_i^+ and ϕ_j^+, i.e. $\frac{1}{2}N(N+1) \times f_s^N$ structures.

The quality of the final results, as well as the relative numerical values of appropriate c_{ij} coefficients, provide reassurance as to the quality of the approximations invoked during the optimization of the virtuals.

The interaction between a helium atom and the LiH molecule has been described using a SCVB* wavefunction built up using just 25 structures. Interaction energies, computed along different approaches of the two moieties, compare extremely well with a corresponding traditional SCVB calculation using many more structures. Even a very small energy minimum of about 0.01 mHartree is perfectly reproduced for He at a distance of $R=11$ bohr from the centre of mass of the LiH molecule (collinear approach of He to H–Li).

In addition to further correlating the ground state of a single molecule, the SCVB* procedure can also be used to describe its excited states. However, a minimization procedure based on a first-order approach tends not to give good convergence in such cases. Instead, we have adopted a stabilized Newton-Raphson scheme, as in the usual SC approach, but we use an approximate expression for the second derivative that requires only density matrices up to third order [12]. The resulting procedure has been shown to be quite stable.

5. MR-SCVB* APPROACH

So far, we have described SCVB-based approaches in which dynamical correlation is introduced by means of excitations from one or more reference functions that are constructed from the occupied and virtual orbitals of one electronic state. A recent advance is the implementation of a multireference

approach involving optimization of a set of properly-bound spin-coupled configurations: these last may be used as 'references functions' for the virtual orbital optimization and for the construction of the final non-orthogonal configuration interaction wavefunctions, which may be termed MR–SCVB*. Rather than use the general multiconfiguration SC procedures that have been used previously for excited states, it turns out to be more appropriate to start from an approximate approach [13] to the excited states problem.

Motivated by the orthogonality of different electronic states, proper bounds may be imposed on excited-state SC configurations by means of orthogonality constraints against the ground-state configuration. We can obtain appropriate SC excited functions simply by imposing orthogonality relations between the orbitals of the 'excited' functions and the orbitals of the ground-state configuration. In this context, we are mainly interested in states characterized by different spatial configurations, simply because those that differ mostly in the mode of spin coupling can already be described by means of different linear combinations of the $\{\Theta^N_{SM,k}\}$.

There is, of course, no shortage of plausible orbital orthogonalization schemes. Applying different constraints on the orbitals results in functions that can have very different energies and which can, in principle, be more appropriate for different excited states. In particular, we have found in practice that the lowest energy ones do indeed turn out to be good representations of the lower-lying excited states. Functions with higher energy lose such correspondence with specific excited states, but they are useful tools for the construction of multireference wavefunctions without problems of linear dependence.

The general strategy is to start with a conventional single-configuration spin-coupled calculation for the lowest state of the given symmetry. Certain of the occupied orbitals are then designated as 'active' for the next stage of the calculations. The 'excited' orbital space is simply the orthogonal complement of the space spanned by the chosen active set, and the dimension of the active set fixes the number of excited orbitals that have to be constrained during optimization of the excited spin-coupled functions. For a three-electron system: we can consider an active set of dimension three and constrain one excited orbital to be orthogonal to those of the ground state; or, we can consider an active set formed by two of the three orbitals (there are three possibilities here) and then constrain two excited orbitals; or, finally, we can take a simple one-dimensional active set (there are again three possibilities) and constrain all the excited orbitals. The actual choice of active set depends on the problem under consideration. Since the approach appears more useful for low-lying excited states, one is mainly interested in orthogonalization schemes that produce low-energy solutions. It is certainly not necessary to test all of the possible orthogonalization schemes, not least because it is often straightforward to identify orbitals that are not likely to be altered substantially between the different states of interest.

In practice, the introduction of the orbital constraints is very simple: it is sufficient to switch from a pure atomic basis set to a projected one, adapted to the decomposition of the one-electron space into an active and an excited space. The orthogonality constraints on the orbitals are thus realized by the expansion of the excited state orbitals within the projected basis set. Good results are obtained employing both the N:1 scheme (N orbitals orthogonal to one ground state orbital) and the 1:N scheme (one excited orbital orthogonal to all the ground state orbitals). The overall computational cost is currently determined by three stages: the (Gram-Schmidt) orthogonalization, the four-index transformation to the projected basis set, and the optimization of the excited SC configurations.

Once the proper spin-coupled excited reference state has been obtained, the type of optimization procedure described in the previous Section may be used to generate virtual orbitals, and thus to introduce dynamical correlation *directly* into the excited states of interest. It should be noted that such optimization has to be modified slightly to avoid the collapse of the doubly-excited configuration towards the ground state. The modifications consist simply in a set of additional orthogonality constraints, analogous to the previous ones, to be imposed during the virtual orbital optimization procedure.

The method has been used to study the LiH_2^+ system [13,14,15] for which the main interest was in the first excited state, which governs the dynamical behaviour of the neutral LiH molecule in the presence of a naked proton. Various nuclear configurations have been sampled, both in the subreactive [14] and reactive regions of the configuration space [13]. It turned out that a simple two-reference VB wavefunction was sufficient for the subreactive study, while the stretching of the LiH bond in the reactive regions required the use of an additional reference function. For this system, the ground state SC wavefunction has the form:

$$\Psi_{SC} = \mathscr{A}\left(\phi_{1s}\phi'_{1s}\phi_{H_A}\phi_{H_B} \sum_{k=1}^{2} c_{0k}\,\Theta^4_{00;k} \right) \qquad (12)$$

in which ϕ_{1s}, ϕ'_{1s} are localized on Li and represent the $1s^2$ core, and ϕ_{H_A}, ϕ_{H_B} are atomic orbitals mostly localized on the hydrogen atoms. In the subreactive domain, the lowest excited spin-coupled reference turned out to be that obtained by applying the N:1 scheme, in which the active orbital was that with the highest orbital energy. The corresponding excited wavefunction takes the form:

$$\Psi_{SC2} = \mathscr{A}\left(\phi_{1s}\phi'_{1s}\phi_{H}\phi_{2s(Li)} \sum_{k=1}^{2} c_{0k}\,\Theta^4_{00;k} \right) \qquad (13)$$

in which ϕ_{H} is based on a $1s$ orbital centred on the H atom closest to the Li site and $\phi_{2s(Li)}$ resembles the somewhat deformed Li(2s) orbital in the isolated LiH molecule. This excited spin-coupled function describes correctly the physical situation of a proton impinging on a neutral LiH molecule. This configuration can

also describe correctly the region of the proton exchange reaction, because of the change of character of the active ϕ_H orbital, from the 1s orbital of the projectile hydrogen to the 1s orbital of the target hydrogen (due to the crossing of the SC orbital energies). In fact, the first and second excited states strongly interact with each other in this region, leading to a maximum or 'bump' in the energy profile of the C_{2v} symmetric configuration. This bump is observed also in full-CI calculations and it is clearly reproduced by the simple (excited) SC curve, as shown in the left-hand panel of Figure 1, in which potentials calculated with only the SC functions are compared with the full-CI data.

r=r$_e$(LiH) and Θ=169.0
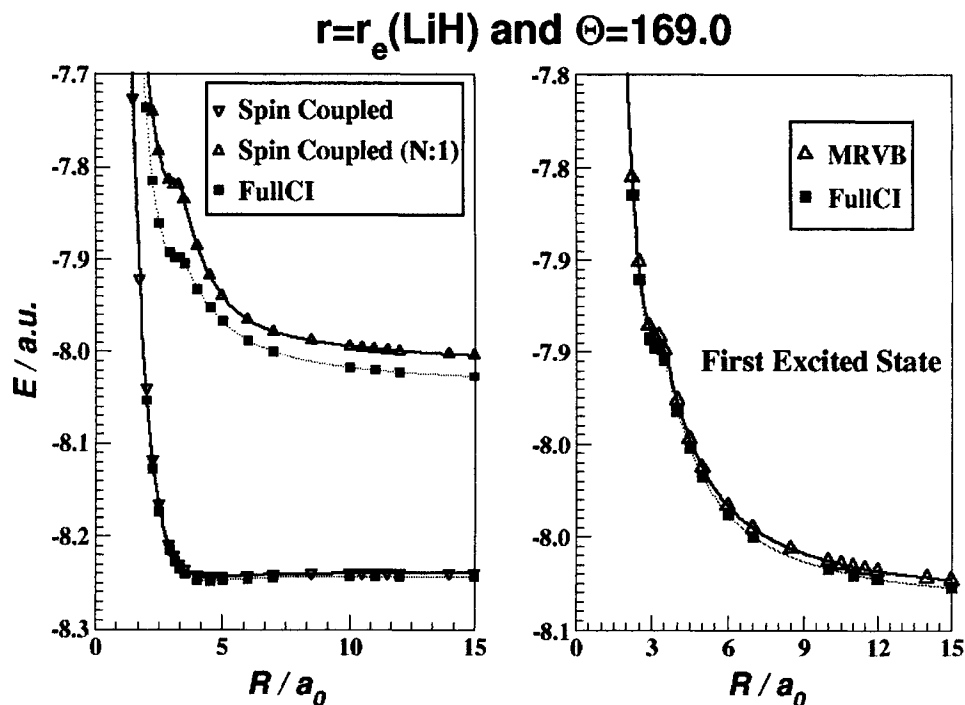
Figure 1. Comparison between VB and full-CI results with the same basis-set for the LiH$_2^+$ system as a function of projectile-target distance. The r(LiH) distance is fixed at the equilibrium distance of the diatomic molecule and the Jacobi angle (the projectile-LiH centre of mass-target H angle) is fixed at the value of 169°.

The right-hand panel of Figure 1 compares the excited curve obtained from the final MR–SCVB* (or, MRVB for short) calculation with that from the full CI. In this study, starting with the double-reference SC functions, we optimized a set of 4 pairs of virtuals for each reference and, at the end, we built a VB wavefunction consisting of 84 spatial configurations for a total of only 125 VB structures. This

contrasts markedly with the 1654650 determinants of a full-CI calculation in the same basis set.

The additional SC reference function required for the reactive domain takes the form

$$\Psi_{SC3} = \mathcal{A}\left(\phi_{1s}\phi'_{1s}\phi_{2s(Li)}\phi_{\sigma_g}(H_2^*) \sum_{k=1}^{2} c_{0k} \Theta^4_{00;k} \right) \tag{14}$$

and is in fact lower in energy than Ψ_{SC2}. The $H_2^+(\sigma_g)$ orbital in Ψ_{SC3} was the outcome of the 1:N orthonormalization scheme.

6. APPLICATIONS OF SCVB* AND MR–SCVB*

Only the lightest elements (H, D, He, Li and trace amounts of Be) are thought to have been present in the early universe, with the chemistry being based on simple binary collisions and processes involving photons (absorption, emission and the scattering of cosmic background radiation) [16]. The small fraction of the atomic gas which had become molecular could lead to radiative cooling, and thereby play an important role in the collapse of protogalactic clouds. We have studied a number of gas phase collision processes that may be important for developing reliable cosmological chemical evolutionary models. In particular, the SCVB* method, either in its single or multireference formulation, has been applied to processes involving LiH, ranging from simple bimolecular reactions to rovibrational energy transfer in inelastic collisions with He.

A full subreactive potential energy surface was computed for the LiH+He system [17,18], avoiding BSSE *a priori* by expanding all orbitals in the properly chosen sets of 'target' and 'projectile' basis functions. The computed points span a wide range of values of the scattering coordinate and of the usual Jacobi angle for each of five chosen Li–H distances in the bottom of the target diatomic well. The orientation dependence of the potential was subsequently expressed in Legendre polynomials and the dependence on scattering coordinate was fitted using Laguerre functions. The dependence on Li–H distance was interpolated with cubic splines and used to compute the vibrational couplings which govern the vibrational energy transfer. The (fitted) PES was used in quantum mechanical calculations of cross sections for rovibrational energy transfer in the LiH molecule by He impact. State-to-state rate constants were generated for a range of temperatures of astrophysical relevance.

The reliability of the PES may be judged by comparing rigid-rotor close-coupling calculations of rotational inelastic scattering cross sections with the experimental data that are available for a collision energy of 0.32 eV [19]. Although the first vibrationally excited channel is open at this high collision energy, the weak vibrational coupling prevents a substantial loss of flux into such excited states, and so very similar results are obtained with V-R close-coupling

calculations. As can be seen from Figure 2, the agreement of the theoretical results with the experimental data is especially good for the lowest Δj transitions. Deviations for higher transitions may reflect imprecision in the experimental data, which could be viewed as lower bounds to the scattering cross sections.

Collision energy 0.32 eV
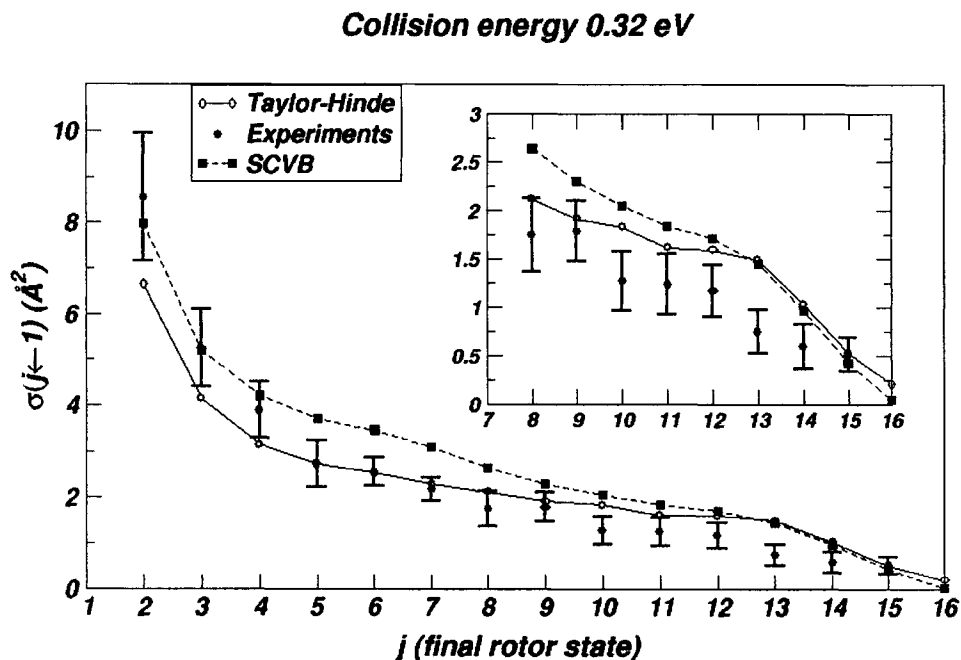
Figure 2 *Experimental and theoretical results for the rotationally inelastic integral cross section in the LiH + He scattering system.*

Also displayed in Figure 2 are results of analogous dynamical calculations using instead a somewhat different coupled-cluster potential energy surface [20]. The authors of Ref. [20] used a rather large basis set that included also bond-functions placed *between* the target and projectile, and they corrected for BSSE with the counterpoise method. The two surfaces are especially different in the region of the well on the Li side of the target: the coupled-cluster potential supports two bound levels, at least for the lower values of the total angular momentum [18], but the rigid-rotor SCVB* potential does not support any. Comparison of data at 0.32 eV tends to suggest that the repulsive wall of the interaction is better represented by the SCVB* surface, but we cannot infer anything about the quality of the low-energy behaviour of the interaction potential. Experiments have been suggested, to settle these matters [18].

The full rovibrational PES has been used in quantum dynamical calculations within the centrifugal sudden approximation for a wide range of total energies of the scattering system. This approximation, which neglects the effect of the collision on the orbital quantum number, reduces the dimension of the problem and makes calculations more feasible. On the other hand, it preserves a reasonable level of accuracy for the rotationally-summed vibrational excitation-relaxation cross sections. The left-hand panel of Figure 3 shows rotationally averaged excitation cross sections from the ground state to the first three excited states, as a function of collision energy in the range 0–2 eV (notice the values of such cross sections relative to the vibrational elastic, rotational inelastic ones shown in Figure 2). The (vibrational) state-to-state rate constants displayed in the right-hand panel have been obtained by averaging over the Boltzmann distribution of the relative velocity of the two colliding partners. These quantities are very important in establishing the cooling function of the LiH molecule, which depends on the collisional heating efficiency and on the radiative properties of the molecule.
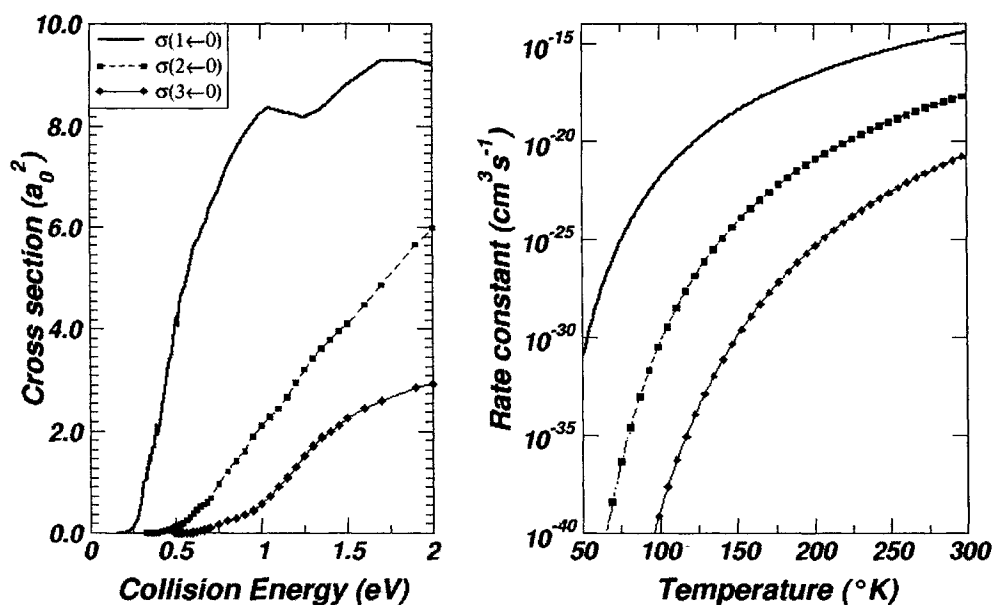
Figure 3. Integral (rotationally averaged) excitation cross sections (left panel) and vibrational state-to-state rate constants (right panel) for the LiH–He scattering system.

In the case of the neutral reaction LiH+H→Li+H$_2$, SCVB* and dynamical studies of the simple collinear arrangement revealed an unusual insensitivity of the reaction to the vibrational energy content of the reagent molecule. Classical and (time-dependent) quantum calculations showed that the reaction probability can be very large, especially in the low collision energy regime. On the other hand, impact on the repulsive wall at high collision energies results mainly in inelastic scattering: this can be attributed to the very deep and narrow channel corresponding to formation of H$_2$. Further study of the LiH$_2$ system revealed that a correct consideration of the lower lying excited states is necessary to understand even the dynamical behaviour of the ground electronic state; indeed, as pointed out by the authors of Ref. [21], the Li(2p)+H$_2$ channel is already open at *zero* collision energy of the LiH+H scattering system.

Finally, we mention preliminary results of MR–SCVB* calculations for full potential energy surfaces of LiH$_2^+$. The ground-state surface describes adiabatically the reaction

$$LiH^+ + H \rightarrow Li^+ + H_2$$
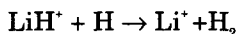
which is driven by the recoupling of the spins associated with the two valence orbitals mostly localized on the hydrogen atoms. We find that the ground state topology is mainly due to the two-body terms of the potential. The first excited potential relates to the adiabatic reaction

$$LiH + H^+ \rightarrow Li + H_2^+$$
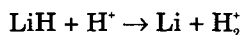
which requires significant deformation of the H-based orbital in LiH so as to form the one-electron bond in the H$_2^+$ product. We find that the three-body potential term (incorporating dipole-charge and charge-induced dipole interactions) plays a very important role in this excited state, and produces local minima in the entrance and exit channels of the reaction.

Important conclusions on the dynamics can already be drawn just by looking at the [Li–H–H]$^+$ collinear cut of the PES displayed in Figure 4. We have found that the large energy gap between the two roots remains substantially unaltered in the other orientations we have sampled so far, and this tends to preclude any significant nonadiabatic interactions between the two states. Further support for this idea comes from the very different nature of the electronic wavefunctions: for example, the charge is always concentrated on the Li atom in the ground electronic state, while it resides on the H atom(s) in the excited state. The absence of significant nonadiabatic interactions suggests that many of the reactions invoked in the current astrophysical literature may have to be considered as *forbidden*, simply because of the resulting very low rate constants. For example, the reactions

$$LiH^+ + H \rightarrow LiH + H^+$$
$$LiH^+ + H \rightarrow Li + H_2^+$$
$$LiH + H^+ \rightarrow Li^+ + H_2$$
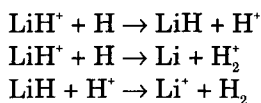
can proceed only by photon-mediated jumping between the two roots, but the rate constants are expected to be very low.

First and second roots
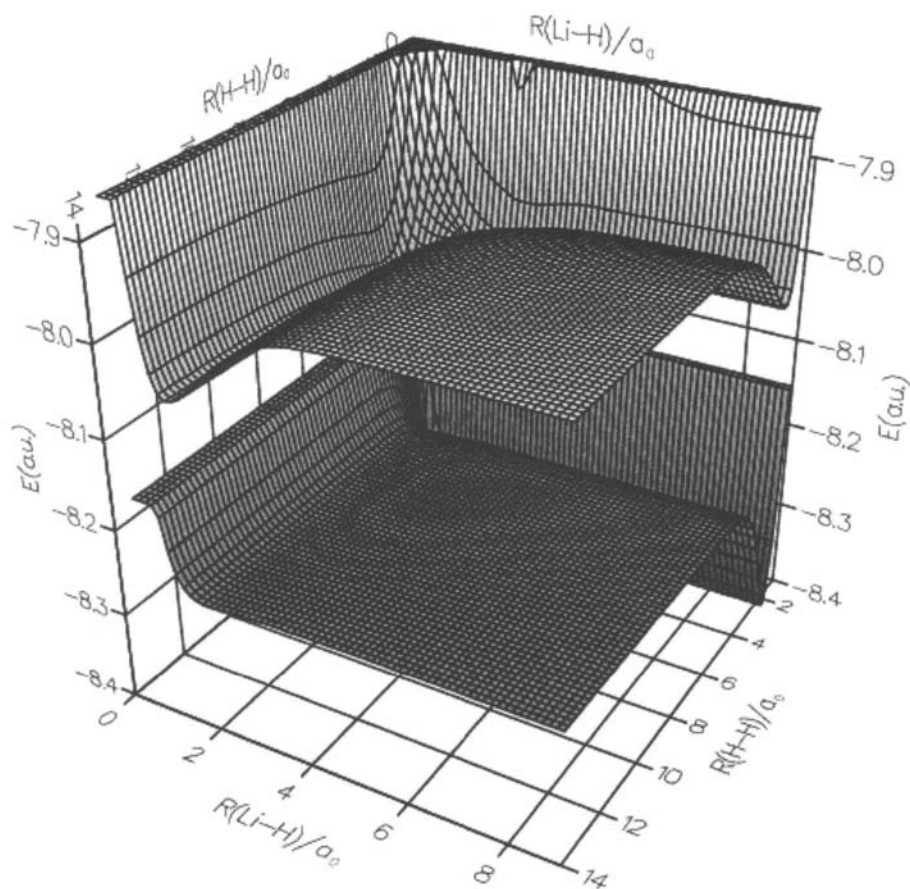
Figure 4. *Potential Energy Surfaces for the first two electronic states of the* LiH_2^+ *system in the Li-H-H collinear geometry, shown as a function of the interatomic distances.*

7. CONCLUSIONS

The *ab initio* spin-coupled valence bond (SCVB) approach continues to provide accurate ground and excited state potential energy surfaces for use in a variety of subsequent applications, with particular emphasis on intermolecular forces and reactive systems. The compactness of the various wavefunctions allows direct and clear interpretation of the correlated electronic structure of molecular systems. Recent developments, in the form of SCVB* and MR–SCVB*, involve the optimization of virtual orbitals via an approximate energy expression. These 'improved' virtuals lead to still higher accuracy for the final variational wavefunctions, but with even more compact wavefunctions.

References

1. J.Gerratt, *Adv. Atom. Mol. Phys.* **7**, 141 (1971).
2. a) D.L. Cooper, J. Gerratt and M. Raimondi, *Chem. Revs* **91**, 929 (1991); b) J. Gerratt, D.L. Cooper, P.B. Karadakov and M. Raimondi, *Chem. Soc. Rev.* **26**, 87 (1997).
3. S.F. Boys and F. Bernardi, *Mol. Phys.* **19**, 553 (1970).
4. E. Gianinetti, M. Raimondi and E. Tornaghi, *Int. J. Quant. Chem.* **60**, 157 (1996).
5. M. Raimondi, A. Famulari and E. Gianinetti, *Int. J. Quant. Chem.* **74**, 259 (1999).
6. J. Gerratt and M. Raimondi, *Proc. Roy. Soc. (Lond.) A* **371**, 525 (1980).
7. M. Raimondi, W. Campion and M. Karplus, *Mol. Phys.* **34**, 1483 (1977).
8. D.L. Cooper, J. Gerratt and M. Raimondi, *Adv. in Chem. Phys.* **69**, 319 (1987).
9. a) B. Zygelman, P.C. Stancil, N.J. Clarke and D.L. Cooper, *Phys. Rev. A* **56**, 457 (1997); b) P.C. Stancil, A.R. Turner, D.L. Cooper, D.R. Schultz, M.J. Raković, W. Fritsch and B. Zygelman, *J. Phys. B* **34**, 2481 (2001); c) D.L. Cooper, N.J. Clarke, P.C. Stancil and B. Zygelman, *Adv. Quant. Chem.* **40**, 37 (2001), and references therein.
10. M. Raimondi, M. Sironi, J. Gerratt and D.L. Cooper, *Int. J. Quant. Chem.* **60**, 225 (1996).
11. D.L. Cooper, J. Gerratt, M. Raimondi, M. Sironi and T. Thorsteinsson, *Theor. Chim. Acta* **85**, 261 (1993).
12. N.J. Clarke, M. Raimondi, M. Sironi, J. Gerratt and D.L. Cooper, *Theor. Chem. Acc.* **99**, 8 (1998).
13. R. Martinazzo, A. Famulari, M. Raimondi, E. Bodo and F.A. Gianturco, *J. Chem. Phys.* **115**, 2917 (2001).

14. E. Bodo, F.A. Gianturco, R. Martinazzo, A. Forni, A. Famulari and M. Raimondi, *J. Phys. Chem. A* **104**, 11972 (2000).

15. a) E. Bodo, F.A. Gianturco, R. Martinazzo and M. Raimondi, *J. Phys. Chem. A* **105**, 10986 (2001); b) E. Bodo, F.A. Gianturco, R. Martinazzo and M. Raimondi, *Chem. Phys.* **271**, 309 (2001).

16. S. Lepp and P.C. Stancil, in *The molecular astrophysics of stars and galaxies* ed. T.W. Hartquist and D.A. Williams (Clarendon Press, Oxford, 1998).

17. F.A. Gianturco, S. Kumar, S.K. Pathak, M. Raimondi, M. Sironi, J. Gerratt and D.L. Cooper, *Chem. Phys.* **215**, 227 (1997).

18. E. Bodo, F.A. Gianturco, R. Martinazzo, F. Paesani and M. Raimondi, *J. Chem. Phys.* **113**, 11071 (2000).

19. P.J. Dagdigian, B.E. Wilcomb and M.H. Alexander, *J. Chem. Phys.* **71**, 1670 (1979).

20. B.K. Taylor and R.J. Hinde, *J. Chem. Phys.* **111**, 973 (1999).

21. H.S. Lee, Y.S. Lee and G-Hi Jeung, *J. Phys. Chem. A* **103**, 11080 (1999).

This Page Intentionally Left Blank

Chapter 10

The Generalized Multiconfiguration Spin-Coupled method, STO optimization, and the electronic structure of BH_3 in its ground state

F.E. Penotti[*]

CNR-CSRSRC, Via Golgi 19, 20133 Milano, Italy

The Optimized Basis Set – Generalized Multiconfiguration Spin-Coupled method, or OBS-GMCSC for short, offers a practical approach to the direct variational calculation of non-orthogonal multiconfiguration electronic wavefunctions. Simultaneous optimization of STO exponential parameters enables high accuracy with rather small basis sets and ensures strict compliance with the virial theorem. OBS-GMCSC wavefunctions can yield compact and accurate descriptions of atomic and molecular electronic structures, and neatly resolve symmetry-breaking difficulties, as illustrated by a brief review of previous results for the boron anion and the dilithium molecule, and by newly obtained results for BH_3.

1. INTRODUCTION

The goal of computing accurate yet compact electronic wavefunctions has motivated the development of many Modern VB methods, as is amply documented by many other contributions to this volume.

The present article is devoted to a discussion of a multiconfiguration approach, the Optimized Basis Set – Generalized Multiconfiguration Spin-Coupled (OBS-GMCSC) method [1]-[2], that can join the flexibility of non-orthogonal orbitals with the use of simultaneously optimized Slater-type basis functions (STFs).

The method is referred to simply as GMCSC when a fixed basis set is used. In this case, it can be viewed as a non-orthogonal variant of the Multiconfiguration Self-Consistent Field (MCSCF) approach. However, GMCSC's methodological roots are firmly planted in the Modern VB camp, and more specifically in the late Joe Gerratt's Spin-Coupled theory [3]-[4].

---

[*]Please address all correspondence to F.E. Penotti, Via Montegani 7, I-20141 Milano, Italy

The latter was developed as a single-configuration method, complemented by non-orthogonal configuration-interaction calculations exploiting "virtual" orbitals in the "Spin-Coupled Valence Bond" (SCVB) approach [5] (for a review, see *e.g.* Ref. [6]). More recently, the use of "perturbative" virtuals has been introduced, giving rise to the SCVB* variant of the method [7][8]. There are further accounts of SCVB* in this volume.

One of the earliest SC papers [4], however, did include some multiconfiguration calculations on diatomic molecules (LiH, BH and Li_2). For each molecule, the wavefunction consisted of a main configuration supplemented by a pair of symmetry-equivalent $(\sigma,\sigma') \rightarrow (\pi,\pi')$ double excitations out of it. Thanks to the fact that different configurations were thus mutually orthogonal, and that in fact corresponding orbitals in different configurations were either identical or mutually orthogonal (by symmetry), the calculations were possible with the limited computing power available at the time, and presumably required only limited adaptations of programs implementing the spin-coupled approach, and of the underlying theory.

The theoretical framework needed to deal with more general and mutually non-orthogonal configurations, while retaining the full-fledged second-derivative energy-minimization procedure adopted in the spin-coupled approach for the optimization of variational parameters, was only developed more than fifteen years later, by the present author [1][2], when the ready availability of greater computing power made calculations employing such an approach finally practical.

In an attempt to exploit fully the flexibility afforded by the lack of any orthogonality constraints, the new theoretical framework included from the very start the possibility of variationally optimizing STF exponential parameters as well, simultaneously with all other parameters entering the wavefunction. Optimization of the exponential parameters removes at least some of the arbitrariness involved in choosing a basis set and ensures the best possible results for a given choice of the number of basis functions of each type (and location) to be included. Moreover, since the basis-function exponential parameters are thus implicitly scale-optimized, the electronic wavefunction rigorously satisfies the virial theorem. Rigorous virial compliance ensures in turn the proper balance between kinetic and potential contributions to the electronic energy. This can be a definite advantage when striving for meaningful physical interpretation of the electronic structure, since it is essentially this balance that determines how contracted or diffuse the electronic wavefunction, and thus presumably individual orbitals as well, actually should be.

Basis-set optimization is thus the hallmark of the present author's approach. Nevertheless, GMCSC wavefunctions can otherwise be viewed as more flexible versions of Resonating Generalized Valence Bond (R-GVB) wavefunctions [9]. The extra flexibility arises from GMCSC's freedom from the constraint of

orthogonality between orbitals belonging to different pairs in the same configuration. On the other hand, GMCSC wavefunctions are essentially equivalent to Valence Bond Self Consistent Field (VBSCF) wavefunctions [10]-[12]; the main difference between the two methods, aside from basis-set optimization, is GMCSC's use of a full-fledged second derivative energy minimization procedure. There are also parallels to the BOVB(N,V) wavefunctions of McDonald, described elsewhere in this volume.

The Complete Active Space Valence Bond (CASVB) method [13]-[15] offers another approach to the computation of non-orthogonal multiconfiguration wavefunctions, as exemplified in various applications [16]-[19]. In fact, for fixed basis sets, CASVB, which is based on the use of similarity transformations from an underlying Complete Active Space Self Consistent Field (CASSCF) wavefunction, may well be more efficient than GMCSC, as stated in Ref. [16]. The ability to take advantage of CASSCF as an especially efficient, orthogonal, "computational engine" is perhaps CASVB's main strength; however, this may prevent it from achieving rigorous simultaneous basis-set optimization, given that basis-set variation brings about a first-order breakdown of orthogonality [20].

CASVB has been shown to be applicable to electronically excited states as well [18], by the adoption of a clever generalization [21] of the second-order stabilized Newton-Raphson optimization procedure [22] used by it, SC [4], and OBS-GMCSC [1][2]. It turns out that essentially the same procedure works for OBS-GMCSC as well [23], allowing it to exploit basis-set optimization where it can be especially advantageous, i.e. for excited states.

An alternative computational scheme for excited-state multiconfiguration wavefunctions employing non-orthogonal orbitals has also been developed [24]. The approach, restricted to fixed basis sets, is based on iterative optimization of a single set of spin-coupling coefficients, common to all configurations, of the orbitals in each configuration, and of the configuration coefficients, through a series of non-orthogonal configuration-interaction calculations, without any use of energy derivatives.

The present article is organized as follows: immediately after this Introduction, Section 2 describes the main aspects of the OBS-GMCSC method, trying to limit the number of equations and thus without entering into many "technicalities". The interested reader will find full details in previous publications [1][2][25].

A third Section briefly reviews previous OBS-GMCSC results that illustrate how, in certain cases, a multiconfiguration description can be essential to a truly meaningful discussion of molecular electronic structure, even at a qualitative level.

A fourth Section presents the results of eight-electron multiconfiguration calculations on the electronic ground state ($^1A_1'$) of BH_3, and discusses their

implications for the nature of the B-H bond in this simple molecule, both to buttress the argument for the necessity of multiconfiguration descriptions, and to demonstrate OBS-GMCSC's applicability to polyatomic molecules.

A final Section briefly presents the Conclusions.

2. THE GMCSC METHOD

As stated in the Introduction, the GMCSC method [1][2][25] is, in its roots, a multiconfiguration generalization of the well known spin-coupled approach [3]-[6].

2.1 The OBS-GMCSC wavefunction

The GMCSC wavefunction for a system of N_e electrons coupled to a resultant spin of S, with projection M (atomic units) along any given axis, can be written as [2]:

$$\Psi_{S,M}(\mathbf{x}) = \sum_{a=1}^{N_c} [d_a \ \Psi_{S,M;a}(\mathbf{x})] \tag{1}$$

In the above equation, N_c is the fixed, but arbitrary, number of configurations included in the wavefunction, d_a the a-th configuration coefficient and

$$\Psi_{S,M;a}(\mathbf{x}) \equiv \sqrt{N_e!} \ A \left[\Phi_a(\mathbf{r}) \Theta_{S,M;a}(\mathbf{\sigma}) \right] \tag{2}$$

is a separately antisymmetrized space-spin configuration, which we shall refer to simply as a "GMCSC configuration".

Note x is used to denote collectively the space and spin coordinates of all electrons, while r denotes their space coordinates and σ their spin coordinates.

Also, A stands for the antisymmetrizer in its usual idempotent form (hence the $\sqrt{(N_e!)}$ in front of it in Eq. (2)), and Φ_a is a product of N_e orbitals (orbital string, or orbital configuration),

$$\Phi_a(\mathbf{r}) \equiv \prod_{\mu=1}^{N_e} \varphi_{a,\mu}(r_\mu), \tag{3}$$

where r_μ denotes the three spatial coordinates of the μ-th electron. Each orbital is expressed as a linear combination of basis functions:

$$\phi_{a,\mu}(r_\mu) \equiv \sum_{i=1}^{N_{bf}} c_{a,\mu,i} \chi_i(r_\mu;\zeta_i) \tag{4}$$

Here $c_{a,\mu,i}$ is the coefficient with which the i-th basis function $\chi_i(r_\mu;\zeta_i)$ (usually a Slater-type function, or STF for short) enters the μ-th orbital of the a-th configuration, ζ_i is an adjustable parameter (usually the STF's exponential parameter), and N_{bf} the fixed but otherwise arbitrary number of basis functions.

Finally, $\Theta_{S,M;a}$ is the linear combination of Yamanouchi-Kotani (YK) spin functions associated with the a-th configuration

$$\Theta_{S,M;a}(\sigma) \equiv \sum_{k=1}^{f(N_e,S)} c_{k,a}^S \, \Theta_{S,M;k}^N(\sigma_1,\ldots\sigma_{N_e}) \tag{5}$$

where $f(N_e,S)$ denotes the total number of linearly independent spin functions for given values of N_e and S and an acceptable, but otherwise arbitrary, value of M. It is given in general by (see e.g. Kotani et al. [27]):

$$f(N_e,S) = \frac{(2S+1)(N_e!)}{(\frac{1}{2}N_e + S + 1)!(\frac{1}{2}N_e - S)!} \tag{6}$$

and is equal to 14 for a system of eight electrons coupled to a singlet ($S=0$), such as the ground state of BH_3.

The $c_{k,a}^S$ are the "spin-coupling" coefficients of the a-th configuration. One should mention that in the earlier "MCSC" version of the method [1] all orbital configurations shared the same linear combination of the $f(N_e,S)$ Yamanouchi-Kotani spin functions: there was a single set of $f(N_e,S)$ spin-coupling coefficients, denoted simply c_k^S, just as in single-configuration spin-coupled theory.

A GMCSC configuration can be viewed as a linear combination, with adjustable coefficients, of $f(N_e,S)$ structures with a common "orbital string", each of them analogous to a classic-VB structure except for orbital optimization and for the use of YK spin functions. Note the latter is not actually a limitation inasmuch as all of them are included, since they span the full spin space for N_e electrons with given values of S and M. One should perhaps note that for $N_c=1$ the wavefunction in Eq. (1) reduces to a single-configuration spin-coupled wavefunction [3]-[6], and d_1 then becomes simply a normalization constant.

2.2 Practical computation

It is computationally convenient to leave individual configurations unnormalized, as implied by the above equations, since explicit normalization constants would complicate the expressions for the derivatives of the energy with respect to various optimization parameters. It is however always possible to express the final wavefunction as a linear combination of individually normalized configurations: this only requires appropriately scaling each configuration coefficient. Configuration overlaps quoted in the following Sections always refer to such individually normalized configurations.

The GMCSC orbitals are in general all distinct, though "double occupancy" may be imposed by constraining any two of them in the same configuration to be identical. They are also in general not mutually orthogonal, though selective orthogonality constraints may be imposed within any configuration, with no loss of generality, when it includes one or more pairs of identical orbitals [2], and orbitals may of course be orthogonal by symmetry. Barring similar circumstances, the configurations are also, in general, not mutually orthogonal.

Variational parameters in a GMCSC wavefunction thus include:

- configuration coefficients (d_a, $a=1,...N_c$)
- spin-coupling coefficients ($c_{k,a}^S$, $k=1,..f(N_e,S)$, $a=1,...N_c$)
- orbital coefficients ($c_{a,\mu,i}$, $a=1,..N_c$, $\mu=1,..N_e$, $i=1,..N_{bf}$)

and, in the OBS-GMCSC variant of the method:

- STF exponential parameters (ζ_i, $i=1,..N_{bf}$).

These are all simultaneously optimized by minimization, either directly of the energy as a function of the variational parameters, for the lowest-energy state compatible with any parameter constraints, or of a suitably defined "image function" [21] for higher-energy states (see Subsection 2.4). The minimization proceeds via an iterative second-order method [22] that requires the availability of all first and second derivatives of the electronic energy with respect to the variational parameters themselves, all cross-terms included. These derivatives are computed analytically. Explicit expressions for them are somewhat involved, and have been published elsewhere [1][2]. Their computation, repeated at every iteration, is one of the two main sources of computational effort, the other being, in the OBS variant, the similarly repeated computation of the STF-based integrals (discussed in the next Subsection). As more configurations are added for a given basis set size, however, integral computation accounts for a smaller fraction of the computational effort, that becomes increasingly dominated by the calculation of the energy derivatives.

The essence of the iterative optimization procedure [22] is actually fairly simple. It is briefly reviewed here for reference in the next Subsection. Focusing attention on the ground state for simplicity, at every iteration the vector of corrections **δc** to the variational parameters is obtained by solving the linear system

$$(G + \alpha I)\, \delta c = -g \tag{7}$$

where the gradient vector g collects the first derivatives of the energy with respect to the variational parameters, the Hessian matrix G collects the corresponding second derivatives, I is the identity matrix and α is an eigenvalue shift parameter. This is defined in terms of the minimum eigenvalue λ_{min} of the Hessian, of the gradient's norm g and of an adjustable "step size control parameter" R as

$$\alpha = Min(\lambda_{min}, 0) + R \cdot g \tag{8}$$

The "step size control parameter" R, initially set to a value of order unity, is adaptive, in the sense that it is decreased (or increased) at each iteration depending on how well (or how badly) the energy change actually brought about by the corrections accords with the value predicted from a second-order Taylor expansion in the corrections themselves. In extreme cases, the corrections are rejected and recomputed with an increased value of R. Otherwise, any updates to R apply from the next iteration. The precise set of rules used to control R may affect efficiency but is not critical to the success of the minimization procedure, as long as the rules provide the correct qualitative behaviour (*e.g.* see Refs. [22] and [18]).

Without the Hessian eigenvalue shift α, the procedure would simply reduce to the well-known Newton-Raphson method (*e.g.* see Ref. [28]), as can be seen by setting α to zero in Eq. (7). The Hessian shift, with adaptive step size, dampens the corrections when needed, removing the risk of divergence that makes pure Newton-Raphson not very reliable. As can be seen from Eq. (7), for large values of α the method reduces essentially to a timid application of steepest descent (small corrections in the direction of -g). Convergence on a minimum is assumed when the Hessian is positive definite and the largest component of the gradient falls below a given threshold (typically 10^{-8} a.u.).

2.3 STF-based integrals

When, in the OBS variant of GMCSC, the STF exponential parameters are treated as variational parameters, energy integrals over the STFs, and the first and second derivatives of these integrals with respect to the exponential parameters themselves, must be recomputed at every iteration of the energy-minimization procedure. Since differentiating an STF-based integral with respect to the exponential parameter of any of the intervening STFs is essentially equivalent to raising the STF's principal quantum number by one, one needs to

be able to compute such integrals for values of the principal quantum number that exceed (by up to two) the actual basis-set values.

In previous applications, restricted to atoms [1][2] and diatomic molecules [26], this was done by inserting directly in the OBS-GMCSC program the necessary blocks of integration code, specially written by the present author, implementing for the two-centre integrals accuracy-controlled variants of time-honoured methods [29]. Although applying analogous accuracy control to a polyatomic generalization [30] of those methods proved feasible [31], the resulting code turned out to be too slow for practical use, except perhaps in the case of linear molecules.

Fortunately, a highly efficient, accurate, and sufficiently general program, *m2cnew* [32][33], based on the use of Gaussian expansions of Slater-type basis functions, became available, and has been adopted for the OBS-GMCSC calculations reported in this paper. This only required writing a simple interface program to transform *m2cnew*-generated integral files to a format suitable for use by the OBS-GMCSC program, and adding to the latter simple routines to generate, at each iteration, suitable data files for the *m2cnew* program and the interface program. In practice, at every iteration one needs to run *m2cnew* twice, for enlarged basis-sets consisting of the basis functions themselves and of the STFs obtained by increasing their principal quantum numbers by one, or by two. Though this does produce some unnecessary integrals, *e.g.* those involving second derivatives of two or more basis functions, it does not increase the computational load all that much, due to the reduced accuracy required of integrals involving such derivatives, see below. Besides, this waste is hard to avoid when using a ready-made program for the integrals, unless one is willing to invest the time and effort to subject the program to *ad hoc* modifications. Cyclic execution of the *m2cnew*, interface and OBS-GMCSC programs can of course be controlled by a simple operating-system procedure, i.e. a "shell script" for Unix or a "batch script" for MS Windows.

As hinted above, the derivatives of the energy integrals do not need to be computed to the same accuracy as the energy integrals themselves and, even for the latter, limited accuracy may be adequate in the first phase of the energy minimization procedure, if far from convergence. In general, the accuracy of, and the computational effort for, the *m2cnew* integrals rises with the number of Gaussians used to interpolate each STF. Accordingly, the OBS-GMCSC program specifies, in the *m2cnew* data files it sets up at every iteration, varying numbers of interpolating Gaussians, smaller for the first derivatives of the basis functions than for the basis function themselves, and smaller still for their second derivatives. The actual number of Gaussians used for each kind of STF varies between iterations, according to the size of the predicted energy change.

Table 1

Number of Gaussians used to interpolate each Slater-type basis function [a]

Predicted Energy Change ΔE / E_h	Energy integrals	1st derivatives of energy integrals	2nd derivatives of energy integrals
$\Delta E > 10^{-2}$	9	7	5
$10^{-2} \geq \Delta E > 10^{-4}$	13	9	7
$10^{-4} \geq \Delta E > 10^{-6}$	17	13	11
$10^{-6} \geq \Delta E > 10^{-8}$	21	17	15
$\Delta E \leq 10^{-8}$	25	21	19

[a] The actual number of Gaussians used for a given STF may be lower, especially for higher quantum numbers, due to current limitations of the *m2cnew* program.

A side benefit of this is that, given that decreases in the size of the corrections usually reduce the energy change, the number of STF-interpolating Gaussians ends up being adaptively controlled, indirectly, by the "step size control parameter" R of Eq. (8). The tendency is for more accurate integrals when the reliability of the truncated Taylor series prediction of the energy change falls appreciably, and vice versa. Higher-accuracy integrals in turn increase the accuracy of the recomputed energy and of the energy derivatives to be used in the next iteration, thus guarding against the possibility that their insufficient accuracy may be causing the adoption of an unnecessarily small step size. On the other hand, under favourable conditions, increases in the step size tend to lead to a reduction in the number of required Gaussians, and thus of the computational effort for the integrals. Calibrating the number of Gaussians to use for the STFs and for their derivatives, in varying circumstances, proved surprisingly easy, thanks to published results of accuracy tests for SCF energies [32], supplemented by some specific OBS-GMCSC tests. The latter were aimed mostly at gauging the accuracy needed for the derivatives. The specifications adopted by the current version of the OBS-GMCSC program are given in Table 1. Though there may be some room for improvement, they do appear to be fairly satisfactory.

2.4 Excited states

Although published applications of the OBS-GMCSC method have been limited so far to the ground states of He, Be, B, B⁻, Li_2 and, as described in Section 4, BH_3, the approach is obviously applicable to the lowest electronic state of each spin multiplicity and spatial symmetry. The latter can be selected with the imposition of appropriate constraints [2][25]. Moreover, as already

noted, OBS-GMCSC is actually applicable to any electronically excited state [23], through the adoption of a clever, and easily implemented, generalization (the so-called Trust Region Image Minimization, or TRIM, procedure [21]) of the optimization method [22]. This is the same approach successfully adopted by T. Thorsteinsson and D.L. Cooper for CASVB [18]. A concise "how to" guide can be found in the Appendix to their paper [18], but one should note that "min" has been misprinted for "max", in the definition of the Hessian shift parameter α; the correct version is described in the text.

3. THE NEED FOR MULTICONFIGURATION DESCRIPTIONS OF THE ELECTRONIC STRUCTURE

When unconstrained energy minimization leads to a symmetry-broken single-configuration solution, one may obviously solve the problem by imposing symmetry constraints to force it to assume the required symmetry properties.

OBS-GMCSC offers the alternative possibility of including, in a non-orthogonal multiconfiguration calculation, all configurations that can be generated from a symmetry-broken one by applying to it the relevant symmetry operations in the molecular point group. Orbitals can be "relaxed" within the multiconfiguration wavefunction, because all variational parameters are re-optimized by energy minimization.

But even when no symmetry breaking is apparent at the single-configuration level, the need for multiconfiguration descriptions may be inescapable, as will be shown here.

3.1 Evidence from previous OBS-GMCSC work

For instance, GMCSC calculations on the boron anion [2] and on the dilithium molecule [26], both in their ground states, have shown how single-configuration wavefunctions, including spin-coupled ones, can be hard-put to provide a "robust description" of certain highly-symmetric systems. By "robust description", we mean one that will not change, at least qualitatively, as more configurations are added to the wavefunction.

In both cases mentioned above, adding a single pair of symmetry-related configurations to the fully-symmetric spin-coupled configuration in an OBS-GMCSC calculation led to an energy lowering that was comparable to that obtained in going from the SCF to the spin-coupled solution.

For B^- (X^3P), the fully symmetric configuration was the obvious ($s_1 s_2 s_3 s_4 p_x p_y$), with s_1 and s_2 a pair of strongly overlapping inner orbitals, s_3 and s_4 more diffuse, but nodeless, "valence" s orbitals, and (p_x, p_y) a pair of symmetry-equivalent $2p$ orbitals. The two symmetry-related configurations were ($s_1' s_2' s_3'$

$s_4^!$ $p_x^!$ $p_y^"$) and ($s_1^!$ $s_2^!$ $s_3^!$ $s_4^!$ $p_x^"$ $p_y^!$), the $2p$ orbitals in one of them being inequivalent and symmetry-related to those in the other.

Similarly for Li_2 ($X^1\Sigma_g^+$): the two symmetry-related configurations, which, like the fully symmetric one, included σ orbitals only, were connected by inversion through the molecular centre. The three configurations, far from being orthogonal, had large mutual overlaps.

In both cases, the extra pair of configurations entered the multiconfiguration wavefunction with a "weight" that was comparable to that assumed in it by the fully symmetric configuration. Here and in what follows, a configuration's weight is defined as its Chirgwin-Coulson occupation number [34][2] (for alternative definitions, see *e.g.* Refs. [35] and [36]).

Obviously, both the fully symmetric and the pair of symmetry-related configurations had to be viewed as reference configurations, and taken into account in qualitative discussions of the electronic structure.

For Li_2 [26], a highly correlated multiconfiguration wavefunction was built by supplementing the three reference configurations, briefly described above, with double and quadruple excitations out of them, plus an SCF-like configuration. The wavefunction was dominated by the reference configurations, all three retaining comparable weights. This suggested that supplementing the single-configuration SC solution with just a few aptly chosen configurations was both necessary and sufficient to produce a multiconfiguration wavefunction that did have the "qualitative robustness" lacked, in these cases, by the former.

As hinted above, such behaviour may occur even when no symmetry constraints are necessary to ensure full symmetry of the single-configuration spin-coupled solution, so that single-configuration calculations may not always provide hints of the solution's shortcomings. For Li_2, whether or not the single-configuration spin-coupled solution is spontaneously fully symmetrical depends on the internuclear distance, while at all internuclear distances the three reference configurations turn out to have similar weights in the multiconfiguration wavefunction [26]. For B^-, at the single-configuration level there is no need to constrain the two p orbitals to be equivalent, as they spontaneously turn out to be symmetry-related under energy minimization. Nor is there any need to force them to be triplet coupled. Thus, the single-configuration spin-coupled wavefunction for B^- spontaneously assumes the required ^3P symmetry when four of the orbitals are taken to be s orbitals, and the other two a p_x and a p_y orbital. Still, the energy lowering brought about by adding the two symmetry-related configurations described above, and the 0.25 occupation number each of them assumes in the three-configuration wavefunction [2], make it hard to ascribe "qualitative robustness" to the single-configuration spin-coupled solution.

4. THE ELECTRONIC STRUCTURE OF BH$_3$ (^{1}A$_1'$)

4.1 Why BH$_3$?

One of the questions implicitly raised by the studies summarized in the previous Section was, of course, whether similar behaviour is exceptional or, in fact, fairly common, at least in highly symmetric systems.

As a first step toward answering this question, it seems reasonable to investigate a high-symmetry polyatomic. BH$_3$ is an obvious candidate, given its D$_{3h}$ equilibrium geometry (experimentally verified by photoelectron-spectroscopy studies of BH$_3^-$ [38] and by gas-phase spectroscopic observations of the neutral molecule itself [39][40]). Besides, its small size makes all-electron OBS-GMCSC calculations on it easily feasible, nowadays, even on a run-of-the-mill Personal Computer. Moreover, the fact that BH$_3$ is an electron-deficient system, and of course that it spontaneously dimerizes to the ever-intriguing diborane, implies that a study of its electronic structure may be of intrinsic interest.

Over the past fifteen years or so, increasingly accurate *ab initio* studies of this molecule have been published [41]-[46]. This makes it possible to assess the accuracy of the OBS-GMCSC results. At the same time, it does not pre-empt a study of the molecule's electronic structure, notably of the nature of its chemical bonds. These admittedly qualitative aspects seem to have been somewhat neglected in otherwise quite thorough investigations, a fact that is not too surprising given that the prevailing orthogonal-orbital approaches, efficient though they are at producing accurate numerical results, do not lend themselves too readily to physical interpretation, once one moves away from the most elementary levels of description.

One should perhaps note in passing that quantitative questions on the molecule's infrared spectrum remain open, essentially for want of further experimental investigation. On one hand, Kawaguchi and co-workers' gas-phase spectroscopic measurements [39][40] of two of the four vibrational fundamentals have essentially resolved the discrepancy between argon-matrix experimental values [47] for those fundamentals and *ab initio* results (see [41] for an early reference). On the other hand, though, the larger discrepancy between theoretical values of the doubly-degenerate asymmetric-bend harmonic frequency ω_4 and the only experimental value available for the corresponding fundamental v_4, also from those argon-matrix studies [47], still stands (see Ref. [45] for an overview up to 1993, and Ref. [46] for later *ab initio* results).

In any case, obvious questions remain on the theoretical side, such as the nature of the B-H bonds in this deceptively simple molecule. Are they really the straightforward "sigma" bonds elementary considerations would suggest? On the basis of the OBS-GMCSC results, the present author will argue that the molecule's electronic structure is not quite that simple.

4.2 Geometry and basis set

All calculations have been carried out for D_{3h} geometries, with the B-H internuclear distance fixed, unless otherwise noted, at 2.24 a_0 (where a_0 denotes the atomic unit of distance, or Bohr: 1 a_0 = 0.5291772 x 10^{-10} m [37]). This choice is based on what is perhaps the highest-level *ab initio* optimization of this molecule's geometry to date [46], which predicted an equilibrium value R_e = 2.2416 a_0 (1.1862 Å, 1 Å = 1.000014 x 10^{-10} m [37]). Though there is at present no experimental value for R_e, the expectation value R_0 of the B-H internuclear distance in the vibrational ground state has been spectroscopically determined to be 2.24882 a_0 (1.19001 Å) [40] and provides an obvious experimental upper bound for R_e, inasmuch as the potential well can be safely assumed to be steeper on the inside.

The basis set consisted of two $1s$, two $2s$, two sets of $2p$ and one set (five components) of $3d$ real Slater-type basis functions (STFs) on boron, two $1s$ and one set of $2p$ STFs on each hydrogen. It was thus of double-zeta plus polarization quality. The z axis was taken to be perpendicular to the plane of the nuclei.

Exponential parameters were optimized at the SCF level, at the single-configuration spin-coupled (SC) level, and for a valence- and core-correlated OBS-GMCSC wavefunction that included eight configurations. Intermediate GMCSC wavefunctions, including three, six and seven configurations, used the exponential parameters that had been optimized at the SC level.

Note that basis functions and orbitals are designated as σ if they are invariant under reflection in the plane of the nuclei, and as π if they do change sign under the same reflection.

4.3 The SC solution

At the single-configuration level, the optimized wavefunction spontaneously displays full ${}^1A_1'$ symmetry. As could easily be anticipated, the eight orbitals are all σ orbitals, and consist of two "inner" orbitals, essentially $1s$ orbitals on boron, and six "valence" orbitals. The latter are neatly organized in three symmetry-equivalent pairs, related to one another by rotation about the ternary axis. Each pair consists essentially of an sp^2-like orbital centred on boron and pointing towards one of the hydrogens, and of a distorted $1s$ orbital on that hydrogen, polarized towards boron. However, while the two inner orbitals include only minor contributions from basis functions centred on the hydrogens, each valence orbital has sizable contributions from basis functions centred on both boron and one of the hydrogens, and non-negligible contributions from the rest of the basis set as well. Orbitals are depicted in Fig. 1. Orbital overlaps are given in Table 2. Note the appreciable overlap between sp^2-like orbitals (0.355).
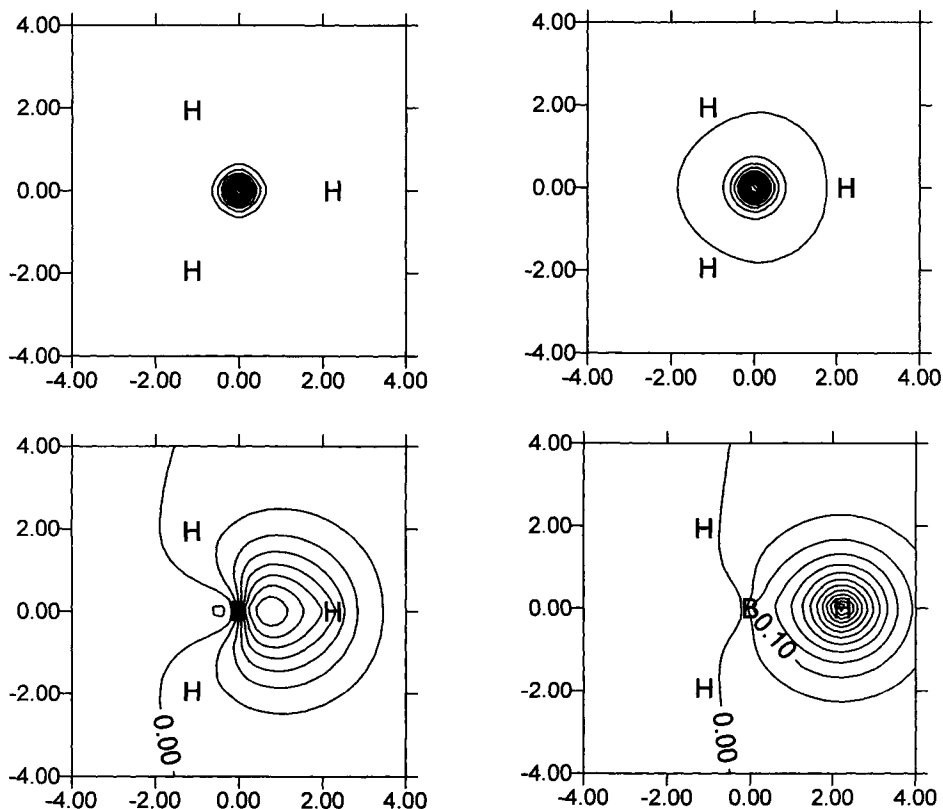
Fig. 1. Contour plots of the four unique orbitals in the single-configuration spin-coupled solution for BH_3, at R_{BH}=2.24 a_0. All plots are drawn in the plane of the nuclei. The upper two plots (contours every 0.2 a.u.) depict the two fully-symmetric "inner" orbitals. The lower two plots (contours every 0.05 a.u.) depict one of the three symmetry-related orbital pairs. The other two pairs can be obtained by rotations through ±120° about an axis going through each orbital plot's origin and perpendicular to the plane of the paper (the molecule's C_3 axis). All orbitals are normalized.

There is no need for orbital constraints to enforce the fully symmetric nature of the two inner orbitals or the symmetry relations between the three pairs of valence orbitals. The fully-symmetric SC solution corresponds to a proper minimum in the unconstrained SC optimization space. It has been verified to be stable against symmetry-breaking perturbations, including the admixture of π basis functions into the orbitals, in the sense that energy minimization from such a perturbed initial guess spontaneously restores the orbitals to purely σ character and to full symmetry, converging back onto the unperturbed solution.

Table 2

Orbital overlaps – single-configuration spin-coupled solution (R_{BH}=2.24 a_0). [a]

	σ_1	σ_2	σ_3	σ_4	$C_3\,\sigma_3$	$C_3\,\sigma_4$	$C_3^2\,\sigma_3$	$C_3^2\,\sigma_4$
σ_1	1.000							
σ_2	0.961	1.000						
σ_3	0.171	0.217	1.000					
σ_4	0.073	0.081	0.816	1.000				
$C_3\,\sigma_3$	0.171	0.217	0.355	0.153	1.000			
$C_3\,\sigma_4$	0.073	0.081	0.153	0.013	0.816	1.000		
$C_3^2\,\sigma_3$	0.171	0.217	0.355	0.153	0.355	0.153	1.000	
$C_3^2\,\sigma_4$	0.073	0.081	0.153	0.013	0.153	0.013	0.816	1.000

[a] Orbitals are identified by their spontaneous symmetry relationships (σ_3 and its two symmetric counterparts resemble sp^2 hybrids on boron, see Fig. 1).

When the orbitals are ordered so that the first two are the inner orbitals and, if a valence orbital is even-numbered (odd-numbered), its symmetry-equivalent counterparts also are even-numbered (odd-numbered), then the spin part of the SC wavefunction is dominated by the perfect-pairing Yamanouchi-Kotani (YK) spin function, with a coefficient exceeding 0.99. The coefficients of the other 13 YK functions are all smaller than 0.01.

Because, for this configuration, rotation about the ternary symmetry axis is equivalent to an even permutation of the orbitals among themselves, the configuration will be invariant under C_3 if, and only if, the vector of spin-coupling coefficients is an eigenvector, with eigenvalue +1, of the matrix representation $U(P^{-1})$ of the inverse permutation in the basis of YK spin functions [3][25]. This requirement is a direct consequence of the antisymmetry principle. The theory of such matrix representations is discussed e.g. in Ref. [27], and practical algorithms for their computation are given e.g. in Refs. [48] and [49].

One needs to consider only one of the two C_3 rotations, since they are mutual inverses. With the orbitals ordered as above, the relevant permutation can be taken to be

$$P = \begin{pmatrix} 1 2 3 4 5 6 7 8 \\ 1 2 7 8 3 4 5 6 \end{pmatrix} \tag{9}$$

Similarly, invariance under reflection in one of the σ_v symmetry planes requires the vector of spin-coupling coefficients to be an eigenvector, with eigenvalue +1, of the matrix representing the self-inverse permutation

$$Q = \begin{pmatrix} 1 2 3 4 5 6 7 8 \\ 1 2 3 4 7 8 5 6 \end{pmatrix} \tag{10}$$

in the basis of YK spin functions. Consideration of other symmetry elements is unnecessary, inasmuch as all orbitals are pure-σ.

$U(P^{-1})$ admits the eigenvalue +1 with degeneracy six, while $U(Q)$ admits the same eigenvalue with degeneracy eight. The intersection of the two eigenspaces has dimension four, so the two conditions are equivalent to ten independent linear constraints on the fourteen spin-coupling coefficients (once normalization is taken into account, only three of the spin-coupling coefficients are truly independent). Methods to reach this conclusion, and find explicit expressions for the constraints, have been described in a previous paper [25]. One should perhaps note that $U(P^{-1})$ is not a symmetric matrix. Though it is obviously diagonalizable, like all U matrices, because of its orthogonality, its eigenvalues, and eigenvectors, are not all real. Of course, the only possible eigenvalues are the three cube roots of +1, since the corresponding permutation is cyclic with period three. It is possible to find a set of eigenvectors of $U(P^{-1})$ that span its +1 eigenspace by careful application of the "inverse iteration" method, as suggested in Ref. [25] for the non-symmetric case, and this is actually all that is required in the present context. However, it is in fact easier to diagonalize the matrix through reduction to Hessenberg form. This is especially true since public-domain subroutines implementing the latter approach are easily available (*e.g.* EISPACK's "RG" [50]; EISPACK is available on the Internet at www.netlib.org, a veritable trove of such packages). As for $U(Q)$, it is symmetric and thus even easier to diagonalize.

In any case, at convergence, the spin-coupling coefficients spontaneously satisfy the two conditions. This is as expected for the single-configuration case [3][25]: if the orbital symmetry is such that conditions on the spin-coupling coefficients suffice for the configuration to display the appropriate symmetry for the lowest-energy state of a given spin multiplicity, energy minimization will lead to spin-coupling coefficients that satisfy them. Constraints on the spin-coupling coefficients should then be unnecessary.

Table 3

Optimized values [a] of STF exponential parameters for BH_3 (R_{BH}=2.24 a_0)

		SCF	Spin-Coupled	GMCSC (8 confs.)
B	1s	8.30452	7.68779	5.71602
B	1s	4.66474	4.35109	4.98762
B	2s	4.07990	5.31368	5.02672
B	2s	1.55101	1.51168	1.57509
B	2p	3.51901	3.73289	6.60964
B	2p	1.42234	1.46023	1.56948
B	3d	1.89654	1.98763	1.91502
H	1s	1.24014	1.20172	1.33187
H	1s	0.77056	0.70319	0.91074
H	2p	1.75392	1.74880	1.65682

[a] not all digits may be always significant

The SC solution can be referred to, more precisely, as an OBS-SC solution, inasmuch as the basis set exponential parameters have been optimized simultaneously with the coefficients with which they enter the eight orbitals (and with the spin-coupling coefficients). Values are given in Table 3.

The OBS-SC energy lies about 1.47 eV below the SCF energy, as computed with a corresponding, and similarly optimized, basis set (the OBS-SCF energy), see Table 4.

To take into account the basis-set size, the OBS-SCF energy will be taken to define the correlation-energy zero. It lies only about 0.02 eV above the SCF energy computed [46] with a large basis set [51] at essentially the same bond length (2.2416 a_0 compared with the value of exactly 2.24 a_0 used in the present work).

The single-configuration spin-coupled solution provides a simple, and intuitively appealing, picture of the molecule's electronic structure and of the three equivalent B-H bonds, smoothly generalizing the obvious "Old VB" model. Of course, quantitative accuracy would require a detailed description of correlation through the addition of "excited" configurations. Nevertheless, one would be tempted to assume that the essential physical picture is held by this one configuration, thanks to the adoption of non-orthogonal orbitals. This not only leads to an energy that is significantly lower than the SCF energy, but also, in all-electron calculations, makes the orbitals unambiguously fixed by the variational principle. Even the inclusion of spin-coupling modes other than perfect pairing appears, in this case, somewhat redundant.

Table 4

Numerical results for BH_3 (R_{BH}=2.24 a_0)

Method	Number of configurations	Number of independent configurations	E / E_h [a]	E_{corr} [b] / eV [c]	θ_0 [d] / (e·a_0^2) [e]
OBS-SCF	1	1	-26.401577	0.0	1.8013
OBS-SC	1	1	-26.455489	1.467	1.8453
MCSC [f]	3	1	-26.490584	2.422	1.9241
MCSC [g]	3	1	-26.494263	2.522	1.8176
VB-CI	6	1	-26.500629	2.695	1.8122
MCSC	6	1	-26.515263	3.093	1.8416
VB-CI	7	2	-26.515331	3.095	1.8413
GMCSC	7	2	-26.518927	3.193	1.8273
GMCSC	8	3	-26.522410	3.288	1.8271
OBS-GMCSC	8	3	-26.533024	3.577	1.9151

[a] E_h denotes the atomic unit of energy, or hartree: 1 E_h = 4.35975 x 10^{-18} J [37]
[b] correlation energy
[c] 1 eV = 1.602177 x 10^{-19} J [37]
[d] electric-quadrupole m=0 spherical-tensor component, the only non-zero component.
[e] atomic units (1 e·a_0^2 = 0.4486553 x 10^{-39} C·m^2 [37])
[f] all orbitals constrained to be σ
[g] includes $\sigma \pm \lambda \pi$ orbitals and is symmetry-contaminated (fully symmetric in C_{3h} subgroup only)

This somewhat lengthy discussion of the SC solution's spontaneous full symmetry has been included, at least in part, to stress that the solution shows no hint of symmetry breaking. Similarly, the convergence process onto it is uneventful, and requires no special precautions (for the present work, the very different OBS-SCF solution, with canonical orbitals, was taken as starting guess). At the single-configuration level, there is thus no intimation that something qualitatively important may be missing.

4.4 Glimmers of complexity: three-configuration solutions

The molecule's symmetry, however, does suggest the possibility of a three-configuration solution, each configuration connected to the other two by rotations through ±120° about the molecule's ternary axis. With suitable symmetry constraints, it is in fact possible to obtain a GMCSC solution that consists of three such equivalent configurations. When the basis-set exponential parameters are fixed to the values that have been optimized for the single-configuration spin-coupled solution, the three-configuration GMCSC solution lies 2.42 eV below the OBS-SCF energy, almost 1 eV below the OBS-SC energy (see Table 4). Each configuration's orbital structure resembles that of the fully symmetric single-configuration solution: three "valence" pairs, each

Table 5

Orbital overlaps for one (any) of the three equivalent "all-sigma" MCSC configurations (R_{BH}=2.24 a_0).

	σ_1	σ_2	σ_3	σ_4	σ_5	σ_6	σ_7	σ_8
σ_1	1.000							
σ_2	0.918	1.000						
σ_3	0.123	0.153	1.000					
σ_4	0.057	0.093	0.691	1.000				
σ_5	0.060	0.132	0.214	0.195	1.000			
σ_6	0.044	0.047	0.169	0.063	0.682	1.000		
σ_7	0.060	0.132	0.214	0.195	0.240	-0.185	1.000	
σ_8	0.044	0.047	0.169	0.063	-0.185	-0.436	0.682	1.000

consisting essentially of an sp^2-like hybrid mostly centred on boron and what looks like a strongly polarized hydrogen orbital, and a pair of "inner" orbitals, essentially localized on boron. However, within each configuration, only two "valence" orbitals, making up one "bonding pair", are now invariant under reflection in the σ_v plane that contains their "bond axis". The same reflection swaps the other two "bonding pairs", which are thus symmetry-equivalent. They are not, however, equivalent to the first "bonding pair", and their orbitals are somewhat distorted with respect to their respective "bond axes". Thus, each of the three configurations is fully symmetric only under one of the three C_{2v} subgroups of the molecular point group (the two inner orbitals display a corresponding symmetry reduction, being invariant under the same σ_v reflection as the first "valence" pair, but not under the other two σ_v's, or C_3).

The overlap between any two individually-normalized configurations is 0.874. Orbital overlaps are given in Table 5.

Symmetry requires the same vector of spin-coupling coefficients to be used for all three configurations, a fact that reduces the GMCSC [2] calculation to a MCSC calculation [1]. This common vector spontaneously meets the requirement for each configuration to be fully symmetric in one of the C_{2v} subgroups, given the symmetry relationship among the orbitals of each configuration. That is, the vector is an eigenvector, with eigenvalue +1, of the

matrix representing the relevant (even) permutation, namely that corresponding to the swap, within each configuration, of the two symmetry-equivalent orbital pairs, Eq. (10). The overall wavefunction is obviously C_3-invariant and σ_h-invariant, by construction, so it has the full symmetry required for a $^1A_1'$ state. Perfect pairing is by far the dominant mode of spin-coupling (YK coefficient 0.999).

This interesting solution, however, is not stable against the mixing-in of π-type basis functions. When this is allowed, while still constraining the three configurations to be connected by C_3 rotations, six orbitals in each configuration do spontaneously remain pure σ orbitals, but two orbitals turn into a ($\sigma\pm\lambda\pi$) pair. These two orbitals are not individually invariant under reflection in the plane of the nuclei. Such a reflection actually swaps them. Their nature allows each configuration to include correlation "across the nuclear plane" for one of the three bonding pairs. A different pair is thus correlated in this way by each of the three symmetry-equivalent configurations. Roughly speaking, this reduces the probability that two electrons can be found, within a "bond region", on the same side of the plane of the nuclei, correspondingly enhancing the probability that they be found on opposite sides of the plane, and thus reduces their electrostatic repulsion.

Table 6

Orbital overlaps for one (any) of the three equivalent "σ-π mixed" MCSC configurations (R_{BH}=2.24 a_0).

	σ_1	σ_2	σ_3	σ_4	σ_5	σ_6	$\sigma+\lambda\pi$	$\sigma-\lambda\pi$
σ_1	1.000							
σ_2	0.919	1.000						
σ_3	0.109	0.123	1.000					
σ_4	0.050	0.076	0.666	1.000				
σ_5	0.055	0.120	0.205	0.197	1.000			
σ_6	0.057	0.067	0.249	0.126	0.736	1.000		
$\sigma+\lambda\pi$	0.057	0.077	-0.015	-0.009	-0.072	-0.112	1.000	
$\sigma-\lambda\pi$	0.057	0.077	-0.015	-0.009	-0.072	-0.112	0.711	1.000
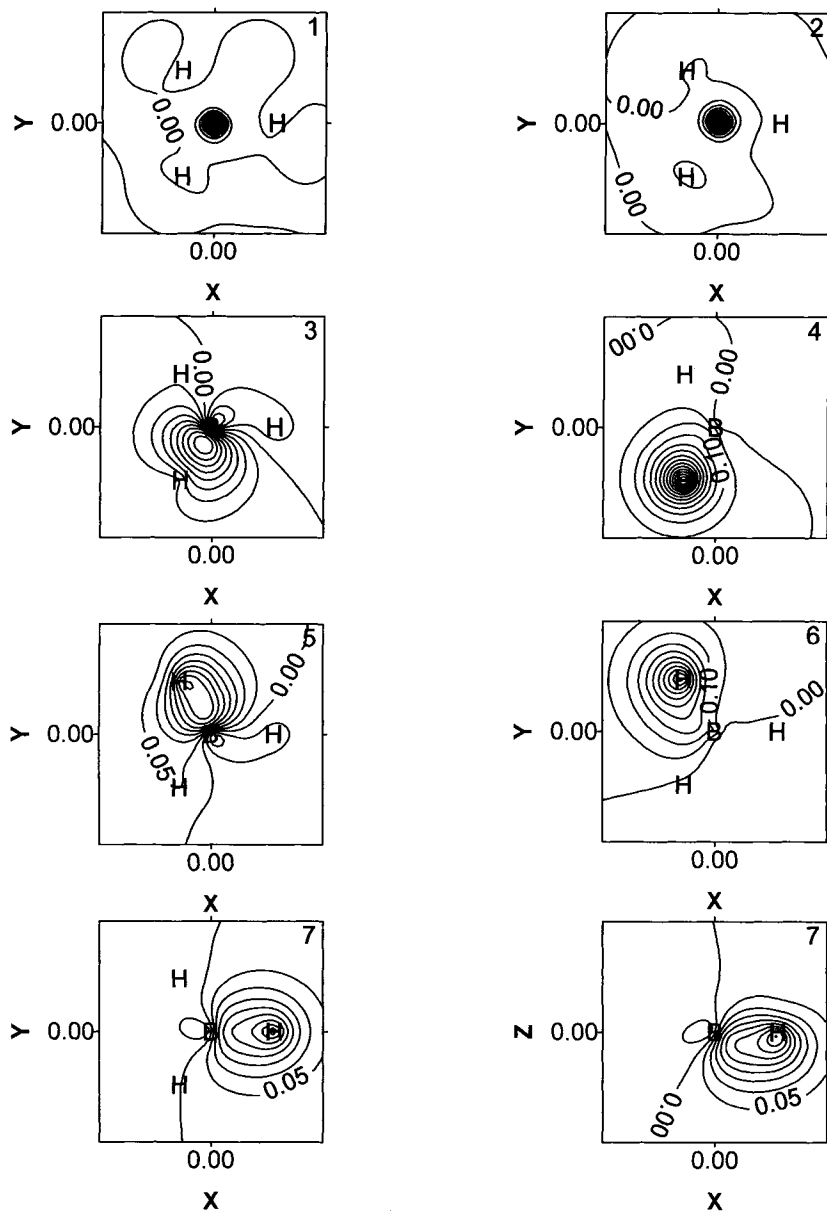
Fig. 2. Contour plots of the seven unique orbitals in one of three symmetry-equivalent configurations, at R_{BH}=2.24 a_0. The first six orbitals are pure σ, and are plotted only in the plane of the nuclei (xy). Orbital 7 is not pure σ, and is plotted both in the xy plane and in the xz plane. Orbital 8 can be obtained from orbital 7 by a reflection in the xy plane. Contours are drawn every 0.2 a.u. for the uppermost two plots (depicting the two "inner" orbitals), every 0.05 a.u. for the other plots. The other two configurations can be obtained by applying C_3 and its inverse, respectively, to this one. The overall wavefunction has C_{3h}, but not D_{3h}, symmetry.

At the same time, the two ($\sigma \pm \lambda \pi$) orbitals in each configuration, being related by a reflection in the molecular plane, provide no "along the bond" correlation in the plane of the nuclei, though this is of course provided, for the other two bonds, by the other two valence pairs in the same configuration. Among them, the three configurations provide both "along the bond" and "across the plane" correlation for all three "bond regions".

Each configuration's orbitals are also distorted in such a way that even their C_{2v} symmetry becomes only approximate. The seven unique orbitals of one of the three equivalent configurations are plotted in Fig. 2. Orbital overlaps are given in Table 6. The overlap between any two configurations is 0.883. For this solution, perfect pairing becomes even more the dominant mode of spin-coupling (YK coefficient 0.9999). Moreover, the vector of spin-coupling coefficients, still necessarily identical for all configurations, spontaneously satisfies the symmetry requirement that the last two orbitals must be singlet-coupled. This ensures that each configuration is invariant under reflection in the plane of the nuclei (σ_h), given that the last two orbitals of each configuration are swapped by such a reflection. The overall wavefunction is of course C_3-invariant as well, by construction.

However, it is *not* invariant under reflection into any of the three σ_v symmetry planes. It thus does *not* have the full symmetry required for an A'_1 state, and it is only fully symmetric in the C_{3h} subgroup of the D_{3h} molecular point group. The energy lies a further 0.10 eV below that of the "all-sigma" three-configuration solution (see Table 4).

4.5 Symmetry remediation as a path to variational improvement

One can obtain a properly symmetric wavefunction from the symmetry-broken three-configuration solution by adding three more configurations, in such a way that the list of six configurations is then closed under all symmetry operations of the D_{3h} molecular point group. These three extra configurations can be obtained *e.g.* by reflecting each of the three original configurations in anyone of the σ_v symmetry planes. Alternatively, one of the three configurations can be obtained by such a σ_v reflection, and the remaining two can then be obtained from it by successive application of C_3 rotations. Either way, the same set of six configurations is obtained, but in a different order.

If these six configurations are used in a non-orthogonal configuration-interaction calculation (VB-CI), the resulting energy is about 0.17 eV lower than that of the symmetry-contaminated three-configuration MCSC wavefunction.

A significant variational improvement can be obtained if orbital and spin-coupling coefficients are simultaneously relaxed in a corresponding MCSC calculation, using six configurations constrained to be related by C_3 and σ_v as above. Six orbitals of each configuration spontaneously remain pure-σ. The last two orbitals of each configuration retain the ($\sigma \pm \lambda \pi$) nature they had in the three-

configuration solution, and remain exactly singlet-coupled, just as spontaneously. Each configuration is thus invariant under σ_h. Symmetry mandates that all configurations share the same set of spin-coupling coefficients, making a GMCSC calculation strictly equivalent to a MCSC calculation, as was the case for the three-configuration calculations. The overall wavefunction then has the symmetry required for a $^1A_1'$ state in the full D_{3h} molecular point group, just as its VB-CI counterpart. In both cases, perfect pairing is by far the dominant mode of spin coupling (YK coefficient greater than 0.9999 for the VB-CI wavefunction, and equal to about 0.999 for its MCSC counterpart).

With basis-set exponential parameters still fixed at the values optimized for the single-configuration spin-coupled solution, the energy falls by 0.40 eV in going from the VB-CI to the MCSC solution. The correlation energy, at 3.09 eV, more than doubles that recovered by the single-configuration spin-coupled wavefunction. One should perhaps stress that only one of the six configurations is truly independent. The full set can be viewed as arising by symmetry adaptation of a single configuration. The significant drop in energy as one goes from VBCI to MCSC illustrates the quantitative importance of relaxation, or, if one wishes, the well-known fact that direct optimization of a symmetry-adapted wavefunction usually yields better results than projection of a properly symmetric component out of an already optimized wavefunction.

4.6 The importance of being relaxed: a seven-configuration solution

A somewhat surprising result emerges as one tries to merge the fully-symmetric single-configuration spin-coupled solution with the six-configuration "σ-π mixed" MCSC wavefunction discussed in the previous Subsection.

One can obviously carry out a non-orthogonal configuration-interaction calculation including the 7x14=98 VB structures that arise from these seven configurations. However, the resulting energy is less than 0.002 eV lower than that of the six-configuration MCSC wavefunction (see Table 4). Moreover, the fully-symmetric configuration enters this "VB-CI" solution with a small and negative Chirgwin-Coulson occupation number (-0.026), and is less than 50% perfect-paired, the YK coefficient of the perfect-paired spin function being about 0.69. All this implies that the fully-symmetric configuration obtained at the single-configuration spin-coupled level plays here only a minor correlation-refinement role, despite a basis set biased towards it (since it was optimized for it alone). On the other hand, each of the six symmetry-equivalent configurations has an occupation number of 0.171 and is essentially perfect-paired (YK coefficient 0.998).

A way out of this apparent conundrum is offered by a GMCSC calculation using these seven configurations as a starting guess. In such a calculation, one can maintain the configurations' essential identity by suitable symmetry constraints. Thus, one configuration is made fully symmetric, in the same way

as the single-configuration spin-coupled solution, by applying suitable constraints. Firstly, all its orbitals are constrained to be pure σ. Two of them are also constrained to be invariant under both C_3 rotations and σ_v reflections, like the two "inner" orbitals in the single-configuration solution. Two other orbitals are constrained to be invariant under one of the σ_v reflections only, as a prototypical "bonding pair". Two more "bonding pairs" are then constrained to be related to the prototypical one by successive applications of C_3 rotations. Suitable constraints on the spin-coupling coefficients [25] then ensure full D_{3h} symmetry. The other six configurations are constrained to be connected to one another by C_3 rotations and σ_v reflections, and to have identical spin-coupling coefficients. Each of these six equivalent configurations is based on six mutually-independent pure-σ orbitals and a pair of σ_h-related ($\sigma \pm \lambda \pi$) orbitals.

At convergence, the GMCSC configurations can thus be considered "fully-relaxed" versions of their VB-CI forerunners and, sure enough, they all turn out to be almost exclusively perfect-paired. Moreover, the fully-symmetric configuration takes on a healthy 0.28 occupation number, the remaining six splitting equally between them, as they must, the 0.72 complement to 1.00 (0.12 each). Configuration overlaps are given in Table 7.

Relaxation brings about a non-negligible 0.10 eV lowering of the energy, with respect to the seven-configuration VBCI result, to 3.19 eV below the OBS-SCF energy, more than doubling the correlation energy recovered by the single-configuration spin-coupled wavefunction (see Table 4).

4.7 Inner correlation: an eight-configuration solution

What is obviously missing from the seven-configuration wavefunction described in the previous Subsection is some correlation "across the plane of the nuclei" for the two "inner" orbitals, analogous to that already included for the three "valence" pairs. The most economical way to provide this missing correlation is of course through the addition of a fully-symmetric configuration consisting of three symmetry-equivalent pairs of σ orbitals and a pair of identical C_3- and σ_v-invariant π orbitals.

Table 7

Configuration overlaps for the seven-configuration GMCSC solution (R_{BH}=2.24 a_0).

1.000						
0.716	1.000					
0.716	0.594	1.000				
0.716	0.594	0.594	1.000			
0.716	0.341	0.557	0.541	1.000		
0.716	0.541	0.341	0.557	0.594	1.000	
0.716	0.557	0.541	0.341	0.594	0.594	1.000

Table 8

Configuration overlaps for the eight-configuration GMCSC solution (R_{BH}=2.24 a_0).

1.000							
0.744	1.000						
0.744	0.631	1.000					
0.744	0.631	0.631	1.000				
0.744	0.435	0.606	0.599	1.000			
0.744	0.599	0.435	0.606	0.631	1.000		
0.744	0.606	0.599	0.435	0.631	0.631	1.000	
0.000	-4.5E-6	-4.5E-6	-4.5E-6	-4.5E-6	-4.5E-6	-4.5E-6	1.000

Such an eight-configuration GMCSC calculation, with basis-set exponential parameters as optimized for the single-configuration spin-coupled solution, gives an energy about 0.10 eV lower than that of the seven-configuration solution described in the previous Subsection.

Basis-set optimization, in a proper OBS-GMCSC calculation, leads to a further lowering of the energy by about 0.29 eV, and a non-negligible change in the quadrupole moment as well (see Table 4). The re-optimised values of the exponential parameters are given in Table 3; one should perhaps note the large increase in that of the more contracted of the two $2p$ functions on boron, consequent to its being 'put to use' for inner-shell correlation. In fact, the eighth configuration can be viewed as a double-excitation out of the all-sigma fully-symmetric configuration's "inner-shell" orbitals: even after full reoptimization, the overlaps between corresponding "valence" orbitals in the two configurations remains 95% or higher.

Chirgwin-Coulson occupation numbers for the first seven configurations turn out to be essentially the same as those of their counterparts in the seven-configuration wavefunction (0.248 for the fully-symmetric configuration, and 0.125 for each of the other six), while the eighth configuration achieves only a puny 0.0002 occupation number. Configuration overlaps are given in Table 8. Note the eighth configuration is orthogonal to the all-sigma first configuration, but is not strictly orthogonal to the other six configurations, each of which includes a ($\sigma\pm\lambda\pi$) orbital pair. It is however nearly orthogonal to them as well.

The first seven configurations remain almost exclusively perfect-paired. As for the eighth configuration, it too turns out to be almost exclusively perfect-paired; the coefficient of the perfectly-paired YK spin function is in fact 0.982. In any case, the fact that its first two orbitals are identical rules out nine YK spin functions out of fourteen, and symmetry requirements further mandate three linear constraints on the coefficients of the five allowed spin functions, so that only two of them are truly independent. Anyway, one can legitimately conclude that the seven-configuration wavefunction is "qualitatively robust" with respect to the inclusion of this kind of "inner shell" correlation.
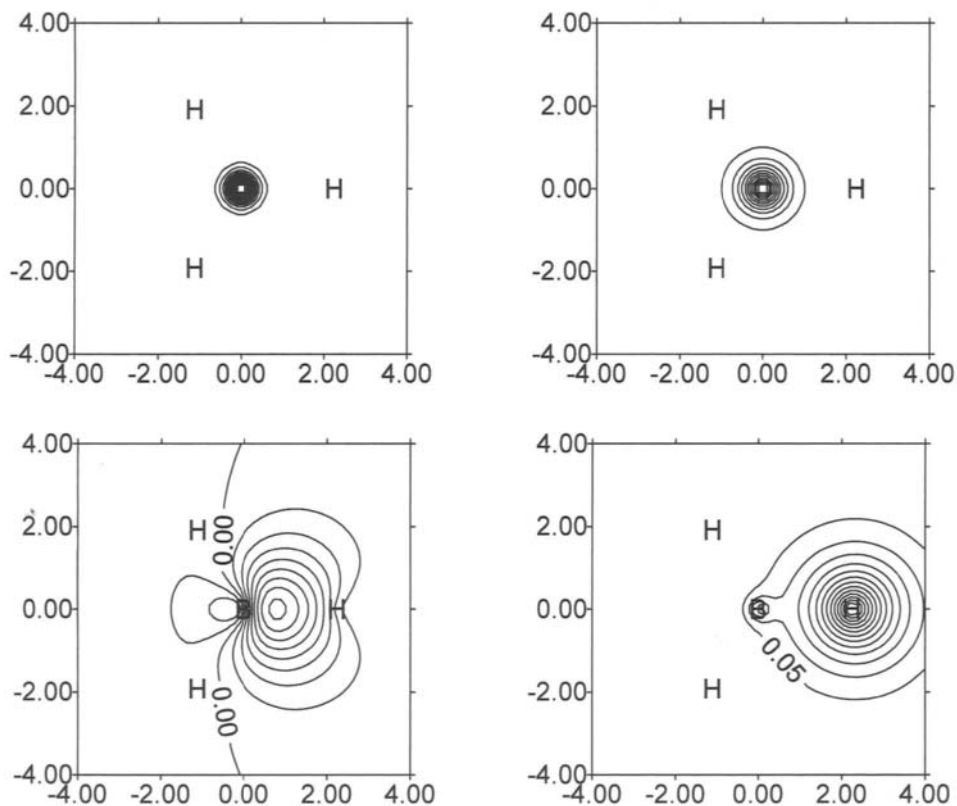
Fig. 3. Contour plots of the four unique orbitals in the fully-symmetric all-σ configuration of the eight-configuration OBS-GMCSC wavefunction for BH_3, at R_{BH}=2.24 a_0. All plots are drawn in the plane of the nuclei. The upper two plots (contours every 0.2 a.u.) depict the two fully-symmetric "inner" orbitals. The lower two plots (contours every 0.05 a.u.) depict one of the three symmetry-related orbital pairs. The other two pairs can be obtained by rotations through $\pm 120°$ about an axis going through each orbital plot's origin and perpendicular to the plane of the paper (the C_3 axis). All orbitals are normalized.

Contour plots of the orbitals are reproduced in the present and following pages. As has been said, the "main", fully-symmetric, configuration includes only σ orbitals, and corresponds to the single-configuration spin-coupled solution. A comparison of Fig. 3 on this page with Fig. 1 will show similarities and differences between corresponding orbitals. Each of the six symmetry-equivalent configurations, on the other hand, includes a $(\sigma \pm \lambda \pi)$ orbital pair in addition to six σ orbitals. The latter are depicted, for one of these configurations, in Fig. 4 on the next page, while Fig. 5 on the following page depicts one of the two symmetry-related orbitals in the same configuration's $(\sigma \pm \lambda \pi)$ pair. A comparison of Fig. 3 (above) with Fig. 4 should persuade the reader that the
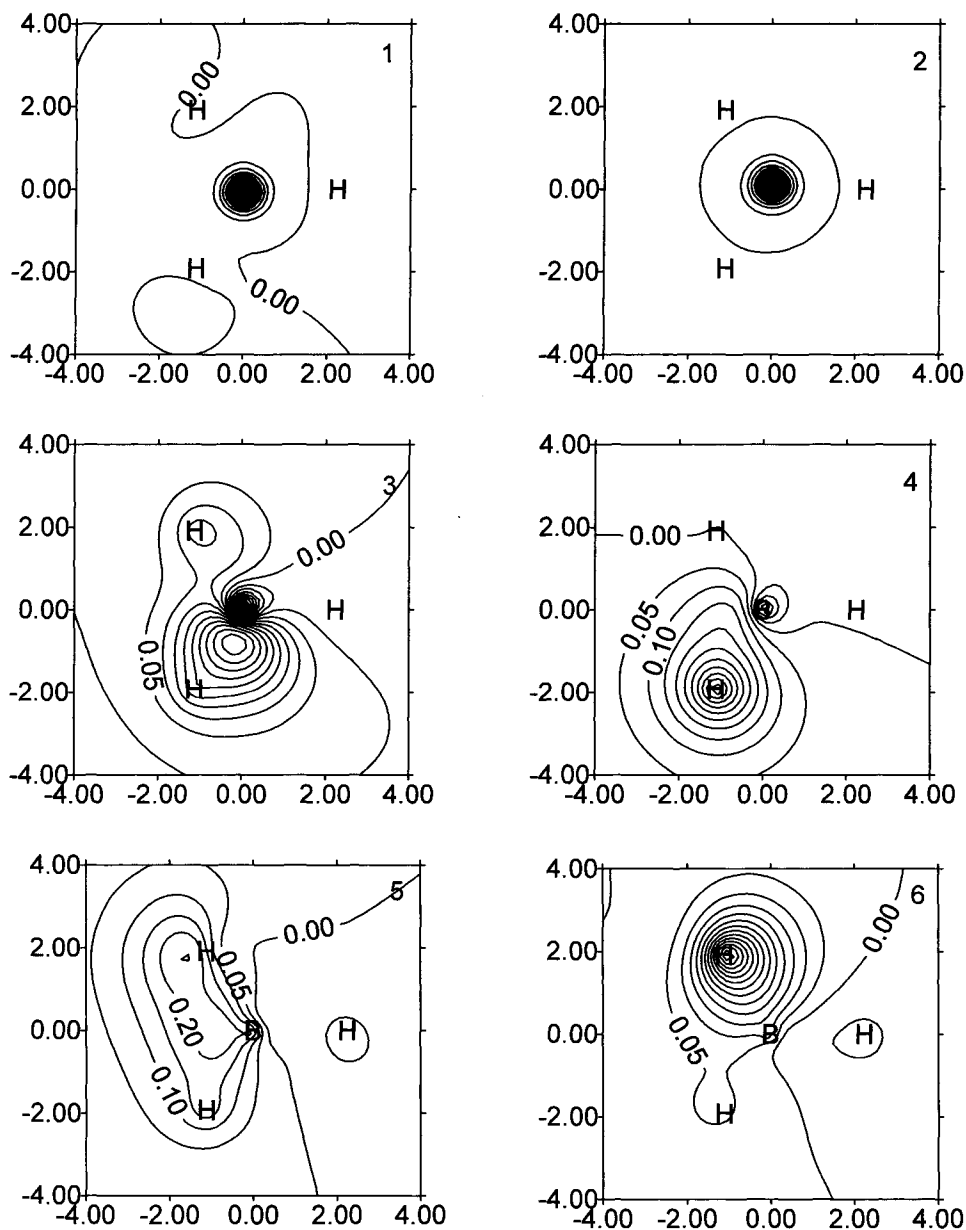
Fig. 4. Contour plots of the six pure-σ orbitals in one of the six symmetry-equivalent configurations of the eight-configuration OBS-GMCSC wavefunction, at R_{BH}=2.24 a_0. All plots are drawn in the plane of the nuclei. Contours join orbital-amplitude levels spaced 0.2 a.u. apart for the uppermost two plots (depicting the two "inner" orbitals), 0.05 a.u. apart for the other plots. All orbitals are normalized. One of the two equivalent ($\sigma\pm\lambda\pi$) orbitals that complete the space part of this configuration is depicted in Fig. 5.
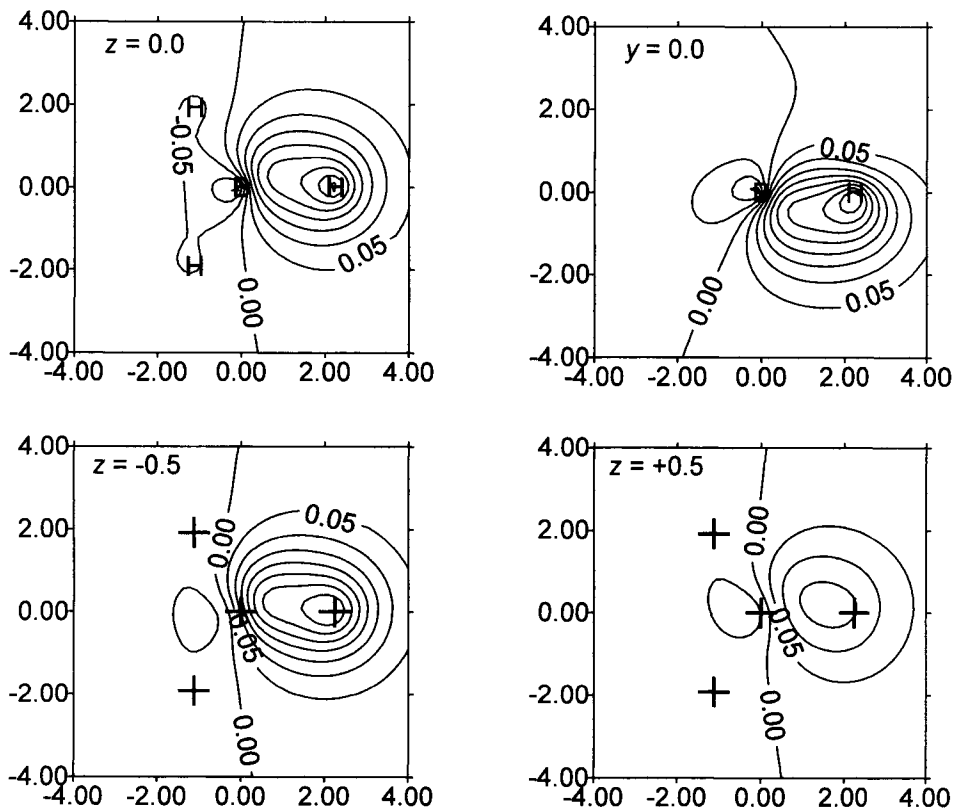
Fig. 5. Contour plots of orbital 7 in one of the six symmetry-equivalent configurations of the eight-configuration OBS-GMCSC wavefunction, at R_{BH}=2.24 a_0. Orbital 7 is not pure σ, and is plotted: in the plane of the nuclei, the xy plane, in the upper left plot, in the xz plane in the upper right plot, and in the two z=±0.5 a_0 planes in the lower two plots. In the upper right plot, only the boron nucleus and the rightmost hydrogen nucleus of the upper left plot are visible. In the two lower plots, crosses mark the projections, onto the plane of the plot, of the nuclear positions. Note that orbital 8 can be obtained from orbital 7 by reflecting it in the xy plane. Thus, to depict orbital 8, the upper left plot should be left unchanged, the upper right plot should be reflected in the line through B and H, while the two lower plots should have their z=±0.5 labelling interchanged. Contours are drawn every 0.05 a.u., for a normalized orbital. The six pure-σ orbitals that complete the spatial part of this configuration are depicted in Fig. 4.

orbitals in the latter are recognizable distortions of those in the fully-symmetric "main" configuration. As can be seen, not even the "inner" orbitals depicted in Fig. 4 on the previous page are exempt from some in-plane distortion. Also, within each of the two σ "valence bonding pairs", what is still recognizable as essentially an sp^2-like hybrid on boron is perhaps more distorted and delocalised than its "mostly-hydrogen" counterpart.
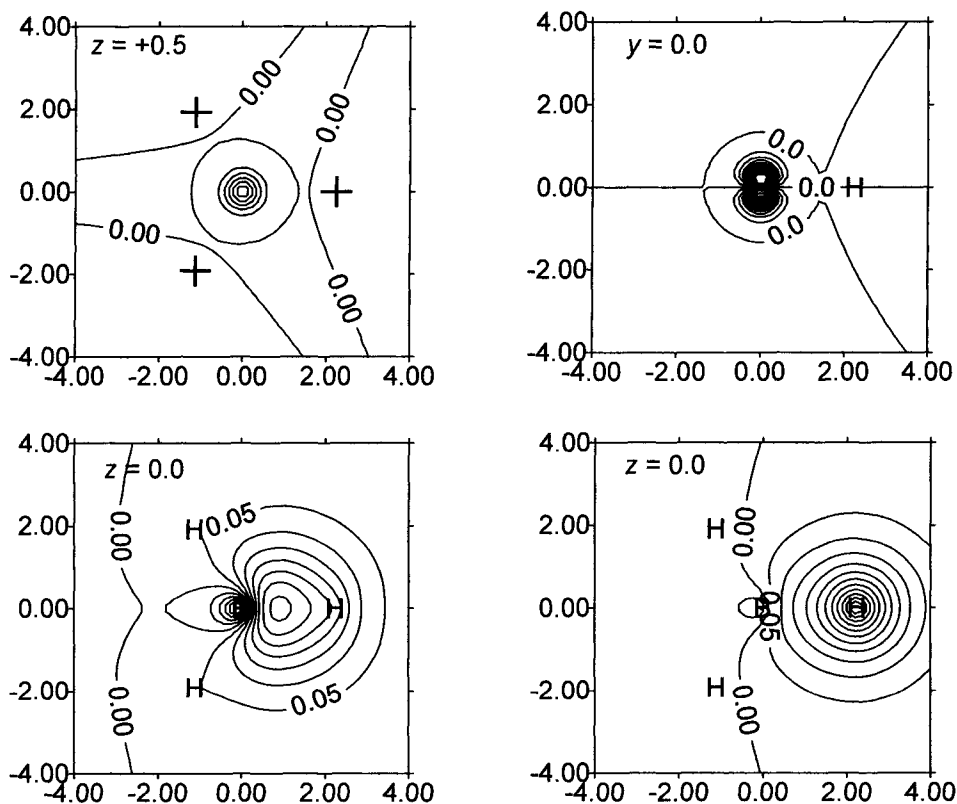
Fig. 6. Contour plots of the three unique orbitals in the "doubly-excited" fully-symmetric configuration of the eight-configuration OBS-GMCSC wavefunction for BH_3, at $R_{BH}=2.24$ a_0. The lower two plots (contours every 0.05 a.u.) depict one of the three symmetry-related σ orbital pairs, in the plane of the nuclei (xy). The other two pairs can be obtained by rotations through $\pm120°$ about an axis going through each orbital plot's origin and perpendicular to the plane of the paper (the C_3 axis). The upper two plots (contours every 0.2 a.u.) depict one of the two identical, C_3-invariant, π "inner" orbitals. The upper left plot is drawn in the plane $z=0.5$ a_0: crosses mark the projections on this plane of the positions of the hydrogen nuclei. The upper right plot is drawn in the xz plane. All orbitals are normalized.

Fig. 5 on the previous page shows that the $\sigma\pm\lambda\pi$ orbital pair seems to have suffered less in-plane distortion than its all-σ counterparts in the same configuration. This supports the idea of a "subdivision of roles" within the configuration, with all-σ orbitals providing most in-plane correlation, while the ($\sigma\pm\lambda\pi$) pair provides very little of that, but all of the across-the-plane correlation (the plane referred to here is of course that of the nuclei).

The three unique orbitals in the last of the eight configurations are drawn in Fig. 6. A comparison with Fig. 3 will confirm that corresponding "valence" orbitals in the two configurations are fairly similar, supporting the claim that this

eighth configuration can be viewed essentially as a double excitation out of the main configuration's "inner" orbitals. These last are replaced by a pair of identical π orbitals which, as expected, turn out to be quite contracted. This eighth configuration does therefore provide across-the-plane correlation for the inner shell, as previously suggested.

4.8 Comparison with previous results

Table 9 compares the eight-configuration OBS-GMCSC results with what are, in the present author's best knowledge, the best previous theoretical results [45][46]. For perspective, OBS-SCF and OBS-SC values computed in the present work are also included. The Table gives the minimum value of the potential energy for nuclear motion, U_e, the B-H distance at which the minimum occurs, R_e, and the harmonic frequency for the fully-symmetric stretch, ω_1.

The latter is the only harmonic frequency that could be easily and accurately computed in the present work, given that the derivatives of the STF-based integrals with respect to the nuclear coordinates were not available. This frequency was obtained by analytical differentiation of the natural-cubic-spline interpolant of the first derivative of the energy with respect to the common length of the three equivalent bonds, with all bond angles fixed at 120°. Analytical values of this first derivative were obtained in turn by applying the virial theorem to the results of eight-configuration OBS-GMCSC calculations at a few bond lengths around equilibrium, all carried out in D_{3h} geometry.

Unfortunately, this harmonic frequency is also the only one for which no experimental value has been obtained, a fact that is hardly surprising given that the relevant transitions are essentially forbidden. However, comparison with the CISDTQ and CCSD(T) values given in Table 9 leads one to infer that the OBS-GMCSC value should not be in error by more than a few cm^{-1}, or about 0.2%. The error on R_e similarly appears to be of the order of 0.2%, or 0.003 Å at most. As already noted, the only experimental value of the bond length refers to R_0 (1.19001 Å [40]), and thus constitutes only an upper bound to R_e.

As for U_e, there is some computational evidence, from calculations with limited basis sets on BH_3 itself [45], and on comparable systems [52], that the CCSD(T) method may yield energies within a few millihartrees of the full-CI limit. This suggests the last line of Table 9 may provide an energy value fairly close to the Born-Oppenheimer non-relativistic limit, given the high quality of the basis set [51] used in Ref. [46]. If that is so, then the total correlation energy can be estimated at about 4.8 eV, and the eight-configuration OBS-GMCSC wavefunction would be recovering about 75% of the total. There is obviously scope for improvement, but 75% of the total correlation energy would appear to be a reasonably good result for such a compact wavefunction. Moreover, despite its merits, the CCSD(T) method, as a variant of the coupled-cluster approach, yields energy values that are not variational upper bounds to the exact energy.

Table 9

Comparison with previous theoretical results for the X ^{1}A$'_1$ state of BH$_3$

Method	Basis Set	U_e / E$_h$	R_e / Å	ω_1 / cm^{-1}	Reference
OBS-SCF	Slater, double-zeta plus polarization.	-26.401580	1.1867	2639	Present work
OBS-SC	Slater, double-zeta plus polarization.	-26.456209	1.2090	2466	Present work
CISDTQ	Gaussian, B(10s6p2d/5s3p2d) H(5s2p/3s2p)	-26.528716	1.1890	2563	[45]
OBS-GMCSC (8 configs.)	Slater, double-zeta plus polarization.	-26.533045	1.1890	2570	Present work
CCSD(T)	Gaussian, B(14s9p4d3f/7s7p4d3f) H(8s4p3d/6s4p3d) [51]	-26.578848	1.1862	2575	[46]

Therefore, the eight-configuration OBS-GMCSC result appears to be the lowest *variationally-bound* value of the energy published so far. Though this distinction may be short-lived, the fact remains that the eight-configuration OBS-GMCSC value lies about 4.3 millihartree (0.12 eV) below a Configuration-Interaction value [45] obtained including all single, double, triple and quadruple excitations out of the SCF wavefunction, with a not-so-small basis set (see Table 9).

5. CONCLUSIONS

The OBS-GMCSC method offers a practical approach to the calculation of multiconfiguration electronic wavefunctions that employ non-orthogonal orbitals. Use of simultaneously-optimized Slater-type basis functions enables high accuracy with limited-size basis sets, and ensures strict compliance with the virial theorem. OBS-GMCSC wavefunctions can yield compact and accurate descriptions of the electronic structures of atoms and molecules, while neatly solving symmetry-breaking problems, as illustrated by a brief review of previous results for the boron anion and the dilithium molecule, and by newly obtained results for BH$_3$.

The latter provide, to the best of my knowledge, the lowest variationally-bound value of the electronic energy, and the only value of the electric quadrupole moment that has been published so far for ground-state BH$_3$. These results support a description of the molecule's electronic structure in terms of "resonance" between eight different orbital configurations. The main configuration is a fully-symmetric configuration, closely related to the single-configuration spin-coupled solution, and consisting of σ orbitals only. It

provides "along the bond" correlation for each of the three equivalent "bonding regions", as the two orbitals in each bonding pair are different, but no correlation "across the plane of the nuclei" for any of them. This configuration also provides some "in-out" correlation for the inner shell. Six similar but distorted configurations that are symmetry-equivalent to one another, and include a $(\sigma \pm \lambda \pi)$ orbital pair each, provide the missing across-the-plane correlation, and supplemental in-plane correlation, both within each bonding pair, and among different orbital pairs. They also provide somewhat more directional in-plane correlation for the inner shell. Each of the six symmetry-equivalent configurations enters the wavefunction with a weight that is more than half that of the "main" configuration. Together, they recover more than twice the correlation energy obtained at the single-configuration spin-coupled level (see Table 4). Finally, an eighth configuration, also fully symmetric, provides across-the-plane correlation for the inner shell, through what is essentially a conventional double excitation out of the two main-configuration inner orbitals into a pair of identical π orbitals. This last configuration enters the overall wavefunction with a decidedly small weight. Nevertheless, it does lead to a significant further lowering of the energy.

The final wavefunction for BH_3 can thus be said to consist of two fully-symmetric configurations, one of them essentially a double excitation out of the other, and a symmetry-adapted linear combination of six equivalent low-symmetry configurations. The latter can be viewed as distortions of the "main" configuration. The wavefunction therefore includes only three truly independent configurations, and is thus readily amenable to physical interpretation, while achieving an accuracy that vouches for the significance of such interpretations.

It is hoped that similar characteristics will be achieved by applications of the OBS-GMCSC method to other systems.

Acknowledgments

REFERENCES

[1]   F.E. Penotti, Intl. J. Quantum Chem., 46 (1993) 535.
[2]   F.E. Penotti, Intl. J. Quantum Chem., 59 (1996) 349.
[3]   J. Gerratt, Adv Atomic Mol. Phys., 7 (1971) 141.
[4]   N.C. Pyper and J. Gerratt, Proc. R. Soc. Lond. A, 355 (1977) 407.
[5]   J. Gerratt, J. and M. Raimondi, Proc. R. Soc. Lond. A, 371 (1980) 525.

[6] J. Gerratt, D. L. Cooper, P.B. Karadakov and M. Raimondi, Chem. Soc. Rev., 26 (1997) 87.

[7] M. Raimondi, M. Sironi, J. Gerratt and D.L. Cooper, Intl. J. Quantum Chem., 60 (1996) 225.

[8] N. J. Clarke, M. Raimondi, M. Sironi, J. Gerratt and D.L. Cooper, Theor. Chem. Acc., 99 (1998) 8.

[9] A.F. Voter and W.A. Goddard III, Chem. Phys., 57 (1981) 253.

[10] J.H. van Lenthe and G.G. Balint-Kurti, J. Chem. Phys., 78 (1983) 5699.

[11] J. Verbeek, Ph.D. Thesis, University of Utrecht, Utrecht, 1990.

[12] J. Verbeek and J.J. Van Lenthe, Mol. Struct. (Theochem), 229 (1991) 115.

[13] T. Thorsteinsson, D.L. Cooper, J. Gerratt, P.B. Karadakov and M. Raimondi, Theor. Chim. Acta, 93 (1996) 343.

[14] T. Thorsteinsson and D.L. Cooper, Theor. Chim. Acta, 94 (1996) 233.

[15] T. Thorsteinsson and D.L. Cooper in: A. Hernández-Laguna, J. Maruani, R. McWeeny and S. Wilson (eds.), Quantum Systems in Chemistry and Physics. Volume 1: Basic problems and models systems, Kluwer, Dordrecht, 2000, pp. 303-326.

[16] D.L. Cooper, T. Thorsteinsson and J. Gerratt, Intl. J. Quantum Chem., 65 (1997) 439.

[17] T. Thorsteinsson and D.L. Cooper, J. Math. Chem., 23 (1998) 105.

[18] T. Thorsteinsson and D.L. Cooper, Intl. J. Quantum Chem., 70 (1998) 637.

[19] F. Ogliaro, S.D. Loades, D.L. Cooper and P.B. Karadakov, J. Phys. Chem. A, 104 (2000) 7091.

[20] R. McWeeny, Methods of Molecular Quantum Mechanics, 2nd ed., Academic Press, London, 1989.

[21] T. Helgaker, Chem. Phys. Letters, 182 (1991) 503.

[22] S.M. Goldfeld, R.E. Quandt, and H.F. Trotter, Econometrica, 34 (1966) 541.

[23] F.E. Penotti, to be published.

[24] F. R. Manby and G. Doggett, J .Phys. B: At. Mol. Opt. Phys., 31 (1998) 949.

[25] F.E. Penotti, Intl. J. Quantum Chem., 78 (2000) 24.

[26] F.E. Penotti, Intl. J. Quantum Chem., 78 (2000) 378.

[27] M. Kotani, A. Amemiya, E. Ishiguro and T. Kimura, Tables of Molecular Integrals, Maruzen, Tokyo, 1955, Chapter 1.

[28] W.H. Press, S.A. Teukolski, W.T. Vetterling and B.P. Flannery, Numerical Recipes - The Art of Scientific Computing, 2nd ed., Cambridge University Press, Cambridge, 1992

[29] A.C. Wahl, P.E. Cade and C.C.J. Roothaan, J. Chem. Phys., 41 (1964) 2578.

[30] A.C. Wahl and R.H. Land, Intl. J. Quantum Chem., 1S (1967) 375.

[31]   F.E. Penotti, unpublished work.

[32]   J.F. Rico, R. López, A. Aguado, I. Ema and G. Ramírez, J. Comp. Chem., 19 (1998) 1284.

[33]   J.F. Rico, R. López, A. Aguado, I. Ema and G. Ramírez, to be published.

[34]   B.A. Chirgwin and C.A. Coulson, Proc. R. Soc. Lond. A, 201 (1950) 196.

[35]   G.A. Gallup and J.M. Norbeck, Chem. Phys. Lett., 21 (1973) 495.

[36]   T. Thorsteinsson and D.L. Cooper, J. Math. Chem., 23 (1998) 105.

[37]   E.R. Cohen and B.N. Taylor, J. Phys. Chem. Ref. Data, 17 (1988) 1795.

[38]   C.T. Wickham-Jones, S. Moran and G.B. Ellison, J. Chem. Phys., 90 (1989) 795.

[39]   K. Kawaguchi, J.E. Butler, C. Yamada, S.H. Bauer, T. Minowa, H. Kanamori and E. Hirota, J. Chem. Phys., 87 (1987) 2438.

[40]   K. Kawaguchi, J. Chem. Phys., 96 (1992) 3411.

[41]   J.F. Stanton, R.J. Bartlett and W.N. Lipscomb, Chem. Phys. Lett., 138 (1987) 525.

[42]   P. Botschwina in: J.P. Maier (Ed.), Ion and Cluster Ion Spectroscopy and Structure, Elsevier, Amsterdam, 1989, pp. 59-108.

[43]   M. Shen and H.F. Schaefer III, J. Chem. Phys., 96 (1992) 2868.

[44]   J.M.L. Martin and T.J. Lee, Chem. Phys. Lett., 200 (1992) 502.

[45]   J.M. Galbraith, G. Vacek and H.F. Schaefer III, J. Mol. Struct., 300 (1993) 281.

[46]   G.L. Gutsev and R.J. Bartlett, Polish J. Chem., 72 (1998) 1604.

[47]   A. Kaldor and R.F. Porter, J. Am. Chem. Soc., 93 (1970) 1562.

[48]   J.C. Manley and J. Gerratt, Comp. Phys. Comm., 31 (1984) 75.

[49]   P.B. Karadakov, J. Gerratt, D.L. Cooper and M. Raimondi, Theor. Chim. Acta, 90 (1995) 51.

[50]   B.T. Smith, J.M. Boyle, J.J. Dongarra, B. S. Garbow, Y. Ikebe, V.C. Klema and C. B. Moler, Matrix Eigensystem Routines - EISPACK Guide, Springer-Verlag, 1976.

[51]   P.O Widmark, P.A. Malmqvist and B.O. Roos, Theor. Chim. Acta, 77 (1990) 291.

[52]   R.J. Bartlett, J.D. Watts, S.A. Kucharski and J. Noga, Chem. Phys. Letters, 165 (1990) 513.

Chapter 11

Ab initio computational approaches to weakly interacting systems in the framework of the valence bond theory: from small to large van der Waals molecules

Antonino Famulari, Roberto Specchio, Ermanno Gianinetti, Mario Raimondi

Dipartimento di Chimica Fisica ed Elettrochimica and Centro CNR – CSRSRC
Università degli Studi di Milano, via Golgi 19 -20133 Milano – Italy

The research accomplished by our group in the field of van der Waals molecules is here summarised. The modification of the Roothaan equations to avoid the *basis set superposition error* (BSSE) at the Hartree-Fock level of theory (SCF-MI) and the successive development to take account of electron correlation effects by a compact multistructure size consistent valence bond wavefunction (MO-VB) are reviewed. The central idea of both the SCF-MI and MO-VB methods is the expansion of the orbitals in the partitioned basis set to exclude BSSE in an *a priori* fashion, while taking properly into account orbital and geometry relaxation effects and the *natural* non orthogonality of the MOs of the interacting fragments. Significant applications on large molecular systems of the SCF-MI approach and MO-VB studies on H-bonded complexes (water dimer and hydrogen fluoride) and on the He-CH$_4$ van der Waals complex, are reviewed. The very promising extension of the MO-VB scheme to fully exploit the capability of the virtual space spanned by the basis set is also presented, including explorative calculation on the helium dimer system.

1. INTRODUCTION

The study of van der Waals and hydrogen bonded molecules is one of the very important fields of chemistry where computational quantum chemical methods have increased our understanding both in a quantitative and qualitative way. The interest in the subject is emphasised by the impressive number of reviews, monographs and books that have recently appeared [1]. An accurate knowledge of the interaction potential between the individual molecules is in fact essential to the treatment of both finite clusters and condensed matter properties in the broad field of computer simulations.

In addition, hydrogen bond interactions play a fundamental role in the life sciences. These interactions are in fact responsible for biomolecular structures and related chemical processes: it would be practically impossible to find important biological phenomena in which these interactions do not play an important role [2].

The use of semi-empirical or even force field methods, which are generally used for problems of this size, is nevertheless not apt for the description of these systems [3]. On the other hand, the application of *ab initio* methods requires a considerable computational effort so that attempts to improve the efficiency of computational techniques are well worthwhile.

The interaction energy involved in weakly interacting systems is a very small fraction of the total energy; as a consequence, a great challenge is set to the accuracy of the quantum mechanical methods employed for its theoretical determination. For this reason, methods based on perturbation theories, which compute the interaction directly rather than as a difference between the energies of the complex and that of the separated systems, are frequently applied. Moreover, the majority of calculations involving complexes and clusters of molecules adopt the supermolecular approach, in which the interaction energy is computed as the difference between the energy of the complex and the total energy of the monomers. Variational procedures have the possibility to rely on the power of the variational theorem, but the appearance of the *basis set superposition error* (BSSE), which can be of the same order of magnitude of the interaction energy itself, represents a major inconvenience.

The BSSE is due to the use of all the basis functions located on the molecular centres of each monomer to compute the molecular orbitals of the complex considered as a single system, the so called supermolecule. In this way, however, when the molecules approach one another, the basis functions centred on the approaching "projectile" partner become better suited to describe the wavefunction also of the "target" partner, particularly in the region where the interaction becomes stronger. This involves a *de facto* use of an artificially too flexible functional space at shorter intersystem distances, causing a bias which is the origin of the BSSE. This error has a strong effect; in particular, it upsets the predicted binding energy and the anisotropy of the forces, quantities that are important in determining the geometry of clusters in both finite systems and in the liquids.

There have been many attempts to formulate a procedure to correct for BSSE and both *a posteriori* and *a priori* schemes are available [4]. The counterpoise approach (CP) [5], based on the use of "ghost orbitals", is the most common *a posteriori* procedure. Nevertheless, the addition of the partner's functions or ghost orbitals to counterbalance the BSSE does not provide a definite solution to the problem [6]. The introduction of the "secondary superposition error", upsetting the multipole moments and polarisabilities of the

monomers, is particularly important in the case of anisotropic potentials for charged species, where these errors can contribute to changing the shape of the PES, and thus the resulting physical picture [7].

In this context, the SCF-MI (Self Consistent Field for Molecular Interactions) [8] was proposed as an *ab initio* variational method that avoids the onset of BSSE in an *a priori* fashion. The very essence of the method consists of partitioning the full basis set into subsets centred on each fragment; the molecular orbitals of the different fragments are then expanded only in their own set, avoiding the BSSE. Because of this partitioning, the orbitals of the different fragments do overlap, reflecting the physics of the problem; the expected computational cost of this non-orthogonal procedure is well alleviated by the SCF-MI strategy. A definite advantage of the *a priori* SCF-MI method is that it is always exact, contrary to the CP procedure that is exact only in the case of Full CI wavefunctions [4]; in addition, geometry relaxation effects are naturally taken into account, without computational penalty. Recently, the algorithm was implemented into the GAMESS suite of programs [8b, 9]. Another important characteristic of the SCF-MI approach is that the schemes for first and second derivative evaluation at the Hartree Fock level are successfully applicable to the SCF-MI wavefunction: the intrinsic features of the method are in fact consistent with those required by the standard procedures for computing gradients and Hessians. This makes it possible to explore the shape of intermolecular potential energy surfaces as well as to determine vibrational frequencies and related properties within a BSSE-free procedure.

The complete description of hydrogen bond and van der Waals interactions requires of course the inclusion of electron correlation effects. Generally it is assumed that a very useful starting point is represented by the Hartree Fock description, which serves as the basis for both perturbation theory and variational configuration interaction approaches to the treatment of electron correlation; we have adopted this assumption in the context of the SCF-MI theory, presenting variational MO-VB *ab initio* approaches [10] to the solution of the problem. A compact, size consistent, multistructure VB - non-orthogonal CI - wavefunction, where the effect of the overlap between the orbitals of the fragments is naturally taken into account, is generated. A general scheme for the intermediate generation of virtual orbitals optimal to describe the interaction between pairs of electrons is devised: it is based on the separate determination of a pair of virtual orbitals that optimises the energy of the configuration interaction wavefunction between the SCF-MI zero-order wavefunction and a doubly excited configuration arising from simultaneous single excitations localised on each monomer. These optimal virtual orbitals can be generated both by *variational* or *perturbative* approaches, the choice mainly depending on the size of the system under study and on the computational cost. Here we shall review the variational approach only. The use of SCF-MI orbitals, where each

orbital belongs by construction to just one fragment, gives to the method extra physical insight. The *variational* procedure ends up by being a specialisation of the Independent Electron Pair Approximation (IEPA), in the framework of the SCF-MI strategy. Finally, the optimised virtual orbitals are employed to generate a MO-VB wavefunction consisting of all the localised single and double excitations involving the valence space: the configuration mixing of the multistructure wavefunction incorporates the coupling of the separately optimised configurations corresponding to each double excitation. The final estimate of the energy, as well as the wavefunction itself, is thus BSSE free. As the orbital pairs are optimal to provide an estimate of intermolecular correlation effects, the overall procedure can be viewed as a variational coupled-electron pair approach to the intermolecular interaction calculation in the framework of the VB theory.

It can be questioned whether the SCF-MI and the MO-VB approaches are able to take into consideration the possibility of a charge transfer. Considering a two-fragment system, with the basis functions of A and B kept strictly partitioned, there is the justifiable concern as to whether the electrons of one fragment can delocalize over the other. However, thanks to the tails of the functions centred on fragment A which extend into the space of fragment B, and vice versa, it is to be expected that, due to the non-orthogonality of the MO's of the different fragments, electronic transfer will not be strictly forbidden. Bader analysis has confirmed this, demonstrating that, even in unfavourable cases, the computed total charge located on A and B is of the same order of magnitude for both standard supermolecular SCF and SCF-MI wavefunctions [11].

In the following sections, the generalisation to an arbitrary number of interacting systems is outlined for the SCF-MI and the MO-VB theories and very recent extensions to reach saturation of the optimal virtual space are discussed. Several applications on large hydrogen bonded complexes and van der Waals systems, including explorative calculations on the helium dimer are then presented. In particular, the results for various DNA basis pairs and their complexes with various mono and divalent metal cations (H^+, Na^+, K^+, free and hydrated Mg^{++}, Ca^{++} and *cis*-$Pt(NH_3)_2$) and with solvating water molecules are reported. As an example of the use of the SCF-MI approach to the study of solvation problems and clustering processes, the calculations on lithium and potassium cations coordinated by ammonia molecules are described. We also comment on calculations for various simple H-bonded complexes such as water and hydrogen fluoride dimer, and the molecular dynamics simulation of water at several conditions, and a study of the He-CH_4 van der Waals complex.

2. THEORY

2.1. The SCF-MI wavefunction

In this section, a brief introduction to the most relevant elements of the SCF-MI theory is reported; for a more detailed account of the method see Ref. 8.

A supersystem of K closed shell interacting fragments $a_1 \ldots a_K$ containing $2N$ electrons ($N=N_1+N_2+\ldots+N_K$) is described by the one determinant SCF-MI wave function

$$\Psi(1\ldots 2N) = \mathbf{A}\left[\varphi_{1,1}(1)\overline{\varphi}_{1,1}(2)\ldots\varphi_{K,N_K}(2N-1)\overline{\varphi}_{K,N_K}(2N)\right] \tag{1}$$

where $\mathbf{A}$ is the total antisymmetrizer operator. The method is based on the partitioning of the total basis set

$$\chi = (\chi_1 \mid \chi_2 \mid \ldots \chi_K) \tag{2}$$

where $M=M_1+\ldots+M_K$ is the basis set size. Accordingly, the N_k doubly occupied molecular orbitals of the fragment k, $\varphi_k = \left(\varphi_{k,1}\ldots\varphi_{k,N_k}\right)$,

$$\varphi_k = \chi_k \, \mathbf{T}_k \tag{3}$$

are expanded in the set $\chi_k = \left(\chi_{k,1}\ldots\chi_{k,M_k}\right)$, where $\mathbf{T}_k$ is an $M_k \times N_k$ matrix and M_k is the number of basis orbitals centred on the fragment k. The total ($M \times N$) matrix of the partitioned molecular orbital coefficients $\mathbf{T}$, defined as

$$\varphi = (\varphi_1 \mid \varphi_2 \mid \ldots \varphi_K); \quad \varphi = \chi \, \mathbf{T} \tag{4}$$

has a block diagonal form
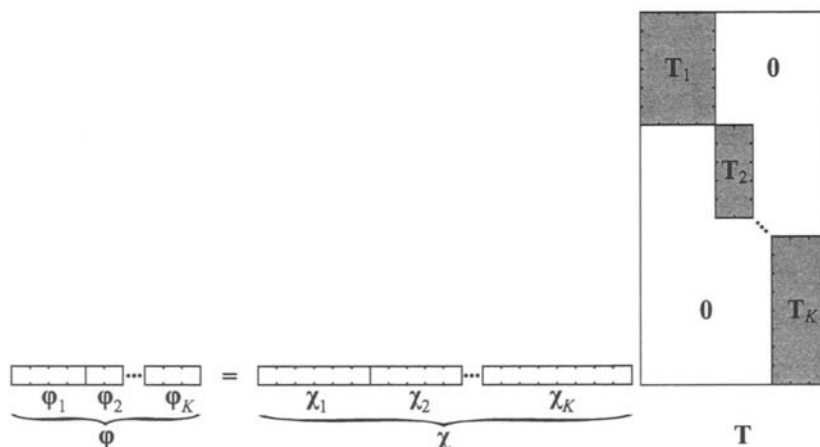
By using symmetric Löwdin orthonormaliazation we can define the new matrix $\underline{\mathbf{T}} = \mathbf{T}\left(\mathbf{T}^\dagger \mathbf{S}\mathbf{T}\right)^{-\frac{1}{2}}$ that is apt for the construction of the correct density matrix $\mathbf{D}$ (the Schmidt method could also be used) that can be easily calculated as

$$D = \underline{T}\,\underline{T}^\dagger = T\left(T^\dagger ST\right)^{-1}T^\dagger \tag{5}$$

satisfying the general idempotency condition ($\mathbf{DSD} = \mathbf{D}$).

As a consequence, the total energy of the SCF-MI wavefunction, Eq. (1),

$$E = Tr[\mathbf{D}\cdot\mathbf{h}] + Tr[\mathbf{D}\cdot\mathbf{F}(\mathbf{D})] \tag{6}$$

can be written in term of the usual Fock ($\mathbf{F}$) and one-electron integral ($\mathbf{h}$) matrices expressed in the atomic orbitals basis set; the density matrix $\mathbf{D}$, is as defined above.

The BSSE is avoided by assuming, and then maintaining, the orbital coefficient variation matrix in a block diagonal form. The stationary condition $\delta E = 0$ is equivalent to K secular problems

$$\begin{cases} \mathbf{F}_k^{'}\mathbf{T}_k^{'} = \mathbf{S}_k^{'}\mathbf{T}_k^{'}\mathbf{L}_k \\ \mathbf{T}_k^{'\dagger}\mathbf{S}_k^{'}\mathbf{T}_k^{'} = \mathbf{1}^{N_k} \end{cases} \tag{7}$$

in terms of effective Fock and overlap matrixes $\mathbf{F}_k^{'}$ and $\mathbf{S}_k^{'}$. These matrices are Hermitian and possess the correct asymptotic behaviour: in the limit of infinite separation of the fragments, $\mathbf{F}_k^{'}$ and $\mathbf{S}_k^{'}$ become the Fock and overlap matrices of the individual systems.

The SCF-MI binding energy can be expressed as

$$\Delta E_{SCF-MI} = E_{SCF-MI} - \sum_{k=1}^{K} E_{SCF}^k \tag{8}$$

taking naturally into account geometry relaxation effects. The validity of the method extends from the long range to the region of the minimum and of short distances.

Following the scheme proposed by Gerratt and Mills [12], see also Pulay [13] and Yamaguchi et al. [14], the calculation of first and second derivatives was implemented [8b] and inserted into the GAMESS-US package [9].

As usually, first derivatives can be written in the AO basis $\{\chi_k\}_{k=1}^M$ as:

$$\frac{\partial E_{elec}}{\partial a} = 2\sum_{\mu\upsilon}^M D_{\mu\upsilon}\frac{\partial h_{\mu\upsilon}}{\partial a} + \sum_{\mu\upsilon\rho\sigma}^M \{2 D_{\mu\upsilon} D_{\rho\sigma} - D_{\mu\rho} D_{\upsilon\sigma}\}\frac{\partial (\mu\upsilon|\rho\sigma)}{\partial a} - 2\sum_{\mu\upsilon}^M W_{\mu\upsilon}\frac{\partial S_{\mu\upsilon}}{\partial a} \qquad (9)$$

where "a" stands for a nuclear coordinate, $\mathbf{W}$ is a symmetric Lagrangian matrix defined as

$$W_{\mu\upsilon} = \sum_{i=1}^N T'_{\mu i} T'_{\upsilon i}\, \varepsilon_i \qquad (10)$$

and $\mathbf{T'}$ and ε are the eigenvectors and eigenvalues of the Fock matrix in the basis of the φ orbitals defined in Eq (4).

Level shifting [15] and DIIS [16] techniques have been adopted to increase convergence performance [17]. The SCF-MI option is also incorporated in the particularly efficient PC GAMESS version [18] of the GAMESS-US quantum chemistry package.

2.2. The MO-VB wavefunction

The MO-VB wavefunction [10] is a non-orthogonal CI expansion resulting from single and double excitations from the SCF-MI determinant into a set of *optimal virtual* orbitals. In order to avoid BSSE, the optimal virtual orbitals are also generated within the SCF-MI strategy by a procedure which closely resembles the IEPA approach. The validity of the method extends from the long range to the region of the minimum and of short distances. The resulting wavefunction is also size consistent.

For each pair of active occupied SCF-MI orbitals located on the fragments, a pair of virtual orbitals Φ_{a*}^A and Φ_{b*}^B is determined by minimising the variational energy corresponding to the following two-configuration wavefunction:

$$\Psi' = C_0\Psi^0 + C_{ab}\Psi_{ab}^{a*b*} \qquad (11)$$

representing the configuration interaction between the SCF-MI ground state

$$\Psi^0 = |\, \Phi_1^A\overline{\Phi}_1^A..\Phi_a^A\overline{\Phi}_a^A..\overline{\Phi}_{Na}^A\Phi_1^B\overline{\Phi}_1^B..\Phi_b^B\overline{\Phi}_b^B..\overline{\Phi}_{Nb}^B > \qquad (12a)$$

and the doubly excited configuration

$$\Psi_{ab}^{a^*b^*} = | \Phi_1^A \overline{\Phi}_1^A .. \Phi_a^A \Phi_{a*}^A .. \overline{\Phi}_{Na}^A \Phi_1^B \overline{\Phi}_1^B .. \Phi_b^B \Phi_{b*}^B .. \overline{\Phi}_{Nb}^B \Theta_{00}^4 > \tag{12b}$$

in which electrons are excited from the occupied SCF-MI orbitals Φ_a^A and Φ_b^B to the unknown virtual orbitals Φ_{a*}^A and Φ_{b*}^B, respectively.

According to the SCF-MI strategy, the virtual Φ_{a*}^A - Φ_{b*}^B orbitals are expanded in the partitioned basis set located on their own fragment:

$$\Phi_{a*}^A = \sum_{p=1}^{M_A} \chi_p^A T_{pa*}^A \qquad \Phi_{b*}^B = \sum_{q=1}^{M_B} \chi_q^B T_{qb*}^B \tag{13}$$

It follows that, if there are na and nb SCF-MI active orbitals on fragments A and B, we obtain a total of $na*nb$ optimised virtual orbitals. The spin space is described by the spin wavefunction

$$\Theta_{00}^4 = C_1 \Theta_{0,0;1}^4 + C_2 \Theta_{0,0;2}^4 \tag{14}$$

where $\Theta_{0,0;k}^4$ ($k=1,2$) are the two spin eigenfunctions corresponding to the singlet state of the four electron system.

During the optimisation, the virtual orbitals Φ_{a*}^A and Φ_{b*}^B, see Eq. (13), are left non-orthogonal.

The variational expression of the energy:

$$E = \frac{<\Psi'|H|\Psi'>}{<\Psi'|\Psi'>} = E_{CORE} + E_{CORE-VAL} \tag{15}$$

is partitioned into two terms: the first is a fixed core electron term; the second is the mixed core-valence term. Leaving the wavefunction invariant, we orthogonalize the SCF-MI virtual space to the core, while the doubly occupied core orbitals are kept orthogonal. At convergence, the core components, included in the optimised virtuals by the orthogonalization step, are deleted leaving the energy unchanged due to the double occupation of the core. This ensures that the process remains BSSE free.

To determine the virtual orbitals which minimise the variational energy (15), the derivatives with respect to the basis set expansion, see Eq. (13), and the configuration coefficients, Eq. (11) are computed. Analytic gradients and second derivatives, including mixed terms, are computed and inserted into the Newton-Raphson stabilised algorithm [19]. The detailed expression of the derivatives

have been reported in Ref 10e. The convergence and stability of the implemented algorithm are satisfactory.

The virtual orbitals are then employed to construct the set of singly- and doubly-excited configurations which provide the final MO-VB wavefunction, where the SCF-MI determinant represents the zero order state. The final wavefunction has a general Molecular Orbital-Valence Bond form:

$$\Psi = C_0 \Psi^0 + \sum_{a=1}^{Na} \sum_{b=1}^{Nb} C_{ab} \Psi_{ab}^{a^*b^*} + \sum_{a=1}^{Na} C_a \Psi_a^{a^*} + \sum_{b=1}^{Nb} C_b \Psi_b^{b^*} \tag{16}$$

The localised single vertical excitations

$$\Psi_a^{a^*} = | \Phi_1^A \overline{\Phi}_1^A .. \Phi_a^A \Phi_{a^*}^A .. \overline{\Phi}_{Na}^A \Phi_1^B \overline{\Phi}_1^B .. \Phi_b^B \overline{\Phi}_b^B .. \overline{\Phi}_{Nb}^B \Theta_{0,0;1}^2 >$$

$$\tag{17}$$

$$\Psi_b^{b^*} = | \Phi_1^A \overline{\Phi}_1^A .. \Phi_a^A \overline{\Phi}_a^A .. \overline{\Phi}_{Na}^A \Phi_1^B \overline{\Phi}_1^B .. \Phi_b^B \Phi_{b^*}^B .. \overline{\Phi}_{Nb}^B \Theta_{0,0;1}^2 >$$

are included to relax the occupied SCF-MI orbitals, which were kept fixed during the determination of optimal virtuals. The energy of such a wavefunction is calculated by solving the corresponding secular problem, which includes the determination of the Hamiltonian and overlap matrixes between non-orthogonal VB structures by means of standard VB techniques [20]. The wavefunction remains size consistent and asymptotically converges to the SCF wavefunctions of the two subsystems.

The configurations included can be therefore directly associated to specific energy contributions: Coulomb-exchange, polarisation or induction (Ψ^0), extra polarisation ($\Psi_a^{a^*}$ and $\Psi_b^{b^*}$) and dispersion ($\Psi_{ab}^{a^*b^*}$).

The MO-VB dimerisation energy is calculated as

$$\Delta E_{VB} = E_{VB}^{AB} - E_{SCF}^A - E_{SCF}^B \tag{18}$$

and takes account of the geometry relaxation effects.

The accuracy of the MO-VB wavefunction is expected to be close to that of a full SD-CI wavefunction involving excitations to the full virtual spaces of each monomer (vertical excitations). Very recently, a new version of the MO-VB optimization scheme has been developed that is apt to guarantee that the wavefunction approaches as close as possible the full SD-CI limit, via saturation of the optimal virtual space. Explorative calculations on the very challenging helium dimer system are encouraging.

2.3. Extension of the MO-VB scheme: saturation of the optimal virtual space

Once the first pair of optimal virtuals Φ_{a*}^A and Φ_{b*}^B is determined, a new optimal pair , say Φ_{a**}^A and Φ_{b**}^B, is optimised by expanding it in the orthogonal complement space to the previously determined pair.

The whole procedure can be repeated n times generating - for each pair of occupied orbitals - n optimised virtual orbital pairs, whose contribution to the interaction energy is strictly decreasing up to saturation of the space, i.e. up to the full use of the SCF-MI virtual orbital space. Consistent with the employed basis set, the final MO-VB wavefunction (16) can be so improved to the desired degree of accuracy.

3. EXAMPLES OF APPLICATIONS

In the present section, several applications of SCF-MI and MO-VB approaches are presented and discussed. Most calculations were performed with the SCF-MI procedure we implemented in the GAMESS-US package [9]. This version of the code can perform conventional and direct energy calculations, analytic gradients, numerical Hessian evaluation and geometry optimisation; vibrational analysis is also available. The increase in complication and computation time with respect to standard SCF algorithms is minimal. The SCF-MI option is also incorporated in the particularly efficient PC GAMESS version [18] of the GAMESS-US quantum chemistry package. The MO-VB calculations reported here have been carried out employing the programs described in Refs. 10d and 10e.

3.1. Large Van der Waals molecules of biological interest

The *performance* of the SCF-MI procedure was tested on large van der Waals systems, such as clusters of biological interest. In particular, DNA base pairing also in the presence of different interacting charged and neutral species was analysed.

The structure of the DNA molecule is basically determined by nucleic acid base interactions. Although the three-dimensional double helix structure of DNA is influenced by various contributions, the hydrogen bonding in DNA base pairs is of particuar importance. Because it is difficult to obtain gas phase experimental data for isolated base pair characterisation (only a limited number of experimental studies are available [21]) quantum chemical calculations can represent a useful tool to obtain reference data on the structure, properties and interactions of nucleic acid pairs. Theoretical studies can help us to understand the properties of nucleic acids and they are fundamental for verification

(validation) and parameterisation of empirical potentials for molecular modelling of larger biomacromolecules, and of interactions between them.

The presence of ions not only affects canonical base pairs [22], but promotes the formation of triplexes and other non-canonical DNA structures [23]. The effects of these interactions span from modifications of the renaturation kinetics of thermally denatured DNA [24] to the known anti-tumoral and mutagenic activity of cisplatin [25].

The complete description of hydrogen bond and van der Waals interactions requires of course the inclusion of electron correlation effects; however, almost always, a very useful starting point for subsequent refinements is represented by a Hartree-Fock description, which serves as the basis for both perturbation theory and variational configuration interaction approaches to the treatment of electron correlation.

For systems of this size, the SCF-MI method is particularly advantageous, as a standard SCF supermolecule CP-corrected approach requires five single point energy evaluations, if geometry relaxation effects are to be included [6, 26]. As will be showed in the following, the SCF-MI algorithm turned out to be particularly efficient: one of the main results was that a small basis set, such as the 3-21G basis, could provide structural and energetic results comparable to those obtained by much more expensive standard SCF/6-31G** CP-corrected calculations.

A number of systematic and accurate studies were accomplished on the H-bonding of DNA bases [27]; for these systems the paper by Sponer, Leszczynski and Hobza [28] represents the most extended benchmark study and it was used for comparison.

Our calculations [11b] were carried out on base pairs made up from several possible combinations of the neutral major tautomers of adenine (A), cytosine (C), guanine (G), thymine (T) and uracil (U) bases. The structures were fully optimised using 3-21G standard basis set. Table 1 reports the corresponding SCF-MI interaction energies and the geometrical parameters characterising the hydrogen bonds formed in the different pairs. These data are compared with the structures optimised at the SCF 6-31G** or 6-31G* levels (CP corrected with deformation terms). SCF-MI interaction energies and structures agree very well with the literature results [28,29] for all the systems considered.

Table 1

Optimised base pairs intermolecular geometrical parameters (distances in Å / angles in degrees) and interaction energies (kcal/mol)

Base pairs	H-bonds	SCF-MI [11b] 3-21G	Ref. 28 6-31G**	ΔE_{SCF-MI} [11b] 3-21G	Ref. 28 6-31G**
GCWC	N2(H)...O2'	2.97/171.9	3.02/178.1	-22.5	-23.4
	N1(H)...N3'	3.04/173.8	3.04/176.1		
	O6...(H)N4'	2.94/172.4	2.92/177.0		
ATWC	N6(H)...O4'	3.09/170.2	3.09/172.0	-9.5	-9.6
	N3'(H)...N1'	3.01/176.7	2.99/178.8		
CC	N3...(H)N4'	3.05/174.2	3.05/173.2	-15.6	-15.9
	N4(H)...N3'	3.05/174.2	3.05/173.2		
GCH	N1'(H)...O2	2.83/177.2	2.82/175.0	-19.1	-20.6
	O6'...(H)N1	2.95/170.1	2.92/179.0		
AA	N6(H)...N1'	3.14/179.1	3.16/179.4	-8	-8.1
	N1...(H)N6'	3.14/179.2	3.16/179.4		
GG	N1(H) ...O6'	2.87/177.7	2.87/178.1	-20.7	-22.5
	O6 ...(H)N1'	2.90/177.7	2.87/178.1		
AUWC	N6(H)...O4'	3.09/170.2	3.08/172.9(a)	-9.5	-10.2(a)
	N3'(H)...N1'	3.01/176.7	3.00/178.4(a)		
TT	O2'...(H)N3	2.95/159.1	2.98/166.2	-8.9	-8.5
	O2...(H)N3'	2.96/158.8	2.98/166.6		
AG	O6'...(H)N6	2.95/175.2	2.95/179.9	-10.7	-11.5
	N1...(H)N1'	3.19/176.4	3.19/179.3		
TAH	O4'...(H)N6	3.11/171.8	3.14/170.1	-9.5	-10.2
	N3'(H)...N7	2.96/176.5	2.95/175.6		

(a) From Ref. 29.
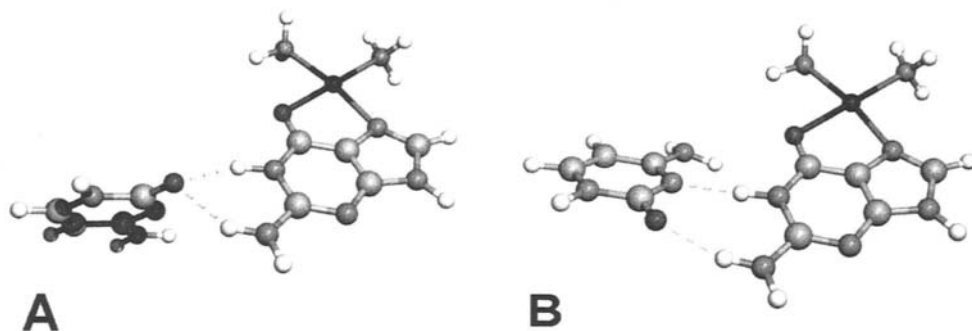
Fig. 1: The two SCF-MI optimised structures of the cis-[Pt(NH$_3$)$_2$GC]$^{2+}$ complex: cisplatin-1 (A) and cisplatin-2 (B). Broken lines represent hydrogen bond bridges.

Such good performance of the SCF-MI method was also highlighted in a study of the coordination of *cis*-[Pt(NH$_3$)$_2$]$^{2+}$ (cisplatin) to the N7 and O6 sites of guanine in the CG base pair [30]. The results (confirmed also by SCF, DFT and MP2 calculations) showed that the coordination of cisplatin causes significant changes in the interaction between guanine and cytosine compared to the Watson-Crick (WC) H-bonding pattern. In particular DFT, MP2 and SCF-MI geometry optimisations agree in finding two conformations that are both characterised by the breaking of the N4'-H-O6 H-bond and by a substantial non-planarity of the base pair (see Fig. 1). In the first structure (cisplatin-1), there is an evident "opening" of the base pair, held together only by a bifurcated hydrogen bond; in the latter (cisplatin-2) the relative position of guanine and cytosine is closer to the standard WC structure. It is to be emphasised that standard SCF fails to find a minimum for the cisplatin-2 conformation.

The structures and energetics of other complexes between GCWC base pairs and various Ia and IIa group cations were also investigated. In particular the N7 and/or O6 coordination of H$^+$, Na$^+$, K$^+$, Mg^{++} and Ca^{++} was analysed, showing that these cations can also generate non-WC hydrogen bonding patterns [31]. As an example, the coordination of guanine by a magnesium cation generated two distorted conformations of the pair, characterised by essentially the same binding energy (43.14 and 43.12 kcal/mol). The first of these is almost identical to the cisplatin-1 complex with the bifurcated hydrogen bond. The other structure is characterised by the same hydrogen bond pattern but with the bases retaining a coplanar arrangement (Fig. 2). These conformations persisted also when considering the effect of cation hydration by four or five water molecules, even if water-induced softening of the cation altered significantly the energetics of the system [32].

The SCF-MI method was also employed to study the influence of hydration on the WC cytosine-guanine base pair, investigating the ability to reproduce the hydration pattern present in the real system (the base pair in the DNA framework) [33]. The calculated water positions around the base pair were compared to those predicted by a knowledge-based approach employing crystallographic data [34]. The correspondence between averaged crystallographic data and our "isolated" system (Fig. 3) corroborated the hypothesis that the hydration pattern of bases in B-DNA strongly depends on the chemical nature of the bases themselves and not as much on the environment [34]. It was also shown that the saturation of the first hydration shell results in a negligible variation of the pair conformation. Despite this, the hydration causes more than 4 kcal/mol enhancement in the CG binding energy, emphasising the important role of the surrounding water in base pair matching and mismatching.
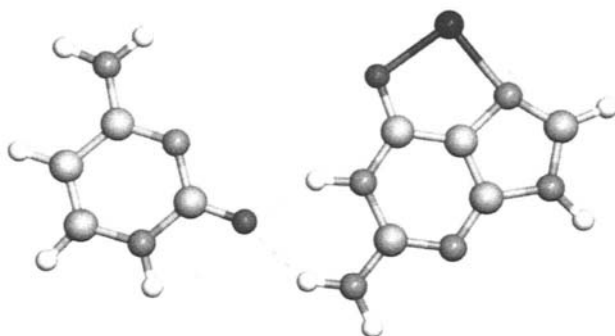
Fig. 2. The structure of the planar CG-Mg^{++} complex. Broken lines represent hydrogen bond bridges.
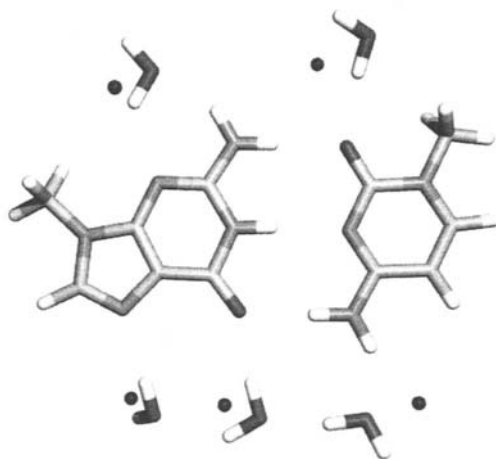
Fig. 3. SCF-MI optimised structure of the penta-hydrated CG pair with methylated bases. Dark circles represent average crystallographic hydration sites in B-DNA.

3.2. The structure of lithium and potassium cations coordinated by ammonia molecules

In order to characterise ion solvation processes, gas phase studies can be performed providing detailed information about individual interactions. These studies can explore changes in some properties between the complexes in the gas phase and the solvated systems in the liquid phase. Theoretical methods can thus provide valuable complementary information not accessible to experimental approaches, both in the characterization of the complexes and in the specific mechanism of the relevant interactions.

Since the first preparation of potassium-ammonia solution (Sir Humphrey Davy, in 1808) alkali metal–ammonia solutions have been at the centre of much theoretical and experimental interest. Novel properties include low density, high electrical conductivity, liquid–liquid phase separation, and a concentration driven metal–nonmetal transition [35].

The structure of Li and K ammonia solution has been recently studied by neutron diffraction experiments [36]. The results show, for saturated lithium–ammonia solutions, that the cation is tetrahedrally solvated by ammonia molecules. On the other hand, from the data of the microscopic structure of potassium–ammonia solutions, the potassium is found to be octahedrally coordinated with ammonia molecules. The Li^+ is a "structure making" ion and K^+ is a "structure breaking" ion in alkali metal–ammonia solutions [37, 38].

We report our results on the $[Li(NH_3)_n]^+$ and $[K(NH_3)_n]^+$ (n=1-6) clusters. Stability and structure of $[Li(NH_3)_n]^+$ and $[K(NH_3)_n]^+$ clusters have been

investigated by the SCF-MI method, ensuring BSSE-free optimizations. The standard 6-31+G* basis set was adopted.

3.2.1. Optimized structures for the $[K(NH_3)_n]^+$ and $[Li(NH_3)_n]^+$ clusters

As can be seen in Figs. 4-8, the ammonia molecules surround the central ion to form the so-called "interior" structures [39]. The molecules are orientated so that the nitrogen atom lone pair faces the cation, as expected from the positive charge of the ion and the electronegative character of nitrogen. The dipole moment of ammonia pointing towards the positive charge of the ion, favours charge-dipole interaction, which is the main contribution to the interaction. The $[K(NH_3)_2]^+$ complex possesses a linear structure, i.e. it exhibits a linear N-K-N atom sequence. In the cluster with $n=3$, the solvent molecules lie symmetrically around the central cation; this is an almost planar structure, where the three nitrogen atoms form an equilateral triangle. The $[K(NH_3)_4]^+$ complex is tetrahedral, with the hydrogens as far apart as possible (see Fig. 4). The cluster with $n=5$ adopts a bipyramidal conformation (see Fig. 5) and that with $n=6$ an octahedral one (see Fig. 6): no hydrogen bonds are formed in the clusters. The variation of Löwdin atomic charge of K^+ with the number of ammonia molecules in the cluster shows that the cation possesses a smaller charge in the cluster than in isolation, and that a part of the charge is transferred from the NH_3 molecules, to an extent that increases with the increasing size of the cluster.
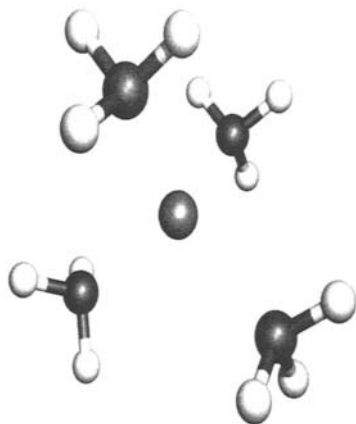
Fig. 4. Lowest energy SCF-MI optimized structure of the tetrahedral complex of the K^+ or Li^+ cations with four ammonia molecules
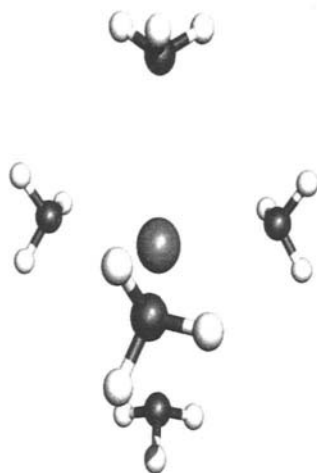
Fig. 5. Lowest energy SCF-MI optimized structure of the bipyramidal complex of the K^+ cation with five ammonia molecules
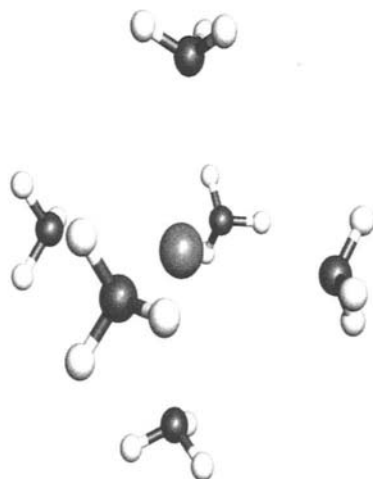
Fig. 6. Lowest energy SCF-MI optimized structure of the octahedral complex of the K^+ cation with six ammonia molecules

Because the ionic radius of Li^+ is smaller than that of K^+, the Li^+ cation allows solvent molecules to come closer to it. In addition because of its smaller size, Li^+ is able to accommodate fewer ammonia molecules in its first coordination shell.
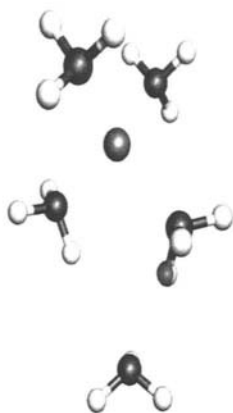
Fig. 7. Lowest energy SCF-MI optimized structure of the complex of the Li$^+$ cation with five ammonia molecules

Fig. 8. Lowest energy SCF-MI optimized structure of the complex of the Li$^+$ cation with six ammonia molecules

The complexes with $n=5$ and $n=6$ exhibit marked differences from the corresponding K$^+$ systems with the fifth and sixth molecules located in the second coordination shell forming bifurcated H-bonds with the first solvation sphere (as shown in Figs. 7 and 8).

From the computed Löwdin charge of Li$^+$ for clusters of different sizes, it follows that Li$^+$ complexes behave as K$^+$ complexes, but a greater amount of charge is transferred in this case.

3.2.2. Interaction energy of [K(NH₃)ₙ]⁺ and [Li(NH₃)ₙ]⁺ clusters

The interaction energy increases as the size of the cluster grows. In order to examine the variation of the interaction energy in the process of formation of the clusters, the difference between the energy in the clusters containing n and n-1 ligands was plotted against n (see Fig. 9).

As can be seen, the magnitude of the stabilising effect of each new molecule in the cluster diminishes with increasing n. Consequently, while the total binding energy of the complex increases as further molecules are incorporated into the cluster, the interaction of each successive ammonia molecule with the ion gradually weakens, as one would expect.

It is evident that for [Li(NH₃)ₙ]⁺ clusters the interaction energies are much greater than those obtained for the K$^+$ complexes, consistent with the smaller size of the Li$^+$ ion, which establishes stronger interactions with the ligands.
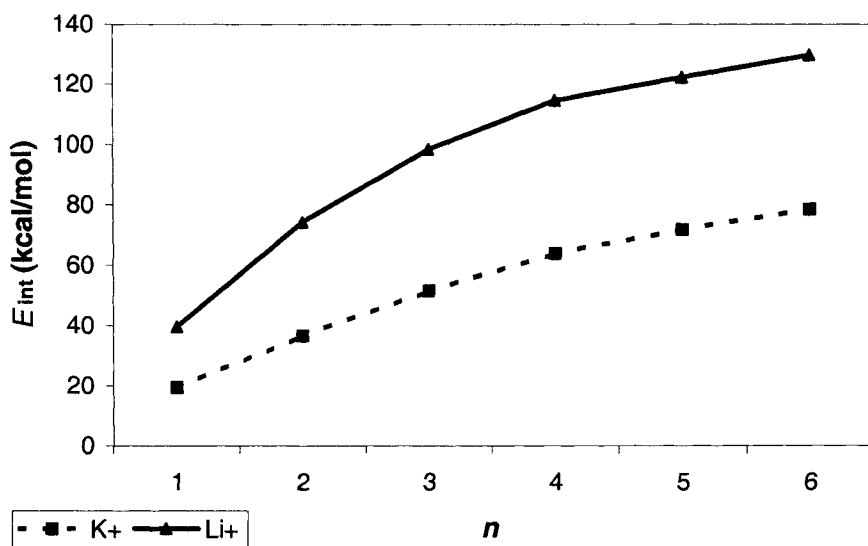
Fig. 9. Variation of SCF-MI interaction energies (E_{int}) with the number of complexing ammonia molecules (n).
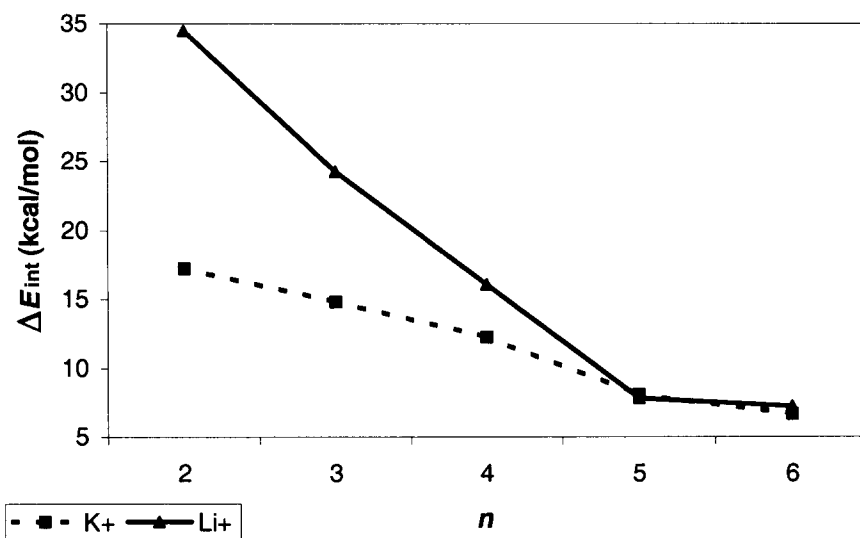
Fig. 10. Changes (ΔE_{int}) in the SCF-MI interaction energy of the systems upon addition of successive solvent molecules.

Fig. 10 shows changes in interaction energy caused by the incorporation of successive ammonia molecules.

For the $[Li(NH_3)_5]^+$ cluster, the stabilisation gained in forming the bipyramidal complex is smaller than that for the structure on which one molecule is placed out of the first solvation shell. In principle, the fifth molecule, which cannot interact directly with the ion, should have a considerably less marked stabilizing effect. However, because the molecules in the coordination shell are strongly polarized and distorted by the ion, the hydrogen-bonding with the outer molecule is stronger.

3.3. The water dimer system

3.3.1. The calculation of the PES

The PES of the water dimer system is characterised by three main stationary points: the "quasi-linear" structure, representing the global minimum (Fig. 11), and the cyclic and bifurcated configurations (saddle points).
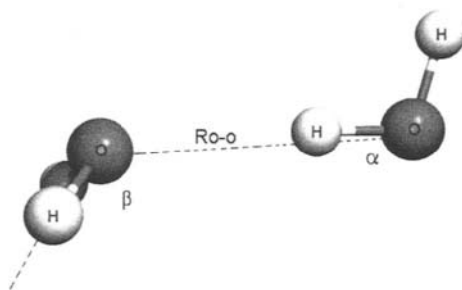
Fig. 11: Transilinear C_s minimum energy geometry of the water dimer system. The relevant intermolecular coordinates are indicated.

To achieve a balanced description of the complex and the of separated fragments, we have augmented the 7s4p2d/4s2p basis set proposed by Millot and Stone [40] as used in our previous calculations [10d], by adding optimised diffuse polarisation functions: f and g functions on oxygen atoms and d and f on the hydrogens. The final basis set provides a monomer energy close to the Hartree-Fock limit and reproduces well the optimal SCF-MI energetic and geometric parameters obtained in our previous calculations employing a large basis set of 548 even tempered functions [10a].

In the MO-VB step, we consider an active space of four MOs, leaving the oxygen $1s^2$ electrons frozen. The resulting dimension of the virtual space of each fragment is 16, implying a set of 32 singly and 256 doubly vertical excited spatial configurations. The final MO-VB wavefunction consists of 289 configurations and, by taking the spin space into account, the size of the MO-VB matrix is 545.

The geometries are initially optimised at the SCF-MI level by gradient techniques. The C_s global minimum (see Fig. 11) was studied thoroughly via additional point-by-point minimisation at the MO-VB level, varying the oxygen-oxygen distance R_{O-O} and the two angles α and β. The OH bonds of the donor monomer were also optimised. The predicted equilibrium geometry, corresponding to R_{O-O} =2.954 Å, β = 134.5° and α= 2.5°, turns out to be in very good agreement with experimental values corrected for anharmonicity effects. As expected, the inclusion of correlation shortens the intermolecular separation. The R_{O-O} distance compares very well with the MP2 value reported by van Duijneveldt-van de Rijdt and van Duijneveldt [41] and with the SAPT result due to Mas and Szalewicz [42].

Table 2

Optimised MO-VB geometrical parameters for the C_s global minimum of the water dimer system (see Fig. 11) compared with some values reported in the literature.

	MO-VB	Exp.[a]	SAPT[b]	MP4[c]	MP2[d]
R_{O-O}(Å)	2.954	2.946[e]/2.952[f]	2.953	2.949	2.978
β°	134.5	122.0±10	124	124.8	134.6
Φ°	2.5	0.0±10	6.8	5.35	5.7

(a) Refs. 49 and 50.
(b) Ref. 45
(c) Ref. 42.
(d) Ref. 51
(e) After correction for the anharmonicity Ref. 50.
(f) After correction for the anharmonicity Ref. 42.

The harmonic vibrational frequency of the OH donor is 4001 cm^{-1}, in agreement with calculated values reported in the literature [43]; by including the usual scale factor of 0.89 [9], the resulting frequency is 3561 cm^{-1}, to be compared with the experimental value of 3601±11 cm^{-1} [44].

The binding energy of the global minimum, obtained by means of our largest basis set, is -5.02 kcal/mol. Using zero-point vibrational and thermal energies based on *ab initio* calculations, experimental binding energies of -5.44±0.7 kcal/mol or 5.2±0.7 kcal/mol have been obtained [45-48]. By employing the most recent estimate for thermal contributions, our predicted enthalpy becomes -3.22 kcal/mol, well inside the experiment range (-3.59±0.5 kcal/mol [46-48]).

The interaction energies and the geometrical parameters corresponding to the minimum are reported in Table 2. The results are in accordance also with very recent calculations [52].

3.3.2. Molecular dynamics simulation of water at critical and supercritical conditions

A preliminary molecular dynamics simulation was performed. To this end, SCF-MI and MO-VB calculations were carried out on water dimers and trimers and a new parameterisation of a NCC-like (Niesar-Corongiu-Clementi) [53] potential was accomplished [10d]. The 7s4p2d/4s2p small basis set proposed by Millot and Stone [40] was employed. The Hartree Fock limit results obtained in our previous work were reproduced using this compact basis set; also equilibrium geometry and binding energy values compared well with the experimental results.

By fitting the MO-VB *ab initio* results, the parameters of a new NCC-like potential have been determined. The *ab initio* MO-VB calculations include the determination of the interaction energy relative to 225 configurations of the

water dimer and of the non-additive three-body contributions relative to 28 trimer configurations. By taking into account that the main contribution to the three-body non-additive terms derives from induction effects, such contributions have been determined at the SCF-MI level.

The molecular dynamics simulation was performed using the MOTECC suite of programs [54] in the context of a microcanonical statistical ensemble. The system considered is a cube, with periodic boundary conditions, which contains 343 water molecules. The molecular dynamic simulation of water performed at ambient conditions revealed good agreement with experimental measurements. The main contribution to the total potential energy comes from the two-body term, while the many-body polarisation term contribution amounts to 23% of the total potential energy. Some of the properties calculated during the simulation are reported in Table 3.

Although still incompatible with the experimental data, the computed internal pressure is greatly improved with respect to previously published simulation results [54-56]. The variation of the computed pressure with or without inclusion of many body polarisation terms (553±131 and 724±156 atm) can be assumed to be an improvement when comparing it with the corresponding values (7900 and -2160±364 atm) [55, 56] computed using the same simulation procedure but different quantum mechanical energy values. The calculated geometry of the water molecule in liquid and gas phase, and the correlation functions $g_{OO}(r)$, $g_{OH}(r)$ and $g_{HH}(r)$, were also in good agreement with the experimental data.

The number of first "neighbours" around a central water molecule, calculated by integrating the correlation function $g_{OO}(r)$ up to the position of the first minimum, was 5.5, consistent with a local tetrahedron (with addition of contributions from some interstitial coordination).

Table 3
Properties of water at ambient conditions.

	ΔU (kJ/mol)	Pressure (atm)	μ (D)	ε	C_V (cal/molK)
two body only (a)	-38.89±0.21	553±131	-	-	18.7
complete (a)	-40.56±0.22	724±156	2.48±0.01	54±10	22.2
MCYL (b)	-35.40±0.6	7900	2.259	26±14	26.5
NCC-flex (c)	-44.88±0.25	-2160±364	3.08	-	17.6
Experiment	-41.5 (d)	~1	2.4-2.6	80	17.9 (e)

(a) Ref. 10c.
(b) Ref. 55.
(c) Ref. 56.
(d) Ref. 57.
(e) Ref. 58.

By integrating $g_{OH}(r)$ up to the first minimum, a value of 1.92 was obtained. This means that each water molecule can form 3.84 hydrogen bonds with its first neighbours, a result compatible with a local structure of water at room temperature of four nearest molecules oriented in a tetrahedron configuration.

As expected, comparisons between the simulations carried out with or without inclusion of the many-body term showed equivalent results for most of the calculated properties of the liquid phase: the many-body contributions played a fundamental role only in determining the position of the second peak of the site-site pair correlation function $g_{OO}(r)$, so as to producee a better agreement with experiment.

Figs. 12, 13 and 14 show the correlation functions $g_{OO}(r)$, $g_{OH}(r)$ and $g_{HH}(r)$ at four different points on the phase diagram, as reported in Table 4 together with the values of the total potential energy and of the molecular dipole moment predicted by the simulations.
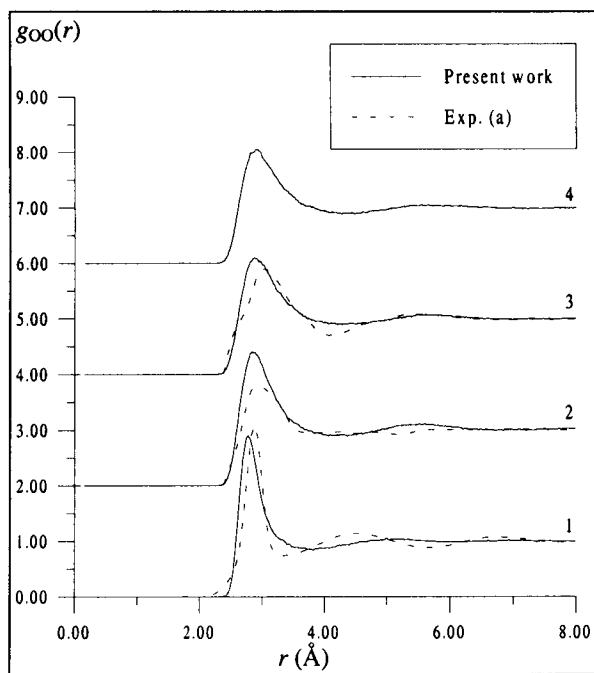
Fig. 12: Calculated (solid line) site-site $g_{OO}(r)$, pair correlation function of water (many body contribution included) in comparison with the corresponding experimental (dashed line) data. The ordinate scale refers to Run 1. Each of the remaining plots have been shifted upwards by an arbitrary unit. (a) Ref. 59.
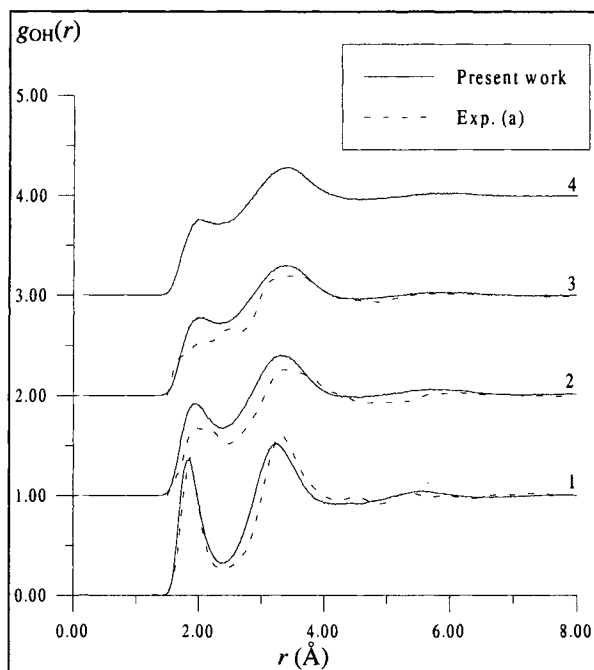
Fig. 13. Calculated (solid line) site-site $g_{OH}(r)$, pair correlation function of water (many body contribution included) in comparison with the corresponding experimental (dashed line) data. The ordinate scale refers to Run 1. Each of the remaining plots have been shifted upwards by an arbitrary unit. (a) Ref.59.

As can be seen from Fig. 13, the first peak of the $g_{OH}(r)$ correlation function broadens and shifts to longer distances, while the first minimum rises on approaching the critical conditions. In the supercritical state, represented in plot 3, a sharp decrease in the intensity of the first peak can be observed. Although it does not correspond exactly to a complete collapse of the peak, such behaviour is undoubtedly in much closer qualitative accordance with the experimental findings and with the recent simulations performed by Chialvo and Cummings [60] by means of a properly modified model potential.

Table 4
Dynamic simulation results at several conditions (see Refs. 7c and 7d).

Run label	T (K)	ρ (g/cm^3)	ΔU (kJ/mol)	ΔU_{exp} (kJ/mol)	μ(D)	μ_{exp} (D)
Run 1	298	0.998	-40.56±0.22	-41.5	2.48±0.01	2.4-2.6
Run 2	573	0.71796	-22.43±0.39	-22.2	2.29±0.01	
Run 3	673	0.66112	-15.87±0.45		2.22±0.01	
Run 4	730	0.64	-13.95±0.50		2.21±0.01	
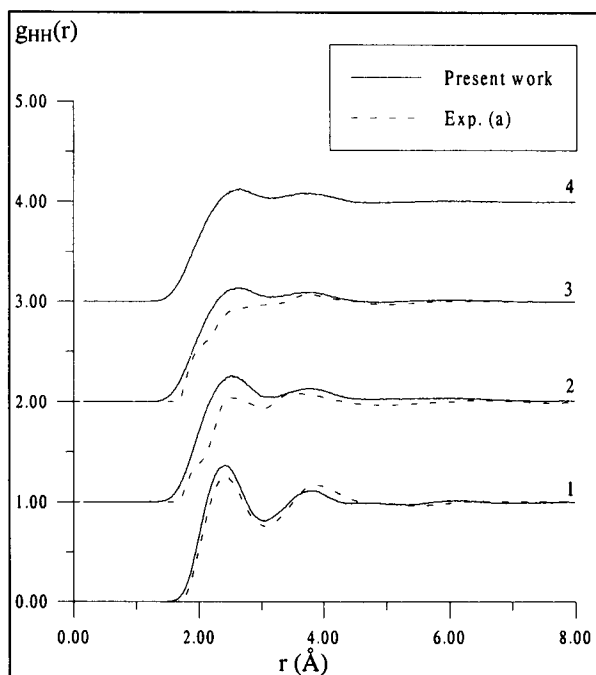
Fig. 14. Calculated (solid line) site-site $g_{HH}(r)$, pair correlation function of water (many body contribution included) in comparison with the corresponding experimental (dashed line) data. The ordinate scale refers to Run 1. Each of the remaining plots have been shifted upwards by an arbitrary unit. (a) Ref. 59.

Table V shows the number of hydrogen bonds per water molecule calculated by integrating the $g_{OH}(r)$ up to the first minimum, in the conditions of the four different simulations.

Although the average number of hydrogen bonds of each water molecule is notably reduced, it is possible to draw the conclusion that the hydrogen bond network persists partially also in the supercritical state, in qualitative agreement with the interpretation of new neutron diffraction experiments [61] and also with the measurements of the proton NMR chemical shifts [62].

Table 5

Number of hydrogen bonds per molecule. See Refs. 10c and 10d.

Run label	Number of bonds
Run 1	3.84
Run 2	2.80
Run 3	2.41
Run 3(two body)	2.00
Run 4	2.30

3.4 The hydrogen fluoride system

Hydrogen fluoride dimer, like with the water dimer, is one of the most frequently studied complexes. Both extensive theoretical and experimental data are available for analysis. The PES of the hydrogen fluoride dimer (see Figs. 15 and 16), if compared with that of water, is simpler; two stationary points exist: the "quasi-linear" structure (see Fig. 15) and the cyclic structure (see Fig. 16).

The former structure corresponds to the energy minimum while the latter one is a transition structure separating two equivalent minima. The energy difference between these two points reveals important information. We have determined the relative stability of these two structures at the MO-VB level. It is to be noted that it has been reported very recently that optimization on the standard PES can yield a structure that is qualitatively wrong for this system [51]. The calculations were performed employing a large basis set of the quality 6s5p4d1f1g on F atoms and 4s3p1d on H atoms.

The stationary structures obtained are consistent with literature and experimental results. Our best estimate of the dimerisation energy for the global minimum in its quasi-linear structure (Fig. 15) from the MO-VB calculations (4.51 kcal/mol) agrees well with the experimental value (4.54 kcal/mol, Ref. 16) and with the calculated values [51].
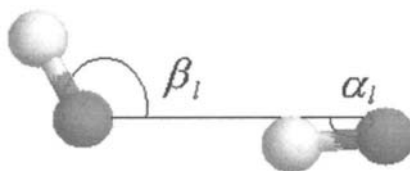
Fig. 15. The quasi-linear structure of the hydrogen fluoride dimer.
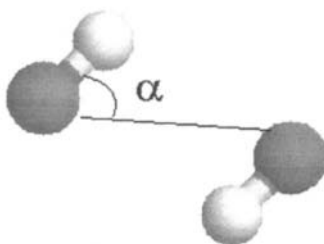
Fig. 16. The cyclic structure of the hydrogen fluoride dimer.

As regards the calculated geometry, we mention from the recent theoretical literature the study by Peterson and Dunning [64] using MP2 and CCSD(T) methods with an extended aug-cc-pVQZ basis set. MP2 and CCSD(T) intermolecular distances R were found to be 2.737 and 2.732 Å, respectively. After correcting for the BSSE, slightly larger values were found (2.753 and 2.745 Å) very close to our values. As regards the cyclic structure (Fig. 16), the calculated MO-VB results (D_E=-3.50 kcal/mol, d_{FF}=2.78 Å and α=55.2°) agree very well with recent literature results (D_E=-3.04 kcal/mol, d_{FF}=2.74 Å and α=52.9°) [51].

Work is in progress in our laboratory to provide an accurate intermolecular potential surface for molecular dynamics studies of liquid hydrogen fluoride.

3.5 The van der Waals complex He-CH$_4$

As another example, the potential surface of the He-CH$_4$ complex (studied in Ref. 10e) is described. In these calculations a basis set 7s6p3d1f1g on the C atom, 4s3p1d on the H atoms, and 8s4p2d1f on the He atom, consisting of a total 182 functions, was adopted. The s and p functions were optimised so as to reproduce energies close to the Hartree-Fock limit of the CH$_4$ molecule and He atom, respectively. The exponents of high-order polarisation functions were determined by maximising directly the dispersion contribution.

The points of the PES were chosen along three different approaches of the helium atom to the CH$_4$ molecule: face, edge and vertex approaches. The interaction energies at the SCF-MI level are all repulsive confirming that the forces are dominated by dispersion contributions. The global minimum occurs for the face approach at R= 3.6 Å θ = 180°, ϕ = 0°. The interaction energy in this geometry is -18.7 cm^{-1}. Other stationary points were found corresponding to the edge and vertex approaches with a well depths of -14.7 cm^{-1} and -12.0 cm^{-1}, respectively. The order of stability of the stationary points found by Buck *et al.* [65] is thus confirmed by the present MO-VB calculations.

A new accurate fitting of the calculated PES was realised by a Newton-Raphson procedure adopting the same potential form as used by Buck *et al.* [65]. The agreement between the MO-VB *ab initio* potential and the Buck potential, determined by direct fitting of the experimental data, is very satisfactory.

The reliability of the newly-developed rigid-rotor potential was tested by means of close-coupling calculations of rotational state-to-state integral cross sections. The MOLSCAT code was used [66]. The results were compared with those obtained using the semiempirical potential of Buck, and with the available experimental data.

Close-coupling equations were solved using the hybrid modified log-derivative / Airy propagator of Alexander and Manolopulos [67]. The agreement

of the calculated cross-sections with experimental values is good. The new potential provides a better accuracy for the low Δj transitions. For the highest Δj transitions the agreement is reduced: however, this could be ascribed to near-elastic secondary collisions in the experimental measurement or, more probably (see for example results for E symmetry where each j value remains non-degenerate up to $j = 7$), to the lack of higher anisotropic potential terms that can directly couple rotor states for high Δj transitions. In order to check the validity of this hypothesis, additional *ab initio* calculations are in progress to extract V_6 and V_8 radial coefficients.

The main difference between the new potential and that of Buck *et al.*, i.e. the depth of potential wells, cannot be verified by this 'high' energy scattering calculation; in order to provide major insights, work is in progress to compute the MO-VB PES at a higher level of theory and to calculate differential cross-sections at the lower collision energy of 275 cm^{-1} [69], where total inelastic and some state resolved differential cross sections are available [65].

3.6 The helium dimer

The study of the interactions among closed shell systems (van der Waals forces) represents a benchmark for theories of electron correlation. We report here the results of our variational MO-VB study of the interaction between two helium atoms [70]. Up to $n=10$ optimal virtuals are calculated and employed to generate MO-VB final wavefunctions of higher and higher accuracy, in the usual MO-VB form:

$$\Psi = C_0\Psi^0 + \sum_{a=1}^{n} C_a\Psi_a^{a*} + \sum_{b=1}^{n} C_b\Psi_b^{b*} + \sum_{a,b=1}^{n} C_{ab}\Psi_{ab}^{a*b*} \tag{24}$$

The energy of such wavefunctions is calculated by solving the final secular problem by means of usual standard VB techniques [20].

The calculations have been realised with the aug-cc-pv5z basis set of Dunning [71], consisting of [6s5p4d3f2g] functions on wich helium atom. The MO-VB wavefunction is built up from the SCF-MI ground state plus single and double vertical excitations arising from the direct product of atomic SCF and singly-excited configurations on the monomer. The resulting wavefunction is very compact, as the number of VB structures increases approximately with n^2. As it is shown in Fig. 17, the contributions to the interaction energy have already converged at $n=3$.
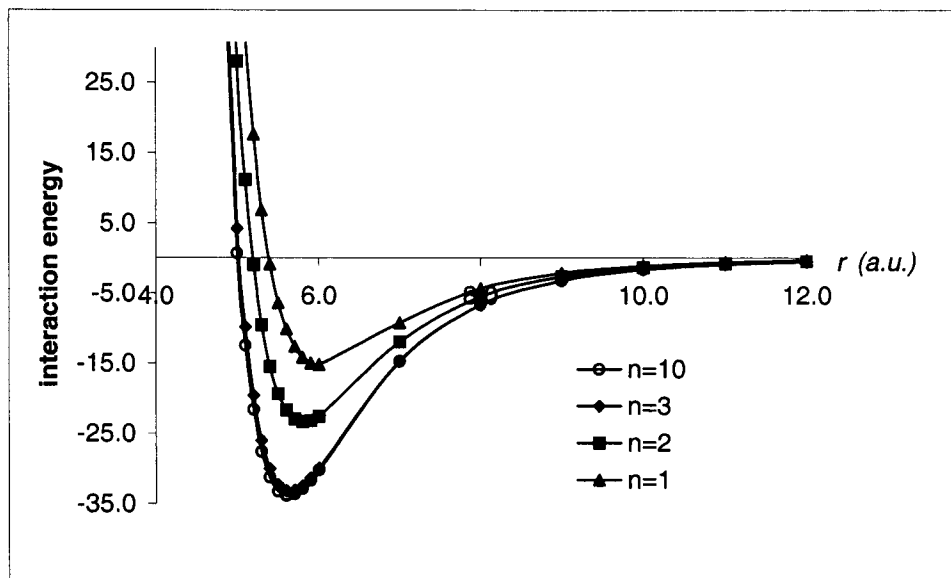
Fig. 17. The calculated MO-VB interaction potential (μE_h) for the helium dimer system.

The well depth of the interaction potential is therefore strongly dependent on the number n of virtuals included, varying from 15.2 μE_h at the equilibrium distance of about 6.00 a.u. for $n=1$ to 33.2 μE_h and 5.60 a.u. for $n=3$. The corresponding values at convergence - at $n=10$ - are 33.8 μE_h at the distance of 5.60 a.u.

The results obtained are in acceptable agreement with Aziz's potential [72] which possesses a well of 34.7 μE_h at 5.60 a.u. These calculations suggest that a complete accordance with the experimental and accurate theoretical results of Korona et al. [73] can be reached by the improved MO-VB wave function, once the appropriate number of virtuals is included and a more extended basis set with h functions is employed. Work is in progress in our laboratory on this problem.

4. CONCLUSIONS

In this review, research in the field of van der Waals molecules accomplished by our group in the last few years was summarised. On the basis of the results obtained so far, it appears that the modification of the Roothaan equations to avoid *basis set superposition error* at the Hartree-Fock level of theory is a promising approach. The fundamental development of the SCF-MI strategy to deal with electron correlation treatments in the framework of the valence bond theory has been described. A compact multistructure and size

consistent valence bond wavefunction (namely MO-VB) has been presented. The central idea of both the SCF-MI and MO-VB approaches is the expansion of the orbitals in the partitioned basis sets centred on each of the interacting molecules. In this way, both the methods provide an *a priori* elimination of the BSSE, while taking properly into account orbital and geometry relaxation effects and the *natural* non-orthogonality of the MOs of the interacting systems.

The SCF-MI method turns out to be efficient in computing binding energies on systems of dimension of biological interest (where most of the times the interaction is dominated by polarisation effects) with an accuracy which compares well with corresponding standard SCF calculations employing larger basis sets. It is also shown that the method is particularly reliable and computationally efficient to determine geometrical conformations, whithout the complications of BSSE. The method appears able to deal with large molecular systems made up of many fragments and so is particularly useful to study the effect of hydration at the molecular level. DNA base pairs have been investigated: the results of a study on the complexes between guanine...cytosine Watson-Crick pair (GCWC) with various mono and divalent metal cations (H^+, Na^+, K^+, free and hydrated Mg^{++}, Ca^{++} and $[cis\text{-}Pt(NH_3)_2]^+$) and with solvating water molecules have been reviewed. The case of the hydrated cytosine-guanine base pair showed that the theoretical SCF-MI results compare well with those provided by knowledge-based approachesemploying crystallographic data. The use of the SCF-MI approach to study solvation problems and clustering processes is supported by calculations on lithium and potassium cations coordinated by ammonia molecules.

The development of the SCF-MI method to properly take account of electron correlation effects by the compact, size consistent and BSSE free MO-VB wavefunction has been shown to provide accurate results as well. Several applications of the MO-VB approach were presented and discussed. In particular, calculations of geometries and stabilisation energies of various simple H-bonded complexes (water dimer and hydrogen fluoride) and a study of the He-CH$_4$ van der Waals complex are reported. The very promising extension of the MO-VB scheme to fully exploit the capability of the virtual space spanned by the basis set is also reviewed, including explorative calculation on the emblematic case of the helium dimer system. The study of water and hydrogen fluoride dimers, other representative cases of hydrogen bonded systems, demonstrated that the MO-VB wavefunction provides results in agreement with the experiments, as well as reliable intermolecular potentials to be used in molecular dynamics studies of the liquid state of these highly structured liquids.

344

REFERENCES

[1]   a) P. Hobza and R. Zahradnik (eds.), Intermolecular Complexes, Elsevier, Amsterdam, 1988; b) P. Hobza and R. Zahradnik, Chem. Rev., 88 (1988) 871; c) S. Scheiner: Calculating the Properties of Hydrogen Bonds by *ab initio* Methods, in Reviews in Computational Chemistry II, K.B. Lipkowitz and D.B. Boyd (eds.), VCH Publisher, New York, 165, 1991; d) S. Scheiner, Annu. Rev. Phys. Chem., 45 (1994) 23; e) A.W. Castleman Jr. and P. Hobza (eds), van der Waals Molecules II, Chem. Rev. 94 (1994); f) S. Scheiner, Molecular Orbital Theory of Hydrogen Bonded Systems and Proton Transfer Reactions, Oxford University Press, New York, 1997; g) D. Hadzi, Theoretical Treatments of Hydrogen Bonding, Wiley Research Series in Theoretical Chemistry, John Wiley & Sons Ltd Publishers, Chichester-England, 1997.

[2]   a)J.O. Hirschfelder (ed.), Adv. Chem. Phys., Interscience Publisher, New York, vol. 12, 1967; b) Discuss. Faraday Soc. 40 (1965), 62 (1977), 73 (1982); c) G.C. Maitland, M. Rigby, V. Smith and W. A. Wakeham (eds), Intermolecular Forces, Claredon Press, Oxford, 1997; e) Chem. Rev. 88 (1988), Chem. Rev. 94 (1994); f) S. Scheiner (ed), Molecular Interactions, from van der Waals to strongly Bound Complexes, Wiley, Chichester, 1997; g) A. J. Stone, The theory of Intermolecular Forces, Claredon Press, Oxford, 1996.

[3]   a) P. Hobza, F. Hubálek, M. Kabelác, P Mejzlík, J. Šponer and J. Vondrášek, Chem Phys. Lett., 257 (1996) 31; b) P. Hobza, M. Kabelác,, P Mejzlík, J. Šponer and J. Vondrášek, J. Comput. Chem., 18 (1997) 1136; c) J. Šponer, J. Leszczynski and P. Hobza, J. Biomol. Struct. Dyn., 14 (1996) 117.

[4]   a) F.B. van Duijneveldt, J.M.C.M. van Duijneveldt-van de Rijdt and van J.H. Lenthe, Chem. Rev., 94 (1994) 1873; b) I. Mayer, P. R. Surjan, In. J. Quantum Chem., 36 (1989) 225; c) J. Almlöf, P. R. Taylor, J. Chem. Phys., 86 (1987) 553; d) W. Saebø, P. Pulay, J. Chem. Phys., 105 (1988) 1884,.

[5]   S.F. Boys and F. Bernardi, Mol Phys., 19 (1970) 553.

[6]   a) S.S. Xantheas, J. Chem. Phys., 104 (1996) 8821; b) S. Simon, M., Duran and J. J. Dannenberg, J. Chem. Phys. 105 (1996) 11024.

[7]   G. Karlström and A.J. Sadlej, Theor. Chim. Acta, 61 (1982) 1.

[8]   a)E. Gianinetti, M. Raimondi and E. Tornaghi, Int. J. Quantum Chem., 60 (1996) 157; b)A. Famulari, E. Gianinetti, M. Raimondi, and M. Sironi, Int. J. Quantum Chem., 69 (1998) 151; c)A. Famulari, E., Gianinetti, M., Raimondi and M. Sironi, Theor. Chem. Acc., 99 (1998) 358; d) E. Gianinetti, I, Vandoni, A. Famulari, and M. Raimondi, Adv. Quantum Chem., 31 (1998) 251; e) E. Gianinetti, I. Vandoni, A. Famulari, M. Raimondi, "Self Consistent Field Theory of Weakly Bonded Systems" in Computational Chemistry: Reviews of Current Trends. J. Leszczynski Ed., World Scientific, SINGAPORE (2000). Vol. 5, p. 141-170. ISBN 981-02-4371.

[9]   M. W. Schmidt, K. K. Baldridge, J. A. Boatz, S. T. Elbert, M. S. Gordon, J. Jensen, S. Koseki, N. Matsunaga, K. A. Nguyen, S. J. Su, T. L. Windus, M. Dupuis, J. A. Montgomery, J. Comput. Chem., 14 (1993) 1347.

[10]   a) A. Famulari, M. Raimondi, M. Sironi and E. Gianinetti, Chem. Phys. 232, 275 (1998); Chem. Phys. 232, 289 (1998); b) A. Famulari, R. Specchio, M. Sironi and M. Raimondi, J. Chem. Phys. 108 (1998) 3296; c)M. Raimondi, A. Famulari, E. Gianinetti, M. Sironi, R. Specchio and I. Vandoni, Adv. Quantum Chem., 32 (1998) 263; d) R. Specchio, A. Famulari, M. Sironi and M. Raimondi, J. Chem. Phys., 111 (1999) 6204; e) R. Specchio, A. Famulari, R. Martinazzo, and M. Raimondi, J. Chem. Phys., 113 (2000) 6724; f) A. Famulari, M. Sironi, and M. Raimondi, in: A. Hernádez-

Laguna et al. (Eds.), Quantum Systems in Chemistry and Physics vol. 1: Basic Problems and Model Systems, Kluwer Academic Publishers, Dordrecht, p. 361 (2000); f) R. Specchio, A. Famulari, M. Raimondi, J. Mol. Struct. (THEOCHEM) (2001). In press; g) M. Raimondi, A. Famulari, R. Specchio, M. Sironi, F. Moroni and E. Gianinetti, J. Mol. Struct. (THEOCHEM), (2001). In press.

[11]   a) C. Gatti, A. Famulari, "Interaction Energy and Density in the Water Dimer. A Quantum Theory of Atoms in Molecules Insight on the Effect of Basis Set Superposition Error Removal". Kluwer book series: UNDERSTANDING CHEMICAL REACTIVITY; Chapter 6, Volume21: Electron, Spin and Momentum Densities and Chemical Reactivity. Paul G. Mezey, Beverly E. Robertson Editors ; Hardbound, ISBN 0-7923-6085-0, March 2000; b) Famulari, A., Sironi, M., Gianinetti, E., and Raimondi, M. 2001, "Hartree Fock study of hydrogen bonded systems in the absence of basis set superposition error: the nucleic acid base pairs", in New Trends in Chemistry and Physics. J. Maruani, R. McWeeny, M. Minot Eds. Volume 1, 313-333, Kluwer Academic Publishers.

[12]   J. Gerratt and I.M. Mills, J. Chem. Phys., 49 (1968) 1719.

[13]   a)P. Pulay, Mol. Phys., 17 (1969) 197; b)P. Pulay, Adv. Chem. Phys., 69 (1987) 241.

[14]   Y. Yamaguchi, Y. Osamura, J.D. Goddard and H.F. Schaefer, in A New Dimension to Quantum Chemistry: Analytic Derivative Methods in Ab Initio Molecular Electronic Structure Theory, Oxford University Press. Oxford, UK, 1994.

[15]   a) I.-H. Hillier and V.-R. Saunders, Int. J. Quantum Chem., 4 (1970) 503; b) V.-R. Saunders and I.-H. Hillier, Mol. Phys., 28 (1974) 819.

[16]   a)P. Pulay, Chem. Phys. Lett., 73 (1980) 393; b) P. Pulay, J. Comput. Chem., 3 (1982) 556.

[17]   A. Famulari, G. Calderoni, F. Moroni, M. Raimondi, P. Karadakov, J. Mol. Struct. (THEOCHEM), (2001). In press.

[18]   A.A.Granovsky,wwwhttp://classic.chem.msu.su/gran/gamess/index.html

[19]   Goldfeld S.M., R.E. Quandt, H.F. Trotter, Econometrica 34 (1966) 541.

[20]   M. Raimondi, W. Campion and M. Karplus, Mol. Phys., 34 (1977) 1483.

[21]   a) I. K. Yanson, A. B., Teplitsky, L. F. Sukhodub, Biopolymers, 18 (1970) 1149; b) M. Dey, F., Moritz, J., Grotemeyer and E. W. Schloag, J. Am. Chem. Soc., 116 (1994) 9211; c) W. Nerdal, D. Hare and B. Reid, Nuc. Acid Res., 28 (1989) 10008.

[22]   M. Egli and R. V. Gessner, Proceeding of the National Academy of Science U.S.A., 92 (1995) 180.

[23]   a) V. N. Potaman and V. N. Soyfer, J. Biomol. Struct. Dyn., 11 (1994) 1035; b) W. Guschlbauer, J. F. Chantot, and D. Thiele, J. Biomol. Struct. Dyn., 8 (1990) 491.

[24]   M. Langlais, H. A. Tajmir-Riahi R. and Savoie, Biopolymers, 30 (1990) 743.

[25]   a) S. Mansy B. Rosenberg and A. J. Thomson, J. Am. Chem. Soc., 95 (1973) 1633; b) B. Rosenberg, Biochemie 60 (1975) 859.

[26]   I. Mayer, P. R. Surján, Chem. Phys. Lett., 191 (1992) 497.

[27]   a)P. Hobza and C. Sandorfy, J. Am. Chem. Soc., 109 (1987) 1302; b)P. Hobza, J. Sponer, and M. Polasek, J. Am. Chem. Soc., 1117 (1995) 792; c)J. Sponer, J. Leszczynski, and P. Hobza, J. Biomol. Struct., Dyn. 14 (1996) 117; d)P. Hobza, J. Sponer, Chem Phys. Lett., 288 (1997) 7; e)P. Hobza, Prog. Phys. Chem. 93 (1997) 257; f) J. Sponer and P. Hobza, Encyclopedia of Computational Chemistry, P. v R. Schleyer (ed), Wiley, Chirchester, 1998.

[28]   J. Sponer, J. Leszczynski, and P. Hobza, J. Phys. Chem. 100 (1996) 1965.

[29]   N. U. Zhanpeisov and J. Leszczynski, J. Phys. Chem., 102 (1998) 6167.

[30] A. Pelmenschikov, I. Zilberberg, J. Leszczynski, A. Famulari, M. Sironi and M. Raimondi, Chem. Phys. Lett., 314 (1999) 496.

[31] A. Famulari, F. Moroni, M. Sironi, and M. Raimondi, Comput. Chem., 24 (2000) 341.

[32] A. Famulari, F. Moroni, M. Sironi, E. Gianinetti, and M. Raimondi, J. Mol. Struct. (THEOCHEM), 529 (2000) 209.

[33] F. Moroni, A. Famulari, M. Raimondi, J. Phys. Chem., A 105 (2001) 1169.

[34] B. Schneider and H. M. Berman, Biophys., J. 69 (1995) 2661.

[35] P. P. Edwards, Phys. Chem. Liq., 10 (1981) 189; N. F. Mott, Metal-insulator Transitions, Taylor and Francis, London; 1990; Z. Deng, G. J. Martyna, and M. L. Klein, Phys. Rev. Lett., 71 (1993) 267; J. Jortner and M. H. Cohen, Phys. Rev. B, 13 (1976) 1548; P. Chieux and H. Bertagnolli, J. Phys. Chem., 88 (1984) 3726.

[36] J. C. Wasse, S. Hayama, N. T. Skipper, C. J. Benmore and A. K. Soper, J. Chem. Phys., 112 (2000) 7147.

[37] a) J. D. Bernal and R. H. Fowler, J. Chem. Phys., 1 (1933) 515; b) H. S. Frank and W. Wen, Discuss. Faraday Soc., 24 (1957) 133.

[38] G. W. Neilson and N. T. Skipper, Chem. Phys. Lett., 114 (1985) 35.

[39] a) K. Hashimoto, K. Morokuma, J. Am. Chem. Soc., 116 (1994) 11436; b) K. Hashimoto, S. He, K. Morokuma, Chem. Phys. Lett., 206 (1993) 297; c) K. Hashimoto, K. Morokuma, Chem. Phys. Lett., 223 (1994) 423; d) A. Garcia-Muruais, M. Cabaleiro-Lago, J. M. Hermida-Ramon, M. A. Rios, Chem. Phys., 254 (2000) 109.

[40] C. Millot and A. J. Stone, Mol. Phys. 77 (1992) 439.

[41] E.M. Mas and K. Szalewicz, J. Chem. Phys., 104 (1996) 7606.

[42] J.G.C.M. van Duijneveldt-van de Rijdt and F.B. van Duijneveldt, J. Chem. Phys., 97 (1992) 5019.

[43] K.S. Kim, B.J. Mhin, U.C. Choi and K. Lee, J. Chem. Phys., 97 (1992) 6649.

[44] F. Huisken, M. Kaloudis, A. Kulcke, J.Chem. Phys., 104 (1996) 17.

[45] E.M. Mas and K. Szalewicz, J. Chem. Phys., 104 (1996) 7606.

[46] L.A. Curtiss, D.J. Frurip and M. Blander, J. Chem. Phys., 71 (1979) 2703.

[47] L.A. Curtiss, D.J. Frurip and M. Blander, Chem. Phys. Lett., 54 (1978) 575.

[48] L.A. Curtiss and J.A. Pople, J. Mol. Spectrosc., 55 (1975) 1.

[49] T.R. Dyke, K.M. Mack and J.S. Muenter, J. Chem. Phys., 66 (1977) 498.

[50] J.A. Odutola and T.R.Dyke, J. Chem. Phys., 72 (1980) 5062.

[51] P. Hobza, and Z. Havles, Theor. Chim. Acc., 99 (1998) 372.

[52] E. M. Mas, R. Bukowski, K. Szalewicz, G. C. Groenenboom, P. E. S. Wormer, and A. van der Avoird, J. Chem. Phys., 113 (2000) 6687.

[53] U. Niesar, G. Corongiu, E. Clementi, G. R. Kneller and D. K. Bhattacharya, J. Phys. Chem., 94 (1990) 7949.

[54] F. Sciortino and G. Corongiu, Modern Techniques in Computational Chemistry: MOTECC-94, E. Clementi (ed) ESCOM, Leiden, The Netherlands, 1994.

[55] G. C. Lie and E. Clementi, Phys. Rev. A, 33 (1986) 2679.

[56] G. Corongiu, Int. J. Quantum Chem. , 44 (1992) 1209.

[57] W. L. Jorgensen, J. Chandrasekhar, J. Madura, R. W. Impey, and M. L. Klein, J. Chem. Phys., 79 (1983) 926.

[58] G. S. Kell (ed), Water: a comprehensive treatise, Vol. 1, 363. Franks, F., Ed. Plenum, New York, 1971.

[59] A. K. Soper, F. Bruni, and M. A. Ricci, J. Chem. Phys., 106 (1997) 247.

[60] a) A. A. Chialvo and P. T. Cummings. J. Chem. Phys., 101 (1994) 4466; b) A. A. Chialvo and P. T. Cummings. J. Phys. Chem., 100 (1996) 1309.

[61] M.-C. Bellissent-Funel, T. Tassaing, H. Zhao, D. Beysens, B. Guillot, and Y. Guissani. J. Chem. Phys. 107 (1997) 2942.

[62] M. M. Hoffmann and M. S. Conradi, J. Am. Chem. Soc., 119 (1997) 3811.

[63] Howard BJ, Dyke TR, Klemperer W, J Chem Phys., 81 (1984) 5417.

[64] Peterson KA, Dunning TH Jr, J Chem Phys., 10 (1965) 2032.

[65] U. Buck, K.H. Kohl, A. Kohlase, M. Faubel, V. Staemmler, Mol. Phys., 55 (1985) 1255.

[66] J.M.Hutson and S.Green, MOLSCAT computer code, version 14 (1995), distributed by Collaborative Computational Project No.6 of the United Kingdom Science and Engineering Research Council.

[67] M.H.Alexander and D.E.Manolopoulos, J.Chem.Phys., 86 (1987) 2044.

[68] D.J.Nesbitt, J.W.Nibler, A.Schiffman, W.B.Chapman, J.M.Hutson, J.Chem.Phys., 98 (1993) 9513.

[69] R. Martinazzo, R. Specchio, A. Famulari, M. Raimondi (2001). Manuscript in preparation.

[70] M. Raimondi, A. Famulari, G. Calderoni, F. Cargnoni (2001). Manuscript in preparation.

[71] D. E. Woon and T.H. Dunning, Jr., J. Chem. Phys., 100, 2975 (1994).

[72] A.R. Janzen and R.A. Aziz, J. Chem. Phys., 107 (1997) 914.

[73] T. Korona, H.L. Williams, R. Bukowski, B. Jeziorski and K. Szalewicz, J. Chem. Phys., 106 (1997) 5109.

This Page Intentionally Left Blank

Chapter 12

Valence bond structures for some molecules with four singly-occupied active-space orbitals: electronic structures, reaction mechanisms, metallic orbitals

Richard D. Harcourt

School of Chemistry, University of Melbourne, Victoria 3010, Australia

Qualitative valence-bond (VB) descriptions of the electronic structures of molecules are often able to provide "primitive patterns of understanding" [1] of the origin of various molecular properties. In this chapter, we shall give consideration to VB structures for some molecular systems that involve four active-space orbitals. The discussion will include VB formulations of the electronic structures of isolated molecules, reaction mechanisms, and types of "metallic orbitals" that can be used in VB representations for electron conduction in metallic lithium. For the latter topic, the results of STO-6G VB calculations are reported in order to make a provisional comparison of two conduction mechanisms.

Where appropriate, increased-valence structures [2-5] will be used to provide qualitative VB representations of electronic structure. Increased-valence structures involve localised one-electron and fractional electron-pair bonds, as well as "normal" electron-pair bonds [2-5]. These features will be re-described by reference to HCNO.

We remind the reader that, with one hybrid or non-hybrid atomic orbital (AO) per atomic centre, the most-general singlet spin ($S = 0$) wavefunction of the Heitler-London type for the electron-pair bond $A\!-\!B$ or $A : B$ is given by Eq.(1).

$$\Psi(A\!-\!B) = \left|\psi'_{ab}{}^{\alpha}\psi''_{ba}{}^{\beta}\right| + \left|\psi''_{ba}{}^{\alpha}\psi'_{ab}{}^{\beta}\right| \tag{1a}$$

$$\equiv (k'k'' + 1)(\left|a^{\alpha}b^{\beta}\right| + \left|b^{\alpha}a^{\beta}\right|) + 2k''\left|a^{\alpha}a^{\beta}\right| + 2k'\left|b^{\alpha}b^{\beta}\right| \tag{1b}$$

In this wavefunction, a and b are the overlapping AOs, $\psi'_{ab} = a + k'b$ and $\psi''_{ba} = b + k''a$ are Coulson-Fischer molecular orbitals (MOs) [7], α and β are the $m_s = +1/2$ and $m_s = -1/2$ electron spin wavefunctions, and k' and k'' are variational polarity parameters. In some of the discussion here, it will be assumed that $k' = k'' = 0$, to give the Heitler-London AO wavefunction $\left|a^{\alpha}b^{\beta}\right| + \left|b^{\alpha}a^{\beta}\right| \equiv \left|a^{\alpha}b^{\beta} + b^{\alpha}a^{\beta}\right|$ for a covalent electron-pair bond. However it should be noted that in Eqs.(2),(3),(5)-(7) and elsewhere, the orbital designations a and b do not refer necessarily only to AOs

1. SINGLET AND TRIPLET SPIN WAVEFUNCTIONS FOR FOUR SINGLY-OCCUPIED ACTIVE SPACE ORBITALS

The phenomenon of four singly-occupied active-space orbitals (AO or MO) arises in many seemingly-unrelated molecular situations. The singlet spin ($S = 0$) Rumer diagrams for these orbitals indicate that there are two linearly-independent or canonical spin-pairings schemes. These spin-pairings are well-exemplified by the π-electrons of butadiene, for which two canonical Lewis VB structures with different π-electron spin pairings are those of **1** and **2**.

$$H_2C\!\!=\!\!=\!\!CH\!\!-\!\!CH\!\!=\!\!=\!\!CH_2 \qquad\qquad H_2\overset{\text{\tiny .}}{C}\!\!-\!\!CH\!\!=\!\!=\!\!CH\!\!-\!\!\overset{\text{\tiny .}}{C}H_2$$

$$\mathbf{1} \qquad\qquad\qquad\qquad\qquad \mathbf{2}$$
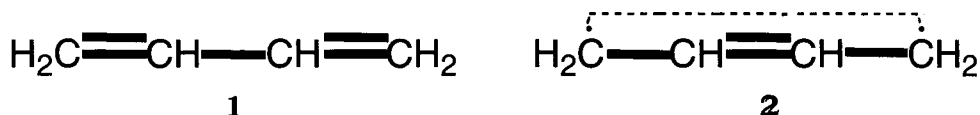
These structures are examples of Kekulé and Dewar type Lewis structures, respectively. In general, if a, b c and d are the orbitals (AOs and/or MOs), the $S = 0$ wavefunctions for the four electrons of these two types of spin-pairings are given by the linear combinations of four Slater determinants, as in Eqs.(2) and (3),

$$^1\Psi_1 \equiv \Psi_1(\text{a-b,c-d}) = \left|(a^\alpha b^\beta + b^\alpha a^\beta)((c^\alpha d^\beta + d^\alpha c^\beta)\right| \tag{2a}$$

$$\equiv \left|a^\alpha b^\beta c^\alpha d^\beta\right| + \left|a^\beta b^\alpha c^\beta d^\alpha\right| - \left|a^\alpha b^\beta c^\beta d^\alpha\right| - \left|a^\beta b^\alpha c^\alpha d^\beta\right| \tag{2b}$$

$$^1\Psi_2 \equiv \Psi_2(\text{a-d,b-c}) = \left|(a^\alpha d^\beta + d^\alpha a^\beta)(b^\alpha c^\beta + c^\alpha b^\beta)\right| \tag{3a}$$

$$\equiv \left|a^\alpha b^\alpha c^\beta d^\beta\right| + \left|a^\beta b^\beta c^\alpha d^\alpha\right| - \left|a^\alpha b^\beta c^\alpha d^\beta\right| - \left|a^\beta b^\alpha c^\beta d^\alpha\right| \tag{3b}$$

The variational linear combinations of Eq.(4)

$$^1\Psi_i = C_{i1}{}^1\Psi_1 + C_{i2}{}^1\Psi_2 \qquad\qquad i = 1,2 \tag{4}$$

are associated with the ground-state and excited-state resonances between the two associated ($S = 0$) VB structures. In Sections 2-4, we shall discuss some of the other phenomena that involve this type of resonance scheme, several of which have been considered previously (cf. Sections 3.4 and 4.2). We shall also give attention to a number of triplet spin ($S = 1$) phenomena that involve four singly-occupied orbitals. There are three linearly-independent $S = M_S = 1$ wavefunctions, which are given by Eqs.(5)-(7). These wavefunctions will be used in Section 5.

$$^3\Psi_1 \equiv {}^3\Psi_1(\text{a-b,c}\!\uparrow\!,\text{d}\!\uparrow) = \left|(a^\alpha b^\beta + b^\alpha a^\beta)c^\alpha d^\alpha\right| \equiv \left|a^\alpha b^\beta c^\alpha d^\alpha\right| - \left|a^\beta b^\alpha c^\alpha d^\alpha\right| \tag{5}$$

$$^3\Psi_2 \equiv {}^3\Psi_2(\text{d-c,a}\!\uparrow\!,\text{b}\!\uparrow) = \left|(c^\alpha d^\beta + d^\alpha c^\beta)a^\alpha b^\alpha\right| \equiv \left|a^\alpha b^\alpha c^\alpha d^\beta\right| - \left|a^\alpha b^\alpha c^\beta d^\alpha\right| \tag{6}$$

$$^3\Psi_3 \equiv {}^3\Psi_3(\text{b-c,a}\!\uparrow\!,\text{d}\!\uparrow) = \left|(b^\alpha c^\beta + c^\alpha b^\beta)a^\alpha d^\alpha\right| \equiv \left|a^\alpha b^\alpha c^\beta d^\alpha\right| - \left|a^\alpha b^\beta c^\alpha d^\alpha\right| \tag{7}$$

2. VALENCE BOND CONSIDERATIONS FOR HCNO

2.1 Kekulé, Dewar and increased-valence structures for HCNO

The electronic structures of C_2-symmetry N_6 and quasi-linear $(CNO)_2$ have attracted some attention recently [8,9]. The results of *ab initio* MO studies [8,9] indicate that these two species are respectively unstable and bound relative to their N_2 and CNO dissociation products. The VB structures that we shall use to represent the primary features of the electronic structures of N_6 and $(CNO)_2$ are examples of increased-valence structures [2-5]. Such structures may be generated from familiar (Kekulé-type) Lewis structures by delocalising non-bonding electrons into bonding localised MOs (LMOs).

To establish the framework for the subsequent treatment in this chapter, VB descriptions of the electronic structure of HCNO [2,10] will initially be re-described. HCNO is isoelectronic with N_2O and HN_3, for which parallel descriptions have been presented previously [2,3(b),4,11-14].

Kekulé-type or standard Lewis-type VB structures which involve atoms of first-row elements, locate electron-pair bonds between pairs of adjacent atoms, and have the maximum number of electron-pair bonds permitted by the Lewis-Langmuir octet rule. For 1,3-dipolar HCNO, there are four Kekulé structures, **3-6** [2,10]
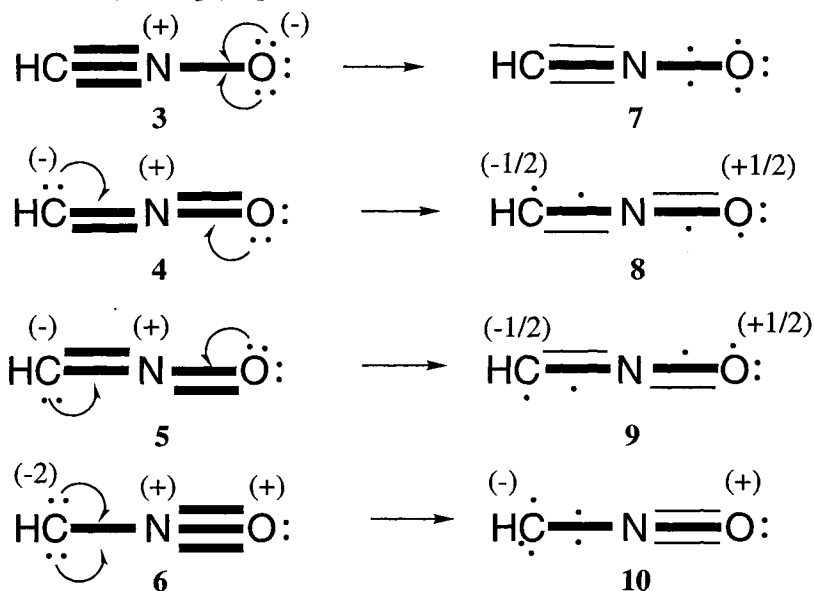
from which increased-valence structures **7-10** may be constructed via the one-electron delocalisations of non-bonding $2p\pi_x$ and $2p\pi_y$ electrons into bonding LMOs, as is indicated in the Kekulé structures. For illustrative purposes, it is assumed that bonding electrons are shared equally by pairs of adjacent atoms. The resulting formal charges of structures **7-10** are then integer or half-integer in magnitude. Appeal to the electroneutrality principle [15] implies

that structure **7** with no formal charges is the primary increased-valence structure, but of course it participates in resonance with structures **8-10**.

HC═N─O: HC═N─O: HC─N─O:

11   **12**   **13**
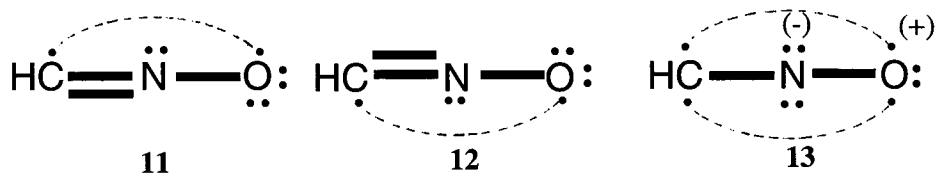
When Heitler-London AO-type wavefunctions (i.e. $|...a^{\alpha}b^{\beta}|$ + $|...b^{\alpha}a^{\beta}|$ in which a and b are AOs) are used to represent electron-pair π_x(CN) and π_y(CN) bonds, it can be deduced [2,4,16, cf. also Eq.(11) below] that VB structure **7** is equivalent to resonance between the Kekulé Lewis structure **3** and the Dewar or "long-bond" Lewis structures **11-13**. Only nearest-neighbour spin-pairing is indicated in increased-valence structures [2-5,10]. When the "long" or formal bonds are omitted from structures **11-13**, these structures are designated as singlet diradical structures [2-4].

Because **7** ≡ **3**↔**11**↔**12**↔**13**, increased-valence structure **7** involves fractional π_x(CN) and π_y(CN) electron-pair bonds [2,4,10-14,16]. Therefore its C-N bond-number, or bond-order is less than 3. A thin bond line is used to represent a fractional electron-pair bond [2-4]. An N-O double bond, which consists of an electron-pair σ bond, and one-electron π_x and π_y bonds, is also present in this VB structure. With these bond properties, the N-O and C-N bond-lengths that are implied by increased-valence structure **7** are in accord with the following observations with regard to its bond-lengths [17]:
(a) The N-O bond length of 1.21 Å is similar to a length of 1.20 Å [18] for an N=O double bond.
(b) The C-N bond length of 1.16 Å is longer than an estimate of 1.13 Å for HCN with the same nitrogen σ-bond hybridisation (sp) as occurs in HCNO (cf. discussion of AO hybridisation and N-N bond lengths for HN_3 and N_2 [13]).

The importance of Dewar-type (or singlet diradical) canonical Lewis structures, as well as the Kekulé-type (or zwitterionic) Lewis structures for VB descriptions of the electronic structures of 1,3-dipolar (or zwitterionic diradical hybrid [19]) molecules has been often stressed in our publications [2-4,10,16], and a similar type of conclusion has been obtained by others [20]. In contrast, the results of spin-coupled [21] and biorthogonal [22] VB calculations have provided a contrary result However because the orbitals used in the latter calculations are primarily either 2-centre or multicentre in form, they disguise the presence of the singlet-diradical character [3(a),4,13,23].

Qualitative VB formulations of various types of reaction mechanisms differ according to whether Kekulé-type or Dewar-type Lewis structures are implicated primarily in the electronic reorganisation processes [2-4,10,19,23]. Some further comparisons are provided here in Sections 3.3 and 4.1.

The effect of solvent polarity on the weights of Lewis VB structures for 1,3-dipolar molecules has been studied in Ref. [24], where it is shown that

polar solvents can stabilize the zwitterionic structures (such as **3-5**) at the expense of the singlet diradical structure(s).

2.2 Some $S = 0$ wavefunctions for the π-electrons of HCNO

In the Kekulé structure **3** there are four singly-occupied carbon and nitrogen $2p\pi_x$ and $2p\pi_y$ AOs. Labelling these orbitals as $p_x(C)$, $p_x(N)$, $p_y(C)$ and $p_y(N)$, the primary $S = 0$ Heitler-London wavefunction for the π electrons which occupy these orbitals is given by Eq.(8),

$$\Psi_3\{p_x(C)\text{-}p_x(N),\ p_y(C)\text{-}p_y(N),\ p_x(O)\text{-}p_x(O),\ p_y(O)\text{-}p_y(O)\}$$
$$= \left|\{p_x(C)^\alpha p_x(N)^\beta + p_x(N)^\alpha p_x(O)^\beta\}\{p_y(C)^\alpha p_y(N)^\beta + p_y(N)^\alpha p_y(O)^\beta\}\right.$$
$$\left.\times\{p_x(O)^\alpha p_x(O)^\beta p_y(O)^\alpha p_y(O)^\beta\}\right|$$
$$= \left|p_x(C)^\alpha p_x(N)^\beta p_y(C)^\alpha p_y(N)^\beta p_x(O)^\alpha p_x(O)^\beta p_y(O)^\alpha p_y(O)^\beta\right|$$
$$+ \left|p_x(C)^\beta p_x(N)^\alpha p_y(C)^\beta p_y(N)^\alpha p_x(O)^\alpha p_x(O)^\beta p_y(O)^\alpha p_y(O)^\beta\right|$$
$$- \left|p_x(C)^\alpha p_x(N)^\beta p_y(C)^\beta p_y(N)^\alpha p_x(O)^\alpha p_x(O)^\beta p_y(O)^\alpha p_y(O)^\beta\right|$$
$$- \left|p_x(C)^\beta p_x(N)^\alpha p_y(C)^\alpha p_y(N)^\beta p_x(O)^\alpha p_x(O)^\beta p_y(O)^\alpha p_y(O)^\beta\right| \tag{8}$$

in which the doubly-occupied $p_x(O)$ and $p_y(O)$ AOs are also included. For the four singly-occupied orbitals, this wavefunction is an example of Eq.(2), in which a $= p_x(C)$ and b $= p_x(N)$ are spin-paired, as are c $= p_y(C)$ and d $= p_y(N)$.

The corresponding wavefunction for the π-electrons of increased-valence structure **7** is given by Eq.(9),

$$\Psi_7\{p_x(C)\text{-}p_x(N),\ p_y(C)\text{-}p_y(N),\ \pi_x(NO),\ p_x(O),\ \pi_y(NO),\ p_y(O)\}$$
$$= \left|p_x(C)^\alpha p_x(N)^\beta p_y(C)^\alpha p_y(N)^\beta \pi_x(NO)^\alpha p_x(O)^\beta \pi_y(NO)^\alpha p_y(O)^\beta\right|$$
$$+ \left|p_x(C)^\beta p_x(N)^\alpha p_y(C)^\beta p_y(N)^\alpha p_x(O)^\alpha \pi_x(NO)^\beta p_y(O)^\alpha \pi_y(NO)^\beta\right|$$
$$- \left|p_x(C)^\alpha p_x(N)^\beta p_y(C)^\beta p_y(N)^\alpha \pi_x(NO)^\alpha p_x(O)^\beta p_y(O)^\alpha \pi_y(NO)^\beta\right|$$
$$- \left|p_x(C)^\beta p_x(N)^\alpha p_y(C)^\alpha p_y(N)^\beta p_x(O)^\alpha \pi_x(NO)^\beta \pi_y(NO)^\alpha p_y(O)^\beta\right| \tag{9}$$

in which the LMOs $\pi_x(NO) = p_x(N) + k p_x(O)$ and $\pi_y(NO) = p_y(N) + k p_y(O)$, are bonding LMOs, with k as a variational parameter. These LMOs accommodate the electrons which form the one-electron N-O bonds in VB structure **7**. Unitary transformations of pairs of nitrogen and oxygen p_x and p_y AOs in Eq.(9) generate the equivalent $S = 0$ wavefunction of Eq.(10),

$$\Psi_7\{p_x(C)\text{-}\pi^*_x(NO),\ p_yC)\text{-}\pi^*_y(NO),\ \pi_x(NO)\text{-}\pi_x(NO),\ \pi_y(NO)\text{-}\pi_y(NO)\}$$
$$\propto \left|p_x(C)^\alpha \pi^*_x(NO)^\beta p_y(C)^\alpha \pi^*_y(NO)^\beta \pi_x(NO)^\alpha \pi_x(NO)^\beta \pi_y(NO)^\alpha \pi_y(NO)^\beta\right|$$
$$+ \left|p_x(C)^\beta \pi^*_x(NO)^\alpha p_y(C)^\beta \pi^*_y(NO)^\alpha \pi_x(NO)^\alpha \pi_x(NO)^\beta \pi_y(NO)^\alpha \pi_y(NO)^\beta\right|$$
$$- \left|p_x(C)^\alpha \pi^*_x(NO)^\beta p_y(C)^\beta \pi^*_y(NO)^\alpha \pi_x(NO)^\alpha \pi_x(NO)^\beta \pi_y(NO)^\alpha \pi_y(NO)^\beta\right|$$
$$- \left|p_x(C)^\beta \pi^*_x(NO)^\alpha p_y(C)^\alpha \pi^*_y(NO)^\beta \pi_x(NO)^\alpha \pi_x(NO)^\beta \pi_y(NO)^\alpha \pi_y(NO)^\beta\right| \tag{10}$$

in which $\pi^*_x(NO) = k^*p_x(N) - p_x(O)$ and $\pi^*_y(NO) = k^*p_y(N) - p_y(O)$ are anti-bonding LMOs that are orthogonal to the $\pi_x(NO)$ and $\pi_y(NO)$. Inspection of Eq.(10) shows that the a, b, c and d orbitals for Eq.(2) now correspond to the $p_x(C)$, $\pi^*_x(NO)$, $p_y(C)$ and $\pi^*_y(NO)$ orbitals, respectively.

When $p_x(N) + kp_x(O)$ and $p_y(N) + kp_y(O)$ are substituted for $\pi_x(NO)$ and $\pi_y(NO)$ in Eq.(9), we obtain the linear combination of Eq.(11).

$$\Psi_7 = \Psi_3 + k(\Psi_{11} + \Psi_{12}) + k^2\Psi_{13} \tag{11}$$

Because structures **11-13** do not involve C-N triple bonds, Eq.(11) shows that in Eq.(9), the $p_x(C)$-$p_x(N)$ and $p_y(C)$-$p_y(N)$ spin-pairings form fractional $\pi_x(CN)$ and $\pi_y(CN)$ electron-pair π-bonds via Heitler-London AO formulations of the bond wavefunctions.

A lower-energy expression for an Eq.(11) type formulation of Ψ_7, with two variational parameters can be obtained by using $\pi'_x(NO) = p_x(N) + k'p_x(O)$, $\pi'_y(NO) = p_y(N) + k'p_y(O)$, $\pi''_x(NO) = p_x(N) + k''p_x(O)$ and $\pi''_y(NO) = p_y(N) + k''p_y(O)$ instead of the $\pi_x(NO)$ and $\pi_y(NO)$. Four structures of type **7** are then needed.

The formulation of Eq.(9) can be generalized and improved by replacing the $p_x(C)$, $p_x(N)$, $p_y(C)$ and $p_y(N)$ AOs with the Coulson-Fischer [7] type MOs $p_x(C) + \mu'p_x(N)$, $p_x(N) + \nu'p_x(C)$, $p_y(C) + \mu''p_y(N)$ and $p_y(N) + \nu''p_y(C)$ in one structure of type **7**, and $p_x(C) + \mu''p_x(N)$, $p_x(N) + \nu''p_x(C)$, $p_y(C) + \mu'p_y(N)$ and $p_y(N) + \nu'p_y(C)$ in a second equivalent structure of type **7**. These two type **7** structures participate in resonance, and introduce more variational flexibility into the wavefunction via the inclusion of four parameters (μ', ν', μ'' and ν'') and additional canonical Lewis structures [2,10].

3 ONC-CNO AND ISOELECTRONIC MOLECULES

3.1 ONC-CNO

For quasi-linear $(CNO)_2$, as ONC-C'N'O', the Kekulé and increased-valence structures **14** and **15**
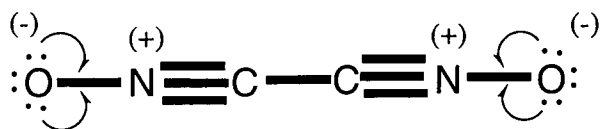
14

15

correspond to the HCNO structures **3** and **7**, respectively. There are eight singly-occupied π electron orbitals, which consist of the two sets of four $p_x(C)$, $\pi^*_x(NO)$, $p_y(C)$ and $\pi^*_y(NO)$ orbitals of each CNO moiety. As a consequence,

there are 14 Rumer $S = 0$ spin-pairing schemes. In four of them, the π_x electrons are spin-paired with each other, as are the π_y electrons. Increased-valence structure **15** involves one of these four spin-pairing schemes, namely that of Eq.(2) for each set of four π electrons. Thus for the π_x electrons, a = $p_x(C)$, b = $\pi^*_x(NO)$, c = $p_x(C')$ and d = $\pi^*_x(N'O')$ in Eq.(2). Similarly for the π_y electrons, the Eq.(2)-type orbital designations are a = $p_y(C)$, b = $\pi^*_y(NO)$, c = $p_y(C')$ and d = $\pi^*_y(N'O')$. (The other three intra π_x and intra π_y spin-pairing schemes involve Eq.(3) either once or twice.)

The C-N and N-O bond-lengths implied by increased-valence structure **15** are similar to those implied by increased-valence structure **7** for HCNO. The calculated MP4SDQ [8] C-N and N-O bond lengths, 1.172 Å and 1.215 Å [8] are similar to the observed lengths (1.16 Å and 1.21 Å) [12] for HCNO. However the MP4SDQ length of 1.351-1.365 Å [8] for the C-C bond is significantly shorter than an estimated length of 1.48 Å for a C-C single bond with (approximately) s-p hybridised carbon atoms [25]. Therefore less-important VB structures with C-C π bonding must also make a significant contribution to the ground-state resonance scheme. Possibly these latter structures are four equivalent "co-ionic" increased-valence structures of type **17**,

16

17
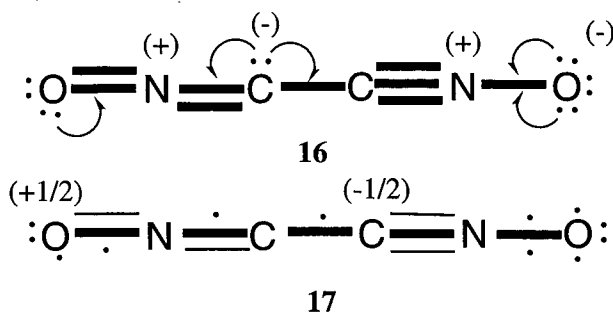
with non-adjacent spatial separation of opposite formal charges and increased-valence representations for two 8-electron 6-centre bonding units. These co-ionic structures can be derived from four Kekulé structures of type **16** via the one-electron delocalisations that are indicated in **16**.

3.2 OCN-NCO and NCO-OCN

Schulz and Klapötke [5,26] have provided direct evidence for the intermediate formation of OCN-NCO, which is isoelectronic with $(CNO)_2$ and N_6. Preparation of OCN-NCO has also been reported by Maier et al. [27]. Important Lewis VB structures for the NCO monomer radical locate the odd electron in either a nitrogen or an oxygen $2p_x$ or $2p_y$ AO, as in **18** with a $2p_x$ odd electron.

18
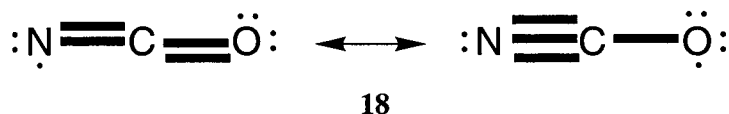
The results of RHF and UHF MO, and STO-6G VB calculations for NCO [28] indicate that the odd-electron is more substantially localised on nitrogen than it is on oxygen. Therefore it is to be expected that when NCO dimerizes, the primary dimer should be OCN-NCO, rather than NCO-OCN (or NCO-NCO). This expectation is in accord with the results of *ab initio* MO calculations [26], which show that OCN-NCO is the more stable isomer. The OCN-NCO isomer is calculated to have C_{2h} symmetry [26,27], with N-N, N-C and C-O bond-lengths of 1.385, 1.238 and 1.181 Å. The N-C and C-O bond lengths are in qualitative accord with those implied by the Kekulé structure* **19**. But as is the case for ONC-CNO, consideration needs also to be given to OCN-NCO VB structures with some N-N π bonding (which can occur for C_{2h} symmetry) to account for the existence of an N-N bond which is shorter than an N-N single bond One such structure is **20**, and the resulting **19** $\leftrightarrow$ **20** resonance is analogous to the **1** $\leftrightarrow$ **2** resonance for butadiene.

19   **20**

21

22   **23**
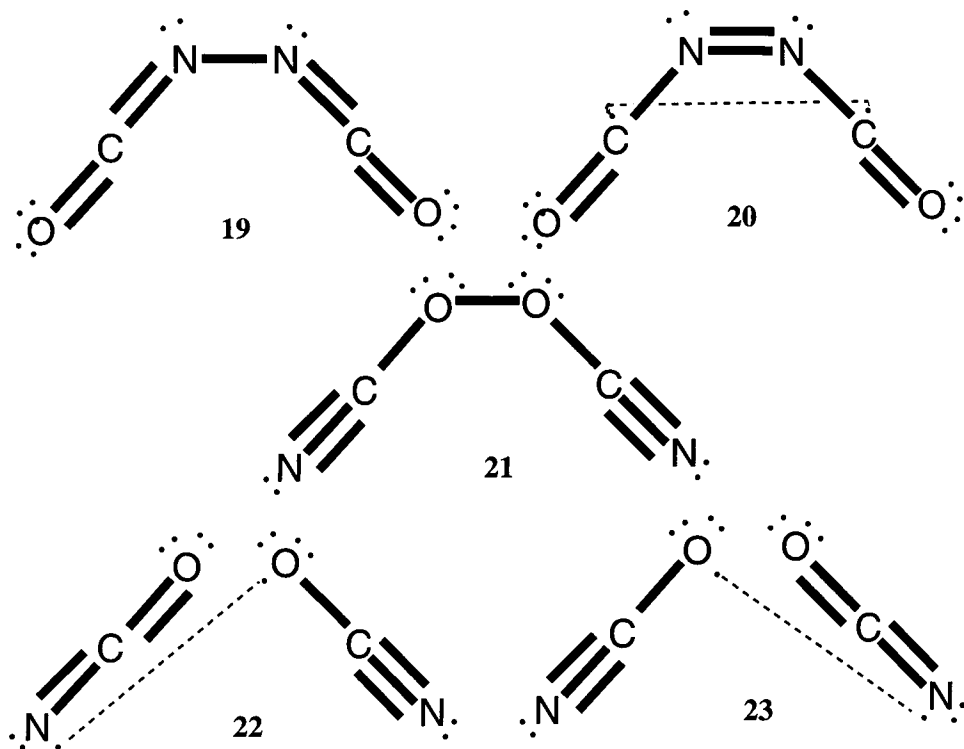
The Kekulé structure **21** is the primary O-O bonded VB structure for C_2 symmetry NCO-OCN. Its calculated O-O bond-length of 1.622 Å [26] is appreciably longer than the N-N bond-length of 1.385 Å [26] for OCN-NCO. This difference must be related, at least partly, to the distribution of the odd electron of NCO. With STO-6G VB estimates of 0.596 and 0.357 for the

*For convenience here, VB structures **19-29** for the NCO dimers and N$_6$ are displayed with C_{2v} symmetry.

nitrogen and oxygen odd-electron densities of NCO [28(c)], the resulting N-N and O-O bond-numbers of OCN-NCO and NCO-OCN are 0.36 and 0.13, if it is assumed that the dimerization processes involve primarily the spin-pairing of the odd-electrons of two NCO radicals.The small O-O bond-number implies that structures **22** and **23** must participate in resonance with structure **21** to an appreciable extent. Each of **21 ↔ 22** and **21 ↔ 23** involves a change in the spin-pairings for four electrons according to Eqs.(2) and (3).

3.3 Open-chain N_6 and $N_6 \rightarrow 3N_2$ dissociation

N_6 is isoelectronic with $(CNO)_2$, and consideration will be given here to the most-stable isomer of N_6, namely a twisted open-chain C_2 isomer [8], which we designate as $N_aN_bN_c$-$N'_cN'_bN'_a$. From the Kekulé structure **24**, the increased-valence structure **25**, with zero atomic formal charges, can be generated by delocalising N_c and N'_c p_x and p_y electrons into the bonding LMOs $\pi_x(N_bN_a)$, $\pi_x(N'_bN'_a)$, $\pi_y(N_bN_a)$ and $\pi_y(N'_bN'_a)$, as is indicated in structure **24**. (N.B. The p_y and π_y designations correspond to those which would obtain if the isomer were linear.) For the π_x electrons, $a = p_x(N_a)$, $b = \pi^*_x(N_bN_c)$, $c = \pi^*_x(N'_bN'_c)$, and $d = p_x(N'_a)$. As discussed in Ref. [13], the bond-orders that are implied by this structure are in accord with calculated estimates for the lengths of the N_a-N_b, N_b-N_c and N_c-N'_c bonds. In Ref. [9]. these lengths are 1.155, 1.262 and 1.463 Å.
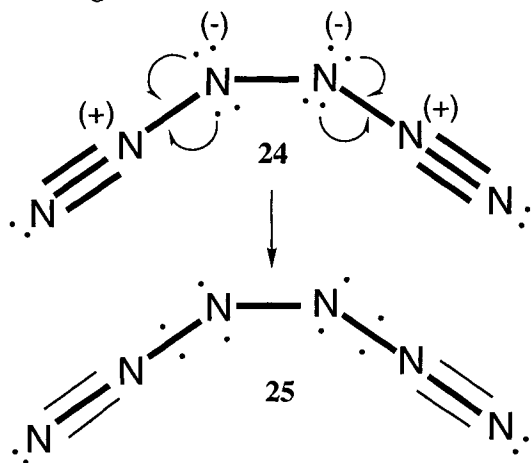
The Kekulé-type Lewis structure **24** is a component of the primary increased-valence structure **25**. The presence of lone-pair electrons on the N_c and N'_c atoms of structure **24** correlates with the calculated bending that occurs at these atoms to generate the C_2 geometry. For $(CNO)_2$, the N_c and N'_c atoms of N_6 are replaced by the carbon atoms, and the absence of lone-pair electrons for these atoms in the Lewis structure **14** permits the molecule to adopt either a linear or a quasi-linear geometry.

VB formulations for the decomposition of N_6 according to [**24 ↔ 26**] →

$3N_2$ and **25** → [**27** ↔ **28** ↔ **29**] → $3N_2$, involve heterolytic and homolytic dissociations of N-N bonds, respectively.
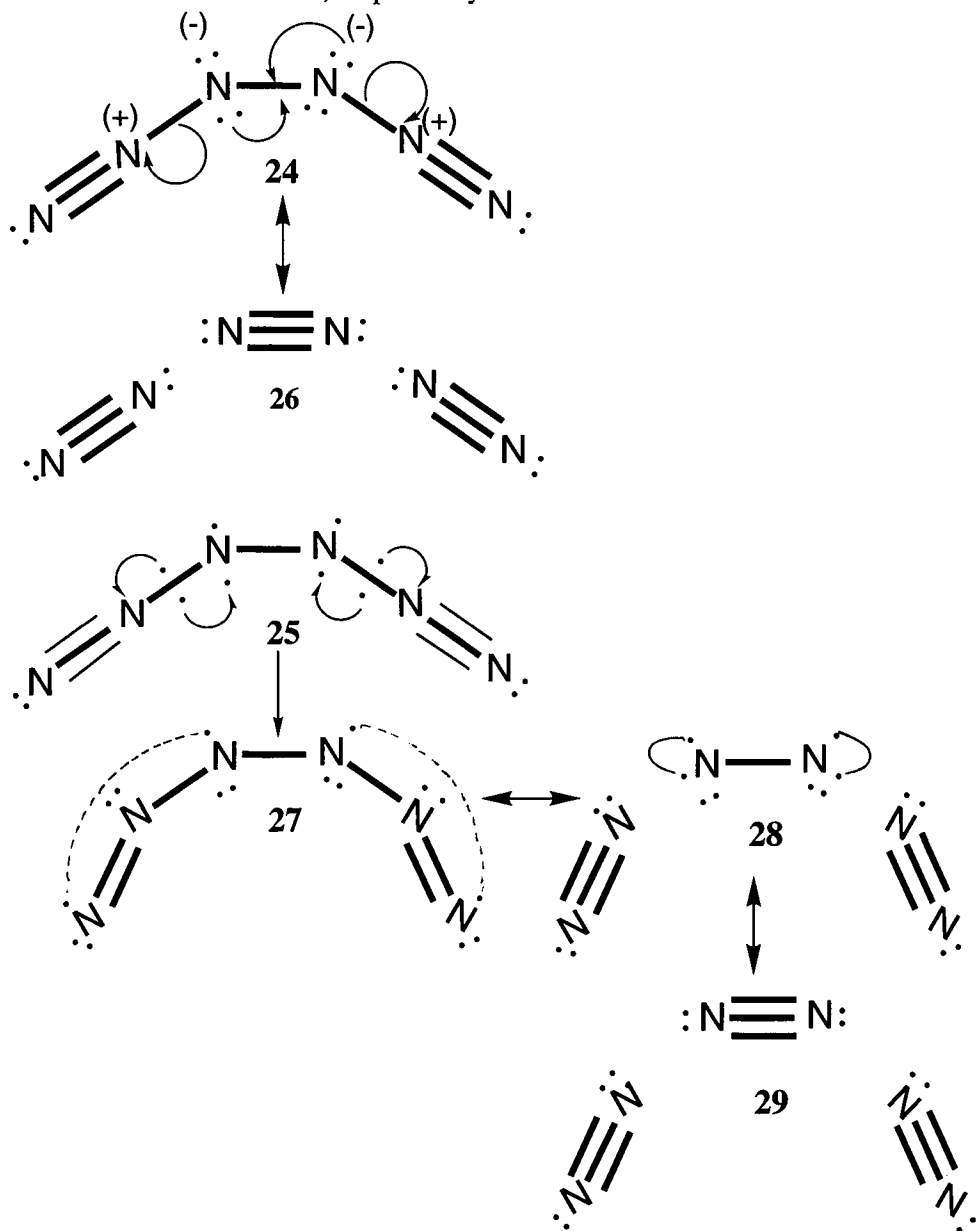
The spin theory which is associated with the homolytic dissociations of the N_b-N_c and N'_c-N'_b bonds corresponds to the use of Eq.(2) for the electrons of the N_b-N_c and N'_c-N'_b bonds in structure **27**, and Eq.(3) for these electrons

in structure **28**. For the **28** ↔ **29** resonance, Eq.(2) obtains for the four unpaired N_C and N'_C electrons of structure **28**, and Eq.(3) refers to these electrons in structure **29**, where they form two N_C-N'_C π-bonds. Which of the homonuclear and heteronuclear formulations is to be preferred will depend on which of the Lewis structures **24** and **27** has the lower energy.

Homolytic dissociations of N-N bonds have been used in Ref. [29] to provide VB formulations for the $N_{12} \rightarrow N_{10} \rightarrow N_8$ decompositions. Presumably the decomposition of each of the polymers of N_2 is assisted by the thermodynamic stability of the N_2 products.

3.4 Thermal decomposition of $O(N_3)_2$

The preparation of $O(N_3)_2$ has been reported recently [30]. The mechanism of Eq.(12) has been suggested [30] to account for the formation of N_2 and $N_2O(C_{\infty v})$ [30] as decomposition products.

$$O(N_3)_2(C_2) \rightarrow 2N_2 + N_2O(cyclic, C_{2v}) \qquad (12)$$
$$N_2O(cyclic, C_{2v}) \rightarrow N_2O(C_{\infty v})$$
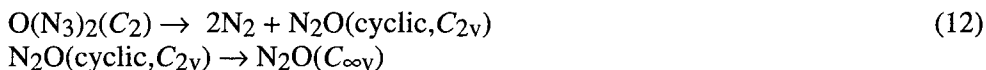
For $O(N_3)_2$, VB structures **30** and **31** are a Kekulé-type Lewis structure and the associated increased-valence structure, respectively [31]. Commencing with the latter structure, we can provide [31] the VB formulations of **32** → [**33** ↔ **34**] → $N_2O(cyclic, C_{2v})$ + $2N_2$ and $N_2O(cyclic, C_{2v})$ → **35** → **36** for the mechanism of Eq.(11). At each stage along the reaction coordinate, Eqs.(2) and (3) apply prior to and after the homolytic dissociations of N-N bonds.

Increased-valence structure **36** for $N_2O(C_{\infty v})$ is analogous to increased-valence structure **7** for isoelectronic HCNO. It has been used recently to develop a VB representation for the $N_2O(C_{\infty v}) \rightarrow N_2O(cyclic, C_{2v}) \rightarrow$ NON($D_{\infty h}$) isomerization process [32]. In Ref. [10], comparisons are made between **36** and other VB structures with apparently quinquevalent nitrogen atoms, and in Section 4.3, **36** provides the VB representation for N_2O when it is formed in NCO-NO and OCN-NO$_2$ decomposition reactions.

4. SOME OTHER SINGLET-SPIN CONSERVATION REACTIONS

4.1 Thermal decomposition of CH_2N_2, and the $CH_3NO_2 \rightarrow CH_3ONO$ isomerization

VB formulations for the spin-allowed thermal decomposition $N_2O(\Sigma_g^+)$ → $N_2(\Sigma_g^+)$ + $O^*(^1D)$, with heterolytic and homolytic dissociations of the N-O bond, have been provided in Ref. [33] The corresponding VB formulations for the spin-allowed thermal decomposition of CH_2N_2 are those of [**37** ↔ **38**] → $CH_2^*(S = 0)$ + N_2, and **39** → [**40** ↔ **41**] → $CH_2^*(S = 0)$ + N_2, respectively.

30

31

32

33

34

35

36
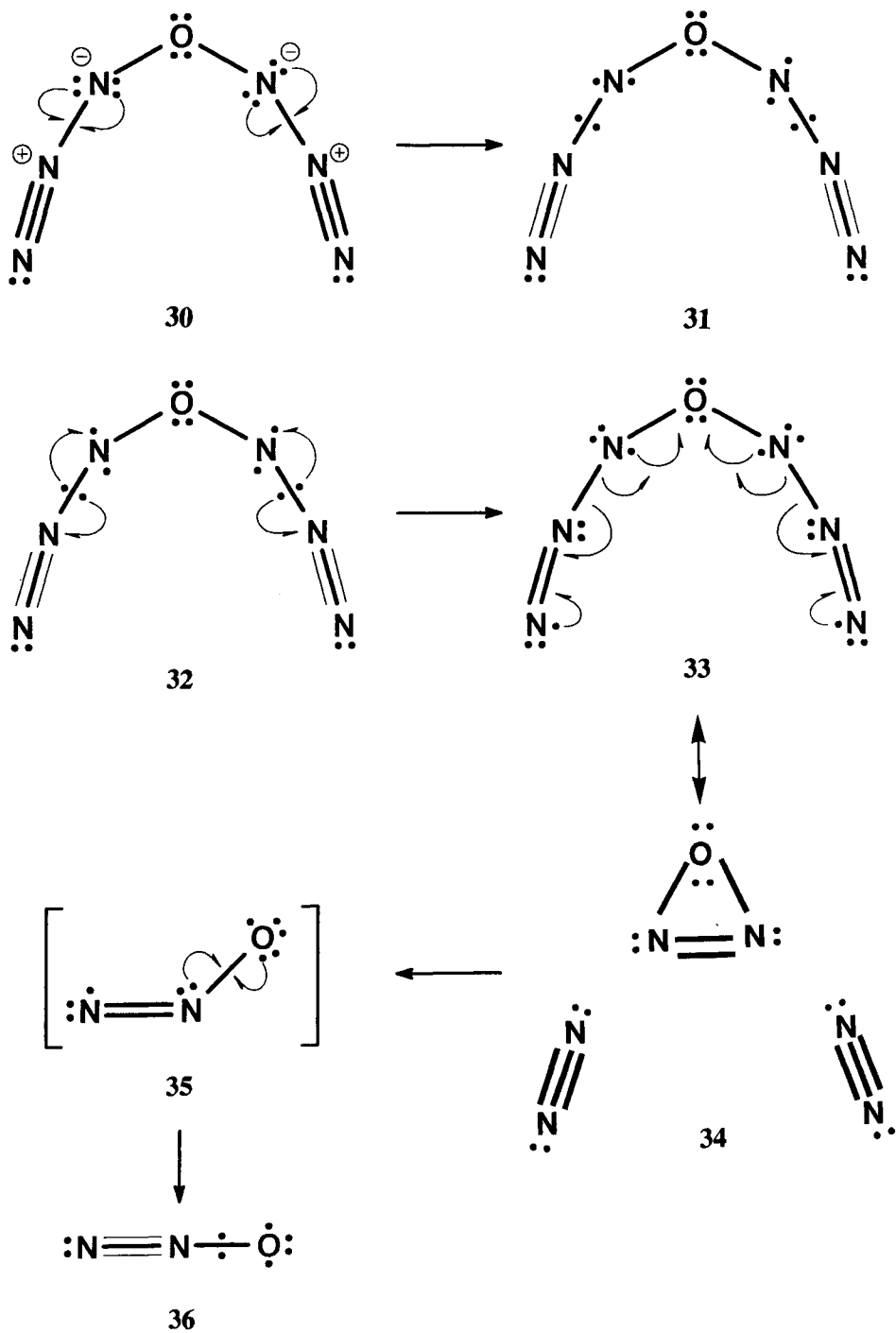
Similarly, the corresponding VB formulations for the $CH_3NO_2 \rightarrow CH_3ONO$ isomerization are those of $[\mathbf{42} \leftrightarrow \mathbf{43}] \rightarrow \mathbf{44}$, and $\mathbf{45} \rightarrow \mathbf{46} \rightarrow \mathbf{44}$, respectively. But no change in electron spin couplings occurs for this reaction.

37

38

39

40

41

42

43

44

45

46
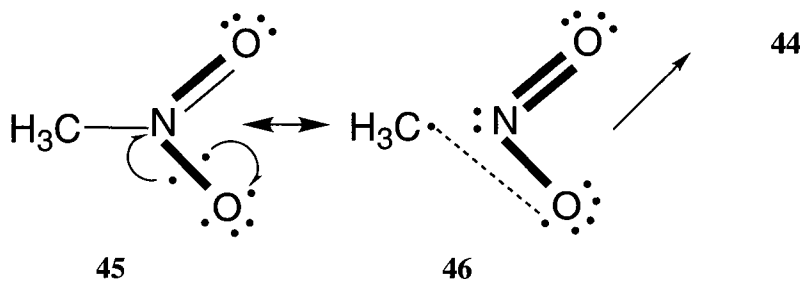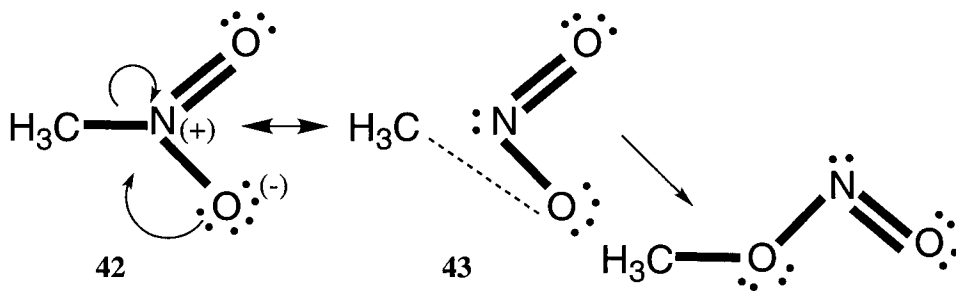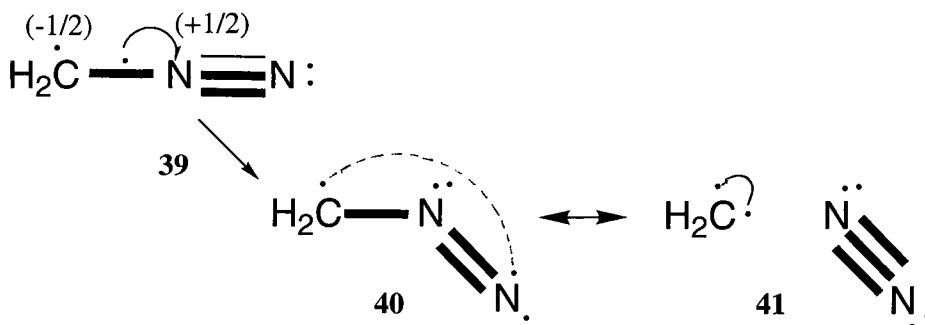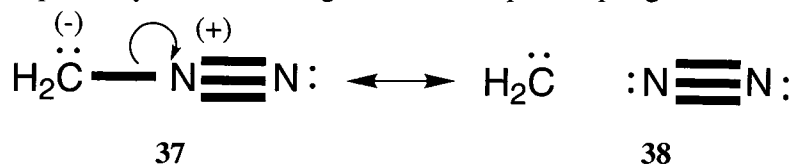
As is the case for the examples considered in the previous sections, and below, the VB formulation to be preferred for dissociation will depend on the relative energies of the Kekulé and Dewar-type Lewis structures.

The increased-valence structures **39** and **45** for CH_2N_2 and CH_3NO_2 are generated from the Kekulé-type Lewis structures **37** and **42** via the one-electron delocalisations that are indicated in structures **47** and **48**. More

complete increased-valence representations for the electronic structure of CH_2N_2 are provided in Refs. [2,19].

47 **39**

48 **45**
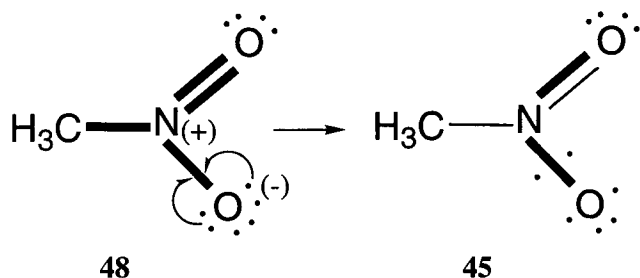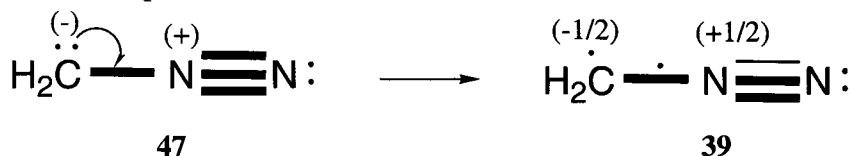
4.2 1,3-dipolar cycloaddition reactions

49 **50** **51**
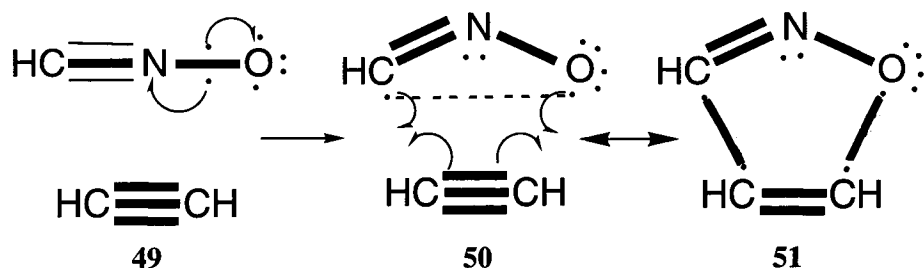
1,3-dipolar (or zwitterionic diradical hybrid [19]) cycloaddition reactions, such as the addition of HCNO to HCCH to generate the cyclo-isoxazole product, involve singlet states for the reactants and products. The primary active space electrons for the separated reactants are four π electrons (π_x for example) for the HCNO, and two π_x electrons for HCCH. As was done in Ref. [10], we shall assume here that increased-valence structure **7** provides the primary VB representation for HCNO. In Eq.(10), $\pi_x(NO)$ is doubly-occupied, and therefore the simplest description of the active space orbitals for this structure are then a = $p_x(C)$ and b = $\pi^*_x(NO)$ (cf. Eq.(10)). For HCCH, the active space AOs, c and d, are $p_x(C)$ AOs. The a-b and c-d spin-pairings of Eq.(2) then obtain for the separated reactants that are indicated in structure **49**.

As cycloaddition proceeds according to the electronic reorganization indicated in VB structures **49** → [**50** ↔ **51**] → isoxazole, changes in the spin-pairings occur - a with c and b with d - and Eq.(3) is associated with this spin-pairing [19,34]. Geometrical changes also occur, and these lead to the introduction of s-p hybridisation into the component AOs that are associated

with all of the active-space orbitals, as well as the π_y AOs. At each stage along the reaction coordinate, the reaction profile is then given by Eq.(4) with $C_2 = 0$ at the commencement of the reaction, and $|C_2| >> |C_1|$ when cycloaddition has occurred.

For simplicity of representation only, we have assumed that the electronic organization indicated in structure **49** has gone to completion in structures **50** and **51**. Of course, the extent to which the electronic reorganization occurs differs at each stage along the reaction coordinate.

We can elaborate this VB formulation for the cycloaddition by replacing the nearest-neighbour active-space AOs in VB structures **50** and **51** with Coulson-Fischer orbitals [34(b)]. Thus if a and b are now the singly-occupied carbon and oxygen AOs of HCNO, and c and d are the singly-occupied carbon AOs of HCCH, the c and d AOs in structure **50** can be replaced by the Coulson-Fischer MOs c + k'd and d + k"c. In structure **51**, a + λd, b + λc, c + κ'b and d + κ"a can replace the a, b c and d AOs. Use of these orbitals permits additional canonical Lewis VB structures to be included in the equivalent Lewis structure resonance scheme. The mechanism can then accommodate some charge transfer between the HCNO and HCCH reactants. The more-flexible wavefunction of Eq.(13),

$$\Psi = C_1(\Psi_{50})_R + C_2(\Psi_{51})_P + C_3(\Psi_{50})_P + C_4(\Psi_{51})_R \qquad (13)$$

in which the subscripts "R" (reactant-like) and "P" (product-like) refer to the spin-pairings of Eqs.(2) and (3), replaces the $\Psi = C_1(\Psi_{50})_R + C_2(\Psi_{51})_P$ of Eq.(4). The latter wave-function obtains when AOs rather than the Coulson-Fischer MOs are used in each of the VB structures

Alternative VB representations for the cycloaddition process are displayed and discussed in Refs. [2,10,19,34]. Some of them also include the less-important increased-valence structures, such as **8-10** here, in the resonance schemes. Recent MO [35] and spin-coupled VB [36] studies for this process do not give consideration to the concerted diradical formulation. The VB studies of Ref. [37] correspond to the concerted diradical mechanism discussed in Ref. [34].

4.3 NCO-NO → N₂O + CO* and OCN-NO₂→ N₂O + CO₂

Gaseous N_2O and CO are among the products that are obtained when HCN(g) reacts with $NO_2^+BF_4^-$(s) [38]. VB representations for the formation of these products, and also N_2 and CO_2, via the decomposition of an OCN-NO intermediate, have been provided in Ref. [2b]. In Figures 1 and 2, we display similar types of VB representations for the reactions NCO-NO → N_2O + CO* and OCN-NO₂→ N_2O + CO_2, one or both of which has been studied in Refs. [5,39,40]. Except for the resonance between the reactant OCN-NO₂ structures of Figure 2, each ↔ resonance symbol relates two VB structures which differ
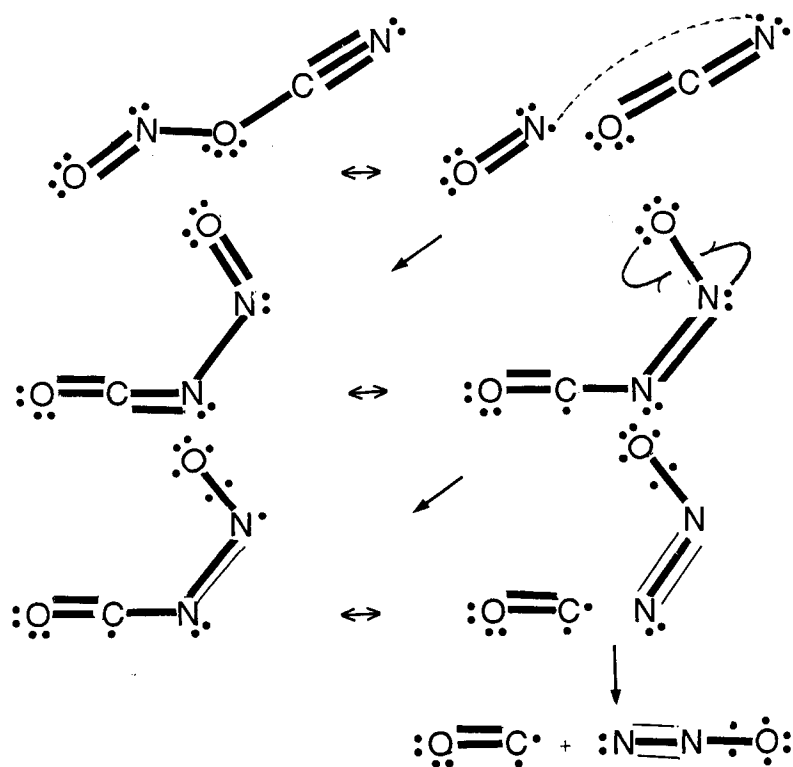
Fig. 1. VB representation for NCO-NO → N₂O + CO*.
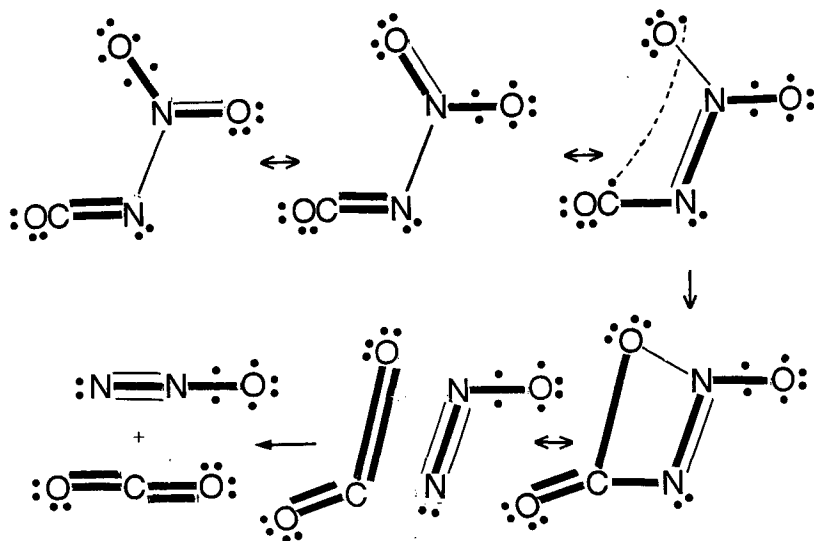
Fig. 2. VB representation for OCN-NO₂ → N₂O + CO₂.

in their spin pairings for four electrons, according to Eqs.(2) and (3). In Figure 1, the CO is formed in an electronically excited state.

5 $O_2(S = 1) + 2X(S = 1/2) \rightarrow XO_2X(S = 0)$ or $O_2(S = 1) + Y(S = 1) \rightarrow YO_2(S = 0)$
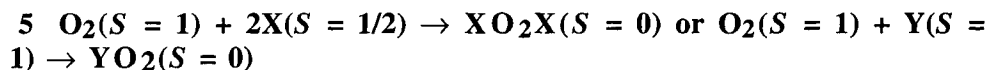
5.1 Wavefunctions

For the 1,3-dipolar cycloaddition reaction, the reactants involved ($S = 0$) closed-shell configurations. We now give consideration to the spin theory for reactions between open-shell systems, using as examples the reactions of $^3\Sigma_g^-$ O_2 with either two univalent radicals (X, for example, H, CH_3, F and Cl) or an ($S = 1$) divalent radical (Y, for example, $O(^3P)$, $O_2(^3\Sigma_g^-)$, and intermediate-spin Fe^{II} as in oxyhaemoglobin or oxymyoglobin [2,4,41-43]).

For Eqs.(2) and (3), the b and c orbitals are the singly occupied antibonding π^*_x and π^*_y MOs of $^3\Sigma_g^-$ O_2. These orbitals overlap respectively with the singly-occupied a and d orbitals of either two X($S = 1/2$) radicals, or one Y($S = 1$) radical. With R equal to either X + X, or Y, and the S and M_S spin quantum numbers indicated as (S, M_S), the wavefunctions of Eqs.(2) and (3), which describe two types of spin-pairings, can be expressed in terms of spectroscopic states for the separated reactants, according to Eqs.(14) and (15) [43],

$$\psi_1 = -\left|\psi_R(1,1)\psi_{O_2}(1,-1)\right| - \left|\psi_R(1,-1)\psi_{O_2}(1,1)\right|$$
$$+ \left\{\left|\psi_R(1,0)\psi_{O_2}(1,0)\right| + \left|\psi_R(0,0)\psi_{O_2}(0,0)\right|\right\}/2 \qquad (14)$$

$$\psi_2 = \left|\psi_R(0,0)\psi_{O_2}(0,0)\right| \qquad (15)$$

Neither of these wavefunctions generates the uncontaminated spectroscopic ground-states of the separated reactants. These states are obtained via the linear combination $\Psi = \psi_1 - \psi_2/2$ which ensures that each of the the three degenerate $M_S = 1$ components of both O_2 and R contributes to the ground-state resonance scheme for the reactants. This linear combination is orthogonal to ψ_2, which generates $S = 0$ excited states for the reactants.

5.2 O_2 and increased-valence structures for O_3, $Fe^{II}O_2$ and FO_2F

| 52 | 53 | 54 | 55 | 56 |
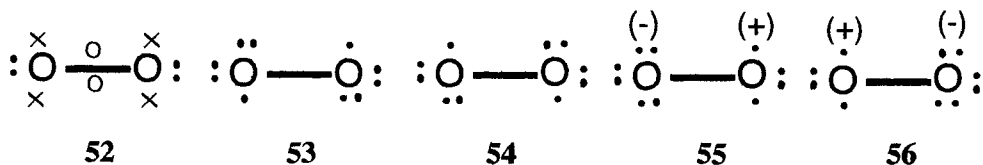
The Linnett VB structure 52 for O_2 [2-4,44,45] corresponds to the ground-state MO configuration, $(\sigma s)^2(\sigma^* s)^2(\sigma p_z)^2(\pi_x)^2(\pi_y)^2(\pi^*_x)^1(\pi^*_y)^1$ for the valence-shell electrons of O_2 when $S = M_S = 1$. The crosses and circles (x

and o [45,46]) represent π electrons with α and β spin wavefunctions. Structure **52** is equivalent to resonance between the Lewis VB structures **53-56**.
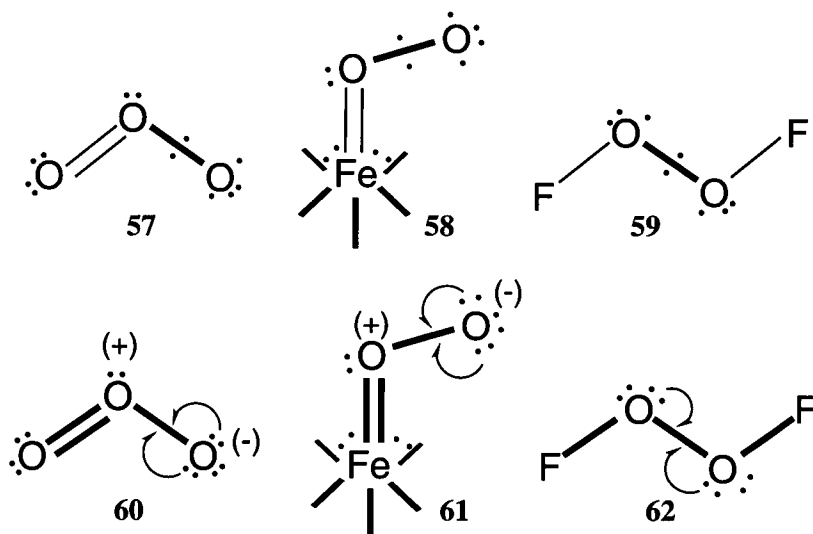
Increased-valence structures **57-59** for O_3, an $Fe^{II}O_2$ linkage of oxyhaemoglobin and FO_2F, can be constructed [2,3(a),3(b),4] either by spin-pairing the unpaired π^*_x and π^*_y electrons of VB structure **52** for O_2, with the unpaired electrons of $O(S = 1)$, $Fe^{II}(S = 1)$ and $2F(S = 1/2)$, or by delocalising oxygen non-bonding electrons of the Kekulé-type Lewis structures **60-62** into O-O bonding LMOs as is indicated in these structures. Bond properties (for example, stretching frequencies and/or bond lengths) that are implied by these increased-valence structures are in qualitative accord with experimental estimates of the values for these properties [2,3(b),42]. The origin of the difference in the O-O bond properties for HO_2H relative to those of FO_2F has been discussed [2,3(b)] in terms of differences in O-H versus O-F bond strengths.

5.3 $Fe^{II}O_2Fe^{II}(S = 1) \to 2Fe^{II}O(S = 1)$ and $Cu^IO_2Fe^{II} \to Cu^IO + Fe^{II}O$

The mechanism of Eq.(16) [46] has been postulated to account for the irreversible oxidation of various Fe^{II} complexes by O_2.

$$Fe^{II} + O_2 \to Fe^{II}O_2$$
$$Fe^{II}O_2 + Fe^{II} \to Fe^{II}O_2Fe^{II} \qquad\qquad (16)$$
$$Fe^{II}O_2Fe^{II} \to Fe^{II}O$$
$$Fe^{II}O + Fe^{II} \to Fe^{II}OFe^{II}$$

Using the intermediate-spin $S = 1$ state as the valence state of the Fe^{II} complex, (cf. $Fe^{II}(S = 1) + O_2(S = 1) \to Fe^{II}O_2(S = 0)$ for the bonding of O_2

to haemoglobin), a VB representation for this mechanism has been presented elsewhere on several occasions [2,4,47]. It utilizes the $S = 0$ increased-valence structure **58** to represent the $Fe^{II}O_2$. The reaction of $Fe^{II}O_2(S = 0)$ with $Fe^{II}(S = 1)$ initially generates increased-valence structure **64** to represent $Fe^{II}O_2Fe^{II}(S = 1)$. Reorganization of the electron distribution to increase the number of bonding electrons generates VB structure **65**, with a weakened O-O bond. On dissociation of this bond, the $Fe^{II}O$ species of structure **66** are formed.

63   +   **Fe**   →   **64**

66   +   ←   **65**
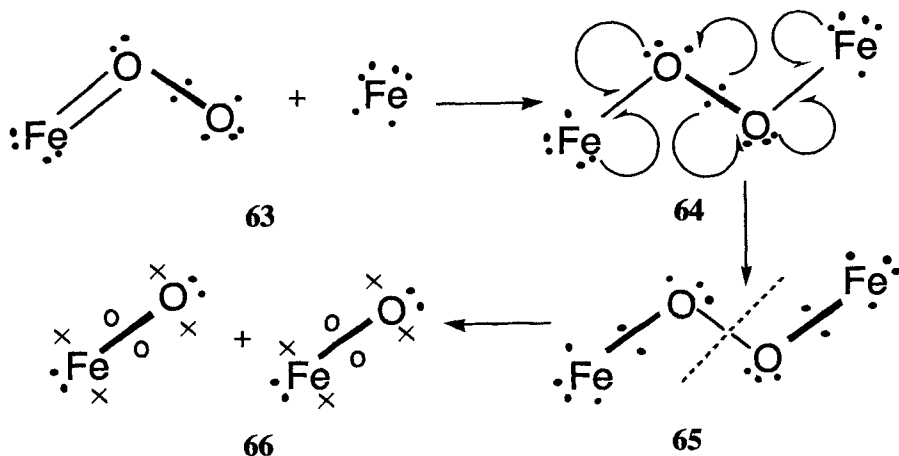
We now deduce that each $Fe^{II}O$, with 16 valence shell electrons (cf. O_2) and two singly-occupied antibonding π_g MOs is generated in its $S = 1$ ground-state. If these MOs are designated as $a = \pi^*_x$ and $d = \pi^*_y$ for one $Fe^{II}O$ moiety of VB structure **66**, and as $b = \pi'^*_x$ and $c = \pi'^*_y$ for the other moiety, then the three linearly independent $S = 1$ wavefunctions of Eqs.(5)-(7) can be constructed to represent the four active-space electrons of VB structure **66**. Due to symmetry, $^3\Psi_1$ and $^3\Psi_2$ are degenerate, and the $\pm$ linear combinations of Eqs.(17)-(20),

$$^3\Psi_- = {}^3\Psi_1 - {}^3\Psi_2 = \left|a^\alpha d^\alpha (b^\alpha c^\beta + b^\beta c^\alpha)\right| - \left|(a^\alpha d^\beta + a^\beta d^\alpha)b^\alpha c^\alpha\right| \tag{17}$$

$$= \left|\psi_{FeO}(1,1)\psi_{Fe'O'}(1,0)\right| - \left|\psi_{FeO}(1,0)\psi_{Fe'O'}(1,1)\right| \tag{18}$$

$$^3\Psi_+ = {}^3\Psi_1 + {}^3\Psi_2 = \left|a^\alpha d^\alpha (b^\beta c^\alpha - b^\alpha c^\beta)\right| + \left|(a^\alpha d^\beta - a^\beta d^\alpha)b^\alpha c^\alpha\right| \tag{19}$$

$$= \left|\psi_{FeO}(1,1)\psi_{Fe'O'}(0,0)\right| + \left|\psi_{FeO}(0,0)\psi_{Fe'O'}(1,1)\right| \tag{20}$$

can be constructed, in which (1,1) etc. designate the S and M_S spin quantum numbers for the $Fe^{II}O$ and $Fe'^{II}O'$ moieties. Similarly, the $^3\Psi_3$ of Eq.(5) can be expressed according to Eq.(21).

$$^3\Psi_3 = \left|a^\alpha d^\alpha (b^\alpha c^\beta + c^\alpha b^\beta)\right| = \left|\psi_{FeO}(1,1)\psi_{Fe'O'}(0,0)\right| \tag{21}$$

At infinite separation between the $Fe^{II}O$ and $Fe'^{II}O'$ moieties, $^3\Psi_-$ and $^3\Psi_+$ do not interact with $^3\Psi_3$. Hund's rule requires that $^3\Psi_-$ gives the dissociation products of lowest energy. Eq.(18) indicates that each of them involves an $S = 1$ state*. A variation on the derivation of this result is provided in Ref. [47(a)], where three $S = 1$ and $M_S = 0$ wavefunctions are used to describe the electronic structure of the $Fe^{II}O_2Fe^{II}(S = 1)$ complex.

An alternative electronic mechanism, which involves $Fe^{II}O_2Fe^{II}(S = 0)$ instead of $Fe^{II}O_2Fe^{II}(S = 1)$, is discussed below in Section 5.6.

A similar type of VB approach can be used to represent the breaking of the O-O bond of O_2 via the cytochrome c oxidase catalysis of the reduction of O_2 to H_2O [2,4,47(b)]. One of the $Fe^{II}(S = 1)$ of VB structure **64** is replaced by $Cu^I(S = 1)$, as in VB structure **67**, and the electronic reorganization indicated in this structure generates VB structure **68** with a weakened O-O bond.

67   **68**
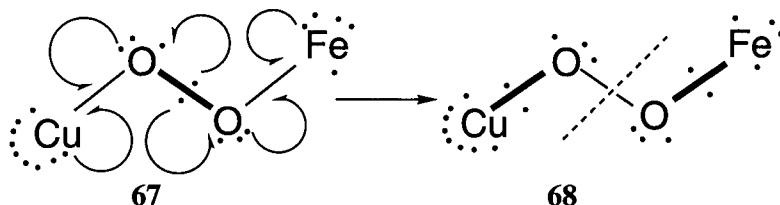
5.4 Thermal dissociation of $(^3\Sigma_g^-) \, O_2$

The VB theory for the dissociation of $(^3\Sigma_g^-) \, O_2$ to generate two $O(^3P)$ atoms, has been considered by Byrman and van Lenthe [48], and will be reconsidered here in terms of the theory presented in the previous section. For large internuclear separations, the "co-ionic" Lewis structures **55** and **56** make essentially no contribution to the ground-state resonance scheme, and the uncharged structures **53** and **54** essentially do not interact with each other. There are four active space AOs which are involved in the dissociation of either of the latter structures. These AOs are the two AOs that participate in the formation of the O-O σ-bond, the singly-occupied $2p_x$ AO of one atom and the singly-occupied $2p_y$ AO of the other atom. Designating these AOs as a = $2p\sigma$, b = $2p'\sigma$, c = $2p'_x$ or $2p'_y$, and d = $2p_y$ or $2p_x$ respectively, then the appropriate $S = M_S = 1$ wavefunctions are those of Eqs.(17), (19) and (21), in which the a electron is spin-paired with the b electron, but parallel spins obtain for the c and d electrons. The resulting theory for the dissociation of $(^3\Sigma_g^-)$ O_2 is identical with that described in Section 5.3 for the dissociation of $Fe^{II}O_2Fe^{II}(S = 1)$ and leads to the generation of $S = 1$ oxygen atoms as the dissociation products.

5.5 Photochemical decomposition of O_3

For O_3, two equivalent increased-valence structures **57** and **69** can be

---

* For simplicity, both $Fe^{II}O$ species in VB structure **66** are displayed for $S = M_S = 1$, each of which involves one Slater determinant. According to Eq.(18), $S = 1$ with $M_S = 0$ and +1. $S = 1$ with $M_S = 0$ involves two Slater determinants, to give two $(S = 1 \pm S = 0)/2$ VB "structures".

constructed, and resonance between these structures generates a $^1A_1$ symmetry ground-state and a $^1B_2$ symmetry excited state. The wavefunction for the ground-state resonance is $\Psi(^1A_1) = \Psi_{57} + \Psi_{69}$, when it is assumed that $\sigma_v\Psi_{57} = \Psi_{69}$ and $\sigma_v\Psi_{69} = \Psi_{57}$ in which σ_v is the reflection symmetry operator for the C_{2v} symmetry group. With Heitler-London AO wavefunctions to represent the fractional O=O bonds in structures **57** and **69**, This resonance is equivalent to resonance between the Lewis structures **70-76**, according to Eq.(22),
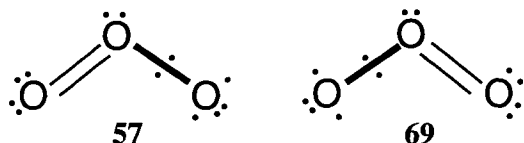
$$\Psi(^1A_1) = \Psi_{57} + \Psi_{69}$$

$$= \kappa(\Psi_{70} + \Psi_{71}) + 2k\Psi_{72} + \Psi_{73} + \Psi_{74} + k\kappa(\Psi_{75} + \Psi_{76}) \qquad (22)$$

in which $\psi_{ab} = b + ka$ and $\psi_{a'b'} = b' + \kappa a'$ type LMOs accommodate the electrons that form the two one-electron bonds in the increased-valence structures. (For free O_2, a and b are the $2p\pi_x$ AOs, a' and b' are the $2p\pi_y$ AOs, and $k = \kappa = 1$ in the ground-state MO configuration. For O_3, the a and a' AOs are located on the central atom, a' acquires some 2s character, and $k \neq \kappa \neq 1$.) The results of both semi-empirical [16] and ab-initio VB calculations [20,49] indicate that the Dewar structure **72** is the dominant Lewis structure, and this is the VB structure which is needed to conserve molecular C_{2v} symmetry.
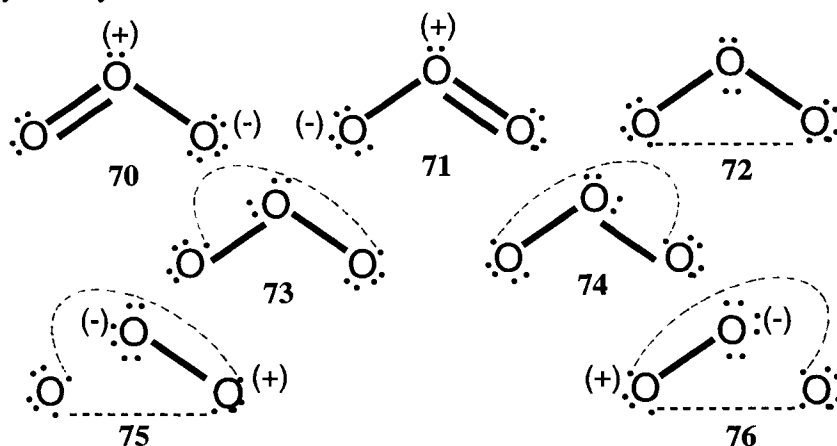
Photochemical dissociation of O_3 can generate $O_2(^3\Sigma_g^-) + O(^3P)$ as well as $O_2(^1\Delta_g) + O(^1D)$ [50]. A low-energy $S = 0$ excited state has $^1B_2$ symmetry. In terms of resonance between the increased-valence structures, the wavefunction for this state is $\Psi(^1B_2) = \Psi_{57} - \Psi_{69}$, which can be expressed according to Eq.(23),

$$\Psi(^1B_2) = \Psi_{57} - \Psi_{69} = \kappa(\Psi_{70} - \Psi_{71}) + \Psi_{73} - \Psi_{74} + k\kappa(\Psi_{75} - \Psi_{76}) \qquad (23)$$

in which Ψ_{72} for the Dewar structure **72** is absent. Therefore C_{2v} symmetry need no longer be conserved, and the stretching of one O-O bond relative to the other can now occur, to generate the wavefunction $\Psi = C_{57}\Psi_{57} - C_{69}\Psi_{69}$. The Ψ_{57} can be expressed as $\Psi_{57} = |C_1|\psi_1 + |C_2|\psi_2$, in which the ψ_1 and ψ_2 are given by Eqs.(14) and (15). If the left-hand O=O bond is stretched, then $C_{69} = 0$ when dissociation of this bond occurs, and Ψ_{57} is equal to $\psi_1 - \psi_2/2$ which generates $O_2(^3\Sigma_g^-) + O(^3P)$ as dissociation products.

5.6 S_2O_2, O_4 and $Fe^{II}O_2Fe^{II}$ ($S = 0$)

Each of $Fe^{II}O_2Fe^{II}$, O_4 and S_2O_2 has 24 valence shell electrons. The ground-states of the latter two species have D_{2h} and C_{2v} symmetries, respectively, and $S = 0$ states. The $S = 0$ wavefunctions for the four active space electrons of each of O_4 and S_2O_2 are given by Eqs.(2)-(4), with a = π^*_x, b = $\pi^{*'}_x$, c = π^*_y and d = $\pi^{*'}_y$. Using the spin theory of the type described above for the photochemical dissociation of O_3, it can be deduced that $S = 0$ O_4 and S_2O_2 dissociate to form $S = 1$ O_2 and SO radicals, respectively. An increased-valence structure for S_2O_2 has been derived and displayed on several occasions elsewhere [2,4,51]. The corresponding increased-valence structure **79** for D_{2h} O_4 can be constructed either by π^*_x-$\pi^{*'}_x$ and π^*_y-$\pi^{*'}_y$ spin pairings of the unpaired electrons of the $^3\Sigma_g^-$ O_2 radicals of **52**, or from the Kekulé-type Lewis structure **77** via structure **78**.
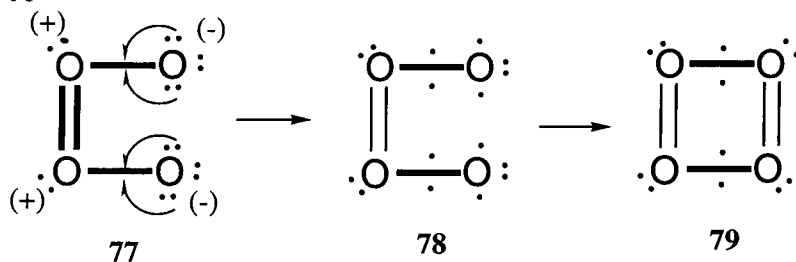
Increased-valence structure **79** retains the double-bond character for each of the O_2 moieties. This structure also involves fractional intermolecular O=O bonds - their σ and π bond-numbers are both equal to 0.25 [43] - thereby implying that the latter bonds should be substantially longer than normal O=O bonds. These bond properties are in accord with calculated estimates of the O-O bond-lengths for O_4 (1.21 and 3.2-3.5 Å [43]). However the results of STO-6G VB calculations show that the π^*_x-$\pi^{*'}_x$ and π^*_y-$\pi^{*'}_y$ spin-pairings alone are not sufficient to stabilize the dimer relative to the two monomers [43]. Dispersion and charge-transfer interactions are also needed to generate a small binding energy (14-154 cm^{-1}) for the dimer (cf. [43(b)] and Refs. therein, for example).

By analogy with S_2O_2 and O_4, an $S = 0$ state for $Fe^{II}O_2Fe^{II}$, with an increased-valence structure of type **65**, but with opposed spins for the two

unpaired electrons of this structure, would also generate $Fe^{II}O(S = 1)$ radicals when its O-O bond is broken. Measurements of the magnetic susceptibilities for several $Fe^{II}O_2Fe^{II}$ species indicate that the electron spins are coupled antiferromagnetically (for example $J = -33$ cm^{-1} [52]), but because the value of the magnetic exchange parameter J is small, an $S = 1$ state is thermally accessible. When this spin state is attained, the spin theory described earlier is relevant to account for the formation of the $Fe^{II}O(S = 1)$ radicals.

With S=S replacing O=O in VB structure **78**, the primary increased-valence structure for C_{2v} symmetry S_2O_2 is obtained [2,4,51].

5.7 $S_2O_3(S = 1)$
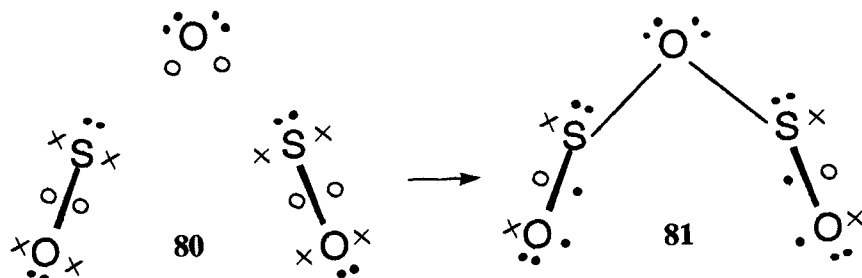
Isomers of S_2O_3 have been studied recently [53.]. An OSOSO($S = 1$) isomer is the ground-state, and it decomposes to form SO($S = 1$) and SO$_2$($S = 0$). An increased-valence structure for this isomer is obtained by bonding two SO($S = M_S = 1$) monomers to an $^3P(M_S = -1)$ oxygen atom, as indicated in **80** $\rightarrow$ **81**. A VB formulation for OSOSO($S = 1$) $\rightarrow$ SO($S = 1$) + SO$_2$($S = 0$).is provided in **82** $\rightarrow$ **83**. For SO$_2$, the increased-valence structure of **83** and its mirror-image are identical to structures **57** and **69** for O$_3$.
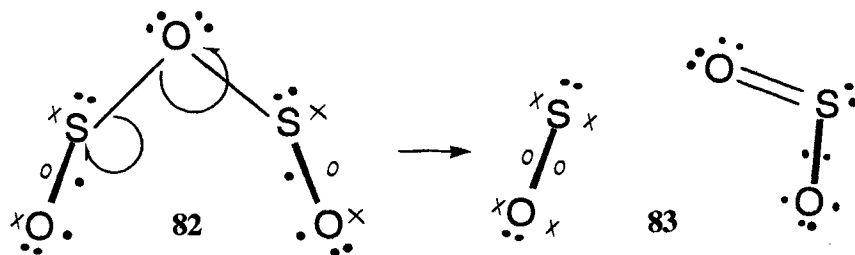
When proceeding from **80** to **81**, the singly-occupied in-plane π^*_x(SO), 2p(O), 2p'(O) and π^*_x(S'O') orbitals are the active space orbitals which correspond to the a, b, c and d orbitals of Eqs.(2) and (3). For structure **81**, the spin-pairing scheme corresponds to that of Eq.(2). The active space orbitals for the dissociation of **82** $\rightarrow$ **83** are the π^*_x(SO), 2p(O) and π^*_y(S'O') of the planar S_2O_3, with geometrical changes occurring in order that the 2p(O) and π^*_y(S'O') orbitals can overlap.

6. ELECTRON CONDUCTION IN ALKALI METALS

(a) Pauling 2pσ AO mechanism

$(+)$ $(-)$
Li   Li   Li — Li   Li — Li   Li — Li

$(+)$ $(-)$
Li   Li — Li — Li   Li — Li   Li — Li

$(+)$ $(-)$
Li   Li — Li   Li — Li — Li   Li — Li

(b) Antibonding σ*2s MO mechanism

$(\sigma)^1$ $(\sigma)^2(\sigma^*)^1$ $(\sigma)^2(\sigma^*)^0$ $(\sigma)^2$
$(+)$ $(-)$
Li • Li   Li • Li   Li — Li   Li — Li

$(\sigma)^1$ $(\sigma)^2$ $(\sigma)^2(\sigma^*)^1$ $(\sigma)^2(\sigma^*)^0$
$(+)$ $(-)$
Li • Li   Li — Li   Li • Li   Li — Li

$(\sigma)^1$ $(\sigma)^2$ $(\sigma)^2$ $(\sigma)^2(\sigma^*)^1$
$(+)$ $(-)$
Li • Li   Li — Li   Li — Li   Li • Li
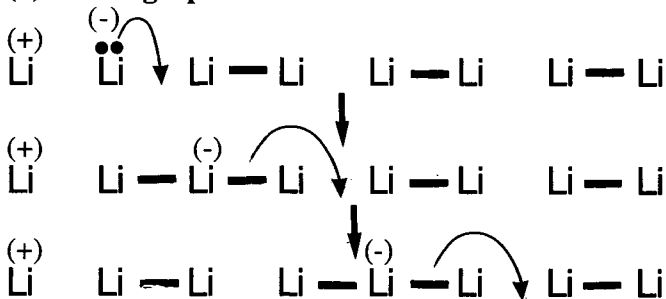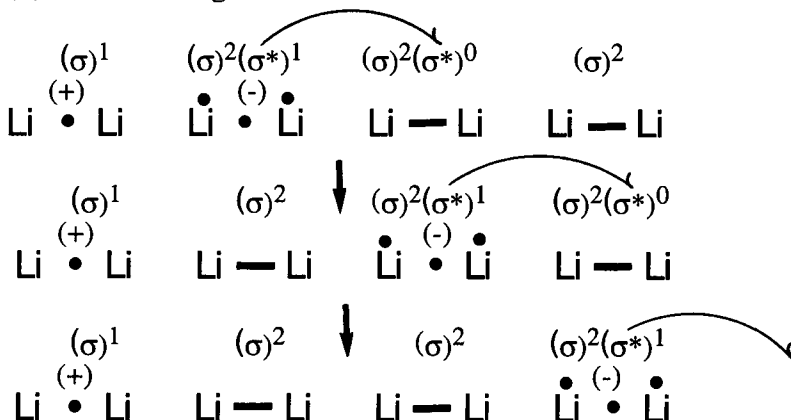
Fig. 3. VB mechanisms for electron conduction in lithium with (a) 2pσ AOs and (b) σ*2s MOs as "metallic orbitals". For simplicity in (b), the MO configuration $(\sigma)^2$ is used to designate each electron-pair bond, i.e. $k' = 1/k''$ in the Coulson-Fischer MOs $\sigma' \equiv \psi'_{ab} = a + k'b$ and $\sigma'' \equiv \psi''_{ba} = b + k''a$ Cathode (-) on left, anode (+) on right. See Appendix to this Chapter for an elaboration of the antibonding orbital mechanism.

Pauling has introduced a "metallic" orbital [54] in order to provide a VB representation for electron conduction in alkali metals. For lithium, this orbital is a 2pσ AO, and use of it enables "bicovalent" VB structures such as

$$Li^{(+)}Li\text{-}Li^{(-)}\text{-}Li$$

to be implicated in the conduction process. The results of VB calculations [55] show that bicovalent structures help to provide an appreciable contribution to the cohesive energy for the metallic solid. However whether or not such structures are of primary importance for the conduction process has yet to be determined. For a linear arrangement of atoms, use of the bicovalent structures implies that electron conduction proceeds according to Figure 3(a).

One of several alternative mechanisms involves the delocalisation of an electron from the antibonding σ^* MO of $Li_2^+ Li_2^-$ into the vacant antibonding σ^* MO of Li_2 [2,3(c),56)]. In its simplest formulation, this is the σ^*2s MO. The formulation of Ref. [3(b)] is displayed in Figure 3(b), for which the conduction band has been entered via a $[(\sigma)^2][(\sigma)^2] \rightarrow [(\sigma)^1][(\sigma)^2(\sigma^*)^1]$ excitation*. However to simplify the subsequent VB treatment, the formulation of Refs. [2,56] is used, in which $Li^{(+)}Li_3^{(-)}$ replaces $Li_2^{(+)}Li_2^{(-)}$.

We report here the results of STO-6G VB calculations for linear $Li^{(+)}Li_3^{(-)}$ as $Li^{(+)}(Li_Y Li_A Li_B)^{(-)}$ in order to compare aspects of the first step for the two mechanisms, i.e. the transfer of an $Li_Y^{(-)}$ electron into either the Li_A $2p\sigma$ AO, or into the antibonding $Li_A Li_B$ σ^*2s MO. The calculations were performed using Roso's ab initio program [57], with Slater exponents for the 1s, 2s(neutral) and 2s(negative) AOs, but with the exponent for the 2p(negative) AO energy-optimized. The nine canonical Lewis structures of Table 1 were initially included in the calculations, with Li-Li internuclear separations of 3.03 Å (as occurs in the bulk metal). The bicovalent structure **VII** involves four singly-occupied AOs, and its $S = 0$ wavefunctions is given by Eq.(2), with a = $2s_Y$, b = $2p\sigma_A$, c = $2s_A$ and d = $2s_B$. Structure **VIII** also has four singly-occupied AOs, and its $S = 0$ wavefunction is given by Eq.(3). The weight for each VB structure ($W_i = C_i^2/\Sigma C_i^2$ [58]), is reported in Table 1, for which the Ψ_i and Ψ_f are the wavefunctions prior to and after the transfer of an electron from the $Li_Y^{(-)}$ into an AO centred on either Li_A or Li_B.

The results of the calculations show that prior to electron transfer, the dominant structure is structure **I**. On delocalising an electron from the $Li_Y^{(-)}$ of structure **I** into either a Li_A or a Li_B AO, structures **II** and **III** are calculated to have larger weights than has the bicovalent structure **VII**.

We now demonstrate that, in the simplest treatment, it is more favourable energetically to delocalise an electron into an antibonding σ^*2s MO rather than into the 2p AO. To do this, we have performed separate calculations using structures **I-V**, and **I, IV, V** and **VII**. The results (Table 1) show that 0.100 a.u. of energy is needed to transfer an electron from $Li_Y^{(-)}$ into the σ^*2s MO whereas the $Li_Y^{(-)} \rightarrow Li_A(2p)$ delocalisation requires 0.114 a.u.

Of course the above treatment is not definitive, but it does suggest that the antibonding σ^*2s MO mechanism can compare favourably with the pivotal resonance mechanism as the primary VB formulation for electron conduction in metallic lithium.

One way to include the $2p\sigma_A$ as well as the 2s AOs in the antibonding MO mechanism involves an initial formulation of the wavefunction for the four valence-shell electrons of

$$Li^{(+)} \ \overset{..}{Li}^{(-)} \ Li\text{-}Li$$

---
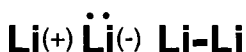
*An alternative entry into the conduction band is via a $[(\sigma)^2][(\sigma)^2] \rightarrow [(\sigma)^1(\sigma^*)^1][(\sigma)^2]$. excitation. With 1s and 2s AOs, the $(S = 0)$ STO-6G energy separation between $[(\sigma)^1][(\sigma)^2(\sigma^*)^1]$ and $[(\sigma)^1(\sigma^*)^1][(\sigma)^2]$ is -0.054 eV for non-polar MOs.

Table 1.
Shifted STO-6G electronic energies ($E' = -E - 36.0$ a.u.), and VB structural weights for resonance between VB structures **I-IX**. Structures **VII-IX** involve $(2s)^1(2p)^1$, $(2s)^1(2p)^1$ and $(2p)^2$ configurations for the $Li^{(-)}$. The wavefunctions for the electron-pair bonds involve Heitler-London AO formulations.

		Ψ_i	Ψ_f	Ψ_i	Ψ_f	Ψ_i	Ψ_f
I	Li+ Li⁻̈ Li —Li	0.907	0.146	0.959	0.071	0.979	0.043
II	Li+ Li˙ Li⁻̈ Li˙	0.008	0.234	0.009	0.410		
III	Li+ Li —Li Li⁻̈	0.053	0.193	0.017	0.101		
IV	Li+ Li⁻̈ Li+ Li⁻̈	0.000	0.128	0.015	0.333	0.001	0.404
V	Li+ Li⁻̈ Li⁻̈ Li+	0.010	0.230	0.001	0.085	0.013	0.569
VI	Li+ Li+ Li⁻̈ Li⁻̈	0.015	0.043				
VII	Li+ Li —Li⁻—Li	0.006	0.022			0.006	0.008
VIII	Li+ Li˙ ˙Li⁻ Li˙	0.000	0.003				
IX	Li+ Li˙ Li⁻̈ Li˙	0.000	0.000				
E'		0.421	0.330	0.418	0.318	0.418	0.304

as $\left| y^\alpha y^\beta \psi_{a'b}{}^\alpha \psi_{a'b}{}^\beta \right|$. In this wavefunction, y, a and b are 2s AOs centred on the atomic nuclei Y, A and B, $p = 2p\sigma_A$, $\psi_{a'b} = a + \lambda p + kb \equiv a' + kb \equiv \psi_{ab} + \lambda p$, and λ is a 2s-2p hybridisation parameter. With $\langle \kappa a' - b | a' + kb \rangle = 0$, the orthogonal antibonding MO, $\psi^*_{a'b} = \kappa a' - b$, may then be constructed. When a y electron is delocalised into $\psi^*_{a'b}$, the $S = 0$ wavefunction of Eq.(24),

$$\Psi(\mathbf{YAB})^- = \left| y^\alpha \psi^*_{a'b}{}^\beta \psi_{a'b}{}^\alpha \psi_{a'b}{}^\beta \right| + \left| y^\beta \psi^*_{a'b}{}^\alpha \psi_{a'b}{}^\beta \psi_{a'b}{}^\alpha \right| \quad (24a)$$

$$\equiv (k\kappa + 1)\left(\left| y^\alpha a'^\beta \psi_{a'b}{}^\alpha b^\beta \right| + \left| y^\beta a'^\alpha \psi_{a'b}{}^\beta b^\alpha \right| \right) \quad (24b)$$

is obtained for a $(\mathbf{YAB})^-$ 4-electron 3-centre bonding unit. On substitution of $a + \lambda p$ for a' into Eq.(24), we obtain the linear combination of Eq.(25).

$$\Psi(\mathbf{YAB})^- = (k\kappa + 1)\{ \Psi(y\text{-}\psi^*_{ab}, \psi_{ab}\text{-}\psi_{ab})/(kk^* + 1)$$
$$+ \lambda(\Psi_{VIII} + k\Psi(y\text{-}p, b\text{-}b)) + \lambda^2 \Psi_{IX} \} \quad (25)$$

in which $\psi^*_{ab} = k^*a - b$ is orthogonal to ψ_{ab}, and Ψ_{VIII} and Ψ_{IX} are the wavefunctions for the p-orbital structures **VIII** and **IX** of Table 1. However the Pauling bicovalent structure **VII** of Table 1 does not participate in this formulation of the antibonding MO mechanism.

Recent presentations of new theory for 4-electron 3-centre bonding units are provided in Refs. [4,59] for example. In them, alternative VB formulations for electron transfer are described and discussed.

7. CONCLUSIONS

We have given consideration (with some speculation) to a variety of phenomena whose primary active space orbitals involve four singly-occupied AOs and/or MOs. Examples have been provided of homopolar versus heteropolar bond cleavages, for which different types of VB structures are involved. Other phenomena that we have considered elsewhere include (a) the π-electrons of triple bonds, where for N_2, it has been demonstrated that resonance between the VB structures $:N \overset{\bullet}{\underset{\bullet}{-}} \dot{N}:$ and $:\dot{N} \overset{\bullet}{\underset{\bullet}{-}} N:$ generates a lower energy than does the usual triple-bond structure with Coulson-Fischer orbitals to accommodate the four π-electrons [60], and (b) $S_1 + S_1 \rightarrow S_2 + S_0$ energy transfer via vibronic coupling [61]. Although some theory has been outlined in this chapter, the primary purpose has been to focus attention on the dictum that "a picture is worth 500 words"[62] via the use of qualitative VB descriptions of electronic structure.

REFERENCES

[1] C.A. Coulson, Revs. Mod. Phys. 32 (1960) 170.
[2] R.D.Harcourt, Qualitative Valence Bond Descriptions of Electron-Rich Molecules, Lecture Notes in Chemistry, Springer-Verlag, Berlin 1982,Vol. 30.
[3]. R.D. Harcourt in (a) Valence Bond Theory and Chemical Structure, D.J. Klein, N. Trinajstić, (eds.) Elsevier New York 1990, p. 251. (b) Quantum Mechanical Methods in Main-Group Chemistry, (T.M. Klapötke, A. Schulz) Wiley, Chichester 1998, p. 217. (c) Pauling's Legacy- Modern Theory (Modelling) of Chemical Bonding, Z.B. Maksić, W.J. Orville-Thomas, (eds.) Elsevier, New York 1999, p. 443.
[4] R.D. Harcourt, Eur. J. Inorg. Chem. (2000) 1901 and Refs. 6(a)-(6f) therein. (Omit "thermal" on p. 1906.) See also Ref. [6] below for a recent review of use of other qualitative VB methods.
[5] A. Schulz, Trends in Inorg. Chem. 6 (1999) 137.
[6] A.C. Pavão, C.A. Taft, T.C.F. Guimarães, M.B.C. Leão, J.R. Mohallem and W.A. Lester, Jr. J. Phys. Chem. (A) 105 (2001) 5.
[7] C.A. Coulson and I. Fischer, Phil. Mag. 40 (1949) 396.
[8] T. Pasinszki and N.P.C. Westwood, (a) J. Am. Chem. Soc. 117 (1995) 8425 (b) J. Chem. Phys. 103 (1995) 3335.

[9] T.M. Klapötke, J. Mol. Struct. Theochem. 499 (2000) 99 and Refs. [8-17] therein.

[10] R.D. Harcourt and A. Schulz, J. Phys. Chem. (A) 104 (2000) 6510

[11] Refs. [1(s), 2, 8, 14(a), 9 and 20] of Ref. [10] above for N_2O.

[12] Refs. [2(b),2(c), and 9(c)] of Ref. [10] above for HN_3.

[13] R.D. Harcourt, J. Mol. Struct. (Theochem) 300 (1993) 245

[14] T.M. Klapötke, Chem. Ber./Recueil 130 (1997) 443.

[15] (a) I. Langmuir, Science, 51 (1929) 605. (b) L. Pauling, J. Chem. Soc. (1948) 1461.

[16] R.D. Harcourt and J.F. Sillitoe, Aust. J. Chem. 27 (1974) 691.

[17] P.R. Bunker, B.M. Landsberg and B.P. Winnewisser, J. Mol. Spectr. 74 (1979) 19.

[18] L. Pauling, The Nature of the Chemical Bond, 3rd edition, Cornell 1960

[19] R.D. Harcourt, J. Mol. Struct. 12 (1972) 351.

[20] (a) P.C. Hiberty in Valence Bond Theory and Chemical Structure, D.J. Klein, N. Trinajstić, (eds.) Elsevier New York 1990, p. 221. (b) R.D. Harcourt and N. Hall, J. Mol. Struct. (Theochem) 342 (1995) 59 and Refs. [66-69 therein].

[21] D.L. Cooper, J. Gerratt and M. Raimondi in Pauling's Legacy- Modern Theory (Modelling) of Chemical Bonding, Z.B. Maksić, W.J. Orville-Thomas, (eds.) Elsevier, New York 1999, p. 537 and Refs. therein.

[22] N.O.J. Malcolm and J.W. McDouall, J. Comput. Chem. 15 (1994) 1365.

[23] R.D. Harcourt, J. Mol. Struct. (Theochem) 259 (1992) 155..

[24] R.M. Parrondo, P. Karafiloglou, R.R. Papparlado and E. Sanchez-Marcos, J. Phys. Chem. 99 (1995) 6461 .

[25] R. McWeeny, Coulson's Valence, 3rd edition. Oxford University Press, 1979, p. 230.

[26] A. Schulz and T.M. Klapötke, Inorg. Chem.35 (1996) 4791.

[27] G. Maier, M. Naumann, H.P. Reisenauer and J. Eckwert, Angew. Chem. Int. Ed. Engl. 35 (1996) 1696.

[28] (a) C. Thomson and B. Wishart, Theor. Chim. Acta, 35 (1974) 361. Odd-electron densities: N, 0.648; O, 0.099 (b) P.P. Wolynec, UHF/cc-pVQZ, Gaussian 94, private communication. Spin densities: N, 0.865; O, 0.412 (c) R.D. Harcourt, see text.

[29] T.M. Klapötke and R.D. Harcourt, J. Mol. Struct. (Theochem) 541 (2001) 237.

[30] M.-J. Crawford and T.M. Klapötke, Inorg. Chem. 38 (1999) 3006.

[31] R.D. Harcourt, F.Wang and T.M. Klapötke, J. Mol. Model. (2001) in press.

[32] F.Wang and R.D. Harcourt, J. Phys. Chem. (A) 104 (2000) 1304.

[33] (a) R.D. Harcourt and N. Hall, J. Mol. Struct. (Theochem) 342 (1995) 59; 369 (1996) 217.(b) R.D. Harcourt, J. Mol. Struct. (Theochem) 398-399 (1997) 93.

[34] (a) R.D. Harcourt and R.D. Little, J. Am. Chem. Soc. 104 (1984) 41 and Refs. 5-8 therein. (b) R.D. Harcourt, (2001), submitted for publication.

[35] (a) M.T. Nguyen, A.K. Chandra, S. Sakai and K. Morokuma, J. Org. Chem. 64 (1999) 65. (b) K. Sakata, J. Phys. Chem. A 104 (2000) 10001.

[36] P.B. Karadakov, D.L. Cooper and J. Gerratt, Theoret. Chem. Acc. 100 (1998) 222.

[37] (a) F. Bernardi, M. Olivucci, J.J.W. McDouall and M.A. Robb, J. Am. Chem. Soc. 109 (1987) 544. (b) D.L. Cooper, M.A. Robb and I. Williams, Chem. Brit. 26 (1990) 1085, in which the discussion for 1,3-dipolar cycloadditions is identical to one of those described in Ref. 34 above.

[38] T.M. Klapötke, G. McIntyre and A. Schulz, J. Chem. Soc., Dalton Trans. (1996) 3237.

[39] (a) A.A. Korkin, J. Leszczynski and R.J. Bartlett, J. Phys. Chem. 101 (1996) 19840. (b) A.A. Korkin, A. Lowrey, J. Leszczynski, D.B. Lempert and R.J. Bartlett, J. Phys. Chem. A 101 (1997) 2709.

[40] T.M. Klapötke and A. Schulz, Inorg. Chem. 35 (1996) 7897.

[41] D.S. McClure, Rad. Res. Suppl. 2 (1960) 218

[42] R.D. Harcourt, (a) Int. J. Quantum Chem., Quantum Biol. Symp. 4, (1977) 143. (Omit "singly occupied" from line 12 of p. 145.) (b) Chem. Phys. Letts. 167 (1990) 374 and Refs. 4-9 and 12 therein..

[43] (a) R.D. Harcourt, Int. J. Quantum Chem. 63 (1997) 547. (b) R.D. Harcourt and N. Pyper, Int. J. Quantum Chem. 68 (1998) 129.

[44] M.Green and J.W. Linnett, J. Chem. Soc. (1960) 4959.

[45] R.D. Harcourt, J. Chem. Ed. 62 (1985) 99.

[46] J.P. Collman, R.R. Gagne, C.A. Reed, T.R. Halbert, G. Lang and W.T. Robinson, J. Am. Chem. Soc. 97 (1975) 1427.

[47] (a) R.D. Harcourt, J. Inorg. Nucl. Chem.39 (1977) 243. (b) A. van der Putten, A. Elzing, W. Visscher and R.D. Harcourt, J. Mol. Struct. (Theochem) 180 (1988) 309.

[48] C.P. Byrman and J.H. van Lenthe, Int. J. Quantum Chem. 58 (1996) 351. See also R. McWeeny, J. Mol. Struct.(Theochem) 229 (1991) 29.

[49] (a) R.D. Harcourt, F.L. Skrezenek, R.H. Flegg and R.M. Wilson, J. Chem. Soc. Faraday Trans. 82 (1986) 495 (b) Ref. [3b] and Refs. [43,44,52] therein

[50] B.J. Finlayson-Pitts and J.N. Pitts, Jr., Chemistry of the Upper Atmosphere, Academic Press, San Diego, 2000, p. 91 and Refs. therein.

[51] R.D. Harcourt, (a) J. Mol. Struct. (Theochem) 169 (1988) 193 . (b) idem. 186 (1989) 131. (c) Croat. Chem. Acta, 64 (1991) 399.

[52] N. Kitajima, N. Tamura, H. Amagai, H. Fukui, Y. Moro-oka, Y. Mizutani, T. Kitagawa, R. Mathur, K. Heerwegh, C.A. Reed, C.R. Randall, L. Que Jr., and K. Tatsumi, J. Am. Chem. Soc. 116 (1994) 9071.

[53] F. Cacace, R. Cipollini, G. de Petris and M. Rosi, J. Am. Chem. Soc. 128 (2001) 478.

[54] L. Pauling , J. Solid. State Chem. 54 (1984) 297.

[55] J.R. Mohallem, R.O. Vianna, A.D. Quintão, A.C. Pavão and R. McWeeny, Z. für physik D- atoms, molecules and clusters, 42 (1997) 135.

[56] R.D. Harcourt, J. Phys. B, 7 (1974) L41-45.

[57] R.D. Harcourt and W. Roso, Canad. J. Chem. 56 (1978) 1093.

[58] V. Bachler, Theor. Chem. Acc. 92 (1997) 223, and Refs. [55,56] therein.
[59] R.D. Harcourt, (a) J. Phys. Chem. (A) 103 (1999) 4293. In Table 2, $T_{I,II}$ and $T_{I,III}$ should be -0.0964774 and +0.0896127, respectively. (b) Int. J. Quantum. Chem. 60 (1996) 553.
[60] R.D. Harcourt, J. Chem. Soc. Faraday Trans. 88 (1992) 1119.
[61] R.D. Harcourt, K.P. Ghiggino, G.D. Scholes and R.P. Steer, J. Chem. Phys. 109 (1998) 1310.
[62] R.L. DeKock, 201st ACS Meeting, Atlanta, GA., American Chemical Society 1991, Abstract 200 CHED.
[63] R.D. Harcourt, J. Mol. Struct. (THEOCHEM) 206 (1990) 253.
[64] R.D. Harcourt and P.P. Wolynec, J. Phys. Chem. A, (a) 104 (2000) 2138, 2144. (b) 105 (2001) 4974.

APPENDIX

(a) The results of minimal basis-set VB calculations [51(c),63,64] for N_2O_2, N_2O_3 and FNO show that lengthenings of the N-N and N-F bonds of these molecules relative to those of N_2H_4 and NH_2F (with "normal" N-N and N-F single bonds) are, to a considerable extent, associated with the nature of the hybridisation of the nitrogen AOs. The optimum hybridisations lead to non-co-linear orientations of the overlapping AOs that form the N-N and N-F σ-bonds, thereby forming "bent" bonds. Whether or not the nature of the oxygen hybridisation has some relevance for the lengthening of the O-O bond of NCO-OCN (cf. Section 3.2) has yet to be determined.

(b) An elaboration of the antibonding mechanism of Figure 3(b) for electron conduction is displayed below. It enables positive hole transfer as well as electron transfer to occur.
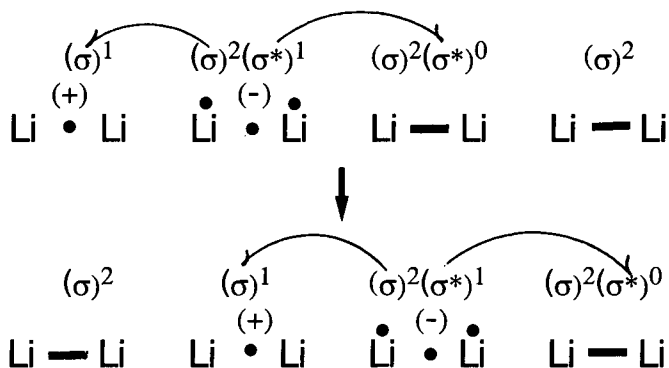
Chapter 13

The spin–free valence bond method: applications to metallic and electron rich systems

Reinaldo O. Vianna[a] and Andréa D. Quintão[b]

[a]Departamento de Física, ICEx, Universidade Federal de Minas Gerais, C.P. 702, CEP 30161–970, Belo Horizonte, MG, Brazil

[b]Instituto de Física, Universidade de São Paulo, C.P. 66318, CEP 05315–970, São Paulo, SP, Brazil

We discuss the application of the valence bond method to systems with delocalized bonds, namely, *metallic* and anionic systems. We show that the admittance of extra orbitals in these systems is necessary, leading to new types of structures, which are related to processes of charge transfer.

1. INTRODUCTION

The valence bond (VB) theory, originally introduced by Heitler and London [1], is a natural tool for studying the formation and breaking of chemical bonds. The VB wave function is a linear combination of structures that can be formally interpreted as the former Lewis structures, therefore furnishing an intuitive localized and chemical description of the molecular system. On the other hand, this chemical appeal costs a high price, for the atomic orbitals used in the wave function must be nonorthogonal, which leads to the so–called *N! problem* in the calculation of matrix elements [2–5]. If we try to circumvent the problem by orthogonalizing the orbitals, they will not overlap and therefore will not bind. If we insist on using orthogonal orbitals, then we are obliged to introduce many polar or ionic structures to recover the binding, but it costs the compactness and the chemical appeal of the wave function. Whatever the case, either with nonorthogonal or orthogonal orbitals, the VB wave function will reproduce exactly the same results of a molecular orbital (MO) based wave function, as long as both are carried to the full–CI limit. VB and MO theories are complementary and, in the end, are just different ways of expanding the

molecular wave function.

According to Pauling [6–9], valence bond theory can also be used to describe metallic systems. At a first glance, this seems to be contradictory, since VB deals with localized chemical bonds and a metallic bond is thought of as completely delocalized. Pauling's argument is that the metal atoms in the crystal have an available orbital to receive an extra electron and thus form an extra covalent bond, through a mechanism he called unsynchronized resonance.

In the present chapter, we explore the Pauling ideas in the context of an *ab initio* valence bond formalism. We do so by admitting extra orbitals in the constituent atoms of molecular systems, and devising the new types of VB structures that can be set allowing the atoms to form more bonds than their "atomic valences" admit. We will see that these Pauling's structures, as we named them, are important to describe some kinds of delocalized bonds and that they give some information about possible processes of charge transfer in the molecular systems.

From all the applications we have done in recent years [10–12], we review those that show the essence of our methodology. After introducing the VB formalism, we study the four electrons problem, a cluster of hydrogen, in an unusual limit, in order to address the problem of insulator to metal transition in solid hydrogen under pressure. Then we proceed to the applications to neutral and anionic lithium clusters, which are systems with very delocalized bonds.

1.1. The VB formalism

Now we briefly outline the McWeeny's spin–free valence bond machinery[2–4] used in our works. From the standard Young tableaux [2–4, 13] we obtain f_s^N orthogonal spin eigenfunctions $\{\Theta_k\}$, for N electrons coupled for total spin S, that carries an irrep D_s of the permutation group S_N. Where we have

$$f_s^N = (2S+1)N!/[(N/2+S+1)!(N/2-S)!]$$

A valence bond structure is defined as

$$\Phi_k = \rho_{11}\,\Omega_k,$$

where ρ_{11} is the Wigner projection operator,

$$\rho_{11} = (f_s^N/N!)\Sigma_p(-1)^p D_s(P)_{11} P\ ,$$

associated with the first spin eigenfunction in $\{\Theta_k\}$, and Ω_k is a product of N nonorthogonal atomic orbitals,

$$\Omega_k = \Phi_{k1}\Phi_{k2}\Phi_{k3}...\Phi_{kN}.$$

The VB wavefunction can be written as

$$\Psi = \Sigma_k C_k \Phi_k \quad .$$

The matrix elements to be evaluated are

$$H_{kl} = \langle \Phi_k | H | \Phi_l \rangle$$

and

$$S_{kl} = \langle \Phi_k || \Phi_l \rangle \, ,$$

where H is the electronic Hamiltonian in the Born–Oppenheimer approximation. These matrix elements are calculated through a permutation driven algorithm due to McWeeny [2–4]. The structure coefficients C_k are obtained solving the secular equation:

HC = ESC .

As the VB structures are nonorthogonal ($S_{kl} \neq 0$), we define the weight (W_k) of a structure as [14]

$$W_k = C_k^2 + \Sigma_{l \neq k} C_k C_l S_{kl} \quad .$$

Thus,

$$\Sigma_k W_k = 1 \quad .$$

In our calculations, only the valence electrons are treated at the VB level. The *inactive* electrons are kept in a frozen core obtained through an atomic Hartree–Fock (HF) calculation. All geometry optimizations or relaxations are also performed at the HF level.

The atomic orbitals that form the VB wave function are written as linear combinations of the atomic centered gaussian basis functions (Gaussian Type Orbitals – GTO) of all atoms in the system, with no constraints of orthogonality or localization, except for orthogonality against the core orbitals. The orbital and structure coefficients are determined simultaneously by solving the secular problem through a hybrid method of diagonalization and *brute force* energy

minimization (David–Fletcher–Powell (DFP) variable metric method [15] mixed with the Pulay's Direct Inversion of Iterative Subspace (DIIS) procedure for accelerating convergence [16]). The required gradient vector in the energy minimization is obtained through the generalized Brillouin theorem [17]. To avoid bias in the orbital optimization, the initial guess is usually a combination of s GTOs centered in one atom. The orbitals so obtained are highly directional and delocalize over a few atoms. On the other hand, this simultaneous optimization of orbitals and structures can be a computationally very difficult task and, sometimes, it is more sensible to break the wave function into different sets of structures, usually related by symmetry, and to optimize the orbitals for these distinct sets separately, therefore reducing the number of parameters to be determined in this nonlinear problem. Once this is done, the VB wave function is rebuilt and the structure coefficients are determined as in a traditional CI calculation. As a consequence of orbital delocalization, coefficients for conventional ionic structures (i.e., VB structures with doubly occupied orbitals) tend to be very small. The ionic structures we use in our works allow two valence electrons in the same centre but occupying different orbitals.

2. INSULATOR TO METAL TRANSITION IN HYDROGEN UNDER PRESSURE

If we imagine a solid insulator whose lattice constant could be arbitrarily reduced, by application of pressure, for instance, then it would eventually become a metal as a consequence of the increasing atomic orbitals overlap: the so–called *Mott transition*. Hydrogen is known to form a highly compressible molecular solid, whose volume can be reduced more than tenfold in the pressure range of 0 to 150 GPa, the band gap being reduced by more than 10 eV [18]. It is believed to become a metal under such high pressures and, therefore, its structural and electronic properties have been the subject of intensive investigation. At about 150 GPa, a discontinuity is observed in the frequency of the intramolecular stretching (vibron) modes [19], accompanied by the onset of infrared activity by the same modes [20]. A possible explanation for these effects have been recently proposed by Edwards and Ashcroft [21], namely, a structural transition in which the hydrogen molecules spontaneously polarize in the solid.

We apply Pauling's ideas to this problem in order to understand the valence bonding between hydrogen molecules in high–density hydrogen. We focus our attention to a pair of neighbor molecules in the solid and study the behavior of the chemical bonds as the intermolecular separation is decreased as a consequence of pressure. We perform *ab initio* valence bond calculations on the cluster H_2H_2 (Fig.1) with a small set of carefully chosen VB structures (Fig.2), able to reproduce all possibilities of bonding in the system. Our inferences are based on the weights of the structures as the intermolecular separation is varied. The results we obtain allow the identification of four regimes of bonding in the

system, corresponding to different ranges of the intermolecular separation. Each regime can be associated to the possibility of infrared activity in the solid.
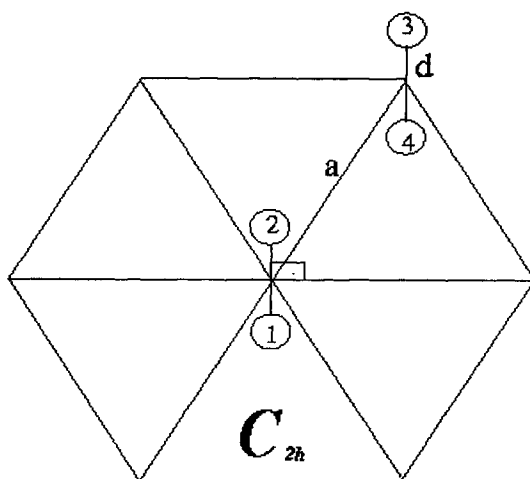
Fig.1. Geometry of the hydrogen cluster used in the calculations.
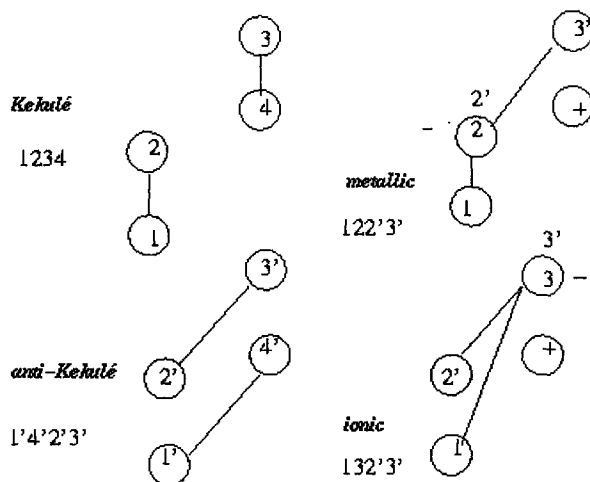
Fig.2. Examples of the valence bond structures adopted in the calculations. The lines represent chemical bonds. The + sign means that one atom has lost its electron to another atom signaled with −.

We note that the *four electrons problem*, a cluster of four hydrogen atoms, is a prototype for testing correlation methods in electronic structure. McWeeny [2] had already addressed this problem in the context of a valence bond formalism and here we tackle the problem in a quite unusual range of intermolecular separations.

2.1. Calculations

We have applied Pauling's theory to the molecular hydrogen cluster as follows: the nonmetallic cluster is well described by the usual Kekulé structure (1–2 3–4) (Fig.2), where orbitals 1 and 2 are at one hydrogen molecule and 3 and 4 are at the other one. The *synchronized resonance* is the mechanism in which the system alternates between structures (1–2 3–4) and (1–4 2–3) (anti–Kekulé) (Fig.2), breaking simultaneously the two original covalent bonds and forming two new ones.

In the *unsynchronized resonance*, just one bond is broken, with the concomitant transfer of one electron from one molecule to another and the formation of a new bond (Fig.2). In order for this to occur, one atom has to lose an electron, say atom 4, becoming a positive ion, and another atom must have an extra orbital to receive the extra electron, say atom 2, becoming a negative ion. Thus we form the structure (1–2 2'–3), that we will call *metallic structure*, where 2', the *metallic orbital*, is the extra atomic orbital on atom 2. In a molecular hydrogen crystal, the unsynchronized resonance would provide a mechanism for charge transport and confer metallic properties to the system.

We investigate the possibility of metallic structures and charge fluctuations as two hydrogen molecules approach each other. To do so, we associate two atomic orbitals to each hydrogen atom and select 14 VB structures from a total of 266 that can be formed with the set of 8 orbitals.

Arranging the two hydrogen molecules in the geometry shown in Fig.1, and labeling the atoms in one molecule as 1 and 2, and in the other molecule as 3 and 4, the 14 structures are as follows (Fig.2). Assuming labels 1, 2, 3 and 4 for the *normal* valence orbitals on each atom, we adopt labels 1', 2', 3' and 4' for the metallic orbitals. The main structure is (*1–2 3–4*), of Kekulé type, bonding atom 1 to 2, and atom 3 to 4. We have another Kekulé type structure, namely, (1'–4' 2'–3'), with two intermolecular bonds, and we call this structure anti–Kekulé. Then we have 8 metallic structures, allowing for intermolecular hopping of one electron, which are (1–2 3'–2'), (3–4 1'–4'), (1–2 1'–4'), (3–4 3'–2'), (1–2 2'–4'), (3–4 2'–4'), (1–2 1'–3'), (3–4 1'–3'). Finally, we have 4 ionic structures, allowing for intramolecular hopping of one electron, which are (1–3 3'–2'), (1–3 1'–4'), (2–4 1'–4'), (2–4 3'–2'). With this small set of structures, we cover all possibilities of bonding and charge fluctuations in the system.

In order to form the set of 8 atomic orbitals to be used in the VB calculations, we proceed as follows. We associate to each atom a (8s1p) atomic centered gaussian basis set contracted to [2s1p] (Table 1). Each orbital is ex–

Table 1
Atomic centered cartesian gaussian basis set.

	Exponents	Contraction Coefficients
S type		
	6.686331	0.0016700
	20.0855369	0.0048500
	6.0496475	0.0219600
	1.8221188	0.0874200
	0.5488116	0.2605400
	0.1652989	0.2295000
	0.0497871	0.0220900
S type		
	0.1000000	1.0000000
P type		
	1.0000000	1.0000000

panded in the basis functions of all centres and optimized variationally, that is, for a given intermolecular separation, the total energy is minimized with respect to the form of the orbitals. We note, again, that the orbitals are allowed to delocalize during the optimization, which leads to vanishing coefficients for the conventional ionic structures, that is, VB structures with doubly occupied orbitals. The ionic structures we use are of *Pauling–type*, in the sense that there are two electrons in the same atom, but in different orbitals.

The valence orbitals (1, 2, 3 and 4) and the metallic orbitals (1', 2', 3' and 4') are optimized separately, using a VB calculation with just one structure, namely, the Kekulé structure for the former and the anti–Kekulé for the later. It is done for each intermolecular separation a (Fig.1), which varies from 1.5 Å to 6.0 Å. The molecular bond distance d was kept fixed to 0.74 Å for all intermolecular separations. We verified that if d is allowed to relax, at the SCF level, it varies at most by a few hundredths of an angstrom and the energy lowers by about 10^{-4} Hartree. It therefore does not affect our results. Once the orbitals are obtained, we form the 14 structures and solve the VB secular equation.

The geometry adopted for the cluster has symmetry C_{2h} (Fig.1) and the set of structures spans symmetry species A_g and B_u. All the point energy calculations we performed resulted in wave functions of symmetry species A_g for the ground state, as would be expected. The energy for selected points are listed in Table 2, where we have included Hartree–Fock results for comparison.

2.2. Results

We start by comparing the relative structure weights as the intermolecular separation is varied (Fig.3). Taking the weight of the main Kekulé structure as unity, we plot, in Fig.3, the absolute value of the anti–Kekulé structure, and for the ionic and metallic structures we plot the total summation of the absolute values of structure weights for each individual set. We can distinguish four regions with different bonding schemes in Fig.3. For intermolecular separations around 5.0 Å, the contributions of the anti–Kekulé and ionic structures increase slightly, reaching a maximum at around 2.6 Å. The weights drop from 0.002 at 5.0 Å to 0.08 at 2.6 Å for the anti–Kekulé structure, and from 0.003 to 0.01 for the ionic structures. The contribution of the metallic structures arises only at around 2.0 Å, increasing abruptly and reaching a maximum at 1.7 Å. These intermolecular separations correspond to pressures around 200 GPa [22]. Below 1.7 Å, the contributions of all structures are appreciable. The same results could be drawn from a plot based on the squared structure coefficients.

Table 2
Ground state (C_{2h} ^1A_g) total energy (a.u.) for some intermolecular separations (Å).

Intermolecular Separation	VB energy	HF energy
1.5000000	–2.2238278	–2.1893468
1.6000000	–2.2434224	–2.2087074
1.7000000	–2.2585167	–2.2232051
1.8000000	–2.2698090	–2.2340706
1.9000000	–2.2782549	–2.2422125
2.0000000	–2.2845541	–2.2483061
3.0000000	–2.3015468	–2.2647516
4.0000000	–2.3021682	–2.2653591
5.0000000	–2.3021833	–2.2653744
6.0000000	–2.3021831	–2.2653742
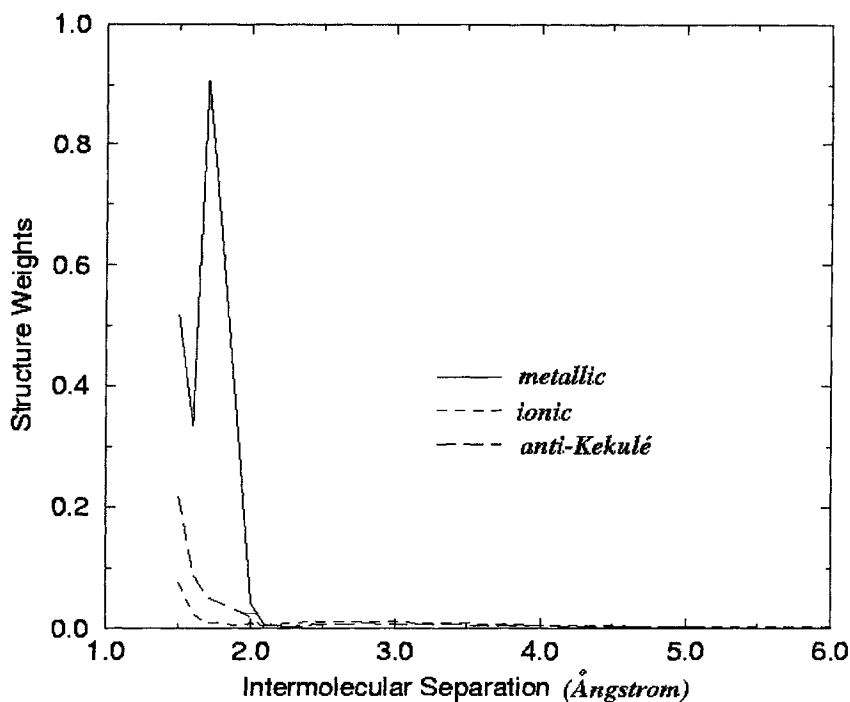
Fig. 3. Weight of VB structures versus intermolecular separation.

The most interesting feature of Fig.3 is the sharp peak in the weight of the metallic structures around 1.7 Å. Each metallic structure has two polarized H_2 molecules as a result of the transfer from a molecular valence bond to a new bond to a neighbor molecule (Fig.2). Our results therefore support a hypothesis, previously made [20], that the ground state wave function will have a component of charge–transfer states at pressures around 150 GPa. Moreover, our results indicate that small variations of the intermolecular separation around 1.7 Å (as a result of a structural modification, for instance) can induce sizeable changes in the polarization of the H_2 molecules. This is fully consistent with the spontaneous polarization predicted by Edwards and Ashcroft [21], and it provides an explanation for this phenomenon in terms of the chemical bonding in the solid.

The other interesting feature of Fig.3 is the increase of the weights for the

anti–Kekulé and ionic structures around 3.0 Å. It means that intermolecular interactions have become stronger (anti–Kekulé structure) and that the hydrogen molecules can polarize (ionic structures), although there is no charge transfer (metallic structures) between them. It is consistent with experimental observations of small infrared absorption for pressures below 150 GPa [23].

It is to be noted that with the C_{2h} symmetry (Fig.1), the cluster does not have a total dipole moment. However, an appreciable weight of the metallic or ionic structures (Fig.2), which is the case around an intermolecular separation of 1.7 Å (Fig.3), will strongly contribute to the polarizability of the system. On the other hand, a small polarizability will arise if only the Kekulé–type structures contribute to the ground state wave function.

We can explore our calculations in more detail so as to understand better the origin of the sharp peak in Fig.3. Let us look at the behavior of the overlap of the metallic orbitals with intermolecular separation (Fig.4). The overlap can vary from zero, no overlap at all, to unity, perfectly overlapped orbitals. In order for metallic binding to take place, the metallic orbitals should have an overlap comparable to that between valence orbitals forming the covalent bond in the
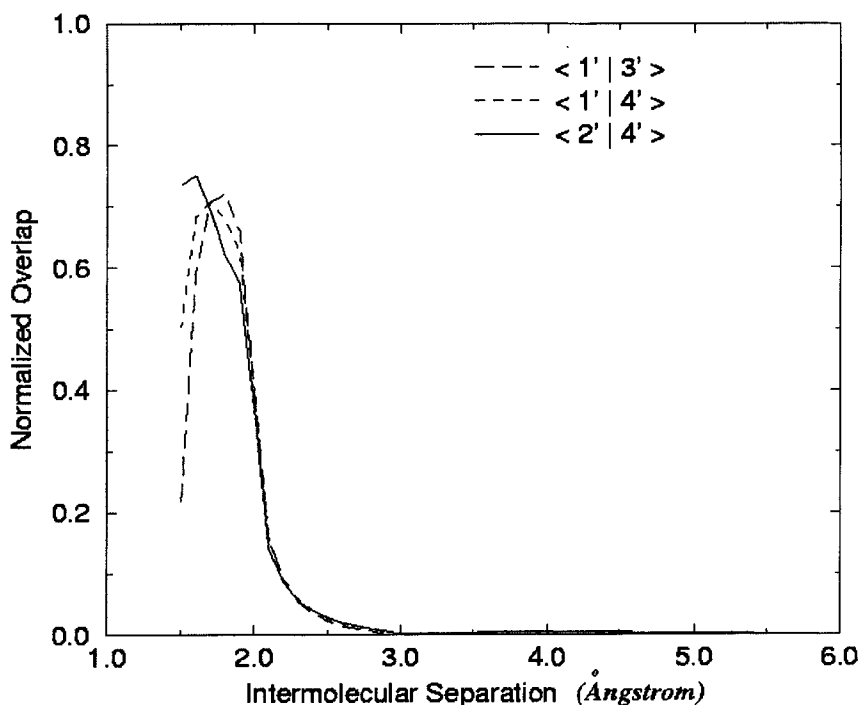
Fig. 4. Metallic orbitals overlap versus intermolecular separation.

hydrogen molecule, that is 0.8. The metallic orbitals overlap appreciably only below 2.0 Å. At 1.7 Å, all the metallic orbitals have an overlap of about 0.7 with each other, steadily decreasing for smaller intermolecular separations. This explains why the metallic structures reach a peak at 1.7 Å. That is where the metallic orbitals have the appropriate overlap to form the metallic bonds, and the decrease of this overlap will weaken these bonds. The re–increase of the metallic structures at 1.5 Å is a consequence of the great proximity of the molecules compensating the smaller metallic orbitals overlap. This interpretation is corroborated by the relevant contribution of the anti–Kekulé structure at that intermolecular separation. Note that, at 1.5 Å, atoms 2 and 4 are separated by just 0.94 Å.

3. STUDY OF THE ELECTRONIC STRUCTURE OF ANIONIC LITHIUM CLUSTERS

We apply the VB methodology to the study of the electronic structure of the small anionic lithium clusters Li_n^- $(2 \leqslant n \leqslant 5)$. These clusters, in their lowest energy state conformations, are shown in Fig.5. In this section, we show how to choose appropriately the VB structures and orbitals, how to understand the structure weights, what the aim of the metallic orbital is and, finally, how to get information about excited states of the systems.

3.1. Calculation details

In our calculations we associate to each Li atom a (10s2p) atomic centered gaussian basis set contracted to [4s,2p] (Table 3). We treat only the valence electrons at the VB level and keep the inner shell electrons (Li1s) in a core obtained by HF calculations. Therefore we are neglecting the core–core and core–valence correlation effects, which are small for these small lithium clusters (Fig.5).

The geometries of the Li_n^- clusters were determined by analytical gradient minimization procedure at HF level [24]. As usual, such geometries were also used in the VB calculations. Theoretical vibrational analysis has been performed at the HF level to check whether the stationary points on the Born–Oppenheimer (BO) surface are a local minima.

3.2. Choosing the structures and characterizing the electronic state of the system

The VB structures are the principal tool of the method, as they represent the possible chemical bonds present in the systems, and choosing them requires some care. Essentially, this choice will depend on the symmetry of the system at a specific electronic state and on its possible dissociation channels. In general, studying the main structures of smaller clusters is useful to give us a hint of the
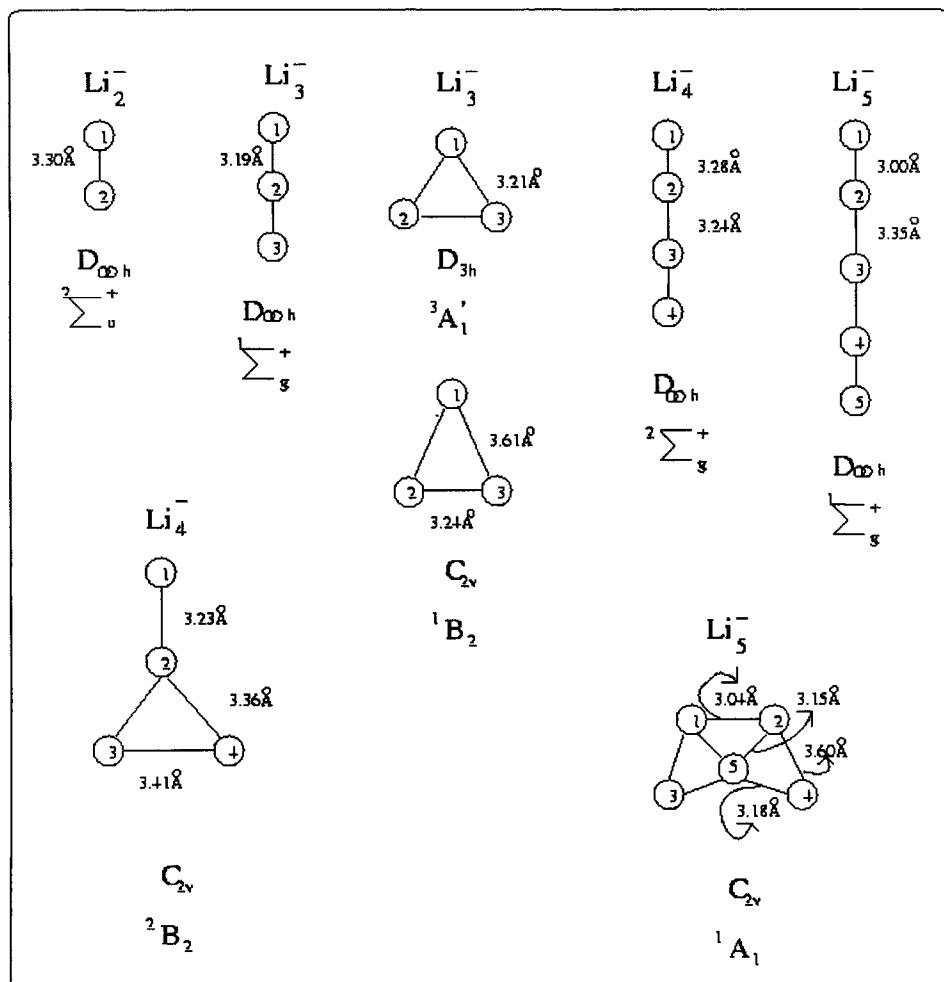
Fig.5. Geometry, point group and electronic state of some small anionic lithium clusters. Up to Li_4^-, the most stable conformations are linear. The most stable conformation of Li_5^- is planar.

probable structures of more complex systems, that may be formed out of these smaller clusters.

There are several types of structures: the conventional covalent (also called Kekulé structures), the ionic and the newest Pauling's structures (*metallic structures*). Below, the main structures of each small anionic cluster, shown in Fig.5, are discussed.

Table 3
The [4s,2p] basis set.

Exponents	Contraction coefficients
S type	
921.30	0.001367
138.70	0.010425
31.940	0.049859
9.3530	0.160701
3.1580	0.344604
1.1570	0.425197
0.4446	0.169468
S type	
0.0200	1.000000
S type	
0.0472	1.000000
S type	
1.0514	1.000000
P type	
0.1135	1.000000
P type	
0.0700	1.000000

3.2.1. The Li_2^- cluster

The minimum set of structures needed to describe the ground state $^2\Sigma_u^+$ of the simplest anionic cluster Li_2^- is shown in Fig.6, where a line represents a pairing of electrons (a covalent bond) and a single dot represents an unpaired electron. Two dots around the same centre represent two electrons at the same atom, with paired spins, as in an ionic bond, but occupying different orbitals. This characterizes the unconventional ionic structure that will be adopted by us, as we have already discussed.

In the case of the ground state $^2\Sigma_u^+$, the final VB wave function is given by the following linear combination of those structures shown in Fig.6 :

$$\Psi_{VB} = C_1(E_1 - E_2) + C_2(E_3 - E_4) \quad .$$

It is shown in Fig.6 that the most important structures that describe the Li_2^- cluster, in its ground state, are the ionic symmetric pair E_1 and E_2, which is almost six times more important than the covalent symmetric pair E_3 and E_4.

We observe that combinations of structures like $(E_1 + E_2)$ and $(E_3 + E_4)$ would lead to the excited state $^2\Sigma_g^+$.

To form the structures of Fig.6, we need, in principle, two orbitals centered on each atom. However, the pairs of structures are of very different nature, ionic and covalent, and thus it becomes necessary to optimize a set of 4 orbitals for each symmetric pair of structures separately, amounting to a total of 8 orbitals.

In Fig.7, we show the two pairs of VB orbitals optimized for atom 1 (Fig.5), corresponding to the two pairs of ionic and covalent structures of Fig.6.

3.2.2. The Li_3^- clusters

The Li_3^- cluster has several stable states for different geometric conformations: $D_{\infty h}$, C_{2v} and D_{3h}. The most stable cluster is linear (symmetry group $D_{\infty h}$), although the planar conformations, a triplet of symmetry A'_1 (symmetry group D_{3h}) and a singlet of symmetry B_2 (symmetry group C_{2v}), are also sufficiently interesting to be studied. These clusters are shown in Fig.5. The preference of Li_n^- clusters $(2 \leqslant n \leqslant 4)$ for linear geometries is an interesting property that will be discussed in detail soon. The structures that represent these clusters in their most stable geometries are shown in Fig.8.

$$Li_2^-$$

Ground State: $^2\Sigma_u^+$

Structures: Weights:

◇ ○·	E1	
		1.000
◇ ·○·	E2	
◇—○	E3	
		0.170
○—○·	E4	
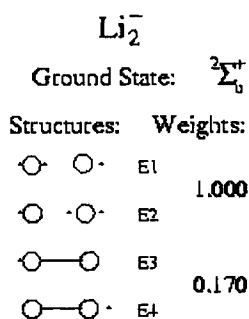
Fig.6. Minimum set of VB structures needed to describe the ground state $^2\Sigma_u^+$ of Li_2^-. A line represents a covalent bond and a single dot represents an unpaired electron. Two dots around the same centre represent two electrons with paired spins near the same atom, as in an ionic bond, but in this case occupying different orbitals.

Orbital 1 – Ionic Structure	Orbital 2 – Ionic Structure

Orbital 1 – Covalent Structure	Orbital 2 – Covalent Structure
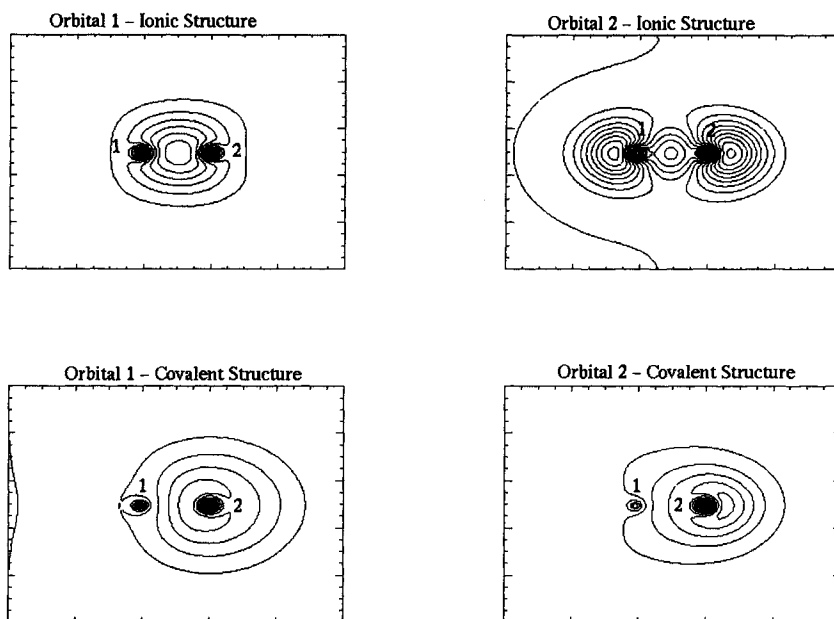
Fig.7. Orbitals on the same centre (atom 1 of Fig.5) of $D_{\infty h}$ Li_2^- cluster. The pair of orbitals of the first line correspond to the ionic structures of Fig.6. The appropriate pair of orbitals of the covalent structures are also shown on the second line. The "black spots" are over the nuclei.

The wave function of the ground state $^1\Sigma_g^+$ of the Li_3^- cluster is given by

$$\Psi_{VB} = C_1\left(E_1 + E_2\right) + C_2\left(E_3 + E_4\right) + C_3\left(E_5\right) + C_4\left(E_6\right) \quad .$$

We see, in Fig.8a, that the structures E_1 and E_2 (ionic structures) for the $D_{\infty h}$ Li_3^- cluster are the most important. This is the first anionic lithium cluster that needs a Pauling type structure (E_6) in its total VB wave function. There is no structure like that in the neutral case. Note that in the anionic case it is necessary to use two orbitals on the central atom. As long as the size of the ionic clusters increases, the role of the Pauling's structures becomes more important, as we will see.

In Fig.9, the orbitals of the central atom for several structures are shown. The first pair of orbitals is optimized for structures E_1, E_2 and E_6. The orbitals for the structure E_5 are also shown.

The planar Li_3^- cluster of lowest energy is a stable conformation of symmetry D_{3h}, state $^3A'_1$. The VB wave function is given by

$$\Psi_{VB} = C_1\left(E_1 + E_2 + E_3\right) + C_2\left(E_4 + E_5 + E_6 + E_7 + E_8 + E_9\right) + C_3\left(E_{10} + E_{11} + E_{12}\right) \quad .$$
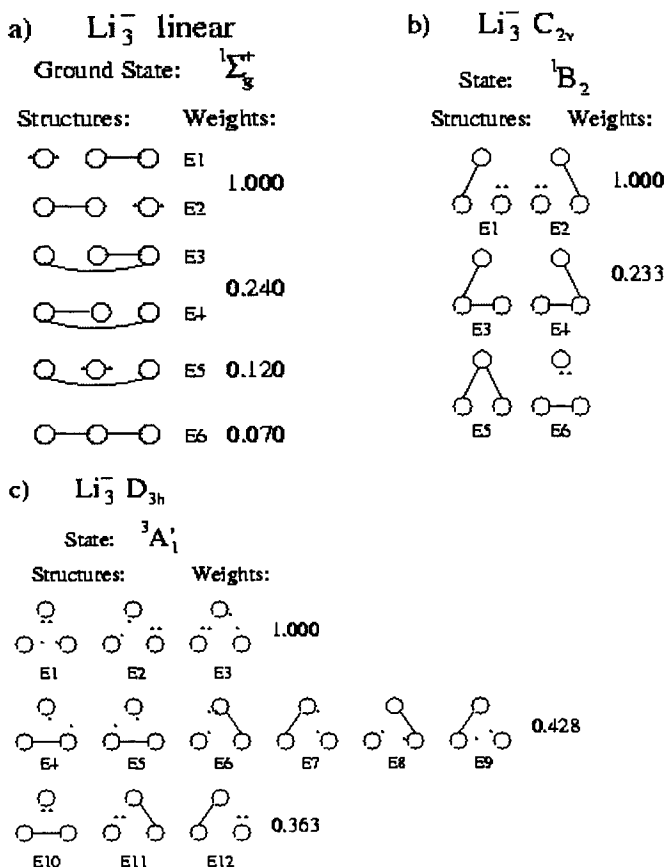
Fig.8. (a) Minimum set of structures needed to describe the ground state $^1\Sigma_g^+$ of the most stable conformation $D_{\infty h}$ Li_3^-, (b) as well as the transition state $^1B_2$ C_{2v} and (c) the stable state $^3A'_1$ D_{3h} Li_3^-.

We need two orbitals centered on each atom to form each set of structures of the D_{3h} Li_3^- cluster. They are delocalized on specific neighbor orbitals. A diagram of them is shown in Fig.10. In the optimization, orbital 1 is allowed to bind (covalent bond) just to orbital 2, orbital 2' is restricted to 3 and 1' to 3'. As the lowest energy state is a triplet, there are no Pauling's structures in this case. So, the structures of Fig.8c for the D_{3h} Li_3^- cluster can be written as: (1–1' 2' 3) (E_1), (3–3' 1 2) (E_2), (2–2' 1' 3') (E_3), (2–'3 1 3') (E_4), (2'–3 2 1) (E_5), (1'–3' 1 2) (E_6), (1–2 1' 3') (E_7), (1'–3' 2' 3) (E_8), (1–2 2' 3) (E_9), (2'–3 1 1') (E_{10}), (1'–3' 2 2') (E_{11}) and (1–2 3 3') (E_{12}). According to this representation, the first two electrons are paired and the other two are unpaired.
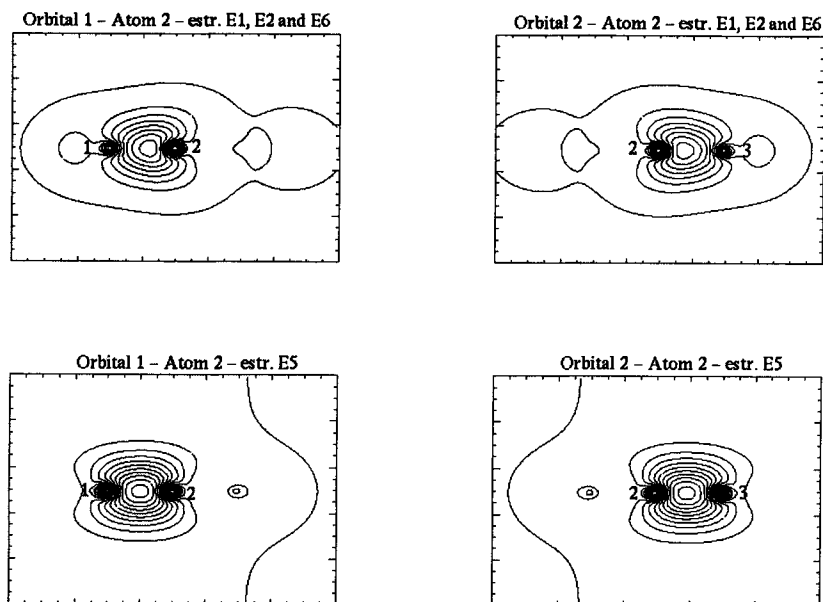
Fig.9. Orbitals of the central atom (atom 2) of $D_{\infty h}$ Li_3^- cluster. The orbitals of the first line of this figure correspond to structures E_1, E_2 and E_6 of Fig.8a. The orbitals of atom 2 for structure E_5 are also shown. The "black spots" are over the nuclei, which are numbered.
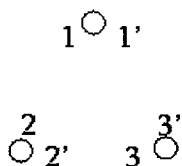
Fig.10. Diagram representing the numbering of VB orbitals of D_{3h} and C_{2v} Li_3^- clusters.

In fact, the $^1E'$ state of the D_{3h} Li_3^- cluster is affected by Jahn–Teller distortion, which reduces the symmetry of the cluster to C_{2v} and creates two distinct electronic states, $^1A_1$ and $^1B_2$, corresponding to triangles of internal angles (69.85°, 69.85°, 40.30°) and (63.34°, 63.34°, 53.32°), respectively.

On the other hand, the 1^1B_2 state of the C_{2v} Li_3^- cluster is indeed a transition state. In Fig.8b, we also show the set of VB structures that describes this state, which has the particularity that the weights of structures E_5 and E_6 are null, as they do not have the symmetry of the electronic state. Therefore, the VB wave

function in this case is

$$\Psi_{VB} = C_1(E_1 - E_2) + C_2(E_3 - E_4) \quad .$$

3.2.3. The Li_4^- clusters

Although the C_{2v} Li_4^- cluster is stable, once more the linear conformation is the one of lowest energy. The set of VB structures that best describes the $^2\Sigma_g^+$ ground state of the $D_{\infty h}$ Li_4^- cluster and their corresponding weights are given in Fig.11a. The ground state VB wave function is

$$\Psi_{VB} = C_1(E_1 + E_2) + C_2(E_3 + E_4) + C_3(E_5 + E_6) + C_4(E_7 + E_8) + C_5(E_9 + E_{10}) \quad .$$

It is important to point out that, starting from the $D_{\infty h}$ Li_4^- cluster, more than one set of structures becomes important to describe correctly the system. As for the other linear clusters, two orbitals centered on each atom are necessary to form the structures in the case of the $D_{\infty h}$ Li_4^-.

The wave function of the $^2E'$ state of the D_{3h} Li_4^- cluster (MO electronic distribution $a'_1{}^2e'{}^2e'$) suffers the Jahn–Teller distortion, which reduces the symmetry of the cluster to C_{2v} and gives rise to two distinct electronic states: $^2B_2$
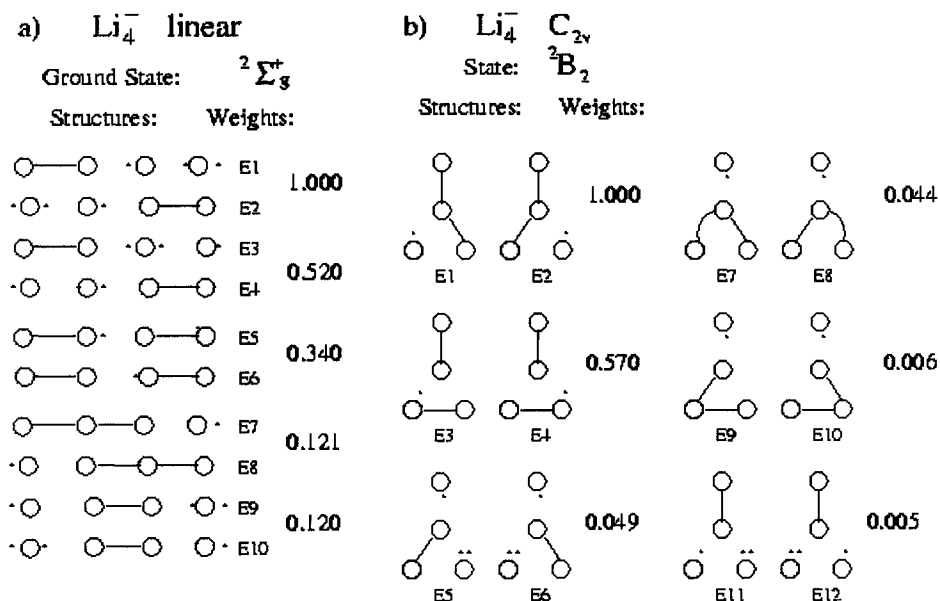
Fig.11. Minimum sets of structures needed to describe (a) the ground state $^2\Sigma_g^+$ of $D_{\infty h} Li_4^-$ and (b) the stable state $^2B_2$ of $C_{2v} Li_4^-$ cluster.

and $^2A_1$. $^2B_2$ is the state of lowest energy and its VB wave function (Fig.11b) is

$$\Psi_{VB} = C_1(E_1 - E_2) + C_2(E_3 - E_4) + C_3(E_5 - E_6) + C_4(E_7 - E_8) + C_5(E_9 - E_{10})$$
$$+ C_6(E_{11} - E_{12}) \quad .$$

Structures similar to E_3 or E_4, but with the extra electron near the central atom, which would result in totally symmetric structures, must vanish to represent the $^2B_2$ state.

The VB calculations describing the $^2B_2$ state were performed using at most seven atomic orbitals for the pair of structures. To form structures E_1 and E_2, we need two different orbitals on the central atom (atom 2 in Fig.5). These orbitals are shown in Fig.12. One of them points toward the top atom and the other is spread inside the lower triangle. In this case, the orbitals are distinct, one being more delocalized than the other. The most diffuse orbital could be a typical "metallic orbital", because atom 2 is performing a metallic bond with atoms 3 and 4 through it. Only one orbital on the first atom (atom 1 in Fig.5) is enough to form each pair of structures of the planar Li_4^- shown in Fig.11b. On the other hand, if we want an excited state of symmetry A_1, for instance, we must use the totally symmetric structures like those mentioned above and the sum of the symmetric pairs instead of the subtraction.

3.2.4. The Li_5^- clusters

The ground state, $^1A_1$ C2v, of the Li_5^- cluster is practically degenerate with the state $^1\Sigma_g^+$ D$_{\infty h}$. The latter is found to be, in fact, an unstable state, in disagreement with the literature [25]. In order to check this, we have made tests with several basis sets, starting from the [3s,1p] of Ref.25, up to 6–311G(d). In all cases, we verify the presence of imaginary frequencies at the SCF level.

Fig.12. Two different orbitals on the central atom of the planar Li_4^-: a) one of them points toward the top atom and b) the other one, the most diffuse, spreads inside the lower triangle. The "black spots" are over the nuclei, which are numbered.

The VB description of the $D_{\infty h}$ Li_5^- system is given by (Fig.13a)

$$\Psi_{VB} = C_1(E_1 + E_2) + C_2(E_3 + E_4) + C_3(E_5) \quad .$$

The VB wave function for the ground state (C_{2v}) is (Fig.13b)

$$\Psi_{VB} = C_1(E_1) + C_2(E_2 + E_3) + C_3(E_4 + E_5) + C_4(E_6) + C_5(E_7 + E_8) + C_6(E_9 + E_{10})$$

For the C_{2v} Li_5^- cluster, we need 3 distinct orbitals on the central atom (atom 5 of Fig.5) to form each set of VB structures, because this atom participates in at least 3 different bonds: one pointing toward the middle of the top pair (see orbital 3 of Fig.14, obtained from a VB calculation with structures E_4 and E_5 of Fig.13b) and the other two bonds associated with atoms 3 and 4 (like in E_1) of the base of the cluster (see orbitals 1 and 2 in Fig.14, which are optimized for structures E_1, E_2, E_3, E_9 and E_{10}).
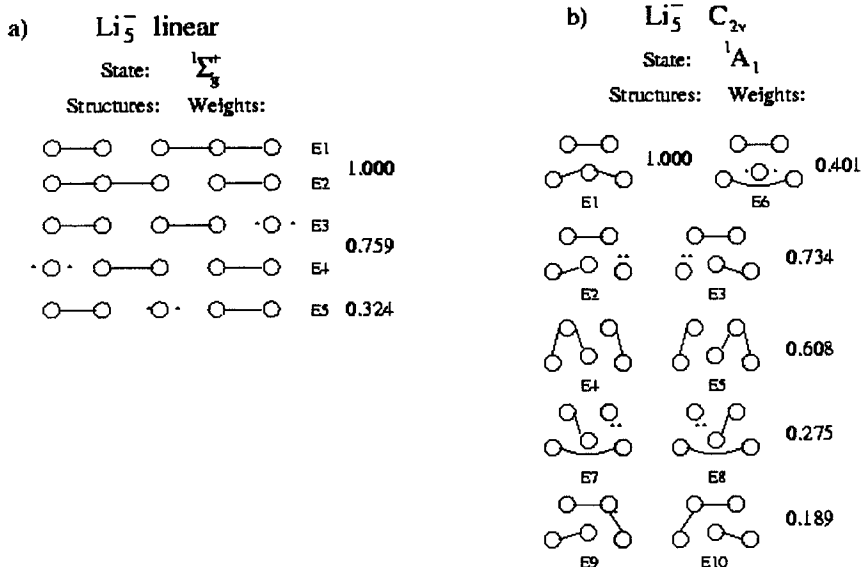
Fig.13. Minimum set of structures needed to describe (a) the unstable state $^1\Sigma_g^+$ of $D_{\infty h}$ Li_5^- and (b) the ground state of C_{2v} Li_5^- .
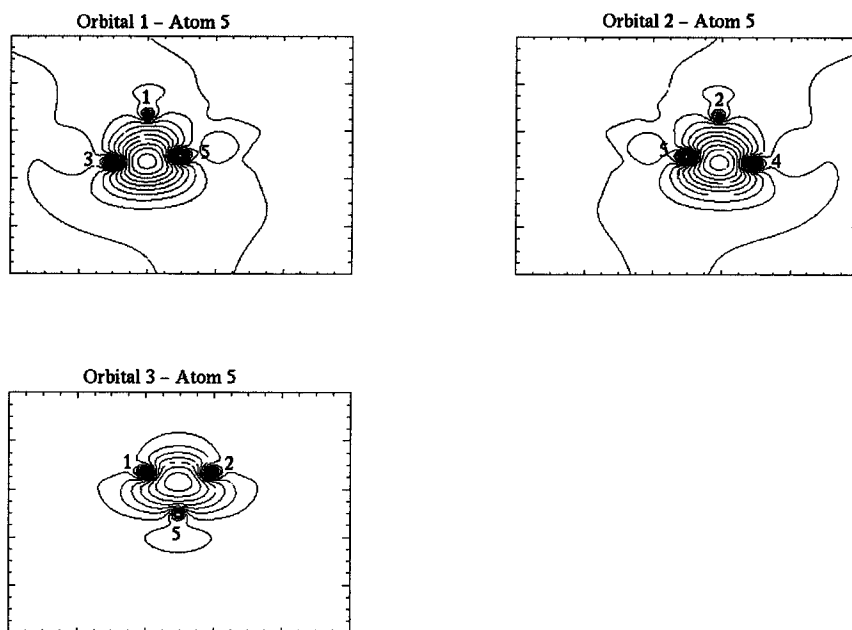
Fig.14. Orbitals of the central atom of C_{2v} Li_5^-.

It is important to clarify that we used 3 orbitals on the central atom of the C_{2v} Li_5^- cluster because the nature of the bonds involved are quite different, although not more than 2 orbitals on an atom are occupied simultaneously. This choice of orbitals accelerates convergence and improves the accuracy of the calculated energies. The metallic character of this sort of cluster increases with the number of atoms, which makes necessary the use of an increasing number of VB orbitals centered on the same atom. Therefore, the number of resonating VB structures also increases for the planar Li_5^- cluster. In this case, note that all structures have considerable weights in Fig.13b.

It is interesting to notice that as the systems become bigger and more compact, a larger number of VB structures becomes necessary to describe them. It means that the metallic character of these systems is increasing (that is why we usually say that small lithium clusters could be prototypes of metals). At the same time, Pauling's structures are showing their importance. From the C_{2v} Li_4^- cluster onwards, it is already possible to observe this tendency. Mainly for this reason, it becomes clear that the VB description that allows the existence of structures in which an atom is able to bind simultaneously with two neighbor atoms is fundamental to describe anionic metallic clusters.

3.3. The influence of the extra electron on the shape of the small anionic lithium clusters

The existence of linear species as the most stable ones is, as a matter of fact, intriguing. Most of all, the presence of an extra electron changes not only the electronic structure but also the shapes of the clusters when compared to their neutral counterparts. Up to the Li_4^- cluster, the $D_{\infty h}$ species are in fact energetically preferable. The ground state $^1A_1$ of the C_{2v} Li_5^- cluster, as was already mentioned, is practically degenerate with the $^1\Sigma_g^+$ state of the $D_{\infty h}$ Li_5^- cluster, although this latter is, in fact, an unstable state. From Li_6^- onwards, it is known that the anionic clusters have similar shapes to the corresponding neutral systems. In this case, there are no linear geometries, as we will discuss in section 4.
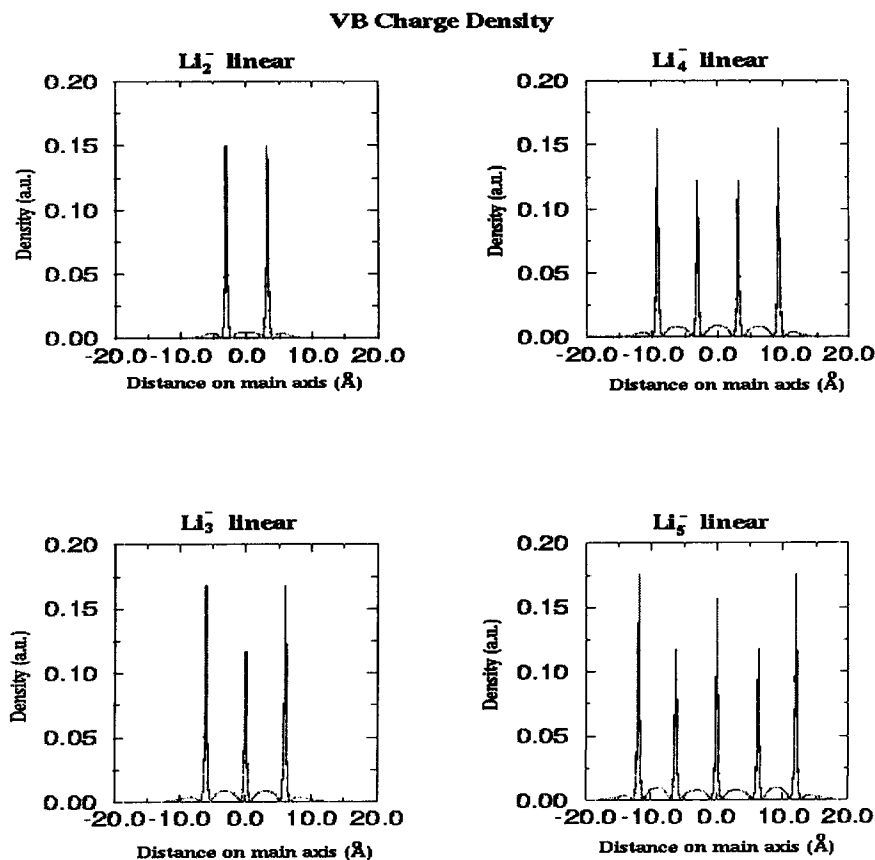
VB Charge Density

Fig.15. VB charge densities along the molecular axis of $D_{\infty h}$ Li_n^- clusters.
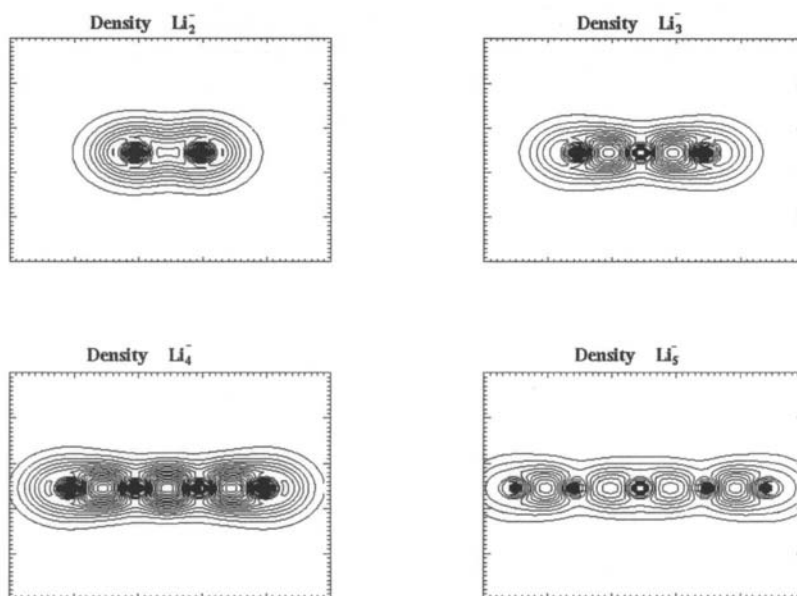
Fig.16. Maps of electronic charge density of linear anionic lithium clusters.

One of the reasons for the preference for less compact structures can be seen from the VB distribution of electronic charge in the linear Li_n^- ions in Fig.15. Observe higher peaks of charge at the extremes of their principal axis. The upper views of these charge densities are also shown in Fig.16.

The electrostatic repulsion is relatively weak for such linear geometries, making the linear clusters the most stable ones. In the Li_5^- case, a tendency of the charge density to turn out more compact can be observed because the central peak is almost similar to the end ones (see Fig.15). We could say that in this case we are in a threshold situation: from the Li_5^- cluster onwards, the lowest energy conformations are no longer the linear ones; the $D_{\infty h}$ Li_5^- structure is in fact an unstable state.

The charge density for planar Li_3^-, Li_4^- and Li_5^- clusters are shown in Fig.17. Observe the presence, in Fig.17, of three–body bonds [26], as they are named, common in planar clusters. They are characterized by peaks of charge inside triangles delimited by 3 atoms. The C_{2v} Li_5^- charge density is more delocalized, clarifying the necessity of using a larger number of structures, as already
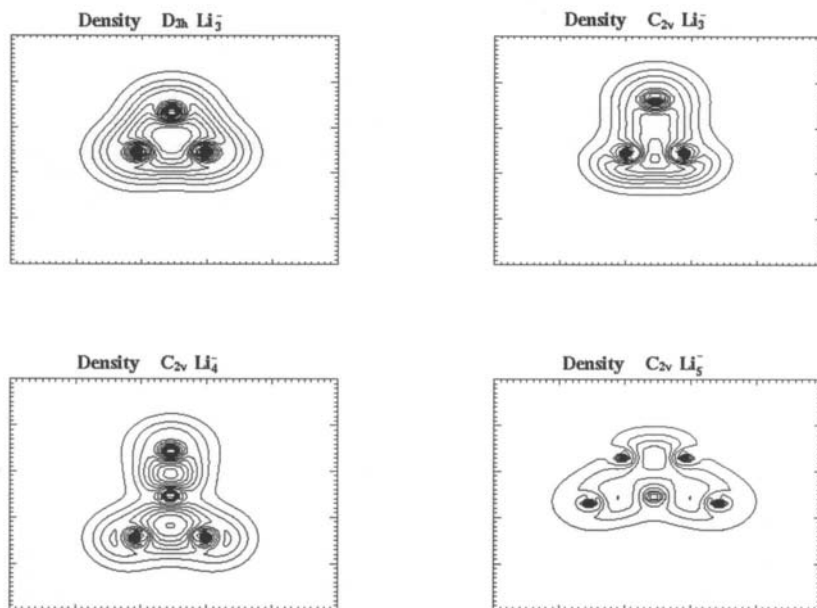
Fig.17. VB charge densities of D_{3h} Li_3^-, C_{2v} Li_3^-, C_{2v} Li_4^- and C_{2v} Li_5^- clusters.

discussed. The main reason is the considerable metallic character of this system.

We have seen that the weights of all the structures in this case are relevant, which means that there is no principal structure that by itself could represent the VB wave function as a whole, as happens for practically every cluster up to Li_4^-. On the other hand, for all anionic clusters studied, except Li_5^-, the preference for linear geometries is a consequence of a localized wave function, as the density maps show in Figs. 16 and 17.

3.4. The VB energies

In Table 4, total energies are given for several Li_n^- clusters, with different basis sets and various levels of calculation.

The VB energy values are lower than the HF values (Table 4), as expected, but they are higher than the QCISD values. This is explained by the fact that we are using a minimum set of VB structures. If we were using a complete set, the MO and VB results would be equivalent. On the other hand, we believe that the use of a small well–chosen set of structures is already appropriate for getting a correct description of the bonding in the system, with a compact and intuitive wave function. The $D_{\infty h}$ Li_5^- case is very illustrative. Using 10 orbitals, we can build 1050 VB structures. However, just 5 structures are sufficient to describe the properties of the system, as is shown in Fig.13a. Numerical results can be improved by enlarging the initial set of structures without any further orbital

Table 4
Energy (a.u.) of ground and first excited states of the anionic lithium clusters.

Cluster	Simmetry	State	$E^{\text{HF(a)}}$	$E^{\text{VB(b)}}$	$E^{\text{HF+corr (c)}}$	$E^{\text{QCISD(d)}}$
Li_2^-	$D_{\infty h}$	$^2\Sigma_u^+$	−14.88018	−14.88875	−14.79592	−14.90652
Li_3^-	$D_{\infty h}$	$^1\Sigma_g^+$	−22.31938	−22.35205	−22.22021	−22.37836
	D_{3h}	$^3A'_1$	−22.32759	−22.33109		−22.36139
	C_{2v}	$^1B_2$	−22.32034	−22.32664		−22.35508
Li_4^-	$D_{\infty h}$	$^2\Sigma_g^+$	−29.78694	−29.80279	−29.63000	−29.83340
	C_{2v}	$^2B_2$	−29.77854	−29.79509	−29.57176[e]	−29.82730
Li_5^-	$D_{\infty h}$	$^1\Sigma_g^+$	−37.20089	−37.25616	−37.04217	−37.28067
	C_{2v}	$^1A_1$	−37.20554	−37.25654	−37.04342	−37.29677

(a) Hartree–Fock energy using the [4s,2p] basis set (Table 3).
(b) VB energy using the [4s,2p] basis set (Table 3). All structures shown in Figs 6, 8, 11 and 13 were used.
(c) Hartree–Fock energy plus Davidson correlation energy calculated using the [3s,1p] basis set of Ref. 25.
(d) CISD energy calculated with quadratic convergence using the [4s,2p] basis set (Table 3).
(e) There is an inconsistency in Ref. 25: The UHF energy calculated with the [3s,1p] basis set of Ref. 25 is −29.55251 a.u. Redoing the calculations, using the same [3s,1p] basis set, we found −29.57176 a.u. So, this result of Ref. 25 was ignored.

optimization (VB–CI). If we had used all possible VB structures, we would have reached a result equivalent to that obtained from a MO full–CI calculation. The great advantage of working with the VB method appears when we want to study qualitative aspects. Looking at the charge densities in Fig.15, for instance, we could say that the $D_{\infty h}$ Li_5^- cluster prefers to dissociate according to the channel $Li_5^- \rightarrow Li_2 + Li_3^-$, because the bonds between the central atom and its first neighbors are weaker than the other ones. This behavior is in accordance with the linear Li_5^- structures of Fig.13a and with the literature [25].

We will investigate the stability of the anionic lithium clusters in Section 5. A relevant quantity is the dependence of the binding energy per atom on the number of atoms, as well as the electron affinity of neutral Li_n clusters. From the latter, we evaluate whether these neutral clusters are able to receive an extra electron and to form an anionic system.

4. STUDY OF THE ELECTRONIC STRUCTURE OF NEUTRAL LITHIUM CLUSTERS

Before starting an investigation of the stability of small anionic lithium clusters, it is necessary to study the conformations of lowest energy of the neutral Li_2, Li_3, Li_4 and Li_5 clusters using the VB approach.

4.1. The small neutral lithium clusters

Several works about neutral and positively charged lithium clusters can be found in the literature (see, for instance, Refs. 10, 12, 27–29), while there are not so many references for the anionic clusters. The main reason is that, for the anionic lithium clusters, experimental results are unusual and if they exist, they are related to the physical observables indirectly.

Up to the Li_5 cluster, the most stable conformations are planar. Theoretical studies agree that the basic topologies of clusters such as Li_n, Na_n and K_n are identical (see Ref. 30). The geometries of the ground state of clusters up to Li_5, calculated with the [4s,2p] basis set (Table 3), are shown in Fig. 18.

4.1.1. The Li_2 cluster

The ground state of the Li_2 cluster is well known: $^1\Sigma_g^+$. To describe it, we need 3 structures, shown in Fig.19. The VB and MO energy values will be compared later, after discussing the properties of each neutral lithium cluster.

It is necessary to use two VB orbitals to build the structure E_1 and 4 orbitals for structures E_2 and E_3. In this latter case, a pair of orbitals is centered on each lithium atom. The VB wave function for the system, in its ground state, is

$$\Psi_{VB} = C_1(E_1) + C_2(E_2 + E_3) \quad .$$

4.1.2. The Li_3 cluster

The D_{3h} conformation of the Li_3 cluster is affected by a Jahn–Teller deformation, producing a more stable C_{2v} conformation of symmetry $^2B_2$. The VB structures needed to describe the ground state are shown in Fig. 20.

It is necessary to include at most 6 VB orbitals to form each pair of structures, with one pair of orbitals centered on each lithium atom. The VB wave function is

$$\Psi_{VB} = C_1(E_1 - E_2) + C_2(E_3 - E_4) + C_3(E_5 - E_6) + C_4(E_7 - E_8) + C_5(E_9 - E_{10}) \quad .$$

Li$_2$ Li$_3$ Li$_+$ Li$_5$

D$_{\infty h}$ C$_{2v}$ D$_{2h}$ C$_{2v}$

$^1\Sigma_g^+$ ^{2}B$_2$ ^{1}A$_g$ ^{2}A$_1$
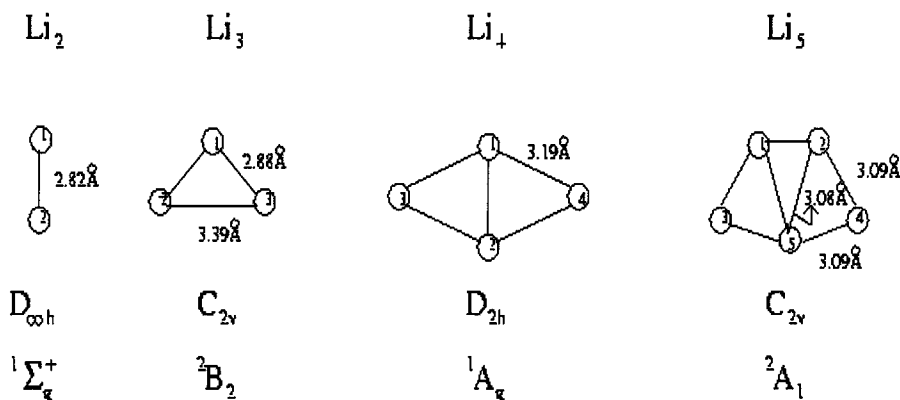
Fig.18. Equilibrium geometries of some small neutral lithium clusters. Their lowest energy states and symmetry groups are also shown.

Li$_2$ D$_{\infty h}$

Ground State: $^1\Sigma_g^+$

Structuress: Weights:

 E1   1.000

 E2

0.210

 E3
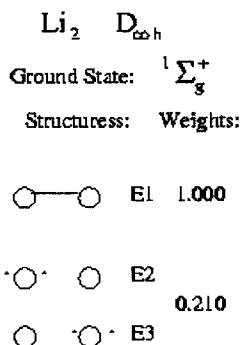
Fig. 19. Minimum set of VB structures needed to describe the ground state $^1\Sigma_g^+$ of the Li$_2$ system. As for anionic clusters already shown, a line represents a covalent bond and two dots around the same centre represent two electrons with paired spins near the same atom, as in an ionic bond, but in this case occupying different orbitals.

4.1.3. The Li$_4$ cluster

The most stable conformation of the Li$_4$ cluster is a rhombus (Fig. 18). Its ground state is ^{1}A$_g$ D$_{2h}$, which can be seen as a Jahn–Teller distortion of the D$_{4h}$ conformation.

The main VB structures are shown in Fig.21, and the VB wave function is

$$\Psi_{VB} = C_1(E_1 + E_2) + C_2(E_3 + E_4) + C_3(E_5 + E_6 + E_7 + E_8) + C_4(E_9 + E_{10})$$
$$+ C_5(E_{11} + E_{12} + E_{13} + E_{14}) + C_6(E_{15} + E_{16} + E_{17} + E_{18}) \quad .$$
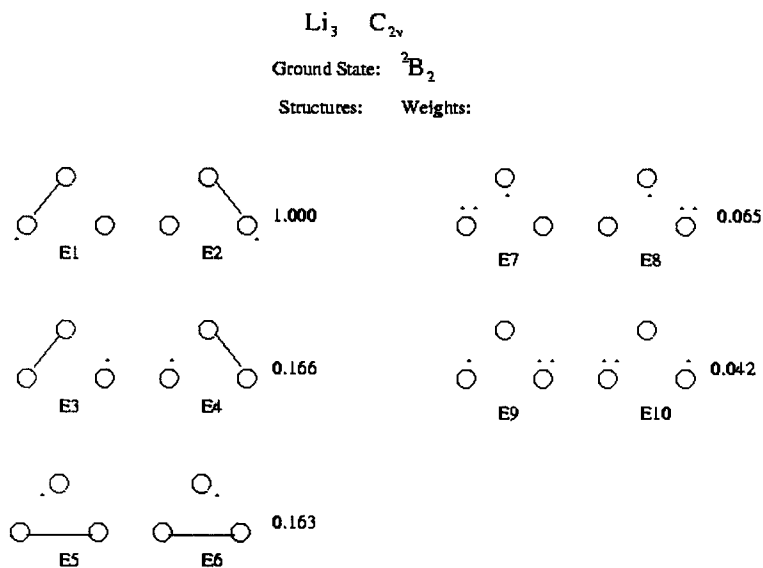
Fig. 20. Minimum set of VB structures needed to describe the ground state $^2B_2$ of the Li_3 system.
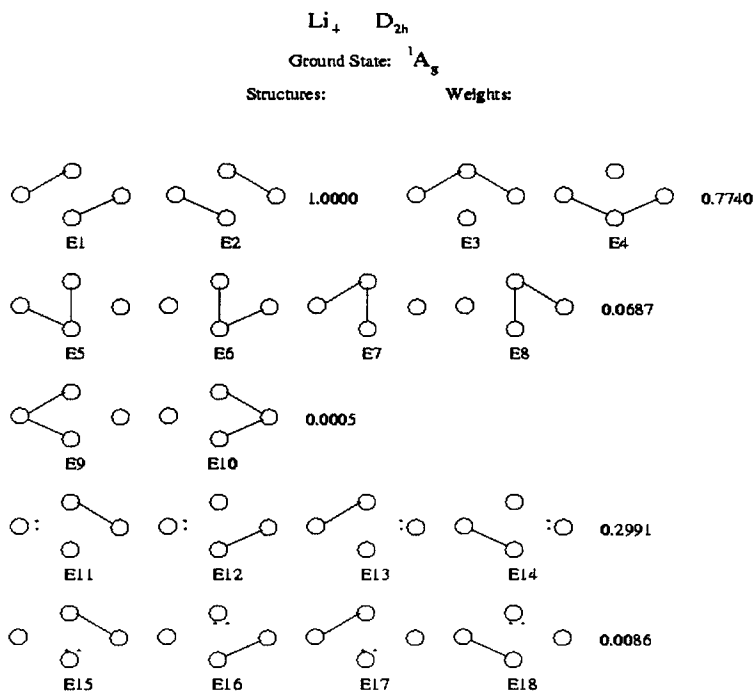
Fig. 21. Minimum set of VB structures needed to describe the ground state ^1A_g of the D_{2h} Li_4 cluster.

We showed, in the last section, that Pauling's structures get more relevant as the size of the anionic clusters increases, being the most important for clusters with more than four atoms. For instance, in the case of the neutral Li_4, the Pauling's structures E_3 and E_4 (Fig. 21) have large weights (0.774). The symmetric ionic structures E_{11}, E_{12}, E_{13} and E_{14} also have considerable weights (0.299). The other structures, E_9, E_{10} and E_{15} to E_{18}, are not so relevant for the ground state conformation, although they should be considered in order to give us a complete representation of the system.

Let us describe briefly how to select the VB orbitals to be used in the structures of Fig.21. First of all, we have 18 structures grouped in 6 sets. The structures in each set are related by symmetry and, therefore, share the same weight. For each set, we perform a separate VB calculation with orbital optimization (the brute force energy minimization we mentioned before). In Fig. 22, each arrow represents a possible direction in which the orbitals are pointing. We have 4 valence electrons that should be arranged in those orbitals. Structures E_1 and E_2 are represented as (1–7 4–10), which means that we have a bond of a particular type between electrons in orbitals 1 and 7 and another one between electrons in orbitals 4 and 10, and similarly for (2–9 3–8). For this set we construct 8 orbitals. For structures E_3 and E_4, represented as (1–7 2–9) and (3–8 4–10), we have also 8 orbitals. The ionic structures E_{11} to E_{14} are represented as (2–9 7–8), (4–10 7–8), (1–7 9–10) and (3–8 9–10), respectively, and again we have 8 orbitals. The sets E_9, E_{10} and E_{11} to E_{14} have also 8 orbitals each. The exception is the set E_5 to E_8, structures (5–6 3–8), (5–6 4–10), (5–6 1–7) and (5–6 2–9).
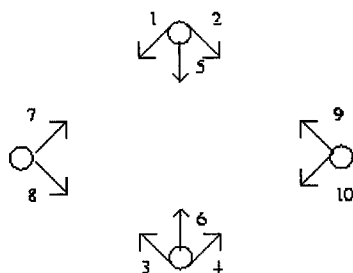
Fig. 22. Representation of the possible orientations of the VB orbitals that are used to describe the most stable conformation D_{2h} of Li_4 system. Observe that on top and bottom atoms are centered three orbitals, although at most 2 of them are used in the representation of structures in Fig. 21.

Table 5
Binding energy per atom (E_b/n) for the neutral Li$_4$ cluster[a].

Cluster	HF [b]	CI [c]	QCISD[d]	VB [e]	RVB [f]	SCVB [g]	Exp.[h]	Exp.[i]
D$_{2h}$ Li$_4$	4.30	12.77	13.43	10.94	7.75	9.10	14.75	19.60

(a) Values in kcal/mol. ($E_b/n=[nE_1-E_n]/n$, where E_n is the energy of the neutral cluster with n atoms, and E_1 is -7.43121 a.u.).
(b) HF values calculated using the [4s,2p] basis set (Table 3).
(c) MRD–CI from Ref. 25.
(d) QCISD values calculated using the [4s,2p] basis set (Table 3).
(e) Our VB result calculated using the [4s,2p] basis set (Table 3).
(f) Best VB result from Ref. 10.
(g) Single–configuration SCVB from Ref. 28.
(h) Experimental value from Ref. 31. (i) Experimental value from Ref. 32.

This last set requires 10 orbitals, as is clearly seen. In the end, we have 50 VB orbitals. Now we "rebuild" the VB wave function and diagonalize the CI problem, producing the weights shown in Fig.21. This procedure should be repeated for each geometry of the cluster.

In Table 5, we compare our results with the literature through the *binding energy per atom*.

It is important to note (Table 5) that even the experimental values [30,31] show discrepancies between them, and that among the VB approaches, ours is the one which describes the system best.

4.1.4. The Li$_5$ cluster

The most stable geometry of Li$_5$ is shown in Fig.18, corresponding to the ground state ($^2A_1$). Indeed this shape is similar to that of C$_{2v}$ Li$_5^-$ (Fig.5), and the choice of orbitals is also similar to that employed for that cluster. The VB structures used to describe this system are shown in Fig.23, and the VB wave function is

$$\Psi_{VB} = C_1(E_1 + E_2) + C_2(E_3) + C_3(E_4 + E_5) + C_4(E_6 + E_7) + C_5(E_8 + E_9)$$
$$+ C_6(E_{10} + E_{11}) + C_7(E_{12} + E_{13}) + C_8(E_{14} + E_{15}) + C_9(E_{16} + E_{17})$$
$$+ C_{10}(E_{18} + E_{19}) + C_{11}(E_{20} + E_{21}) \quad .$$
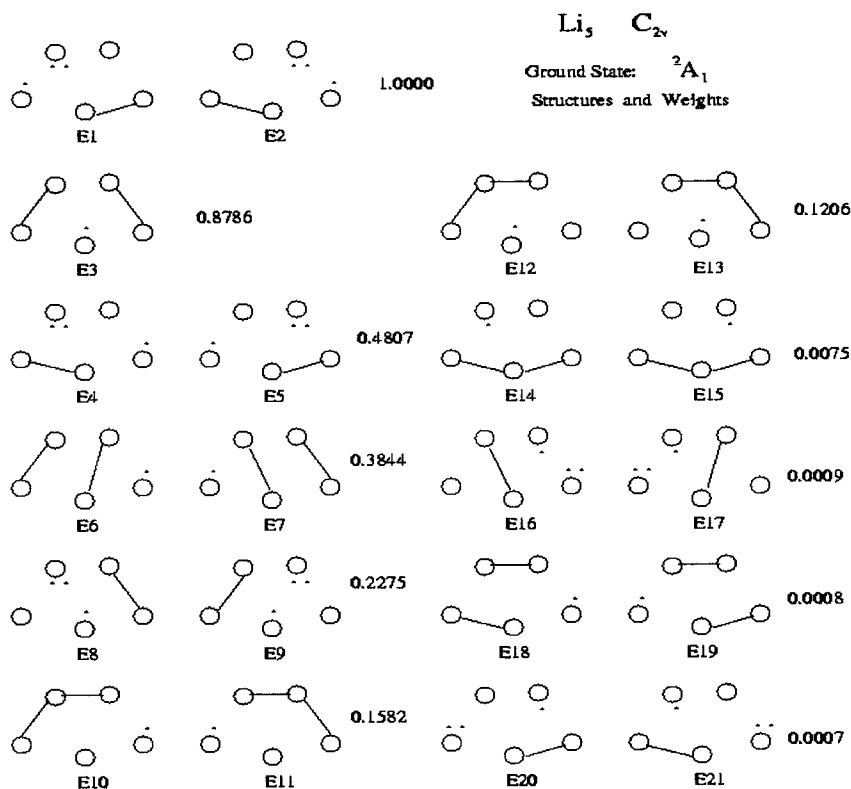
Fig.23. Minimum set of structures that describes the C_{2v} Li_5 cluster at its most stable geometry.

From the structures shown in Fig. 23, we optimized the orbitals for the three symmetric pairs of highest weight and for structure E3, with is also very important. The other structures participate in the VB–CI, but without proper optimized orbitals. We realized later that it affected undesirably the VB results for this cluster, as we will see soon.

The total energies are given in Table 6 and the VB charge densities for the neutral clusters are shown in Fig. 24.

Table 6
Energy of small neutral lithium clusters (a.u.)

Cluster	State	$E_{HF}(a)$	$E_{VB}(b)$	$E_{QCISD}(c)$
$D_{\infty h}$ Li$_2$	$^1\Sigma_g^+$	-14.86789	-14.88479	-14.89355
C_{2v} Li$_3$	$^2B_2$	-22.30920	-22.32465	-22.33895
D_{2h} Li$_4$	^1A_g	-29.75221	-29.79458	-29.81043
C_{2v} Li$_5$	$^2A_1$	-37.21148	-37.24040	-37.26734

(a) HF energy calculated using the [4s,2p] basis set of Table 3.
(b) VB energy calculated using the [4s,2p] basis set of Table 3.
(c) QCISD energy calculated using the [4s,2p] basis set of Table 3.
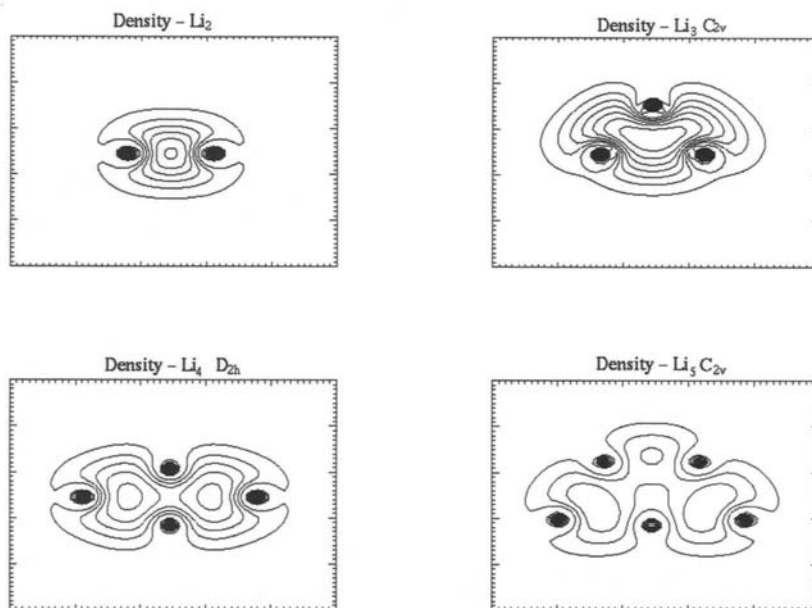
Fig.24. Charge densities of the Li$_2$, C_{2v} Li$_3$, D_{2h} Li$_4$ and C_{2v} Li$_5$ clusters.

5. STUDY OF THE STABILITY OF LITHIUM CLUSTERS

5.1. Binding energy per atom

Due to the lack of experimental results, quantities like the dependence of the *binding energy per atom* with the number of atoms are useful for giving us hints as to the quality of our VB results. Let us study the anionic and neutral clusters separately.

5.1.1. Anionic clusters

The function E_b^-/n is defined as:

$$E_b^-/n = [E_1^- + (n-1) E_1 - E_n^-] / n$$

where E_n^- is the energy of the anionic cluster with n atoms (Table 4). The value of E_1 calculated with the [4s,2p] basis set (Table 3) is -7.43121 a.u.. E_1^- is calculated as $E_1^-(\text{VB}) = -7.43469$ a.u., and $E_1^-(\text{QCISD}) = -7.44673$ a.u.. The results are reported in Table 7.

The VB values of Table 7 show a trend that agrees with the QCISD results and with the literature [25]: they increase regularly without significant even/odd alternations, as the nuclearity increases. In fact, with the lack of experimental results, these results indicate the stability of these clusters.

5.1.2. Neutral clusters

The function E_b/n is defined as:

$$E_b/n = [nE_1 - E_n] / n$$

where E_n is the energy of the neutral cluster with n atoms (Table 6). The results are reported in Table 8. According to that Table, both the experiment and the theory confirm the stability of these small neutral clusters. Except for the C_{2v} Li_5 cluster, the trend of our VB results agrees with the other CI and SCVB values. The discrepancy of the binding energy per atom of the C_{2v} Li_5 cluster is a consequence of the poor basis of VB orbitals used in the calculation. It stresses the importance of the proper choice and optimization of orbitals. It is certainly the most difficult part of our methodology, but it is rarely a problem for the smaller systems.

Table 7
Binding energy per atom E_b^-/n (kcal/mol) of the small anionic lithium clusters.

Cluster	State	$E^{\text{HF(a)}}$	$E^{\text{VB(b)}}$	$E^{\text{QCISD(c)}}$	$E^{\text{CI-Dav(d)}}$
$Li_2^- D_{\infty h}$	$^2\Sigma_u^+$	8.06	7.17	8.97	9.77
$Li_3^- D_{\infty h}$	$^1\Sigma_g^+$	7.05	11.49	14.48	16.02
$Li_4^- D_{\infty h}$	$^2\Sigma_g^+$	10.99	11.68	14.60	16.14
$Li_5^- C_{2v}$	$^1A_1$	7.21	12.17	15.71	16.96

(a) Calculated using the HF energy (Table 4) and the [4s,2p] basis set of Table 3.
(b) Calculated using the VB energy (Table 4) and the [4s,2p] basis set of Table 3.
(c) Calculated using the QCISD energy (Table 4) and the [4s,2p] basis set of Table 3.
(d) MRD–CI result from Ref. 25.

Table 8

Binding energy per atom E_b/n (kcal/mol) of the small neutral lithium clusters.

Cluster	$E^{HF(a)}$	$E^{VB(b)}$	$E^{QCISD(c)}$	$E^{CI-Dav(d)}$	$E^{SCVB(e)}$	Exp. [f]	Exp. [g]
Li_2 $D_{\infty h}$	1.72	7.02	9.77	8.66		12.68	12.45
Li_3 C_{2v}	3.26	6.49	9.48	8.01	3.84	13.84	11.53
Li_4 D_{2h}	4.30	10.94	13.43	12.77	9.10	19.60	14.75
Li_5 C_{2v}	6.96	10.59	13.97	13.78	9.74	22.14	[h]

(a) HF energies calculated using the [4s,2p] basis set (Table 3).
(b) VB energies calculated using the [4s,2p] basis set (Table 3).
(c) QCISD energies calculated using the [4s,2p] basis set (Table 3).
(d) MRD–CI with Davidson corrections of Ref. 25.
(e) Single–configuration SCVB from Ref. 28.
(f) Experimental result from Ref. 31.
(g) Experimental result from Ref. 32.
(h) It reports a $3-D$ structure as the most stable one, instead of that of symmetry C_{2v}.

5.2. Electron affinities

Values of electron affinities of the neutral clusters are also an indication of the stability of the corresponding anionic clusters. In fact, it is important to check if the neutral system is able to attach an extra electron to form a stable species. The adiabatic electron affinity is given by the difference between the energy of the neutral system Li_n, at its most stable geometry, and of the anionic Li_n^- cluster, also at its most stable conformation. In general, a greater electron affinity implies a lower tendency of the atom to accept an extra electron. In Table 9, experimental results of the electron affinities of some neutral clusters are shown, as well as *ab initio* results. All of the results confirm the stability of the anionic lithium species.

Table 9

Adiabatic electron affinities (EA_a) (kcal/mol) of the small neutral lithium clusters.

Cluster	VB [a]	HF [b]	QCISD [c]	MRD–CI [d]	Exp. [e]
Li_2 $D_{\infty h}$	2.48	7.71	8.14	2.47	10.15
Li_3 C_{2v}	17.19	6.39	24.73	22.43	23.17
Li_4 D_{2h}	5.11	21.79	14.41	12.04	
Li_5 C_{2v}	10.23	3.73	18.47	14.75	

(a) Calculated with VB energies (Tables 4 and 6) and using the [4s,2p] basis set of Table 3.
(b) Calculated with HF energies (Tables 4 and 6) and using the [4s,2p] basis set of Table 3.
(c) Calculated with QCISD energies (Tables 4 and 6) and using the [4s,2p] basis of Table 3.
(d) Results of Ref. 25.
(e) Experimental results of Ref. 29.

6. CONCLUSION

Following Pauling, we have admitted extra orbitals on monovalent atoms involved in molecular systems with some *metallic* character or very delocalized bonds. In conjunction with a spin–free valence bond formalism, these extra orbitals have allowed us to devise new kinds of VB structures, the Pauling's structures, as we call them. These structures permit the monovalent atoms to form two covalent bonds simultaneously, as a consequence of electron transfer from neighbors and, thus, give information about delocalization of charge in the system, that is not directly inferred from the usual Kekulé or ionic structures. Therefore, the Pauling's structures complement the VB description of molecular systems.

In the case of the hydrogen cluster, we have obtained, through the Pauling's structures, a description of the *metallization* of the system under pressure, that is completely consistent with other sophisticated *ab initio* calculations and with experiments.

For the lithium clusters, we have seen that the Pauling's structures can have the highest weights in the VB wave function, *e.g.* the C_{2v} Li_4^- and C_{2v} Li_5^- clusters. The structures are certainly very important when three–body bonds are present. According to our results, a VB description of the anionic or neutral lithium clusters without the Pauling's structures would be incomplete or would result in a less compact wave function.

In the methodology we have developed, the "orbital optimization" can be a source of grief, as is obvious in our results for the neutral Li_5 cluster, but it is rarely a problem for smaller systems. Therefore, this is a point that deserves additional attention in the future.

REFERENCES

[1] W.Heitler and F.London, Z. Phys., 44(1927)455.
[2] R.McWeeny, Int. J. Quantum. Chem., 34(1988)25.
[3] R.McWeeny, Int. J. Quantum. Chem., S24(1990)733.
[4] R.McWeeny, Methods of Molecular Quantum Mechanics, 2nd ed., Academic, London, 1992.
[5] P.O.Löwdin, Adv. Quantum Chem., 17(1985)285.
[6] L.Pauling, Nature, 161(1948)1029.
[7] L.Pauling, Proc. R. Soc. London, A196(1949)343.
[8] L.Pauling, J. Solid State Chem., 54(1984)2197.
[9] L.Pauling, Phys. Rev. Lett., 59(1987)225.
[10] J.R.Mohallem, R.O.Vianna, A.D.Quintão, A.C.Pavão, R.McWeeny, Z. Phys., D42(1997)135.
[11] R.O.Vianna and H.Chacham, J. Chem. Phys., 109(1998)23.

414

[12] A.D.Quintão, R.O.Vianna, J.R.Mohallem, Eur. Phys. J., D6(1999)89; A.D.Quintão, PhD Thesis, UFMG, Brazil, 1999; A.D.Quintão and R.O.Vianna, Int. J. Quantum Chem., 81(2001)76.

[13] R.Pauncz, Spin Eigenfunctions: Construction and Use, Plenum, New York, 1979.

[14] B.H.Chirgwin and C.A.Coulson, Proc. R. Soc. London, A201(1950)196.

[15] W.H.Press, S.A.Tenkolsky, W.T.Vetterling, B.P.Flannery, Numerical Recipes, Cambridge University, Cambridge, 1992.

[16] P.Pulay, Chem. Phys. Lett., 73(1980)393; T.P.Hamilton, P.Pulay, J. Chem. Phys. 84(1986) 5728.

[17] B.Levy, G.Berthier, Int. J. Quantum Chem., 2(1968)307.

[18] H.Chacham, L.M.Falicov, B.Koiller, Phys. Rev., B50(1994)7195; H.Chacham and S.G.Louie, Phys. Rev. Lett., 66(1991)64; H.Chacham, X.Zhu, S.G.Louie, Phys. Rev., B46(1992)6688.

[19] R.J.Hemley and H.K.Mao, Phys. Rev. Lett., 61(1988)857; H.E.Lorenzana, I.F.Silvera, K.A.Goettel, Phys. Rev. Lett., 63(1989)2080.

[20] M.Hanfland, R.J.Hemley, K.K.Mao, Phys. Rev. Lett., 70(1993)3760; R.J.Hemley, Z.G.Soos, M.Hanfland, H.K.Mao, Nature, 369(1994)384.

[21] B.Edwards and N.W.Ashcroft, Nature, 388(1997)652.

[22] J.van Strassen and I.F.Silvera, Phys. Rev., B37(1988)1989.

[23] J.van Kranendonk, Solid Hydrogen, Plenum, New York, 1983; M.Hanfland, R.J.Hemley, H.K.Mao, G.P.Williams, Phys. Rev. Lett., 69(1992)1129.

[24] Gaussian 92/DFT, Revision F.4, M.J.Frisch, G.W.Trucks, H.B.Schlegel, P.M.W.Gill, B.G.Johnson, M.W.Wong, J.B.Foresman, M.A.Robb, M.Head–Gordon, E.S.Replogle, R.Gomperts, J.L.Andres, K.Raghavachari, J.S.Binkley, C.Gonzalez, R.L.Martin, D.J.Fox, D.J.Defrees, J.Baker, J.J.P.Stewart, J.A.Pople, Gaussian, Inc., Pittsburgh PA, 1993.

[25] I.Boustani, J.Koutecký, J. Chem. Phys. 88 (1998) 5657.

[26] C.Gatti, P.Fantucci, G.Pacchioni, Theor. Chim. Acta 72 (1987) 433.

[27] E.Tornaghi, D.L.Cooper, J.Gerratt and M.Raimondi, Croat. Chim. Acta 64 (1991) 429; M.Raimondi, E.Tornaghi, D.L.Cooper and J.Gerratt, J. Chem. Soc. Faraday Trans. 88 (1992) 2309; B.Petch, D.L.Cooper, J.Gerratt, P.B.Karadov and M.Raimondi, J. Chem. Soc. Faraday Trans. 91 (1995) 3751.

[28] E.Tornaghi, D.L.Cooper, J.Gerratt, M.Raimondi and M.Sironi, J. Mol. Struct. (THEOCHEM) 259 (1992) 383.

[29] M.Gutowski, J.Simons, J. Chem. Phys. 101 (1994) 6.

[30] V.Bonacic–Koutecký, P.Fantucci, J.Koutecký, Chem. Rev. 91 (1991) 1035.

[31] C.Brechignac, H.Busch, P.Cahuzac, J.Leygnier, J. Chem. Phys. 101 (1994) 6992.

[32] C.H.Wu, J. Chem. Phys. 91 (1989) 546.

Chapter 14

VB analysis of wavefunctions calculated for chemical reactions in solution

Claudio Amovilli

Dipartimento di Chimica e Chimica Industriale, Università di Pisa, Via Risorgimento 35, I-56126 Pisa, Italy

In the last few years, the polarizable continuum model for the study of solvation has been extended to consider multideterminantal wavefunctions. Such novel techniques allow the study of the most important solvent effects on chemical reactions. In this context, the valence bond theory provides a way to analyze such effects through the transcription of the, generally, complicated multiconfigurational wavefunctions into sums of few selected classical structures, which are, in fact, more useful to understand the electron distribution rearrangement along a reaction path. In this chapter, the valence bond analysis of CASSCF wavefunctions calculated for chemical reactions in solution is discussed in details. By way of example, the results for some basic chemical processes are also reported.

1. INTRODUCTION

After Valence Bond (VB) theory was formulated for the first time [1, 2, 3], the meaning of chemical bonding [4] became rapidly simple and comprehensive to all chemists. The result has been the development of a key mode of interpretation which is still a solid basis for the explanation of a great variety of chemical reactions, namely the processes for which bonds can break or form allowing the matter, regarded as an assembly of molecules, to change. The great advantage of such a mechanistic approach is that, regardless of an enormous quantity of known data on chemical reactions, everything can be handled in terms of a relatively small number

of guidelines [5].

The aim of this chapter is to illustrate some of the most important solvent effects on a reaction path, for a chemical reaction in solution, from a typical VB point of view. The reaction path is a walk representing the variation of the geometrical configuration of reactants in the transformation to products; the position of the system on this walk is given by a parameter called the reaction coordinate and the path chosen by the system is the most energetically convenient. A plot of the free energy against the reaction coordinate is the basic diagram that experimentalists would like to know in order to define, for example, a strategy for the synthesis of products of chemical interest. From a computational point of view, the above plot can be obtained by analyzing a portion of the potential energy surface (PES), namely the surface representing the dependence of the electronic energy on nuclear positions. The knowledge of the PES allows the determination of both the minimal energy path and the nuclear vibrational contribution to the free energy along the path itself. In this chapter the latter contribution will not be considered because it is less important for a VB analysis of a reaction mechanism.

The accurate calculation of the electronic energy requires the averaging of the Hamiltonian onto a good approximation of the electronic wavefunction; it is well known that far from the equilibrium geometry the PES depends strongly on the quality of the wavefunction itself.

The simplest method, namely the Hartree-Fock method, which describes the wavefunction in terms of a single Slater determinant within a mean field theory, although is used for many practical purposes, especially in large molecular systems, cannot be applied in principle for PES evaluation. Woodward and Hoffmann [6] have shown that the presence of a high free energy barrier along a reaction path is evidence of strong changes in the wavefunction when the system overcomes the barrier. Although these authors focused their attention on orbital symmetries, it is a general fact that such strong changes cannot be described within a one determinantal approximation and then, to correctly reproduce the curvature of a PES, one has to resort to a multiconfiguration method.

The more interesting opportunities for interpreting a chemical process come out at this point. A multiconfigurational wavefunction can be decomposed into a sum of contributions with which to describe the main variations when the nuclear geometry changes. Each individual term could describe reactants, intermediates or products, and commonly the energy surface for each of them turns out to be much simpler. The plot of all these energies against the reaction coordinate is a kind of correlation diagram; in Figure 1 a typical plot is shown. In this example the wavefunction is decomposed into three contributions according to

$$\Psi = c_1\Psi_1 + c_2\Psi_2 + c_3\Psi_3 \tag{1}$$

where c_1, c_2 and c_3 depend on the reaction coordinate. The energies E_j are given by

$$E_j = <\Psi_j|\hat{H}|\Psi_j>, \tag{2}$$

with $\hat{H}$ being the electronic Hamiltonian.

Looking at Figure 1 it is clear that the reactants, in order to evolve towards the products of the reaction, must overcome two barriers passing through a minimum, at which is located an intermediate, in this case described by Ψ_2. This simple diagram shows clearly how the presence of crossings between the energy curves E_j (diabatics) of the partial contributions Ψ_j leads to the appearance of maxima in the expectation value of the Hamiltonian and, consequently, to barriers along the reaction path. It is important to remark that these maxima are saddle points with respect to full variations of nuclear positions while minima are true minima.
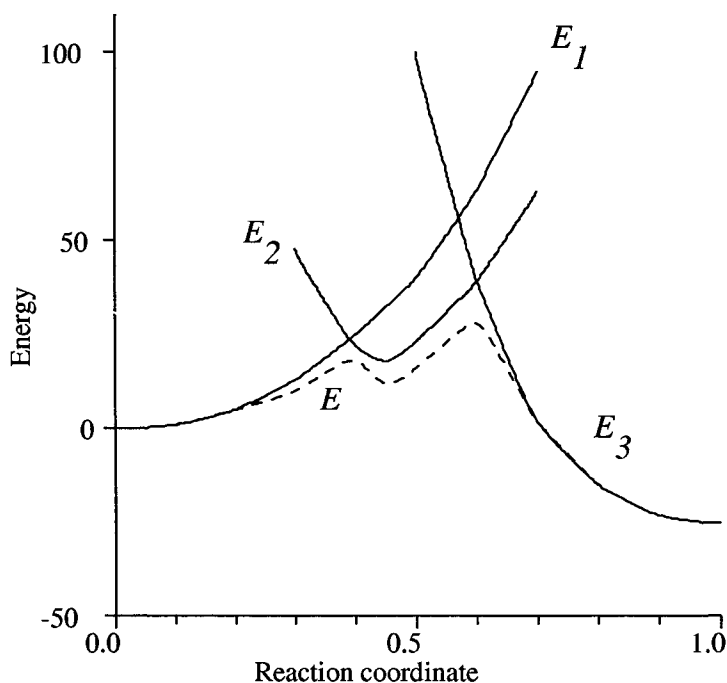
Figure 1. Generic energy diagram for a reaction which involves the formation of an intermediate. The dashed curve corresponds to the expectation value of the Hamiltonian for the electronic wavefunction Ψ.

Very often, as in the case of the Woodward-Hoffmann rules, the crossing between the diabatic curves can be predicted without resorting to complicated calculations. A simple and interesting review on VB correlation diagrams has been recently given by Shaik and Shurki [7] (see also other useful Chapters in this volume).

Another type of diagram, often used in combination with the energy diagram, is the plot of the weights of partial contributions Ψ_j against the reaction coordinate. The definition of a weight is not unique; the one most commonly used is the following

$$W_j = c_j^2 + \sum_{k \neq j} c_j c_k < \Psi_j | \Psi_k >$$ (3)

where W_j is the weight of the term Ψ_j assuming that the Ψ_j and Ψ are all normalized. The sum of all W_j is thus equal to unity. A good choice of Ψ_j leads to positive weights but it is important to remark that this is not guaranteed by Eq. (3) when the functions Ψ_j are not orthogonal.
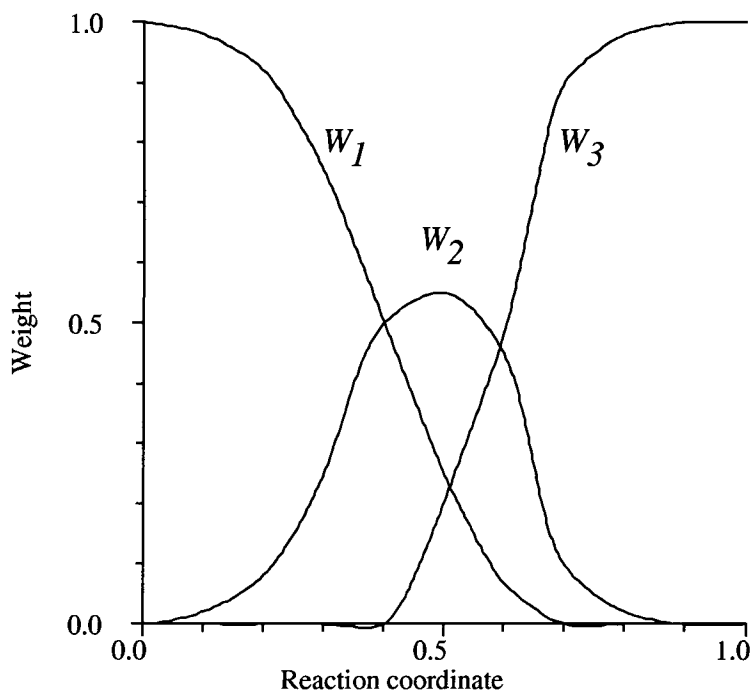
Figure 2. Generic weight diagram for a reaction which involves the formation of an intermediate.

Referring again to the example of Fig. 1, the plot of weights W_{1-3} against the reaction coordinate is shown in Figure 2.

This diagram shows in a clear cut way how the wavefunction changes along the reaction coordinate: it starts from the reactancts' wavefunction Ψ_1, then moves towards the products' wavefunction Ψ_3, passing through an intermediate represented by a function which results from the resonance of all the contributions, but with a predominance of Ψ_2.

Having recalled these few basic concepts, which are important in a VB analysis of a reaction mechanism when the contributions Ψ_j to the wavefunction are classical VB structures, we can now move our attention to the solvent.

The solvent effects are essentially of two types: *physical*, when they allow the reactants to show a different behaviour with respect to the gas phase, and *chemical*, when the solvent itself participates in the reaction. Moreover, it is generally observed, for reactions in the condensed phase that the conversion rate constants are better described by transition state theory than for reactions in the gas phase [8], a consideration that enforces the importance of determining energy diagrams like that of Figure 1 by quantum theory calculations.

The physical effects are always present: they are in fact the effects of a condensed state environment, and are the more complicated to study. The main difficulty arises from the dynamical response of the solvent in the presence of a molecular system which is transforming under a chemical reaction. Actually, no one has so far developed a general method that can treat in detail this difficult aspect, but the literature is dense with contributions which try to study the solvent dynamics (see for example Reference [9]).

In the present chapter, the solvent will be considered always at equilibrium with the reacting system.

2. SOLVENT EFFECT

One of the first attempts to introduce the solvent effect in a VB analysis for the comprehension of a chemical reaction in solution has been given by Warshel and Weiss [10]. These authors introduced the Empirical Valence Bond method (EVB) for the modeling of proton transfer processes in enzymatic reactions in aqueous environment.

The EVB method is a semiempirical method based on the construction of the wavefunction by solving a secular problem in which the Hamiltonian matrix elements are written in terms of empirical parameters. In order to obtain these parameters, the reaction is first studied in the gas phase with the most convenient method, *ab initio* when possible, and

then the energy along the reaction path is reproduced by diagonalization of an effective Hamiltonian built on a basis of well selected VB classical structures as diabatic functions. This effective Hamiltonian contains parameters which allow the correct reproduction of bond dissociation energy curves. When the solvent is included, the diagonal effective Hamiltonian matrix elements are modified in order to consider the solvent electrostatic polarization in such a way that the stronger is the ionic character of a VB structure, the larger is the correction to the relevant diagonal Hamiltonian matrix element. In the EVB method, the contribution of solvation to the off diagonal elements is instead neglected.

Later, in 1990, Kim and Heynes [11] investigated the role of solvent polarization in fast electron transfer processes and pointed out that, when the solvent is instantaneously equilibrated to the quantum charge distribution of the solute, the Hamiltonian itself is a functional of the wavefunction, giving a non-linear Schrödinger equation. The resulting solvent contribution to the Hamiltonian matrix on the diabatic basis thus cannot be simply described as in the former EVB method.

Nowadays the solvent effect is introduced in multiconfiguration quantum calculations in two ways: (i) directly from Monte Carlo or molecular dynamics simulations [12] or (ii) by means of the dielectric model [11, 13]. In the first method, the solvent is represented by a system of point charges that can interact with the solute as in a standard simulation. The main problem arises by the formal requirement to solve a Schrödinger equation every time that a solvent configuration is generated. This fact limits enormously the range of applicability of the method to small reacting systems and to small basis sets. Very recently Mo and Gao [12] studied in this way a prototype proton transfer reaction in water by using a mixed Molecular Orbital Valence Bond (MOVB) methodology for the solute and Monte Carlo simulation for the solvent. Some discussion on this study will be given in Section 4.

The methodology that uses the dielectric model is instead the simpler and in principle the more suitable for the study of chemical reactions involving large molecular systems. In 1998, Amovilli et al [13] developed a computer code in which the solvent reaction field, including all the basic solute-solvent interactions, has been considered for Complete Active Space Self Consistent Field (CASSCF) calculations.

Following this method, the electronic wavefunction is obtained by minimizing self-consistently the free energy functional

$$
\begin{aligned}
G_n &= <\Psi_n|\hat{H}_{vac} + \sum_{i=1}^{N}\hat{V}_0(\vec{r}_i) + \frac{1}{2}\sum_{i=1}^{N}\hat{V}_1(\Psi_{n-1};\vec{r}_i)|\Psi_n> \\
&\quad + \frac{1}{2}\sum_{\alpha}^{nuclei}Z_\alpha V_{pol}(\Psi_{n-1};\vec{R}_\alpha)
\end{aligned}
\tag{4}
$$

where $\hat{H}_{vac}$ is the free molecule Hamiltonian, $\hat{V}_0$ and $\hat{V}_1$ are the contributions to the effective potential due to the solvent and acting on the solute electrons, and the term outside the brackets represents the contribution to the free energy given by the interaction between the solute nuclei and the polarized solvent. Here $\hat{V}_0$ does not change during approach to self-consistency while $\hat{V}_1$ is determined by Ψ_{n-1}, the function calculated at iteration $n-1$. At convergence, Ψ_n and Ψ_{n-1} must be the same.

Adopting the usual decomposition of the solute-solvent interaction energy, $\hat{V}_0$ contains contributions arising from repulsion and dispersion while $\hat{V}_1$ contains those from polarization and dispersion. In terms of a given basis set $\{\chi_r\}$ the matrix elements of each of these contributions are defined as follows:

$$(V_{0,rep})_{rs} = \kappa_r \left(S_{rs} - S_{rs}^{(in)} \right) \tag{5}$$

$$(V_{0,dis})_{ru} = -\frac{\kappa_d}{2} \sum_{st} \{rs|tu\} S^{-1}{}_{st} \tag{6}$$

$$(V_{1,dis})_{ru} = \frac{\kappa_d}{2} \sum_{st} \{rs|tu\} P_{st} \tag{7}$$

$$(V_{1,pol})_{ru} = \int d\vec{r} \chi_r^*(\vec{r}) V_\sigma(\vec{r}) \chi_u(\vec{r}) \tag{8}$$

in which

$$S_{rs}^{(in)} = -\frac{1}{4\pi} \oint_{S(C)} E_{rs}(\vec{r}) da \tag{9}$$

$$\{rs|tu\} = \frac{1}{2} \oint_{S(C)} da \quad [V_{rs}(\vec{r}) E_{tu}(\vec{r}) + V_{tu}(\vec{r}) E_{rs}(\vec{r})] \tag{10}$$

$$V_\sigma(\vec{r}) = \oint_{S(C)} da_1 \frac{\sigma(\vec{r}_1)}{|\vec{r} - \vec{r}_1|} \tag{11}$$

where $\mathbf{P}$ is the solute electron density matrix, $\mathbf{S}$ is the overlap matrix, and V_{rs} and E_{rs} are, respectively, the potential and the outward component of the field due to the distribution $\chi_r \chi_s$. σ is the apparent surface charge density induced by the charge distribution of the solute on the surface of the cavity and depends on the dielectric constant of the solvent. It should be noted that in this polarizable continuum model (PCM), the solute is embedded in a cavity of a dielectric medium which is defined in terms of interlocking spheres centered on the solute nuclei. The integrals (9), (10) and (11) are surface integrals defined over the surface of this cavity [14] and they are computed by exploiting a partitioning of the surface itself in terms of tesserae.

For κ_r and κ_d, in atomic units, the expressions are [15]

$$\kappa_r = 0.063 \; \rho_B \frac{n_{val}^B}{M_B} \tag{12}$$

$$\kappa_d = 0.036 \; \frac{(\eta_B^2 - 1)}{\eta_B(\eta_B + \frac{\omega_A}{I_B})} \tag{13}$$

where ρ_B is the density of the solvent relative to the density of water at 298 K, n_{val}^B and M_B are the number of valence electrons and the molecular weight of the solvent, η_B and I_B are the refractive index and the ionization potential of the solvent, and finally ω_A is a suitable average transition energy for the solute.

To the quantum mechanical contribution to the solvation free energy (4) it is also necessary to add the work required to create the cavity in which the solute is placed; this quantity, namely the cavitation free energy, is calculated with the Pierotti-Claverie formula [16, 17].

All the details on the PCM, here only summarized, can be found in the source papers (see Refs. [13, 14, 15]).

The CASSCF wavefunction obtained by minimization of G in Eq. (4) can be transcribed, in the spirit of Eq. (1), in terms of diabatic contributions, resorting to a given set of VB structures. A standard spin-free VB calculation (see for example [18]) can be performed in the space of the previous active orbitals, freezing the MCSCF core. The localization of the active orbitals can also be enhanced by a VB calculation with a restricted set of structures. It is important to remark that in this process the valence orbitals lose their orthogonality and the minimal energy of a wavefunction expanded in terms of the selected VB structures is reached. The VB structures must be selected in order to have the best pairing of electrons. The quality of this choice can easily be tested by calculating the percentage of the CASSCF correlation energy recovered, where 100 % corresponds to the CASSCF result.

Actually the transcription of a MCSCF function into a VB formalism, instead of a direct optimization of a VB function, is preferable in order to exploit the capabilities of the standard packages for *ab initio* calculations which, in fact, work with orthogonal orbitals [19].

In the next few sections, the role of the solvent in a reaction mechanism is shown by analyzing, from a VB point of view, the electron cloud rearrangement in some basic chemical processes.

3. TWO ELECTRON - TWO CENTRE BOND BREAKING

The simplest chemical process is the breaking of a bond between two atoms involving two electrons. In this dissociation there is a competition between the homolytic fission, in which each atom maintains one electron, and the heterolytic fission, in which one of the atoms retains the electrons. This competition is very sensitive to the polarization of the environment because in the heterolytic dissociation there is a separation of charges. In order to focus the problem let us take two atoms, A and B, initially bonded through a classical resonance scheme involving three structures written in terms of two hybrids, χ_A and χ_B, located on different atoms. Denoting all electrons not involved in the bond as 'core' the wavefunction can be well approximated by

$$\Psi = c_1\Psi_{cov} + c_2\Psi_{ion} + c_3\Psi'_{ion} \tag{14}$$

with

$$\Psi_{cov} = K_1\hat{A}(core)\chi_A(\vec{r}_1)\chi_B(\vec{r}_2)[\alpha(\sigma_1)\beta(\sigma_2) - \beta(\sigma_1)\alpha(\sigma_2)] \tag{15}$$

$$\Psi_{ion} = K_2\hat{A}(core)\chi_A(\vec{r}_1)\chi_A(\vec{r}_2)[\alpha(\sigma_1)\beta(\sigma_2) - \beta(\sigma_1)\alpha(\sigma_2)] \tag{16}$$

$$\Psi'_{ion} = K_3\hat{A}(core)\chi_B(\vec{r}_1)\chi_B(\vec{r}_2)[\alpha(\sigma_1)\beta(\sigma_2) - \beta(\sigma_1)\alpha(\sigma_2)] \tag{17}$$

where the K_j denote suitable normalization constants, $\hat{A}$ the full anti-symmetrizer and α and β the usual one electron spin functions. The first of the three functions in the Equations (15-17) is normally referred as a covalent structure while the other two are ionic structures; they are perfectly analogous to those given in the Heitler-London treatment of the H_2 molecule [1].
Although a single covalent structure written in terms of new hybrids obtained by mixing χ_A and χ_B could reproduce the wavefunction Ψ of Eq. (14), as Coulson and Fischer did in their H_2 VB study [20], in this Section the role of each contribution will be examined separately in order to analyze the solvent effect.

3.1 Dissociation of LiF

The first illustrative example is the dissociation of LiF. It is well known that alkali halides are compounds with strong ionic character and that they dissociate as neutral atoms *in vacuo* but as a pair of ions in aqueous solution. By means of the model shown in the previous Section, this effect can be observed quantitatively. In the example the LiF has been studied

both *in vacuo* and in the dielectric medium at a CASSCF level distributing two active electrons in two valence orbitals and using a good even tempered basis set. The VB transcription has been performed localizing the two active valence orbitals on the separate atoms. In this particular case, one of the two ionic structures does not contribute to the wavefunction because the situation in which the lithium is negatively charged and the fluorine is positively charged is energetically too unfavourable.

In Figure 3 the plot of the diabatic energies referring to the two main VB structures is shown against the LiF interatomic distance. It is quite evident looking at this diagram that at the equilibrium geometry ($d_{LiF} = 1.7$Å), both *in vacuo* and in solution, that the molecule is characterized by essentially an ionic description: Ψ_{ion} dominates in the expression for Ψ, while, at dissociation *in vacuo*, the molecule gives two neutral atoms, because in this case the wavefunction is represented by Ψ_{cov}.
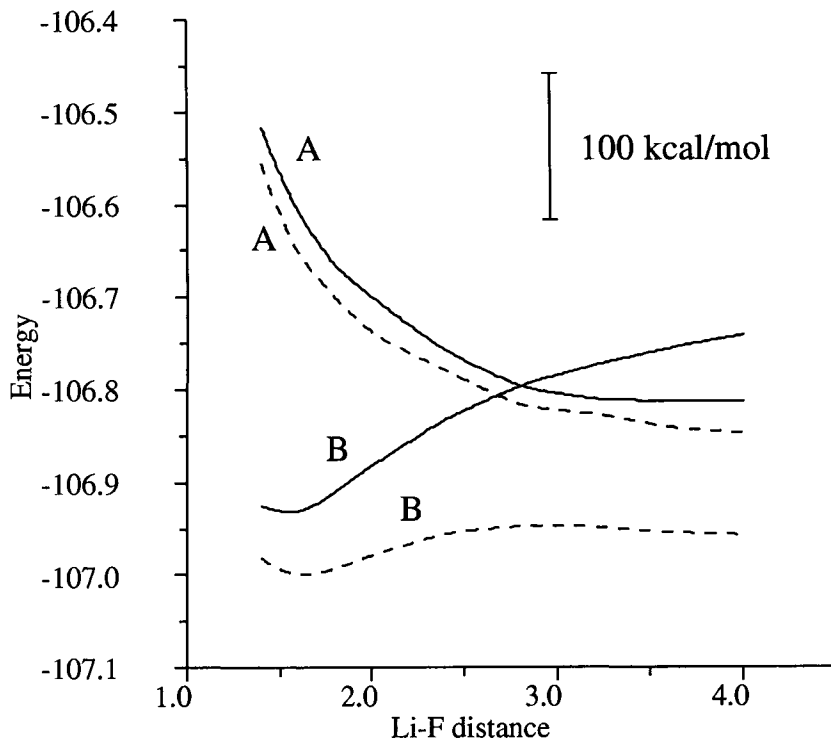
Figure 3. Diabatic energy curves (hartree) for the dissociation of LiF *in vacuo* (solid line) and in aqueous solution (dashed line). The LiF distance is measured in Å. Curves A refer to the covalent structure and curves B to the ionic structure corresponding to Li$^+$F$^-$.

The solvent water instead allows the LiF to dissociate into Li^+ and F^-, compensating the energy required for the separation of opposite charges with the polarization interaction.

It is important to note at this point the quantitative effect on the energy surfaces of solute-solvent interactions. As already anticipated, the dominant effect is due to electrostatic polarization; in fact, in the range of distances of Fig. 3, the fluctuations of dispersion, repulsion and cavitation contributions are respectively 0.3 kcal/mol, 1.1 kcal/mol and 0.9 kcal/mol, which must be compared with 100 kcal/mol, the order of magnitude of variation of polarization in this case.

Turning to the VB analysis, the behaviour of the wavefunction along the path to dissociation is more evident in Fig. 4, where the weights of VB structures, calculated as defined in Eq. (3), are plotted against the interatomic distance. The ionic contribution at equilibrium is more or less the same in the two cases, close to 90 percent, while it falls rapidly to zero *in vacuo* and it is enhanced in water as the distance increases.
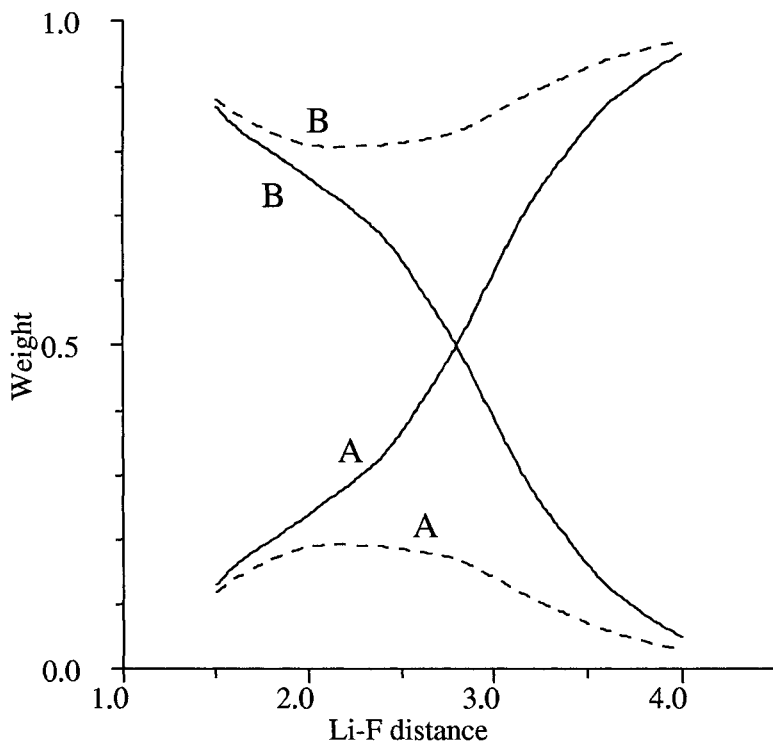
Figure 4. Weight curves for the dissociation of LiF *in vacuo* (solid line) and in aqueous solution (dashed line). The LiF distance is measured in Å. Curves A refer to the covalent structure and curves B to the ionic structure corresponding to Li^+F^-.

3.2 Dissociation of the CF bond in CH$_3$F

The second example of this Section shows instead an opposite behaviour. In this example, the dissociation of the methyl fluoride (CH$_3$F) CF bond in methanol (CH$_3$OH) solution is illustrated. Similar reactions, namely the production of carbocations in polar solvents from alkyl halides, are important in organic synthesis where very often they are favoured by the presence of a catalyst, normally a metal cation. Methanol is a polar solvent: the dielectric constant ϵ is 32.6 at 298 K, about half of that of water, but the ratio $(\epsilon - 1)/\epsilon$ is close to unity, showing a strong capability to polarize in a static external electric field. Nevertheless this dissociation is energetically unfavourable.

The carbon-fluorine bond is a polar covalent bond in the sense that it exhibits a not negligible ionic character. This polarity is reflected in the weight of the ionic VB structure, $\Psi_{ion}(\text{H}_3\text{C}^+\text{F}^-)$, which is calculated to
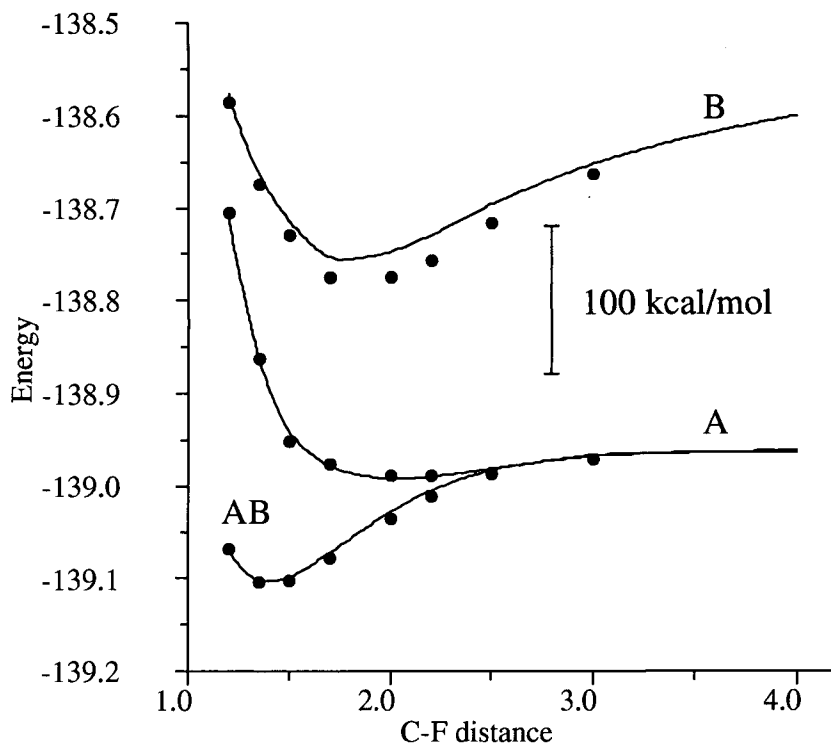
Figure 5. Energy curves (hartree) for CH$_3$F dissociation *in vacuo* (solid line) and in methanol (filled circles) against the CF distance (Å). Curves A refer to the covalent structure, curves B to the ionic structure corresponding to H$_3$C$^+$F$^-$, and curves AB to the adiabatic electronic wavefunction.

be 0.39 at the equilibrium geometry in free space. For this calculation, a standard 6-311G** basis set has been used.

The energy curves are plotted in Fig. 5. For this case, the diabatic curve corresponding to the ionic structure is the higher at all the distances considered. For this reason, the polarization of the solvent is less pronounced than for LiF because it depends on a wavefunction which is dominated by covalent character.

The solvation contributions to the free energy functional of Eq. (4) cannot be distinguished on the scale of Fig. 5 for the lower two curves, which are respectively, the total free energy and the covalent structure diabatic curve. Instead in the region of the minimum of the upper curve, the solvent lowers the free energy by about 15 kcal/mol, but this effect is not sufficient to product a particularly significant variation in the total wavefunction.

In Table 1, the individual contributions to the total free energy in solvent, for various CF interatomic distances, are presented according to the decomposition made in Ref. [15].

It is clear from Table 1 that, for this example, the solvent does not change significantly the solute wavefunction. Looking first at the internal energy change, which is a measure of the change of the wavefunction in passing from vacuo to the solvent, being the change of the expectation value of the free solute Hamiltonian, one sees that 0.3 kcal/mol is a very small effect and it is largely within the precision of the model. The main changes to solvation free energy due to the solute wavefunction, when the CF distance increases, come from polarization and dispersion, but their effects are restricted only to a small change in the value of the PES.

The presence of a metal cation in close proximity of CH_3F alters significantly the shape of the curves in Fig. 5 but it is important to remark that a metal cation is better solvated than a carbocation because of the

Table 1

Solvation free energies and their components (kcal/mol) for methyl fluoride in methanol at 298 K, calculated at various C–F interatomic distances (Å).

C–F distance	iec*	components				total
		polarization	repulsion	dispersion	cavitation	
1.20	0.0	−1.1	1.1	−5.2	5.3	0.1
1.35	0.1	−2.4	1.1	−5.3	5.4	−1.1
1.50	0.1	−3.8	1.1	−5.5	5.6	−2.5
1.70	0.2	−5.5	1.1	−5.8	5.8	−4.2
2.00	0.3	−6.2	1.1	−6.5	6.0	−5.3
2.20	0.2	−5.1	1.2	−7.2	6.2	−4.7
2.50	0.1	−2.5	1.3	−8.6	6.5	−3.2
3.00	0.0	−1.0	1.4	−9.6	6.9	−2.3

*iec – internal energy change

smaller radius. This fact could render useless the metal ion for catalysis in solution, because in this case the exchange of F^- ion between CH_3F and the metal remains energetically unfavourable. A different situation is offered by transition metal complexes, which instead can play a different role owing to their larger size.

4. FOUR ELECTRON - THREE CENTRE REARRANGEMENTS

Reactions involving four electrons and three centres can include the formation of a chemical bond at the expenses of another bond which is consequently broken. A large variety of reactions can be explained by such a mechanism, by way of example attention here will be focused on bimolecular nucleophilic substitutions (S_N2) and proton transfers. Typically a four electron - three centre unit AXB, in which the central atom X could be a hydrogen or a carbon atom, is mainly described by the resonance of the following three classical VB structures

$$A: \quad X - B \quad , \quad A^+ - X \quad :B^- \quad , \quad A: \quad X^+ \quad :B^- \tag{18}$$

to which, according to the notation given in the previous section, one can associate the three functions

$$\Psi_1 = K_1 \hat{A}(\text{core}) \chi_A \chi_A \chi_X \chi_X \chi_B [\alpha\beta - \beta\alpha][\alpha\beta - \beta\alpha] \, , \tag{19}$$

$$\Psi_2 = K_2 \hat{A}(\text{core}) \chi_A \chi_X \chi_X \chi_B \chi_B [\alpha\beta - \beta\alpha][\alpha\beta - \beta\alpha] \tag{20}$$

and

$$\Psi_3 = K_3 \hat{A}(\text{core}) \chi_A \chi_A \chi_X \chi_B \chi_B [\alpha\beta - \beta\alpha][\alpha\beta - \beta\alpha] \, , \tag{21}$$

now written in terms of three hybrids located on A, X and B. Of course, for four electrons displaced in three orbitals, three other structures can be generated, but those given above remain the most important.

One of the problems in studying a PES by using multiconfiguration methodologies comes from the balance of correlation energy for all the nuclear configurations considered. Clearly, an unbalanced PES, could lead to wrong estimates of barrier heights and reaction energies. In principle it should be better to allow single occupancies of orbitals in the active space because electrons tend to repel each others. Therefore the above proposal, for the study of a reaction involving a four electron - three centre rearrangement, could be improved by a CASSCF calculation distributing the four active electrons in four orbitals. The studies of the π system of 1,3-dipolar molecules using the increased valence structures [21] and the spin coupled valence bond (SCVB) approach [22] meet the latter consideration.

4.1 Menshutkin reaction between NH_3 and CH_3Cl

Recently Amovilli *et al* [13] studied the Menshutkin reaction (MR) in aqueous solution using a similar approach.

The MR is in a special S_N2 reaction where the reactants are neutral, as opposed to most usual S_N2 reactions where one of the reactants is charged. Thus, while along the reaction coordinate of usual S_N2 reactions there is a charge migration, in MRs there is a creation of two ions of opposite sign, followed by their separation. In gas phase, this reaction is an extremely unfavorable process due to Coulombic interactions, with a huge energy barrier. As a matter of fact, MRs have never been reported in the gas phase. However, hydration very significantly reduces the energy barrier, and the reaction becomes largely exothermic. These experimentally observed solvent effects and also some other specific features of the MRs have been put forward in computational studies.

In the present chapter a preliminar study, made on an approximate reaction path of the MR between ammonia and methyl chloride in aqueous solution, is reported. In this study a deeper VB analysis than that given in Ref. [13] by Amovilli *et al* is attempted.

As in the earlier paper, because C_{3v} symmetry is maintained for all the geometries studied, the active orbitals are taken to be of a_1 type. The complete active space is then spanned by all the configurations arising by distributing four valence electrons in four orbitals. This choice is able to reproduce correctly, for reactants, a lone-pair and a diffuse orbital on nitrogen and a bonding and an anti-bonding orbital between carbon and chlorine; and, for products, a lone-pair and a diffuse orbital on chlorine and a bonding and an anti-bonding orbital between carbon and nitrogen. The calculations have been performed using a 6-311G** basis set.

In Figure 6, the energy curves for the reaction *in vacuo* and in solution are plotted against the CCl distance.

The approximate reaction coordinate has been characterized by keeping the NCl distance at the fixed value of 4.3 Å and optimizing all other geometrical parameters.

In Ref. [13] the CASSCF wavefunction was transcribed in terms of VB structures. The localization of the active orbitals was imposed by making a calculation with one perfect pairing structure. Comparing the energy of this calculation with that obtained using all 20 Weyl-Rumer configurations, corresponding to the full-CI limit of four electrons in four orbitals coupled to singlet as in the CASSCF, the authors recovered 99 % of the correlation energy. This was the most important result of their VB analysis because it shows that this MR may be formulated according to a mechanism in which one VB structure is used to describe the rearrangement of the electronic distribution along the reaction path. With the notation used in this chapter, this perfect pairing structure can be
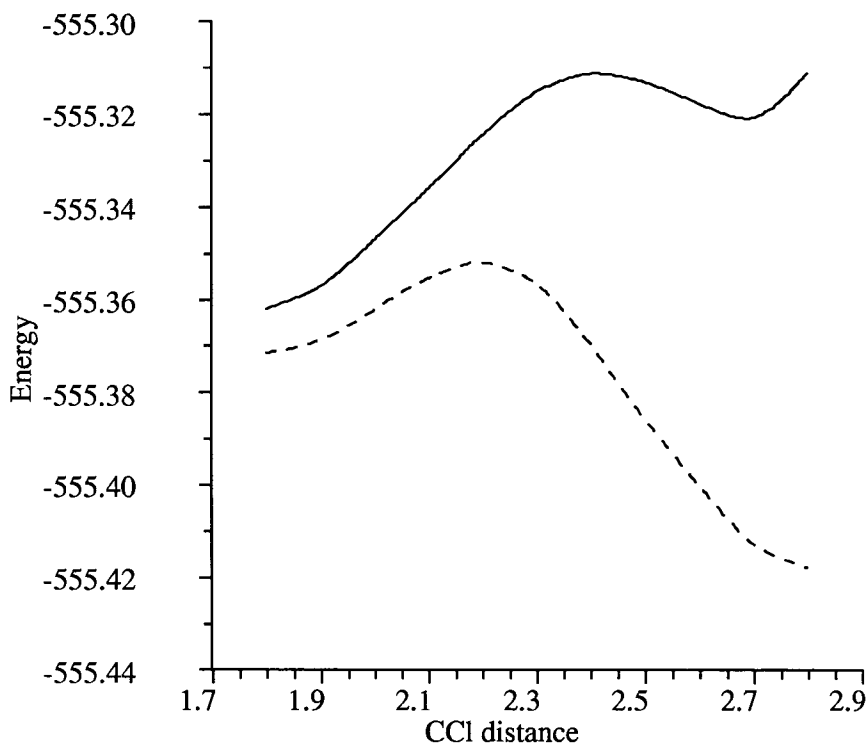
Figure 6. Energy curves (hartree) against the CCl distance (Å) for the reaction between ammonia and methyl chloride *in vacuo* (solid line) and in aqueous solution (dashed line). The NCl distance is fixed at 4.3 Å.

written as

$$\Psi = K \hat{A}(\text{core})\phi_1\phi_2\phi_3\phi_4[\alpha\beta - \beta\alpha][\alpha\beta - \beta\alpha] , \qquad (22)$$

where the final orbitals ϕ_{1-4} were shown to be of the form

$$\phi_1 = \chi_N \qquad (23)$$

$$\phi_2 = a\,\chi_C + b\,\chi_N' \qquad (24)$$

$$\phi_3 = a'\,\chi_C' + b'\,\chi_{Cl} \qquad (25)$$

$$\phi_4 = \chi_{Cl}' \qquad (26)$$

where $\chi_N, \chi_N', \chi_C, \chi_C', \chi_{Cl}, \chi_{Cl}'$, are six hybrids located on nitrogen, carbon and chlorine atoms, and where the coefficients a, b, a', b' play the role of bond polarization parameters which change along the reaction coordinate.

Looking at the composition of these orbitals, the VB structure (22) is very similar to that involved in the Linnett-type non-paired spatial orbital representation for a four electron, three-centre bonding unit [23], discussed by Harcourt in Ref. [24]. The only difference is related to the number of hybrids involved; in the Harcourt paper only three hybrids, one for each atom, are considered while here, owing to the use of an extended basis set, the four localized orbitals in Eq. (22) derive from the six hybrids described above.

The same scheme applies to the reaction in the gas phase, the main difference being the degree of the polarization of the orbitals ϕ_2 and ϕ_3, corresponding to the different location of the transition state.

The great flexibility of the orbitals ϕ_{1-4} makes it difficult to compare the present result with the weights obtained by Shaik et al [25] in their classical VB scheme.

Turning to the expression of orbitals ϕ_2 and ϕ_3, it is of interest now to analyze the solvent effect on CN and CCl bond polarization. Because of the simplicity of Equations (24) and (25), it is convenient to perform a Mulliken population analysis (see for example [26]) on the above orbitals at different CCl distances in $vacuo$ and in solution. In terms of contributions coming only from ϕ_2 and ϕ_3, the Mulliken charges on nitrogen and chlorine turn out to be as follows

$$q_N = b^2 + ab < \chi_C | \chi'_N > \tag{27}$$

$$q_{Cl} = b'^2 + a'b' < \chi'_C | \chi_{Cl} > . \tag{28}$$

Fig. 7 shows the behaviour of these charges with variation of the CCl distance. As was to be expected in going towards the products, namely $CH_3NH_3^+$ and Cl^-, q_N tends to a minimal value while q_{Cl} tends to unity. The effect of water, the solvent, results in a further enhancement of q_{Cl} and in a further reduction of q_N with the increase of CCl distance. This effect is completely due to the solvent polarization when the ionic products begin to form. It is important to note that such small changes in the Mulliken charges (27) and (28) correspond instead to a strong change in the value of the energy along the reaction path (see Fig. 6). Repulsion and dispersion contributions to the solvation free energy do not have any visible effects on the solute wavefunction in this reaction.

The apparently strange behaviour of q_N, namely the presence of a minimum at the CCl distance of 2.1 Å, could be a sign of resonance of structures involving diffuse orbitals on nitrogen, with the perfect pairing function (22) being representative of a more complex CASSCF wavefunction, or it could be simply related to the quality of the basis set. As anticipated, this is a preliminary result of work in progress: a full account will be published elsewhere in due course.
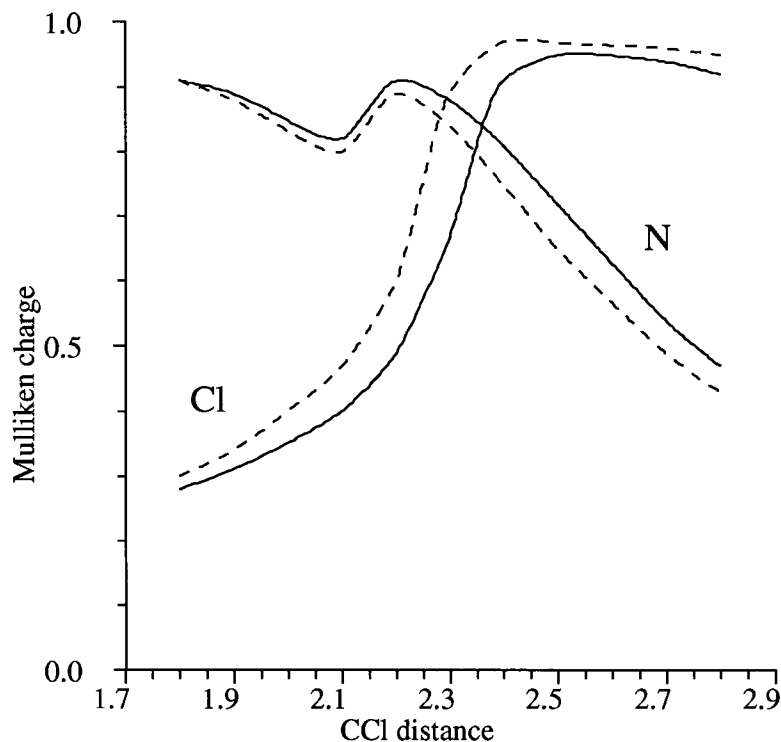
Figure 7. Mulliken charges on nitrogen (N) and chlorine (Cl) derived from orbitals ϕ_2 and ϕ_3 (see text) against the CCl distance for the reaction between ammonia and methyl chloride *in vacuo* (solid line) and in aqueous solution (dashed line).

4.2 Proton transfer between H_2O and $[FeH(CO)_4]^-$

When the central atom X in structures (18) is a hydrogen, the reaction involved is a proton transfer (PT) process. This kind of reaction is very similar to S_N2 reactions, the main difference being that the proton is much smaller in size and mass than a CH_3 group and thus a proton transfer can be influenced by quantum effects like tunneling. Nevertheless the PES can be calculated in the same way as in the previous MR case.

Although, from a classical VB point of view, it is difficult to imagine a hypervalent hydrogen atom, from a computational point of view there are no difficulties in using a perfect pairing structure in which a hydrogen atom is simultaneously bonded to atoms A and B. This situation corresponds exactly to the interpretation of a CASSCF calculation, performed on a system in which a proton is exchanged, with an active space generated by distributing four electrons in four orbitals as in the MR. Such a

description could be insufficient only in cases when the proton migration is coupled to electron transfer or more complicated bonds reorganization, a frequent situation in biological systems (see for example [27]).

The effect of solvents on PT is complicated by the fact that usually the solvents which exhibit a strong activity are both proton donor and proton acceptor, like water, and thus can participate in the reactions. A model of proton transport in water which uses the EVB model has been recently published by Schmidt and Voth [28].

One of the first *ab initio* calculations on a PT in aqueous solution has been presented by Mo and Gao [12]. Those authors developed a mixed MOVB method to treat the solute and a Monte Carlo method for the solvent, the latter described by a system of point charges. In Ref. [12] they report a calculation on a PT reaction between the NH_4^+ ion and NH_3. It is important to remark that they used the classical VB scheme (18). Because reactants and products are the same species, the solvent effect is small, although a large percentage of the barrier height, which is low. The effect increases the activation energy by about 1 kcal/mol. Such a value cannot correspond to significant changes in the solute wavefunction, as shown in this chapter, and so it is not necessary to solve again the Schrödinger equation for the reacting system every time that a solvent configuration is generated, like Mo and Gao did in their calculation. The large computational effort restricted them to a small and consequently poor basis set.

The solvent effects on PT reactions begin to become important when reactants and products are solvated differently as in the example below involving iron complexes.

The proton transfer reaction

$$[FeH(CO)_4]^- + H_2O \rightarrow FeH_2(CO)_4 + OH^- \tag{29}$$
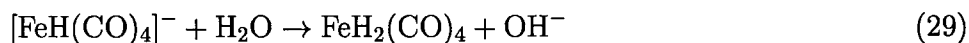
is the slow step of the water gas shift reaction (WGSR), a key process for the production of hydrogen for the chemical industry, and catalyzed by $Fe(CO)_5$ [29, 30]. The homogeneous catalysis by $Fe(CO)_5$ allows the WGSR to be carried out at considerably lower temperatures, with water present as a liquid. Experimental data reported by Sunderlin and Squires [31] suggested that the above process (29), largely endothermic in the gas phase, is considerably less endothermic in aqueous solution owing to the strong solvation of the species OH^- which is a smaller ion than $[FeH(CO)_4]^-$.

The mechanism of the WGSR catalyzed by $Fe(CO)_5$ in the gas phase has been analyzed in detail through a quantum mechanical study published by Torrent *et al* [32]. In that paper, the authors confirmed, for the catalytic cycle, the following scheme:

$$Fe(CO)_5 + OH^- \rightarrow Fe(CO)_4COOH^-$$
$$Fe(CO)_4COOH^- \rightarrow FeH(CO)_4^- + CO_2$$
$$FeH(CO)_4^- + H_2O \rightarrow FeH_2(CO)_4 + OH^-$$
$$FeH_2(CO)_4 \rightarrow H_2 + Fe(CO)_4$$
$$Fe(CO)_4 + CO \rightarrow Fe(CO)_5 . \tag{30}$$
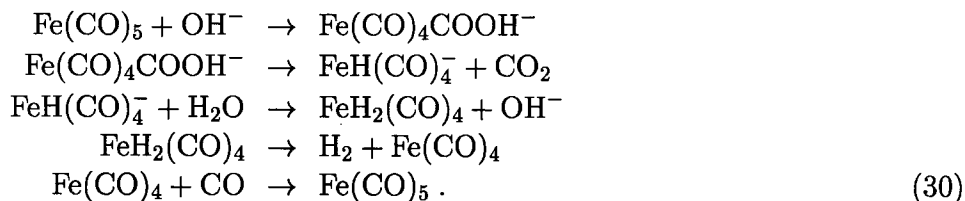
The global process was found to be exothermic, while the step (29) was found to be endothermic, in good agreement with experiments.

Most of the energy required to overcome the process (29) is provided by the initial formation of the ion $Fe(CO)_4COOH^-$ from $Fe(CO)_5$ and OH^-, which is a highly exothermic process.

In a very recent paper, Amovilli *et al* [33] analyzed the effect of water as solvent on the slow step (29) by means of the polarizable continuum model used for the MR.

Their results confirmed a considerable lowering of the endothermicity although, for a final consideration about the energy balance on the WGSR,
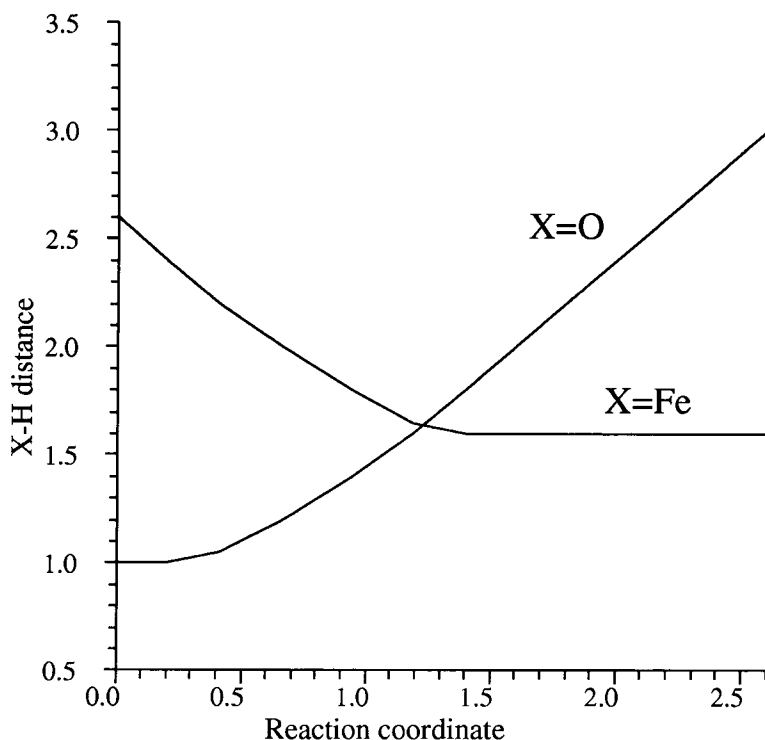
Figure 8. FeH and HO distances (Å) againsts the reaction coordinate (Å) for the proton transfer between H_2O and $[FeH(CO)_4]^-$.
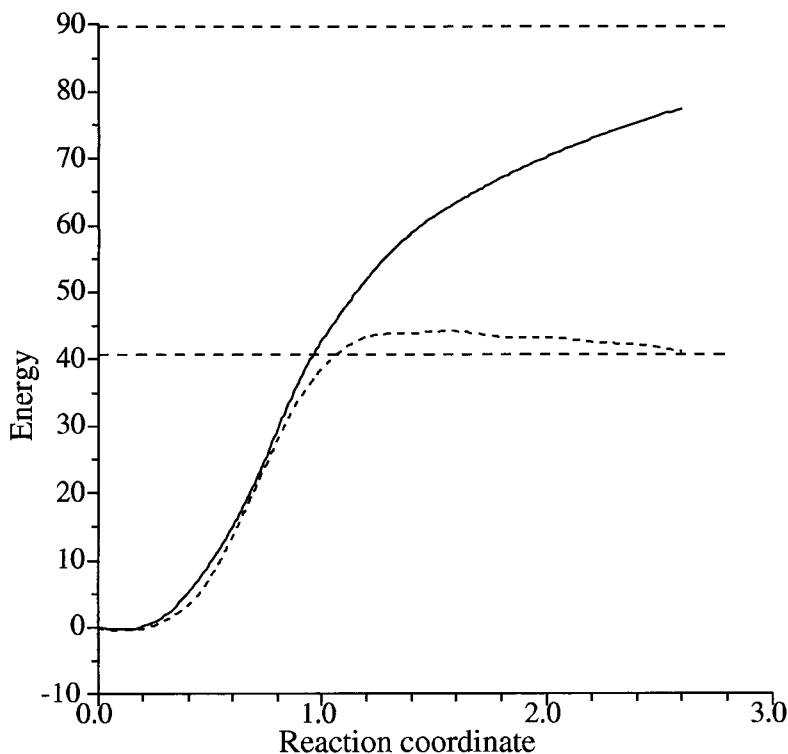
Figure 9. Energy (kcal/mol) profiles along the reaction coordinate (Å) *in vacuo* (solid line) and in aqueous solution (dashed line) for the proton transfer reaction between H_2O and $[FeH(CO)_4]^-$. The horizontal lines correspond to the energies of the products at infinite separation.

a complete PCM study of all the other processes of the scheme (30) will be necessary.

In Ref. [33] a reaction coordinate has been defined by constraining the motion of the transferred hydrogen to a line connecting the oxygen of water to iron. In such a way, a two dimensional map of the energy, in terms of the distance of hydrogen from iron (FeH) and the distance of hydrogen from oxygen (HO), has been derived. Each position on the map corresponds to a geometry in which the above distances are fixed and all the other internal coordinates are optimized to the best energy. For simplicity in Fig. 8, the variation of the FeH and HO distances with the selected reaction coordinate is shown. Fig. 9 instead shows the energy curves for the transfer in the gas phase and in aqueous solution. Here, for a better comparison, the two curves start from the same point at which the energy is set to zero.

All the computational details for this reaction can be found in the source

436

paper [33] while, in this chapter, the same more-refined VB analysis is presented as for the reaction between ammonia and methyl chloride described earlier.

The same perfect pairing scheme used to study the previous MR applys also to this PT reaction. Now there is a hydrogen atom simultaneously bonded to iron and oxygen with different polarization depending on the reaction coordinate. If the orbital ϕ_1 is located on iron and orbital ϕ_4 on oxygen, then orbitals ϕ_2 and ϕ_3 show the following modifications:

$$\phi_2 \; : \; \chi'_{Fe} \rightarrow a\chi'_{Fe} + b\chi_H \rightarrow \chi_H$$
$$\phi_3 \; : \; \lambda\chi_O + \chi'_H \rightarrow a'\chi_O + b'\chi'_H \rightarrow \chi_O$$

$$(31)$$

where the mixing coefficients are arranged to give the best overlap with the partner orbitals ϕ_1 and ϕ_4 in the perfect-pairing structure (22) for all geometries.
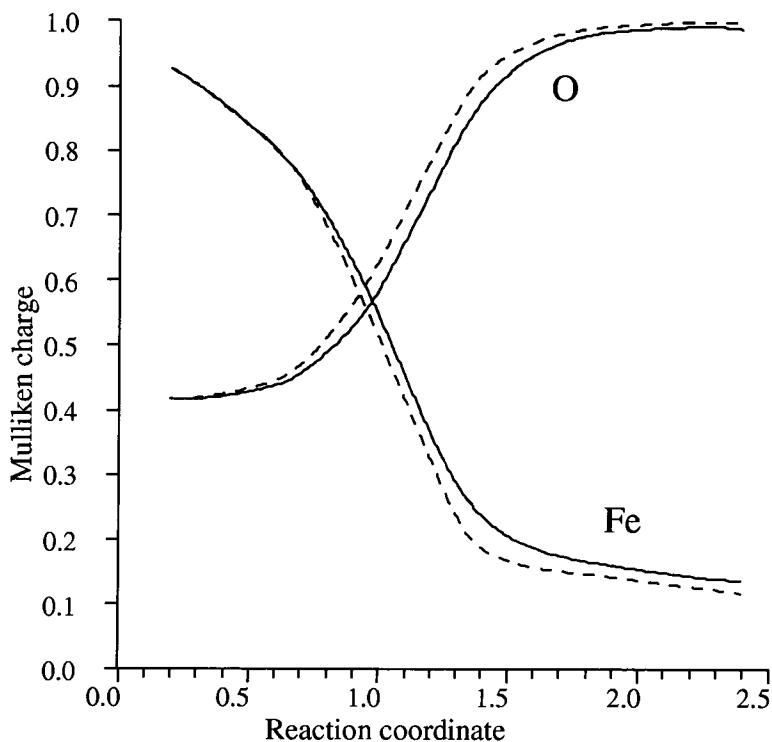
Figure 10. Mulliken charges on iron (Fe) and oxygen (O) derived from orbitals ϕ_2 and ϕ_3 (see text) against the reaction coordinate (Å) for the proton transfer reaction between H_2O and $[FeH(CO)_4]^-$ in the gas phase (solid line) and in aqueous solution (dashed line).

Performing a Mulliken population analysis on hybrids ϕ_2 and ϕ_3, the following charges on iron and oxygen are derived:

$$q_{Fe} = b^2 + ab < \chi_H | \chi'_{Fe} > \tag{32}$$

$$q_O = b'^2 + a'b' < \chi'_H | \chi_O > \quad . \tag{33}$$

A plot of these against the reaction coordinate is given in Fig. 10: it is evident that the solvent, again through the polarization contribution to the solvation, 'anticipates' the transformation (31) of orbitals ϕ_2 and ϕ_3, in comparison with the gas phase behaviour. This effect is less pronounced than in the MR; it is important to remark that in this PT process the solvent lowers the reaction energy by about 50 kcal/mol while in the MR this lowering is stronger.

5. ELEMENTARY PROCESSES INVOLVING MORE THAN FOUR ELECTRONS

An elementary process of a reaction is commonly described by chemists as a concerted mechanism in which the electron distribution rearrangement is schematically shown resorting to graphical symbols like points, lines and arrows. In chemistry it is difficult to find a concerted step which involves more than six or eight electrons although the six electrons rearrangements are very frequently encountered. In the previous sections some processes have been analyzed in order to show the effect of a solvent on VB structures and hybrids. It is clear now that the solvent becomes important only when it can determine a strong variation of the reacting system free energy along the reaction path. At present, such strong variations are observed only when ionic products are formed starting from neutral reactants or when the ions involved change significantly their volume along the reaction walk.

In order to study more complicated bond rearrangements, by using the same approach shown in previous sections, one needs to pay attention to the following two points: (i) the MCSCF calculation must be performed using an appropriate but limited active space and (ii) to elaborate a comprehensible and reliable analysis it is now very important to exploit the full flexibility of the VB methodologies. At this level in fact, with more than four active electrons, the complexity of the problem does not allow a simple description like that given in the cases discussed so far and proliferation of optimization parameters could lead to a difficult analysis.

5.1 Electrophilic attachment of chlorine to ethylene

An illustrative example is the electrophilic attachment of chlorine to the carbon-carbon double bond of ethylene.

It is well known that in polar solvents this attachment determines the formation of the chloronium ion intermediate starting from an initially neutral T-shaped intermolecular complex, while in the gas phase the same mechanism is unfavourable. It has been shown [34] that once the solvent polarization compensates the energy requested for the separation of opposite charges, a reaction path can be found which maintains the C_{2v} symmetry of the T-shaped complex and which exhibits a low barrier. Thanks to such symmetry constraints, the Woodward-Hoffmann rules can be applied in order to define a reliable active space for the PCM-MCSCF calculation. Amovilli *et al* in Ref. [34] distributed six electrons in five selected orbitals. Their choice was sufficient to describe, for the reactants, the C–C π-bond and anti-bond, the Cl–Cl σ-bond and anti-bond and a p orbital on the approaching chlorine atom lying in the C_2Cl plane; and, for the intermediate, the two C–Cl bonds and anti-bonds of the ring and an axial p orbital on the detached chlorine atom. This CAS(6,5) falls into two limiting CAS(4,4) descriptions in the regions of the reactants and of the intermediate: the p orbital on the approaching Cl for the T-shape complex and the p orbital on the detached Cl when the chloronium ion is formed are doubly occupied in these two limits.

After the CASSCF calculation with the above choice of orbitals, in order to perform an efficient VB analysis, it is better in this case to resort to an overcomplete non-orthogonal hybrid set. The five active orbitals, in fact, can be split into ten hybrids, in term of which the VB transcription of the wavefunction turns out to be the simplest and the most compact. Such kinds of overcomplete basis sets are commonly used in constructing the so called non-paired spatial orbital structures (NPSO, see for example [35]), but it should be remarked that their use is restricted to gradient methods of wavefunction optimization, such as steepest descent, because other methods, which need to invert the hessian matrix (like Newton--Raphson) clearly have problems with singularities.

Turning to the electrophilic attachment of chlorine to ethylene, Amovilli *et al* in [34] recovered between 93 and 99 % of the CAS(6,5) correlation energy using four structures and ten hybrids with the following classical coupling scheme

$$\Psi_1 = K_1\hat{A}(\text{core})\phi_3\phi_3\phi_1\phi_2\phi_4\phi_5[\alpha\beta - \beta\alpha][\alpha\beta - \beta\alpha][\alpha\beta - \beta\alpha]\,, \tag{34}$$

$$\Psi_2 = K_2\hat{A}(\text{core})\phi_{10}\phi_{10}\phi_6\phi_8\phi_7\phi_9[\alpha\beta - \beta\alpha][\alpha\beta - \beta\alpha][\alpha\beta - \beta\alpha]\,, \tag{35}$$

$$\Psi_3 = K_3\hat{A}(\text{core})\phi_{10}\phi_{10}\phi_9\phi_9\phi_6\phi_8[\alpha\beta - \beta\alpha][\alpha\beta - \beta\alpha][\alpha\beta - \beta\alpha]\,, \tag{36}$$
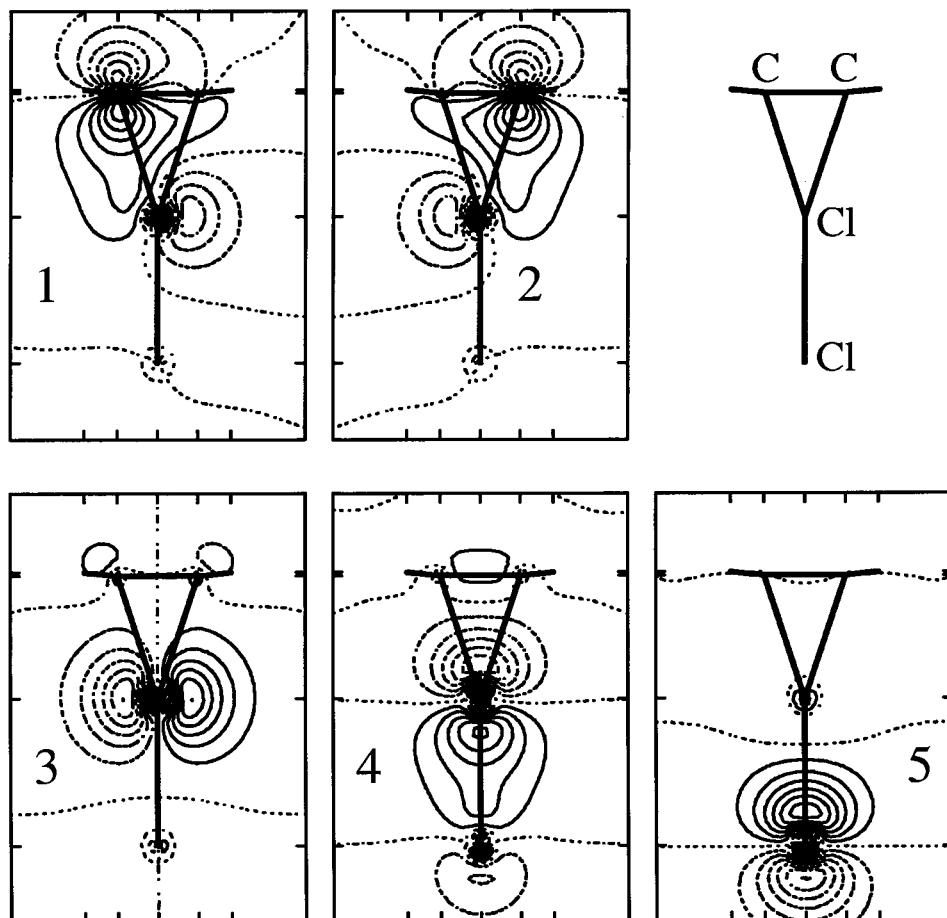
Figure 11. Contour map of hybrids ϕ_{1-5} used for the VB structure Ψ_1 obtained by analyzing the CASSCF wavefunction at the transition state geometry for the electrophilic attachment of chlorine to ethylene in aqueous solution.

$$\Psi_4 = K_4\hat{A}(\text{core})\phi_{10}\phi_{10}\phi_8\phi_8\phi_7\phi_9[\alpha\beta - \beta\alpha][\alpha\beta - \beta\alpha][\alpha\beta - \beta\alpha] \,. \qquad (37)$$

The countour maps of the ten hybrids are shown in Figures 11 and 12 at the transition state geometry, when resonance of reactant and product structures is strong. It is evident, looking at the shape of orbitals ϕ_{1-10}, that the configuration Ψ_1 is able to describe the reactants very well, while the configurations Ψ_{2-4} are the most important for the description of the chloronium ion intermediate; in particular Ψ_2 represents a C_2Cl ring configuration, while in Ψ_3 and Ψ_4 the ring is opened with the consequent localization of the positive charge on one of the two carbon atoms.

The orbitals plotted in Figures 11 and 12 are generalized hybrids: they are mainly defined on one atom but they show contributions also from neighbouring centres.
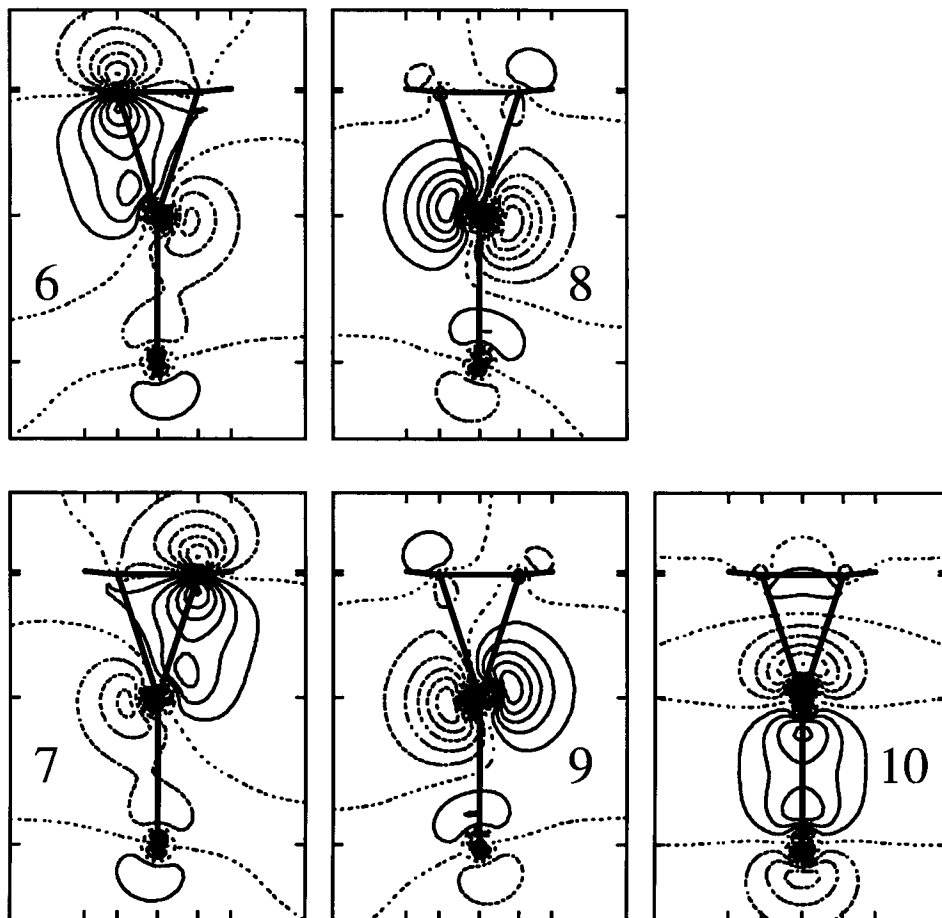
Figure 12. Contour map of hybrids ϕ_{6-10} used for the VB structures Ψ_{2-4} obtained by analyzing the CASSCF wavefunction at the transition state geometry for the electrophilic attachment of chlorine to ethylene in aqueous solution.

The localization of such hybrids comes from the combination of the CASSCF orbitals minimizing the energy for a wavefunction written in terms of structures Ψ_{1-4}; the degree of polarization can thus be easily studied for all geometries through these kinds of plots.

In Ref. [34], this attachment is discussed in detail along an optimized path obtained for reaction in aqueous solution; here, instead, a comparison with the reaction in gas phase will be presented. It is useful to recall that the ring structure has a maximum weight at a geometry close to that of the transition state, while Ψ_{3-4} increase monotonically, starting from zero at the T-shaped complex and arriving at a maximum when the chloronium ion intermediate is formed. The wavefunction of the intermediate is very well represented by the resonance of structures Ψ_2, Ψ_3 and Ψ_4 with the

same weights.

The reaction coordinate in Figures 13 and 14 refer to a portion of the path studied in [34], more precisely to that in which the Cl-Cl distance (x) and the C-C bond midpoint Cl distance (y) vary according to

$$
\begin{aligned}
x &= 2.2 + \frac{1}{\sqrt{2}}\,\lambda \\
y &= 2.4 - \frac{1}{\sqrt{2}}\,\lambda
\end{aligned}
$$

$$(38)$$

where λ is the present reaction coordinate and all distances are in Å. All other geometric parameters are optimized to the best energy after λ is fixed.

Figure 13 shows the energy diagrams calculated with the same basis set used in Ref. [34]. The plot [a] of the figure refers to adiabatic curves for reaction *in vacuo* and in aqueous solution. As expected, owing to the separation of opposite charges, the process is unfavourable in the gas phase but can occur in water, where a modest barrier must be overcome. The plot [b] of the same Figure shows instead the diabatic curves obtained from structures Ψ_{1-4}. The ionic structures Ψ_{2-4} in the total wavefunction determine a strong polarization of the solvent, which changes significantly the diabatic energy curves in going from the gas phase to the solution; curve 1 increases more rapidly with the reaction coordinate but curves 2, 3 and 4 become much lower in energy. In this analysis, curves 3 and 4 coincide because they refer to equivalent structures and do not correspond to curve III+IV of Ref. [34] which is given by

$$
E_{\text{III+IV}} = \frac{< \Psi_3 + \Psi_4 | \hat{H} | \Psi_3 + \Psi_4 >}{< \Psi_3 + \Psi_4 | \Psi_3 + \Psi_4 >} \; .
$$

$$(39)$$

Finally, in Figure 14, the plot of the weights of reactancts and products against the reaction coordinate is shown. The weight of products, shown as the curve $(2+3+4)$ of the Figure, is taken to be the sum of the weights W_2, W_3 and W_4. From this diagram, it is evident that the solvent water 'anticipates' the formation of the chloronium ion intermediate.

Repulsion, dispersion and cavitation contributions to the solvation free energy do not affect significantly the shape of the PES, their effect being about two orders of magnitude smaller than the polarization effect in this reaction. For non-polarization contributions, it is possible to conclude that they are not important in variations of wavefunctions when studying thermochemical reactions, where only the ground state is considered.
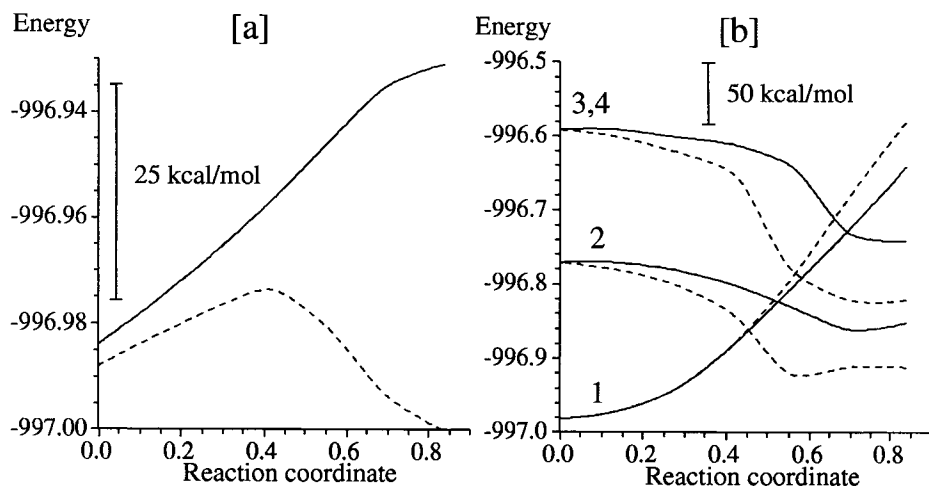
Figure 13. Adiabatic ([a]) and diabatic ([b]) energy curves (hartree versus Å) for the electrophilic attachment of chlorine to ethylene *in vacuo* (solid line) and in aqueous solution (dashed line). Curves 1-4 correspond to VB structures Ψ_{1-4}.
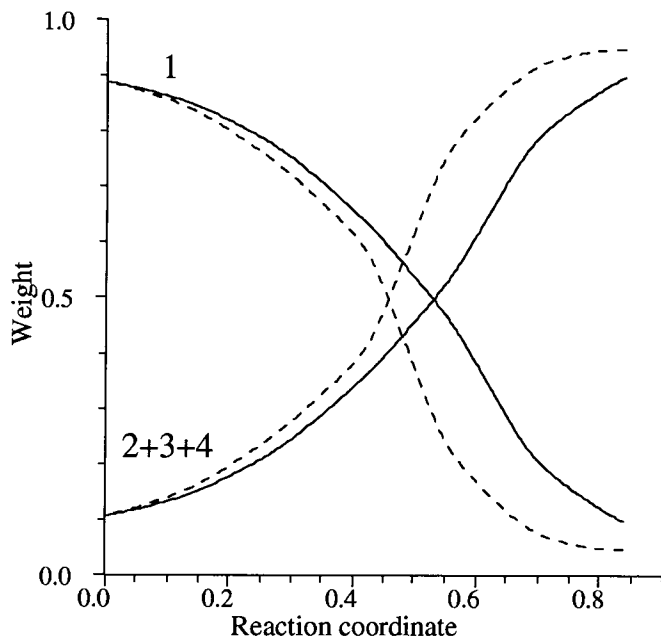
Figure 14. Weights of reactant (1) and product (2+3+4) VB structures against the reaction coordinate (Å) for the electrophilic attachment of chlorine to ethylene *in vacuo* (solid line) and in aqueous solution (dashed line).

6. CONCLUDING REMARKS

The detailed study of electron distribution rearrangements in a chemical reaction needs a multiconfiguration *ab initio* method, because one determinantal wavefunctions are unreliable away from equilibrium geometries. By means of the CASSCF method it is possible to focus attention on the electrons more directly involved in the reaction, allowing the calculation to be done with a relatively limited number of Slater determinants. Moreover, CASSCF uses orthogonal orbitals which are simpler than non-orthogonal orbitals in the development of computer codes. Nowadays CASSCF is, in fact, efficiently included in practically all distributed packages for molecular quantum calculations.

The calculations presented in this chapter have been done using the MCSCF code of the package GAMESS [36] which contains also the more recent developments, made in our laboratory, on the solvent dielectric model for the study of solvation (see for example [37]). Our solvation model implemented in GAMESS allows a CASSCF calculation with the inclusion of all the basic solute-solvent interactions.

The CASSCF wavefunctions correspond to limited but complete configuration interaction and, when are not too complicate, they can be transcribed in a VB formalism through a transformation of the active orbitals. There are several ways in which this transformation can be applied; in this chapter it has been done by the minimization of the energy of a function corresponding to a restricted sum of selected VB classical structures. The selected structures must be sufficient to describe bonding in the reactants and products. The accuracy of this choice can be measured by checking the percentage of CASSCF correlation energy recovered: if 100 % corresponds to CASSCF, the restricted VB calculation must give more than 90 % in order to be acceptable. The result of such a procedure is a localization of orbitals mainly on atoms; these orbitals lose their orthogonality and can be viewed as generalized hybrids in the sense given by Coulson and Fischer in their H_2 study, which is of course also the modern VB point of view.

The interpretation of reactions can be made at this point by analyzing the weights of VB structures, calculated according to Eq. (3), along the reaction path. This type of study shows immediately how the electronic wavefunction changes with nuclear configuration within the adiabatic approximation.

The energy profile in terms of the reaction coordinate is taken instead from the CASSCF calculation. The importance of this diagram is related to the shape of the curve. The presence of a barrier is relevant to the reaction kinetics: it is well known in fact that the higher is such a barrier, the smaller is the conversion rate constant. 'Forbidden' thermochemical

reactions show typically high energy barriers.

The solvent, through solute-solvent interactions, can modify significantly the potential energy surface, thus influencing the kinetics. When this occurs it is interesting to study the solvent effect on the diabatic energy curves which come out from the above VB transcription of the CASSCF wavefunction. Because the solvent reaction field depends on the wavefunction itself, it is difficult to predict the changes on diabatic energies and, consequently, the suggested method of calculation presented in this chapter becomes an important new theoretical tool for the understanding of solvent effect on chemical reactions.

The examples treated in this chapter have shown that only the Coulombic polarization of the solvent, represented as a continuum medium, is responsible for significant changes of the behaviour of reacting systems in passing from the gas phase to the solution. Dispersion, Pauli repulsion and cavitation do not lead to significant effects.

The reader should notice that in this chapter only thermochemical reactions have been considered. A completely different situation is expected with photochemical reactions because of the excited states involved. The solvent model included in the MCSCF code of GAMESS package can work with excited states, but it is important to remark that the model in this case is incomplete and needs substantial improvements. The intermolecular interactions, when one of the molecules is in an excited state, are not yet fully understood and solute-solvent interactions in this case must account for complicated charge transfer and resonance effects.

REFERENCES

[1] W. Heitler and F. London, Z. Phys., 44 (1927) 455.

[2] E. Hückel, Z. Phys., 60 (1930) 423.

[3] L. Pauling, J. Am. Chem. Soc., 53 (1931) 1357.

[4] L. Pauling, The Nature of Chemical Bond, Cornell University Press, New York, 1948.

[5] P. Sykes, A Guidebook to Mechanism in Organic Chemistry, Longmans, London, 1961.

[6] R. B. Woodward and R. Hoffmann, The Conservation of Orbital Symmetry, Verlag, Germany, 1970.

[7] S. Shaik and A. Shurki, Angew. Chem. Int. Ed., 38 (1999) 586.

[8] W. C. Gardiner Jr., Rates and Mechanisms of Chemical Reactions, W. A. Benjamin Inc., New York, 1969.

[9] D. F. Calef and P. G. Wolynes, J. Phys. Chem., 87 (1983) 3387.

[10] A. Warshel and R. M. Weiss, J. Am. Chem. Soc., 102 (1980) 6218.

[11] H. J. Kim and J. T. Heynes, J. Phys. Chem. 94 (1990) 2736.

[12] Y. Mo and J. Gao, J. Phys. Chem. A, 104 (2000) 3012.

[13] C. Amovilli, B. Mennucci and F. M. Floris, J. Phys. Chem. B, 102 (1998) 3023.

[14] R. Cammi and J. Tomasi, J. Comp. Chem., 16 (1995) 1449.

[15] C. Amovilli and B. Mennucci, J. Phys. Chem. B, 101 (1997) 1051.

[16] R. A. Pierotti, Chem. Rev., 76 (1976) 717.

[17] J. Langlet, P. Claverie, J. Caillet and A. Pullman, J. Phys. Chem., 92 (1988) 1617.

[18] R. McWeeny, Int. J. Quantum Chem., 34 (1988) 25.

[19] T. Thorsteisson and D. L. Cooper, Theor. Chim. Acta, 94 (1996) 233.

[20] C. A. Coulson and I. Fischer, Philos. Mag., 40 (1949) 306.

[21] R. D. Harcourt, J. Mol. Struct. (Theochem), 259 (1992) 155.

[22] D. L. Cooper, J. Gerratt and M. Raimondi, J. Chem. Soc. Perkin Trans. 2, (1989) 1187.

[23] R. D. Harcourt and A. Harcourt, J. Chem. Soc. Faraday Trans. II, 70 (1974) 743.

[24] R. D. Harcourt, J. Mol. Struct. (Theochem), 229 (1991) 39.

[25] S. Shaik, A. Ioffe, A. C. Reddy and A. Pross, J. Am. Chem. Soc., 116 (1994) 262.

[26] A. Szabo and N. S. Ostlund , Modern Quantum Chemistry: Introduction to Advanced Electronic Structure Theory, McGraw Hill, New York, 1989.

[27] A. Soudackov and S. Hammes-Schiffer, J. Am. Chem. Soc., 121 (1999) 10598.

[28] U. W. Schmidt and G. A. Voth, J. Phys. Chem. B, 102 (1998) 5547.

[29] H. Kang, C. Mauldin, T. Cole, W. Slegeir and R. Petit, J. Am. Chem. Soc., 99 (1977) 8323.

[30] D. C. Gross and P. C. Ford, Inorg. Chem., 21 (1982) 1704.

[31] L. S. Sunderlin and R. R. Squires, J. Am. Chem. Soc., 115 (1993) 337.

[32] M. Torrent, M. Solà and G. Frenking, Organometallics, 18 (1999) 2801.

[33] C. Amovilli, F. M. Floris, M. Solà and J. Tomasi, Organometallics, 20 (2001) 1310.

[34] C. Amovilli, F. M. Floris and B. Mennucci, Int. J. Quantum Chem., 74 (1999) 59.

[35] C. Amovilli, R. D. Harcourt and R. McWeeny, Chem. Phys. Lett., 187 (1991) 494.

[36] M. W. Schmidt, K. K. Baldridge, J. A. Boatz, S. T. Elbert, M. S. Gordon, J. H. Jensen, S. Koseki, S.; N. Matsunaga, K. A. Nguyen, S. J. Su, T. L. Windus, M. Dupuis and J. A. Montgomery, J. Comp. Chem., 14 (1993) 1347.

[37] C. Amovilli, V. Barone, R. Cammi, E. Cancès, M. Cossi, B. Mennucci, C. S. Pomelli and J. Tomasi, Adv. Quantum Chem., 32 (1998) 227.

This Page Intentionally Left Blank

Chapter 15

Resonating Valence-Bond theories for carbon π-networks and classical/quantum connections

D. J. Klein

Texas A&M University at Galveston, Galveston, Texas 77553-1675, USA

1. INTRODUCTORY HISTORICAL SURVEY

Modern quantum-mechanical Valence-Bond (VB) theory has firm roots back to classical ideas even of a century and a half ago. These connections are of special interest, especially if greater general insight and extension of the classical concepts can be made. The interconnecting simpler semiempirical approaches, such as are of the prime focus here, are historically inextricably mixed with that of the *ab initio* theory, and the development has been *via* a peculiarly torturous road toward quantitative relevance. Thence here some brief historical commentary which also sets some nomenclature and ideas is first made.

1.1. Quantum-mechanical genesis & promise

The idea of *valence structures* goes back to classical chemistry. And indeed it was even then at the heart of chemistry, primitive in many ways though the theory was in rationalizing molecular structure. There are both brief surveys [1,2,3] encompassing this history, as well as whole books on the subject [4,5]. Indeed before 1925 the main achievements seem to have been primarily concerned with the structural possibilities, with considerations for individual molecules being of a quite qualitative nature.

Then quantum mechanics in the mid-1920s brought a prospect for the quantitative treatment of molecular electronic structure. Quite early on in 1926 Heitler & London [6] developed a quantitative "valence-bond" (VB) description for the H_2 molecule, though at this stage the quantitative agreement was not perfect - the equilibrium distance was accurate to within a few percent (which was as good as the then accepted experiments), the force constant for vibrational motion was good to ~10% (which was comparable to what was earlier accepted and somewhat worse than results from experiments only coming to be properly interpreted), and the dissociation energy was too small by roughly a factor of 2 (which was seemed

notably worse than experiment). But the treatment of Heitler & London was evidently only an approximation, with a clear-cut (variational) approach to improvement, and the variational form of the solution combined with the essentially exact treatment of the separated atom limit of two H atoms indicated that the computed dissociation energy was only a lower bound to a more accurately computed one. Thus this held out much promise for quantitative agreement, and in addition there were notable aspects of Heitler & London's approach which were quite consistent with classical chemical bonding theory. Soon there were several even more approximate VB treatments of more complicated molecules. Then in 1932 Rumer [7] identified key aspects of VB theory that correlated with a large body of which correlated well with classical chemical ideas. And on the fully *ab initio* front very satisfactory high accuracy close agreement had been achieved (by Hyleraas [8]) for a variety of aspects of the He atom, and during this same period of time James & Coolidge [9] surmounted (then current) immense computational difficulties to achieve great accuracy (notably <1%) in the already-mentioned physical properties of H_2, though the complexity of their computations was daunting, and tended to loose site of simple pictures. Further properties (& small atoms & molecules) were beginning to be treated by several researchers with evident promise of further quantitative agreement with experiment. Rumer's VB-theoretic ideas were then further discussed by Pauling [10] and by Eyring & Kimball [11]. And especially Pauling & Wheland [12] went ahead with the VB picture, introducing the idea of "resonance" as of central chemical significance in understanding the so-called "aromaticity" not only of benzene but of other benzenoid molecules. It was emphasized that the general VB ideas merged neatly with pre-quantum mechanical theory concerning bonding and electron pairs, as of Lewis [13] & Langmuir [14], and even the idea of resonance merged neatly with the classically developed ideas, *e.g.*, of Armitt & Robinson [15] or Fries [16], which in turn derived from much even earlier work back into the 1800s. (Again see [1,2,3] for some earlier history.) By the late 1930s Pauling had extended the "resonance" concept to apply in describing bonding for a great variety of molecular structures, all as explicated in a qualitative format in Pauling's masterwork [17] *The Nature of the Chemical Bond*, emphasizing the neatness with which it connected with & extended classical chemical-bonding concepts. And Wheland followed up with a more detailed consideration [18] of resonance for conjugated hydrocarbon π-networks, again emphasizing the connection with & extension of classical chemical concepts. With all this qualitative success and promise for the resonance-theoretic VB approach. much less attention seems to be found in purely chemical texts (before say 1950) for an alternative molecular orbital (MO) approach. For example in the now classic quantum chemistry text [19] of Eyring, Walter, & Kimball of 1941 one finds a discussion of the VB

approach, while the self-consistent-field (MO-like) approach is quite subdued (being largely confined to a mention of Hartree's work on atoms).

1.2. Eclipse of VB theory by MO theory

Despite the promise of VB theory the MO approach had been applied in several papers [20] by E. Hückel in the early 1930s to treat the same type of benzenoid hydrocarbons as considered by Pauling & Wheland [12], while further Hückel neatly rationalized the evident scarcity of 4-membered rings in conjugated systems as well as the special stability of rings with 6 π electrons. More comprehensively Hückel's contributions are very nicely covered by Berson [21]. Also F. Hund had been [22] an early advocate of the MO-theoretic approach, though he considered it mostly in a formal framework for diatomics, and R. Mulliken went on through the 1930s with rather detailed semi-quantitative MO-based considerations [23] for whole families of (ground- & excited state) potential curves for one diatomic molecule after another. Yet further starting about 1930 a number of physicists such as F. Bloch [24] and J. C. Slater [25] formally developed MO theory for crystalline solids (integrally incorporating the consequences of translational symmetry), and the resultant *band theory* was utilized in developing the functional expressions for a variety of physical properties of metals (where the theory seemed to work best). Still in the bulk of chemistry for a period of time not so much attention was paid to MO theory, because a number of the treated systems (Mulliken's oft exotic unstable diatomics, and the physicists' metals) seemed more physical than chemical, while Pauling & Wheland [12] had indicated connections of the alternative VB theory to classical chemical-bonding ideas. Many of the workers were viewed more as physicists than chemists. Still some few theoretical chemists paid attention to the MO approach for general chemically interesting molecules, with Hall [26] & Roothaan [27] developing an efficient (self-consistent-field Hartree-Fock) computational matrix formalism.

Then in 1950 Coulson's influential book [28] on *Valence* appeared, ushering in the era of widespread recognition of the chemical utility of MO theory. Thereafter MO theory became of ever increasing interest, and with the emerging electronic digital computers it seemed that both semiempirical & *ab initio* MO computations (following Roothaan's & Hall's formulations) could be relatively readily be implemented (as compared to VB theory). Further in the 1950s a wide appreciation developed (as in [29,30]) for the diverse applicability of Hückel's qualitative rules concerning the correlation between chemical stability & number of π-electrons in a ring of a conjugated organic molecule. Much qualitative, semi-quantitative, and quantitative MO theory then followed, with many texts emphasizing different aspects then appearing. The English school of Coulson , Longuet-Higgins, and Dewar especially in the 1950s obtained numerous

qualitative MO-framed theorems for conjugated hydrocarbons - see, *e.g.*, [31-34]. Even more generally in the 1960s Woodward & Hoffmann's [35] "orbital symmetry conservation" rules and Fukui's [36] "frontier orbital" ideas developed significantly the qualitative aspects of MO theory. And at the same time the accuracy of the MO-theoretic self-consistent-field computational approach kept developing in pace with the ever improving electronic computers. By the 1970s canned MO-based computer programs became ever more widely available, not only for molecules but also in the band-theoretic formulation of physics for solids.

Thence during the 1950s and on through the 1960s & 1970s VB theory came to be largely eclipsed by MO theory. Some nice early articles by Hartmann [37] in 1947, by Vrolent & Daudel [38] in 1949, and by Kasteleyn [39] in 1952, approached VB-theoretic models from then-novel many-body viewpoints, but these articles seem to have been largely ignored and almost completely forgotten - with the many-body techniques these researchers developed later independently rediscovered. Similarly much work [40,41,42] by McConnell and his students starting in the late 1950s used the VB model presented as the Heisenberg model so that much of this work seems to have been classified by most researchers of the day as semiempirical work on exotic molecular species, often presumed to be without much relation to VB theory, though quite clearly McConnell realized the relation [42]. Of course too there was a great quantity of work in the physics literature on the Heisenberg model as applied to magnetism, though the solution techniques looked vastly different than those envisaged by Pauling & Wheland, and in addition primary focus was on non-zero temperature magnetic properties for quite different systems (such as transition-metal or rare-earth oxides and salts) - thence this too was typically viewed by chemists as unrelated to VB theory, or at least unrelated to resonance theory. Several theoretical criticisms of VB theory spread, concerning not only computational difficulties but also perceived conceptual conondrums, *e.g.*, involving exchange-integral signs as well as nonorthogonality & size-consistency. That Hartmann [37] and Vrolent & Daudel [38] and Kasteleyn [39] had in fact quite neatly resolved some of these many-body problems in a VB framework went unnoticed, and much more attention was paid to parallel many-body resolutions in the MO framework in the mid-1950s (by Brueckner, Goldstone, Hubbard, Bethe, and others, as reviewed in a multiplicity of many-body books, *e.g.*, as in [43]). In fact Kasteleyn's Ising-related cluster function [39] was also treated even earlier (in 1938) in two seldom noted sections of Hülthen's article [44] which is often otherwise noted for its *tour de force* exact ground-state solution of the infinite linear-chain Heisenberg model. And enormous numbers of many-body MO-based (or more especially band-based) applications were made, so that the impression was left that non-trivial advances had been made in many-body theory, while VB theory remained anachronistically

computationally difficult. From a more traditional quantum-chemical view some few workers sought to overcome the computational difficulties seemingly inherent in the VB approach, and the *ab initio* results were often limited to disappointingly small molecules, as in the (relatively accurate) computations of Matsen's group [45] on LiH & (several states of) He_2 , entailing discouraglingly much configuration interaction. Or similar disappointment seemingly was registered for Poshusta's work [46] on small (chemically somewhat exotic) polyatomic ions (of say ≤ 4 electrons), though the results were quite accurate. In the mid-1960s Fisher & Murrell [47] obtained a VB analogue (at least for ionic rings) of Hückel's fundamental correlation between π-electron count and stability, and about 1970 Oosterhoff 's group explicated [48] a VB-theoretic analogue of the Woodward-Hoffmann rule for Cope-reaction cyclo-additions. But this VB work was somewhat special and came sometime after the same developments *via* MO theory, which in the meantime had been pushed to yet further insights. Thorson & co-workers [49] consideration of distinctive natural-geminal eigen-distributions for VB wave-functions was deemed by many to be an esoteric mathematical curiosity, and thence largely ignored. Around 1970 Goddard [50] & Gerratt [51] started advocating formulations for VB computations with variationally optimized orbitals, but this first work was largely formal. These optimal orbitals were to remedy McWeeny's [52] rather disappointing semiempirical VB-based computations in the 1950s as well as the (~1970) quantitative all-electron *ab initio* computations of Gallup [53] for benzene, as had seemed to confirm VB theory's short-comings - the resonance-theoretically anticipated important resonance structures seemed in fact to be of relatively minor importance, so that a great multiplicity of higher-order VB structures seemed to be required for quantitative results. From 1950 through 1980 the ratio of MO-theoretic to VB-theoretic computations may have been as great as 100 to 1. Quantum chemistry texts came to focus almost entirely on MO theory, with some sort of brief discussion and cursory dismissal of VB theory (one book being somewhat exceptional in this approach being that of McWeeny & Sutcliffe [54]). MO/band-theoretic approaches completely dominated in physics, and physics texts. The still frequent occurrence of qualitative resonance-theoretic arguments in most introductory text-books for general chemistry & for organic chemistry seemed to many to be merely an anachronism which would surely fade away in future decades.

1.3. Reemergence of VB theory

Of course there was a reason for the retention of resonance-theoretic explanations in text-books; such explanations offered conceptual simplicity and connection with the classical chemical-bonding ideas. Moreover starting in the 1970s and more especially so in the 1980s there turned out to be dramatic

successes for resonating VB theory. As a first point Epiotis identified [55] the appropriate modification to rectify the difficulties McWeeny & Gallup had found, Epiotis (working in a semiempirical mode) emphasizing how the chemically anticipated important resonance-theoretic structures should indeed be more dominant if the structures were built using appropriately "anti-orthogonalized" atomic orbitals rather than bare atomic orbitals, or even worse orthogonalized atomic orbitals. And this expectation was also somewhat implicit in the formalisms of Goddard [50] & of Gerratt [51] in utilizing orbitals obtained through an energy optimization. As discussed more fully elsewhere in this volume, both Goddard [56] & Gerratt [57] as well as others [58-61] pursued such ideas with several concrete *ab initio* computations by the 1980s, though at first there often were limitations, say as to perfect-pairing wave-functions in Goddard's group's work, and to fairly small molecules in Gerratt's and Harcourt's work. Ultimately the relevance of such optimal orbitals in the context of resonance was dramatically verified in the highly accurate quantitative *ab initio* computations of Cooper *et al* [62] in 1985 on benzene. And thereafter many more computations further supported this favorable conclusion, as further discussed in many other chapters in this book. Goddard's group also computationally implemented his "generalized VB" theory in an *ab initio* framework by the end of the 1970s, and (successfully) used the resultant program in application to a fair number of molecules, with some modest degree of distribution of the programs. This theory which usually entailed a single VB structure (sometimes referred to as "perfect pairing") then differed from the less frequent *ab initio* computations based on the approach centered around Gerratt & Cooper. Such *ab initio* approaches are discussed more fully in other chapters in the present book.

There too were some developments along semiempirical lines. Some theorems [63,64,65] concerning the semi-empirical Pauling-Wheland VB model for conjugated hydrocarbons were established, one having been proposed by Ovchinnikov [66] and indicated to imply interesting results concerning radicaloid conjugated hydrocarbon structures. Especially the consequent ground-state spin multiplicity predictions were quite favorably tested, initially with full configuration interaction computations on Hubbard-PPP models [67,68]. Moreover in the early 1980s, Malrieu & Maynau [69,70] published several articles making approximate (Neel-state-based) solutions to the Heisenberg model for application to conjugated hydrocarbons. And there was a degree of related work on full covalent-space VB models by others [71-74]. It may also be mentioned that in the early 1980s a variety of accumulated criticisms of VB theory were in turn (supposedly cogently) criticized [75].

Further in 1986 P. W. Anderson suggested [76] that resonating VB theory would be crucial to the understanding of high-temperature superconductivity. This

suggestion quickly led to a great out-pouring of several hundreds of papers concerning "many-body" VB theory in the physics literature, as discussed in several reviews [77], and other chapters here. Some brief aspects of overlappings of this work in physics with the theory of conjugated π-networks also are mentioned in [78] and in the present chapter.

But approaches from a more nearly classical point of view were also developed, for application to the benzenoids, which provide the prototypical example of non-localized bonding. In particular, in the mid-1970s Herndon [79] & Randić [80] independently developed a fairly successful quantitative resonance theory for stable (*i.e.*, non-radicaloid) benzenoids. And there have been a number of uses of this approach (including work on fullerenes [81]). Further a great number of "chemical graph-theoretic" articles appeared giving a variety of neat methods to enumerate the resonance-theoretically relevant Kekule structures - Cyvin & Gutman's book [82] gives a few hundred references in this area, up through 1987, with much discussion of selected methods of enumeration - and a more recent survey is found in the article of Cyvin *et al* [83], applying several techniques to an examplar class of benzenoid fragments of a certain selected shapes. Novel many-body long-range ordering aspects of resonance-theoretic descriptions were noted [71,72,84,85]. Numerous additional articles on very simple approaches appeared (*e.g.*, [86-90]) in the 1980s, and on up to the present. A further example of a much simplified theoretical framework [91] is found in a what might be termed a "mean-field" resonance-theoretic view, applied especially to extended systems. The general area involving the simplest most nearly classical ideas particularly as applied to conjugated π-networks is in fact a primary focus of the present chapter.

2. VB THEORETIC FRAMEWORK

There are a number of frequently occurring ideas in VB theory which often are used in slightly different manners by different authors, so that it may be well to try to formulate such ideas in a clear and precise manner, at least for use in this present chapter. These ideas include that of VB bases, of VB diagrams (especially those more readily relatable to classical chemical bonding ideas), of VB models, of VB-theoretic solutions (or wave-functions for various models), of resonance, of resonating VB wave-functions, *etc.*

2.1. VB bases and diagrams

First, a VB basis may be defined to consist of configurations constructed from spin-paired localized orbitals, at least for the overall spin singlet case, while

for higher spins there are additional unpaired spins. Such a basis configuration is developed in terms of (singlet) *spin-pairings*, which most simply vewed take the form

$$\Delta_{a,b} = \chi^+_{a\alpha} \chi^+_{b\beta} + \chi^+_{b\alpha} \chi^+_{a\beta} \tag{1}$$

where $\chi^+_{c\sigma}$ is a Fermion creation operator for the (c,σ)th spin-orbital which first is localized in the neighborhood of an atomic region also labelled by c and which second has spin σ (which can be spin-up or -down, α or β). In general the $\chi^+_{c\sigma}$ need not generate bare (or simple) atomic orbitals, but may generate be linear combinations of such so as to give a result in the general region of the site c. Indeed the simple form of the spin-free pairing may sometimes be replaced by a more general geminal with density still localized primarily in the region of sites a & b. Then a (generalized unnormalized) *VB configuration* is

$$|V\rangle = \prod_a^{\in V_+} \Delta_{a,a'} \prod_c^{\in V_o} \chi^+_{c\alpha} |0\rangle \tag{2}$$

where a' is the second site in a spin-pairing in which a is the first site, V_+ is the set of first sites in the configuration, V_u is the set of unpaired orbitals in the configuration, and $|0\rangle$ is the so-called "vacuum" (from which the state $|V\rangle$ is obtained by the application of the various operators $\Delta_{a,a'}$ & $\chi^+_{c\alpha}$). Such configurations exhibit an overall spin S which is just half the number of unpaired orbitals (in V_u). If the spin-pairings take the simple geminal form of Eq. (1), then (with S and the overall set of spin-free orbitals fixed) a *VB basis* is a maximal set of linearly independent such VB configurations. Within the assumption of the fixed set of atomic orbitals, these are a sufficient set of configurations to treat the systems described by an ordinary spin-free Hamiltonian.

As an aside, it may be noted that our notation of Eq. (1) & Eq. (2) is of the so-called "second-quantized" form. This is convenient in different ways, including the suppression of electron indices - electrons being indistinguishable according to the Pauli Exclusion principle. If the "first-quantized" notation is used instead, then in place of $\Delta_{a,b}$ one has spin-pairings $\{\chi_a(i)\chi_b(j) + \chi_b(i)\chi_a(j)\}\alpha(i)\beta(j)$ with $\chi_c(k)\sigma(k)$ a spin-orbital for site c & electron k, and one worries about some sort of correspondence between sites & electrons, though after antisymmetrization the electron labels also appear permuted about in all possible ways. In the second-quantized approach antisymmetrization is implicit throughout.

To each VB configuration $|V\rangle$ there is a corresponding *VB spin-pairing diagram* V which is a graph with the orbital labels identified to sites and the spin-paired sites corresponding to edges. *E.g.*, for the case of six electrons in six orbitals (as for the six occupied atomic π-orbitals of benzene) one has
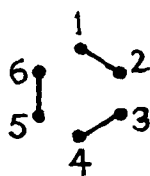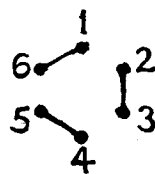
$$\Delta_{1,2}\,\Delta_{3,4}\,\Delta_{5,6}\,|0\rangle \qquad\qquad \Delta_{2,3}\,\Delta_{4,5}\,\Delta_{6,1}\,|0\rangle$$

which displays an evident close analogy to the primary classical *valence structures* for benzene, especially if augmented with the rest of the spin-pairing diagram for the σ-orbitals. Rumer [7] focused on the singlet case with orbitals singly occupied, it being recognized that the extension to states with doubly occupied orbitals is trivial. Too Pauling [10] early pointed out the ready extension to the overall spin doublet case, and the approach taken hinted at further extension, *e.g.*, as done in Simonetta's group [92]. But it is to be emphasized that there are other possibilities - such as that of Rumer, Weyl, & Teller [93] which though providing a neatly exactly complete basis does not generally provide basis structures corresponding so closely to classical VB structures. That is, such Rumer (or Weyl) bases are often developed in terms of orbitals arranged around a cycle, and in many cases a chemical structure may have little to do with a simple cycle. More important should be spin-pairing patterns involving pairing between nearer pairs of localized orbitals, independently of a relation to the formal basis of Rumer *et al* [93]. That is, a basis related to the particular molecular graph G under consideration would in general be desirable. The subject of different means by which to build up overall spin bases is nicely considered by R. Pauncz [94], where he also deals much with the alternative Young-Yamanouchi basis [95], which does not build up the overall spin functions from local spin-pairing structures but rather involves an iterative construction obtaining all N-spin functions from the set of all N-1-spin functions. This alternative basis is widely used, especially in the context of "unitary-group" methods [96], and if related to any molecular structure, it presumably would be that for a linear chain. Also, as has long been noted [97,50], the first (or last, depending on convention) of the Young-Yamanouchi functions corresponds to a Rumer type spin-pairing function. VB bases made to incorporate more local spin pairings on other graphical structures are largely undeveloped, though there are some limited results [98] on linear independence for suitable relatively small subsets of near-neighbor spin-paired patterns for certain classes of interesting (benzenoid) graphs.

2.2. VB models

Granted a VB basis, a semiempirical model represented on such a basis often

is described as a *VB model*. Of course such models can be represented on any basis spanning the same space, but the semiempirical integral approximations are (usually) motivated from considerations in terms of the localized (atomic) orbitals as appear in VB basis states. One such case is the VB model of Pauling and Wheland [10] expressed on the covalent space of configurations built from singly-occupied orbitals. Indeed the model so developed turns out to be essentially the Heisenberg spin Hamiltonian, as long ago noted by Van Vleck & Sherman [99], though Heisenberg's original formulation [100] was spin-free. The model may be viewed to be expressed on a basis of what is essentially Slater determinants of atomic orbitals, but especially in physics the model may be re-represented (following Dirac [101] & Van Vleck [102]) equivalently to act just on spin space. This spin formulation takes the general form

$$H = \sum_P J_P P^{\text{spin}} \tag{3}$$

where the P^{spin} are spin space permutations and the J_P are parameters. And this may be viewed as an approximation to a more complete representation including all structures covalent or ionic built out of the given set of orbitals, which for the benzenoids would be the set of π orbitals one for each π center. One systematic manner of derivation [103,104] is to consider these orbitals to be orthogonal, and develop H of (3) *via* degenerate perturbation theory from a PPP-type model, but for the typical parameter values for benzenoids there is a problem with the adequacy of such an approximation. But there is a related cluster-expansion procedure for the derivation which yields an improved result for the various J_P which arise, as discussed in [105,70,106]. There are a number of other derivations [107] which incorporate improvements on the standard (degenerate) perturbation-theoretic expansion. A type of derivation which sticks closer to the ideas of Pauling & Wheland is discussed in [108], and a more abbreviated fashion in section 3 here.

Approximations for the covalent-space model retain only lower-order permutations, from Eq. (3). Most simply (and most commonly) just the terms involving a transposition $P=(ab)$ exchanging the ath & bth (site) indices are retained, whence the exchange parameter can [109] be nicely approximated to be of the form

$$J_{(ab)} = \{ES_{ab} - \langle \Phi | (ab)H | \Phi \rangle \} / \{1 - S_{ab}^2\} \tag{4}$$

with $E \equiv \langle \Phi | H | \Phi \rangle$, $Sab \equiv \langle \Phi | (ab) | \Phi \rangle$, and Φ most simply being taken as a product of non-orthogonal atomic-like orbitals, one assigned to each center. Often i & j may be restricted to nearest neighbors, and the interaction operator may be recast

as

$$(ab)^{\text{spin}} = 2\,s_a \cdot s_b + 1/2 = 2\,s_a^z s_b^z + s_a^+ s_b^- + s_a^- s_b^+ + 1/2 \tag{5}$$

in terms of the (usual) spin operators s_c^z, s_c^+, s_c^-, & s_c for site c. Then the Hamiltonian (with a further shift of energy 0) is written as

$$H = \sum_{a \sim b} J_{ab}\, 2\,s_a \cdot s_b \tag{6}$$

which is the more commonly presented form, whence it is known as the Heisenberg spin Hamiltonian. Evidently reference to Rumer or VB bases is now quite hidden, and many other bases are used - those involving "spin-waves" are not uncommon in physics. Working with representations on such alternative bases can lead to non-locally interpreted wave-functions, and results can end up being rather far divorced from apparent classical-chemical connection and interpretation. In the physics literature there has been much study of this model from a many-body viewpoint. A simple traditional approach [110] identifies approximate eigenstates of the system as simple products of site spins - for the antiferromagnetically signed case (*i.e.*, for $J_{ab}>0$, with $a \sim b$). A still quite traditional refinement to this picture is the [111,112] spin-wave representations (as well as not unrelated more recent "slave boson" schemes [113] from solid-state physics) embed the physical space in a much larger one, and typical approximate methods of solution of H inter-mix non-physical with physical states - and the contact with chemical interpretation of the wave-functions seemingly becomes quite opaque. Generally the problem of solution of the Hamiltonian of Eq. (4) may be viewed in a variety of mathematical ways, with those (few) based on Kekule structures consistent with the particular molecular structure being those which offer most promise for contact with classical chemical-bonding ideas.

2.3. Resonance

Resonating VB theory should make use of a VB model treated in terms of VB states, especially the more *chemical* basis states corresponding to more the more local spin-pairing patterns. This really is the focus of this review, including attention to the *many-body* case. The use of *VB theory* (without the adjective *resonating*) should be more general, but in order to connect it most directly back to classical chemical-bonding ideas, it would be preferable to use a VB basis accommodated to the molecular structure under consideration, though often researchers refer to anyting using the Rumer basis as "VB theory". Often the spin-pairing patterns where all spin-pairings are between nearest neighbors are termed a *Kekule structures*, at least in dealing with benzenoids. Again elegant systematic

methods for a VB basis including Kekule structures plus some additional patterns based preferentially on more local spin pairings have not yet been developed. The Kekule structures for benzenoid graphs have been proven [98] to be linearly independent, and for even a variety of other chemically interesting molecular frameworks they often empirically appear [114] as linearly independent.

A question of the adequacy of resonance theory naturally arises. In the *ab initio* realm this question is addressed in other chapters in this book. But in the semiempirical realm the Pauling-Wheland model (for benzenoids) turns out to be mathematically equivalent to the Heisenberg model of magnetic theory, where seemingly quite different (approximate) solutions have long been used. For the antiferromagnetically signed Heisenberg model on a bipartite (alternant) network, this traditional approach thinks about the Neel state [110], which corresponds (in spin space) to a simple product of up & down spins on the two respective types (starred & unstarred) of sublattices. In much of the physics magnetism literature there may be developed "spin-waves" on top of this. That is, there is no mention of spin-pairing, as in resonance theory, and these Neel-state-based approaches have met with great success in solid-state magnetic theory. Moreover for extended bipartite lattice networks, these two types of approaches must be fundamentally quite different in that they associate [71,72] to two different (likely mutually exclusive) types of long-range order. Thus a question of which approach is (more nearly) "correct" arises. And rather interestingly the resolution [115] of this seeming paradox appears to be that each approach is "correct" in different structural realms. That is, if one compares simple resonance-theoretic and Neel-state approaches for the nearest-neighbor Pauling-Wheland model on bipartite lattices one finds an interesting behavior as a function of the average number z of nearest neighbors, as displayed in figure 1. Here the Neel-state and single Kekule-structure curves (each independent of the details of the structure beyond the value of z) are variational upper bounds for the exact ground-state energy, and the resonance-theory curve (including the effects solely of Kekule structures) is an upper bound for a particular class of benzenoid polymers of a whole range of widths. Evidently one finds that:

* resonance-theory does better for small degree z (say for $z \leq 3$, as for all benzenoids) when there are many Kekule structures; and
* Neel-state-based approaches do better for higher z (say for $z > 3$, as for the realized systems of classical solid-state magnetic theory).

Thence a neat resolution arises of what at first sight might seem quite ominous (because of the great success of the Neel-state-based approaches).
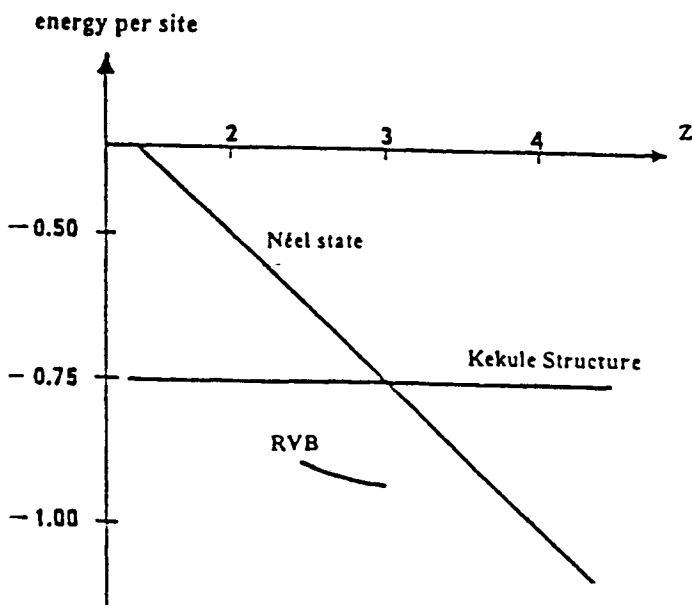
Figure 1 - Plots of resonance energies per site for several simple ground-state approximants. The single-Kekule-structure plot applies for general graphs, the Neel-state plot for general bipartite graphs, and the RVB plot for a special class [115] of benzenoid polymers.

The relevance of resonance-theoretic wave-functions naturally suggests at least one more derivative VB model, obtained by restriction of the covalent-space (Heisenberg) VB model to the subspace of (neighbor-paired) Kekule structures. In fact a whole hierarchy of models begins to emerge, as discussed a little more in the next section.

3. HIERARCHY OF VB MODELS

There are a variety of VB- or resonance-theoretic models which have been considered at one time or another, and for which a systematic organization might be desired. Preferably the organization should also indicate their derivation and relation to one another.

3.1. Restriction & Orthogonalization

The general idea of restriction to a model space underlies the development

of most model Hamiltonians. That is, a restricted model space which is a subspace of the full space of the parent Hamiltonian is identified, and it is sought to treat eigen-levels which have states with much overlap with this subspace. Typically the space includes the ground state and a few low-lying excited states, and one seeks to obtain their energies exactly through solution of a suitable effective Hamiltonian restricted to the subspace. In some cases one identifies a whole sequence of

of subspaces, the overall collection of which spans the full space, and the effective Hamiltonian model is to be defined on the whole space in such a way that it is block-diagonal on the different model subspaces. Indeed this is what is imagined with degenerate perturbation theories, with the various model subspaces being identified as the 0-order eigenspaces.

In fact degenerate perturbation theory provides a systematic scheme to obtain such model Hamiltonians, say as discussed in general in [116]. This folds in the effects of the interactions between the different 0-order eigenspaces, so that the restriction is in principle not an approximation but rather a recasting of the Hamiltonian, as has been done [70,103-107] to proceed from a Hubbard-PPP model to the Heisenberg model. But in applying perturbation theory there generally is a question of convergence of the series for the so expanded transformed Hamiltonian - and one expects this to occur if: first, the perturbed states of the full Hamiltonian have much overlap with correspondent 0-order eigenspaces; and second, the perturbed eigen-energies associated to different 0-order eigen-space are separated in energy from one another. But notably one expects these conditions never to be met for realistic many-body systems. That is, if for a N-body system where the 0-order picture corresponds to N independent subsystems, the energy corrections may be expected to be size-extensive (*i.e.*, $\sim N$) so that the energy splittings arising from a 0-order level should be $\sim \lambda N$ with λ the strength of the perturbation, whereas the 0-order difference between the energies of the ground-eigenspace and the first-excited-eigenspace should be an excitation energy $\sim N^0 = 1$. Thus for sufficiently large N the perturbation splittings $\sim \lambda N$ exceed the 0-order splittings ~ 1, even if the perturbation with strength λ is small. But despite this difficulty many-body effective Hamiltonians are very useful, and in a number of cases capture the essence of the physics involved. Indeed some undeniably many-body areas such as magnetism have the understanding of the whole subject both qualitative & quantitative based on such models (as the Heisenberg model for the magnetic case). Basically the degenerate perturbation formulas may be expected to give reasonable approximate results in low order, while higher orders lead to instabilities associated with the interpenetration of the different 0-order eigenspaces. And indeed we note a cluster expansion approach

to the development of many-body model Hamiltonians, this approach presumably often should being better than corresponding degenerate-perturbation-theoretic treatments, such as has been now been applied [103,104] done in developing the VB-theoretic Heisenbery model from a PPP-Hubbard model. Still this approach ultimately should suffer from this same problem interpenetration if pressed to too high an order of approximation, and one hope eventually for a better resolution. Indeed this interpenetration problem is a disease of all many-body models, VB- or MO-theoretic. In any event the restriction to a model space is a general key step in building models.

Sometimes the model space has a natural basis which is not orthogonal, and a transformation to achieve orthogonalization may be desired. There are different orthogonalization procedures, *e.g.*, as reviewed by Löwdin [117], but generally orthogonalization results in a transformation of the initial Hamiltonian H with overlap operator S to a new Hamiltonian

$$\mathcal{H} = S^{-1/2} H S^{-1/2} \tag{7}$$

This new Hamiltonian is with respect to an orthonormal basis. If the square-root is that of Löwdin orthogonalization [117,118], then the new basis is [117,119] "as similar as possible" (in a well-defined mathematical sense) to the initial basis subject to the constraint of orthogonality.

3.2. The hierarchy of models

The restriction and orthogonalization constructions may be repeated several times to yield a whole hierarchy of model Hamiltonians. This hierarchy is indicated in fig. 2. It may be noted that older criticisms concerning non-orthogonality or size-consistency "catastrophes" connected with several of the intermediate models are largely irrelevant or misleading, responses to these (and other) criticisms of VB theory having been presented elsewhere [75]. The atomic orbitals on the different sites are best imagined to be non-orthognoal, and perhaps not even bare atomic orbtials, but rather anti-orthogonalized from this stage. The first restriction in figure 2 is from the space of covalent & ionic valence structures to the space of purely covalent structures, as discussed more thoroughly in [120] (along with the subsequent orthogonalization step). This restriction is most reasonable in the absence of hetero-atoms (and to some degree the approximation may be a little better in the absence of odd cycles). The next step in the hierarchical scheme of figure 2 indicates an orthogonalization of the different covalent-space Slater determinants to one another. The third step in figure 2 is the restriction of Pauling & Wheland [12] to the subspace of nearest-neighbor spin-

paired Kekule structures, every one of which has a non-zero overlap with every other, as is neatly computable *via* Pauling's island counting scheme [10]. The subsequent orthogonalization of these Kekule structures has been shown [120] to lead to the Herndon-Simpson model [79,121], which in turn with a proper ground-state wave-function *ansatz* leads to the so-called "conjugated circuits" model, such as discussed in section 5 here. A *conjugated circuit* in a Kekule structure K of a graph G may be identified to a cycle of G such that every other edge of the cycle is in K, and it is called a conjugated *n-circuit* of K if there are *n* sites in this cycle (and thence $n/2$ of its edges in K). There is [121] another motivation and derivation of sorts for the Herndon-Simpson model: one takes the classical ideas seriously as well as quantum mechanics, and on the basis of the classical evidence for benzene notes that the symmetric & antisymmetric combinations of the exact $^1A_{1g}$ ground state and the exact $^1B_{2u}$ excited state yields two (orthogonal) states with many of the characteristics of the two Kekule structures - so that postulating these two combinations as the "exact" Kekule structures for benzene Simpson identified an exact model for benzene on this basis, and through seemingly reasonable arguments involving transferability of interaction matrix elements from one system to another, Simpson built up much the same form of model as arises from the derivation indicated in figure 2. The next restriction to a yet smaller subspace of so-called "Clar structures" is possible, as suggested in [108]. Such a *Clar structure* may be described as a spanning subgraph of G with every component either a 6-cycle or an edge, and such that no triplet of isolated edges forms a conjugated 6-circuit. The states labelled by such a Clar structure C may be viewed as a linear combination of the different Kekule structures having spin-pairings corresponding to each isolated edge and pairs of conjugated-6-circuit structures corresponding to each 6-cycle of C. That is, the Clar-structure state $|C\rangle$ is taken as a sum over all $|K\rangle$ for Kekule structures $K \subseteq C$, so that if C has n cycles, then $|C\rangle$ is a sum over 2^n different $|K\rangle$. Thence this subspace of Clar structures is typically substantially smaller than that of the Kekule structures. In a lucid & charming book [122] E. Clar called the 6-cycles in such structures "aromatic sextets" in as much as the greater the number of such sextets in a Clar structure C, the greater importance he ascribed to C. It is amusing that if one tries to quantify Clar's qualitative ideas (which are classically derived, more from Robinson's pre-quantum-mechanical work [13] than from Pauling's work), one is rather naturally led to conjugated-circuit theory, as discussed elsewhere [123]. Thus the quantum-chemically based derivation of figure 2 touches on classical ideas not only at the Pauling-Wheland model (as often emphasized by Pauling), but also perhaps even more closely at the conjugated-circuits model, which again arises directly from the Herndon-Simpson model for a suitable wave-function *ansatz*. The Clar structures taken as the indicated linear combinations of orthogonalized Kekule structures turn
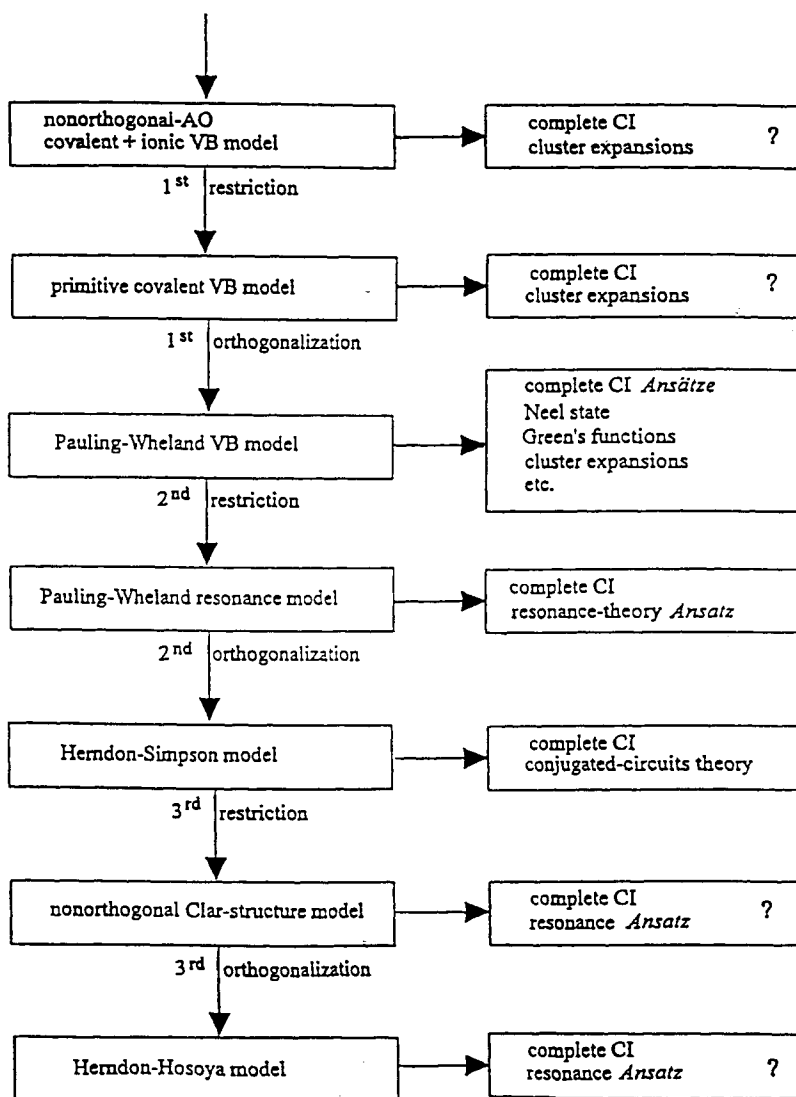
Figure 2 - Fundamental hierarchical scheme for VB models, and an indication of their methods of solution (with question marks marking less explored possibilities).

out themselves to be non-orthogonal, but can be orthogonalized to yield what we have [108] termed a "Hosoya-Herndon" model, which with a suitable wave-function *ansatz* (as an equally weighted sum over all Clar structures) should lead to the energetic form actually considered by Herndon & Hosoya [124]. It may be noted that there is even another model possible, based on *Fries* structures, defined [125] following Fries ideas [15] as those Kekule structures κ of a benzenoid graph G such that these κ achieve the maximum number (for the given graph G) of conjugated 6-circuits. Notably for catacondensed benzenoids [125] and for some important fullerenes there is a unique such Fries structure, and Fries (classically based arguments) would seem to suggest [108] that such a model might work reasonably well for benzenoids, while there is also some interesting support for this idea based on recent computations [114] for buckminsterfullerene (a non-alternant). All the models here involve explicit electron correlation. And numerous many-body solution techniques are possible, as summarily indicated in the boxes on the right in figure 2, solution methods marked with a "question mark" being relatively little explored.. Some discussion of some solution methods for the covalent-space VB (or Heisenberg) model are found in Refs. [62,106]. Most other models in figure 2 have been comparatively less studied, though there is some discussion for the Herndon-Simpson model, and conjugated-circuit methodology in section 5 here.

3.3. Further inter-relations

The various models of our hierarchy in figure 2 may be related to a number of other models of one sort or another. This is indicated in figure 3. As already mentioned, the derivation from the Hubbard or PPP model to the Heisenberg (covalent VB) model has in the last few decades been done *via* a variety of methods [70,103-107]. Standard degenerate perturbation theories, which through second-order yield the simple nearest-neighbor Heisenberg model, really do not apply for the values of the parameters appropriate applicable to conjugated hydrocarbons (at equilibrium geometries) - that is, the values of the Hubbard or PPP model parameters seem to be out of the range of the usual perturbation expansions, (disregarding the many-body full-convergence problems mentioned in section 3.1). But the general form of the model is believed to be suitable, and reasonably valued quantitative results for the Heisenberg model parameters in terms of the Hubbard or PPP model parameters are obtained *via* a fairly simple cluster expansion [105,106]. The so-called tJ-model (with a tremendous literature [126] since about 1990), is defined on a space of size intermediate between that of the full Hubbard model and the ordinary Heisenberg model, it includes low-lying ionic structures, and it has engendered much interest in connection with the perovskite high-temperature superconductors, though there in fact was some earlier
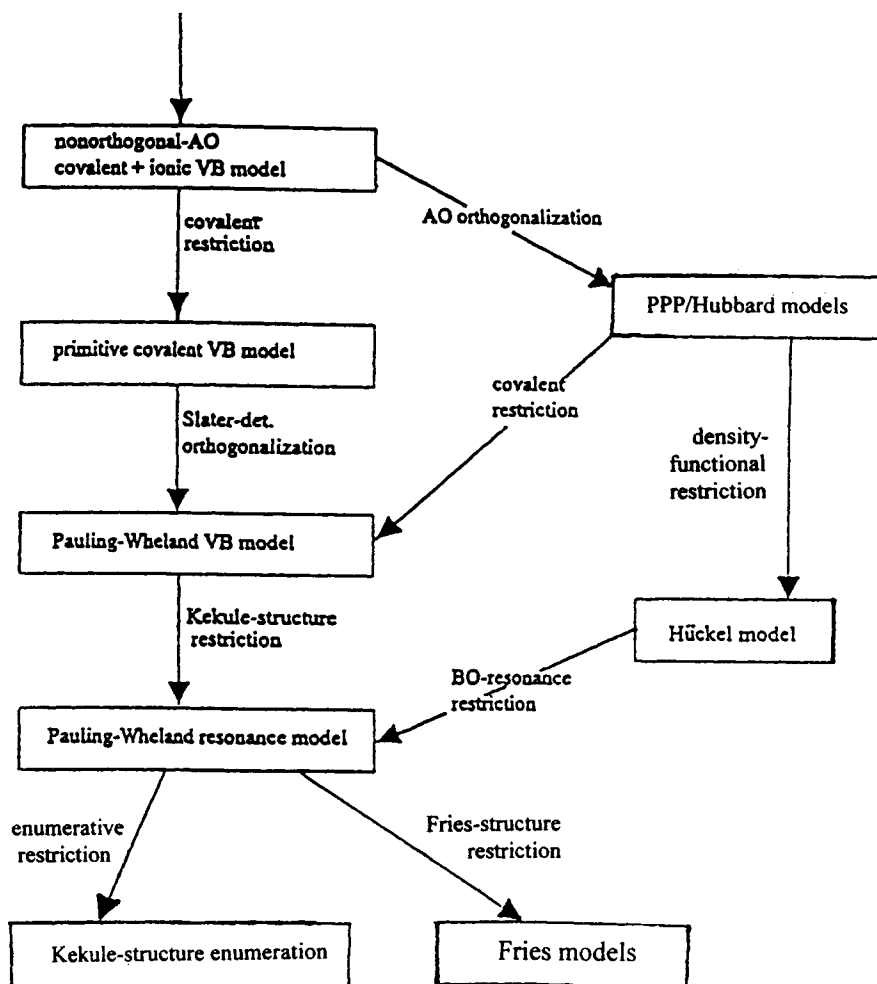
Figure 3 - Some additional inter-relations to further models.

consideration [127]. The derivation from the Hückel (or even Hubbard) model to the conjugated circuits model is accomplished in a somewhat unusual manner, as described in several articles by Zivković [128]. The lower-level model of simply

enumerating Kekule structures is that advocated most notably by Pauling [12], and is rationalized in that the greater the number of Kekule structures, the greater the potential for resonance. Of course the resonance also depends on how strongly the various Kekule structures interact and admix, and this additional aspect is just what is taken into account in the Herndon-Simpson and conjugated-circuits models. Though Pauling most commonly advocates Kekule-structure counting for qualitative purposes, one may also utilize it in a quantitative format, so that one would imagine the resonance energy to be some specified function of the number of Kekule structures. Now for independent subsystems U & V of a total system G, the total Kekule-structure count is $K(G)=K(U) \cdot K(V)$, while resonance energies should be additive $E_G=E_U+E_V$ (at least if the two subsystems really are independent). That is, $K(G)$ may be anticipated to be multiplicative while resonance energy is additive, so that one naturally imagines [129,130] that the functional dependence of E_G on $K(G)$ is

$$E_G \approx c \cdot \log K(G) \tag{8}$$

with c an appropriate constant. Indeed if one presumes that the functional form is continuous and differentialble (with respect to $K(G)$ viewed as a variable), then this functional form is required. Thence one naturally expects the number of Kekule structures for stable benzenoid systems typically to increase exponentially with system size, so that even for moderately sized systems it can be a challenge to generate all these Kekule structures. (If the number does not increase exponentially with system size, then for sufficiently large systems one anticipates a less stable benzenoid, which would be reactive to form one with an appropriately greater number of structures.) Even just the simplest traditional approach, namely that of Kekule-structure enumeration might prove a challenge, at least without a suitable computational algorithm (e.g., there being 12500 Kekule structures [81] for buckminsterfullerene C_{60}). And this counting problem is discussed in the next section.

4. ENUMERATION OF KEKULE STRUCTURES

The computational methods developed to deal with the various (explicitly correlated) resonance-theoretic models turn out to be most powerful for the more highly simplified models, of the preceding section **2**. It is emphasized that these more highly simplified schemes need not necessarily entail significant approximation or loss of accuracy when properly parameterized. Moreover, these more simplified schemes often allow general conclusions for whole sequences or sets of molecules. For the higher-level models the manner of solution turns out to

be such a serious problem that there are many methods advocated and under development, including: various many-body perturbation methods; various Green's function methods; various Monte-Carlo methods; various fragment extrapolation and moment methods; various wave-function cluster expansion methods ; various renormalization group methods; and more. The on-going development of these sophisticated many-body ideas is discussed elsewhere [78,131], while here focus is on more traditionally chemical methods, including the enumeration of Kekule structures and of conjugated circuits. As such these enumeration problems are mathematically neatly defined problems of interest not just in the quantum-chemical context discussed here but also in statistical mechanics and even in mathematics.

4.1. General recursion

Evidently the earliest [132-134] and now quite extensively considered [82,135-138] method for Kekule-structure enumeration is based on a recursion to smaller graphs. Let e be any edge of graph G, let G – e be the graph obtained from G by deleting e, and let G⊖e denote the graph obtained by deleting e as well as the sites at its ends (so that all the edges incident to e are also deleted). Then there is a simple recursion

$$K(\mathrm{G}) = K(\mathrm{G} - \mathrm{e}) + K(\mathrm{G} \ominus \mathrm{e}) \tag{9}$$

which is readily seen and also is readily implementable in a computer program. But also this general recursion may be advantageously manipulated in different ways for different special types of graphs. It is noteworthy that if the recursion is iterated with a choice for a sequence of edges so as to disconnect the resultant graphs into disconnected fragments then the fragments are separately treatable. For regular polymer graphs it can be used [133,136-138] to yield recursions on Kekule structure counts for chains of different lengths. Typically with K_L defined as the number of Kekule structures in a polymer chain of L monomer units one finds linear recursions of the form

$$K_N = \sum_{n=1}^{M} a_n K_{N-n} \tag{10}$$

with the coefficients a_n being largely fixed for the particular type of monomer unit. The ends of the polymer chain make a difference in the values of the counts, and such ends identify a polymer to one of a few "long-range-order" classes (discussed in section **6.2**) such that all those within the same class satisfy the same monomer-unit-dependent recursion, with different ends of the same class influencing the K_L through initial values of the first smaller K_L. From such recursions quite explicit

formulas for K_L as a function of L may often be developed, and perhaps the bulk of Cyvin & Gutman's book [82] is given over to the such development for a fair number of different particular polymer strips. Often the formulas are for a range of strip widths w which then also appears in these formulas. Often also the formulas are for particular "long-range-order" classes, with notable modifications when the ends of a polymer chain are changed from one such class to another.

Even for non-regular polymer graphs and especially catacondensed species there are elegant results, *e,g.*, described in chap. 6 of ref. [82]. This scheme of Gordon & Davison [133] has a neat pictorial presentation which might be illustrated for a catacondensed polyhex chain:
* first, given the displayed graph one begins to write in a sequence of numbers in the hexagons starting from one end with a 2 in the first hexagon and a 1 adjacent to it (in a 0*th* hexagon);
* second, each number in subsequent hexagons then is the sum of that immediately preceding and the 1*st* preceding number around a "kink" in the chain; and
* third, the (desired) number appearing in the last hexagon is $K(G)$.

For instance,
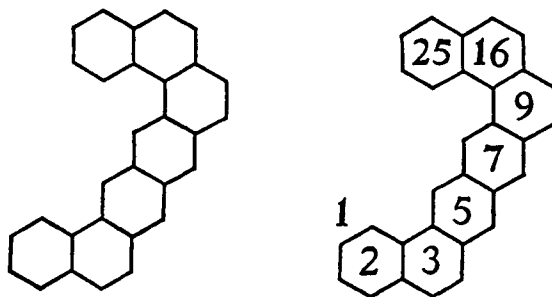
so that for this species $K(G) = 25$. Also there is a quite easy to use extension [135] to branched catacondensed polyhex species.

4.2. Transfer-Matrix Methods

The recursions of the preceding section can be alternatively cast into an especially elegant form for polymer graphs. The Kekule-structure count K_L for a polymer chain of length L monomers can [139-144] quite generally be cast into the form of a trace

$$K_L = \text{Tr}(\mathbb{p} \cdot \mathbb{T}^L) \tag{11}$$

where $\mathbb{T}$ is a *transfer* matrix characteristic of the monomer unit and $\mathbb{p}$ is a matrix

encoding the character of the boundary conditions, *i.e.*, of the polymer chain ends. Basically $\mathbb{T}$ gives the number of ways a Kekule structure can propagate from one local pattern at the boundary of one monomer unit to another local pattern at the subsequent boundary of the next monomer unit. For narrow chains of say a couple hexagons width there are but a few such patterns, so that $\mathbb{T}$ is of a small size (say no more than 4×4), and upon diagonalization of $\mathbb{T}$ one has a quite explicit expression for arbitrary length L. From eq. (11) one may often find asymptotic long-chain behavior for K_L in terms of the maximum eigenvalue Λ of $\mathbb{T}$,

$$K_L \approx A \cdot \Lambda^L \tag{12}$$

where the chain-end dependence (for all ends of a given long-range-order class, discussed in **6.2**) occurs in A. In somewhat "exceptional" cases where the maximum eigenvalue of $\mathbb{T}$ occurs in a Jordan block of dimension $d>1$, an extra factor of N^{d-1} occurs in Eq. (12). In the "common" case that Λ is nondegenerate the factor A is given in terms of the normalized maximum-eigenvalue (columnar) eigenvector c to $\mathbb{T}$ (and the transpose $c^\dagger$) as

$$A = c^\dagger \,\mathbb{p}\, c \tag{13}$$

Moreover, for a $(M{\times}M)$ transfer matrix $\mathbb{T}$ with characteristic polynomial

$$p(x) \equiv \det\{x\mathbb{I}-\mathbb{T}\} = x^M - \sum_{n=1}^{M} a_n x^{M-n} \tag{14}$$

it turns out that the number K_N of Kekule structures for a polymer chain of N satisfy the recursion of Eq. (10), with the a_n of Eqs. (10) & (14) the same. In fact, the recursion can oft-times be made even briefer using the minimal polynomial of $\mathbb{T}$ in place of the characteristic polynomial. Thus the transfer-matrix is intimately related to such recursions as also are encountered [82,83,133,136-138]. As strip width w increases (as measured in terms of the number of bonds crossing a monomer boundary) the size of $\mathbb{T}$ increases exponentially with w, but the technique is still readily applicable for w up to about a dozen.

Here the technique was first developed in a statistical mechanical framework [141], with in fact applications of the technique to other lattice combinatorial problems going back [145] to the 1940s. In this area the most focus has been on the infinite-length infinite-width limit as the solution for an extended 2-dimensional surface. In the resonance-theoretic context the treatment of some polymer chains of arbitrary width has also been made [142]. A flow chart for subroutines for the recursion of the preceding section and its use in developing transfer matrices for finite-width chains is described in [143]. Ref. [145] gives a

listing of transfer-matrix results for a few dozen different polymers.

4.3. Kasteleynian Adjacency-matrix-based methods

The most general Kekule-structure-count method of the present type was devised by Kasteleyn [146], though there is slightly earlier work for different special cases [33,147]. This too involves certain matrices, most simply the graph adjacency matrices $A(G)$ with rows & columns that are labelled by the sites of G and elements that are all 0 except those $A_{ab}=+1$ with a & b adjacent sites in G. Then Kastelyn shows how for "planar" graphs to set up a "signed" version $S(G)$ of this matrix with half of its +1 elements replaced by − 1 such that

$$\det\{S(G)\} = \pm\{K(G)\}^2 \tag{15}$$

The signs appearing in $S(G)$ are to be such that:
* first, $S(G)$ is antisymmetric; and
* second if for an embedding of G in the plane one follows the edges of S around any even face (*i.e.*, minimal ring) of this embedding, then the number of times a minus sign is encountered is odd.

That is, if one proceeds around a ring of sites $i(1),i(2),...,i(n)$ then

$$S_{I(1)i(2)} S_{i(2)i(3)} \cdot \ldots \cdot S_{i(n-1)i(n)} S_{i(n)i(1)} = -1 \tag{16}$$

Kasteleyn [146] describes how this "odd orientation" is readily achievable for any planar graph. For instance, if one inserts arrows on edges of G so that an arrow from a to b indicates $S_{ab}=+1$ while $S_{ba}=-1$, then an example of one such odd orientation is
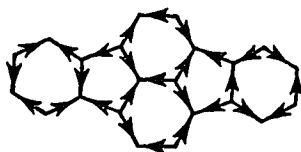
For the special case of polyhex benzenoid structures (such as is of importance for chemical applications) the determinantal formula for $K(G)$ holds but in fact one need not even go through the signing procedure, using just $A(G)$ in place of $S(G)$, as was earlier noted by Dewar & Longuet-Higgins [33].

4.4. John-Sachs Determinantal Method

This scheme rather readily lends itself to hand computation on polyhex benzenoids of up to a dozen or so hexagonal rings, and of course even larger systems when computer automated   The scheme is based on a 1-to-1

correspondence between Kekule structures and certain sets of mutually self-avoiding directed walks on the graph, and indeed this correspondence was noted earlier on in special contexts [133,134,148], and was utilized [141] in a statistical mechanical context in modelling collections of partly disordered polymer chains. The walks proceed from "peak" to "valley" without any regression - the correspondence between a Kekule structure and two such sets of 2 mutually self-avoiding directed walks is illustrated by
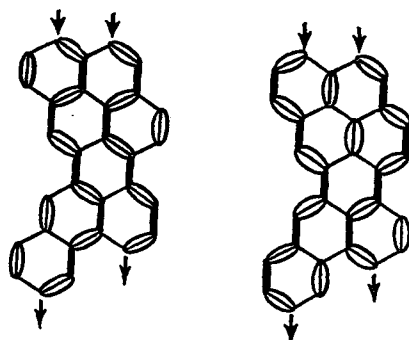
where the diagonal-oriented double bonds and (bold-face) vertical single bonds are the steps of the walks. Granted this correspondence John and Sachs [149] developed a neat algorithm to give the Kekule-structure count as the determinant of a small matrix W whose elements count the numbers of possible directed (individual) walks from a position on one side of the polyhex graph G to each position on the other side (independently of any other such walks). Also see [150,151]. Moreover, the elements of this matrix are conveniently obtained *via* a simple construction, not unlike that involved in "Pascal's triangle". For example the path enumerations from either "peak" to either "valley" of the benzenoid structure below are readily obtained as indicated
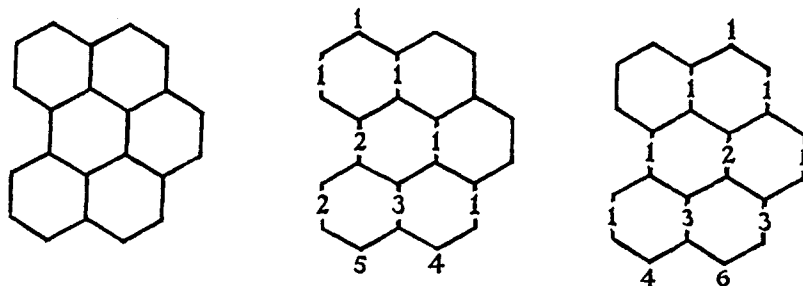
and then there follows a Kekule-structure count as

$$K(G) = det(\mathbf{W}) = det \begin{pmatrix} 5 & 4 \\ 4 & 6 \end{pmatrix} = 14 \tag{17}$$

The consideration of the sets of mutually self-avoiding walkers has a wider import in revealing a fundamental invariant (the number of walkers) which turns out to be important in transfer-matrix solutions, as applied to polymer graphs extending even to the 2-dimensional limit [141,142]. Also this invariant or "order" has physical implications [71,72,84,85,152].

4.5. Other Methods

Really very few significantly different other schemes for computation of Kekule structures or conjugated-circuit counts seem to have been explored to any great extent, presumably because the preceding schemes have been so successful. Dewar & Longuet-Higgins [33] and Herndon [153] describe an enumeration method based on the identification of non-bonding MOs for radical fragments of the graph under consideration. Randić [154] has considered a Monte-Carlo scheme, but the range of sizes of benzenoids up to a couple dozen rings are really quite easily treated exactly by the John-Sachs scheme - still the Monte-Carlo scheme is more evidently extendable to the treatment of the higher-level VB-theoretic models. There are some other less common schemes, *e.g.*, as in [155]. Various special recursions are discussed in [82]. Several different schemes (most of which are as in the preceding sections) are applied to the enumeration problem for a particular set of benzenoids with particular edge-types but variable latitudinal & longitudinal dimensions.

There are some notable special schemes for determining *Pauling bond orders*, which for a given bond e of a π-network G is defined to be the fraction f_e of Kekule structures of G which have a spin-pairing at e. Of course, f_e may be given as $K(G-e)/K(G)$, so that it might be imagined that such f_e are readily obtained. In this regard an extension of the Gordon-Davison algorithm to obtain bond orders of a linear catacondensed polyhex has been made [156]. Especially neatly for a general benzenoid (*i.e.*, polyhex) graph G, Ham [157] has shown that these f_e are given as the corresponding elements $[A^{-1}]_{ij}$ (for $e=\{i,j\}$) of the inverse of the adjacency matrix A for G. A related result applies [158] for all planar graphs G, giving the bond order f_{ij} as $[S^{-1}]_{ij}$ with S the Kasteleyen matrix of the preceding subsection. Moreover, correlations of Pauling bond orders with MO-theoretic Coulson bond orders (for benzenoids) have been empirically observed [159], as also have correlations with experimental bond lengths [160].

Other powerful approximative many-body techniques which are more

standard in other quantum chemical areas such as renormalization group or wave-function cluster expansions are surely applicable to enumerating Kekule structures, such techniques having already been applied to some extent for the treatment of the higher-level models noted in sections **2 & 3**. Indeed the more powerful methods of the preceding subsections **4.2→4.5** seem to be limited to certain general classes of graphs, so that applications to Kekule structure counts for other types of graphs (particularly of a non-planar type representing 3-dimensional crystal structures) likely will make use of such approximation methods. Indeed Kamb & Pauling [161] have used a type of mean-field approximation for 3-dimensional lattices arising in conjunction with Pauling's resonating VB theory of metals. Different mean-field resonance-theoretic approaches are returned to in subsections **6.4 & 6.4** here.

5. CONJUGATED-CIRCUITS THEORY

The conjugated-circuits model is one of the simplest quantitative models that has been reasonably well studied. As already mentioned this model may be motivated from classical chemical bonding theory (extended *a la* Clar's classical empiricist argument) or from Simpson's existential quantum-theoretic argument [121], or from a quantum chemical derivation indicated in our hierarchy of section **3.2**. But beyond derivation of the model there is the question of its solution, such as we now seek to address.

5.1. Herndon-Simpson model

To solve the Herndon-Simpson model a more precise description of the model is desirable. Being defined on a space with a basis of orthonormal Kekule structures, the model Hamiltonian is naturally built from operators which transform different Kekule structures about amongst one another, presumably in a "local" way. This condition of locality means that we are interested in (interaction) operators which act on a Kekule structure only locally, in the sense that such an operator rearranges only a few nearby spin-pairings in a Kekule structure. The simplest operator $\Lambda_d(a\text{-}b)$, for $a\text{-}b$ an edge of G, is such that when applied to a Kekule-structure state $|K\rangle$ the result is merely either $|K\rangle$ back if the edge $a\text{-}b$ is in K or else 0 if the edge $a\text{-}b \notin K$. There are of course of course similar diagonal operators for two or more bonds, *e.g.*, for two disjoint bonds $a\text{-}b$ & $c\text{-}d$, one has $\Lambda_d(a\text{-}b\ c\text{-}d) = \Lambda_d(a\text{-}b)\Lambda_d(c\text{-}d)$. But of course these are diagonal, and we naturally need off-diagonal operators also. For a benzenoid system the simplest off-diagonal operators give a nonzero result if a given circuit has alternating double & single bonds whence it simply move the double bonds of this conjugated circuit one step around the circuit, and the sum over all such off-diagonal circuit

operators for all cycles of size n we denote by $\Lambda_{od}(n)$. Similarly the sum over all diagonal $n/2$-fixed-bond operators for all cycles of size n is denoted by $\Lambda_d(n)$. For benzenoids all the "basic" rings are of size 6, and the only size conjugated circuits which arise are [162] Hückeloid in the sense that they are all of a size $n=4m+2$ for m an integer, so that the only operators which occur are $\Lambda_{od}(n)$ & $\Lambda_d(n)$ with $n=4m+2$. Then for benzenoids the Herndon-Simpson model up through "5$\underline{th}$ order" turns out to be [120]

$$H_{HS} = \gamma_1 \Lambda_{od}(6) + \gamma_1' \Lambda_d(6) + \gamma_2 \Lambda_{od}(10) \tag{18}$$

At the next higher stage (at "2 orders" higher) a 10-site diagonal term $\Lambda_d(10)$ appears along with off-diagonal circuit operators for each of the three possible types of 14-cycles. That is, there arise 14-site operators $\Lambda_{od}(14a)$, $\Lambda_{od}(14ph)$, & $\Lambda_{od}(14py)$ each with different coefficients and each associated to different 14-cycles taking the respective shapes of anthracene, phenanthrene, or pyrene:
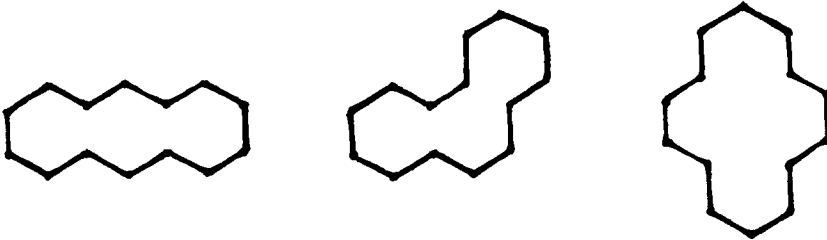
The derivation *via* the hierarchy of section **3.2** catches the diagonal terms and the distinction between the different types of 14-circuits, which in other formulations were not included. They can of course be imagined to be included *via* the other approaches, though they were not. The diagonal terms are perhaps the most subtle in other approaches, because seeking for a resonance energy to result from the conjugated-circuits model, one realizes that the diagonal terms for a single edge should be 0.

For non-benzenoids a Herndon-Simpson model is also possible, though less well explored in a fundamental way. Indeed Rothksar & Kivelson [163] have given the very first terms, through "2$\underline{nd}$ order". The diagonal term $\Lambda_d(4)$ plays a key role and occurs with a negatively signed coefficient, so as to counteract the "effect" of the off-diagonal term $\Lambda_d(4)$, with a smaller coefficient and such as to otherwise enhance stability. In a derivation from the Hubbard model the 2$\underline{nd}$-order form appears only to be reasonable perhaps up through $|t|/U \approx 1/4$, which is

considerably smaller than is appropriate for a conjugated carbon network (for which $|t|/U \approx 2/3$, at equilibrium bond lengths). Such small $|t|/U \lesssim 1/4$ may however be appropriate for the couplings between Cu^{2+} ions of the Perovskite lattices of interest to Rokhsaar & Kivelson [163]. For non-alternants there is a yet further complication in that there are questions about the choice of phase of VB structures, even of Kekule structures. Still of course one could move ahead with a more empirically motivated form of the conjugated-circuits model, and indeed this is what now often has been done - see, *e.g.*, the reviews [123,164], or the C_{60} computations [81].

5.2. Solution of the model

One approach to solving the Herndon-Simpson model is to simply go through standard matrix diagonalizations. This is what was considered by Simpson [121], and so long as there are not too many Kekule structures this is quite reasonable. Indeed, this is applicable for all well-characterized benzenoid molecules, which seem to so far be limited to ~20 rings, with no more than a few thousand Kekule structures. But larger benzenoids surely occur in various pyrolysis mixtures, and benzenoid polymers are starting to be prepared, and of course graphite itself is viewable as an extra large benzenoid (infinite to a first approximation).

A second approach to solving the Herndon-Simpson model is to make a wave-function *Ansatz* which then leads to an upper bound to the ground state. The simplest *Ansatz* (of Pauling & Wheland [12]) is a uniform sum over all Kekule structures,

$$|\Psi_1\rangle \equiv \sum_{K}^{G} |K\rangle \tag{19}$$

From a classically motivated view this should in fact be a good approximation to the ground state, and as it turns out it has the correct phase relationship between all the Kekule structures (if we make the restriction to alternants, and choose the phase such that in Pauling's spin-pairing diagrams all spin-pairing arrows are directed from starred to unstarred sites). An improved *Ansatz* is

$$|\Psi_x\rangle \equiv \sum_{K}^{G} x^{c(K)} |K\rangle \tag{20}$$

where x is a variational parameter, and $c(K)$ is the number of conjugated 6-circuits in K. This is a reasonable *Ansatz*, with the expectation that $0 < x < 1$, while for $x = 1$ it reduces to the simpler Pauling-Wheland *Ansatz*. Even better, for the coefficient of $|K\rangle$ one could include an additional term $y^{c'(K)}$ with y a further variational parameter and $c'(K)$ the number of conjugated 10-circuits in K. But such cluster

expanded wave-functions have been relatively little explored. One such cluster expansion developed [165] for a homologous sequence of benzenoid polymers has been developed, and found to yield an exact ground state, for a specific choice of Hamiltonian parameters, not overly different from those actually preferred. For the usual parameterizations the *Ansatz* is very close to the exact ground state of these polymers, with the Pauling-Wheland *Ansatz* even being quite reasonable. Another related *ansatz* which has been proposed [166] entails $c(K)$ in place of the coefficient $x^{c(K)}$ in Eq. **(20)**, and is expected to be quite decent for not overly large molecules. In addition, with such a variational ground state as $|\Psi_x\rangle$, as in Eq. **(20)**, there arises [167] a neat description for excited states, in terms of so-called "single" excitations (where the "single" here refers to single local rearrangements of spin-pairings).

Indeed the vast bulk of work with the Herndon-Simpson model has been in terms of the simple uniform sum $|\Psi_1\rangle$. For this case one finds

$$\langle \Psi_1 | \Psi_1 \rangle = K(G) \tag{21}$$

and

$$\langle \Psi_1 | H_{HS} | \Psi_1 \rangle = \sum_K^G \{(\gamma_1 + \gamma_1') \, \#_6(K,G) + \gamma_2 \#_{10}(K,G)\} \tag{22}$$

where $\#_n(K,G)$ is the number of conjugated n-circuits of K in G. But (as emphasized in [89]) this is just the conjugated circuits model, such as used by Herndon [79] and by Randić [80] with parameters interpreted as

$$R_1 \equiv \gamma_1 + \gamma_1' \quad \& \quad R_2 \equiv \gamma_2 \tag{23}$$

With higher order terms in the model additional counts $\#_n(K,G)$ arise.

For various non-benzenoids the model has been more or less empirically extended. One simply includes [79,80,168] additional terms $\#_4(K,G)$ & $\#_8(K,G)$ with associated additional coefficients, $-Q_1$ & $-Q_2$ respectively, where the negative sign emphasizes (with the Q_1 & Q_2 of the same sign as R_1 & R_2) the resonance-destabilizing nature of the new terms. See, *e.g.*, [123,164] for reviews referencing a number of applications.

5.3 Matrix Element Evaluation Schemes

There are different methods to evaluate the numerator $\langle \Psi_1 | H_{HS} | \Psi_1 \rangle$ in the conjugated-circuits expression for the resonance energy. One approach is simply to go through each Kekule structure identifying and counting up conjugated n-circuits as occur in each. In another approach this numerator is recast as

$$\langle \Psi_1 | H_{HS} | \Psi_1 \rangle = \sum_C^6 R_1 K(G \ominus C) + \sum_C^{10} R_2 K(G \ominus C) \qquad (24)$$

where the sums are over conjugated 6- & 10-circuits, and the $K(G \ominus C)$ are Kekule-structure counts for $G \ominus C$ (much as in section **4.1**).

Thence all the various methods we have noted for the enumeration of Kekule structures also apply for obtaining the conjugated-circuit numerators. For polymer graphs recursions on the polymer length can be developed, as *e.g.*, in [136]. The special pictorial Gordon-Davison algorithm (as described in section **4.1**) extends [139,143] nicely to conjugated circuit counts. In the context of conjugated-circuits counts for a regular length-L polymer graph, the conjugated n-circuit count $\#_L(n)$ is obtained as

$$\#_L(n) = \sum_{i=1}^L \mathrm{Tr}(\mathbb{p} \cdot \mathbb{T}^{i-1} \cdot \mathbb{C} \cdot \mathbb{T}^{L-i}) \qquad (25)$$

where $\mathbb{C}$ is a *connection* matrix also characteristic of the monomer unit. Really $\mathbb{C}$ can be viewed as a sum of modified transfer matrices each with a different n-cycle deleted within the considered cell. (If n is sufficiently big or the monomer cells are sufficiently small, the n-cycle deleted structure may span two monomer units so that $\mathbb{C}$ would instead replace two powers of $\mathbb{T}$.) Again this leads to quite explicit solutions, at least for polymer chains of not too great a width. And sometimes arbitrary width polymeric systems can be relevantly treated, as in [169], for a sequence of polymers which then converge toward graphite. The recursion method for regular linear polymers also extends neatly, so that

$$\#_{L+1}(n) = \sum_i b_i \#_{L+1-i}(n) \qquad (26)$$

with the unit-cell dependent coefficients b_i given as

$$\{p(x)\}^2 = x^{2M} - \sum_{i=1}^{2M} b_i x^{2M-i} \qquad (27)$$

where the polynomial $p(x)$ is the same as that of Eq. **(14)**. That is, the linear recursion for conjugated-circuit counts has a characteristic polynomial which is simply the square of that for the Kekule-structure enumeration.

Notably Kasteleyn's method [146] of Kekule-structure enumeration extends [158] neatly & computationally efficiently to the solution for conjugated-circuits counts for general planar graphs. One inverts the matrix $\mathcal{S}(G)$ and computes determinants for submatrices associated with each cycle for which conjugated-circuit counts are sought. That is, the mean conjugated circuit count for a particular cycle C of a graph G is given as

$$\langle C \rangle_G = \det(\mathbb{S}^{-1})_C \tag{28}$$

where a subscripted matrix M_C indicates just the submatrix of a matrix M for the rows and columns associated to the sites in C. The method has been applied to several thousands [170] of fullerenes (many with more than a million Kekule structures), to numerous polymeric systems [171], and also [172] to a couple dozen different extended (*i.e.*, infinite) planar carbon- network graphs, most with some 5- & 7-membered rings. All this proceeds with the difficult part of the computation being the inversion of the adjacency-like matrix $\mathbb{S}$, and as a consequence the computations are of comparable difficulty as ordinary Hückel-theoretic (or tight-binding) ones.

Thus many of the Kekule-structure enumeration methodologies of section 4 have been shown to rather neatly extend to conjugated-circuits enumerations, with but modest trouble beyond the overall Kekule-structure count $K(G)$.

6. MISCELLANEOUS QUALITATIVE APPROACHES

As it turns out though even the simplified VB-theoretic formulations giving rise to conjugated-circuit theory or even just Kekule-structure enumeration, may become challenging for sufficiently large (perhaps formally infinite) systems, or for non-Kekulean (*i.e.*, radicaloid) systems. It might oft be convenient if explicit enumeration of Kekule structures could be avoided. Notably for such cases there are some few alternative sorts of means by which to obtain some partial information about the system, within a VB-theoretic context.

6.1. Isoresonance
One ultimately simply applicable theoretical tool is that of "isoresonance". Naturally isoresonance should be a type of equivalence for which two different so equivalent molecular structures exhibit especially similar resonance interactions. Clearly such interactions depend on superpositions between pairs of VB pairing patterns (as early considered by Pauling [10]). But the most important Kekule structures to superimpose typically are the nearest-neighbor spin-pairing ones, the Kekule structures. Such a superposition between K & K' is conveniently graphically represented by a spanning subgraph S of G such that the edge set of S is the union of that for K & K' together. *E.g.*, for naphthalene

Then [173] two molecular graphs G & G' are said to be *isoresonant* iff the set of superposition graphs for the two are in one-to-one correspondence such that corresponding pairs of superpositions are isomorphic as graphs. This condition of isoresonance is notably stronger than the condition that G & G' have the same number of Kekule structures, this weaker condition having been termed [174] *isoarithmicity*, and considered as a condition for similarity of two conjugated networks. In terms of our simple definition azulene and 10-annulene would be isoresonant (each having two Kekule structures, with two different alternation patterns around the 10 cycle), and also isoarithmic. In fact one may modify the definition of isoresonance to strengthen it, *e.g.*, so that the correspondence between superposition graphs S & S' is required to be augmented with a correspondence between some additional edges of the π-network graphs G & G' not appearing in S & S' (especially these additional edges might be required to occur between correspondent relative locations of components in the superposition of S & S'). Such additional possibilities are considered in more detail elsewhere [173]. In any event any of these definitions of isoresonance imply that for two isoresonant molecules G & G':

* first the conjugated circuits energies are the same; and
* second there is a correspondence between Pauling bond orders (specified for a
   bond e as the *f* fraction of Kekule structures which contain that bond).

Indeed there are correspondences within different levels of approximation for higher-level models too, as discussed in [173]. Thence there indeed is a consequent degree of equivalence between two such structures, G & G'.

Notably there are certain types of benzenoid structures which can be recognized as isoresonant by theorem without recourse to the explicit generation of superposition diagrams, or even of Kekule structures. These special benzenoids involve those with chains of cata-condensed hexagons, such a chain being identifiable by a sequence of labels for each non-terminal hexagon specifying the manner of cata-condensation of the hexagon to the hexagons on either side, either as *para*-fused (as for the center ring of anthracene) or as *meta*-fused (as for the center ring of phenanthrene). Thence tetracene would bear the fusion label *para-para*, or more simply just *pp*, whereas both of the species
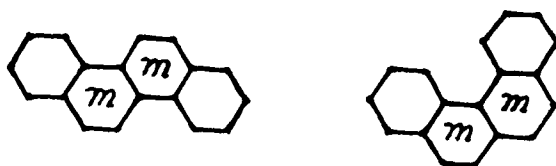
would be labelled as *meta-meta*, or more simply just *mm*. Then the theorem is that: two benzenoid cata-condensed chains are isoresonant if they each have the same such fusion label (with the sequence for a label recognized as the same in either forward or reverse order). Indeed such benzenoid structures have long been noted to satisfy the weaker condition of isoarithmicity (as is readily evident, *e.g.*, from the Gordon-Davison enumerative scheme [134] for cata-condensed chains). But being isoresonant implies of itself a greater degree of similarity. And this is bourne out in comparisons [173] involving a great variety of different computational schemes, and even of some experimental data on reactivities of such benzenoids. Thence at least for this subclass of benzenoids this qualitative bit of information as to similarity is very easily obtainable.

6.2. Theorematics for Pauling-Wheland resonance theory

Within the presumption of the resonance theory of Pauling & Wheland there are some results which reveal a type of long-range spin-pairing order, with some apparent chemico-physical consequences. This ordering in fact may be seen to be of a long-range nature and to have some interesting consequences, as regards different ground states with different degrees of this order and as regards novel excited states, which can under suitable circumstances be of a solitonic nature, thereby making possible the dissipationless propagation of information from one end of a polymer chain to the other. As such this suggests the possibility of quantum computation at a very small scale without generation of much (resistive) heating.

These ordering ideas may developed in terms of some fundamental graph-theoretic notions. A *cutset c* of a connected graph G is defined to be a set of edges such that if deleted from G (without deleting any sites of G) the result $G-c$ is unconnected, with disconnected parts G_+ and G_- such that every edge of c has one end in G_+ and one in G_-. As earlier, let $\mathcal{A}$ & $\mathcal{B}$ denote the two sets of types (starred & unstarred) of sites when G is bipartite (or alternant). Also let $c_{\mathcal{A}+}$ denote the subset of c consisting of edges with an end in $\mathcal{A}$ also in G_+, and let $c_{\mathcal{B}+}$ denote the subset of edges of c with an end in $\mathcal{B}$ in G_+. Let the edge set of a Kekule structure K be denoted $\mathcal{E}(K)$. Then we have:

Ordering Theorem — Let c be a cutset in a bipartite graph G with a Kekule structure K. The difference $\Delta(G,c)$ between the orders of $\mathcal{E}(K) \cap c_{A+}$ & $\mathcal{E}(K) \cap c_{\mathcal{B}+}$ is independent of the particular Kekule structure κ.

That is, for each cutset e as defined above, the quantity $\Delta(G,c)$ is a type of (c-dependent) characteristic for each Kekule structure of G such that the value is independent of the Kekule structure. Proofs are given in Refs. [85,175]. An example may be of interest, such as for ovalene, for which we might consider a cut

set c of edges as intersected by the dashed line:
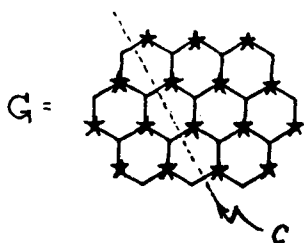
Then for a selection of 4 of the 50 Kekule structures
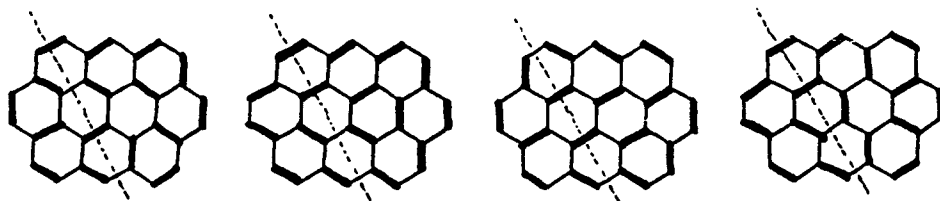
we evidently have $\Delta(G,c)=2$ double bonds in the cut. This evidently places constraints on Pauling bond orders, with consequences for bond lengths. But of special interest is that sometimes the value for such $\Delta(G,c)$ influence those for other $\Delta(G,c')$ with c & c' very distant and independent of some features of G, as is soon to be evidenced.

Of special interest is the case where the graph G is quasi-1-dimensional (*i.e.*, a polymer chain, strip, or tube). The dividing sets e of edges can be conveniently composed from the sets of edges intersected by unit-cell boundaries. The invariance theorem as considered involves the assumption that the graph be finite, so that to apply it one also needs polymer ends, or if considerations independent of ends are desired, then cyclic boundary conditions might be invoked. With ends the polymer can be divided in two by a set of edges intersected by a single "unit-cell" boundary, whereas with cyclic boundary conditions the polymer is divided in two by a set of edges intersected by a pair of unit-cell boundaries. A *regular* polymer graph is defined as one which is translationally symmetric when cyclic boundary conditions are chosen (or possibly in place of the primitive translation one may use a glide translation, to admit an even smaller unit cell), and in a regular polymer one speaks of different sites (or bonds) as being *equivalent* if when there are cyclic boundary conditions they are transformed into one another by a

translation (or perhaps by a glide translation). A set e of edges intersected by a single "unit-cell" boundary is called a *boundary* set. Each boundary has two sides, one called the + side and the other the − side, and when two boundaries are translationally equivalent the + sides of each are also presumed to be chosen so as to be translationally equivalent (whence the − sides are also translationally equivalent). Let $e_{\mathcal{A}+}$ denote the subset of e with edges have starred sites at the end on one side (the + side) of the boundary, and let $e_{\mathcal{B}+}$ denote the similar set of edges with unstarred sites at the end on that same side of the boundary. Then we have [85]:

Theorem — Let G be a bipartite regular polymer graph G with cyclic boundary conditions and with a Kekule structure K, which has edge set $\mathcal{E}(K)$. Then the difference $\delta(G,e,K)$ between the orders of $e_{\mathcal{A}+} \cap \mathcal{E}(K)$ and of $e_{\mathcal{B}+} \cap \mathcal{E}(K)$ for translationally equivalent boundary sets e varies with a period of no more than 2. The period can only be 2 if the primitive translation interchanges starred & unstarred sites.

As an example we may note:
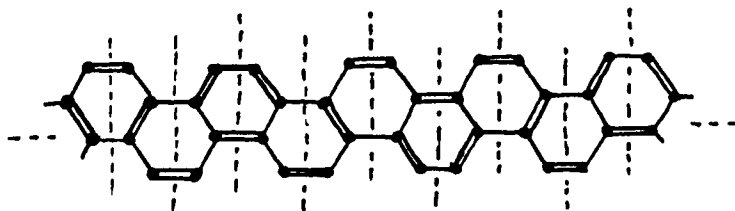
The difference $\delta(G,e,K)$ evidently describes a type of *long-range order* for the Kekule structure. Thence for cyclic boundary conditions the different Kekule structures fall into a finite number of different classes depending on their long-range-order parameters. As such a polymer becomes ever longer, Kekule structures in such different classes exponentially rapidly approach non-interaction via any "local" interaction operator, because such Kekule structures in different classes differ from one another in every unit cell. Thence in approaching the high-polymer limit each different such class of Kekule structures gives rise to its own separate and independent ground state. The value for the lowest ground-state energy level is of special interest, and also whether or not there is degeneracy is of special interest. Degeneracy can arise *via* a symmetry argument, most simply recognized if the period of oscillation of the relevant long-range-order parameter $\delta(G,e,K)$ is 2, for then there is a second class of Kekule structures with the same oscillation pattern but off-set by one unit cell (*i.e.*, by one step of the primitive

translation). There are a few discussions [72,162,169,176] of the relevance of this long-range ordering in the theory of conjugated polymers. Also long-range ordering in resonating VB states has also often been suggested [85,152,177] to be of relevance for the perovskite high-temperature-superconducting structures.

The long-range-ordering theorems can be broadened to allow (in place of the Kekule structures) any VB structure with spin-pairings always between starred and unstarred sites. The utility in the identification of a long-range-order parameter needs however a limitation to (or at least a strong preference for) shorter range spin pairings contributing to a wave-function. Some discussion is found in the chapter by Garcia-Bach in the present book. The theorems can also be broadened to allow G non-bipartite, so long as one of the two parts arising from a dividing set is bipartite.

Anderson & Fazekas [178] also early mentioned the possibility of some sort of long-range order for resonating VB wave-functions. And even earlier Thorson, & co-workers [49] suggest a long-range order in such wave-functions. Quite convincing demonstration of a long-range ordering for the linear-chain nearest-neighbor Heisenberg model have been achieved [179], though this really seems to be of the type discussed in the preceding paragraphs.

Finally a different category of theorematic result concern spin-space Kekule structures occurring as exact ground states to spin Hamiltonians with short-range interactions. Indeed around 1970 Majumdar & Ghosh noted [180] that for even cycles with a next-nearest exchange coupling of 1/2 the strength of the nearest neighbor coupling, the two available Kekule structures turn out to be ground states for even cycles up to 12, while for larger even cycles these two states where demonstrated to be eigenstates, which they conjectured to be the ground state. Subsequently a proof of their conjecture was obtained [181] with the proof technique [182,183,184] applying for additional special (still short-range) models, even in 2 or 3 dimensions. As such one may imagine such models as of utility in a perturbative approach, where the Kekule-structure space is split in first order. Even for higher site spins than s=1/2 some analogues to Kekule structures have been suggested [71], and found [185] to sometimes be ground states to suitable special Heisenberg Hamiltonians for higher spins. Indeed such resonance-theoretic wave-functions solve [186] some special Hubbard-like models. These results might also be viewed as categorizable under the next section.

6.3. Theorematic results for the Heisenberg model

As it turns out for general bipartite (or alternant) molecular graphs, there are some rigorous theorems using a fairly general model, the nearest neighbor simple covalent VB model. There is an initial fundamental "working" theorem [187] which characterizes what might be termed the "nodal structure" of the ground-state

wave-function on the spin-product basis. But of more directly manifest experimental relevance is the theorem [63,64] for which the ground-state spin is given in terms of the orders of the starred & unstarred sets of sites, as

$$S_{VB} = |\,|\mathcal{A}| - |\mathcal{B}|\,|/2 \qquad (29)$$

In fact this applies even if the nearest-neighbor exchange interactions are of different sizes (as one might imagine if a degree of bond localization is considered to lead to slight variations in bond lengths). Moreover this theorem extends for the half-filled nearest neighbor Hubbard model for which all the sites have the same on-site electron-repulsion parameter U. Yet further for a more general PPP model this result is found (*via* brute force complete configuration-interaction computation [67,68]) to persist for all (92) chemically plausible alternants of 10 or fewer sites. This and further (even experimental) comparisons are discussed elsewhere [67,188].

There are some further theorems concerning the signs of various ground-state expectation values (still for bipartite graphs). First [64] for expectations over an exchange operator for an arbitrary pair of sites

$$\langle \Psi | s_i \cdot s_j | \Psi \rangle \begin{cases} <0 & , i \ \& \ j \text{ on unlike sites } (\mathcal{A} \ \& \ \mathcal{B}, \text{ or } \mathcal{B} \ \& \ \mathcal{A}) \\ >0 & , i \ \& \ j \text{ on like sites } (\mathcal{A} \ \& \ \mathcal{A}, \text{ or } \mathcal{B} \ \& \ \mathcal{B}) \end{cases} \qquad (30)$$

where s_k is a spin operator for site k. Next for spin densities (maximal expectations over the z-component of site spin operators), there is [65] the theorem

$$\langle \Psi | s_j^z | \Psi \rangle \begin{cases} <0 & , j \text{ in } \mathcal{A} \\ >0 & , j \text{ in } \mathcal{B} \end{cases} \qquad (31)$$

where s_j^z is the z-component of s_j and there are imagined to be at least as many type $\mathcal{A}$ sites as type $\mathcal{B}$ sites. Further there are two theorems given in [64] concerning point-group-like symmetries of the ground state. All these have simple extensions to nearest neighbor antiferromagnetically signed Heisenberg models for arbitrary site spins (other than site spin 1/2). All these theorems are quite simply applied, though the overall-spin result requires a finite molecular graph.

For infinite systems there is another type of result concerning long-range magnetic order, which is implicated in making a material "magnetic" in the sense that there be a phase transition at the onset, as well as hysteresis. This Neel-state type of ordering concerns the spin correlation function

$$m(i,j) \equiv (\pm) \langle s_i^z s_j^z \rangle \to m_\infty \quad \text{as } d(i,j) \to \infty \tag{32}$$

where the $\pm$ sign applies as the sites are $(+)$ or are not $(-)$ of the same type (starred or unstarred), where $d(i,j)$ is the distance between the sites i & j, and where the expectations are for the (temperature-dependent) thermodynamic average, for the nearest-neighbor Heisenberg model (in the limit of 0 external magnetic field). Then for infinite translationally symmetric bipartite lattices in 1- or 2-dimensions Mermin & Wagner have shown [189] that at all positive temperatures $m_\infty = 0$, and this result has been extended [67] to apply also to all possible subgraphs of such lattices. That is, for these species classical antimagnetic behavior is precluded. But it is to be emphasized that with a relaxation of the assumptions of the theorem, especially at the borderline case of 2 dimensions, this conclusion may be voided. *E.g.*, if there are secondary weaker interactions amongst a whole set of such molecular networks, then magnetic ordering would not be in violation of this theorem.

Finally it may be mentioned that there have been efforts to extend these theorems to higher order models than the nearest-neighbor Heisenberg model (on bipartite graphs). Most notable in this regard is Lieb's [190] spin result in agreement with Eq. (23) for the ground state of the half-filled Hubbard model. For yet higher order models, the results [190] are quite meagre, for linear chains or simple cycles.

6.4. Mean-field resonance theory

Some aspects of the resonance-theoretic approach may be distilled to a form useable without reference to individual Kekule structures, especially for the case of alternant systems. For these alternant or bipartite systems there are two subsets of sites $\mathcal{A}$ & $\mathcal{B}$ such that sites in one set are bonded solely to sites in the other set, and the (antiferromagnetically signed) exchange interactions of the simple Heisenberg model occur solely between sites of these different sets.. Further it is important to realize that the spin-pairing of the various VB clusters may be stipulated in the ground state to occur solely between sites in the $\mathcal{A}$ & $\mathcal{B}$ subsets. For our bipartite benzenoid graphs the pairing-stabilizing interactions occur solely between these subsets, so that spin pairing may be expected to be maximized to the extent consistent with this stipulation. Further [7] a double spin-pairing one within $\mathcal{A}$ and one within $\mathcal{B}$ may be reexpressed as a linear combination of two inter-set double spin-pairings, so that there is a basis of VB functions with any intra-set spin-pairings canceled out between the two sets. Moreover spin pairing beyond the extent dictated by our stipulation (say with spin pairings within the more numerous set, say $\mathcal{A}$, while there are none within $\mathcal{B}$) would introduce constraints

on the wave-function, so that it is more energetically favorable to allow the freedom foregone by such constraints. Yet further it may be viewed to be the content of the finite-molecule Lieb-Mattis analysis [63,64] as explicated to some degree in [91] that the ground state may be stipulated to be comprised from VB structures solely with spin pairings between the two sets functions, and of those only those with the maximum number of such intra-set spin pairings. As a further consideration, the greater the number of low-energy such VB patterns the greater the stabilization (because of mutual "configuration interaction" amongst these patterns), this phenomenon [12,17] being termed *resonance*. But even patterns with non-neighbor pairing can contribute to this resonance especially if they are not too different from a maximally neighbor-spin-paired pattern and there are a greater number of such resonance structures. Thus to achieve overall energetic stability we might make [91] three considerations:

   (Alt) the spin pairing occurs to the maximum extent between sites from different sets $\mathcal{A}$ & $\mathcal{B}$;

   (Loc) the spin-pairing is preferably between nearer sites; and

   (Res) the number of resonance (or VB) structures should be a maximum.

The first rule provides a framework in which the next two points may in general be in conflict, so that the contribution from non-neighbor spin-pairing may be somewhat enhanced in order to allow more resonance. It is understood that beyond neighbor pairing there is a weakened preference to a slightly more distant local "vicinity" pairing. If a pairing between very distant sites makes a contribution, then this spin pairing provides little stabilization so that at a very slight energy above the spin-paired wave-functions there should be a state with the electron pair truly unpaired - *i.e.*, triplet coupled, thereby leading to an excited state with additional unpaired spin density and an overall spin greater by 1 than in the ground state.

   The question of the competition between maximization of neighbor pairing and resonance may be rephrased [91,192] in terms of "mean resonance fields" arising from whole sets of resonance structures. This approach is conveniently managed in terms of resonance-theoretic "bond orders" and "free valences". The *resonance bond order* for a neighbor pair $\{i,j\}$ of orbitals is putatively identified as the fraction p_{ij} of ground-state contributing structures which have the electrons of these two orbitals spin-paired; and the *free valence* for a site i is the fraction v_i of ground-state contributing structures which have no spin-pairing to another electron in the vicinity of site i. What is meant by "vicinity" here may be given different interpretations. If the vicinity is taken as the limit of nearest neighbors with all spin-pairing between such neighbors (and each of the maximally spin-paired bonding patterns is taken to contribute equally to the ground state), then these "1*st*-order" p_{ij} are called [157,159,160] *Pauling bond orders*, and the

associated "1*st*-order" v_i might be called *Pauling free valences*. For instance, for benzene, naphthalene, and trimethylene-methyl, Pauling bond-orders and free valences for three different species are as in figure **4** (as obtained directly from examination of all the nearest-neighbor spin-pairing patterns). It has been demonstrated [160] that for a variety of non-radicaloid benzenoids the Pauling bond-orders correlate closely with experimental bond lengths. Too any remnant free valence may be indicative of unpaired spin density, as in the third trimethylene-methyl case of figure **4**, for which it is known both experimentally [193] and theoretically [194] to be a triplet ground state with spin density primarily on the terminal atoms. For these Pauling bond orders and Pauling free valences one often imagines examining the full set of Kekule structures (or maximally paired spin-pairing VB diagrams).

The maximization of the number of neighbor-paired sites clearly minimizes the free valences. The maximization of resonance is also somewhat intuitively clear: resonance is greatest when the bonding patterns are as delocalized as possible. That is, for maximal resonance one might anticipate that the probability (or bond-order) of a double bond along any one of the directions away from a site to its nearest neighbors is equally likely. For benzenoids (and many of the other organic species we consider) the maximum number of neighbors is 3 so that resonance would seem greatest the more nearly the π-bond orders are to 1/3. Then even without explicit consideration of the Kekule structures of a species, the maximization of resonance might lead one to (tentatively) assign *0-order* bond orders of 1/3 and corresponding *0-order* free valences as deficits from 1 of the
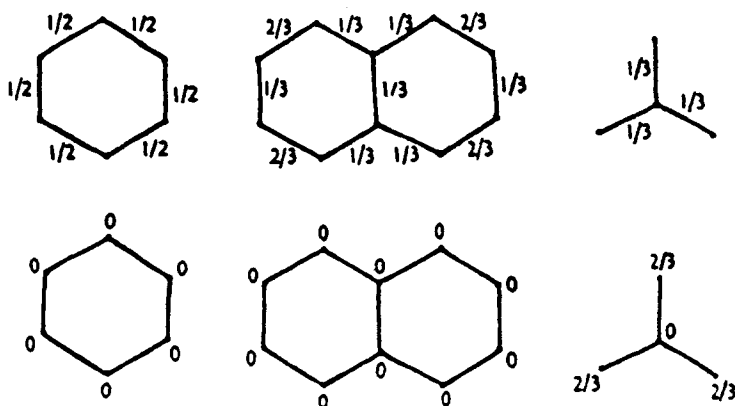
Figure **4** – Pauling bond orders and free valences for benzene, naphthalene, and trimethylene-methyl.

sums of these 0-order bond orders incident at a site. That is, this 0-order free valence for a site i turns out to be just 1 minus one third of the π-network degree of site i. In many cases additional pairing between neighbor sites may further reduce the free valences, yielding *1st-order* bond orders and *1st-order* free valences. For instance for naphthalene, we may take each 0-order bond order to be 1/3 whence one obtains remnant 0-order free valences, as
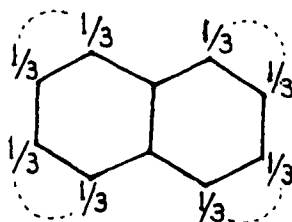
where also we indicate the possibility for additional *1st*-order spin pairing to the extent of 1/3 of a pairing for each of the curved dashed lines. Thence one is immediately led to (*1st*-order) bond orders coincident with the Pauling bond orders noted in figure 4. The avoidance of direct reference to individual Kekule structures is of little relevance for naphthalene, but proves quite valuable for extremely large conjugated networks.

Generally one may further introduce spin-pairings between $\mathcal{A}$ & $\mathcal{B}$ sites even if not neighbors (though preferably as close as possible). That is, the free valences on one type of sites are (at least partly) satiated by other free valences located on the other type of sites (*i.e.*, $\mathcal{A}$ vs. $\mathcal{B}$ sites). As a consequence it is just the difference between the net free valence on the two sets which results in unpaired spins (in the ground state). And this difference is the same for the full free valences as well as for the 0-order ones. But the $i \in \mathcal{A}$ & $j \in \mathcal{B}$ site sums for the 0-order free valences can be neatly expressed in terms of the numbers a_z & b_z of degree-z sites on the $\mathcal{A}$- & $\mathcal{B}$-sets of sites (for $z=1,2,3$ being the only possibilities). That is, the overall number of unpaired spins is [91,192] predicted to be

$$u_{\mathrm{RT}} = |\{\sum_i^{\mathcal{A}} v_i - \sum_j^{\mathcal{B}} v_j\}| = |\{2a_1 + a_2 - 2b_1 - b_2\}|/3 \tag{33}$$

Notice too that in the present argument the (unpaired-electron) spin density should appear primarily on the sites with an excess free-valence sum, especially for those such sites more well separated from opposite-type sites with non-zero free valence. Yet further too if distant sites need to be spin-paired, then there should be a low-lying higher-spin excited state where the spin-pairing is violated. For finite conjugated molecules this further leads to agreement with the spin result of Eq.

(25), of section **6.3**. But in the present formulation a wider range of predictions even for extended infinite systems, and also there are some indications of the location of the unpaired electrons. Such additional predictions would seem to be a major value of the present resonance-theoretic framework, so that such matters we now consider.

6.5. Application of Mean-Field Resonance Theory to Defected Graphites

One application where the resonance-theoretic formulation turns out to be significantly more transparently useful than the fundamental theorems for ground-state spin involves infinite (or large) networks where the count of $\mathcal{A}$ & $\mathcal{B}$ sites is either balanced though not locally, or perhaps even the difference between the $\mathcal{A}$ & $\mathcal{B}$ counts may be indeterminant. These examples then include graphitic networks with a local defect or a semi-infinite edge (which maybe viewed as a line of defects). For the case of translationally symmetric edges, our resonance-theoretic approach also quite easily makes predictions, about the number of unpaired spins per unit cell of edge. For instance, for the two types of edges in figure **5** one may apply the resonance-theoretic arguments to reveal 1/3 of an unpaired electron per unit cell in the first (zig-zag) case, or 0 in the second (corrugated) case. The application of the resonance-theoretic argument, showing the first-order bond orders & unpaired spin densities for a single unit cell are given in figure **6**, where also the analysis is repeated for a third type of edge, with 2/3 of
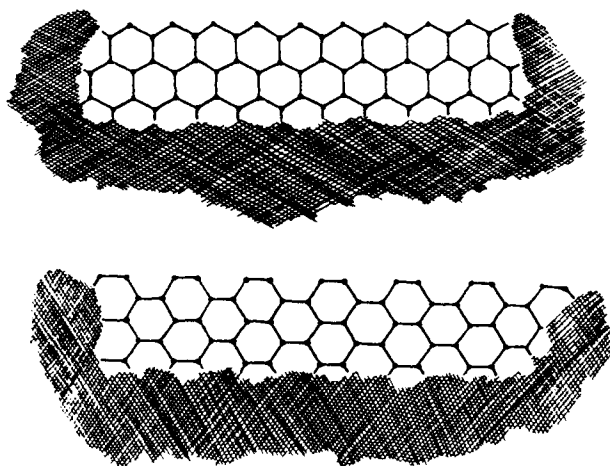
Figure **5** - Portions of zig-zag & arm-chair edges of graphite.
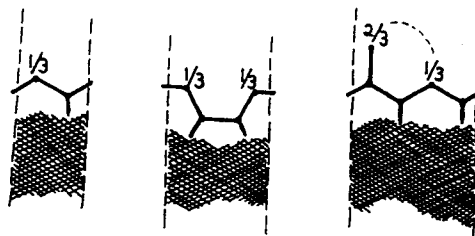
Figure **6** - Unit cells for three graphitic edges showing 0-order free valences, and additional higher-order spin pairings indicated by dashed lines.

an unpaired electron per unit cell of edge. Interestingly again, predictions [91,195] for these cases (as well as several others) end up in agreement [91,194,196] with unrestricted-Hartree-Fock (UHF) band-theoretic results for the Hubbard or PPP models for such edges. That is, when one looks at UHF band structures for rather wide strips with these various types of edges it seems to turn out (in case after case that there are edge-localized non-bonding band orbitals with unpaired electrons of the same spin all along each edge, such as to match that predicted by our resonance theory. But the band-theoretic argument is somewhat more involved and typically is of a numerical nature. The simple mean-field result for edges also seems to be in agreement with slightly more elaborated resonating VB-theoretic arguments [197].

The case of vacancy defects in graphite is also of interest. Most simply one may consider a graphite lattice with a single π-center deleted, whence our resonance-theoretic approach predicts 1 unpaired electron, localized near the hole with density primarily on the three sites adjacent to the deleted π-center, as in figure **7(a)**. Indeed this prediction is confirmed [45] from solutions to the conventional Hückel model for such a single hole in graphite. If a Y-shaped (trimethylene-methane) unit is deleted, then our resonance-theoretic argument predicts 2 unpaired electrons, with density on the 6 sites adjacent to the Y-shaped hole, as in figure **7(b)**. If a single pair of adjacent sites is deleted, then one has the situation in **7(c)**, then the resonance-theoretic argument yields to first-order unpaired electrons on the 4 sites adjacent to the deleted pair, but it is seen that this unpaired spin density may in second order be paired up (between next-next-nearest neighbors sites, in different $\mathcal{A}$ & $\mathcal{B}$ sets). Notably with cases **7(a)** or **(c)** it is seen that such local spin-pairing cannot be accommodated (in finite order) without
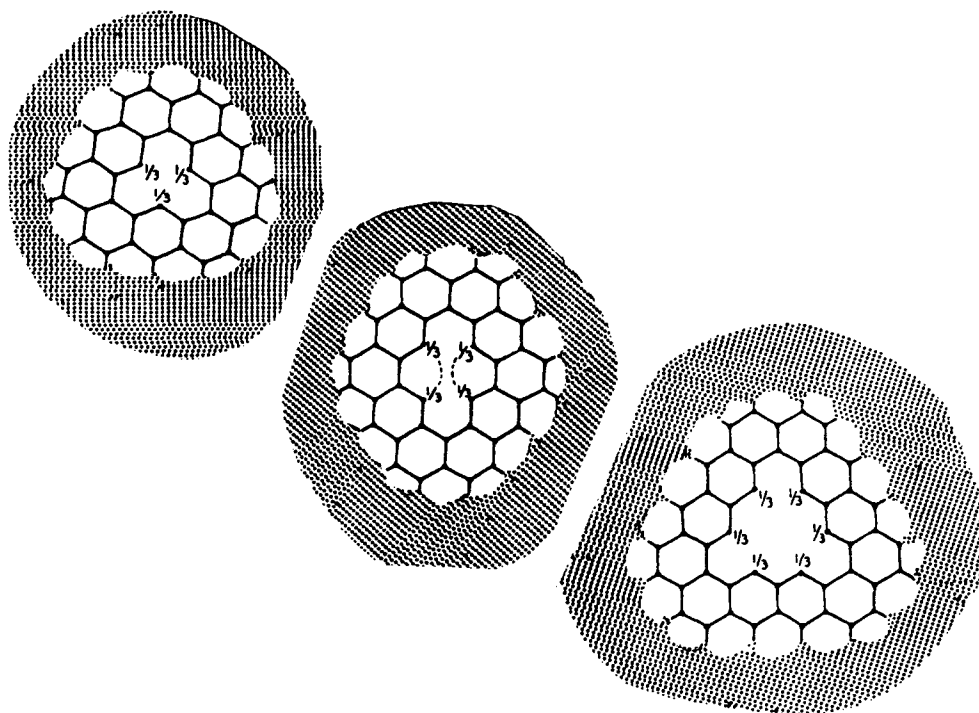
Figure 7 - Vacancy defects of 1, 2, & 4 sites in graphite. Again 0-order free valences are shown with higher-order spin pairing indicated by dashed lines.

compromising the resonance pattern of uniform bond orders in the bulk of the graphite. Overall it turns out that for molecule R with $a(R)$ & $b(R)$ sites of A & B sets, the corresponding vacancy denoted by Я has a number of unpaired spins localized in the general area of the defect as given by

$$u(Я) = |a(R) - b(R)| \qquad (34)$$

This corresponds to the number of unpaired electrons in R also, and we term Я the graphitic *anti-molecule* corresponding to R.

Beyond these two example applications a number of others have been described. These concern not only ordinary radicaloid (finite) molecules, but also polymer ends, graphitic corners, carbene containing systems (with ferromagnetic couplings between the singly-occupied σ-orbitals and the π-network), and even some systems with transition metal centers involved in the exchange network. See Refs. [195,198].

7. PROGNOSIS & OUTLOOK

Overall it seems that there is utility for both resonance-theoretic and MO-theoretic approaches. To some at one time (say around the 1960s) it may have been thought that resonance theory and VB theory would fade away, though this has not occurred, and the trend may have even been reversed, now with a variety of dramatic successes for resonating VB theory, both in semi-empirical & *ab-initio* modes. Most of the preceding book [3], much of the present chapter, and most of the present book document this modest resurgence of VB theory. There are a variety of VB- & resonance-theoretic models which are seen to fit into an overall hierarchy. And for each model there may be a variety of solution or computational techniques. Particularly in the semi-empirical mode there seem to be some novel conceptual results (*e.g.*, as concerns long-range ordering and theorems governing numbers & partial locations of unpaired spins in the ground state) - and there are some quite powerful methods for making numerous quantitative computations (*e.g.*, for Kekule-structure & conjugated-circuit counts).

Despite the VB-theoretic successes of recent decades there still seems a domination by MO theory. *Ab-initio* VB theory seems weak in comparison to *ab-initio* MO-based theory in consideration of general availability of canned programs. Semi-empirical VB theory (the simplest versions of which are the focus of the present chapter) seems weak in comparison to semi-empirical MO-based theory when consideration is made of a comprehensive semiempirical model to make quantitative estimates for heats of formation, geometries, or excitation spectra, all for a diversity of chemical species.

Semiempirical VB theory seems to have reached its greatest success where it has treated systems for which the classical chemical-bonding ideas are most useful - in particular it has been especially successful in application to conjugated π-networks. But there is much promise for other systems including: additional organic molecules; magnetic systems (especially when low-dimensional or frustrated); and some perovskite systems which are of relevance in high-temperature superconductivity. Especially this last area has received an incredible amount of theoretical attention beyond even what we have briefly indicated in this section, some of this being indicated in the reviews [77], and other chapters in the current book. Another area in which Pauling was [161,199] enthusiastic for the relevance of resonance theory was that of metals, but rather little has been done by others in this area - perhaps his ideas would be especially relevant for the special (but difficult & interesting) case of "narrow-band" conductors. In this regard we may mention the seeming close correspondence [176] between resonance- & band-theoretic predictions for solitonic conduction in conjugated polymers. But even in application to conjugated π-networks there is much more work than we have

covered in this chapter, with Cyvin & Gutman's book [82] identifying many more papers concerned with Kekule-structure enumerations. And other chapters of the current book are more concerned with methods of solution of the Heisenberg spin Hamiltonian (or equivalently the Pauling-Wheland VB model) for such conjugated π-networks, and thence cover many references not indicated here. The current chapter emphasizing the simplest semiempirical approaches indicates especially strongly the connections of classical chemical-bonding ideas to the underlying quantum-mechanical framework. A few of these semiempirical approaches are seen to have been independently developed from classical or quantum-theoretic researches.

Surely the continuing VB-theoretic successes which have been achieved in the last few decades indicate much promise for future extensions. Resonating VB theory & MO theory may be seen as complementary descriptions, each with greater utility in different circumstances.

REFERENCES

[1] H. M. Leicester, J. Chem. Ed. **36** (1959) 328.
    D. F. Larder, J. Chem. Ed. **44** (1967) 661.
[2] S. R. La Paglia, in chap.1 of *Introductory Quantum Chemistry* (Harper & Row, NY, 1971).
    L. Pauling, J. Chem. Ed. **61** (1984) 201.
    D. J. Klein & N. Trinajstić, J. Chem. Ed. **67** (1990) 633.
    various chapters in [3], especially those by D. J. Klein & N. Trinajstić, and by R. McWeeny.
[3] *Valence-Bond Theory & Chemical Structure*, ed. D. J. Klein & N. Trinajstić (Elsevier, Amsterdam, 1990).
[4] C. A. Russell, *The History of Valency* (University Press, Leicester, 1971).
[5] A. N. Stranges, *Electrons and Valence*, (Texas A&M University Press, College Station, 1982).
[6] W. Heitler & F. London, Zeit. Physik **44** (1927) 455.
[7] G. Rumer, Gött. Nach. Ges. Wiss. (1932) 337.
[8] E. A. Hylleraas, Zeit. Physik **65** (1930) 299.
[9] H. M. James & A. S. Coolidge, J. Chem. Phys. **3** (1935) 129.
[10] L. Pauling, J. Chem. Phys. **1** (1933) 280.
[11] H. Eyring & G. E. Kimball, J. Chem. Phys. **1** (1933) 239.
[12] L. Pauling & G. W. Wheland, J. Chem. Phys. **1** (1933) 362.
[13] G. N. Lewis, J. Am. Chem. Soc. **38** (1916) 762.
[14] I. Langmuir, J. Am. Chem. Soc. **41** (1919) 1543.
[15] J. W. Armit & R. Robinson, J. Chem. Soc. (1922) 827; (1925) 1604.
[16] K. Fries, Liebigs Ann. Chim. **545** (1927) 121.
[17] L. Pauling, *The Nature of the Chemical Bond* (Cornell University Press, Ithaca, NY, 1939).

[18] G. W. Wheland, *Resonance in Organic Chemistry* (John Wiley & Sons, NY,1955).

[19] H. Eyring, J. Walter, & G. E. Kimball, *Quantum Chemistry* (J. Wiley & Sons, NY, 1944).

[20] E. Hückel, Zeits Phys. **72** (1932) 310; **76**, 628.

[21] J. A. Berson, Angew. Chemie Int. Edn. **35** (1996) 2750.

[22] F. Hund, Zeit. Physik **51** (1928) 759.

F. Hund, Zeit. Physik **73** (1931-32) 565.

[23] R. S. Mulliken, Phys. Rev. **32** (1928) 761.

R. S. Mulliken, Rev. Mod. **4** (1932) 1.

R. S. Mulliken, J. Chem. Phys. **1** (1933) 492; **2** (1934) 782; **3**(1935) 573 & 720.

[24] F. Bloch, Zeit. Physik **57** (1929) 545.

[25] J. C. Slater, Rev. Mod. Phys. **6** (1934) 209.

J. C. Slater & W. Shockley, Phys. Rev. **50** (1936) 705.

[26] G. G. Hall, Proc. Phys. Soc. (London) A **205** (1951) 541.

[27] C. C. J. Roothaan, Rev. Mod. Phys. **23** (1951) 69.

[28] C. A. Coulson, *Valence* (Oxford University Press, Oxford, 1950).

[29] W. von Doering, pages 35-50 in *Theoretical Organic Chemistry Kekule Symposium* (Butterworths, London, 1953).

W. von Doering & C. H. Depuy, J. Am. Chem. Soc. **75** (1953) 5955.

M. J. S. Dewar & R. Petit, Chem. Ind. (London) (1955) 199.

J. K. Dauben, F. A. Gadecko, L. M. Harmon, & D. L. Pearson, J. Am. Chem. Soc. **79** (1957) 4557.

C. R. Ganellin & R. Petit, J. Am. Chem. Soc. **79** (1957) 1767.

R. Breslow & E. Mohacsi, J. Am. Chem. Soc. **85** (1963) 431.

F. Sondheimer, Pure & Appl. Chem. **7** (1963) 363.

[30] A. Streitwieser, *Molecular Orbital Theory* (John Wiley & Sons, NY, 1961).

[31] C. A. Coulson & G. S. Rushbrooke, Proc. Camb. Phil. Soc. **36** (1940) 193.

[32] C. A. Coulson & C. H. Longuet-Higgins, Proc. Roy. Soc. (London) A **191** (1947) 39; A **192** (1947) 16; A **193** (1948) 447 & 456; A **195** (1948) 188.

[33] C. H. Longuet-Higgins, J. Chem. Phys. **18** (1950) 265.

M. J. S. Dewar & H. C. Longuet-Higgins, Proc. Roy. Soc. A **214** (1952) 482.

[34] M. J. S. Dewar, J. Am. Chem. Soc. **74** (1952) 3341, 3345, 3350, 3353, 3355, & 3357.

[35] R. B. Woodward & R. Hoffmann, J. Am. Chem. Soc. **87** (1965) 395 & 2511.

R. B. Woodward & R. Hoffmann, Angew. Chem. Intl. Ed. Engl. **8** (1969) 781.

[36] K. Fukui, T. Yonezawa, & H. Shingu, J. Chem. Phys. **20** (1952) 722.

K. Fukui, T. Yonezawa, & C. Nagata, Bull. Chem. Soc. Japan **27** (1954) 423.

K. Fukui, T. Yonezawa, & C. Nagata, J. Chem. Phys. **27** (1957) 1247.

[37] H. Hartmann, Zeit. Naturforschung A **2** (1947) 259.

[38] C. Vroelant & R. Daudel, Bull. Soc. Chim. **16** (1949) 36.

[39] P. W. Kasteleyn, Physica **28** (1952) 104.

[40] H. M. Lynden-Bell & H. M. McConnell, J. Chem. Phys. **36** (1962) 2393.

H. M. McConnell, J. Chem. Phys. **39** (1963) 1910.

P. L. Nordio, Z. G. Soos, & H. M. McConnell, Ann. Rev. Phys. Chem. **17** (1966) 237.

[41] D. B. Chesnut & W. D. Phillips, J. Chem. Phys. **35** (1961) 1002.

Z. G. Soos, J. Chem. Phys. **43** (1965) 1121.

Z. G. Soos, Phys. Rev. **149** (1966) 330.

D. B. Chesnut & R. W. Mosley, Theor. Chim Acta **13** (1969) 230.

[42] H. M. McConnell, J. Chem. Phys. **30** (1959) 126.

R. Lefebrev, H. H. Dearman, & H. M. McConnell, J. Chem. Phys. **32** (1960) 176.

H. Sternlicht & H. M. McConnell, J. Chem. Phys. **35** (1961) 1793.

[43] D. Pines, *The Many-Body Problem* (W. A. Benjamin Pub., NY, 1962).

N. H. March, W. H. Young, & S. Sampanthar, *The Many-Body Problem in Quantum Mechanics* (reprinted: Dover, NY, 1997).

[44] L. Hülthen, Arkiv Mat. Astron. Fiz. A **26** (1938) 1.

[45] G. H. Brigman, S. J. Brient, & F. A. Matsen, J. Chem. Phys. **34** (1961) 589.

J. C. Browne & F. A. Matsen, J. Phys. Chem. **66** (1962) 2332.

P. N. Reagan, J. C. Browne, & F. A. Matsen, Phys. Rev. **132** (1963) 304.

J. C. Browne & F. A. Matsen, Adv. Chem. Phys. **23** (1973) 161.

[46] R. D. Poshusta, J. A. Haugen, D. F. Zetik, J. Chem. Phys. **51** (1969) 3343.

D. F. Zetik & R. D. Poshusta, J. Chem. Phys. **52** (1970) 4920.

R. D. Poshusta & W. F. Siems, J. Chem. Phys. **55** (1971) 1995.

W. I. Salmon & R. D. Poshusta, J. Chem. Phys. **59** (1973) 4867.

[47] H. Fisher & J. N. Murrell, Theor. Chim. Acta **1** (1963) 463.

[48] J. J. C. Mulder & L. J. Oosterhoff, Chem. Commun. (1970) 305 & 307.

W. J. van der Hart, J. J. C. Mulder, & L. J. Oosterhoff, J. Am. Chem. Soc. **94** (1972) 5724.

[49] J. H. Choi & W. Thorson, J. Chem. Phys. **57** (1972) 252.

W. R. Thorson, J. H. Choi, & R. G. Hake, Intl. J. Quantum Chem. S **1** (1967) 487.

[50] W. A. Goddard, III, Phys. Rev. **157** (1967) 73, 87, & 93.

[51] J. Gerratt & J. N. Lipscomb, Proc. Natl. Acad. USA **59** (1968) 332.

J. Gerratt, Adv. At. & Mol. Phys. **7** (1971) 141.

[52] R. McWeeny, Proc. Roy. Soc. (London) A **223** (1954) 63 & 306.

[53] G. A. Gallup, Intl. J. Quantum Chem. **6** (1973) 899.

G. A. Gallup & J. M. Norbeck, J. Am. Chem. Soc. **96** (1974) 11; **97** (1975) 970.

[54] R. McWeeny & B. C. Sutcliffe, *Methods of Molecular Quantum Mechanics* (Academic Press, London, 1969).

[55] N. D. Epiotis, *Unified Valence Bond Theory of Electronic Structure*, Lect. Notes Chem. **29** (Springer-Verlag, Berlin, 1982).

[56] W. R. Wadt & W. A. Goddard, III, J. Am. Chem. Soc. **97** (1975) 3004.

L. B. Harding & W. A. Goddard, III, Chem. Phys. Lett. **55** (1978) 217.

L. McElwee-White, W. A. Goddard, III, J. Am. Chem. Soc. **108** (1984) 2830.

M. H. McAdon & W. A. Goddard, Phys. Rev. Lett. **55** (1985) 2563.

[57] N. C. Pyper & J. Gerratt, Proc. Royal Soc. (London) A **355** (1977) 407.

J. Gerratt & M. Raimondi, Proc. Roy. Soc. A **371** (1980) 525.

D. L. Cooper, M. J. Ford, J. Gerratt, & M. Raimondi, Phys. Rev. A **34** (1986) 1752.

[58] R. D. Harcourt & W. Roso, Can. J. Chem. **56** (1978) 1093.

R. D. Harcourt, J. Am. Chem. Soc. **100** (1978) 8060.

R. D. Harcourt, J. Am. Chem. Soc. **102** (1980) 5195.

R. D. Harcourt, J. Am. Chem. Soc. **103** (1981) 5623.

R. D. Harcourt & R. D. Little, J. Am. Chem. Soc. **106** (1984) 41.

[59] P. C. Hiberty & C. Leforestier, J. Am. Chem. Soc. **109** (1978) 2012.

P. C. Hiberty & G. Ohanessian, J. Am. Chem. Soc. **194** (1982) 66.

P. C. Hiberty & D. L. Cooper, J. Mol. Str. **169** (1988) 437.

[60] S. Shaik, Nouv. J. Chim. **6** (1982) 159.

S. Shaik, P. C. Hiberty, J. Am. Chem. Soc. **107** (1985) 3089.

S. Shaik, Progr. Phys. Org. Chem. **15** (1985) 197.

[61] D. M. Chipman, B. Kirtman, & W. E. Palke, J. Chem. **65** (1976) 2556.

R. L. Vance & g. A. Gallup, Chem. Phys. Lett. **81** (1981) 98.

J. R. Collins & G. A. Gallup, J. Am. Chem. Soc. **104** (1982) 1530.

J. H. van Lenthe & G. G. Balint-Kurti, J. Chem. Phys. **78** (1983) 5699.

C. M. Cao & R. P. Messmer, Chem. Phys. Lett. **106** (1984) 183.

B. Kirtman & W. E. Palke, Croat. Chem. Acta **57** (1984) 1247.

R. P. Messmer, P. A. Schultz, R. C. Tatar, & H. J. Freund, Chem. Phys. Lett. **126** (1986) 176.

J. J. W. McDouall, K. Peasley, & M. A. Robb, Chem. Phys. Lett. **148** (1988) 183.

[62] D. L. Cooper, J. Gerratt, & M. Raimondi, Nature **323** (1986) 699.

J. Gerratt, D. L. Cooper, & M. Raimondi, pages 287-350 in ref. [3].

[63] E. H. Lieb & D. C. Mattis, J. Math. Phys. **3** (1962) 749.

[64] D. J. Klein, J. Chem. Phys. **77** (1982) 3098.

[65] V. O. Cheranovskii, Teor. Eksp. Kh. **20** (1984) 468.

D. J. Klein & S. A. Alexander, pages 404-419 in *Graph Theory & Topology in Chemistry*, ed. R. B. King & D. H. Rouvray (Elsevier, Amsterdam, 1987).

[66] A. A. Ovchinnikov, Theor. Chim. Acta **47** (1978) 297.

[67] D. J. Klein, C. J. Nelin, S. A. Alexander, & F. A. Matsen, J. Chem. Phys. **77** (1982) 3101.

[68] D. Döhnert & J. Koutecky, J. Am. Chem. Soc. **102** (1980) 1789.

J. Koutecky, D. Dohernt, P. E. S. Wormer, J. Paldus, J. Cizek, J. Chem. Phys. **80** (1984) 2244.

[69] J. P. Malrieu & D. Maynau, J. Am. Chem. Soc. **104** (1982) 3021 & 3029.

D. Maynau, M. Said, & J. P. Malrieu, J. Am. Chem. Soc. **105** (1983) 5244.

M. Said, D. Maynau, & J. P. Malrieu, J. Am. Chem. Soc. **106** (1984) 580.

P. Karafiloglou & J. P. Malrieu, Chem. Phys. **104** (1986) 383.

[70] R. D. Poshusta & D. J. Klein, Phys. Rev. Lett. **48** (1982) 1555.

D. Maynau, Ph. Durand, J. P. Daudey, & J. P. Malrieu, Phys. Rev. A **28** (1983) 3193.

J. P. Malrieu, D. Maynau, & J. P. Daudey, Phys. Rev. B **38** (1984) 1817.

[71] D. J. Klein & M. A. Garcia-Bach, Phys. Rev. B **19** (1979) 877.

[72] D. J. Klein, Intl. J. Quantum Chem. **13** (1979) 293.

[73] S. R. Bondeson & Z. G. Soos, Chem. Phys. **44** (1979) 403.

S. Mazumdar & Z. G. Soos, Phys. Rev. B **23** (1981) 2810.

S. Ramesha & Z. G. Soos, Intl. J. Quantum Chem. **25** (1984) 1003.

Z. G. Soos, S. Kuwajima, & J. E. Mihalick, Phys. Rev. B **32** (1985) 3124.

Z. G. Soos, S. Kuwajima, & R. H. Harding, J. Chem. Phys. **85** (1986) 601.

[74] S. Kuwajima, J. Am. Chem. Soc. **106** (1984) 6496.

[75] D. J. Klein, Pure & Appl. Chem. **55** (1982) 299.

[76] P. W. Anderson, Science **287** (1987) 1196.

[77] E. Mansosakis, Rev. Mod. Phys. **63** (1991) 1.

T. Barnes, Intl. J. Mod. Phys. C **2** (1991) 659.

G. Senatore & N. H. March, Rev. Mod. Phys. **66** (1994) 445.

E. Dagotto, Rev. Mod. Phys. **66** (1994) 763.

[78] D. J. Klein, pages 403-421 of *Pauling's Legacy - Modern Modelling of the Chemical Bond*, ed. Z. B. Maksić & W. J. Orville-Thomas (Elsevier, Amsterdam, 1999).

[79] W. C. Herndon, Thermochimica Acta **8** (1974) 225.

W. C. Herndon, Tetrahedron **29** (1973) 3.

[80] M. Randić, J. Am. Chem. Soc. **99** (1977) 444.

M. Randić, Chem. Phys. Lett. **128** (1986) 193.

[81] D. J. Klein, T. G. Schmalz, W. A. Seitz, & G. E. Hite, J. Am. Chem. Soc. **108** (1986) 319.

T. G. Schmalz, W. A. Seitz, D. J. Klein, & G. E. Hite, J. Am. Chem. Soc. **110** (1988) 1113.

[82] S. J. Cyvin & I. Gutman, *Kekule Structures in Benzenoid Hydrocarbons* (Springer-Verlag, Berlin, 1988).

[83] R. S. Chen, S. J. Cyvin, B. N. Cyvin, J. Brunvoll, & D. J. Klein, Topics Curr. Chem. **153** (1990) 227.

[84] N. E. Bonesteel, Phys. Rev. B **40** (1989) 8954.

[85] D. J. Klein, T. P. Zivković, & R. Valenti, Phys. Rev. B **43** (1991) 723.

[86] Y. Pipeng, Kexue Tongbao **27** (1982) 961.

A. S. Shawali, C. Parkanyi, & W. C. Herndon, J. Org. Chem. **47** (1982) 734.

Y. Pipeng, Theor. Chim. Acta **77** (1990) 213.

[87] W. Gründler, Zeit. Chem. **19** (1979) 236; **20** (1980) 425; **21** (1981) 198.

W. Gründler, Theor. Chem. Acta **63** (1983) 439.

[88] Y. Jiang & H. Zhu, & G. Wang, J. Molec. Struct. **297** (1993) 327.

S. Li, J. Ma, Y. Jiang, Chem. Phys. Lett. **146** (1995) 221.

S. Li, J. Ma, Y. Jiang, J. Phys. Chem. **101** (1997) 5567.

[89] L. J. Schaad & B. A. Hess, Pure & Appl. Chem. **54** (1982) 1097.

[90] J. Cioslowski, Chem. Phys. Lett. **134** (1987) 507.

[91] D. J. Klein & L. Bytautas, J. Phys. Chem. **103** (1999) 5196.

[92] M. Simonetta, E. Gianinetti, & I. Vandoni , J. Chem. Phys. **48** (1968) 1579.

[93] G. Rumer, E. Teller, & H. Weyl, Gött. Nach. ges. Wiss. (1932) 499.

[94] R. Pauncz, *Spin Eigenfunctions* (Plenum Press, NY, 1979).

[95] A. Young, Proc. London Math. Soc. **28** (1928) 255; **31** (1930) 253 & 273; **34** (1932) 196; **37** (1934) 441.

T. Yamanouchi, Proc. Phys. Math. Soc. Japan **19** (1937) 436.

[96] J. Paldus, pp. 131-190 in *Theoretical Chemistry: Advances and Perspectives*, Ed. H. Eyring & D. Henderson (Academic Press, NY, 1976).

F. A. Matsen & R. Pauncz, *The Unitary Group in Chemistry* (Elsevier, Amsterdam, 1986).

[97] M. Kotani, A. Amemiya, E. Ishiguro, & T. Kimura, *Tables of Molecular Quantum Mechanics* (Maruzen, Tokyo, 1955).

F. A. Matsen, Adv. Quantum Chem. **1** (1963) 59.

[98] J. T. Chayes, L. Chayes, & S. A. Kivelson, Commun. Math. Phys. **123** (1989) 53.

[99] J. H. Van Vleck & A. Sherman, Rev. Mod. Phys. **7** (1935) 167.

[100] W. Heisenberg, Zeit. Physik **49** (1928) 619.

[101] P. A. M. Dirac, section 58 of *Quantum Mechanics* (Clarendon Press, Oxford, 3*rd* edn.,1949).

[102] J. H. Van Vleck *Theory of Electric and Magnetic Susceptibilities* (Clarendon Press, Oxford, 1932).

[103] J. Linderberg & Y. Ohrne, J. Chem. Phys. **49** (1966) 716.

B. H. Brandow, Intl. J. Quantum Chem. **15** (1979) 207.

[104] D. J. Klein & W. A. Seitz, Phys. Rev. B **8** (1973) 2236.

[105] L. N. Buleavski, Zh. Eksp. Fiz. **51** (1966) 230.

[106] R. D. Poshusta, T. G. Schmalz, & D. J. Klein, Mol. Phys. **66** (1989) 317.

N. H. March, M. P. Tosi, & D. J. Klein, Phys. Rev. B **52** (1995) 9115.

[107] W. C. Mullin, Phys. Rev. A **136** (1963) 1126.

M. D. Girardeau, J. Math. Phys. **17** (1976) 431.

498

E. N. Economu & P. Mihas, J. Phys. C **10** (1977) 5017.

D. J. Klein, W. A. Seitz, M. A. Garcia-Bach, J. M. Picone, & D. C. Foyt, Intl. J. Quantum Chem. S **17** (1983) 555.

[108] D. J. Klein, Topics Curr. Chem. **153** (1990) 59.

[109] W. T. Simpson, J. Chem. Phys. **25** (1956) 1124.

P. O. Löwdin, Adv. Phys. **5** (1956) 1.

[110] L. Néel, Ann. phys. (Paris) **5** (1936) 232.

[111] T. Holstein & H. Primakoff, Phys. Rev. **58** (1940) 1098.

[112] P. W. Anderson, Phys. Rev. **84** (1952) 694.

R. Kubo, Phys. Rev. **87** (1952) 568.

[113] G. Kotlar & A. E. Ruckenstein, Phys. Rev. Lett. **57** (1986) 1362.

T. Li, P. Wölfe, & P. Hirschfeld, Phys. Rev. B **40** (1989) 6817.

M. Lavagna, Intl. J. Mod. Phys. B **6** (1991) 885.

[114] N. Flocke, T. G. Schmalz, & D. J. Klein, J. Chem. Phys. **109** (1998) 873.

[115] D. J. Klein, S. A. Alexander, W. A. Seitz, T. G. Schmalz, & G. E. Hite, Theor. Chim. Acta **69** (1986) 393.

[116] B. H. Brandow, Rev. Mod. Phys. **39** (1967) 771.

P. Jørgensen, Mol. Phys. **29** (1975) 1137.

[117] P. O. Löwdin, Adv. Quantum Chem. **5** (1970) 185.

[118] P. O. Löwdin, J. Chem. Phys. **18** (1950) 365.

[119] B. C. Carlson & J. H. Keller, Phys. Rev. **105** (1957) 102.

[120] D. J. Klein & N. Trinajstić, Pure & Appl. Chem. **61** (1989) 2107.

[121] W. T. Simpson, J. Am. Chem. Soc. **75** (1953) 597.

W. T. Simpson & C. W. Looney, **76** (1954) 6285.

[122] E. Clar, *The Aromatic Sextet* (John Wiley & Sons, NY, 1972).

[123] D. J. Klein, J. Chem. Ed. **69** (1992) 691.

[124] W. C. Herndon & H. Hosoya, Tetrahedron **40** (1984) 3987.

[125] F. Harary, D. J. Klein, & T. P. Zivković, J. Math. Chem. **6** (1991) 295.

[126] Y. Hasegawa & D. Poilblanc, Phys. Rev. B **40** (1989) 9035.

A. V. Markelov, JETP Lett. **51** (1990) 365.

V. J. Emery, S. A. Kivelson, & H. Q. Lin, Phys. Rev. Lett. **64** (1990) 475.

P. Schlottmann, Phys. Rev. **41** (1990) 4164.

S. Sarkar, J. Phys. A **23** (1990) L409.

A. Moreo & E. Dagotto, Phys. Rev. B **42** (1990) 4786.

P. A. Bares & G. Blatter, Phys. Rev. Lett. **64** (1990) 2567.

N. Kawakami & S-K. Yang, Phys. Rev. Lett. **65** (1990) 2309.

J. P. Rodriguez & B. Doucot, Phys. Rev. **42** (1990) 8724.

W. Stephan & P. Horsch, Phys. Rev. B **42** (1990) 8736.

A. G. Rojo, J. O. Sofo, & C. A. Balseiro, Phys. Rev. B **42** (1990) 10241.

N. E. Bonesteel & J. W. Wilkins, Phys. Rev. Lett. **66** (1991) 1232.

R. Eder, Phys. Rev. B **44** (1991) 12609.

[127] D. J. Klein & W. A. Seitz, Phys. Rev. B **10** (1974) 3217.

V. Ya Krivnov, A. A. Ovchinnikov, & V. O. Cheranovskii, Synth. Metals **33** (1989) 65.

F. C. Zhang & T. M. Rice, Phys. Rev. B **37** (1989) 4548.

W. J. Caspers & P. L. Iske, Physica A **157** (1989) 1033.

[128] T. P. Zivković, Theor. Chim. Acta **62** (1983) 335.

T. P. Zivković, Croatica Chem. Acta **56** (1983) 29 & 525.

T. P. Zivković, Croatica Chem. Acta **57** (1984) 387 & 1553.

T. P. Zivković, J. Math. Phys. **25** (1984) 2749.

[129] P. G. Carter, Trans. Faraday Soc. **45** (1949) 597.

R. Swinbourne-Sheldrake, W. C. Herndon, & I. Gutman, Tetrahedron Lett. (1949) 755.

[130] W. A. Seitz, D. J. Klein, T. G. Schmalz, & M. A. Garcia-Bach, Chem. Phys. Lett. **115** (1985) 139.

[131] D. J. Klein, H-Y. Zhu, R. Valenti, & M. A. Garcia-Bach, Intl. J. Quantum Chem. **65** (1997) 421.

[132] G. W. Wheland, J. Chem. Phys. **3** (1936) 356.

[133] R. H. Fowler & G. S. Rushbrooke, Trans. Faraday Soc. **33** (1937) 1272.

[134] M. Gordon & W. H. T. Davison, J. Chem. Phys. **20** (1952) 428.

[135] D. J. Klein & W. A. Seitz, J. Molec. Struc. **169** (1988) 167.

[136] M. Randić, Intl. J. Quantum Chem. **27** (1980) 549.

[137] E. J. Farrell, Disc. Math. **25** (1979) 121.

J. L. Hock & R. B. McQuistan, Disc. Appl. Math. **8** (1984) 101.

A. J. Phares, J. Math. Phys. **25** (1984) 1756.

T. P. Zivković, M. Randić, D. J. Klein, H.-Y. Zhu, & N. Trinajstić, J. Comp. Chem. **16** (1995) 517.

[138] H. Hosoya & A. Motoyama, J. Math. Phys. **26** (1985) 157.

[139] D. J. Klein, T. G. Schmalz, & G. E. Hite, J. Comp. Chem. **7** (1986) 443.

[140] D. Babić & A. Graovac, Croat. Chim. Acta **7** (1986) 731.

[141] J. F. Nagle, Proc. Royal Soc. (London) A **337** (1974) 569.

J. F. Nagle, Phys. Rev. Lett. **34** (1975) 1150.

C. S. O. Yokoi, J. F. Nagle, & S. R. Salinas, J. Stat. Phys. **44** (1986) 729.

[142] D. J. Klein, G. E. Hite, W. A. Seitz, & T. G. Schmalz, Theor. Chim Acta **69** (1986) 409.

D. J. Klein & T. G. Schmalz, Phys. Rev. B **41** (1990) 2244.

D. J. Klein & T. P. Živković, Mathl. Comp. & Mod. **17** (1993) 113.

D. J. Klein & H. Zhu, Disc. Appl. Math. **67** (1996) 157.

[143] D. J. Klein, W. A. Seitz, & T. G. Schmalz, pages 127-147 in *Computational Graph Theory*, ed. D. H. Rouvray (Nova Science Pub., New York, 1990).

[144] W. A. Seitz & T. G. Schmalz, pages 525-551 in Ref. [3].

[145] E. W. Montroll, J. Chem. Phys. **9** (1941) 706.

G. H. Wannier, Rev. Mod. Phys. **17** (1945) 50.

L. Onsager, Phys. Rev. **65** (1944) 117.

[146] P. W. Kasteleyn, chap. 2 in *Graph Theory & Theoretical Physics*, ed. F. Harary (Academic Press, NY, 1967).

[147] C. A. Hurst, & H. S. Green, J. Chem. Phys. **33** (1960) 1059.

P. W. Kasteleyn, Physica **27** (1961) 1209.

M. E. Fisher, Phys. Rev. 124 (1961) 1664.

P. W. Kasteleyn, J. Math. Phys. **4** (1963) 287.

[148] T. F. Yen, Theor. Chim Acta **10** (1971) 399.

H. Sachs, Combinatorica **4** (1984) 89.

[149] P. John & H. Sachs, pages 85-101, in *Graphen in Forschung & Unterricht*, ed R. Bodendiek, H. Schumacher, & G. Walther (Franzbecker-Verlag, Bad Salzdetfurth, 1985).

[150] P. John, H. Sachs, & H. Zernitz, Zast. Mat. Appl. Mat. **19** (1987) 405.

[151] D. J. Klein & N. Trinajstić, J. Mol. Struct. **206** (1990) 135.

H. Sachs, P. Hansen, & M. Zheng, Match **33** (1996) 169.

[152] D. J. Klein, T. G. Schmalz, M. A. García-Bach, R. Valenti, & T. P. Živković, Phys. Rev. B **43** (1991) 719.
[153] W. C. Herndon, Tetrahedron **29** (1973) 3.
[154] M. Randić, Chem. Phys. Lett. **128** (1986) 193.
[155] J. K. Percus, J. Math. Phya. **10** (1969) 1881.
    B. Džonova-Jerman-Blažić & N. Trinajstić, Comp. Chem. **6** (1982) 121.
    V. Elser, J. Phys. A **17** (1984) 1509.
    G. G. Hall, Chem. Phys. Lett. **145** (1988) 168.
[156] D. J. Klein & W. A. Seitz, J. Molec. Struc. (TheoChem) **169** (1988) 167.
[157] N. S. Ham, J. Chem. Phys **29** (1958) 1229.
[158] D. J. Klein & X. Liu, J. Comp. Chem. **12** (1991) 1260.
[159] N. S. Ham & K. Ruedenberg, J. Chem. Phys. **29** (1958) 1215.
[160] L. Pauling, sec. **7.5** & **7.6** of 3_rd_ edition of Ref. [17].
    L. Pauling, Acta Cryst.B **36** (1980) 1898.
    W. C. Herndon & M. L. Ellzey, J. Am. Chem. Soc. **16** (1974) 6631.
[161] B. Kamb & L. Pauling, Proc. Natl. Acad. Sci. USA **82** (1985) 8284.
[162] A. Graovac, I. Gutman, M. Randić, & N. Trinajstić, J. Am. Chem. Soc. **95** (1973) 6267.
[163] D. S. Rokhsar & S. A. Kivelson, Phys. Rev. Lett. **61** (1988) 2376.
    S. A. Kivelson, Phys. Rev. B **39** (1989) 259.
    S. A. Kivelson, pages 113-124 in *Field Theories in Condensed matter Physics*, ed. Z. Tesanović (Addison Wesley, Reading, Massachusetts, 1990)
[164] S. Nikolić, N. Trinajstić, & D. J. Klein, Comput. Chem. **14** (1990) 313.
    N. Trinajstić, S. Nikolić, & D. J. Klein, J. Molec. Struc. (TheoChem) **229**
      (1991) 63.
[165] D. J. Klein & T. G. Schmalz, Intl. J. Quantum Chem. **35** (1989) 373.
[166] M. Randić, D. J. Klein, S. El-Basil, & P. Calkins, Croat. Chem. Acta **69** (1996) 1639.
[167] D. J. Klein, M. A. Garcia-Bach, & W. A. Seitz, J. Molec. Struct. (TheoChem) **185** (1989) 275.
    M. A. Garcia-Bach, R. Valenti, & M. A. Garcia-Bach, J. Molec. Struct. (TheoChem) **185** (1989) 287.
[168] M. Randić, S. Nikolić, & N. Trinajstić, p. 429 in *Graph Theory & Topology in Chemistry*, ed. R. B. King & D. H. Rouvray (Elsevier, Amsterdam, 1987).
[169] G. E. Hite, T. P. Zivković, & D. J. Klein, Theor. Chim. Acta **74** (1988) 349.
[170] X. Liu, D. J. Klein, W. A. Seitz, & D. J. Klein, J. Comp. Chem. **12** (1991) 1265.
    X. Liu, D. J. Klein, & T. G. Schmalz, Full. Sci. & Tech. **2** (1994) 405.
[171] H. Y. Zhu & D. J. Klein, Commun. Math. Chem. (MatCh) **101** (1994) 205.
    M. Randić, D. J. Klein, H.-Y. Zhu, N. Trinjastić, & T. P. Zivković, Theor. Chim. Acta **90** (1995) 1.
[172] H. Y. Zhu, A. T. Balaban, & D. J. Klein, J. Chem. Phys. **101** (1994) 5281.
[173] T. P. Zivković, D. J. Klein, & T. G. Schmalz, Polycyclic Arom. Compd. **13** (2000) 457.
    T. P. Zivković, T. G. Schmalz, & D. J. Klein, Polycyclic Arom. Compd. **18** (2000) 13.
[174] A. T. Balaban & I. Tomescu, Commun. Math. Chem. (MatCh) **14** (1983) 155.
    M. Randić, p.469 in Ref. [3].
[175] P. Hansen & M. L. Zheng, Disc. Math. **122** (1993) 179.
[176] D. J. Klein, T. G. Schmalz, W. A. Seitz, & G. E. Hite, Intl. J. Quantum Chem.S **19** (1986) 707.
[177] S. A. Kivelson, D. S. Rokhsar, & J. P. Sethna, Phys. Rev. B **35** (1987) 8865.

D. J. Thouless, Phys. Rev. B **36** (1987) 7187.

S. Tang & H. Q. Lin, Phys. Rev. B **38** (1988) 6863.

B. Sutherland, Phys. Rev. B **38** (1988) 7192.

N. Read & S. Sachdev, Nucl. Phys. B **316** (1989) 609.

[178] P. W. Anderson, Mat. Res. Bull. **8** (1973) 153.

P. W. Anderson & Fazekas, Phil. Mag. **30** (1974) 423.

[179] J. C. Talstra, S. P. Strong, & P. W. Anderson, Phys. Rev. Lett. **74** (1995) 5256.

[180] C. K. Majumdar & D. K. Ghosh, J. Math. Phys. **18** (1969) 1388.

[181] P. M. van den Broek, Phys. Lett. A **77** (1980) 261.

[182] D. J. Klein & T. L. Welsher, J. Stat. Phys. **24** (1981) 555.

[183] D. J. Klein, J. Phys. A **15** (1982) 661.

[184] G. S. Shastry & B. Sutherland, Physica B **108** (1981) 1069.

W. J. Caspers, Physica **115** (1982) 275.

B. Sutherland & G. S. Shastry, J. Stat. Phys. **33** (1983) 477.

I. Kanter, Phys. Rev. B **39** (1989) 7270.

M. P. Gelfand, R. R. P. Singh, & D. A. Huse, Phys. Rev. B **40** (1989) 10801.

I. Bose, Phys. Rev. B **45** (1992) 13072.

P. Orland, Phys. Rev. B **47** (1993) 11280.

T. Oguchi & H. Kitatani, J. Phys. Soc. Japan **64** (1995) 612.

U. Bhaumik & I. Bose, Phys. Rev. B **52** (1995) 12489.

[185] I. Affleck, T. Kennedy, E. H. Lieb, & H. Tasaki, Phys. Rev. Lett. **59** (1987) 799.

T. Kennedy, E. H. Lieb, & H. Tasaki, J. Stat. Phys. **53** (1988) 383.

P. L. Iske & W. J. Caspers, Mod. Phys. Lett. B **2** (1988) 1223.

[186] H. Tasaki, Phys. Rev. Lett. **70** (1994) 3303.

[187] W. Marshall, Proc. Roy. Soc. (London) A **232** (1955) 48.

[188] S. A. Alexander & D. J. Klein, J. Am. Chem. Soc. **110** (1988) 3401.

[189] N. D. Mermin & H. Wagner, Phys. Rev. Lett. **17** (1966) 1133.

[190] E. H. Lieb, Phys. Rev. Lett. **62** (1989) 1201.

[191] E. H. Lieb, J. Math. Phys. **8** (1967) 2339.

D. J. Klein & N. Trinjastić, J. Am. Chem. Soc. **106** (1984) 8050.

[192] D. J. Klein, pages 33-50 in *Theoretical Organic Chemistry*, ed. C. Párkanyi (Elsevier, Amsterdam, 1998).

[193] S. B. Auster, , R.P. Dowd, J. Am. Chem. Soc. **88** (1966) 2587.

[194] R. Yarkony & H. F. Schaeffer, III, J. Am. Chem. Soc. **96** (1974) 3754.

D M. Pitzer, M. S. Platz, J. Am. Chem. Soc. **100** (1982) 3812.

P. G. Weinhold, J. Hu, R. R. Squires, & W. C. Lineberger, J. Am. Chem. Soc. **118** (1996) 475.

[195] O. Ivanciuc, L. Bytautas, & D. J. Klein, J. Am. Chem. Soc. (submitted, 2000).

O. Ivanciuc, D. J. Klein, & L. Bytautas, (in preparation, 2001).

[196] D. J. Klein, Chem. Phys. Lett. **217** (1994) 261.

M. Fujita, K. Wakabayashi, K. Nakada, & K. Kusakabe, J. Phys. Soc. Japan **65** (1996) 1920.

K. Wakabayashi, M. Fujita, & K. Kusakabe, Czech. J. Phys. **46** (1996) 1865.

K. Nakada, M. Fujita, K. Wakabayashi,& K. Kusakabe, Czech. J. Phys. **46** (1996) 2429.

K. Nakada, M. Fujita, G. Dresselhaus, & M. S. Dresselhaus, Phys. Rev. B **54** (1996) 17954.

[197] W. A. Seitz, D. J. Klein, T. G. Schmalz, & M. A. Garcia-Bach, Chem. Phys. Lett. **115**

(1985) 139.

[198] D. J. Klein & N. H. March, Intl. J. Quantum Chem. (submitted).

[199] L. Pauling, Phys. Rev. **54** (1938) 899.

L. Pauling, Nature **161** (1948) 1019.

L. Pauling, Proc. Royal Society (London) A **196** (1949) 343.

L. Pauling, Physica **15** (1949) 23.

L. Pauling & Z. Herman, p. 569 in Ref. [3].

Chapter 16

Clar's π-aromatic sextet revisited *

Milan Randić

Department of Mathematics and Computer Science, Drake University,
Des Moines, IA 50311, USA

We consider the recently proposed mathematical definition of Clar's π-sextet structures based on the concept of the innate degree of freedom and in particular extend this approach to generalized Clar structures in which the number of the π-sextets need not be the maximal. It is conjectured that the mathematical definition of Clar structure and the geometrical definition which has been hitherto used are equivalent. The novel definition of Clar's structure, which allows only superposition of those Kekulé valence structures which have the same innate degree of freedom, leads to generalized Clar's structures which differ from the earlier considered generalized Clar's structures of Herndon and Hosoya. Construction of generalized Clar structures is outlined based on re-examination of Herndon-Hosoya type Clar's structures. It is believed, having finally arrived at a mathematical definition of the Clar structures for the first time after over forty years since the pioneering work of Clar in advocating π-sextets was initiated in late 1950's, that this particular characterization of benzenoid hydrocarbons will attract due attention not only of experimental chemists but also theoretical chemists. Given a Clar structure of a benzenoid hydrocarbons having k π-sextets it is not difficult to decompose it into a set of 2k Kekulé valence structures. The proposed mathematical characterization of Clar structures represents the solution to the inverse problem concerning Clar's structures: How to determine in advance which Kekulé valence structures contribute to Clar structure of a benzenoid hydrocarbon.

1.   INTRODUCTION

The idea of π-aromatic sextet was introduced in 1925 by Armitt and Robinson [1] but really came to life in 1958 with the pioneering work of Clar and Zander [2] on benzenoid hydrocarbons which displayed unusual stability having 6n π-electrons (n= 1, 2, . . .). Clar continued to develop the π-aromatic sextet model and convincingly argued in favor of characterization of benzenoid hydrocarbons by structural properties of its π-sextets [3]. Prior to this benzenoid hydrocarbons were represented by sets of Kekulé valence structures, but according to Clar only a subset of

* This paper is honoring Professor Ivan Gutman, a dedicated warrior for a better recognition of Clar's insights into the nature of benzenoids dominate properties of benzenoid systems.

504

Fig. 1   Benzenoid hydrocarbons that have a single Clar structure consisting of only inscribed circles
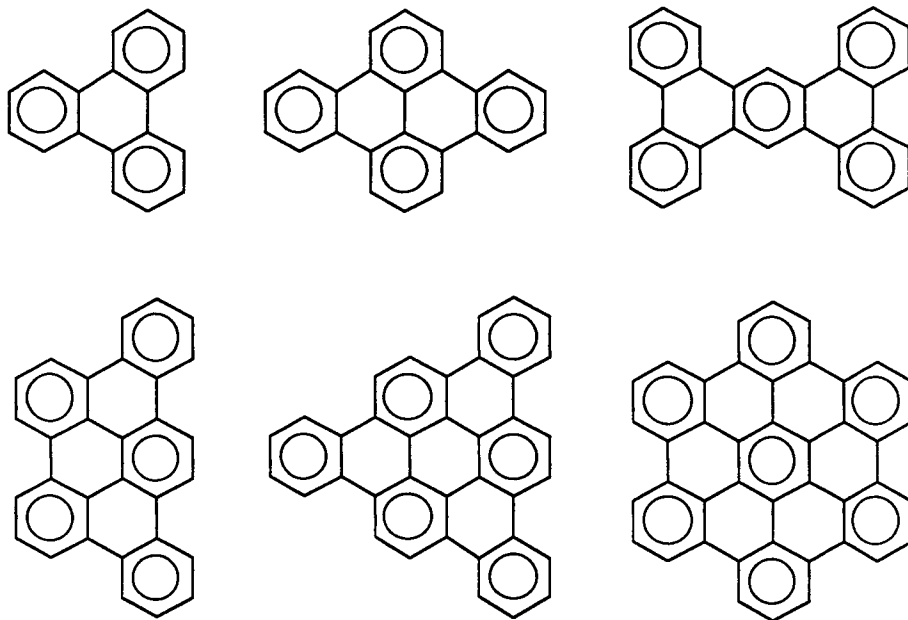
Fig. 2   Cata- and peri-condensed benzenoid hydrocarbons with Clar structure needing both the inscribed circles and CC double bonds
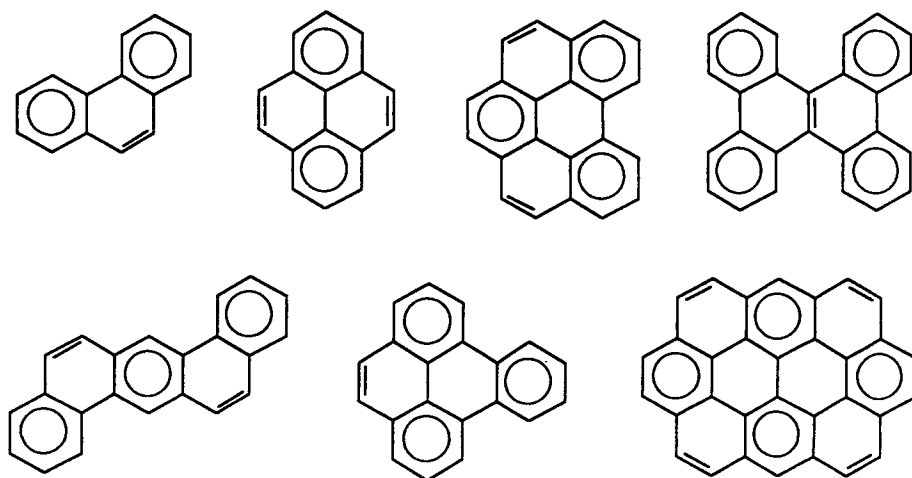
Kekulé valence structures, which contribute to so called Clar structures, Clar valence structures are depicted with inscribed circles in some benzene rings obeying the following rule. Inscribe as many circles as possible subject to two restrictions: (i) No adjacent rings should have inscribed circles; and (ii) CC bonds not involved in rings with inscribed circles should allow completion of valence structure by assignment of CC double bonds wherever possible.

In Fig. 1 we illustrate Clar structures for several smaller benzenoids in which only inscribed circles appear. These are the unusually stable 6n π-electron benzenoids which Clar called "fully benzenoid." In Fig. 2 we illustrate Clar structures for smaller benzenoids in which besides inscribed circles representing aromatic sextets also appear one or more CC double bonds. Finally in Fig. 3 we illustrate benzenoid hydrocarbons for which one can draw several Clar valence structures. In such cases the overall Clar structure is obtained as a superposition of the "component" valence structures in an analogous way as one represents molecules by superposition of several Kekulé valence structures. Clar represented the final superposition of component structures by drawing a single structure to which one or more arrows are added to suggest delocalized π-sextets.

The above descriptive definition of Clar structures has been satisfactory and does not cause ambiguities in applications. Nevertheless, it seems desirable to have in addition to such descriptive characterization of Clar structures also a mathematical characterization that can reveal relationships between Clar structures and the underlying Kekulé valence structures. That there is such an apparently subtle relationship has only very recently been recognized [4]. As is well known, not all Kekulé valence structures are involved in the construction of the Clar structure of a benzenoid hydrocarbon, but until recently a mathematical characterization of Clar structures, that is the characterization of Kekulé valence structures involved and those not involved in formation of Clar structures, was not known. It turns out that the superposition of all Kekulé valence structures having "the largest degree of freedom," a concept that has been around for a while [5], constitutes Clar structures. In view of this finding in this contribution we will revisit Clar structures and will consider how is this recognition of Kekulé valence structures important for construction of Clar structures and how is it reflected in the characterization of benzenoid hydrocarbons.

2. INNATE DEGREE OF FREEDOM OF KEKULÉ STRUCTURES

The novel definition of Clar structures to be outlined in the next section, is based on the concept of the *"degree of freedom"* (df) of a

506

Kekulé valence structure. The degree of freedom has been defined as the smallest number of choices to be made in the assignment of CC double bonds which determine a Kekulé valence structure completely. For example, all three Kekulé valence structures of naphthalene have df = 1, because if one assigns CC double bond character to any of the three vertical CC bonds in the naphthalene diagram (Fig. 4) the location of the remaining four CC bonds is completely determined. The same is true for anthracene, tetracene, and other linearly fused benzenoids.

In phenanthrene (Fig. 5), however, four out of five Kekulé structures have df = 2, and one structure has df = 1. Clearly by selecting a bond in one of the peripheral benzene rings of phenanthrene as a CC

Fig. 3   Cata-condensed benzenoid hydrocarbons with more than one Clar structure
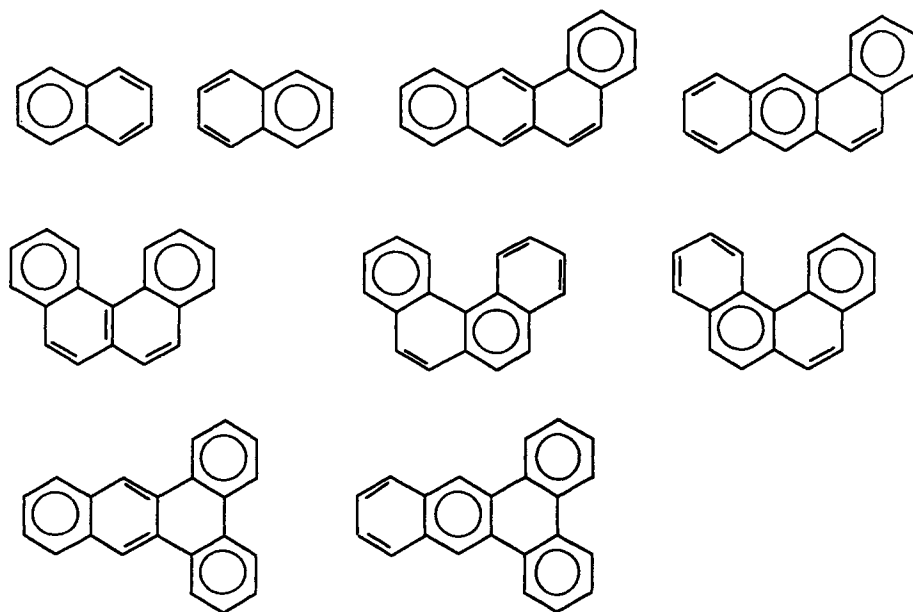
Fig. 4   The Kekulé valence structures of naphthalene and their innate degrees of freedom

df = 1   df = 1   df = 1
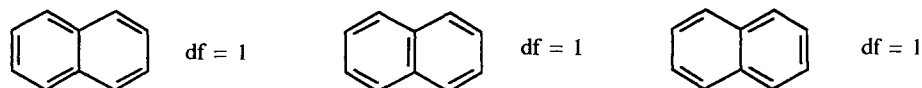
Fig. 5   The Kekulé valence structures of phenanthrene and their innate degrees of
            freedom

df = 2   df = 2   df = 2   df = 2   df = 1
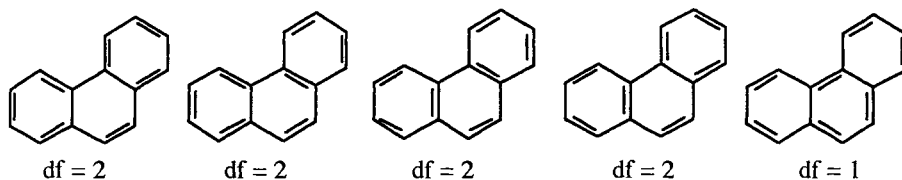
double bond, the CC bond type of none of CC bonds in the other peripheral benzene rings has been determined.   The situation is different for the last Kekulé structure of phenanthrene for which df = 1.   By assigning to CC double bond character to the central CC bond that connects two peripheral rings the CC double and CC single bond character for all the remaining CC bonds of phenanthrene is determined, which completely determines Kekulé valence structure.   Additional illustration of df values for Kekulé structures of several smaller benzenoids are shown in Fig. 6.

Observe that in cata-condensed benzenoid hydrocarbons Kekulé valence structures that have the maximal degree of freedom also have the largest possible number of disjoint conjugated circuits.   On the other hand Kekulé valence structures that have the smallest degree of freedom also have the smallest number of disjoint conjugated circuits.   That the degree of freedom in cata-condensed benzenoid hydrocarbons is determined by the number of disjoint Kekulé benzene rings has been recently recognized by Hansen and Zheng [6] who were able to prove a theorem that gives the degree of freedom in cata-condensed benzenoid hydrocarbons as the number of disjoint benzene rings in which one can independently assign three CC double bonds.   We should also mentioned that the so called Fries Kekulé valence structure [7], which is defined as the Kekulé valence structure having the largest number of rings with three CC double bonds (i.e., Kekulé benzene rings), is always one of the Kekulé valence structures having the maximal innate degree of freedom.   On the other hand most chemists would easily recognized Kekulé structures with the smallest innate degree of freedom as valence structures of limited interest for characterization of benzenoids systems.

In   Fig.   7   we   show   all   Kekulé   valence   structures   of benzo[ghi]perylene and their degrees of freedom.   The first eight structures have df = 3, the next five Kekulé valence structures have df = 2, and the last Kekulé valence structure has df = 1.   The individual Kekulé valence structures have quite different count of conjugated circuits R_i, which can be as high as five (in the first Kekulé valence structure) and as low as one (in the last Kekulé valence structures). A close look at these

508

Fig. 6   A selection of Kekulé valence structures of smaller benzenoid hydrocarbons
         and their innate degrees of freedom

df = 1   df = 1

df = 2

df = 3   df = 1   df = 1

df = 2   df = 2   df = 2   df = 2

df = 3   df = 2   df = 1

df = 3   df = 2   df = 2
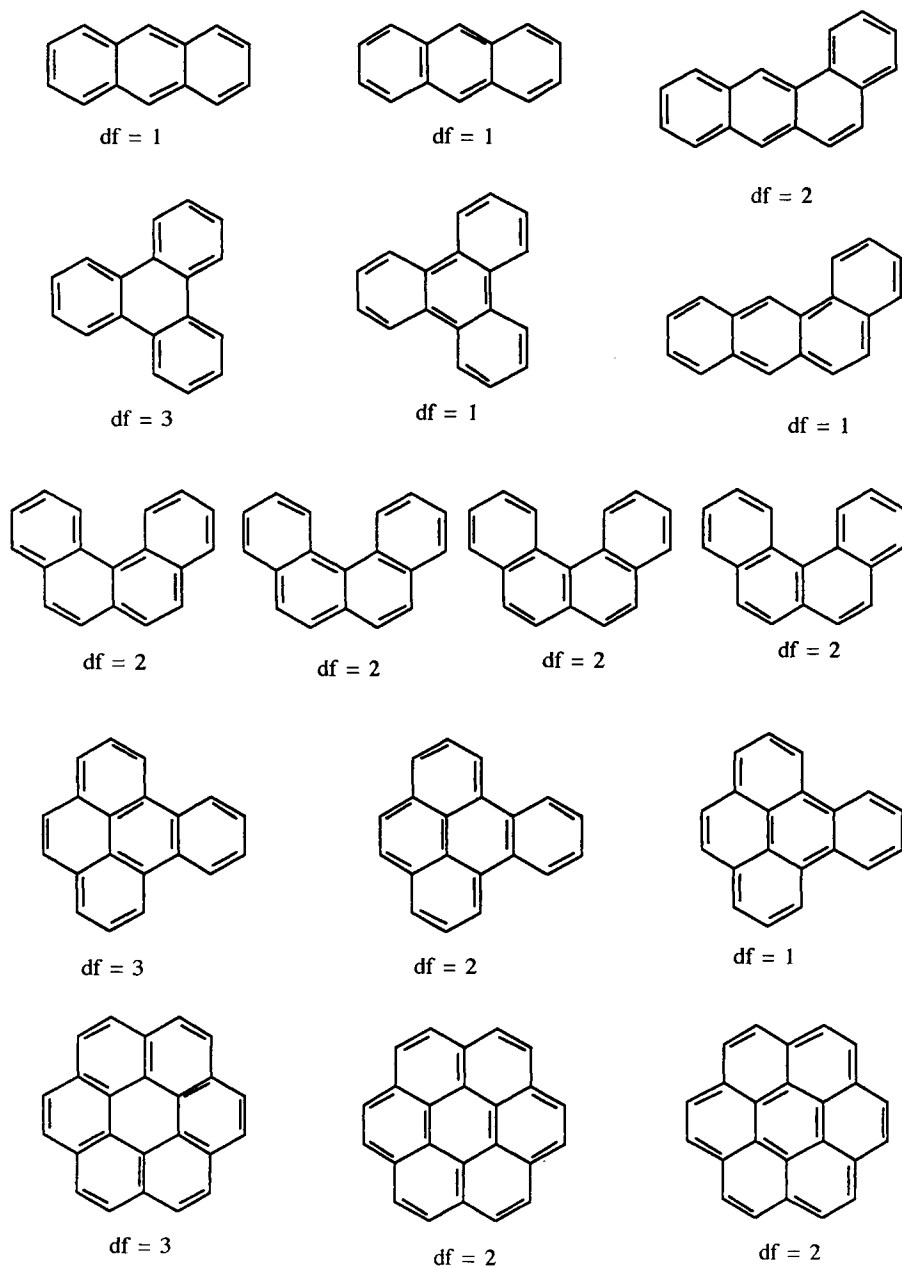
Fig. 7   The Kekulé valence structures of benzo[ghi]perylene and their innate
          degrees of freedom
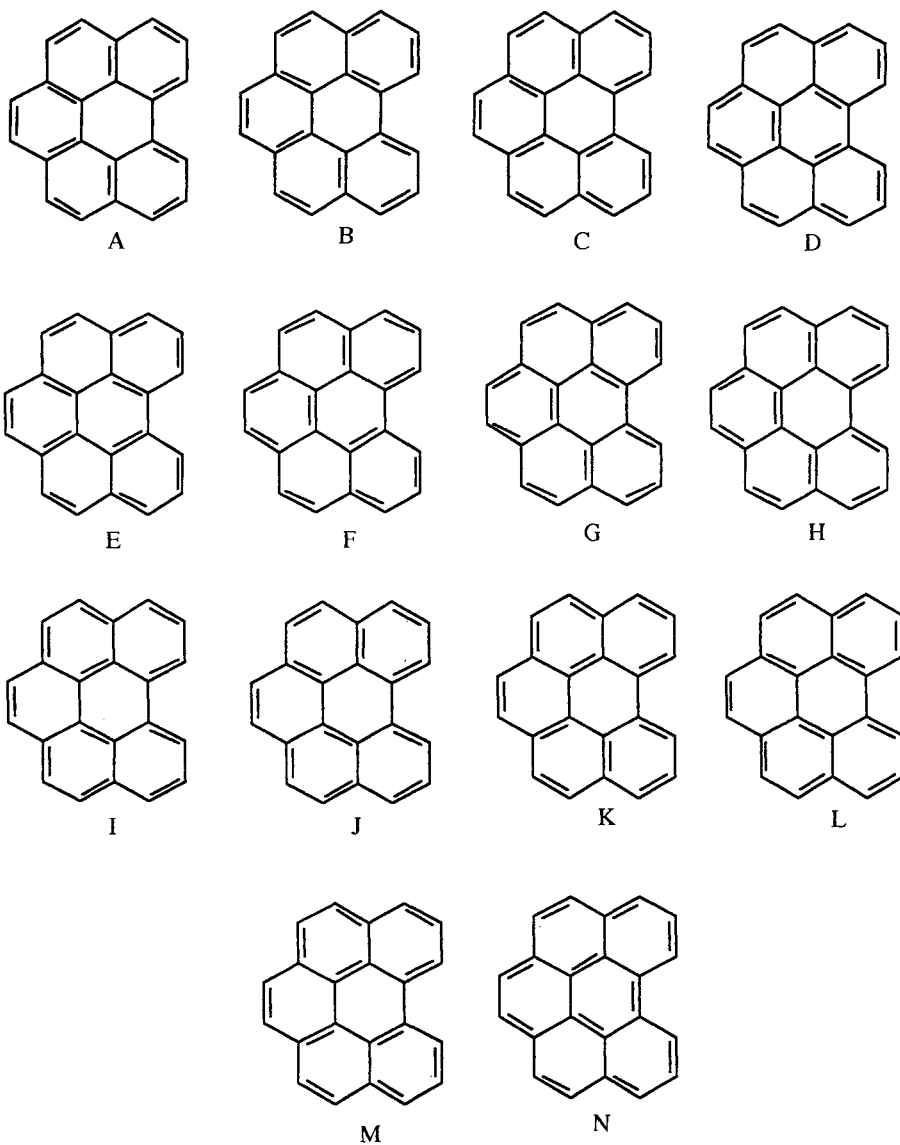
structures shows that the number of disjoint R_1 conjugated circuits is three for the first eight structures all of which have innate degree equal three, and that the number of disjoint R_1 conjugated circuits in the following five Kekulé structures is two and all of these structures have innate degree equal two, and finally the last valence structure has only one disjoint conjugated circuit and has df = 1. This observation suggest the following Conjecture:

Conjecture: The degree of freedom of a Kekulé valence structure is given by the maximal number of disjoint conjugated circuits.

This is certainly true for cata-condensed benzenoids, as it follows from the work of Hansen and Zheng. In all cases that we considered we found the conjecture true, which of course, proofs nothing, but strengthen our belief that the conjecture may be true. That one should focus attention to conjugated circuits rather than to "benzene rings having three CC double bonds" (which are the smallest conjugated circuits R_1) can be seen from Fig. 6 in which we have included three symmetry non equivalent Kekulé valence structures of coronene. By inspection on can see that the degree of freedom of the last of Kekulé valence structure of coronene is two, and the structure has two disjoint conjugated circuits: R_1 in the central ring and R_3 along the molecular periphery.

3. ON SUPERPOSITION OF KEKULÉ STRUCTURES

Simple VB method is based on superposition of all Kekulé valence structures. Similarly Pauling bond orders are obtained by the count of CC double bond character for individual CC bonds assuming superposition of all Kekulé valence structures. Both these approaches assume that all Kekulé valence structures have the same weight, but already the empirical Fries rule suggested that this may not be the case. Moreover, Clar's valence structures, like those shown in Fig. 1 - Fig. 3 imply importance of some Kekulé valence structure only. Thus Clar's structure of phenanthrene decomposes into four Kekulé valence structures which implies that the fifth Kekulé valence structure of phenanthrene is ignored. Formally in this case we can say that four Kekulé structures have weight equal one, and one has weight equal zero. In the case of Clar's structures of Fig. 3 for benzenoids having more than one Clar structure the situation is even more complicated because besides the weights zero and one also other non-zero weights may arise.

Because Clar structures can be viewed as a superpositions of selected Kekulé valence structures we will briefly examine pair-wise superposition of the five Kekulé valence structures of phenanthrene (shown in Fig. 5). In all we can construct ten combinations illustrated in Fig. 8. First,

Fig. 8   All pair-wise combinations of the five Kekulé valence structures of
            phenanthrene.

a + b   a + c   a + d   a + e

b + c   b + d   b + e   c + d

c + e   d + e
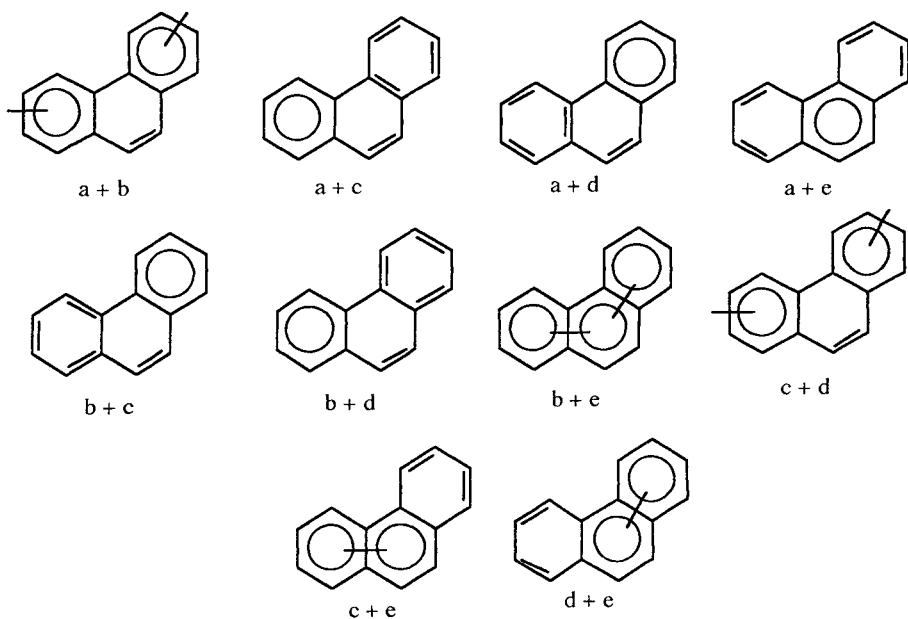
observe that in five cases we have a single π-sextet, in two cases we have
conjugated circuits of size n=10 and in one case conjugated circuit n = 14.
Finally in two cases we have two disjoint conjugated circuits n = 6 which
both represent the same valence structure obtained either as combination
(a, b) or (c, d). The valence structures (a, b) and (c, d) appear identical to
Clar structure of phenanthrene but with an important distinction. Clar
structure is obtained by superposition of *four* Kekulé valence structures,
while the combinations (a, b) and (c, d) are obtained as a superposition of
two Kekulé valence structures. Because of this distinction the
combinations (a, b) and (c, d) have been drawn by crossing sextet circles in
order to avoid confusion with Clar structure built from disjoint circles
using two Kekulé structures for each sextet. In addition to excluding the
combinations (a, b) and (c, d) we will also exclude combinations which
result in 10-member and 14-member conjugated circuits. This leaves for
close examination the following five combinations of Kekulé valence
structures: (a, c), (a, d), (a, e), (b, c) and (b, d) in which appears only a
single π-sextet. The combination (a, e), however, shows π-sextet in the
"wrong" ring and has to be excluded. Observe that Kekulé structures *a*

and *e* have different df values, which suggests that we restrict superposition of Kekulé valence structures to those having the same degree of freedom. With this restriction we are left with four combinations (a, c), (a, d), (b, c) and (b, d) which we may call 1-sextet structures which can be characterized by the following definition:

Definition: 1-Sextet structure is valence structure obtained by superposition of *two* Kekulé valence structures having the same degree of freedom *and* having CC double bonds in the same locations except for one benzene ring.

After arriving at 1-sextet structures we continue to consider superpositions of 1-sextet structures. All such structures already have the same df thus according to our approach can be superimposed. However, we will continue to restrict superpositions by demanding that all CC double bonds have the same locations except for one benzene ring. This restriction, preclude us to consider superpositions of (a, c) and (a, d), and in general any pair of 1-sextet structures unless they also have π-sextet in the same benzene ring. Therefore in the case of phenanthrene we can only superimpose the pair (a, c) and (b, d) or the pairs (a, d) and (b, c). In both case we obtain the same Clar structure of phenanthrene which is combination of Kekulé valence structures (a, b, c, d) already depicted in Fig. 2. Clearly the order in which we superimpose the four Kekulé valence structures is immaterial. Moreover, if we consider the "rejected" superpositions (a, b) and (c, d), which have "half-bread" π-sextets in the same positions, we see that their superposition leads to the same Clar structure (a, b, c, d), and hence, can be viewed as legitimate.

Superposition of 1-sextet structures results in 2-sextet structures, which in the case of phenanthrene represents the Clar's structure of phenanthrene. For benzenoids having larger number of benzene rings this process is continued till one arrives at k-sextet structures which have the maximal number of disjoint π-sextets. We can define k-sextet structure a follows:

Definition: k-Sextet structure is valence structure obtained by superposition of *two* (k-1) Kekulé valence structures having (k-1)-sextets in the same benzene rings *and* having CC double bonds in the same locations except for one benzene ring.

In Fig. 9 we illustrate all 1-sextets for benzo[ghi]perylene. Under each structure are the labels indicated the Kekulé valence structures involved. In all there are twelve 1-sextet structures to be used in the next step for construction of 2-sextet structures shown in Fig. 10. The first

Fig. 9   All 1-sextet structures of benzo[ghi]perylene obtained by pair-wise superposition of Kekulé valence structures of the maximal degrees of freedom
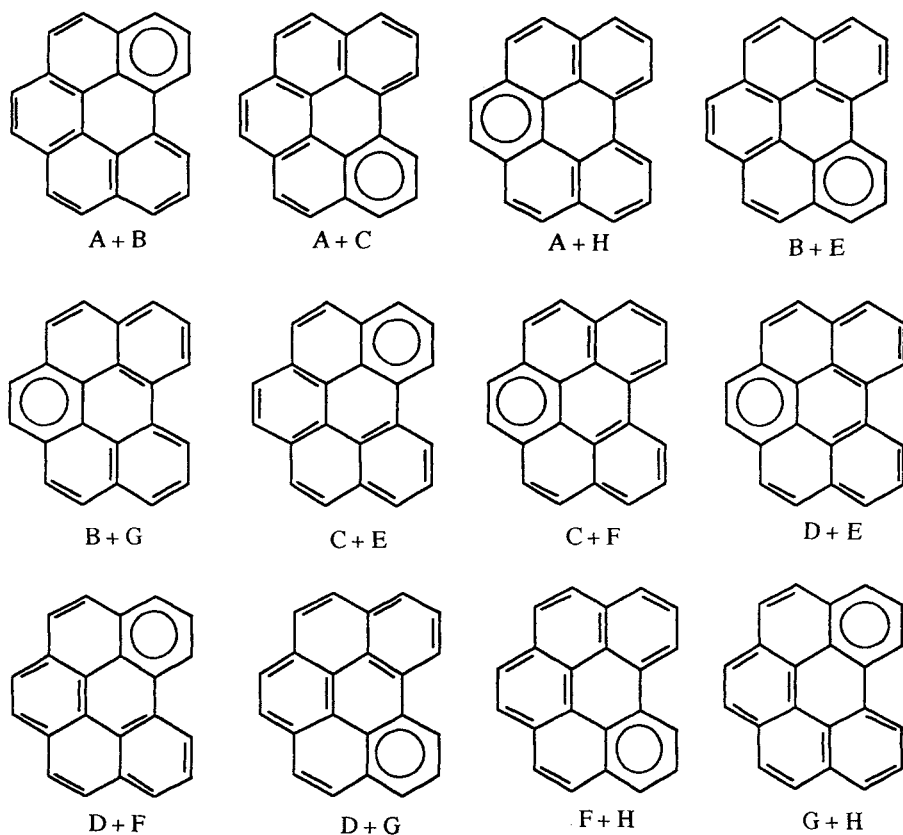
structure (A, B, C, E) is obtained by superposition of (A, B) and (C, E), which as we can see from Fig. 9 have π-sextet and all CC double bonds in the same location except for the last benzene ring of perylene fragment. The same 2-sextet structure can be obtained by superposition of (A, C) and (B, E). By continuing the process we continue to superimpose pair of 2-sextet structures to obtain 3-sextet structure (A, B, C, D, E, F, G, H) by combining (A, B, C, D) and (D, F, G, H) which have both π-sextets in the same location and differ in distribution of CC bonds only within a single ring. The same structure can be obtained alternatively by combining (A, B, G, H) and (C, E, D, F) or (A, C, F, H) and (B, E, D, G). The 3-sextet structure (A, B, C, D, E, F, G, H) of Fig. 11 has the maximal number of

514

Fig. 10   All distinct 2-sextet structures of benzo[ghi]perylene obtained by pair-wise
                superposition of 1-sextet structures

A + B + C + E   D + F + G + H   A + H + B + G   C + F + D + E

A + H + C + F   B + G + D + E
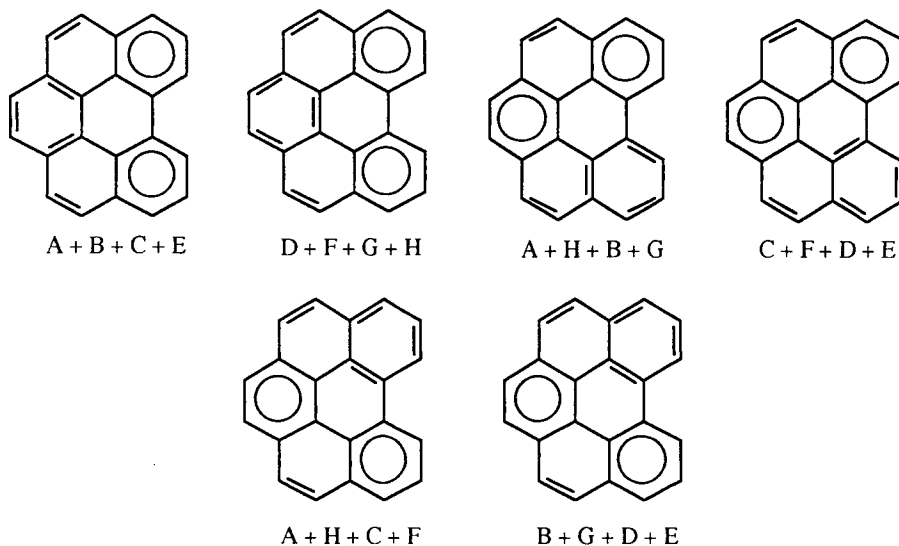
Fig. 11   The 3-sextet structure of benzo[ghi]perylene obtained by superposition of
                any of the three pairs of 2-sextet structures of Fig. 10

A + B + C + D + E + F + G + H
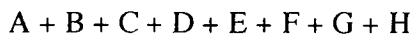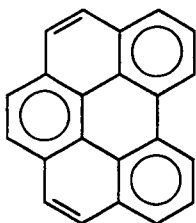
disjoint   π-sextets   and   therefore   represents   Clar   structure   of
benzo[ghi]perylene.

4.   NOVEL DEFINITION OF CLAR STRUCTURES

With use of the concept of the innate degree of freedom, or shortly
degree of freedom, we can characterize Clar's structures as follows: Clar

structure is valence structure obtained as a linear combination of all Kekulé valence structures having the highest degree of freedom.

This characterization suffice to determine Clar structure if there is but one such structure (the cases illustrated in Fig. 1 and Fig. 2). In order to define Clar structure in a general case we have to find which Kekulé valence structure are used more than once in a superposition. The concept of k-sextet structure considered in the previous section allow us to arrive at the mathematical definition of Clar's structure shown below which we are comparing with the geometrical definition of Clar's structure:

Definition (mathematical): Clar valence structure is obtained by superposition of k-sextet structures having the maximal k possible.

Definition (geometrical): Clar valence structure is constructed by placing the maximal number of disjoint circles inside benzene rings of benzenoid system subject to completion of valence structure by assigning CC double bonds if necessary.

The two definition leads to a following conjecture:

Conjecture: The mathematical definition of Clar structure and the geometrical (constructive) definition are equivalent.

We believe, or we should say, we conjecture, that the novel definition of Clar structure, which can be referred to as axiomatic and the original definition, which can be referred to as constructive are equivalent. In all the cases that we examined this has been the case, but that, of course, proofs nothing. The above is certainly true for the class of cata-condensed benzenoid hydrocarbons for which Hansen and Zheng [6] proved that df is given by the maximal number of disjoined benzene rings having three CC double bonds. Such rings are equivalent to the smallest conjugated circuits R_1 of the Conjugated Circuits Model [8]. The smallest conjugated circuits R_1 is trivially related to the inscribed circles of Clar.

We will leave the proof of the conjecture to mathematically inclined readers interested in this problem and will focus attention on consequences of the novel definition of Clar structures. If the two definitions of Clar structure are equivalent (as we conjecture) there should be identical consequences and the new definition is not to make a difference. However, the new definition does offer a mathematical characterization of Kekulé valence structures involved in construction of Clar structure, something that has been hitherto missing.

One area in which the novel definition of Clar structures may have an advantage over the "geometrical" counterpart is in computer manipulations with Kekulé and Clar structures. There are several algorithms and computer programs that enumerate, and even construct, all Kekulé valence structures for benzenoid hydrocarbons [9]. These programs can now be combined with evaluation of the degree of freedom of Kekulé structure, and such information can be combined into a scheme to produce list of Clar valence structures.

5. ON GENERALIZED CLAR STRUCTURES

We will now investigate the role of the new definition of Clar structures for Clar-type structures that do not posses the maximal number of inscribed π-aromatic sextets. Already Clar, in discussing properties of benzo[a]coronene, evoked a structure that has less than the maximal number of π-sextets [10]. While the *proper Clar structure* of benzo[a]coronene has four π-sextets, which is the maximal number for benzo[a]coronene, Clar considered also a structure having three sextets (Fig. 12). Such "imperfect" Clar structures were introduced into "Clar Sextet Theory" systematically by Hosoya and Yamaguchi [11].

Generalized Clar's Structures of Hosoya and Yamaguchi

Hosoya and Yamaguchi generalized Clar structures by removing the restriction that Clar structures have to have the maximal number of π-aromatic sextets. We will refer to these as HY-Clar structures, or briefly HY-structures (HY for Hosoya-Yamaguchi) in order to differentiate them from other generalizations of Clar structures that will be discussed later. In Fig. 13 we show the set of generalized HY-Clar formulas for

Fig. 12´   Clar structure of benzo[a]coronene and a Clar-type structure that has less than the maximal number of π-sextets considered by Clar
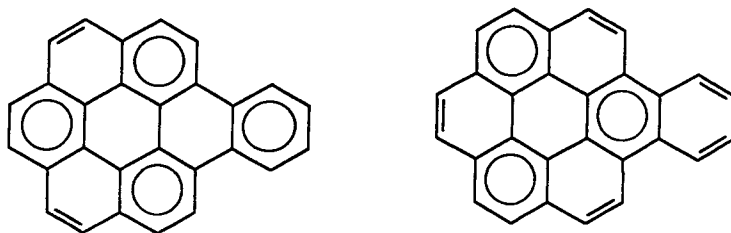
benzo[ghi]perylene, which are constructed by inserting one or more circles in different benzene rings such that no adjacent rings have inscribed circles. The last structure in Fig. 13 which does not include any inscribed circles completes the set of generalized Clar formulas of Hosoya and Yamaguchi. Observe that only the first formula represents proper Clar structure. Of the 14 HY-Clar structures of Fig. 13 only five (which are shown in Fig. 14) allow one to complete CC double bond assignments while

Fig. 13   Generalized Clar structures introduced by Hosoya-Yamaguchi illustrated on benzo[ghi]perylene.

518
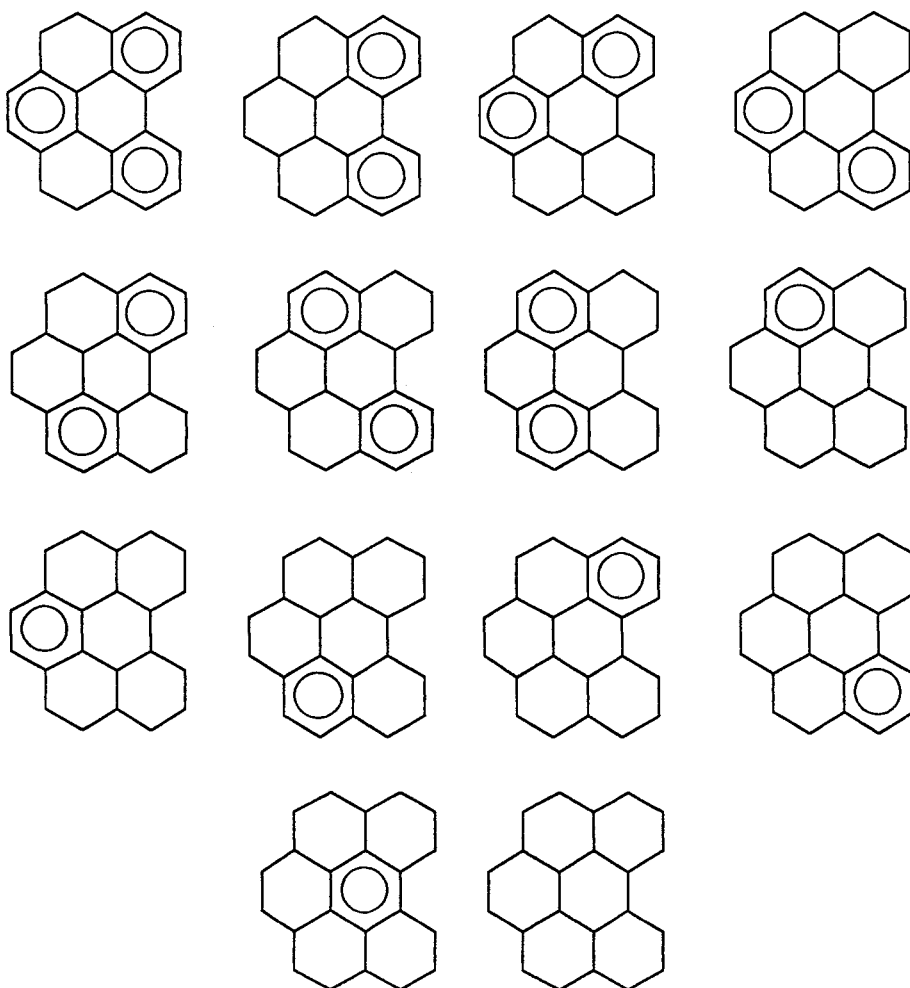
Generalized Clar structures introduced by Herndon and Hosoya illustrated on benzo[ghi]perylene.
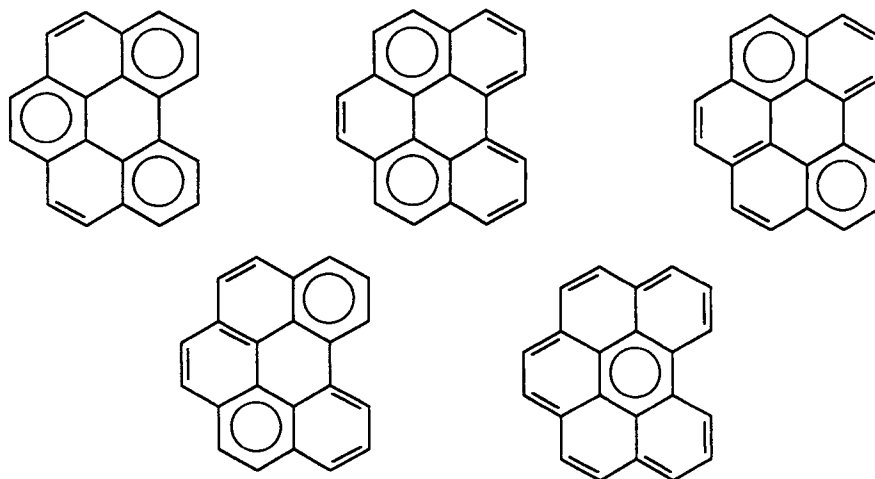
for the remaining nine HY-Clar formulas there is more than one way of assigning CC double bond type.   For this reason no CC double bond are shown in Fig. 13.   A one-to-one correspondence between Kekulé and sextet patterns has been recognized and is reflected in the sextet polynomial, which is the counting polynomial for generalized HY-Clar structures [12].

Generalized Clar's Structures of Herndon and Hosoya

A more restrictive definition of generalized Clar structures was proposed by Herndon and Hosoya about ten years later [13].   We will refer to these generalized Clar structures as HH-Clar structures, or briefly HH-structures (HH for Herndon-Hosoya).   Herndon and Hosoya have restricted the set of Clar-type structures by requiring that upon insertion of inscribed circles all the remaining CC double bonds should have a uniquely determined location.   Of the nine Clar patterns shown in Fig. 13 only the first four satisfy the new requirements.   This can be readily verified by completing the assignment of CC double bonds which for these fours structures result in a single possibility.   Herndon and Hosoya have defined the novel generalized Clar structures as follows:

Definition: Clar structures are defined to be structural diagrams in which all the carbon atoms of an aromatic hydrocarbon are spanned *uniquely* either by an aromatic sextet (designated by a circle) or by a π electron pair (designated as a double bond).

We have inserted in their definition the word "uniquely" for added precision. In other words, once the positions of inscribed circles have been selected the rest of the molecule should have the residual degree of freedom equal one, that is, positions of all CC double bonds are unique. In Fig. 14 we illustrate the five HH-Clar structures of benzo[ghi]perylene. In the case of benzo[ghi]perylene the first structure is the proper Clar structure that has the maximal number of π-sextets. Of the four generalized HH-Clar structures three have two π-sextet and one has but a single π-sextet.

Generalized Clar's Structures of the same Degree of Freedom

Even more restrictive definition of generalized Clar structures, than that of Herndon and Hosoya is possible by considering only superpositions of Kekulé valence structures of the same innate degree of freedom. This latest generalization of Clar structure naturally follows from the novel mathematical definition of Clar structures [4]. We will refer to these most recent generalization as the k-Clar structures, where k indicates the number of π-sextets in a structure. The restriction requires that only Kekulé valence structures having the same degree of freedom are combined in formation of Clar structures. In Fig. 15 we show k-Clar structures of benzo[ghi]-perylene. As we see the last k-Clar structure is one of the Kekulé valence structures. This particular Kekulé valence structure has no other structure having the same innate degree of freedom for superposition and therefore qualifies as 0-Clar structure. This is a consequence of the condition that k-Clar structures can only be obtained by superimposition of structures having the same value of the degree of freedom. Therefore Kekulé valence structures which have no structure to be combined with have to be included in the set of k-Clar structures, being structures having k = 0 value. The reason why several HH-Clar structures do not qualify as k-Clar structure is because they are obtained by superposition of Kekulé structures having different degree of freedom.

As we can see by comparing the HH-Clar structures and k-Clar structures they offer a distinctive basis for representation of benzenoid hydrocarbons. Each of the two approaches have their own merits, and as we will see in the next section, although the structures arising in the two models are quite different, the two approaches can be related in some respect. Both approaches use the same basis Kekulé structures and differ

Fig. 15   Generalized k-Clar structures of benzo[ghi]perylene

ABCDEFGH	IJ	JL	IK

KM	N
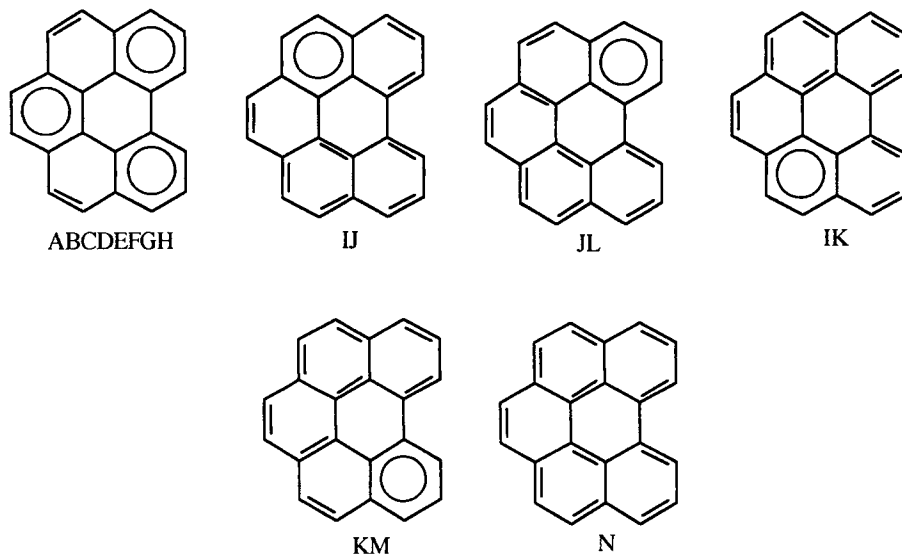
in selecting the subset of Kekulé structures used.   Thus the five HH structures of benzo[ghi]perylene shown in Fig. 14 involve superposition of (A, B, C, D, E, F, G, H); (A, I, J, K), (A, C, K, M), (A, B, J, L) and (D, N), total of 22 Kekulé structures: 4A + 2B + 2C + 2D + E + F + G + H + I + 2J + 2K + L + M + N.   In contrast the six generalized k-Clar structures of benzo[ghi]perylene obtained by superposition of Kekulé valence structures of the same degree of freedom (shown in Fig. 15) involve superposition of (A, B, C, D, E, F, G, H); (I, J), (J, L), (I, K), and (K, M), while Kekulé structure n remains isolated, total of 17 Kekulé structures: (A + B + C + D + E + F + G + H) + (2I + 2J + 2K + L + M) + N.   We have grouped Kekulé structures of the same df to emphasize that only superposition of Kekulé structures within the same group is allowed. As a consequence we do not have in case of benzo[ghi]perylene 2-Clar structures, but only one 3-Clar structure, four 1-Clar structures and a single 0-Clar structure.

6.   ON CONSTRUCTION OF k-CLAR STRUCTURES

Already in the case of smaller benzenoids, such as benzo[ghi]-perylene, it may be somewhat tedious to find by inspection of all the

Kekulé valence structures all the combination of Kekulé valence structures of interest. The same is also true for finding combinations of Kekulé valence structures involved in HH-Clar structures. A better way to obtain the correct combinations of Kekulé valence structures instead of construction of various superpositions is to first write down k-Clar structures (or HH-Clar structures) and then decompose them into underlying Kekulé valence structures. The apparent difficulty that remains in such an approach, that cannot be avoided, is the case of benzenoids having a large number of Kekulé valence structures which results in large number of decomposition.

A straightforward procedure for construction of k-Clar valence structures is similar to previously described construction of k-sextet structures. In the first step one considers pair-wise superposition of all Kekulé valence structures having the same degree of freedom but excluding combinations that lead to conjugated circuits having more than six π-electrons. Such superposition was illustrated in Fig. 9 and Fig. 10 for construction of 1-sextet and 2-sextet structures of benzo[ghi]perylene, respectively. We apply the same process now by considering Kekulé valence structures of a lesser degree of freedom. Superposition of a pair of Kekulé structures will produce 1-Clar structure for all combinations for which the process can not be continued. The structures with 1-sextet for which the process continues will lead to 2-Clar structures if no combinations between such structures can yield, by continuation, 3-Clar structures, and so on.

A direct construction of k-Clar structures by repeated superposition of a smaller number of Kekulé valence structures, while straightforward is not very efficient, because it offers duplicate combinations of k-Clar structures to obtain fewer number of (k+1)-Clar structures. For benzenoids having dozen or more Kekulé valence structures we need a more efficient approach. Hence it would be nice to have a more practical algorithm for construction of k-Clar structures. It turns out that a more efficient algorithm in which one takes advantage of HH-Clar structures is possible. Construction of Herndon-Hosoya Clar structures appears not to be so tedious as is the case with k-Clar structures. In fact, for not too large benzenoid construction of HH Clar structures is relatively simple. Hence, we will view HH-Clar structures to be readily available, at least for benzenoids of moderate size. We are going to take advantage of this situation and will base construction of k-Clar structures on HH-Clar structures. As we will see the HH-Clar structures contain indirectly also k-Clar structures, not necessarily all as the members of the same set, but as derivatives of some of the members of HH-Clar structures.

Let us clarify what we mean as the "derivative" structure by returning to Fig. 15 in which we listed the six k-Clar structure of

522

benzo[ghi]perylene. The four 1-Clar structures, the combinations IJ, JL, IK, and KM, are clearly not members of the set of HH-Clar structures of benzo[ghi]perylene (Fig. 14). Let us consider the structure (A, B, J, L), illustrated in Fig. 16, which is one of the three HH-Clar structures having two π-sextets. We can decompose this structure in two structure by selecting the encircled rings for which we write the two underlying Kekulé valence structures of benzene. This is illustrated in the lower part of Fig. 16 for the HH-Clar structure having two π-sextets. Observe that combinations (A, J) and (B, L) "mix" Kekulé valence structures of different df. The combination AB is obtained by mixing structures of the same df, but is not completed because it has no maximal possible number of sextets. The structure JL is a legitimate 1-Clar structures, however having one π-sextet less, hence, of a "lower" hierarchical level. Because the labels that indicate structure as ABJL can be permuted we can have three different decomposition: AB + JL, AJ + BL and AL + BJ. All three possibilities are depicted in Fig. 16. The combination AL + BJ shows two identical components having two sextets but obtained from superposition of only two Kekulé structures, rather than four. To emphasize the distinction we have drawn these "improper" sextets by crossed the circles with short line.

Fig. 16   Decomposition of one of the Herndon-Hosoya generalized Clar structures having two π-sextets

ABJL

AL   BJ

AJ   BL   or   AB   JL
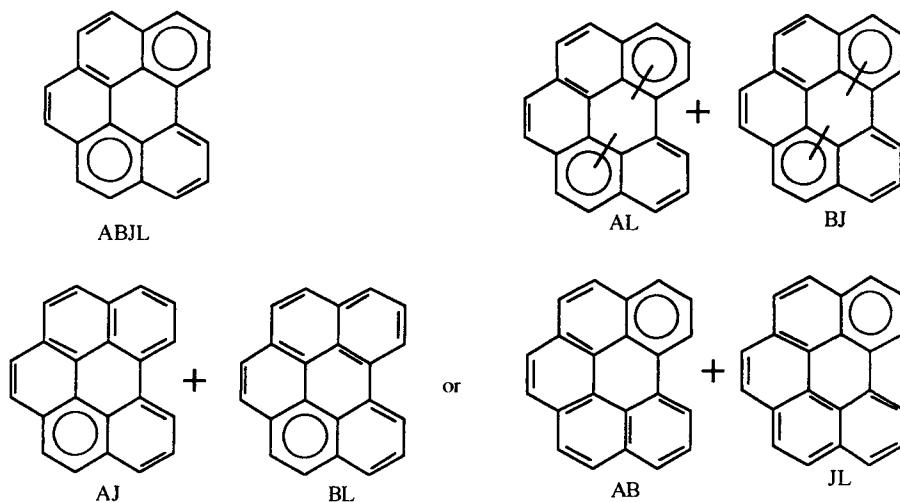
The above illustration suggests an algorithm for construction of k-Clar structures that can be outlined as follows:

(i)   Construct all HH-Clar structures.   This step is here assumed as reasonably straightforward, although for large benzenoids even this step can be quite difficult [14];

(ii)   Decompose individual HH-Clar structures by representing one of inscribed circles by the two underlying Kekulé valence structures, to be referred as derivative structures;

(iii)   If both derivative structures have the same degree of freedom (df) keep the parent structure as k-Clar structure;

(iv)   If one of the derivative structure has the same df value as the original structure and the other has increased df value, retain the structure with the same df value as k-Clar structure and discard the other structure.

This algorithm as stated can be readily implemented in a computer program, even though it may be somewhat demanding when applied to systems having a larger number of Kekulé structures.

7.   ILLUSTRATION OF k-CLAR STRUCTURES FOR SMALLER BENZENOID HYDROCARBONS

In Fig. 17 we illustrate k-Clar structures for a selection of smaller benzenoid hydrocarbons.   For molecules having symmetry only symmetry non equivalent Clar structures are shown.   In cases when all Kekulé valence structures have the same degree of freedom, clearly there is no difference between HH-Clar structures and k-Clar structures, because all the Kekulé structures are allowed to be superimposed.   This is the case not only of linear acenes, like naphthalene, anthracene, tetracene, etc., but also of chrysene, benzo[b]chrysene, dibenzo[bk]chrysene, and related cata-condensed systems having two adjacent "kink" rings.   "Kink" rings, introduced by Gordon and Davison [15], are those rings in unbranched cata-condensed benzenoid for which adjacent rings have phenanthrene geometry.

There are number of smaller benzenoids in which the set of HH-Clar structures and the set of k-Clar structures almost coincide.   For example, this is the case with dibenzo[bc,kl]coronene, one of smaller benzenoid with large number of CC double bond "fixation" in its leading (i.e., the proper) Clar structure.   Its Clar structure has three π-sextets but six CC double bonds.   In Fig. 18 we illustrated seven out of nine HH-Clar structures of dibenzo[bc,kl]-coronene.   Of the nine HH structures one has three π-sextets, six have two π-sextets (see Fig. 18) and two have a single π-sextet (shown in Fig. 19).   Interestingly, there are also nine k-Clar structures, seven of which coincide with the first seven HH-Clar structures of Fig. 18. However, instead of the last two HH-Clar structures having a single π-

524

Fig. 17   Generalized k-Clar Structures for several smaller benzenoid hydrocarbons
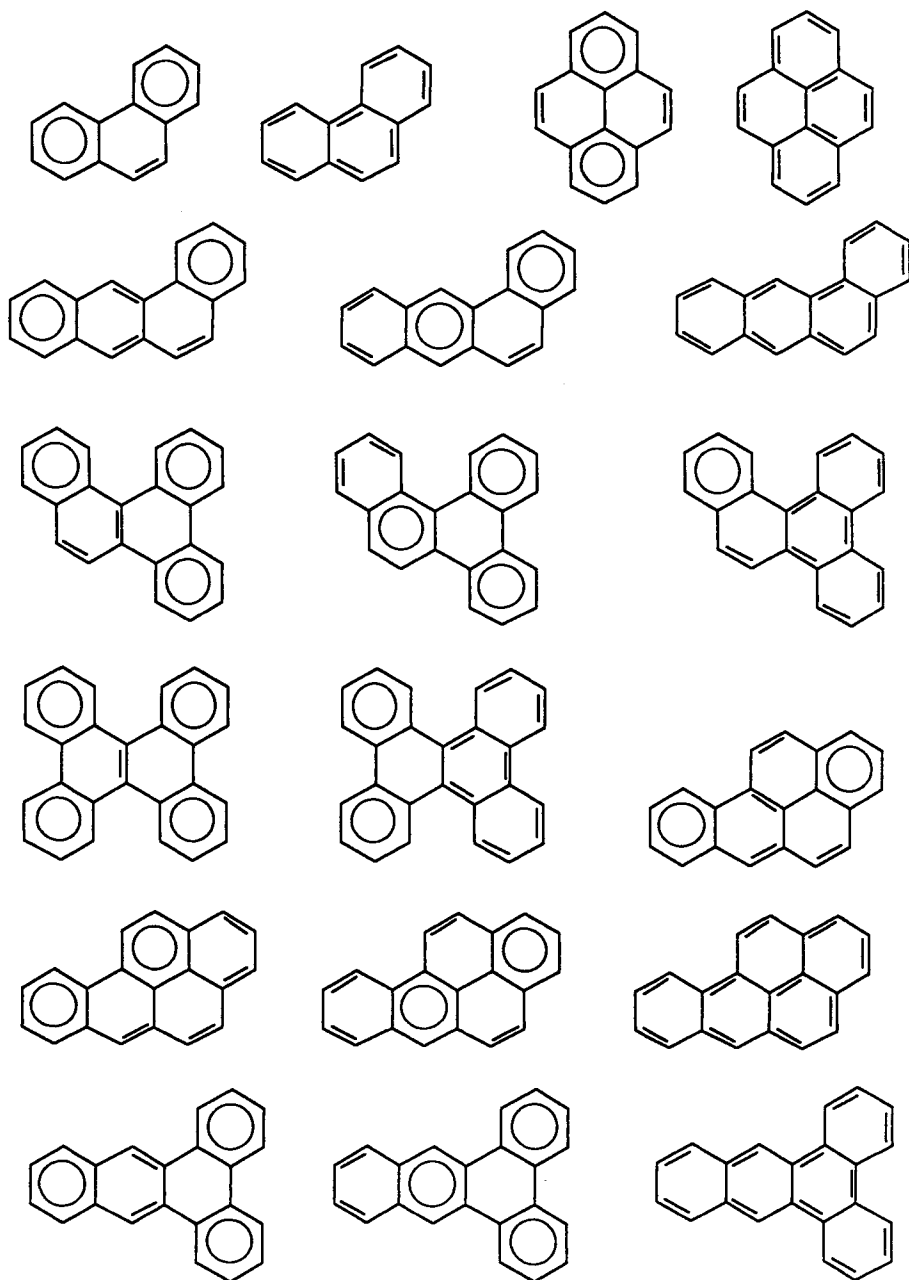
sextet shown in Fig. 19 we have two (symmetry equivalent) Kekulé valence structures showing "long range" order [16] referred to also as anti-Fries [17] structures which qualify as 0-Clar structures. Is the coincidence between the number of HH-Clar structures and k-Clar structures accidental? As we will see later there is a one-to-one correspondence between the HH-Clar structures and k-Clar structures.

Fig. 18   The seven of the nine HH Clar structures of dibenzo[bc,kl]coronene which coincide with seven generalized k-Clar structures
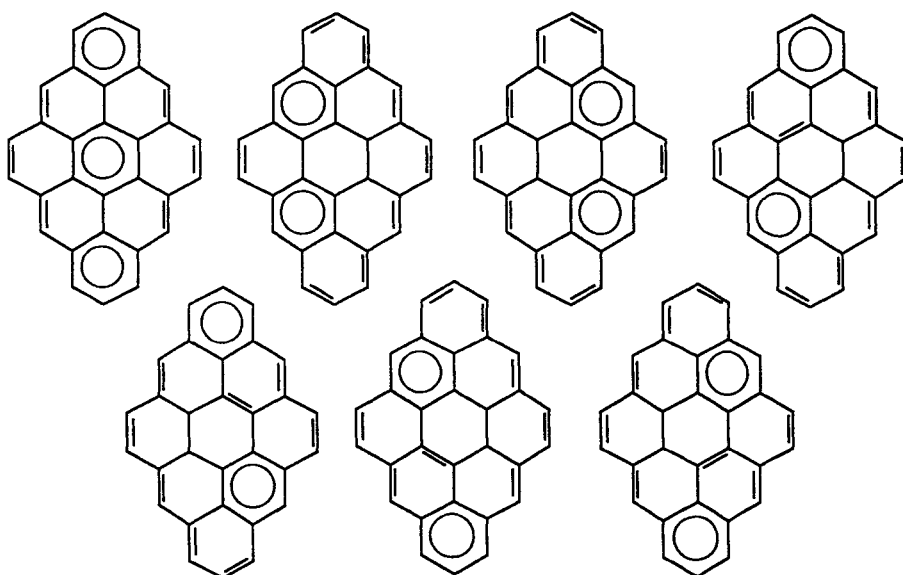
The algorithm for construction of k-Clar structures when applied to benzenoids having several inscribed sextets in each Clar structures may become time consuming. Can we speed up the procedure for decomposition of π-sextet somehow? In Fig. 20 and 21 we illustrate the HH-Clar structures of dibenzo[bc,ef]-coronene. There are 11 such structures: five having three π-sextets, five having two π-sextets, and one having a single π-sextet. There are also 11 k-Clar structures, six of which coincide with the six HH Clar structures of Fig. 20. Of the remaining five k-Clar structures four are 1-Clar structures (with a single π-sextet) and one is 0-Clar structure (i.e., a Kekulé valence structure). They are shown in Fig. 22.

526
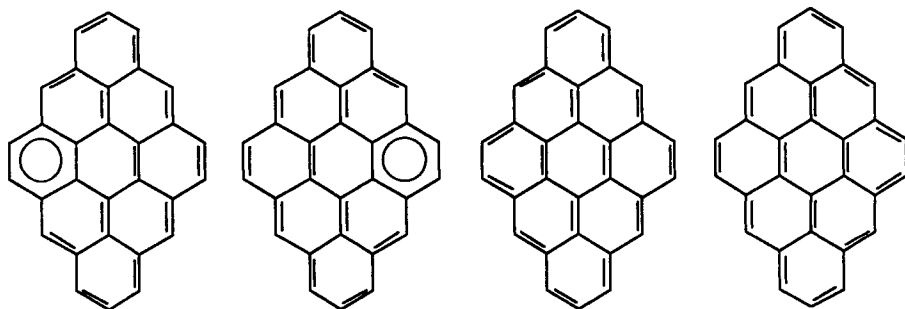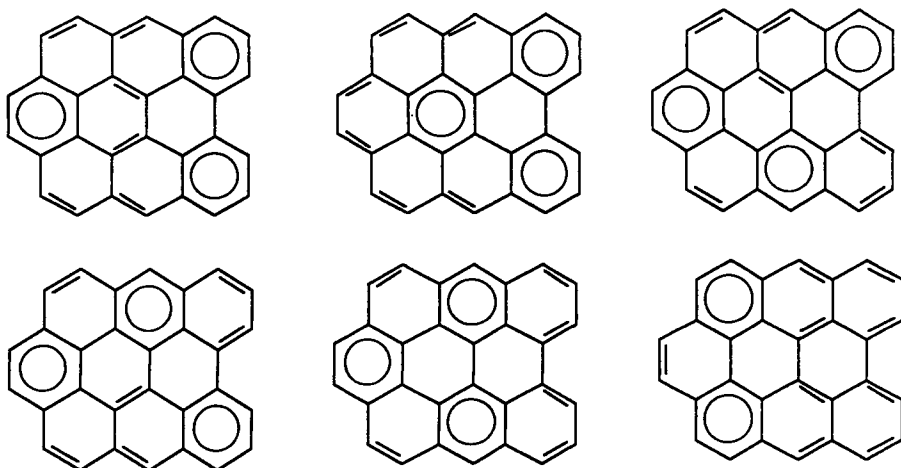
A coincidence between the number of HH-Clar structures and k-Clar structures is again evident. To each of the five HH-Clar structures of Fig. 21 corresponds a k-Clar structure having one π-sextet less (shown in Fig. 22). We have indicated by asterisk sextets of HH Clar structures that have not "survived" more restrictive definition of k-Clar structures which

restricts a superposition of Kekulé valence structures only to those having the same degree of freedom. We will refer to π-sextets with an asterisk as "vulnerable," for reasons that will become soon clarified. Observe that the immediate environment of the four "vulnerable" rings in HH-Clar structures having two π-sextets rings is identical to the CC double bond distribution in the HH-Clar structures of phenanthrene in which the π-sextet is assigned to the central benzene rings. The immediate environment of the "vulnerable" ring in the last HH-Clar structures having a single π-sextets rings is identical to the CC double bond distribution in the HH-Clar structures and triphenylene in which the π-sextet is assigned to the central benzene rings. The HH-Clar structures indicated by asterisk do not qualify as k-Clar structures, for the same reason that the corresponding HH-Clar structures of phenanthrene and triphenylene do not qualify. When the π-sextet with asterisk is decomposed into the underlying Kekulé valence structures one of the component structure will have a higher df value and the other structure will have a lower df value. The structure with the lower df qualifies as k-Clar structure having one less π-sextet than the parent HH-Clar structure. The other component having higher df is discarded because it should not be "mixed" with Kekulé valence structure of lower degree of freedom.

Fig. 21   The Herndon-Hosoya Clar structures of dibenzo[bc,ef]-coronene obtained by superposition of Kekulé valence structures of different degree of freedom

528
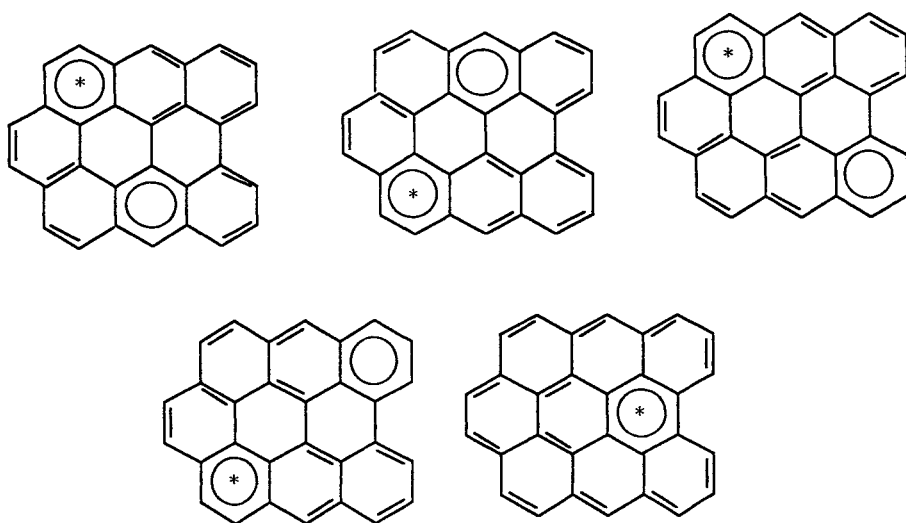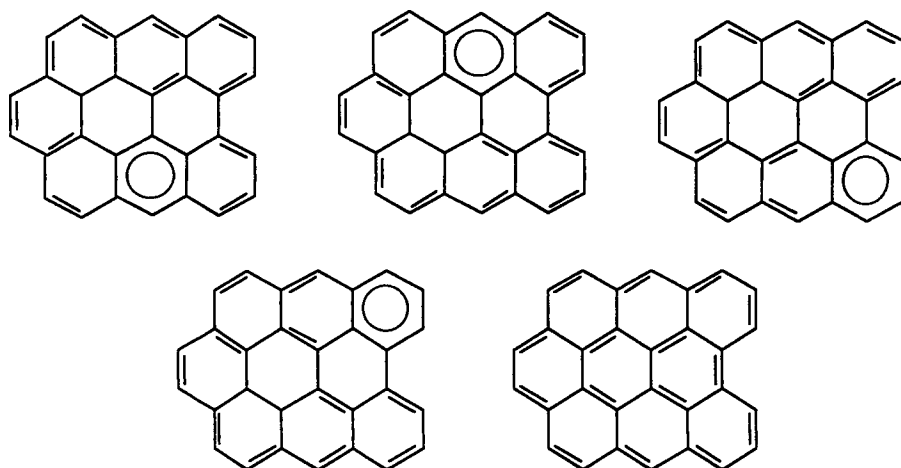
As we see one can quickly identify vulnerable π-sextet of HH-Clar structures by inspecting adjacent rings to see if they correspond to HH-Clar structures of phenanthrene and triphenylene which have inscribed circle in the central rings. By replacing in those Clar structures the inscribed circle by the Kekulé component having smaller df one immediately transform HH-Clar structures into k-Clar structure. If HH-Clar structure has no vulnerable π-sextets it qualifies as k-Clar structure. On the other hand, if HH-Clar structure has a vulnerable π-sextet each such structure by decomposition will produce one k-Clar structure having one π-sextet fewer. This establishes a one-to-one correspondence between HH-Clar structure and k-Clar structures. Hence, to write down quickly k-Clar structures for larger benzenoid one should first find all HH-Clar structure. Then one should look for distribution of CC double bonds in adjacent rings in order to identify the vulnerable benzene rings within such structures. Finally these HH-Clar structures are transformed into k-Clar structures.

In Fig. 23 we have illustrated several HH-Clar structures of smaller benzenoids and have indicated their vulnerable rings. Each of the Kekulé valence structure having a single vulnerable ring will produce the corresponding 0-Clar structure (i.e., a Kekulé valence structure that qualifies as Clar structure). In Fig. 24 are shown additional HH-Clar structures having besides vulnerable ring additional π-sextets. These structures will reduce to k-Clar structures when π-sextet of the vulnerable

Fig. 23   Several Herndon-Hosoya Clar structures in which the vulnerable rings have been indicated by asterisk which reduce to 0-Clar structures
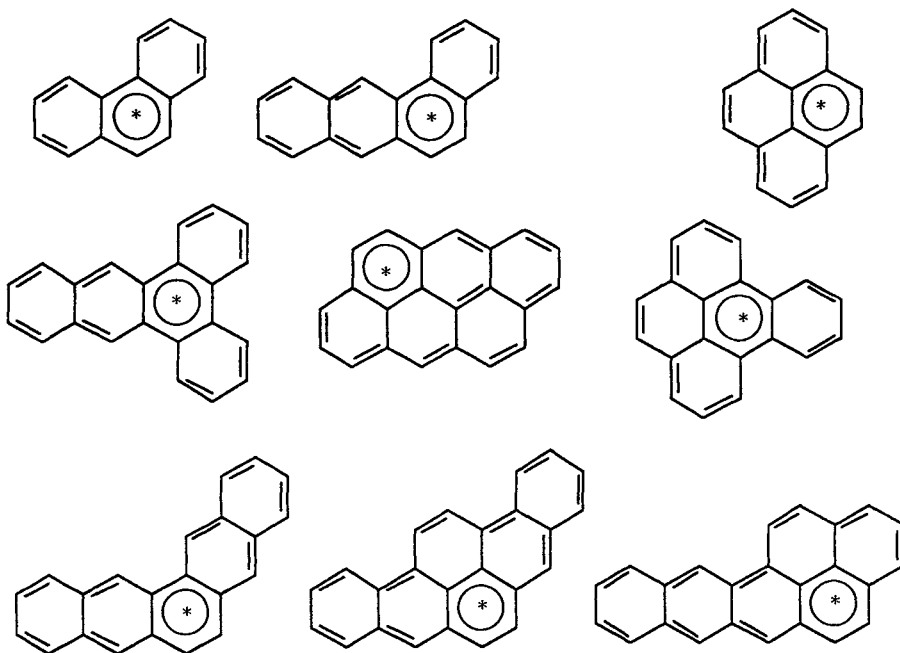
rings are replaces by one of Kekulé valence structures of benzene. For compounds considered only symmetry non equivalent k-Clar structures are shown. The compounds shown include benzo[a]-coronene, which is the benzenoid for which Clar speculated possible role of valence structure having less than the maximum number of π-aromatic sextets. Vulnerable rings have been recognized as critical in enumeration of Kekulé valence structures as outlined by Polansky and Gutman [18].

In fact, Polansky and Gutman [18] in their article on the number of Kekulé structures in fully benzenoid hydrocarbons, refer to such rings as "starred" rings and designated them by asterisk, the symbol that we have also adopted here. Vulnerable rings have been recognized also as critical for enumeration conjugated circuits as reported by Balaban and Tomescu [19]. They are the rings which participate in the so called "linearly dependent" conjugated circuits obtained by considering alternation of CC double and CC single bonds along periphery of phenanthrene, triphenylene and larger fragments (involving phenanthrene or triphenylene sub units) [20]. The same "vulnerable" rings apparently are associated with the

Fig. 24   Additional Herndon-Hosoya Clar structures in which the vulnerable rings have been indicated by asterisk which reduce to k-Clar structures (k ≠ 0)
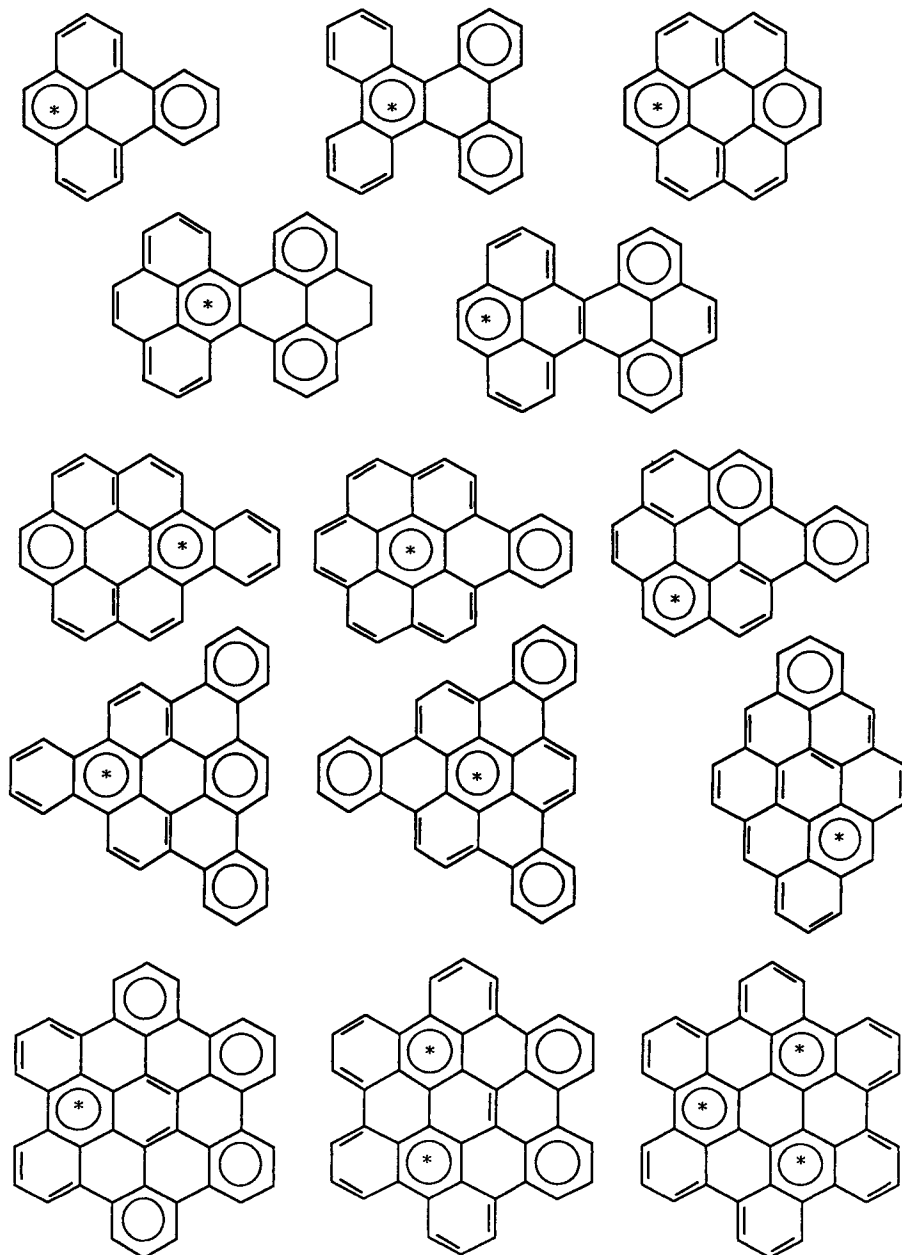
smallest Clar's index values. Clar index has been introduced by Randic, Plavsic and Trinajstic [21] as a measure of local benzenoid character for polycyclic benzenoid hydrocarbons. The index measures the relative contribution to the molecular resonance energy attributed to individual benzene rings.

6. CONCLUDING REMARKS

Probably the major hindrance to a wider acceptance of Clar's notions on characterization of benzenoid hydrocarbons by π-aromatic sextets in some circles is the apparent lack of the mathematical rigor behind the intuitive approach of Clar. One expect that "sound" theoretical model should be accompanied by some "sound" mathematical description. Hosoya and Yamaguchi, who introduced the sextet polynomial, were the first to cast some aspects accompanying Clar's model based on π-aromatic sextets, into appropriate mathematical formalism, but their approach was concerned with properties of generalized Clar structures, not the *proper* Clar structures. Among others who contributed to study of Clar's structures and generalized Clar's structures Gutman in particular devoted much of his talent to explore in greater fullness the mathematics behind this model. Because most of these mathematical explorations were concerned with generalized Clar-type structures, rather than "proper" Clar structures, this has left Clar π-electron sextets theory in very embryonic form. The basic concept and the foundations were based on argumentation derived from experimental observations, that is, being empirical. A theoretical approach to chemical structure using Clar's π-sextet was missing. With the novel mathematical definition of Clar structures, however, in our opinion the situation has been dramatically changed, for better, of course. At last, we can say, Clar's π-aromatic sextet has become a mathematical model. Hence the potential objection that critics may have considered in the past, that the model is a qualitative at best no longer holds as Clar's π-aromatic sextet emerges as legitimate variant of VB model. The task that remains is to see how this particular VB variants compares with other VB descriptions of benzenoid systems. We have to await for the answer, meanwhile, precisely because Clar's model evolved from considerations a selection of experimental data on UV and NMR spectral of benzenoid hydrocarbons we may expect that it may be supported by such experimental findings.

While in this contribution we focused attention to k-Clar structures, and to their relation to the Herndon-Hosoya type Clar structures, one can anticipate a number of interesting problems to emerge from the proposed innovation for π-aromatic sextets. It would be of interest to see, for instance, how k-Clar structures as a basis for semi-empirical VB

calculations of molecular RE compare with the calculations reported by Herndon and Hosoya when, what we call now HH-Clar structures, were used as a basis. Another area of exploration is to consider how the Model of Conjugated Circuits relates the contributions to RE of Kekulé valence structures of different degree of freedom. Apparently the novel definition of Clar structures highlights the concept of the innate degree of freedom, which thus comes to play a significant role in considerations of benzenoid hydrocarbons.

We may say that we have passed a long way from the early qualitative descriptions of aromatic compounds by a single, dominant, Kekulé structure, such as the Fries structures. We have also passed a long way from accepting a more "democratic" descriptions of benzenoids, in which all Kekulé valence structures play equal role. It appears that final solution is given by an obvious compromise that implies that "the truth is probably somewhere in between." But where "in between" has remained somewhat disputable. Different models, different quantum chemical calculations, different parametrizations of semi-empirical approaches, all suggest somewhat different answers. Among such alternative the notions of Clar π-aromatic sextet, which points to Kekulé valence structures of maximal degree of freedom as the most relevant, has a unique position. It offers a non-parametric characterization of benzenoid hydrocarbons, that may represent the ultimate characterization of benzenoids, and that may yield novel insights into chemistry of benzenoid hydrocarbons.

The successful accomplishments of Müllen and coworkers [22-25] who synthesized several giant benzenoid hydrocarbons will undoubtedly stimulate further theoretical interest in benzenoid hydrocarbons. It is not surprising that all the giant benzenoids that have been synthesized have 6n π-electrons, which Clar predicted to be unusually stable. Now that the "inverse" problem of Clar structures has been solved we may expect novel theoretical developments in this area that may continue to expand experimentally beyond expectations. For example, the Conjugated Circuit Model, that has already been applied to giant benzenoids [26-28], may have to be modified so to take into account the prominent role of the Clar structures of benzenoids rather then considering all Kekulé valence structures as equally important. Construction and enumeration of giant benzenoids and their Kekulé valence structures has also received some attention [29, 30].

REFERENCES

[1]   T. W. Armitt and R. Robinson, J. Chem. Soc. (1925) 1604.

[2]   E. Clar and M. Zander, J. Chem. Soc. (1958) 1861.

[3]   E. Clar, The Aromatic Sextet, John Wiley and Sons, London, 1972.

[4]   M. Randić, J. Chem. Inf. Comput. Sci. (submitted)

[5]   M. Randić and D. J. Klein, "Mathematical and Computational Concepts in Chemistry N. Trinajstic (ed.), Ellis Horwood Ltd., Chichester, England, pp. 274.

[6]   P. Hansen and M. Zheng (Prepint)

[7]   M. Randić, Chem. Phys. Lett. 38 (1976) 68.

[8]   K. Fries, Justus Liebigs Ann. Chem. 454 (1927) 121.

[9]   N. Trinajstić, Chemical Graph Theory (2nd ed.), CRC Press, Boca Raton, Fl., (1992) Chapter 8, pp. 161-198.

[10]   E. Clar, The Aromatic Sextet, John Wiley and Sons, London, 1972, p. 66.

[11]   H. Hosoya and T. Yamaguchi, Tetrahedron Lett., (1975) 4659.

[12]   N. Ohkami, A. Motoyama, T. Yamaguchi, H. Hosoya and I. Gutman, Tetrahedron, 37 (1981) 1113.

[13]   W. C. Herndon and H. Hosoya, Tetrahedron, 40 (1984) 3995.

[14]   M. Randić, H. Hosoya and K. Nakada, Polycyclic Aromatic Comp. 4 (1995) 249.

[15]   M. Gordon and W. H. T. Davison, J. Chem. Phys., 20 (1952) 428.

[16]   D. J. Klein, Int. J. Quantum Chem. Quantum Chem. Symp. 13 (1979) 293.

[17]   M. Randić and T. Pisanski,. Rep. Mol. Theory, 1, (1990) 107-114.

[18]   O. R. Polansky and I. Gutman, MATCH, 8 (1980) 269.

[19]   A. T. Balaban and I. Tomescu, Discrete Appl. Math. 19 (1988) 5.

[20]   X. Guo, M. Randić, and D. J. Klein, Int. J. Quantum Chem. 60, (1996) 943.

[21]   M. Randić, D. Plavšić and N. Trinajstić, Gazz. Chim. Ital., 118 (1988) 441.

[22]   F. Morgenroth, E. Reuther and K. Müllen, Angew. Chem. Int. Ed. Engl. 36, (1997) 631.

[23]   V. S. Iyer, M. Wehmeier, J. Brand, M. A. Keegstra, and K. Müllen, Angew. Chem. Int. Ed. Engl. 36, (1997) 1604.

[24]   M. Müller, V. S. Iyer, C. Kubel, V. Enkelmann and K. Müllen, Angew. Chem. Int. Ed. Engl. 36, (1997) 1607.

[25]   M. D. Watson, A. Fechtenkötter and K. Müllen, Chem. Rev. (2001)

[26]   M. Randić, Acta Chim. Slovenica, 44 (1997) 361.

[27]   M. Randic and X. Guo, New J. Chem. 23 (1999) 251.

[28]   M. Randić and X. Guo, Int. J. Quantum Chem. 74, (1999) 697.

[29]   C. Lin, J. Chem. Inf. Comput. Sci. 40 (2000) 778.

[30]   J. R. Dias, J. Chem. Inf. Comput. Sci. 39 (1999) 144.

This Page Intentionally Left Blank

Chapter 17

A valence bond view of fullerenes

T. G. Schmalz

Texas A&M University at Galveston,
Galveston, Texas 77553-1675, USA

1. INTRODUCTION

Since their discovery in 1985 [1] and subsequent isolation in macroscopic quantities [2], fullerenes and related forms of carbon such as nanotubes have been the subject of enormous numbers of both theoretical and experimental studies. This chapter describes a series of theoretical studies of fullerenes, concentrated on C_{60} buckminsterfullerene, the original and still the most common form, which are tied together by an underlying valence bond picture of chemical structure. This work has attempted to identify characteristics of fullerenes which are more easily discerned in a valence bond than in a molecular orbital picture, and to see how far these valence bond ideas can be pushed before they break down.

A number of fullerenes have been the subject of fully ab initio theoretical studies, and no attempt will be made here to review this work. However, for any but the smallest fullerenes these remain tremendously challenging computations due to the shear size of the molecules. Were it not for the extremely high icosahedral symmetry of buckminsterfullerene, most of the ab initio calculations which have been performed on it would still be impossibly time consuming even with modern computational resources. Even the largest of these, such as the TZP-MP2 (triple zeta plus polarization basis with electron correlation at the Moeller-Plesset 2nd order level) calculation on buckminsterfullerene of Häser, Almlöf, and Scuseria [3], are still short of the basis set and correlation levels normally desired to be confident that the calculation is converged to chemical accuracy. As a result, semiempirical theoretical methods have played, and likely will continue to play, a major role in theoretical work on fullerenes.

One semiempirical method which has been a workhorse in studies of fullerenes is the MNDO (Modified Neglect of Differential Overlap) method [4], which treats all valence electrons explicitly but within an essentially molecular

orbital framework. The MNDO method has proven quite good at predicting the energy ordering of closely related fullerene structures, but has been much less successful when used to compare rather diverse structures. In particular, it gives heats of formation for fullerenes relative to graphite in substantial quantitative disagreement with experiment [5]. This behavior is most likely related to the fact that the method does not include electron correlation in an explicit fashion. Thus in comparing atoms in similar chemical bonding environments, where correlation is likely to be of roughly the same importance, correlation effects can be modeled by suitable choices of parameter values, but when comparing atoms in rather different environments, with different degrees of correlation, discrepancies appear.

One of the goals of the studies described in this chapter has been to assess the importance of electron correlation in fullerenes, and so we have looked for theoretical methods in which electron correlation plays an explicit role. This has led us to focus on another widely applied class of semiempirical methods, those which attempt a sigma-pi separation of the electrons in a fullerene. While the advantages of such an approach are obvious – buckminsterfullerene is immediately reduced from a 360 to a 60 electron problem – the possibility of this kind of separation at first glance is not so obvious. Fullerenes clearly lack the usual requirement for such a separation, a planar, conjugated pi-electron system. However, they share many of the characteristics of molecules which are usually thought of in sigma-pi terms. Each carbon atom is bonded to three neighbors by an essentially localized bond which can be considered to result from overlap of nearly sp^2 hybridized orbitals between neighbors. Each atom has in addition one electron accommodated in a p-like orbital oriented normal to the fullerene surface. Although not perfectly aligned, these orbitals overlap significantly with the corresponding orbital on all three nearest neighbor atoms, so that these orbitals with their associated electrons form a rather delocalized bonding system, which will be termed the pi system.

There is substantial experimental evidence that many of the physical and chemical properties of fullerenes are strongly determined by these pi-like electrons. For example, all of the observed low-lying electronic excitations in buckminsterfullerene can be related to one electron excitations of pi electrons [5]. Much of the pattern of chemical reactivity of buckminsterfullerene has also been related to the greater pi electron density on the bonds lying on the edge of two hexagonal faces relative to that on an edge bounding a hexagon and a pentagon [6]. It thus seems useful to attempt theoretical studies within the framework of an assumed sigma-pi separation, and this is the approach which will be followed in this chapter. Of course, this approach has been very widely used in studies of fullerenes, but almost always in one particular guise, that of Hückel molecular orbital theory. But a pi electron view of fullerenes does not in any way limit one to Hückel theory, and if the goal is to include electron

correlation it is essential not to be limited to Hückel theory. Instead, it is important to investigate the valence bond treatment of the pi electrons.

2. HÜCKEL VERSUS VALENCE BOND PI ELECTRON MODELS

2.1 The Hückel Model

The Hückel molecular orbital (HMO) model of pi electrons goes back to the early days of quantum mechanics [7], and is a standard tool of the organic chemist for predicting orbital symmetries and degeneracies, chemical reactivity, and rough energetics. It represents the ultimate uncorrelated picture of electrons in that electron-electron repulsion is not explicitly included at all, not even in an average way as in the Hartree Fock self consistent field method. As a result, each electron moves independently in a fully delocalized molecular orbital, subject only to the Pauli Exclusion Principle limitation to one electron of each spin in each molecular orbital.

Quantitatively, HMO theory has proven to be of limited utility for fullerenes. HMO calculations have been performed for thousands of fullerenes, and one important correlation has emerged: fullerenes with zero or small HOMO-LUMO (Highest Occupied Molecular Orbital-Lowest Unoccupied Molecular Orbital) gaps at the Hückel level are almost never found experimentally, presumably because of high reactivity. Unfortunately the reverse correlation does not hold. For fullerenes with reasonably large HOMO-LUMO gaps there does not seem to be a correlation between the size of the gap and the likelihood that the fullerene will be formed. Additionally, the total pi electron energies of all fullerene isomers with a given carbon number are usually close, and there does not seem to be a strong correlation between the computed total energy and the stability of the isomer.

2.2 The Valence Bond Model

There is, however, another pi-electron model with an historical pedigree comparable to that of Hückel theory. In the valence bond (VB) view [8, 9], the electrons are viewed to interact so strongly that there is negligible probability of finding two electrons in the same atomic orbital. The wave function is thus considered to be dominated by purely covalent contributions in which each electron is spin paired to one other electron. The most important of these are the spin pairings limited to nearest neighbor (bonded) atom pairs, namely the Kekulé structures. The delocalized nature of the wave function then results from resonance among these different localized spin-paired structures. This picture represents the ultimately correlated picture of pi electrons, in that motion of any one electron requires concerted reorganization of the entire, or at least a substantial portion of, the pi electron system.

In practice, the valence bond picture has probably exerted more influence on how chemists actually think than the HMO picture. However most early applications were primarily qualitative in nature. This qualitative VB picture can be summarized under the name of resonance theory [10]. The basic concept is that in general the more ways one has of arranging the spin pairing in the VB wave function, the more stable the molecule is likely to be. Thus, VB theory predicts that phenanthrene with 14 carbon atoms and 5 Kekulé structures should be more stable than anthracene with 14 carbon atoms but just 4 Kekulé structures, in complete accord with the experimental evidence. It also predicts that benzenoid hydrocarbons with no Kekulé structures should be unstable and highly reactive, and in fact no such compounds are known. Extensions of this qualitative picture appear, for example, in Clar's ideas of resonant sextets [11], which seem to be very powerful in rationalizing much of the chemistry of benzenoid aromatic hydrocarbons. The early ascendancy of HMO theory was thus largely based on the ease with which it could be used for quantitative computations rather than on any inherent superiority of its fundamental assumptions.

2.3 Resonance Models

An important step forward was introduced by Herndon [12] who, building on the work of Simpson [13], showed how to express the resonance stabilization due to conjugated rings in terms of a few simple empirical parameters, an approach which he called Quantitative Resonance Theory. This approach was subsequently recast in a computationally more useful form by Randic´ [14] and is widely used under the name of Conjugated Circuit Theory [15]. This model expresses the resonance energy of a molecule in terms of contributions from each conjugated circuit, where a conjugated circuit refers to a closed path of alternating single and double bonds within any of the Kekulé structures of the molecule. Each size of circuit is given an empirical energy weighting in accordance with the Hückel $4n/4n+2$ rule: circuits of size 4,8,12... are destabilizing while those of size 6,10,14... are stabilizing, with diminishing contributions as the size of the circuit grows. Finally, Klein [16] showed how all of the needed structural information about the molecule can easily be extracted from a few minors of the adjacency matrix. Thus Conjugated Circuit computations require as input only the pattern of connectivity of the conjugated atoms in the molecule, the same input information needed for Hückel theory, and can be carried out in a comparable amount of computer time. They are therefore an attractive complement to Hückel calculations since, though also highly approximate, they approach the solution from the opposite, highly correlated, valence bond limit.

2.4 The Heisenberg Model

An even more quantitative application of VB theory can be developed from the realization that the nearest-neighbor VB model as developed, for example, by Pauling [10], can be mapped exactly onto a Heisenberg spin Hamiltonian [17]. The Heisenberg spin Hamiltonian has long been used to study the interaction between magnetic atoms in transition metal compounds and other paramagnetic substances [18], and can be written most simply as

$$H'_{Heis} = \Sigma_{i<j} J_{ij} S_i \cdot S_j \qquad (1)$$

where each atom is assumed to have only one active orbital contributing one electron to the spin system, J_{ij} is a (positive for antiferromagnetic) spin-spin coupling constant, and S_i is the ordinary spin operator for an electron in the orbital on atom i. However to represent the valence bond model of hydrocarbons it is useful to shift the spectrum and to restrict the interaction to nearest neighbor carbon atoms (ie., those directly connected by a sigma bond). Therefore we take the Heisenberg Hamiltonian in the form

$$H_{Heis} = J \Sigma_{i\sim j} (2S_i \cdot S_j - 1/2) \qquad (2)$$

where the notation i~j denotes summation over bonds. The choice of the value for the coupling constant J will be discussed in the next section.

Solution of the Schrödinger equation with the Hamiltonian of Eq. (2) can be carried out in a variety of ways, but the most compact representation of the wave function is achieved by using a basis which is symmetry adapted to either the symmetric group (Young-Yamanouchi basis) or the unitary group (Gelfand basis). Programs are available which utilize the same graphical lookup techniques which have been developed for ab initio molecular orbital calculations to efficiently organize the evaluation of integrals [19,20]. These programs make possible the exact (to within a predefined adjustable error limit) solution for the ground state energy and wave function of molecules with up to about 30 pi centers.

2.5 The Pariser-Parr-Pople/Hubbard Model

Finally, for purposes of comparison, it is useful to have a pi electron model which makes neither the Hückel nor the VB assumptions about the strength of the electron-electron interaction. Such a model can provide a smooth bridge between the Hückel and Heisenberg models as the relative strength of the chemical bonding and electron repulsion interactions between electrons are changed. Such a role is played by the Pariser-Parr-Pople (PPP) model [21,22], and its close relative, the Hubbard model [23]. The PPP model can be

considered to result from a systematic application of the zero differential overlap (ZDO) approximation to the pi electron Hamiltonian expressed in a basis of orthogonalized atomic orbitals.

The one electron part of the Hamiltonian is treated as in Hückel theory. Only one center and two center one electron integrals are given nonzero values, and the latter are restricted to nearest neighbor (bonded) pairs of atoms. These integrals represent the kinetic energy and effective attraction of an electron moving in the potential of the nuclei and sigma bonds. For molecules with only one kind of atom such as fullerenes, the one center integrals (the α's of Hückel theory) just introduce a uniform shift in the spectrum and can be taken as zero. The two center integrals, usually denoted t, are responsible for chemical bonding and are identical to the β's of Hückel theory.

The two electron part of the Hamiltonian (which is missing completely in Hückel theory) introduces the effects of electron-electron repulsion, and hence electron correlation. Within the ZDO approximation all two electron integrals which contain a two center overlap distribution are set to zero, on the grounds that such integrals are small for orthogonal orbitals. The remaining integrals are all of the coulomb form, but are usually taken as a simple function of the value of the one center coulomb integral and the distance between the atoms. The two most common expressions used in the literature (in atomic units) are those of Ohno [24]:

$$\gamma_{ij} = 1/(\gamma_0^{-2} + r_{ij}^2)^{1/2} \tag{3}$$

and of Mataga and Nishomoto [25]:

$$\gamma_{ij} = 1/(\gamma_0^{-1} + r_{ij}) \tag{4}$$

where γ_{ij} is the coulomb repulsion integral for two orbitals separated by a distance r_{ij} and γ_0 is the one center coulomb integral which is taken as an empirical parameter.

The PPP Hamiltonian can then be written in second quantized form as

$$H_{PPP} = \Sigma_{<ij>} t_{ij} E_{ij} + \Sigma_i \gamma_0 a^\dagger_{i\alpha} a^\dagger_{i\beta} a_{i\beta} a_{i\alpha} + \Sigma_i \Sigma_{j<i} \gamma_{ij}(E_{ii}-1)(E_{jj}-1) \tag{5}$$

where the notation $<ij>$ means the first double sum is nonzero only when atom i and atom j are nearest neighbors, $\sigma = \alpha, \beta$, and $E_{ij} = \Sigma_\sigma a^\dagger_{i\sigma} a_{j\sigma}$, in terms of usual creation and annihilation operators. The PPP model Hamiltonian is believed to be the simplest model which includes all of the most important physical effects in conjugated pi electron systems, and has been widely and successfully used to the study the electronic properties of aromatic hydrocarbons.

Formally, the Hubbard model can be derived from the PPP Hamiltonian by setting all two center coulomb integrals γ_{ij} equal to zero. However, a more informative derivation recognizes that the remaining coulombic term is in essence a measure of the energy cost of moving an electron from a covalent state with one electron per atom to an ionic state in which one atomic orbital is empty and that on a nearby site is doubly occupied. The energy cost for doing this is approximately γ_0-γ_1 where γ_1 is a typical nearest neighbor coulomb integral, because the electron which moves now feels a repulsion from the other electron in its new orbital but none from the orbital which it has vacated. The Hubbard Hamiltonian thus involves only the first two terms of Eq. (5), and for equivalent atoms can be written as

$$H_{Hubb} = \Sigma_{<ij>} t_{ij} E_{ij} + U \Sigma_i a^\dagger_{i\alpha} a^\dagger_{i\beta} a_{i\beta} a_{i\alpha} \qquad (6)$$

with $U \approx \gamma_0$-γ_1 representing the effective strength of the electron repulsion.

The exact FCI (full configuration interaction) solution of the PPP or Hubbard model is possible for molecules with up to about 16 atoms in the pi system. Any of the standard methods for performing approximate ab initio calculations, such as limited configuration interaction, Moeller-Plesset perturbation theory, or coupled cluster theory, may be applied to these models as well. All are expected to be very accurate at low order when U is small, but all will have to be pushed to higher order as U increases.

2.6 Relations among the models

The Hubbard model is essentially a one parameter model in the ratio $U/|t|$ where t is an average t_{ij}, since the magnitude of t just sets the energy scale, and is the simplest many body Hamiltonian to include electron correlation explicitly. When U is equal to zero it reduces exactly to the Hückel model, while for large U many body perturbation theory or cluster expansion methods can be used to map its spectrum exactly onto the Heisenberg model. If the t_{ij} are taken the same for all bonds, perturbation theory gives $J=2t^2/U$ for the Heisenberg model [26], while the cluster expansion derivation gives $J=((U^2 + 16t^2)^{1/2} - U)/4$ [27,28]. The latter expression has the advantage of accurately tracking the Hubbard model to much smaller values of U than the perturbation theory expression. The Hubbard model thus spans the entire range from independent particle to highly correlated electron behavior as a function of the ratio $U/|t|$, and has been of great value in studying the role of correlation effects.

An instructive view of the relation between the spectra of the Hückel model (U=0), the Heisenberg model (U large) and the Hubbard model is provided in Fig. 1. Those states described by the Heisenberg model are all of covalent

542
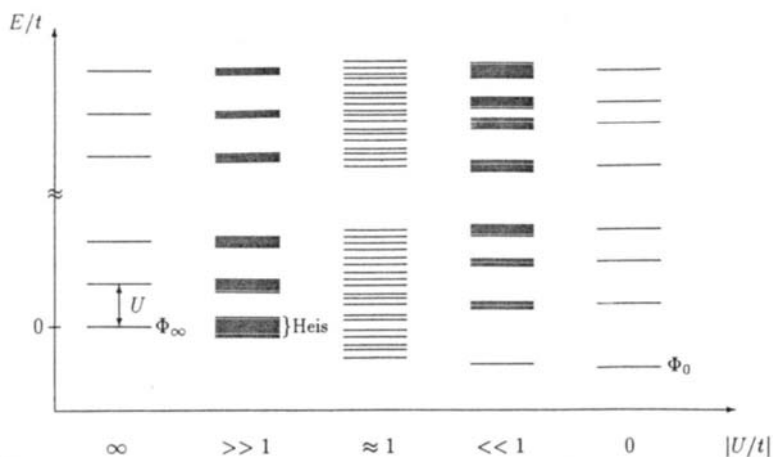
Fig. 1. A schematic representation of the spectrum of the Hubbard model as the effective electron repulsion U varies from very large (Valence Bond limit) to zero (Hückel limit).

parentage, since for large U the energy cost of doubly occupying a site is too large. For small U all low-lying states can be clearly identified as one electron excitations from the Hückel orbitals. But in the physically realistic regime in which U is approximately of the same magnitude as t, neither of these limits is easily discernable. In fact, it has been shown that the Hubbard model itself does not accurately describe excited states with significant ionic parentage [29], the long range coulomb interactions dropped in going from the PPP model to the Hubbard model being much more important for ionic than for covalent states. However, for the ground state, and usually for several of the lowest-lying excited states, it is often possible to draw a correlation diagram which goes smoothly from the lowest manifold in the MO limit to the lowest manifold in the VB limit, without avoided crossings, and for these states the Hubbard model is quite useful.

In the following sections results will be reported of conjugated circuit calculations on a variety of fullerenes, of Heisenberg calculations on buckminsterfullerene, some of its isomers and derivatives, and a few smaller fullerenes, and of Hubbard/PPP calculations primarily on buckminsterfullerene, while attempting to emphasize both the strengths and the limitations of the VB picture of these molecules.

3. CONJUGATED CIRCUIT RESULTS

Conjugated circuit calculations have been performed for all 1812 isomers of C_{60} fullerene [30,31]. As expected, the largest (most negative) resonance energy value occurs for buckminsterfullerene, the only experimentally stable isomer. These results provide strong evidence in support of one of the most important structural rules concerning fullerene stability, the "isolated pentagon rule". So far, all fullerenes which have been prepared in significant quantity with the exception of the recently produced C_{36} [32] have only pentagonal rings surrounded completely by hexagonal rings. Buckminsterfullerene itself is the smallest fullerene for which this is possible, and this observation was part of the original rationale for believing in the fullerene structure of the prominent C_{60} mass spectral peak prior to the isolation and structural characterization of C_{60}. We originally proposed this rule in light of the conjugated circuit analysis of resonance energy, which shows that destabilizing conjugated eight circuits develop around the periphery of any two pentagons which share an edge [33]. Kroto has shown that abutting pentagons also lead to greater strain in the sigma bond system [34], so taken together these two factors strongly mitigate against fullerene isomers containing fused pentagons.
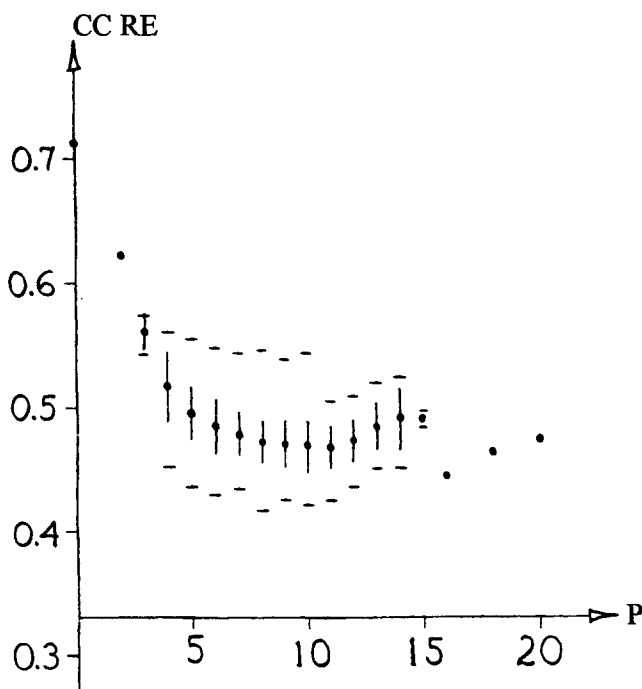
Fig. 2. The resonance energy per site, relative to graphite, computed from conjugated circuit theory as a function of p, the number of bonds contained in two pentagonal rings.

Fig. 2 shows the resonance stabilization per atom of C_{60} isomers relative to graphite as computed from conjugated circuit theory using the parameters of Herndon (uncorrected for curvature), plotted versus p, the number of carbon-carbon bonds shared between two pentagonal faces. At least for small p, the general decrease in resonance stabilization with p is quite obvious. A similar comparison at the all electron level using MNDO theory [35] shows the same decreasing trend of stability with increasing p for p less than or equal to 4, and there now seems to be agreement based on ab initio calculations that each pentagon-pentagon contact involves an energy cost in the vicinity of 1.5 ev [5].

On the other hand, the trend of decreasing pi electron stability with p is not at all evident from HMO total pi electron energies. While buckminsterfullerene does have the largest total energy, the HMO pi electron energies per site (also without correction for curvature) of almost all C_{60} isomers lie between 97% and 99% of that of graphite, and it is difficult to detect the dependence on p. Thus the isolated pentagon rule is one case where a valence bond based analysis reveals an important trend which is much more difficult to discern in the MO picture. (To be fair, it is possible to elucidate the dependence on p from HMO energies by defining more sophisticated measures of resonance energy, but these methods involve resonance concepts based on Kekulé structures, and essentially try to restore the missing VB concepts to Hückel theory.)

A second structural trend in pi electron stability emerges from an analysis of conjugated circuit calculations for isolated pentagon isomers of fullerenes in the size range of 60 – 100 carbon atoms which can also be given a valence bond interpretation. Although there is considerable scatter in the resonance energy values for different isomers, and no clear trend with size, certain structures clearly stand out as possessing unusual pi electron stability. We have called these isomers "Clar sextet" fullerenes [36], but they are elsewhere referred to as "leapfrog" isomers [37, 38]. In resonance theoretic terms these isomers possess special Kekulé structures in which every double bond participates in two conjugated six circuits [36]. Stated in another way, these fullerenes possess the property that if all atoms contained in five-membered rings were removed, the remaining portions of the carbon skeleton (if any) would be "fully aromatic" in Clar's sense [11], and thus presumably especially stable. Buckminsterfullerene is the smallest fullerene which possesses one of these special Kekulé structures, and can be viewed as the first member of a family with $v=60 + 6n$ carbon atoms, with n any integer except one.

The special stability of the pi system for the Clar sextet isomers stands out clearly in the conjugated circuit computations [36], and in this case is also evident from HMO calculations, particularly from the HOMO-LUMO gaps which are uniformly large for these isomers. Unfortunately, the relevance of the Clar sextet criterion to experimental stability is not yet proven. While buckminsterfullerene is certainly especially stable, C_{72} has not been prepared in

macroscopic quantities, and the Clar sextet isomer of C_{78} is not one of the experimentally observed isomers [39]. Examination of models of these latter two structures reveals them to be rather "squashed" and thus probably relatively highly strained. Unlike the isolated pentagon rule where increased pi stability and decreased sigma strain apparently go together, there does not seem to be any such correlation for Clar sextet cages. It is thus quite possible that sigma strain energy, rather than pi stability, will turn out to be the dominant factor in determining the relative stability of larger isolated pentagon cages. Including a reasonable measure of sigma strain in pi electron calculations of fullerenes – by any pi electron theory - remains an unsolved problem which warrants further research.

4. HEISENBERG CALCULATIONS

4.1. The Kekulé basis

Quantitative implementation of the valence bond model for pi electron systems is most conveniently achieved by solving a Heisenberg spin Hamiltonian. In the simplest valence bond model the Hamiltonian is limited to products of spin operators for two atoms linked by a sigma bond in the molecule under study. The exact ground state energy and wave function for such a Hamiltonian can most easily be found using a complete spin basis symmetry adapted to orthogonal irreducible representations of the unitary or symmetric group. Calculations are feasible for molecules with up to about 30 atoms in the pi system [19,20]. Although much easier to solve than a Hamiltonian not limited to the covalent space, the Heisenberg model cannot be solved exactly for a molecule as large as buckminsterfullerene, so some approximate method is needed for fullerene studies. Even for small molecules, the wave function expressed in unitary or symmetric group form is not easily interpreted in chemical terms, so an attractive approach is to investigate the model in truncated basis sets motivated from valence bond theory. The most important such functions are the Kekulé functions, which are found by partitioning the set of N (even) atoms in the molecule into N/2 disjoint nearest-neighbor pairs and forming a singlet spin pairing for each pair of sites. A Kekulé function, up to sign, is just the product of the singlet functions for each such pair of sites.

For molecules of more than a few atoms the number of Kekulé functions is orders of magnitude smaller than the size of the complete spin basis, and finding the variational ground state of the Heisenberg model within the space of Kekulé functions is quite feasible for molecules the size of buckminsterfullerene which has 12,500 Kekulé functions [40]. Yet this type of simple resonating valence bond (RVB) approximation often yields a surprising good variational estimate of the ground state energy. Table 1 presents a comparison of the exact FCI ground

Table 1

Full CI ground state energy of the Heisenberg model (Eq. 1) in units of J

Molecule	Complete basis	Kekulé basis	percent
benzene	-2.8028	-2.7000	96.33
pentalene	-3.5483	-3.2500	91.59
azulene	-4.4440	-3.9265	88.35
naphthalene	-4.7700	-4.4352	92.98
anthracene	-6.7252	-6.0750	90.33
phenenthrene	-6.7613	-6.2624	92.62
naphthacene	-8.6791	-7.6650	88.32
benz[a]anthracene	-8.7222	-7.9489	91.13
benzophenanthrene	-8.7466	-8.0470	92.00
chrysene	-8.7475	-8.0470	91.99
triphenylene	-8.7697	-8.1534	92.97
coronene	-11.9755	-10.8218	90.37
benz[a]coronene	-13.9764	-12.6688	90.64
C_{20} (I_h)	-9.7222	-8.9658	92.22
C_{24} (D_{6d})	-11.7194	-10.4781	89.41
C_{26} (D_{3h})	-12.6090	-10.9596	86.92
C_{28} (T_d)	-13.5749	-11.7230	86.36
C_{28} (D_2)	-13.8602	-12.3118	88.83
C_{30} (D_{5h})	-14.8873	-13.2328	88.89

state energy to the energy calculated from the Kekulé basis, using the unshifted Heisenberg Hamiltonian Eq. 1, for a series of small molecules on which the exact calculation is feasible [41,42]. Included are several small fullerenes and some other nonalternant molecules as well as several classical benzenoids. Although the Kekulé basis seems to do slightly better for the benzenoid aromatics, the difference is not great, and for all molecules except the very small benzene where the Kekulé basis is nearly complete, the limited basis recovers between 88% and 93% of the exact energy. Yet for C_{30} the Kekulé basis has just 151 functions compared to 9,694,845 in the complete basis!

Accordingly, the solution of the Heisenberg model for buckminsterfullerene in the Kekulé basis is expected to yield a reasonable first approximation to the exact solution. This calculation has been carried out [43], yielding a ground state energy of $-27.899051J$ for the Hamiltonian of Eq. 1. If it is assumed that this represents approximately 90% of the exact energy for the unshifted Hamiltonian, then the VB energy corresponding to Eq. 2 should be something in the vicinity of $-107J$. If we assume a typical value of J for hydrocarbons of about 1.75 ev, this gives an estimate of the total VB pi electron energy for buckminsterfullerene of about -187 ev. This can be compared with the value of -93.162β from simple Hückel theory, which with a standard value of β of -2.5 ev would translate to about -233 ev, a considerable difference. The spin-spin correlation functions (proportional to the negative of the spin bond order) are also readily computed from the Kekulé wave function, giving $<S_i \cdot S_j> = -0.5328$

for the 6-6 bonds separating two hexagons and $<S_i S_j> = -0.1960$ for the 6-5 bonds separating a pentagon and a hexagon [43]. This indicates a substantial tendency for the pi bonds to localize on the 6-6 positions, in agreement with the chemical evidence. The difference in bond order is significantly larger than that computed from Hückel theory, which is consistent with the smaller resonance stabilization (less negative pi energy) predicted by the Heisenberg model.

The Kekulé wave function also yields considerable insight into the structure of buckminsterfullerene. Since buckminsterfullerene is a Clar sextet molecule, it has the special Kekulé structure which places double bonds on all 30 of the 6-6 edges. Since the pi electrons tend to localize to these positions, this Kekulé function should be the most important single contributor to the ground state wave function, while Kekulé functions with many double bonds in 6-5 positions should be less important. Fig. 3 shows the absolute value of the wave function coefficient for each Kekulé structure as a function of the number of double bonds in 6-5 positions. The expected decreasing trend is clearly observed, but something else stands out as well. The Kekulé functions divide into two classes, separated by the solid line in the figure. This separation is a reflection of the nonalternant character of a fullerene.

A hydrocarbon is said to be alternant if the carbon atoms can be separated into two groups, usually designated starred and unstarred, such that starred atoms are bonded only to unstarred atoms and vice versa. All benzenoid
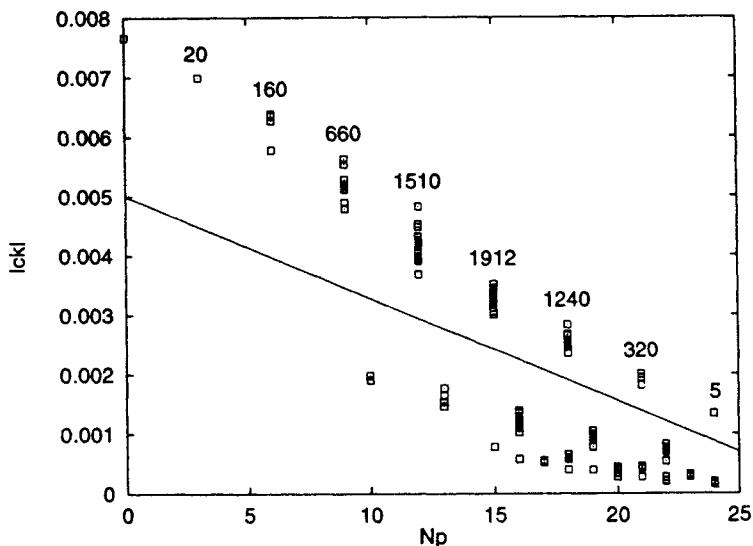
Fig. 3. Wave function coefficients as a function of the number of 6-5 bonds in a Kekulé structure. Numerical values show the number of Kekule functions in each group.

hydrocarbons have this property but any molecule containing a ring with an odd number of atoms does not. Since fullerenes contain 5-membered rings to produce the curvature needed to close them into a spherical structure, all fullerenes are nonalternant. The definition of a Kekulé function given at the beginning of this section defines a Kekulé structure only up to its sign. For alternant molecules there is a natural way to assign the signs so that all Kekulé functions have a positive overlap with each other, and it is found [44] that all functions contribute to the ground state wave function with the same sign. It is just necessary to build each spin function in the Kekulé function in the form $\alpha_i\beta_j-\beta_i\alpha_j$ with i always a starred atom and j always an unstarred atom.

On the other hand, for nonalternant molecules it is generally not possible to choose signs for the Kekulé functions so that all pairs of functions have a positive overlap. Indeed, for buckminsterfullerene the Kekulé functions divide into two classes. One group, containing 5,828 of the 12,500 Kekulé structures including the special structure with no double bonds on 5-5 edges, can be given signs so that they have positive overlap with all other members of the group. All of the other Kekulé functions, no matter how chosen, have negative overlap with some members of the first group. This first group of "aromatic" functions, which behave like those in traditional aromatic benzenoids, can be given a simple graphical interpretation. They are all of the Kekulé functions which can be derived from the special starting function by interchange of single and double bonds in disjoint 6-membered rings, ie., by moving bonds only in rings which share no edges. Interestingly, in the ground state wave function, the weights of all of the aromatic Kekulé functions lie above the solid line in Fig. 3, while the weights of all of the remaining functions lie below the line. If the Heisenberg energy is computed using just the 5,828 aromatic functions, the value found is 99.82% of the energy computed with the full Kekulé basis [43]. Thus the ground state wave function is effectively totally dominated by these classically aromatic functions. The perturbation introduced into the resonance pattern by the 5-membered rings is essentially negligible.

The Heisenberg model in the Kekulé basis has also been used to study isomers and derivatives of buckminsterfullerene. It agrees with other theoretical methods [5] in showing the isomer derived from buckminsterfullerene via one Stone-Wales rotation to be the next most stable C_{60} fullerene [43]. Addition products are modeled [41] simply by removing all bonds to the saturated sites from the Hamiltonian, and the Heisenberg model also agrees with other methods in showing addition to the ends of a bond along the edge of two hexagons to be most favored. It differs from some other methods in predicting further addition to atoms in the same hexagonal ring to be favored over additions to 6-6 bonds in other parts of the molecule. This is consistent with the resonance theoretic interpretation of the wave function, because once conjugation around one ring is

destroyed further additions to that hexagon do the least damage to resonance structures in the remainder of the molecule. On the other hand, strain in the sigma system, which is not included in the Heisenberg model, is probably minimized when the addition sites are far apart, so we may have here another situation where the experimental addition pattern is determined by a subtle balance between resonance and strain. This emphasizes again the need for semiempirical methods which treat both pi energy and sigma strain accurately.

4.2. Larger basis sets

Though chemically informative, the Kekulé basis is clearly not a complete description of the ground state of fullerenes, since the energy derived from it for buckminsterfullerene is well short of variational bounds for the Heisenberg energy available from Monte Carlo calculations using the Gutzwiller wave function anzatz [45,46]. In the Gutzwiller approach the wave function is optimized with respect to a single variational parameter, which however introduces a weight for every function in the complete basis, rather than allowing independent variations for each of a restricted subset of basis functions. To approach the complete basis limit using unconstrained variation, it is necessary to include functions with longer bonds, that is with spin pairings between atoms which are not connected by sigma bonds. The importance of functions with one long bond has been investigated [42], and as expected, there is a general decrease in importance as the length of the long bond increases. However, there is a strong even-odd modulation. Functions with odd-length bonds, which of course include the Kekulé functions, are much more important than functions with even-length long bonds. This is additional evidence of the minor role played by the nonalternant character of buckminsterfullerene. In an alternant molecule the wave function can be expressed completely in terms of structures with odd-length bonds only, and the fact that even-length functions are not very important in buckminsterfullerene is additional evidence of the similarity of buckminsterfullerene to traditional benzenoid aromatics.

Even inclusion of all functions with one long bond in the basis does not reach the full CI complete basis limit of the Heisenberg model, so additional functions with two or more long bonds would have to be added in a quantitatively accurate treatment of the model. Just as the importance of functions decreases with the length of the long bond, it should also decrease with the number of long bonds. Numerical results for small molecules [42] indicate that addition of functions with just two length three long bonds, in addition to the single long bond and Kekulé functions, might be adequate, but this results in a basis more than a thousand times bigger than the Kekulé basis, and is beyond present computational capabilities for buckminsterfullerene. However expansion of the basis seems unlikely to alter the basic picture of the ground state wave function,

which can usefully be viewed as dominated by the RVB resonance combination of Kekulé structures.

5. HUBBARD CALCULATIONS

5.1. Correlation methods

The last section addressed efforts to approach the exact wave function and energy of the Heisenberg model Hamiltonian, but this Hamiltonian itself is, of course, only an approximate model, most valid when the effective repulsion between electrons is large compared to the bonding interaction between them. Unfortunately, reasonable parameter values for carbon atoms indicate that while the effective repulsion energy is probably larger than the bonding energy, it is not much larger. Buckminsterfullerene, as well as other fullerenes and hydrocarbons, are likely to fall near the middle of Fig. 1, perhaps at a $U/|t|$ ratio of 1.5-2.0. In this region the electronic spectrum is at its most complicated, it is difficult to recognize either the Hückel or Heisenberg limit parentage of most states, and the computational demands of even approximate quantum chemical calculations are most extreme. One possible approach to a better description of molecules under these conditions is to extend the perturbation theory or cluster expansion derivations of the Heisenberg model to higher order to include more than two particle interaction terms in an effective Hamiltonian. Presumably Kekulé based RVB methods and resonance theory ideas from valence bond theory can be extended to provide approximate solutions for these more accurate model Hamiltonians. Unfortunately, such methods are not yet well developed computation tools, so we have elected to approach the solution of more accurate Hamiltonians from the opposite independent particle limit.

The advantage of approaching the solution of semiempirical pi electron model Hamiltonians from the IPM (independent particle model) limit is that many highly developed computational methods from ab initio quantum chemistry can be taken over bodily. In ab initio calculations on most stable closed shell molecules, using ab initio rather than empirically adjusted values for all electronic integrals, it is usually found that the independent particle Hartree-Fock description of the wave function is an excellent starting approximation. Several standard methods with different strengths and weaknesses are available for adding electron correlation, including configuration interaction (CI), Moeller-Plesset perturbation theory, and coupled cluster (CC) theory. While these methods are frequently accurate at low order in ab initio computations, all will break down if the strength of the electron correlation becomes too large, so an important first question is to investigate their adequacy for pi electron model Hamiltonians. The Hubbard model is well suited for this task, since it includes electron correlation with a strength which can be varied via a single parameter, the $U/|t|$ ratio.

Table 2
Hubbard model energy of fluoranthene at different levels of correlation (in units of $|t|$)

U/|t|	0.5	1.0	1.5	2.0	4.0	8.0
E_{HF}	-20.4982	-18.5962	-16.4943	-14.4923	-6.4845	9.5310
E_{SD}	-20.5598	-18.7357	-17.0103	-15.3624	-9.2234	2.2755
+DD	-20.5605	-18.7461	-17.0585	-15.5006	-10.6557	-9.1756
MP2		-18.7456		-15.4902		
E_{SDTQ}	-20.5605	-18.7459	-17.0566	-15.4898	-10.2155	-1.7868
E_{FCI}	-20.5605	-18.7461	-17.0589	-15.5015	-10.6192	-5.9423
CE	-22.0350	-19.4889	-17.2979	-15.4267	-10.3391	-5.8925
PT	-99.8436	-49.9218	-33.2812	-24.9609	-12.4804	-6.2402

Table 2 shows results [47, 48] for the total ground state energy of the Hubbard model of fluoranthene, with electron correlation treated by several approximate methods, as a function of the ratio $U/|t|$. Fluoranthene is near the size limit for which the FCI energy can be computed, and its carbon skeleton can be considered to be a fragment of the surface of buckminsterfullerene, but the results are quite typical of other small molecules. One of the simplest correlation methods is to mix, variationally, the Hartree-Fock SCF (Self Consistent Field) determinant with all of those which differ from it by replacement of just a small number of atomic orbitals. By the Brillouin theorem, single replacements (singly excited determinants) do not mix directly with the SCF function, denoted Φ_0, but doubly excited determinants mix both with Φ_0 and with single excitations, so the lowest-order nontrivial configuration interaction treatment can be denoted SDCI. For fluoranthene this treatment is seen to be essentially exact when $U/|t|$ is equal to 0.5, since Φ_0 itself is the exact ground state wave function when U=0, and it is still very accurate when $U/|t|$=1.0. But in the important range of $U/|t|$ between 1.5 and 2.0 significant errors begin to appear and for larger ratios this treatment is clearly inadequate.

Additional correlation can be included in the wave function by adding triple and quadruple excitations (SDTQCI), but such computations are much more time consuming. Table 2 shows two much cheaper methods to estimate the effects of higher excitations, a generalization of the Davidson correction [49] due to Duch and Diercksen [50] (denoted DD), and Moeller-Plesset 2nd order perturbation theory [51]. Both are in excellent agreement with the SDTQCI result, as well as the FCI limit, through $U/|t|$=2.0 and may still be quite useful at $U/|t|$=4.0, but of course all of these limited methods break down when U becomes very large. Nevertheless, it seems that IPM methods based on either generalized Davidson or perturbation corrections to the SDCI wave function may be sufficient in the experimentally relevant range of $U/|t|$ values, at least for small molecules. Of course, the SDCI method is not size extensive, meaning that it recovers an increasingly small fraction of the correlation energy relative

to the SCF wave function, as the size of the molecule increases. Thus either the DD or MP2 methods must "work harder" for larger molecules, and we cannot guarantee that they will be as successful for a molecule as large as buckminsterfullerene.

Before considering the Hubbard model for fullerenes, it is of some interest to compare the Hubbard model results to those of the Heisenberg model for fluoranthene, which are shown in the bottom half of Table 2. The Hubbard model maps exactly onto the Heisenberg model for very large U, but for smaller U we can still approximate the Hubbard model by a nearest-neighbor Heisenberg Hamiltonian using either the perturbation theory or cluster expansion expressions for J as a function of t and U given in section 2.6. As can be seen, $U/|t| > 8.0$ is needed to make these approximations fully quantitative, but both are much better than the IPM approaches at large U. The perturbation based treatment (PT) becomes wildly inaccurate at smaller U, but the Heisenberg model with the cluster expansion (CE) value for J is a good approximation – certainly much better than the Hartree-Fock approximation – down to $U/|t|=1.5$, and it is not completely unreasonable all the way down to zero correlation! This provides strong evidence that the VB model itself is physically reasonable and is not just a mathematical artifact of the empirical integral rescalings used to generate the pi electron Hamiltonian. It also emphasizes again the importance of considering correlated methods such as VB theory in the experimentally relevant region around $U/|t|=1.5$, rather than relying exclusively on SCF theory.

5.2. The Hubbard model of buckminsterfullerene

Results for the ground state energy of the Hubbard model of buckminsterfullerene [48] are summarized in Table 3. Values are shown at $U/|t|$ ratios of 1.0, 2.0, and 3.0 both for uniform and alternating bond lengths. While all atoms in buckminsterfullerene are equivalent under I_h symmetry, those bonds separating two hexagons need not be the same length as those separating a hexagon and a pentagon, and experimentally the 6-6 bonds are found to be noticeably shorter than the 6-5 bonds. A shorter bond should in turn correspond to a stronger bonding interaction. The results labeled "alternating" were generated by setting $t_{hh}=1.2t$ and $t_{hp}=0.9t$ to model this difference. It is highly encouraging that the generalized Davidson corrected and MP2 energies are in excellent agreement. These values are also below variational bounds [52,53] available from Monte Carlo calculations using the Gutzwiller wave function anzatz at $U/|t|$ equal to 1.0 and 2.0, and are probably very close to the FCI limit at these ratios. The effect of electron correlation at $U/|t|=2.0$ is by no means small. For a standard t value of –2.5 ev it contributes almost 8 ev of stabilization.

Table 3
Ground state energy of the Hubbard model of buckminsterfullerene in units of |t|

U/|t|	Uniform			Alternating		
	1.0	2.0	3.0	1.0	2.0	3.0
E_{HF}	-78.1616	-63.1616	-48.1616	-80.6942	-65.6942	-50.6942
E_{SDCI}	-78.8603	-65.4137	-52.2857	-81.4144	-68.0225	-54.9608
+DD	-78.9474	-66.2908	-55.1779	-81.5018	-68.9222	-57.9545
MP2	-78.9489	-66.3106	-55.2468	-81.5017	-68.9245	-57.9624

While calculations were not done for U/|t|=1.5, the ratio most appropriate for direct comparison to the Heisenberg and Hückel results of the last section, the energy at that ratio for uniform bond lengths can be interpolated to about −72.6t, which with t=−2.5 ev gives a total energy around -182 ev. This is in much better agreement with the Heisenberg energy of −187 ev than with the Hückel limit of −233 ev, and indicates that the VB model has got the energetics of the ground state essentially right. Bond alternation is seen to stabilize the molecule at all values of U, but increasingly so as the electron correlation increases. At U/|t|=2.0 it adds an additional stabilization of nearly 7 ev, not counting, of course, any changes in the sigma strain energy which unequal bond lengths may induce.

Bond orders and spin-spin correlation functions may also be extracted from the ground state wave function. The bond order on the 6-6 bonds is found to be about 25% larger than on the 6-5 bonds, with only a very slow increase with U. Bond alternation has a much more dramatic effect, making the 6-6 bond order almost 75% larger than the 6-5 bond order. The spin-spin correlation, as expected, is negative for both types of bonds, with a substantially larger magnitude for 6-6 bonds. The only other significant correlation is between atoms on opposite corners of a hexagon, and it is negative as it would be in a purely antiferromagnetic system. The other correlations are small and of random sign, and there is no clear long range spin order.

The Hubbard model also opens up the study of the low-lying electronic spectrum of buckminsterfullerene, which is not accessible through the purely VB Heisenberg model. The lowest singlet and triplet excitations are found to lie at 0.769|t| and 0.694|t| for uniform bonds and at 0.916|t| and 0.836|t| for alternating bonds. With the standard t value of −2.5 ev these translate to 1.9 ev (uniform) and 2.3 ev (alternating) for the singlet and 1.7 ev (uniform) and 2.1 ev (alternating) for the triplet. Experimentally, the singlet is found between 1.92 ev [54] and 2.00 ev [55] while values of 1.63±0.20 ev [55], 1.7 ev [56], and 1.57 ev [57] have been reported for the triplet. The uniform bond length Hubbard values are fortuitously in almost perfect agreement with experiment, but the agreement of the presumably more realistic alternating bond length excitation energies must be accounted as quite satisfactory. The Hubbard model can be expected to

describe excited states less well than ground states because excited states are typically much more seriously admixed with ionic character, necessitating the retention of the long range coulomb integrals of the PPP model if they are to be treated accurately. The PPP model of buckminsterfullerene will be treated in the next section.

6. PPP CALCULATIONS

6.1. PPP model parameters for fullerenes

While the Hubbard model successfully models several aspects of buckminsterfullerene, it does not have the capability to describe the full range of chemical and physical properties which one would like to be able to extract from a semiempirical model. To begin with, it makes no predictions of geometry. Instead, the experimental bond lengths must be used to estimate the differences in t values for different bonds. As mentioned above, the model also fails to describe states with significant ionic character, and thus often gives poor electronic spectra. The same limitation applies to ionization potentials and electron affinities, which of necessity introduce ionic character into the wave function. These latter limitations can be largely removed by returning to the full PPP model which allows electrons to interact via effective coulomb repulsions at all distances. To make the model predictive of geometry, the pi electronic energy must be coupled in some way to the energy of the sigma system. For a general three dimensional molecule this is a difficult task, but for planar conjugated hydrocarbons such as polyenes and benzenoid aromatics this can be done in a rather simple way. It turns out that because of the rather special symmetry of buckminsterfullerene this simple approach can be applied with only minimal modification to it as well.

For planar polyenes and aromatics it is reasonable to assume that bond angles remain very close to the ideal $120°$ angles generated by sp^2 hybridization. Given the quite localized nature of sigma electron pair bonding, it is then reasonable to assume that the energy of a sigma bond couples to the geometric structure of the molecule only through a stretching force constant. Accordingly, we treat each sigma bond as a spring, and write the total energy of the molecule as

$$E = \Sigma_{i \sim j}\{Ee_{ij} + 1/2k_{ij}(r_{ij} - re_{ij})^2\} + E^\pi \qquad (7)$$

where Ee_{ij} is the energy of a bond at its equilibrium bond length re_{ij} in the absence of the pi electrons, r_{ij} is its bond length in the presence of the pi electrons, k_{ij} is a force constant, and E^π is the energy computed from the pi electron Hamiltonian. The notation $i \sim j$ again denotes summation over atom pairs connected by a sigma bond. For molecules such as those discussed here

with only bonds between sp^2 hybridized carbon atoms, all of the Ee_{ij}'s, re_{ij}'s and k_{ij}'s can be replaced with common values E_e, r_e, and k.

If values are known for E_e, r_e, and k, and if the dependence of the parameters in the PPP Hamiltonian on distance is also known, then the total energy may be minimized with respect to all of the bond lengths to find the most stable molecular structure. In fact, the value of E_e need never be elucidated since it contributes equally to the energy of all states at all geometries, so just two additional parameters, r_e and k, need to be added to the PPP model to carry out this program. The distance dependence of the electron repulsion integrals in the PPP model is already prescribed by the choice of the Ohno or Mataga-Nishomoto forms given in Eq. 3 and Eq. 4, so we need only consider the distance dependence of the resonance integrals t which account for the strength of bonding.

It is often assumed that resonance integrals are proportional to the overlap between the atomic orbitals which formally underlie the pi Hamiltonian [58]. If these are assumed to be ordinary $2p_\pi$ atomic orbitals for carbon, the distance dependence of the overlap can be calculated analytically, and the distance dependence of the t parameters is often taken to be of this form, as for example in Extended Hückel Theory [59]. But there is no need to make this assumption since the parameters in the pi Hamiltonian should more properly be thought of as rescaled effective integrals, and there is evidence that the model performs better if the t values are allowed to vary more rapidly with distance. Accordingly, we have adopted the form

$$t_{ij} = t_o[1 - \delta(r_{ij} - r_o)] \tag{8}$$

with t_o the value of the resonance integral at the reference length r_o, usually taken to be the bond length of benzene, and δ a third new parameter. Values of k, r_e, and δ can be found by fitting to the bond lengths of any convenient test set of molecules. In all of the work described here the accurately known gas phase carbon-carbon bond lengths of ethylene (1.339A°), benzene (1.399A°), and butadiene (1.349A°, 1.467A°) [60] were used for this purpose.

To apply the PPP model to a fullerene, it is then necessary to consider how the parameters which appear in the model might be modified by the curvature of the fullerene surface. For most fullerenes it is to be expected that strain introduced into the sigma system will alleviate itself both through changes in bond lengths and in bond angles. But buckminsterfullerene is rather special in this regard. It can be shown that except for the unavoidable Gaussian curvature required to form a closed sphere, other forms of strain are minimized by the icosahedral symmetry of the molecule [61, 62]. There is thus no tendency to distort bond angles as the molecule relaxes to its minimum energy geometry.

On the other hand the I_h symmetry imposes no constraint on the lengths of the 6-6 and 6-5 bonds, other than that all 6-6 bonds must be identical and all 6-5 bonds must be identical. There are thus just two geometric degrees of freedom, and both can be represented by stretching force constants just as in planar hydrocarbons.

The curvature is also unlikely to seriously effect the electron repulsion integrals which are rather isotropic. Indeed in CNDO theory all electron repulsion integrals are modeled by those computed for s orbitals to maintain local coordinate invariance [63]. However the resonance integrals are quite likely to be sensitive to curvature. In the simplest picture of the origin of the resonance interaction the t integrals are viewed as being proportional to the overlap between atomic 2p orbitals. While the work described here did not make that assumption for the distance dependence of the t's, it does suggest that less than perfect alignment of atomic orbitals on adjacent atoms should result in a reduced pi bonding capacity. Eq. 8 was therefore modified to

$$t_{ij} = t_o[1 - \delta(r_{ij} - r_o)]f(\theta_{ij}) \tag{9}$$

To estimate the angular dependence of the t integrals it was assumed that each carbon atom has a p_π-like atomic orbital oriented along the line from the center of the molecule to the atomic nucleus. But since the three neighboring carbon atoms are not in the same plane as the nucleus due to the curvature of the surface, the carbon orbitals forming the sigma bonds are not purely sp^2 and must be rehybridized slightly [64]. Then in addition to being out of alignment with their neighbors by an angle θ_{ij} which is determined by the distance of the atoms from the molecular center and the bond length between them, the π-like orbitals are also not purely p_z in character. Nevertheless, the overlap $s(\theta_{ij})$ between two such orbitals can be worked out analytically and $f(\theta_{ij})$ was taken simply as $s(\theta_{ij})/s(0)$. For the angles encountered in medium to large fullerenes, it turns out that this ratio is very accurately approximated by the two leading terms in its expansion in powers of θ_{ij}, leading to the very simple final result

$$f(\theta_{ij}) = 1 - 3\theta_{ij}^2/4 \tag{10}$$

and the PPP model was applied to buckminsterfullerene with no additional modification.

Correlated calculations using SDCI plus generalized Davidson or MP2 corrections as described for the Hubbard model were first performed for buckminsterfullerene using a standard literature set of PPP parameters [65], namely t_o = -2.6 ev at the benzene reference bond length r_o, γ_o = 11.13 ev, and the Ohno form for the two center γ's. While t_o is more commonly chosen as

−2.5 ev or even lower, Tavan and Schulten [65] have found better success at fitting spectra with the larger value, and our experience confirms this observation.` The fit to the bond lengths of ethylene, benzene, and butadiene, using the FCI solution to the PPP model for these molecules yielded $r_e = 1.5190$ A°, $k = 55.841$ ev/(A°)^2, and $\delta = 1.8$ (A°)$^{-1}$. The value of r_e is in excellent agreement with other estimates of the length of a pure sigma bond between sp^2 hybridized carbon atoms, though the value of δ is somewhat larger than that employed in most other studies. All four bond lengths in the fitted set were reproduced to within 0.001 A° of their experimental values. No experimental information about buckminsterfullerene itself was used in deriving any of the parameter values.

6.2. Ground state structure of buckminsterfullerene

Geometry optimization was performed for the ground state of buckminsterfullerene at the Hartree-Fock/SCF, SDCI and MP2 levels [66], giving equilibrium bond lengths which are shown in Table 4 along with the results from some other theoretical treatments. The bond lengths computed from the PPP model at the MP2 level with the parameterization described here are in outstanding agreement with experiment, being within the experimental errors for both bonds as measured by gas phase electron diffraction [67]. They are also in excellent agreement with those calculated with ab initio methods when electron correlation is included [3]. While electron correlation does not produce as large changes for the PPP model, the trends are the same as for the ab initio results [68], with correlation serving primarily to lengthen the 6-6 bonds. This is an important observation since most SCF based methods underestimate the length

Table 4
Bond lengths in buckminsterfullerene in A°

Method	r_{66}	r_{65}	reference
Experiment	1.401±0.010	1.458±0.006	67
Ab initio			
HF/TZP	1.370	1.448	68
MP2/TZP	1.406	1.446	3
PPP model			this work
SCF	1.398	1.454	
SDCI	1.403	1.453	
MP2	1.407	1.452	
PPP model	1.398	1.439	69,70
	1.396	1.443	71

of the 6-6 bond [5]. Also shown in Table 4 are the results from earlier PPP studies [69-71] which used somewhat different parameterizations and estimated bond lengths from empirical bond order-bond length relations, but without correlation. The agreement with the SCF level bond lengths found here is reasonable, indicating that the geometry is probably not overly sensitive to the choice of PPP parameters.

Bond orders are not much different than those found from the Hubbard model and are not very sensitive to electron correlation. At the MP2 level they are 0.424 for the 6-5 bonds and 0.692 for the 6-6 bonds, favoring pi electron density on the 6-6 bonds as expected. The spin-spin correlation functions, though, show interesting behavior. Any SCF calculation of necessity gives all negative spin-spin correlations, so a VB or correlated electron approach is necessary to observe the true spin behavior. The correlated PPP wave functions for buckminsterfullerene show the strong negative spin correlation for nearest-neighbors found with the Hubbard model, with a larger magnitude for the 6-6 bonds. But they also show clear evidence of longer-range antiferromagnetic correlation. The average correlation with all atoms located d bonds away from a given site is negative for all odd d and positive for all even d out through d=5. Only for the very small correlations with d greater than 5 are some sign reversals observed, and these may be below the accuracy of the calculation. It thus appears that at least locally buckminsterfullerene preserves an antiferromagnetic spin ordering. Additionally, the positive correlations for even d are much smaller in magnitude than the negative correlations. For an alternant antiferromagnetic system they would be zero, so this result provides additional evidence that buckminsterfullerene is "almost" alternant and that the 5-membered rings introduce quite minor perturbations into the pi electron wave function.

6.3. Electronic spectrum of buckminsterfullerene

It thus seems that the PPP model provides a very satisfactory description of the structure of buckminsterfullerene. Unfortunately when we turn to the excitation spectrum the results are not yet so encouraging. Due to the high degeneracy of the HOMO and LUMO under I_h symmetry, there are four states, with symmetries T_{1g}, T_{2g}, G_g, and H_g, which trace their parentage to the HOMO-LUMO excitation, and all are apparently very close in energy. Transitions to any of them from the ground state are dipole forbidden, but both the lowest singlet and triplet have been observed experimentally. Table 5 presents the transition energies calculated from the present version of the PPP model at various levels of correlation, again with some other theoretical calculations for comparison purposes.

The simplest approach to obtaining excitation energies theoretically is to introduce configuration interaction with singly excited determinants. This

Table 5

Lowest singlet and triplet excitation energies of buckminsterfullerene in ev

Method	singlet		triplet		reference
Experiment	1.92		--		54
	2.00		1.63±0.20		55
	--		1.7		56
	--		1.57		57
6-31G+s/SCI	2.97	T_{2g}	1.69	T_{2g}	72
MNDO/SCI	3.17	T_{2g}	3.03	T_{2g}	73
PPP/SCI	2.87	T_{1g}	2.46	T_{2g}	69
PPP/SCI	2.61	T_{1g}	2.23	T_{2g}	70
PPP/SCI	2.69	T_{1g}	--		71
PPP					this work
SCI	2.80	T_{2g}	2.24	T_{2g}	
SDCI	3.08	T_{2g}	2.83	T_{2g}	
MP2	1.65	T_{2g}	1.31	T_{2g}	
MP3	2.66	G_g	2.35	T_{2g}	

produces no change in the SCF energy of the ground state but gives a first order estimate of excited state energies. Transition energies calculated at this level from the PPP model with the parameter set described here and the complete set of single excitations give values at least 0.5 ev too high for the triplet and as much as 0.9 ev too high for the singlet compared to experiment. However they are in good agreement with SCI excitation energies found from other parameterizations of the PPP model with more limited CI [69-71]. An ab initio computation [72], which is limited to a small basis set, does better for the triplet but is even higher for the singlet, while MNDO gives higher values for both states [73]. It should be noted that the various methods identify different symmetries for the lowest excited singlet state, but the separation between T_{1g}, T_{2g}, and G_g is very small.

Given that single and double CI introduces fairly substantial energy corrections for the ground state, it may well be that doubly excited CI corrections for the excited states are necessary to produce accurate excitation energies. Accordingly, the excitation energies have been recalculated at both the SDCI and MP2 levels [66], but the results are disappointing. The SDCI corrections actually raise both transition energies, making the agreement with experiment even worse, while the MP2 corrections drop both values below experiment. The downward shifts of 1.5 ev from the MP2 corrections are disconcerting, as is the fact that the Duch-Diercksen corrected ground state energy differs noticeably from the MP2 energy. This strongly suggests that the

CI treatment is not converged, and we have confirmed this by computing the MP3 corrections, which shift the transition energies back up by 1.0 ev! The failure of the SDCI/MP2 method to deliver well converged results for the PPP model is rather surprising given that it was apparently quite well converged for a Hubbard model designed to contain the same strength of electron correlation.

6.4. Ionization potential and electron affinity of buckminsterfullerene

Two other properties of buckminsterfullerene, the ionization potential (IP) and electron affinity (EA), are also of interest. Since each involves a change in the number of electrons, they can be found from the PPP model only if the site energy terms (the α integrals of Hückel theory), which have been dropped from Eq. 5, are restored. However the difference between them, IP-EA, is independent of α, and can readily be computed at the SDCI level, giving a value of 6.60 ev. Experimentally, the ionization potential is accurately measured to be very close to 7.6 ev [74-77], while the electron affinity is found to be 2.65±0.05 ev [78]. Thus the experimental difference IP-EA = 4.95±0.05 ev, is quite far from the PPP value. We can try to identify the source of the discrepancy by estimating a value for α from PPP calculations on small hydrocarbons for which the ionization potential is known experimentally and assuming that α is unchanged in a fullerene. For buckminsterfullerene this gives IP = 7.3 ev in reasonable agreement with experiment, but EA = 0.7 ev which is much too small. These results are consistent with the observation that the SDCI is not well converged, since convergence problems are expected to be much more serious for the anion than for the cation.

6.5. Improved treatment of long range electron-electron interaction

It is impossible to say with certainty why the second order correlation methods perform as poorly as they do for the PPP model of buckminsterfullerene, given their success with the Hubbard model, but it appears that the problem may be related to the use of the Ohno formula for the two center electron repulsion integrals. The Ohno formula was introduced to model the relative repulsions between atoms which are not too far apart, and it seems to be quite successful at that. On the other hand it may will give overly large values for the effective repulsion between electrons located on widely separated atoms. In small molecules where few if any atoms are far apart inadequacies in the long range form of the repulsion are unlikely to be important, but in a molecule as large as buckminsterfullerene the cumulative effect of many overly large repulsions from distantly separated atom pairs may significantly overestimate the strength of the electron-electron interaction, thus contributing to the poor convergence of low-order correlation treatments. In the physics literature this problem is often addressed by introducing an effective dielectric constant to represent the extra

screening produced by other charge centers, but this is really only appropriate for condensed phases. Instead, for fullerenes it might be more appropriate to use the Mataga-Nishomoto form for the electron repulsion integrals given in Eq. 4. This functional form dies off with distance more sharply than the Ohno function.

While examples of the use of the Mataga-Nishomoto function in PPP studies can be found in the literature, it seems not to be generally recognized that replacement of the Ohno with the Mataga-Nishomoto function with no other change in parameters cannot be expected to give reasonable results. The steeper fall off with distance reduces the nearest neighbor γ's with respect to the one center γ, thus sharply increasing the short range correlation strength as measured by the Hubbard model effective U parameter. The result is to make the model much more strongly correlated, rather than to weaken the correlation as is desired. Thus use of the Mataga-Nishomoto form requires a reduction in the value of the one center coulomb integral to restore the balance between on-site and nearest-neighbor repulsions, and this is likely to require a reoptimization of all parameters in the PPP Hamiltonian to maintain good agreement with experiment for small molecules.

A systematic reoptimization of the PPP Hamiltonian for fullerenes using the Mataga-Nishomoto function for the electron repulsion integrals has not yet been carried out. But some test calculations have been performed, using an arbitrarily chosen value of $\gamma_0 = 9.5$ ev, and the results are encouraging. The ground state geometry is little changed, and the agreement with experiment remains excellent. On the other hand, the excitation energies at the SCI level are somewhat reduced and both the MP2 and MP3 corrections are substantially smaller, though the MP3 correction is still larger than would be desired. The calculated electron affinity is also increased to a value much nearer experiment. There is thus reason for optimism that when properly reparameterized the PPP model will prove capable of giving a quantitatively useful description of the electronic properties of buckminsterfullerene.

7. CONCLUSION

The valence bond picture of fullerenes has certainly proven to be valuable. The basic mental model of a fullerene, consisting of a cage of sigma bonds supporting a delocalized resonance superposition of many Kekulé functions formed from mobile pi-like electrons, is supported at many levels. At its most qualitative level it rationalizes an important component of the isolated pentagon rule for fullerene structures. In more quantitative forms it explains the preference for pi electron density to lie on 6-6 bonds, which underlies much of the chemical reactivity of fullerenes, and at least for buckminsterfullerene shows a strong tendency towards antiferromagnetic spin ordering. This latter fact,

along with the observation of a special families of Kekulé structures, argues strongly that the 5-membered rings in fullerenes, though essential to the spherical physical structure, are rather minor perturbations to the electronic structure.

In addition, comparison to solutions of the Hubbard and PPP models including electron correlation shows the VB wave function to be a more accurate initial approximation than the Hartree Fock solution at the correlation strengths likely to be encountered in realistic semiempirical models. In spite of the qualitative superiority of the VB wave function, systematic computational approaches to more accurate treatment of correlation are still most readily achieved when starting from the independent particle limit, but the correlated wave functions thus built up are likely to be interpretable in valence bond terms.

Finally, the outlook for semiempirical pi electron models as useful tools for studying fullerenes is good. They are apparently capable of quite accurate predictions of molecular geometry, and there is reason for optimism that when properly parameterized they will be useful predictors of electronic properties as well.

REFERENCES

[1] H. W. Kroto, J. R. Heath, S. C. O'Brien, R. F. Curl, and R. E. Smalley, Nature, 368 (1985) 6042.
[2] W. Krätschmer, L. D. Lamb, K. Fostiropoulos, and D. R. Huffman, Nature, 347 (1990) 354.
[3] M. Häser, J. Almlöf, and G. E. Scuseria, Chem. Phys. Lett., 181 (1991) 497.
[4] M. J. S. Dewar and W. Thiel, J. Am. Chem. Soc., 99 (1977) 4899.
[5] J. Cioslowski, Electronic Structure Calculations on Fullerenes and Their Derivatives, Oxford University Press, New York, 1995.
[6] R. Taylor (ed.), The Chemistry of Fullerenes, World Scientific, Singapore, 1995.
[7] E. Hückel, Z. Physik, 70 (1931) 204; 76 (1932) 628.
[8] W. Heitler and F. London, Z. Physik, 44 (1927) 455.
[9] G. Rumer, Gött. Nach. Ges. Wiss. (1932) 337.
[10] L. Pauling, J. Chem. Phys., 1 (1933) 280.
[11] E. Clar, The Aromatic Sextet, John Wiley, London, 1972.
[12] W. C. Herndon, J. Amer. Chem. Soc., 95 (1973) 2404; Thermochimica Acta, 8 (1974) 225.
[13] W. T. Simpson, J. Amer. Chem. Soc., 75 (1953) 597.
[14] M. Randic´, Tetrahedron 31 (1975) 1477.
[15] M. Randic´ and N. Trinajstic´, J. Amer. Chem. Soc., 106 (1984) 4428.
[16] D. J. Klein and X. Liu, J. Comp. Chem., 12 (1991) 1260.
[17] J. H. Van Vleck and A. Sherman, Rev. Mod. Phys., 7 (1953) 167.

[18] See, for example, D. C. Mattis, The Theory of Magnetism, Harper and Rowe, New York, 1965.

[19] S. A. Alexander and T. G. Schmalz, J. Amer. Chem. Soc., 109 (1987) 6933.

[20] N. Flocke, Comp. Phys. Comm., 106 (1997) 114.

[21] R. Pariser and R. G. Parr, J. Chem. Phys., 21 (1953) 767.

[22] J. A. Pople, Trans. Faraday Soc., 42 (1953) 1375.

[23] J. Hubbard, Proc. R. Soc. London, Ser. A 276 (1963) 238; 281 (1964) 401.

[24] K. Ohno, Theor. Chim. Acta, 2 (1964) 219.

[25] K. Nishimoto and N. Mataga, Z. Physik. Chem. (Frankfurt), 12 (1957) 335.

[26] L. N. Buleavski, Zh. Eksp., Teor. Fix., 51 (1966) 230.

[27] R. D. Poshusta and D. J. Klein, Phys. Rev. Lett., 48 (1982) 1555.

[28] D. J. Klein, W. A. Seitz, M. A. Garcia-Bach, J. M. Picone, and D. C. Foyt, Int. J. Quantum Chem. 17S (1983) 555.

[29] R. D. Poshusta, T. G. Schmalz, and D. J. Klein, Mol. Phys., 66 (1989) 317.

[30] X. Liu, D. J. Klein, W. A. Seitz, and T. G. Schmalz, J. Comp. Chem., 12 (1991) 1265. Note that these results were corrected in X. Liu, T. G. Schmalz, and D. J. Klein, Chem. Phys. Lett., 192 (1992) 331.

[31] T. G. Schmalz, D. J. Klein, and X. Liu, Mat. Res. Soc. Symp. Proc., 270 (1992) 129.

[32] C. Pistoti, J. L. Yarger, and A. Zettl, Nature, 393 (1998) 771.

[33] T. G. Schmalz, W. A. Seitz, D. J. Klein, and G. E. Hite, Chem. Phys. Lett., 130 (1986) 203.

[34] H. W. Kroto, Nature, 329 (1987) 529.

[35] K. Raghavachari and C. M. Rohlfing, J. Phys. Chem., 96 (1992) 2463.

[36] X. Liu, D. J. Klein, and T. G. Schmalz, Fullerene Sci. Tech., 2 (1994) 405.

[37] P. W. Fowler, Chem. Phys. Lett., 131 (1986) 444.

[38] P. W. Fowler, J. E. Cremona, and J. I. Steer, Theor. Chim. Acta, 73 (1988) 1.

[39] K. Kikuchi, N. Nakahar, T. Wakabayashi, S. Susuki, H. Shiromaru, Y. Miyake, K. Saito, I. Ikemoto, M. Kainosho, Y. Achiba, Nature, 357 (1992) 142.

[40] D. J. Klein, T. G. Schmalz, G. E. Hite, and W. A. Seitz, J. Amer. Chem. Soc., 108 (1986) 1301.

[41] T. G. Schmalz, N. Flocke, and D. J. Klein, (K. M. Kadish and R. S. Ruoff eds.), Fullerenes, Volume 6, The Electrochemical Society, Pennington, NJ, 1998, pp 47-59.

[42] N. Flocke and T. G. Schmalz, Chem. Phys. Lett., 298 (1998) 71.

[43] N. Flocke, T. G. Schmalz, and D. J. Klein, J. Chem. Phys., 109 (1998) 873.

[44] L. Pauling and G. W. Wheland, J. Chem. Phys., 1 (1933) 362.

[45] D. N. Sheng, Z. Y. Weng, C. S. Ting, and J. M. Dong, Phys. Rev. B 49 (1994) 4279.

[46] V. Y. Krivnov, I. L. Shamovsky, E. E. Tornau, and A. Rosengren, Phys. Rev. B 50 (1994) 12144.

[47] N. Flocke and T. G. Schmalz, Int. J. Quant. Chem., 76 (2000) 83.

[48] N. Flocke, T. G. Schmalz, and D. J. Klein, J. Chem. Phys., 112 (2000) 8233.

[49] R. Langhoff and E. R. Davidson, Int. J. Quant. Chem., 8 (1974) 61.

[50] W. Duch and G. H. F. Diercksen, J. Chem. Phys., 101 (1994) 3018.

[51] C. Moeller and M. S. Plesset, Phys. Rev., 46 (1934) 618.

[52] B. Srinivasan, S. Ramasesha, and H. R. Krishnamurthy, J. Phys. Chem. 100 (1996) 11260.

[53] B. Srinivasan, S. Ramasesha, and H. R. Krishnamurthy, Phys. Rev. B 54 (1996) 1692.

[54] Z. Gasyna, P. N. Schatz, J. P. Hare, T. J. Dennis, H. W. Kroto, R. Taylor, and D. R. M. Walton, Chem. Phys. Lett., 183 (1991) 283.

564

[55] J. W. Arbogast, A. P. Darmanyan, C. S. Foote, Y. Rubin, F. N. Diedrich, M. M. Alvarez, S. J. Anz, and R. L. Whetten, J. Phys. Chem., 95 (1991) 11.

[56] R. E. Haufler, L.-S. Wang, L. P. F. Chibante, C. Jin, J. Conceicao, Y. Chai, and R. E. Smalley, Chem. Phys. Lett., 179 (1991) 449.

[57] Y. Zeng, L. Biczok, and H. Linschitz, J. Phys. Chem., 96 (1992) 5237.

[58] M. Wolfsberg and L. Helmholz, J. Chem. Phys., 20 (1952) 837.

[59] R. Hoffmann, J. Chem. Phys., 39 (1963) 1397; 40 (1964) 2474, 2480, 2745.

[60] (D. R. Lide, ed.), CRC Handbook of Chemistry and Physics, 78th edition, CRC Press, Boca Raton, 1997.

[61] D. J. Klein and X. Liu, Int. J. Quant. Chem., S28 (1994) 501.

[62] D. J. Klein and H.-Y. Zhu, (A. Balaban, ed.), From Chemical Topology to Three-Dimensional Geometry, Plenum Press, New York, 1997.

[63] J. A. Pople and D. L. Beveridge, Approximate Molecular Orbital Theory, McGraw-Hill, New York, 1970.

[64] R. C. Haddon, L. E. Brus, and K. Raghavachari, Chem. Phys. Lett., 131 (1986) 165.

[65] P. Tavan and K. Schulten, Phys. Rev. B 36 (1987) 4337.

[66] N. Flocke, T. G. Schmalz, and D. J. Klein, unpublished.

[67] K. Hedberg, L. Hedberg, D. S. Bethune, C. A. Brown, H. C. Dorn, R. D. Johnson, and M. deVries, Science, 254 (1991) 410.

[68] G. E. Scuseria, Chem. Phys. Lett., 176 (1991) 423.

[69] I. Lazlo and L. Udvardi, Chem. Phys. Lett., 136 (1987) 418.

[70] I. Lazlo and L. Udvardi, J. Mol. Struct. (Theochem), 183 (1989) 271.

[71] M. Kataoka and T. Nakajima, Tetrahedron, 42 (1986) 6437.

[72] H. Weiss, R. Ahlrichs, and M. Häser, J. Chem. Phys., 99 (1993) 1262.

[73] R. Saito, G. Dresselhaus, and M. S. Dresselhaus, Chem. Phys. Lett., 210 (1993) 159.

[74] J. A. Zimmerman, J. R. Eyler, S. B. H. Bach, and S. W. McElvany, J. Chem. Phys., 94 (1991) 3556.

[75] D. L. Lichtenberger, M. E. Jatco, K. W. Nebesny, C. D. Ray, D. R. Huffman, and L. D. Lamb, Mat. Res. Soc. Symp. Proc., 206 (1991) 673.

[76] J. de Vries, H. Steger, B. Kamke, C. Menzel, B. Weisser, W. Kamke, and I. V. Hertel, Chem. Phys. Lett., 188 (1992) 159.

[77] R. K. Yoo, B. Ruscic, and J. Berkowitz, J. Chem. Phys., 96 (1992) 911.

[78] L. S. Wang, J. Conceicao, C. Jin, and R. E. Smalley, Chem. Phys. Lett., 182 (1991) 5.

Chapter 18

Valence Bond Calculations and Their Applications to Medium-sized Conjugated Hydrocarbons

Y. Jiang and S. Li

Department of Chemistry, Nanjing University, Nanjing, 210093, P. R. China

1. INTRODUCTION

The valence bond (VB) theory is a general theory of chemical bonding parallel with the molecular orbital (MO) theory. It origins from the Heitler-London treatment of the hydrogen molecule and regards the chemical bond to the spin pairing of the shared electrons localized around the linking atoms (or atomic cores) [1,2]. During the 1930s and 1940s, Pauling and his collaborators generalized the ideas introduced by Heitler and London in their hydrogen molecule calculation to general many-electron molecules and laid the foundations of VB theory [3,4]. In VB theory, the exchange of atomic spins and the resonance mixture of covalent VB structures result in energy lowering and the formation of molecule. In contrast, the MO theory accounts for bonding in terms of a delocalized picture in which electrons move around all nuclei of the molecule. In comparison, one sees that the VB model is closer to the concept of valence traditionally adopted by chemists that molecules are ensembles of atoms held together by localized two-center and three-center bonds [3-5].

Over the past decades, MO theory has been predominantly developing due to the computational advantage that the basis sets are orthogonal. Various semi-empirical and ab initio SCF schemes as well as some MO-based correlation methods are available to explore the physical and chemical behaviors of molecules [6-8]. In contrast, the development of the VB theory has been seriously hindered by the non-orthogonal atomic wave functions and the exponentially increased configuration space for many-electron molecules. In the early days of VB theory, in order to make energy calculations possible, Pauling and his contemporaries assumed that the orbitals could be considered orthogonal to each other [3,4]. This assumption resulted in a dramatic simplification for VB calculations and the resultant form of VB theory is now termed the classical VB theory. Even though, since the number of covalent VB structures rapidly increases with the number of valence electrons, the exact solution of the classical VB model for many-electron molecules except a few small systems

was prohibited before powerful computers appeared. Hence, the simple versions of VB theory [9,10] such as the enumeration of Kekulé structures or the conjugated-circuit model [9], have been used instead to give qualitative discussions on some properties of chemical systems, especially for the benzenoid hydrocarbons (BHs). On the other hand, due to the early success of VB theory [1,3,4,11], chemists have never lost their confidence in developing new forms of VB theory and solving various VB models via a strict approach for larger molecules and thus elaborating the applications of VB theory to these systems.

The difficulties with the VB theory went on until the last thirty years. There have been several threads of development in semi-empirical [12-22] and ab initio [23-28] VB frameworks with much widening interest in applying VB theories. New forms of VB theory, under the name of modern VB theory, have emerged, in all of which overlap integrals are explicitly considered and all required one- and two-electron integrals are precisely evaluated. While for the VB theory in its classical semi-empirical form, its applications to general molecules have been overshadowed by its new forms. Nevertheless, for conjugated systems in which π-electrons are mainly responsible for their special properties [29,30], the classical VB model could be considered to approximately represent the many-electron Hubbard model [31], a simplified PPP model for describing π-electrons, in the strongly correlated limit. On the other side, the simple Hückel MO (HMO) theory is an approximation of the Hubbard Hamiltonian in the weakly correlated limit. As the structure-property relationships for conjugated systems have been well established using simple and sophisticated MO theories [29,30], it would be still valuable to investigate some properties of conjugated molecules from exact solutions of the classical VB model so that the effects of electron correlation on π-conjugation interactions could be assessed. Unless otherwise stated, hereafter the VB model refers to the classical VB model throughout this chapter. With the advent of powerful computers, use of the graphical unitary-group technique has led to exact VB ground-state energies for BHs up to N=24 sites [16]. To extend VB calculations to larger species, an efficient strategy is to reduce the size of the VB matrix by using the molecular point group and spin symmetry, and then applying the powerful methods developed for treating large sparse matrices for diagonalization. In addition, if the VB model is solved in various spin subspaces with conserved z-component of total spin S, efficiently coding the Slater determinants also aids in saving computational time and required memory. Recently, by employing a combination of these techniques we have obtained the VB energies and wave functions of the ground and lowest excited states for a large number of conjugated systems with up to 28 π-electrons [22].

The exact VB solutions offer the possibility for the reinterpretation of

various molecular behaviors and the validation of approximate VB versions [9,10]. Both the energies and wave functions of the lower-lying states are instrumental in property-structure investigations. In this chapter, we firstly describe the VB model in detail and then introduce the computational techniques to enable VB calculations feasible for conjugated systems having 28 π-electrons. Then for closed-shell BHs we demonstrate that their bond lengths, reactivity, low-lying electronic spectra, and aromaticity could be interpreted in a systematic way. And for open-shell conjugated radicals, their spin coupling strength could be easily calculated within the VB model, which is difficult to obtain in conventional MO approaches.

2. METHODOLOGY

2.1. VB model

2.1.1. The origin of the VB model: the Heitler-London treatment of the hydrogen molecule

For the hydrogen molecule, the Hamiltonian operator is as follows

$$\hat{H} = \hat{h}(1) + \hat{h}(2) + \hat{g}(1,2) \tag{1}$$

where

$$\hat{h}(i) = -\frac{1}{2}\nabla_i^2 + r_{ai}^{-1} + r_{bi}^{-1} \tag{2}$$

$$\hat{g}(1,2) = r_{12}^{-1} \tag{3}$$

Here $\hat{h}(i)$, $i=1$ or 2, stands for the core Hamiltonian for electron i moving in the field of nuclei a and b separated by distance R, and $\hat{g}(1,2)$ is the repulsion potential between two electrons away from each other by distance r_{12}.

According to Heitler and London [1], the electronic states of the hydrogen molecule can be formed by distributing the two electrons between the atomic orbitals (AOs), $1s_a$ and $1s_b$ (abbreviated by a and b), on the two hydrogen atoms. The singlet wave function characterized by quantum numbers S=0 and M=0 (M denotes the z-component of total spin S) can be described using the form

$$\psi_{00} = (|a\bar{b}\rangle - |\bar{a}b\rangle)/\sqrt{2} \tag{4}$$

where the symbol $|\ \rangle$ denotes a normalized Slater determinant in which the spin

orbitals are used, for example, $(a,\bar{a}) = (a\alpha, a\beta)$. For simplicity electronic variables (space and spin) are implicitly taken to be in natural order $\mathbf{r}_1$ and $\mathbf{r}_2$ or, for spins, s_1 and s_2 in all determinants. In the same way, one can write out the three components of the triplet wave function, for example, the one with S=1 and M=0 being

$$\psi_{t0} = (|a\bar{b}\rangle + |\bar{a}b\rangle)/\sqrt{2} \tag{5}$$

The variational energy of either the singlet or the triplet can be computed by

$$E = \langle\psi|\hat{H}|\psi\rangle/\langle\psi|\psi\rangle \tag{6}$$

On substituting functions (4) and (5) into Eq. (6), we get the singlet and triplet energies E_S and E_T as follows

$$E_S = \frac{Q+K}{1+S_{ab}^2} \qquad\qquad E_T = \frac{Q-K}{1-S_{ab}^2} \tag{7}$$

In Eq. (7), S_{ab} is the overlap integral between two atomic orbitals a and b, defined by Eq. (8), Q and K are coulomb and exchange integrals defined by Eqs. (9) and (10), respectively.

$$S_{ab} = \langle a|b\rangle \tag{8}$$

$$Q = 2\langle a|\hat{h}|a\rangle + \langle ab|\hat{g}|ab\rangle \tag{9}$$

$$K = 2\,S_{ab}\langle a|\hat{h}|b\rangle + \langle ab|\hat{g}|ba\rangle \tag{10}$$

Here, for instance, ab means the simple product of atomic orbitals a and b occupied by electrons 1 and 2 respectively, i.e., $a(1)b(2)$. Besides, $\langle a|h|a\rangle = \langle b|h|b\rangle$ valid for the hydrogen molecule has been used to simplify Q.

The energy gap between singlet and triplet states is obtained directly from Eq. (7)

$$E_S - E_T = 2K \tag{11}$$

if the square of the atomic overlap, S_{ab}^2, is negligible in Eq. (7). For the real hydrogen molecule, the exchange integral K is negative, thus the singlet state is

the ground state of the hydrogen molecule. But for other two-electron model systems, K may be positive, and as a consequence the triplet state will be the ground state.

2.1.2. Equivalent spin-Hamiltonian

The Hamiltonian (1) is spin free, commutative with the spin operator $\hat{S}^2$ and its z-component $\hat{S}_z$ for one-electron and many-electron systems. The total spin operator of the hydrogen molecule relates to the constituent one-electron spin operators as

$$\hat{S}^2 = \left(\hat{S}_1 + \hat{S}_2\right)^2 = \hat{S}_1^2 + \hat{S}_2^2 + 2\hat{S}_1 \cdot \hat{S}_2 \qquad (12)$$

Suppose ψ denotes the common eigenfunction with quantum number S of four operators, $\hat{S}^2$, $\hat{S}_z$, $\hat{S}_1^2$ and $\hat{S}_2^2$, being commutative with each other, then we have

$$\left\langle \psi \middle| \hat{S}_i^2 \middle| \psi \right\rangle = 2^{-1}(2^{-1}+1) = 3/4, \qquad i = 1, 2 \qquad (13)$$

$$\left\langle \psi \middle| \hat{S}^2 \middle| \psi \right\rangle = S(S+1) \qquad (14)$$

Thus, combining Eqs. (12), (13) and (14) leads to

$$\left\langle \psi \middle| \hat{S}_1 \cdot \hat{S}_2 \middle| \psi \right\rangle = 2^{-1} S(S+1) - 3/4 \qquad (15)$$

Evidently, if one defines a Hamiltonian operator containing only spin operators and numerical parameters as follows

$$\hat{H}_S = Q - K/2 - 2K\,\hat{S}_1 \cdot \hat{S}_2 \qquad (16)$$

then this spin-only Hamiltonian can reproduce the energies of the singlet and triplet states of the hydrogen molecules obtained above provided that S_{ab}^2 in Eq. (7) can be neglected, i.e., $\left\langle \psi_{00} \middle| \hat{H}_S \middle| \psi_{00} \right\rangle = Q + K$, $\left\langle \psi_{10} \middle| \hat{H}_S \middle| \psi_{10} \right\rangle = Q - K$. In this sense, we say that the Hamiltonian defined by Eq. (16) is an equivalent Hamiltonian to the true Hamiltonian (1) in the Heitler-London treatment, or in other words, the Hamiltonian (16) defines the VB model for the hydrogen molecule.

It was Pauling and his collaborators who generalized the Heitler-London treatment of the hydrogen molecule to general polyelectronic systems and gave the rules for evaluating the Hamiltonian matrix elements [3,4], which could also

be derived using the following artificial equivalent spin-only Hamiltonian [8,11].

$$\hat{H}_S = \hat{H}_{VB} = (-1)\sum_{i\sim j} K_{ij}(2\hat{S}_i \cdot \hat{S}_j - 1/2) \tag{17}$$

Here $i\sim j$ denotes a specified nearest-neighbor pair of AOs and K_{ij} is the corresponding exchange integral, and $(Q - \sum_{i\sim j} K_{ij})$ is taken as the zero of energy. The VB model (17) is the basis of nearly all semi-empirical applications of VB theory to polyatomic molecules.

2.1.3. The VB model for conjugated molecules

It is well known that the properties of conjugated molecules are principally determined by their π-electrons. Furthermore, planar conjugated molecules are prototypical in that their π-electrons could be separately treated from the remaining σ-electrons. Hence, semiempirical theoretical models developed mainly for conjugated molecules treated only the π-electrons explicitly but incorporated the effects of the σ-electrons and the nuclei into some adjustable parameters featuring these models. The VB model (17) could be such a model, which may be further simplified as

$$\hat{H}_{VB} = J\sum_{i\sim j}(2\hat{S}_i \cdot \hat{S}_j - 1/2) \tag{18}$$

where the exchange integral K_{ij} in Eq. (17) is now replaced with minus J (thus J is a positive exchange parameter), implicitly assuming that the exchange integral has the same value for the two $2p_\pi$ orbitals of any two carbon atoms bonded to each other.

We would like to point out that the VB model (18) has also proven to be the second-order effective Hamiltonian of the many-electron Hubbard model in the strongly correlated limit via degenerate perturbation theory [31] and other methods [32,33]. These methods can lead to systematic procedures for improving the VB model (18) by introducing higher order corrections [13]. On the other side, a geometry-dependent VB model [14], analogous to the model Hamiltonian (18), has also been proposed, in which the σ and π energy dependence to the bond length and bond twisting are incorporated into the parameters. Despite that these variants of the VB model (18) can usually provide slightly better descriptions for a certain conjugated molecule [13,14,19,21], the VB model (18) is appropriate for studying a group of conjugated molecules to probe structure-property relationships, and consequently will be employed as

our working VB model in subsequent sections.

Now we are concerned with how the VB model (18) can be solved for a given conjugated system. In fact, the model Hamiltonian (18) actually acts on the space of pure spin functions, either of the Weyl-Rumer (WR) form [34] or the simple product of one-electron spin functions. The matrix element between any two WR functions can be obtained by using Pauling's graphical rules [4], while the matrix element between two simple spin products is easily available using the following expression

$$2\hat{S}_i \cdot \hat{S}_j = \hat{S}_{i+}\hat{S}_{j-} + \hat{S}_{i-}\hat{S}_{j+} + 2\hat{S}_{iz}\hat{S}_{jz} \tag{19}$$

Expanding the "wave function" in a linear combination of pure spin functions could yield the correct secular equations and thus correct eigenvalues. However, such spin-only "wave functions" could not be considered complete since complete wave functions must describe both the spatial and spin motions of electrons and must be antisymmetric under exchange of any two electrons. It would be better to rewrite the VB model (18) in the second quantization form as given in Eq. (20), in which its eigenstates can be taken as a linear combination of Slater determinants or neutral VB structures. Then

$$\hat{H}_{VB} = \hat{H}_D + \hat{H}_I \tag{20}$$

where

$$\hat{H}_D = -J\sum_{i-j}(a_i^+ a_j^+ a_j a_i + a_i^+ a_j^+ a_j a_i) \tag{21}$$

$$\hat{H}_I = J\sum_{i-j}(a_i^+ a_j^+ a_j a_i + a_i^+ a_j^+ a_j a_i) \tag{22}$$

Here a_i^+ and a_i are the creation operator of the spin-down electron and the annihilation operator of the spin-up at site i, respectively. In the derivation, we have employed the relationships such as $\hat{S}_{j+} = a_j^+ a_{\bar{j}}$, $\hat{S}_{j-} = a_{\bar{j}}^+ a_j$, $\hat{S}_{jz} = 1/2(a_j^+ a_j - a_{\bar{j}}^+ a_{\bar{j}})$, and so on, which are easily confirmed by testing the effect of each side of these expressions on the two spin orbitals $\phi_j(r_j)\alpha(s_j)$ and $\phi_j(r_j)\beta(s_j)$, $\phi_j(r_j)$ being the $2p_\pi$ orbital of the jth carbon atom.

The model Hamiltonian (20) can be solved in various spin spaces in which S or its z-component M is conserved. For a given conjugated molecule with N π-electrons, the number of linearly independent covalent VB structures in a certain

S subspace is known to be $f_S^N = (2S+1)N!/(N/2+S+1)!(N/2-S)!$ [34], while the number of neutral Slater determinants with quantum number M, n(M), equals the binomial coefficient $n(M)=C_{N/2-M}^N$. It is clear that in either case the dimension of the Hamiltonian matrix is exponentially proportional to the size of the system. In this chapter, the Slater determinants are chosen to be the N-electron basis functions, in which the VB model (20) is solved for various S_z spaces respectively.

To illustrate the VB method, we consider several small conjugated molecules in the following. For larger conjugated molecules, the solution of the VB model (20) needs efficient computational techniques, which will be described in the next subsection.

Ethylene. The π-electron network of ethylene has electronic states completely analogous to those of the hydrogen molecule. For convenience, we simply use 1, 2, ..., instead of $2p_{\pi a}, 2p_{\pi b}, ...$, to specify atomic orbitals on various carbon sites in the following. Clearly, ethylene has four Slater determinants built from two AOs, which can be designated by $|1\bar{2}\rangle, |\bar{1}2\rangle, |12\rangle, |\bar{1}\bar{2}\rangle$. According to the above discussions, the wave function can be written as a linear combination of Slater determinants limited to the subspace of conserved z-component of total spin, namely,

$$\psi = \sum_{i=1}^{n} c_i \varphi_i \tag{23}$$

In this subsection, for simplicity we take the energy in units of J so that the elements of the Hamiltonian matrix are all integers. Thus, in the subspace M=0, the VB secular equation is

$$\begin{vmatrix} -1-E & 1 \\ 1 & -1-E \end{vmatrix} = 0 \tag{24}$$

The expansion of this equation yields $(-1-E)^2-1=0$, giving two eigenvalues, $E_{1,2}$= -2, 0, with their corresponding eigenstates $\psi_1 = (|1\bar{2}\rangle - |\bar{1}2\rangle)/\sqrt{2}$ and $\psi_2 = (|1\bar{2}\rangle + |\bar{1}2\rangle)/\sqrt{2}$, respectively. While in subspaces of M=+1, -1, the wave functions are simply $|12\rangle$, $|\bar{1}\bar{2}\rangle$, with both eigenvalues equal to zero. In summary, ethylene has two electronic states in the VB model, one is the singlet state ψ_1 with the energy -2, the other is the triplet state (ψ_2, or $|12\rangle$, or $|\bar{1}\bar{2}\rangle$) with the energy 0.

Butadiene. There are a total of 16 Slater determinants in the neutral VB

space which split into five groups consisting of 1, 4, 6, 4, 1, associated with M=-1, -2, 0, 1, 2, respectively, in which those having equal but opposite M values have identical numbers. Because of the spin-inversion symmetry, the VB model only needs to be solved in M=0, 1, 2 subspaces.

The energy matrix entries can be evaluated by simple rules. For a given determinant, the diagonal entry equals the negative value of the number of spin-alternations for nearest-neighbor pairs of carbon atoms in the determinant, i.e.,

$$\langle \varphi_k | \hat{H} | \varphi_k \rangle = -(\text{number of spin-alternations for all carbon-carbon bonds in } \varphi_k) \qquad (25)$$

The off-diagonal entry between two Slater determinants always takes the value 1 or 0

$$\langle \varphi_k | \hat{H} | \varphi_l \rangle = 1 \text{ or } 0 \qquad (26)$$

in which 1 results only if the two Slater determinants differ by just one spin-exchange on a specified carbon-carbon bond and otherwise 0 results. Suppose the carbon atoms of butadiene are numbered as 1, 2, 3, 4, from left to right, then applying the above rules easily leads to all matrix entries of the VB Hamiltonian. For example, $\langle 1\overline{2}3\overline{4}|\hat{H}|1\overline{2}3\overline{4}\rangle = -3$, $\langle \overline{1}23\overline{4}|\hat{H}|\overline{1}23\overline{4}\rangle = -2$, $\langle 1\overline{2}3\overline{4}|\hat{H}|\overline{1}23\overline{4}\rangle = 1$, $\langle 12\overline{3}\overline{4}|\hat{H}|1\overline{2}\overline{3}4\rangle = 0$.

Because the Hamiltonian matrix is sparse and its elements are simply integers, one can specifically map it to a "configuration interaction" graph. The graph is a collection of points and lines. Each Slater determinant maps to a point with its degree, the number of lines incident to the point, equal to the negative value of the diagonal entry. Each line defines a non-zero off-diagonal entry, 1, between two points. In this way, two graphs representing the Hamiltonian matrices of butadiene in spin spaces M=0 and 1 respectively are shown below, along with their corresponding secular equations aside each graph.

(1) M=0

$$\begin{vmatrix} -1-E & 1 & 0 & 0 & 0 & 0 \\ 1 & -3-E & 1 & 1 & 0 & 0 \\ 0 & 1 & -2-E & 0 & 1 & 0 \\ 0 & 1 & 0 & -2-E & 1 & 0 \\ 0 & 0 & 1 & 1 & -3-E & 1 \\ 0 & 0 & 0 & 0 & 1 & -1-E \end{vmatrix} = 0$$

(2) M=1
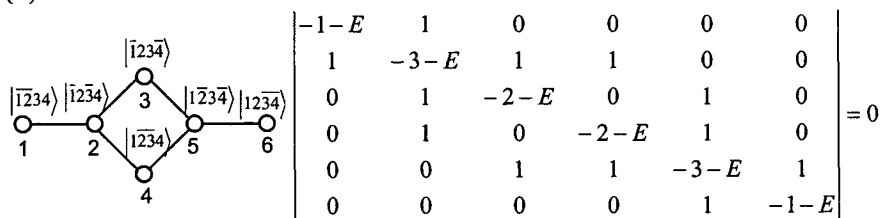
$$\begin{vmatrix} -1-E & 1 & 0 & 0 \\ 1 & -2-E & 1 & 0 \\ 0 & 1 & -2-E & 1 \\ 0 & 0 & 1 & -1-E \end{vmatrix} = 0$$

The expansion of the secular equations shown above results in two polynomials, $E^6 + 12E^5 + 52E^4 + 100E^3 + 84E^2 + 24E = 0$ for M=0 and $E^4 + 6E^3 + 10E^2 + 4E = 0$ for M=1. While for M=2, the eigenstate is just $|1234\rangle$, with the energy $E=0$. Classifying the roots obtained from these polynomials by spin multiplicity and point group C_s, we have eigenvalues of butadiene in the increased energy order, $^1A'$ ($-3-3^{1/2}$), $^3A''$ ($-2-2^{1/2}$), $^3A'$ (-2), $^1A'$ ($-3+3^{1/2}$), $^3A''$ ($-2+2^{1/2}$), and $^5A'$ (0). For these eigenvalues, one can also derive corresponding wave functions without difficulty.

Trimethylene-cyclopropane. By the same procedure outlined above, we have obtained the eigenvalues of trimethylene-cyclopropane classified by spin multiplicity and the irreducible representations of its point group D_{3h} as follows: $^1A'_1$ (-8.000), $^3E'$ (-6.529), $^3A'_1$, $^3A'_2$, $^1E'$ (-5.000), $^5E'$ (-4.303), $^3E'$ (-3.833), $^1A'_1$, $^1A'_2$ (-3.000), $^5A'_1$, $^3A'_1$ (-2.000), $^3E'$ (-1.639), $^5E'$ (-0.697), $^7A'_1$ (0.000).

2.2 Computational methods

2.2.1. Lanczos method

It is instructive to solve the VB model in the space of conserved z-component of total spin because Slater determinants are orthogonal to each other. The central idea of the Lanczos method [35] is to transform a general quantum model to a chain model or, in matrix language, to convert a general symmetric matrix into a tridiagonal matrix via an orthogonal transformation. By recursion, the eigenvalue can be effectively computed from a well-behaved initial state, ψ_0. If ψ_0 (normalized to 1) has a nonzero projection over the true ground state, ψ, the recursion can give a good approximation to the ground state as accurate as possible. Otherwise, it will converge to an excited state. Since the larger the number of spin-alternations in a determinant, the lower its energy will be (see Eq. (25)), the classical Néel state is usually chosen as an initial state to determine the ground state. For low-lying excited states, the same procedure can proceed in other subspaces of different M. Comparing the energies of these states, the first excited and other low-lying excited states can be picked out [20].

Let's describe this recursion process. By operating with $\hat{H}$ on ψ_0, we define a state ψ_1 as follows

$$\psi_1 = (\hat{H}\psi_0 - a_o\psi_0)/b_1 \tag{27}$$

where

$$a_0 = \left\langle \psi_0 \middle| \hat{H} \middle| \psi_0 \right\rangle \tag{28}$$

$$b_1^2 = \left\langle (\hat{H}\psi_0 - a_0\psi_0) \middle| (\hat{H}\psi_0 - a_0\psi_0) \right\rangle \tag{29}$$

It is obvious that ψ_1 is normalized and orthogonal to ψ_0.

Once we have obtained ψ_0 and ψ_1, we can construct a set of orthonormal states $\{\psi_2, \psi_3, ..., \psi_n\}$ in succession defined by the following relation

$$\psi_n = (\hat{H}\psi_{n-1} - a_{n-1}\psi_{n-1} - b_{n-1}\psi_{n-2})/b_n \tag{30}$$

where

$$a_{n-1} = \left\langle \psi_{n-1} \middle| \hat{H} \middle| \psi_{n-1} \right\rangle \tag{31}$$

$$b_n^2 = \left\langle (\hat{H}\psi_{n-1} - a_{n-1}\psi_{n-1} - b_{n-1}\psi_{n-2)} \middle| (\hat{H}\psi_{n-1} - a_{n-1}\psi_{n-1} - b_{n-1}\psi_{n-2}) \right\rangle \tag{32}$$

Obviously, all $\psi_i (i \leq n)$ span a tridiagonal symmetric matrix of $\hat{H}$ with diagonal entries $\{a_0, a_1, ..., a_{n-1}\}$ and their nearest-neighbor off-diagonal entries $\{b_1, b_2, ..., b_n\}$ represented by a chain graph. Then the secular equation for the chain model is solved for the eigenvalues instead of the original Hamiltonian matrix.

For a tridiagonal matrix, less entries, $3n$, rather than $n \times n$, have to be stored. If we limit ourselves to the ground state and a few excited states, the recursive calculation can terminate at some early stage under recursions much less than n, giving the eigenvalues steadily converging toward exact results. In other words, the calculated eigenvalues within a given precision are no longer changed on increasing the number of recursions. The tridiagonal Hamiltonian matrix facilitates the computation for the corresponding eigenvectors in terms of the transformed basis set expressed by Eqs. (27) and (30). In order to obtain the eigenvectors in the original Hilbert space, we must repeat the recursion procedure accumulating the basis vectors with their corresponding weights. Then the resultant wave functions can be employed for evaluating various quantities of interest, with the purpose of gaining the structure-property

relationships for conjugated molecules.

2.2.2. Coding of the Slater determinants

For a conjugated molecule with N π-electrons (or carbon atoms), the wave function (Eq. (23)) spans the subspace characterized by quantum number M with dimension $n(M)$ equal to a binomial coefficient $n(M)=C_{N/2-M}^{N}$. This implies that the dimension for the subspace of M increases exponentially with the size of the system. For examples, we have n(0)=184,765, n(1)=167,960 for N=20, which increase to n(0)=40,116,600, n(1)=37,442,160 when N=28. Obviously, the storage of such an enormous number of determinants is first of importance for the efficient implementation of VB calculations. For this purpose, we introduce an algorithm of coding the Slater determinants for minimizing the searching time and saving the storing space in the central memory of the computer [22].

As we have mentioned, each Slater determinant is defined by a unique array of site numbers 1, 2, ..., N with specific spin distribution. Apparently, one can extract the sequence of spin-up (or spin-down) sites to specify a determinant. For example, when N being even and M=0, this spin-up site sequence consists of N/2 numbers, $\{\alpha_1, \alpha_2, ..., \alpha_{N/2}\}$ where α_i (i=1, 2, ..., N/2) satisfies $\alpha_1 < \alpha_2 < ... < \alpha_{N/2}$ and $i \le \alpha_i \le N/2+i$. For illustration, we list the twenty Slater determinants and their spin-up sequences, $\{\alpha_1, \alpha_2, \alpha_3\}$ for N=6 and M=0 in Table 1.

Let us demonstrate the coding of 20 Slater determinants in Table 1. We have arranged them one by one sequential entries: we put $\{\beta_1, \beta_2, \beta_3\}$ ahead of $\{\gamma_1, \gamma_2, \gamma_3\}$, if $\beta_1 < \gamma_1$ or $\beta_1 = \gamma_1$, but $\beta_2 < \gamma_2$, or if $\beta_1 = \gamma_1, \beta_2 = \gamma_2$, but $\beta_3 < \gamma_3$. Thus, for the whole set of determinants we can define ordinal numbers from 1 to 20 shown in the third column of Table 1. There is a one-to-one correspondence between the spin-up site sequence and the ordinal number, and in fact we can derive an analytical formula to connect them. In the following, we exemplify one of the determinants, $|\bar{1}2\bar{3}4\bar{5}6\rangle$, with the spin-up sequence {246} and the ordinal number 15.

At first, we notice when α_1=1, α_2 and α_3 can be either 2 or 3 up to 6 in constraint to $\alpha_2 < \alpha_3$, thus the total number of combinations with α_1=1 is equal to the binomial coefficient

$$C_{3-1}^{6-1} = C_2^5 = 10 \tag{33}$$

Such ten determinants are labeled in Table 1 with ordinal numbers 1 to 10. Similarly, if α_1=2, α_2 and α_3 are to be integers satisfying $3 \le \alpha_2 < \alpha_3 \le 6$ which

result in six determinants numbering from 11 to 16 in Table 1. Obviously, $\{246\}$ is located between 10 and 16. Then $\{246\}$ has an ordinal number greater than 13 rather than 10, because the sequences with $\alpha_1=2$, $\alpha_2=4$ follow those with $\alpha_1=2$, $\alpha_2=3$ while the latter cover three determinants due to the fact that α_3 can be 4, 5, or 6. Thus, 13 is a sum of two binomial coefficients

$$C_{3-1}^{6-1} + C_{3-2}^{6-2-1} = C_2^5 + C_1^3 = 10+3 = 13 \tag{34}$$

Meanwhile, if $\alpha_1=2$, $\alpha_2=4$, then α_3 can be either 5 or 6. Since $\{246\}$ is preceded by $\{245\}$, $\{246\}$ corresponds to the ordinal number 15.

The evaluation of the ordinal number of $\{246\}$ suggests that 15 can be summed stepwise as 10+3+1+1, in which "10" denotes the number of sequences with $\alpha_1=1$ (<2), "3" signifies the number of sequences with $\alpha_1=2$, $\alpha_2=3$ (<4), "1" represents the sequence with $\alpha_1=2$, $\alpha_2=4$, $\alpha_3=5$ (<6), and the last "1" comes from $\{246\}$ itself. In general, the ordinal number, δ, of the sequence $\{\alpha_1\alpha_2\alpha_3\}$ can be analytically written as

$$\delta\{\alpha_1\alpha_2\alpha_3\} = \sum_{j=1}^{\alpha_1-1} C_{3-1}^{6-j} + \sum_{j=1}^{\alpha_2-\alpha_1-1} C_{3-2}^{6-\alpha_1-j} + \sum_{j=1}^{\alpha_3-\alpha_2-1} C_{3-3}^{6-\alpha_2-1} + 1 \tag{35}$$

Table 1
The coding of Slater determinants for M=0 and N=6

Slater determinant	$\alpha_1\,\alpha_2\,\alpha_3$	Coset	Ordinal number	Slater determinant	$\alpha_1\,\alpha_2\,\alpha_3$	Coset	Ordinal number
$\|123\overline{4}\overline{5}\overline{6}\|$	123	E	1	$\|\overline{1}23\overline{4}\overline{5}6\|$	234	A	11
$\|12\overline{3}4\overline{5}\overline{6}\|$	124	C	2	$\|\overline{1}23\overline{4}5\overline{6}\|$	235	C	12
$\|12\overline{3}\overline{4}5\overline{6}\|$	125	C	3	$\|\overline{1}23\overline{4}\overline{5}6\|$	236	C	13
$\|12\overline{3}\overline{4}\overline{5}6\|$	126	A	4	$\|\overline{1}2\overline{3}45\overline{6}\|$	245	D	14
$\|1\overline{2}34\overline{5}\overline{6}\|$	134	C	5	$\|\overline{1}2\overline{3}4\overline{5}6\|$	246	B	15
$\|1\overline{2}3\overline{4}5\overline{6}\|$	135	A	6	$\|\overline{1}2\overline{3}\overline{4}56\|$	256	D	16
$\|1\overline{2}3\overline{4}\overline{5}6\|$	136	C	7	$\|\overline{1}\,\overline{2}345\overline{6}\|$	345	B	17
$\|1\overline{2}\overline{3}45\overline{6}\|$	145	D	8	$\|\overline{1}\,\overline{2}34\overline{5}6\|$	346	D	18
$\|1\overline{2}\overline{3}4\overline{5}6\|$	146	D	9	$\|\overline{1}\,\overline{2}3\overline{4}56\|$	356	D	19
$\|1\overline{2}\overline{3}\overline{4}56\|$	156	B	10	$\|\overline{1}\,\overline{2}\,\overline{3}456\|$	456	E	20

Here the upper bounds of the summations are, $\alpha_1 - 1 = 1$, $\alpha_2 - \alpha_1 - 1 = 1$, and $\alpha_3 - \alpha_2 - 1 = 1$, respectively, with exceptions for $\alpha_i = \alpha_{i-1} + 1 \, (\alpha_0 = 0)$, in which the corresponding term vanishes.

This coding procedure can be extended to systems having N π-electrons. The spin-up site sequence $\{\alpha_1, \alpha_2, ..., \alpha_i, ..., \alpha_{N/2-M}\}$ with $\alpha_1 < \alpha_2 < ... < \alpha_{N/2-M}$ is extracted from the Slater determinant of quantum number M. No matter how huge the dimension of the subspace is, an ordinal number can be defined uniquely for every determinant to maintain the one-to-one correspondence with the spin-up sequence. The general formula is as follows

$$\delta\{\alpha_1, \alpha_2, ..., \alpha_i, ..., \alpha_{N/2-M}\} = \sum_{i=1}^{N/2-M} \sum_{j} C_{N/2-M-i}^{N-\alpha_{i-1}-j} + 1 \tag{36}$$

where $1 \le j \le \alpha_i - \alpha_{i-1} - 1$ and $\alpha_0 \equiv 0$. Obviously, Eq. (36) generates natural numbers from 1 to n(M), mapping one-to-one to the Slater determinants of conserved M, as displayed in Table 1 for N=6.

In summary, we can use natural numbers obtained using Eq. (36) instead of the spin-up sequences to store the n(M) Slater determinants in the central memory of the computer. As a result, the time consumed in searching the determinants and the space needed to store the determinants are minimized.

2.2.3. Symmetry adapted linear combinations (SALCs) of the determinants

The VB Hamiltonian matrix can split into N+1 blocks characterized by M=0, ± 1, ± 2, ..., $\pm N/2$ for even N. Each block of dimension n(M) can be reduced again by utilizing the molecular point symmetry. Eigenvalues of each eigenlevel are found in the M=0 block, in which the spin-inversion symmetry can be employed for further simplification.

One can deal with the reduction by constructing SALCs of the Slater determinants via the projection operator approach. In other words, we factorize n(M) Slater determinants into disjoint invariant subspaces under the point group of the molecule. An invariant subspace includes a subset of determinants generated by operating on an arbitrary determinant with all symmetry elements of the molecular point group G. Because a single determinant generating one of these invariant subspaces S may be invariant under a subgroup H of G, the basis determinants of S correspond to cosets of H in G. Often coset representatives of H in G may be themselves chosen to form a group, called the factor group. For illustration, the 20 determinants of M=0 for trimethylene-cyclopropane have been partitioned into six invariant subspaces under the point group D_{3h}, symbolized by A, B, C, D, E, and F in Table 1. The factor groups for A (B), C (D) and E (F) are C_3, C_{3v} and identity group, respectively. The sum of factor

group orders equals the dimension of M=0 block, n(0), i.e., 20=3+3+6+6 +1+1.

After the factorization, one can derive SALCs within each invariant subspace via the action of the projection operator. The projection operator for irreducible representation j is defined as

$$\hat{P}^j = (N)^{-1/2} \sum_R \sigma(R) \chi^j(R) R \tag{37}$$

where N is the normalizing factor, the summation runs over all symmetry operations of the factor group, $\chi^j(R)$ is the character of the jth irreducible representation and $\sigma(R)$ is a phase factor equal to +1 or −1 depending on whether R refers to an even or odd permutation of atom sites. For the computation of low-lying states, we can limit our attention to one-dimensional irreducible representations. Consider trimethylene-cyclopropane as an example. It is easy to derive six SALCs of A_1' by using the operator (37) on each of the six invariant subspaces and two SALCs of A_2' from C and D displayed in Table 1 under point group D_{3h}. Thus, we simplify the calculation by reducing the original 20×20 matrix to smaller matrices, 6×6 and 2×2, provided we deal with the lowest singlet and triplet states only.

For medium-sized molecules such as hexacene of 26 π-electrons, n(0) is equal to 10,400,600. By means of symmetry, the ground state is solved from the block of A_g under point group D_{2h} with a dimension of 2,600,612. Thus the Hamiltonian matrix can be considerably reduced for those molecules with higher symmetry. For hexacene and two other benzenoids, the dimensions of one-dimensional irreducible representations in subspaces of M=0, 1, and 2 are listed in Table 2.

In addition, the spin-inversion symmetry is available for M=0. The operator $\hat{O}$ is defined when it acts on a Slater determinant, transforming all spin-up sites to spin-down sites and vice versa. Thus the space of M=0 is invariant under the group $[I, \hat{O}]$ which consists of identity and spin-inversion operations. Let us discuss the 20 determinants of M=0 for trimethylene-cyclopropane, the spin-inversion operator transforms A to B, C to D, and E to F, or vice versa, respectively. Under the compounded group $D_{3h} \otimes [I, \hat{O}]$, a pair of Slater determinants that are transformable via the spin-inversion operation should combine, as represented by $A \pm B$, $C \pm D$ and $E \pm F$ respectively. Thus blocks A_1' and A_2' are further reduced to two 3×3 and two 1×1 blocks belonging to irreducible representations $A_1'^+$, $A_1'^-$ and $A_2'^+$, $A_2'^-$ of group $D_{3h} \otimes [I, \hat{O}]$.
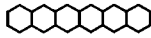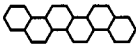
The combination of Slater determinants in different invariant subspaces to simplify the secular equation has been called the "half-projected Hartree-Fock"

method [36,37]. In general, under the compounded group of point group and spin-inversion, all irreducible subspaces have smaller dimensions: nearly half of those in the point group alone. These are illustrated in Table 2 for three molecules.

After the SALCs of the Slater determinants have been obtained, the Lanczos method is employed for diagonalization.

Table 2
Dimensions of each irreducible representation in the various S_Z spaces.

D_{2h}	A_g $(A_g^+)^a$	B_{1g} (B_{1g}^+)	B_{2u} (B_{2u}^+)	B_u (B_u^+)	Total dimensions in S_Z space
$S_Z = 0$	2,600,612 (1,302,354)	2,599,688 (1,309,756)	2,599,688 (1,309,756)	2,600,612 (1,314,514)	10,400,600
$S_Z = 1$	2,415,712	2,413,996	2,413,996	2,413,996	9,657,700
$S_Z = 2$	1,931,936	1,931,144	1,931,144	1,931,936	7,726,160

C_{2h}	A_g (A_g^+)	B_u (B_u^+)	Total dimensions in S_Z space
$S_Z = 0$	5,200,300 (2,602,198)	5,200,300 (2,606,294)	10,400,600
$S_Z = 1$	4,827,992	4,829,708	9,657,700
$S_Z = 2$	3,863,080	3,863,080	7,726,160

D_{2h}	A_g (A_g^+)	B_{1g} (B_{1g}^+)	B_{2u} (B_{2u}^+)	B_u (B_u^+)	Total dimensions in S_Z space
$S_Z = 0$	10,032,648 (5,020,420)	10,027,368 (5,013,684)	10,027,368 (5,013,684)	10,029,216 (5,010,512)	40,116,600
$S_Z = 1$	9,362,256	9,358,824	9,358,824	9,362,256	37,442,160
$S_Z = 2$	7,608,483	7,603,896	7,603,896	7,605,480	30,421,755

[a] The values in brackets are the dimensions of the totally symmetric irreducible representation, according to the point group plus spin-inversion symmetry $G \otimes \hat{o}$.

3. APPLICATIONS TO THE π-CONJUGATED MOLECULES

Using the effective computational methods introduced above, the VB energies and wave functions of the ground and the lowest excited states have been calculated for a large number of conjugated systems with up to 28 π-electrons (Fig. 1). We will demonstrate that these results can be used to account for some physical and chemical properties such as the bond lengths, kinetic reactivities, low-lying electronic spectra, and local and global aromaticities of BHs. In addition, we illustrate that the VB model provides a feasible way of calculating the spin coupling strength of the π-conjugated radicals.

3.1. Bond lengths

Analogous to the bond orders in the MO approaches, p_{ij}^s, as defined in Eq. (38), which stands for the probability of finding a singlet arrangement between atoms i and j [38], has been introduced as an index to correlate with the bond lengths of BHs.

$$p_{ij}^s = \left\langle \Psi \left| \tfrac{1}{2}(a_i^+ a_j^+ - a_{\bar{i}}^+ a_{\bar{j}}^+)(a_{\bar{j}} a_i - a_j a_{\bar{i}}) \right| \Psi \right\rangle \tag{38}$$

The reason for choosing this index is because the VB energy of a molecule can be partitioned into the sum of the probabilities of finding local singlet arrangements on its various bonds, as shown in Eq. (39).

$$
\begin{aligned}
E_\pi &= \left\langle \Psi \left| J \sum_{i-j} (2\hat{S}_i \cdot \hat{S}_j - \tfrac{1}{2}) \right| \Psi \right\rangle = \left\langle \Psi | H_D + H_I | \Psi \right\rangle \\
&= -2J \sum_{i-j} P_{ij}^s
\end{aligned}
\tag{39}
$$

As a result, one may expect that p_{ij}^s could measure the strength of the i-j bond and correlate with the i-j bond length. A good linear correlation (Fig. 2) between the calculated ground-state p_{ij}^s and the experimental bond lengths of several BHs (displayed later in Table 3) encouraged us to apply these p_{ij}^s values to predicting carbon-carbon bond lengths. In order to do so, we must establish the appropriate empirical formula between the bond length and the corresponding ground-state p_{ij}^s. Since the VB model (18) homogenizes all sites and all bonds, it is suitable to select two typical species, benzene (1) and pyrene (5), to determine this formula. A least-square procedure results in an excellent linear relationship below

582
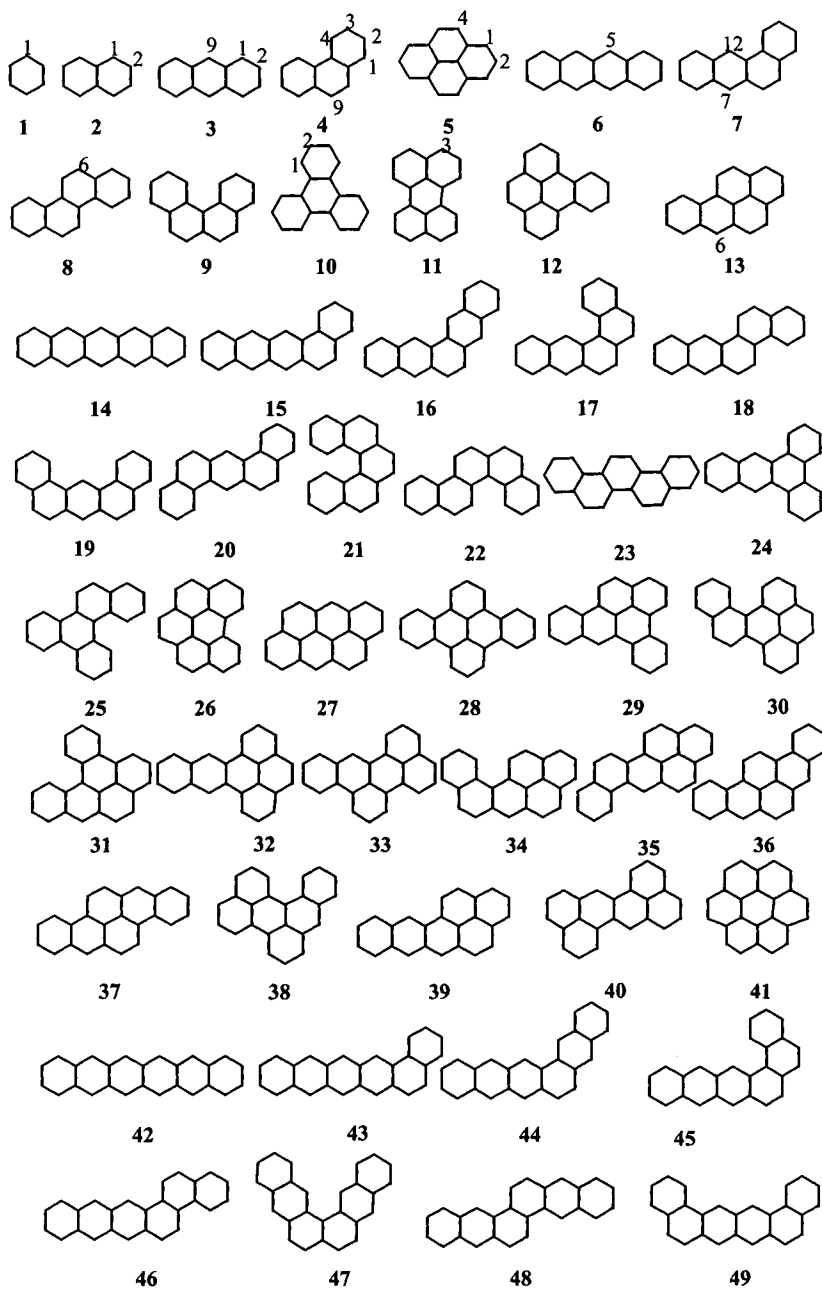
Fig. 1. Selected benzenoid hydrocarbons (to be continued).
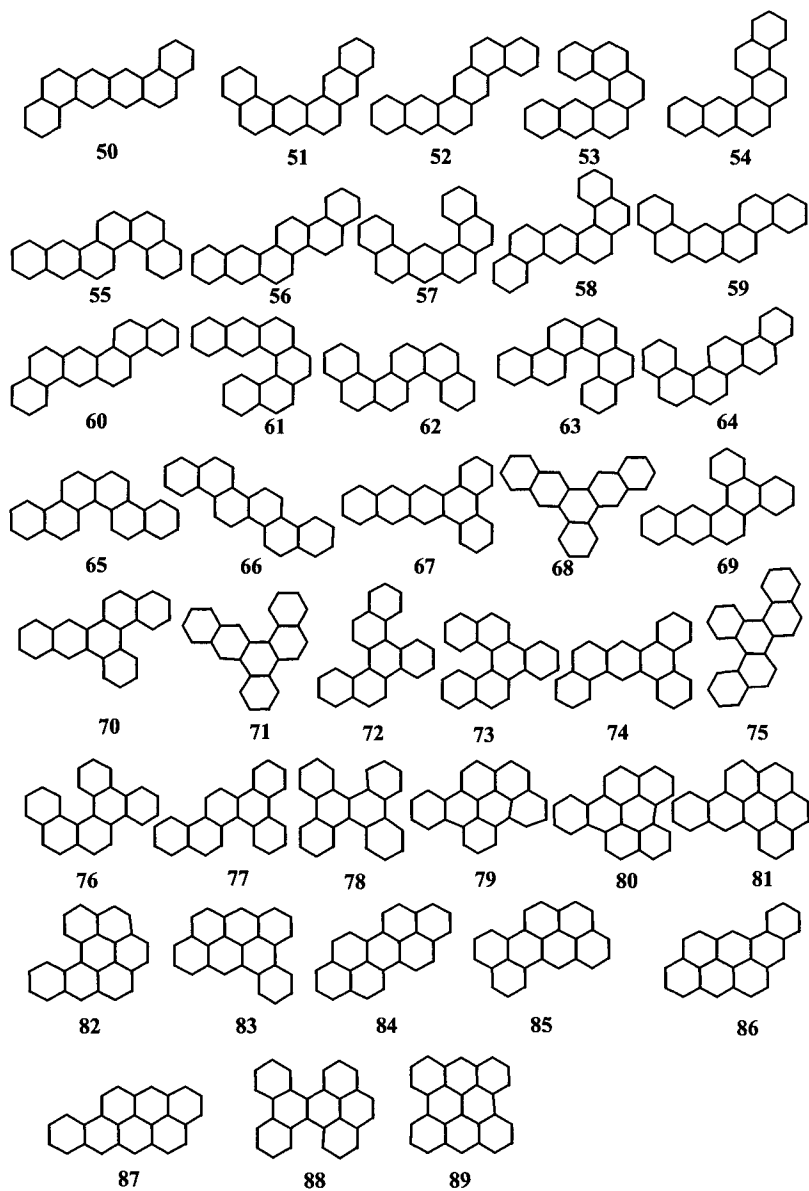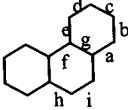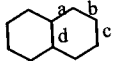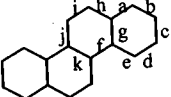
Fig. 1. Selected benzenoid hydrocarbons (continued).

Table 3
Bond lengths in benzenoid hydrocarbons (Å)

Compound	Bond	P^s_{ij}	Bond length		Compound	Bond	P^s_{ij}	Bond length	
			Exptl[a]	Calcd				Exptl[a]	Calcd
Benzene		0.717	1.397	1.395	Phenanthrene	a	0.646	1.423	1.418
Pyrene						b	0.751	1.386	1.385
	a	0.718	1.395	1.395		c	0.678	1.394	1.408
	b	0.666	1.406	1.411		d	0.748	1.401	1.386
	c	0.616	1.425	1.427		e	0.655	1.409	1.415
	d	0.586	1.438	1.437		f	0.557	1.465	1.446
	e	0.615	1.430	1.428		g	0.634	1.420	1.422
	f	0.807	1.367	1.367		h	0.588	1.453	1.436
Naphthalene						i	0.807	1.350	1.367
	a	0.628	1.422	1.423	Chrysene				
	b	0.766	1.371	1.380		a	0.640	1.428	1.420
	c	0.661	1.412	1.413		b	0.754	1.363	1.384
	d	0.619	1.420	1.426		c	0.673	1.394	1.409
Anthracene						d	0.751	1.381	1.385
	a	0.613	1.444	1.428		e	0.649	1.409	1.417
	b	0.775	1.375	1.377		f	0.571	1.468	1.442
	c	0.649	1.418	1.417		g	0.629	1.409	1.423
	d	0.673	1.405	1.409		h	0.599	1.421	1.433
	e	0.594	1.433	1.434		i	0.792	1.369	1.372
Tetracene						j	0.611	1.428	1.429
	a	0.608	1.420	1.430		k	0.655	1.401	1.415
	b	0.777	1.381	1.376	Triphenylene				
	c	0.646	1.459	1.418		a	0.665	1.410	1.412
	d	0.586	1.420	1.437		b	0.739	1.381	1.388
	e	0.681	1.390	1.407		c	0.688	1.397	1.405
	f	0.655	1.404	1.415		d	0.646	1.413	1.418
	g	0.574	1.460	1.441		e	0.531	1.458	1.454

[a] Values are from Ref. 18 and references therein.

$$d_{ij}(\overset{\circ}{A}) = 1.622 - 0.316 p^s_{ij} \tag{40}$$

where d_{ij} denotes the length of the i-j bond. By applying this relationship, the bond lengths of these two molecules and several other BHs have been calculated and listed in Table 3.

The average deviation of the calculated and experimental values, ±0.009Å, is slightly larger than the average estimated experimental error of ±0.008Å and comparable to the results given by Cioslowski based on the ab initio VB approach [39]. Deviations between calculated and experimental bond lengths depend on the approximate extent of the Hamiltonian (18) in which equal J for each C-C bond is assumed. For examples, in triphenylene almost all bond lengths are predicted in remarkable agreement with the observed values because this molecule may be regarded as being composed of three benzene rings joined together through single bonds and consequently to a larger extent it satisfies the approximation made in the Hamiltonian (18). While the bond lengths predicted
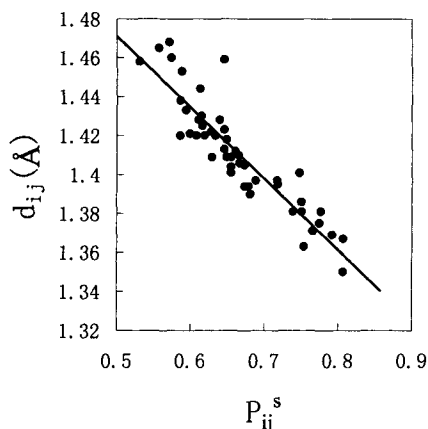
Fig. 2. Relation between the ground-state singlet probabilities and experimental bond lengths for BHs listed in Table 3.

by Eq. (40) is less satisfactory for tetracene because its diminished aromatic character leads to larger differences among the bond lengths, which conflicts with the equal J-value assumption.

3.2. Reactivities

Electrophilic aromatic substitution is a typical reaction for BHs. In the MO treatment, some indices such as free valence [40], localization energy [41], and other quantities [42,43] have been introduced to predict the orientation of electrophilic aromatic substitution. Within the VB framework, several indices have also been formulated [44]. Here we introduce an alternative index, which is available from accurate VB wave functions, and demonstrate its applicability in accounting for the electrophilic aromatic substitution.

According to Eq. (39), the total VB energy could also be partitioned into the sum of the quantities with respect to each site, i.e.,

$$E_\pi = -2J\sum_i \sum_{j>i} p_{ij}^s$$
$$= \sum_i E_i \tag{41}$$

where

$$E_i = -J\sum_{i-j} P_{ij}^s \tag{42}$$

Since p_{ij}^s was proven to be a well-behaved local index of a certain i-j bond, E_i (negative) might be feasibly understood as the local site-energy of the ith atom. When an electrophilic substitution occurs, primary concern is to the change of the total energy as an electrophilic group attacks a certain carbon atom. Supposing lengths of those bonds bound to the ith atom are equally varied in the preliminary stage of the electrophilic attack, resulting in a small variation of exchange parameter J, the first-order change in the total π-energy of this molecule can be easily evaluated with

$$\Delta E = \Delta J(-2\sum_{i-j} P_{ij}^s) = 2\frac{\Delta J}{J}E_i \tag{43}$$

Thus ΔE (positive) is proportional to the site-energy E_i of the ith atom defined by Eq. (42), indicating that the site-energy E_i may be anticipated to serve as a reactivity index for electrophilic aromatic substitution, i.e., a site is more reactive the smaller is the absolute value of its site-energy. For a few selected BHs, the calculated site-energy values and Hammett's σ^+ constants [30], which were derived from the empirical fitting of experimental data, are given in Table 4. Evidently, there exists a good correlation between the calculated E_i and Hammett's σ^+ constants as shown in Fig. 3.

Table 4
Reactivity indices for selected BHs[a]

Compound	Position	E_i^b	σ^{+c}	Compound	Position	E_i^b	σ^{+c}
1	1	1.434	-7.8	5	1	1.383	6.1
2	1	1.394	0.0		2	1.436	
	2	1.427	-3.4		4	1.393	
3	1	1.388	1.1	6	5	1.336	9.8
	2	1.424	0.0	7	7	1.350	6.6
	9	1.346	8.1		12	1.355	6.6
4	1	1.397	-0.2	8	6	1.391	2.6
	2	1.429	-2.5	10	1	1.404	-0.8
	3	1.426	-0.5		2	1.427	-2.3
	4	1.403	-2.7	11	3	1.377	8.4
	9	1.395	0.5	13	6	1.339	11.1

[a] The numbering of compounds and their positions (C atoms) are shown in Fig. 1. [b] In units of $-J$. [c] Values are from Ref. 30.

3.3. Low-lying electronic spectra

Compared with ground states of BHs, the low-lying excited states of these systems have been less studied from the semiempirical VB approaches. This is not accidental because even for benzene (1) the descriptions of the classical VB
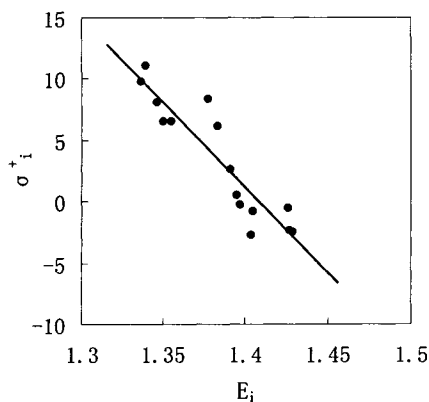
Fig. 3. Correlation of E_i values with experimental reactivities.

theory for its lowest excited state are not satisfactory [13]. The inclusion of nonadjacant and cyclic six-body contributions into the classical VB model has been proven to be necessary for improving the low-lying electronic spectra of benzene [13]. Meanwhile, the effect of higher order corrections was found to become gradually smaller with the increase in the size of benzenoids, and the classical VB model could yield reasonably accurate results for the low-lying excited states, especially for the lowest excited states of BHs with more than 14 π-electrons [19].

For all BHs with up to 26 π-electrons and two species having 28 electrons (Fig. 1), we have calculated the energies of the singlet ground states and lowest triplet states, which are tabulated in Table 5. For some BHs, we compare the calculated singlet-triplet (S-T) energy gaps ΔE_{S-T} (in units of J) with the available experimental spectra (in units of eV) in Table 6. As shown in Fig. 4, the calculated energy gaps exhibit a good linear correlation with experimental data. From this correlation, we obtain the realistic value of the exchange parameter J to be about 3.15 eV for BHs in the VB model. The predicted S-T energy separations using this parameter are also collected in Table 6. One can see that our predicted lowest triplet spectra compare well with the available experimental spectra with the average deviation of only ±0.13eV, being comparable to the results of the semiempirical PPP MO calculations [45].

The calculated S-T energy gap may also be employed to deduce the kinetic reactivities of a given BH. One might notice that those BHs with large S-T gaps commonly behave relatively inert toward the various reactions, while those BHs

Table 5

Energies of the singlet ground and lowest triplet states and the corresponding S-T energy gaps for all benzenoid hydrocarbons shown in Fig. 1

Compd[a]	E_s[b]	E_T[b,c]	ΔE_{S-T}[d]	Compd[a]	E_s[b]	E_T[b,c]	ΔE_{S-T}[d]
1	-8.60555	-7.23607	1.36948	46	-40.82553	-40.23698	0.58855
2	-15.03997	-14.03395	1.00602	47(C_{2v})	-40.83301	-40.21604(A_1)	0.61697
3	-21.45050	-20.67185	0.77865	48(C_{2h})	-40.83521	-40.22167(B_u)	0.61354
4	-21.52250	-20.64475	0.87775	49(C_{2v})	-40.85050	-40.23585(A_1)	0.61465
5	-25.13256	-24.41103	0.72153	50(C_{2h})	-40.85058	-40.23672(B_u)	0.61386
6	-27.85819	-27.22240	0.63579	51	-40.85894	-40.21862	0.64032
7	-27.94444	-27.20543	0.73901	52	-40.85930	-40.22098	0.63832
8	-27.99497	-27.21658	0.77839	53	-40.88914	-40.24138	0.64776
9	-27.99314	-27.20919	0.78395	54	-40.88999	-40.24151	0.64848
10	-28.03938	-27.21988	0.81951	55	-40.89019	-40.24242	0.64777
11	-31.60319	-30.98949	0.61370	56	-40.89190	-40.24721	0.64469
12	-31.65132	-30.94675	0.70457	57	-40.90432	-40.24684	0.65748
13	-31.59204	-30.96224	0.62960	58	-40.90448	-40.24751	0.65697
14	-34.26652	-33.72357	0.54295	59	-40.90616	-40.25075	0.65541
15	-34.35497	-33.72939	0.62558	60	-40.90648	-40.25313	0.65335
16	-34.36970	-33.70609	0.66361	61	-40.94197	-40.26271	0.67926
17	-34.41313	-33.73185	0.68128	62(C_{2h})	-40.94246	-40.26236(B_u)	0.68010
18	-34.41514	-33.73779	0.67735	63	-40.94323	-40.26551	0.67772
19	-34.43451	-33.73109	0.70342	64	-40.94415	-40.26660	0.67755
20	-34.43483	-33.73365	0.70118	65(C_{2v})	-40.94431	-40.26655(A_1)	0.67776
21	-34.46809	-33.74483	0.72326	66(C_{2h})	-40.94598	-40.27243(B_u)	0.67355
22	-34.46908	-33.74615	0.72293	67(C_{2v})	-40.88045	-40.25706(B_2)	0.62339
23	-34.47083	-33.75256	0.71827	68(C_{2v})	-40.89934	-40.23911(B_2)	0.66023
24	-34.46838	-33.74775	0.72063	69	-40.92131	-40.27544	0.64587
25	-34.50282	-33.77033	0.73249	70	-40.93073	-40.27045	0.66028
26	-35.28475	-34.65456	0.63019	71	-40.93073	-40.27145	0.65928
27	-35.19345	-34.66378	0.52967	72	-40.96899	-40.29443	0.67456
28(D_{2h})	-38.16881	-37.48431(B_{3u})	0.68450	73(C_{2v})	-40.97003	-40.29997(B_2)	0.67006
29	-38.11672	-37.48465	0.63207	74	-40.95613	-40.27137	0.68476
30	-38.11525	-37.46932	0.64593	75(C_{2v})	-40.96865	-40.29234(B_2)	0.67631
31	-38.10104	-37.48538	0.61566	76	-40.97999	-40.28980	0.69019
32(C_{2v})	-38.08140	-37.43523(B_2)	0.64617	77	-40.98104	-40.29205	0.68899
33	-38.08381	-37.50029	0.58352	78(D_{2h})	-41.00554	-40.32046(B_{3u})	0.68508
34	-38.07192	-37.46434	0.60758	79	-41.79631	-41.18568	0.61063
35	-38.07579	-37.47899	0.59680	80(C_{2v})	-41.78128	-41.20091(B_2)	0.58037
36(C_{2v})	-38.05767	-37.48564(B_2)	0.57203	81	-41.75342	-41.18156	0.53633
37(C_{2h})	-38.04832	-37.49477(B_u)	0.55355	82	-41.73391	-41.17928	0.55463
38	-38.04258	-37.52352	0.51906	83	-41.71789	-41.18156	0.53633
39	-38.01145	-37.45350	0.55795	84(D_{2h})	-41.71585	-41.22052(B_{2u})	0.49533
40(C_{2h})	-37.96759	-37.54490(B_u)	0.42269	85	-41.70826	-41.19810	0.51016
41(D_{6h})	-38.95098	-38.34755(B_{1u})	0.60343	86	-41.66739	-41.17575	0.49164
42(D_{2h})	-40.67565	-40.19577(B_{3u})	0.47988	87	-41.64940	-41.18108	0.46842
43	-40.76389	-40.22198	0.54191	88(C_{2v})	-44.61813	-44.00645(B_2)	0.61168
44	-40.78130	-40.19558	0.58572	89(D_{2h})	-45.31055	-44.90399(B_{3u})	0.40656
45	-40.82351	-40.23290	0.59061				

[a] The point groups are given in parentheses. [b] Energies of the singlet ground states (E_S) and the lowest triplet states (E_T) are in units of J. [c] The irreducible representations are given in parentheses. [d] The lowest singlet-triplet energy gaps are in units of $-J$.

Table 6
The lowest triplet spectra for some benzenoid hydrocarbons

Compd	ΔE_{S-T}[a]	Lowest triplet spectra[b]			Compd	ΔE_{S-T}[a]	Lowest triplet spectra[b]		
		VB[c]	Exptl[d]	MO[d]			VB[c]	Exptl	MO[d]
5	0.72153	2.27	2.11	1.79	**16**	0.66361	2.09	2.08	2.07
6	0.63579	1.26	1.26	1.24	**17**	0.68128	2.15		1.89
7	0.73901	2.33	2.04	2.03	**18**	0.67735	2.13	2.23	1.95
8	0.77839	2.45	2.47	2.20	**19**	0.70342	2.22	2.30	2.33
9	0.78395	2.47	2.49		**20**	0.70118	2.21	2.26	2.29
10	0.81951	2.58	2.89	2.76	**21**	0.72326	2.28	2.45	
11	0.61370	1.93	1.56	1.67	**22**	0.72293	2.28	2.52	2.35
12	0.70457	2.22	2.29		**23**	0.71827	2.26	2.49	2.35
13	0.62960	1.98	1.82	1.65	**24**	0.72063	2.27	2.20	2.13
14	0.54295	1.08	<1.24		**25**	0.73249	2.31		2.27
15	0.62558	1.97			**26**	0.63019	1.99	1.99	2.11

[a] Singlet-triplet energy gaps are in units of −J. [b] In units of eV and referring to their ground-state energies. [c] All molecules, except for naphthacene (**6**) and pentacene (**14**) (J=1.99 eV [19b]), are calculated by taking J=3.15 eV. [d] Ref. 19b and references therein.

with very narrow S-T gaps might be very reactive or even difficult to synthesize [30]. For instance, S-T gaps from VB calculations suggest that for sufficiently long polyacenes their ground and lowest triplet states will become nearly degenerate and thus they may be elusive to synthesize [46].
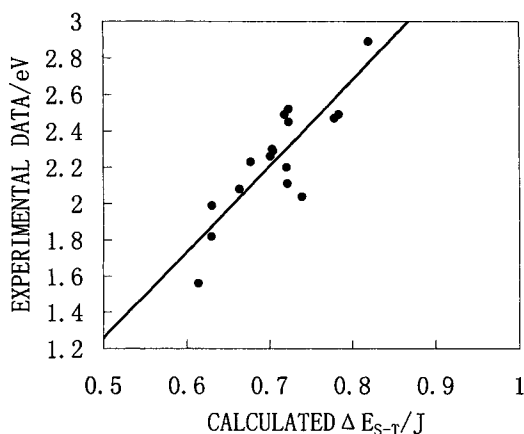

Fig. 4. Correlation of the calculated S-T gaps with experimental data.

3.4. Aromaticity

The concept of aromaticity has rooted in the thought of chemists for a long time. Aromaticity, which is associated with high thermodynamic stability and low reactivity, is helpful in unearthing structure-activity relations and designing novel molecular systems [47,48]. It is easier to describe the nature of aromaticity of a single-ring system than that of polycyclic systems, which has an additional complication due to the local aromaticity for individual hexagons [47,49]. For example, phenanthrene, as a whole entity, is usually considered to be aromatic, but its central ring behaves more like an olefin than the other two terminal rings which resemble benzene to a large degree. Therefore it is necessary to further subdivide the concept of aromaticity into local and global aromaticities. For a certain hexagon within a polycyclic compound, its local aromaticity could be understood as to what extent it chemically behaves like benzene [47]. Local aromaticity has been studied for many years, several indices based on either approximate VB [10,50] or simple MO calculations[51,52] have been put forward to account for local aromaticity.

Global aromaticity, or conventionally termed aromaticity in short, is usually assumed to reflect the thermodynamic stability and kinetic reactivity of a species as a whole [53]. Quantitative descriptions of global aromaticity usually start from consideration of the thermodynamic stability of aromatic compounds relative to reference acyclic olefins. Traditionally, resonance energy (RE) per π electron (REPE) [54] has been extensively employed as a quantitative measure of global aromaticity. Resonance energy is defined as the difference between the total π-electron energy of a given conjugated molecule and that of its corresponding hypothetical reference structure. Several strategies for determining the reference structure and its energy have been reported [54-58], and resultant REPE values correlate reasonably well with each other, giving predictions consistent with chemical facts. Besides the REPE index, absolute hardness and relative hardness [53], indices that could simultaneously cover stability and reactivity, have been shown to be good measures of global aromaticity. Interestingly, it was demonstrated that absolute hardness (or relative hardness) correlates with REPE in general, thus yielding similar predictions in most cases [53].

It is worth pointing out that measures to quantify local and global aromaticities have been principally calculated by means of MO theory, although their definitions are also generally applicable to VB theory. The predominance of MO theory is certainly due to its computational simplicity, e.g., the total π-electron energy of a given conjugated system with N π-electrons is easily obtained by diagonalizing only a $N \times N$ Hamiltonian matrix. Here, we demonstrate that with exact VB results for 89 BHs we obtained it is now

plausible to discuss local and global aromaticities for these BHs from a strict VB model.

3.4.1. Local aromaticity

Similar to Herndon-Ellzey's definition of local aromaticity [10b], we define the relative local hexagon energy (RLHE) as the ratio of the local hexagon energy to the ground-state energy of benzene to measure the local aromaticity of individual rings [18]. Due to the additivity of singlet probabilities on various bonds as indicated in Eq. (39), the local energy of each hexagon in the ground state of a given BH can be directly calculated by

$$E_r = -2J \sum_{i-j} P_{ij}^s \tag{44}$$

where the summation goes over the bonds in the rth hexagon.

The calculated RLHE values of several BHs have been given in Fig. 5. For the polyacene series, the local aromaticity of each hexagon reflected by its corresponding RLHE monotonously decreases from the terminal toward the central, verifying the idea of the "aromatic dilution" of Clar's sextet concepts [47]. Along this series, the local aromaticity of the end hexagons becomes weaker gradually and finally arrives at a constant value with the increasing number of rings, while the decrease in the local aromaticity of the middle rings is more noticeable. Thus, the ease on addition reaction occurring across the para positions in the central rings of long chain polyacenes could be anticipated, in accord with the observed increasing reactivity upon the annelation of hexagons [49].

For triphenylene (10) and perylene (11), their central rings have the lowest RLHE values, 0.821 and 0.814, respectively (Fig. 5). As we know, for hypothetical non-aromatic cyclohexatriene with three localized bonds, whose energy should be the same as the energy of either one Kekulé structure of benzene, the ratio of its energy to the total π-electron energy of benzene is 0.871. Hence, the central hexagons of triphenylene and perylene are less stable than the non-aromatic cyclohexatriene, numerically confirming the concept of Clar's "empty" ring [47].

It has been shown that a linear relationship between the present RLHEs and the $\bar{r}_L^P$ values (normalized benzene character in PPP-MO theory [51]) holds very well. Very recently, Suresh and Gadre [49] suggested a new local aromaticity index based on the molecular electrostatic potential topography (MESP) of the π regions of BHs, which is obtainable from ab initio MO calculations. This index was also found to bear linear correlation with the RLHE values. As a result, one
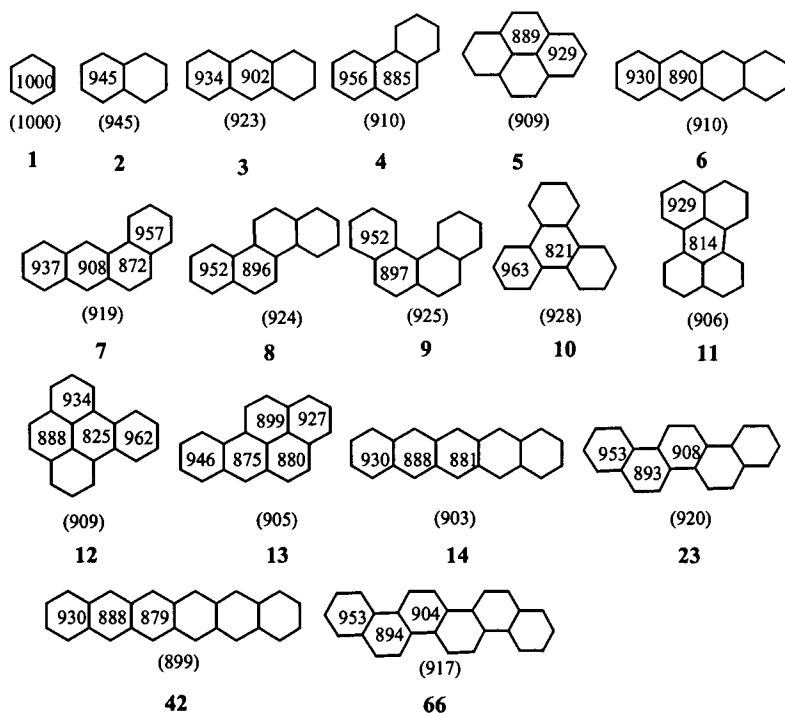
Fig. 5. RLHE values of selected BHs. Values are given as 1000RLHE. The av. RLHE values are listed in the parentheses.

can see that VB and MO models give consistent interpretations on the local aromaticity of BHs. Moreover, it is encouraging that the RLHE index avoids the limitations of those VB indices [10b,50] based solely on the enumeration of the Kekulé structures, which provide unsatisfactory predictions of local aromaticity for individual rings within some BHs such as polyacene series and benz[a]anthracene.

3.4.2. Global aromaticity

As done in MO theory, REPE values can be computed within the VB model if an appropriate reference structure and its energy are determined [22]. Then

$$REPE = RE/N \qquad (45)$$

where

$$RE = E_\pi - E_\pi(\text{ref}) \qquad (46)$$

and E_π is the VB ground state energy of the studied molecule, and $E_\pi(ref)$ is the VB ground state energy of the acyclic π-conjugated reference system.
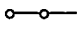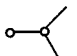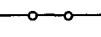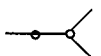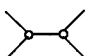
A number of strategies [54-58] for determining the energy of the reference structure have been proposed, among which the scheme, due to Jiang, Tang, and Hoffmann (JTH in short) [58], is unique in parameterizing and independent of Kekulé structures and consequently will be employed here. According to this scheme, the π-electron energy of the acyclic reference system is evaluated by

$$E_\pi(ref) = n_{12}E_{12} + n_{13}E_{13} + n_{22}E_{22} + n_{23}E_{23} + n_{33}E_{33} \qquad (47)$$

where E_{ij} is the π-electron energy in units of J for a bond i-j in which two vertices are of degrees i and j, and n_{ij} is the number of such kind of bonds in the studied molecule. The values of E_{ij} can be obtained by a least-square fit of ground state VB energies of acyclic polyenes as the sum of bond energies, as shown in Eq. (47). The determined E_{ij} values are listed in Table 7. Actually, only three types of bonds, i.e., 2-2, 2-3, and 3-3 occur in BHs.

Table 7
The E_{ij} values (in units of J) determined by a least-square procedure

	E_{12}	E_{13}	E_{22}	E_{23}	E_{33}
Bond type					
VB bond energy	-1.6701	-1.5433	-1.3837	-1.2769	-1.1783
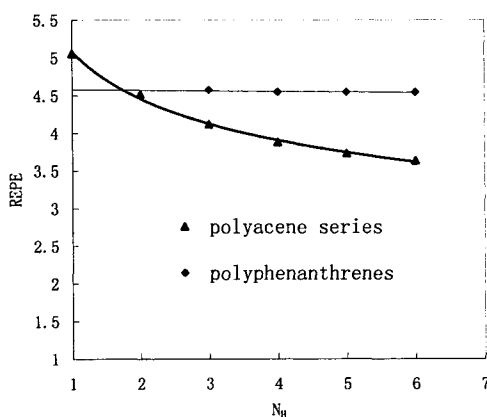
Fig.6. The REPE values vs. the number of hexagons (N_H) for polyacene and polyphenanthrene series

According to the JTH scheme, the calculated RE and REPE values are listed in Table 8. Encouragingly, our VB RE values bear an excellent linear correlation with the delocalization energies obtained by Wiberg [59] at the B3LYP/6-311G** level (the correlation coefficient=0.994) for the first four members of polyacene and polyphenanthrene series, respectively. Thus it appears that the VB RE is a good measure of the thermodynamic stability for isomeric BHs.

However, for comparing the global aromaticity of BHs of different size, REPE values are needed. For the polyacene and polyphenanthrene series, the variation of their REPE values with the number of hexagons is displayed in Fig. 6. One can notice that polyacenes exhibit a descending trend of the global aromaticity with the increase in the number of hexagons, in good accord with corresponding experimental facts and MO-based REPE values [54-58]. Nevertheless, VB REPEs of [n]phenanthrenes remain constant with variation of n, while corresponding REPE scales within the simple MO theory show a slight decrease in the global aromaticity along the series, at least for the members we studied [54-58].

The inconsistency between predictions made by MO REPEs and VB REPEs may be attributed to the different natures of simple MO and VB theories, i.e., the simple MO theory is a one-electron model, free of electron correlation, but VB theory is a many-electron, correlation model. This difference may result in the different topological dependence of π-conjugation in MO and VB models, as illustrated by the [n]phenanthrene series.

As stated above, a new scale is desirable to describe quantitatively the global aromaticity in the VB model. Since the global aromaticity measures the average benzene character of a conjugated system, resonance energy per hexagon (REPH), as defined by Eq. (48), may be a natural choice for BHs [22].

$$REPH = RE/N_H \qquad (48)$$

where N_H stands for the number of hexagons for a given BH. In this way, for all BHs under study, we calculated their VB REPHs, which are tabulated in the fourth and eighth columns of Table 8. The slightly descending trend of the global aromaticity for the first four members of polyphenanthrenes (if phenanthrene is taken as the first member) is now clearly brought out by their corresponding REPH values. In general, the consistency between VB REPHs and MO REPEs is obvious, as shown in Fig. 7 for all BHs with up to 22 π-electrons.

Table 8

The calculated RE, REPE, and REPH values (in J) of BHs shown in Fig. 1

Molecule	RE	REPE ($\times 10^{-2}$)	REPH	Molecule	RE	REPE ($\times 10^{-2}$)	REPH
1	0.30335	5.056	0.30335	46	1.07820	4.147	0.17970
2	0.45187	4.519	0.22594	47	1.08570	4.176	0.18095
3	0.57650	4.118	0.19217	48	1.08798	4.185	0.18133
4	0.64030	4.574	0.21343	49	1.10316	4.243	0.18386
5	0.72366	4.523	0.18092	50	1.10328	4.243	0.18388
6	0.69829	3.879	0.17457	51	1.11162	4.275	0.18527
7	0.77634	4.313	0.19409	52	1.11198	4.277	0.18533
8	0.81867	4.548	0.20467	53	1.13358	4.360	0.18893
9	0.81684	4.538	0.20421	54	1.13448	4.363	0.18908
10	0.85488	4.749	0.21372	55	1.13466	4.364	0.18911
11	0.89199	4.460	0.17840	56	1.13634	4.371	0.18939
12	0.94012	4.701	0.18802	57	1.14876	4.418	0.19146
13	0.88904	4.445	0.17781	58	1.14894	4.419	0.19149
14	0.82072	3.731	0.16414	59	1.15062	4.425	0.19177
15	0.90097	4.095	0.18019	60	1.15092	4.427	0.19182
16	0.91570	4.162	0.18314	61	1.17822	4.532	0.19637
17	0.95093	4.322	0.19019	62	1.17870	4.533	0.19645
18	0.95294	4.332	0.19059	63	1.17948	4.536	0.19658
19	0.97231	4.420	0.19446	64	1.18038	4.540	0.19673
20	0.97263	4.421	0.19453	65	1.18056	4.541	0.19676
21	0.99769	4.535	0.19954	66	1.18224	4.547	0.19704
22	0.99868	4.539	0.19974	67	1.12494	4.327	0.18749
23	1.00043	4.547	0.20009	68	1.14378	4.399	0.19063
24	0.99798	4.536	0.19960	69	1.15752	4.452	0.19292
25	1.02422	4.656	0.20484	70	1.16694	4.488	0.19449
26	1.04685	4.758	0.17448	71	1.16694	4.488	0.19449
27	0.96375	4.381	0.16062	72	1.19700	4.604	0.19950
28	1.15596	4.817	0.19266	73	1.19808	4.608	0.19968
29	1.11210	4.634	0.18535	74	1.19238	4.586	0.19873
30	1.11066	4.628	0.18511	75	1.19664	4.602	0.19944
31	1.09644	4.569	0.18274	76	1.20804	4.646	0.20134
32	1.08498	4.521	0.18083	77	1.20906	4.650	0.20151
33	1.07922	4.497	0.17987	78	1.22532	4.713	0.20422
34	1.07550	4.481	0.17925	79	1.25685	4.834	0.17955
35	1.07940	4.498	0.17990	80	1.24180	4.776	0.17740
36	1.06128	4.422	0.17688	81	1.22220	4.701	0.17460
37	1.05192	4.383	0.17532	82	1.20267	4.626	0.17181
38	0.93936	3.914	0.15656	83	1.18664	4.564	0.16952
39	1.02330	4.264	0.17055	84	1.18461	4.556	0.16923
40	0.97122	4.047	0.16187	85	1.17705	4.527	0.16815
41	1.18713	4.946	0.16959	86	1.14436	4.401	0.16348
42	0.94476	3.634	0.15746	87	1.12637	4.332	0.16091
43	0.98370	3.783	0.16395	88	1.31131	4.683	0.18733
44	1.04220	4.008	0.17370	89	1.24448	4.445	0.15556
45	1.07616	4.139	0.17936				

596
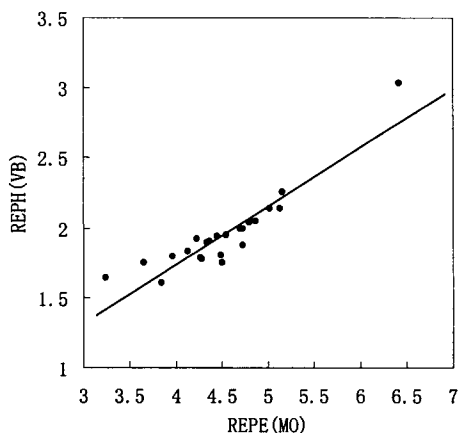
Fig. 7. Correlation of VB REPHs with REPEs from simple MO caluclations.

It is also instructive to look into the global aromaticity of a BH by averaging the local aromaticity of all hexagon rings. Accordingly, the global aromaticity may be measured by an average:

$$av.RLHE = \sum_{i=1}^{N_H} (RLHE)_i / N_H \qquad (49)$$

where the summation runs over all hexagons of total number N_H. For those BHs in Fig. 5, we also list their av. RLHE values in Fig. 5. It is not unexpected that av. RLHE values linearly correlate with REPH values, as exemplified in Fig. 8 by those BHs collected in Fig. 5.

The indices proposed above, the REPH and the av. RLHE, mainly concentrate on characterizing the thermodynamic stability aspect of the global aromaticity. As we pointed out in the above subsection, the S-T gap could be utilized to correlate with the kinetic reactivity of a given BH. Meanwhile, it appears that a linear correlation holds reasonably well between S-T gaps and REPHs. This is shown in Fig. 9 for all 89 BHs we investigated. Hence, the S-T energy gap could also serve as a good measure of the global aromaticity in the VB model, playing a similar role as absolute hardness [53] (which is approximately half the HOMO-LUMO gap) in the simple MO theory.
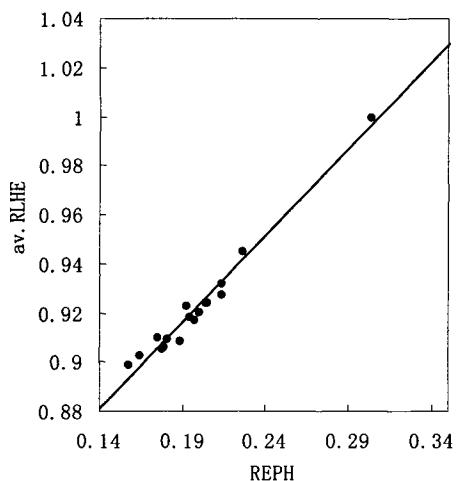
Fig. 8. Correlation of av. RLHE values with REPH values.
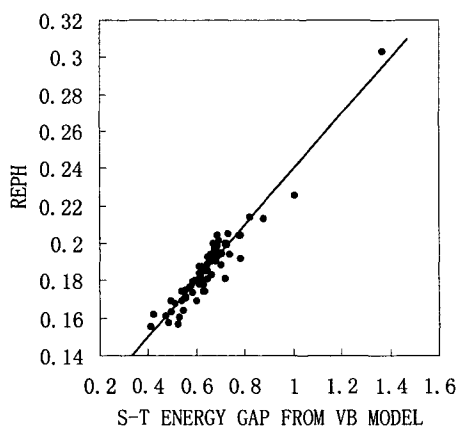
Fig. 9. Relation between S-T gaps and REPH values of BHs shown in Fig. 1.

3.5. Spin coupling in radicals

Chemists have long recognized that a diradical or polyradical can be built up from two elements [60-62]: the spin-containing unit that provides the unpaired electrons, and the spin-coupling unit that couples any two or more spin-containing units. Accordingly, a diradical could be assumed to be composed of two "unpaired" electrons coupled through a spin-coupling unit, characterized by a coupling constant J_{cc} (J_{cc} is used here to denote the coupling constant, differing

from J in Eq. (18)). For example, m-quinodimethane (**90**) can be schematically represented by the following reduced "molecule", in which J_{cc} is the spin-coupling constant through m-phenylene.

90
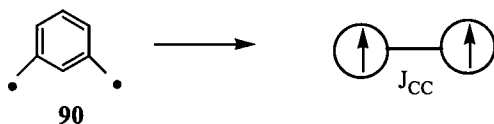
Similarly, a polyradical might be viewed as many "unpaired" electrons coupled through spin-coupling units with different coupling constants.

Obviously, calculating theoretically spin coupling constants in diradicals and their homologous polyradicals (even related polymers) is very helpful for designing stable high-spin organic molecules and high temperature organic ferromagnets in practice [62]. A strategy commonly used for obtaining coupling constants in radicals [20,21,63] is as follows: (1) Compute the energy gaps between the ground and lowest excited states by using available theoretical methods; (2) Derive coupling constants in radicals from the obtained energy gaps by using the classical VB model. In principle, step (2), a "renormalization" process, could actually be derived by applying a cluster expansion technique [64].

Usually, in step (1) one uses various MO-based correlation methods, primarily because MO-based methods dominate in molecular electronic structure calculations. Nevertheless, for open-shell radicals available MO-based approaches are not free of drawbacks [6,7]. Unrestricted Hartree Fock (UHF) theory and those UHF-based correlation methods usually suffer from spin contamination to some extent. Truncated configuration interaction (CI) methods are not size-consistent and therefore cannot be utilized to compare the spin coupling constants for molecules of different size. On the other hand, VB theory could avoid these problems by solving exactly the VB model in different spin subspaces. As a result, we have applied various VB models in discussing the spin coupling problem for a series of conjugated radicals [20,21]. Here we just choose m-phenylene as the spin-coupling unit, and illustrate how coupling constants in related radicals, depicted below, can be estimated.

90   **91**   **92**   **93**
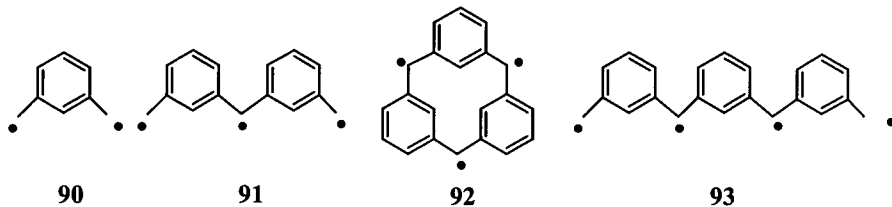
Since m-phenylene (**90**) is a ferromagnetic coupling unit, radicals **91-93** all

have high-spin ground states. The coupling constant through m-phenylene in diradical **90** (m-quinodimethane) is easy to obtain from the singlet-triplet energy gap ΔE_{ST} by the relation $\Delta E_{ST} = -2J_{cc}$. In an analogous way, the coupling parameters in linear triradical **91** and circular triradical **92** can be derived from the relations $\Delta E_{DQ} = -J_{cc}$ and $\Delta E_{DQ} = -3J_{cc}$ (ΔE_{DQ} is the energy separation between the ground quartet and lowest doublet states), respectively. For linear tetraradical **93**, the coupling parameter through the terminal m-phenylene may differ from that through the middle m-phenylene. A reasonable treatment is to assume that the coupling constant through the terminal m-phenylene has the same value as that in the linear triradical **91**. This assumption allows for the coupling constant through the middle m-phenylene to be determined from the calculated triplet-quintet gap. For these radicals, we have listed the calculated energy gaps and coupling constants in Table 9. The data show that about two-thirds of the coupling constant in diradical **90** is maintained in the linear triradical **91** and half in the circular triradical **92**. Here we would like to mention the related experimental results obtained by Ishida and Iwamura [65]. In their experiments, nitroxide groups were introduced as radical centers in species **90** and **91**. They found that J_{cc} in the diradical is about half that in the triradical, basically consistent with our estimates for model systems **90** and **91**. For the linear tetraradical **93**, one can see that the magnitude of the coupling constant through the central m-phenylene is lower than that through the terminal m-phenylene in **91**, indicating that the coupling constant decreases with the connectivity of radical sites. Reasonably, we may expect that the coupling constant through the central m-phenylene in **93** is a good approximation to that in infinite poly(m-phenylmethylene) system.

Table 9
Energy gaps between the ground and lowest excited states and coupling constants through m-phenylene for molecules **90-93**[a]

Radicals	$\Delta E(J)$	coupling constant (-J)	ratio
90	0.718	0.359	
91	0.245	0.245	0.68
92	0.578	0.193	0.54
93[b]	0.129	0.205	0.57

[a] The ratio of coupling constants between polyradicals and diradical is also listed for comparison. [b] The coupling constant through the central m-phenylene is given.

4. CONCLUDING REMARKS

In this chapter, a combination of effective computational methods have been invoked to solve the VB model exactly for the ground and first excited states of conjugated molecules with up to 28 π-electrons. These methods include: (1) coding all Slater determinants in a spin subspace with conserved M as a set of

natural numbers to minimize the searching time and storing space; (2) reducing the size of the Hamiltonian matrix by using molecular point group and spin-inversion symmetry; (3) diagonalizing the large sparse matrix by employing the Lanczos technique.

The focus of this chapter is to interpret systematically some physical and chemical properties of conjugated hydrocarbons by means of the obtained VB energies and wave functions of the ground and lowest excited states. For all BHs containing up to 26 π-electrons and two BHs of 28 π-electrons, their bond lengths, orientation of electrophilic aromatic substitution, and local aromaticities have been well accounted for by defining corresponding local indices, which are available from the ground-state wave functions. For lowest triplet states of BHs, which are primarily covalent in nature, our VB results are able to give satisfactory descriptions, in good agreement with available experimental data. In addition, our results indicate that some BHs with very narrow VB S-T energy gaps should be very reactive or hard to synthesize, as predicted from MO calculations.

For describing the global aromaticity of BHs, three indices including a wave function-based av. RLHE, the ground-state energy-based REPH, and the energy gap between the ground and lowest triplet states, were introduced. They all lead to predictions agreeing with the known experimental facts. The traditionally adopted REPE scale, although it is successful in the simple MO theory, gives less satisfactory descriptions in some cases within the VB model, revealing the different nature of VB and MO approaches.

The last application is devoted to calculating the spin coupling constants in conjugated radicals, which is a difficult task in MO approaches. Our calculations illustrated here and reported elsewhere [20,21] first revealed the topological dependence of coupling constants in a number of di- and poly-radicals, and the variation of coupling constants through some spin-coupling units from related diradicals to their homologous polyradicals.

In summary, our work collected in this chapter leads us to conclude that VB theory can also make very valuable predictions for some properties of conjugated hydrocarbons, either closed-shell BHs or open-shell radicals, although most of these properties were believed to belong to MO theory's province. Finally, we would like to point out that the exact solution of the VB model for larger conjugated systems is becoming feasible with the advent of more powerful methods such as the density-matrix renormalization group method [66]. Thus, more applications of the VB theory to the conjugated systems could be expected in the near future.

ACKNOWLEDGEMENT

REFERENCES

[1] W. Heitler and F. London, Z. Phys., 44 (1927) 445.

[2] D.J. Klein and N. Trinajstic (eds.), Valence Bond Theory and Chemical Structure, Elsevier, Amsterdam, 1990.

[3] L. Pauling, The Nature of the Chemical Bond, Cornell University Press, Ithaca, 1960.

[4] (a) L. Pauling and G.W. Wheland, J. Chem. Phys. 1 (1933) 362. (b) L. Pauling, J. Chem. Phys. 1 (1933) 280.

[5] R. McWeeny, Coulson's Valence, Oxford, 1979.

[6] A. Szabo and N.S. Ostlund, Modern Quantum Chemistry, Dover, Mineola, New York, 1996.

[7] I.N. Levine, Quantum Chemistry, Prentice Hall, New Jersey, 2000.

[8] R. McWeeny, Methods of Modern Quantum Mechanics, Academic Press, London, 1992.

[9] (a) M. Randić, Chem. Phys. Lett. 38 (1976) 68. (b) M. Randić, Tetrahedron (1977) 1905. (c) M. Randić, J. Am. Chem. Soc. 99 (1977) 444.

[10] (a) W.C. Herndon, J. Am. Chem. Soc. 95 (1973) 2404. (b) W.C. Herndon and M. L. Jr. Ellzey, J. Am. Chem. Soc. 96 (1974) 6631.

[11] J. H. Van Vleck and A. Sherman, Rev. Mod. Phys. 7 (1935) 167.

[12] D. J. Klein and M.A. Garcia-Bach, Phys. Rev. B 19 (1979) 877.

[13] (a) J.P. Malrieu and D. Maynau, J. Am. Chem. Soc. 104 (1982) 3021. (b) D. Maynau and J.P. Malrieu, J. Am. Chem. Soc. 104 (1982) 3029.

[14] M. Said, D. Maynau, J.P. Malrieu and M.A. Garcia-Bach, J. Am. Chem. Soc. 106 (1984) 571.

[15] S. Kuwajima, J. Chem. Phys. 77 (1982) 1930.

[16] S.A. Alexander and T.G. Schmalz, J. Am. Chem. Soc. 109 (1987) 6933.

[17] D.J. Klein, Top. Curr. Chem. 153 (1990) 59 and references therein.

[18] S. Li and Y. Jiang, J. Am. Chem. Soc. 117 (1995) 8401.

[19] (a) J. Ma, S. Li, Y. Jiang, J. Phys. Chem. 100 (1996) 15068. (b) J. Ma, S. Li, Y. Jiang, J. Phys. Chem. A 101 (1997) 4970.

[20] S. Li, J. Ma, Y. Jiang, J. Phys. Chem. 100 (1996) 4775.

[21] (a) S. Li and Y. Jiang, Chem. Phys. Lett. 211 (1995) 246. (b) S. Li, J. Ma, Y. Jiang, J. Phys. Chem. A 101 (1997) 5567.

[22] J. Wu and Y. Jiang, J. Compt. Chem. 21 (2000) 856.

[23] D.L. Cooper, J. Gerratt and M. Raimondi, Nature 323 (1986) 699.

[24] J. Gerratt, D.L. Cooper, P.B. Karadakov and M. Raimondi, Chem. Soc. Rev. 97 (1997) 87.

[25] Q. Zhang and X. Li, J. Mol. Struct. 198 (1989) 413.

[26] (a) W.A. Goddard, Phys. Rev. 157 (1967) 73. (b) W.A. Goddard, Phys. Rev. 157 (1967) 81.

[27] G.A. Gallup, Adv. Quantum Chem. 16 (1973) 229.

[28] J.H. van Lenthe and G.G. Balint-Kurti, Chem. Phys. Lett. 76 (1980) 138.

[29] L. Salem, The Molecular Orbital Theory of Conjugated System, Benjamin, New York, 1966.

[30] A. Streitweiser, Molecular Orbital Theory for Organic Chemists, Wiley, New York, 1961.

[31] J. Hubbard, Proc. Roy. Soc. London A 276 (1963) 283.

[32] J. Linderberg and Y. Öhrn, Propagators in Quantum Chemistry, Academic Press, New York, 1973.

[33] (a) R.D. Poshusta and D.J. Klein, Phys. Rev. Lett. 48 (1982) 1555. (b) D.J. Klein, W.A. Seitz, M.A. Garcia-Bach, J.M. Picone, D.C. Foyt, Int. J. Quantum Chem. 17S (1983) 555. (c) Ph. Durand, Phys. Rev. A 28 (1983) 3184. (d) D. Maynau, Ph. Durand, J.P. Daudey, J.P. Malrieu, Phys. Rev. A 28 (1983) 3193.

[34] (a) H. Weyl, The Theory of Groups and Quantum Mechanics, Dover, New York, 1956. (b) G. Rumer, Nachr Ges Wiss Gölfingen, Math. Phys. KL (1932) 337.

[35] C.J. Lanczos, Res. Nat. Bur. Stand 45 (1950) 255.

[36] Y.G. Smeyers and L. Doreste-Suares, Int. J. Quantum Chem. 7 (1973) 687.

[37] Y.G. Smeyers and G. Delgado-Barrio, Int. J. Quantum Chem. 8 (1973) 733.

[38] D. Maynau, M. Said, J.P. Malrieu, J. Am. Chem. Soc. 105 (1983) 5244.

[39] J. Cioslowski, Theor. Chim. Acta 75 (1989) 271.

[40] C.A. Coulson, Proc. Roy. Soc. London A 169 (1939) 413.

[41] G.W. Wheland, J. Am. Chem. Soc. 64 (1942) 900.

[42] Y. Jiang and H. Zhang, Theor. Chim. Acta 75 (1989) 279.

[43] K. Fukui, T. Yonezawa, C. Nagata, J. Chem. Phys. 27 (1957) 1247.

[44] (a) W.C. Herndon, J. Org. Chem. 40 (1975) 3583. (b) W.C. Herndon, Int. J. Quantum Chem., Quantum Biol. Symp. 1 (1974) 123.

[45] M.J.S. Dewar and N. Trinajstić, J. Chem. Soc. A (1971) 1220.

[46] S. Astilean, V. Chitta, A. Corval, R.J.D. Miller, H.P. Trommsdroff, Chem. Phys. Lett. 219 (1994) 95.

[47] E. Clar, The Aromatic Sextet, Wiley, New York, 1972.

[48] P.J. Garratt, Aromaticity, John Wiley & Sons, New York, 1986.

[49] C.H. Suresh and S.R. Gadre, J. Org. Chem. 64 (1999) 2505.

[50] M. Randić, Tetrahedron 30 (1974) 2067.

[51] M. Aida, H. Hosoya, Tetrahedron 36 (1980) 1317.

[52] O.E. Polansky, G. Derflinger, Int. J. Quantum Chem. 1 (1967) 379.

[53] Z. Zhou and R.G. Parr, J. Am. Chem. Soc. 111 (1989) 7371.

[54] M.J.S. Dewar and C.J. de Llano, J. Am. Chem. Soc. 91 (1969) 789.

[55] B.A. Hess and L.J. Schaad, J. Am. Chem. Soc. 93 (1971) 305.

[56] J.I. Aihara, J. Am. Chem. Soc. 98 (1976) 2750.

[57] I. Gutman, M. Milun, N. Trinajstić, J. Am. Chem. Soc. 99 (1977) 1692.

[58] Y. Jiang, A. Tang, R. Hoffmann, Theor. Chim. Acta 66 (1984) 183.

[59] K.B. Wiberg, J. Org. Chem. 62 (1997) 5720.

[60] D.A. Dougherty, Pure Appl. Chem. 62 (1990) 519.

[61] H. Iwamura, Advan. Phys. Org. Chem. 26 (1990) 179.

[62] A. Rajca, Chem. Rev. 94 (1994) 871.

[63] D.A. Dixon, T.H. Dunning, R.A. Eades, D.A. Kleier, J. Am. Chem. Soc. 103 (1981) 2878.

[64] D.J. Klein, C.J. Nelin, S. Alexander, F.A. Matsen, J. Chem. Phys. 77 (1982) 3101.

[65] T. Ishida, H. Iwamura, J. Am. Chem. Soc. 113 (1991) 4238.

[66] S. R. White, Phys. Rev. Lett. 69 (1992) 2863.

Chapter 19

Symmetric group approach to the theory of Heisenberg lattices

Norbert Flocke[a] and Jacek Karwowski[b]

[a]Quantum Theory Project, University of Florida,
Gainesville, FL 32611, USA
[b]Instytut Fizyki, Uniwersytet Mikołaja Kopernika,
Grudziądzka 5, PL-87-100 Toruń, Poland

1. INTRODUCTION

Theoretical studies on spectroscopic properties of polyenes and polyacenes, investigations of magnetic properties of crystalline lattices, analyses of carcinogenic power of unsaturated organic compounds, and the search for organic ferromagnets have one feature in common: they are based on an analysis of the eigenvalue problem of simple model Hamiltonians such as the Pariser-Parr-Pople Hamiltonian, the Hubbard Hamiltonian and the Heisenberg Hamiltonian. After the discovery of high-temperature superconductivity in cuprates, the interest in the model Hamiltonians, particularly in the Heisenberg Hamiltonian, increased considerably since this Hamiltonian is appropriate for describing specific properties of compounds with highly correlated electrons, which are believed to be responsible for the superconductivity-related phenomena.

Most interesting in this context are properties of Heisenberg lattices of mesoscopic dimensions, i.e. containing hundreds, if not thousands, of nodes. Unfortunately, except for some simple model cases, an exact theoretical description of the spectrum of the corresponding Hamiltonian is extremely difficult. In the majority of cases the only way to get some insight into the bulk limit properties is by extrapolation of the results obtained for small lattices. The number of spins in a lattice which can be treated exactly is severely limited by the combinatorial explosion of the dimension of the basis [1] and exact calculations for more than 30 spins without explicitly using symmetry properties of the lattice are next to impossible. In order to circumvent this problem several approximation methods were designed, like the resonating valence bond (RVB) method [2, 3], perturbational approaches [4, 5], or methods based on renormalization group techniques like, for example, the density matrix renormalization group (DMRG) approach [6]. The usual procedure for testing these approximate methods is to compare their results with the ones derived from exact calculations obtained for

lattices for which the exact calculations are feasible. Therefore, designing methods aimed at obtaining exact results for lattices as large as possible is of particular interest and importance.

In this chapter we address the problem of the construction and diagonalization of model Hamiltonian matrices using the so called symmetric group approach (SGA) to the theory of many-electron systems [7, 8]. A general N-electron Hamiltonian eigenvalue problem has been formulated and successfully solved within the SGA for both spin-independent [7, 8] and spin-dependent [9, 10] interaction operators. These general methods may, in principle, also be applied to the case of model Hamiltonians. However, simplifications resulting from the simple structure of the Pariser-Parr-Pople, Hubbard and Heisenberg Hamiltonians are so essential that a detailed discussion of their independent treatment within the SGA-based scheme is highly justified. The physical model becomes particularly simple and meaningful if the electrons are described by localized atomic orbitals. In this kind of formulation SGA leads to a valence-bond-like theory. In fact, valence-bond-like models are then applicable to handling the pertinent eigenvalue problem. Therefore a presentation of this approach among other valence-bond methods seems to be most appropriate and useful to a reader.

Heisenberg Hamiltonians describing systems of N spins are closely related to the symmetric group $\mathcal{S}_N$. In fact, these Hamiltonians represent elements of the $\mathcal{S}_N$ algebra. This property, when related to SGA, appears to be essential for designing efficient computational methods. However, in a majority of studies, relations between the Heisenberg Hamiltonian and the symmetric group are put in a context of some fundamental, group-theoretical rather than numerical problems [11, 12]. Only very recently has SGA been applied to construct an algorithm applicable to studies on Heisenberg lattices [13]. The resulting method has been implemented as an efficient computer code [14] and has been used to solve exactly Heisenberg eigenvalue problems of dimensions up to 10^7. A demonstration that the SGA-based theory, apart from giving new insights into the structure of the Hamiltonian matrices, allows us to formulate compact and efficient algorithms for the exact numerical treatment of the Heisenberg lattices is one of the aims of this work.

In cases where Heisenberg Hamiltonian matrix dimensions prohibit their exact treatment one can use for energy states which are predominantly antiferromagnetic, an approximate method based on the idea of forming bonds between different lattice sites. These bonds, or rather the wave functions formed for these bonds, are then allowed to resonate giving rise to the RVB method mentioned earlier. The RVB method is very useful, since not only it makes possible a treatment of lattices which are out of reach by

the exact methods but also gives some insight into the structure of the exact wave function by identfying from the very beginning its major components. Therefore, in Section 4 of this chapter, the exact SGA approach is compared with the RVB method. Besides, differences in computational strategies for both methods are briefly discussed.

2. GENERAL DEFINITIONS

We are concerned with the eigenvalue problem

$$\mathsf{H}\,\Psi_\kappa = \mathcal{E}_\kappa\,\Psi_\kappa \tag{1}$$

of a clamped-nuclei spin-independent N-electron Hamiltonian

$$\mathsf{H}(\mathbf{r}) = \sum_{i=1}^{N} \mathsf{h}_1(\mathbf{r}_i) + \sum_{i>j}^{N} \mathsf{h}_2(\mathbf{r}_i, \mathbf{r}_j), \tag{2}$$

where $\mathbf{r} = \{\mathbf{r}_1, \mathbf{r}_2, \ldots, \mathbf{r}_N\}$ is a shorthand notation for the collection of all electronic space coordinates, $\mathsf{h}_1(\mathbf{r}_i)$ includes the kinetic energy and interactions of the i-th electron with an external field and $\mathsf{h}_2(\mathbf{r}_i, \mathbf{r}_j)$ describes the interaction between electrons i and j. Usually, in atomic units,

$$\mathsf{h}_2(\mathbf{r}_i, \mathbf{r}_j) = \frac{1}{r_{ij}}. \tag{3}$$

Two universal symmetry properties of the Hamiltonian are particularly significant in designing methods of solution of its eigenvalue problem: the invariance with respect to rotations in the spin space and the invariance with respect to permutations of electrons. As a consequence of these symmetries the Hamiltonian commutes with spin operators and with permutation operators. In particular, the Hamiltonian, the square of the total spin operator (S^2) and the projection of the total spin operator (S_z) form a set of commuting operators:

$$\left[\mathsf{H}, \mathsf{S}^2\right] = \left[\mathsf{H}, \mathsf{S}_z\right] = \left[\mathsf{S}^2, \mathsf{S}_z\right] = 0. \tag{4}$$

The permutational invariance results in

$$[\mathsf{H}, \mathsf{P}] = \left[\mathsf{S}^2, \mathsf{P}\right] = [\mathsf{S}_z, \mathsf{P}] = 0, \tag{5}$$

but different permutations $\mathsf{P} \in \mathcal{S}_N$, where $\mathcal{S}_N$ is the $N!$-element symmetric group, in general do not commute with each other.

The eigenvalue problem of the Hamiltonian operator (1) is defined in an infinite-dimensional Hilbert space $\mathcal{G}$ and may be solved directly only for very few simple models. In order to find its bound-state solutions with energies not too distant from the ground-state it is reduced to the corresponding eigenvalue problem of a matrix representing H in a properly constructed finite-dimensional model space, a subspace of $\mathcal{G}$. Usually the model space is chosen to be spanned by N-electron antisymmetrized and spin-adapted products of orthonormal spinorbitals. In such a case it is known as the full configuration interaction (FCI) space [8, 15]. The model space $\mathcal{H}^{\mathrm{A}}(N, K, S, M)$ may be defined as the antisymmetric part of the N-fold tensorial product of a one-electron space

$$\mathcal{H}^{\mathrm{A}}(N, K, S, M) = \left[\mathcal{H}^{\mathrm{so}}(1, 2K)^{\otimes N}\right]^{\mathrm{A}}_{SM}, \tag{6}$$

where the superscript A stands for antisymmetry and S and M refer to the respective eigenvalues of the total spin operators S^2 and S_z. The $2K$-dimensional one-electron space $\mathcal{H}^{\mathrm{so}}(1, 2K)$ is spanned by a set of orthonormal spinorbitals and is a tensorial product of the two-dimensional one-electron spin space $\mathcal{H}^{\mathrm{s}}(1, 2) = \{\alpha, \beta\}$ spanned by the two one-electron spin functions, and the K-dimensional one-electron orbital space $\mathcal{H}^{\mathrm{o}}(1, K) = \{\phi_j; j = 1, \ldots, K\}$, i.e.

$$\mathcal{H}^{\mathrm{so}}(1, 2K) = \mathcal{H}^{\mathrm{s}}(1, 2) \otimes \mathcal{H}^{\mathrm{o}}(1, K). \tag{7}$$

Eqs.(6) and (7) imply that the basis in the model space is formed by spin-adapted combinations of Slater determinants. This way of constructing the model space is specific for the unitary group approach to the theory of N-electron systems [15, 16].

Alternatively the model space may be constructed as

$$\mathcal{H}^{\mathrm{A}}(N, K, S, M) = \mathsf{A}\left[\mathcal{H}^{\mathrm{o}}(N, K) \otimes \mathcal{H}^{\mathrm{s}}(N, 2, S, M)\right], \tag{8}$$

where $\mathcal{H}^{\mathrm{o}}(N, K)$ is the N-electron orbital space spanned by all Hartree products of the orbitals and

$$\mathcal{H}^{\mathrm{s}}(N, 2, S, M) = \left\{\Theta_k^{SM}; k = 1, 2, \ldots, f\right\} \tag{9}$$

is the N-electron spin space spanned by the eigenfunctions Θ_k^{SM} of the total spin operators, where

$$f \equiv f(S, N) = \frac{2S + 1}{N + 1} \binom{N + 1}{N/2 - S} \tag{10}$$

is the dimension of $\mathcal{H}^s(N, 2, S, M)$ [17, 18]. The construction of the model space according to Eq.(8) is specific for the SGA and results in a neat separation of the orbital and spin space contributions to the Hamiltonian matrix elements. This independent handling of the orbital and spin spaces constitutes the key to the compact structure of the SGA matrix element formulas for a general spin-dependent Hamiltonian [9, 10]. The N-electron basis functions are defined in the SGA as

$$\Psi_{\lambda k}^{SM}(\mathbf{r}, \mathbf{s}) = \xi_\lambda \mathsf{A} \left[\Phi_\lambda(\mathbf{r}) \Theta_k^{SM}(\mathbf{s}) \right], \tag{11}$$

where $\mathbf{s} = \{\mathbf{s}_1, \mathbf{s}_2, \ldots, \mathbf{s}_N\}$ denotes the collection of spin variables,

$$\mathsf{A} = \frac{1}{N!} \sum_{\mathsf{P} \in \mathcal{S}_N} \epsilon(\mathsf{P}) \mathsf{P} \tag{12}$$

is the idempotent antisymmetrization operator with $\epsilon(\mathsf{P}) = \pm 1$ being the parity of the permutation P and ξ_λ is the normalization constant. The orbital part of the basis functions in (11) corresponding to $\mathcal{H}^o(N, K)$ is defined as

$$\Phi_\lambda(\mathbf{r}) = \prod_{j=1}^{N} \phi_{\lambda_j}(\mathbf{r}_j), \tag{13}$$

where $\lambda = \{\lambda_j; j = 1, 2, \ldots, N\}$ is referred to as the orbital configuration. The antisymmetry condition implies that an orbital may appear in λ at most twice. The occupation number n_p^λ of ϕ_p in λ may thus take only one of three possible values: 0, 1, or 2. The orbitals with $n_p^\lambda = 2$ are referred to as doubly occupied or *doubles* and the ones with $n_p^\lambda = 1$ as singly occupied or *singles*. The numbers of singles (s_λ) and doubles (d_λ) are connected by the obvious relation $s_\lambda + 2d_\lambda = N$. As one can easily check [7], the normalization constant is equal to

$$\xi_\lambda = \sqrt{\frac{N!}{2^{d_\lambda}}}. \tag{14}$$

We adopt a convention that in all products of orbitals the position index of an orbital in the product is equal to the designation index of

the electron described by this orbital, i.e. if $\phi_{\lambda_i}(\mathbf{r}_j)$ is contained in the product, then $i = j$. As a consequence of this convention we usually omit the electron designation indices in the products of orbitals. We assume that in the orbital products the electron coordinate indices of singles are always smaller than those of doubles and that both singles and doubles stand in an ascending order of their orbital indices, i.e.

$$\lambda_1 < \lambda_2 < \ldots < \lambda_s, \quad \lambda_{s+1} = \lambda_{s+2} < \ldots < \lambda_{N-1} = \lambda_N, \tag{15}$$

where $s \equiv s_\lambda$. Let us note that the number of different basis functions in (11) associated with an orbital configuration λ is equal to $f(S, s_\lambda)$ rather than $f(S, N)$. This is because the antisymmetry requirement restricts the spin coupling schemes in the parts of Θ_k^{SM} which corresponds to doubles in Φ_λ. Since Φ_λ is symmetric upon transpositions within doubles, the corresponding parts of the spin functions must be antisymmetric. Therefore the spins of those electron pairs that correspond to doubles must be coupled in Θ_k^{SM} to two-electron singlets, i.e.

$$\Theta_k^{SM}(\mathbf{s}_1, \mathbf{s}_2, \ldots, \mathbf{s}_N) = \Theta_k^{SM}(\mathbf{s}_1, \mathbf{s}_2, \ldots, \mathbf{s}_{s_\lambda}) \prod_{j=1}^{d_\lambda} \Theta_1^{00}(\mathbf{s}_{s_\lambda+2j-1}, \mathbf{s}_{s_\lambda+2j}). \tag{16}$$

The Hamiltonian in the model space may be represented in second-quantized form as

$$\mathsf{H} = \sum_{pq}^{K} (p|q)\, {}^1\mathsf{E}_q^p + \tfrac{1}{2} \sum_{pqrs}^{K} (pq|rs)\, {}^2\mathsf{E}_{qs}^{pr}, \tag{17}$$

where $(p|q)$ and $(pq|rs)$ are the respective one- and two-electron integrals expressed in terms of the orbitals. The operators

$${}^1\mathsf{E}_q^p = \sum_{\sigma} \mathsf{a}_{p\sigma}^\dagger \mathsf{a}_{q\sigma} \tag{18}$$

and

$${}^2\mathsf{E}_{qs}^{pr} = \sum_{\sigma_1,\sigma_2} \mathsf{a}_{p\sigma_1}^\dagger \mathsf{a}_{r\sigma_2}^\dagger \mathsf{a}_{s\sigma_2} \mathsf{a}_{q\sigma_1} \tag{19}$$

are, respectively, the first- and the second-order reduced density operators and $\mathsf{a}_{p\sigma}^\dagger / \mathsf{a}_{p\sigma}$ are the fermion creation/annihilation operators with $\sigma = \alpha, \beta$

referring to the spin state of the electron. Expressing the reduced density operators in terms of shift operators [19], also known as replacement operators [8],

$$\mathsf{E}_{pq} = \mathsf{a}^\dagger_{p\alpha}\mathsf{a}_{q\alpha} + \mathsf{a}^\dagger_{p\beta}\mathsf{a}_{q\beta},\tag{20}$$

we get $^1\mathsf{E}^p_q = \mathsf{E}_{pq}$ and

$$^2\mathsf{E}^{pr}_{qs} = \mathsf{E}_{pq}\mathsf{E}_{rs} - \delta_{qr}\mathsf{E}_{ps}.\tag{21}$$

From the definition of E_{pq} we further obtain the commutation rule

$$[\mathsf{E}_{pq}, \mathsf{E}_{rs}] = \delta_{rq}\mathsf{E}_{ps} - \delta_{ps}\mathsf{E}_{rq},\tag{22}$$

which is specific for the generators of the unitary group $\mathcal{U}(K)$. Therefore the shift operators can also be viewed as unitary group generators [15]. Consequently, $\mathcal{H}^A(N, K, S, M)$ is a carrier space for the representations of the unitary group $\mathcal{U}(K)$ labeled as $\{2^y 1^{x-y}\}$, with

$$x = \frac{N}{2} + S, \quad y = \frac{N}{2} - S.\tag{23}$$

Therefore the dimension of the model space is equal to the dimension of the pertinent representation and is given by the Weyl-Paldus dimension formula [20, 21]

$$D = D(N, K, S) = \frac{2S+1}{K+1}\binom{K+1}{N/2-S}\binom{K+1}{N/2+S+1}.\tag{24}$$

Dimensions of the spin-adapted FCI spaces grow up exponentially with the number of orbitals and electrons reaching the order of Avogadro's number at about $N = K = 50$ (if $S = 0$).

The shift operators in the spin space act as unit operators (Eq.(20) corresponds to an integration over spin variables) and their action in the orbital space may be expressed in terms of the orbitals as [19]

$$\mathsf{E}_{pq} = \sum_{i=1}^N |\phi_p(\mathbf{r}_i)\rangle \langle\phi_q(\mathbf{r}_i)|.\tag{25}$$

According to Eqs.(20) and (25), E_{pq}, when acting on Φ_λ, raises by 1 the occupation number n_p^λ and lowers by 1 the occupation number n_q^λ, i.e. it replaces ϕ_q by ϕ_p. In particular $\mathsf{E}_{pq}\Phi_\lambda = 0$ if $n_q^\lambda = 0$ and

$$\mathsf{E}_{pq}\phi_p\phi_q = \phi_p\phi_p, \tag{26}$$

$$\mathsf{E}_{qp}\phi_p\phi_p = \phi_q\phi_p + \phi_p\phi_q. \tag{27}$$

From Eqs.(26) and (27) one can easily deduce that

$$(\mathsf{E}_{qp}\mathsf{E}_{pq} - \mathsf{I})\,\phi_p\phi_q = \phi_q\phi_p, \tag{28}$$

where I is the unit operator. Consequently, if $n_p^\lambda = n_q^\lambda = 1$ then

$$(\mathsf{E}_{qp}\mathsf{E}_{pq} - \mathsf{I})\,\Phi_\lambda = (\mathsf{p},\mathsf{q})\,\Phi_\lambda, \tag{29}$$

where (p,q) is the transposition operator. Besides,

$$\mathsf{E}_{pp}\Phi_\lambda = n_p^\lambda\,\Phi_\lambda, \tag{30}$$

thus $\mathsf{E}_{pp} = \mathsf{n}_p$ is the orbital occupation number operator.

The eigenvalue problem of Eq. (1), projected onto $\mathcal{H}^A(N, K, S, M)$, may be expressed as

$$\sum_j^D [\langle \Psi_i^{SM}|\mathsf{H}|\Psi_j^{SM}\rangle - \delta_{ij}E_\kappa]C_{j\kappa} = 0, \tag{31}$$

where $j = \{\lambda k\}$, $i = \{\mu\ell\}$ and $i, \kappa = 1, \ldots, D$. The resulting wave functions are

$$\Psi_\kappa^{SM} = \sum_j^D \Psi_j^{SM}C_{j\kappa} = \sum_{\lambda k}^D \Psi_{\lambda k}^{SM}C_{\lambda k,\kappa}, \tag{32}$$

where $C_{\lambda k,\kappa} = \langle\Psi_{\lambda k}^{SM}|\Psi_\kappa\rangle$ are the coefficients representing the solutions of the system of equations (31). The corresponding energies fulfill the variational condition, that is we have $E_\kappa \le \mathcal{E}_\kappa$ if $\mathcal{E}_\kappa \le \mathcal{E}_{\kappa+1}$ and $E_\kappa \le E_{\kappa+1}$, where $\mathcal{E}_\kappa$ are the exact eigenvalues of the Hamiltonian defined in Eq. (1).

3. THE MODEL HAMILTONIAN

The one- and two-electron integrals appearing in the second-quantized form of the Hamiltonian carry all information about the specific features of the quantum system. The one-electron integrals are defined as

$$(p|q) = \int d\mathbf{r}_1 \phi_p^*(\mathbf{r}_1) \mathsf{h}_1(\mathbf{r}_1) \phi_q(\mathbf{r}_1), \tag{33}$$

and the two-electron ones as

$$(pq|rs) = \int d\mathbf{r}_1 d\mathbf{r}_2 \phi_p^*(\mathbf{r}_1) \phi_r^*(\mathbf{r}_2) \mathsf{h}_2(\mathbf{r}_1, \mathbf{r}_2) \phi_q(\mathbf{r}_1) \phi_s(\mathbf{r}_2) \tag{34}$$

In the *ab-initio* approaches the orbitals ϕ_q are usually constructed as linear combinations of some primitive basis functions. Consequently, the evaluation of the two-electron integrals is associated with the so called four-index transformation, a procedure both time- and space-consuming. Modern group-theory-based algorithms for construction and analysis of the Hamiltonian eigenvalue problem in the FCI space, combined with the development in computer technology, resulted in considerable progress in solving the CI eigenvalue equations. However, though the length of tractable CI expansions have grown up during the last two decades by several orders of magnitude reaching up to 10^9 Slater determinants [22], only systems of several electrons may be treated this way with a sufficient accuracy. For larger systems the use of simplified semiempirical approaches is necessary.

In semiempirical theories the number of one- and two-electron integrals is drastically reduced. In consequence, their evaluation and handling becomes a trivial task. The basic idea of these theories may be formulated as follows [23]. Let us assume that there exists a set of orbitals such that the majority of the one- and two-electron integrals, when evaluated within these orbitals, is either very small or equal to 0. Then let us assume that our theory has been formulated in terms of these orbitals. We do not have to know the specific form of these orbitals, since the integrals need never be evaluated. They are treated as empirical parameters of the theory and determined by fitting the results obtained for some reference systems to the experimental data. Among semiempirical theories, models based on the zero-differential-overlap (ZDO) approximation leading to neglect of all three- and four-center integrals belong to the most commonly used. They are particularly useful in describing lattices composed of regularly distributed identical atoms. To this category belongs the Pariser-Parr-Pople theory of π-electron systems in unsaturated hydrocarbons as well as the Heisenberg and the Hubbard models used extensively in solid state

physics. In the case of π-electron systems of conjugated hydrocarbons one can choose an orbital basis in which all but the Coulomb two-electron integrals may be neglected. This approximation is best fulfilled for symmetrically orthogonalized localized $2p\pi$ orbitals, often referred to as the Löwdin orbitals [24]. In order to describe the magnetic properties of the molecules, one also has to retain the exchange integrals, since these are primarily responsible for removing degeneracies between different spin states.

The two-electron integrals in the Löwdin basis are then assumed to be given by

$$(pq|rs) = \gamma_{pr}\,\delta_{pq}\delta_{rs} + J_{pq}\,\delta_{qr}\delta_{ps} - \gamma_{pp}\,\delta_{pq}\delta_{rs}\delta_{pr}, \tag{35}$$

where $\gamma_{pr} = (pp|rr)$ are the Coulomb integrals and $J_{pq} = (pq|qp)$ are the exchange integrals. Substituting Eqs.(35) and (21) into Eq.(17) gives the semiempirical model Hamiltonian:

$$\mathsf{H} = \sum_{p,q}^{K}\left[\beta_{pq}\mathsf{E}_{pq} + \tfrac{1}{2}\gamma_{pq}\mathsf{E}_{pp}(\mathsf{E}_{qq}-\delta_{pq})\right] + \tfrac{1}{2}\sum_{p\neq q}^{K} J_{pq}\left(\mathsf{E}_{qp}\mathsf{E}_{pq}-\mathsf{E}_{qq}\right), \tag{36}$$

where $\beta_{pq} = (p|q)$ are the resonance integrals. The Löwdin orbitals are localized on individual atoms. Therefore each orbital product Φ_λ corresponds to a specific distribution of electrons over the atomic orbitals. Each configuration λ may be interpreted as a set of valence-bond-type structures. The structures are purely covalent if all the orbital occupation numbers are equal to 1. If some of the occupation numbers are 2 or 0, we have ionic structures with the degree of ionicity equal to the number of doubly occupied orbitals. This model is frequently referred to as a semiempirical orthogonal valence bond (VB) method [25, 26].

The localized atomic orbitals are associated with specific centers of the lattice or molecule and the corresponding charge densities decrease exponentially with increasing distance from these centers. In most cases one can therefore retain only those resonance and exchange integrals which correspond to neighboring centers. Another simplification may be obtained if we assume that the Coulomb integrals are asymptotically equal to the interaction energy of two non overlapping spheres of unit charge. This leads to interpolation formulas for γ_{pr}, $p \neq r$, of the form $\gamma_{pr} = (\gamma_{pp}^{-x} + R_{pr}^{x})^{-1/x}$, where R_{pr} is the distance between the centers and γ_{pp} is determined empirically. For $x = 1$ we get the Mataga-Nishimoto formula [27], and for $x = 2$ the Ohno formula [28]. In essence this simplification can be viewed as condensing the parameter set γ_{pr}, $p \neq r$ into a single parameter x describing the optimum form of decay of the Coulomb interaction energy with distance. Hamiltonians describing several different models may be obtained

as special cases of the semiempirical Hamiltonian defined in Eq.(36). In particular, setting $J_{pq} = 0$ we obtain the Pariser-Parr-Pople Hamiltonian [29, 30] describing properties of π-electron systems. Assuming additionally $\gamma_{pq} = 0$ for $p \neq q$ we get the Hubbard Hamiltonian [31] useful in solid state physics. Finally, by restricting the model space to a single configuration with all orbitals singly occupied, we get the Heisenberg Hamiltonian [17] describing ferromagnetic properties of spin lattices (formally the Heisenberg Hamiltonian may be obtained from Eq. (36) by putting $\beta_{pq} = \gamma_{pq} = 0$). An excellent review about use of different model Hamiltonians and different approximation methods for solving the electron correlation problem in molecular and solid state physics can be found in [32].

3.1. Matrix elements

In order to solve the eigenvalue problem in Eq.(31) we need to evaluate Hamiltonian matrix elements between the N-electron basis functions Ψ^{SM}. Combining Eqs.(11), (12), (14), (16) and (17) we get

$$H_{k\ell}^{\lambda\mu} = \langle \Psi_{\lambda k}^{SM} | \mathsf{H} | \Psi_{\mu\ell}^{SM} \rangle = \frac{\xi_\lambda \xi_\mu}{N!} \sum_{\mathsf{P} \in \mathcal{S}_N} \epsilon(\mathsf{P}) \langle \Theta_k^{SM} | \mathsf{P} | \Theta_\ell^{SM} \rangle \langle \overline{\mathsf{P}} \Phi_\lambda | \mathsf{H} | \Phi_\mu \rangle, \qquad (37)$$

where $k = 1, 2, \ldots, f(S, s_\lambda)$, $\ell = 1, 2, \ldots, f(S, s_\mu)$ and $\overline{\mathsf{P}}\Phi_\lambda$ means that P acts on the orbital indices in the product Φ_λ rather than on the electron coordinates. Due to the hermitian nature of H we can assume without loss of generality that $s_\lambda \geq s_\mu$, i.e. the number of singles in Φ_λ is greater than or equal to the number of singles in Φ_μ. The orbital function Φ_λ is invariant with respect to the subgroup Π_λ of $\mathcal{S}_N$ consisting of transpositions within doubles. Permutations of this subgroup acting on the spin functions Θ_ℓ^{SM} either change their sign (if the permutation is odd) or leave it invariant (in the even case). It is easy to observe that permutations belonging to a double coset $\Pi_\lambda \mathsf{P} \Pi_\mu$ of $\mathcal{S}_N$ give identical contributions to $H_{k\ell}^{\lambda\mu}$. Therefore Eq. (37) may be simplified to

$$H_{k\ell}^{\lambda\mu} = \sum_q \epsilon(\mathsf{P}_q) \alpha_{\lambda\mu}(\mathsf{P}_q) \langle \Theta_k^{SM} | \mathsf{P}_q | \Theta_\ell^{SM} \rangle \langle \overline{\mathsf{P}}_q \Phi_\lambda | \mathsf{H} | \Phi_\mu \rangle, \qquad (38)$$

where the sum runs over a complete set of distinct double coset representatives P_q and

$$\alpha_{\lambda\mu}(\mathsf{P}_q) = 2^{(d_\mu - d_\lambda)/2 + t_q}, \qquad (39)$$

.where t_q is equal to the number of doubles in Φ_λ being broken by P_q [7].

As one can see from Eq.(36), three classes of matrix elements over the orbital variables appear in Eq.(37):

1. Matrix elements associated with the Coulomb integrals γ_{pq}. These are expressed in terms of the orbital occupation number operators. Since Φ_μ is an eigenfunction of E_{pp} we get

$$\langle \overline{P}\Phi_\lambda | F(E_{pp}) | \Phi_\mu \rangle = \begin{cases} F(n_p^\mu)\delta_{\lambda\mu}, & \text{if } \overline{P} \in \Pi_\lambda | \Pi_\lambda, \\ 0, & \text{otherwise,} \end{cases} \qquad (40)$$

where F denotes a general function of its arguments.

2. Matrix elements associated with the exchange integrals J_{pq}. Due to Eq.(29), and its generalization valid for doubly occupied orbitals (see [8] for details),

$$\langle \overline{P}\Phi_\lambda | E_{qp}E_{pq} - E_{qq} | \Phi_\mu \rangle = \begin{cases} \delta_{\lambda\mu}, & \text{if } \overline{P} \in \Pi_\lambda(p,q)\Pi_\lambda, \\ 0, & \text{otherwise.} \end{cases} \qquad (41)$$

The matrix elements vanish if $n_p^\lambda n_q^\lambda = 0$.

3. Matrix elements associated with the resonance integrals β_{pq}. For $p = q$ these matrix elements are of the same kind as in class 1. For $p \neq q$, $\langle \overline{P}\Phi_\lambda | E_{pq} | \Phi_\mu \rangle = 1$ if $\overline{P}\Phi_\lambda = E_{pq}\Phi_\mu$. In the opposite case the integral vanishes. Thus, the integral does not vanish if $n_p^\lambda = n_p^\mu + 1$, $n_q^\lambda = n_q^\mu - 1$ and $\overline{P} = \Pi_\lambda \overline{P}_0 \Pi_\mu$, where P_0 is the so called line-up permutation, bringing the orbitals of Φ_λ into a complete coincidence with the orbitals of $E_{pq}\Phi_\mu$. One may easily demonstrate [8] that P_0 may always be expressed as a single cycle, where a cycle is defined as follows:

$$(p \cdots q) = (p, p-1)(p-1, p-2)\cdots(q+1, q), \quad p > q. \qquad (42)$$

In order to evaluate integrals over spin variables let us note that Eq. (5) implies that the symmetric group $\mathcal{S}_N$ is an invariance group for the total spin operators S^2 and S_z. Consequently, the eigenfunctions of these operators form bases for representations of $\mathcal{S}_N$. In particular,

$$P\Theta_\ell^{SM} = \sum_{i=1}^{f} V_S^N(P)_{i\ell}\Theta_i^{SM}, \qquad (43)$$

where $\mathbf{V}_S^N(\mathsf{P})$ are the matrices of such a representation. Indices S and N label the representation and f is its dimension. We assume that the set of spin functions $\{\Theta^{SM}\}$ is orthonormal. Then the matrices $\mathbf{V}_S^N$ are orthogonal. As one can show (see e.g. [18]) the representations generated by $\{\Theta^{SM}\}$ are irreducible, M-independent, and correspond to two-row Young diagrams with x boxes in the first row and y boxes in the second row, where x and y are defined in Eq.(23). Now, from Eq.(43) we readily get

$$\langle \Theta_k^{SM} | \mathsf{P} | \Theta_\ell^{SM} \rangle = V_S^N(\mathsf{P})_{k\ell}. \tag{44}$$

According to Eqs.(38) – (41) the non-vanishing matrix elements of the semiempirical Hamiltonian (36) are given by two kinds of equations:

- If $\lambda = \mu$ then

$$
\begin{aligned}
H_{k\ell}^{\lambda\lambda} &= \delta_{k\ell} \left[\sum_{p=1}^K \left(n_p^\lambda \beta_{pp} + \tfrac{1}{2} n_p^\lambda (n_p^\lambda - 1) \gamma_{pp} \right) + \sum_{p<q}^K n_p^\lambda n_q^\lambda \gamma_{pq} \right. \\
&\quad \left. - \tfrac{1}{2} \sum_{p<q}^{K}{}' n_p^\lambda n_q^\lambda J_{pq} \right] - \sum_{p<q}^{K}{}'' J_{pq} V_S^N((\mathsf{p},\mathsf{q}))_{k\ell},
\end{aligned}
\tag{45}
$$

  where the prime indicates that only terms with $\max\left(n_p^\lambda, n_q^\lambda\right) = 2$ are included and the double prime means that only terms with $n_p^\lambda = n_q^\lambda = 1$ are included.

- If λ and μ differ by one orbital, for example $n_p^\lambda = n_p^\mu + 1$ and $n_q^\lambda = n_q^\mu - 1$, then

$$H_{k\ell}^{\lambda\mu} = \epsilon(\mathsf{P}_0)\, \alpha_{\lambda\mu}(\mathsf{P}_0)\, \beta_{pq}\, V_S^N(\mathsf{P}_0)_{k\ell}, \tag{46}$$

  where $k = 1, 2, \ldots, f(S, s_\lambda)$ and $\ell = 1, 2, \ldots, f(S, s_\mu)$.

Eqs.(45) and (46) show a very simple structure of the semiempirical Hamiltonian matrix. The the one-site resonance integrals β_{pp} and the Coulomb integrals γ_{pq} appear only in the diagonal elements. The exchange integrals J_{pq} are present only in the diagonal blocks of dimensions $f(S, s_\lambda) \times f(S, s_\lambda)$. Pairs of the diagonal blocks corresponding to configurations λ and μ differing by one orbital are coupled by the off-diagonal blocks of matrix elements given by Eq.(46). These elements are proportional to the resonance integrals β_{pq}. In general, the Hamiltonian matrix is very sparse since majority of configurations differ by more than one orbital.

The structure of the matrix is particularly simple in the Hubbard model, when the only type of non-vanishing Coulomb integrals is γ_{pp}. In this case the energy difference between two configurations, one with $n_p = 2$, $n_q = 1$ and another one with $n_p = n_q = 1$, is equal to γ_{pp}. The energetic sequence of the diagonal matrix elements is determined by the value of d_λ: the smaller is the number of doubly occupied centers in λ, the lower is the energy of this configuration. Thus, if $\beta_{pq} = 0$, the ground state corresponds to the covalent structures in which all orbitals are singly occupied, the first excited state is composed of the ionic configurations, in which one orbital is doubly occupied and one is empty, and the highest energy state is related to the configuration in which $N/2$ centers are doubly occupied and $N/2$ are empty. Configurations of the same degree of ionicity which differ by one orbital ($n_p^\lambda = n_p^\mu + 1$, $n_q^\lambda = n_q^\mu - 1$) are coupled by the off-diagonal matrix element (46). This coupling removes the degeneracy of the same ionicity configurations. Configurations λ and μ with adjacent degrees of ionicity, i.e. the ones for which $|s_\lambda - s_\mu| = 1$, may also be coupled by the matrix elements (46). However, unless the values of β_{pq} are unreasonably large compared to γ_{pp}, in the eigenvectors the dominant ionic character of the "parent" configuration is retained. In particular, the ground state usually remains covalent. If the lattice is composed of identical or similar atoms, then the more uniform the valence electron distribution is (i.e. the larger the number of singles) the lower is the energy. The ground state is dominated by the orbital configuration in which all orbitals are singly occupied by the valence electrons. For a strongly correlated system, when $|\beta_{pq}| << \gamma_{pp}$, the coupling between different configurations is weak, giving rise to energy bands for each configuration. The energy level splittings within each band depend on the relative magnitudes between the exchange and resonance integrals. If the exchange integrals are included they contribute, in the first order of the perturbation theory, to the energy level splitting (in this model the resonace integrals contribute in the second order only). In particular, if $J_{pq} > |\beta_{pq}|$, the energy level splittings will only be slightly affected by the resonance integrals and will be given to a very good approximation by considering only the diagonal blocks $\mathbf{H}^{\lambda\lambda}$ given by Eq.(45). Large atomic exchange integrals favor the parallel alignment of spins, hence the ground state will be in this case of a ferromagnetic nature. On the other hand, if $|\beta_{pq}| >> J_{pq}$, then the off-diagonal blocks $\mathbf{H}^{\lambda\mu}$ will have a considerable effect on the energy level splittings and cannot simply be neglected. In this case, and if we assume still that $\gamma_{pp} >> |\beta_{pq}|$, one proceeds by performing perturbation [33] or cluster expansions [34] in β_{pq}/γ_{pp} leading to effective Heisenberg type operators in the λ configuration space describing a predominantly antiferromagnetic ground state. For simplicity let us assume that we are dealing with the ferromagnetic case,

that is we simply neglect the off-diagonal blocks $\mathbf{H}^{\lambda\mu}$ of Eq.(46). If we are interested in the lowest energy configuration of a neutral system, then we take $K = N$ and $n_p^\lambda = 1$ for $p = 1, 2, \ldots, K$. In such a case the relevant matrix elements in (45) become

$$H_{k\ell}^{\lambda\lambda} = \epsilon\,\delta_{k\ell} - \sum_{p<q}^{N} J_{pq}\,V_S^N((\mathsf{p}, \mathsf{q}))_{k\ell}, \tag{47}$$

where

$$\epsilon = \sum_{p=1}^{N} \beta_{pp} + \sum_{p<q}^{N} \gamma_{pq} \tag{48}$$

is a (k, ℓ)-independent contribution to the diagonal elements of the Hamiltonian matrix, shifting all eigenvalues of H by ϵ.

When the long-range interactions (i.e. the Coulomb integrals for non-neighboring centers) are included, the simple correlation between the degree of ionicity of a configuration and its energy is frequently broken. For example, if we take the values of the Coulomb integrals derived from a least square fit to the π-electron spectrum of benzene [35], then in the limit of $\beta_{pq} = 0$ the ground state configuration of a linear chain of 6 atoms is ionic with occupation numbers on consecutive atoms equal to $[2, 0, 1, 1, 0, 2]$.

4. THE HEISENBERG HAMILTONIAN

The matrix defined in Eq.(47) represents a general, non-relativistic spin-independent N-electron Hamiltonian given by Eq.(2) in a specifically defined model space. The one-electron orbital space is spanned by N orthonormal localized orbitals $\{\phi_j; j = 1, 2, \ldots, N\}$ and the N-electron orbital space is one-dimensional with the basis function

$$\Phi(\mathbf{r}) = \prod_{j=1}^{N} \phi_j(\mathbf{r}_j). \tag{49}$$

This basis function is associated with $f(S, N)$ different spin functions $\{\Theta_k^{SM}; k = 1, 2, \ldots, f(S, N)\}$. Thus, in this case the N-electron antisymmetric model space may be expressed as

$$\widetilde{\mathcal{H}}^{\mathsf{A}}(N, N, S, M) = \mathsf{A}\left[\widetilde{\mathcal{H}}^o(N, N) \otimes \mathcal{H}^s(N, 2, S, M)\right], \tag{50}$$

618

where $\widetilde{\mathcal{H}}$ means that all orbital occupation numbers are equal to 1. Consequently, the dimension of the model space is equal to $f(S, N)$, i.e. to the dimension of the N-electron spin space. The basis in the model space may be interpreted as a set of $f(S, N)$ covalent structures corresponding to the orbital configuration (49). In principle, this is also the main idea of Anderson's resonating valence bond model [2, 3].

The specific form of the Hamiltonian matrix depends upon the choice of the spin coupling scheme. Thus, one can use a non-orthogonal basis of the spin functions specific for the classical valence-bond-type models [36, 37, 38] with a possibility of drawing the corresponding covalent structure diagrams, the Serber basis [39] with diagonal representation matrices for a selected set of commuting transpositions, the genealogically constructed Yamanouchi-Kotani basis described by Van Vleck's branching diagram [40, 41, 42] or the basis described by the reversed branching diagram [8, 41]. Detailed review of a large variety of different spin coupling schemes may be found in the monographs by Pauncz [18, 43]. All these bases are related by similarity transformations and therefore give the same results if the Hamiltonian matrix is exactly diagonalized. However, for specific applications, particularly when the exact diagonalization procedure is prohibitive to perform, the choice of the basis functions may be very essential. This point will be discussed in the next section.

The procedure leading from the exact N-electron Hamiltonian (2) to the Heisenberg Hamiltonian matrix (47) is very instructive, but it is rather lengthy. Much simpler is the use of effective Hamiltonians which in the space of N-electron eigenfunctions of S^2 and S_z are represented by the same matrix. Furthermore, using the effective Hamiltonians may bring another insight into the nature of the interactions described by the model. The simplest effective Hamiltonian in the pure spin is

$$\mathsf{H}_1^{\mathrm{eff}} = -\sum_{p<q}^{N} J_{pq}(\mathsf{p}, \mathsf{q}), \tag{51}$$

where, relatively to Eq. (47), the energy scale has been chosen such that $\epsilon = 0$. This form of the Heisenberg Hamiltonian is most appropriate for group-theory-based formulations. In particular, Eq.(51) shows that, although the Heisenberg Hamiltonian does not commute with all $\mathsf{P} \in \mathcal{S}_N$, it is an element of the symmetric group algebra. As a consequence, the matrix of $\mathsf{H}_1^{\mathrm{eff}}$ is block-diagonal in an $\mathcal{S}_N$-adapted basis of N-electron spin functions. The blocks are labeled by irreducible representations of $\mathcal{S}_N$ (i.e. by pairs of S, M quantum numbers) [14, 44]. This property of the Heisenberg Hamiltonian also results, in a rather obvious way, from its construction presented in sections 2 and 4 of this chapter.

Another form of the Heisenberg Hamiltonian may be obtained by means of the so called Dirac identity [45]

$$(\mathsf{p}, \mathsf{q}) = \tfrac{1}{2} + 2\, \vec{S}_p \cdot \vec{S}_q, \tag{52}$$

where $\vec{S}_p \equiv \vec{S}(\mathsf{s}_p)$ is the total one-electron spin operator corresponding to the p-th electron. The identity is valid if the operators act only in the spin space. Then, Eq.(51) may be rewritten as

$$\mathsf{H}_2^{\mathrm{eff}'} = -2 \sum_{p<q}^{N} J_{pq}\, \vec{S}_p \cdot \vec{S}_q - \tfrac{1}{2} \sum_{p<q}^{N} J_{pq}. \tag{53}$$

By changing again the origin of the energy scale we get

$$\mathsf{H}_2^{\mathrm{eff}} = -2 \sum_{p<q}^{N} J_{pq}\, \vec{S}_p \cdot \vec{S}_q. \tag{54}$$

The effective operators defined in Eqs.(51) and (54) were first introduced by Heisenberg [17], Dirac [45] and Van Vleck [46] in order to formulate a quantum theory of ferromagnetism based on exchange effects. As explained in the discussion following Eq.(46), the antiferromagnetic situation can also be cast in form of a Heisenberg Hamiltonian, the same as in Eq.(51) but with a negative value of the exchange integral. For a unified treatment we will henceforth absorb the sign into J_{pq} and simply refer to J_{pq} as the Heisenberg exchange parameters with negative/positive values for ferromagnetic/antiferromagnetic treatment. The exchange parameters form the $N \times N$ Heisenberg exchange parameter matrix.

As long as the model space is constructed according to Eq.(50), the matrices representing Hamiltonians defined in Eqs.(2), (17), (36), (51) and (54) are the same (up to a constant added to all diagonal elements) and in this sense they are equivalent. In the SGA-based formalism, the form given by Eq.(51) is most convenient and this form will be used in our further discussion.

The geometry of the lattice determines the structure of the Heisenberg exchange parameter matrix. In most cases only nearest-neighbor interactions are taken into account and all non-vanishing Heisenberg exchange parameters are set equal, i.e. we set

$$J_{pq} = \begin{cases} J & \text{if } p \text{ and } q \text{ are nearest-neighbors,} \\ 0 & \text{otherwise.} \end{cases} \tag{55}$$

In such a case

$$H_1^{\text{eff}} = J \sum_{p<q}^{N\,'} (\mathsf{p}, \mathsf{q}), \tag{56}$$

where the prime means that the sum is extended over the nearest-neighbors only.

Some sums of the transposition operators are represented by very simple matrices. For example the operator

$$A_k = \sum_{s=1}^{k} (\mathsf{s}, \mathsf{k}), \quad k = 1, 2, \ldots, N \tag{57}$$

in the Yamanouchi-Kotani basis is represented by diagonal matrices [10]. Consequently, the eigenvalue problem describing a lattice constructed in such a way that the corresponding Hamiltonian (56) is a combination of the A_k operators may be easily solved analytically. In most cases however one has to set up the Heisenberg Hamiltonian matrix and solve for its eigenvalues.

4.1. The matrix

As one can see from Eq.(47), the Heisenberg Hamiltonian matrix is a linear combination of the appropriate representation matrices of $\mathcal{S}_N$. Only the matrices which correspond to transpositions of nearest-neighbor particles are needed. In principle, the representation matrices may be constructed using one of the techniques developed over several decades by many different authors (for reviews see the monographs by Pauncz [18, 43] and references therein). However, to our knowledge, the most efficient approach is based on using graphical techniques in model spaces [47] based on the Yamanouch-Kotani wave functions [48, 49]. This methodology has been developed in connection with designing general SGA-based CI programs [8, 9, 10] and was also successfully applied in studies on Heisenberg Hamiltonians [13, 14].

The Yamanouchi-Kotani basis in the N-electron $\mathcal{S}_N$-adapted spin space is closely related to the standard Young tableaux used in characterizing irreps of the symmetric group [50] and is conveniently represented by Van Vleck's branching diagram [18, 42]. To a basis function Θ_{ℓ}^{SM} we assign an array

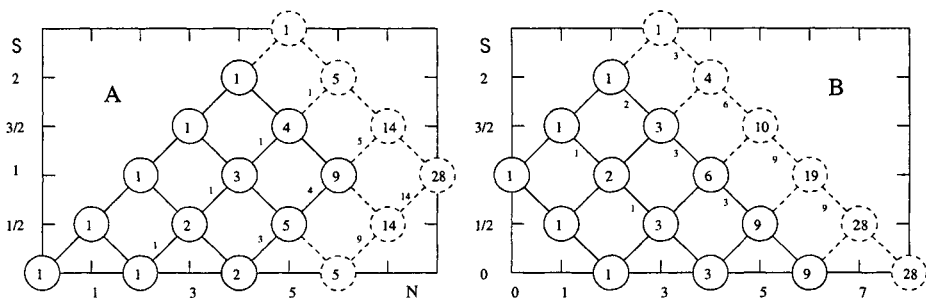$$\mathbf{T}^S(\ell) = [S_0, S_1, \ldots, S_N], \tag{58}$$

Figure 1: Van-Vleck's branching diagram (A) and the reversed branching diagram (B) for $S = 1$, $N = 8$. Either 6 (full lines) or 8 (full and broken lines) spins are coupled in all ways allowed by the Yamanouchi-Kotani scheme. At vertices and arcs their weights (if different from 0) are shown.

where S_k is the resultant spin obtained by coupling the spins of the first k electrons. The array may be represented graphically on a grid in which the vertical position equals S_k and the horizontal one k. The graphical representation of $\mathbf{T}^S(\ell)$ is a directed path which starts at the $(0, 0)$ vertex, joins consecutive vertices $(k, S_k); k = 0, 1, \ldots, N$, and ends at the (N, S) vertex. To a (k, S_k) vertex we assign the lexical weight of the vertex defined as

$$d(k, S_k) = d(k - 1, S_k - \tfrac{1}{2}) + d(k - 1, S_k + \tfrac{1}{2}). \tag{59}$$

If the coordinates of a vertex correspond to a point outside the diagram then its weight is equal to 0. To the arc of slope $+1$ contained between the $(k - 1, S_k - \tfrac{1}{2})$ and (k, S_k) vertices we assign the lexical arc index $y(+1, k, S_k) = d(k - 1, S_k - \tfrac{1}{2})$ and to the arc of slope -1 contained between the $(k - 1, S_k + \tfrac{1}{2})$ and (k, S_k) vertices we assign the lexical arc index $y(-1, k, S_k) = 0$. The overall lexical index I_ℓ^S of the complete path representing $\mathbf{T}^S(\ell)$ is then given by

$$I_\ell^S = 1 + \sum_{k=1}^{N} y(p_k, k, S_k), \tag{60}$$

where $p_k = 2(S_k - S_{k-1}) = \pm 1$. An example of a branching diagram is shown in Fig. 1 A. The branching diagram makes possible the representation of very large bases of spin functions in terms of a few arcs and vertices and is thus of great practical importance.

As one can see by analyzing Fig. 1 A, a change in the number of spins results in changing the lexical numbers of all paths in the branching diagram. In particular, adding to the system of spin functions described by the branching diagram some singlet-coupled pairs results in renumbering of all spins in the system. This inconvenience may be removed by a simple change of the structure of the branching diagram: the reverse numbering of the spins and the reverse lexical ordering of the spin functions. The resulting diagram, referred to as the reversed branching diagram, is shown in Fig. 1 B. It has two important features:

- Let us assume that we have two sets of Yamanouchi-Kotani spin functions: one describing a system of N spins and the other one describing a system of $(N + 2)$ spins, both coupled to the same value of S. The functions of the $(N + 2)$-spin system may be divided into two sets: set I containing $f(S, N)$ functions coupled according to the same scheme as in the N-spin system with two additional spins forming a singlet-coupled pair and set II containing the remaining $f(S, N+2) - f(S, N)$ functions. In the corresponding reversed branching diagrams, the lexical indices of the functions belonging to set I of the $(N + 2)$-spin system are the same as the lexical indices of the functions describing the N-spin system.

- Adding an arbitrary number of singlet-coupled pairs to a reversed branching diagram changes neither the indexing of the remaining part of the diagram nor the numbering of the spin functions.

The reversed branching diagram is of crucial importance in setting up the Hamiltonian matrix for CI calculations. In this case we have to deal with orbital configurations having varying numbers of singly occupied orbitals. The reversed branching diagram allows one to find the spin representation matrices in Eq.(44) corresponding to $N - 2, N - 4, \ldots$ electrons simply as upper left subblocks of $\mathbf{V}_S^N(\mathrm{P})$, a fact which makes superfluous the generation of spin matrices corresponding to the overall number of electrons. Rather only those corresponding to the maximum number of singles are needed [8]. To treat the Heisenberg Hamiltonian the reversed branching diagram offers no particular advantage, since the number of electrons corresponding to singly occupied orbitals is fixed from the very beginning. Hence, in what follows, we will base our discussion on the branching diagram as presented in Fig. 1 A.

A transposition $(\mathsf{k} - 1, \mathsf{k})$ which interchanges two adjacent elements is called an elementary transposition. When this elementary transposition acts on a branching diagram spin function Θ_ℓ^{SM}, it affects only the arcs corresponding to $k - 1$ and k, that is the path segments contained between

vertices with abscissae $k-2$ and k. It may be easily demonstrated [13, 18] that

$$(k-1,k) \quad \text{⟋⟍} \;=\; \text{⟋⟍} \,, \qquad (k-1,k) \quad \text{⟍⟋} \;=\; \text{⟍⟋} \,, \tag{61}$$

$$(k-1,k) \quad \text{⟍⟋} \;=\; -\,a_k\,\text{⟍⟋} + b_k\,\text{⟋⟍} \,, \tag{62}$$

$$(k-1,k) \quad \text{⟋⟍} \;=\; +\,b_k\,\text{⟍⟋} + a_k\,\text{⟋⟍} \,, \tag{63}$$

where only the path segments contained between $k-2$ and k are shown and

$$a_k = \frac{1}{2S_k + 1}, \quad b_k = \sqrt{1 - a_k{}^2}. \tag{64}$$

From Eqs.(61) – (64) one can see that

$$V_S^N((k-1,k))_{ii} = \begin{cases} 1, & \text{Eq.(61),} \\ -a_k, & \text{Eq.(62),} \\ a_k, & \text{Eq.(63),} \end{cases} \tag{65}$$

where the equation number refers to the way the i-th spin function is transformed by the transposition $(k-1,k)$. The representation matrices are orthogonal. Therefore, if $V_S^N((k-1,k))_{ii} = a_k$ and $V_S^N((k-1,k))_{jj} = -a_k$ then $V_S^N((k-1,k))_{ij} = V_S^N((k-1,k))_{ji} = b_k$ and the remaining off-diagonal elements corresponding to the i,j rows and columns are equal to 0. This implies that the representation matrices of elementary transpositions have either a 1 on the diagonal or have 2×2 blocks composed of $\pm a_k$ and b_k. Matrices corresponding to other transpositions may be obtained by multiplication of the elementary transposition matrices. For example, $(k-1, k+1) = (k-1,k)(k,k+1)(k-1,k)$, etc. A description of an algorithm which couples the procedure of evaluation of the representation matrix elements with a method of solving the eigenvalue problem of the Heisenberg Hamiltonian matrix is given in the next section.

The Yamanouchi-Kotani basis is best suited if we want to solve the Heisenberg problem in the complete spin space. However, the number of spins that can be handled this way, soon reaches an end due to the rapid growth of the spin space dimension $f(S,N)$. Even with the present day computers, the maximum number of spins that can be treated clusters around $N = 30$. For larger values of N one must resort to approximate treatments, one of which, as described hereafter, is based on the idea of resonating valence bonds (RVB) coming from the classical VB model developed by Pauling and Wheland back in the early 1930's [37, 51]. In essence,

it consists in identifying the most important contributions from the entire spin space to the relevant part of the Heisenberg spectrum that one wants to treat. Thus, it can be viewed as a similarity transformation on the Heisenberg matrix with the goal of isolating its most important subblocks.

Suppose that we have a system for which N is even and that we are interested in the singlet ($S = 0$) ground state of a Heisenberg Hamiltonian describing an antiferromagnetic material. Since in Eq.(56) the sum is only over nearest-neighbor spin pairs, a hypothetical wave function containing singlet spin functions between all these pairs would give the lowest energy, though it is generally not possible to build such a wave function, except for the obvious case of disconnected spin pairs. However, this idea of pairing the spins leads to the concept of the RVB space. To construct this space we index the sites of the system with the positive natural numbers from 1 to N and partition the resulting set of positive numbers $\{P\}$ into $N/2$ disjoint two-numbered sets $P_{k\ell}$ in all possible ways. Each such partition is then associated with a spin product function ϕ, in which each two-numbered set $P_{k\ell}$ of the partition gives rise to a singlet spin pairing between sites k and ℓ:

$$\{P\} = \bigoplus_{k,\ell}^{N/2} P_{k\ell} \quad \longrightarrow \quad \phi = \prod_{k,\ell}^{N/2} \frac{1}{\sqrt{2}}(\alpha_k\beta_\ell - \beta_k\alpha_\ell). \tag{66}$$

The resulting set of RVB functions $\{\phi\}$ has the following properties:

- Each $\phi \in \{\phi\}$ is a singlet function, i.e. it belongs to the $S = 0$ subspace of the complete N-particle spin basis.

- The order of the set $\{\phi\}$ is equal to $(N-1)!!$ but its dimension is given by $f(0, N) = N!/(N/2 + 1)!(N/2)!$. Hence $\{\phi\}$ constitutes a linearly dependent set for $N > 2$.

- The overlap between any two RVB functions is different from zero, that is $\langle \phi_i | \phi_j \rangle \neq 0$ for all i, j.

- If G denotes a point group of the system and if $g \in G$ is any of its symmetry elements, then $g\phi = \pm\phi^g$, where ϕ^g denotes the RVB function in $\{\phi\}$ obtained from ϕ in Eq.(66) by permuting and rearranging to their original order all the index pairs $\{k, \ell\}$ according to g; the $+$ or $-$ sign holding if an even or odd number of index pair rearrangements needs to be performed.

The importance of the RVB space lies in the fact that we can now identify its most important parts characterizing the ground state wave function

of an antiferromagnetic system. Obviously, since the Heisenberg Hamiltonian involves only nearest-neighbor exchange interactions, we expect a RVB function to make a substantial contribution to the ground state wave function if we maximize the spin pairings between nearest-neighbor sites. This leads directly to the important notion of the so called Kekulé subspace $\{\phi^K\}$ contained in $\{\phi\}$, and we define this subspace as the space containing all those RVB functions in which all spin pairings are between nearest-neighbors. The order of $\{\phi^K\}$ is usually much smaller than the RVB basis dimension but using $\{\phi^K\}$ alone one recovers typically $\approx 90\%$ of the exact ground state energy together with a very good description of the wave function. This has lead to formulation of qualitative rules concerning properties of π-electronic systems in organic chemistry, like for example the Clar sextet concept [52] in connection with relative stability of aromatic hydrocarbons or Herndon's structure count method [53] for predicting reactivities of polycyclic hydrocarbons. Further improvement over the Kekulé subspace can be anticipated with the inclusion of the subspace consisting of all those RVB functions possessing one excited bond, i.e. having one spin pairing between non-nearest-neighbors, then next with the inclusion of those possessing two excited bonds and so on. Note, however, that by doing so the linear dependency problem of the spin basis comes more and more into play, although one can usually assume, with some confidence, that the Kekulé subspace is linearly independent. Examples of such type of restricted RVB Heisenberg Hamiltonian calculations performed on fullerene-type carbon cages in the range $20 \leq N \leq 60$ and on two-, three- and four-legged spin-1/2 ladders are presented in [54, 55, 56].

Note, that one can always choose a basis within the RVB space as the subset consisting of all RVB functions corresponding to the Rumer diagrams [36]. However, from the way of constructing the Rumer diagrams as a set of directed noncrossing arrows on a circular array of lattice nodes, the Kekulé space is generally not contained in the Rumer basis, except for some trivial cases like the Heisenberg chain. The Rumer basis is thus inadequate for designing approximate treatments of large Heisenberg lattices. In case of exact treatments, however, it can be used and has resulted in the diagrammatic valence bond (DVB) approach developed by Soos and coworkers (see [57] and references therein) and applied successfully to Heisenberg problems [58]. The DVB approach has the same underlying structure as the RVB method, hence all that follows regarding RVB also applies to DVB.

A major drawback of RVB calculations is the fact that RVB functions cannot be cast into a compact graphical form as it is possible in SGA using the branching diagram. Each RVB function has to be generated explicitly and special techniques (e.g. bit representation) have to be used

to store them efficiently on a disk. As a consequence, recalculation of matrix elements between RVB functions during iterative diagonalization procedures (see the next section) becomes prohibitive due to excessive disk I/O that would have to be performed.

A last point worth mentioning about RVB functions is their easy transformation under the symmetry operations of the system point group G. As stated above, every RVB function transforms under such an operation into only one other RVB function. Moreover, each RVB subspace, labeled by the number of bond excitations, is closed under G, i.e. any $g \in G$ does not create or destroy extra excited bonds. Hence, application of group projection operators, in particular the ones corresponding to the one-dimensional irreps of G, is easy to perform. This makes the point group adaptation of restricted RVB Heisenberg Hamiltonian calculations rather trivial. Consequnetly, the adaptation can be done for RVB spaces of very large dimensions (see for example [54]). This nice feature is not shared by the Yamanouchi-Kotani spin functions. Each Yamanouchi-Kotani spin function gives a *linear combination* of many other Yamanouchi-Kotani spin functions under the action of an element of G, a fact which makes the point group adaptation a very demanding task, except for very small systems where projection operator methods may be used [11]. For exact calculations we would thus prefer a method which combines the nice features of both SGA (a compact graphical representation of an orthogonal basis) and RVB (an easy G-adaptation) approaches. To our knowledge this has not yet been achieved so far.

4.2. The eigenvalue problem

In a recent series of papers [13, 14, 44, 54, 55, 56] SGA- and RVB-based algorithms of construction and solving the eigenvalue problem of a Heisenberg Hamiltonian matrix have been formulated and successfully applied to lattices containing up to 30 (in case of SGA) and up to 60 nodes (in case of RVB), with dimensions of the corresponding matrices ranging up to 2.5×10^7 and 3.8×10^6, respectively. In this section we describe only the main ideas of the methods. For details the reader is referred to the original papers and references therein.

For the Heisenberg matrices **H** of low dimensions (up to orders of a few thousands) one can determine their full spectrum by using any one of the methods available for complete diagonalization, as discussed for example in [59]. For much bigger matrices one must make use of iterative diagonalization methods, which are able to extract several of the lowest or highest eigenvalues together with the corresponding eigenvectors. Most of these iterative methods are based on the original Lanczos scheme [60] or on one of its modifications [61, 62]. The key idea of these iterative

schemes is to expand the eigenvectors of interest in terms of so called correction vectors at each iteration step by solving a small eigenvalue problem and repeating this process until convergence has been achieved. A central step during this procedure is the repeated construction of products $\mathbf{HC}$, where $\mathbf{C}$ is a vector of the same dimension as $\mathbf{H}$. Since $\mathbf{H}$ in SGA is a linear combination of transposition matrices $\mathbf{V}_S^N((\mathsf{p},\mathsf{q}))$, each of which, in turn, is built up multiplicatively from elementary transposition matrices $\mathbf{V}_S^N((\mathsf{k}-1,\mathsf{k}))$, the problem of constructing an efficient SGA-based algorithm depends on finding a way of rapidly performing multiplications of the type $\mathbf{V}_S^N((\mathsf{k}-1,\mathsf{k}))\mathbf{C}$. To this end we note from Eqs.(61)-(63) that the only relevant contributions to this multiplication come from the bent-shaped segments in Eqs.(62) and (63). These contributions can be schematically represented as a two-segment loop in the branching diagram, as shown in Fig. 2 A, in which $\{I_\ell\}$ and $\{I_r\}$ denote the collection of lexical indices of all left and right subpaths reaching the corresponding leftmost and rightmost vertices v_ℓ and v_r of the loop, and I_1, I_2 are the non-zero lexical arc indices of the loop. An algorithm can now be set up for evaluating $\mathbf{D} = \mathbf{V}_S^N((\mathsf{k}-1,\mathsf{k}))\mathbf{C}$:

loop over all vertices v_ℓ at $k-2$

if vertex v_r exists at k, then

$$\text{calculate} \begin{cases} a_k & = & (2S_k + 1)^{-1} \\ b_k & = & \sqrt{1 - a_k^2} \end{cases}$$

determine I_1, I_2, $\{I_\ell\}$ and $\{I_r\}$

loop over all I_ℓ and I_r

$$\text{calculate} \begin{cases} i & = & I_1 + I_\ell + I_r \\ j & = & I_2 + I_\ell + I_r \end{cases}$$

$$\text{calculate} \begin{cases} D_i & = & -a_k C_i + b_k C_j \\ D_j & = & b_k C_i + a_k C_j \end{cases}$$

continue

endif

continue

This algorithm entirely avoids multiplications with zeros and repeated evaluation of identical a_k and b_k constants. The most time consuming part is the search through the paths reaching v_ℓ and v_r in order to evaluate the respective sets $\{I_\ell\}$ and $\{I_r\}$. Timings for evaluating the product
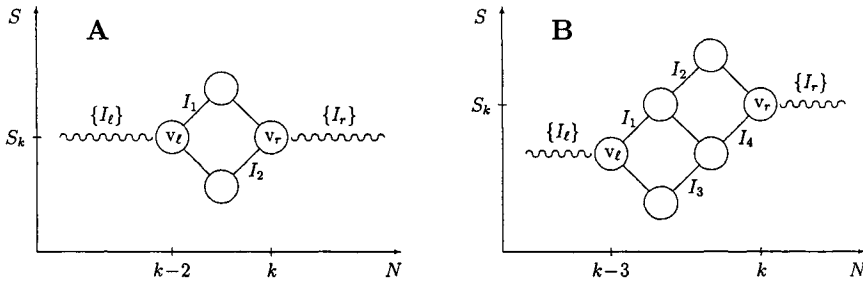
628

Figure 2: Two-segment (A) and three-segment (B) loop in the branching diagram

$\mathbf{V}_S^N((1,N))\mathbf{C}$, with the most dense transposition matrix, for several S and N, can be found in [14]. These timings show that the main limiting factor in a Heisenberg lattice calculation is the computer core memory available rather than the waiting time for each **HC**. Note, that one needs to hold at least three large vectors in the core memory, due to the multiplicative buildup of the transposition matrices. A further improvement in algorithmic efficiency can be achieved by explicit coding of larger segment loops corresponding to consecutive cycle matrices. The three-segment loop in Fig. 2 B would be used, for example, to evaluate contributions coming from the consecutive cycle matrix $\mathbf{V}_S^N((k-2,k-1,k))$. The gain is twofold: 1) the number of paths which have to be searched to establish the sets $\{I_\ell\}$ and $\{I_r\}$ are reduced and 2) some of the loop contributions are equal to zero and need not be considered explicitly. Of course, coding of the loop contributions, in terms of the relevant sets of a_k and b_k, soon becomes tedious, but it can be eased using any of the symbolic mathematical packages available. A program based on the above algorithm has been written including an explicit three-segment loop coding and is available from CPC [14].

Having established an efficient algorithm for performing the product **HC**, there remains the issue of how to start the iterative diagonalization procedure, i.e. how to select appropriate starting vectors $\mathbf{C}_0$ for each of the states required. This issue should never be underestimated since a bad choice of $\mathbf{C}_0$ almost always leads to many more iterations needed to achieve the convergence. When dealing with Hamiltonians defined in model spaces constructed out of multidimensional N-electron orbital spaces this problem is of minor importance when dealing with the lowest part of the spectrum, since usually one has a good zero order description of the wave functions in terms of Hartree-Fock type determinants or excitations therefrom. In these cases **H** is diagonally dominant and $\mathbf{C}_0$ can be set equal to the coefficients of the Hartree-Fock wave function. For the Heisenberg Hamiltonian

expressed in the Yamanouchi-Kotani basis the situation is quite different. The Hamiltonian is no longer diagonally dominant and one does not know in advance, which of the Yamanouchi-Kotani spin functions play a major role in the final wave function. One way to proceed is to subdivide the Heisenberg lattice into several noninteracting sublattices, each of which can be solved exactly. A zero order wave function for the overall lattice can then be constructed simply as a product of the sublattice wave functions. This procedure works well if the spin correlations corresponding to the neglected interactions are small in the final wave function. Otherwise considerable iteration time might be spent in building up these correlations. Another possibility would be to use as a starting point the wave function obtained from a RVB calculation within the Kekulé space $\{\phi^K\}$ expressed in terms of the Yamanouchi-Kotani spin functions. This procedure would avoid the need of large extra spin correlation buildup between any two sites and would probably be the optimum way to start the Heisenberg iterations. However, in order to express the Kekulé wave function in terms of the Yamanouchi-Kotani basis one needs to find efficient overlap expressions between these two bases and work is still underway to see if such expressions can be found.

When trying to perform the Heisenberg RVB calculations the algorithmic problems are entirely different in nature. The main difference, as compared to the SGA, is the necessity to evaluate the overlap matrix in addition to the Heisenberg matrix. Detailed formulas for both types of matrix elements can be found in [63, 64]. The overlap matrix poses a severe problem in RVB calculations: it is 100% dense, with no zeros. This fact prohibits its recalculation during an iterative diagonalization procedure, a similar situation holding for the Heisenberg matrix. Thus, partial evaluation and storage of conveniently sized subblocks of both matrices is essential. Hence, for a Heisenberg RVB calculation the disk space is the main limiting factor. As mentioned earlier effective use of the lattice point group G can be made here quite easily, reducing the dimensions and matrix evaluation cost roughly by a factor of $|G|$ and hence the disk storage requirements by a factor of $|G|^2$. Such a G-adaptation of the RVB space made it possible to perform a RVB study on the icosahedral buckminsterfullerene $C_{60}(I_h)$, where the largest calculation involving RVB Heisenberg and overlap matrices of dimension 3 840 260 were reduced to a manageable size of 32 520 in I_h-adapted space [55]. For details regarding the necessary algorithmic changes to perform iterative diagonalizations in the presence of overlap and the choice of iteration starting vectors we refer to [54].

5. SPECTRAL DENSITY DISTRIBUTIONS

As we could see in the previous sections, the construction of the Heisenberg Hamiltonian matrix within the SGA formalism in the (SM)-adapted model space is very simple – it is merely a linear combination of $\mathcal{S}_N$ representation matrices corresponding to transpositions. Despite this, however, the problem is far from being trivial. The dimension of the model space grows explosively with N. For example, $f(1,16) = 3\,432$, $f(1,32) = 94\,287\,120$, $f(1,40) = 17\,902\,146\,600$. Exact diagonalizations for lattices containing considerably more than, say, 32 nodes does not seem to be feasible in the foreseeable future. Therefore alternative ways of describing spectra have to be developed. One of them, originated in nuclear physics, is the statistical theory of spectra [65]. In this approach information about spectra is derived from the knowledge of spectral density distribution moments. The moments are defined as traces of Hamiltonian powers. In the case of the Heisenberg Hamiltonian their evaluation is rather simple and the complexity of the approach does not depend upon the size of the lattice.

The n-th spectral density distribution moment of a general Hamiltonian is defined as

$$M_n(\mathsf{H}) = \frac{1}{D} Tr(\mathsf{H}^n), \tag{67}$$

where D denotes the corresponding Hilbert space dimension in which H is represented. The n-th power of the Heisenberg Hamiltonian may be expressed in terms of products of n transpositions

$$\mathsf{H}^n = \frac{1}{2^n} \sum_{\{i\},\{j\}}^{N} J_{i_1 j_1} J_{i_2 j_2} \cdots J_{i_n j_n} (\mathsf{i_1 j_1})(\mathsf{i_2 j_2}) \cdots (\mathsf{i_n j_n}), \tag{68}$$

where $\{i\} = i_1, i_2, \ldots, i_n$ and $\{j\} = j_1, j_2, \ldots, j_n$ and all J's with equal indices are defined to be equal to zero. After further development Eq.(68) leads to

$$M_n = \frac{1}{2^n} \sum_{C} X_{[C]}^{[xy]} \sum_{\{i\},\{j\}}^{N} J_{i_1 j_1} J_{i_2 j_2} \cdots J_{i_n j_n}, \tag{69}$$

where the first sum is extended over those classes $[C]$ of $\mathcal{S}_{2n} \subset \mathcal{S}_N$ which can be generated by products of n transpositions,

$$X_{[C]}^{[xy]} = \frac{\chi_{[C]}^{[xy]}}{f(S,N)} \tag{70}$$

are the normalized irreducible characters, introduced and studied by Klein et al [25], $\chi_{[C]}^{[xy]}$ denote characters of the representation of $\mathcal{S}_N$ corresponding to the two-row Young shape defined in Eq.(23) and the sums over $\{i\}$ and $\{j\}$ extend to those combinations of the indices $i_1, i_2, \ldots, i_n$ and $j_1, j_2, \ldots, j_n$, which result in permutations belonging to the appropriate class. In particular [66],

$$M_1 = \tfrac{1}{2} X_{[2]}^{[xy]} \sum_{ij}^{N}{}' J_{ij}$$

$$M_2 = \tfrac{1}{4} X_{[2^2]}^{[xy]} \sum_{ijkl}^{N}{}' J_{ij} J_{kl} + X_{[31]}^{[xy]} \sum_{ijk}^{N}{}' J_{ij} J_{jk} + \tfrac{1}{2} X_{[1^4]}^{[xy]} \sum_{ij}^{N}{}' J_{ij}^2,$$

$$M_3 = \tfrac{1}{8} X_{[2^3]}^{[xy]} \sum_{ijklmn}^{N}{}' J_{ij} J_{kl} J_{mn} + \tfrac{3}{2} X_{[321]}^{[xy]} \sum_{ijklm}^{N}{}' J_{ij} J_{jk} J_{lm}$$

$$+ \; X_{[21^4]}^{[xy]} \left[\tfrac{1}{2} \sum_{ij}^{N}{}' J_{ij}^3 + \sum_{ijk}^{N}{}' (3 J_{ij}^2 J_{jk} + J_{ij} J_{jk} J_{ki}) + \tfrac{3}{4} \sum_{ijkl}^{N}{}' J_{ij}^2 J_{kl} \right]$$

$$+ \; X_{[41^2]}^{[xy]} \sum_{ijkl}^{N}{}' (J_{ij} J_{ik} J_{il} + 3 J_{ij} J_{jk} J_{kl}),$$

where primes indicate that all the summation indices are different and classes $[C]$ of $\mathcal{S}_N$ are defined by the corresponding partitions in $\mathcal{S}_{2n}$. In the simplest case $\chi_{[1^q]}^{[xy]} = f(S, N)$. In a general case, the characters $\chi_{[C]}^{[xy]}$ may be expressed in terms of binomial coefficients involving N, S and the partition numbers defining $[C]$ using a recently developed method [67].

If all nearest-neighbor exchange parameters are equal to J and all the others vanish, then J_{ij}/J is the $N \times N$ topological matrix of the molecule (its elements are 1 for neighboring atoms and 0 otherwise). In this case the summation over all exchange parameter combinations in Eq.(69) can be explicitly performed leading to

$$M_n = J^n \sum_C X_{[C]}^{[xy]} W_{[C]}. \tag{71}$$

where the coefficients $W_{[C]}$ carry the information about the topology of the molecule. They may be determined from a knowledge of the topological matrix and are referred to as the topological invariants of the molecule. In particular, if a denotes the number of bonds in the molecule, b_i the number of bonds connected to the i-th atom,

$$\beta_p = \sum_{i=1}^{N} b_i^p, \quad \alpha = \frac{1}{J} \sum_{i,j}^{N} b_i b_j J_{ij}$$

and $n(\triangle)$ is the number of three-member cycles formed by the bonds, then [66]

$$
\begin{aligned}
W_{[2]} &= 2a, \\
W_{[2^2]} &= a(a+1) - \beta_2, \\
W_{[31]} &= -2a + \beta_2, \\
W_{[1^4]} &= a, \\
W_{[2^3]} &= a(a^2 + 3a + 4) - 3(a+2)\beta_2 + 3\alpha + 2\beta_3 - n(\triangle), \\
W_{[321]} &= -6a(a+2) + 3(a+5)\beta_2 - 6\alpha - 3\beta_3 + 3n(\triangle), \\
W_{[41^2]} &= 10a - 9\beta_2 + 3\alpha + \beta_3 - 3n(\triangle), \\
W_{[21^4]} &= a(3a-2) + n(\triangle).
\end{aligned}
$$

The normalized irreducible characters $X_{[C]}^{[xy]}$ express the way in which these specific features propagate when N and S change. Therefore they are called propagation coefficients [65].

In principle, having the complete set of spectral density distribution moments one has complete information about the Hamiltonian spectrum. The moments are not affected by the combinatorial explosion: they may be expressed in a closed form with the dimension of the model space, quantum numbers and topological characteristics of the system appearing as parameters. The theory in which information about spectra is derived from the knowledge of spectral density distribution moments is known as the statistical theory of spectra. In statistical spectroscopy densities of spectral distribution rather than locations of individual energy levels are studied. However, also individual eigenvalues may be approximated using several lowest moments [66]. A comparison of the real energy levels with those derived from the spectral density distribution moments leads to notions of the secular eigenvalue density and of fluctuations [65]. The secular density is defined by a small number of moments. Usually three or four moments are sufficient to obtain a correct secular density. If the secular density is accurate enough, then the fluctuations are small, energy-independent and insensitive to an increase in the number of moments used to describe the spectrum. Therefore only several (usually not more than four) moments are of some practical importance.

6. FINAL REMARKS

In this chapter we gave a brief review of several applications of SGA to a desription of spectra of the Heisenberg Hamiltonian. There are three topics in which using SGA is particularly useful: (1) establishing relations

between the Heisenberg model and other semiempirical methods, particularly the Hubbard and the Pariser-Parr-Pople ones; (2) designing efficient algorithms for the exact solving of the Heisenberg Hamiltonian eigenvalue problem; (3) construction of the statistical theory of the Heisenberg Hamiltonian spectra. Several aspects of this formulation, in particular developing an approach which combines the most attractive features of the RVB method and the SGA-based theory, or including the point-group symmetry adaptation of the wavefunction to the SGA formalism, remain to be interesting challenges for further developments of the theory.

REFERENCES

[1] J. Karwowski, Intern. J. Quantum Chem. 51 (1994) 425.
[2] P. W. Anderson, Mat. Res. Bull. 8 (1973) 153.
[3] P. W. Anderson, Science 235 (1987) 1196.
[4] T. Oguchi, H. Kitatani and H. Nishimori, J. Phys. Soc. Japan 56 (1987) 3858.
[5] R. F. Bishop, R. G. Hale and Y. Xian, Intern. J. Quantum Chem. 57 (1996) 919.
[6] S. R. White, Phys. Rev. B 48 (1993) 10345.
[7] J. Karwowski, Theoret. Chim. Acta (Berlin) 29 (1973) 151.
[8] W. Duch and J. Karwowski, Comp. Phys. Reports 2 (1985) 93.
[9] N. Flocke, M. Barysz, J. Karwowski and G. H. F. Diercksen, Intern. J. Quantum Chem. 61 (1997) 1, 11, 21.
[10] N. Flocke, Intern. J. Quantum Chem. 61 (1997) 747.
[11] W. A. Seitz and D.J. Klein, Intern. J. Quantum Chem. 7 (1973) 647.
[12] P. Tavan, Z. Phys. B: Condensed Matter, 72 (1988) 277.
[13] N. Flocke and J. Karwowski, Phys. Rev. B 55 (1997) 8287.
[14] N. Flocke, Comp. Phys. Commun. 106 (1997) 114.
[15] J. Paldus, Many-Electron Correlation Problem. A Group Theoretical Approach, in Theoretical Chemistry: Advances and Perspectives, H. Eyring and D. J. Henderson (eds.) Academic, New York 1976, pp 131-297.
[16] M. A. Robb and U. Niazi, Comp. Phys. Reports 1 (1984) 127.
[17] W. Heisenberg, Z. Phys. 49 (1928) 619.
[18] R. Pauncz, Spin Eigenfunctions, Plenum, New York 1979.
[19] F. A. Matsen, Adv. Quantum Chem. 11 (1978) 223.
[20] H. Weyl, The Theory of Groups and Quantum Mechanics, Dover, New York 1950.
[21] J. Paldus, J. Chem. Phys. 61 (1974) 5321.
[22] J. Olsen, P. Jørgensen and J. Simons, Chem. Phys. Lett. 169 (1990) 463.
[23] R. G. Parr, The Quantum Theory of Molecular Electronic Structure, Benjamin, New York 1963.
[24] P. O. Löwdin, J. Chem. Phys. 18 (1950) 365.
[25] D. J. Klein, W. A. Seitz, M. A. Garcia-Bach J. M. Picone and D. C. Foyt, Intern. J. Quantum Chem. S 17 (1983) 555.
[26] S. Ramasesha and Z. G. Soos, Intern. J. Quantum Chem. 25 (1984) 1003.
[27] N. Mataga and K. Nishimoto, Z. Physik. Chem. (Frankfurt) 13 (1957) 140.
[28] K. Ohno, Theoret. Chim. Acta 2 (1964) 219.
[29] R. Pariser and R. G. Parr, J. Chem. Phys. 21 (1953) 466.
[30] J. A. Pople, Trans. Faraday Soc. 49 (1953) 1375.
[31] J. Hubbard, Proc. Roy. Soc. London A 276 (1963) 238.

634

[32] P. Fulde, Electron Correlations in Molecules and Solids, Springer Series in Solid-State Sciences 100, Springer, Berlin 1993.

[33] J. H. Van Vleck, in Quantum Theory of Atoms, Molecules and the Solid State, P. O. Löwdin (ed.), Academic Press, New York 1966.

[34] L. N. Buleavski, J. Exptl. Theor. Phys. (USSR) 51 (1966) 230.

[35] J. Karwowski, J. Mol. Structure 19 (1973) 143.

[36] G. Rumer, Göttinger Nachr. (1932) 337.

[37] L. Pauling, J. Chem. Phys. 1 (1933) 280.

[38] M. Simonetta, E. Gianinetti and I. Vandoni, J. Chem. Phys. 48 (1978) 1579.

[39] R. Serber, Phys. Rev. 45 (1934) 461; J. Chem. Phys. 2 (1934) 697.

[40] T. Yamanouchi, Proc. Phys. Math. Soc. Japan 19 (1937) 436.

[41] M. Kotani, A. Amemiya, E. Ishiguro and T. Kimura, Table of Molecular Integrals, Maruzen, Tokyo 1955.

[42] J. H. Van Vleck and A. Sherman, Rev. Mod. Phys. 7 (1935) 167.

[43] R. Pauncz, The Symmetric Group in Quantum Chemistry, CRC Press, Boca Raton 1995.

[44] N. Flocke, Phys. Rev. B 56 (1997) 13673.

[45] P. A. M. Dirac, Proc. Roy. Soc. (London) A123 (1929) 714.

[46] J. H. Van Vleck, Phys. Rev. 45 (1934) 405.

[47] W. Duch, GRMS or Graphical Representation of Model Spaces, Lecture Notes in Chemistry 42, Springer, Berlin 1986.

[48] W. Duch, Intern. J. Quantum Chem. 27 (1985) 59.

[49] W. Duch, Chem. Phys. Letters 124 (1986) 442.

[50] B. E. Sagan, The Symmetric Group, Wadsworth & Brooks/Cole, Pacific Grove, California 1991.

[51] L. Pauling and G. W. Wheland, J. Chem. Phys. 1 (1933) 362.

[52] E. Clar, The Aromatic Sextet, Wiley-Interscience, London, New York, Sydney, Toronto 1972.

[53] W. C. Herndon, J. Am. Chem. Soc. 95 (1973) 204.

[54] N. Flocke, T.G. Schmalz and D.J. Klein, J. Chem. Phys. 109 (1998) 873.

[55] N. Flocke and T.G. Schmalz, Chem. Phys. Lett. 298 (1998) 71.

[56] N. Flocke, J. Phys.: Condensed Matter 11 (1999) 6945.

[57] Z. G. Soos and S. Ramasesha, in Valence Bond Theory and Chemical Structure, D. J. Klein and N. Trinajstić (eds.), Elsevier, New York 1990.

[58] Z. G. Soos, S. Kuwajima and J. E. Mihalick, Phys. Rev. B 32 (1985) 3124.

[59] J. H. Wilkinson, The Algebraic Eigenvalue Problem, Clarendon Press, Oxford 1965.

[60] C. Lanczos, J. Res. Nat. Bureau Standards B 45 (1950) 225.

[61] E. R. Davidson, J. Comput. Phys. 17 (1975) 87.

[62] N. Kosugi, J. Comput. Phys. 55 (1984) 426.

[63] I. L. Cooper and R. McWeeny, J. Chem. Phys. 45 (1966) 226.

[64] B. T. Sutcliffe, J. Chem. Phys. 45 (1966) 235.

[65] T. A. Brody, J. Flores, J. B. French, P. A. Mello, A. Pandey and S. S. M. Wong, Rev. Mod. Phys. 53 (1981) 385.

[66] J. Karwowski, D. Bielińska-Wąż and J. Jurkowski, Intern. J. Quantum Chem. 60 (1996) 185.

[67] B. G. Wybourne, N. Flocke and J. Karwowski, Intern. J. Quantum Chem. 62 (1997) 261.

Chapter 20

Valence Bond Theory of Quantum Cell Models

S. Ramasesha[1] and Z.G. Soos[2]
[1]Solid State and Structural Chemistry Unit,
Indian Institute of Science, Bangalore 560 012, India
[2]Department of Chemistry,
Princeton University, Princeton, NJ 08544, USA

Contents:

1 Introduction

The Hückel Hamiltonian introduced in 1931 was probably the first quantum cell model in chemistry. Hückel models approximate the electronic structure of conjugated molecules with one $2p_z$ orbital per carbon and take the Hamiltonian matrix elements from experiment. The same procedure is called tight-binding in the theory of metals, now with an ns orbital per alkali atom. Cell models based on a frontier orbital per molecule are in the same spirit and confer great generality to such models. The $4n+2$ rule and countless Hückel computations are classic examples of important results arrived at from a simple model. Tight-binding theory for simple metals provides similar triumphs that are sometimes close to quantitative. The approximate nature of models is emphasized in theoretical chemistry, where a major goal has been the development of quantitative electronic-structure methods for molecules. The inherent complexity of extended systems, on the other hand, provides challenges for correlated models of magnetic or optical properties, phase transitions and other collective phenomena. The wide scope and mathematical complexity of quantum cell models belies their humble origins as the simplest approximation to the problem at hand.

Hückel's familiar ansatz for π-electrons illustrates the phenomenological nature of models in general. The number of p_z orbitals fixes the order of the Hamiltonian matrix, $\mathbf{H}$. Diagonal elements α correspond to orbital energies that can be estimated from ionization data. Off-diagonal elements β are restricted to π-bonded atoms, without distinguishing between partial single and double bonds. The remaining elements are presumed to vanish. The eigenvalues and eigenfunctions of $\mathbf{H}$ are obtained and compared to experiment. The β integrals describe π electron transfer between bonded atoms and become $t(R)$ in solid-state models. The dependence on bond-length is crucial in polymers such as polyacetylene and generates electron-vibrational coupling[1, 2]. The magnitude of β obtained from thermochemistry or spectroscopy is so useful that different values are used in the two fields[3]. This underscores the limitations of non-interacting π electrons, as indeed has been

recognized all along. A larger basis is an obvious improvement and much work has been devoted to practical, accurate and flexible bases. Another improvement concerns electron- electron interactions, or correlations, that are particularly important for excited states. Correlations can be added directly to quantum cell models and quickly raise the stakes for accurate solutions.

Coulomb interactions dominate the electronic structure of molecules. The total spin S^2 and S_z are nearly conserved for light atoms. We will consider spin-independent interactions in models with one orbital per site. In the context of π electrons, the operators $\hat{a}_{p\sigma}^+$ and $\hat{a}_{p\sigma}$ create and annihilate, respectively, an electron with spin σ in orbital p. The Hückel Hamiltonian is

$$\hat{H}_{\text{Hückel}} = \sum_{p\sigma} \epsilon_p \hat{a}_{p\sigma}^\dagger \hat{a}_{p\sigma} + \sum_{<pq>\sigma} t_{pq}(\hat{a}_{p\sigma}^\dagger \hat{a}_{q\sigma} + \hat{a}_{q\sigma}^\dagger \hat{a}_{p\sigma}) \tag{1}$$

The sum is over all sites p and bonded sites $< pq >$; the orbital energy ϵ_p and transfer integrals t_{pq} are used instead of α and β. The Hückel problem is to solve (1) for a given number of electrons, often one per orbital. Coulomb interactions between electrons are

$$\hat{H}_{\text{Coul.}} = \frac{1}{2} \sum_{pqkl\sigma\sigma'} [pq|kl](\hat{a}_{p\sigma}^\dagger \hat{a}_{q\sigma} \hat{a}_{k\sigma'}^\dagger \hat{a}_{l\sigma'} - \delta_{qk} \hat{a}_{p\sigma}^\dagger \hat{a}_{l\sigma}) \tag{2}$$

The two-electron integrals $[pq|kl]$ are $< \phi_p(1)\phi_k(2)|e^2/r_{12}|\phi_q(1)\phi_l(2) >$ and may involve as many as four orbitals. The models of interest are restricted to one and two-center terms. Two electrons in the same orbital, $[pp|pp]$, is γ in Pariser-Parr-Pople (PPP) theory[4] or U in Hubbard models[5], while $[pp|qq]$ are the two-center integrals kept in PPP. The zero-differential-overlap (ZDO) approximation[3] can be invoked to rationalize such simplification. In modern applications, however, and especially in the solid state, models are introduced phenomenologically. Particularly successful models are apt to be derived subsequently and their parameters computed separately.

We have interacting π-electrons in the PPP model and on-site repulsion in Hub-

bard models. Their relation to Hückel models is[6]

$$\hat{H}_{Hub.} = \hat{H}_{\text{Hückel}} + \frac{U}{2} \sum_p \hat{n}_p (\hat{n}_p - 1) \tag{3}$$

$$\hat{H}_{PPP} = \hat{H}_{Hub.} + \sum_{p>q} V_{pq} (\hat{n}_p - z_p)(\hat{n}_q - z_q) \tag{4}$$

The number operators $\hat{n}_p = \sum_\sigma \hat{a}_{p\sigma}^+ \hat{a}_{p\sigma}$ indicate that the interactions do not depend on spin. The constant V_{pq} depends on the distance R_{pq} between the orbitals and is U at $R_{pq} = 0$; different interpolations have been proposed by Ohno[7] and by Mataga-Nishimoto[8]. The local chemical potential z_p specifies the occupancy for a neutral site and is unity in hydrocarbons. Hubbard invoked strong shielding in d-electron metals for on-site only Coulomb interactions. Hubbard models are applied instead to high-T_c superconductors and generic systems[9] with interesting correlations of variable magnitude. The PPP model for hydrocarbons has no adjustable parameters, and hence has predictive capabilities[10]. Both models conserve spin. Their solutions require comparable effort and, with the notable exception of the one-dimensional Hubbard chain, are restricted to finite systems. The special case of one electron per orbital, or a half-filled band, is closely related to Heisenberg spin systems. Other modifications lead to the $U - V$ models, Kondo lattices, donor-acceptor crystals with valence instabilities, and ion-radical salts with diverse magnetic properties.

The shared features of quantum cell models are specified orbitals, matrix elements and spin conservation. As emphasized by Hubbard[5] for d-electron metals and by Soos and Klein[11] for organic crystals of π-donors or π-acceptors, the operators $\hat{a}_{p\sigma}^+$ and $\hat{a}_{p\sigma}$ in (1), (3) and (4) can rigorously be identified with exact many-electron states of atoms or molecules. The provisos are to restrict the solid-state basis to four states per site (empty, doubly occupied, spin α and spin β) and to stop associating the matrix elements with specific integrals. The relaxation of core electrons is formally taken into account. Such generalizations increase the plausibility of the models and account for their successes, without affecting their solution or interpretation.

Correlated states are not easily visualized even when, for example, the appropriate linear combination of Slater determinants is known. Here again, conjugated molecules and their ubiquitous representation as valence bond (VB) diagrams prove to be instructive. VB diagrams specify at a glance the location and pairing of all π-electrons and fully describe a particular many-electron state. Quite generally, VB diagrams with N sites (orbitals) and N_e π-electrons with total spin S form a complete basis for quantum cell models[12, 13]. The proof is based on writing diagrams as N_e-fold products over $\hat{a}_{p\sigma}^+$. The intuitive reasoning is illustrated in Fig. 1 for benzene. The Kekulé diagrams $|1>$ and $|2>$ are two possible singlets with paired
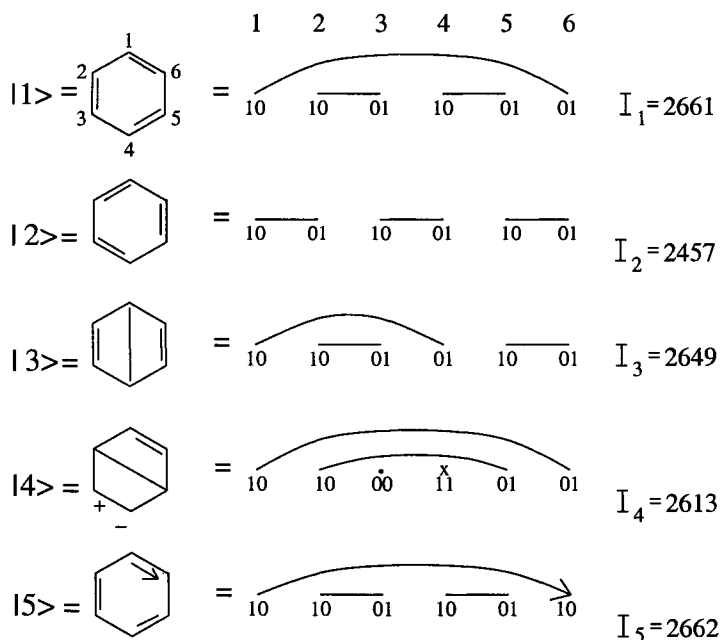
Figure 1: Representative valence bond diagrams for benzene, their bit representation using two bits per site, and the integer I_k that encodes these correlated states with six π-electrons. The Kekulé diagrams $|1>$ and $|2>$ are covalent singlets, as is the Dewar diagram $|3>$, with one electron at each site. Diagram $|4>$ is an ionic singlet, while $|5>$ is a covalent triplet.

spins at adjacent sites. They have $n_p = 1$ at all sites in molecules with $N = N_e$. Such diagrams are called covalent and occur only in half-filled systems. The Dewar diagram $|3>$ is one of three singlets with spin-pairing between nonbonded carbons. Rumer and Pauling found the number of covalent singlets for even $N = N_e$ and covalent doublets for odd $N = N_e$. Diagrams such as $|4>$ with one or more empty (C^+) or doubly-occupied (C^-) sites are called ionic and are singlets by inspection when the $n_p = 1$ sites are spin-paired. The covalent triplet $|5>$ has parallel spins indicated by an arrow and has $n_p = 1$ for all n. Larger S can be represented by an arrow connecting $2S$ sites, and any number of $n_p = 0$ or 2 sites can be inserted[13]. The generalization of Rumer-Pauling rules for covalent singlets to arbitrary S and $N \neq N_e$ is straightforward.

These introductory remarks establish the connection between VB diagrams and quantum cell models. In principle, any eigenstate of (3) or (4) is a linear combination of spin-adapted diagrams. The order of the PPP, Hubbard and Hückel Hamiltonian matrices are the same and they differ only in the diagonal matrix elements since the VB basis is diagonal both in the site energy terms and in the interaction terms. The many-electron basis increases a bit more slowly than 4^N for N orbitals, with significant but modest symmetry reductions. The large size of $\mathbf{H}$ is offset to some extent by the sparseness due to one-electron off-diagonal terms. The implementation of the VB basis for quantum cell models is summarized in the following sections, along with applications. The underlying idea of representing molecular states as linear combinations of VB diagrams dates back to Pauling and Eyring. So we are combining ideas from the dawn of quantum chemistry to discuss correlated states of molecular, polymeric and solid-state systems. Recent studies[14, 9] go beyond excitation energies to include nonlinear optical susceptibilities, magnetic susceptibilities, structural instabilities, charge and spin densities, and vibronic contributions. The necessary matrix elements over correlated states of quantum cell models can also be evaluated using VB methods.

The Hückel Hamiltonian matrix from (1) is of order N and its solution yield

N molecular orbitals that are linear combinations of the p_z functions. The ground state is a Slater determinant obtained by assigning the N_e electrons in pairs to the lowest-energy MOs. Slater determinants are overwhelmingly used for molecular computations. They describe independent electrons that, nowadays, move in self-consistent potentials. Slater determinants conserve S_z, but not S^2, and SCF potentials have well known limitations. The MO ground state of H_2 yields H^+, H^- ions as well as neutral H atoms with increasing bond length or decreasing $t(R)$. The Heitler-London function for H_2 is surely the original covalent singlet, with paired electrons on two protons, and is a linear combination of two determinants. VB diagrams with p spin-paired electrons at p pairs of different sites (each pair represented as a line), are linear combinations of 2^p Slater determinants with fixed phases. Such phase relations and the nonorthogonality of VB diagrams hindered early attempts in which diagrams were expanded as Slater determinants. We work instead directly in the Hilbert space of VB diagrams to obtain correlated states and only resort to determinants for computing matrix elements. As emphasized in textbooks for H_2, the MO theory plus full configuration interaction (CI) is equivalent to VB theory with all covalent and all ionic diagrams. Quantum cell models with a large but finite basis can be solved exactly either way.

The review is organized as follows. Given the scarcity of VB treatments, we start with their general applicability to quantum cell models such as (4). The VB basis in Section 2 is introduced for covalent diagrams that are appropriate for Heisenberg spin exchange in insulators and then generalized to ionic and covalent diagrams that apply to many-fermion problems. We comment on the dimensions of the basis and on symmetry adaptation. The eigenvalue problem is presented in Section 3 for sparse unsymmetric matrices and solved iteratively. Matrix elements over correlated states are found separately for observables that contain number and spin operators. The dynamical properties in Section 4 are based on correction vectors that are illustrated by linear and nonlinear responses to applied electric and magnetic fields. Section 5 summarizes VB results for $\pi - \pi^\star$ excitations of conjugated hydrocarbons using PPP theory, including such familiar examples as naphthalene,

anthracene, polyenes, stilbene, and pyrene. Recent modeling of ring currents in annulenes illustrates the contrasting goal of molecular and extended systems. The electronic structure of conjugated polymers has been intensively studied over the past two decades. We comment in Section 6 of correlation effects such as spin-charge separation, fluorescence and vibronic coupling. In Section 7 we discuss VB applications to organic donors and acceptors whose lowest electronic excitation is a charge-transfer (CT) state. Neutral-ionic or valence transitions in CT salts are typically described by a modified Hubbard model with three state per site. Related models for chains of S = 1 spins or Kondo chains in Section 8 with localized spins and delocalized electrons are other examples of specialized VB bases. We comment in Section 9 on VB applications to organic ferromagnetism. Quantum cell models provide a flexible approach to correlated electronic states and extended systems, while VB diagrams provide for easy visualization.

2   The VB basis

The dimension of the Fock space grows as 4^N for a system with N orbitals, since each orbital can be empty, doubly occupied or singly occupied with spin α or β. The Hilbert space of quantum cell models with N_e electrons, total spin S and z-component M_S is a projection of the Fock space. Slater determinants with a spin-orbital basis automatically conserve N_e and M_S. The construction of spin adapted functions (SAFs) with fixed S is a longstanding problem in theoretical chemistry[15, 16, 17]. Working with SAFs has the advantages of reducing the size of the basis and of knowing the spin multiplicity for comparisons with experiment. Several methods for constructing SAFs have been proposed. Löwdin's approach[15] is based on projection operators to eliminate undesired spin states. Either the symmetric[16] or the unitary[17] group can be used to obtain SAFs. These techniques are equivalent and yield an orthonormal basis of SAFs. They share the drawback of functions whose chemical meaning is not transparent for nonspecialists.

The VB technique[18] of constructing SAFs is simple in comparison and directly

based on familiar chemical structures. The main limitation is that VB diagrams are not orthogonal even for an orthonormal orbital basis. This technical problem turns out not to be serious, while the chemical transparency of VB diagrams and the sparseness of matrices in the nonorthogonal basis actually proves to be advantageous.

We discuss first the VB basis of covalent diagrams for systems with $N = N_e$. The physical situation is large $U/|t| > 0$ in (3), which gives a large energy cost for two electrons on any site. Low-energy states with $n_p = 1$ for all p retain a spin degree of freedom. There are 2^N spin or covalent states with S ranging from 0 to $N/2$ for even N. Antiferromagnetic (AF) Heisenberg exchange, $J = 2t^2/U$, stabilizes singlets through admixture with virtual states with an empty and doubly-occupied site that are not accessible to parallel spins. There are many realizations of $s = 1/2$ systems[11]: clusters, chains, ladders, or lattices in two or three dimensions with interactions $J\hat{s}_p \cdot \hat{s}_q$ between neighbors p and q. All spin states can rigorously be represented by covalent diagrams with fixed S. For $N = 2n$, we clearly have $(2n)!/(n!\, n!)$ state with $M_S = 0$ and n spins α, n spins β. The number of $S = 0$ diagrams is $(n + 1)$ times smaller according to Rumer's formula[19],

$$P_S(N) = (2S + 1)\frac{N!}{(\frac{N}{2} - S)!(\frac{N}{2} + S + 1)!} \tag{5}$$

which gives the number of states with a given S from N spins. This formula is easily derived as the difference in number of states with $M_S = S$ and $M_S = (S + 1)$. The two Kekulé and three Dewar diagrams in Fig. 1 are the covalent singlets for $N = 6$, and the other 15 covalent states with $M_S = 0$ have $S > 0$.

To construct covalent singlets for $N = 2n$, we take a regular polygon with $2n$ vertices and draw n lines connecting any two vertices. Each diagram corresponds to spin-pairing the connected vertices. The Rumer-Pauling rules show that the number of diagrams without any intersecting lines (legal diagrams) gives the number of singlets and that diagrams with intersecting lines (illegal diagrams) can be expanded in terms of legal diagrams. These and related rules can readily be derived by using second quantization. Covalent diagrams contain N-fold products of $\hat{a}_{p\sigma}^+$ in which p is never repeated.

In practice, a computer generates, manipulates and stores VB diagrams[13]. The scheme for covalent singlets is very simple, thanks to the non-crossing rule. We associate a bit with each of $N = 2n$ vertices of the polygon, which are numbered consecutively. The n lines of a legal diagram are encoded by setting the state of the bits as "1" and "0" for the lower and higher-numbered vertex, respectively. Each covalent singlet becomes a $2n$-digit binary integer with n bits "0" and n bits "1". The association is in fact unique if we decipher the bit pattern of the integer from the inside out, much like expanding an algebraic expression with multiple parentheses. Covalent diagrams are generated on a computer by checking whether $2n$-bit patterns satisfy the criteria for the desired S. Diagrams with $S \geq 1$ contain an arrow connecting $2S$ sites with parallel spins and $(n - S)$ lines for paired spins. We take $2S$ more bits "1" than "0", draw lines as before for paired spins, and associate the arrow with the remaining vertices "1", which are not adjacent in general. The special case $S = 1/2$ is handled with a phantom site and $(n + 1)$ lines. The non-crossing rule for legal diagrams thus yields the complete, linearly independent basis of covalent VB diagrams with any S. The phase information for 2^n Slater determinants for singlets is preserved by the $2n$ bits. Moreover, the association of diagrams with integers yields ordered sequences that greatly facilitate searching operation involved in setting up the Hamiltonian matrix as well as in manipulations of the eigenstates of the Hamiltonian.

Covalent diagrams illustrate the salient features of the VB basis. The generalization to fermionic systems with $n_p = 0$ or 2 sites is straightforward. When ionic diagrams are included, we first consider how many ways N_e electrons can be distributed in N orbitals and then pair up $n_p = 1$ sites as before. Legal diagrams have no crossing lines. A bit representation is again possible, now with two bits for each of the N sites. We use "00" and "11" for empty and doubly-occupied sites, respectively, and "10" and "01" for the lower and higher-numbered vertex of lines that represent spin-paired sites. The bit representation of VB diagrams is illustrated in Fig. 1. The correspondence between VB diagrams with fixed S and $2N$-bit binary integers is again unique. The integers I_k fully encode these six-electron functions.

With increasing basis size, VB diagrams are efficiently generated by manipulating the bits directly to generate only legal diagrams. Rapid generation of 10^8 diagrams is now routine with a workstation.

The Weyl formula gives the dimensions $P_S(N, N_e)$ of the basis for N orbitals with N_e electrons and total spin S,

$$P_S(N, N_e) = \frac{2S+1}{N+1} \binom{N+1}{\frac{1}{2}N_e - S} \binom{N+1}{N - \frac{1}{2}N_e - S} \tag{6}$$

in terms of binomial coefficients. This formula is also obtained in a manner similar to the Rumer's formula[19], as a difference in the number of Slater determinants with $M_S = S$ and those with $M_S = S + 1$. This can be easily calculated since N spin-orbitals are made up of N α-spin orbitals and N β-spin orbitals. The number of Slater determinants with M_S is then given by

$$P_{M_S}(N, N_e) = \frac{N!}{(N - N_\alpha)! N_\alpha!} \cdot \frac{N!}{(N - N_\beta)! N_\beta!}. \tag{7}$$

N_α (N_β) are the number of α (β) spin electrons that make up $N_e = N_\alpha + N_\beta$ and $M_S = N_\alpha - N_\beta$.

The general result provides a check on diagram generation. $P_S(N, N_e)$ is the order of $\mathbf{H}$, the Hamiltonian matrix in the many - electron basis, for any model that conserves S and has no additional symmetry. The eigenstates of $\mathbf{H}$ are consequently model exact and correspond formally to CI to all orders. We clearly require finite N and hence a large but finite active space. On the other hand, choices in (3) or (4) about transfer between bonded sites or two-center interactions are incidental. The order of $\mathbf{H}$ remains $P_S(N, N_e)$ in general, but approximations yield sparser matrices that are easier to generate. The Hückel limit, for example, has the same order and constant diagonal elements for alternant hydrocarbons. The VB solution is enormously more complicated than the conventional MO treatment and the latter serves as a check on the VB method. But the VB solution does not become more difficult for interacting models (with diagonal interactions in real space as in the PPP model), where it is far more convenient than CI to all orders in a conventional Slater-determinantal basis with MOs as one-electron functions. The VB treatment that

will be discussed here is equally applicable to configuration interaction calculations that can be carried out in the MO basis with spin symmetry adaptation. In this case, however, we would lose the advantage of the interaction part of the models being diagonal in the basis[20].

We exploit the real space representation of VB diagrams to construct spatial symmetry adapted linear combination of VB diagrams. Linear combinations of two Kekulé or three Dewar structures of benzene in Fig. 1 are readily found for D_{6h} symmetry. The restriction to finite N implies that the system belongs to a point group. Spatial symmetry adaptation further reduce the dimensions $P_S(N, N_e)$ of the full basis. Although there is no general result, a group G of order g yields irreducible representations Γ whose dimensions satisfy

$$P_S(N, N_e) = \sum_{\Gamma=1}^{g} D_\Gamma(S, N, N_e) \sum_m \sum_{\Gamma=1}^{g} D_m(\Gamma). \tag{8}$$

The estimate $D_\Gamma(S, N, N_e) \approx P_S(N, N_e)/g$ can be confirmed directly by generating the symmetry-adapted VB basis. The general problem of constructing symmetry adapted VB functions is that a group operation $\hat{R}_i$ often transforms a legal diagram into an illegal diagram. While the expansion of any illegal diagram in terms of legal diagrams is easy, visual symmetry relations are no longer self-evident.

The first step in the general problem[18] of constructing spatial - symmetry adapted linear combinations of VB diagrams is to break up the total spin space for a given S, N, N_e into disjoint invariant subspaces $D_m(S, N, N_e)$. The subspace $D_m(S, N, N_e)$ contains $|k >$ and all diagrams $|k' >$ generated by repeated applications of all symmetry operations R_j of the group on these diagrams. The symmetry operations of the group can now be expressed as matrices in the legal VB basis of the disjoint invariant subspace $D_m(S, N, N_e)$. The subspaces $D_m(S, N, N_e)$ in (8) are far smaller in general than $D_\Gamma(S, N, N_e)$. The order of $D_m(S, N, N_e)$ is not fixed by G, however, but depends on which sites are interchanged by $\hat{R}_i$. Hence systems with identical G, N and N_e may have different invariant subspaces[21]. Systems with the largest number of subspaces have the smallest matrices $D_m(S, N, N_e)$ and are the easiest to symmetry adapt. The projection operator for a given irreducible

representation is

$$\hat{P}_\Gamma = \sum_{i=1}^{g} \chi(\Gamma, R_i)\hat{R}_i \tag{9}$$

where $\chi(\Gamma, R_i)$ is the character under the group operation $\hat{R}_i$ in the irreducible representation Γ. The linearly independent set of symmetry adapted VB functions can be obtained from the projected states in the invariant space either by *brute force* using Gram-Schmidt orthonormalization or by devising rules[18, 21] for recognizing linear independence among a group of linear combinations of VB functions, which allow weeding out dependent states just by inspection. This procedure when applied to all disjoint invariant subspaces yields the symmetry adapted VB functions for the full space $P_S(N, N_e)$.

Linear systems such as trans-polyenes in Fig. 2 are particularly simple, since inversion amounts to reading a legal diagram backwards and thus relates pairs of diagrams $|k>$ and $\hat{\sigma}|k> = |k'>$.

The inversion operation does not produce illegal VB diagrams. The electron-hole (e-h) symmetry[22] operator $\hat{J}$ of half-filled models of alternant π-conjugated hydrocarbons also relates pairs $|k>$ and $\hat{J}|k> = e^{i\eta\pi}|k'>$, with $n_p = 0$ and 2 sites in $|k>$ interchanged to obtain $|k'>$. In the phase factor $e^{i\eta\pi}$, η is the sum of the number of doubly occupied sites and the number of singly occupied sites on one of the two sublattices (starred or unstarred) of the bipartite system. Again, the operator $\hat{J}$ also does not produce illegal VB diagrams.

The conjugated systems in Fig. 2 have inversion and e-h symmetry. The acenes are the prototypical systems of molecular exciton theory[23]. The photophysics of stilbene and polyparaphenylene vinylene (PPV) have been extensively studied[14], separately at first and together since the preparation[24] of light-emitting diodes based on PPV. Pyrene and perylene appear in many contexts, while the polydiacet-

acenes (n=0,1,2,3)

polythiophenes (PT)

rylenes , polyperinapthalene (PPN)

polyparaphenylenevinylene (PPV)
stilbene

pyrene
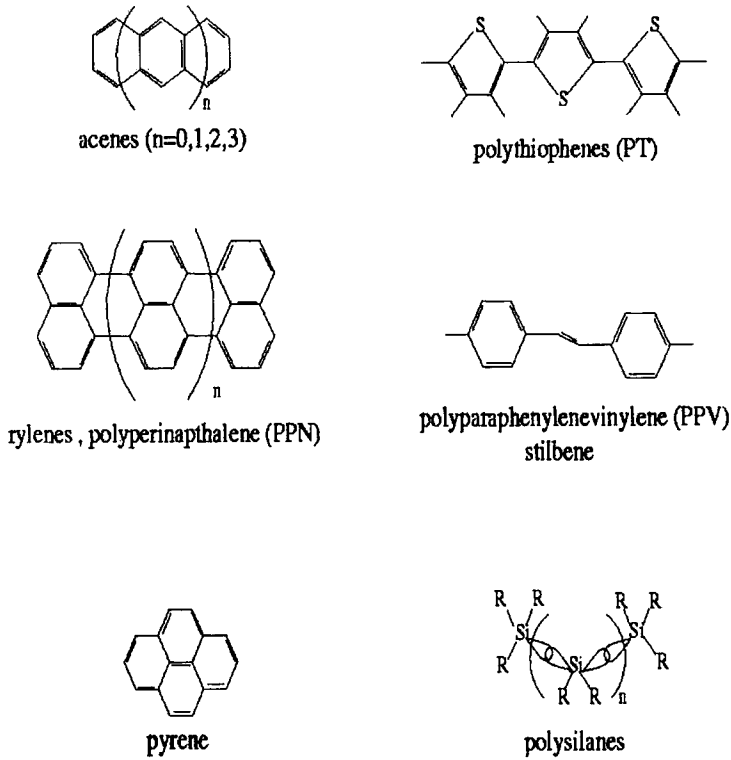
polysilanes

Figure 2: Planar π-systems of representative conjugated molecules and polymers, and σ-conjugated polysilanes. Polyenes, acenes and rylenes have variable length. Polydiacetylenes, polythiophenes, polyparaphenylenevinylenes and polysilanes give families with similar backbones and different nonconjugated side groups.

ylenes (PDAs) are the only conjugated polymers available so far as single crystals[25]. Linear combinations of VB diagrams with inversion and e-h symmetry can be done by inspection. Additional symmetry in D_{2h} requires invariant subspaces and careful analysis. VB diagrams and their bit representation provides a general approach to any quantum cell model with point-group symmetry, but symmetry adapted linear combination of VB functions have only been found for a few systems with more than inversion and e-h symmetry. The symmetry adapted many-electron basis

still increases rapidly with N and the eigenvalue problem sets the limit on what is possible.

3 The eigenvalue problem

The Hückel or one-electron Hamiltonian (1) describes electron transfers without spin flips and thus connects VB diagrams with fixed total spin, S. The remaining terms in the quantum cell models (3) or (4) are otherwise diagonal in the VB basis. More generally, two-electron operators such as exchange K_{ij} produce off-diagonal elements[26] in the VB basis that can be treated in a similar way as the transfer terms. As originally suggested by Pauling[27] for conjugated molecules, we expand the wavefunction of quantum cell models in terms of normalized VB diagrams

$$|\psi> \ = \ \sum_k C_k |k> \tag{10}$$

The sum is over the $P_S(\text{N,N}_e)$ diagrams and C_k is real. Normalization of $|\psi>$ requires care since the basis is nonorthogonal. Any two VB diagrams with *different* pairings or lines for *identical* charge distributions have nonzero overlaps that are found for any S by the island-counting method.

Since the many-electron basis of quantum cell models is finite and complete, we have

$$\hat{H}|\psi> \ = \ \sum_{kk'} C_k H_{kk'} |k'> \ = \ E_\psi \sum_k C_k |k> \tag{11}$$

The matrix elements $H_{kk'}$ follow directly from (1) and correspond to directional cosines in a vector space. Transfers between adjacent sites $<pq>$ are proportional to t_{pq}. The local structure of VB diagrams limits the outcome to possibilities for $H_{kk'}$ that can readily be enumerated[13]. Spin problems in the covalent basis have even simpler[28] $H_{kk'}$. The matrix **H** is not symmetric when the basis is not orthogonal, but it is extremely sparse. This follows because N sites yield about N bonds and each transfer integral gives at most two diagrams. There are consequently $\sim 2N$ off-diagonal $H_{kk'}$ in matrices of order $\sim P_S(N, N_e)/4$ for systems with inversion and

e-h symmetry. We exploit sparse-matrix methods to obtain the lowest eigenvalues in a given symmetry, as summarized below.

The textbook approach to eigenvalue problems is to express H_{ij} in an orthonormal basis. Linear equations such as (11) then yield secular determinants on multiplying by $|k' >$ from the left and integrating. The impulse to obtain a symmetric secular determinant must be resisted for the nonorthogonal VB basis since this leads to a generalized eigenvalue problem $\mathcal{H}\vec{X} = \lambda S\vec{X}$ with overlap matrix S. Sparseness is completely lost in the case of covalent or spin problems for an orthogonal basis and is considerably reduced in general. The keys to solving (11) are to work with nonsymmetric $H_{kk'}$ and to avoid overlap while finding a specified number of eigenvalues. Rettrup[29] extended Davidson's efficient coordinate - relaxation algorithm[30] for the eigenvalues of sparse symmetric matrices to nonsymmetric ones. We summarize below Rettrup's small-matrix algorithm that we have extensively used for VB treatments of quantum cell models.

The storage of large matrices such as H is a problem. We take advantage[31] of sparseness and of the small number of model parameters. Hubbard models usually have a single U/t. Site energies or interactions V_{nm} appear in PPP models, as indicated in (4). In practice, we have fewer than a thousand distinct elements, and this fact can be used to advantage from both accuracy and storage view points. We create a list of finite matrix elements and in the variable corresponding to the column address of the element, we reserve ten bits for storing the address of the value of the matrix element and the remaining bits for storing the column index. This way of storing both the value and the column index in a single 4-byte integer holds up to matrices of $\sim 8 \times 10^6$ columns and $\sim 10^3$ distinct elements. We avoid storing the row index of each element by grouping the nonzero elements by their row index and keeping track of the number of nonzero elements in each row. Such compact storage methods are essential for solving large systems on modern workstations.

We seldom need the full spectrum in CI calculations, since most experiments probe only a few electronic states. Rettrup's method[29] is well suited for the low-

est few ($\sim$ 5 to 10) eigenstates of nonsymmetric matrices and follows Davidson's approach to symmetric matrices[30]. They are similar in spirit to the Lanczos algorithm, which relies on a small matrix and iteration. The order of the small matrix that represents the full problem is augmented in each iteration until convergence is achieved for the desired low-lying eigenstate. Davidson augments the subspace in which the small-matrix is set up, by using the component of the coordinate relaxation vector which is orthogonal to the subspace of the small-matrix at the previous iteration. The coordinate relaxation vector is the steepest descent correction to the eigenvector at any given iteration.

Ramasesha and coworkers[32] applied the Rettrup algorithm to solve (11) for either the ground state in each symmetry subspace or several of the lowest eigenstates. One starts with a set of m orthogonal vectors $\{\vec{Q}_i : i = 1, ..., m\}$ and constructs a small matrix $\mathbf{h}$ such that, $h_{ij} = (\vec{Q}_i, \mathbf{H}\vec{Q}_j)$. This small matrix $\mathbf{h}$ is diagonalized using standard library routines for exact diagonalization (in core). The eigenvectors $\vec{c}_k^{(m)}$ of $\mathbf{h}$ are arranged in ascending order of eigenvalues $e_k^{(m)}$. The corresponding approximate eigenvectors of the large matrix are given by,

$$\vec{C}_l^{(m)} = \sum_{i=1}^m c_{i,l}^{(m)} \vec{Q}_i \tag{12}$$

where $c_{i,l}^{(m)}$ is the ith component of the lth eigenvector $\vec{c}_l^{(m)}$. If we are interested in the lth eigenvalue, we construct i^{th} component of correction vector $\vec{P}_l^{(m)}$ as,

$$P_{i,l}^{(m)} = \frac{R_{i,l}^{(m)}}{(E_l^{(m)} - H_{ii})} \tag{13}$$

Here $R_{i,l}^{(m)}$ is the ith component of the residue vector for the lth eigenvalue,

$$\vec{R}_l^{(m)} = (\mathbf{H} - \vec{e}_l^{(m)}\mathbf{I})\vec{C}_l^{(m)} \tag{14}$$

The initial space is now augmented with a normalized vector $\vec{Q}_{m+1}$ obtained from Gramm-Schmidt orthonormalization of $\vec{P}_l^{(m)}$ to the set of vectors $\{\vec{Q}_i : i = 1, ..., m\}$, i.e.,

$$\vec{Q}_{m+1} = \frac{\vec{Q}'_{m+1}}{||\vec{Q}'_{m+1}||} \quad , \quad \vec{Q}'_{m+1} = \vec{P}_l^{(m)} - \sum_{k=1}^m (\vec{P}_l^{(m)}, \vec{Q}_k)\vec{Q}_k \tag{15}$$

This procedure is iterated until no component of the residue vector is greater than a certain threshold. When the augmented matrix $\mathbf{h}$ reaches a large dimension, $M \sim 30$, the procedure can be restarted by choosing m eigenvectors $\vec{C}_1^{(M)}, \vec{C}_2^{(M)}, \ldots \vec{C}_m^{(M)}$ with lowest eigenvalues as the basis $\{\vec{Q}_i\}$. The initial choice $\{\vec{Q}_i\}$ can be made on the basis of the diagonal elements of $\mathbf{H}$. We could set the component of $\vec{Q}$ corresponding to the lowest diagonal element to unity, with other components being some small number $\sim 10^{-3}$ to obtain $\vec{Q}_1$. Choosing the second lowest diagonal element could give $\vec{Q}_2$ and so on.

The iterative solution of (11) yields eigenvalues and eigenfunctions whose normalization leads to

$$1 \; = \; <\psi|\psi> \; = \; \sum_{kk'} C_k \, C_{k'} \, S_{kk'} \tag{16}$$

The coefficients C_k are real and $S_{kk'} \; = <k|k'>$ is the overlap of normalized VB diagrams with identical electron distributions $\{n_j\}$. Normalization illustrates the general problem of finding matrix elements between correlated states. We express an operator in second-quantized notation and consider exact eigenstates $|\psi>$ and $|\chi>$ that may be in the same or different symmetry subspaces. The matrix elements $A_{kk'}$ of $\hat{A}$ are obtained as shown in (11) to give

$$<\chi|\hat{A}|\psi> = \sum_{p,k,k'} C_p \, A_{kk'} \, C_{k'} \, S_{pk'} \tag{17}$$

where C_p are the coefficient in $|\chi>$. Normalization or matrix elements require a matrix multiplication that is prohibitive for large nonorthogonal bases in the millions.

Fortunately, the VB basis is orthogonal in the charge variables for quantum cell models (3) or (4) in an orthonormal basis of Wannier functions $|\phi_p>$. The overlap matrix $\mathbf{S}$ is block diagonal, with each block containing diagrams with precisely the same electron distribution. We reorder[33] the diagrams so that the sums in (16) or (17) are confined to manageable blocks along the diagonal. The blocks are repeated many times, since each represents the covalent diagrams for $2p$ singly-occupied sites

for a distribution of $N - 2p$ empty and doubly-occupied sites. Hence the Rumer-Pauling rules for covalent singlet diagrams suffice for $S_{kk'}$,

$$S_{kk'} = (-1)^m 2^{(l-p)}. \tag{18}$$

Here p is the number of lines in $|k>$ or $|k'>$, l is the number of islands formed when the diagrams are superimposed as shown in Fig. 3, and m is the number of arrow reversals defined below. The overlap shown is between a Kekulé diagram (dashed
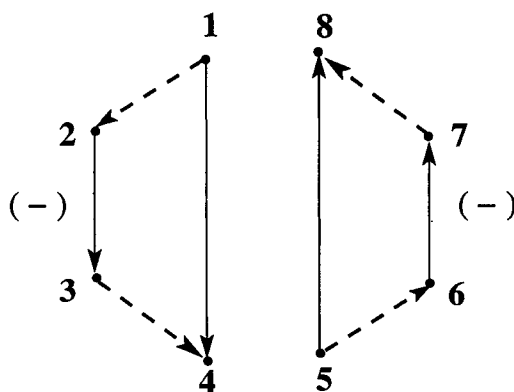
Figure 3: Island counting for overlap integral of two valence bond diagrams. The superposition of two covalent singlets for $N = N_e = 8$ yields two islands. The associated phase factor $(-1)^2$, since two arrows 2-3 and 6-7 need to be reversed.

line) for $N = N_e = 8$ and a covalent singlet (solid line) with two long bonds; there are two islands. We associate an arrow with each singlet line $[n \, n']$ for spin-paired sites and take its direction to be from n to n' if $n < n'$. When $|k>$ and $|k'>$ are superimposed, two arrows appear at each site in an island. The phase m in (18) is the number of reversals needed so that every site has either two heads or tails. Overlaps between triplet or other $S > 0$ diagrams require simple generalizations.

Island counting is well suited for normalization or for matrix elements of spin-independent properties such as dipole moments, transition dipoles or charge-charge

correlation functions. Any operator that can be expressed exclusively through the number operators $\hat{n}_p$ is diagonal in the VB basis and leads to simple overlaps. On the other hand, matrix elements for spin densities[34] or spin-spin correlation functions[35] are quite involved because the spin operators of sites connect VB diagrams with different total S. New rules must consequently be developed[35] for determining the resultant when a combination of site-spin operators acts on VB diagrams. For example, when site j in a singlet $|k>$ has a line, the operation $\hat{s}_j^z|k>$ yields a triplet $|k'>$ with parallel spins at j and the site to which it is connected. Matrix elements of $\hat{s}_j^z\hat{s}_i^z$ are frequently encountered and can be reduced to overlaps of two triplets[36], one resulting from the operation of $\hat{s}_j^z$ on the *bra* state and the other from the operation of $\hat{s}_i^z$ in the *ket* state. Nevertheless, the direct VB computation of spin dependent matrix elements is rather cumbersome.

To circumvent this problem, we expand the eigenstate $|\psi>$ in terms of Slater determinants. As already noted, each spin-paired line in VB diagrams corresponds to two Slater determinants that, in turn, can be represented uniquely by binary integers and generated as an ordered sequence. A diagram with p lines yields 2^p determinants and, once converted to Slater determinants, matrix elements are simple because the basis is orthonormal. The procedure is general[37] and obviates the need for direct VB computation of matrix elements. It illustrates nicely the different priorities of the eigenvalue problem. VB diagrams $|k>$ represented as an ordered sequence of binary integers allow one to set up, symmetry adapt and solve for the eigenstates of the sparse matrix $\mathbf{H}$. A different ordering of diagrams yields matrix elements of spin-independent operators. Individual eigenstates in the VB basis are then transformed to the Slater determinant basis to obtain general matrix elements. Efficient computation of matrix elements of model-exact states has been as important as energies in diverse applications such as spin densities, polarization assignments, electroabsorption and nonlinear (NLO) optical spectra.

4 Dynamical properties of interacting models

The dynamics of interacting electron systems pose major challenges. Linear responses or susceptibilities must usually be approximated in extended systems of interacting fermions. In finite systems, responses are often estimated using a few low-lying eigenstates. The formal problem of applied electric or magnetic fields leads to a perturbation series and sums over states (SOS), as discussed extensively for NLO coefficients[38]. The complete spectrum of Hubbard, PPP or other correlated models is almost as inaccessible for large model systems as the exact wavefunctions of the corresponding molecules. As summarized below, model-exact responses for the ground state $|G>$ can nevertheless be found using correction vectors.

The Lanczos method has been widely applied to the dynamics in Hubbard and Heisenberg model Hamiltonians[39]. The spectral intensity for an operator $\hat{O}$ is given by

$$I(\omega) = -\frac{1}{\pi}\text{Im}[< G|\hat{O}^{\dagger}\frac{1}{(\omega + E_0 + i\epsilon - \hat{H})}\hat{O}|G >] \qquad (19)$$

where $|G>$ is the ground state of $\hat{H}$ with eigenvalue E_0, ω is the frequency of the response sought, and ϵ is a life-time parameter. The Lanczos method for computing $I(\omega)$ is through a continued fraction

$$I(\omega) = -\frac{1}{\pi}\text{Im}[\cfrac{< G|\hat{O}^{\dagger}\hat{O}|G >}{z - a_0 - \cfrac{b_1^2}{z - a_1 - \cfrac{b_2^2}{z - a_2 - \ldots}}}] \qquad (20)$$

where $z = \omega + i\epsilon$. The coefficients a_i and b_i are, respectively, the diagonal and off-diagonal elements of the $L \times L$ Lanczos small matrix that represents the Hamiltonian, $\hat{H}$, of the system. The Lanczos scheme relies on the symmetric tridiagonal approximation to the Hamiltonian. Since $L \ll P_S(N, N_e)$, there is an implicit truncation of the Hilbert space that is akin to truncation in the SOS method. Approximate dynamic quantities are consequently obtained even for an exact $|G>$.

Correction vectors[40], as introduced by Dirac[41], provide a model-exact approach to dynamical NLO coefficients of Hubbard or PPP models with a large but

finite basis. The formal problem, given a known $|G>$, is to introduce the correction vector $\phi^{(1)}(\omega)$ through the inhomogeneous linear equation

$$(\hat{H} - E_0 - \omega - i\epsilon)\phi^{(1)}(\omega) = -\hat{O}|G> \tag{21}$$

The spectral function can be expressed as,

$$I(\omega) = -\frac{1}{\pi}\text{Im} < G|\hat{O}^{\dagger}|\phi^{(1)}(\omega) > \tag{22}$$

We regain SOS expressions by expanding $\phi^{(1)}(\omega)$ in the basis of the eigenstates of the Hamiltonian[40]. However, this difficult step is avoided by the direct solution of $\phi^{(1)}(\omega)$ from (21) in the VB basis. A single correction vector is inherently more accessible than many exact excited states, although it remains out of reach for extended interacting systems. The correction vector can be found in the same VB basis used for $|G>$, since the dimensions of (21) with $\epsilon = 0$ are comparable to those of symmetry-adapted subspaces. Coordinate relaxation can be applied to (21) as shown below.

In the context of NLO responses, we note that $\phi^{(1)}(\omega)$ and higher corrections provide a systematic analysis[40]. We choose $\hat{O}$ to be the jth component of the dipole displacement operator, $\tilde{\mu}- < G|\tilde{\mu}|G >$, and solve (21) for $\phi_j^{(1)}(\omega)$. The frequency dependent polarizability tensor is

$$\alpha_{ij}(\omega) = [< G|\hat{\mu}_i|\phi_j^{(1)}(\omega) > + < G|\hat{\mu}_i|\phi_j^{(1)}(-\omega) >]/4 \tag{23}$$

The correction vectors $\{\phi_i^{(1)}(\omega)\}$ also suffices for the first hyperpolarizability,

$$\beta_{ijk}(\omega_1, \omega_2) = \hat{P} < \phi_i^{(1)}(-\omega_1 - \omega_2)|\hat{\mu}_j|\phi_k^{(1)}(-\omega_2) > /8 \tag{24}$$

where the operator $\hat{P}$ permutes the pairs $[-(\omega_1 + \omega_2), i]$, $[\omega_1, j]$ and $[\omega_2, k]$. The frequency-dependent responses of Hubbard or PPP models can be obtained rigorously this way.

Higher-order NLO coefficients are given by higher-order correction vectors, starting with $\phi_{ij}^{(2)}(\omega_1, \omega_2)$. It satisfies the inhomogeneous linear equation

$$(\hat{H} - E_0 - \omega_2 - i\epsilon)\phi_{ij}^{(2)}(\omega_1, \omega_2) = -\hat{\mu}_i|\phi_j^{(1)}(\omega_1) > \tag{25}$$

and can also be obtained in the large but finite VB basis. The second hyperpolarizability is

$$\gamma_{ijkl}(\omega_1, \omega_2, \omega_3) = \hat{P} < \phi_i^{(1)}(-\omega_1 - \omega_2 - \omega_3)|\hat{\mu}_j|\phi_{ij}^{(2)}(-\omega_1 - \omega_2, -\omega_1) > /24 \quad (26)$$

where now $\hat{P}$ is all permutations of $[-(\omega_1 + \omega_2 + \omega_3), i]$, $[\omega_1, j]$ and $[\omega_2, k], [\omega_3, l]$. Suitable choices of frequencies, in (26), including static fields, yield NLO coefficients for third harmonic generation, two-photon absorption, four-wave mixing and electroabsorption. Linear polyenes and conjugated polymers frequently have large transition dipoles connecting $|G >$ to a few odd-parity singlets[42] that in turn have strong dipole transitions to a small number of even-parity states. SOS expressions based on model-exact energies and transition moments of a few states and their vibronics are then more convenient for simulations of NLO spectra[43]. Since correction vectors give the collective contribution of all excited states, we can readily assess the accuracy of using selected eigenstates. The correction vector technique is quite general and not limited to any particular method or model. It has been employed in obtaining NLO coefficients of semiempirical quantum chemical models as well as for correlated one-dimensional systems in different approximations such as the DMRG (density matrix renormalization group) method[44].

Aromatic ring currents[45, 46] or the charge stiffness[47] provide a related application of correction vectors, now associated with magnetic fields. Ring currents are the diamagnetic susceptibility of $4n+2$ systems. The correction vector in monocycles is obtained from

$$(\hat{H} - E_0)|\phi^{(1)} >= \hat{v}_-|G > \quad (27)$$

where $\hat{v}_-$ is the velocity operator, $i\sum_{p\sigma} t(\hat{a}_{p\sigma}^+ \hat{a}_{p+1\sigma} - \hat{a}_{p+1\sigma}^+ \hat{a}_{p\sigma})$. The summation is over all sites and cyclic boundary conditions are assumed. The susceptibility is proportional to the second-order correction to E_0,

$$E^{(2)} =< G|\hat{v}_+|G > -2 < G|\hat{v}_-|\phi^{(1)} > \quad (28)$$

The first term is essentially the total π-electron bond order for bonded sites, since $\hat{v}_+$ is the Hückel model (1) for a ring with $\epsilon = 0$ and $t = $ -1 between neighbors.

Correction vectors lead to inhomogeneous linear equations of the form $\mathbf{A}\vec{x} = \vec{b}$ that involve sparse matrices in the VB representation. An iterative small matrix method gives rapid convergence using coordinate relaxation that resembles the Davidson algorithm for eigenvalues. We summarize the procedure here[48, 40]. We begin with a set of m orthonormal N-vectors $\{\vec{Q}_i : i = 1 \ldots m\}$ and construct $\vec{x}^{(0)}$, the zeroth approximation to the true solution $\vec{x}$ as,

$$\vec{x}^{(0)} = \sum_{j=1}^{m} C_j \vec{Q}_j. \tag{29}$$

The matrix equation $\mathbf{A}\vec{x} = \vec{b}$ can be rewritten, using the trial solution, as,

$$\sum_{j=1}^{m} C_j \mathbf{A}\vec{Q}_j = \vec{b}. \tag{30}$$

From (30) we can construct a small matrix $\mathbf{a}$ such that,

$$a_{ij} = \left(\vec{Q}_i, \mathbf{A}\vec{Q}_j\right) \quad ; \quad \sum_{j=1}^{m} C_j \left(\vec{Q}_i, \mathbf{A}\vec{Q}_j\right) = \left(\vec{Q}_i, \vec{b}\right). \tag{31}$$

Since the matrix $\mathbf{a}^{(m)}$ thus constructed is small enough to be inverted using conventional algorithms, the coefficients C_i and consequently $\vec{x}^{(0)}$ can be obtained. Knowing $\vec{x}^{(0)}$, the residue vector $\vec{r}^{(0)}$ defined as,

$$\vec{r}^{(0)} = \vec{b} - \mathbf{A}\vec{x}^{(0)} \tag{32}$$

is determined. The vector $\vec{x}^{(0)}$ is used as the trial solution in the Jacobi iteration scheme to obtain the correction vector $\vec{\alpha}^{(0)}$, whose i^{th} component is given by,

$$\alpha_i = \left(r_i^{(0)}/a_{ii}\right) \tag{33}$$

The correction vector $\vec{\alpha}^{(0)}$ is Schmidt orthogonalized with the basis set and the resultant is normalized. This new vector $\vec{Q}_{m+1}$ is used to augment the set $\{\vec{Q}_i\}$. The new basis, $\{\vec{Q}_i : i = 1, \ldots, m + 1\}$ is used to construct a new augmented small matrix $\mathbf{a}^{(m+1)}$. Inverting $\mathbf{a}^{(m+1)}$ gives $\vec{x}^{(1)}$ and this iterative procedure is continued until all components of the residue vector are found to be below a previously chosen threshold. If the set of vectors $\{\vec{Q}_i\}$ becomes too large to handle, the procedure can

be restarted with $m = 1$ and taking $\vec{Q}_1$ as the most recent solution after normalization. The initial dimension m of the space of trial vectors $\{Q\}$, could also be just one with components $Q_{i,1}$ proportional to b_i/A_{ii}, for nonzero A_{ii} and zero otherwise.

In contrast to the Lanczos method, correction vectors are not limited to tridiagonal matrices and form a hierarchy for solving responses of any order. They make accessible the exact dynamics of finite models and within restricted configuration spaces, unlike techniques that rely on truncations over and above that imposed by the choice of configurations. In correction vector applications, it is important to exploit the system's full symmetry as this avoids spurious singularities in the linear algebraic system of equations. Spin symmetry, for example, avoids singularities in (21) that would otherwise occur at frequencies corresponding to triplet excitations. VB theory in conjunction with correction vectors has afforded a powerful, efficient and exact way for computing the dynamic responses of systems with strong interactions that span a finite-dimensional Hilbert space.

5 π-Electronic structure of conjugated molecules

Conjugated hydrocarbons were synonymous with theoretical chemistry until advent of reliable all-electron computations, when molecules such as benzene became accessible to *ab initio* treatment. Pentacene and substituted perylenes are now considered to be "small molecules" in contrast to conjugated polymers. Direct analysis is possible for most ground state and some excited state properties. Purely π -electronic models focus on quantities that are not easily calibrated, such as correlation effects, extended systems, and comparisons among conjugated systems. Since suitable models must also reproduce π-π^* spectra, conjugated hydrocarbons provide a rich data base that, for example, unequivocally favors the Pariser-Parr-Pople (PPP) model over either Hückel or Hubbard models. Molecular comparisons are an effective way to calibrate quantum cell models for extended systems, especially in conjugated systems that evolve smoothly with size and typically saturate in the range of 50-100 π-electrons.

Conjugated hydrocarbons contain sp^2 carbons with similar bond lengths and occasionally some sp centers. A few phenomenological inputs then suffice in quantum cell models such as (4). "Standard" PPP parameters were obtained decades ago using bond lengths and linear absorption of small test molecules. Small (10%) parameter variations have been suggested since, but the robustness and predictive capabilities of a standard set far outweigh small improvements. These parameters have proved to be remarkably reliable[43, 13, 10] in entirely different contexts when combined with exact VB solutions. They hold for two-photon and NLO spectra of large hydrocarbons and conjugated polymers, as well as for oscillator strengths, spin densities, ring currents, electron-vibration coupling and other π-electronic features. Transferable PPP parameters for hydrocarbons stand in striking contrast to solid-state models. Hubbard, Heisenberg and related models are more broadly applicable, but parameters are chosen case by case. They address electronic correlations in narrow-band systems in general, while the PPP model describes a particular class of molecules in a predictive manner.

The structure polycyclic hydrocarbons (eg. Fig. 2) is taken with benzene bond lengths $R_0 = 1.397$Å and bond angles $2\pi/3$. The Ohno formula[7] for $V(R_{pq})$ is

$$V(R_{pq}) = 14.397[\frac{7.1985}{U^2} + R_{pq}^2]^{-\frac{1}{2}} \qquad (34)$$

where distance is in Å and energy in eV. $V(R_{pq})$ interpolates between on-site re-pulsion $U = 11.26eV$, taken from atomic gas-phase data, and Coulomb interactions e^2/R between distant carbon atoms. The PPP model (4) has $V_{pq} = V(R_{pq})$, transfer integrals t$(R_0) = -2.40eV$ between bonded sites in (1), and site energies $\epsilon_p = 0$. Half-filled systems have electron-hole symmetry when there are no odd-membered rings. We typically find the lowest 2-5 eigenstates in each symmetry subspace, as this covers the available spectroscopic range. All eigenstates are explicitly given as linear combinations (10) of VB diagrams and can be used for calculating matrix elements.

The naphthalene results[35] in Table 1 illustrate the scope and success of standard PPP parameters for a classic series of experiments[49, 50, 51]. $N = N_e = 10$

yields 42 purely covalent singlet diagrams. There are about 20,000 singlets and 30,000 triplets when ionic diagrams are included. The small oscillator strength of the $^1B_{3u}$ excitation, which is forbidden by electron-hole symmetry, is properly given for slightly different site energies at the fused carbons, $\epsilon_9 = \epsilon_{10} = -0.15eV$. Although electron-hole symmetry is approximate for molecules, it has far reaching consequences that carry over into all-electron treatments. The location and large intensity of $^1B_{2u}$ are properly given, as are the fine structure constants and spin densities of the $^3B_{2u}$ triplet.

The VB basis for anthracene and pyrene is larger by two and three orders of magnitude, respectively. Linear $\pi - \pi^*$ spectra of these D_{2h} molecules are polarized along the long ($^1B_{2u}$) and short ($^1B_{3u}$) axes. Two-photon transitions to X^1A_g and $^1B_{1g}$ differ in having parallel and perpendicular transition dipoles, respectively, to virtual odd-parity singlets. Assignment as ^1A_g or $^1B_{1g}$ is based on the relative intensities with parallel or circularly polarized light. The experimental[52] and PPP[21] excitation energies of pyrene in Table 2 reflect both energy and symmetry. The "±" superscript is the electron-hole index[22], which changes in dipole-allowed transitions to $^1B_{2u}^-$ or $^1B_{3u}^-$. The forbidden $^1B_{3u}^+$ transition at 3.3 eV is in fact 400-fold weaker[53] than allowed transitions; as in the case of naphthalene, it becomes weakly allowed on breaking electron-hole symmetry by changing the site energies of fused carbons. The agreement in Table 2 is remarkable as it also reproduces the two-photon excitations in the ^1A_g and $^1B_{1g}$ subspaces. The only exception is the 4.535 eV excitation that we assign as $^1B_{1g}$ rather than ^1A_g. These PPP excitations for pyrene are competitive with the state-of-the-art all-electron theory.

Similarly good agreement with experiment is found for biphenyl[37], ith 12 pi electrons, anthracene[54] or trans-stilbene[55], with 14 π-electrons. The even-parity singlets of anthracene are systematically reassigned to lower energy and show strong correlation effects. The bond order p_{nm} of sites n and m in the model-exact eigenstate $|X>$ is,

$$p_{nm}(X) = \frac{1}{2} \frac{\partial E(X)}{\partial t_{nm}} = -\sum_\sigma < X|a_{n\sigma}^\dagger a_{m\sigma} + a_{m\sigma}^\dagger a_{n\sigma}|X > \qquad (35)$$

Table 1. Experimental and Pariser-Parr-Pople results for naphthalene[35]: ΔE is the 0-0 excitation energy, D and E are fine structure constants, ρ is the spin density, and f is the oscillator strength.

State	Property	PPP	Expt:
$^3B_{2u}$	ΔE (eV)	2.522	2.64
Fine Structure	D (cm^{-1})	0.1140	0.1012[49]
	E (cm^{-1})	-0.0063	-0.0141[49]
Spin Density	ρ_1	0.4060	0.438[49]
	ρ_2	0.1164	0.125[49]
	ρ_9	-0.0451	-0.126[49]
$^1B_{3u}$	ΔE (ev)	3.604	3.96[50]
	f[†]	0.00063	0.0005[50]
$^1B_{2u}$	ΔE (ev)	4.463	4.45[51]
	f	0.2129	0.18[51]
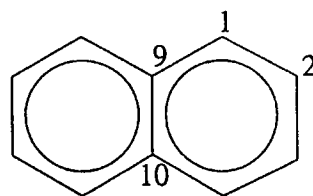
[†] For site energy $\epsilon = -0.15eV$ at carbons 9 and 10.

Table 2. Exact Pariser-Parr-Pople results[21] with standard parameters for the first three singlet excitations (in eV) of pyrene (Fig. 2) in D_{2h} and electron-hole symmetry. In parenthesis, experimental excitations and assignments, from[52]. The ground state is $1^1A_g^+$.

n	$(n+1)^1A_g^+$	$n^1B_{1g}^+$	$n^1B_{3u}^-$	$n^1B_{2u}^-$	$n^1B_{3u}^+$	$n^1B_{2u}^+$	$n^1A_g^-$	$n^1B_{1g}^-$
1	3.81	4.171	4.945	3.755	3.063	5.321	5.396	4.524
	(3.468)	(4.116)	(4.550)	(3.707)	(3.339)		(5.396)	(4.535)
2	4.911	4.239	6.943	5.411	5.180	6.282	6.259	5.791
	(5.155)	(4.287)		(5.145)				
3	5.551	5.412	7.324	6.379	5.503	6.789	6.977	6.584
	(5.777)	(4.939)						

Large p_{nm} (1^1A_g) in the ground state indicate increased double-bond character and reduced bond lengths in the actual structure. Thus equal bond lengths and transfer integrals suffice for refinements that hardly change when $t(R)$ is modulated according
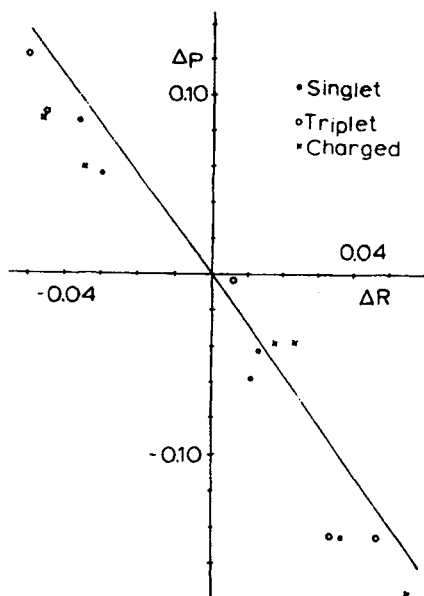
Figure 4: Correlation between Pariser-Parr-Pople bond orders (35), and Parameter Method 3 bond lengths of anthracene. ΔP is the bond-order change between the ground state and the singlet, triplet and charged states discussed in the text for the five distinct bonds of anthracene; ΔR is the corresponding bond-length change. The line has slope $\Delta P/\Delta R = -0.36$[58].

to X-ray data. The bond orders for $|X> = 1^1B_{2u}^-$, $1^3B_{2u}^+$ and 1^1A_g (diion) refer, respectively, to the lowest dipole-allowed singlet, the lowest triplet, and the ground state of the dianion or dication, whose bond orders are equal due to electron-hole symmetry. Since these are ground states in various subspaces, bond lengths can readily be calculated by conventional methods such as PM3 and changes ΔR from the 1^1A_g bond lengths are directly related to excited-state relaxation. The bond-order change, $p_{nm}(X) - p_{nm}(1^1A_g)$, are shown in Fig. 4 as a function of PM3

bond-length changes for the five distinct bonds of anthracene.

The linear correlation with slope $\Delta R/\Delta p = -0.36$ shows that PPP bond orders can be used for excited-state relaxation. The comparable graph of $\Delta R/\Delta p$ for trans-stilbene has a linear correlation with slope -0.25. Similarly, it is seen in biphenyl[37] that the lowest triplet state has a bond order pattern corresponding to the quinonoidal structure, implying a planar geometry in the triplet state in conformity with the prediction of Lewis and Kasha[56].

Planar hydrocarbons are certainly the most favorable applications of PPP models. They highlight the fact that accurate excitation energies are possible using simple basis and exact solutions that correspond formally to CI to all order. Table 1 shows the range of accessible electronic properties, while Fig. 4 shows that π-electrons account for excited-state relaxation in the conjugation plane. Polyenes have partial single and double bonds of 1.35 and 1.45 Å, respectively, and transfer integrals of $t_0(1 - \delta)$ and $t_0(1 + \delta)$ with $\delta = 0.07$ in the PPP model. Gas-phase[57] and matrix[58] studies have provided accurate one and two-photon spectra up to 8 double bonds, as given in Table 3. Contrary to the expectations of single-particle theory, even at the Hartree-Fock level, the even-parity 2^1A_g state is below the intense odd-parity 1^1B_u state. This paradigm of electron-electron correlations has consequently been extensively studied, notably by Kohler's group. As seen in Table 3, standard PPP parameters and exact correlated states account for these excitations. The constraints of standard structures and parameters based on small molecules are now evident. Slightly smaller alternation, bandwidth and Coulomb interactions would improve the description of large molecules.

Hückel theory confers special stability and diamagnetism to $4n + 2$ systems, as recognized by London[59]. Half-filled systems have the largest ring currents, since all bonding orbitals are filled and antibonding orbitals are empty. Annulenes with $4 \leq n \leq 6$ are large enough to form tetraanions whose ring currents[60] are distinctly larger than in the neutral molecule. The observed ring currents are in accord with PPP theory[45, 46, 47] and reflect electron-electron correlations. As seen from (5),

the VB basis for $N = N_e = 18$ has over 10^8 singlets that contain more than 2.3×10^9 Slater determinants with $S_z = 0$.

Table 3. One and two-photon thresholds (in eV) of trans-polyenes, C_nH_{n+2}, in alkane matrices[58] and in the Pariser-Parr-Pople model[21]. The solid-state shift of $0.40eV$ of the ionic $1^1B_u^-$ state yields gas-phase values up to $n = 12$; covalent $2^1A_g^+$ shifts of $\sim 0.05eV$ are neglected.

	matrix	PPP	matrix + 0.40	PPP
n	$2^1A_g^+$	$2^1A_g^+$	$1^1B_u^-$	$1^1B_u^-$
16	2.216	2.835	3.223	3.698
14	2.437	2.962	3.388	3.831
12	2.683	3.137	3.677	4.001
10	3.10^a	3.391	3.998	4.234
8	3.541	3.775	4.380	4.561

^{a} Gas phase[57]

The idealized D_{18} symmetry reduces the basis to manageable blocks of $\sim 6 \times 10^6$ symmetry-adapted diagrams[47]. The PPP model (4) has equal bonds of length R_0, uniform transfer integrals $t(R_0)$, and Ohno potential $V(R)$ based on a regular polygon. Figure 5 shows exact ring currents of $4n + 2$ annulenes as a function of $z = U/4t_0$, the ratio of on-site correlations to the bandwidth. The Hückel ($z = 0$) diamagnetism increases linearly with the ring size. The PPP result for $U = 11.26eV$ is the doted line $z = 1.17$, where $N = 18$ hardly exceeds $N = 14$. Stronger correlations (larger z) shows decreasing ring currents with increasing size. Covalent diagrams increasingly dominate in the ground state for $U \gg 4t_0$ and such diagrams cannot support charge flow.

Experimental ring currents[60] are associated with the anisotropy of ^{1}H shifts at protons pointing inside and outside the annulene. The virtually equal shifts of 13.78 and 13.46 ppm in 14 and 18 annulenes clearly support the PPP results in Fig. 5, which also rationalize the decreasing shifts of 10.03 and 6.41 ppm for 22 and 26 annulenes. Moreover, the PPP ring current[47] of the anion $[18]^{-4}$ is 1.49 times that of neutral [18], while the measured ^{1}H shift increases 1.57 times[60]. In general, the identification of ring currents in conjugated molecules requires careful atten-

tion to contributions from all other sources to chemical shifts. Accurate molecular wavefunctions[61] are required for local contributions.

In the context of solid-state models, on the other hand, ring currents correspond to the charge stiffness introduced by Kohn[62] to distinguish between conductors and insulators. Exact analysis[63] of the infinite Hubbard chain (only on-site interactions, $U > 0$), yields an insulator with vanishing ring current. Although there are no exact results for an infinite PPP chain, its electron-hole symmetry leads to the same conclusion. We expect that Fig. 5 becomes a delta function at $z = 0$ as $N \longrightarrow \infty$. This counterintuitive result has its roots in Hückel's $4n$, $4n + 2$ rule. The orbital degeneracy of $4n$ rings leads to paramagnetic ring currents flowing in the opposite direction. Although ring currents or stabilization that alternates between $4n$ and $4n + 2$ is perfectly sensible in small molecules, they cannot persist in extended systems that are insulators and Coulomb interactions suppress aromatic stabilization in large annulenes. Bond length alternation is a closely related problem. The Jahn-Teller instability of $4n$ rings is due to orbital degeneracy, while $4n+2$ rings have nondegenerate ground state. Thus cyclobutadiene distorts and benzene does not. The orbital spacing decreases with ring size, however, and bond-length alternation always wins at large N, as recognized by Longuet-Higgins and Salem[64] for polyenes and more generally by Peierls[65] for one-dimensional metals. In all-electron theory[66], the crossover from uniform bond lengths to partial single and double bonds in annulenes occurs in the same range of about 50 π-electrons found in simple models.

6 Conjugated Polymers

The synthesis and characterization of polyacetylene (PA) provided new incentive for understanding π-electronic spectra, electron-phonon interactions and electronic correlations[1, 2, 14]. The electrical conductivity of chemically doped PA rivals that of metals. Families in Fig. 2 such as polydiacetylenes (PDAs), polythiophenes (PTs), σ-conjugated polysilane (PSs) and polyparaphenylene vinylene (PPVs), among
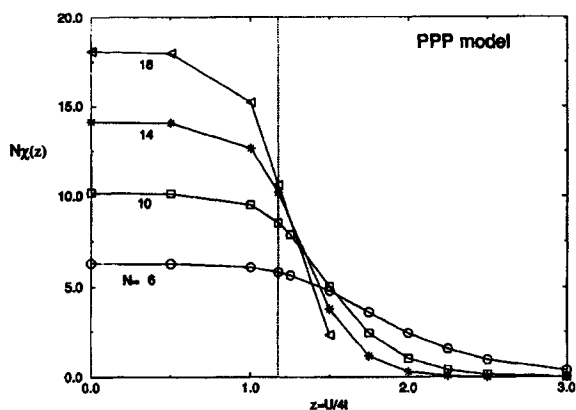
Figure 5: Diamagnetic rings currents, $N\chi(z)$, of half-filled Pariser-Parr-Pople models for regular polygons with D_{Nh} symmetry. The dashed line at $z = U/4|t_0| = 1.17$ corresponds to standard parameters; $z = 0$ is the Hückel limit of free electrons, while $z \gg 1$ is the strong-correlation limit of antiferromagnetic Heisenberg spin chain with vanishing ring currents[50].

others, have provided new opportunities based on large NLO responses, on applications as thin-film transistors[67], and above all as organic light-emitting diodes (OLED). Molecules such as α-sexithiophene (α-6T), perylenetetracarboxylic acid dianhydride (PTCDA), or tris(8-hydroxy-quinoline)aluminum (Alq$_3$), also make excellent OLEDs[68]. Recent studies on vapor-grown acenes[69], notably pentacene and tetracene, have produced an organic injection laser and high enough mobility at low temperature to observe superconductivity and the fractional quantum Hall effect. A great deal of work has been done and even more is in progress. Our interest here is limited to quantum cell models.

Conjugated polymers and organic molecular crystals or thin films are extended systems whose electronic structure is beyond direct *ab initio* theory, although many valuable treatments of oligomers have been reported. Simple models are advanta-

geous for extended systems for purely computational reasons. More importantly, however, models focus on key physical aspects and thus unite polymers, complexes, and crystals whose chemistry is entirely different. Molecular PPP parameters, for example, are quite suitable for conjugated polymers; this focuses attention to the relevant sector of parameter space and makes possible predictions for any backbone. Model-exact results for oligomers completely avoid the problem of size consistency in NLO applications, which currently limit the self-consistent treatment of large systems to first order. The price, of course, is the necessity of extrapolating from oligomers to infinite systems.

The 1^1B_u and 2^1A_g excitation energies in Table 3 decrease as $1/N$ and extrapolate sensibly to PA excitations whose widths are about $\sim 0.2eV$. The limited agreement for finite systems is sufficient for polymer spectra of amorphous films. These excitations of pristine chains clearly require correlations just to get the proper order of one and two-photon thresholds. The successes of the Su-Schrieffer-Heeger (SSH) model[70, 1] of electron-phonon coupling in Hückel chains, on the other hand, are for chains in which chemical doping or photoexcitation produces new excitations below the optical gap (below 1^1B_u). Solitons, polarons and bipolarons account for the number and approximate energies of these gap states in many polymers. Their precise location or vibronic structure is not known accurately. Detailed comparisons consequently await both experimental and theoretical advances.

Ring currents in Fig. 4 illustrate extrapolations whose convergence is far from obvious. Many simple models such as $4n$ and $4n + 2$ Hückel rings or various spin chains can be used to demonstrate slow or problematic convergence with increasing length. These are mathematical challenges for models. Physical considerations often provide guidance that, however, need not be decisive. Recent debates[71] about band or exciton theory or binding energies or the roles of interchain interactions or electron-phonon versus electron-electron models reflect the difficulties of extended systems and of low-resolution spectra. Such discussions rely on quantum cell models to pose questions precisely and to illustrate specific consequences of extended

interacting systems.

As noted above, exact solution[72] of the infinite Hubbard chain with uniform transfer integrals shows the ground state to be an insulator for any $U > 0$. Hence we have $E(1^1B_u) > 0$ for arbitrarily small on-site repulsion. But the excitation threshold of triplets or of even-parity singlets, $E(2^1A_g)$, rigorously vanishes[72] for arbitrarily large U. The electron-hole symmetry of Hubbard and PPP models ensures similar thresholds[73] in regular PPP chains, although $E(1^1B_u) > 0$ is not known for the infinite chain. The conjugated backbones of polymers have unequal bond lengths. PA has alternating single and double bonds, as in polyenes ($\delta = 0.07$), while PDAs and PTs have four t's per unit cell. The σ-conjugated backbone of PS (Fig. 2) is alternating with larger δ due to inter and intra-atomic overlaps. A PPP model with U for Si in (34) now accounts[74] for low-energy excitations and illustrates similarities between polymer families that at chemically quite different. The PPV backbone requires at least six t's per repeat unit; there is increased alternation at bridgehead carbons, where $t\sqrt{2}$ follows from the topology[75]. In all these polymers, alternation opens gaps in the spectrum of triplets and even-parity singlets. The gaps are tiny for $U \gg t_0$, when these states correspond to spin excitations of Heisenberg antiferromagnetic chains, and substantial for $U < t_0$, where the single-particle gap of $4t_0\delta$ is the threshold for all excitations.

Spin-charge separation with increasing U has been extensively discussed in Hubbard models, which indeed were introduced to study the formation of local moments with increasing U/t_0. The infinite chain with equal transfer integrals is strongly correlated for $U > 0$ and such reasoning has been applied to conjugated polymers. Alternation produces a qualitative change, since finite U is now required for strong correlations. We have comparable correlations in polymers with variable backbones and single-particle gaps[73]. Theorists usually turn on correlations in noninteracting models rather than vary $4t_0\delta$ at fixed U, but the two procedures are completely equivalent and π-conjugated polymers illustrate variable δ at fixed U and t_0.
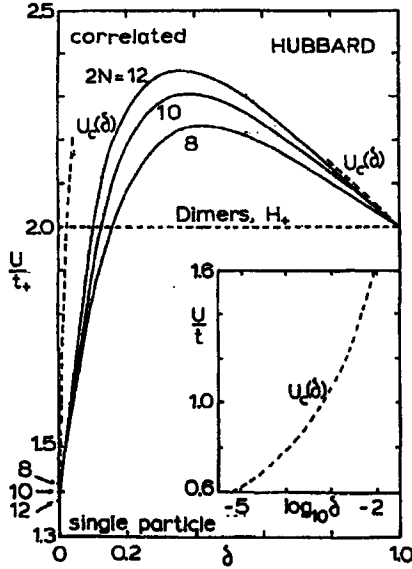
Figure 6: Band-to-correlated crossover based on $E(1^1B_u) = 2E(1^3B_u)$ of N-site Hubbard chains with alternating transfer integrals $t_\pm = t_0(1 \pm \delta)$. The $U = 0$ and $2t_+$ points are exact for the infinite chain and dimers, respectively. The dashed $U_c(\delta)$ line is based on perturbation theory at large δ and (inset) separate estimates of the singlet and triplet thresholds at small δ[80].

We can estimate correlations in polymers with centrosymmetric backbones by comparing the relative energies of $E(1^1B_u)$ and $E(2^1A_g) \sim 2E(1^3B_u)$. The one-photon excitation is lower for weak correlations. The two-photon excitation is lower for strong correlations and 2^1A_g can be viewed as two odd-parity triplets with total spin zero. Fig. 6 shows the $(U/t_0, \delta)$ values for Hubbard chains[76] at which $E(1^1B_u) = 2 E(1^3B_u)$. The dashed line is the extrapolation to infinite chains. It necessarily passes through the origin, where it can be estimated analytically as shown in the inset. All low-energy excitations of the infinite chain can be obtained near $\delta = 1$ by perturbation theory in dimers[77] and rapid convergence with N is

both expected and seen at large alternation. The line $E(1^1B_u) = 2E(1^3B_u)$ and a similar line $E(1^1B_u) = E(2^1A_g)$ represent excited-state crossovers in models with centrosymmetric backbones. An excited-state crossover is a simple general result with direct physical implications: Since 1^1B_u is dipole allowed and fluorescence is usually from the lowest singlet, fluorescent polymers[75] have $E(1^1B_u) < E(2^1A_g)$ and exhibit intermediate correlations. This has proved to be the case. PS, PPV and PT in Fig. 2 are families whose fluorescence can be modulated by the choice substituents or morphology, while PA, polyenes and PDAs emit orders of magnitude more weakly (from 2^1A_g in the case of polyenes[78]) at cryogenic temperatures.

The PPP model yields $E(1^1B_u) = 2E(1^3B_u)$ curves and extrapolations similar to Fig. 5. Since there are no new parameters, the model predicts fluorescence and agrees with experiment. In oligomers[79], the relative energies of $E(1^1B_u)$ and $E(2^1A_g)$ are almost independent of N at alternation $\delta = 0.20$, which in fact is a typical value in polymers. The two-photon state is slightly lower in PDAs and slightly higher in PTs or PPVs. The weak N dependence is clearly fortuitous for extrapolations.

The Taylor expansion of $t(R)$ about R_0, the benzene bond length, gives the linear coupling $\alpha = t'(R_0)$ in first order and $t''(R_0)$ in second order. Solid-state models for polarons or excitons typically consider linear coupling, which in harmonic lattices leads to displaced harmonic oscillators with unchanged frequencies. The SSH model[1] has $\alpha \sim 5eV/\mathring{A}$. The $t''(R_0)$ term is clearly required[80] to interpret the Raman spectra of PA and follows for wavefunctions that decay exponentially, but is difficult to incorporate into models. An accurate force field is required and has been obtained for PA and its isotopes [43]. The effective conjugation coordinate[81] of conjugated polymers and infrared active vibrational (IRAV) modes[82] have been extensively studied using quantum cell models. The PPP potential also has corrections in $V'(R_0)$ for the distance dependence of Coulomb interactions[83]. Vibronic contributions[43] improve markedly the modeling of NLO spectra even at the level of the Condon approximation[84].

To conclude these comments about modeling polymers, we mention rylenes (Fig. 2) and other D_{2h} systems whose π-electrons can be separated into two subsystems. The Hückel MOs of acenes in Fig. 2 or pyrene in Table 2 are even and odd with respect to reflection about the plane normal to the conjugation and containing the long axis. Rylenes are peri-linked naphthalenes that start with perylene ($n = 0$ in Fig. 2, $C_{20}H_{12}$), terrylene ($n = 1$) and quatterylene ($n = 2$) and extend to a poorly characterized polymer, polyperinaphthalene (PPN), with a very small calculated optical gap[85]. The repeat unit is the 10 π-electrons of naphthalene and rylenes have electron-hole symmetry. A simple canonical transformation[86] of $\hat{H}_{\text{Hückel}}$ leads to $5(n + 2)$ filled bonding orbitals, of which $n + 2$ are localized on individual naphthalenes, $2n + 4$ are even under reflection and $2n + 4$ are odd under reflection. Since both the HOMO and LUMO are odd under reflection, the optical gap of rylenes or pyrenes depends on a subset of π-electrons in precisely the same sense that $\pi - \pi^*$ excitations involve a subset of all electrons. In the spirit of $\sigma - \pi$ separation, we keep the subset of odd MOs and introduce Coulomb interactions in the zero-differential approximation. The odd subspace of perylene becomes a conjugated chain similar to octatetraene, and longer rylenes or pyrenes map into longer polyenes[86].

Since the Hückel model in the odd subspace is precisely that of a polyene, we can immediately understand strong coupling[87] in Table 4 of rylenes or pyrenes to the characteristic $0.18eV$ vibration of polyenes or PA. This out-of-phase stretch of single and double bonds is excited on promoting an electron from the HOMO, which is weakly bonding for double bonds and weakly antibonding for single bonds, to the LUMO, which is just the opposite. The electronic excitation is delocalized over two strands in rylenes, one strand in polyenes. Linear coupling and harmonic oscillators then imply excited-state (1^1B_u) displacements that are factor $\sim \sqrt{2}$ smaller in rylenes. The $0 - p$ intensity for displaced harmonic oscillators goes as $g^{2^p}/p!$ and comparable 0-0, 0-1 intensities in polyenes corresponds to $g \sim 1$. The expected intensities[86] for $g' = g/\sqrt{2}$ are then 10:5:1.25 and rationalize at once the measured patterns in Table 4. The lower optical gap of rylenes requires going beyond the

Table 4. Excitation energy to 1^1B_u, vibronic spacing and relative intensities of polycyclic aromatics in solution[87]; 1^1B_u threshold for polyenes in alkane matrices[86]. Value of n in the tables refers to Fig. 2.

Molecule	DE(0-0) (eV)	h_n (eV)	10 In/I0	Polyenes, (eV)
perylene $(n = 0)$	2.86	0.17	10/7.2/3.3/1.3	3.98
terrylene $(n = 1)$	2.21	0.18	10/5.0/1.7	3.28
quaterrylene $(n = 2)$	1.85	0.19	10/5.0/2.0	2.82
pyrene $(C_{16}H_{10})^a$	3.72	0.18	10/5.7/2.2/0.08	4.67
peropyrene $(C_{26}H_{14})$	2.80	0.18	10/5.7/1.5/0.06	3.60

^{a} p-band, 18° C

Hückel model, which gives equal $E(1^1B_u)$. Since the transformation leads to expanded sites that contain two or three carbons, we expect smaller reduced Coulomb interactions in the PPP model. Standard parameters for expanded sites account for reduced $E(1^1B_u)$ in Table 4 for rylenes and places their $E(2^1A_g)$ at higher energy, consistent with their strong fluorescence[86]. Although reduced in rylenes, correlations lead to $E(2^1A_g) < E(1^1B_u)$ in longer rylenes or PPN and to an insulating ground state. The sharply reduced fluorescence[88] of a substituted quaterrylene may signal the crossover to be at $n = 4$.

7 Neutral - ionic transition in organic charge - transfer salts

Diagrammatic VB theory[12] was introduced to model organic charge-transfer (CT) and ion-radical salts instead of conjugated molecules. Organic π-donors (D) and acceptors (A) often crystallize as face-to-face stacks[11]. Solid CT complexes contain mixed $\cdots$ DADA $\cdots$ stacks, while ion-radical salts form segregated $\cdots D^+D^+D^+ \cdots$ or $\cdots A^-A^-A^- \cdots$ stacks with counterions between the stacks. The relevant orbitals for quantum cell models (4) are now the HOMO of D and LUMO of A. Segregated stacks yield Hubbard or PPP models[11] that are half-filled in the case of simple 1:1 salts and have other filling in complex salts. Double occupancy in delocalized

orbitals leads to $U \approx 1eV$, which is an order of magnitude smaller than in conjugated molecules, but π-π overlap around 3.3Å reduces transfer integrals, t to $\approx 0.2eV$. So correlations are comparable or stronger in these crystals. Radical ions lead to magnetic properties that are described by linear Heisenberg antiferromagnetic chains with exchange $J = 2t^2/U$ between neighbors. The lowest optical features are CT transitions polarized along the stack; both simple and complex salts have self-exchange leading to a doubly-occupied site around energy U; the latter have even lower energy CT bands that involve singly-occupied and empty sites. Organic conductors have segregated stacks with uniform or nearly uniform transfer integrals and nonintegral oxidation states, while half-filled systems are Mott insulators.

The combination of mixed or segregated stacks, of simple or complex stoichiometry, and of regular, dimerized or tetramerized stacks offers many possibilities that have all been realized[11]. Indeed, a few key acceptors such a TCNQ (tetracyanoquinodimethane) or CA (chloranil) and donors such as TTF (tetrathiofulvalene) or TMPD (tetramethyl-p-phenylene- diamine) are sufficient. TTF-TCNQ is a conductor[89] with two segregated stacks, ionicity $\rho = 0.59$, and separate metalinsulator transitions on each stack at low temperature. Organic superconductors[90] are 2:1 salts based on substituted TTFs. TMPD-ClO$_4$ and alkali-TCNQ salts with dimerized stacks show triplet spin excitons[91] with resolved fine structure in electron paramagnetic resonance spectra. TTF-CA is a special CT salt[92] that undergoes a valence transition at 81 K or under pressure between a largely neutral and a largely ionic ground states. The ionic phase corresponds to a dimerized $\cdots D^+A^-D^+A^- \cdots$ stack, while the neutral phase is a regular $\cdots DADA \cdots$ stack.

The generalization of the Hückel model (1) to a donor-acceptor stack is through a site energy, $e_p = (-1)^p\Delta$, that lowers the energy of electrons on odd-numbered D sites for $\Delta > 0$. In principle we have different on-site U in (3) for donors and acceptors, but a single U is usually assumed. The Coulomb terms in (4) now have $z_p = 2$ and 0 at odd and even sites, respectively, because neutral D and A require two and no electrons. The complete basis for a stack is identical to the PPP basis

and has recently been studied up to 16 sites[93]. Since electron transfer is from D
to A, it is an excellent approximation to discard VB diagrams containing D^{2+} sites
with two holes or A^{2-} sites with two electrons. The reduced basis has three states
per sites and makes exact results for 22 sites accessible[93]. Spin-pairing is now
between singly-occupied sites that correspond to ion radicals and doubly-occupied
or empty sites are neutral.

The neutral-ionic transition (NIT) at $t = 0$ occurs abruptly[94] when the Madelung
energy M of the ionic lattice exceeds the energy $I - A$ to transfer an electron form
D to A. Long-range Coulomb interactions are treated self-consistently as part of Δ
in the modified Hubbard model[95],

$$\hat{H}_{mod.} = \sum_{p\sigma}\{(-1)^p \Delta \hat{a}_{p\sigma}^\dagger \hat{a}_{p\sigma} - (\hat{a}_{p\sigma}^\dagger \hat{a}_{p+1\sigma} + \hat{a}_{p+1\sigma}^\dagger \hat{a}_{p\sigma})\} + \sum_p U\hat{n}_p(\hat{n}_p - 1)/2. \quad (36)$$

We take the parameters Δ and U in units of t, which sets the energy scale. Long-
range Coulomb interactions can also be included explicitly, at least for single chains[96].
The NIT of modified Hubbard model (36) is continuous[97, 98, 99] as a function of Δ;
it occurs around $U = 2\Delta$ when DA and D^+A^- become degenerate. A discontinuous
change of ionicity requires long-range interactions or strong coupling to molecular
vibrations. There are marked $4n$ / $4n + 2$ variations here also. The ground state of
(36) for $U \ll 2\Delta$ is totally symmetric ($k = 0$) on the neutral side, but transforms
as $k = \pi$ in $4n$ rings with periodic boundary conditions for $U \gg \Delta$. The degener-
acy at the symmetry crossover marks the NIT as $\Delta_c(U)$ for $4n$ rings. There is no
crossover in $4n+2$ rings with periodic boundary conditions. Antiperiodic or Möbius
boundary conditions in which N-fold rotation changes the sign of the wavefunction
are achieved by changing the sign of t_{1N}. Now $4n + 2$ rings have degenerate ground
states at $\Delta_c(U)$ that mark the NIT and there is no crossover in $4n$ rings.

As seen in Fig. 7, crossovers[93] for periodic and antiperiodic boundary condi-
tions separate the neutral and ionic regimes. The dashed line is the extrapolated
behavior of the infinite chain. The narrow ionic region at small U becomes a point
at $U = 0$ for the noninteracting system that can readily be solved exactly. Finite
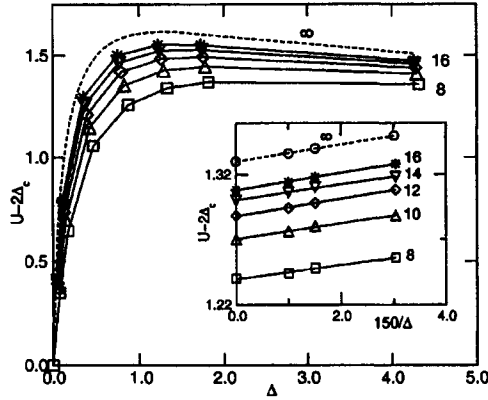
Figure 7: Ground-state crossover, $U(\Delta_c, N)$, of the modified Hubbard model (36), with periodic and antiperiodic boundary conditions for $N = 4n$ and $4n + 2$, respectively. The dashed lines are extrapolations to the infinite chain and rigorously passes through the origin. The inset shows the behavior at large site-energy Δ; the limit $\Delta \longrightarrow \infty$ corresponds to the restricted basis in which D^{+2} and A^{-2} sites are excluded[97].

$U > 1$ is needed to stabilize an ionic ground state. Although slightly on the ionic side for finite $U \gg 1$, the NIT for $U > 2$ is almost independent of Δ, with $U - 2\Delta_c \approx 1.5$. The inset shows the crossovers at large Δ. The restricted basis gives the NIT in the limit[100] that both U and Δ diverge such that $\Gamma = \Delta - U/2$ remains finite. The ground-state charge density ρ of (36) is the partial derivative of the energy with respect to Δ, or the expectation value of electrons on A sites. It changes discontinuously at symmetry crossover; $\Delta\rho$ decreases with increasing N and is continuous in this infinite chain. As noted above, finite $\Delta\rho$ at the NIT is found in models with long-range interactions or mean-field contributions that yield $\Delta(\rho)$ and nonlinearities. There are systems with both continuous and discontinuous valence transitions. Organic CT salts have small $U > 1$, while inorganic oxides[101]

have $U \approx 1$ and NITs close to the origin in Fig. 7.

Having identified the NIT in terms of a symmetry crossover, we can study excitations at that transition. The lowest singlet excitation is a CT between the $k = 0$ and π ground states[102]. The lowest triplet[103] is finite in a band insulator, the simple $U = 0, \Delta > 0$ case of (6.1), and vanishes in a Mott insulator, the $U > 0, \Delta = 0$ case of a Hubbard model or Heisenberg spin chain for large U. The exact singlet-triplet gaps[93] in Fig. 8 are in the restricted basis and show the gap to open at, or very near, the crossover. At each N, periodic and antiperiodic boundary conditions yield a system with a crossover whose singlet-triplet gap is shown with open symbols and a system without a crossover whose singlet-triplet gap is shown with close symbols. The two sets are extrapolated separately. The singlet-triplet gap opens with $0.1t$ of the NIT. Similar analysis of CT gaps up to $N = 22$ gives a tighter bound of $0.05t$. The charge gap, $I(N) - A(N)$, is the energy for transferring an electron between two noninteracting rings. It is finite on the neutral or ionic side and vanishes precisely at the NIT. Ionization potentials and electron affinities up to $N = 18$ in the restricted basis shows vanishing charge gaps at the NIT with a $0.2t$ bound[93]. Moreover, the charge stiffness at the NIT of (36) indicates a metal with correlations reduced by 40% from free electrons $(U = \Delta = 0)$.

Experimental and theoretical studies of valence transitions are current topics with many open points. Different roles are expected for Coulomb or interchain interactions and coupling to molecular or lattice phonon in various systems. Direct solutions of models are one of several methods for studying the NIT. Magnetic, dielectric and thermal properties can be obtained exactly, albeit for finite systems of increasing size. Extrapolations to infinite chains require care and guidance from related analytical results.

The exclusion of D^{+2} and A^{-2} sites on physical grounds leads to three possible states per site in the restricted basis. It exceeds the basis of covalent diagrams used for $s = 1/2$ sites, but is far smaller than the fermion basis for one orbital per site. $S = 1$ sites also have three states that may be considered as a pair of $s = 1/2$ sites
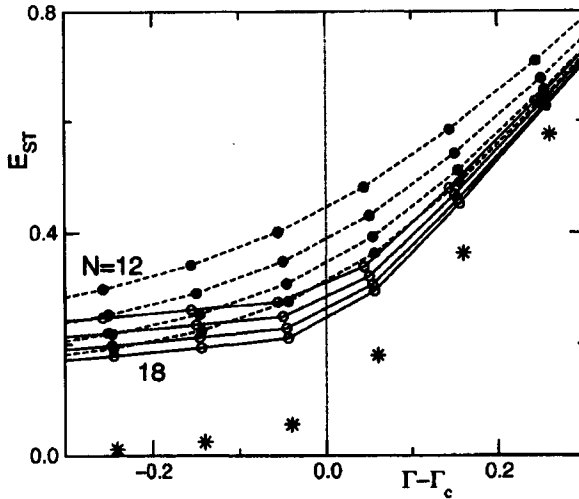
Figure 8: The singlet-triplet gap, E_{ST}, near the neutral-ionic transition of (36) in the restricted basis as a function of $\Gamma = \Delta - U/2$. Open and closed symbols refer to boundary conditions with and without crossovers, respectively, and the stars as joint $N \longrightarrow \infty$ extrapolations based on both[97].

in which spin pairing, or a line connecting the sites, is excluded. Although nearest-neighbor exchange in a chain of $S = 1$ spins leads to exchange between first, second and third neighbors of the $s = 1/2$ spins, the necessary transformation rules for VB diagrams can readily be found. Large reductions in basis size are achieved by conserving total spin[113]: the Hamiltonian is ~ 100 times smaller for a chain of 15 $S = 1$ spins. Thus N sites with $S = 1$ correspond to the covalent subspace of $2N$ sites with $s = 1/2$. The $s = 1/2$ sites are labeled such that $2n - 1$ and $2n$ correspond to $S_n = 1$. We generate the covalent VB basis as indicated in Section 2 and obtain the $S = 1$ basis by discarding all VB diagrams that contain one or more lines between $2n - 1$ and $2n$, with $n = 1, 2, \cdots N$. In these examples, the simplest

way to find the appropriate VB basis is to generate a larger set and discard the unwanted diagrams.

8 Kondo Chains and Magnetic Clusters

One of the puzzling features of dilute magnetic impurities in nonmagnetic hosts was the vanishing of the magnetic moment of the guest in some cases such as iron dissolved in aluminum[104, 105]. The Anderson model[106] introduced to study such systems, consists of a tight-binding s-band of the host hybridizing with the correlated d-orbital of the guest atom. In the limit of strong d-electron correlation, the interaction between the electron in the d-orbital and the electron in the s-band is given by $J\hat{S} \cdot \hat{s}$, where $\hat{S}$ is the spin of the electron in the d orbital, $\hat{s}$ is the spin of the conduction electron at the guest site and J is an antiferromagnetic exchange constant[107, 108]. The model for studying stoichiometric alloys of magnetic and non-magnetic metals involves a lattice of the magnetic spins immersed in a bath of conduction electrons of the nonmagnetic metal. The magnetic moment has an antiferromagnetic interaction with the electron in the itinerant orbital, whenever it is singly occupied. The Hamiltonian of this system can be written as,

$$
\begin{aligned}
H = -t \sum_{<ij>,\sigma} (\hat{a}_{i,\sigma}^{\dagger}\hat{a}_{j,\sigma} + H.C.) \\
+J[(\hat{a}_{i,-\sigma}^{\dagger}\hat{a}_{i,\sigma}\hat{S}_i^+ + \hat{a}_{i,\sigma}^{\dagger}\hat{a}_{i,-\sigma}\hat{S}_i^-) + (\hat{a}_{i,\sigma}^{\dagger}\hat{a}_{i,\sigma} - \hat{a}_{i,-\sigma}^{\dagger}\hat{a}_{i,-\sigma})\hat{S}_i^z]
\end{aligned}
\tag{37}
$$

There also exist molecular systems involving transition metal phthalocyanine complexes which behave like Kondo chains away from half-filling[109]. The conducting electrons reside in the π-subsystem while the spins are localized on the transition metal ions. The band-filling of the conduction band is controlled by using varying composition of bromine which acts as an oxidizing agent.

The Kondo-lattice Hamiltonian conserves total spin and being an interacting model is nontrivial to solve. However, as with the conjugated systems, it is possible to solve finite Kondo chains efficiently by employing the VB method. The VB

basis now requires three bits per site: two for the fermionic subsystem and one for the subsystem spanned by the localized spins, assumed to be spin-1/2 objects. It is straightforward to obtain rules for operating by individual terms on the Kondo chain VB diagrams, necessary to set up the Hamiltonian matrix[110]. The VB studies on Kondo chains show that the spin quenching of the site spins by the conduction electrons occurs for any finite J/t. Introduction of electron correlations in the conduction band promotes singlet pairing by increasing the probability for single occupancy of the conduction orbital.

The VB basis can also be constructed using Rumer-Pauling rules for systems in which the on-site spin is greater than 1/2 and there is on-site spin-spin interaction between singly occupied itinerant orbitals on the site and the site spin. This situation arises in manganites which exhibit giant magnetoresistance[111]. High-spin sites are also encountered in the study of Haldane gap in integer and half-odd integer spin chains[112].

We can extend the VB rules to spin clusters containing sites with different spins. If the spin at a site is s_i, then we replace this site by a set of $2s_i$ sites, each with spin-half. We then proceed with constructing the VB basis[113, 114], as though the system is made up entirely of spin-half objects, with one difference, namely, we impose the additional constraint that there should be no singlet lines within the subset of $2s_i$ sites which replace the spin s_i at site i. The VB diagrams with total spin $S \geq 1/2$ are constructed as before with the help of phantom sites. Some examples of the legal VB diagrams involving higher site spins are shown in Fig. 9. While computing properties such as spin densities and spin-spin correlations, the VB diagrams can be expanded in the constant M_S basis using appropriate Clebsch-Gordon coefficients.

We see that additional orbitals or spins can readily be introduced in quantum cell models. The real constraint is the total number of orbitals, which governs the

exponential growth of the many-electron basis as discussed in Section 2. What distinguishes one situation from another is the model that is employed. In models which employ the ZDO approximation, the VB basis is diagonal in the interaction part and the Hamiltonian is sparse. In cases where the VB basis is off-diagonal in the interaction part, or the noninteracting part involves electron transfer between nonsequential orbitals in the VB diagram, the sparseness of the matrix reduces dramatically and this could decide the size of the problem that can be managed.
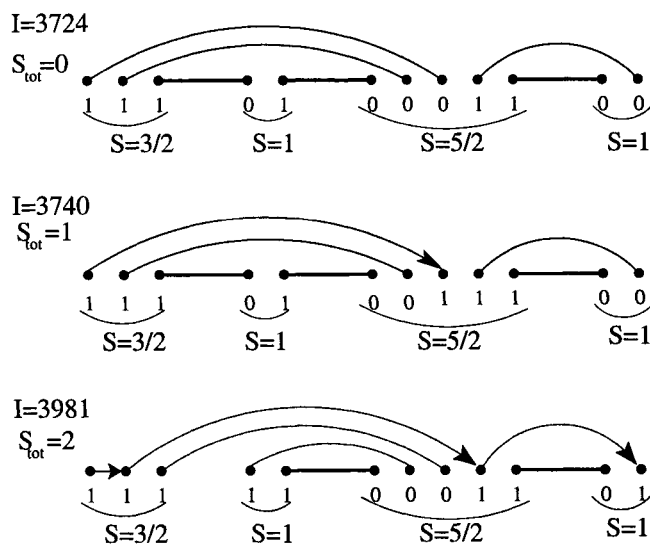
Figure 9: VB diagrams for site spins $> 1/2$. The four site system has site spins of $3/2$, 1, $5/2$ and 1. The VB diagrams and their bit-representation are for three different total spins ($S_{tot} = 0$, 1, and 2).

9 Ferromagnetism in Organic Systems

One of the challenges for organic chemistry is the synthesis of a fully organic ferromagnet. Several models of conjugated organic systems have been proposed in which the high-spin state of the conjugated system is expected to be the ground state. McConnell proposed two early schemes[115, 116]. In one he suggested that the existence of a high-spin virtual state below a low-spin virtual state would stabilize the high-spin ground state resulting in an effective exchange constant which is ferromagnetic[115] (Fig. 10). In the other, ferromagnetic exchange involved stacking
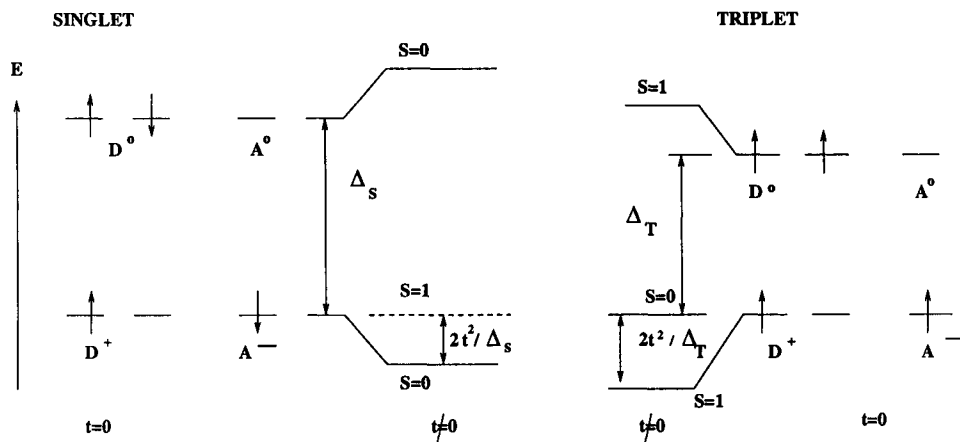
Figure 10: McConnell's mechanism for ferromagnetic exchange between ion-radicals[115]. Δ_T is less than Δ_S because of direct exchange involving the degenerate donor orbitals. This results in greater stabilization of the lowest triplet state compared to lowest singlet state upon turning on electron transfer between the donor and acceptor orbitals.

organic radicals such that negative spin density sites are directly above those of the positive spin density sites[116]. Such stacking allows delocalization of the electrons via the intervening singlet bonds while retaining parallel alignment of the spins on the radical. Mataga[117] proposed several alternant conjugated structures (Fig. 11) in which the nonbonding MOs are nondisjoint. In this situation, introducing electron

correlations results in parallel alignment of spins in the nonbonding MOs as this
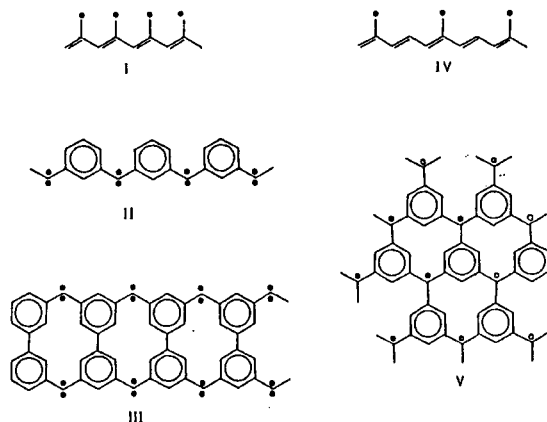
Figure 11: Examples of Mataga[117] systems involving radicals and diradicals expected to be in the high-spin ground state.

would avoid two electrons coming together on the same site. Ovchinnikov[118] also suggested alternant systems in which the number of starred and unstarred sites are unequal. Antiferromagnetic exchange interactions along the bonds leads to a spin arrangement which is reminiscent of ferrimagnetism in solids. The spin in the ground state of such a system is $S_G = |N_o - N_*|/2$, where N_o and N_* are the number of unstarred and starred sites in the alternant system.

The above models are based on physical insights gained from analysis of typically two site problems under simplified assumptions. To provide a quantitative basis for these models, it becomes necessary to deal with larger and more realistic systems. In this context, VB method becomes an invaluable tool, being a spin adapted method. Exact solution of large model systems afforded by the VB method allows introducing parameters that make the models more realistic.

We have studied McConnell's kinetic exchange mechanism by dealing with a one-

dimensional mixed stack of donors and acceptors[119], with the active donor orbital being doubly degenerate while the active acceptor orbital is nondegenerate. The noninteracting ground state of a donor-acceptor dimer would correspond to their ion-radicals D^+A^-. The direct exchange interaction among the degenerate donor orbitals implies that virtual triplet intermediate state corresponding to D^0A^0 would be lower in energy compared to the corresponding singlet state. The Hamiltonian which captures the essentials of the model thus involves besides the Hubbard and site energy parameters for the donors and acceptors U_D, ϵ_D, U_A, ϵ_A, the direct exchange integral for the degenerate donor orbitals K_D as well as the repulsion between electrons in separate donor orbitals on the same site, U_{DD}. The magnitude of U_{DD} is comparable to U_D and it is not necessary to treat it as an additional parameter. In the mixed stack, the transfer parameters connect the donor orbitals to the acceptor orbital on the neighboring sites. Hitherto, the interaction part of the model Hamiltonians we encountered were diagonal in the real space VB basis. The direct exchange term associated with K_D leads to off-diagonal terms resulting from two types of processes; (i) a double hop of electrons from one donor orbital to the other and (ii) a hop from one donor orbital to the other followed by a reverse hop. These terms can be easily handled within the VB framework.

The VB calculations of the model described above on two, three and four DA units leads to some interesting conclusions[119]. When all the Hubbard on-site correlations are taken to be equal $U_A = U_D = U_{DD}$ then, for weak ($U/t \leq 2$, $K_D/t \leq 0.4$), the ground state is low-spin state in all the cases. For ($2 < U/t \leq 6$, $K_D/t \leq 0.4$), the ground state is an intermediate spin state and for the high-spin state to be the ground state, the on-site correlations have to be very strong ($U/t > 10$). We also find that as the system size increases, stronger on-site repulsion is required for stabilizing the high-spin state relative to the low-spin state. It can be argued that with increase in system size, the phase space for singlet delocalization increases more rapidly than that of the high-spin state, with $S = N$, where N is the number of DA units. When we vary U_{DD}/t independently, we find that the high-spin state is favored for smaller values of U_{DD}/t, since this favors single occupancy of the

doubly degenerate orbitals over an empty and a doubly occupied degenerate donor orbital configuration.

The Mataga-Ovchinnikov systems can also be modeled using quantum cell models. The prediction of the high-spin ground state in these systems revolves around a few idealizations such as uniform bond lengths and identical carbon site energies implied by electron-hole symmetry. What is important from a practical standpoint is the stability of the high spin ground state when these symmetries are broken. VB theory is well suited for such studies[37]. Numerically also, it is seen that the state with spin S_G is the ground state in the idealized cases. The lowest excitation is to the state with spin $S_G - 1$ and the gap extrapolates to zero in the thermodynamic limit. The excitation gap between the ground state and the lowest energy state with spin $S_G + 1$ remains finite in the thermodynamic limit and so does the gap between the ground state and the nonmagnetic state with spin $S = 0$. For Hubbard models, the magnetic gap peaks near $U/t = 4$. Electron-hole symmetry is broken by introducing different nonzero site energies at the dangling carbon sites and the nodal carbon sites. Even when the site energy difference between these sites is a few eV, the magnetic gap hardly changes. The Mataga-Ovchinnikov systems are stable with respect to electron-hole symmetry breaking. It is also observed that the bond orders vary substantially from the uniform limit. When the transfer integrals for the bonds are changed so that the computed bond-orders are in the same ratio as the transfer parameters, the nonmagnetic state becomes the ground state for larger system sizes. Thus, it is unlikely (at least in quasi-one-dimensional systems which are more prone to lattice distortions), that in real systems one would succeed in synthesizing a ferromagnet or ferrimagnet based on the Mataga polymers.

Substituted cyclophanes are the simplest systems in which opposite pin densities are stacked at sites directly above each. The spin resonance of several cyclophanes have been studied to test the McConnell[120] idea. Introducing a dicarbene substitution at each of the phenyl rings leads to unpaired electrons in the molecule. Following McConnell, we should expect the carbene spins to be aligned parallel if the substi-

tution is pseudo-ortho or pseudo-para. The ground state will be nonmagnetic, if the substitution is pseudo-meta. This system can be easily modeled using quantum cell models. Indeed, one obtains a robust quintet ground state for pseudo-ortho and pseudo-para isomers and a singlet ground state for the pseudo-meta isomer[121]. The exchange interactions between nonbonded sites governs the magnetic gap and this could be rather small in organic systems. Thus, while this model does have a robust magnetic ground state we should expect the Curie temperature for magnets based on this mechanism to be rather low.

10   Concluding remarks

Quantum cell models are idealizations that capture some fundamental features of molecular, polymeric or solid-state systems at a phenomenological level. While quantitative descriptions are occasionally realized, models are typically semiquantitative and aim at understanding large or extended systems. We have shown that Hubbard, Pariser-Parr-Pople, Heisenberg models and their variants are widely used in chemistry and physics for diverse magnetic, optical and electrical properties. Most current models conserve total spin, except for anisotropic spin systems. The valence bond basis then provides an attractive and efficient real-space representation of correlated many-electron states. We have summarized VB procedures and applications that over the past two decades have yielded model-exact solutions to quantum cell models, including dynamic responses and matrix elements between correlated states. Modern workstations can now handle, in a matter of hours, systems of 30 spins or 16-18 electrons or an intermediate number of sites in models with three states per site. Exact analysis of large active spaces avoids entirely difficulties encountered in conventional single-particle schemes, but introduces finite-size considerations that can be problematic. The VB method is limited by the basis set size which is dictated by the number of active orbitals or sites. Given this, the number of unit cells with a few orbitals per site that can be treated exactly is larger in one dimension than in higher dimensions. Thus, it is no accident that we have focused on conju-

gated polymers, on polyenes, annulenes, and polycyclic hydrocarbons, on CT and ion-radical solids with one-dimensional stacks, and on spin chains. Linear systems and low-lying states are the simplest to extrapolate. They have considerable scope, as we have illustrated in this review.

Simply by changing hopping integrals or correlations, we can apply quantum cell models such as (3) or (4) to entirely different kinds of systems or phenomena and make contact with exact results for extended systems. Models provide a unification that is both pleasing and important, and that for many purposes outweighs their approximate nature. Solid-state models have in fact become objects of extensive research in several fields, notably in statistical physics, and this will continue in the future. In a wider context, we have classical and quantum models, discrete and continuum models, and many other possibilities than the mainly electronic models considered here. We anticipate improvements in VB methodology along with greater computational power. Model-exact results provide calibration for approximations such as the quantum Monte Carlo or the DMRG methods that can be applied to larger systems and should remain one of the tools for investigating correlated electronic or spin systems.

References

[1] A.J. Heeger, S. Kivelson, J.R. Schrieffer and W.P. Su, Rev. Mod. Phys. **60**, 781 (1988).

[2] T.A. Skotheim, (Ed.) *Handbook of Conducting Polymers*, (Marcel Dekker, New York, 1986) Vols. 1 and 2.

[3] L. Salem, *The Molecular Orbital Theory of Conjugated Systems*, (Benjamin, New York, 1966).

[4] R. Pariser and R.G. Parr, J. Chem. Phys. **21**, 767 (1953); J.A. Pople, Trans. Faraday Soc. **42**, 1375 (1953).

[5] J. Hubbard, Proc. Phys. Soc. Lond. **A276**, 238 (1963); **A277**, 237 (1964); **A281**, 401 (1964); M. C. Gutzwiller, Phys. Rev. **A134**, 993 (1964).

[6] Z.G. Soos and S. Ramasesha, Phys. Rev. **B29**, 5410 (1984).

[7] K. Ohno, Theor. Chim. Acta **2**, 219 (1964).

[8] N. Mataga and K. Nishimoto, Z. Physik Chem. (Frankfurt) **13**, 140 (1957).

[9] D. Baeriswyl, D. K. Campbell and S. Mazumdar, in *Conjugated Conducting Polymers*, H. G. Kiess (Ed.), (Springer, Berlin 1992); Y. Anusooya, B. Srinivasan and S. Ramasesha, in *Strongly Correlated Electron Systems in Chemistry*, S. Ramasesha and D. D. Sarma (Eds.), (Narosa Publishing House, New Delhi, 1996) p. 67.

[10] Z.G. Soos and G.W. Hayden, in *Electroresponsive Polymeric Systems* T.A. Skotheim, (Ed.) (Marcel Dekker, New York, 1988) p.197; S. Etemad and Z.G. Soos, in *Advances in Spectroscopy: Spectroscopy of Advanced Materials*, R.J.H. Clark and R.E. Hester (Eds.), (Wiley, New York, 1991) p. 87.

[11] Z.G. Soos and D.J. Klein, in *Molecular Association*, R. Foster, (Ed.) (Academic, London, 1975), p. 1.

[12] S. Mazumdar and Z.G. Soos, Synthetic Metals **1**, 77 (1979).

[13] Z.G. Soos and S. Ramasesha, in *Valence Bond Theory and Chemical Structure*, D.J. Klein and N. Trinajstic, (Eds.) (Elsevier, Amsterdam 1989), p. 81.

[14] T. A. Skotheim, R. Elsenbaumer and J.R. Reynolds, (Eds.) *Handbook of Conducting Polymers*, 2nd Ed. (Marcel Dekker, New York, 1997).

[15] P.O. Löwdin, Rev. Mod. Phys. **36**, 966 (1964).

[16] R. Pauncz, *Spin Eigenfunctions: Construction and Use*, (Plenum, New York 1979); W. Duch and J. Karwowski, Comput. Phys. Rep., **2**, 93 (1985).

[17] J. Paldus, J. Chem. Phys., **61**, 5321 (1964); B. R. Brooks and H. H. Schaefer, *ibid*, **70**, 5092 (1979); M. A. Robb and U. Niazi, Comput. Phys. Rep., **1**, 127 (1984).

[18] S. Ramasesha and Z.G. Soos, J. Chem. Phys. **98**, 4015 (1993).

[19] G. Rumer, Gottingen Nachrich. Tech. 377 (1932).

[20] B. Srinivasan and S. Ramasesha, Solid State Commun., **81**, 831 (1992).

[21] G. Wen and Z.G. Soos, J. Chem. Phys. **108**, 2486 (1998).

[22] A.D. McLachlan, Mol. Phys. **2**, 276 (1959); O.J. Heilmann and E.H. Lieb, Trans. N.Y. Acad. Sci. Ser. II **33**, 116 (1971); S.R. Bondeson and Z.G. Soos, J. Chem. Phys. **71**, 3807 (1979); **73**, 598 (1980).

[23] M. Pope and C.E. Swenberg, *Electronic Processes in Organic Crystals* (Clarendon, Oxford, 1982); E.A. Silinsh and V. Capek, *Organic Molecular Crystals: Interaction, Localization and Transport Phenomena* (Am. Inst. Phys., New York, 1994).

[24] J. H. Burroughes, D. D. C. Bradley, A. R. Brown, R. N. Marks, K. Mackay, R. H. Friend, P. L. Burns, and A. B. Holmes, Nature, **347**, 539 (1990).

[25] D. Bloor and R. Chance, (Eds.) *Polydiacetylenes*, NATO ASI Series E012, (Martinus Najhoff, Dordrecht, The Netherlands, 1985); D.J. Sandman, (Ed.) *Crystallographically Ordered Polymers*, ACS Symposium Series 337 (ACS, Washington, D.C. 1987).

[26] B. Srinivasan and S. Ramasesha, Solid State Commun., **81**, 831 (1992).

[27] L. Pauling, J. Chem. Phys. **1**, 180 (1933); L. Pauling and G. W. Wheland, *ibid*, 362 (1933).

[28] S. R. Bondeson and Z. G. Soos Phys. Rev. **B 22**, 1793 (1980).

[29] S. Rettrup, J. Comput. Phys. **45**, 100 (1982).

[30] E.R. Davidson, J. Comput. Phys. **17**, 87 (1975).

[31] S. Ramasesha and Z.G. Soos, Intern. J. Quant. Chem., **XXV**, 1003 (1984).

[32] K. Das and S. Ramasesha, Solid State Commun., **66**, 1047 (1988); I.D.L. Albert and S. Ramasesha, Phys. Rev. **B40**, 8516 (1989); S. Ramasesha and I.D.L. Albert, Phys. Rev. **B42**, 8587 (1990); I.D.L. Albert, P.K. Das and S. Ramasesha, Chem. Phys. Letts., **176**, 217 (1991).

[33] S. Ramasesha and Z.G. Soos, J. Chem. Phys. **80**, 3278 (1984).

[34] Z.G. Soos and S. Ramashesha, Phys. Rev. Letters **51**, 2374 (1983).

[35] S. Ramasesha and Z.G. Soos, Chem. Phys. **91**, 35 (1984).

[36] S. Ramasesha and K. Das, Chem. Phys. Letts., **138**, 462 (1987).

[37] S. Ramasesha, I.D.L. Albert and B. Sinha, Mol. Phys., **72**, 537 (1991)

[38] J.F. Ward, Rev. Mod. Phys. **37**, 1 (1965); B.J. Orr and J. F. Ward, Mol. Phys. **20**, 513 (1971); D.C. Hanna, M.A. Yuratich and D. Cotter, *Nonlinear Optics of Free Atoms and Molecules*, (Springer, Berlin, 1979); S.P. Karna and A.T. Yeates,

Eds. *Nonlinear Optical Materials: Theory and Modeling*, (American Chemical Society, Washington, D.C., 1994)

[39] H. H. Roomany and H. W. Wyld, Phys. Rev. **D21**, 3341 (1980); E. Dagotto, Rev. Mod. Phys. **66**, 763 (1994).

[40] Z.G. Soos and S. Ramasesha, J. Chem. Phys. **90**, 1067 (1989).

[41] P.W. Langhoff, S.T. Epstein and M. Karplus, Rev. Mod. Phys. **44**, (1972).

[42] J.R. Heflin, K.Y. Wong, O. Zamani-Khamari and A.F. Garito, Phys. Rev. **B38**, 1573 (1988); S.N. Dixit and S. Mazumdar, Phys. Rev. **B43**, 6781 (1991); P.C.M. McWilliams, G.W. Hayden and Z.G. Soos, Phys. Rev. **B43**, 9777 (1991).

[43] Z.G. Soos, D. Mukhopadhyay, A. Painelli and A. Girlando, in ref. 15, p. 165.

[44] S. Ramasesha, Z. Shuai and J.L. Brédas, Chem. Phys. Letts., **245**, 224 (1995); S.K. Pati, S. Ramasesha, Z. Shuai and J. L. Bredas, Phys. Rev. **B59**, 14827 (1999).

[45] S. Kuwajima and Z.G. Soos, J. Amer. Chem. Soc. **109**, 107 (1987).

[46] Y. Anusooya, A. Chakrabarti, S. K. Pati and S. Ramasesha, Intern. J. Quant. Chem. **70**, 503 (1998).

[47] Z.G. Soos Y. A. Pati and S.K. Pati, J. Chem. Phys. **112**, 3133 (2000).

[48] S. Ramasesha, J. Comput. Chem., **11**, 545 (1990); S.K. Pati, S. Ramasesha, Z. Shuai and J. L. Bredas, Phys. Rev. **B59**, 14827 (1999).

[49] C.A. Hutchison and B.W. Mangum, Chem. Phys. **34**, 908 (1961).

[50] D.S. McClure, Chem. Phys. **22**, 1668 (1954); J. Wessel and D.S. McClure, Mol. Cryst. Liq. Cryst. **58**, 121 (1980).

[51] H.B. Klevens and J.R. Platt, Chem. Phys. **17**, 470 (1949).

[52] P.R. Salvi, P. Foggi and E Castelucci, Chem, Phys. Lett. **98**, 206 (1983).

[53] J.B. Birks, Ed. *Organic Molecular Photophysics*, (Wiley, London, 1973), Vol. 1, p. 13.

[54] S. Ramasesha, D.S. Galváo and Z.G. Soos, J. Phys. Chem. **97**, 2823 (1993).

[55] Z.G. Soos, S. Ramasesha, D.S. Galváo, and S. Etemad, Phys. Rev. **B47**, 1742 (1993).

[56] G.N. Lewis and M. Kasha, J. Amer. Chem. Soc., **66**, 2100 (1944).

[57] K.L. D'Amico, C. Manos and R.L. Christensen, J. Amer. Chem. Soc. **102**, 1777 (1980).

[58] B.E. Kohler, C. Spangler and C. Westerfield, J. Chem. Phys. **89**, 5422 (1988).

[59] F. London, J. Phys. Radium **8**, 397-409 (1937).

[60] K. Müllen, W. Huber, T. Meul, M. Nakagawa and M. Iyoda, J. Amer. Chem. Soc. **104**, 5403 (1982).

[61] D. B. Chesnut, Reviews in Computational Chemistry 8, 245 (1996); Chem. Phys. **231**, 1 (1998); P.v.R. Schleyer, C. Maerker, A. Dransfeld, H. Jiao and N.J.R. van Eikema Hommes, J. Amer. Chem. Soc. **118**, 6317 (1996); M. Bilde and A. E. Hansen, Mol. Phys. 92, 237 (1997).

[62] W. Kohn, Phys. Rev. **133**, A171 (1964).

[63] B.S. Shastry and B. Sutherland, Phys. Rev. Lett. **65**, 243 (1990).

[64] H.C. Longuet-Higgins and L. Salem, Proc. Roy. Soc. Lond. **A251**, 172 (1959).

[65] R.E. Peierls, *Quantum Theory of Solids*, (Clarendon, Oxford, 1955), p.108.

[66] C.H. Choi and M. Kertesz, J. Chem. Phys. **108**, 6681 (1998).

[67] G. Horowitz, Advanced Mat. **10**, 365 (1998).

[68] S.R. Forrest, Chem. Rev. **97**, 1793 (1997).

[69] J.H. Schon, C. Kloc and A. Dodabalapur, Science **289**, 599 (2000); J.H. Schon, C. Kloc and B. Batlogg, Science **288**, 2338 (2000).

[70] W.P. Su, J.R. Schrieffer and A.J. Heeger, Phys. Rev. Lett. **44**, 1698 (1979); Phys. Rev. **B22**, 2099 (1980).

[71] N.S. Sariciftci, (Ed.) *Primary Photoexcitations in Conjugated Polymers: Molecular Exciton versus Semincoductor Band Model* (World Scientific, Singapore, 1997) and references therein.

[72] E.H. Lieb and F.Y. Wu, Phys. Rev. Lett. **25**, 1445 (1968); A.A. Ovchinnikov, Sov. Phys. JETP **30**, 1160 (1970).

[73] Z.G. Soos, D.S. Galváo, and S. Etemad, Advanced Mat. **6**, 280 (1994).

[74] R.G. Kepler and Z.G. Soos, in *Relaxation in Polymers*, T. Kobayashi, (Ed.) (World Scientific, Singapore, 1994), p. 100.

[75] Z.G. Soos, S. Etemad, D.S. Galváo, and S. Ramasesha, Chem. Phys. Lett. **194**, 341 (1992).

[76] Z.G. Soos, S. Ramasesha, and D.S. Galváo, Phys. Rev. Lett. **71**, 1609 (1993).

[77] D. Mukhopadhyay, G.W. Hayden, and Z.G. Soos, Phys. Rev. **B51**, 9476 (1995).

[78] B.S. Hudson and B.E. Kohler, Ann. Rev. Phys. Chem. **25**, 437 (1974).

[79] Z.G. Soos, Mol. Cryst. Liq. Cryst. **256**, 35 (1994); Z.G. Soos, D.S. Galváo and S. Etemad, in *Advanced Photonic Materials for Information Technology*, S. Etemad, (Ed.) (SPIE Proceedings 2144, 1994), p. 115.

[80] A. Girlando, A. Painelli, G.W. Hayden, and Z.G. Soos, Chem. Phys. **184**, 139 (1994); Z.G. Soos, G.W. Hayden, A. Girlando and A. Painelli, J. Chem. Phys. **100**, 7144 (1994).

694

[81] M. Gussoni, C. Castiglioni and G. Zerbi, in *Advances in Spectroscopy: Spectroscopy of Advanced Materials*, R.J.H. Clark and R.E. Hester, (Eds.), (Wiley, New York, 1991) p. 251.

[82] B. Horovitz, Solid State Comm. **41**, 729 (1982); E. Ehrenfreund, Z. Vardeny, O. Brafman and B. Horovitz, Phys. Rev. **B36**, 1533 (1988).

[83] A. Painelli, A. Girlando, L. Del Freo, and Z. G. Soos Phys. Rev. B 56, 15100-15108 (1997).

[84] Z.G. Soos and D. Mukhopadhyay, J. Chem. Phys. **101**, 5155 (1994); D. Mukhopadhyay and Z.G. Soos, ibid. **104**, 1600 (1996).

[85] M. Baumgarten, S. Karabunarliev, K.H. Koch, K. Müllen and N. Tyutyulkov, Synth. Met. **47**, 21 (1992); J.L. Bredas and R.H. Baughman, J. Chem. Phys. **83**, 1316 (1984).

[86] Z.G. Soos, M.H. Hennessy, and G. Wen, Chem. Phys. Lett. **274**, 189 (1997); Chem. Phys. **227**, 19 (1998).

[87] E. Clar, *Polycyclic Hydrocarbons*, (Academic, London, 1964) Vol. 2.

[88] K.H. Koch and K. Müllen, Chem. Ber. **124**, 2091 (1991).

[89] D. Jerome and L. G. Caron (Eds.), *Low Dimensional Conductors and Superconductors*, NATO Advanced Study Institute, Series B, Vol. 155, (Plenum, New York 1987); J.T. Devreese (Ed.), *Highly Conducting One-Dimensional Solids*, (Plenum, New York/London 1979); G. Grüner, *Density Waves in Solids* (Addison-Wesley, London, 1994)

[90] J. M. Williams, J. R. Ferraro, R. J. Thorn, K. D. Carlson, U. Geiser, H. H. Wang, A. M. Kini, and M.-H. Whangbo, *Organic Superconductors* (Prentice-Hall, Englewood Cliffs, NJ, 1992); H.S. Nalwa (Ed.),*Organic Conductive Molecules and Polymers* (Wiley, Chichester, NY, 1997); H. Tanaka, A. Kobayashi, T. Saito, K. Kawano, T. Naito, and H. Kobayashi, Adv. Mater. **8**, 812 (1996).

[91] Z.G. Soos and S.R. Bondeson, in *Extended Linear Chain Compounds*, J.S. Miller, (Ed.) (Plenum, New York, 1983), Vol. III p. 193.

[92] J. B. Torrance, A. Girlando, J. J. Mayerle, J. I. Crowley, V. Y. Lee, P. Batail, and S. J. LaPlaca, Phys. Rev. Lett. 47, 1747-1750 (1981); J.B. Torrance, J.E. Vazquez, J.J. Mayerle and V.Y. Lee, Phys. Rev. Lett. **46**, 253 (1981); K. Nasu, (Ed.), *Relaxations of Excited States and Photo-Induced Structural Phase Transitions*, Springer series in Solid-State Sciences 124 (Springer-Verlag, Heidelberg, 1997).

[93] Y. A. Pati, Z.G. Soos and A. Painelli, Phys. Rev. **B63**, 205118 (2001)

[94] H.M. McConnell, B.M. Hoffman and R.M. Metzger, Proc. Natl. Acad. Sci. US, **53**, 46 (1965); P. L. Nordio, Z.G. Soos, and H.M. McConnell, Ann. Rev. Phys. Chem. **17**, 237 (1966).

[95] P.J. Strebel and Z.G. Soos, J. Chem. Phys. **53**, 4077 (1970).

[96] Z.G. Soos, S. Kuwajima and R.H. Harding, J. Chem. Phys. **87**, 1705 (1986).

[97] A. Painelli and A. Girlando, Phys. Rev. **B37**, 5748 (1988); *ibid* **B39**, 9663 (1989); *ibid* Phys. Rev. B63, 205118 (2001).

[98] N. Nagaosa and J. Takimoto, J. Phys. Soc. Japan **55**, 2737, 2747 (1986); N. Nagaosa, ibid. **55**, 2756 (1986)

[99] M. Avignon, C. A. Balseiro, C. R. Proetto, and B. Alascio, Phys. Rev. **B33**, 205 (1986); E.R. Gagliano, C.A. Balseiro and B. Alascio, Phys. Rev. **B37**, 5697 (1988).

[100] Z.G. Soos and S. Mazumdar, Phys. Rev. **B18**, 1991 (1978).

[101] T. Egami, S. Ishihara and M. Tachiki, Science **261**, 1307 (1993); T. Egami and M. Tachiki, Phys. Rev. **B49**, 8944 (1994); R. Resta and S. Sorella, Phys. Rev. Lett. **74**, 4738 (1995); ibid. **82**, 370 (1999).

[102] A. Girlando and A. Painelli, Phys. Rev. **B34**, 2131 (1986)

[103] Z.G. Soos, S.R. Bondeson, and S. Mazumdar, Chem. Phys. Letters **65**, 331 (1979).

[104] A. M. Clogston, B. T. Mathias, M. Peter, H. J. Williams E. Corenzwit, and R. C. Sherwood, Phys. Rev. **125**, 541 (1962).

[105] A. J. Heeger, Solid State Phys. **23**, 283 (1969).

[106] P. W. Anderson, Phys. Rev., **124**, 41 (1961).

[107] J. R. Schrieffer and P. A. Wolf, Phys. Rev. **149**, 491 (1966).

[108] J. Kondo, Progr. Theor. Phys. **28**, 846 (1962); *ibid*, **32**, 37 (1964); J. Kondo, J. Solid State Phys., **23**, 183 (1969).

[109] M. Y. Ogawa, J. Martinsen, S. M. Palmer, J. L. Stanton, J. Tanaka, R. L. Greene, B. M. Hoffman, and J. A. Ibers, J. Am. Chem. Soc., **109**, 1115 (1987).

[110] S. Ramasesha and K. Das, Phys. Rev. **B42**, 10682 (1990).

[111] J. Inoue and S. Maekawa, Phys. Rev. Lett. **74**, 3407 (1995).

[112] F.D.M. Haldane, Phys. Lett. **A93**, 464(1983).

[113] K. Chang, I. Affleck, G.W. Hayden, and Z.G. Soos, J. Phys: Condens. Matter **1**, 153 (1989).

[114] S.K. Pati, S. Ramasesha and D. Sen, Phys. Rev. **B55**, 8894 (1997);C. Raghu, I. Rudra, S. Ramasesha and D. Sen, Phys. Rev. **B62** 9484 (2000); *ibid* (in press).

[115] H.M. McConnell, Proceedings of the Robert A. Welch Foundation Conference on Chemical Research, **11**, 144 (1967).

[116] H.M. McConnell, J. Chem. Phys., **39**, 1910 (1963).

[117] N. Mataga, Theor. Chim. Acta, **10**, 372 (1968).

[118] A.A. Ovchinnikov, Theor. Chim. Acta, **47**, 297 (1978).

[119] B. Sinha and S. Ramasesha, Phys. Rev. **B48**, 16410 (1993).

[120] A. Izuoka, S. Murata, T. Sugawara and H. Iwamura, J. Am. Chem. Soc., **107**, 1786 (1985); Y. Teki and K. Itoh in *Magnetic Properties of Organic Materials*, P.M. Lahti (Ed.) (Marcel Dekker, New York, 1999) Ch. 12.

[121] B. Sinha and S. Ramasesha, Chem. Phys. Letts., **182**, 180 (1991).

This Page Intentionally Left Blank

Chapter 21

Spin permutation technique in the theory of strongly correlated electron systems

V.O.Cheranovskii

Institute of Chemistry, Kharkov National University 61077 Kharkov, The Ukraine

1. INTRODUCTION

The theoretical description of electron correlations in the strong coupling regime is a long standing problem. This is of great importance for adequate study of electron properties of quasi-1D systems like organic polymers with conjugated bonds and stacked charge-transfer salts (e.g. tetracyanquinodimethane complexes) [1-4]. The unexpected discovery of high-temperature superconductivity in lightly doped antiferromagnets (cuprate oxides) has sparked renewed interest in the theory of strongly correlated electron systems. Many scientists believe that the Hubbard model with strong electron repulsion already contains at least some of the important physics governing the properties of high-T_c materials [5,6]. Unfortunately, there are only a few exact solutions for the theoretical models used to describe the above systems [7]. Therefore the corresponding description is rather incomplete even in the zero temperature case and there are many unsolved important physical questions despite the huge number of different theoretical approaches that have been applied.

One of the simplest models describing a system of strongly correlated electrons on a crystal lattice is the Hubbard Hamiltonian [8]:

$$\mathbf{H} = \sum_{i,j,\sigma} t_{ij}(\mathbf{a}_{i\sigma}^+ \mathbf{a}_{j\sigma} + \mathbf{a}_{j\sigma}^+ \mathbf{a}_{i\sigma}) + U \sum_i \mathbf{a}_{i\sigma}^+ \mathbf{a}_{i\sigma} \mathbf{a}_{i-\sigma}^+ \mathbf{a}_{i-\sigma} \qquad (1)$$

where t_{ij} is a matrix element of the electron transfer between the states of i-th and j-th sites, U is the one-site repulsive potential as a simple approximation to the Coulomb interaction between the electrons, $\mathbf{a}_{i\sigma}^+$ is a creation operator for an electron with spin σ on the i-th site.

At infinite electron repulsion, if the total numbers of electrons and lattice sites are coincident (half-filled band), each site is occupied by one electron only.

Thus no hopping processes are allowed and the ground state energy is highly degenerate and independent of the orientation of the individual spins. For $U \gg \max(t_{ij})$, as in the case of compounds of transition metals, perturbation theory (PT) can be applied and in the second PT order in t_{ij} the Hamiltonian (1) is reduced to a Heisenberg spin Hamiltonian [9] which is formally identical to the covalent-space Pauling-Wheland VB model [10,11].

$$\mathbf{H} = \sum_{i<J} J_{ij} \mathbf{S}_i \cdot \mathbf{S}_j, \quad J_{ij} = \frac{4t_{ij}^2}{U} \geq 0 \tag{2}$$

where $\mathbf{S}_i$ is the one-electron spin operator and J_{ij} is an exchange parameter. Note, that the Hamiltonian (2) can be written in terms of permutations of spin variables $\mathbf{P}_{ij}$ if the Dirac identity $\mathbf{P}_{ij} = 2\mathbf{S}_i \cdot \mathbf{S}_j + 1/2$ is taken into account. If $U \sim \max(t_{ij})$, as in the case of conjugated hydrocarbons, higher order PT terms and convergence of the perturbation expansion should be considered. The corresponding generalized effective VB Hamiltonian acting in covalent space contains renormalized exchange parameters and additional terms having a form of products of transposition permutations $\mathbf{P}_{ij}$ [12-15]. For lattice systems, which contain even member rings, the most important additional terms can be expressed in the form of cyclic permutations of spin variables. Covalent VB Hamiltonians with additional cyclic spin permutations were successfully applied to the study of the aromaticity problem [13,16].

The dimensionality of the space spanned by covalent states is much less than the full number of basis states of the Hubbard model. This is one of the reasons of the success in the application of the above VB Hamiltonians to the study of low-lying energy levels of the transition metal compounds and organic molecules with conjugated bonds. The covalent VB approach is very useful especially for predictions as to ground state spin multiplicity and spin ordering [14, 17-20].

For strongly correlated electron systems with non half-filled bands there are electron hops between occupied and unoccupied lattice sites. In the general case these hops lift spin degeneracy in first PT order in t_{ij}. This leads to more complicated structures of perturbative Hamiltonians in comparison with the half-filled case. One of the simplest representatives of such Hamiltonians is a well-known t-J model for a one-dimensional lattice [21]. Nevertheless in certain cases it is possible to reduce the initial Hubbard model to a spin model and carry out the study of low-lying energy states similarly to the covalent case [22-26].

The purpose of these notes is to show how some strongly correlated electron models like the one-band Hubbard model with infinite electron repulsion on rectangular and triangular lattices can be described in terms of spinless fermions and the operators of cyclic spin permutations. We will consider in detail the

properties of corresponding effective Hamiltonians. Special attention will be paid to the description of the ground state spin and lowest excitations of the lattices formed by weakly interacting segments (e.g. ladder compounds). Because of quasi-degenerate energy spectra of these lattices, approximate methods can give inaccurate conclusions about their ground state spin. We will show how a simple physical idea about the appearance of magnetic polarons in such systems due to competition of different types of the interactions of neighboring segments may be used for an accurate description of the dependence of the ground state spin on the Hamiltonian parameters.

2. CYCLIC SPIN PERMUTATION FORMALISM FOR HUBBARD MODEL WITH INFINITE REPULSION

The Hubbard model with infinite electron repulsion represents restricted hopping in a space with no doubly occupied sites. For the N-electron system on the lattice formed by L sites the model Hamiltonian has the form [27]

$$
\mathbf{H} = \sum_{i,\sigma} \alpha_i \, \mathbf{a}_{i\sigma}^+ \mathbf{a}_{i\sigma} (1 - \mathbf{a}_{i-\sigma}^+ \mathbf{a}_{i-\sigma})
$$
$$
+ \sum_{i,j,\sigma} t_{ij} (\mathbf{a}_{i\sigma}^+ \mathbf{a}_{j\sigma} + \mathbf{a}_{j\sigma}^+ \mathbf{a}_{i\sigma})(1 - \mathbf{a}_{i-\sigma}^+ \mathbf{a}_{i-\sigma})(1 - \mathbf{a}_{j-\sigma}^+ \mathbf{a}_{j-\sigma}) \tag{3}
$$

where α_i is the one-site energy. Because of particle-hole symmetry we may restrict our consideration to electron systems with $N \le L$. The wave function of this lattice system can be written as

$$
\Psi_r(L, N, M) = \sum_{l=1}^{D} A_l^r (n_1, n_2, \ldots, n_N | \sigma_1, \sigma_2, \ldots, \sigma_N) \prod_{i=1}^{N} a_{n,\sigma_i}^+ |0\rangle
$$
$$
= \sum_{l=1}^{D} A_l^r (n_1, n_2, \ldots, n_N | \sigma_1, \sigma_2, \ldots, \sigma_N) \Phi(n_1, n_2, \ldots, n_N) \times |\sigma_1, \sigma_2, \ldots, \sigma_N\rangle. \tag{4}
$$

$$
D = \frac{L!}{(L-N)!(N/2-M)!(N/2+M)!}
$$

Here $\Phi(n_1, n_2, \ldots, n_N)$ is a coordinate function that describes the distribution of N electrons over the L lattice sites; n_i labels the i-th singly occupied lattice site; M is the z-projection of total spin of a lattice; D is the dimensionality of the space spanned by the eigenvectors of (3); and $|\sigma_1, \sigma_2, \ldots, \sigma_N\rangle$ is a function of spin variables σ_i, describing the spin configuration of the electrons

$$
\mathbf{S}_i^z |\sigma_1, \sigma_2 \ldots \sigma_N\rangle = \sigma_i |\sigma_1, \sigma_2, \ldots, \sigma_N\rangle, \quad \sigma_i = \pm 1/2,
$$

where S_i^z is an operator of the z projection of the spin for the i-th electron.

Despite the simple algebraic structure of the model, the study of its spectrum is a complicated task. The simplest case is a linear lattice fragment with free ends (segment). Let us enumerate its electrons in succession along the segment. It is easily seen that any electron hop does not change this numeration. In other words the Hamiltonian (1) does not act on $|\sigma_1,\sigma_2,...,\sigma_N\rangle$ and we have spin degeneracy of the exact energy spectrum of the segment. If all $\alpha_i = \alpha$, $t_{ii+1} = t$ (one-site unit cell) the spectrum of the segment has a very simple structure for arbitrary values of L and N:

$$E_r(N,L) = 2t \sum_{i=1}^{N} \cos\left(\frac{\pi\, r_i}{L+1}\right) + N\alpha, \quad 1 \le r_1 < r_2 < ... < r_N \le L, \quad (5)$$

$$\Psi_r(L,N,M) = \sum_{l=1}^{D} A_l^r(n_1,n_2,...,n_N)\prod_{i=1}^{N} a_{n_i,\sigma_i}^+|0\rangle, \quad 1 \le n_1 < n_2 < ... < n_N \le L,$$

$$A_l^r(n_1,n_2,...,n_s) = \det[f(r_1 n_1)f(r_2 n_2)...f(r_s n_s)], \quad (6)$$

$$f(r_i,n_j) = \sqrt{\frac{2}{n+1}}\sin\left(\frac{\pi r_i n_j}{n+1}\right),$$

where the index r enumerates all the orderings of numbers r_i. For $t < 0$ the set of numbers $r_i = i$ corresponds to the ground state of the segment.

In the case of nonlinear lattice topology, electron hops mix different spin configurations and the corresponding eigenvalue problem becomes much more complicated. A complete analytical solution of this problem is known only for some special cases (e.g. for the linear chain with periodic boundary conditions [22]). In the absence of exact results a reliable way to describe the properties of nonlinear systems is to perform a numerical study of the electron structure for finite lattice clusters.

2.1. Rectangular lattice

Our approach to the study of the Hamiltonian (3) is based on the direct consideration of the processes of electron hopping between neighboring lattice sites with the restriction to the states without doubly occupied lattice sites [23]. Let us consider a rectangular lattice strip with 8 sites and 5 electrons and enumerate all the variables of the lattice wave function in succession along the lattice rows beginning from the upper one.

When the Hamiltonian (3) acts upon the function Ψ_r, the electrons hop to neighboring unfilled lattice sites. For example, the first electron can hop to the second site along the lattice or to the fifth site. With our enumeration over the
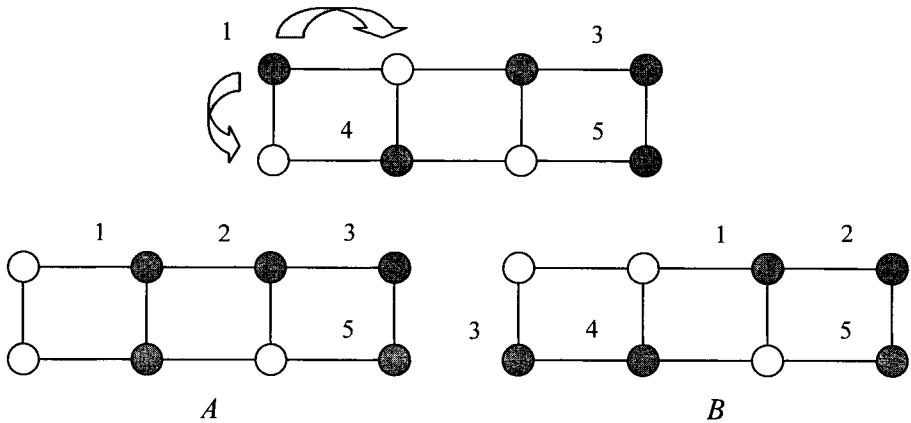
Fig. 1. Electron hopping between neighboring lattice sites (shaded sites specify the positions of electrons).

lattice rows, two new electron configurations A and B appear as a result of these processes (Fig.1). It is easily shown that all the electron numbers are fixed in the case of electron transfer between the states at the first and second sites. Therefore, this process leads to a change of the variable n_i in the coordinate function only. If the electron hops to the fifth site, the first electron becomes the third one, the second electron becomes the first one, and the third electron becomes the second one. Thus, to retain the chosen numeration, we need to perform the cyclic permutation of numbers of electrons, which are situated between the first and fifth lattice sites. This process leads to the cyclic permutation of the three spin variables in the function $|\sigma_1, \sigma_2, ..., \sigma_N\rangle$ and to an obvious change of the coordinate function.

The considered spin permutation can be written in the following form:

$$\mathbf{Q}_{1,3} = \begin{pmatrix} 1\,2\,3 \\ 3\,1\,2 \end{pmatrix}, \quad \mathbf{Q}_{1,3}\,|\sigma_1, \sigma_2, \sigma_3\rangle = |\sigma_3, \sigma_1, \sigma_2\rangle,$$

where the upper row determines the initial spin configuration while the lower row corresponds to the final one ($\mathbf{P}_{ij}$ transposes only two spin variables).

Making use of this treatment for all electrons and sites, one obtains that the Hubbard Hamiltonian with infinite repulsion can be written in the form

$$\mathbf{H} = \sum_{i=1}^{L} \alpha_i \mathbf{b}_i^+ \mathbf{b}_i + \sum_{i<J}^{L} t_{ij} (\mathbf{b}_i^+ \mathbf{b}_j \mathbf{Q}_{m,n}^+ + \mathbf{b}_j^+ \mathbf{b}_i \mathbf{Q}_{m,n}) \qquad (7)$$

Here $\mathbf{b}_i$ is a spinless Fermi operator which acts only on the coordinate part of (4), $Q_{m,n}$ is the cyclic permutation of spin variables of electrons, located on the

lattice sites from the interval (i, j), where i-th and j-th sites are neighbors $(t_{ij} \neq 0)$.

All cyclic permutations can be rewritten in the form of a product of spin transpositions $\mathbf{P}_{ij}$. Therefore, using the Dirac identity, the cyclic permutation of n spin variables can be expressed in the form of a scalar product of one-electron spin operators $\mathbf{S}_i$

$$\begin{pmatrix} 1 & 2 & 3 \ldots & n \\ n & 1 & 2 \ldots & n-1 \end{pmatrix} = \prod_{i=1}^{n-1}\left(2\mathbf{S}_i \cdot \mathbf{S}_n + \frac{1}{2}\right) = \prod_{i=1}^{n-1}\left(2\mathbf{S}_{n-i} \cdot \mathbf{S}_{n-i+1} + \frac{1}{2}\right) \quad (8)$$

The Eq.(7) is an exact representation of the Hamiltonian (3). Because of the scalar character of (7) we can exploit the conservation of the value of total spin S and its z-component M and consider separately different spin-symmetry subspaces. Therefore one can substitute spin-symmetry-adapted basis functions Θ_α^{SM} for a set of functions $|\sigma_1, \sigma_2, ..., \sigma_N\rangle$ in (4) and construct the matrix elements of (7) by means of the branching diagram technique [23, 28] or VB spin-pairing (Rumer) diagrams [29]. This simplifies calculations of the exact spectra of small lattice clusters because of the reduction of the dimensionality D of the corresponding eigenvalue problem. It is also useful for the analytical study of some special type of lattices. It should be noted that Fermi operators and cyclic spin permutations act simultaneously on the basis functions. Therefore we cannot obtain "separation" of charge and spin variables in our representation of the Hubbard model excepting some special cases [22-26]. Note also that the representation (3) is valid for other types of lattices, say the triangular one. A similar representation as an extension of the Jordan-Wigner transformation for $U=\infty$ one-dimensional Hubbard model has been proposed by Long and Zotos [30].

2.2. $U=\infty$ Hubbard model for polyallyl chain

One of the simplest π-electron models of a conjugated polymer with a macroscopic ground state spin is a polyallyl chain (Fig.2) described by the Hubbard Hamiltonian [20]:

$$\begin{aligned}
\mathbf{H} = \sum_{i=1}^{L}&\left(t_1\, \mathbf{a}_{3i-2,\sigma}^+ + t_2\, \mathbf{a}_{3i,\sigma}^+ + t_3\, \mathbf{a}_{3i+1,\sigma}^+\right)\mathbf{a}_{3i-1,\sigma} + H.c. \\
&+ U\sum_{j=1}^{3L}\mathbf{a}_{j,\sigma}^+\mathbf{a}_{j,\sigma}\mathbf{a}_{j,-\sigma}^+\mathbf{a}_{j,-\sigma}
\end{aligned} \quad (9)$$

where index i labels 3-site unit cell (allyl), $\mathbf{a}_{3L+1}^+ = 0$.

According to Lieb's theorem [31], the ground state spin of this Hamiltonian
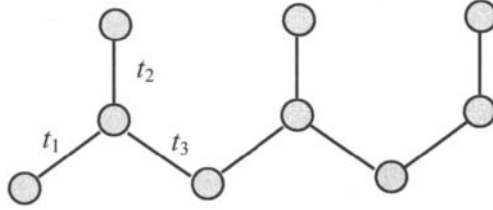
Fig.2. Fragment of polyallyl chain.

equals half the number of unit cells if the half-filled band is considered. For real materials, a filling of the band may be less than half as the result of the influence of acceptor admixtures. Therefore the question arises as to how the holes in the half-filled band of the model influence the energy spectrum. Here we will consider only the strongly correlated limit of (9) – the $U=\infty$ Hubbard model for polyallyl chain. The case of big finite values of U (t-J model for polyallyl chain) is described in [24].

Let us enumerate all the electrons of the chain in succession along the cells of the chain. Making use of the spin permutations, one can obtain the Hamiltonian (8) with $U = \infty$ in the form

$$H = \sum \left\{ t_1 \mathbf{b}_{3i-2}^+ + t_2 \mathbf{b}_{3i}^+ + t_3 \left[1 - \mathbf{b}_{3i}^+ \mathbf{b}_{3i} \left(1 - \mathbf{Q}_{l,l+1} \mathbf{b}_{3i+1}^+ \right) \right] \right\} \mathbf{b}_{3i-1} + H.c. \quad (10)$$

For one hole in the half-filled band, the exact energy spectrum of the chain with free ends formed by L unit cells is spin-degenerate, similar to the spectrum of the uniform Hubbard chain with $U = \infty$. In the case of periodic boundary conditions an electron hopping between the first and the last unit cells of the chain leads to the additional term to the Hamiltonian (9). For one hole in the half-filled band this term has the following form:

$$\mathbf{b}_{3L-1}^+ \mathbf{b}_1 \mathbf{Q}_{1,3L-1} + \mathbf{b}_1^+ \mathbf{b}_{3L-1} \mathbf{Q}_{1,3L-1}^+$$

In the case of periodic boundary conditions the chain Hamiltonian commutes with the operator that displaces all electrons by one unit cell cyclically. Therefore, its eigenfunctions must be characterized by the hole quasi-impulse $k = \dfrac{2\pi m}{L}$ ($m=1,2,...L$). The symmetry-adapted basis functions corresponding to a fixed value of k have the form

$$\Psi_\alpha^{SM}(k) = \sum_{l=1}^{L-1} \exp(-ikl) \mathbf{Q}_{1,3L-1}^{-3l} \left(c_1 \mathbf{b}_{3l+1}^+ + c_2 \mathbf{b}_{3l+2}^+ + c_3 \mathbf{b}_{3l+3}^+ \right) |0\rangle \Theta_\alpha^{SM}, \quad (11)$$

where $|0\rangle$ is a vacuum state for holes, and the c_i are arbitrary numbers.

After simple manipulations with the cyclic permutations, one obtains the following Hamiltonian:

$$\mathbf{H} = \begin{pmatrix} 0 & \mathbf{h}_1^+ & 0 \\ \mathbf{h}_1 & 0 & \mathbf{h}_2 \\ 0 & \mathbf{h}_2 & 0 \end{pmatrix}, \quad \mathbf{h}_1 = t_1 \mathbf{I} + t_3 \exp(ik) \mathbf{Q}_{3L-1}^3 \mathbf{Q}_{2,3}, \quad \mathbf{h}_2 = t_2 \mathbf{I} \quad (12)$$

It is easily shown that $\mathbf{h}_1$ is a normal operator ($\mathbf{h}_1^+ \mathbf{h}_1 = \mathbf{h}_1 \mathbf{h}_1^+$). Therefore, the spectrum of $\mathbf{H}$ is determined by the following expression:

$$\lambda_i = \pm\left(t_2^2 + \omega_i^2\right)^{1/2}, \quad 0, \quad (13)$$

where ω_i is an i-th singular value of matrix $\mathbf{h}_1$.

For $t_2 = 0$ the Hamiltonian $\mathbf{H}$ describes a one-dimensional Hubbard lattice (chain) with the alternating values of hopping integrals. Evidently, the spectrum of such a system must coincide with the set of singular values ω_i. This spectrum is known for arbitrary values of L. Consequently, the exact spectrum of (12) is determined by Eq.(13), where ω_i are the energies of a dimerized Hubbard chain containing $2L$ sites and $2L-1$ electrons. The full spin of the state with the energy λ_i is determined by

$$S_\lambda = |S_\omega \pm m|, \quad (14)$$

where S_ω is the spin of the state of a dimerized chain with energy ω_i, $m=1/2$, $3/2, \dots L/2$ for odd L and $m=0,1, \dots L/2$ for even L.

The ground state of the polyallyl chain is spin degenerate and has the energy

$$E_0 = -\left[(t_1 + t_3)^2 + t_2^2\right]^{1/2} \quad (15)$$

Some excited states are partially spin-degenerate because of partial spin degeneracy of corresponding states of the dimerized chain.

For several holes, spin permutations $\mathbf{Q}_{l,l+1}$ occuring in (9) lead to the mixing of different spin configurations, even in the case of the polyallyl chain with free ends (in contrast to the uniform chain).

3. EFFECTIVE HAMILTONIANS FOR THE LATTICES FORMED BY WEAKLY INTERACTED SEGMENTS

As has been shown by Nagaoka [32] and Thouless [33], for some types of lattices, the ground state of the $U=\infty$ Hubbard model with one hole in a half-filled band, has a maximal value of total spin. The generalization of this result was given by Tasaki [34]. The possibility of saturated ferromagnetism for some holes in the band is a delicate issue depending on the lattice structure and the density of electrons. Thus, for the $U=\infty$ Hubbard model on the rectangular lattices consisting of weakly interacted n-site segments, there is a cascade of concentration transitions with regular oscillation of the ground state multiplicity between minimal and maximal values [23,35]. In other words a multiband
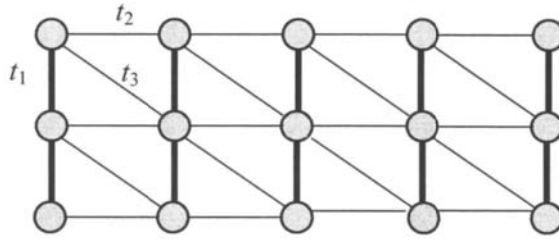
Fig.3. Triangular lattice strip formed by weakly interacting 3-site segments.

anisotropic model shows ferromagnetism for finite concentrations of holes. A similar result has been proved for the case $n=2$ in the limit of the large interchain hopping [36]. The consideration of anisotropic triangular lattice strips is more complicated but is of interest because some new lattice models with the ferromagnetic ground state contain triangles, the importance of which for the stabilization of ferromagnetism has been widely recognized [37, 38].

Let us consider a triangular lattice strip formed by weakly interacting linear n-site segments (Fig.3), the energy spectrum of which is described by the Hubbard Hamiltonian (3) with $\alpha_i = 0$. In the absence of interaction between segments (t_2, $t_3=0$) all states of the strip are spin degenerate and corresponding energies are sums of quantities (4). The interaction between segments leads to electron hops. If electrons are numbered in succession over the segments, these hops lead to cyclic spin permutations similarly as in the above consideration. As a result of these permutations, mixing of spin configurations and splittings of the spin-degenerate energy levels take place. For $|t_2|, |t_3| \ll |t_1|$ this splitting can be considered by means of perturbation theory (PT). In the absence of interaction between segments the most regular distribution of electrons through the segments corresponds to the lowest energy (naturally, in general we have several different distributions with the same energy). Therefore, for the lowest energy states the filling of the neighbor segments cannot differ by more than one electron, and there are two different cases: interaction of neighbor segments with different numbers of electrons and the interaction of the segments with equal fillings.

3.1 Two neighbor segments with different filling

It is easily seen that for the lattice formed by two neighbor segments with s and $s+1$ electrons the spin degeneracy is resolved in the first PT order in t_2, t_3. By making use of the cyclic spin permutations similar to the above consideration of rectangular lattice strips, one can construct the corresponding effective Hamiltonians describing low energy states of the lattice.

For simplicity, let us first consider the case of two-site segments with 3 electrons and $t_3=0$. Because of infinite electron repulsion there are only two
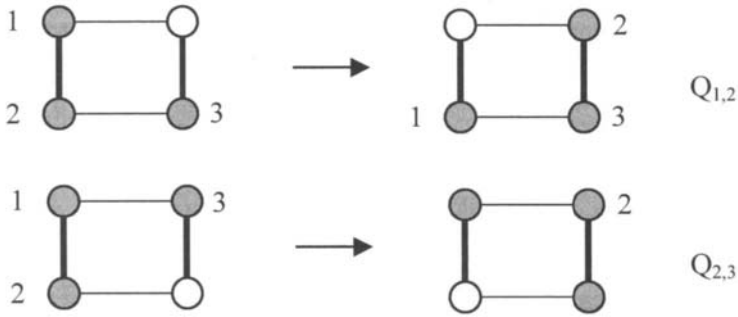
Fig.4. Electron hops in the system of two weakly interacted segments with three electrons

different distributions of electrons through the segments (two electrons may be situated on the first or the second segments). The corresponding wave functions of the segments are specified by Eq.(6). If two electrons are on the first segments only the electron transfer from the first one to the second segment is possible (Figure 4). Carrying out summation over the lattice variables n_i one can obtain the following first PT order Hamiltonian

$$H_{1,3} = -\frac{t_2}{2}\left(Q_{1,2} + Q_{2,3}\right)\left(a_1^+ a_2 + a_2^+ a_1\right),$$ (16)

where the spin-free Fermi operator a_i^+ creates the two-electron state on the i-th segment.

The Hamiltonian (8) can also be rewritten in a "pure" spin form if the spin space of double dimensionality is taken into account

$$\mathbf{H}(1,3) = -\frac{t_2}{2}\begin{pmatrix} 0 & Q_{1,2} + Q_{2,3} \\ Q_{1,2} + Q_{2,3} & 0 \end{pmatrix}.$$ (17)

For $t_3 \neq 0$ the Hamiltonian describing the interaction of two neighbor two-site segments with one and two electrons has the form

$$\mathbf{H}(1,3) = \begin{pmatrix} 0 & \mathbf{A} \\ \mathbf{A}^+ & 0 \end{pmatrix}, \quad \mathbf{A} = -\frac{t_2}{2}\left\{Q_{1,2} + Q_{2,3} + \mu\, Q_{1,3}\right\}, \quad \mu = \frac{t_1 t_3}{|t_1||t_2|}.$$ (18)

It is easily seen, that to change the numeration of electrons we can obtain similar Hamiltonian $\mathbf{H}^*$ with Hermitian matrix $\mathbf{A}^*$

$$\mathbf{A}^* = -\frac{t_2}{2}\left\{Q_{1,2} + Q_{2,3} + \mu \mathbf{I}\right\}$$

This Hamiltonian has the same spectrum because of the identity

$$\mathbf{H}^* = \mathbf{R}^+ \mathbf{H} \mathbf{R}, \quad \text{where } \mathbf{R} = \begin{pmatrix} Q_{1,3}^+ & 0 \\ 0 & Q_{1,3} \end{pmatrix},$$ (19)

and there is a simple relation between eigenvalues λ_i of $\mathbf{H}^*$ and eigenvalues ε_j of the matrix $\mathbf{A}^*$: $\lambda_i = \pm\varepsilon_j$, $i = 1,2...6$; $j = 1,2,3$. To use this relation it can be shown that Hamiltonian $\mathbf{H}^*$ has the ground state spin $S_0 = 3/2$ only if $\mu \geq -0.5$. Therefore for positive values of all hopping integrals $\mathbf{H}^*$ gives a ferromagnetic spin alignment of interacting neighbor segments.

For $n=3$ the same consideration after simple manipulations gives the effective Hamiltonian:

$$\mathbf{H}(1,3) = \begin{pmatrix} 0 & \mathbf{A} \\ \mathbf{A}^+ & 0 \end{pmatrix},$$

$$\mathbf{A} = -\frac{t_2}{16}\left\{9(\mathbf{Q}_{1,2} + \mathbf{Q}_{2,3}) - \mathbf{Q}_{1,3} - I - \mu\, 2\sqrt{2}\left(\mathbf{Q}_{1,2} + \mathbf{Q}_{2,3} - 2\mathbf{Q}_{1,3}\right)\right\}. \quad (20)$$

For two neighbor n-site segments with s and $s+1$ electrons a similar consideration gives the Hamiltonian:

$$\mathbf{H}(1,2s+1) = \begin{pmatrix} 0 & \mathbf{A} \\ \mathbf{A}^+ & 0 \end{pmatrix}, \quad \mathbf{A} = \sum_{k,l=1}^{s+1} J(k,l)(\mathbf{Q}_{l,k+s}^+ + \mathbf{Q}_{k,l+s}) \quad (21)$$

$$J(k,l) = \left\{ t_2 \sum_{i=1}^{n} G_{00}(i,k,s+1)G_{00}(i,l,s+1) \right.$$

$$\left. + t_3 \sum_{i=1}^{n-1} G_{00}(i+1,k,s+1)G_{00}(i,l,s+1) \right\}(-1)^{k+l+s}$$

$$G_{rp}(i,m,s) = \sum_{1 \leq n_1 < n_2 ... < n_s \leq n} A_r(n_1,n_1,...n_{m-1},i,n_{m+1},...n_s)A_p(n_1,n_1,...n_{m-1},n_{m+1},...n_s)$$

Here each ordering set of integer number r_i corresponds to a possible eigenstate of isolated linear n-site segments, described by the Hamiltonian (1). All these states are spin-degenerated and are specified by Eq.(5). Index 0 corresponds to the ground state of the segment with the energy

$$E_0(s) = -2|t_1|\cos(\beta(s+1))\frac{\sin(\beta s)}{\sin(\beta)}, \quad \beta = \frac{\pi}{2(n+1)}$$

In the case of the anisotropic rectangular lattice formed by two weakly interacted segments (t_3=0), there arise effective exchange integrals $J(k,l)$ subject to the condition [23]

$$\sum_{k,l=1}^{s+1} J(k,l) = (-1)^s t_2 \tag{22}$$

Because of the symmetric form of the state with the maximal value of total spin all the spin permutations give the same contributions to the ferromagnetic energy. Therefore the energy of the lowest ferromagnetic state of the rectangular lattice formed by two weakly interacting segments with $2s+1$ electrons, equals $-|t_2|$ independently of s and n. Obviously, this is a minimal possible eigenvalue of (21). Therefore, among the ground states of (21) there is one with the maximum value of total spin. The exact diagonalization study of the spectra of the Hamiltonian (21) at different values of s and n ($2 \le n < 7$) shows that all the ground states are unique (apart from the trivial ($2S+1$)–fold degeneracy) and have maximal values of total spin [28].

3.2 Two neighbor segments with equal filling

Let us now consider the interaction of two n-site segments with s electrons per segment. Single electron hopping between neighboring segments leads to an inhomogeneous distribution of electrons through the segments. Therefore the splitting of spin-degenerate energy levels appears only in the second PT order in t_2, t_3. Using the proposed spin permutation technique, one may sum over the lattice variables to obtain the lattice Hamiltonian in a "pure" spin form:

$$\mathbf{H}(1,2s) = \sum_{kp=1}^{s} \sum_{lq=1}^{s+1} J_1(k,l,p,q)\mathbf{Q}_{k,l+s-1}^{+}\mathbf{Q}_{p,q+s-1} + J_2(klpq)\mathbf{Q}_{l,k+s}\mathbf{Q}_{q,p+s}^{+} \tag{23}$$

$$J_\alpha(k,l,p,q) = \sum_{rt} \frac{B_{rt}^{ss+1}(k,l,\alpha)B_{rt}^{ss+1}(p,q,\alpha)}{2E_0(s) - E_r(s-1) - E_t(s+1)}, \quad \alpha = 1,2$$

$$B_{rt}^{su}(k,l,1) = \left\{ t_2 \sum_{i=1}^{n} G_{0r}(i,k,s)G_{t0}(i,l,u) + t_3 \sum_{i=1}^{n-1} G_{0r}(i,k,s)G_{t0}(i+1,l,u) \right\}(-1)^{k+l}$$

$$B_{rt}^{su}(k,l,2) = \left\{ t_2 \sum_{i=1}^{n} G_{0r}(i,k,s)G_{t0}(i,l,u) + t_3 \sum_{i=1}^{n-1} G_{0r}(i+1,k,s)G_{t0}(i,l,u) \right\}(-1)^{k+l}$$

For the case $s=1$ and $n=2$ this Hamiltonian has the following form:

$$\mathbf{H}(1,2) = \frac{t_2^2}{4|t_1|}\left(2(1-\mu)\,\mathbf{Q}_{1,2} - (1-\mu)^2 - 1\right) \qquad (24)$$

Rewriting the spin permutation with the help of the Dirac identity, one can obtain the following spin Hamiltonian:

$$\mathbf{H} = J_1\,\mathbf{S}_1\cdot\mathbf{S}_2 - J_2, \quad J_1 = \frac{t_2^2}{|t_1|}(1-\mu), \quad J_2 = \frac{t_2^2}{4|t_1|}\left[(1-\mu)^2 - (1-\mu) + 1\right]$$

When n is increased, the form of the exchange integrals J_1 and J_2 is changed only. For example in the case of $n=3$ and $\mu = 0$ $J_1 = \frac{J_2}{4} = \frac{7\sqrt{2}}{6}\frac{t_2^2}{|t_1|}$.

The increase in s leads to more complicated spin Hamiltonians. Thus, in the case of $s=2$, $n=3$ and $\mu = 0$, this Hamiltonian is of the form

$$\mathbf{H}_{1,2} = 2J(\mathbf{P}_{13} + \mathbf{P}_{24}) + \frac{J}{9}(\mathbf{Q}_{1,2} + \mathbf{Q}_{3,4}) - \frac{44J}{9} + J\begin{pmatrix}1\,2\,3\,4\\2\,4\,1\,3\end{pmatrix} \qquad (25)$$

$$-\frac{J}{6}\left[\begin{pmatrix}1\,2\,4\\2\,4\,1\end{pmatrix} + \begin{pmatrix}1\,2\,3\\3\,1\,2\end{pmatrix} + \begin{pmatrix}2\,3\,4\\3\,4\,2\end{pmatrix} + \begin{pmatrix}1\,3\,4\\4\,1\,3\end{pmatrix}\right] + H.c., \qquad J = \frac{3t_1^2}{16\sqrt{2}|t|}$$

For $\mu = 0$ effective exchange integrals $J_1(k,l,p,q) = J_2(k,l,p,q) = J(k,l,p,q)$ obey the condition [23]

$$\sum_{kp=1}^{s}\sum_{lq=1}^{s+1} J(k,l,p,q) = 0. \qquad (26)$$

Therefore, the ferromagnetic state energy of the rectangular lattice formed by weakly interacting segments with equal filling should be equal to zero in the second PT order in t_2.

According to the results of the exact diagonalization study of the lattice Hamiltonian (23), it has a singlet ground state for $2 \le n \le 5$ and $1 \le s \le 3$ [28]. For $n=5$, $s=4$ and $n=6$, $s=5$ the ground state spin S_0 has the values 3 and 4 respectively. For the case $n=6$ and $s=4$, $S_0=0$. Therefore we can suppose that

$$S_0 = \begin{cases} 0 & , \quad s/n < 0.8 \\ S_{\max} - 1, & s/n \ge 0.8 \end{cases}$$

3.3 Anisotropic lattice strips and magnetic polarons

Let us consider triangular lattice strips formed by L two-site weakly interacted segments at electron density $\rho \le 0.5$ $\left(\rho = \frac{N}{2L}\right)$. The total lattice Hamiltonian has a form of a sum of Hamiltonians that describe the interaction of neighboring segments:

$$\mathbf{H} = \mathbf{H}_1 + \mathbf{H}_2, \quad \mathbf{H}_1 = (2 - \mu) t_2 \sum_{i=1}^{L-1} \left(\mathbf{a}_i^+ \mathbf{a}_{i+1} + \mathbf{a}_{i+1}^+ \mathbf{a}_i \right) - N \frac{t_2^2 \mu^2}{4|t_1|},$$

$$\mathbf{H}_2 = (1 - \mu) \frac{t_2^2}{|t_1|} \sum_{i=1}^{L-1} \left\{ \left(\mathbf{S}_j \cdot \mathbf{S}_{j+1} - \frac{1}{4} \right) (2\mathbf{a}_i^+ \mathbf{a}_i - \mathbf{a}_i^+ \mathbf{a}_{i+2} - \mathbf{a}_{i+2}^+ \mathbf{a}_i) \mathbf{a}_{i+1}^+ \mathbf{a}_{i+1} \right\}, \quad (27)$$

where a_i^+ is a spinless Fermi operator describing the creation of a one-electron state on the i-th lattice segment (this state corresponds to the j-th electron of the lattice).

Making use of the consideration proposed by Klein and Seitz [39] for the atomic limit of the linear Hubbard chain one performs averaging over the ground state of $\mathbf{H}_1$ and obtains the following effective Hamiltonian that describes low-lying states of (27):

$$\mathbf{H} = -\frac{L|t_2|}{\pi}(2 - \mu)\sin(2\pi\rho) + \frac{2t_2^2}{|t_1|}(1 - \mu)\left(\rho - \frac{\sin(4\pi\rho)}{4\pi}\right)\sum_{i=1}^{N}\left(\mathbf{S}_i \cdot \mathbf{S}_{i+1} - \frac{1}{4}\right) - N\frac{t_2^2\mu^2}{4|t_1|} \quad (28)$$

It is easily seen that (28) has a form of uniform one-dimensional Heisenberg spin Hamiltonian with a well-known spectrum. Therefore the ground state spin of our lattice has a minimal value at $\mu < 1$ and a maximal value at $\mu > 1$.

The above consideration can be generalized to systems of n-site segments. Thus, for the rectangular lattice strip ($\mu = 0$) there is an analytical formula for the exchange integrals of the Heisenberg spin Hamiltonian describing the interaction of neighboring segments with $s=1$ at arbitrary n [23]. An effective Heisenberg spin Hamiltonian which is similar to (28) can be derived. Obviously, the ground state of this Hamiltonian has a minimal value of total spin and a gapless excitation spectrum.

For $t_2 = t_3$

$$\mathbf{H}(1,2) = \begin{cases} -\dfrac{t_2^2}{4t_1}, & t_1 > 0 \\[3mm] -\dfrac{2t_2^2}{t_1}\left(\mathbf{S}_1 \cdot \mathbf{S}_2 - \dfrac{3}{8}\right), & t_1 < 0 \end{cases} \quad (29)$$

Total lattice Hamiltonian is the sum of the Hamiltonians describing the interaction of neighbor segments. Therefore in the second PT order in t_2 for positive values of t_1 the lattice with one electron per segment has a degenerate energy spectrum (because of hole-particle symmetry, positive values of t_1 correspond to the model with more than one electron per site). This degeneracy

is resolved in 4-th PT order in t_1 and the corresponding effective spin Hamiltonian for two interacting segments has the form

$$\mathbf{H}(1,2) = -\frac{t_2^4}{16t_1^3}\left(\mathbf{Q}_{12} + \frac{11}{4}\right),$$

with a triplet ground state. If we have lattice strips with more than two segments, there are 4-th order processes, which include three segments. For example for the lattice formed by three segments we have the following effective Hamiltonian:

$$\mathbf{H}(1,3) = \frac{t_2^4}{128t_1^3}\left\{4\left(\mathbf{Q}_{1,3}^+ + \mathbf{Q}_{1,3}\right) + 3\left(\mathbf{Q}_{1,2} + \mathbf{Q}_{2,3}\right) - 6\mathbf{P}_{13} - 40\right\}$$

This Hamiltonian has a ground state with $S_0=1/2$. Therefore, if for the strip we take into account only interactions between nearest segments (i.e., a two-particle approximation) we obtain the ferromagnetic ground state. Only the inclusion of three-segment interactions leads to the correct ground state spin of the lattice strip.

For negative values of t_1 we obtain the uniform Heisenberg spin chain with antiferromagnetic coupling which has a nondegenerate singlet ground state.

Unfortunately, for s>1 the corresponding effective Hamiltonians have a much more complicated form and the study of corresponding electron systems can be provided numerically only. Also, for triangular lattice there are no simple sum rules for the effective exchange integrals, which have been derived for a rectangular lattice (Eq. (22,26)).

As has been shown by Takahashi [38], the isotropic case of the triangular lattice with a positive value of hopping integrals has a dominantly ferromagnetic character. Therefore, increasing the value of t_2 $(t_2 = t_3)$ can lead to the changing of the ground state total spin of the lattice strip.

According to the numerical calculations of the exact spectra of finite lattice clusters [26], there is a critical value of t_2 near which a ferromagnetic state of the lattice is stable against a few spin flips, but the ground state is a singlet. In other words we can suppose that the depolarization of the ferromagnetic ground state of the infinite lattice strips for some electron concentrations cannot be considered to be a continuous process. The extrapolation of the numerical estimations of the critical values of t_2 gives for the infinite lattice formed by two-site segments the critical value $t_2 \approx 0.63$ [26]. For the case $n=3$, $s=1$ there is no such transition. Nevertheless it appears again at $s=2$, $n=3$, and it can be expected there are transitions with the hopping of the ground state spin mostly between the marginal values for corresponding infinite lattice strips. Thus, at $t_2 = t_3$ for triangular lattice strips we have obtained a complicated dependence of S_0 on model parameters.

When $1/2 < \rho < 1$ there can be one or two electrons at each segment. At $N=L+1$ there is one pair. Let us first consider this case in detail. Omitting simple but cumbersome manipulations with the spin permutations in the first and second order in t_2 we can write the lattice Hamiltonian for this filling in the form

$$\mathbf{H} = \mathbf{H}_1 + \mathbf{H}_2$$

$$\mathbf{H}_1 = \sum_{j=1}^{L-1} \left\{ -\frac{t_2}{2} \left[\left(\mathbf{Q}_{j,j+1} + \mathbf{Q}_{j+1,j+2} + \mu \mathbf{Q}_{j,j+2} \right) \mathbf{b}_{j+1}^+ \mathbf{b}_j + H.c. \right] \right.$$

$$\left. + \frac{t_2^2}{4|t_1|} \mathbf{b}_j \mathbf{b}_j^+ \mathbf{b}_{j+1} \mathbf{b}_{j+1}^+ \sum_{l=1}^{L-1} \left[2(1-\mu) \mathbf{Q}_{i,i+1} - (1-\mu)^2 - 1 \right] \right\},$$

$$i = \sum_{k=1}^{l-1} \delta(j-k) + l,$$

$$\mathbf{H}_2 = -\frac{t_2^2}{8|t_1|} \left\{ \sum_{j=1}^{L-2} \left[(1-\mu) \mathbf{Q}_{j,j+1} - 1 \right] \left[(1-\mu) \mathbf{Q}_{j+2,j+3} - 1 \right] \mathbf{b}_{j+2}^+ \mathbf{b}_j + H.c. \right.$$

$$+ \sum_{j=1}^{L-1} \left[A(j) - 2\mu \mathbf{Q}_{j,j+1} \right] \mathbf{b}_j^+ \mathbf{b}_j + \left[A(j) - 2\mu \mathbf{Q}_{j+1,j+2} \right] \mathbf{b}_{j+1}^+ \mathbf{b}_{j+1} \right\},$$

$$A(j) = 2 + \mu^2 - \mathbf{Q}_{j,j+2} - \mathbf{Q}_{j,j+2}^+ + 2\mu \, \mathbf{P}_{jj+2},$$

where $\delta(i, j)$ is a Kronecker symbol; $\mathbf{b}_i^+$ is a spin-free operator creating a pair of electrons on the i-th segment $\left(\left(\mathbf{b}_i^+ \right)^2 \equiv 0 \right)$.

The numerical study of the exact spectra of the finite lattice strips with different values of parameters t_1, t_2 and t_3 shows that for $1 > \mu > -0.5$ there is a monotonic decrease in the ground state total spin with the increase of the interaction between segments [26,40]. The increase in the total number of segments L leads to the same result. Therefore we can study the stability of the ferromagnetic state of a strip, comparing the energies of the lowest states with $S = S_{\max}$ and $S = S_{\max} - 1$ at fixed values of L, μ and $\alpha = \left| \frac{t_2}{t_1} \right|$. The coincidence of these energies gives us an estimation of the critical value of model parameters, which corresponds to the boundary of the stability region. This estimation can be obtained to use the following single spin-flip wave function with the correct space and spin symmetry:

$$\Psi = \frac{1}{\sqrt{2}}\left[\Theta^1_{1,N}\left(\frac{L-1}{2},\frac{L-1}{2}\right)\sum_{n=2}^{L}a_n|n\rangle \pm \Theta^2_{1,N}\left(\frac{L-1}{2},\frac{L-1}{2}\right)\sum_{n=1}^{L-1}a_n|n\rangle\right], \quad (32)$$

$$\Theta^1_{1,N}\left(\frac{L-1}{2},\frac{L-1}{2}\right) = \frac{1}{\sqrt{2L}}\left[\left|\frac{1}{2}\right\rangle\Theta^1_{2,N}(\frac{L}{2},\frac{L}{2}-1) - \sqrt{2L-1}\left|-\frac{1}{2}\right\rangle\Theta^1_{2,N}(\frac{L}{2},\frac{L}{2})\right]$$

$$\Theta^2_{1,N}\left(\frac{L-1}{2},\frac{L-1}{2}\right) = \frac{1}{\sqrt{2L}}\left[\Theta^1_{1,L}(\frac{L}{2},\frac{L}{2}-1)\left|\frac{1}{2}\right\rangle - \sqrt{2l-1}\,\Theta^1_{1,L}(\frac{L}{2},\frac{L}{2})\left|-\frac{1}{2}\right\rangle\right]$$

$$a_n = \sqrt{\frac{2}{L}}\sin\left(\frac{\pi n}{L}\right),$$

where index n labels a segment with two electrons. For large L this function corresponds to the energy

$$E_1 = -\frac{t_2^2\mu^2}{4|t_1|}(L-1) - t_2(2+\mu)\cos\left(\frac{\pi}{L}\right) - \frac{t_2^2(1-\mu)}{2|t_1|} \quad (33)$$

At $\alpha \ll 1$ and large L the lowest ferromagnetic energy is

$$E_2 = -\frac{t_2^2\mu^2}{4|t_1|}(L-1) - |t_2|(2+\mu)\cos\left(\frac{\pi}{L+1}\right) \quad (34)$$

Hence at $E_1=E_2$ we have the following relation between Hamiltonian parameters and the total number of the segments:

$$L = \left(\frac{2(2+\mu)\pi^2}{(1-\mu)}\left|\frac{t_1}{t_2}\right|\right)^{1/3} \quad (35)$$

It should be noted that the same formula could be obtained if we consider only the Hamiltonian $\mathbf{H}_1$ specified by Eq. (30). It agrees with the results of numerical calculations, which show that the estimations of critical value of α are slightly modified if only $\mathbf{H}_1$ is taken into consideration.

In the vicinity of $\mu = -0.5$, the numerical calculations show that an increase in the value of α leads to a jump of the ground state total spin from the maximum to the minimum value [41]. Therefore Eq. (35) is not valid for the estimation of the stability of the ferromagnetic state of the strip in this region of the values of parameter μ.

The results of numerical calculations are in a good agreement with Eq.(35). For example, for the strips with L=10-18 at μ=0.5 they are fitted by the formula $L = 3.29\alpha^{-0.34}$ [40].
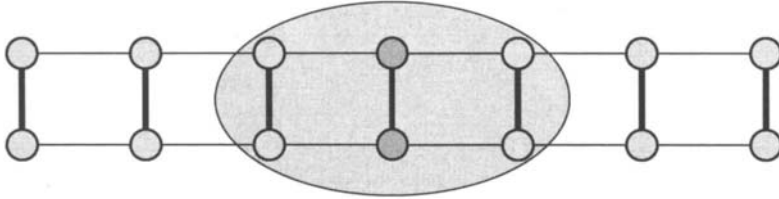
Fig.4 Magnetic polaron (big shaded region) for the rectangular strip with $N=L+1$.

For the lattice strip with $N=L+1$ described by the Hamiltonian (31) there are a few kinds of interactions of neighboring segments. The first one corresponds to the interaction of the segments with equal filling ($s=1$) and leads to an "antiferromagnetic" spin ordering at $\mu < 1$. The second one corresponds to the interaction between the segment with $s=1$ and the segment with $s=2$ (the interaction between the "unit" and the "pair") and produces a ferromagnetic spin ordering at $\mu > -0.5$. The lattice spin structure is formed by the competition between these interactions. For the rectangular lattice strip of a two-leg ladder type ($n=2$, $\mu = 0$) according to Krivnov and Ovchinnikov [22] this competition leads to the formation of a region with ferromagnetic ordering around the pair (spin polaron) with sharp boundaries as is shown schematically in Fig.4. Let suppose, that for the triangular lattice strip at $1 > \mu > -0.5$ we have a similar spin ordering and the ferromagnetic region includes X segments. In the polaron approximation [22,26], the total ground state energy of a lattice could be written in the form

$$E(X) = -(L-X)(1-\mu)\frac{t_2^2}{|t_1|}\ln 2 - |t_2|(2+\mu)\cos\frac{\pi}{X+1} - (L-1)\frac{\mu^2 t_2^2}{4|t_1|} \qquad (36)$$

To minimize this function at $|t_2|, |t_3| \ll |t_1|$ we obtain the following estimation for X:

$$(X+1)^3 = \frac{(2+\mu)\pi^2}{(1-\mu)\ln 2}\left|\frac{t_1}{t_2}\right| \qquad (37)$$

The total ground state spin of the lattice strip is proportional to X. When X coincides with L it takes a maximum possible value. In this case one can easily obtain the corresponding relation between Hamiltonian parameters and the total number of segments L

$$L = \left(\frac{(2+\mu)\pi^2}{(1-\mu)\ln 2}\left|\frac{t_1}{t_2}\right|\right)^{1/3}, \qquad (38)$$

which is close to the estimation (35).

If $N>L+1$, there are several pairs. It can be shown that all the pairs form a common ferromagnetic region [22]. Omitting manipulations which are similar to
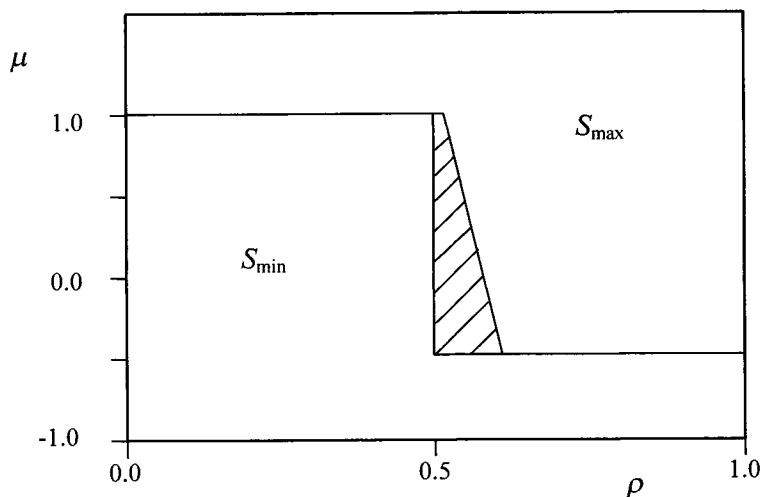
Fig.5. The ground state phase diagram of the triangular lattice strip with $n=2$. The shaded region associates with the intermediate values of the ground state spin.

the above consideration, it can be shown that our lattice at $N>L$ has the ferromagnetic ground state if the electron concentration ρ obeys the condition

$$\rho > \frac{1}{2} + \frac{1}{2}\left(\frac{3(1-\mu)\ln 2}{(2+\mu)\pi^2}\left|\frac{t_2}{t_1}\right|\right)^{1/3} \qquad (39)$$

Let us consider the case $\mu = 1$. The difference between the lowest singlet and ferromagnetic states of the two-electron systems on two neighbor segments is proportional to $\frac{t_2^4}{t_1^3}$. Therefore, according to the polaron description of the ground state, it has a ferromagnetic ground state at arbitrary values of the electron concentration ρ from the interval $(0.5+O\left(\frac{t_2}{t_1}\right), 1)$.

The main results of the above PT analysis are shown in the phase diagram in the parameter space of electron density and μ (Fig.5).

Let us now consider the case of the anisotropic rectangular lattice strips with $n>2$. For $\rho \le 1/n$ it is described by the antiferromagnetic Heisenberg spin Hamiltonian and S_0 takes a minimum possible value ($S_0=0$ for even N). When $1/n < \rho < 2/n$ there is a competition between the interactions of the neighbor segments similar to the case $s=2$, that leads to the formation of the magnetic polaron. Therefore in the vicinity of $\rho = 1/n$ the increase in ρ leads to a monotonic increase in the value of S_0. When ρ approaches the critical value specified by the analog of Eq.(38) for given n, S_0 takes a maximum value.
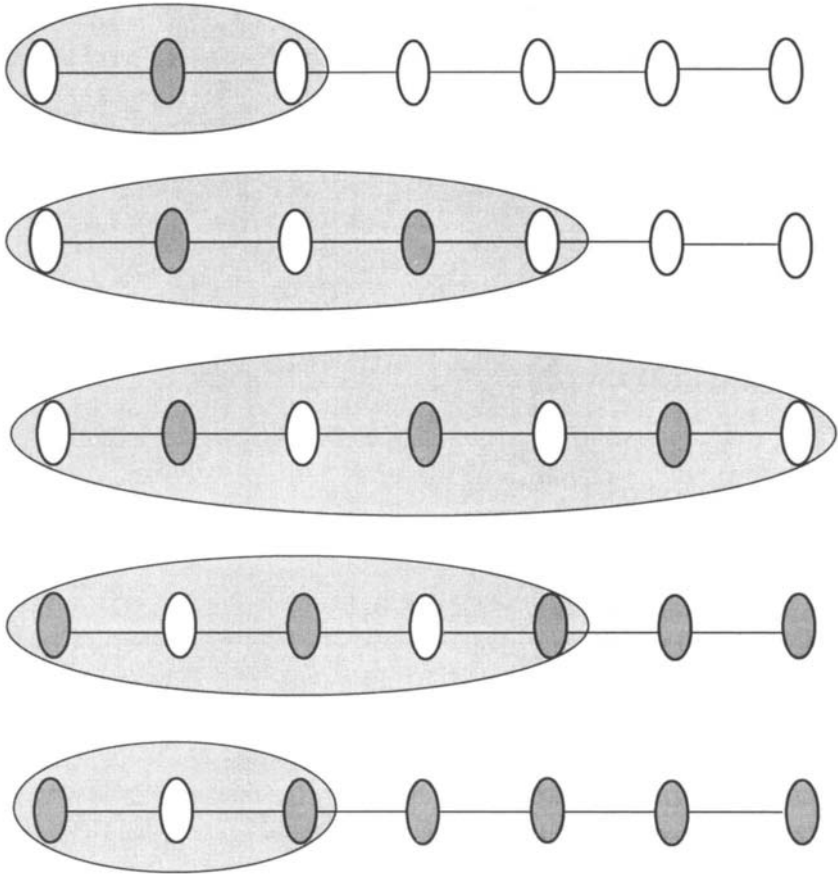
Fig. 6. Magnetic polarons (big shaded regions) for different values of electron concentration ρ in the interval $1/n < \rho < 2/n$. The small ellipses correspond to the two-electron states of the segments.

Nevertheless, there is an important distinction. Two segments with $n=2$ and $s=2$ cannot interact because all the electron hops between segments are forbidden. In contrast to this, at $n>2$ the neighbor segments with the equal filling $s=2$ interact to decrease the value of S_0. Therefore, at $\rho = 2/n$ $S_0 = 0$, and in the vicinity of the value of $\rho = 2/n$ the polaron is formed by units on the background of pairs as is depicted in Fig.6. As a result, for infinite L the increase in the value of ρ in the vicinity of $\rho = 2/n$ decreases S_0 to destroy the ferromagnetic spin ordering of the lattice. Thus in interval $1/n < \rho < 2/n$ there is a non-monotonic behavior of S_0 as a function of electron concentration ρ.

The further increase in ρ leads to the appearance of segment states with three electrons on the background of the pairs. The competition among the

$S_0=1/2$ $S_0=3/2$
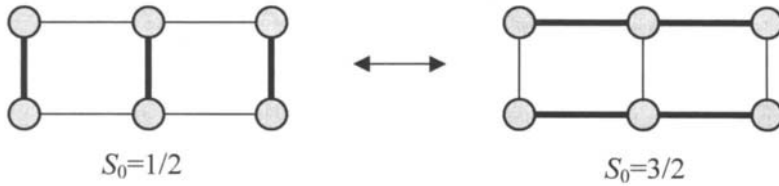
Fig.7 The dependence of S_0 on the geometry of the lattice.

interactions of these segments with pairs and between pairs leads again to the creation of the magnetic polaron and to the increase in S_0 and so on. Therefore, for the lattice formed by n-site weakly interacting segments there is a cascade of concentration transitions with regular oscillations of spin multiplicity between minimal and maximal values. The ground state spin of the lattice takes a maximum value if ρ obeys the following condition:

$$A_+(s, n, t_1, t_2) < \rho < A_-(s+1, n, t_1, t_2), \tag{40}$$

where

$$A_\pm(s, n, t_1, t_2) = s\,n^{-1} \pm \frac{1}{n\pi}\left[\frac{3\pi|\varepsilon(r, n)|}{2}\right]^{1/3} \alpha^{1/3}, \quad \alpha = \left|\frac{t_1}{t_2}\right|, \quad s = 1, 2 \ldots n-1,$$

$\varepsilon(s, n)$ is a dimensionless ground state energy per unit cell for the lattice formed by n-site segments with s electrons per segment.

Let us consider the lattice consisting of 3 two-site segments (Fig.7) and suppose that $N=3$. If $|t_1| >> |t_2|$, the lowest energy corresponds to the homogeneous distribution of electrons through segments (one electron per segment), and the ground state spin takes a minimal value $S_0=1/2$. On the other hand, if $|t_1| << |t_2|$ we can consider the same lattice as one formed by two 3-site segments with inhomogeneous distribution of electrons. The ground state spin of the lattice in this case takes a maximal value $S_0=3/2$. Hence the multiplicity of the lattice ground state is a function of the ratio of hopping integrals t_1 and t_2. To generalize this consideration to a L_1 by L_2 rectangular lattice it can be shown that in two limiting cases $|t_1| >> |t_2|$ and $|t_1| << |t_2|$ this lattice has different values of the ground state spin if the electron density ρ satisfies the condition

$$\max[A_+(l_1, L_1), A_-(l_2, L_2)] < \rho < \min[A_-(l_1+1, L_1), A_+(l_2, L_2)] \tag{41}$$

3.4 Lattices formed by segments with alternating values of α

Quite recently the ferromagnetic ground state in a class of Hubbard systems on decorated lattices that contain flat or nearly flat lowest energy bands has been found [42,43]. Obviously such multiband systems have more degrees of freedom than the one-band model considered by Nagaoka, and we can expect the appearance of unusual effects even in the case of infinite electron repulsion.

Assume that the rectangular lattice consists of two weakly interacting segments, one of them having a nonzero value of α. This lattice may be considered as a simple correlated electron model for stacked donor-acceptor crystals. For $\alpha \gg |t_2|$ one can use the cyclic spin permutation technique within the framework of PT. As a result, for $2|t_1| \neq \alpha$ it can be shown that the effective Hamiltonian describing the interaction between two neighbor segments with s and s+1 electrons has the form

$$\mathbf{H}(1,2s+1) = \sum_{klpq=1}^{s+1} J_1(k,l,p,q)\mathbf{Q}_{k,l+s}^+ \mathbf{Q}_{p,q+s} + \sum_{kp=1}^{s}\sum_{lq=1}^{s+2} J_2(k,l,p,q)\mathbf{Q}_{l,k+s+1}^+ \mathbf{Q}_{q,p+s+1} \quad (42)$$

where

$$J_1(k,l,p,q) = \sum_{rt} \frac{B_{rt}^{s+1s+1}(k,l)B_{rt}^{s+1s+1}(p,q)}{E_0^1(s+1) + E_0^2(s) - E_r^1(s) - E_t^2(s+1)}$$

$$J_2(k,l,p,q) = \sum_{rt} \frac{B_{rt}^{ss+2}(k,l)B_{rt}^{ss+2}(p,q)}{E_0^1(s+1) + E_0^2(s) - E_r^1(s+2) - E_t^2(s-1)}$$

$$B_{rp}^{st}(m,n) = t_2 \sum_{i=1}^{n} G_{0r}(i,m,s)G_{r0}(i,n,t)(-1)^{m+n}$$

$$E_0^1(s) = -2|t_1|\cos(\beta(s+1))\frac{\sin(\beta s)}{\sin(\beta)}, E_0^2(s) = s\alpha + E_0^1(s)$$

For example, in the case of $n=2$ $s_1=2$ and $s_2=1$ this Hamiltonian can be expressed in the form

$$\mathbf{H}(1,3) = J\big[(\mathbf{Q}_{13} + \mathbf{Q}_{13}^+)|t_1| + 2(\alpha + |t_1|)\big]; \quad J = -\frac{t_2^2}{2\alpha(\alpha + 2|t_1|)}. \quad (43)$$

This Hamiltonian has only non-positive matrix elements and its matrix in the space of spin configurations cannot be represented in a block-diagonal form after any permutation of the basis functions. Therefore, according to the Perron-Frobenius theorem its ground state must be nondegenerate. Obviously, the minimal eigenvalue of (43) equals $-\frac{t_2^2}{\alpha}$. Hence the Hamiltonian (43) has the ferromagnetic ground state.

For the lattice consisting of L unit cells and $N=2L+1$ we have

$$H = \sum_{i=1}^{L-1} H(6i-5,6i-3) + H(6i-3,6i-1) + H(6i-2,6i) + H(6i,6i+2) \qquad (44)$$

with the ferromagnetic ground state energy

$$E_0 = -\frac{t_2^2}{\alpha}(L-1) \qquad (45)$$

and a one-magnon spectrum

$$\Delta E(k) = E(k) - E_0 = \frac{2t_2^2}{\alpha(\alpha + 2|t_1|)}\left(1 - \frac{\varepsilon}{4}\right),$$

$$\varepsilon = \begin{cases} 1 \pm \sqrt{1 + 8\cos^2(k/2)}; & k = \frac{4\pi\lambda}{L}, \lambda = 0,1...L/2-1 \\ -2 \end{cases}$$

Note, that the similar result may be found for the lattice formed by two segments with different hopping integrals t_1 and t_1' respectively and $\alpha = 0$. For example, in the case of two-site segments with $s_1 = 2$ and $s_2 = 1$ ($t_1' - t_1 \gg |t_2|$) the lattice Hamiltonian has the form

$$H(1,3) = J\big[(Q_{13} + Q_{13}^+)t_1' + 2t_1\big]; \quad J = \frac{t_2^2}{2\big|(t_1)^2 - (t_1')^2\big|}$$

The ground state spin of this Hamiltonian takes a maximal value independently of the nonvanishing value of $|t_1 - t_1'|$.

Let us consider now a rectangular lattice strip consisting of two-site weakly interacting segments with the same value of t_1 and alternating values of one-site energies α (two-leg ladder). For $N = L+1$ and $L > 2$ the segment with two electrons interacts in the second order of PT in t_2 with nearest and next-nearest segments. The corresponding Hamiltonian for a three-segment system has the following form at $2|t_1| - \alpha \gg |t_2|$:

$$H = H_1 + H_2, \qquad (46)$$

where H_1 is described by formula (43),

$$H_2 = -\frac{t_2^2}{2\alpha(\alpha + 2|t_1|)}\big[(Q_{13} + Q_{24})(\alpha + |t_1|) + (I + Q_{34}Q_{12})|t_1|\big]a_3^+ a_1 + H.c..$$

Here a_i^+ is a spinless Fermi operator describing the creation of a two-electron state on the i-th lattice segment.

The interaction between neighboring segments with one electron per segment is described by the following spin Hamiltonian:

$$\mathbf{H}_3(1,2) = \frac{2|t_1||t_2^2|}{4t_1^2 - \alpha^2}(\mathbf{Q}_{12} - \mathbf{I}) \tag{47}$$

As a result we have obtained the effective Hamiltonian with the two types of interaction of neighboring segments. The competition between these types of interactions leads to the formation of a magnetic polaron similar to the anisotropic one band $U=\infty$ Hubbard model.

It should be noted that for the last case the ferromagnetic interaction terms appear in the first order of PT in $|t_2|$. If the polaron includes X segments the total ground state energy of a lattice could be written in the form

$$E_0 = -t_2^2 \left\{ \frac{2}{\alpha} \left[1 + \cos\left(\frac{2\pi}{X+1} \right) \right] + (L - X) \frac{4|t_1|\ln 2}{\left(4t_1^2 - \alpha^2\right)} \right\} \tag{48}$$

(The term $\mathbf{H}_3$ gives zero contribution to the ferromagnetic region energy).

To minimize this function, we can evaluate the size of the ferromagnetic region and the energy and spin of the lattice ground state. For large values of X when $\alpha \ll |t_1|$ such a minimization gives

$$X = \left(\frac{2\pi^2\left(4t_1^2 - \alpha^2\right)}{\alpha|t_1|\ln 2} \right)^{\frac{1}{3}} \tag{49}$$

For $2|t_1| = \alpha$ neighbor segments interact in the first order in $|t_1|$. The corresponding Hamiltonian has the form

$$\mathbf{H} = \begin{pmatrix} 0 & \mathbf{A} \\ \mathbf{A} & 0 \end{pmatrix}, \quad \mathbf{A} = \frac{t_1 t_2}{2|t_1|}(\mathbf{Q}_{12} - \mathbf{I}) \tag{50}$$

It is easily shown that the ground state energy of H equals $-\lambda$, where λ is the spectral radius of the matrix A. Therefore (50) gives the ground state with a minimal value of total spin. It is of interest, because the first-PT-order terms for such lattices lead usually to the ferromagnetic ground state.

Hence, the small clusters of anisotropic rectangular lattice with $n=2$ have a minimal ground state spin at $2|t_1| = \alpha$ and intermediate values of S_0 at $2|t_1| > \alpha$. The corresponding results of the exact diagonalization study for the small lattice clusters described by the Hamiltonian (1) are in agreement with this conclusion [26].

Let us consider an anisotropic triangular lattice with alternating values of the one-site energy α. The corresponding general formulas for the interaction between n-site segments are more cumbersome because of a more complicated dependence on the distribution of electrons through the lattice in zero PT order.

We will study only one simple case: the triangular lattice formed by two-site segments with the one electron per segment. Omitting cumbersome calculations, which are similar to the above one, we obtain the following effective spin Hamiltonians:

$$\mathbf{H}(1,2) = \frac{|t_1|t_2^2}{4t_1^2 - \alpha^2}\left\{2(1-\mu)\mathbf{Q}_{12} - 1 - (1-\mu)^2\right\}, \quad 2|t_1| - \alpha \gg \max\left(|t_2|,|t_3|\right) \quad (51)$$

$$\mathbf{H}(1,2) = \frac{-2t_1 t_2^2}{\alpha(\alpha + 2t_1)}\mathbf{Q}_{12} - \frac{t_2^2(3\alpha^2 - 2\alpha t_1 - 6t_1^2)}{\alpha(\alpha^2 - 4t_1^2)}, \quad \alpha - 2|t_1| \gg |t_2|, t_2 = t_3 \quad (52)$$

Note, that (51) is a generalization of the Hamiltonian (24). For positive t_1 it has a ferromagnetic ground state. Note that we have obtained this ferromagnetic Hamiltonian in the second PT order in t_2, which usually gives antiferromagnetic coupling.

In the case of $\varepsilon = 2|t_1|$ at $N=L$, even segments may contain one or two electrons. Therefore neighbor segments interact in the first order of PT, and the corresponding Hamiltonian has a form [40]

$$\widetilde{\mathbf{H}} = \begin{pmatrix} 0 & \mathbf{A}_{1,2} \\ \mathbf{A}_{1,2} & 0 \end{pmatrix}, \quad \mathbf{A}_{1,2} = \frac{t_1 t_2}{2|t_1|}\left[(1-\mu)\mathbf{Q}_{12} - I\right] \quad (53)$$

It is easily shown that the ground state energy of $\widetilde{\mathbf{H}}$ equals $-\lambda$, where λ is the spectral radius of the matrix $\mathbf{A}$. Hence Hamiltonian (53) has a ground state with a minimal value of total spin S_0 at $\mu<1$ and a maximal value of S_0 at $\mu>1$.

For the strip formed by L segments the lattice Hamiltonian can be written as

$$\mathbf{H}'' = \sum_{i=1}^{L-1}\left(\mathbf{R}_i + \mathbf{R}_i^+\right)\mathbf{A}_{i,i+1} \quad (54)$$

This Hamiltonian acts in the space spanned by the basis vectors

$$\varphi_i = \left| m_1, m_2 ... m_L\right\rangle \otimes \left| \sigma_1, \sigma_2 ... \sigma_L\right\rangle \quad (55)$$

The coordinate part of these vectors $\left| m_1, m_2 ... m_L\right\rangle$ describes the distribution of electrons through the segments in zero-order of PT ($m_{2l-1} = 1, 2; m_{2l} = 0, 1$). The operators $\mathbf{R}_i$ act upon the coordinate part of these basis functions only. Its non-zero elements are determined by the following equations:

$$R_{2l-1}\left| m_1, ... m_{2l-2}, 1, 1 ... m_L\right\rangle = \left| m_1, ... m_{2l-2}, 2, 0 ... m_L\right\rangle$$

$$R_{2l}\left| m_1, ... m_{2l-1}, 1, 1 ... m_L\right\rangle = \left| m_1, ... m_{2l-1}, 0, 2 ... m_L\right\rangle$$

It can be shown that the energy spectrum of (54) does not depend on the sign of the product $t_1 t_2$. If we choose a positive sign of $t_1 t_2$, none of the off-diagonal elements of the Hamiltonian matrix in the space spanned by the basis functions (55) is positive at $\mu > 1$. Besides, for two arbitrary basis states χ and φ with the same value of the z-projection of total spin M and finite values of model parameters, there always exists an integer n with $\langle \chi | \mathbf{H}^n | \varphi \rangle \neq 0$. This means that we have no additional decoupling in the subspace with a specified value of M. Therefore, according to the Perron-Frobenius theorem, at $\mu > 1$ Hamiltonian (54) has unique ground state and all the components of its eigenvector have the same sign, say positive. It is true for any subspace with a specified M. Such a subspace includes all the states with $S \geq M$. It can be shown that in the basis (55) the lowest ferromagnetic state of the Hamiltonian (54) has all the components of the same sign. Obviously it is not orthogonal to the ground state. Therefore at $\mu > 1$, Hamiltonian (54) has a unique ferromagnetic ground state.

3.5 Two-dimensional systems

Let us consider a fragment of the two-dimensional rectangular lattice such that the sites are weakly interacting n-site segments situated perpendicularly to the plane of the lattice (Fig.8). One can suppose that similar to the rectangular lattice strips, at $N > L$ the ground state spin of the lattice can be described by means of the polaron hypothesis [44]. Making use of this hypothesis it can be shown that the lattice ground state spin takes a maximum value if electron concentration ρ is taken from one of the intervals

$$A_-(r, n, t_\perp, t) < \rho < A_+(r + 1, n, t_\perp, t), \tag{56}$$

where

$$a(r, n) = \frac{1}{n}\left[-\frac{\varepsilon(r, n)}{2\pi}\right]^{0.5} \quad A_\pm(r, n, t_\perp, t) = r\, n^{-1} \pm a(r, n)\alpha^{0.5},$$

$$\alpha = \left|\frac{t_\perp}{t}\right|, \quad r = 1, 2 \ldots n - 1,$$

$\varepsilon(r, n)$ is a dimensionless ground state energy per unit cell for the lattice formed by n-site segments with r electrons per segment. For the square lattice there is a numerical estimate: $\varepsilon(1, 2) = -1.17$ [45].

To check the adequacy of this polaron estimate we performed a direct numerical study of the exact lowest energy spectra of small $\sqrt{L} \times \sqrt{L}$ clusters of rectangular and triangular lattices formed by weakly interacting two-site segments. The least squares fit of the results of this study gives the following dependence between number of segments and a critical value of the anisotropy parameter α [44]:
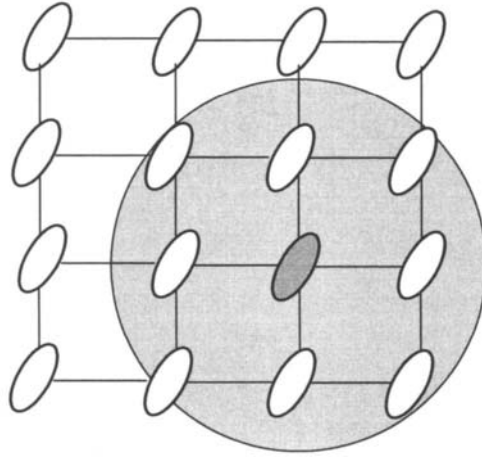
Figure 8. A fragment of two-dimensional rectangular lattice with $N=L+1$. The shaded circle corresponds to the region with ferromagnetic spin ordering around the segment with an additional electron (the shaded ellipse).

Square lattice: $L = 2.69\alpha^{-0.47}$

Triangular lattice: $L = 3.50\alpha^{-0.35}$

4. EMERY MODEL

One of the simple models of high-T_c superconducting copper oxides is a two-band Hubbard Hamiltonian (so called Emery model) [46]

$$H = t_{pd} \sum_{ij\sigma} \left(\mathbf{p}_{i,\sigma}^+ \mathbf{d}_{j,\sigma} + \mathbf{d}_{j,\sigma}^+ \mathbf{p}_{i,\sigma} \right) + \alpha \sum_{i\sigma} \mathbf{p}_{i,\sigma}^+ \mathbf{p}_{i,\sigma} + U_p \sum_i \mathbf{p}_{i,\sigma}^+ \mathbf{p}_{i,\sigma} \mathbf{p}_{i,-\sigma}^+ \mathbf{p}_{i,-\sigma}$$
$$+ t_{pp} \sum_{ij\sigma} \left(\mathbf{p}_{i,\sigma}^+ \mathbf{p}_{j,\sigma} + \mathbf{p}_{j,\sigma}^+ \mathbf{p}_{i,\sigma} \right) + U_d \sum_i \mathbf{d}_{i,\sigma}^+ \mathbf{d}_{i,\sigma} \mathbf{d}_{i,-\sigma}^+ \mathbf{d}_{i,-\sigma} \tag{57}$$

Here t_{pd} is the hopping integral, representing the hybridization of oxygen and copper bands, t_{pp} describes direct hops of holes between neighbor oxygen atoms; α is a difference between the orbital energies for oxygen and copper sites, U_p and U_d are Hubbard energies for oxygen and copper sites respectively.

Let us consider a one-dimensional lattice described by (57) with $\left| t_{pd} \right| << \alpha$, $t_{pp}=0$ and $U_d=\infty$ and enumerate the spins of holes in succession over the sites independently of type. In this case, the lattice Hamiltonian with periodic boundary conditions and one hole in an oxygen band can be written in the form [23,47]

$$\mathbf{H} = \sum_l J_1 \mathbf{a}_l^+ \mathbf{a}_l \mathbf{Q}_{l,l+1} + J_2 \left(\mathbf{a}_l^+ \mathbf{a}_{l+1} + \mathbf{a}_{l+1}^+ \mathbf{a}_l \right) + J_2 \left(\mathbf{a}_1^+ \mathbf{a}_N \mathbf{Q}^+ + \mathbf{a}_N^+ \mathbf{a}_1 \mathbf{Q} \right) \tag{58}$$

$$J_1 = \frac{t^2}{\alpha + U_p}, \quad J_2 = \frac{t^2}{\alpha}$$

where $\mathbf{a}_l^+$ is the creation operator for a hole at l-th oxygen atom, while $\mathbf{Q}$ is the cyclic spin permutation of all $N+1$ spin variables of $2N$-site lattice.

The Hamiltonian (58) commutes with the operator that displaces all the spins by one unit cell cyclically. Therefore, the eigenfunctions of (58) must be characterized by hole quasi-impulse $k = 2\pi m / N$ ($m=1,2...N$). The symmetry adapted basis functions corresponding to a fixed value of k can be constructed by the usual group theory technique.

$$\Psi_{k,\lambda} = N^{-\frac{1}{2}} \sum_{l=1}^{N} \exp(ikl)\mathbf{Q}^{l+1}\mathbf{a}_{N-l+1}^+ |0\rangle \Theta_\lambda \tag{59}$$

Omitting simple manipulations with the cyclic permutations, we can rewrite the Hamiltonian (1) in the following form:

$$H = J_1\left(\mathbf{Q}_{1,2} + \mathbf{P}_{1N+1}\right) + J_2\left[\exp(ik)\mathbf{Q}_{1,N+1} + \exp(-ik)\mathbf{Q}_{1,N+1}^+\right] \tag{60}$$

So, to use the spin permutation technique we constructed the symmetry adapted lattice Hamiltonian in a compact operator form and essentially reduced the dimensionality of the corresponding eigenvalue problem. The effects of $t_{pp} \neq 0$ and the additional superexchange of copper holes are considered in [48].

REFERENCES

[1] I.A.Misurkin and A.A.Ovchinnikov, Russ.Chem.Rev., 46 (1977) 967.
[2] H.G. Kiess (eds.), *Conjugated Conducting Polymers*, Springer-Verlag, Berlin, 1992.
[3] L.N.Bulaevskii, A.V.Zvarykina, Yu.S.Karimov, R.B. Lyubovskii and I.F.Shchegolev, Zh.Eksp.Teor.Fiz., 62 (1972) 725.
[4] A.L.Tchougreeff and I.A.Misurkin, Phys.Rev. B46 (1992) 5357.
[5] P.W.Anderson, Science, 235 (1987) 1197.
[6] P.W.Anderson and J.R. Schieffer, Phys. Today, 44 (1991) 54.
[7] E.H.Lieb, ASI NATO Series B: Physics, 343 (1995) 1.
[8] J.Hubbard, Proc.R.Soc. London Ser.A, 276 (1963) 238.
[9] J.H.Van Vleck and A.Sherman Rev.Mod.Phys. 7 (1935) 167.
[10] L.Pauling and G.M.Wheland, J.Chem.Phys., 1 (1933) 362.
[11] D.J.Klein, (Z.B.Maksic and W.J.Orville-Thomas) *Pauling's Legacy: Modern Modelling of the Chemical Bond. Theoretical and Computational Chemistry*, Elsevier, Science B.V. 6 (1999). pp.403-420.
[12] L.N.Bulaevskii, Zh.Eksp.Teor.Fiz., 51 (1966) 230.
[13] S.Kuwajima, J.Chem.Phys., 77 (1982) 1930.
[14] D.Maynau, J.P.Malrieu J.Amer.Chem.Soc. 104 (1982) 3029.
[15] S.Lee, J.Chem.Phys., 90 (1989) 2732.
[16] J.Aihara, J.Chem.Soc.Perk.T., 2 (1994) 971.
[17] E.H.Lieb and D.C.Mattis, J.Math.Phys., 3 (1962) 749.
[18] S.A.Alexander and D.J.Klein, J.Am.Chem.Soc. 110 (1988) 3401.
[19] A.A.Ovchinnikov, Theor.Chim.Acta, 47 (1978) 297.

[20] D.J.Klein, C.J.Nelin, S.A.Alexander and F.A.Matsen, J.Chem.Phys., 77 (1982) 3101.
[21] W.Brinkman and T.M.Rice, Phys.Rev. B, 2 (1970) 1324.
[22] V.Ya.Krivnov, A.A.Ovchinnikov, and V.O.Cheranovskii, Synth.Metals, 33 (1989) 65.
[23] V.O.Cheranovskii, Int.Journ.Quant.Chem., 41 (1992) 695.
[24] V.O.Cheranovskii, Int.Journ.Quant.Chem. 46 (1993) 577.
[25] E.V.Ezerskaya and V.O.Cheranovskii, Sov.J.Low Temp.Phys. 18 (1992) 872
[26] V.O.Cheranovskii, O.Esenturk, H.O.Pamuk, Phys.Rev., B 58 (1998) 12260.
[27] A.B.Harris and R.V.Lange, Phys.Rev., 157 (1967) 295.
[28] V.O.Cheranovskii, Thesis, Kharkov 1993.
[29] S.Ramasesha and Z.G.Soos, Int.J.Quantum Chem., 25 (1984) 1003.
[30] M.W.Long and X.Zotos, Phys.Rev., B 45, (1992) 9932.
[31] E.H.Lieb, Phys.Rev.Lett. 62 (1989) 1201.
[32] Y.Nagaoka, Phys.Rev., 147 (1966) 392.
[33] D.J.Thouless, Proc. Phys. Soc. London, 86 (1965) 893.
[34] H.Tasaki, Phys.Rev., B 40 (1989) 9192.
[35] V.Ya.Krivnov, A.A.Ovchinnikov and V.O.Cheranovskii, Helvetica Physica Acta, 65, (1992) 454.
[36] M.Konho, Phys.Rev., B 56 (1997) 15015.
[37] T.Hanish, B.Kleine, A.Ritzi, and E.Muller-Hartmann, Ann. Phys., 4 (1995) 303.
[38] M.Takahashi, J.Phys.Soc.Jpn., 51 (1982) 3475.
[39] D.J.Klein, W.A.Seitz, Phys.Rev., B 10 (1974) 3317.
[40] V.O.Cheranovskii, E.V.Ezerskaya and M.V.Krikunov, Int.Journ.Quant.Chem. 81 (2001) 253.
[41] V.O.Cheranovskii, E.V.Ezerskaya, and M.V.Krikunov, Low Temp.Phys., 25 (1999) 280.
[42] A.Mielke, J.Phys., A24 (1991) L73.
[43] H.Tasaki, J.Stat.Phys., 84 (1996) 535.
[44] M.V.Krikunov and V.O.Cheranovskii, Kharkov University Bulletin. Chemical Series, 2 (1998) 53.
[45] V.O.Cheranovskii, T.G.Schmalz, and D.J.Klein, J.Chem.Phys., 101 (1994) 5841.
[46] V.J.Emery, Phys.Rev.Lett., 58 (1987) 2794.
[47] V.Ya.Krivnov, A.A.Ovchinnikov and V.O.Cheranovskii, Research Reports in Physics. *Electron-electron correlation effects in low-dimensional conductors and super-conductors*, Springer-Verlag, Heidelberg 1991.
[48] V.Ya.Krivnov and V.O.Cheranovskii, Fiz. Tverd. Tela, 34 (1992) 3101.

This Page Intentionally Left Blank

Chapter 22

Many body VB ansätze. From polymers and ladder materials to the square lattice

M. A. Garcia-Bach

Departament de Física Fonamental, Facultat de Física, Universitat de Barcelona, Diagonal 647, 08028 Barcelona, Catalunya, Spain

SUMMARY

We consider different variational localized-site wave functions, i.e. a cluster-expanded *ansatz* based upon a Néel-state as a zero-order picture, and Resonating Valence Bond *ansätze*, for the spin=1/2 antiferromagnetically-signed Heisenberg Hamiltonian appropriate for square lattice strips and conjugated polymers. For Resonating Valence Bond *ansätze* a Long-Range Spin-Pairing Order can be used to separate the space generated by the covalent Valence Bond configurations into different subspaces. The equivalence among different subspaces when connected by symmetry operations opens the possibility of either twofold degeneracy or spin-Peierls distortions. Degeneracy, energy ordering, and discontinuities in the Long-Range Spin-Pairing Order due to the presence of topological spin-defects rationalize the differences among different strips. Computationally feasible formulae for expectation values are obtained using either a powerful "Transfer-matrix" technique or a "residual-overlap-ratios" technique.

1. INTRODUCTION

Before the discovery, in 1986, by Bednorz and Müller [1] of high-T_c super-conductivity, there was a rather widespread belief that Solid State Theory was satisfactorily built so as to allow the comprehension of any solid state problem, provided the computations to be carried out were feasible. Nourishing this believe there was, on the free quasi-particle side, the Fermi Liquid Theory and tools as Green Functions and Diagrammatic Perturbation Theory, which allowed to study most of the band-theoretic-based solid-state properties. Namely, Diagrammatic Perturbation Theory has

been the major theoretical tool for treating interactions in metals, semi-conductors, itinerant magnets, and low T_c superconductors. Nevertheless, one already could found in the literature some papers pointing to problems needing a deeper understanding (see, for instance the pioneering work of Anderson [2].

In the opposite end, in the strongly correlated domain, magnetic behavior was studied via Ising and Heisenberg-related empirical Hamiltonians, with actual results mainly semi-classical or mean-field-like.

To cover the gap between them the Hubbard model Hamiltonian was quite generally accepted. This Hamiltonian apparently has the ability of mimicking the whole spectrum, from the free quasi-particle domain, at $U=0$, to the strongly correlated one, at $U \to \infty$, where, for half-filled band systems, it renormalizes to the Heisenberg Hamiltonian, via Degenerate Perturbation Theory. Thence, the Heisenberg Hamiltonian was assumed to be acceptable only for rather small t/U values.

However, in the preceding two decades, there have been many experimental discoveries, beside high-T_c superconductivity, evidencing that we do not have yet the proper theoretical skills and tools to deal well with strongly correlated electron systems. For instance, heavy-fermions, fractional quantum Hall effect, ladder materials, and very specially high-T_c superconductivity seem not accessible from the weak coupling limit.

To deal with these systems, the solid state community has turned to effective Hamiltonians, the more paradigmatic being the Hubbard, the t-J and (at half filling) the Heisenberg models. For instance, Anderson [3] suggested that the important features of the undoped High T_c parent compounds can be described by a Heisenberg Hamiltonian on a two-dimensional square lattice with one electron per site. More recently Dagotto [4] proposed that this model on square lattice strips are also relevant to describe the ladder materials.

Meanwhile in Chemistry the Heisenberg Hamiltonian, which is known as the (covalent-structure) valence-bond (VB) model, has also been applied to conjugated systems. Therefore, some parallelism can be established between ladder materials and long conjugated polymers.

Nevertheless, several concerns emerged related about the adequacy or the predictive capability of the model Hamiltonians. Particularly, it has been argued that Coulomb interactions are not strong enough to justify the Heisenberg or the t-J model Hamiltonians for high-T_c superconductivity. However, in the literature one can find different derivations of effective Hamiltonians [5-10] enlarging its validity beyond the generally accepted Degenerate Perturbation Theory limit. Even more, it has also been claimed [11] that the Hubbard Hamiltonian is a good approximation to a

more complete Hamiltonian (with more extended Coulombic interactions) largely when the Heisenberg Hamiltonian is too.

The appropriate parameterization is also essential to the predictive capability of model Hamiltonians. Hence, much progress has been achieved on the computation of reliable appropriate parameterizations [12-15], obtained by accurate electronic structure calculations using as external input the crystal structure only. Here, we will not pursue on these two topics furthermore.

A third concern about correlated systems is related to the task of solving the appropriate effective Hamiltonians and extracting information from them. Our interest here concerns work towards this goal. Thence, in this chapter we focus our attention on some useful tools and different many-body wave functions which allow extracting information from Heisenberg-like Hamiltonians with controlled approximations capable of a systematic improvement. This chapter cannot pretend to be exhaustive, though.

This chapter is organized as follows: The quantum antiferromagnetic spin-1/2 strips and their unit cells are described in Section 2. The Model Hamiltonians considered here are presented in Section 3. The Néel-state based cluster-expanded *ansatz* can be found in Section 4. The resonating valence-bond cluster-expanded *ansätze* and their properties are presented in Section 5. In particular, the model space generated by the covalent valence-bond singlet configurations can be found in Subsection 5.1. The long-range spin-pairing order underlying the covalent VB singlets is developed in Subsection 5.2. The Resonating Valence Bond cluster-expanded *ansatz* are described in Subsection 5.5. The treatment of expectation values by a transfer matrix technique is described in Subsections 6.2. Some results and its discussion can be found in Section 7. Finally, the conclusions are presented in Section 8.

2. QUANTUM ANTIFERROMAGNETIC SPIN-1/2 STRIPS

For the sake of simplicity, we limit ourselves to extended half-filled bipartite systems, with equal number of sites in each sublattice, A (non-starred) and B (starred),

$$N^A = N^B \equiv N, \tag{1}$$

showing finite width and infinite length ($L \to \infty$). We will refer to them as *strips*.

These strips are presumed to be *translationally symmetric* along L, with periodic boundary condition. Each site of the strip is taken to wear a
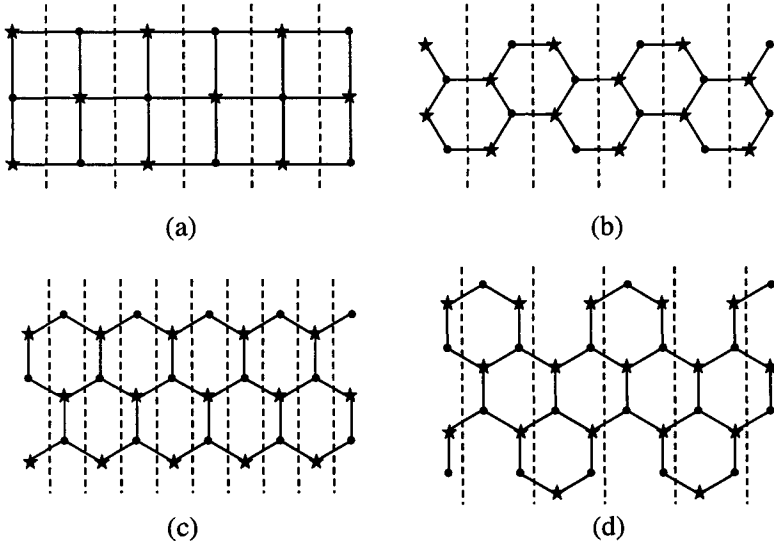
Figure 1: Some examples of fragments of strips: (a) Square lattice strip or ladder of $w=3$, (b) polyphenantrene, (c) polyaceacene, (d) poly(benz[m,n])anthracene. The region between two dashed vertical lines define a (reduced) unit cell

spin$=1/2$. Examples of such strips are CuO_2 square-lattice and carbon honeycomb strips. These include ladder materials as well as conjugated polymers, such as polyacetylene (P), p-polyphenylene, polyacene (PA), polyaceacene (PAA), polyphenantrene (PPh), polyperylene (PPR), poly-(benz[m,n])anthracene (PBA) polymers, or even carbon nanotubes. Some examples of strips can be seen in Fig. 1.

The strips may be divided into *unit cells* or eventually *reduced unit cells* (see Fig. 1), when the *space group* of the strip contains operations involving glide-reflections or screw-rotations, i.e. a combination of an improper reflection or two-fold rotation followed by a non-primitive translation of half a unit cell, which by themselves do not leave the lattice invariant. Each cell will contain w sites, $w \times L = 2N$.

Along with the primitive translations, and glide-reflections when appropriate, there are other symmetry operations belonging to the *space group*. In bipartite systems, it is relevant to classify any symmetry operation according to whether it leaves each sublattice invariant or transforms one into each other (see, for instance, Fig. 2).
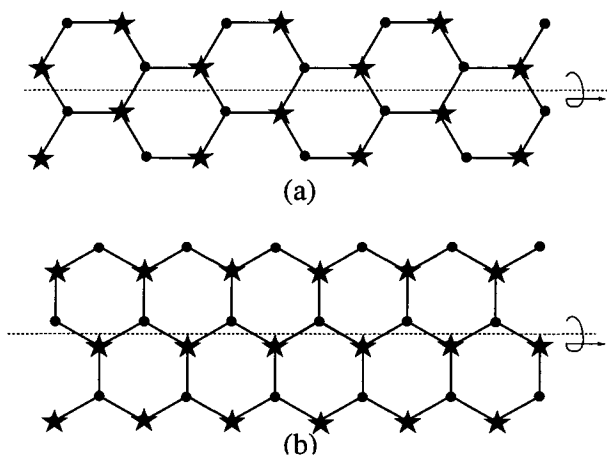
Figure 2: (a) The polyphenantrene polymer with its glide-reflection plane. Here the A and B sublattices are invariant under this symmetry operation. (b) Polyaceacene polymer with its glide-reflection plane. Notice that here the A and B sublattices transform one into each other under this symmetry operation.

3. MODEL HAMILTONIANS FOR QUANTUM SPIN-1/2 STRIPS

The lowest-lying fraction of the strips spectra is assumed to be describable by a spin Hamiltonian

$$H = H_s + H_r, \tag{2}$$

where H_r is a spin-independent distance-dependent term and H_s is the antiferromagnetic quantum spin-$\frac{1}{2}$ Heisenberg Hamiltonian,

$$H_s = \sum_{ni,mj} J_{ni,mj} \, \mathbf{s}_{ni} \cdot \mathbf{s}_{mj}, \tag{3}$$

where $\mathbf{s}_{ni}$ is the spin operator for spin on site ni, n indicating the cell and i the site within the cell, and the $J_{ni,mj}$ are the exchange-coupling parameters. The $J_{ni,mj}$ are assumed to decrease very rapidly with distance. Even more, frequently the Heisenberg Hamiltonian is restricted solely to the nearest-neighbor terms,

$$H_s \to H_{\mathrm{nn}} = \sum_{\langle ni,mj \rangle} J_{\langle ni,mj \rangle} \, \mathbf{s}_{ni} \cdot \mathbf{s}_{mj}, \tag{4}$$

$\langle ni, mj \rangle$ indicating that ni and mj are nearest-neighbor.

Recently the appropriate $J_{ni,mj}$ values for some ladder materials [16,17] as well as for the well-known CuO_2 planes shown by high-T_c superconduc-

tors [14,15] have already been obtained. Meanwhile, for the conjugated polymers, the *ab initio* distance-dependent $J(r)$ as well as the two-body contributions, $R(r_{\langle ni,mj \rangle})$, to the spin-independent term, H_r, were obtained early in 1984 [18],

$$H_r \approx \sum_{\langle ni,mj \rangle} R(r_{\langle ni,mj \rangle}). \tag{5}$$

Since the degrees of freedom for a spin-1/2 system with $2N$ sites grows as 2^{2N}, solving the spin-1/2 Heisenberg Hamiltonian for extended systems, is not an easy task. In fact, exact solutions for spin-1/2 nearest-neighbor Heisenberg models are largely limited to that of Hulthén [19] for the linear chain. Thence approximate solutions are generally required. In doing so, special care must be taken to ensure size-consistency, since we are dealing with extended systems. Therefore, we will focus our attention on wave functions obtained as cluster-expanded 'excitations' acting on an appropriate zero-order wave function.

Rough approximations to the ground state for the Heisenberg Hamiltonian to be used as our zero-order wave-functions are the Néel state and the Kekulé or dimer-covering VB structures. The Néel state is mostly used in Physics. Although it is not a singlet, thence violating the Lieb and Mattis theorem [20], it has the suggestive image of a spin-ordered classical antiferromagnet. The alternative of using the dimer-covering configurations as a rough approximation to the ground state seeks to take advantage of the fact that the Heisenberg Hamiltonian commutes with the total-spin operator and the Lieb and Mattis theorem ensuring that the ground state is a singlet. At this level of approximation, it is seen that the energy expectation value is lower for the Néel state than for a single dimer-covering VB structure when the number of nearest-neighbors is greater than three. A paradigmatic case where the Néel state is far from the actual ground state is that of a linear chain, with a coordination of two. Nevertheless, in the two-dimensional honeycomb fragment or strip, with mixed coordination numbers of two and three, or the square-lattice strips, with coordination of three and four, reasonable doubts emerge about the nature of the ground state. For instance, either the inclusion of next-nearest-neighbor spin interactions or better ground-state wave functions can reverse the rough-level energy ordering.

Therefore, two main different kinds of variational localized-site cluster expanded *ansätze* have so far been considered: first the *Néel-state-based ansätze* (NSBA), where the Néel state is the zero order wave-function from which the trial wave-functions are generated, and second the *Resonating*

VB (RVB) *ansätze*, where the trial wave-functions are a weighted super-position of singlets, each singlet being a product of N two-body singlets on two (not necessarily nearest-neighbor) sites at a time.

4. THE NEEL-STATE-BASED CLUSTER-EXPANDED ANSÄTZE

The cluster expanded wave-function *ansätze* in this section are based upon the Néel state as a zero-order wave-function,

$$|\Phi_N\rangle \equiv \prod_{ni}^{ni \in A} \alpha(ni) \prod_{mj}^{mj \in B} \beta(mj), \tag{6}$$

where $\alpha(ni)$ $[\beta(ni)]$ indicates that the spin of the electron on site ni is $+1/2$ $[-1/2]$.

Starting from $|\Phi_N\rangle$, we notice that it is neither an eigenstate of a Heisenberg Hamiltonian nor an eigenstate of the total spin operator S^2. For instance, the Néel state is not invariant under the action of the nearest-neighbor XY spin terms of the Heisenberg Hamiltonian, which may produce a spin-flip on two nearest-neighbor sites at a time with respect to $|\Phi_N\rangle$. These XY 'excitation operators' from the 'vacuum' $|\Phi_N\rangle$, can be written as

$$F^+_{\langle ni, mj \rangle} \equiv s^-_{ni} s^+_{mj}, \quad ni \in A, \tag{7}$$

where $s^{\pm}_{ni} \equiv s^x_{ni} \pm i s^y_{ni}$. Since $|\Phi_N\rangle$ is invariant under the action of the spin terms involving sites an even number of bonds apart, the relevant excitations above the Néel state would be those between sites an odd number of bonds apart. As it is expected that the spin interactions between sites more than two bonds apart are small, for the sake of simplicity here we will limit ourselves to the excitation operators of Eq. (7).

Therefore, a family of states susceptible to mixing with the Néel state are obtained when applying to the Néel state a product of an arbitrary number of such $F_{\langle ni, mj \rangle}$ excitation operators in an "unlinked" way,

$$F^+_{\Gamma(\mu)} \equiv \prod_{\langle ni, mj \rangle}^{\in \Gamma(\mu)} F^+_{\langle ni, mj \rangle}, \tag{8}$$

where $\Gamma(\mu)$ is a not-necessarily-connected set of μ bonds of the strip with no sites in common. Thence, a lowering of the energy, with respect to that of the Néel state, occurs for an *ansatz* defined within a space spanned by

the family of states of the form

$$|\Phi_N^{\Gamma(\mu)}\rangle \equiv F_{\Gamma(\mu)}^+|\Phi_N\rangle. \tag{9}$$

Notice that the Néel state belongs to this space, $|\Phi_N\rangle = F_\emptyset^+|\Phi_N\rangle$, where $\emptyset$ stands for the empty set.

For a finite system, approximate eigenstates within the space generated by the $|\Phi_N^{\Gamma(\mu)}\rangle$ could be obtained by Configuration Interaction (CI),

$$|\Psi_N\rangle = \sum_{\Gamma(\mu)} C_{\Gamma(\mu)}|\Phi_N^{\Gamma(\mu)}\rangle. \tag{10}$$

For $L \to \infty$, the 'exact' values of the CI weight, $C_{\Gamma(\mu)}$, of each state into the ground state cannot be obtained. Therefore, they are to be written as a function of a few variational parameters. To do so, every $|\Phi_N^{\Gamma(\mu)}\rangle$ can be viewed as made of connected clusters with a spin-flip pattern in each connected cluster. Any spin-flip pattern in a connected cluster can be written as

$$\mathcal{P}_{\xi(\mu,\nu)}^+ \equiv F_{\gamma(\mu)}^+ I_{\eta(\nu)}. \tag{11}$$

In Eq. (11), $I_{\eta(\nu)}$ is the identity operator on the set of sites $\eta(\nu)$, which contain ν sites; $\gamma(\mu)$ is a set of μ bonds with no site in common, and $\xi(\mu, \nu)$ is the connected cluster of the 2μ sites in $\gamma(\mu)$ and the ν sites in $\eta(\nu)$,

$$\gamma(\mu) \cup \eta(\nu) \equiv \xi(\mu, \nu), \tag{12}$$
$$\gamma(\mu) \cap \eta(\nu) = \emptyset. \tag{13}$$

We associate a variational parameter $x_{\xi(\mu,\nu)}$ to the spin-flips pattern $\mathcal{P}_{\xi(\mu,\nu)}^+$.

Thence, variational localized-site cluster expansion *ansätze* based upon the Néel state can be defined as

$$|\Psi_N^M\rangle = \mathcal{U}(e^{\mathcal{P}_M^+})|\phi_N\rangle, \tag{14}$$

where

$$\mathcal{P}_M^+ \equiv \sum_{\xi(\mu,\nu)}^{2\mu+\nu \leq M} x_{\xi(\mu,\nu)} \mathcal{P}_{\xi(\mu,\nu)}, \tag{15}$$

and the summation is limited to connected clusters of no more than M sites. The $x_{\xi(\mu,\nu)}$ are scalars to be optimized, while submitted to appropri-

ate translation-symmetry restrictions. $\mathcal{U}$ indicates that only the unlinked portion of $e^{\mathcal{P}_M^+}$ is to be retained, i.e., a product as $\Pi_{\xi(\mu,\nu)} \mathcal{P}_{\xi(\mu,\nu)}^+$ is to be retained in the Taylor series expansion of $e^{\mathcal{P}_M^+}$ only if none of the sets $\xi(\mu,\nu)$ in the product have a site in common.

Notice that different levels of approximation can naturally be achieved when allowing a set of increasing values of M.

4.1. Linear chain

For the linear chain, any connected cluster $\xi(\mu,\nu)$ is simply a set of consecutive sites $\{n, n+1, \ldots n+m\}$. Numerical results for *ansätze* using connected-cluster patterns involving up to $M = 4$ sites, for alternate chains, and up to $M = 5$ sites, for regular chains, have been obtained so far. The hierarchy of patterns have been defined as

$$\mathcal{P}_{\{n,n+1\}}^+ \equiv x_n F_{\langle n,n+1 \rangle}, \tag{16}$$

$$\mathcal{P}_{\{n,n+1,n+2,n+3\}}^+ \equiv y_n F_{\langle n,n+1 \rangle} F_{\langle n+2,n+3 \rangle} + z_n F_{\{n,n+3\}} I_{\{n+1,n+2\}}, \tag{17}$$

$$\mathcal{P}_{\{n,n+1,n+2,n+3,n+4\}}^+ \equiv t_n F_{\langle n,n+1 \rangle} I_{\{n+2\}} F_{\langle n+3,n+4 \rangle}. \tag{18}$$

The x_n, y_n, z_n and t_n are variational parameters submitted to translational symmetry restrictions, $v_{n+m} = v_n$, $v \equiv x, y, z, t$, where $m = 1$ for a regular chain, and $m = 2$ when alternating translational symmetry conditions are desired.

4.2. Strips with $w > 1$

For strips with $w > 1$, up to now the NSBA has been limited to $M = 2$ *ansätze*. Thence

$$\mathcal{P}^+ \equiv \sum_{\langle ni,mj \rangle} x_{\langle ni,mj \rangle} F_{\langle ni,mj \rangle}. \tag{19}$$

The variational parameters are submitted to translational symmetry restrictions and are assumed to be different when associated to spin-flips on non-equivalent bonds. Several conjugated polymers and square-lattice strips have been treated so far.

5. THE RESONATING-VALENCE-BOND ANSÄTZE

Since the Heisenberg Hamiltonian commutes with the total-spin operators, the 2^{2N}-dimensional spin space can be separated in subspaces with

well defined total spin $\mathbf{S}^2$ and S^z. Trivially, there is only one totally ferromagnetic state, i.e. with spin $S = S^z = N$, $|N, N\rangle$. From it, $2N$ states with $S^z = N - 1$ can be obtained by the action of the s_{ni}^-, ni ranging. Linearly independent combinations of these $s_{ni}^-|N, N\rangle$ yield the $|N, N - 1\rangle$ state plus $2N - 1$ different $|N - 1, N - 1\rangle$ states. Furthermore, applying to the totally ferromagnetic state products such as $s_{ni}^- s_{mj}^-$, $ni \neq mj$, it is easily seen that

$$d_N^{2N} + d_{N-1}^{2N} + d_{N-2}^{2N} = \frac{2N(2N - 1)}{2!} = \frac{(2N)!}{2!(2N - 2)!}, \tag{20}$$

where d_{N-m}^{2N} is the number of states with $S = S^z = N - m$. Following this line of reasoning, it can be easily shown that

$$d_N^{2N} + d_{N-1}^{2N} + \cdots + d_{N-m}^{2N} = \frac{(2N)!}{m!(2N - m)!}. \tag{21}$$

Therefore, with this recursive relations, the dimension of any well-defined spin subspace can be obtained. In particular, since the results of Lieb and Mattis [20] establishes that the ground state of systems with equal number of sites in each sublattice must be a singlet, we will limit ourselves to the singlet subspace. Then, the ground state can be written as a weighted superposition of a non-orthogonal complete basis set of singlets, $|\sigma_i\rangle$, $i = 1$ to d_0^{2N}, where d_0^{2N} can be easily obtained making use of Eq. (21),

$$d_0^{2N} = \frac{(2N)!}{(N + 1)!N!}, \tag{22}$$

and is known as the Catalan number.

In a bipartite system a set of d_0^{2N} independent singlets can be constructed by pairing to a singlet each of the N spins in A to a spin in B, with no site unpaired. We represent one of these spin-pairings (SP) by an arrow from the site in the sublattice A to its partner in B (see, for instance, Fig. 3, where a complete set of linearly-independent singlets for six-site systems are represented).

Although the dimension of the space where the ground state is constructed has been considerably reduced with respect to 2^{2N}, d_0^{2N} still grows too rapidly with N and truncating the covalent VB basis set is required soon. Therefore, the many-body or multiconfigurational (covalent) VB wave functions, i.e. resonating-valence-bond-type (RVB) wave functions, are to be defined in a still smaller VB subspace. In order of selecting the relevant VB configurations in the basis set, we rely on two facts. First,
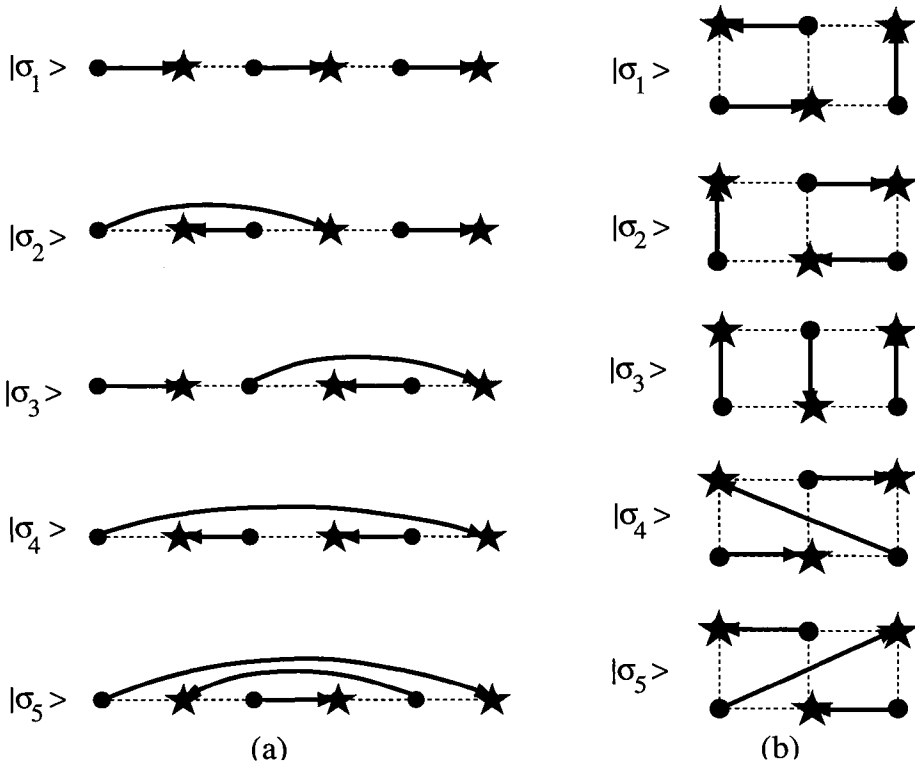
Figure 3: A complete set of linearly independent (covalent) singlets for a six-sites system: a) 1×6; b) 2×3.

the dimer-covering configurations (or Kekulé structures [21], as they have always been termed in Resonance Theory) are the lowest-lying monoconfigurational singlets. Thus, they provide a good zero-order picture upon which the longer-range RVB *ansätze* are based. Second, the VB configurations show a long-range spin-pairing order which allow to separate the VB configurations into different non-interacting sectors.

5.1. The M-range covalent VB structures

Although the dimer-covering configurations are the lowest lying VB structures, the space generated by the dimer-covering configurations alone is not invariant under the Hamiltonian operator. However, on applying the Hamiltonian to any Kekulé structure, it can be noticed that the nearness of spin pairing tends to be preserved. For instance, the XY terms, $s_{ni}^{\pm} s_{mj}^{\mp}$, of the nearest-neighbor Heisenberg Hamiltonian acting on a Kekulé structure yield singlets with SP between sites up to 3 bonds apart (see Fig. 4). Then, as a first step, linearly independent singlets with 3-bond-
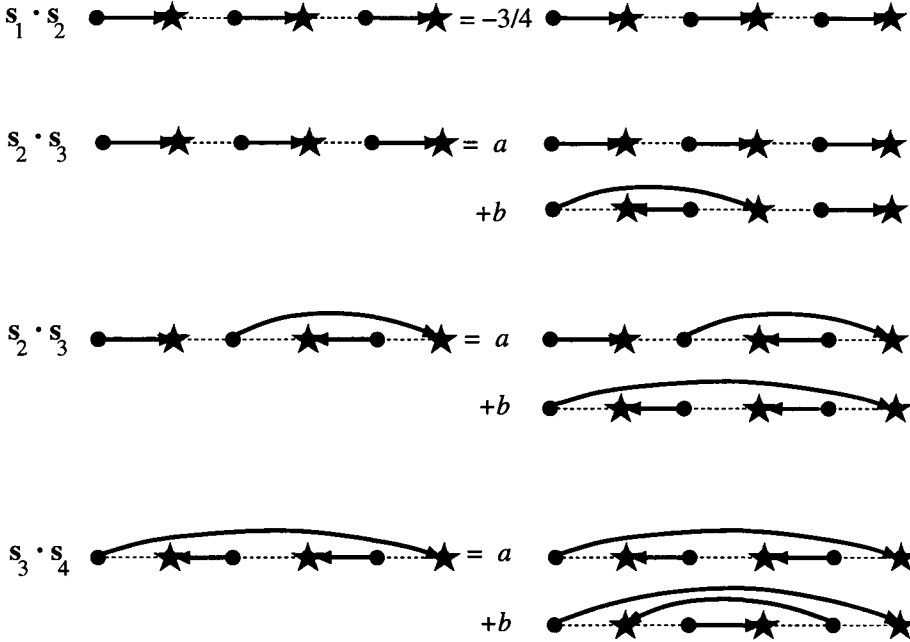
Figure 4: A dimer-covering configuration is an eigenstate of $\mathbf{s}_j \cdot \mathbf{s}_k$ when sites j and k are spin-paired. The "off-diagonal" singlet with (i, l^*) and (k, j^*) pairings is also obtained when $\mathbf{s}_j \cdot \mathbf{s}_k$ acts on a VB configuration with spin-pairings (i, j^*) and (k, l^*).

range (3BR) SP should be incorporated into the model space, $\mathcal{H}$, to go beyond the dimer-covering approximation. These 3BR-SP states allow sites in the A-sublattice to be SP to sites in the B-sublattice no more than 3 bonds apart. These states can be directly generated by the "recoupling" [22,23] of two simply adjacent bond-dimers, i.e. unlinked bond-pairs with one and only one site in a pair being a nearest neighbor to a site in the other pair. It is worth noting that these re-couplings satisfy a generalized non-crossing rule. Thence, the 3BR-SP model space incorporates any singlet obtained from any Kekulé structure when allowing an arbitrary number of unlinked recouplings between simply adjacent bond-pairs. Still longer-range model spaces can be obtained allowing an arbitrary number of recouplings between longer-range SP (see Fig. 4). Thence 5BR-SP, 7BR-SP, ..., would be included into $\mathcal{H}$. Nevertheless, singlets with very long bond-range SP should contribute less, so a reasonable model space will be that including singlets with SP up to M bonds apart, M not necessarily being small. Hence, the RVB wave functions are defined in the space spanned by M-BR-SP, with large but finite M. We refer to this space as the M-BR *model space*. In this context, the Kekulé structures are referred

to simply as the 1-BR configurations.

However, we note that the M-range RVB pictures neglect corrections lying higher than the M order in Perturbation Theory, which could be important for the isotropic nearest-neighbor Heisenberg Hamiltonian for some systems. Although, additional frustrational terms in the Hamiltonian are expected to stabilize the finite-range RVB wave functions with respect to other Néel-based *ansätze* (see Ref. 24 and references therein). Indeed, there exist finite-range Heisenberg models for which short-range Kekulé structures are exact ground states and also short-range RVB *ansätze* certainly apply for so-called "bond-dimer" models (see, for instance, References from 25 to 29).

5.2. Singlets and long-range spin-pairing-order

In order to reduce the dimension of the model space, several attempts have been made to find associated topological quantum numbers which would allow to separate the covalent VB space into non-mixing different subspaces (see Ref. 30 and references therein). For the linear chain, preliminary attempts were made early in 1979 [31], when a parameter measuring the spin-pairing long-range order was suggested,

$$\rho \equiv 2 \lim_{|p-n|\to\infty} (-1)^{p-n} \langle (\mathbf{s}_n \cdot \mathbf{s}_{n+1} - \langle \mathbf{s}_n \cdot \mathbf{s}_{n+1} \rangle)(\mathbf{s}_p \cdot \mathbf{s}_{p+1} - \langle \mathbf{s}_p \cdot \mathbf{s}_{p+1} \rangle) \rangle. \quad (23)$$

Recently, in Ref. 30, it has been shown that monoconfigurational covalent VB structures for ladder materials show a long-range spin-pairing order (LR-SPO). This LR-SPO can be easily generalized to our present strips.

Let us take f_n to be the right boundary of the cell n. Thus, f_n unambiguously break up the strip in two regions: a left region, L_n, and a right region, R_n (see Fig. 1). Furthermore, the f_{n-1} and f_n boundaries delimit the nth cell.

We define P_n^+ (P_n^-) as the number of arrows penetrating the boundary f_n with the arrowhead in the R_n (L_n) region (see Fig. 5). I_n is the number of arrows with both ends in the cell n. l_n (r_n) is the number of arrows starting in R_n (L_{n-1}) and with the arrowhead in L_{n-1} (R_n), i.e. with no partner belonging to the cell nth. Finally, w_n^A (w_n^B) is the number of sites in the cell n belonging to the sublattice A (B). Then

$$P_{n-1}^- - l_n + P_n^+ - r_n + I_n = w_n^A, \quad (24)$$

$$P_{n-1}^+ - r_n + P_n^- - l_n + I_n = w_n^B. \quad (25)$$
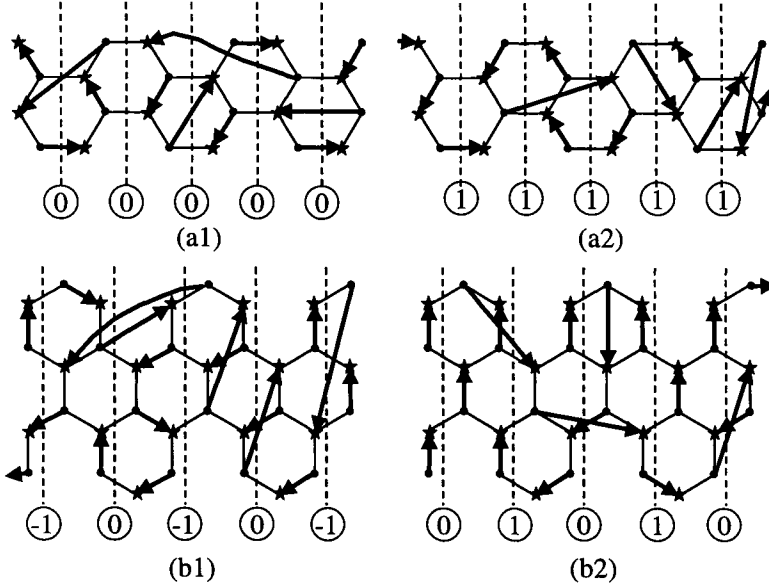
Figure 5: Fragment of VB configurations showing the values of D_n inside circles: (a) Polyphenantrene, with $b = 0$: (1) $D = 0$ and (2) $D = 1$. (b) Poly(benz[m,n]anthracene, with $b_n = -(-1)^n$: (1) $D = -1$ and (2) $D = 0$.

Subtracting Eq. (25) from Eq. (24)

$$P_{n-1}^- - P_{n-1}^+ + P_n^+ - P_n^- = w_n^A - w_n^B. \tag{26}$$

Making use of the *resonance quantum number* at boundary f_n of Klein *et al.* [32],

$$D_n \equiv P_n^+ - P_n^-, \tag{27}$$

we obtain

$$D_n - D_{n-1} = w_n^A - w_n^B \equiv b_n, \tag{28}$$

For translationally symmetric bipartite systems with $N^A = N^B = N$ and cyclic boundary conditions, either b_n is zero or $b_n = -b_{n-1}$, although actual values of b_n for a given strip depend to a certain extend on the unit cell selected. For instance, b_n is even for ladders with an even number of legs, while b_n is odd for ladders with an odd number of legs. In particular,

though, when the unit cells are defined as in Fig. 1, $b_n = 0$ for ladders with an even number of legs, polyacene, polyphenantrene, or polyperylene polymers, while $|b_n| = 1$ for ladders with an odd number of legs, polyaceacene, or poly(benz[m,n])anthracene. Choosing A and B sublattices according to

$$w_1^A - w_1^B \equiv b \geq 0, \tag{29}$$

one has

$$b_n = w_n^A - w_n^B = -(-1)^n b, \tag{30}$$

Thence,

$$w_n^A = \frac{1}{2} \left[w - (-1)^n b \right], \tag{31}$$

$$w_n^B = \frac{1}{2} \left[w + (-1)^n b \right]. \tag{32}$$

Therefore, from Eq. (28) we obtain a recurrence relation for the SPO in any cell boundary,

$$D_{n+1} = D_n + (-1)^n b. \tag{33}$$

Then a SPO parameter $D \equiv D_0$ can be associated to any covalent VB configuration, so that

$$D_n = D + \frac{1}{2} \left[1 - (-1)^n \right] b. \tag{34}$$

Since the shorter range VB structures are expected to contribute to the lower-lying wave functions, the subspaces of interest will contain VB structures with at least one position n where $l_n = r_n = 0$. At this particular position

$$P_n^+ = 0, 1, \ldots w_n^A, \tag{35}$$

$$P_n^- = 0, 1, \ldots w_n^B. \tag{36}$$

Therefore, there generally are $w + 1$ different values of D to be considered,

$$D = \frac{w - b}{2}, \frac{w - b - 2}{2}, \ldots, -\frac{b + w}{2}, \tag{37}$$

and the relevant sector of the VB space can be restricted to these $w + 1$ subspaces, $\mathcal{H}_D^w$, with the values of D from Eq. (37).

For quantum spin-1/2 ladders, it can be seen that there are dimer-covering configurations in any $\mathcal{H}_D^w$ subspace, while that is not so in general. Particularly, when dealing with honeycomb conjugated polymers, it is worthwhile to notice that some subspaces do not contain dimer-covering configurations. Examples of this fact are the $\mathcal{H}_{-1}^4$ and $\mathcal{H}_{-2}^4$ subspaces associated to polyphenantrene.

5.3. LR-SPO of the Eigenstates and Degeneracy

So far, we have separated the relevant model space into $w + 1$ subspaces of different LR-SPO. At this point we note that two singlets from different subspaces must be different repeatedly at every position along the strip. Since the overlap, $\langle \sigma_i | \sigma_j \rangle$, and matrix elements, $\langle \sigma_i | H | \sigma_j \rangle$ can be evaluated using the Pauling's [21,33] superposition rules, by the island-counting technique, two singlets from different subspaces are asymptotically orthogonal and non interacting via any interaction mediated by a few-particle operator. Then, the matrix of the Hamiltonian asymptotically block-diagonalizes, so configurations belonging to different subspaces do not mix in the configuration-interaction sense. Thus D may be taken as a long-range order parameter labeling the eigenstates Ψ_D of the D block.

For a given strip, it may happen that under a symmetry operation one configuration of LR-SPO D transforms into a configuration of different LR-SPO, D'. That happens in particular for symmetry operations that transform one sublattice into each other, since then the arrows representing the SP will change their direction. Sometimes such a symmetry operation may be the one step translation (or the glide reflection when appropriate), $\mathcal{T}$. For instance, when $b \neq 0$, A and B sublattices always must transform one into each other under $\mathcal{T}$,

$$\mathcal{T}A = B, \tag{38}$$

$$\mathcal{T}B = A. \tag{39}$$

On the other hand, for $b = 0$, it may happen either that $\mathcal{T}$ transforms the A- and B-sublattices into each other, as for w=even ladders, or alternatively that A and B sublattices are invariant, as for polyphenantrene (see Fig. 2). Thence, for any strip with $b \neq 0$ and those with $b = 0$ such that the sublattices are not invariant under $\mathcal{T}$, the $\mathcal{H}_D^w$ subspace transforms into the $\mathcal{H}_{-b-D}^w$ subspace,

$$\mathcal{T}\mathcal{H}_D^w = \mathcal{H}_{-b-D}^w. \tag{40}$$

Therefore, there is a one-to-one correspondence among wave functions,

$$\mathcal{T}\Psi_D = \Psi_{-b-D},\tag{41}$$

and the energy of the corresponding wave functions must be

$$E_D = E_{-b-D}.\tag{42}$$

Consequently, degeneracy is expected to occur, unless $2D = -b$ =even. For instance, the D-manifold is spanned by Ψ_D and Ψ_{-b-D}, which are eigenstates of H, but not of $\mathcal{T}$. The eigenstates $\Phi_D^{\pm}$ of the translation operator, are defined in the D-state manifold,

$$\Phi_D^{\pm} \equiv \frac{1}{\sqrt{2}}\left(\Psi_D \pm \Psi_{-b-D}\right),\tag{43}$$

so

$$\mathcal{T}\Phi_D^{\pm} = \pm\Phi_D^{\pm}.\tag{44}$$

with $k = 0$ and $k = \pi$. Even more, if a small variation of the interaction strength occurs, as a result of a distortion, then the accidental degeneracy of Eq. (42) no longer holds. Therefore, either Ψ_D or Ψ_{-b-D} will be lower in energy and completely dominate the wave function, leading to a spin-Peierls broken-symmetry ground state. For instance, early in 1979 [31] it was shown that long linear chains, as seen from the point of view of VB theory, show a long-range order, measured by the parameter ρ in Eq. (23), leading to a ground-state instability to bond alternation. Bond alternation is actually found for polyacetylene (see Ref. 34 and references therein), and it is also expected for other conjugated polymers (see Ref. 23).

5.4. Topological spin defects, excited states and LR-SPO

There are different types of excitations conceivable from a *Maximally-spin-paired* ground state. The common fact of any excitation will be the existence of an even number of *topological spin defects*, i.e. non-paired sites. Preserving half filling (one electron per site), there are primarily *spin excitations*. In this case, two topological spin defects are obtained by breaking one SP to form a triplet state. Away from half filling, hopping terms must be retained in the Hamiltonian and the so-called *t-J model* applies, whence, there are low-energy *spin* and *charge excitations*. For instance, hole doping produces vacant sites, while electron doping produces doubly occupied sites, and in both cases doping produces sites that cannot

be SP. As long the doping is not so strong as to preclude a maximally-spin-paired ground state, either a vacancy or a doubly-occupied site may also be assimilated to topological spin defects in a sea of singlets, although there is no spin associated with them. Still, going up in the hierarchy of Hamiltonians, the Hubbard or even a more general Hamiltonian has to be considered. In this case, still another type of *charge excitations* (though presumably of higher energy if a Heisenberg-like Hamiltonian is assumed to govern the lowest-lying region of the spectrum) can be produced relaxing the single-occupancy restriction. This leads to the *ionic* states, i.e. states with at least a couple of sites, one doubly occupied and the other empty.

Let us now suppose that there is a topological spin defect on site i of cell n, i.e. for any reason the site ni remains not spin-paired. Making use of the freedom of defining the cell and the numbering of the sites in the cell, without lost of generality, let us number the sites such that

$$ni \in \begin{cases} A, & n+i = \text{ even,} \\ B, & n+i = \text{ odd.} \end{cases} \tag{45}$$

Then, Eqs. (24) and (25) become

$$w_n^A = P_{n-1}^- - l_n + P_n^+ - r_n + I_n + \frac{1}{2}\left[1 + (-1)^{n+i}\right], \tag{46}$$

$$w_n^B = P_{n-1}^+ - r_n + P_n^- - l_n + I_n + \frac{1}{2}\left[1 - (-1)^{n+i}\right], \tag{47}$$

and the recurrence relation across the cell n with a topological spin defect on site ni is

$$D_n = D_{n-1} - (-1)^n \left[b + (-1)^i\right]. \tag{48}$$

If the order parameter to the left of the spin defect is D_l, according to Eq. (34), the order parameter to the right of site ni, D_r, will be

$$D_r = D_l - (-1)^{n+i}. \tag{49}$$

Thus, a topological spin defect can be seen as a domain wall separating sectors with order parameters D_l and D_r.

Therefore, when the subspaces D and $-b-D$ are degenerate, the energy per site associated to the sectors to the right and to the left of a spin defect

located at the ni site will be degenerate if

$$D_l = \frac{1}{2}\left[(-1)^{n+i} - b\right]. \tag{50}$$

Since D_l must be an integer, this equation has a solution only when b=odd. Thence, for our bipartite strips with $b = 1$, that is fulfilled when $D_l = 0$ ($D_l = -1$) with the defect in the sublattice A (B) and $D_r = -1$ ($D_r = 0$).

Furthermore, it is possible to form a local region between the cells n and m of LR-SPO $D \pm 1$ placing two spin defects in a wave function of LR-SPO D, one on a site ni and the other on a site mj, with $n + i + m + j$=odd.

Thence, when b=odd and $D = (1 - b)/2$ ($D = -(1 + b)/2$) a local region with $D = -(1 + b)/2$ ($D = (1 - b)/2$) is obtained when $n + i$=even ($n + i$=odd). Since subspaces with $D = (1 - b)/2$ and $D = -(1 + b)/2$ are degenerate, topological spin defects are not confined, though it may happen that they attract one another (with an ordinary short-range potential). For instance, solitons in polyacetylene (with $b = 1$) can be interpreted as a realization of this deconfinement of spin defects.

On the contrary, for a b=even strip, the order parameter of the local region delimited by the pair of spin defects is in general associated to higher energy per site, then the two spin defects should remain as close as possible, predominantly in neighboring sites, so confinement is expected.

5.5. Resonating Valence Bond (RVB) ansätze

Within the RVB scheme for the ground state, the simplest wave function beyond that of a single Kekulé structure can be defined as a simple equally-weighted superposition of Kekulé structures (EWK) within a given LR-SPO subspace,

$$|\Psi_{EWK}^D\rangle = \sum_{K_D} |K_D\rangle. \tag{51}$$

However, this approximation is not expected to yield reasonable results when the strength of the nearest-neighbor J parameters are different in different directions, since then some Kekulé structures can be stabilized with respect to other structures in the same LR-SPO subspace, although it can be of some help as an indication about which LR-SPO subspace is likely to contain the ground state. Thence, removing the equally-weighted constrain is the first step in order of improving the energy expectation value. Still better approximations can be obtained when longer-range VB structures enlarging the model space are considered. Different strategies have already been applied in order of selecting the singlets involved in the

superposition *ansätze* and how their weight contributing to the ground state is written as a function of a few variational parameters. Thence, we distinguish the $w = 1$ from the $w > 1$ *ansätze*.

5.5.1. RVB ansätze for the linear chain

For the linear chain there is only one Kekulé structure in each LR-SPO subspace. Therefore, two main different *ansätze* including long SP may be considered. See, for instance, Refs. 24, 31 and 35.

Five-bond-range RVB ansatz: The M-bond RVB variational localized-site cluster expansion *ansätze* can be defined [31] as

$$|\Psi_{\text{RVB}}^M\rangle = \mathcal{U}_s(e^{\mathcal{P}_M^+})|\phi_{\text{N}}\rangle, \tag{52}$$

where $\mathcal{U}$ indicates that only unlinked terms are to be retained and the subscript s on $\mathcal{U}$ indicates an excitation is to occur on every site. $\mathcal{P}_M^+$ is the excitation operator

$$\mathcal{P}_M^+ \equiv \sum_n \sum_{p=0}^{<M/2} \mathcal{P}_{n(2p+1)}. \tag{53}$$

Numerical results for such *ansätze* with connected-cluster patterns involving up to $M = 5$ bonds have been treated so far. The hierarchy of patterns have been defined as

$$\mathcal{P}_{n(1)}^+ \equiv \frac{1}{2}x_n\left[(1 - (-1)^n)(I - s_n^- s_{n+1}^+) - (1 + (-1)^n)(I - s_n^+ s_{n+1}^-)\right], \tag{54}$$

$$\mathcal{P}_{n(3)}^+ \equiv \frac{1}{2}y_n\left[(1 - (-1)^n)(I - s_n^- s_{n+3}^+)(I - s_{n+1}^+ s_{n+2}^-)\right.$$
$$\left. - (1 + (-1)^n)(I - s_n^+ s_{n+3}^-)(I - s_{n+1}^- s_{n+2}^+)\right], \tag{55}$$

$$\mathcal{P}_{n(5)}^+ \equiv \frac{1}{2}z_n\left[(1 - (-1)^n)(I - s_n^- s_{n+5}^+)(I - s_{n+1}^+ s_{n+2}^-)(I - s_{n+3}^+ s_{n+4}^-)\right.$$
$$\left. - (1 + (-1)^n)(I - s_n^+ s_{n+5}^-)(I - s_{n+1}^- s_{n+2}^+)(I - s_{n+3}^- s_{n+4}^+)\right]. \tag{56}$$

The x_n, y_n and z_n are variational parameters submitted to translational-symmetry constraints, $v_{n+m} = v_n$, $v \equiv x, y, z$, where $m = 1$ for a regular chain, and $m = 2$ when alternating translational symmetry conditions are desired.

Infinite-bond-range RVB ansätze: Infinite range RVB *ansätze* are defined [35] by

$$|\Psi_{RVB\infty}^P\rangle = \sum_\sigma \prod_n \prod_p x_{n,p}^{m(n,p,\sigma)} |\sigma\rangle, \tag{57}$$

where σ is restricted to all the linearly independent overall singlets made as a product of N non-crossing two-body spin-pairings such that, at any boundary f_n, $P_n \leq P$, with $P_n \equiv P_n^+ + P_n^-$; $x_{n,p}$ is the variational parameter, submitted to appropriate symmetry constraints, associated to the occurrence of p sites preceding a site $n+1$ being spin-paired to p sites succeeding site n, i.e. $P_n = p$; finally,

$$m(n,p,\sigma) \equiv \begin{cases} 1, & \text{if in } \sigma \text{ there are } p \text{ SP penetrating the } f_n \text{ boundary,} \\ 0, & \text{otherwise.} \end{cases}$$

Actual *ansätze* has gone up to $P = 4$, while $P = 1$ gives the dimer-covering approximation.

5.5.2. RVB ansätze for $w > 1$

For strips other than the linear chain, i.e. $w > 1$, we start with LR-SPO-adapted 1BR-RVB *ansätze*. These LR-SPO-adapted 1BR-RVB *ansätze* play the fundamental zero order role for the higher-range *ansätze*. Below the 3BR-RVB *ansätze* are developed explicitly. Generalization to higher range *ansätze* is straight forward, albeit quite tedious.

One-bond-range RVB ansätze: A one-bond-range RVB *ansatz* Φ_D showing LR-SPO D is a weighted superposition of dimer-covering configurations with LR-SPO D. They can be written as

$$|\Phi_D\rangle = U_D \prod_{ni}^{\in A} \sum_{mj}^{\langle ni,mj\rangle} x_{\langle ni,mj\rangle} \left(I - S_{ni}^- S_{mj}^+\right) |\Phi_N\rangle. \tag{58}$$

I is the identity operator, U_D projects out all the terms with LR-SPO different than D as well as those where any site appears more than once. It is worth noting that the weight of every specific Kekulé structure contributing to Φ_D is a product of the variational parameters $x_{\langle ni,mj\rangle}$ associated to each of the N spin pairings in Φ_D.

Three-Bond-Range RVB ansätze: Following a strategy parallel to that of the Néel-state based *ansätze*, we try to generate a trial wave function as a superposition, now, of singlets which are obtained from a cluster-

expanded excitation operator acting on the appropriate zero order function, i.e. $|\Phi_D\rangle$. From the Sec. 5.1, the two-body XY terms of the Hamiltonian acting on a covalent VB singlet such as those in the 1BR-RVB wave functions of Eq. (58) may produce "off diagonal" states with next-next-nearest-neighbors pairings. These off-diagonal states can be directly generated by the "recoupling" of two adjacent bond-singlets in Φ_D as indicated in Fig. 4. We denote by $\hat{q}_{ef}$ the operator related to such a recoupling between two bond-singlets e and f. From $|\Phi_D\rangle$ we may build the 3BR-RVB with LR-SPO D allowing an arbitrary number of recouplings of two simply adjacent bond-singlets. Then, the overall 3BR-RVB excitation operator above the 1BR wave function is

$$Q = \sum_{\langle e,f\rangle} y_{ef}\hat{q}_{ef}, \tag{59}$$

with $y_{\langle ef\rangle}$ variational parameters. The corresponding *ansatz* is then

$$|\Psi_D\rangle = \mathcal{U}e^Q|\Phi_D\rangle, \tag{60}$$

where $\mathcal{U}$ indicates that only unlinked terms are to be retained. That is, in the Taylor series expansion of e^Q one retains only products of $\hat{q}_{ef}$ such that no pair index (e or f) appears more than once. And Q and Φ_D are to be optimized simultaneously.

6. THE GROUND STATE ENERGY

In this section the ground-state energy per site in units of a characteristic J of the strip,

$$E(\Psi) \equiv \frac{1}{JLw}\frac{\langle\Psi|H|\Psi\rangle}{\langle\Psi|\Psi\rangle}, \tag{61}$$

is to be computed assuming translational symmetry and cyclic boundary conditions along L. Different strategies are used depending of the kind of *ansatz*.

For the equally-weighted dimer-covering wave function, the *resonance energy*, i.e. the ground-state energy correction below the energy of a single Kekulé structure $[2N(-0.375)]$, is obtained by the Kekulé structures counting method. For the trial wave functions which depend of some variational parameters, the local way our *ansätze* are constructed allows us to deal with the strips locally. Thence, the expectation values of local operators accept a treatment based either on the use of a transfer matrix or on

a residual-overlap-ratios technique [36,37].

6.1. Kekulé structures counting method

Within the dimer-covering approximation the *resonance energy* in units of J, $2N\varepsilon_r(w, D)$ depends on configuration interaction amongst the different Kekulé structures. When an equally-weighted wave function is considered, it has been argued [38,39] that one might consider this energy lowering to depend solely on the dimension of the space spanned by the appropriate Kekulé structures. Let $n(w, D)$ be the dimension of the D block for a strip with w sites per cell. Since $n(w, D)$ is multiplicative in terms of a break up into subsystems while the energy is additive, such a functional dependence should be of the form

$$\varepsilon_r(w, D) \approx -\frac{CJ}{wL} \ln n(w, D), \tag{62}$$

where C is a fitting parameter independent of the structure to some degree. For energy-ordering purposes the value of C is irrelevant. Nevertheless, for the nearest-neighbor isotropic Heisenberg model the value of C have been determined for a class of benzenoid hydrocarbons [38] (with C=0.5667) and for finite square-lattice fragments [39] (with C=0.75), by fitting the logarithm of the Kekulé-structure count to the resonance energy calculated from an equally-weighted Kekulé-structure wave function.

Since the arguments supporting Eq. (62) rely on the fact that the energy is an extensive magnitude, i.e. scales as the system size, while the number of Kekulé structures needs to scale exponentially with the system size, values of C have been determined for the square lattice [30,39] by fitting the logarithm of the Kekulé-structure count to the "exact" energy values of Table II of Ref. 39. This yields C_w=0.84, 1.0 and 0.93 appropriate for square-lattice strips with $L \to \infty$ and w=2, 3 and 4, respectively, and their weighted average $C = 0.94 \pm 0.19$ as a rough estimate of C appropriate for the two-dimensional square lattice.

When the sublattices are invariant under $\mathcal{T}$, $n(w, D)$ is easily obtained as the Lth-power of the highest eigenvalue, Λ_{wD}, of the D block of the square of a dimer-covering-*counting* transfer matrix K_D. Otherwise, i.e. when under the (pseudo) translation $\mathcal{T}$ the sublattices transform one into each other as reported in Eqs. (38) and (39), a symmetry operation of $\mathcal{T}^2$ is needed to leave the sublattices invariant. Thence, the values of $n(w, D)$ can be obtained as the $L/2$ power of the highest eigenvalue, Λ_{wD}^2, of the D block of the square of a dimer-covering-*counting* transfer matrix K_D^2. Then, in general, the resonance energy of the lowest lying state in the

subspace D can be written as

$$\varepsilon_r(w, D) \approx -\frac{CJ}{w} \ln \Lambda_{wD}. \tag{63}$$

6.2. Transfer-Matrix Based Technique

The way the present *ansätze* are defined allows one to deal with the strips locally and the matrix elements can be evaluated by a transfer-matrix technique [22,23,34,35,40-44]. Within this technique one can define transfer and connection matrices that encode the local features and reduce the computation expectation values of any observable accepting a local expression, such as that of Eq. (61) for the energy. The results entails "simple" products of matrices [22,34].

Let's suppose there are imaginary vertical lines cutting the strip on translationally equivalent positions, as for instance it is shown in Fig. 1. We can define the *ansatz*-dependent "local states" according to every possible local configuration around a given position determined by one of the imaginary vertical lines, when computing $\langle\Psi|\Psi\rangle$. Thence these local states contain the contributions from both the *bra* and the *ket*.

By translational symmetry, local states in every symmetrically equivalent position are to be the same. Now, labeling these local states by e_n, n ranging, we let the transfer-matrix element

$$T_{nm} \equiv (e_n|T|e_m), \tag{64}$$

denote a weighted sum over the various ways a local state e_m may succeed a local state e_n. The weight of every contribution is obtained by considering the additional variational parameters (and island-counting in RVB *ansätze* involved in proceeding from e_n to e_m. The transfer matrix is then conveniently used to evaluate the overlap as

$$\langle\Psi|\Psi\rangle = \text{tr}T^L. \tag{65}$$

For $L \to \infty$, the largest eigenvalue Λ of T dominates, and the previous expression (65) reduces to

$$\langle\Psi|\Psi\rangle \simeq \Lambda^L. \tag{66}$$

The Hamiltonian expectation value over $|\Psi\rangle$ can be obtained in a similar

way introducing a connection matrix C defined according to

$$\langle\Psi|H_s|\Psi\rangle = JL\langle\Psi|\sum_{\langle ni,mj\rangle}^{\text{unit cell}} \mathbf{s}_{ni}\cdot\mathbf{s}_{mj}|\Psi\rangle = JL\,\text{tr}\{T^{L-c}C\}, \tag{67}$$

where c measures the range of the interaction within the *ansatz*. In our case $c = 2$. And, the matrix element

$$C_{nm} = (e_n|C|e_m) \tag{68}$$

is a weighted sum over the various ways a local state e_m may succeed a c-transfer-matrix-steps preceding local state e_n when the Hamiltonian operators per cell are present.

In the long-length limit the energy per site of Eq. (61) reduces to:

$$E = \frac{1}{w\Lambda^2}\frac{(\Lambda, l|C|\Lambda, r)}{(\Lambda, l|\Lambda, r)}, \tag{69}$$

where $(\Lambda, l|$ and $|\Lambda, r)$ are left and right eigenvectors corresponding to the maximum eigenvalue Λ of T. This expression is a function of the variational parameters associated to Ψ and an upper bound to the exact ground state energy. Because the matrix element limit is obtained exactly, this result remains a rigorous upper bound upon optimization of the variational parameters.

7. RESULTS AND DISCUSSION

In this section we present some of the results obtained so far, although some numerical results not previously published are now included. They are organized according the sort of strip and the *ansatz* that has been used.

7.1. Linear Chain

Two different problems have already been considered: The spin-1/2 Heisenberg chain with interactions up to next-nearest-neighbor, and the geometry and ground-state energy of polyacetylene. Related with polyacetylene, the alternating-J Heisenberg chain and associated alternating-variational-parameter *ansätze* have also been considered.

7.1.1. Regular chain with next-nearest-neighbor interactions

For the regular chain with nearest- and next-nearest-neighbor spin-interacting terms, with $J_{\langle n,n+1\rangle} \equiv J$ for any n, and $J_{\{n,n+2\}} \equiv \alpha J$, the

Heisenberg ground-state energy per site, in units of J

$$E(\Psi_N) = \frac{1}{J} \sum_{p=1}^{2} J_{\{n,n+p\}} \frac{\langle \Psi_N | \mathbf{s}_n \cdot \mathbf{s}_{n+p} | \Psi_N \rangle}{\langle \Psi_N | \Psi_N \rangle} \equiv \varepsilon_1 + \alpha \, \varepsilon_2, \qquad (70)$$

has been obtain by the NSBA, with up to $M = 5$ sites, and the RVB *ansätze*, including pairing up to $M = 5$ bonds apart, for $-1 \leq \alpha \leq 1$. It is worth noticing that at $\alpha = 1$ the triangular lattice is reached, while for $\alpha = 1/2$ the dimer-covering structure is the exact ground state.

NSB *ansätze*:   The p-neighbor energy per site, ε_p, as a function of the variational parameters x_n, y_n, z_n, and t_n of Sec. 4, with translational-symmetry constraints $v_n \equiv v$ for all n, was obtained by the residual-overlap-ratio method.

   The nearest- and next-nearest-neighbor contributions to the energy, ε_1 and ε_2, can be written as (see, Ref. 45 for more details)

$$\varepsilon_1 \equiv \frac{1}{f f_1} \left[x + 2\zeta + f - 1 + \frac{2t\xi\zeta}{f} + \frac{z^2 + yz + z\zeta^2}{f^2} + \frac{t^2}{f^4} - \frac{f f_1}{8} \right], \qquad (71)$$

$$\varepsilon_2 \equiv \frac{1}{2 f f_1} \left\{ (f-1)^2 + 2f(f-1)\left(f - 1 - \frac{z^2}{f^3} \right) + 1 + 2(x+\zeta)^2 \right.$$

$$+ 4xt\xi + 2t^2\xi + \frac{1}{f}\left[4y(x+\zeta)^2 + 2y^2 + 4z(x+\zeta) \right]$$

$$\left. + \frac{1}{f^2}\left[t^2 + 2t(x+\zeta)^2 + 2z^2 4ty \right] - \frac{f f_1}{4} \right\}, \qquad (72)$$

where the residual-overlap-ratios are

$$f_1 \equiv 1 + 2t\xi^2 + \frac{2}{f}\left(x^2 + 4x\zeta + \zeta^2 \right) + \frac{4}{f^3}\left(y^2 + z^2 \right) + \frac{5t^2}{f^4}, \qquad (73)$$

$$f \equiv 1 + \frac{x^2 + 2x\zeta}{f} + \frac{y^2 + z^2}{f^3} + \frac{t^2}{f^4}, \qquad (74)$$

with

$$\xi \equiv \frac{x}{f^2 - y - t/f}, \qquad (75)$$

$$\zeta \equiv \left(y + \frac{t}{f} \right) \xi. \qquad (76)$$

Table 1: Long-range spin-pairing order ρ as defined by Eq. (23) of the RVB *ansatz* and the energy per site in units of J for the linear spin-1/2 Heisenberg chain with nearest- and next-nearest-neighbor spin interactions yield by the $M = 5$ bonds RVB *ansatz* with SP parterns of Eqs. (54)-(56) and the $M = 5$ sites NSBA *ansatz* with the spin-flip paterns of Eqs. (16)-(18). The lower and upper bounds and the extrapolated results from finite systems of van den Broek et al. [26], the exact results at $\alpha = 0$ of Hulthén [19] and at $\alpha = 0.5$ of Majumdar [25] have been included for comparison. At $\alpha = 0.5$ the RVB *ansatz* yield the exact result $\rho(J = 1/2) = 3/16$.

α	ρ	RVBA	NSBA	lower	upper	extrpol	exact
-1.0	0.0519	-0.6174	-0.6367	-0.6759	-0.6223	-0.6486	
-0.9	0.0531	-0.5987	-0.6156	-0.6526	-0.6020	-0.6267	
-0.8	0.0547	-0.5801	-0.5947	-0.6294	-0.5818	-0.605	
-0.7	0.0565	-0.5615	-0.5739	-0.6061	-0.5615	-0.5835	
-0.6	0.0587	-0.5430	-0.5535	-0.5828	-0.5412	-0.5622	
-0.5	0.0612	-0.5246	-0.5333	-0.5595	-0.521	-0.5412	
-0.4	0.0641	-0.5064	-0.5134	-0.5363	-0.5007	-0.5206	
-0.3	0.076	-0.4883	-0.4939	-0.513	-0.4853	-0.5004	
-0.2	0.0720	-0.4744	-0.4748	-0.4897	-0.4713	-0.4806	
-0.1	0.0776	-0.4529	-0.4562	-0.4664	-0.4572	-0.4614	
0.0	0.0848	-0.4358	-0.4382	-0.4432	-0.4332	-0.4424	-0.44315
0.1	0.0946	-0.4193	-0.4208	-0.4291	-0.4199	-0.4251	
0.2	0.1083	-0.4038	-0.4044	-0.4150	-0.3966	-0.4083	
0.3	0.1282	-0.3900	-0.389	-0.401	-0.3859	-0.3929	
0.4	0.1566	-0.3794	-0.375	-0.3869	-0.3782	-0.3804	
0.5	0.1875	-0.3750	-0.3627	-0.3750	-0.3750	-0.3750	-0.37500
0.6	0.1994	-0.3801	-0.3524	-0.3889	-0.3789	-0.3812	
0.7	0.1926	-0.3944	-0.3446	-0.4154	-0.3906	-0.3963	
0.8	0.1831	-0.4147	-0.3394	-0.4462	-0.4090	-0.4174	
0.9	0.1750	-0.4392	-0.3369	-0.4905	-0.4326	-0.4503	
1.0	0.1684	-0.4667	-0.3368	-0.5348	-0.4602	-0.5016	

The optimal values of the energy as a function of α are presented in Table 1, where it can be noticed that the NSBA is progressively less reliable as a frustrating ($\alpha > 0$) next-nearest-neighbor interaction increases, while it is stabilized with respect to the upper bound of van den Broek by an $\alpha \leq 0.3$ contribution.

RVB *ansätze*: The p-neighbor energy per site ε_p as a function of the variational parameters x, y, z of the $M = 5$ bonds RVB *ansatz* with SP paterns of Eqs. (54)-(56), with translational-symmetry constraints $v_n \equiv v$ for all n, was obtained by the residual-overlap-ratio method (see Ref. 31

for details).

$$\varepsilon_1 \equiv \frac{-3}{4ff_{1,2}} \left[-f + y^2 + \frac{2z^2}{f} + \frac{2\xi}{4f^3 - \zeta} \left(4yz + \frac{\xi(4f^3 + 3\zeta - 4yf^2))}{4f^3 - \zeta} \right) \right], \quad (77)$$

$$\varepsilon_2 \equiv \frac{3\xi}{ff_{1,2}(4f^3 - \zeta)} \left[yz + \frac{\xi(\zeta + zf)}{4f^3 - \zeta} \right], \quad (78)$$

where the residual-overlap-ratios are

$$f \equiv -1 + \frac{y^2}{f} + \frac{z^2}{f^2} + \frac{2\xi^2}{(4f^3 - \zeta)f}, \quad (79)$$

and

$$f_{1,2} \equiv -2 + \frac{4y^2}{f} + \frac{6z^2}{f^2} + \frac{4\xi}{f(4f^3 - \zeta)} \left(\xi + 4yz + \frac{\xi(\zeta + fz + 2z^2)}{4f^3 - \zeta} \right), \quad (80)$$

with

$$\xi \equiv 2f^2 + yz, \quad (81)$$

$$\zeta \equiv 2yf^2 + zf + z^2. \quad (82)$$

The optimal ground-state energy values and the LR-SPO, as measured by ρ in Eq. (23), as a function of α are presented in Table 1. From this table, it can be seen that the RVB *ansatz* is exact at $\alpha = 0.5$, while the error at $\alpha = 0$ is $\sim 1.7\%$. Also, it is noticed that the RVB *ansatz* is clearly stabilized with respect to the NSBA when frustration is present. Also, it is worth noticing that the energy values yield by the RVB *ansatz* are lower than the upper bounds of van den Broek for $-0.7 \le \alpha < -0.1$ and $\alpha > 0.1$, while van den Broek's upper bounds crosses below for $-0.1 \le \alpha < 0.1$, with a maximum difference of less than 1.7% , and for $\alpha < -0.7$, with a maximum difference of less than 0.9% . Therefore, the RVB *ansatz* yield very good ground-state energy values for all the rang $-1.0 \le \alpha \le 1.0$.

7.1.2. Polyacetylene and the alternating-J Heisenberg chain

In Ref. 31 it has been shown that long linear chains, as seen from the point of view of VB theory, show a long-range order, measured by the parameter ρ in Eq. (23), leading to a ground-state instability to bond alternation. From Sec. 5.3 also this is expected to occur.

Polyacetylene is a physical realization of such a system and it is known-that it does present bond alternation [46,47]. Since a parameterization to a model spin Hamiltonian is available [18] for conjugated hydrocarbons, this system is a good test for the NSBA and RVB *ansätze*. Therefore, in Ref. 34 the geometry of polyacetylene has been computed using this sort of *ansätze*.

The total energy per site of polyacetylene has two contributions, i.e. the expectation value of the spin independent term, as given by Eq. (5), which only depends on the interatomic distances,

$$E_r(\Psi) = \frac{1}{2}\left(R(r_1) + R(r_2)\right),$$ (83)

and the expectation value of the spin term of the nearest-neighbor Heisenberg Hamiltonian of Eq. (4),

$$
\begin{aligned}
E_s(\Psi) &\equiv \frac{1}{2}\left(\varepsilon_1 + \varepsilon_2\right) \\
&\equiv \frac{1}{2}\left(J(r_1)\frac{\langle\Psi|\mathbf{s}_1\cdot\mathbf{s}_2|\Psi\rangle}{\langle\Psi||\Psi\rangle} + J(r_2)\frac{\langle\Psi|\mathbf{s}_2\cdot\mathbf{s}_3|\Psi\rangle}{\langle\Psi||\Psi\rangle}\right).
\end{aligned}
$$ (84)

Néel-State-Based Ansatz: The NSBA of Subsec. 4.1, with $M = 2$ and $M = 4$, and alternate translational symmetry conditions, has been used [34] to obtain the energy as a function of the variational parameters and the interatomic distances, r_1 and r_2. Upon optimization, the geometry and the alternating-to-regular geometry transition have been obtain (see Ref. 34).

The alternate value of the energy per site ε_n as a function of variational parameters x_n, y_n, and z_n of Sec. 4 and the interatomic distances, r_1 and r_2, was obtained by the residual-overlap-ratios method,

$$
\begin{aligned}
\varepsilon_n &\equiv \frac{J(r_n)}{f f_{n+1}}\left[f_{n+1}\left(1 - \frac{f}{4}\right) - 1 + \frac{x_n(f_{n+1}f_n + y_n)}{f_{n+1}f_n - y_n} + \frac{z_n^2}{f_{n+1}f_n}\right. \\
&\quad \left. + \frac{y_{n+1}z_{n+1}}{f_n^2} + \frac{x_{n+1}^2 z_{n+1}f_{n+1}^2}{(f_{n+1}f_n - y_{n+1})^2}\right],
\end{aligned}
$$ (85)

where the residual-overlap-ratios are

$$f_n \equiv 1 + \frac{y_n^2 + z_n^2}{f_{n+1}^2 f_n} + \frac{x_n^2(f_{n+1}f_n + y_n)}{f_{n+1}(f_{n+1}f_n - y_n)}$$ (86)

Table 2: Results of Variational Localized-site Cluster expansions from either a Néel-state based *ansätze* or a Resonating Valence Bond *ansatz*. We notice that the lower level NSBA is unable of showing the dimerization of polyacetylene. $\bar{r}_c$ is the critical bifurcation mean bond length, r_1 and r_2 are the optimized short and long bond distances (in Å). E is the energy per carbon atom (in eV), taking the energy of the Néel state with 1.40 Å equal bond lengths as zero of energy. NSB forth order perturbative and Dimer-covering second order perturbative (see Ref. 34), CEPA *ab-initio* estimate of Kønig and Stollhoff [52], and the experimental results [46,47] for r_1 and r_2 have been added for comparison.

ansatz	$\bar{r}_c$	r_s	r_l	E
NSBA $M = 2$	1.46	1.400	1.400	-0.661
NSBA $M = 4$	1.32	1.360	1.443	-0.704
RVBA		1.364	1.436	-0.724
NSB perturbative (4$^{\text{th}}$ order)	1.43	1.401	1.401	-0.616
Dimer-covering perturbative (2$^{\text{nd}}$ order)		1.361	1.438	-0.720
CEPA *ab-initio*		1.343	1.436	
Experimental		1.36	1.44	

and

$$f \equiv 1 + \frac{2(y_n^2 + z_n^2)}{f_{n+1}^2 f_n} + \frac{2(y_{n+1}^2 + z_{n+1}^2)}{f_{n+1} f_n^2} + \frac{x_n^2 y_n (2 f_n f_{n+1} - y_n)}{f_{n+1}(f_n f_{n+1} - y_n)^2}$$
$$+ \frac{x_{n+1}^2 y_{n+1} (2 f_n f_{n+1} - y_{n+1})}{f_n (f_n f_{n+1} - y_{n+1})^2}. \tag{87}$$

When the geometry is optimized, the $M=2$ NSBA ($y_n = z_n = 0$) would predict a regular ground state. The lowest energy is obtained for a non-dimerized geometry $r_1 = r_2 = 1.40$ Å. Meanwhile the $M = 4$ NSBA yield an alternate geometry (see, for instance, Table 2) with interatomic distances that compare very well with the experimental values [46,47].

The study of the energy surface $E(r_1, r_2)$ or $E(\bar{r}, \delta)$, with

$$\bar{r} \equiv \frac{1}{2} (r_1 + r_2), \tag{88}$$

$$\delta \equiv \frac{r_2 - r_1}{r_1 + r_2}, \tag{89}$$

as a function of δ for different values of $\bar{r}$, allows to obtain the critical value $\bar{r}_c$ where the regular-to-dimerized geometry transition takes place. The energy per site, as a function of δ, has been computed [34] at the $M = 2$ and $M = 4$ level of approximation for different values of $\bar{r}$. Results for the $M = 4$ level of approximation are plotted in Fig. 6, and the transition
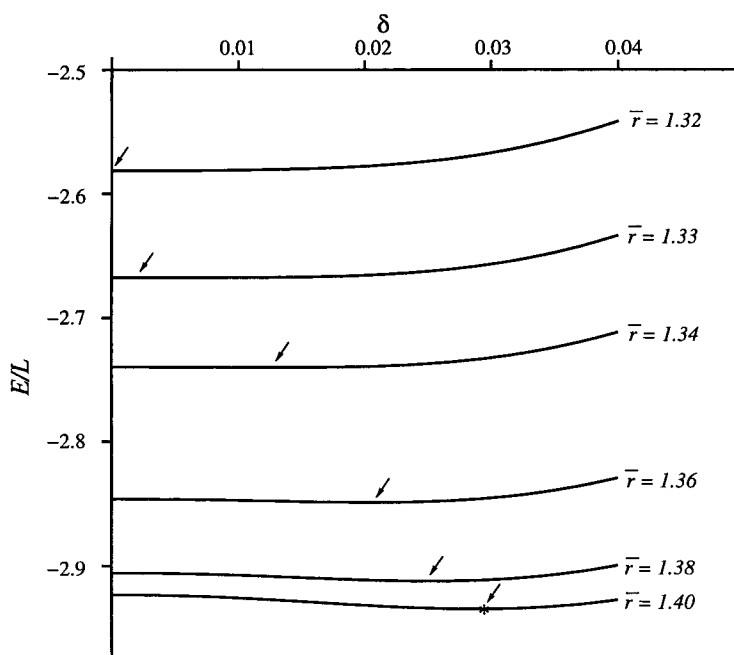
Figure 6: 5-sites Néel based Variational Localized-site Cluster Expansion Energy per atom (in eV) as a function of δ for different values of $\bar{r}$ (in Å), taking the energy of the Néel state with 1.40 Å equal bond lengths as zero of energy. The arrows point to the relative minima, while the star indicates the position of the ground state when the geometry is optimized.

is found for $\bar{r}_c \simeq 1.32$ Å, while at the $M = 2$ level the bifurcation in the energy surface takes place for a stretched system, the critical distance $\bar{r}_c$ being 1.46 Å.

The whole calculated potential energy surface is very flat. In particular for the optimal $\bar{r}$ (1.40 Å), the energy gain brought by the dimerization is ~ 0.0118 eV per C_2H_2 unit. This value is very close to that shown in Table 3, which has been obtained as the difference between the cluster expansion ground-state energies when optimization is performed with and without the $r_1 = r_2$ constraint. Those are about 4 times the value predicted by Mintmire and White using a Local-density-functional approach [48], but still smaller than 0.07 eV suggested by Ashkenazi *et al.* [49] to be compatible with polyacetylene being dimerized well above room temperature, or Suhai (0.09 eV) HF calculation and second order Møller-Plesset perturbation theory [50]. HF stabilization energies brought by dimerization are in general still higher (see Ref. 51 and references therein), though this approximation is not reliable due to the charge density wave HF instability

Table 3: Optimized regular interatomic distance (in Å) and gain in energy per C_2H_2 unit (in eV) of regular polyacetylene by report to the alternating ground state, with the Néel state based higher order and the RVB *ansätze*. Results from Local-density-functional approach of Mintmire and White [48], Hartree-Fock and Møller-Plesset perturbation Theory of Suhai [50], or Ashkenazi [49] are included.

	r	ΔE
NSBA	1.399	0.0118
RVB	1.398	0.0391
LDA		0.003
Ashkenazi		0.07
Suhai		0.09

occurring for $\delta = 0$. Still higher order NSBA should yield higher values of the barrier than the $M = 4$ *ansatz*.

RVB *ansatz*: The $P = 4$ infinite-range RVB *ansatz* of Eq. (57) has been used (see Ref. 34) to obtain the energy as a function of the interatomic distances, r_1 and r_2, and the variational parameters. Upon optimization, this *ansatz* yields better energy evaluation for the distorted region (see, for instance, Table 2). Furthermore, the RVB *ansatz* already yields lower energy than the NSBA even when applied to the regular chain, as reported in Table 4. Thus, one always obtains a reasonable estimate of the dimerized geometry.

Optimizing the geometry with the constraint of equal bond length, the stabilization energy gain by dimerization has also been estimated. The barrier to inversion of dimerization is higher with RVB than with NSBA (see Table 3). While the RVB *ansatz* yields better energy and interatomic distances, it is not suitable for the $r_1 \simeq r_2$ region and the bifurcation of the energy surface $E(\bar{r}, \delta)$. In a general way, all methods which start with a symmetry-broken description are unable to treat correctly the weakly dimerized region and of course the bifurcation point. Such is for the case of RVB *ansätze* with well defined LR-SPO D. A similar problem is found when starting from Hartree-Fock, where a symmetry-breaking takes place for non-dimerized geometries, leading to bond-centered charge density waves, i.e. bond alternation of the density-matrix without any bond-length alternation. Then, any strategy based on the HF solutions will be unable to study the region around $\delta = 0$, since it is symmetry-broken for the non-dimerized geometries. This fact is manifested by the energy cusp for $\delta = 0$ in Ref. 52 or in RVB *ansätze* as also pointed out for the Heisenberg Hamiltonian in Ref. 31.

Table 4: Ground state Heisenberg energies per site for undistorted polymers (see Refs. 22, 23, 34, 35, and 45 and references therein for other available results). EPV stands for Exclusion Principle Violating infinite summation perturbation theory (see Ref. 34 for more details).

Method	P	PA	PAA	PBA	PPR
Néel state	-0.25	-0.3125	-0.333	-0.3214	-0.325
One Kekulé configuration	-0.375	-0.375	-0.375	-0.375	-0.375
RVB 1-bond-range SP	-0.375	-0.375	-0.375	-0.4339	-0.4435
RVB 3-bond-range SP	-0.4269	-0.4480	-0.43395		
EPV (2nd order)	-0.393				
EPV (4th order)	-0.416				
NSBA $M = 2$	-0.4279	-0.4740	-0.4941		-0.4906
One-Kekulé+perturb. (2nd order)	-0.4375				
Néel+perturbative (4th order)	-0.4375				
NSBA $M = 4$	-0.4379				
NSBA $M = 5$	-0.43815				
RVB ∞-range SP $P = 4$	-0.43955				
Exact result of Hulthén [19]	-0.44315				
Néel+perturbative (2nd order)	-0.5000				

7.2. Conjugated hydrocarbon polymers

The possibility of distortions in several polymers, besides polyacetylene, have also been studied using NSBA and RVB *ansätze* (see, for instance Refs. 22 and 23). For the sake of space limitation, here we only report the ground-state Heisenberg energy for the undistorted polymeric strips (see Table 4).

7.3. Spin-1/2 square-lattice strips

In Ref. 30 the values of Λ_{wD} of Sec. 6.1 for w ranging from one to twelve and D from zero to $(w - b)/2$ (with $\Lambda_{w(-b-D)} = \Lambda_{wD}$) have been obtain by a dimer-covering-counting transfer-matrix method as follows.

Let us analyze from a local point of view the dimer-covering singlets. We can identify a dimer-covering local state, $|e_{nI}\rangle$, I ranging, according to which legs have an arrow across the f_n boundary. The direction of any arrow is fixed by n and w. For ladders, it can be seen that there are 2^w different local states for each boundary, which can be classified according to the value of D_n, $|e_{nI}^D\rangle$. Since $\mathcal{T}$ transforms one sublattice into the other, the local states of position $n + 1$ are mirror images of those of position n.

A dimer-covering-*counting* matrix, $\mathcal{K}_n$, is defined as

$$(e_{n-1I}|\mathcal{K}_n|e_{nJ}) = \begin{cases} 1, & |e_{nJ}\rangle \text{ can succeed } |e_{n-1I}\rangle, \\ 0, & \text{otherwise.} \end{cases} \tag{90}$$

Table 5: The absolute value of the resonance energy in units of C, $(\ln \Lambda_D)/w$, for the lowest lying state of subspaces with order parameters from $D = 0$ to $(w - b)/2$ (with $\Lambda_{wD'} = \Lambda_{wD}$, $D' \equiv -b - D$), and the extrapolations to $w \to \infty$ for the lowest lying subspace of both, the w=even and w=odd, series.

$D =$	0	1	2	3	4	5	6
w							
1	0						
3	0.2195	0					
5	0.2529	0.1567	0				
7	0.2656	0.2121	0.1181	0			
9	0.2721	0.2383	0.1762	0.0940	0		
11	0.2760	0.2527	0.2090	0.1491	0.0799	0	
∞	0.2920						
2	0.2406	0					
4	0.2610	0.1849	0				
6	0.2699	0.2331	0.1349	0			
8	0.2748	0.2532	0.1930	0.1048	0		
10	0.2778	0.2637	0.2332	0.1617	0.0852	0	
12	0.2800	0.2700	0.2410	0.1959	0.1382	0.0717	0
∞	0.2913						

Then, the number of dimer-covering states in a $\mathcal{H}_D^w$ subspace is

$$n(w, D) = \sum_{e_{0I}^D} (e_{0I}^D | \mathcal{K}_1 \mathcal{K}_2 \dots \mathcal{K}_L | e_{0I}^D). \tag{91}$$

Since for any dimer-covering singlet $D_{n-1} = D_{n+1}$, $\mathcal{K}_n \mathcal{K}_{n+1}$ is a block-diagonal symmetric matrix which does not depend on n (apart from the direction of the arrows in the local states that it relates) we can omit the sub-index. For $L \to \infty$, the highest eigenvalue Λ_{wD}^2 of the D block $\mathcal{K}_D^2$ dominates, and

$$n(w, D) \approx \Lambda_{wD}^L. \tag{92}$$

Table 5 summarizes the absolute values of the zero order resonance energies $\varepsilon_r(w, D)$, in units of C, as computed from Eq. (63). Since it is unlikely that the zero-order energies are drastically modified by the small corrections to the isotropic nearest-neighbor Heisenberg Hamiltonian, the expected energy ordering would be

$$E_0 < E_1 < \cdots < E_{\frac{1}{2}(w-b)}. \tag{93}$$

Table 6: Ground-state Energy per site in units of J for CuO_2 square-lattice strips. K-C stands for the Kekulé counting method, with $C = 0.75$ and 0.94, NB-M is the $M = 2$ NSBA, RVB-M are the M-bond RVB *ansätze*. Extrapolations of K-C to $w = \infty$ are obtained from the even- and odd-w ground-state energies separately, while extrapolation from NSBA is done with even- and odd-w energies together. Some other results are included for comparison.

w	Néel	K-0.75	K-0.94	NB-2	RVB-1	RVB-3	other
2	-0.375	-0.5555	-0.6012	-0.5507	-0.55696	-0.57317	-0.578 [39]
4	-0.4375	-0.5708	-0.6203	-0.6025	-0.57221		-0.618 [39]
6	-0.4583	-0.5774	-0.6287				
8	-0.4688	-0.5811	-0.6333				
10	-0.4750	-0.5834	-0.6361				
12	-0.4792	-0.5850	-0.6382				
3	-0.4167	-0.5396	-0.5813	-0.5834	-0.56824		-0.594 [39]
5	-0.45	-0.5647	-0.6127				
7	-0.4643	-0.5742	-0.6247				
9	-0.4722	-0.5791	-0.6308				
11	-0.4773	-0.5820	-0.6344				
∞-even		-0.5940	-0.6488				
∞-odd		-0.5935	-0.6495				
∞-any				-0.6626			
							-0.6688 [61]
∞	-0.5						-0.67228 [62]
							-0.7158 [63]

Therefore, for w=even, the ground state belongs to the non-degenerate $D = 0$ subspace, with

$$\mathcal{T}\Psi_0 = \Psi_0, \tag{94}$$

while, for w=odd, the ground-state manifold is spanned by Ψ_0 and Ψ_{-1}, which are eigenstates of H, but not of $\mathcal{T}$. The eigenstates $\Phi_0^{\pm}$ of the translation operator, are defined in the ground-state manifold,

$$\Phi_0^{\pm} \equiv \frac{1}{\sqrt{2}}\left(\Psi_0 \pm \Psi_{-1}\right), \tag{95}$$

so

$$\mathcal{T}\Phi_0^{\pm} = \pm\Phi_0^{\pm}, \tag{96}$$

with $k = 0$ and $k = \pi$. This RVB asymptotic degeneracy for w=odd is consistent with a very wide body of evidence [53-58].

The ground-state energy per site, in units of J, for CuO_2 square-lattice

strips with w=2 to 12 has been computed from the dimer-covering-counting method, assuming the constant C of Sec. 6.1 as 0.75 and 0.94. Also, for some w values the eneergy has been obtained [59,60] by the $M = 2$-sites NSBA and the $M = 1$ and $M = 3$ bond-range RVB *ansätze* by the transfer-matrix technique. Extrapolations to $w = \infty$ of the dimer-covering-counting results are done from the even- and odd-w ground-state energies separately, while extrapolation from NSBA is done with even- and odd-w energies together. These results are presented in Table 6, where the extrapolation to $L = \infty$ from exact results on finite systems of Živković *et al.* [39], the long-range RVB result from Doucot and Anderson [61], the real-space renormalization method of Mattis and Pan [62], and the lower bounds of Tarrach and Valentí [63] have been included for comparison.

Following Subsection 5.4, excitations above the maximally-spin-paired ground state have also been analyzed [30] as local regions delimited by a couple of topological spin defects. When w=odd and D=0 ($D = -1$), there can be local regions with $D = \pm 1$ (D=0,-2). Then, since subspaces D=0 and $D = -1$ are degenerate, it is possible to have a local region with identical per site energy inside and outside the local region. In this case the topological spin defects limiting the local region are not confined, though it may happen that they attract one another (with an ordinary short-range potential). Two conclusions can be drawn from this result. First, for the half filling case, triplets with the two spin defects very far apart from one another are possible. Although breaking a singlet does cost some energy (due to contribution of the diagonal terms), there is a gain in kinetic energy (off-diagonal terms contributions), since (for w=odd) the two spins are not confined and can move independently. Consequently, a gapless triplet spectrum is not inconsistent with these results. This feature can be understood as a generalization to any odd-legged spin-$\frac{1}{2}$ antiferromagnetic ladders of Lieb, Shultz, and Mattis theorem [56,57] holding for one-dimensional systems. Second, away from half filling, removing (adding) an electron to the system yields a *non-confined* pair of sites, one being a vacant (doubly-occupied) site and the other a non-SP site. It is worth noting that the vacant (doubly-occupied) site holds the charge, while the non-SP site holds the up or down spin, leading to charge-spin separation.

In clear contrast, when w=even, the order parameter of the local region limited by the couple of spin defects is always associated to higher energy per site. This indicates that the couple of spin defects should remain as close as possible so confinement is predicted to occur. Hence, at half filling, the energy difference between the triplet and the ground state will be finite, and the w=even ladders are expected to be gapped. Nevertheless the energy difference per site between the lowest lying subspaces decreases

faster than $1/w$. Therefore, a lowering of confinement and the closing of the gap is predicted for increasing values of w. Nevertheless, within the scope of the present treatment it is not able to predict the energy ordering of the lowest singlet and triplet excited states. Now, away from half filling, when removing (adding) one electron the vacant (doubly-occupied) site will be bound to the non-SP spin, forming a "quasi-particle" with charge and spin. Again the lowering of the confinement and the charge-spin separation with increasing values of w is expected. When removing (adding) two electrons, arguments based on the LR-SPO alone are not able to decide if the two-holes (two-electrons) state is described as two quasi-particles or two bound vacant (doubly-occupied) sites. Nevertheless, we expect the two vacant (doubly-occupied) sites to be confined to benefit from the energy lowering due to the hoping term of the Hamiltonian, as has been pointed out in Ref. 64, using numerical results from DMRG techniques on clusters. Another argument to take into account is the range of the RVB. Since the two quasi-particles are expected to couple to a singlet, non-bound quasi-particle would imply a long bond, while a short-range RVB is expected for w=even ladders [65,66].

8. CONCLUSIONS

Although considerable work remains to be done on the intermediate and strongly correlated domains, model Hamiltonians, with reliable parameterization, combined with the cluster expansion *ansätze* wave functions, have proven to be a useful tool to extract information capable of a systematic improvement. The RVB *ansätze* yield fairly good ground-state energies (with errors estimated $\sim 1-2\%$) for the alternating-J Heisenberg chain for the whole range of $-J_{n,n+1} \leq J_{n,n+2} \leq J_{n,n+1}$ and is exact for $J_{n,n+2} = 0.5 J_{n,n+1}$, while still a higher order Néel-state-based *ansätze* would be necessary for frustrating $J_{n,n+2}$ close $J_{n,n+1}$. For Polyacetylene, both, the RVB and the higher order Néel-state-based *ansätze*, yield alternate interatomic distances quantitatively comparable with experimental results, while the lower-level Néel-state-based *ansatz* predicts a regular geometry. It is worth noticing that the Néel-state-based *ansätze* are not symmetry-broken, thence, permitting to analyze the region around $\delta = 0$, although they converge slowly for alternating geometries. The RVB configurations present a long-range spin-pairing order, thence, so do the RVB *ansätze*. Therefore, RVB *ansätze* with different long-range spin-pairing order can be defined, symmetry relations suggesting (non)degeneracy among different RVB wave functions. Topological spin defects can be seen as domain walls separating regions of the strips with long-range spin-pairing

order differing by ± 1. This fact allows one to conceive of the existence of local regions, delimited by a pair of topological spin defects. In terms of energy ordering, (non)degeneracy and the discontinuities introduced in the long-range spin-pairing order by the topological spin defects, the differences between w=even and w=odd strips can be explained in a general and systematic way.

ACKNOWLEGMENTS

REFERENCES

[1] J. G. Bednorz and K. A. Müller, Z. Phys. B 64 (1986) 188.

[2] P. W. Anderson, Mater. Res. Bull 8 (1973) 153.

[3] P.W. Anderson, Science, 235 (1987) 1196.

[4] E. Dagotto and T.M. Rice, Science 271 (1996) 618.

[5] R. D. Poshusta and D. J. Klein, Phys. Rev. Lett. 48 (1982) 1555.

[6] D. J. Klein, W. A. Seitz, M. A. Garcia-Bach, J. M. Picone, and D. C. Foyt, I. J. Quant. Chem. Sym. 17 (1983) 555.

[7] R. D. Poshusta, T. G. Schmalz, and D. J. Klein, Mol. Phys. 66 (1989) 317

[8] R. D. Poshusta and D. J. Klein, J. Mol. Struc. 229 (1991) 103.

[9] S. Kuwajima, J. Chem. Phys. 74 (1981) 6342, and 77 (1982) 1930.

[10] J.-P. Malrieu, The Hierarchy of VB Determinants and How to Exploit it Through Magnetic Hamiltonians, in Valence Bond Theory and Chemical Structure, D. J. Klein and N. Trinajstić (eds.), Elsevier, 1990, pp. 135-175.

[11] R. D. Poshusta, T. G. Schmalz, and D. J. Klein, Mol. Phys. 66 (1989) 317.

[12] F. Illas, J. Casanovas, M. A. Garcia-Bach, R. Caballol, and O. Castell, Phys. Rev. Lett. 71 (1993) 3549.

[13] C. J. Calzado, J. F. Sanz, J.-P. Malrieu, and F. Illas, Chem. Phys. Lett. 307 (1999) 102.

[14] D. Muñoz, I. de P. R. Moreira, and F. Illas, Phys. Rev. Lett. 84 (2000) 1579.

[15] I. de P. R. Moreira, D. Muñoz, F. Illas, C. de Graaf, and M. A. Garcia-Bach, to be publish.

[16] C. de Graaf and F. Illas, Phys. Rev. B 63 (2000) 14404.

[17] C. de Graaf, I. de P.R. Moreira, F. Illas, and R. L. Martin, Phys. Rev. B 60 (1999) 5179.

[18] M. Said, D. Maynau, J.-P. Malrieu, and M. A. Garcia-Bach, J. Amer. Chem. Soc. 106 (1984) 571.

[19] Hulthén, Ark. Mat. Astron. Phys. 26A, (1938) 1.

[20] E. H. Lieb and D. C. Mattis, J. Math. Phys. (N.Y.) 3 (1962) 749.

[21] L. Pauling, The Nature of the Chemical Bond, Cornell University Press, Ithaca, NY, 1958.

[22] M. A. Garcia-Bach, A. Peñaranda, and D. J. Klein, Phys. Rev. B 45 (1992) 10891.

[23] M. A. Garcia-Bach, R. Valentí, and D. J. Klein, Phys. Rev. B 56 (1997) 1751.

[24] M. A. Garcia-Bach and D. J. Klein, Phys. Lett. 89A (1982) 101.

[25] C. K. Majumdar, J. Phys. C 3 (1970) 911.

[26] P. M. van den Broek, Phys. Lett. 77A (1980) 261.

[27] B. Sriram Shastry and B. Sutherland, Phys. Rev. Lett. 47 (1981) 964; Physica 108B (1981) 1069.

[28] D. J. Klein, J. Phys. A 15 (1982) 661.

[29] S. Miyahara and K. Ueda, Phys. Rev. Lett. 82 (1999) 3701.

[30] M. A. Garcia-Bach, Eur. Phys. J. 14 (2000) 439.

[31] D. J. Klein and M. A. Garcia-Bach, Phys. Rev. B 19 (1979) 877.

[32] D. J. Klein, T. P. Živković, and R. Valentí Phys. Rev. B 45 (1991) 723.

[33] L. Pauling, J. Chem. Phys. 1 (1933) 280.

[34] M. A. Garcia-Bach, P. Blaise, and J.-P. Malrieu, Phys. Rev. B 46 (1992) 15645.

[35] M.A. Garcia-Bach, R. Valentí, S.A. Alexander, and D.J. Klein, Croatica Chemica Acta 64 (1991) 415.

[36] D. J. Klein, J. Chem. Phys. 64 (1976) 4868.

[37] D. J. Klein and M. A. Garcia-Bach, J. Chem. Phys. 64 (1976) 4873.

[38] W. A. Seitz, D. J. Klein, T. G. Schmalz, and M. A. Garcia-Bach, Chem. Phys. Lett. 115 (1985) 139; *Erratum*, 118 (1985) 110.

[39] T. P. Živković, B. L. Sandleback, T. G. Schmalz, and D. J. Klein, Phys. Rev. B 41 (1990) 2249 .

[40] D.J. Klein, G.E. Hite, and T.G. Schmalz, J. Comput. Chem. 7 (1986) 443.

[41] M.A. Garcia-Bach, D.J. Klein, R. Valentí, Int. J. Mod. Phys. B, 1 (1988) 1035.

[42] D.J. Klein, M.A. Garcia-Bach, and R. Valentí, Int. Journal Mod. Phys. B, 1 (1989) 2159.

[43] D.J. Klein, M.A. Garcia-Bach, and W.A. Seitz, J. Mol. Struc. 185 (1989) 275.

[44] M.A. Garcia-Bach, R. Valentí, and D.J. Klein, J. Mol. Struc. 185 (1989) 287.

[45] M. A. Garcia-Bach and D. J. Klein, Int. J. Quant. Chem. XII (1977) 273.

[46] C.S. Yannoni and T.C. Clarke, Phys. Rev. Lett. 51 (1983) 1191.

[47] H. Kalhert, O. Lertner, and G. Leising, Synthetic Metals 17 (1987) 467.

[48] J.W. Mintmire and C.T. White, Phys. Rev. B 35 (1987) 4180; Phys. Rev. Lett. 63 (1989) 2532.

[49] J. Ashkenazi, W.E. Pickett, H. Krakauer, C.S. Wang, B.M. Klein, and S.R. Chubb, Pys. Rev. Let. 62 (1989) 2016; Pys. Rev. Let. 63 (1989) 2533.

[50] S. Suhai, Phys. Rev. B 27 (1983) 3506; Int. J. Quant. Chem. 23 (1983) 1239.

[51] M. Springborg, Phys. Rev. B 33 (1986) 8475.

[52] G. Kønig and G. Stollhoff, Phys. Rev. Lett. 65 (1990) 1239.

[53] A. G. Rojo, Phys. Rev. B 53 (1996) 9172.

[54] B. Frischmuth, B. Ammon, and M. Troyer, Phys. Rev. B 54 (1996) R3714.

[55] M. Greven, R. J. Birgeneau, and U.-J. Wiese, Phys. Rev. Lett. 77 (1996) 1865.

[56] E. Lieb, T. D. Shultz, and D. C. Mattis, Ann. Phys. (N.Y.) 16 (1961) 407; reprinted in D. C. Mattis, The Many-Body Problem, World Scientific, Singapore, 1993.

[57] M. Yamanaka, M. Oshikawa, and I. Affleck, Phys. Rev. Lett. 79 (1997) 1110.

[58] E. Manousakis, Rev. Mod. Phys. 63 (1987) 1.

[59] R. Valentí, Ph.D., Universitat de Barcelona, 1989.

[60] D. J. Klein, H. Zhu, R. Valentí, and M. A. Garcia-Bach, Int. J. Quant. Chem. 65 (1997) 421.

[61] S. Liang, B. Doucot, P.W. Anderson, Phys. Rev. Lett. 61 (1988) 365.

[62] D.C. Mattis and C.Y. Pan, Phys. Rev. Lett. 61 (1988) 463.

[63] R. Tarrach and R. Valentí, Phys. Rev. B 41 (1990) 9611.

[64] S. R. White and D. J. Scalapino, Phys. Rev. B 55 (1997) 6504.

[65] D. J. Klein, M. A. Garcia-Bach, R. Valentí, and T. P. Živković, Phys. Rev. B 43 (1991) 719.

[66] S. R. White, R. M. Noack, and D. J. Scalapino, Phys. Rev. Lett. 73 (1994) 886.

Chapter 23

Exact ground states of one- and two-dimensional frustrated quantum spin systems

A.A.Ovchinnikov, V.Ya.Krivnov and D.V.Dmitriev

Joint Institute of Chemical Physics of RAS, 117977 Moscow, Russia
Max-Planck-Institut fur Physik Komplexer Systeme, 01187 Dresden, Germany

Summary

We outline the recent results for the ground states for a class of one- and two-dimensional frustrated quantum spin models with competing ferro(F)- and antiferromagnetic (AF) interactions. Frustrated spin systems are known to have many interesting properties due to large quantum fluctuations. As a result of these fluctuations the usual mean-field approach gives a quite crude (if not false) description of these systems. Therefore, exactly solvable models are very instructive for investigations of such systems. The exact ground state wave function of the proposed models has a structure of the valence-bond state (VBS) type. One of the 1D model describes the transition line between the F and AF phase. The exact singlet ground state on this line has a double-spiral ordering. Using different approximation methods we study the magnetization curve in the AF phase. The second considered set of the 1D and 2D models has an exact non-degenerate ground state with exponentially decaying spin correlations. We also propose the 1D and 2D electronic models with exact ground states represented in terms of singlet bond functions which are a generalization of the RVB functions including ionic states.

1 Introduction

There is currently much interest in quantum spin systems that exhibit frustration [1]. This has been stimulated in particular by the study of the magnetic properties of the cuprates which become high-Tc superconductors when doped. Frustrated spin systems are known to have many interesting properties that are quite unlike those of conventional magnetic systems. The simplest model of such kind is the Heisenberg spin chain with nearest- and next-nearest neighbor interactions J_1 and J_2. This model is well studied for J_1, $J_2 > 0$ [2, 3, 4]. In particular, it has been found that at $J_2 = 0.24J_1$ the transition from the gapless state to the

dimerized one takes place [5]. The point $J_2 = J_1/2$ corresponds to the well-known Majumdar-Ghosh model [6] for which the exact ground state consists of dimerized singlets and there is a gap in the spectrum of excited states.

Less studied are frustrated spin models with competing interactions of ferro- and antiferromagnetic types. The physical interest for these models is connected with the study of the real compounds containing CuO chains with edge-sharing CuO_4 units, like $La_6Ca_8Cu_{24}O_{41}$, Li_2CuO_2 and $Ca_2Y_2Cu_5O_{10}$ [7]. In these compounds the $Cu - O - Cu$ bond angle is nearly 90° and the nearest-neighbor $Cu - Cu$ spin interaction is ferromagnetic according to the Goodenough-Kanamori-Anderson rules [8] while the next-nearest-neighbor interaction is antiferromagnetic. The magnetic properties of these models are very different from those for models with pure antiferromagnetic interactions. Their ground states can be either ferromagnetic or singlet depending on the relation between the exchange integrals. One of the most interesting problems related to these models is the character of the transition between ferromagnetic (F) and antiferromagnetic (AF) phases.

Of a special importance are models for which it is possible to construct an exact ground state. Recently considerable progress has been achieved by using a so-called Matrix-Product (MP) form of the ground-state wave function [9, 10]. The ground-state wave function in the MP method is represented by Trace of a product of matrices describing single-site states. The MP ground state has a structure of the type where each neighboring pair of spins has a valence bond and, in fact, the MP form is a convenient representation of the valence bond states. Its origin can be traced to the S=1 quantum spin chain with bilinear and biquadratic interactions [13]. At present, various 1D spin models with the exact MP ground state have been found [10, 11, 12].

In this paper we present a set of 1D and 2D spin-1/2 models with competing F and AF interactions for which the singlet ground-state wave function can be found exactly. This function has a special form expressed in terms of auxiliary Bose operators. This form of the wave function is similar to the MP one but with infinite matrices. For special values of model parameters it can be reduced to the standard MP form.

One such model is the 1D quantum spin model describing the F-AF transition point. Spin correlations in the singlet ground state show giant spiral magnetic structure with period equal to the system size. On the antiferromagnetic side of this point the ground state can be either gapless with incommensurate spiral ground state [18] or gapped with exponential decay of correlators [24]. There are

regions in the AF phase where the magnetization as a function of magnetic field has jumps.

The second considered model is the special case of the spin ladder with exchange integrals depending on one parameter. The exact ground state of this model is non-degenerated singlet with exponentially decaying spin correlations, and there is an energy gap.

It will be shown that proposed form of the exact wave function can be generalized to higher dimensions and a two dimensional frustrated spin model with exact ground state can be constructed.

It is known that the exact ground state of some 1D and 2D quantum spin models can be represented in RVB form [15, 6, 36, 13, 31]. The RVB function in the Fermi representation consists of homopolar configurations of electron pairs. We generalize this two-particle function to include ionic states and denote it as "singlet bond" (SB) function. It is natural to try to find electronic models with exact ground state formed by SB functions in the same manner as for known spin models. In the paper some models of interacting electrons are presented. The Hamiltonians of these models include the correlated hopping of electrons and spin interactions. One of the 1D models describes the transition point between the phases with and without an off-diagonal long-range order.

The paper is organized as follows. In Sec.2 we consider the frustrated spin chain at F-AF transition point and describe the exact singlet ground-state wave function as well as details of the spin correlation function calculations. We discuss the phase diagram of this model and its magnetic properties in the AF phase. In Sec.3 the special spin ladder will be considered. A two-dimensional frustrated spin model with the exact ground state is considered in Sec.4. Sec.5 is devoted to the construction of the electronic models with the SB type of wave function. The results of this paper are summarized in Sec.6.

2 Zigzag spin model

2.1 Zigzag spin model at F-AF transition point

Let us consider the $s = \frac{1}{2}$ spin chain with nearest- and next-nearest neighbor interactions given by the Hamiltonian

$$H = -\sum_{i=1}^{M}(\mathbf{S}_{2i-1} \cdot \mathbf{S}_{2i} - \frac{1}{4}) + J_{23}\sum_{i=1}^{M}(\mathbf{S}_{2i} \cdot \mathbf{S}_{2i+1} - \frac{1}{4}) + J_{13}\sum_{i=1}^{N}(\mathbf{S}_i \cdot \mathbf{S}_{i+2} - \frac{1}{4}), \quad (1)$$
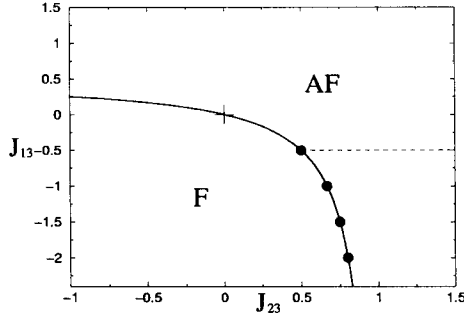
Figure 1: Phase diagram of the 'zigzag' model (1). The solid line is the boundary between the ferromagnetic and singlet phases. Circles correspond to the special cases of the model. On the dotted line the ground state is a product of singlet pairs.

with periodic boundary conditions and an even number of spins $N = 2M$. This model is equivalent to a ladder model with diagonal coupling: the so called a 'zigzag' spin ladder.

If $J_{23} < 1$, then the ground state of (1) is ferromagnetic (singlet) when $\delta < 0$ ($\delta > 0$), where $\delta = J_{23} + \frac{2J_{13}}{1 - 2J_{13}}$ (Fig.1). The equation $\delta = 0$ defines the line of transition points from the ferromagnetic to the singlet state, when energies of these states are zero. The model (1) along this line is given by the Hamiltonian depending on the parameter x ($x > -1/2$):

$$H = -\sum_{i=1}^{M}(\mathbf{S}_{2i-1} \cdot \mathbf{S}_{2i} - \frac{1}{4}) + \frac{2x}{2x+1}\sum_{i=1}^{M}(\mathbf{S}_{2i} \cdot \mathbf{S}_{2i+1} - \frac{1}{4}) - x\sum_{i=1}^{N}(\mathbf{S}_i \cdot \mathbf{S}_{i+2} - \frac{1}{4}), \quad (2)$$

with periodic boundary conditions.

We note that the Hamiltonian (2) has a symmetry: its spectrum coincides with the spectrum of $\widetilde{H}(x)$ obtained by the following transformation

$$\widetilde{H}(x) = -\frac{2x}{2x+1} H(-x - \frac{1}{2}), \qquad -\frac{1}{2} < x < 0$$

This transformation permutes the factors at the first and the second terms in the Hamiltonian (2). Thus, due to the symmetry it is sufficient to consider the range $x \geq -\frac{1}{4}$.

First, we will show that the ground-state energy of (2) is zero. Let us represent the Hamiltonian (2) as a sum of Hamiltonians h_n of cells containing three sites

$$H = \sum_{i=1}^{M}(h_{2i-1} + h_{2i}), \qquad (3)$$

where

$$h_{2i-1} = -\frac{1}{2}(\mathbf{S}_{2i-1} \cdot \mathbf{S}_{2i} - \frac{1}{4}) + \frac{x}{2x+1}(\mathbf{S}_{2i} \cdot \mathbf{S}_{2i+1} - \frac{1}{4}) - x(\mathbf{S}_{2i-1} \cdot \mathbf{S}_{2i+1} - \frac{1}{4}),$$

$$h_{2i} = -\frac{1}{2}(\mathbf{S}_{2i+1} \cdot \mathbf{S}_{2i+2} - \frac{1}{4}) + \frac{x}{2x+1}(\mathbf{S}_{2i} \cdot \mathbf{S}_{2i+1} - \frac{1}{4}) - x(\mathbf{S}_{2i} \cdot \mathbf{S}_{2i+2} - \frac{1}{4})$$

The eigenvalues of each h_n are

$$\lambda_1 = \lambda_2 = 0, \qquad \lambda_3 = \frac{4x^2 + 2x + 1}{4x + 2} > 0$$

We will present a singlet wave function which is an exact zero-energy eigenvector to each h_n and, therefore, it is the exact ground-state wave function of (2). This function has a form

$$\Psi_0 = P_0\Psi, \qquad \Psi = \langle 0_b | \, g_1 \otimes g_2' \otimes g_3 \otimes \ldots \otimes g_N' \, |0_b\rangle \tag{4}$$

Here

$$g_i = b^+ |\uparrow\rangle_i + |\downarrow\rangle_i, \qquad g_i' = (b^+ b - 2x) |\uparrow\rangle_i + b |\downarrow\rangle_i \tag{5}$$

where the spin-configuration space has been augmented with an auxiliary bosonic space, having creation (annihilation) operators $b^+ (b)$ and a vacuum $|0\rangle_b$. This auxiliary space is 'integrated away', so that Ψ is a pure spin-configuration wave function. The direct product $g_1 \otimes g_2' \otimes \ldots \otimes g_N'$ is the superposition of all possible spin configurations multiplied on the corresponding Bose operators, like $b^+ b \, b \, b^+ \ldots |\uparrow\downarrow\downarrow\uparrow \ldots\rangle$. P_0 is a projector onto the singlet state. This operator can be written as [16]

$$P_0 = \frac{1}{8\pi^2} \int_0^{2\pi} d\alpha \int_0^{2\pi} d\beta \int_0^{\pi} \sin\gamma d\gamma \, e^{i\alpha S^z} e^{i\gamma S^x} e^{i\beta S^z}, \tag{6}$$

where $S^{x(z)}$ are components of the total spin operator.

The form of wave function (4) resembles the MP form, but with an infinite matrix which is represented by Bose operators. Therefore, we have to pick out the $\langle 0_b | \ldots |0_b\rangle$ element of the matrix product instead of the usual trace in the MP formalism [9, 10], because the trace is undefined in this case. The function Ψ contains components with all possible values of spin S $(0 \le S \le N/2)$ and, in fact, a fraction of the singlet is exponentially small at large N. This component is filtered out by the operator P_0.

One can easily check that each cell Hamiltonian h_{2i-1} and h_{2i} for $i = 1, \ldots (M-1)$ gives zero when acting on the corresponding part in wave function $\Psi - g_{2i-1} \otimes$

$g'_{2i} \otimes g_{2i+1}$ and $g'_{2i} \otimes g_{2i+1} \otimes g'_{2i+2}$ (one should take care of Bose commutation relations). Since each h_i is a non-negatively defined operator, then Ψ is the exact ground state wave function of an open chain:

$$H_{\text{open}} = \sum_{i=1}^{M-1} (h_{2i-1} + h_{2i}) \tag{7}$$

As mentioned above, the function Ψ contains components of all possible values of total spin S, and, therefore, the ground state of the open chain is multiply degenerate. However it can be proven [14, 11] that for the cyclic chain (3) only the singlet and ferromagnetic components of Ψ have zero energy. Therefore, for the cyclic chain (3) Ψ_0 is the singlet ground state wave function degenerate with the ferromagnetic state.

In particular case, $x = -1/4$, when $J_{12} = J_{23} = -1$ and $J_{13} = \frac{1}{4}$, another form of the exact singlet ground-state wave function has been found in [15]. It reads

$$\Psi = \sum [i,j][k,l][m,n]\ldots, \tag{8}$$

where $[i,j]$ denotes the singlet pair and the summation is made for any combination of spin sites under the condition that $i < j, k < l, m < n \ldots$.

The following general statements relevant to the Hamiltonian (2) can be proved:

1). The ground states of open chain described by (7) in the sector with fixed total spin S are non-degenerate and their energies are zero.

2). For cyclic chains the ground state in the $S = 0$ sector is non-degenerate. The ground-state energies for $0 < S < M$ are non-zero.

3). The singlet ground-state wave function for open and cyclic chains coincide with each other.

2.2 Spin correlations in the ground state

For the sake of simplicity we show the calculation of the spin correlation function in the symmetric case $x = -1/4$, when the Hamiltonian (2) takes the form

$$H = -\sum_{i=1}^{N} (\mathbf{S}_i \cdot \mathbf{S}_{i+1} - \frac{1}{4}) + \frac{1}{4} \sum_{i=1}^{N} (\mathbf{S}_i \cdot \mathbf{S}_{i+2} - \frac{1}{4}), \tag{9}$$

Since in this case there is one spin in each elementary cell, the singlet ground state wave function Ψ_0 can be written in a more simple and symmetric form:

$$\Psi_0 = P_0 \Psi, \qquad \Psi = \langle 0_b | \, g_1 \otimes g_2 \otimes \ldots \otimes g_N \, | 0_b \rangle, \tag{10}$$

where

$$g_i = b^+ \, |\uparrow\rangle_i + b \, |\downarrow\rangle_i \tag{11}$$

One can check that wave functions (10) is the singlet ground-state wave function with zero energy for Hamiltonian (9). Therefore, the equivalence of wave functions (4) and (10) follows from the non-degeneracy of the ground state in the $S = 0$ sector (though functions Ψ in Eqs.(10) and (4) are different).

Now we calculate the norm and correlation function of the wave function Ψ_0 (10). The norm of the singlet wave function Ψ_0 is

$$\langle \Psi_0 | \Psi_0 \rangle = \langle \Psi | \, P_0 \, | \Psi \rangle \tag{12}$$

It is easy to check that the function Ψ has $S^z = 0$. Then the projector P_0 in Eq.(6) takes the form [11]

$$P_0 = \frac{1}{2} \int_0^\pi \sin \gamma d\gamma \, e^{izS^-} e^{iz'S^+}, \tag{13}$$

where $z = \tan \frac{\gamma}{2}$, $z' = \sin \frac{\gamma}{2} \cos \frac{\gamma}{2}$ and $S^{+(-)}$ are the operators of the total spin.

Therefore, the norm takes the form

$$\langle \Psi_0 | \Psi_0 \rangle = \frac{1}{2} \int_0^\pi \sin \gamma d\gamma \, \langle 0_a, 0_b | \prod_{i=1}^N (g_i^+ \, e^{izS_i^-} e^{iz'S_i^+} \, g_i) | 0_a, 0_b \rangle,$$

where

$$
\begin{aligned}
g_i^+ \, e^{izS_i^-} e^{iz'S_i^+} g_i &= (a^+ \, \langle \uparrow_i | + a \, \langle \downarrow_i |) \, e^{izS_i^-} e^{iz'S_i^+} (b^+ \, |\uparrow\rangle_i + b \, |\downarrow\rangle_i) \\
&= a^+ b^+ + (1 - z'z)ab + iza b^+ + iz' a^+ b,
\end{aligned}
$$

and a^+ and a are the Bose operators. Thus the norm can be rewritten as

$$\langle \Psi_0 | \Psi_0 \rangle = \frac{1}{2} \int_0^\pi \sin \gamma d\gamma \, \langle 0 | G^N | 0 \rangle, \tag{14}$$

where $|0\rangle = |0_a, 0_b\rangle$ is the Bose vacuum of a^+ and b^+ particles and

$$G = u(a^+ b^+ + ab) + iv(ab^+ + a^+ b),$$

where $u = \cos \frac{\gamma}{2}$, $v = \sin \frac{\gamma}{2}$.

Let us introduce the auxiliary function $P(\xi)$:

$$P(\xi) = \langle 0 | e^{\xi G} | 0 \rangle, \tag{15}$$

then

$$\langle 0 | G^N | 0 \rangle = \left. \frac{d^N P}{d\xi^N} \right|_{\xi=0}$$

The function $P(\xi)$ can be easily found [17]:

$$P(\xi) = \frac{1}{\sqrt{1 - u^2 \sin^2 \xi}} \tag{16}$$

Integrating Eq.(16) over γ, we obtain

$$\langle \Psi_0 | \Psi_0 \rangle = \frac{1}{2} \int_0^\pi \sin\gamma d\gamma \left. \frac{d^N P}{d\xi^N} \right|_{\xi=0} = \left. \frac{d^N}{d\xi^N} \left(\frac{1}{\cos^2(\frac{\xi}{2})} \right) \right|_{\xi=0} \tag{17}$$

Thus, finally, we arrive at

$$\langle \Psi_0 | \Psi_0 \rangle = 2 \frac{d^{N+1}}{d\xi^{N+1}} \left. \left(\tan\frac{\xi}{2} \right) \right|_{\xi=0} = \frac{4\,(2^{N+2} - 1)}{N + 2} |B_{N+2}| \tag{18}$$

Here B_N are the Bernoulli numbers.

To calculate the spin correlators we need to introduce operators

$$
\begin{aligned}
G_z &= g_i^+ \, e^{izS_i^-} e^{iz'S_i^+} 2S_i^z g_i = u(a^+ b^+ - ab) + iv(ab^+ - a^+ b), \\
G_+ &= g_i^+ \, e^{izS_i^-} e^{iz'S_i^+} S_i^+ g_i = ua^+ b + ivab, \\
G_- &= g_i^+ \, e^{izS_i^-} e^{iz'S_i^+} S_i^- g_i = uab^+ + iva^+ b^+
\end{aligned}
$$

Then, the correlator $\langle \mathbf{S}_1 \cdot \mathbf{S}_{l+1} \rangle$ will be defined by

$$\langle \Psi_0 | \mathbf{S}_1 \cdot \mathbf{S}_{l+1} | \Psi_0 \rangle = \frac{1}{2} \int_0^\pi \sin\gamma d\gamma \, \langle 0 | \frac{1}{4} G_z G^l G_z G^{N-l-2} + \frac{1}{2} G_+ G^l G_- G^{N-l-2} | 0 \rangle \tag{19}$$

(since $\langle 0 | G_- \ldots | 0 \rangle = 0$).

The expectation values in Eq.(19) can be represented as

$$
\begin{aligned}
\langle 0 | \, G_z G^l G_z G^{N-l-2} | 0 \rangle &= \frac{\partial^l}{\partial\xi^l} \frac{\partial^{N-l-2}}{\partial\zeta^{N-l-2}} \left. \langle 0 | G_z e^{\xi G} G_z e^{\zeta G} | 0 \rangle \right|_{\xi=\zeta=0}, \\
\langle 0 | \, G_+ G^l G_- G^{N-l-2} | 0 \rangle &= \frac{\partial^l}{\partial\xi^l} \frac{\partial^{N-l-2}}{\partial\zeta^{N-l-2}} \left. \langle 0 | G_+ e^{\xi G} G_- e^{\zeta G} | 0 \rangle \right|_{\xi=\zeta=0}
\end{aligned} \tag{20}
$$

After a procedure similar to that for the norm and the integration over γ, we obtain

$$\langle \Psi_0 | \mathbf{S}_1 \cdot \mathbf{S}_{l+1} | \Psi_0 \rangle = \frac{\partial^l}{\partial\xi^l} \frac{\partial^{N-l-2}}{\partial\zeta^{N-l-2}} \left. \left(-\frac{3}{8} \frac{\cos(\xi - \zeta)}{\cos^4(\frac{\xi+\zeta}{2})} \right) \right|_{\xi=\zeta=0} \tag{21}$$

It can be shown that in the thermodynamic limit, Eqs.(18) and (21) result in

$$\langle \mathbf{S}_i \cdot \mathbf{S}_{i+l} \rangle = \frac{1}{4} \cos\left(\frac{2\pi l}{N} \right) \tag{22}$$

So, we reproduce the result obtained in [15, 11] that in the thermodynamic limit a giant spiral spin structure is realized, with the period of the spiral equal to the system size.

For the general case of model (2) the calculation of the singlet ground-state correlation functions can be performed in a similar way. The final result in the thermodynamic limit is [14, 11]:

$$
\begin{aligned}
\langle \mathbf{S}_n \mathbf{S}_{n+2l} \rangle &= \frac{1}{4} \cos\left(\frac{4\pi l}{N}\right), \\
\langle \mathbf{S}_n \mathbf{S}_{n+2l-1} \rangle &= \frac{1}{4} \cos\left(\frac{2(2l-1)\pi}{N} + (-1)^n \triangle\varphi\right)
\end{aligned}
\tag{23}
$$

The latter equations mean that the long-range double-spiral order exists in the singlet ground state of Hamiltonian (2). The pitch angle of each spiral is $\frac{4\pi}{N}$ and there is a small shift angle $\triangle\varphi = \frac{2\pi(4x+1)}{N}$ between them. This shift angle reflects the fact that the unit cell contains two sites unless $x = -\frac{1}{4}$.

We note that for special values of the model parameter $x = \frac{1}{2}, 1, \frac{3}{2}, 2 \dots$ Eqs.(23) are not valid and spin correlations decay exponentially. These cases will be considered in Sec.III (see Eqs.(42)).

2.3 Phase diagram of 'zigzag' model

So far we have considered the model (1) at the transition line from ferromagnetic to antiferromagnetic state. Now we discuss the phase diagram of this model. The exact ground state in the AF phase is generally unknown. But it is interesting to note that the ground state on the line $J_{13} = -1/2$ is the product of singlets on ladder diagonals (2,3), (4,5), ... as in the point $J_{13} = -J_{23} = -1/2$ on the transition line. The spectrum of (1) on the transition line is gapless. There are some regions on the plane (J_{13}, J_{23}) which were studied by different approximation methods.

First let us consider the behavior of the system in the transition region near the 'symmetric' point $x = -\frac{1}{4}$, where

$$
J_{12} = J_{23} = -1, \qquad J_{13} = \frac{1}{4} + \delta
\tag{24}
$$

It should be mentioned that several copper oxide compounds are described by this model. These compounds contain CuO chains and $Cu - O - Cu$ angle θ is near $90°$ [7]. In this case the usual antiferromagnetic super-exchange of two nearest-neighbor magnetic Cu ions is suppressed and the exchange integral J_{12} is
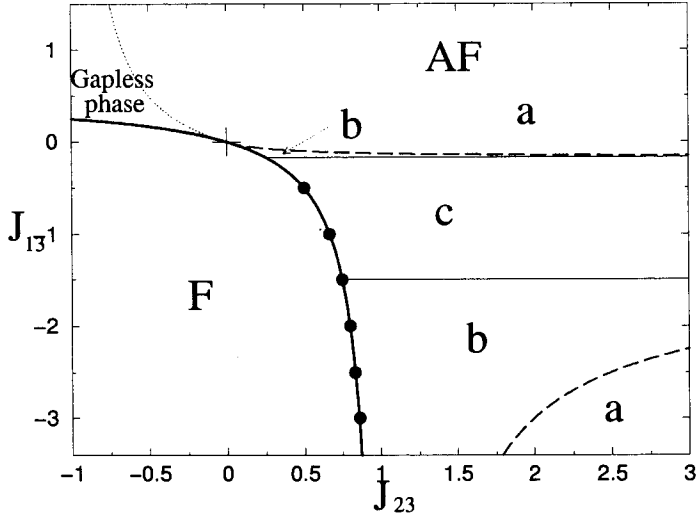
Figure 2: The thick solid line is the boundary between the ferromagnetic and singlet phases. Circles correspond to the special cases of the model. The dotted line denotes the heuristic boundary between gapped and gapless phases. The dashed line is the boundary of the region with a multimagnon bound state.

negative. On the other hand the next-nearest-neighbor interaction J_{13} between Cu ions does not depend on θ and is antiferromagnetic. The estimation of the ratio J_{13}/J_{12} for $La_6Ca_8Cu_{24}O_{41}$ and Li_2CuO_2 gives $\delta = 0.11$ and $\delta = 0.37$ respectively [7].

Though the model (24) is not exactly solvable in this case, its properties for $\delta \ll 1$ can be studied. The consideration is based on the classical approximation. In this approximation the ground-state spin structure is the spiral with period $\sim \delta^{-1/2}$ and the ground-state energy $E = -2N\delta^2$. Using this approach the regular expansion in powers of the small parameter δ can be developed [18, 14]. The second-order quantum corrections coincide with the classical energy. The calculation of higher orders of the perturbation theory in δ leads to infrared-divergent integrals and it is necessary to sum them in all orders to obtain the contributions proportional to $\delta^{5/2}$, δ^3 etc. In particular, the ground-state energy calculated up to terms $\sim \delta^{5/2}$ is

$$E_0 = -4N\delta^2 + 4.14N\delta^{5/2}$$

The excitation spectrum is gapless and has a sound-like behavior [18]. The

corresponding sound velocity is $v = 4\delta^{3/2}$.

The study of the dependence of the ground-state energy $E(m)$ on magnetization $m = S_z/N$ [26] at $\delta \ll 1$ shows that $\frac{\partial^2 E}{\partial m^2} < 0$ in a finite interval of values of m. This implies the thermodynamic instability of the uniform state against phase separation. This instability arises due to the existence of multimagnon bound states. The energy of an n-magnon bound state $(n \gg 1)$ is $\varepsilon_n = -nb$, $b = |\varepsilon_1| + \epsilon_b$, where ε_1 is the energy of one-magnon state and ϵ_b is the binding energy per magnon. For the model (24) $\varepsilon_1 = -8\delta^2$ and $\epsilon_b \sim \delta^{5/2}$. As a result the function $E(m)$ has the form [26]:

$$
\begin{aligned}
E(m) &= E_0 + 2\pi\delta^{3/2}m^2, & m < m_c = \frac{2}{\pi}\sqrt{\delta} \\
E(m) &= -\frac{b}{2}(1 - 2m), & m_c < m < \frac{1}{2}
\end{aligned}
\tag{25}
$$

At $m > m_c$ the system is in a two-phase state consisting of the ferromagnetic ($m = 1/2$) phase and the phase with $m = m_c$. According to (25) the magnetization as a function of magnetic field h has a jump from $m = m_c$ to $m = 1/2$ (metamagnetic transition) at $h = h_c = b$. These values m_c and h_c are close to those obtained in [27] by extrapolation of finite cluster calculations. We stress that the jump of the magnetization exists if there are multimagnon bound states leading to the linear dependence of $E(m)$ for some region of m.

As for properties of the model far from the transition point $\delta = 0$, now-days there is no clear understanding [3, 19, 20], but we believe that the spectrum remains gapless. For the case $\delta \gg 1$ this fact is predicted in [21]. As for the jump in $m(h)$ it is unknown if it remains at $\delta \simeq 1$. Numerical calculations [27] show that, at least, there is an abrupt increase of magnetization at some critical value of magnetic field.

This perturbation theory can be generalized for the vicinity of any point on the transition line. It gives similar properties of the system in the region $J_{23} < 0$, but it diverges at $J_{23} > 0$.

At $J_{13} = 0$ and $J_{23} > 0$ the model (1) reduces to the alternating Heisenberg chain studied in [22]. The lowest excitation is the triplet and there is a gap. At $J_{23} = 0$ and $J_{13} > 0$ the model (1) reduces to the spin ladder with antiferromagnetic interactions along legs and ferromagnetic interactions on rungs. It is evident that there is a gap at $J_{13} \ll 1$ (in this case the model is equivalent to the spin $S = 1$ Heisenberg chain). It was shown in [23] that the gap exists at $J_{13} \gg 1$.

The region $J_{23} > 0$, $J_{13} < 0$ was studied by different methods in [24, 26]. The exact diagonalization of finite chains shows a gap Δ in the excitation spectrum
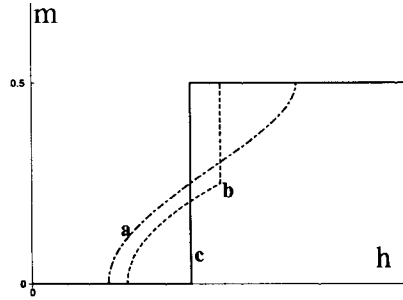
Figure 3: Dependence of magnetization m on magnetic field h for the case: (a) outside the bound-state region; (b) in the bound-state region, but outside the strip $-\frac{1}{2} < J_{13} < -\frac{1}{6}$; (c) inside the strip $-\frac{1}{2} < J_{13} < -\frac{1}{6}$.

which is closed at the transition line. The presence of singlet-triplet gap is also confirmed by calculations with the use of variational wave functions in MP form (39) when all matrix elements are considered as variational parameters. The MP variational function gives very good accuracy [25, 26], besides it gives exact ground-state results for special points on the transition line and for the line $J_{13} = -\frac{1}{2}$ (dimer state).

Another important property of the model with $J_{23} > 0$, $J_{13} < 0$ is the existence of the multimagnon bound states for a definite region of the values J_{23} and J_{13}. This region is shown on Fig.1. On the boundary of this region the multimagnon bound states disappear. As was noted before the existence of the bound states leads to linear regions on the dependence $E(m)$ and to a metamagnetic transition. The dependence for $E(m)$ and $m(h)$ was found using MP variational function. The calculations show that out of the bound-state region the function $m(h)$ is typical for the gapped antiferromagnet, i.e. it is monotonically increasing function (Fig.3). In other words, $m(h) = 0$ for $h < \Delta$ and $m(h) = 1/2$ for $h > |\varepsilon_1|$. In the bound-state region the magnetization curve has the jump. It is interesting that inside the strip $-\frac{1}{2} < J_{13} < -\frac{1}{6}$ this jump takes place immediately from zero to the maximal value $m = \frac{1}{2}$ (Fig.3) at $h_c = |\varepsilon(0)|$ ($\varepsilon(0)$ is a ground-state energy per site). Such behavior of $m(h)$ is explained by the fact that inside this strip $\Delta > |\varepsilon(0)|$ and the transition from the singlet state to the ferromagnetic one passes through states with intermediate values of spin. In the bound-state region outside the stripe the magnetization curve has a form as shown on Fig.(3). In this case the critical field $h_c = \Delta$.

Thus, summarizing all the above, we expect that the phase diagram of the
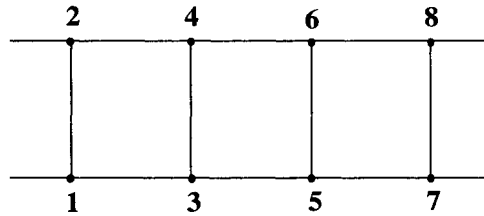
Figure 4: The two-leg spin ladder.

model (1) has the form shown in Fig.(2).

3 Spin ladder model

Let us consider a more general spin-ladder model, for which the 'zigzag' model (2) is a particular case. So, we consider the cyclic ladder model containing $N = 2M$ spins $s = \frac{1}{2}$ (Fig.4). The proposed form of wave function (4) can be generalized for a ladder model as follows:

$$\Psi_0 = P_0 \Psi, \qquad \Psi = \langle 0|\, g_1 \otimes g_2 \otimes \ldots \otimes g_M\, |0\rangle, \tag{26}$$

where each g_i corresponds to the ith rung of the ladder:

$$g_i = -b^+(2x - b^+b)\,|\!\uparrow\uparrow\rangle_i + b\,|\!\downarrow\downarrow\rangle_i + (b^+b - x)\,|\!\uparrow\downarrow + \downarrow\uparrow\rangle_i + y\,|\!\uparrow\downarrow - \downarrow\uparrow\rangle_i \tag{27}$$

where x and y are two parameters of the model. It is obvious that the ladder wave function (26)-(27) reduces to the original function (4) at $y = x$.

Now we will construct the Hamiltonian for which Ψ_{ladder} is the exact ground-state wave function. This Hamiltonian describes the two-leg $s = \frac{1}{2}$ ladder with periodic boundary conditions (Fig.4) and can be represented in a form

$$H = \sum_{i=1}^{N} h_{i,i+1}, \tag{28}$$

where $h_{i,i+1}$ describes the interaction between neighboring rungs. The spin space of two neighboring rungs consists of six multiplets: two singlet, three triplet and one quintet. At the same time, one can check that the product $g_i \otimes g_{i+1}$ contains only three of the six multiplets of each pair of neighboring rungs: one singlet, one triplet and one quintet. The specific form of the singlet and triplet components present in the product $g_i \otimes g_{i+1}$ depends on parameters x and y. The Hamiltonian

$h_{i,i+1}$ can be written as the sum of the projectors onto the three missing multiplets with arbitrary positive coefficients λ_1, λ_2, λ_3:

$$h_{i,i+1} = \sum_{k=1}^{3} \lambda_k P_k^{i,i+1}, \tag{29}$$

where $P_k^{i,i+1}$ is the projector onto the missing multiplets in the corresponding cell Hamiltonian.

The wave function (26) is an exact wave function of the ground state of the Hamiltonian $h_{i,i+1}$ with zero energy, because

$$h_{i,i+1}|\Psi\rangle = 0, \qquad i = 1, ... N - 1 \tag{30}$$

and λ_1, λ_2, λ_3 are the excitation energies of the corresponding multiplets in the cell.

So, Ψ is the exact ground state wave function with zero energy for the total Hamiltonian of an open ladder

$$H_{\text{open}} = \sum_{i=1}^{M-1} h_{i,i+1} \tag{31}$$

$$H_{\text{open}}|\Psi\rangle = 0 \tag{32}$$

Since the function Ψ contains components with all possible values of total spin S $(0 \leq S \leq M)$, then the ground state of the open ladder is multiply degenerate. But for a cyclic ladder (28) only singlet and ferromagnetic components of Ψ have zero energy. Therefore, for a cyclic ladder Ψ_0 is a singlet ground state wave function degenerated with the ferromagnetic state. Further, all the statements given for the 'zigzag' model (2) are valid for ladder model (28).

Since the specific form of the existing and missing multiplets in the wave function (26) on each of the two nearest neighbor spin pairs depends on the parameters x and y, the projectors in (29) also depend on x and y. Each projector can be written in the form

$$P_k^{1,2} = J_{12}^{(k)}(\mathbf{S}_1 \cdot \mathbf{S}_2 + \mathbf{S}_3 \cdot \mathbf{S}_4) + J_{13}^{(k)}(\mathbf{S}_1 \cdot \mathbf{S}_3 + \mathbf{S}_2 \cdot \mathbf{S}_4) + J_{14}^{(k)}\mathbf{S}_1 \cdot \mathbf{S}_4 + J_{23}^{(k)}\mathbf{S}_2 \cdot \mathbf{S}_3$$
$$+ J_1^{(k)}(\mathbf{S}_1 \cdot \mathbf{S}_2)(\mathbf{S}_3 \cdot \mathbf{S}_4) + J_2^{(k)}(\mathbf{S}_1 \cdot \mathbf{S}_3)(\mathbf{S}_2 \cdot \mathbf{S}_4) + J_3^{(k)}(\mathbf{S}_1 \cdot \mathbf{S}_4)(\mathbf{S}_2 \cdot \mathbf{S}_3) + C^{(k)} \tag{33}$$

and this representation is unique for a fixed value of the parameters x and y.

Substituting the above expressions for the projectors into Eq. (29), we obtain the general form of the Hamiltonian $h_{i,i+1}$. Inasmuch as the Hamiltonian $h_{i,i+1}$

have the same form for any i, it suffices here to give the expression for $h_{1,2}$:

$$h_{1,2} = \quad J_{12}(A_{12} + A_{34}) + J_{13}(A_{13} + A_{24}) + J_{14}A_{14} + J_{23}A_{23}$$
$$+ \quad J_1 A_{12} A_{34} + J_2 A_{13} A_{24} + J_3 A_{14} A_{23} \tag{34}$$

where

$$A_{ij} = \mathbf{S}_i \cdot \mathbf{S}_j - \frac{1}{4}$$

and all exchange integrals depend on the model parameters and the spectrum of excited states $J_i = J_i(x, y, \lambda_1, \lambda_2, \lambda_3)$ as follows:

$$J_{12} = -\frac{\lambda_2}{2} + \frac{\lambda_3}{2}\frac{4y^2 - 1}{4y^2 + 1}, \qquad\qquad J_{23} = -\frac{\lambda_2}{2} - \frac{\lambda_3}{2}\frac{(2y - 1)^2}{4y^2 + 1},$$

$$J_{13} = -\frac{\lambda_2}{2} - \frac{\lambda_3}{2}\frac{4y^2 - 1}{4y^2 + 1}, \qquad\qquad J_{14} = -\frac{\lambda_2}{2} - \frac{\lambda_3}{2}\frac{(2y + 1)^2}{4y^2 + 1},$$

$$J_1 = 2J_{12} - \lambda_1\frac{y^4 - x^2(x + 1)^2}{3y^4 + x^2(x + 1)^2}, \qquad J_2 = 2J_{13} + 2\lambda_1\frac{y^4 + y^2 x(x + 1)}{3y^4 + x^2(x + 1)^2},$$

$$J_3 = J_{14} + J_{23} + 2\lambda_1\frac{y^4 - y^2 x(x + 1)}{3y^4 + x^2(x + 1)^2} \tag{35}$$

(one should keep in mind that only positive λ_i can be substituted in these expressions). The model (35) has evident symmetry: the change of sign of y is equivalent to renumbering of sites $1 \leftrightarrow 2$, $3 \leftrightarrow 4 \dots$. Therefore, we will consider only the case $y > 0$.

In general, the Hamiltonian $h_{i,i+1}$ contains all the terms present in (33), but we can simplify it by setting, for example, $J_2 = J_3 = 0$ and solving equations (35) for $\lambda_1, \lambda_2, \lambda_3$. All λ_k turn out to be positive in this case for any x and y except two lines $y = 0$ and $x = -1/2$, where ground state is multiple degenerated. The Hamiltonian $h_{i,i+1}$ in this case takes the form

$$h_{1,2} = J_{12}(A_{12} + A_{34}) + J_{13}(A_{13} + A_{24}) + J_{14}A_{14} + J_{23}A_{23} + J_1 A_{12} A_{34} \tag{36}$$

$$J_{12} = -x(x + 1) + y^2 - \frac{1}{2}, \qquad J_{14} = x(x + 1) - y^2 - y,$$

$$J_{13} = -x(x + 1) - y^2, \qquad\qquad J_{23} = x(x + 1) - y^2 + y,$$

$$J_1 = \frac{[x(x + 1) - y^2]^2}{y^2} - 1$$

The calculation of the norm of (26) and the singlet ground-state correlation functions can be performed in a similar way as the corresponding calculations for

the case $y = x = -1/4$. Therefore, we give here the final result for spin correlation functions at $N \to \infty$

$$
\begin{aligned}
\langle \mathbf{S}_n \cdot \mathbf{S}_{n+2l} \rangle &= \frac{1}{4} \cos\left(\frac{4\pi l}{N} \right), \\
\langle \mathbf{S}_{2n-1} \cdot \mathbf{S}_{2n+2l} \rangle &= \frac{1}{4} \cos\left(\frac{4\pi l}{N} - \triangle\varphi \right)
\end{aligned}
\tag{37}
$$

These equations mean that a spiral on each leg with pitch angle $\frac{4\pi}{N}$ is formed and the shift angle between spirals on the upper and the lower legs is $\triangle\varphi = \frac{8\pi y}{N}$. At $y = 0$, when spins on each rung form a local triplet, the shift angle vanishes and the spirals on both legs become coherent (we note that the shift angles in Eqs.(23) and (37) are defined in different ways).

Thus, there is just one full rotation of the spin over the length of the ladder, independent of the size of the system and for fixed $l \ll N$ at $N \to \infty$ two spins on the ladder are parallel.

We emphasize that the spin correlation function $\langle \mathbf{S}_i \cdot \mathbf{S}_j \rangle$ does not depend on the choice of λ_k for a fixed parameters x, y, because the ground-state wave function of the three-parameter set of Hamiltonians (35) is the same.

3.1 Special cases

There are special values of the parameter x for which Eqs.(37) are not valid. For cases of integer or half-integer $x = j$, which correspond to the special cases of the model (35), in Eq.(27) one can easily recognize Maleev's boson representation of spin $S = j$ operators [28]:

$$
S^+ = b^+(2j - b^+b), \qquad S^- = b, \qquad S^z = b^+b - j
\tag{38}
$$

Generally, the wave functions (4) and (26) resemble the MP form but with infinite matrices represented by the Bose operators. However, in accordance to Maleev's representation in the special cases the infinite matrices formed by the Bose operators b^+ and b can be broken off to the size $n = 2j + 1$, and wave function (26) is reduced to the usual MP form

$$
\Psi_0 = Tr\left(g_1 \otimes g_2 \otimes \ldots \otimes g_N \right),
\tag{39}
$$

where $g = -xT + yS$ is the $n \times n$ matrix describing states of spin pair on corresponding rung of the ladder. The singlet-state matrix is

$$
S = I \, |s\rangle
\tag{40}
$$

where I is unit matrix and $|s\rangle$ is the singlet state. The triplet-state matrix T is expressed by Clebsch-Gordan coefficients $C_{m_1,m_2} = \langle (1, m_1)\,(j, m_2) \,\|\, (j, m_1 + m_2) \rangle$ as follows:

$$T = \frac{1}{C_{0,j}} \begin{pmatrix} C_{0,j}\,|0\rangle & C_{1,j-1}\,|1\rangle & 0 & 0 & 0 \\ C_{-1,j}\,|-1\rangle & C_{0,j-1}\,|0\rangle & . & 0 & 0 \\ 0 & . & . & . & 0 \\ 0 & 0 & . & . & C_{1,-j}\,|1\rangle \\ 0 & 0 & 0 & C_{-1,-j+1}\,|-1\rangle & C_{0,-j}\,|0\rangle \end{pmatrix}, \qquad (41)$$

where $|\sigma\rangle$ is the triplet state with $S^z = \sigma$.

Exact calculation of the correlators in the thermodynamic limit is performed using standard transfer matrix technique and results in

$$\langle S_1 S_2 \rangle = \frac{x(x+1) - 3y^2}{4\omega},$$

$$\langle S_i S_{i+2l} \rangle = \frac{x(x+1)(4y^2-1)}{4\omega^2}\left(\frac{\omega-1}{\omega}\right)^{l-1},$$

$$\langle S_{2i+1} S_{2i+2l+2} \rangle = -\frac{x(x+1)(2y-1)^2}{4\omega^2}\left(\frac{\omega-1}{\omega}\right)^{l-1},$$

$$\langle S_{2i+2} S_{2i+2l+1} \rangle = -\frac{x(x+1)(2y+1)^2}{4\omega^2}\left(\frac{\omega-1}{\omega}\right)^{l-1}, \qquad (42)$$

where

$$\omega = x(x+1) + y^2$$

In the particular case of zero singlet weight, $y = 0$, when spins on each rung form a local triplet, correlation functions (42) coincide with those obtained in [9, 29].

According to Eqs.(42) the spin correlations have an exponential decay and the correlation length r_c is

$$r_c = 2\ln^{-1}\left|\frac{\omega}{\omega-1}\right| \qquad (43)$$

In particular, for special points of the 'zigzag' model (2) with $J_{23} = \frac{2x}{2x+1}$ and $J_{13} = -x$ the correlation length $r_c = -2\ln^{-1}\left(1 - \frac{1}{x(2x+1)}\right)$.

The correlation length r_c diverges when $x \to \infty$ or $y \to \infty$. In these cases the singlet ground state has a collinear or stripe spin structure, i.e. spin-spin correlations are ferromagnetic along legs and antiferromagnetic between them (Fig.5), with a magnetic order m:

$$\langle S_i S_{i+2l} \rangle \simeq - \langle S_i S_{i+1+2l} \rangle \simeq m^2, \qquad m \simeq \frac{xy}{x^2 + y^2}$$
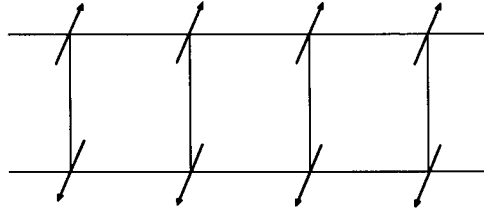
Figure 5: Stripe spin structure on the ladder model.

When $y = x$ (the 'zigzag' model) the magnetic order is equal to the classical value $m = 1/2$.

We note that the wave function (26) shows double-spiral ordering for all values of x and y excluding the special lines $x = j$. The crossover between spiral and stripe states occurs in the exponentially small (at $N \to \infty$) vicinity of the special lines.

3.2 Spectrum of the model

Generally, the excitation spectrum of model (28,36) can not be calculated exactly. It is clear that this spectrum is gapless because, for example, the one-magnon energy is $\sim N^{-4}$ at $N \to \infty$. Moreover, the lowest singlet excitation is gapless as well. For model (28,36) lying on the special lines this fact can be established from the following consideration. As mentioned above, the crossover between spiral and stripe states occurs in the exponentially small vicinity of the special lines. It means that two wave functions $\Psi_0(j)$ and $\Psi_0(j + \delta)$ corresponding to points $(x = j, \ y)$ and $(x = j + \delta, \ y)$ respectively are almost orthogonal at $\delta \sim e^{-N}$. Hence, we can consider a spiral wave function $\Psi_0(j + \delta)$ as a variational function of the excited singlet state at special point $x = j$. The energy of this excited state at a special point $x = j$ is

$$
\begin{aligned}
E_{ex} &= \langle \Psi_0(j + \delta)| \, H(j) \, |\Psi_0(j + \delta)\rangle \\
&\sim \left\langle \Psi_0(j + \delta)| \, H(j + \delta) - \delta\frac{dH(j + \delta)}{dx} \, |\Psi_0(j + \delta)\right\rangle \sim \text{const.} \cdot \delta \sim e^{-N}
\end{aligned}
$$

Thus, on the special lines the stripe ground state of the considered model is asymptotically degenerated with an excited spiral singlet state in the thermodynamic limit. It is not clear if the degeneracy is exponentially large or not. This consideration is valid for any integer or half-integer $x = j$, but it is not valid for

the parameters $x \neq j$, which are outside of special lines. We performed [24] numerical diagonalization of finite ladders for various parameters x and y and found that the exponential degeneracy possibly takes place for all parameters x and y, but we can not confirm it strictly.

It is interesting to note that the singlet wave function (26) can be also represented in a special recurrent form [14, 11]

$$\Psi_0 = P_0 \Psi_M, \tag{44}$$

$$
\begin{aligned}
\Psi_M &= (s_1^+ + \nu_1 s_2^+ + \nu_2 s_3^+ \ldots + \nu_2 s_N^+)(s_3^+ + \nu_1 s_4^+ \ldots + \nu_2 s_N^+) \ldots \\
&\quad (s_{2n-1}^+ + \nu_1 s_{2n}^+ \ldots + \nu_2 s_N^+) \ldots (s_{N-1}^+ + \nu_1 s_N^+) \, |\downarrow\downarrow \ldots \downarrow\rangle
\end{aligned} \tag{45}
$$

where s_i^+ is the $s = \frac{1}{2}$ raising operator. Eq.(45) contains M operator multipliers and the vacuum state $|\downarrow\downarrow \ldots \downarrow\rangle$ is the state with all spins pointing down. The function Ψ_M is the eigenfunction of S_z with $S_z = 0$ but it is not an eigenfunction of $\mathbf{S}^2$. P_0 is a projector onto the singlet state. Two parameters ν_1 and ν_2 in wave function (45) are connected with parameters x and y in (27) as

$$\nu_1 = \frac{1 + x - y}{1 + x + y}, \qquad \nu_2 = \frac{1}{1 + x + y}$$

The norm of the wave function (44) and expectation values can be also calculated with the use of the recursion technique developed in [14, 11]. Certainly, it gives the same expressions (37,42) for spin correlation functions.

3.3 Antiferromagnetic ladder model

Now we should consider in particular the special case [11] $x = 1/2$. In this case the product $g_i \otimes g_{i+1}$ contains only one singlet and one triplet and does not contain any quintet. Therefore, in this case the cell Hamiltonian can be written in the form [31]

$$H = \sum_i h_{i,i+1}, \qquad h_{i,i+1} = \sum_{k=1}^{4} \lambda_k P_k^{i,i+1}, \tag{46}$$

where $P_4^{i,i+1}$ - is a projector onto the quintet state. If all $\lambda_k > 0$, the ferromagnetic state has positive energy $E = M\lambda_4$ and wave function Ψ_0 (26) is now a non-degenerate singlet ground-state wave function for the Hamiltonian (46), while for Hamiltonian (28,29) Ψ_0 is also an exact ground state but degenerate with the ferromagnetic state. Using a freedom in choice of λ_k we can exclude all four-spin

interactions in $h_{i,i+1}$

$$
\begin{aligned}
h_{i,i+1} &= J_{12}\left(\mathbf{S}_{2i-1} \cdot \mathbf{S}_{2i} + \mathbf{S}_{2i+1} \cdot \mathbf{S}_{2i+2}\right) + J_{13}\left(\mathbf{S}_{2i-1} \cdot \mathbf{S}_{2i+1} + \mathbf{S}_{2i} \cdot \mathbf{S}_{2i+2}\right) \\
&\quad + J_{14}\mathbf{S}_{2i-1} \cdot \mathbf{S}_{2i+2} + J_{23}\mathbf{S}_{2i} \cdot \mathbf{S}_{2i+1} + C
\end{aligned} \tag{47}
$$

and all exchange integrals J_{ij} depend on one model parameter $y < 3/2$ (this inequality is necessary to satisfy $\lambda_k > 0$)

$$
\begin{aligned}
J_{12} &= \frac{3}{2}(4y^2 - 1), & J_{14} &= -y(3 + 2y)(2y - 1)^2, \\
J_{13} &= -2y^2(4y^2 - 1), & J_{23} &= y(3 - 2y)(2y + 1)^2, & C &= 9y^2 + \frac{3}{4} \quad (48)
\end{aligned}
$$

It follows from Eq.(42) that the ground state has ultrashort-range correlations with $r_c \sim 1$. For example, $r_c(y = 0) = 2\log^{-1} 3$, which coincides with the correlation length of the AKLT model. But at $y = \frac{1}{2}$ all correlations are zero except $\langle \mathbf{S}_{2i} \cdot \mathbf{S}_{2i+1} \rangle = -\frac{3}{4}$. It implies that at $y = \frac{1}{2}$ the model (46-48) has a dimer ground state.

The value $(\omega - 1)$ changes sign at $y = \frac{1}{2}$, and as follows from Eqs.(42), the correlators show the antiferromagnetic structure of the ground state at $\frac{1}{2} \le y \le \frac{3}{2}$, while at $0 \le y \le \frac{1}{2}$ there are ferromagnetic correlations inside pairs $(1,2), (3,4), \ldots$ and antiferromagnetic correlations between the pairs.

The Hamiltonian (46-48) of the cyclic ladder has a singlet-triplet gap Δ for finite N. It is evident that for $y = \frac{1}{2}$ the gap exists for $N \to \infty$ and $\Delta(\frac{1}{2}) = 4$. The existence of the finite gap at the thermodynamic limit in the range $0 < y < \frac{3}{2}$ follows from the continuity of the function $\Delta(y)$. It is also clear that $\Delta(y)$ at $N \to \infty$ vanishes at the boundary points $y = 0$ and $y = \frac{3}{2}$ when the ground state is degenerate and there are low-lying spin-wave excitations.

Unfortunately, a method for the exact calculation of $\Delta(y)$ in the thermodynamic limit is unknown. For the approximate calculation $\Delta(y)$ we use the trial function of the triplet state in the form

$$
\Psi_t = \sum_n s_n^+ e^{ikn} \Psi_0, \tag{49}
$$

The trial function Ψ_t gives $\Delta(y)$ which at $N \to \infty$ has minima at $k = \pi$ and $k = 0$ for $0 < y < \frac{1}{2}$ and $\frac{1}{2} < y < \frac{3}{2}$, respectively

$$
\begin{aligned}
\Delta(y) &= \frac{32y^2(4y^2 + 1)}{4y^2 + 3}, & 0 < y < \frac{1}{2} \\
\Delta(y) &= \frac{128y^2}{(4y^2 + 1)(4y^2 + 3)}, & \frac{1}{2} < y < \frac{3}{2}
\end{aligned} \tag{50}
$$
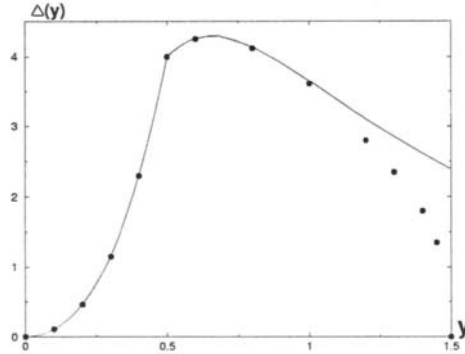
Figure 6: Singlet-triplet gap of the model (48) as a function of the parameter y. The circles denote the results of the extrapolation of exact finite-chain calculations. The solid line represents the dependence $\Delta(y)$ given by Eq.(50).

The dependence of $\Delta(y)$ given by Eq.(50) is shown in Fig.6 together with the results of extrapolations of exact finite-chain calculations. Both dependences agree very well for $y \leq \frac{1}{2}$. However, $\Delta(y)$ given by Eq.(50) is not zero at $y = \frac{3}{2}$, while numerical calculations fit the dependence $\Delta(y) \sim \sqrt{\frac{3}{2} - y}$, $y \to \frac{3}{2}$.

We note that the trial function of the type (49) gives the value 0.7407 for the singlet-triplet gap in the AKLT model. This estimate is close to the value 0.7143 obtained by another approach in [30].

For other special cases one can also construct Hamiltonians for which Ψ_0 is a non-degenerate singlet ground-state wave function. But in these cases one have to introduce more distant interactions.

4 Valence-Bond-State models

4.1 One-dimensional model

We studied previously a one-parameter ladder model (46-48) with non-degenerate singlet ground state. The exact ground state wave function of the cyclic ladder was written in the MP form (39). Now we write the wave function Ψ_0 in a form more suitable for subsequent generalization to other types of lattices [31].

We consider a ladder of $N = 2M$ spins $1/2$. The wave function of this system is described by the Nth-rank spinor

$$\Psi = \Psi^{\lambda\mu\nu\ldots\tau},\tag{51}$$

where the indices λ, μ, ν, ..., $\tau = 1$, 2 correspond to different projections of the spin 1/2.

We partition the system into pairs of spins located on rungs of the ladder. The wave function can then be written as the product of M second-rank spinors

$$\Psi = \Psi^{\lambda\mu}(1)\Psi^{\nu\rho}(2)\ldots\Psi^{\sigma\tau}(M). \tag{52}$$

We now form a scalar from Eq. (52), simplifying the latter with respect to index pairs:

$$\Psi_s = \Psi^{\lambda}{}_{\nu}(1)\Psi^{\nu}{}_{\kappa}(2)\ldots\Psi^{\sigma}{}_{\lambda}(M). \tag{53}$$

Here subscripts correspond to the covariant components of the spinor, which are related to the contravariant components (superscripts) through the metric spinor

$$g_{\lambda\mu} = g^{\lambda\mu} = \begin{pmatrix} 0 & 1 \\ -1 & 0 \end{pmatrix}. \tag{54}$$

$$\Psi_{\lambda} = g_{\lambda\mu}\Psi^{\mu}, \qquad \Psi^{\lambda} = g^{\mu\lambda}\Psi_{\mu}.$$

The scalar function (53) can thus be written in the form

$$\Psi_s = \Psi^{\lambda\mu}(1)g_{\mu\nu}\Psi^{\nu\rho}(2)g_{\rho\kappa}\ldots\Psi^{\sigma\tau}(M)g_{\tau\lambda}. \tag{55}$$

The scalar function Ψ_s obviously describes the singlet state.

The second-rank spinor, describing the pair of spins 1/2, can be written in the form

$$\Psi^{\lambda\mu} = c_t\Psi_t^{\lambda\mu} + c_s\Psi_s^{\lambda\mu}, \tag{56}$$

where $\Psi_t^{\lambda\mu}$ and $\Psi_s^{\lambda\mu}$ are symmetric and antisymmetric second-rank spinors, respectively, and c_t and c_s are arbitrary constants. We know that the symmetric second-rank spinor describes a system with spin $S = 1$, so that the pair of spins 1/2 in this case forms a triplet. If $\Psi^{\lambda\mu}$ is an antisymmetric second-rank spinor reducible to a scalar multiplied by $g_{\lambda\mu}$, the spin pair exists in the singlet state. Consequently, the ratio of the constants c_t and c_s determines the relative weights of the triplet and singlet components on the pair of spins $s = 1/2$ and is a parameter of the model. In particular, for $c_s = 0$ the wave function (56) contains only a triplet component, and for $c_t = 0$ it contains only a singlet component.

We note that the wave function (53) has the MP form (39) with the matrices g_i representing a mixed second-rank tensor:

$$g_i = \Psi^{\lambda}{}_{\nu}(i) = c_t \begin{pmatrix} \dfrac{1}{2}|\uparrow\downarrow + \downarrow\uparrow\rangle_i & |\downarrow\downarrow\rangle_i \\ -|\uparrow\uparrow\rangle_i & -\dfrac{1}{2}|\uparrow\downarrow + \downarrow\uparrow\rangle_i \end{pmatrix} - \frac{1}{2}c_s(|\uparrow\downarrow + \downarrow\uparrow\rangle_i\, I, \tag{57}$$
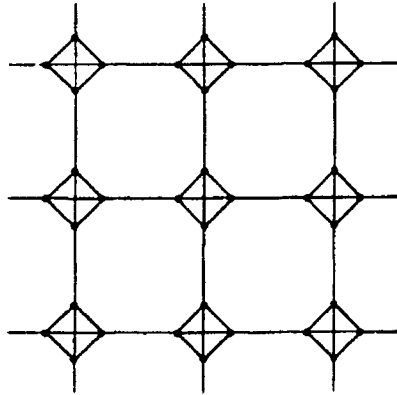
Figure 7: Two-dimensional lattice on which the spin model is defined.

where I is the unit matrix.

We now choose a Hamiltonian H for which the wave function (55) is an exact ground-state wave function. To do so, we consider the part of the system (cell) consisting of two nearest neighbor spin pairs. In the wave function (55) the factor corresponding to the two spin pairs is a second-rank spinor:

$$\Psi^{\lambda\mu}(i)g_{\mu\nu}\Psi^{\nu\rho}(i+1). \tag{58}$$

In the general case, therefore, only two of the six multiplets forming two pairs of spin $1/2$ — one singlet and one triplet — are present in the function (58). Inasmuch as four spins $1/2$ form two singlets and three triplets, the specific form of the singlet and triplet components present in the wave function (58) depends on the ratio c_s/c_t. The cell Hamiltonian acting in the spin space of nearest neighbor spin pairs can be written as the sum of the projectors onto the four missing multiplets with arbitrary positive coefficients λ_k (46). As mentioned above, the general form of the Hamiltonian (46) can be reduced to a more simple form (47) with $c_s/c_t = 2y$.

Thus, the singlet ground-state wave function of the model (46) can be also written in a spinor form (55).

4.2 Two-dimensional model

Now we consider an $N \times N$-site square lattice with cyclic boundary conditions. We replace each site of the lattice by a square (Fig.7) with spins $s = 1/2$ at its corners, making the total number of spins equal to $4N^2$. To avoid misunderstanding, however, from now on we continue to refer to these squares as sites. The wave
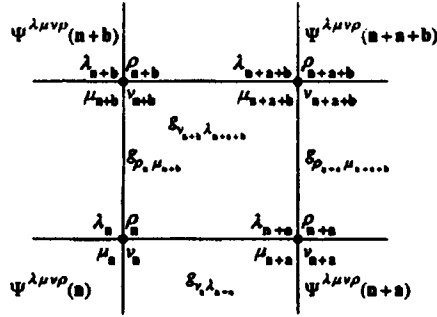
Figure 8: Graphical correspondence of the model wave function. The indices of the site spinors depend on the site index (not shown in the figure).

function of the system is described by the product of fourth-rank spinors

$$\Psi = \prod_{\mathbf{n}} \Psi^{\lambda_{\mathbf{n}} \mu_{\mathbf{n}} \nu_{\mathbf{n}} \rho_{\mathbf{n}}}(\mathbf{n}). \tag{59}$$

By analogy with (55), from Eq. (59) we form the scalar

$$\Psi = \prod_{\mathbf{n}} \Psi^{\lambda_{\mathbf{n}} \mu_{\mathbf{n}} \nu_{\mathbf{n}} \rho_{\mathbf{n}}}(\mathbf{n}) g_{\nu_{\mathbf{n}} \lambda_{\mathbf{n}+\mathbf{a}}} g_{\rho_{\mathbf{n}} \mu_{\mathbf{n}+\mathbf{b}}}. \tag{60}$$

where $\mathbf{a}$ and $\mathbf{b}$ are unit vectors in the x and y directions.

The singlet wave function (60) is conveniently identified graphically with a square lattice, each site corresponding to a fourth-rank spinor $\Psi^{\lambda \mu \nu \rho}$ (whose form is identical for all sites), and each segment linking sites corresponds to a metric spinor $g_{\lambda \mu}$ (Fig.8).

To completely define the wave function (60), it is necessary to know the form of the site spinor $\Psi^{\lambda \mu \nu \rho}$. The specific form of the fourth-rank spinor $\Psi^{\lambda \mu \nu \rho}$ [and, hence, the wave function (60)] describing the system of four spins $s = 1/2$ is governed by 14 quantities [31], which are parameters of the model.

We now choose a Hamiltonian H for which the wave function (60) is an exact ground state wave function. As in the one-dimensional case, we seek the required Hamiltonian in the form of a sum of cell Hamiltonians acting in the space of two nearest neighbor spin quartets:

$$H = \sum_{\mathbf{n}} H_{\mathbf{n},\mathbf{n}+\mathbf{a}} + \sum_{\mathbf{n}} H_{\mathbf{n},\mathbf{n}+\mathbf{b}}. \tag{61}$$

The first term in Eq. (61) is the sum of the cell Hamiltonians in the horizontal direction, and the second term is the same for the vertical. The cell Hamiltonians
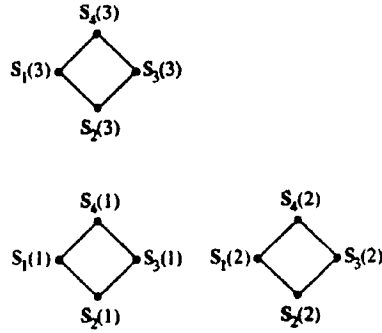
Figure 9: Lattice sites associated with interactions $H_{1,2}$ and $H_{1,3}$.

along each direction have the same form, but the "horizontal" and "vertical" Hamiltonians differ in general. In the following discussion, therefore, we consider only the Hamiltonians $H_{1,2}$ and $H_{1,3}$ (Fig.9), which describe interactions of "sites" in the x and y directions, respectively.

For the wave function (60) to be an exact eigenfunction of the Hamiltonian H, it is sufficient that the sixth-rank spinors

$$\Psi^{\lambda_1\mu_1\nu_1\rho_1}(1)\Psi^{\lambda_2\mu_2\nu_2\rho_2}(2)g_{\nu_1\lambda_2},$$
$$\Psi^{\lambda_1\mu_1\nu_1\rho_1}(1)\Psi^{\lambda_3\mu_3\nu_3\rho_3}(3)g_{\rho_1\mu_3},\tag{62}$$

be eigenfunctions of the corresponding cell Hamiltonians $H_{1,2}$ and $H_{1,3}$.

In general, when the site spinor $\Psi^{\lambda\mu\nu\rho}$ is not symmetric with respect to any indices, the possible states of two quartets of spins $s = 1/2$ consist of 70 multiplets. A wave function represented by a sixth-rank spinor contains only 20 of them. Accordingly, the cell Hamiltonians $H_{1,2}$ and $H_{1,3}$ can be represented by the sum of projectors onto the 50 missing multiplets:

$$H_{1,2} = \sum_{k=1}^{50} \lambda_k P_k^{1,2}, \qquad H_{1,3} = \sum_{k=1}^{50} \mu_k P_k^{1,3},\tag{63}$$

where the positive constants λ_k and μ_k are the excitation energies of $H_{1,2}$ and $H_{1,3}$, and the specific form of the projectors depends on 14 model parameters.

Inasmuch as

$$H_{\mathbf{n},\mathbf{n}+\mathbf{a}}|\Psi_s\rangle = 0, \quad H_{\mathbf{n},\mathbf{n}+\mathbf{b}}|\Psi_s\rangle = 0,\tag{64}$$

for the total Hamiltonian (61) we have the expression

$$H|\Psi_s\rangle = 0.\tag{65}$$

Consequently, Ψ_s is the ground-state wave function of the total Hamiltonian H, because it is a sum of nonnegative definite cell Hamiltonians. Also, it can be rigorously proved [31] that the ground state of H is non-degenerate.

As mentioned above, the specific form of the projectors depends on 14 model parameters, and in general the cell Hamiltonians (63), expressed in terms of scalar products of the type $s_i \cdot s_j$, $(s_i \cdot s_j)(s_k \cdot s_l)$, etc., have an extremely cumbersome form. We therefore consider a few special cases.

When the site spinor $\Psi^{\lambda\mu\nu\rho}$ is a symmetric fourth-rank spinor $Q^{\lambda\mu\nu\rho}$ (corresponding to the two-dimensional AKLT model[13]), only the quintet component out of the six multiplets on each spin quartet is present in the wave function (60). The sixth-rank spinors (62) are symmetric with respect to two triplets of indices and, hence, contain four multiplets with $S = 0$, 1, 2, 3 formed from two quintets. Consequently, the cell Hamiltonian ($H_{1,2}$ and $H_{1,3}$ coincide in this case) has the form

$$H_{1,2} = \sum_{k=1}^{66} \lambda_k P_k^{1,2}. \tag{66}$$

If we set $\lambda_k = 1$ ($k = 1$, 66), we can write Eq. (66) in the form

$$H_{1,2} = P_4(\mathbf{S}_1 + \mathbf{S}_2) + [1 - P_2(\mathbf{S}_1)P_2(\mathbf{S}_2)], \tag{67}$$

where $\mathbf{S}_i$ is the total spin of the quartet of spins $s = 1/2$ on the ith site, $\mathbf{S}_i = s_1(i) + s_2(i) + s_3(i) + s_4(i)$, and $P_l(\mathbf{S})$ is the projector onto the state with spin $S = l$.

If the four spins $s = 1/2$ at each site are replaced by a single spin $S = 2$ and if the wave function (60) is treated as a wave function describing a system of N^2 spins $S = 2$, the second term in the Hamiltonian (67) vanishes, and we arrive at the Hamiltonian of the two-dimensional AKLT model:

$$H_{1,2} = P_4(\mathbf{S}_1 + \mathbf{S}_2) = \frac{1}{28}\mathbf{S}_1 \cdot \mathbf{S}_2 + \frac{1}{40}(\mathbf{S}_1 \cdot \mathbf{S}_2)^2 + \frac{1}{180}(\mathbf{S}_1 \cdot \mathbf{S}_2)^3 + \frac{1}{2520}(\mathbf{S}_1 \cdot \mathbf{S}_2)^4 \tag{68}$$

Another interesting special case is encountered when the system decomposes into independent one-dimensional chains. This happens if the site spinor $\Psi^{\lambda\mu\nu\rho}$ reduces to a product of two second-rank spinors, each describing two spins $1/2$. For example,

$$\Psi^{\lambda\mu\nu\rho}(s_1, s_2, s_3, s_4) = \varphi^{\lambda\nu}(s_1, s_3)\varphi^{\mu\rho}(s_2, s_4). \tag{69}$$

In this case the Hamiltonians $H_{1,2}$ and $H_{1,3}$ contain interactions of four rather than eight spins $1/2$ and have the form (34).
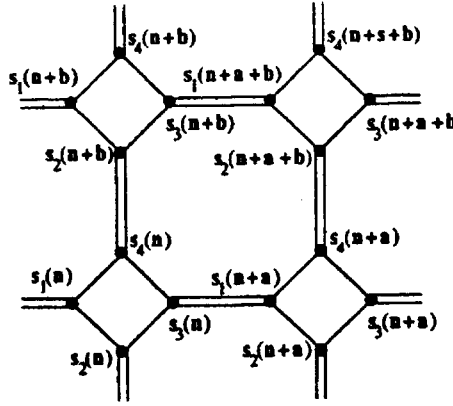
Figure 10: Pattern of independent singlet pairs (double lines).

The simplest case is when the site spinor $\Psi^{\lambda\mu\nu\rho}$ is a product of four first-rank spinors:

$$\Psi^{\lambda\mu\nu\rho}(s_1,\ s_2,\ s_3,\ s_4) = \varphi^\lambda(s_1)\varphi^\mu(s_2)\varphi^\nu(s_3)\varphi^\rho(s_4). \tag{70}$$

Now the system decomposes into independent singlet pairs (Fig.10), and the total Hamiltonian of the system has the form

$$H = \sum_{i,j}\left(\mathbf{s}_i \cdot \mathbf{s}_j + \frac{3}{4}\right), \tag{71}$$

where $\mathbf{s}_i$ and $\mathbf{s}_j$ are the spins forming the singlet pairs.

4.3   Spin correlation functions in the ground state

We now look at the problem of calculating the norm and the correlation function of the model described by the wave function (60). The expression for the norm of the wave function $G = \langle \Psi_s | \Psi_s \rangle$ has the form

$$G = \prod_{\mathbf{n}} \left\langle \Psi^{\lambda'_{\mathbf{n}}\mu'_{\mathbf{n}}\nu'_{\mathbf{n}}\rho'_{\mathbf{n}}}(\mathbf{n}) \middle| \Psi^{\lambda_{\mathbf{n}}\mu_{\mathbf{n}}\nu_{\mathbf{n}}\rho_{\mathbf{n}}}(\mathbf{n}) \right\rangle g_{\nu_{\mathbf{n}}\lambda_{\mathbf{n+a}}} g_{\rho_{\mathbf{n}}\mu_{\mathbf{n+b}}} g_{\nu'_{\mathbf{n}}\lambda'_{\mathbf{n+a}}} g_{\rho'_{\mathbf{n}}\mu'_{\mathbf{n+b}}}$$

$$= \prod_{\mathbf{n}} R^{\lambda'_{\mathbf{n}}\mu'_{\mathbf{n}}\lambda'_{\mathbf{n+a}}\mu'_{\mathbf{n+b}}}_{\lambda_{\mathbf{n}}\mu_{\mathbf{n}}\lambda_{\mathbf{n+a}}\mu_{\mathbf{n+b}}} = \prod_{\mathbf{n}} R_{\alpha_{\mathbf{n}}\beta_{\mathbf{n}}\alpha_{\mathbf{n+a}}\beta_{\mathbf{n+b}}}, \qquad \alpha_i,\ \beta_i = \{1,\ 2,\ 3,\ 4\}, \tag{72}$$

where $R_{\alpha\beta\alpha\beta}$ is a $4 \times 4 \times 4 \times 4$ matrix.

According to the selection rules for the projection of the total spin S^z, only 70 of the 256 elements in the expression $\langle \Psi^{\lambda'\mu'\nu'\rho}(\mathbf{n}) | \Psi^{\lambda\mu\nu\rho}(\mathbf{n}) \rangle$ are non-vanishing. Consequently, the matrix R also contains at most 70 elements. If we regard the elements of R as Boltzmann vertex weights, the problem of calculating the norm

reduces to the classical 70-vertex model. Since the exact solution for the 70-vertex model is unknown, numerical methods must be used to calculate the norm and the expectation values.

To calculate the above-indicated expected values, we carry out Monte Carlo calculations on 20×20-site lattices. As mentioned, the ground-state wave function of the model depends on 14 parameters and, of course, cannot possibly be analyzed completely. We confine the numerical calculations to the case in which the spinor $\Psi^{\lambda\mu\nu\rho}$ depends on one parameter α:

$$\Psi^{\lambda\mu\nu\rho} = \cos\alpha \cdot Q^{\lambda\mu\nu\rho} + \sin\alpha \cdot (A^{\lambda\mu\nu\rho} - Q^{\lambda\mu\nu\rho}), \tag{73}$$

where $\alpha \in [-\pi/2; \ \pi/2]$, the spinor $Q^{\lambda\mu\nu\rho}$ is symmetric with respect to all indices, and

$$A^{\lambda\mu\nu\rho} = \varphi^\lambda(s_1)\varphi^\mu(s_2)\varphi^\nu(s_3)\varphi^\rho(s_4). \tag{74}$$

In this case we have a one-parameter model with two well-known limiting cases. One corresponds to $\alpha = \pi/4$, for which $\Psi^{\lambda\mu\nu\rho} = A^{\lambda\mu\nu\rho}$, and the system decomposes into independent singlet pairs (Fig. 10); the other limiting case corresponds to $\alpha = 0$ (our model reduces to the two-dimensional AKLT model in this case, the spins at each site forming a quintet).

In the given model there are four spins $s = 1/2$ at each site, and the enumeration of each spin is determined by the order number of the lattice site to which it belongs and by its own number at this site. The spin correlation function therefore has the form

$$f_{ij}(\mathbf{r}) = \langle \mathbf{s}_i(\mathbf{n}) \cdot \mathbf{s}_j(\mathbf{n} + \mathbf{r}) \rangle. \tag{75}$$

In determining the spin structure of the ground state, however, it is more practical to consider the more straightforward quantity $F(\mathbf{r})$:

$$F(\mathbf{r}) = \sum_{i,j=1}^{4} \langle \mathbf{s}_i(\mathbf{n}) \cdot \mathbf{s}_j(\mathbf{n} + \mathbf{r}) \rangle = \langle \mathbf{S}(\mathbf{n}) \cdot \mathbf{S}(\mathbf{n} + \mathbf{r}) \rangle. \tag{76}$$

The function $F(\mathbf{r})$ is left unchanged by a change of sign of α. We note, however, that only the total correlation function, and not $f_{ij}(\mathbf{r})$, possesses symmetry under a change of sign of α. This assertion is evident, for example, in Fig. 11, which shows the dependence of $f_{31}(\mathbf{a})$ on α as an illustration.

The correlation function decays exponentially as $\mathbf{r}$ increases, differing from the one-dimensional model in that the pre-exponential factor also depends on $\mathbf{r}$.
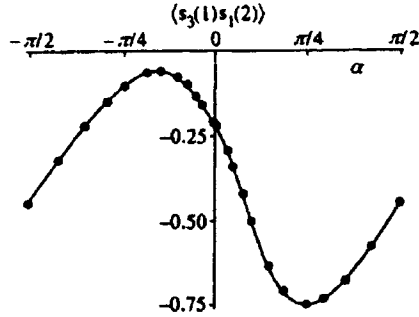
Figure 11: Dependence of the spin correlation function $\langle s_3(1)s_1(2)\rangle$ on the parameter α.

Figure 12 shows the dependence of the correlation length r_c on the parameter α. The correlation length is a maximum at the point $\alpha = 0$ (two-dimensional AKLT model), decreases as α increases, and at $\alpha = \pi/4$, when the system decomposes into independent singlet pairs (Fig. 10), it is equal to zero. With a further increase in α the correlation length increases and attains a second maximum at $\alpha = \pi/2$. Like the correlation function $F(\mathbf{r})$, the function $r_c(\alpha)$ is symmetric with respect to α. It is evident from Fig. 12 that the parameter α has two ranges corresponding to states with different symmetries. In the range $|\alpha| < \pi/4$ the correlation function $F(\mathbf{r})$ exhibits antiferromagnetic behavior:

$$F(\mathbf{r}) \propto (-1)^{r_x+r_y} e^{-|\mathbf{r}|/r_c}, \tag{77}$$

whereas the spins at one site are coupled ferromagnetically, $\langle s_i(\mathbf{n}) \cdot s_j(\mathbf{n})\rangle > 0$. On the other hand, in the range $\pi/4 < |\alpha| < \pi/2$ the correlation function $F(\mathbf{r})$ is always negative:

$$F(\mathbf{r}) \propto -e^{-|\mathbf{r}|/r_c} \tag{78}$$

and all the correlation functions at one site are also negative.

These ranges have two end points in common, $\alpha = \pm\pi/4$, where $r_c = 0$. Whereas $\alpha = \pi/4$ corresponds to the trivial partition of the system into independent singlet pairs, the case $\alpha = -\pi/4$ is more interesting. In this case one can calculate all spin correlations exactly [31]. The correlations of spins located on neighboring 'sites' of lattice at $\alpha = -\pi/4$ are antiferromagnetic, while all other correlators are zero.

The Hamiltonian for model (73) has a very combersome form and for the cases $\alpha = -\pi/4$ and $\alpha = \pi/2$ was given in [31].
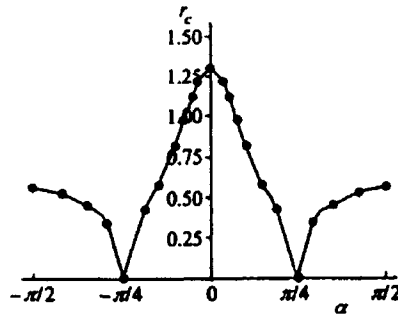
Figure 12: Dependence of the correlation length on the parameter α.

Our results suggest that the spin correlation functions decay exponentially with a correlation length ~ 1 for an arbitrary parameter α. We also assume that the decay of the correlation function is of the exponential type for the 14-parameter model as well, i.e., for any choice of site spinor $\Psi^{\lambda\mu\nu\rho}$. This assumption is supported in special cases: 1) the partition of the system into one-dimensional chains with exactly known exponentially decaying correlation functions; 2) the two-dimensional AKLT model, for which the exponential character of the decay of the correlation function has been rigorously proved [32]. Further evidence of the stated assumption lies in the numerical results obtained for various values of the parameter in the one-parameter model.

4.4 Generalization of the model to other types of lattices

The wave function (55), (60) can be generalized to any type of lattice. The general principle of wave function construction for a system of spins 1/2 entails the following:

1) Each bond on a given lattice has associated with it two indices running through the values 1 and 2, one at each end of the bond.

2) Each bond has associated with it a metric spinor $g_{\lambda\mu}$ with the indices of the ends of this bond.

3) Each site of the lattice (a site being interpreted here, of course, in the same sense as in Sec.IVB) with m outgoing bonds has associated with it an mth-rank spinor with the indices of the bonds adjacent to the site.

4) The wave function is the product of all spinors at sites of the lattice and all metric spinors.

It is obvious that each index in the formulated wave function is encountered twice, so that the wave function is scalar and, hence, singlet.

The wave function so constructed describes a system in which each lattice site contains as many spins $s = 1/2$ as the number of bonds emanating from it.

To completely define the wave function, it is necessary to determine the specific form of all site spinors. The coefficients that determine their form are then parameters of the model.

The Hamiltonian of such a model is the sum of the cell Hamiltonians acting in the spin space of the subsystem formed by the spins at two mutually coupled sites:

$$H = \sum_{\langle ij \rangle} H_{ij}. \tag{79}$$

Each cell Hamiltonian is the sum of the projectors with arbitrary positive coefficients onto all multiplets possible in the corresponding two-site subsystem except those present in the constructed wave function:

$$H_{i,j} = \sum_k \lambda_k P_k^{i,j}. \tag{80}$$

Then $H_{i,j}|\Psi_s\rangle = 0$ and, accordingly, $H|\Psi_s\rangle = 0$.

Consequently, Ψ_s is an exact ground-state wave function.

We note that any two lattice sites can be joined by two, three, or more bonds, because this does not contradict the principle of construction of the wave function. Moreover, the general principle of construction of the wave function is valid not only for translationally symmetric lattices, but for any graph in general. As an example, let us consider the system shown in Fig. 13. The wave function of this system has the form

$$\Psi_s = \Psi^{\lambda_1}(1)\Psi^{\lambda_2\mu_1\nu_1\rho_1}(2)\Psi^{\rho_2\nu_2\tau_1}(3)\Psi^{\mu_2\tau_2}(4)g_{\lambda_1\lambda_2}g_{\mu_1\mu_2}g_{\nu_1\nu_2}g_{\rho_1\rho_2}g_{\tau_1\tau_2} \tag{81}$$

and describes a system containing ten spins $1/2$.

If the given lattice has dangling bonds (as occurs for systems with open boundary conditions), the resulting wave function represents a spinor of rank equal to the number of loose ends. The ground state of this kind of system is therefore 2^l-fold degenerate, where l is the number of loose ends. For an open one-dimensional chain, for example, the ground state corresponds to four functions — one singlet and three triplet components. For higher-dimensional lattices this degeneracy depends on the size of the lattice and increases exponentially as its boundaries grow.
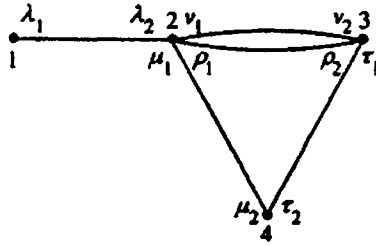
Figure 13: Example of a graph corresponding to the wave function (81).

5   Electronic models

In recent years there has been increasing interest in studying models where at least the ground state can be found exactly [33, 34]. The most popular method for the construction of exact ground state is the so-called optimal ground state approach (OGS) [34]. In the OSG method the ground state of the system is simultaneously the ground state of each local interaction. In this Section we propose new 1D and 2D models of interacting electrons with the exact ground state which are different from those constructed in the OSG method. The ground state wave function of our models is expressed in terms of the two-particle *'singlet bond'* (SB) function located on sites i and j of the lattice:

$$[i, j] = c_{i,\uparrow}^+ c_{j,\downarrow}^+ - c_{i,\downarrow}^+ c_{j,\uparrow}^+ + x \left(c_{i,\uparrow}^+ c_{i,\downarrow}^+ + c_{j,\uparrow}^+ c_{j,\downarrow}^+ \right) |0\rangle, \tag{82}$$

where $c_{i,\sigma}^+$, $c_{i,\sigma}$ are the Fermi operators and x is an arbitrary coefficient. The SB function is the generalization of the RVB function [35] including ionic states. The presence of the ionic states is very important from the physical point of view because, as a rule, the bond functions contain some amount of the ionic states as well.

It is known that for a set of 1D and 2D quantum spin models the exact ground state of which can be represented in the RVB form [15, 6, 36, 13, 31]. It is natural to try to find electronic models with an exact ground state at half-filling formed by SB functions in the same manner as for above mentioned spin models. The electronic models of these types include the correlated hopping of electrons as well as the spin interactions and pair hopping terms.

The model with dimerization.

As the first example we consider the 1D electronic model with the two-fold degenerate ground state in the form of the simple product of SB dimers, similarly to the ground state of the well-known spin-$\frac{1}{2}$ Majumdar-Ghosh model [6]. For the half-filling case the proposed ground state wave functions are:

$$\Psi_1 = [1,2][3,4]...[N-1,N] \tag{83}$$

and

$$\Psi_2 = [2,3][4,5]...[N,1] \tag{84}$$

In order to find the Hamiltonian for which the wave functions (83) and (84) are the exact ground state wave functions, we represent the Hamiltonian as a sum of local Hamiltonians h_i defined on three neighboring sites (periodic boundary conditions are supposed):

$$H = \sum_{i=1}^{N} h_i \tag{85}$$

The basis of three-site local Hamiltonians h_i consists of 64 states, while only eight of them are present in Ψ_1 and Ψ_2. These 8 states are

$$[i, i+1]\, \varphi_{i+2}, \qquad \varphi_i\, [i+1, i+2], \tag{86}$$

where φ_i is one of four possible electronic states of i-th site: $|0\rangle_i,\ |\uparrow\rangle_i,\ |\downarrow\rangle_i,\ |2\rangle_i$.

The local Hamiltonian h_i for which all the functions (86) are the exact ground state wave functions can be written as the sum of the projectors onto other 56 states $|\chi_k\rangle$

$$h_i = \sum_k \lambda_k |\chi_k\rangle \langle \chi_k|, \tag{87}$$

where λ_k are arbitrary positive coefficients. This means that the wave functions Ψ_1 and Ψ_2 are the ground states of each local Hamiltonian with zero energy. Hence, Ψ_1 and Ψ_2 are the 'optimal' ground state wave functions of the total Hamiltonian H with zero energy, similarly to the models in [10, 34, 37, 12]. In general case, the local Hamiltonian h_i is many-parametrical and depends on parameters λ_k and x. We consider one of the simplest forms of h_i including the correlated hopping of electrons of different types and spin interactions between nearest- and next-nearest neighbor sites:

$$\begin{aligned}
h_i \;=\; & 2 - x\left(t_{i,i+1} + t_{i+1,i+2}\right) \\
& + \left(x^2 - (1+x^2)(1-n_{i+1})^2\right) T_{i,i+2} \\
& + 8\frac{1-x^2}{3}(\mathbf{S}_i \cdot \mathbf{S}_{i+1} + \mathbf{S}_{i+1} \cdot \mathbf{S}_{i+2} + \mathbf{S}_i \cdot \mathbf{S}_{i+2}),
\end{aligned} \tag{88}$$

where

$$T_{i,j} = \sum_\sigma (c_{i,\sigma}^+ c_{j,\sigma} + c_{j,\sigma}^+ c_{i,\sigma})(1 - n_{i,-\sigma} - n_{j,-\sigma}),$$

$$t_{i,j} = \sum_\sigma (c_{i,\sigma}^+ c_{j,\sigma} + c_{j,\sigma}^+ c_{i,\sigma})(n_{i,-\sigma} - n_{j,-\sigma})^2 \tag{89}$$

and $\mathbf{S}_i$ is the $SU(2)$ spin operator.

Each local Hamiltonian h_i is a non-negatively defined operator at $|x| \leq 1$. The following statements related to the Hamiltonian (88) are valid:

1. The functions (83) and (84) are the only two ground state wave functions of the Hamiltonian (88) at $N_e = N$ (N_e is the total number of electrons). They are not orthogonal, but their overlap is $\sim e^{-N}$ at $N \gg 1$.

2. The ground state energy $E_0(N_e/N)$ is a symmetrical function with respect to the point $N_e/N = 1$ and has a global minimum $E_0 = 0$ at $N_e/N = 1$.

3. The translational symmetry of (88) is spontaneously broken in the ground state leading to the dimerization:

$$\langle |t_{i,i+1} - t_{i+1,i+2}| \rangle = 2$$

The excited states of the model can not be calculated exactly but we expect that there has to be a gap, because the ground state is formed by the ultrashort-range SB functions. If this is the case, the function $E_0(N_e/N)$ has a cusp at $N_e/N = 1$.

Actually, this model is the fermion version of the Majumdar – Ghosh spin model. Moreover, it reduces to the Majumdar – Ghosh model at $x = 0$ and in the subspace with $n_i = 1$.

For $x = 1$ the Hamiltonian (88) simplifies and takes the form:

$$H = -2\sum_j t_{j,j+1} - \sum_j e^{i\pi n_{j+1}} T_{j,j+2} \tag{90}$$

The 2D model.

We can easily construct the 2D electronic model with the exact ground state which is analogous to the Shastry – Sutherland model [36] (Fig.14). The Hamiltonian of this model is:

$$H = \sum_{\{i,j,k\}} h_{i,j} + h_{i,k} + h_{j,k}^d, \tag{91}$$

where the sum is over all triangles $\{i, j, k\}$, one of which is shown on Fig.14. So, each diagonal line belongs to the two different triangles. The local Hamiltonians
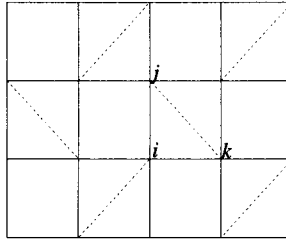
Figure 14: The lattice of the Shastry – Sutherland model

$h_{j,k}^d$ acting on the diagonal of the triangle $\{i, j, k\}$, and $h_{i,j}$, $h_{i,k}$ have the form (for the sake of simplicity we put $x = 1$)

$$
\begin{aligned}
h_{j,k}^d &= -2\, t_{j,k} + 4 \\
h_{i,j} &= -t_{i,j} - e^{i\pi n_k}\, T_{i,j} \\
h_{i,k} &= -t_{i,k} - e^{i\pi n_j}\, T_{i,k}
\end{aligned}
\tag{92}
$$

It is easy to check that

$$
h_{j,k}^d\, |\varphi_i\, [j, k]\rangle = (h_{i,j} + h_{i,k})\, |\varphi_i\, [j, k]\rangle = 0
$$

All other states of the local Hamiltonian $h_{i,j} + h_{i,k} + h_{j,k}^d$ have higher energies. Therefore, the ground state wave function in the half-filling case is the product of the SB functions located on the diagonals shown by dashed lines on Fig.14. This model has non-degenerate singlet ground state with ultrashort-range correlations.

The ladder model.

Let us now consider electronic models with a more complicated ground state including different configurations of short-range SB functions. The form of these ground states is similar to that for spin models proposed in [13] and generalized in [31]. In the 1D case our model describes the two-leg ladder model (Fig.4). Its ground state is a superposition of the SB functions where each pair of nearest neighbor rungs of the ladder is connected by one SB.

The wave function of this ground state can be written in a form (55):

$$
\Psi_s = \psi^{\lambda\mu}(1) g_{\mu\nu} \psi^{\nu\rho}(2) g_{\rho\kappa} \ldots \psi^{\sigma\tau}(N) g_{\tau\lambda}
\tag{93}
$$

The functions $\psi^{\lambda\mu}(i)$ describes the i-th rung of the ladder

$$
\psi^{\lambda\mu}(i) = c_1 \varphi_{2i-1}^{\lambda} \varphi_{2i}^{\mu} + c_2 \varphi_{2i}^{\lambda} \varphi_{2i-1}^{\mu}
\tag{94}
$$

with

$$\varphi_k^\lambda = \begin{pmatrix} |{\uparrow}\rangle_k \\ |{\downarrow}\rangle_k \\ |2\rangle_k \\ |0\rangle_k \end{pmatrix}, \qquad g_{\lambda\mu} = \begin{pmatrix} 0 & 1 & 0 & 0 \\ -1 & 0 & 0 & 0 \\ 0 & 0 & 0 & x \\ 0 & 0 & x & 0 \end{pmatrix} \qquad (95)$$

It is easy to see that

$$g_{\lambda\mu}\varphi_i^\lambda \varphi_j^\mu = [i, j]$$

Therefore, the function Ψ_s is a singlet wave function depending on two parameters x and c_1/c_2. Actually, this form of Ψ_s is equivalent to the MP form with 4×4 matrices $A_{\lambda\nu}(i) = g_{\lambda\mu}\psi^{\mu\nu}(i)$. Moreover, at $x = 0$ and $c_1/c_2 = -1$ the function Ψ_s reduces to the wave function of the well-known AKLT spin-1 model.

In order to find the Hamiltonian for which the wave function (93) is the exact ground state wave function, it is necessary to consider what states are present on the two nearest rungs in Ψ_s. It turns out that there are only 16 states from the total 256 ones in the product $\psi^{\lambda\mu}(i)g_{\mu\nu}\psi^{\nu\rho}(i+1)$. The local Hamiltonian h_i acting on two nearest rungs i and $i + 1$ can be written in the form of (87) with the projectors onto the 240 missing states. The total Hamiltonian is the sum of local ones (85). The explicit form of this Hamiltonian is very cumbersome and, therefore, it is not given here.

The correlation functions in the ground state (93) can be calculated exactly in the same manner as was done for spin models [13]. It can be shown that all of correlations exponentially decay in the ground state. We expect also that this model has a gap.

This method of construction of the exact ground state can be generalized also to 2D and 3D lattices, as was done in Sec.IV. Following [31], one can rigorously prove that the ground state of these models is always a non-degenerate singlet.

1D models with a giant spiral order.

There is one more spin-$\frac{1}{2}$ model with an exact ground state of the RVB type [15]. This is the model (9) describing the F-AF transition point. The exact singlet ground state can be expressed by the combinations of the RVB functions (i, j) distributed uniformly over the lattice points (8). The analog of the wave function (8) in the SB terms is:

$$\Psi_0 = \sum_{i<j\ldots} (-1)^P [i, j][k, l][m, n]\ldots, \qquad (96)$$

where $P = (i, j, k, l, \ldots)$ is the permutation of numbers $(1, 2, \ldots N)$. It is interesting to note that the singlet wave function (96) can be also written in the MP form but with infinite size matrices [17].

In order to find the Hamiltonian for which the wave function (96) is the exact ground-state wave function, let us consider what states are present on the two nearest sites in the Ψ_0. It turns out [17] that there are only 9 states from the total 16 ones in (96). They are

$$|\uparrow\uparrow\rangle, \qquad |\downarrow\downarrow\rangle, \qquad |\uparrow\downarrow + \downarrow\uparrow\rangle, \qquad |20 - 02\rangle,$$
$$|\uparrow\downarrow - \downarrow\uparrow\rangle + x\,|20 + 02\rangle, \qquad |\uparrow\,0 - 0\,\uparrow\rangle,$$
$$|\uparrow\,2 - 2\,\uparrow\rangle, \qquad |\downarrow\,0 - 0\,\downarrow\rangle, \qquad |\downarrow\,2 - 2\,\downarrow\rangle \tag{97}$$

The local Hamiltonian $h_{i,i+1}$ can be written as the sum of the projectors onto the 7 missing states (87). At $|x| > 1$ the most simple form of this total Hamiltonian is:

$$
\begin{aligned}
H \;=\; & \sum_{i=1}^{N} \left(T_{i,i+1} - \frac{2}{x} t_{i,i+1} - 4\,\mathbf{S}_i \cdot \mathbf{S}_{i+1} \right. \\
& \left. + \; \frac{4}{x^2}\eta_i \cdot \eta_{i+1} + 4\frac{x^2 - 3}{x^2}\eta_i^z \eta_{i+1}^z + 1 \right)
\end{aligned}
\tag{98}
$$

We use here η operators:

$$\eta_i^+ = c_{i,\downarrow}^+ c_{i,\uparrow}^+, \qquad \eta_i^- = c_{i,\uparrow} c_{i,\downarrow}, \qquad \eta_i^z = \frac{1 - n_i}{2},$$

which form another $SU(2)$ algebra [38, 39], and $\eta_1 \cdot \eta_2$ is a scalar product of pseudo-spins η_1 and η_2. We note that this Hamiltonian commutes with $\mathbf{S}^2$, but does not commute with η^2. It can be proved [17] that only three multiplets are the ground states of (98): the singlet state (96), the trivial ferromagnetic state $S = N/2$ and the state with $S = N/2 - 1$.

The norm and the correlators of the electronic model (98) in the singlet ground state are exactly calculated [17]. For example, the norm of (96) is:

$$\langle \Psi_0 | \Psi_0 \rangle = \frac{d^N}{d\xi^N} \left(2\frac{1 + \cosh(x\xi)}{\cos^2(\frac{\xi}{2})} \right)\bigg|_{\xi=0}$$

The correlators at $N \gg 1$ are

$$
\begin{aligned}
\langle \eta_i^z \eta_{i+l}^z \rangle \;=\; & O\left(\frac{1}{N^2}\right), \qquad \langle \eta_i^- \eta_{i+l}^+ \rangle = O\left(\frac{1}{N^2}\right), \\
\langle c_{i,\sigma}^+ c_{i+l,\sigma} \rangle \;=\; & O\left(\frac{1}{N}\right), \qquad \langle \mathbf{S}_i \mathbf{S}_{i+l} \rangle = \frac{1}{4}\cos\left(\frac{2\pi l}{N}\right)
\end{aligned}
\tag{99}
$$

The correlator $\langle \eta_i^+ \eta_{i+l}^- \rangle$ which determines the off-diagonal long-range order (ODLRO) [40] vanishes in the thermodynamic limit. At the same time the spin-spin correlations have a spiral form, and the period of the spiral equals the system size as in the spin model (9).

Another electronic model can be obtained by making the canonical transformation $c_{i,\uparrow}^+ \to c_{i,\uparrow}^+$ and $c_{i,\downarrow}^+ \to c_{i,\downarrow}$. As a result of this transformation, the SB function (82) becomes:

$$\{i,j\} = c_{i,\uparrow}^+ c_{i,\downarrow}^+ - c_{j,\uparrow}^+ c_{j,\downarrow}^+ - x \left(c_{i,\uparrow}^+ c_{j,\downarrow}^+ + c_{i,\downarrow}^+ c_{j,\uparrow}^+ \right) |0\rangle , \qquad (100)$$

and the wave function (96) changes to

$$\Psi_0 = \sum_{i<j\ldots} \{i,j\}\{k,l\}\{m,n\}\ldots \qquad (101)$$

The function (101) for $|x| > 1$ is the exact ground state wave function of the transformed Hamiltonian:

$$\begin{aligned}
H &= \sum_{i=1}^{N} \left(-T_{i,i+1} - \frac{2}{x} t'_{i,i+1} - 4\eta_i \cdot \eta_{i+1} \right. \\
&\quad \left. + \frac{4}{x^2} \mathbf{S}_i \cdot \mathbf{S}_{i+1} + 4\frac{x^2-3}{x^2} S_i^z S_{i+1}^z + 1 \right) , \qquad (102)
\end{aligned}$$

where

$$t'_{i,i+1} = \sum_\sigma \sigma (c_{i,\sigma}^+ c_{i+1,\sigma} + c_{i+1,\sigma}^+ c_{i,\sigma})(n_{i,-\sigma} - n_{i+1,-\sigma})^2$$

This Hamiltonian commutes with η^2 but does not commute with $\mathbf{S}^2$. Therefore, the eigenfunctions of the Hamiltonian (102) can be described by quantum numbers η and η^z. For the cyclic model the states with three different values of η have zero energy [17] [as it was for the model (98)]. They include one state with $\eta = 0$ (101), all states with $\eta = N/2$:

$$\Psi_{N/2,\,\eta^z} = (\eta^+)^{N/2-\eta^z} |0\rangle , \qquad (103)$$

and the states with $\eta = N/2 - 1$. Therefore, for the case of one electron per site $(\eta^z = 0)$, the ground state of the model (102) is three-fold degenerate.

The correlation functions in the ground states with $\eta = N/2$ and $\eta = N/2 - 1$ for the half-filling case coincide with each other and at $N \gg 1$ they are:

$$\langle c_{i,\sigma}^+ c_{i+l,\sigma} \rangle = O\left(\frac{1}{N}\right), \qquad \langle \mathbf{S}_i \mathbf{S}_{i+l} \rangle = O\left(\frac{1}{N^2}\right),$$

$$\langle \eta_i^z \eta_{i+l}^z \rangle = O\left(\frac{1}{N}\right), \qquad \langle \eta_i^- \eta_{i+l}^+ \rangle = \frac{1}{4} + O\left(\frac{1}{N}\right) \qquad (104)$$

The existence of the ODLRO immediately follows from the latter equations. The correlation functions in the ground state (101) have similar forms as in Eqs.(99):

$$\langle c_{i,\sigma}^{+}\, c_{i+l,\sigma}\rangle = O\left(\frac{1}{N}\right), \qquad \langle \mathbf{S}_i \mathbf{S}_{i+l}\rangle = O\left(\frac{1}{N^2}\right),$$

$$\langle \eta_i^{-}\eta_{i+l}^{+}\rangle = 2\,\langle \eta_i^{z}\eta_{i+l}^{z}\rangle = \frac{1}{6}\cos\left(\frac{2\pi l}{N}\right) \tag{105}$$

The giant spiral ordering in the last equation implies the existence of ODLRO and, therefore, of superconductivity [40] in the ground state (101).

Similarly to the original spin model (9) [11, 18] the last two electronic models (98),(102) describe the transition points on the phase diagram between the phases with and without a long-range order [ferromagnetic for the model (98) and off-diagonal for the model (102)]. Therefore, we suggest the formation of the ground state with giant spiral order (ferromagnetic or off-diagonal) as a probable scenario of the subsequent destruction of ferromagnetism and superconductivity.

6 Conclusion

We have considered the class of the 1D and 2D spin and electronic models with an exact ground states.

One of these models is the spin-$\frac{1}{2}$ ladder with competing interactions of the ferro- and antiferromagnetic types at the F-AF transition line. The exact singlet ground-state wave function on this line is found in the special form expressed in terms of auxiliary Bose-operators. The spin correlators in the singlet state show double-spiral ordering with the period of spirals equal to the system size.

In the general case the proposed form of the wave function corresponds to the MP form but with matrices of infinite size. However, for special values of parameters of the model it can be reduced to the standard MP form. In particular, we consider a spin-$\frac{1}{2}$ ladder with nondegenerate antiferromagnetic ground state for which the ground state wave function is the MP one with 2×2 matrices. This model has some properties of 1D AKLT model and reduces to it in definite limiting case.

The ground state wave function of the spin ladders can be represented in an alternative form as a product of second-rank spinors associated with the lattice sites and the metric spinors corresponding to bonds between nearest neighbor sites. Two-dimensional spin-$\frac{1}{2}$ model is constructed with exact ground state wave function of this type. The ground state of this model is a nondegenerate singlet

with exponential decay of spin correlators. We believe the model has a gap in the spectrum of excitations.

We propose new models of interacting electrons with the exact ground state formed by the singlet bond functions in the same manner as for some spin models. In particular, we have considered the models describing the boundary points on the phase diagram between the phases with and without long-range order (ferromagnetic or off-diagonal).

In conclusion we note that the construction of considered models is based on the following property. Their Hamiltonians are the sums of the cell Hamiltonians that are local and non-commuting with each other. At the same time the ground-state wave function of the total Hamiltonian is the ground state for each cell Hamiltonian. It is clear that these models are rather special. Nevertheless, the study of them is useful for understanding properties of the real frustrated spin systems and strongly correlated electronic models.

References

[1] E.Dagotto, Int.J.Mod.Phys.B5, 907 (1991).

[2] R.Chitra, S.Pati, H.R.Krishnamurthy, D.Sen, S.Ramasesha, Phys.Rev.B 52, 6581 (1995).

[3] T.Tonegawa and I.Harada, J.Phys.Soc.Japan 56, 2153 (1987); 58, 2902 (1989).

[4] R.Bursill, G.A.Gehring, D.J.J.Farnell, J.B.Parkinson, Tao Xiang and Chen Zeng, J.Phys.Cond.Mat. 7, 8605 (1995).

[5] K.Nomura and K.Okamoto, Phys.Lett.A 169, 433 (1992).

[6] C.K.Majumdar and D.K.Ghosh. J.Math.Phys. 10, 1388, 1399 (1969).

[7] Y.Mizuno, T.Tohyama, S.Maekawa, T.Osafune, N.Motoyama, H.Eisaki, S.Uchida, Phys. Rev. B57, 5326 (1997).

[8] J.B.Goodenough,
Phys. Rev. 100, 564 (1955); J.Kanamori, J.Phys.Chem.Solids 10, 87 (1959); P.W.Anderson, Solid State Phys. 14, 99 (1963).

[9] M.Fannes, B.Nachtergaele, R.F.Werner, Commun. Math. Phys. **144**, 443 (1992).

[10] A.Klumper, A.Schadschneider and J.Zittartz, Z.Phys.B **87** , 281 (1992); Europhys. Lett. **24** (4), 293 (1993); C.Lange, A.Klumper and J.Zittartz. Z.Phys.B **96**, 267 (1994).

[11] D.V.Dmitriev, V.Ya.Krivnov, A.A.Ovchinnikov, Phys. Rev. B **56** 5985 (1997).

[12] A.K.Kolezhuk, H.-J.Mikeska, Int. J. Mod. Phys. B **12**, 2325 (1998).

[13] I.Affleck, T.Kennedy, E.H.Lieb and H.Tasaki. Phys.Rev.Lett. **59**, 799 (1987), Commun.Math.Phys. **115**, 477 (1988).

[14] D.V.Dmitriev, V.Ya.Krivnov, A.A.Ovchinnikov, Z.Phys. B**103**, 193 (1997).

[15] T.Hamada, J.Kane, S.Nakagawa and Y.Natsume. J.Phys.Soc.Jpn. **57**, 1891 (1988); **58**, 3869 (1989).

[16] P.van Leuven. Physica **45**, 86 (1969).

[17] D.V.Dmitriev, V.Ya.Krivnov, A.A.Ovchinnikov, Phys. Rev. B **61**, 14592 (2000).

[18] V.Ya.Krivnov and A.A.Ovchinnikov, Phys.Rev.B **53**, 6435 (1996).

[19] A.V.Chubukov and T.Jolicoeur, Phys.Rev.B **44**, 12050 (1991).

[20] A.V.Chubukov. Phys.Rev.B **44**, 4693 (1991).

[21] S.R.White and I.Affleck, Phys.Rev.B **54**, 9862 (1996).

[22] K.Hida, Phys. Rev. B **45**, 2207 (1992).

[23] D.G.Shelton, A.A.Nersesyan, A.M.Tsvelik, Phys. Rev. B **53**, 8521 (1996).

[24] D.V.Dmitriev, V.Ya.Krivnov, A.A.Ovchinnikov, Eur.Phys.J. B **14**, 91 (2000).

[25] A.K.Kolezhuk, H.-J.Mikeska, S.Yamamoto, Phys. Rev. B **55**, R3336 (1997).

[26] D.V.Dmitriev, V.Ya.Krivnov, A.A.Ovchinnikov, JETP **92**, 146 (2001).

[27] A.A.Aligia, cond-mat/0009175.

[28] F.G.Dyson. Phys.Rev. **102**, 1230 (1956); S.V.Maleev. Sov.Phys. JETP **33**, 1010 (1957).

[29] W.D.Freitag, E.Muller-Hartmann, Z.Phys. B **83**, 381 (1991).

[30] S.Knabe, J.Stat.Phys. **52**, 627 (1988).

[31] D.V.Dmitriev, V.Ya.Krivnov, A.A.Ovchinnikov, JETP **88**, (1999) 138.

[32] T. Kennedy, E. H. Lieb, and H. Tasaki, J. Statist. Phys. **53**, 383 (1988).

[33] R.Strack, D.Vollhardt, Phys. Rev. Lett. **70**, 2637 (1993), Phys. Rev. Lett.**72**, 3425 (1994).

[34] Jan de Boer, A.Schadschneider, Phys. Rev. Lett. **75**, 4298 (1995).

[35] P.W.Anderson, Mater. Res. Bull.**8**, 153 (1972); Science **235**, 1196 (1987).

[36] B.S.Shastry, B.Sutherland, Physica **108B** 1069 (1981).

[37] A.K.Kolezhuk, H.-J.Mikeska, Europ. Phys. Journ. B **5**, 543 (1998); Phys. Rev. Lett. **80**, 2709 (1998).

[38] C.N.Yang, Phys. Rev. Lett. **63**, 2144 (1989).

[39] F.H.L.Essler, V.E.Korepin, K.Schoutens, Phys. Rev. Lett. **68**, 2960 (1992); Phys. Rev. Lett. **70**, 73 (1993).

[40] C.N.Yang, Rev. Mod. Phys. **34**, 694 (1962).

[41] D.V.Dmitriev, V.Ya.Krivnov, A.A.Ovchinnikov, JETP Letters **72**, 82 (2000).

INDEX